SHOUT
SHARE
IT

MBL

Volume 200 Number 1

THE
BIOLOGICAL
BULLETIN

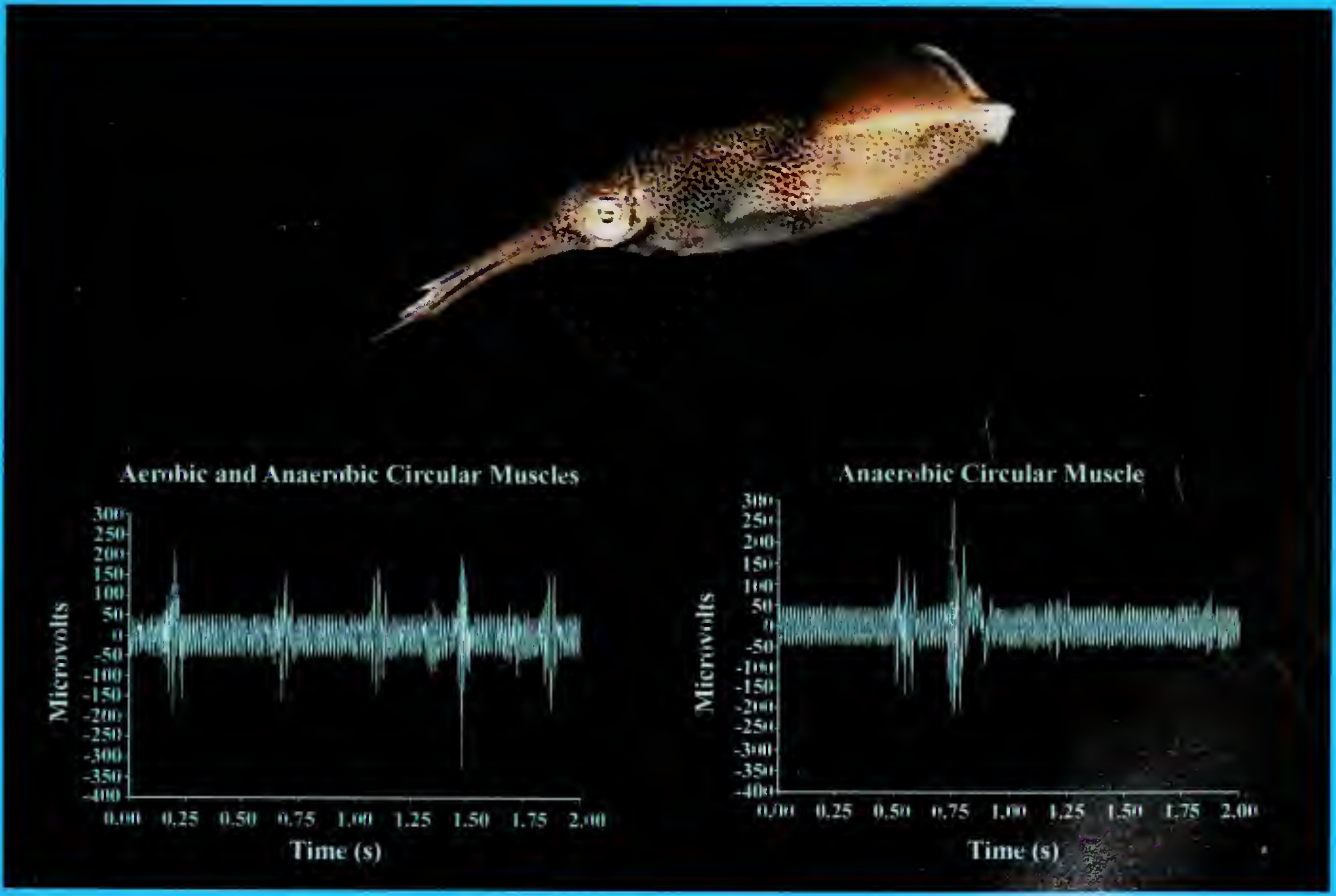

FEBRUARY 2001

Published by the Marine Biological Laboratory

Thanks Galileo, Hooke and Leeuwenhoek for the incentive.

We walk in the footsteps of visionaries.
And see with the eyes of disciples.

Galileo up close: astronomer, physicist, mathematician, dethroner of Aristotle, defender of Copernicus and, yes, credited with making double convex lenses and the first biological observations with a microscope. A compound microscope. In 1624.

Hooke: 43 years later, the compound microscope reveals living things are composed of cells.

Leeuwenhoek: invents the first practical microscope and discovers bacteria.

Armed with the knowledge and inspiration of these and other Olympians, secure in the history of our own accomplishments and aware that the mind's eye should always focus on challenging the enigmatic as well as the undeniable, Olympus has created the BX2 series of clinical and research microscopes, noteworthy for their enhancements in optics, imaging and ergonomics.

And each so individual, it deserves the nomenclature My Microscope.

From possibility to actuality, it is wonderful to behold.
A posse ad esse est mirabile visu.

Welcome to the next golden age of microsopy.

BX2 Microscope Series

The BX41

The new standard in laboratory microscopy vis-a-vis performance, versatility, operation.

Uncanny digitized imaging: enhanced with the **DP11 digital camera**, delivering high-resolution image recording beyond the norm.

Unusually insightful optics: observe magnifications from **1.25x to 100x without changing the condenser.** Choice of condensers includes Abbe, swing-out, phase-contrast and darkfield.

Unerringly precise-motion stage: selectable for right/left hand. Discover speed, ease, touch, comfort, and clinical accuracy.

Uncommonly easy-to-operate controls: extended fine-focus knob; forwarded-positioned illumination intensity dial; tactile X-Y control.

The BX45

The new standard in ergonomic microscopy. A dramatic metamorphosis: innovative, intelligent, insightful design improvements specifically addressing the needs of those spending hours looking through a microscope.

The **lowest low-position stage: three inches lower** than standard microscopes, offering the promise of minimum effort and hand movement when changing specimens.

The **tilting, telescoping observation tube:** a marvel of adjustability, it can be changed to accommodate any observation position. 80mm higher and 70mm closer to the operator than a conventional tilting tube. And the eyepoint can be moved forward by 45mm and inclined from 0–25 degrees.

The BX51

The new standard in research microscopy. The words "new" and "standard" really don't do it justice. How about "ingenious" or "original," "paragon" or "prototypical." Prepare yourself for a higher power.

The **6-position filter cube turret:** Not 4, not 5, but 6, so single and multi-band imaging of new fluorochromes and fluorescent proteins is faster, simpler and exclusively tailored.

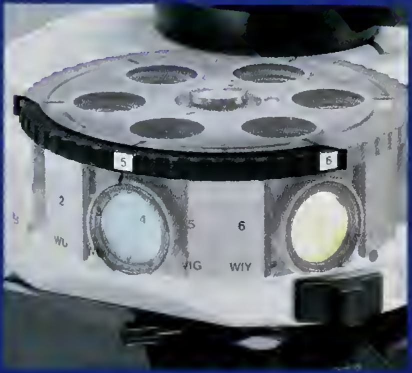

The **rectangular field stop: ours alone**. By cleverly matching the camera's field of view, only the area requiring fluorescence excitation is exposed. Which means that the surrounding areas are protected from photo bleaching.

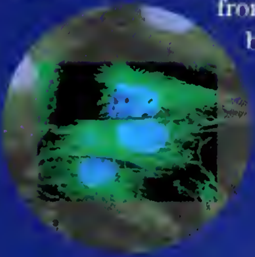

The **fluorescence excitation balancers:** another **Olympus exclusive**. A continuously variable excitation bandwidth. Visualization is enhanced, differentiation of multi-labels is immeasurably improved, capturing of images is at an unheard-of level.

Triple Labeled Specimen (l to r):

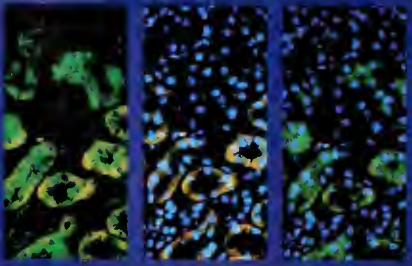

- with prevalent FITC and Cy3
- with prevalent DAPI and Cy3
- with balanced fluorescence emission

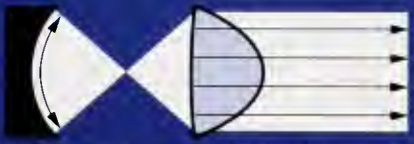

The **aspherical collector lens:** *sui generis*, in a class by itself. Specimens appear **brighter** and **more evenly illuminated**; and achromatic performance now incorporates wavelengths from UV to IR.

The **universal condenser: with 8 positions**, it can accept optical inserts for DIC, phase, brightfield and darkfield illumination. And the advanced Nomarski DIC system has been expanded and optimized to encompass prisms for enhanced contrast and image resolution.

PH1
PH2
DIC10
DIC20
DIC40

OLYMPUS®
FOCUS ON LIFE

Visit us at www.olympusamerica.com
or call 1-800-455-8236

© Olympus America Inc.

THE
BIOLOGICAL BULLETIN
FEBRUARY 2001

FEB 26 2001

Editor	Michael J. Greenberg	The Whitney Laboratory, University of Florida
Associate Editors	Louis E. Burnett	Grice Marine Biological Laboratory, College of Charleston
	R. Andrew Cameron	California Institute of Technology
	Charles D. Derby	Georgia State University
	Michael LaBarbera	University of Chicago
Section Editor	Shinya Inoué, *Imaging and Microscopy*	Marine Biological Laboratory
Online Editors	James A. Blake, *Keys to Marine Invertebrates of the Woods Hole Region*	ENSR Marine & Coastal Center, Woods Hole
	William D. Cohen, *Marine Models Electronic Record and Compendia*	Hunter College, City University of New York
Editorial Board	Peter B. Armstrong	University of California, Davis
	Ernest S. Chang	Bodega Marine Lab., University of California, Davis
	Thomas H. Dietz	Louisiana State University
	Richard B. Emlet	Oregon Institute of Marine Biology, Univ. of Oregon
	David Epel	Hopkins Marine Station, Stanford University
	Gregory Hinkle	Cereon Genomics, Cambridge, Massachusetts
	Makoto Kobayashi	Hiroshima University of Economics, Japan
	Esther M. Leise	University of North Carolina Greensboro
	Donal T. Manahan	University of Southern California
	Margaret McFall-Ngai	Kewalo Marine Laboratory, University of Hawaii
	Mark W. Miller	Institute of Neurobiology, University of Puerto Rico
	Tatsuo Motokawa	Tokyo Institute of Technology, Japan
	Yoshitaka Nagahama	National Institute for Basic Biology, Japan
	Sherry D. Painter	Marine Biomed. Inst., Univ. of Texas Medical Branch
	J. Herbert Waite	University of California, Santa Barbara
	Richard K. Zimmer	University of California, Los Angeles
Editorial Office	Pamela Clapp Hinkle	Managing Editor
	Victoria R. Gibson	Staff Editor
	Carol Schachinger	Editorial Associate
	Carol Marrama	Subscription & Advertising Secretary

Published by
Marine Biological Laboratory
Woods Hole, Massachusetts

Cover

The brief squid, *Lolliguncula brevis*, is a small cephalopod mollusc found in shallow coastal waters from Delaware Bay south to Texas and Brazil. It is the only species of cephalopod frequently caught in estuaries, and is noteworthy for its ability to tolerate euryhaline waters. The brief squid on the cover is swimming by jet propulsion in a water tunnel at intermediate speeds (~15 cm s^{-1}); the image is from a single video frame.

The circular muscles of the mantle of squids and cuttlefishes are responsible for body contractions during jetting and consist of three anatomically and metabolically distinct layers. The inner and outer (peripheral) layers have structural and biochemical features characteristic of aerobic muscle, whereas the middle (central) layer has characteristics of anaerobic muscle. This has led to the hypothesis that the peripheral muscle layers – analogous to the red muscle in fish – are employed in slow, steady swimming and in rhythmic, respiratory contractions, whereas the central layer is analogous to the white muscle in fish and is used during burst swimming, escape, and in the capture of prey.

I.K. Bartol (see p. 59 in this issue) has now tested these predictions about the functional roles of the circular muscle layers of the mantle in swimming squid. Bartol captured brief squid in the Chesapeake Bay and fitted them with paired electrodes embedded either in both the peripheral aerobic and central anaerobic circular muscles or only in the latter. Electromyograms (EMGs) were recorded from the electrodes, while video recordings were made of the squid swimming against a range of steady currents in a water tunnel. The waveforms on the left side of the cover are EMGs recorded over five jet cycles from both muscle layers, whereas the EMGs on the right are recorded over four jet cycles from the central anaerobic circular muscle. In both cases, the steady current was 15 cm s^{-1}. Although central anaerobic circular muscle activity was first detected at these intermediate swimming speeds, it does not occur with each contraction of the mantle at such speeds.

Bartol presents evidence that the peripheral aerobic and the central anaerobic circular muscle fibers in squid have distinct functional roles during swimming that are indeed similar to those of red and white myotomal fibers in fishes. Unlike fishes, however, squids appear to use anaerobic muscle at subcritical speeds. This discovery of functional "gears" in squids – yet another instance of convergent evolution in fishes and cephalopods – suggests that the locomotive muscle in squids is specialized and efficiently used.

CONTENTS

Volume 200, No. 1: February 2001

BIOMECHANICS

Etnier, Shelley
Flexural and torsional stiffness in multi-jointed biological beams 1

Nauen, Jennifer C., and George V. Lauder
Three-dimensional analysis of finlet kinematics in the chub mackerel (*Scomber japonicus*) 9

DEVELOPMENT AND REPRODUCTION

Amano, Shigetoyo, and Isao Hori
Metamorphosis of coeloblastula performed by multipotential larval flagellated cells in the calcareous sponge *Leucosolenia laxa* 20

ECOLOGY AND EVOLUTION

McEdward, L. R., and K. H. Morgan
Interspecific relationships between egg size and the level of parental investment per offspring in echinoderms 33

Kinzie, Robert A., III, Michelle Takayama, Scott R. Santos, and Mary Alice Coffroth
The adaptive bleaching hypothesis: experimental tests of critical assumptions 51

PHYSIOLOGY

Bartol, Ian K.
Role of aerobic and anaerobic circular mantle muscle fibers in swimming squid: electromyography . . . 59

Zielinski, S., F. J. Sartoris, and H. O. Pörtner
Temperature effects on hemocyanin oxygen binding in an Antarctic cephalopod 67

Medler, Scott, and Harold Silverman
Muscular alteration of gill geometry *in vitro*: implications for bivalve pumping processes 77

RESEARCH NOTES

Browne, Kenneth A., and Richard K. Zimmer
Controlled field release of a waterborne chemical signal stimulates planktonic larvae to settle 87

Dawson, Michael N., and David K. Jacobs
Molecular evidence for cryptic species of *Aurelia aurita* (Cnidaria, Scyphozoa) 92

THE BIOLOGICAL BULLETIN

THE BIOLOGICAL BULLETIN is published six times a year by the Marine Biological Laboratory, 7 MBL Street, Woods Hole, Massachusetts 02543.

Subscriptions and similar matter should be addressed to Subscription Manager, THE BIOLOGICAL BULLETIN, Marine Biological Laboratory, 7 MBL Street, Woods Hole, Massachusetts 02543. Subscription per year (six issues, two volumes): $235 for libraries; $95 for individuals. Subscription per volume (three issues): $117.50 for libraries; $47.50 for individuals. Back and single issues (subject to availability): $40 for libraries; $20 for individuals.

Communications relative to manuscripts should be sent to Michael J. Greenberg, Editor-in-Chief, or Pamela Clapp Hinkle, Managing Editor, at the Marine Biological Laboratory, 7 MBL Street, Woods Hole, Massachusetts 02543. Telephone: (508) 289-7428. FAX: 508-289-7922. E-mail: pclapp@mbl.edu.

http://www.mbl.edu/BiologicalBulletin/

The home page for the electronic companion to THE BIOLOGICAL BULLETIN—*the Marine Models Electronic Record*—and other BIOLOGICAL BULLETIN publications is available on the World Wide Web at the address shown above.

THE BIOLOGICAL BULLETIN is indexed in bibliographic services including *Index Medicus* and MEDLINE, *Chemical Abstracts, Current Contents, Elsevier BIOBASE/Current Awareness in Biological Sciences,* and *Geo Abstracts.*

Printed on acid free paper,
effective with Volume 180, Issue 1, 1991.

POSTMASTER: Send address changes to THE BIOLOGICAL BULLETIN, Marine Biological Laboratory,
7 MBL Street, Woods Hole, MA 02543.

Copyright © 2001, by the Marine Biological Laboratory

Periodicals postage paid at Woods Hole, MA, and additional mailing offices.
ISSN 0006-3185

INSTRUCTIONS TO AUTHORS

The Biological Bulletin accepts outstanding original research reports of general interest to biologists throughout the world. Papers are usually of intermediate length (10–40 manuscript pages). A limited number of solicited review papers may be accepted after formal review. A paper will usually appear within four months after its acceptance.

Very short, especially topical papers (less than 9 manuscript pages including tables, figures, and bibliography) will be published in a separate section entitled "Research Notes." A Research Note in *The Biological Bulletin* follows the format of similar notes in *Nature*. It should open with a summary paragraph of 150 to 200 words comprising the introduction and the conclusions. The rest of the text should continue on without subheadings, and there should be no more than 30 references. References should be referred to in the text by number, and listed in the Literature Cited section in the order that they appear in the text. Unlike references in *Nature,* references in the Research Notes section should conform in punctuation and arrangement to the style of recent issues of *The Biological Bulletin*. Materials and Methods should be incorporated into appropriate figure legends. See the article by Lohmann *et al.* (October 1990, Vol. **179:** 214–218) for sample style. A Research Note will usually appear within two months after its acceptance.

The Editorial Board requests that regular manuscripts conform to the requirements set below; those manuscripts that do not conform will be returned to authors for correction before review.

1. ***Manuscripts.*** Manuscripts, including figures, should be submitted in quadruplicate, with the originals clearly marked. (Xerox copies of photographs are not acceptable for review purposes.) The submission letter accompanying the manuscript should include a telephone number, a FAX number, and (if possible) an E-mail address for the corresponding author. The original manuscript must be typed in no smaller than 12 pitch or 10 point, using double spacing (*including* figure legends, footnotes, bibliography, etc.) on one side of 16- or 20-lb. bond paper, 8 by 11 inches. Please, no right justification. Manuscripts should be proofread carefully and errors corrected legibly in black ink. Pages should be numbered consecutively. Margins on all sides should be at least 1 inch (2.5 cm). Manuscripts should conform to the *Council of Biology Editors Style Manual,* 5th Edition (Council of Biology Editors, 1983) and to American spelling. Unusual abbreviations should be kept to a minimum and should be spelled out on first reference as well as defined in a footnote on the title page. Manuscripts should be divided into the following components: Title page, Abstract (of no more than 200 words), Introduction, Materials and Methods, Results, Discussion, Acknowledgments, Literature Cited, Tables, and Figure Legends. In addition, authors should supply a list of words and phrases under which the article should be indexed.

2. ***Title page.*** The title page consists of a condensed title or running head of no more than 35 letters and spaces, the manuscript title, authors' names and appropriate addresses, and footnotes listing present addresses, acknowledgments or contribution numbers, and explanation of unusual abbreviations.

3. ***Figures.*** The dimensions of the printed page, 7 by 9 inches, should be kept in mind in preparing figures for publication. We recommend that figures be about 1 times the linear dimensions of the final printing desired, and that the ratio of the largest to the smallest letter or number and of the thickest to the thinnest line not exceed 1:1.5. Explanatory matter generally should be included in legends, although axes should always be identified on the illustration itself. Figures should be prepared for reproduction as either line cuts or halftones. Figures to be reproduced as line cuts should be unmounted glossy photographic reproductions or drawn in black ink on white paper, good-quality tracing cloth or plastic, or blue-lined coordinate paper. Those to be reproduced as halftones should be mounted on board, with both designating numbers or letters and scale bars affixed directly to the figures. All figures should be numbered in consecutive order, with no distinction between text and plate figures and cited, in order, in the text. The author's name and an arrow indicating orientation should appear on the reverse side of all figures.

Digital art: The Biological Bulletin will accept figures submitted in electronic form; however, digital art must conform to the following guidelines. Authors who create digital images are wholly responsible for the quality of their material, including color and halftone accuracy.

Format. Acceptable graphic formats are TIFF and EPS. Color submissions must be in EPS format, saved in CMKY mode.

Software. Preferred software is Adobe Illustrator or Adobe Photoshop for the Mac and Adobe Photoshop for Windows. Specific instructions for artwork created with various software programs are available on the Web at the Digital Art Information Site maintained by Cadmus Professional Communications at http://cjs.cadmus.com/da/home.html

Resolution. The minimum requirements for resolution are 1200 DPI for line art and 300 for halftones.

Size. All digital artwork must be submitted at its actual printed size so that no scaling is necessary.

Multipanel figures. Figures consisting of individual parts (*e.g.*, panels A, B, C) must be assembled into final format and submitted as one file.

Hard copy. Files must be accompanied by hard copy for use in case the electronic version is unusable.

Disk identification. Disks must be clearly labeled with the following information: author name and manuscript number; format (PC or Macintosh); name and version of software used.

Color: The Biological Bulletin will publish color figures and plates, but must bill authors for the actual additional cost of printing in color. The process is expensive, so authors with more than one color image should—consistent with editorial concerns, especially citation of figures in order—combine them into a single plate to reduce the expense. On request, when supplied with a copy of a color illustration, the editorial staff will provide a pre-publication estimate of the printing cost.

4. ***Tables, footnotes, figure legends, etc.*** Authors should follow the style in a recent issue of *The Biological Bulletin* in preparing table headings, figure legends, and the like. Because of the high cost of setting tabular material in type, authors are asked to limit such material as much as possible. Tables, with their headings and footnotes, should be typed on separate sheets, numbered with consecutive Roman numerals, and placed after the Literature Cited. Figure legends should contain enough information to make the figure intelligible separate from the text. Legends should be typed double spaced, with consecutive Arabic numbers, on a separate sheet at the end of the paper. Footnotes should be limited to authors' current addresses, acknowledgments or contribution numbers, and explanation of unusual abbreviations. All such footnotes should appear on the title page. Footnotes are not normally permitted in the body of the text.

5. ***Literature cited.*** In the text, literature should be cited by the Harvard system, with papers by more than two authors cited as Jones *et al.*, 1980. Personal communications and material in preparation or in press should be cited in the text only, with author's initials and institutions, unless the material has been formally accepted and a volume number can be supplied. The list of references following the text should be headed Literature Cited, and must be typed double spaced on separate pages, conforming in punctuation and arrangement to the style of recent issues of *The Biological Bulletin*. Citations should include complete titles and inclusive pagination. Journal abbreviations should normally follow those of the U. S. A. Standards Institute (USASI), as adopted by Biological Abstracts and Chemical Abstracts, with the minor differences set out below. The most generally useful list of biological journal titles is that published each year by Biological Abstracts (biosis List of Serials; the most recent issue). Foreign authors, and others who are accustomed to using The World List of Scientific Periodicals, may find a booklet published by the Biological Council of the U.K. (obtainable from the Institute of Biology, 41 Queen's Gate, London, S.W.7, England, U.K.) useful, since it sets out the World List abbreviations for most biological journals with notes of the USASI abbreviations where these differ. Chemical Abstracts publishes quarterly supplements of additional abbreviations. The following points of reference style for The Biological Bulletin differ from USASI (or modified World List) usage:

A. Journal abbreviations, and book titles, all underlined (for *italics*)

B. All components of abbreviations with initial capitals (not as European usage in World List *e.g., J. Cell. Comp. Physiol.* NOT *J. cell. comp. Physiol.*)

C. *All* abbreviated components must be followed by a period, whole word components *must not* (*i.e., J. Cancer Res.*)

D. Space between all components (*e.g., J. Cell. Comp. Physiol.*, not *J.Cell.Comp.Physiol.*)

E. Unusual words in journal titles should be spelled out in full, rather than employing new abbreviations invented by the author. For example, use *Rit Vísindafjélags Islendinga* without abbreviation.

F. All single word journal titles in full (*e.g., Veliger, Ecology, Brain*).

G. The order of abbreviated components should be the same as the word order of the complete title (*i.e., Proc.* and *Trans.* placed where they appear, not transposed as in some BIOLOGICAL ABSTRACTS listings).

H. A few well-known international journals in their preferred forms rather than WORLD LIST or USASI usage (*e.g., Nature, Science, Evolution* NOT *Nature, Lond., Science, N.Y.; Evolution, Lancaster, Pa.*)

6. ***Reprints, page proofs, and charges.*** Authors may purchase reprints in lots of 100. Forms for placing reprint orders are sent with page proofs. Reprints normally will be delivered about 2 to 3 months after the issue date. Authors (or delegates for foreign authors) will receive page proofs of articles shortly before publication. They will be charged the current cost of printers' time for corrections to these (other than corrections of printers' or editors' errors). Other than these charges for authors' alterations, *The Biological Bulletin* does not have page charges.

Reference: *Biol. Bull.* **200:** 1–8. (February 2001)

Flexural and Torsional Stiffness in Multi-Jointed Biological Beams

SHELLEY A. ETNIER*

Department of Biology, Duke University, Durham, North Carolina 27708-0338

Abstract. Flexibility, the ability to deform in response to loads, is a common property of biological beams. This paper investigates the mechanical behavior of multi-jointed beams, which are characterized by a linear series of morphologically similar joints. Flexural stiffness and torsional stiffness were measured in two structurally distinct beams, crinoid arms (Echinodermata, Comatulida) and crustacean antennae (Arthropoda, Decapoda). Morphological data from these beams were used to determine the relative contributions of beam diameter and joint density (number of joints per millimeter of beam length) to the flexural and torsional stiffness of these two structures. As predicted by beam theory, beam diameter influenced stiffness in both crinoid arms and crustacean antennae. In crinoid arms, increases in joint density were associated with decreases in stiffness, but joint density had no significant influence on stiffness in crustacean antennae. In both crinoid arms and crustacean antennae, the magnitudes of flexural and torsional stiffness, as well as the ratio of these two variables, were similar to previously reported values for non-jointed biological beams. These results suggest that the structural design of a biological beam is not a limiting factor determining its mechanical properties.

Introduction

Biological beams, which are structures that are long relative to their width, can be divided into three broad groups based on their structural design. *Continuous beams* have no distinct discontinuities in either material or geometry along the length of the beam. These continuous beams, such as leaf petioles and tree trunks, deform relatively evenly along their entire length when loaded. Continuous beams contrast with *jointed beams*, which are characterized by one or a few material or structural discontinuities along their length which allow the beam to deform at particular points. Examples include vertebrate limbs and arthropod appendages. The third structural design is a *multi-jointed beam*, which is characterized by a linear series of morphologically similar joints connected by a series of stiff elements. The vertebrate backbone is the most extensively studied example of a multi-jointed beam (see Gál, 1993; Long *et al.*, 1997); other examples are found in echinoderms (Baumiller and LaBarbera, 1993), cnidarians (Muzik and Wainwright, 1977), and plants (Niklas, 1997).

When loaded, a multi-jointed beam will deform at each of the joints. Yet, because the joints are arrayed in a linear series, the deformation is evenly distributed along the length of the beam. Thus, the overall deformation of the beam resembles that of a continuous beam, although the underlying mechanism (deformation at individual joints) differs dramatically. Ideally, studies of the mechanical properties of a multi-jointed beam should include information on the overall flexibility of the beam as well as on the relative contribution of the individual joints.

Regardless of their structural design, most biological beams are flexible; that is, they deform in response to loads (Vogel, 1984; Denny, 1988). One dictionary (*New Lexicon Webster's Dictionary*, 1987) defines flexibility as the quality of being easily bent, and rigidity as the quality of resisting deformation. These two contrasting states actually reflect a continuum that can be described with a single, more precise term borrowed from engineering beam theory. Stiffness is defined as a mechanical property indicating the resistance of a material or structure to deformation under a given load (Roark, 1943). Flexural stiffness is a measure of the resistance of a structure to bending, and torsional stiffness is a measure of the resistance of a structure to twisting (Roark, 1943).

Received 13 July 2000; accepted 13 December 2000.

* Present address: Department of Biological Sciences, University of North Carolina, 601 S. College Rd., Wilmington, NC 28403. E-mail: etniers@uncwil.edu

Flexural stiffness and torsional stiffness are composite variables whose magnitudes are determined both by material and structural properties (Wainwright *et al.*, 1976). Flexural stiffness is expressed as EI, where E is Young's modulus of elasticity and I is the second moment of area relative to the neutral plane of bending (*i.e.*, the plane that neither shortens nor lengthens during deformation). Torsional stiffness is expressed as GJ, where G is the shear modulus and J is the polar moment of area about the central axis of rotation. I and J reflect the cross-sectional geometry of a beam and are influenced by both size and shape. Size is a very strong determinant of beam stiffness (Roark, 1943; Wainwright *et al.*, 1976), as both I and J are proportional to radius to the fourth power.

Flexural stiffness and torsional stiffness are engineering terms used to describe the stiffness of ideal beams that meet a certain set of criteria (Roark, 1943), none of which are met by either continuous or multi-jointed biological beams (Wainwright *et al.*, 1976). For biological beams, flexural stiffness and torsional stiffness are descriptors of the overall mechanical behavior of the beam, reflecting the amount of deformation observed under a given load. As such, the presence of joints does not negatively impact the overall usefulness of these terms as a means to quantify the stiffness of biological beams.

The stiffness of biological beams can also be characterized by the dimensionless, and thus size invariant, ratio EI/GJ, called the twist-to-bend ratio (Niklas, 1992; Vogel, 1995; Etnier and Vogel, 2000). The twist-to-bend ratio indicates the relative resistance of a beam to bending *versus* twisting, without reference to the absolute magnitude of either. Intuitively, a higher twist-to-bend ratio indicates a structure that twists more readily than it bends. Previous studies have found that the twist-to-bend ratio is a biologically relevant parameter that provides insight into the functional demands on a structure. For example, daffodil stems (Etnier and Vogel, 2000), leaf petioles (Vogel, 1992), and sedges (Ennos, 1993) are characterized by relatively high twist-to-bend ratios. These structures easily twist into low-drag configurations when the wind blows, thus reducing the potential for damage to the organism.

In this paper, values for flexural and torsional stiffness, as well as the twist-to-bend ratio, are reported for crinoid arms (Echinodermata, Comatulida) and crustacean antennae (Arthropoda, Decapoda). Mechanical and morphological data from these beams are used to determine the relative contributions of beam diameter and the number of joints to the flexural and torsional stiffness of these two structures. This broadly comparative study of morphologically distinct structures provides insight into the contribution of a serial arrangement of joints to the mechanical properties of multi-jointed beams.

Comatulid crinoids have long, slender arms composed of a linear series of ossicles connected by muscles and ligaments (Breimer, 1978). The arms move actively in response to muscular contractions (Breimer, 1978) or passively in response to external forces. Crinoids extend their arms into the currents to filter feed passively (Liddell, 1982), thus the arms must be flexible enough to be positioned for feeding, yet stiff enough to maintain that position once obtained (Meyer, 1971). The flexibility of the arms is also relevant during locomotion (Motokawa, 1988), because the arms are bent during swimming and crawling (Breimer, 1978; Shaw and Fontaine, 1990). The dependence of feeding and locomotion on the mechanical properties of the arms suggests that these properties are important to the survival and reproductive success of comatulid crinoids. The only experimental studies of arm mechanics have explored the behavior of isolated joints in the arm (Birenheide and Motokawa, 1994, 1996) without considering how the serial arrangement of the joints affects the mechanics of this multi-jointed beam.

The second antenna of a lobster or crayfish consists of a series of calcified rings, or annuli, connected by flexible arthrodial membranes (Tautz *et al.*, 1981). There are no muscles associated with the annuli of the antennae, although the entire structure can be moved by muscles located at its base (Sandeman, 1985). Hair receptors on each annulus are sensitive to gross water movements, water vibrations, and mechanical deformation of the antenna (Vedel, 1985). In palinurid lobsters, the antennae are not only used as sense organs, but are also actively used as a defensive mechanism to ward off predators (Atema and Cobb, 1980). These two functions may have conflicting mechanical demands in lobsters, because the antenna must be flexible enough to deform in response to water vibrations, but also stiff enough to serve as a defensive weapon. Again, very little is known about how the multi-jointed nature of these beams affects their mechanical properties.

Materials and Methods

Specimens

Crinoids. Specimens of *Comactinia echinoptera* were obtained from the invertebrate collection at Duke University Marine Laboratory, Beaufort, North Carolina, and freshly preserved specimens of *Florometra serratissima* were obtained from Sea Life Supply in Sand City, California. Both species were initially preserved in formalin, and then stored in 70% alcohol. Prior to testing, arms were disarticulated proximally and then transferred through a series of increasingly dilute alcohol solutions, culminating in seawater.

Crustaceans. Specimens of *Procambarus sp.* (freshwater crayfish) were obtained commercially from a local grocer (Wellspring Grocery), and specimens of *Panulirus argus* (spiny lobster) were obtained from investigators at the University of North Carolina, Chapel Hill. Antennae were disarticulated from the carapace and frozen until tested. The

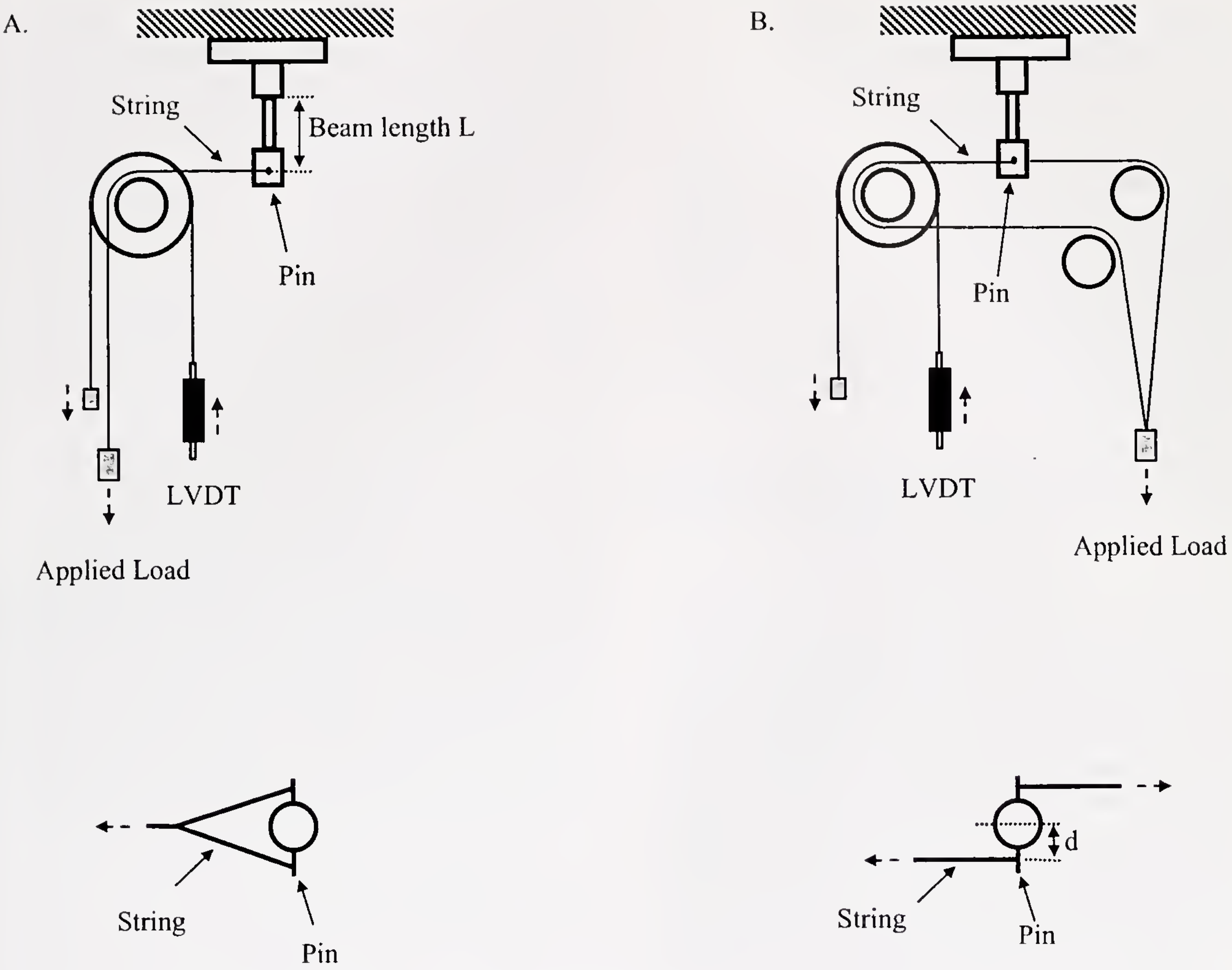

Figure 1. Mechanical apparatus for measuring flexural and torsional stiffness. (A) Flexural stiffness is measured by applying a load to the specimen's free end, causing it to bend. The two pulleys on the left are coaxial. Shown below is a cross section through the free end of the embedding cap, illustrating how the load is applied during flexural tests. (B) Torsional stiffness is measured by applying a load to the specimen's free end, causing it to twist. Shown below is a cross section through the free end of the embedding cap, illustrating how the load is applied during torsional tests. The load is applied simultaneously to the two ends of pin extending through the embedding cap, causing the specimen to twist, but not bend. L = Beam length, d = moment arm, LVDT = linear variable differential transformer. (Based on Vogel, 1992.)

antennae were thawed in seawater or fresh water, as appropriate, before testing.

Mechanical measures

For both flexural and torsional stiffness, the free ends of the specimen were embedded in hard, plastic caps (diameter approximately 11 mm, length 15 mm) with 5-minute epoxy resin. As the epoxy cured, a pin was inserted in the distal cap. The proximal end of the prepared specimen was fixed in place. A load was applied to the pin at the free distal end, causing the specimen to bend or twist (Fig. 1). Through a series of pulleys and strings, the deformation of the specimen was linked to movement of a linear variable differential transformer (LVDT, Pickering 7308-W2-AO), which provided a voltage output proportional to distance traveled (see Vogel, 1992, for full details). The LVDT was calibrated with a micrometer, and each reading was corrected for load-dependent stretching of the string (Berkley Gorilla Braid 10-lb-test fishing line made of braided gelspun polyethylene fibers). All readings were taken on moist specimens 60 s after loading, to allow for initial creep. Specimens were tested with two loads of different magnitude, and data for deformation relative to the load were averaged. This experimental protocol assumes that flexural and torsional stiffness are linear functions of load.

Flexural stiffness (in N · m^2) was calculated with the usual formula for end-loaded cantilever beams:

$$\text{Flexural stiffness} = \frac{FL^3}{3y} \qquad (1)$$

where F is the force applied, L is the length of the beam, and y is the deflection at the free end of the beam (Fig. 1A). The formula is satisfactory for deflections up to about 10% of total specimen length (Gere and Timoshenko, 1984). Crinoid arms and crustacean antennae are radially asymmetric, so flexural stiffness was measured both dorsoventrally (oral/aboral) and laterally. These values were then averaged to provide an overall measure of the flexural stiffness of the system.

Torsional stiffness (in N · m^2) was determined by applying a load to the distal end of the beam, causing the specimen to twist (Fig. 1B). Calculations of torsional stiffness were based on the following formula:

$$\text{Torsional stiffness} = \frac{Fd}{\theta/L} \qquad (2)$$

where F is the force applied at a moment arm d, L is the length of the beam, and θ is the resulting rotation in radians.

A test of the apparatus using a piece of spring steel (0.65 mm in diameter) gave an average EI/GJ value of 1.4 (standard deviation 0.3), close to the expected value of 1.3 (Gere and Timoshenko, 1984). This error indicates a systematic overestimate of about 8% in the ratios given here.

In some cases, the applied loads were so small that they did not overcome the frictional resistance of the pulleys in the test apparatus. For measures of flexural stiffness, data were omitted if (1) the total deflection was less than 1% of the total specimen length, and (2) the load applied over the moment arm of the pulley was less than or equal to 4.9×10^{-3} N (0.5 g). For torsional measures, data were omitted if (1) the total rotation was less than 0.06 radians (3.6°), and (2) the load applied over the moment arm of the pulley was less than or equal to 9.8×10^{-3} N (1 g).

Morphological measures

Immediately after the mechanical tests, beam length (L) and moment arm (d) were measured using digital calipers (resolution 0.1 mm). The beam diameter was recorded as the average diameter of the specimen at the midpoint of the beam. The number of joints in each specimen was counted to calculate joint density (number of joints per millimeter of beam length).

Data analysis

The average twist-to-bend ratio for each species was calculated from the twist-to-bend ratio for each individual. Distributions and variances were normalized using log-transformed values for flexural stiffness, torsional stiffness, the twist-to-bend ratio, and beam diameter (Sokal and Rohlf, 1981). Joint densities were unaltered because of their normal distribution. Student's t tests were used to determine whether there were significant differences in these variables within the crinoids and within the crustacea. Differences between phyla were not tested because distinct preservation methods were used for crinoids and crustaceans.

Morphological and mechanical data from the two species of crinoids and the two species of crustaceans were combined to provide information on the general structural design of each system. Although there are assuredly mechanical and morphological differences within each phylum, these are assumed to be relatively minor compared to the differences between the two. Multiple regressions were used to determine the relative contribution of beam diameter and joint density to flexural and torsional stiffness (Sokal and Rohlf, 1981). Multiple regressions determine whether a linear combination of independent variables explain a significant portion of the variability observed in the original data (Sokal and Rohlf, 1981). Additionally, multiple regressions indicate which of the independent variables contribute significantly to the overall model.

Because of the unequal variances of these data, differences in joint density between crinoid arms and crustacean antennae were examined using a Wilcoxon rank sum test for nonparametric data (Glantz, 1992).

Microsoft Excel 5.0 (1995) was used for all data manipulation, and JMP In (SAS Institute, Inc., Cary, NC) was used for all statistical analyses.

Results

Mechanical measures

Flexural stiffness and torsional stiffness varied greatly from specimen to specimen, as expected based on differences in beam diameter between individuals (Table 1). The coefficients of variation for flexural stiffness ranged from 84% to 196%, whereas those for torsional stiffness ranged from 61% to 110%. The twist-to-bend ratio was also highly variable (Table 1), with coefficients of variation ranging from 41% to 88%. The variability of the twist-to-bend ratio far exceeded that of the test apparatus, suggesting that the variability was real. The magnitudes of flexural stiffness and torsional stiffness varied among all of the species. *Procambarus* was the most flexible beam in both bending and twisting, and *Panulirus* was by far the stiffest in both measures. The two crinoids fall in the middle, with *Florometra* being stiffer than *Comactinia*. This pattern was not observed in the twist-to-bend ratio, where *Panulirus* had the lowest ratio and *Florometra* had the highest. The values for flexural stiffness, torsional stiffness, and twist-to-bend ratio are comparable to those of other continuous biological beams (Table 2), such as leaf petioles and plant stems.

Table 1

Morphological and mechanical values for multi-jointed beams

Species	n	Diameter (mm)	Flexural stiffness ($N \cdot m^2 \times 10^{-6}$)	Torsional stiffness ($N \cdot m^2 \times 10^{-6}$)	Twist-to-bend ratio
Comactinia echinoptera	10	1.33 (0.13)	50 (47)	15 (11)	4.3 (3.8)
Florometra serratissima	6	1.75 (0.10)	392 (383)	51 (31)	6.6 (2.7)
Procambarus sp.	8	0.99 (0.07)	25 (21)	6 (4)	4.5 (3.7)
Panulirus argus	13	2.83 (0.36)	5827 (11466) $n = 12$	2036 (2242)	1.8 (1.3) $n = 12$

Mean values for beam diameter, flexural stiffness, and torsional stiffness for n specimens. In one case, as noted, the number of specimens varied. The mean twist-to-bend ratio is the average calculated from the individual twist-to-bend ratios. The standard deviation for each parameter is given in parentheses.

Mechanical differences between crinoid species

The arms of *Florometra* had significantly higher flexural ($t = -3.88$, $P < 0.002$) and torsional ($t = -3.40$, $P < 0.004$) stiffness than those of *Comactinia* (Table 1). These differences may be associated with differences in the size of the two species, because both flexural and torsional stiffness are highly size dependent. *Florometra* specimens had significantly thicker arms (Table 1) than *Comactinia* specimens ($t = -2.27$, $P < 0.04$). Despite the differences in the magnitudes of flexural and torsional stiffness, the twist-to-bend ratios of these two species were not significantly different ($t = -1.70$, $P < 0.112$).

Mechanical differences between crustacean species

Panulirus antennae were significantly stiffer in flexural ($t = -5.63$, $P < 0.0001$) and torsional ($t = -7.99$, $P < 0.0001$) stiffness than *Procambarus* antennae (Table 1). Again, these differences may be associated with size, because *Panulirus* antennae were significantly larger in diameter (Table 1) than *Procambarus* antennae ($t = -5.05$, $P < 0.0001$). The twist-to-bend ratio of *Panulirus* was significantly higher than that of *Procambarus* ($t = 2.43$, $P < 0.026$). As in the crinoid arms, the magnitudes of flexural and torsional stiffness varied between species, but in this case, the twist-to-bend ratios also differed.

Table 2

Mechanical properties of biological beams

Biological beam	Flexural stiffness ($N \cdot m^2 \times 10^{-6}$)	Torsional stiffness ($N \cdot m^2 \times 10^{-6}$)	Twist-to-bend ratio
Daffodils[1]	11900	890	13.3
Sweet gum petiole[2]	984	199	5.1
Sunflower shoot[2]	73	53	1.4

Mean flexural stiffness, torsional stiffness, and twist-to-bend ratios for a variety of continuous biological beams.

[1] Data from Etnier and Vogel (2000).

[2] Data from Vogel (1992).

Differences between structural designs

Morphology. Joint density differed significantly ($Z = 3.28$, $P < 0.001$) between the crinoid arms and crustacean antennae. Crustacean antennae had an average joint density of 2.04 mm^{-1} (SD = 1.18), whereas crinoid arms had an average joint density of 0.82 mm^{-1} (SD = 0.17). These results correspond to about 200 joints in a 10-cm-long crustacean antenna, but only about 80 joints in a crinoid arm of the same length.

Mechanics. In crinoids, the multiple regression model accounted for a significant portion of the observed variation in both flexural ($R^2 = 0.87$) and torsional ($R^2 = 0.74$) stiffness. Both joint density and diameter contributed significantly to the overall model. Increases in diameter were associated with increases in stiffness, and increases in joint density were associated with decreases in stiffness (Table 3). In crustacean antennae, the model also explained a significant portion of the observed variation in flexural ($R^2 = 0.92$) and torsional ($R^2 = 0.91$) stiffness, although in this case, only beam diameter contributed significantly to the overall model (Table 3). Joint density did not contribute significantly to either flexural or torsional stiffness in the crustacean antennae (Table 3). In summary, beam diameter was an important determinant of stiffness in both multi-jointed beams, as expected for a continuous beam. Joint density, which was expected to affect the mechanical properties of multi-jointed beams, was a determining factor only in the crinoid arms.

Discussion

The results of this study suggest that flexibility in multi-jointed beams is influenced by variables associated with both continuous and jointed beams. As predicted by engineering beam theory, beam diameter contributes to flexural and torsional stiffness in both crinoid arms and crustacean

Table 3

Factors affecting stiffness

Structural design	n	R^2	Model for log (stiffness) P values	Regression coefficients log (diameter)	Regression coefficients Joint density
Flexural stiffness					
Crinoids	16	0.87	0.0001*	2.4*	−2.5*
Crustaceans	15	0.92	0.0001*	4.0*	0.0
Torsional stiffness					
Crinoids	16	0.74	0.0002*	2.1*	−1.3*
Crustaceans	15	0.91	0.0001*	4.4*	0.1

Statistical values for multiple regressions of log (diameter) and joint density against log (stiffness) for both structural designs (n = sample size). The model tests the significance of the overall regression equation, which is in the form $Y = A + BX_1 + CX_2$. Values given for log (diameter) and joint density are standard partial regression coefficients for flexural and torsional stiffness. Regression coefficients that contribute significantly to the overall model ($P < 0.05$) are marked with asterisks. For example, in crustaceans, the linear equation, log (EI) = a + 4.0*log (diameter) + 0.0*joint density, explained 92% of the observed variation in flexural stiffness. Joint density, with a regression coefficient of 0.0, did not contribute significantly to the model.

antennae. In contrast, joint density contributes to beam stiffness only in the crinoid arms. Future studies of multijointed beams must consider both types of variables to fully understand the mechanical properties of these structures.

The flexibility of crinoid arms is influenced both by beam diameter and by joint density, so morphological variation at the level of the entire arm or at the level of the individual ossicles will affect the mechanical properties of the arms. This result is particularly interesting because the evolutionary success of the comatulid crinoids has been attributed to morphological changes that increased arm flexibility relative to the stalked crinoids (Meyer and Macurda, 1977). Increased arm flexibility, coupled with the loss of a stalk, enabled comatulid crinoids to become secondarily mobile (Motokawa, 1988). Today, this mobility allows comatulids to feed in variable water currents and to move in response to undesirable environmental conditions or predators (Meyer and Macurda, 1977). The hypothesis that comatulid crinoid arms are more flexible than stalked crinoid arms could be directly tested in extant crinoids by using the techniques developed in this study. Similarly, arm diameter and joint density may serve as useful proxies for investigating flexibility in fossil specimens, providing valuable insight into changes in arm flexibility over evolutionary time.

The mechanical properties of crinoid arms may determine, in part, the distribution of individuals in the environment. Comatulid crinoids differentially distribute themselves on the basis of flow regime, with some species preferring exposed sites with relatively predictable flows and others preferring more sheltered areas, with unpredictable flow (Meyer, 1973a). *Comactinia* is typically found in the infrastructure of the reef in sheltered areas (Meyer, 1973b). Its arms bend and twist relatively easily, potentially allowing the animals to adjust to flows that change in both velocity and direction. In contrast, *Florometra* tends to be found at the apex of rocky outcroppings (Shaw and Fontaine, 1990) where it is exposed to more regular flow (LaBarbera, 1982). The arms of *Florometra* are stiffer in both bending and twisting than those of *Comactinia*. The flexibility needed to respond to constantly changing flows may not be necessary in a steady current. Instead, the arms may simply need to be stiff enough to maintain their position. Because stiffness is related to arm diameter, these results also suggest that individuals within a species may be differentially distributed on the basis of their size. Larger individuals, with stiffer arms, may be able to live and feed in different areas than smaller, more flexible, individuals. These results suggest that the mechanical properties of crinoid arms may be tuned to the specific loading regime of the animal's preferred habitat.

Although the magnitudes of flexural and torsional stiffness differed between these crinoid species, there were no detectable differences in their twist-to-bend ratios. This constancy suggests that there is a functional advantage to maintaining the relationship between flexural and torsional stiffness across comatulid crinoid species, although the biological relevance of this constancy has yet to be determined. One possibility is that the constant twist-to-bend ratio reflects selective pressure on the ability to passively orient the arms with respect to water currents during feeding. The ability to passively orient the arms may be particularly important for crinoids that live where flow oscillates continuously. Passive orientation of entire organisms has been described in gorgonian corals (Thèodor and Denizot, 1965; Wainwright and Dillon, 1969) and in stalked crinoids (Baumiller and Plotnick, 1989), although the mechanisms differ in these two systems. In comatulid crinoids, passive orientation has been observed in the individual pinnules radiating off of each crinoid arm (Baumiller and Meyer, 2000), suggesting that the mechanical properties of the arms may be less important than the mechanical properties of the pinnules themselves. Passive orientation of comatulid arms has apparently not been investigated. Alternatively, the constant twist-to-bend ratio of comatulid crinoid arms may reflect functional demands of locomotion. Comatulid crinoids use their arms to crawl along the surface of the reef and to swim freely through the water. Each of these activities place different functional demands on the arms, and these demands may be reflected in the constant twist-to-bend ratios.

The mechanical properties discussed here represent the passive properties of the arms. Crinoids may be able to actively alter the mechanical properties of their arms by contracting the muscles that cross from one ossicle to the next or by making changes in the properties of their connective tissue. As in all echinoderms, crinoid ligaments are made up of catch connective tissue that can exhibit dramatic changes in mechanical properties (Diab and Gilly, 1984; Motokawa, 1984). Crinoids might be able to use muscular contractions to position the arms, and then use the mutable properties of catch connective tissue to maintain that position with little muscular effort (Willkie, 1983). Thus, the ability of a crinoid to feed and locomote may depend on both the passive and active properties of the arms.

The crinoids used in this study were initially preserved in formalin, which increases the number of cross-links between the proteins in connective tissue (Presnell and Schreibman, 1997). Such treatment will greatly influence the mechanical properties of these tissues (Wainwright *et al.*, 1976). The reported values for flexural stiffness are within an order of magnitude of values reported for the stalks of living stalked crinoids (Baumiller and LaBarbera, 1993). Yet the stalks were about 3 times larger in diameter than the comatulid arms, suggesting that the values for the flexural stiffness of arms given here are overestimates of the true values. No values were available for comparisons with torsional stiffness. In the multi-jointed vertebrate spine, the magnitudes of both flexural and torsional stiffness increased after preservation in formalin, yet the twist-to-bend ratio remained the same (Wilkie *et al.*, 1996). Thus, although the magnitudes of flexural and torsional stiffness in preserved crinoids may be overestimates, the twist-to-bend ratios may accurately reflect values for living crinoids.

The factors affecting beam stiffness in crustacean antennae differed in part from those affecting crinoid arms. The flexibility of crustacean antennae is dependent on their diameter but not their joint density, suggesting that these beams effectively function as continuous beams. Increases or decreases in the number of joints in the antennae do not significantly affect their mechanical properties. I suggest that the joints of the antenna are not designed to allow appreciable bending or twisting. Previous studies have shown that the mechanoreceptors on the antenna are sensitive to bending deformations of 0.06 degrees at each joint (Tautz *et al.*, 1981). Thus, the joints may allow only very small deformations. Deformations of this magnitude, if they occurred, were below the resolution of the present equipment.

Both *Procambarus* and *Panulirus* use their antennae to collect sensory information, but *Panulirus* also uses its antennae in aggressive interactions with predators (Atema and Cobb, 1980). The antennae of *Panulirus* do not bend or twist easily, which may make them more effective tools for warding off predators. Yet, because stiffness is related to diameter, the ability to ward off predators may be size dependent. In contrast, the antennae of *Procambarus* deform easily in response to loads, ensuring their sensitivity to environmental stimuli. The twist-to-bend ratios differed significantly, with *Panulirus* having a lower ratio than *Procambarus*. A variable twist-to-bend ratio suggests that flexural stiffness and torsional stiffness are not tightly coupled in the crustacean antenna. This decoupling may be indicative of the different functional demands placed on the two antennae, or alternatively, may simply reflect the functional irrelevancy of torsional stiffness in these structures.

Mechanistically, the decoupling of flexural and torsional stiffness in crustacean antennae may be a function of subtle morphological or material changes that affect one of the stiffness variables to a greater degree than the other. For example, the stiffness of a hollow beam, such as a crustacean antenna, is influenced not only by its external cross-sectional shape, but also by the thickness of its walls (Roark, 1943; Niklas, 1998). This study did not investigate wall thickness or other morphological features within each hollow antenna. Thus, the assumption that the two different antennae have the same structural design may be inappropriate despite their external similarity.

The antennae used in this study were frozen and thawed prior to mechanical tests, which could have affected the results. The flexural stiffness reported for *Procambarus* was very similar to values reported for other similarly sized freshwater crayfish that were tested immediately after death (Sandeman, 1989). For torsional stiffness, no data from fresh specimens were available for comparisons. Again, the values reported here reflect the passive properties of the antennae. In crustaceans, no muscles cross over the joints in the antenna, so there is no possibility of active control of the mechanical properties of the structure.

The mechanical properties of multi-jointed beams do not differ dramatically from those of continuous biological beams, despite large differences in underlying morphology. Both multi-jointed and continuous beams have similar mechanical properties despite vastly different structural designs and functional demands. This convergence suggests that the structural design of a biological beam does not necessarily determine the resultant mechanical properties. This commonality also emphasizes the importance of flexibility, both in bending and in twisting, biological beams.

Acknowledgments

I thank Shaun Cain of the University of North Carolina, Chapel Hill, for assistance in obtaining *Panulirus argus* antennae, and Duke University Marine Lab for loaning me specimens of *Comactinia echinoptera* from their invertebrate collection. I am grateful for the comments of Dr. Steve Vogel and Dr. Bill Hoese on early drafts of this manuscript, as well as for the critical comments of two anonymous reviewers.

Literature Cited

Atema, J., and J. S. Cobb. 1980. Social behavior. Pp. 409–450 in *The Biology and Management of Lobsters. Vol 1: Physiology and Behavior*, J. S. Cobb and B. F. Phillips, eds. Academic Press, New York.

Baumiller, T. K., and M. LaBarbera. 1993. Mechanical properties of the stalk and cirri of the sea lily *Cenocrinus asterius. Comp. Biochem. Physiol.* **106A:** 91–95.

Baumiller, T. K., and D. L. Meyer. 2000. Crinoid postures in oscillating current: insights into some biomechanical aspects of passive filter feeding. *Geol. Soc. Am. Abs. Progs.* **32(7):** A372.

Baumiller, T. K., and R. E. Plotnick. 1989. Rotational stability in stalked crinoids and the function of wing plates in *Pterotocrinus depressus. Lethaia* **22:** 317–326.

Birenheide, R., and T. Motokawa. 1994. Morphological basis and mechanics of arm movement in the stalked crinoid *Metacrinus rotundus* (Echinodermata, Crinoida). *Mar. Biol.* **121:** 273–283.

Birenheide, R., and T. Motokawa. 1996. Contractile connective tissue in crinoids. *Biol. Bull.* **191:** 1–4.

Breimer, A. 1978. General morphology, recent crinoids. Pp. 9–58 in *Treatise on Invertebrate Paleontology. Part T, Echinodermata 2.* Geological Society of America, Boulder, CO.

Denny, M. W. 1988. *Biology and the Mechanics of the Wave-swept Environment.* Princeton University Press, Princeton, NJ.

Diab, M., and W. F. Gilly. 1984. Mechanical properties and control of non-muscular catch in spine ligaments of the sea urchin, *Strongylocentrotus franciscanus. J. Exp. Biol.* **111:** 155–170.

Ennos, A. R. 1993. The mechanics of the flower stem of the sedge *Carex acutiformis. Ann. Bot.* **72:** 123–127.

Etnier, S. A., and S. Vogel. 2000. Reorientation of daffodil (*Narcissus:* Amaryllidaceae) flowers in wind: drag reduction and torsional flexibility. *Am. J. Bot.* **87:** 29–32.

Gál, J. 1993. Mammalian spinal biomechanics. I. Static and dynamic mechanical properties of intact intervertebral joints. *J. Exp. Biol.* **174:** 247–280.

Gere, J. M., and S. P. Timoshenko. 1984. *Mechanics of Materials.* Brooks/Cole Engineering Division, Monterey, CA.

Glantz, S. A. 1992. *Primer of Biostatistics,* 3rd ed. McGraw-Hill, New York.

LaBarbera, M. 1982. Metabolic rates of suspension feeding crinoids and ophiuroids (Echinodermata) in a unidirectional laminar flow. *Comp. Biochem. Physiol.* **71A:** 303–307.

Liddell, W. D. 1982. Suspension feeding by Caribbean comatulid crinoids. Pp. 33–40 in *Echinoderms: Proceedings of the International Conference, Tampa Bay.* J. M. Lawrence, ed. A. A. Balkema, Rotterdam.

Long, J. H., Jr., D. A. Pabst, W. R. Shepherd, and W. A. McLellan. 1997. Locomotor design of dolphin vertebral columns: bending mechanics and morphology of *Delphinus delphis. J. Exp. Biol.* **200:** 65–81.

Meyer, D. L. 1971. The collagenous nature of problematical ligaments in crinoids (Echinodermata). *Mar. Biol.* **9:** 235–241.

Meyer, D. L. 1973a. Feeding behavior and ecology of shallow-water unstalked crinoids (Echinodermata) in the Caribbean Sea. *Mar. Biol.* **22:** 105–129.

Meyer, D. L. 1973b. Distribution and living habits of comatulid crinoids near Discovery Bay, Jamaica. *Bull. Mar. Sci.* **23:** 244–259.

Meyer, D. L., and D. B. Macurda, Jr. 1977. Adaptive radiation of the comatulid crinoids. *Paleobiology* **3:** 74–82.

Motokawa, T. 1984. Connective tissue catch in echinoderms. *Biol. Rev.* **59:** 255–270.

Motokawa, T. 1988. Catch connective tissue: a key character for echinoderm success. Pp. 39–54 in *Echinoderm Biology.* R. D. Burke, P. V. Mladenov, P. Lambert, and R. B. Parsley, eds. *Proceedings of the 6th International Echinoderm Conference, Victoria.* A. A. Balkema, Rotterdam.

Muzik, K., and S. A. Wainwright. 1977. Morphology and habitat of five Fijian sea fans. *Bull. Mar. Sci.* **27:** 308–337.

New Lexicon Webster's Dictionary of the English Language. 1987. Lexicon Publications, New York.

Niklas, K. J. 1992. *Plant Biomechanics: An Engineering Approach to Plant Form and Function.* University of Chicago Press, Chicago, IL.

Niklas, K. J. 1997. Relative resistance of hollow, septate internodes to twisting and bending. *Ann. Bot.* **80:** 275–287.

Niklas, K. J. 1998. Modes of mechanical failure of hollow, septate stems. *Ann. Bot.* **81:** 11–21.

Pressnell, J. K., and M. P. Schreibman. 1997. *Humason's Animal Tissue Techniques.* John Hopkins University Press, Baltimore, MD.

Roark, R. J. 1943. *Formulas for Stress and Strain,* 2nd ed. McGraw-Hill, New York.

Sandeman, D. C. 1985. Crayfish antennae as tactile organs: their mobility and the responses of their proprioceptors. *J. Comp. Physiol.* **157A:** 363–373.

Sandeman, D. C. 1989. Physical properties, sensory receptors and tactile reflexes of the antenna of the Australian freshwater crayfish *Cherax destructor. J. Exp. Biol.* **141:** 197–218.

Shaw, G. D., and A. R. Fontaine. 1990. The locomotion of the comatulid *Florometra serratissima* (Echinodermata: Crinoidea) and its adaptive significance. *Can. J. Zool.* **68:** 942–950.

Sokal, R. R., and F. J. Rohlf. 1981. *Biometry: The Principles and Practice of Statistics in Biological Research,* 2nd ed. W. H. Freeman, New York.

Tautz, J., W. M. Masters, B. Aicher, and H. Markl. 1981. A new type of water vibration receptor on the crayfish antenna. I. Sensory physiology. *J. Comp. Physiol.* **144:** 533–541.

Théodor, J., and M. Denizot. 1965. Contribution à l'étude des Gorgones. I. A propos de l'orientation d'organismesmarins fixés végétaux et animaux en fonction du courant. *Vie Milieu* **16:** 237–241.

Vedel, J.-P. 1985. Cuticular mechanoreception in the antennal flagellum of the rock lobster *Palinurus vulgaris. Comp. Biochem. Physiol.* **80A:** 151–158.

Vogel, S. 1984. Drag and flexibility in sessile organisms. *Am. Zool.* **24:** 37–44.

Vogel, S. 1992. Twist-to-bend ratios and cross-sectional shapes of petioles and stems. *J. Exp. Bot.* **43:** 1527–1532.

Vogel, S. 1995. Twist-to-bend ratios of woody structures. *J. Exp. Bot.* **46:** 981–985.

Wainwright, S. A., and J. R. Dillon. 1969. On the orientation of sea fans (Genus *Gorgonia*). *Biol. Bull.* **136:** 130–139.

Wainwright, S. A., W. D. Biggs, J. D. Currey, and J. M. Gosline. 1976. *Mechanical Design in Organisms.* Princeton University Press, Princeton, NJ.

Wilkie, H. J., S. Krischak, and L. E. Claes. 1996. Formalin fixation strongly influences biomechanical properties of the spine. *J. Biomech.* **29:** 1629–1631.

Wilkie, I. C. 1983. Nervously mediated change in the mechanical properties of the cirral ligaments of a crinoid. *Mar. Behav. Physiol.* **9:** 229–248.

Reference: *Biol. Bull.* **200:** 9–19. (February 2001)

Three-Dimensional Analysis of Finlet Kinematics in the Chub Mackerel (*Scomber japonicus*)

JENNIFER C. NAUEN* AND GEORGE V. LAUDER

Department of Organismic and Evolutionary Biology, Harvard University, 26 Oxford Street,
Cambridge, Massachusetts 02138

Abstract. Finlets, which are small non-retractable fins located on the body margins between the second dorsal and anal fins and the caudal fin of scombrid fishes, have been hypothesized to improve swimming performance. The kinematics of three posterior finlets of the chub mackerel, *Scomber japonicus,* were examined using three-dimensional measurement techniques to test hypotheses on finlet rigidity and function during steady swimming. Finlet bending and finlet planar orientation to the *xz*, *yz*, and *xy* planes were measured during steady swimming at 1.2 lengths s^{-1} in a flow tank.

Despite very similar morphology among the individual finlets, there was considerable variability in finlet flexure during a stroke. Several of the finlets were relatively rigid and flat (with intrafinlet angles close to 180° during the stroke), although intrafinlet angle of the proximal portion of the most posterior finlet varied considerably over the stroke and was as low as 140° midstroke. Finlets showed complex orientations in three-dimensional space over a stroke, and these orientations differed among the finlets. For example, during tail deceleration the proximal portion of the fifth finlet achieves a mean angle of approximately 75° with the *xz* plane, while the distal portion of this finlet is oriented at 110°. Our data suggest that the trajectory of local water flow varies among finlets and that the most posterior finlet is oriented to redirect flow into the developing tail vortex, which may increase thrust produced by the tail of swimming mackerel.

Introduction

Finlets are small non-retractable fins characteristic of scombrid fishes including mackerel, bonitos, and tuna (Collette and Nauen, 1983; Joseph *et al.*, 1988). The finlets are situated on the dorsal and ventral body margins adjacent to the tail (spanning the region between the second dorsal and anal fins and the caudal fin, Fig. 1). In the case of the five dorsal and five ventral finlets of the chub mackerel, *Scomber japonicus* (Fig. 1), the summed surface area of the finlets is about 15% of the surface area of the caudal fin (Nauen and Lauder, 2000). Muscles that may actively control finlet motion insert at the base of each finlet (Nauen and Lauder, 2000).

Scombrid fishes are capable of high locomotory performance, including burst speeds from 18 body lengths per second (*bl* s^{-1}) for mackerel (Wardle and He, 1988) to up to 27 *bl* s^{-1} for tuna (Fierstine and Walters, 1968; also see Magnuson, 1978), and cruising speeds from 3.5 *bl* s^{-1} for mackerel (Wardle and He, 1988) to 6–10 *bl* s^{-1} for tuna (Yuen, 1970; summarized in Beamish, 1978). Given the close proximity of finlets to the caudal fin, previous investigators have suggested that finlets play a role in locomotion. Walters (1962) proposed that finlets direct flow longitudinally along the body, and Magnuson (1970) and Lindsey (1978) suggested that finlets direct flow across the caudal peduncle and caudal keels.

A recent study by Nauen and Lauder (2000) using two-dimensional (2-D) kinematic analysis methods to quantify the kinematics of finlets of *S. japonicus* showed that during steady forward locomotion at speeds from 1.2 to 3.0 fork lengths (*l*) s^{-1}, finlet kinematics in the vertical (*xy*) and horizontal (*xz*) plane were independent of speed. Angle of attack calculations using the kinematic measurements and the assumption that the direction of flow incident to the finlet was equal and opposite to the path of motion of the

Received 30 May 2000; accepted 1 December 2000.

* To whom correspondence should be addressed. E-mail: jnauen@oeb.harvard.edu.

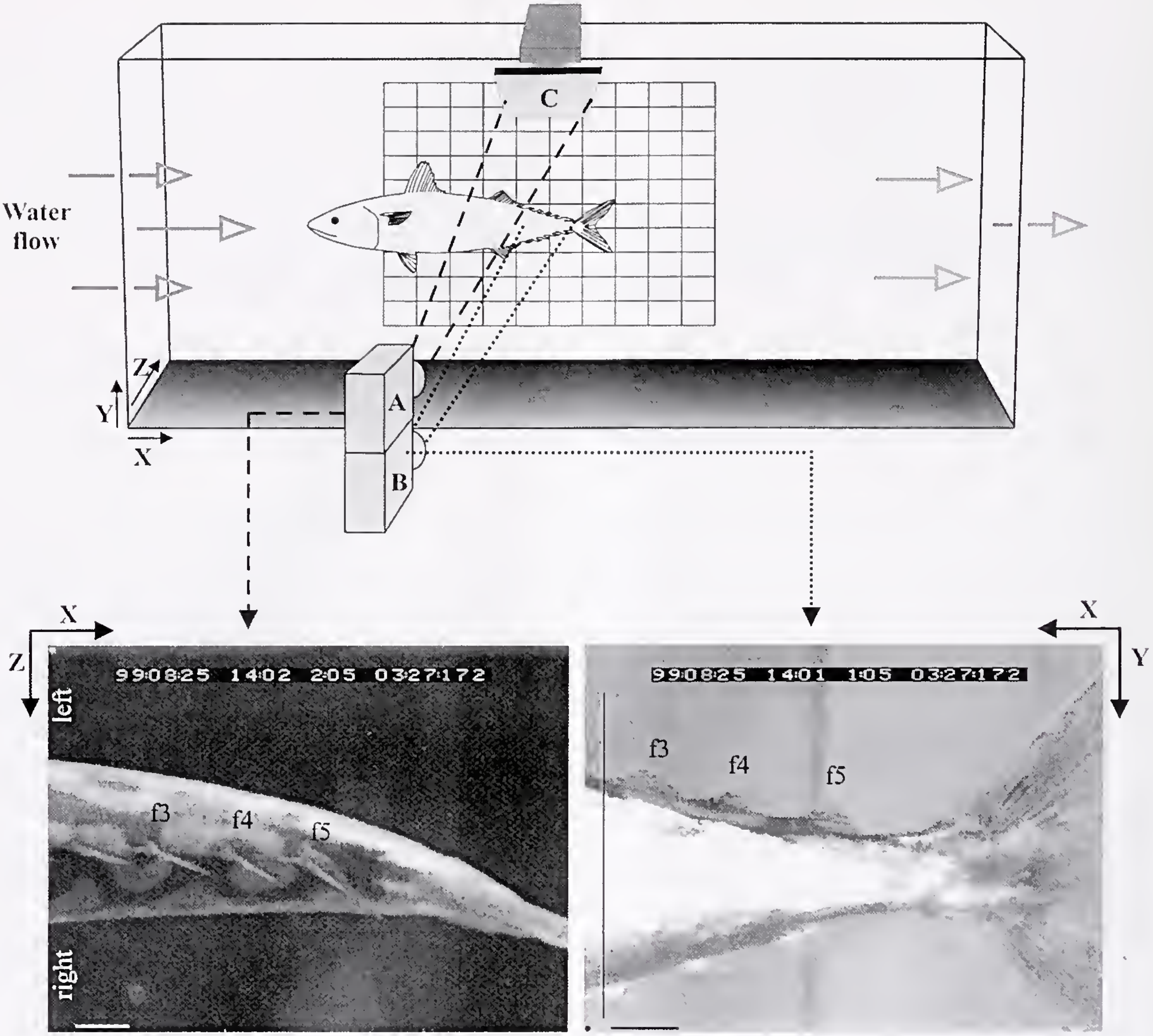

Figure 1. A schematic of the flow tank and camera system showing camera A (dashed line) viewing the mirror (C), which was situated at a 45° angle to the xz plane and showed a dorsal view of the fish. The origin of the dorsal view image (white asterisk in the left image) was in the upper left corner of the image. The viewing area of camera B (dotted line) was a lateral view of the left side of the fish; the origin of the lateral image (black asterisk in the right image) was in the lower left corner of the image. The three posterior finlets are identified in both of the images. Scale bars indicate 1 cm.

fish indicated that finlet oscillation in the horizontal plane is largely passive, and thrust is not created by lift-based mechanisms. However, the position of the finlets as the tail decelerates (at the end of each stroke) suggests that the finlets might direct flow into the developing caudal fin vortex, thus enhancing vortex circulation and thrust.

The 2-D method was useful for determining basic patterns of finlet movement and the independence of these patterns from swimming speed (Nauen and Lauder, 2000). A limitation of this method, however, was that each finlet was considered to be a flat plate that acted as a single functional unit during the tail beat cycle. Thus, any flexion of the finlet in response to hydrodynamic load was neglected. Furthermore, the orientations of the finlets in three-dimensional (3-D) space were not determined. This information is important for understanding finlet hydrodynamic function because it is the motion and orientation of the surface of a fin that creates fluid motion and generates force (Dickinson, 1996). For examples of how 2-D kinematic measurements can be misleading for evaluating fin hydrodynamics, see Ferry and Lauder (1996), Lauder and Jayne (1996), Walker and Westneat, (1997), Gibb *et al.* (1999), Wilga and Lauder (1999), and Lauder (2000).

Thus, the primary goal of this paper is to quantify the movement of finlets in three dimensions and to describe the orientation of the finlet surfaces with respect to three external earth reference planes (*xy*, *xz*, and *yz*). To test the hypothesis that each finlet acts as a single rigid flat plate, we divided each finlet into two separate elements and calculated the internal angle of these elements to each other as an approximation of finlet curvature. *A priori* we expected that finlet deformation would be low, because a dense assembly of fin rays support each finlet (Nauen and Lauder, 2000), and that the magnitude of flexion and 3-D orientation of the finlets would be similar, because the individual finlets are very similar in morphology (see Fig. 1, Fig. 2, and Nauen and Lauder, 2000). Using the 3-D data, we determined the position of the finlets during a critical portion of the stroke cycle when, as predicted by the vorticity enhancement hypothesis described above, the finlets may redirect water flow towards the caudal fin vortex. We then use these data to predict the direction of water motion in the region of the finlets.

Materials and Methods

Animals

Chub mackerel, *Scomber japonicus* (Houttuyn) were collected, using rod and reel, from various locations in coastal southern California. The animals were fed chopped smelt and housed in 1200-l tanks at a water temperature of 18 ± 2 °C in a photoperiod of 12:12 h light:dark. Three individuals (numbered 7, 9, and 10) ranging in fork length (*l*) from 20 to 26 cm were studied here.

3-D kinematic measurements

Experiments were conducted using a 600-l flow tank with a working area 82 cm long × 28 cm wide × 28 cm high (Fig. 1) and a water temperature of 19 ± 1 °C. The speed profile of the flow across and along the working section of the tank has been determined by tracking dye streams on images collected using high-speed video (for details, see Jayne *et al.*, 1996). To accurately image the motion of the finlets for a series of tailbeats, it was necessary that the fish maintain a consistent position relative to the field of view of the cameras. Thus, we used a flow tank rather than have the fish swim in still water through the field of view.

Two cameras that were part of a NAC HSV 500 C^3 video system were mounted on a vertical frame and aimed perpendicular to the flow tank (Fig. 1). The upper camera (Fig. 1A) was focused on a front-surface mirror (Fig. 1C) that was immersed in the flow at a 45° angle to the bottom of the tank (the *xz* plane) and showed a dorsal view of the fish. The lower camera (Fig. 1B) provided a lateral view (the *xy* plane) of the finlets. Using Nikon Micro-Nikkor 55-mm lenses with these cameras, we were able to image the finlets clearly in a field of view that was about 5 cm × 4 cm (Fig. 1). When a mackerel was in the field of view of the cameras and the image was in focus, the animal was necessarily swimming in the center of the working section of the tank. Thus, no data were obtained near the walls or floor of the flow tank, or the upper surface of the water. The fields of view of both cameras were scaled at the start of the experiment using two perpendicularly oriented rulers. The video system electronically synchronized the two cameras and recorded images at 250 Hz. About 12–15 images were collected per stroke of the tail. Video images were recorded continuously until sufficient sequences of steady swimming with the finlets in the fields of view of both cameras were obtained.

We swam the mackerel at speeds of 1.2 and 2.2 fork lengths per second ($l\ s^{-1}$). These speeds are within the range of swimming speeds (0.4–3.5 $bl\ s^{-1}$) that mackerel can sustain for longer than 200 min (Wardle and He, 1988), and match the speeds used in previous kinematic studies of mackerel finlets (Nauen and Lauder, 2000) and tail (Gibb *et al.*, 1999).

The video images were imported into a computer using DT-Acquire software with a Data Translation video card (Data Translation, Inc.). The procedures for calculating 3-D kinematics were adopted from those used in previous studies (Lauder and Jayne, 1996; Wilga and Lauder, 1999; Lauder, 2000). With the Cartesian coordinate system, any point on the video images can be identified by *x*, *y*, and *z* values. The origin was assigned to the lower left corner of the lateral view and the upper left corner of the dorsal view because the dorsal view was recorded using a mirror (the origin is denoted by asterisks in the images in Fig. 1). Because the finlets move over the body midline with each stroke (Nauen and Lauder, 2000), and we viewed the left side of the fish, the finlets were in full view of camera B as the tail was beating from left to right. There is a phase lag in the movement of the finlets relative to the body (Nauen and Lauder, 2000), thus the finlets are in view from about the start of the second quarter of one stroke to the end of the first quarter of the next (as determined by digitizing the dorsal insertion of finlet 5A, see Figs. 3 and 5).

The movements of finlets 3, 4, 5A, and 5B were quantified in this study. Previous kinematic measurements (Nauen and Lauder, 2000) indicated that finlet size and amplitude of finlet movement decrease anteriorly, with finlets 1 and 2 showing small excursions compared to those of finlet 5. In addition, the body of *S. japonicus* tapers posteriorly (Fig. 1). For example, for the fish 23 cm in fork length examined here, the depth of the body at the insertion of finlet 5 was 0.72 cm, which is 30% of the depth of the body at the position of finlet 1. The posterior decrease in the depth of the body and increase in the size and excursion of the finlets result in the posterior finlets moving over a much greater area of the body. The tips of dorsal and ventral finlet 5B actually meet at the lateral midline of the body on the caudal peduncle during their maximum vertical excursion (see fig. 12 of Nauen and Lauder, 2000). Thus, because the posterior finlets have a much larger potential hydrodynamic effect than the anterior finlets, we quantified the 3-D kinematics of finlets 3, 4, and 5.

The fifth finlet in *S. japonicus* is composed of two distinct groups of fin rays joined by a thin, clear membrane (Nauen and Lauder, 2000). Finlet 5 was treated here as two separate elements, 5A and 5B. The geometric relationship between those two elements (the internal angle of finlet 5) was also quantified. Single finlets 3 and 4 were an interesting comparison to the double-finlet structure of finlet 5.

Each finlet was divided into two triangles that were defined by a series of points (Fig. 2). This method gives a very good representation of finlet shape (Fig. 2) and allowed us to estimate finlet curvature by calculating the angle between the two triangular surfaces (angle α in the animal's frame of reference, Fig. 3), given the assumption of spanwise rigidity of the two triangles. Angle α for finlet 5 as a whole was the angle between finlets 5A and 5B (Fig. 2). The angles made by each of the eight triangular surfaces to the three orthogonal planes in the earth frame of reference (xy, xz, and yz) were also determined (Fig. 3).

Downloaded video images were digitized using a customized program. The coordinates were imported into Excel (Microsoft) to calculate the internal angles of the finlets and the angles of the finlet triangles to the three external reference planes. Each calculated angle was verified in a customized 3-D visualization program. All angle measurements were made from the upstream left side of the triangular surface to the plane of interest (Fig. 3). Under this measurement convention, if the left finlet surface was positioned to the right of the body midline (as shown in Fig. 3) the yz angle was less than 90°; a yz angle greater than 90° indicated that the left finlet surface was on the left side of the body midline. An xz measurement greater than 90° indicated that the surface was tilted away from the floor of the tank (or the frontal plane of the fish, Fig. 3). An xy angle measurement less than 90° indicated that the surface was oriented to the left of the body midline. Values of xy angles decreased to 0° as the finlet moved parallel to the body midline and then abruptly increased to about 120° as the finlet crossed to the right of the body midline. This abrupt increase (see Fig. 5A) is solely due to the measurement convention and does not reflect a large change in orientation of the finlet.

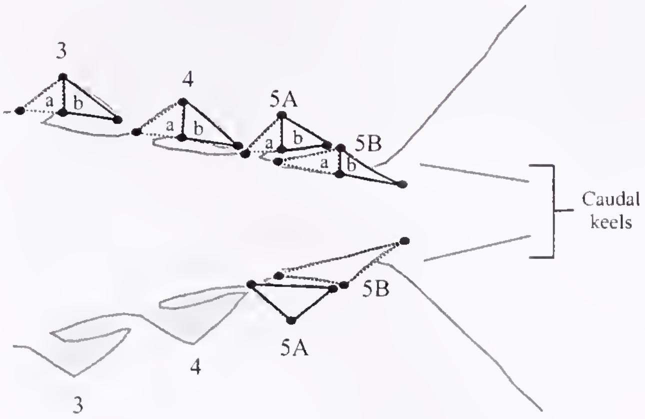

Figure 2. An outline of *Scomber japonicus* (gray lines) traced from a video image showing finlets 3, 4, 5A, 5B, and the caudal keels for reference. Note that the fifth finlet is morphologically composed of two distinct units (5A and 5B) that are bound by a clear membrane (Nauen and Lauder, 2000). Each set of four points (black circles) defined two triangular surfaces shown by the solid and dotted lines. Three of the points on finlets 5A and 5B (illustrated on the ventral finlets for clarity) were used to determine the rigidity of the fifth dorsal finlet as a whole. The thin, clear membrane that covers each of finlets 1–5 and attaches to the body is depicted in gray on ventral finlets 3 and 4.

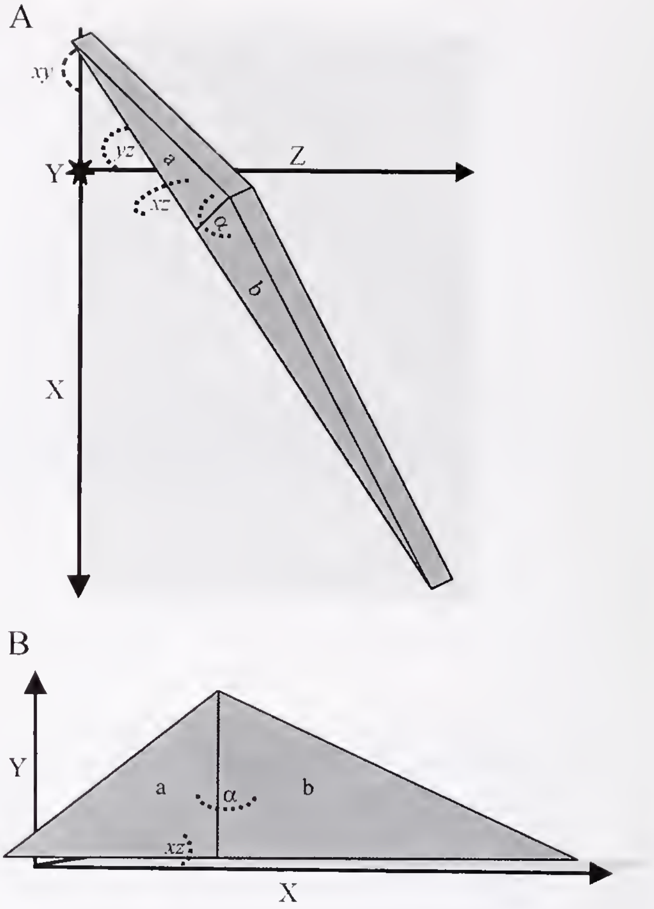

Figure 3. Diagram of a finlet (dark gray triangle) from a dorsal (A) and lateral (B) view. From the dorsal view (A) the y axis (indicated by an asterisk) is coming straight out of the page; in both views the xz plane is light gray. The internal angle (α), and the xy, xz, and yz angles (dotted lines), shown here in the dorsal view of triangle A, were calculated from digitized points (Fig. 2). See the text for further explanation.

Initial comparisons of a time series of the 3-D angles over a complete stroke for a single individual swimming at 1.2 and 2.2 $l\ s^{-1}$ indicated that the general patterns of finlet kinematics were not affected by speed. This observation is supported by our previous finding (based on a statistical analysis of 2-D measurements) that finlet kinematics were independent of speed over a speed range of 1.2 to 3.0 $l\ s^{-1}$ (Nauen and Lauder, 2000). On the basis of this information we focused on the 3-D kinematics of the finlets at the speed of 1.2 $l\ s^{-1}$.

Three to six tail strokes were digitized for each fish. The strokes were from sequential tailbeats for two of the fish; for the third fish we analyzed strokes from two sequential tailbeats and a third, single tailbeat. The digitized position values were not filtered. To determine the digitizing error, we digitized a single finlet 5 times. The calculated angle to the xy, xz, and yz planes were 23.0° ± 0.7°, 91.1° ± 1.0°, and 113.0° ± 0.8° (mean + SD, $n = 5$). Therefore, the digitizing error is approximately 1°. Finlet movement over an entire stroke was determined for one individual; finlet position as the tail was decelerating was determined for multiple strokes from all three individuals.

Statistics

Statistical analyses were performed using Statgraphics (v. 3.0 for Windows, STSC, USA). To determine if the mean values of intrafinlet angles averaged over a tailbeat cycle for a single individual were significantly different from 180°, t tests were performed on the time series data. The purpose of this analysis was to determine the general trend of finlet flexibility over the course of a tail stroke. The probability values of the t tests were established using the sequential Bonferroni method of Rice (1989) to control for conducting multiple comparisons. A multivariate ANOVA could not be performed on all of the angle data for the multiple individuals because of insufficient degrees of freedom; therefore, the data for each plane (xy, xz, and yz) were separately analyzed using two-way ANOVAS. The position of the finlet on the body (finlet number) was considered a fixed effect, and the individuals were considered random effects. The data at the specific time at 75% of the tail beat cycle—the time when the posterior finlets are in position to influence flow according to the vorticity enhancement hypothesis (Nauen and Lauder, 2000)—were also analyzed using this method. Tukey-Kramer *post hoc* tests were performed on each variable that showed significant effects of speed, finlet number, or structure.

Results

Kinematics over a stroke

Given that the magnitude of digitizing error was about 1° (detailed in the methods section), intrafinlet angle (α) values over a complete stroke for one individual (fish 10) swimming at a slow cruising speed of 1.2 $l\ s^{-1}$ indicate changes in finlet flexure over the stroke and variability in flexure among finlets. The variability in finlet flexibility is not directly attributable to the finlets' position on the body (Fig. 4) given that the greatest difference in α values from 180° (representing a flat plate) were about 40° for finlet 5A and about 15° for finlet 5B, and these two finlets are directly adjacent to each other (Fig. 2). Mean α values over a stroke, which represent a general index of finlet flexion, were not significantly different from 180° for finlets 3 ($\alpha = 179 \pm 6°$, mean ± SD, $n = 11$) and 5B ($\alpha = 182 \pm 10°$, mean ± SD, $n = 10$, t test, $P = 0.61$ and 0.52, respectively). The mean α values of finlet 4 ($174 \pm 6°$, mean ± SD, $n = 13$) and finlet 5A ($160 \pm 18°$, mean ± SD, $n = 10$) were significantly different from 180° (t test, $P = 0.003$, and 0.006, respectively). The flexion of finlet 5A was largest three-quarters of the way through the stroke (at about 0.75 s in Fig. 4) and decreased to close to zero ($\alpha = 180°$) at the end of the stroke (at about 0.1 s in Fig. 4).

The mean α value of finlet 5 over one stroke for fish 10, measured as the angle between finlet 5A and finlet 5B (see Fig. 2), was significantly different from 180° (t test, $P < 0.001$), indicating that the coupling between the two finlets is not rigid. The α for finlet 5 was relatively low throughout the stroke ($\alpha = 157 \pm 8°$, mean ± SD, $n = 10$).

The time series of the orientation of the finlets to the planes xy (Fig. 5A, B), yz (Fig. 5C, D), and xz (Fig. 5E, F) also indicate variability in orientation among the different finlets during different stages in the stroke. The more posterior finlets tended to make greater angles to the xy (longitudinal) plane (Fig. 5A, B). The phased increase in xy angle to values greater than 90° reflects the finlets crossing the longitudinal body midline to the right side of the fish at the end of the stroke (see Fig. 2). Relative to the yz (transverse) plane (Fig. 5C, D), the angles of the finlets decreased throughout the stroke, and were less than 90° for the first quarter of the next stroke. As the xy angle increases to greater than 90°, the yz angle decreases to less than 90° (Fig. 5A, B), indicating that the finlet has crossed to the right side of the body midline.

The time series of the angle of finlets 3, 4, and 5B to the xz plane during a stroke (Fig. 5E, F) suggests that the angles of finlets 3, 4, and 5B were at a slightly obtuse angle to the xz plane, while finlet 5A made an acute angle to the xz plane. However, when the mean values of the xz angle over a stroke were tested using adjusted probability values to control for conducting a series of simultaneous t tests (Rice, 1989), this observation was not statistically significant (Table 1). When averaged over an entire tail-beat, the angle of triangles 3A, 3B, 4A, and 4B to the xz plane were significantly different from 90° (Table 1), whereas the angles of finlets 5A and 5B were not (Table 1). This surprising statistical result is due to (1) averaging values over the

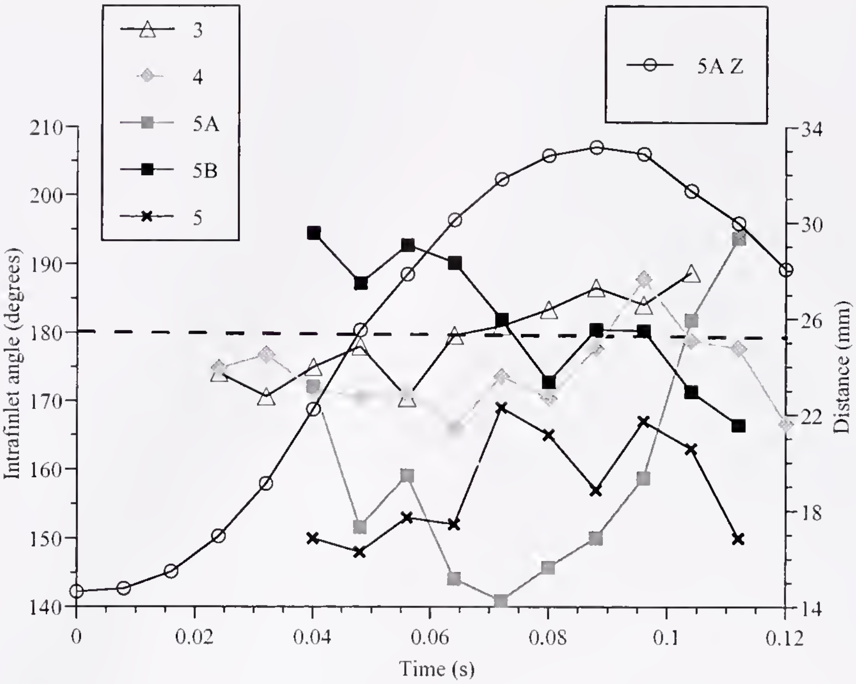

Figure 4. The internal angle (α) of finlets 3 (triangle), 4 (diamond), 5A (gray square), and 5B (black square) of a single individual over a tail stroke at 1.2 l s^{-1}. The angle between 5A and 5B (crosses) is also plotted. The dashed line indicates 180°. Axial body bending is indicated by the position of the body (at the insertion of finlet 5A) on the z axis (circles, 5A Z).

entire tail stroke and (2) the fact that the P value at which significance is achieved decreases with an increasing number of tests (Rice, 1989). We investigated this further by determining whether the intrafinlet angle differed from 90° at a specific time in the stroke.

Kinematics during tail deceleration

Three-quarters of the way through a stroke, the tail decelerates (Nauen and Lauder, 2000). Intrafinlet angle (α) values averaged from three fish indicate that finlet flexure was low at this point in the stroke, because α values were generally close to 180° (Fig. 6). Individual variation in the α value for finlet 5A was high, however: two of the individuals showed relatively low mean α values (mean ± SD of 151 ± 6° and 153 ± 7°, for fish 10 (n = 6) and fish 9 (n = 3), respectively), similar to the value of 144° seen at that point in the time series of a single stroke for Fish 10 (Fig. 4); in contrast, individual 7 showed a mean α value of 182 ± 1° (n = 3). This variation was reflected in the significant individual effect on α for finlets 4, 5A, 5B, and 5 (F = 15.9, $P < 0.0001$, Table 2). The significant interaction effect (F = 5.4, P = 0.0024, Table 2) indicates that there was no consistent change among individuals in α with position on the body (*i.e.*, finlet number, Fig. 6). There was no significant effect of finlet position on the body on α (F = 3.0, P = 0.16).

At this point in the stroke, the xy angle of the posterior finlets tended to be larger than those of the anterior finlets (Fig. 7A). This difference is reflected in the significant finlet effects (F = 9.2, P = 0.0016, Table 3). There were also significant individual (F = 30.6, $P < 0.0001$, Table 3) and individual × finlet interaction effects (F = 2.98, P = 0.0046, Table 3). The yz angles tended to be greater than 90° (Fig. 7B); the ANOVA indicated significant individual (F = 20.2, $P < 0.0001$) and individual × finlet (F = 9.5, $P < 0.0001$) effects but not significant finlet effects (F = 2.53, P = 0.0996) on the yz angles (Table 3). The xz angles of finlet 5B tended to be greater than 90°, whereas finlet 5A tended to be less than 90° (Fig. 7C). The ANOVA indicated significant finlet (F = 8.12, P = 0.0027, Table 3) and individual × finlet effects (F = 3.64, P = 0.0009, Table 3) but not significant individual effects (F = 1.56, P = 0.2190, Table 3) on the xz angles.

To illustrate the position of the finlets three-quarters of the way through the tail stroke, the coordinates of finlets 4, 5A, and 5B from the time series in Figure 5 are plotted in 3-D space in Figure 8. The data shown here are the highlighted points in the time series (Fig. 5). Although from a lateral view the finlets appear roughly flat and oriented normal to the xz plane (Fig. 8A), the flexure of finlets 4 and 5, the flexure between 5A and 5B, and the acute angle of 5A

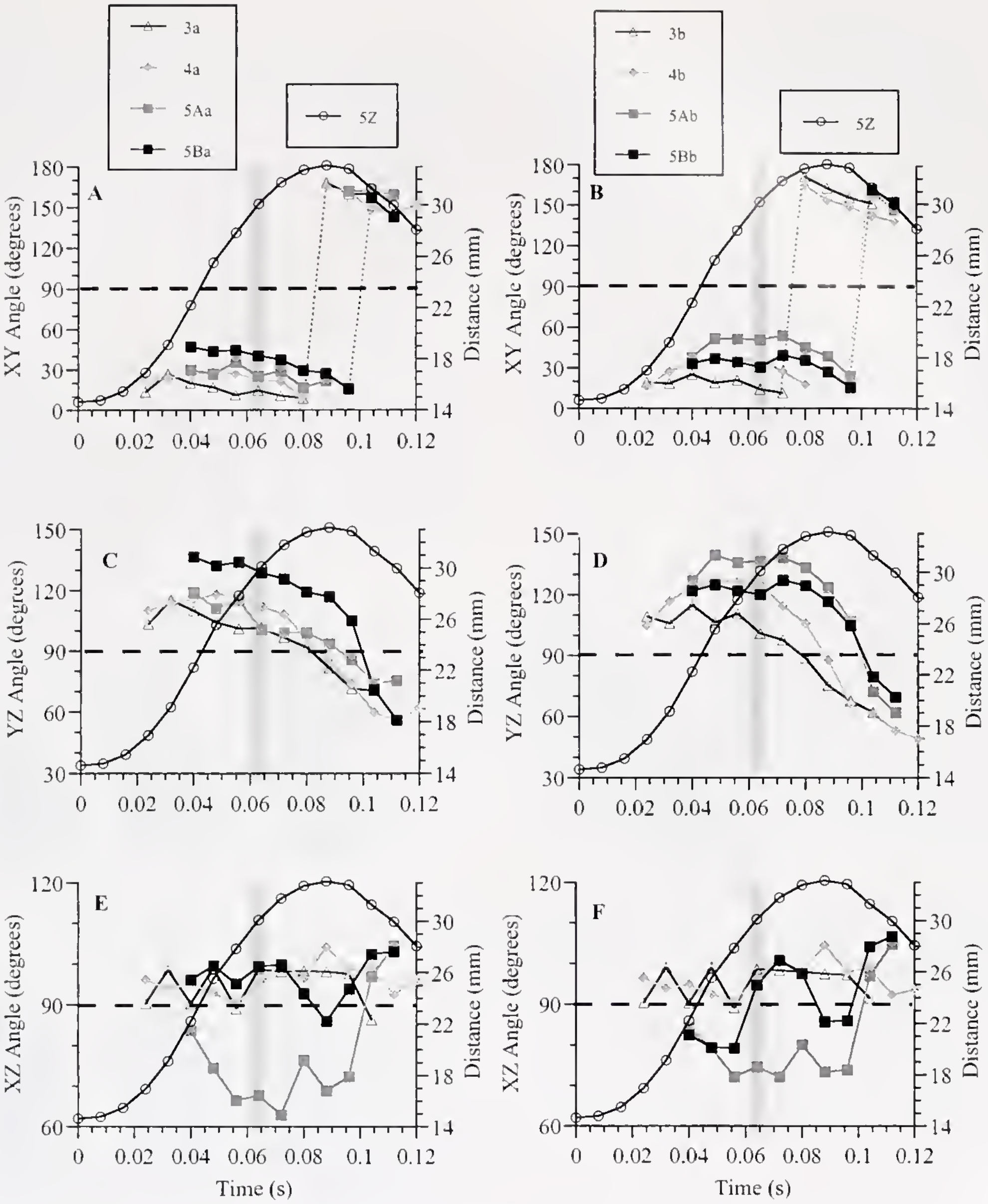

Figure 5. The angle of finlets 3 (triangle), 4 (diamond), 5A (gray square) and 5B (black square) to the *xy* (A, anterior triangles, B, posterior triangles), *yz* (C, D), and *xz* (E, F) planes over a stroke by a single individual at 1.2 l s^{-1}. Axial body bending is indicated by the position of the body (at the insertion of finlet 5A) on the *z* axis (circles). The tail stroke is defined from minimum to maximum values of 5A Z; the duration of this stroke was approximately 0.09 s. The angles at the time highlighted by the gray bar are plotted in 3-D space in Figure 8. The abrupt change in angles to the *xy* plane in panels A and B (indicated by the dotted lines) is due to our measurement convention (see Fig. 3 and the methods section) and reflects the transition of the planar finlet orientation across the body midline relative to the *xy* reference plane, not a large movement by the finlets.

to the *xz* plane are visible when the lateral view is rotated about 30° clockwise (Fig. 8B).

Discussion

Finlet morphology

A detailed morphological description of the finlets of *Scomber japonicus* is available in Nauen and Lauder (2000), and is useful for interpreting the three-dimensional pattern of movement. In brief, the finlets are on the order of 1 cm in length. A thin, clear membrane covers each finlet and attaches to the body. Jointed bony fin rays that extend to the distal tip of the fin stiffen each finlet. These rays articulate on a cartilaginous pad and are associated with muscles that appear to be homologous to the inclinator, depressor, and

Table 1

Results of t tests of the angle of each finlet to the XZ plane over a stroke

Finlet	*P*
4A	0.000035
4B	0.000086
3A	0.0087
3B	0.0021
5Aa	NS
5Ab	NS
5Ba	NS
5Bb	NS

NS indicates not significant according to $P = 0.05/k\text{-}i$ where k = the number of t tests performed and i = the order number of the variable based on its calculated P value (Rice, 1989).

Table 2

Results (F values) of the three-way ANOVA on intrafinlet angle during tail deceleration

Variable	Individual	Finlet #	Individual × finlet
df	2, 27	2, 4	4, 27
Intrafinlet angle (α)	15.9*	3.0	5.4*

df is the degrees of freedom.
* Statistically significant effect ($P < 0.05$).

erector muscles of the dorsal fin (Jayne *et al.*, 1996). This structure is identical for finlets 1 through 4.

The fifth (most posterior) finlet of *S. japonicus* has an interesting structural difference from the anterior four finlets. Finlet 5 is actually two finlets (5A and 5B) that each have a separate set of the structural components described above (Fig. 2). Finlets 5A and 5B are bound together by the clear membrane that covers the other finlets. Considered as a single functional unit, the fifth finlet is significantly larger than the anterior four finlets.

Finlet kinematics

On the basis of the presence of the fin rays throughout each of the finlets, the membrane binding finlets 5A and 5B, and the movement patterns of the finlets inferred from separate measurements in the *xy* and *yz* planes, we previously considered the fifth finlet to be a single functional unit and each finlet to move as a flat plate normal to the *xz* and *xy* planes (Nauen and Lauder, 2000). The present data show that this characterization was oversimplified. All of the finlets display considerable flexion and tilting to the *xz* and *yz* planes during locomotion, with finlets 5A and 5B showing distinct patterns of flexion and movement.

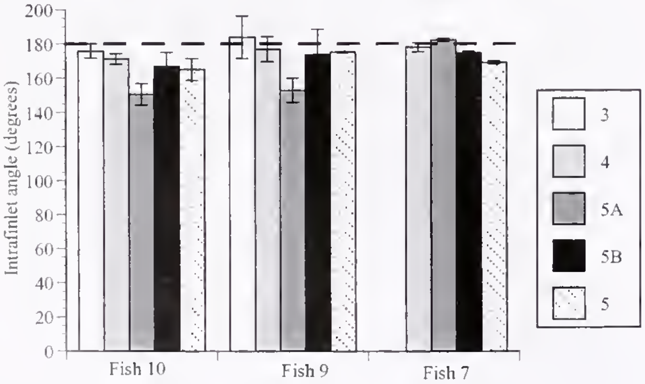

Figure 6. Means and standard deviations of the intrafinlet angle (α) for the finlets of three individuals at a single time point three-quarters of the way through the stroke as the tail is decelerating (n = 6, 3, and 3 strokes for fish 10, 9, and 7, respectively). The dashed line indicates an intrafinlet angle of 180° when the finlet elements are coplanar.

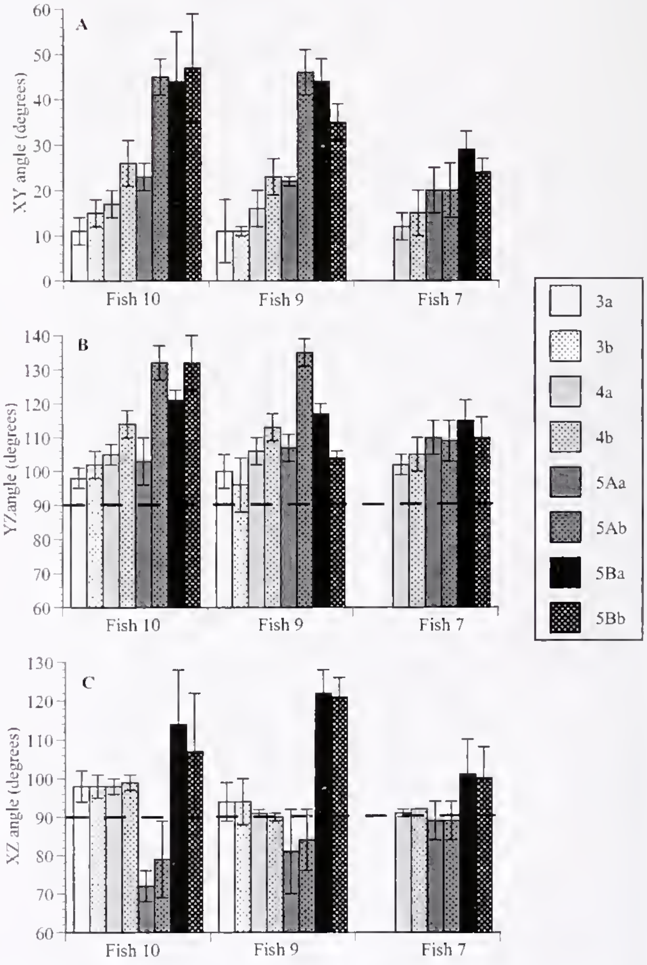

Figure 7. Means and standard deviations of the angles of the anterior (a, solid bars) and the posterior (b, dotted bars) elements of finlets 3 (white), 4 (light gray), 5A (dark gray), and 5B (black) to the three reference planes as the tail is decelerating three-quarters of the way through the stroke (n = 6, 3, and 3 strokes for fish 10, 9, and 7, respectively). The dashed lines in B and C indicate 90°.

Table 3

Results (F values) of the three-way ANOVAs on xy, yz and xz angles during tail deceleration

Variable	Individual	Finlet #	Individual × finlet
df	2, 54	5, 10	10, 54
xy angle	30.6*	9.2*	2.98*
yz angle	20.2*	2.5	9.49*
xz angle	1.6	8.12*	3.64*

df is the degrees of freedom.
* Statistically significant effect ($P < 0.05$).

A priori we expected that the stiffness of finlets 3, 4, 5A, and 5B would be similar because they are structurally identical, but that the stiffness of finlet 5 as a whole would be less than that of the individual finlets because the double-finlet structure is supported only by a clear membrane. In some cases this expectation was corroborated by the lack of bending seen in finlets 3 and 5B, and the slight bending ($\alpha = 174 \pm 6°$, mean ± SD, $n = 13$) of finlet 4. However, in two of the three fish examined, finlet 5A displayed significant bending during the tail stroke, with α values as low as 145° (compared with 180° for a flat plate). This variability in the stiffness of finlet 5 among individuals was unexpected. As anticipated, there was considerable flexion

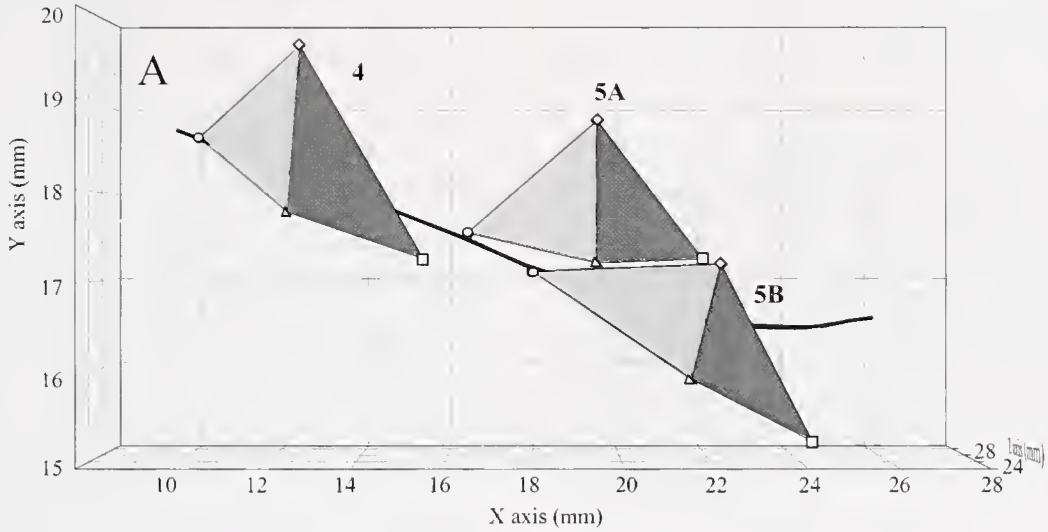

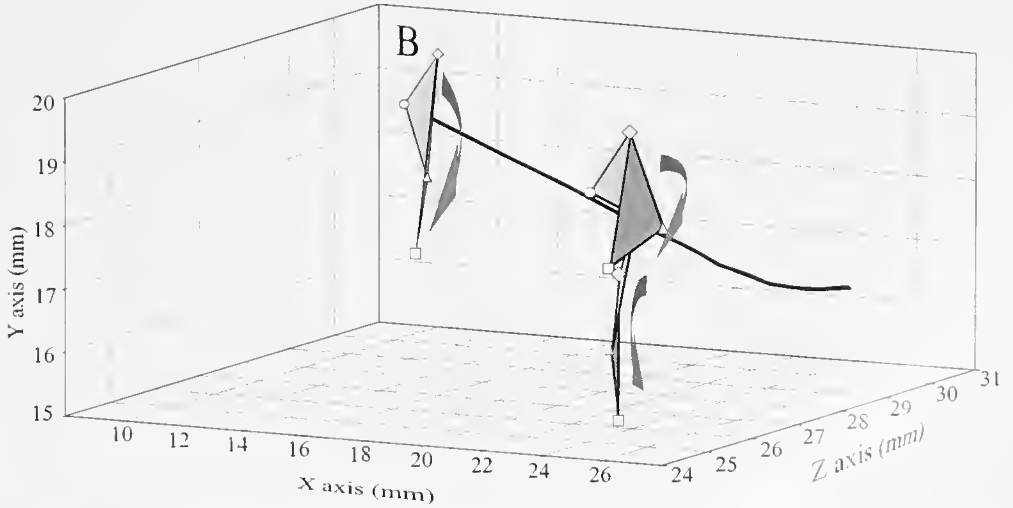

Figure 8. Three-dimensional orientation of finlets 4, 5A, and 5B as the tail is decelerating three-quarters of the way through the stroke. The thick solid line indicates the position of the body midline. The tail is beating into the page. The anterior element of each finlet is shaded light gray, while the posterior element is shaded dark gray. The lateral view (A) is rotated 30° clockwise relative to the xz plane in panel B. The arrows in B depict the hypothesized fluid motion based on finlet orientation.

between finlet 5A and 5B, given that mean α values were about 160°. This resulted in a complex, concave structure for the entire fifth finlet for over half of the stroke (see Fig. 8).

Fin deformation during movement has been demonstrated for the pectoral fins of elasmobranchs (Rosenberger and Westneat, 2000; Wilga and Lauder, 2000), chondrosteans (Wilga and Lauder, 1999), and teleosts (Webb, 1973; Geerlink, 1983; Gibb *et al.*, 1994; Lauder and Jayne, 1996; Walker and Westneat, 1997). The caudal fins of elasmobranchs (Ferry and Lauder, 1996), chondrosteans (Wilga and Lauder, 2000) and teleosts (Gibb *et al.*, 1999; Lauder, 2000) are also flexible, to a greater or lesser extent. Although the surface areas of these fins are considerably larger than the finlets studied here, in some cases the finlets also showed significant deformation during steady swimming despite their apparent morphological stiffness. The lack of rigidity during motion greatly complicates our understanding of swimming kinematics, and thus of swimming mechanics, in fish. The motion of a flexible structure is more difficult to predict and much more complex to model mathematically than the motion of a rigid object, and patterns of energy transfer from fins to fluid are greatly affected by the time-dependent deformation of the fins (Triantafyllou *et al.*, 1993; Barrett *et al.*, 1999; Walker and Westneat, 2000). Integrating experimental data on fin flexibility (such as that presented here and in the previous studies listed above) with unsteady hydrodynamic models of fish swimming will result in a more complete understanding of fin function during locomotion.

Active versus passive movement of the finlets

The orientation of the finlets during the stroke may be a combination of active and passive responses of the structure. For example, during the tail beat shown in Figure 8 the tail is beating into the plane of the page and water is flowing over the tail from the right to the left. Flexion of the finlets to the left is consistent with a passive response of the finlet to the water movement. However, the different orientations of finlet 5A and 5B might reflect active forces generated by the musculature at the base of the finlet rays. Bending of the finlets might also result from differential motion of the two bony jointed hemitrich elements that compose a single fin ray in teleost fishes (Arita, 1971). Asymmetrical action of the right and left side finlet musculature such as the erector, depressor, or inclinator muscles would act to slide one hemitrich past the other, causing the fin rays within the finlet to bend and thus change finlet shape. This may be the source of the individual variation seen in the intrafinlet angle of finlet 5A.

The finlet oscillates around its anterior insertion point on the dorsal body midline, thus the angles of the finlets to the xy and yz planes reflect the orientation of the finlets to the body midline. The present data indicate that the maximum xz and yz angles are larger in the posterior finlets and show phased anteroposterior changes to values respectively greater than and less than 90° over a tail stroke. These data agree with previous measurements showing a posterior increase in finlet oscillation amplitude and a posterior phase lag in finlet oscillation (Nauen and Lauder, 2000).

Implications for finlet function

On the basis of the high locomotory performance of scombrid fishes and the position of the finlets immediately anterior to the caudal fin, it has been hypothesized that finlets increase locomotory efficiency by directing flow longitudinally along the body (Walters, 1962), and across the caudal peduncle (Magnuson, 1970) and caudal keels (Lindsey, 1978). Direct tests of finlet function require quantitative flow visualization data on the tail and finlets (*e.g.*, see Drucker and Lauder, 1999; Wilga and Lauder, 1999; Lauder, 2000). However, the present data offer some insights into a possible hydrodynamic function of the finlets.

At the time of tail deceleration, the angles made to the xz plane by both elements of finlet 5B are significantly higher than the angle made by finlet 5A. The higher angles to the xz plane reflect the bending between finlets 5A and 5B, as well as the "bent" orientation of the entire fifth finlet at this point in the stroke (Fig. 8). Such a configuration may affect the pattern of water flow over the caudal peduncle. Finlet 5B is relatively planar in conformation at the time when water flow is expected to be crossing the midline and encountering the finlet surface (Fig. 8B). The differences in the orientation of finlets 5A and 5B suggest that the direction of water flow is more cross-peduncular at 5A and more parallel to the longitudinal body axis at 5B (Fig. 8B). Flow passing posterolaterally and ventrally over the trailing edge of finlet 5A would encounter the relatively planar surface of finlet 5B, which would redirect flow along the midline of the caudal peduncle into the developing tail vortex, as suggested on the basis of two-dimensional data by Nauen and Lauder (2000) as well as to some extent by Walters (1962), Magnuson (1970), and Lindsey (1978). The amount of redirected fluid is likely to be small but—when summed over the many tail strokes executed during daily activity by scombroid fishes—it may increase thrust production significantly relative to a fish without finlets.

This hypothesis can be tested by swimming mackerel in fluid with small reflective particles and tracking the trajectory of the particles as they move past the finlets and the caudal peduncle. Such future experiments with flow visualization will reveal whether the finlets alter the path of water flow in their vicinity and whether that water is directed into the tail vortex, potentially increasing swimming efficiency.

Acknowledgments

The authors thank Cheryl Wilga for assistance with obtaining the mackerel for this study, and Laura Farrell for assistance with data analysis. We also thank Jimmy Liao, Cheryl Wilga, Laura Farrell, Tonia Hsieh, and Ellen Freund for helpful comments during the course of this project. Three reviewers provided useful comments for improving the manuscript. Support was provided by NSF grant 9807021 to GVL.

Literature Cited

Arita, G. S. 1971. A re-examination of the functional morphology of the soft-rays in teleosts. *Copeia* **1971:** 691–697.

Barrett, D. S., M. S. Triantafyllou, D. K. P. Yue, M. A. Grosenbaugh, and M. J. Wolfgang. 1999. Drag reduction in fish-like locomotion. *J. Fluid Mech.* **392:** 183–212.

Beamish, F. W. H. 1978. Swimming capacity. Pp. 101–189 in *Locomotion, Vol. VII, Fish Physiology,* W. S. Hoar and D. J. Randall, eds. Academic Press, New York.

Collette, B. B., and C. E. Nauen. 1983. *Scombrids of the World,* Vol. 2. United Nations Development Programme, FAO, Rome.

Dickinson, M. H. 1996. Unsteady mechanisms of force generation in aquatic and aerial locomotion. *Am. Zool.* **36:** 537–554.

Drucker, E. G., and G. V. Lauder. 1999. Locomotor forces on a swimming fish: three-dimensional vortex wake dynamics quantified with digital particle image velocimetry. *J. Exp. Biol.* **202:** 2393–2412.

Ferry, L. A., and G. V. Lauder. 1996. Heterocercal tail function in leopard sharks: a three-dimensional kinematic analysis of two models. *J. Exp. Biol.* **199:** 2253–2268.

Fierstine, H. L., and V. Walters. 1968. Studies in locomotion and anatomy of scombroid fishes. *Mem. South. Calif. Acad. Sci.* **6:** 1–31.

Geerlink, P. J. 1983. Pectoral fin kinematics of *Coris formosa* (Teleostei, Labridae). *Neth. J. Zool.* **39:** 166–193.

Gibb, A. C., B. C. Jayne, and G. V. Lauder. 1994. Kinematics of pectoral fin locomotion in the bluegill sunfish *Lepomis macrochirus. J. Exp. Biol.* **189:** 133–161.

Gibb, A. C., K. A. Dickson, and G. V. Lauder. 1999. Tail kinematics of the chub mackerel *Scomber japonicus:* testing the homocercal tail model of fish propulsion. *J. Exp. Biol.* **202:** 2433–2447.

Jayne, B. C., A. F. Lozada, and G. V. Lauder. 1996. Function of the dorsal fin in bluegill sunfish: motor patterns during four distinct locomotor behaviors. *J. Morphol.* **228:** 307–326.

Joseph, J., W. Klawe, and P. Murphy. 1988. *Tuna and Billfish: Fish Without a Country.* Inter-American Tropical Tuna Commission, La Jolla, CA.

Lauder, G. V. 2000. Function of the caudal fin during locomotion in fishes: kinematics, flow visualization, and evolutionary patterns. *Am. Zool.* **40:** 101–122.

Lauder, G. V., and B. C. Jayne. 1996. Pectoral fin locomotion in fishes: testing drag-based models using three-dimension kinematics. *Am. Zool.* **36:** 567–581.

Lindsey, C. C. 1978. Form, function, and locomotory habits in fish. Pp. 1–100 in *Locomotion, Vol. VII, Fish Physiology,* W. S. Hoar and D. J. Randall, eds. Academic Press, New York.

Magnuson, J. J. 1970. Hydrostatic equilibrium of *Euthynnus affinis,* a pelagic teleost without a gas bladder. *Copeia* **1970:** 56–85.

Magnuson, J. J. 1978. Locomotion by scombrid fishes: hydromechanics, morphology, and behavior. Pp. 239–313 in *Locomotion, Vol. VII, Fish Physiology,* W. S. Hoar and D. J. Randall, eds. Academic Press, New York.

Nauen, J. C., and G. V. Lauder. 2000. Locomotion in scombrid fishes: morphology and kinematics of the finlets of the chub mackerel *Scomber japonicus. J. Exp. Biol.* **203:** 2247–2259.

Rice, W. R. 1989. Analyzing tables of statistical tests. *Evolution* **43:** 223–225.

Rosenberger, L. J., and M. W. Westneat. 2000. Functional morphology of undulatory pectoral fin locomotion in the stingray *Taeniura lymma* (Chondrichthyes: Dasyatidae). *J. Exp. Biol.* **202:** 3523–3539.

Triantafyllou, G. S., M. S. Triantafyllou, and M. A. Grosenbaugh. 1993. Optimal thrust development in oscillating foils with application to fish propulsion. *J. Fluids Struct.* **7:** 205–224.

Walker, J. A., and M. W. Westneat. 1997. Labriform propulsion in fishes: kinematics of flapping aquatic flight in the bird wrasse *Gomphosus varius* (Labridae). *J. Exp. Biol.* **200:** 1549–1569.

Walker, J. A., and M. W. Westneat. 2000. Mechanical performance of aquatic rowing and flying. *Proc. R. Soc. Lond. B.* **267:** 1875–1881.

Walters, V. 1962. Body form and swimming performance in the scombroid fishes. *Am. Zool.* **2:** 143–149.

Wardle, C. S., and P. He. 1988. Burst swimming speeds of mackerel, *Scomber scombrus* L. *J. Fish Biol.* **32:** 471–478.

Webb, P. W. 1973. Kinematics of pectoral fin propulsion in *Cymatogaster aggregata. J. Exp. Biol.* **59:** 697–710.

Wilga, C. D., and G. V. Lauder. 1999. Locomotion in sturgeon: function of the pectoral fins. *J. Exp. Biol.* **202:** 2413–2432.

Wilga, C. D., and G. V. Lauder. 2000. Three-dimensional kinematics and wake structure of the pectoral fins during locomotion in leopard sharks *Triakis semifasciata. J. Exp. Biol.* **203:** 2261–2278.

Yuen, H. S. H. 1970. Behavior of a skipjack tuna, *Katsuwonus pelamis,* as determined by tracking with ultrasonic devices. *J. Fish. Res. Board Can.* **27:** 2071–2079.

Reference: *Biol. Bull.* **200:** 20–32. (February 2001)

Metamorphosis of Coeloblastula Performed by Multipotential Larval Flagellated Cells in the Calcareous Sponge *Leucosolenia laxa*

SHIGETOYO AMANO[1,*] AND ISAO HORI[2]

[1] *Cancer Research Institute, Kanazawa University, 13-1 Takaramachi, Kanazawa, Ishikawa 920-0934;*
and [2] *Department of Biology, Kanazawa Medical University, Uchinada, Ishikawa 920-0265, Japan*

Abstract. The calcareous sponge *Leucosolenia laxa* releases free-swimming hollow larvae called coeloblastulae that are the characteristic larvae of the subclass Calcinea. Although the coeloblastula is a major type of sponge larva, our knowledge about its development is scanty. Detailed electron microscopic studies on the metamorphosis of the coeloblastula revealed that the larva consists of four types of cells: flagellated cells, bottle cells, vesicular cells, and free cells in a central cavity. The flagellated cells, the principal cell type of the larva, are arranged in a pseudostratified layer around a large central cavity. The larval flagellated cells characteristically have glutinous granules that are used as internal markers during metamorphosis. After a free-swimming period the larva settles on the substratum, and settlement apparently triggers the initiation of metamorphosis. The larval flagellated cells soon lose their flagellum and begin the process of dedifferentiation. Then the larva becomes a mass of dedifferentiated cells in which many autophagosomes are found. Within 18 h after settlement, the cells at the surface of the cell mass differentiate to pinacocytes. The cells beneath the pinacoderm differentiate to scleroblasts that form triradiate spicules. Finally, the cells of the inner cell mass differentiate to choanocytes and are arranged in a choanoderm that surrounds a newly formed large gastral cavity. We found glutinous granules in these three principal cell types of juvenile sponges, thus indicating the multipotency of the flagellated cells of the coeloblastula.

Introduction

All major sponge groups emerged on the earth in the late Precambrian, about 580 million years ago (Li *et al.*, 1998). Thereafter they have changed in different ways and adapted the structure of their larvae and process of metamorphosis to survive through the subsequent geologic eras. As a result of adaptation, sponge development is greatly diversified among higher taxonomic groups (Brusca and Brusca, 1990). Most sponges are viviparous, but some are oviparous. Some viviparous sponges release crawling larvae, but most release swimming larvae, of which there are a number of types. An amphiblastula or coeloblastula is produced by calcareous sponges; a parenchymella is the larva of the majority of demosponges, but several other larval types are known; and a trichimella is exclusive to hexactinellid sponges. The modes of metamorphosis of these larvae are also quite variable (Simpson, 1984). In spite of such variations, recent molecular evidence shows that all sponges are of monophyletic origin (Müller, 1997).

Because all adult sponges are sessile animals, their free-swimming larval period is a critical one for habitat selection. After the free-swimming period, larvae settle on the substratum and initiate metamorphosis. The layer of flagellated cells is a larval organ for swimming, therefore those cells disappear soon after settlement. Because the sponge larvae are generally minute and their nutritive materials are limited, it seems very disadvantageous to discard the flagellated cells during metamorphosis. The developmental fate of these cells in the parenchymellae of demosponges has long been debated. One view holds that the flagellated cells are transformed into the choanocytes of juvenile sponges (Borojevic and Levi, 1965; Boury-Esnault, 1976; Amano and Hori, 1994, 1996), but the opposing view contends that they are lost by exfoliation or phagocytosis during metamorphosis (Bergquist and Glasgow 1986; Misevic *et al.*, 1990; Kaye and Reiswig, 1991). The flagellated cells in the coeloblastulae of calcareous sponges cannot, however, be discarded, because these cells make up the greater part of the larva.

---

* To whom correspondence should be addressed. E-mail: samano@kenroku.kanazawa-u.ac.jp

The coeloblastulae of calcareous sponges have been studied very rarely, and we know little about the process of their metamorphosis (Minchin, 1896; Tuzet, 1947; Borojevic, 1969). In this study we will show the fine structure of the coeloblastula, metamorphosing larva, and juvenile sponge of *Leucosolenia laxa* in clear electron micrographs. After settlement, the larval flagellated cells dedifferentiate into a simple cell mass on the substratum; thereafter they differentiate again into the three principal cell types of a juvenile sponge. We discuss the multipotency of the larval flagellated cells of *L. laxa* by comparing them with the developmental potency of the larval flagellated cells of other sponges.

Materials and Methods

Sponges and larvae

In early September, specimens of *Leucosolenia laxa* were collected from rafts in Mutsu bay in northern Japan. *L. laxa* is one of the most common calcareous sponges in this region. Immediately after collection, the sponges were placed in containers with seawater, brought to the laboratory of Asamushi Marine Biological station within 1 h, and kept in running seawater.

To collect larvae, in the early morning sponges were placed in glassware with seawater. Under the natural illumination, about one-tenth of them released larvae, beginning soon after dawn and ceasing by noon. So the larval release of this calcareous sponge is probably controlled by light cycles, as it is in certain demosponges (Amano, 1986, 1988; Maldonado and Young, 1996). The larvae, which began swimming immediately upon release, were placed in petri dishes with filtered seawater; the seawater was changed daily. The larvae and juveniles can be reared for a week under these conditions.

Electron microscopy

Released larvae swam around mainly under the water surface, and after a swimming period, settled on the glass surface or beneath the air-water interface. Free larvae were picked up on a platinum loop and placed into fixative. Settled larvae were collected from beneath the air-water interface in the same way. This procedure minimized the mechanical stress of the larvae during collection.

It is quite difficult to preserve the ultrastructure of the larvae of this species satisfactorily. After trying a number of fixatives, we found the following formula to be the best: 1% paraformaldehyde, 7.5% glutaraldehyde, and 14% sucrose in 0.1 *M* cacodylate buffer, pH 7.4. Larvae or juvenile sponges were fixed in the ice-cold fixative for 1 h. Then the samples were rinsed twice in the same buffer and postfixed in 1% osmium tetroxide in 0.1 *M* cacodylate buffer, pH 7.4, for 1 h. They were dehydrated through a graded ethanol series, cleared in propylene oxide, and embedded in Spurr epoxy resin (Spurr, 1969). Semithin sections were stained with toluidine blue for light microscopy. Ultrathin sections were stained with uranyl acetate and lead citrate, then examined and photographed under a Hitachi H-500 electron microscope.

Results

Free-swimming larva

The calcareous sponge *Leucosolenia laxa* releases free-swimming coeloblastulae through the osculum with the excurrent water. The free larvae were fixed soon after release and on the next day. We examined larvae collected after different periods of swimming but found no morphological difference; thus we show only the images of the free larvae fixed soon after release. The coeloblastula is a hollow spheroid consisting of a layer of flagellated cells around a large central cavity (Fig. 1). This larva, which is about 90 μm in length and about 50 μm in width, is entirely ciliated—including its posterior pole. The coeloblastula contains three additional types of cells: bottle cells, vacuolar cells, and free cells in the central cavity. Figure 1 also shows the polarity of the larva. Its anterior pole consists exclusively of flagellated cells, and its posterior pole includes several vacuolar cells.

Flagellated cells. Figure 2 shows the flagellated cells of the coeloblastula of *L. laxa.* These cells are organized in a pseudostratified cell layer that is about 15-μm thick and

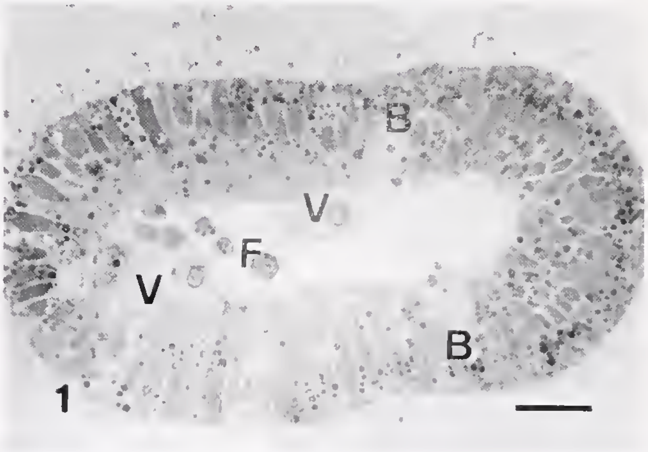

Figure 1. Coeloblastula of *Leucosolenia laxa.* The pseudostratified layer of flagellated cells surrounds a large central cavity. B: bottle cell. F: free cell in the central cavity. V: vacuolar cell. Scale bar = 10 μm.

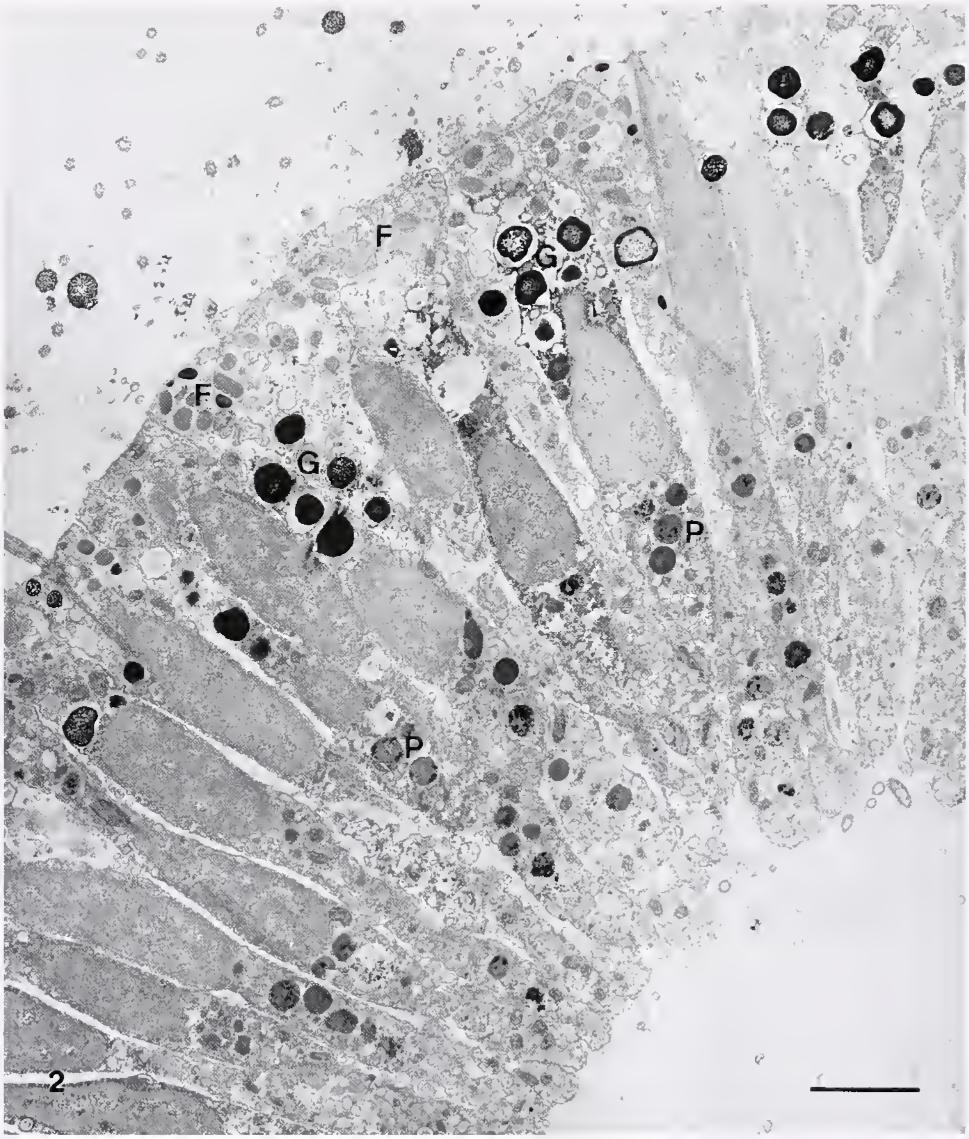

Figure 2. The pseudostratified layer of flagellated cells in the coeloblastula of *Leucosolenia laxa*. F: fibrous granule in the outermost cytoplasm, G: glutinous granule in the apical cytoplasm, P: phagosome-like granule in the basal cytoplasm. Scale bar = 2 μm.

lacks a basal lamina. One flagellum emerges from the outer surface of the cell. There are glutinous granules in the apical cytoplasm and fibrous granules in the outermost cytoplasm. An elongated nucleus, about 5 × 2 μm, has a nucleolus and heterochromatin masses. The basal cytoplasm contains phagosome-like granules, and the innermost region of the cell is filled with many small (about 0.25 μm) vesicles and a few lipid droplets (Fig. 3). There are mitochondria in both the apical cytoplasm and the basal cytoplasm.

Figures 4 and 5 show magnified images of the apical region of flagellated cells. It is apparent that one flagellum emerges from the flat outer surface of the cell. The most proximal portion of the flagellum is somewhat electron-dense. From a basal body, two rootlets extend downward to the sides of a nucleus. The rootlets are striated, with a distance of about 40 nm between the midpoints of two neighboring striae. There is a basal foot running parallel to the outer surface. The Golgi apparatus is always located vertically along the rootlet. Only in the apical region are the neighboring flagellated cells united, by simple apposition (Figs. 4 and 5); in the deeper region, there is a wide space between the cells (Fig. 2).

We found a consistent arrangement and orientation in the apical region of larval flagellated cells. One side of the outermost portion of the cell protrudes toward a neighbor cell, and the protrusion is regularly directed to the anterior end of the larva (Figs. 4 and 5). A basal foot consistently extends in the opposite direction—that is, to the posterior

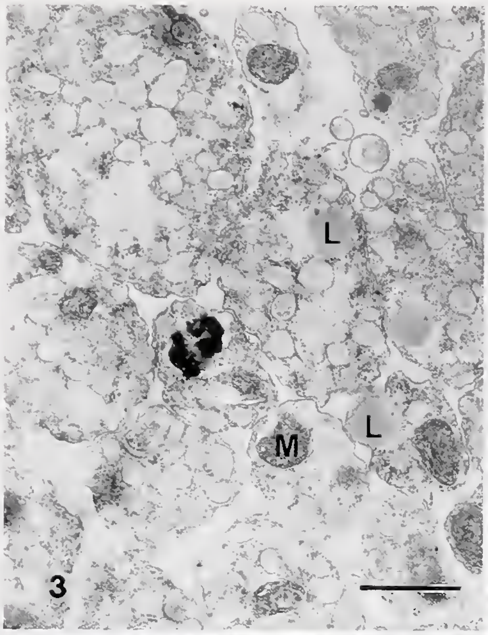

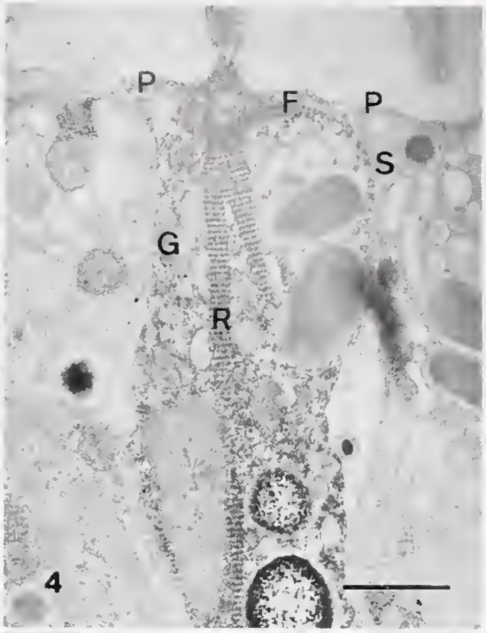

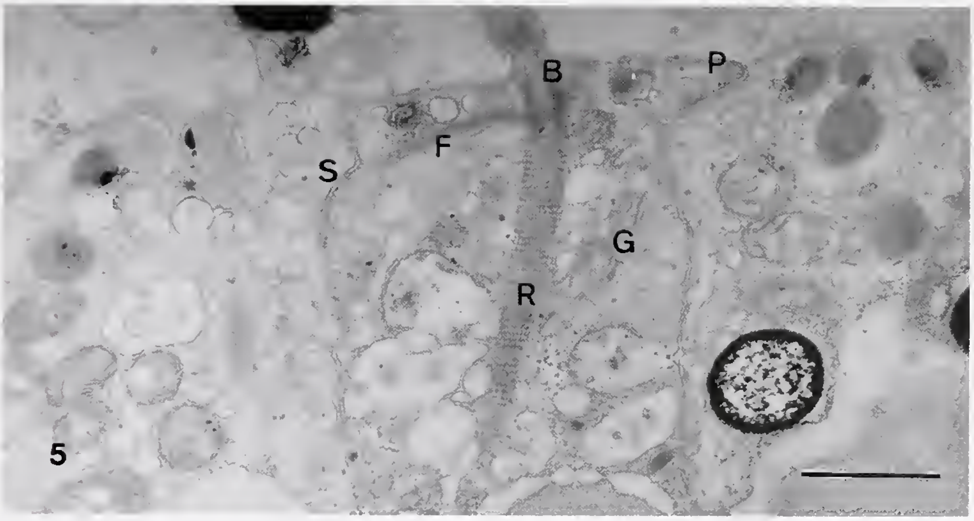

Figure 3. The innermost region of flagellated cells in the coeloblastula of *Leucosolenia laxa*. L: lipid droplet, M: mitochondrion. Scale bar = 1 μm.

Figure 4. Apical region of flagellated cells in the coeloblastula of *Leucosolenia laxa* showing two basal rootlets (R) and a basal foot (F). G: Golgi apparatus, P: protrusion of the outermost portion of flagellated cells, S: simple apposition. Scale bar = 1 μm.

Figure 5. Flagellar basal apparatus of *Leucosolenia laxa*. B: basal body, F: basal foot, G: Golgi apparatus, P: protrusion of the outermost portion of flagellated cells, R: basal rootlet, S: simple apposition. Scale bar = 1 μm.

end of the larva. The Golgi apparatus is always located anteriorly to the rootlet (Fig. 4). These precise spatial arrangements seem to be essential for aligning the direction of an effective stroke.

Figure 6 shows glutinous granules of about 1-μm diameter in the apical cytoplasm of flagellated cells. Their surface layer is very electron-dense, and the inner part is made of the loose network of a fine granular substance. The name glutinous granules was chosen because they are made of a very sticky substance. When paraformaldehyde was omitted from the fixative, some of these granules were discharged from the cell, and their content was released into the water. The released content was found to be glutinous because it adhered to flagella and made them very sticky. The sticky flagella became crooked and tangled with each other in the fixative. Figure 7 shows fibrous granules of about 1.0 × 0.5 μm. They are yolk granules filled with a fibrous substance

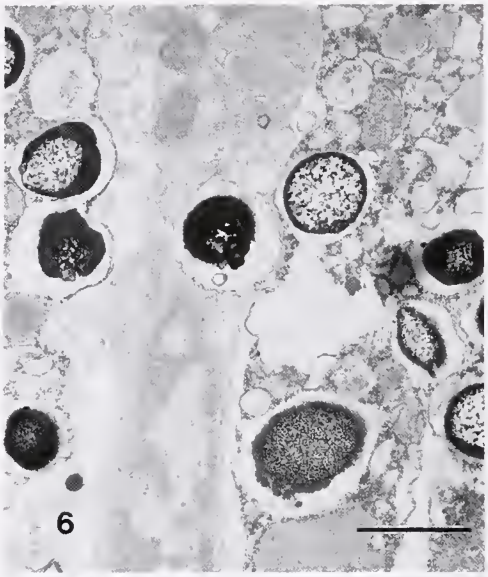

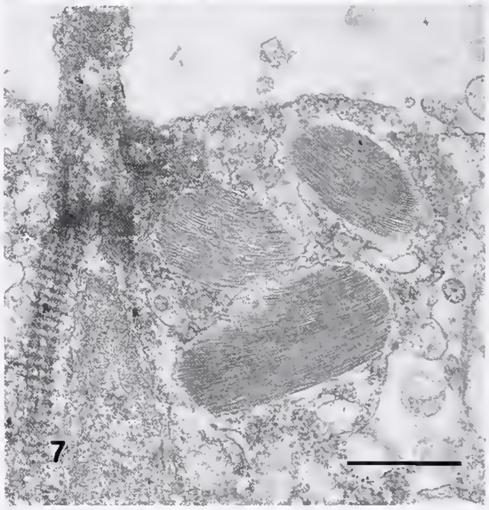

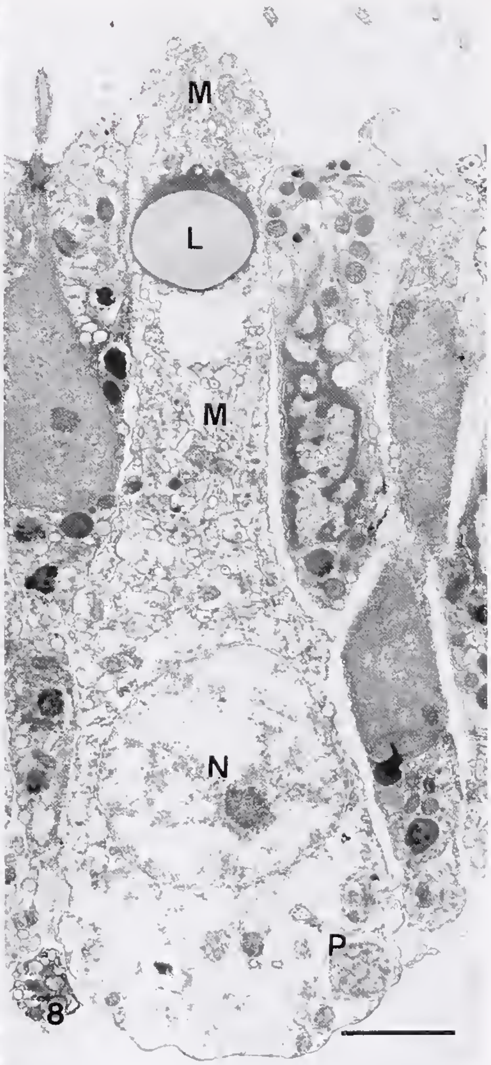

Figure 6. Glutinous granules in the apical cytoplasm of flagellated cells in the coeloblastula of *Leucosolenia laxa.* Scale bar = 1 μm.

Figure 7. Fibrous granules in the outermost cytoplasm of flagellated cells in the coeloblastula of *Leucosolenia laxa.* Scale bar = 0.5 μm.

Figure 8. A bottle cell between flagellated cells in the coeloblastula of *Leucosolenia laxa.* L: lipid droplet, M: membranous structure, N: nucleus, P: phagosome-like granule. Scale bar = 2 μm.

that runs parallel with the long axis. These granules are located in the outermost cytoplasm of flagellated cells (Fig. 2).

Bottle cells. Bottle cells are large (about 18 × 6 μm) cells that are located between flagellated cells but have no flagellum themselves (Fig. 8). There are several bottle cells in a larva. These cells are longer than flagellated cells and protrude outside and into the central cavity. Their nucleolated nucleus is usually located in the basal region. The apical and middle cytoplasm are filled with membranous structures, and the cell shown in Figure 8 has a large lipid droplet. In the basal cytoplasm there are phagosome-like granules, some of them have digested their content.

Vacuolar cells. These cells, having an irregular form, are filled with large vesicles (Fig. 9). Their nucleolated nucleus has a large number of heterochromatin masses. There are about 10 vacuolar cells in a larva, most of them concentrated in the posterior region (Fig. 1). In most cases, a part of the cell is inserted between flagellated cells, but the greater part protrudes into a central cavity.

Free cells in a central cavity. There are a few free cells in a central cavity (Fig. 1). These cells are small, with scanty cytoplasm (Fig. 10). They have an undeveloped Golgi ap-

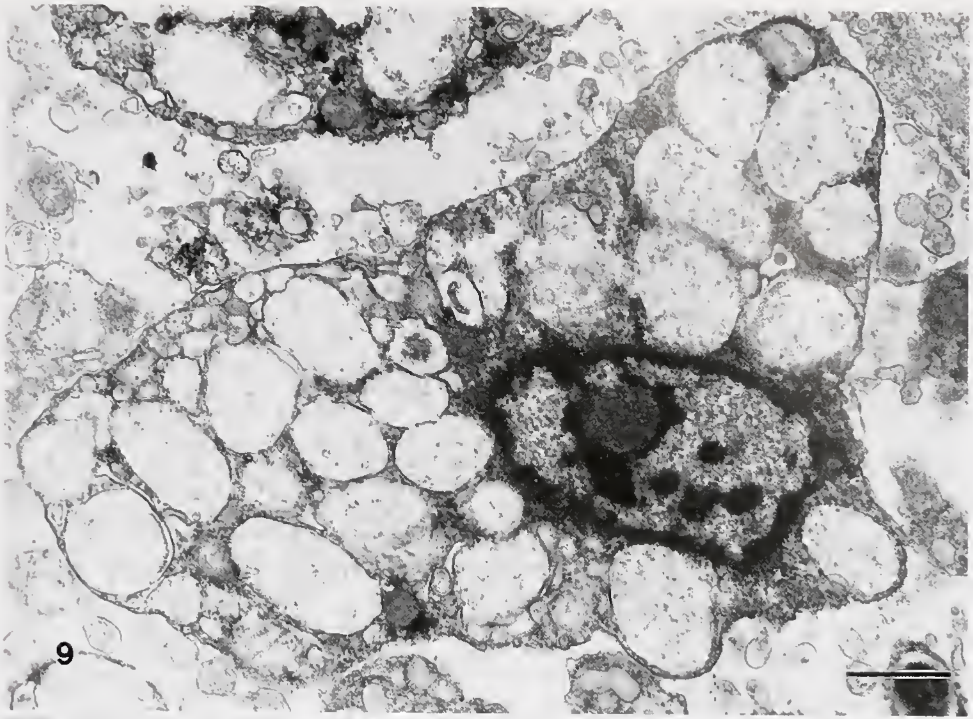

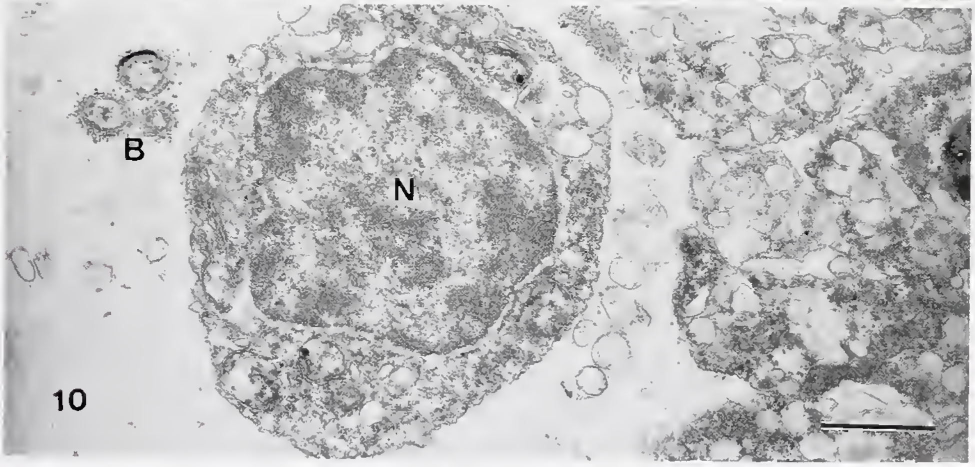

Figure 9. A vesicular cell in the coeloblastula of *Leucosolenia laxa*. Scale bar = 1 μm.

Figure 10. A free cell in the central cavity of the coeloblastula of *Leucosolenia laxa*. B: symbiotic bacteria. N: nucleus. Scale bar = 1 μm.

paratus and a small number of mitochondria. Figure 10 also shows symbiotic bacteria in the central cavity.

Metamorphosis

The coeloblastulae of *L. laxa* begin to settle after a free-swimming period of about 36 h or more, and the settling larvae soon spread out on the substratum. Figure 11 shows a larva that has rounded up about 18 h after settlement. The larva of this stage consists of a peripheral layer of pinacocytes and an inner cell mass (Fig. 12). About 36 h after settlement, choanocytes are differentiated in the inner cell mass and formation of the choanocyte chamber begins. Figure 13 shows a juvenile sponge about 72 h after settlement. It has a large choanocyte chamber, or gastral cavity, with an osculum. Its body wall is very thin and transparent, hence the characteristic triradiate spicules are clearly visible.

Pinacocytes. Soon after settlement, larvae lose their flagella and become a mass of dedifferentiated cells. The cells at the surface become flattened and cover the inner cell mass. Figure 14 shows a part of a settled larva consisting of a pinacoderm and an inner cell mass. It is apparent that both cell types have glutinous granules, thus showing their origin. The pinacocytes have already begun to flatten but are

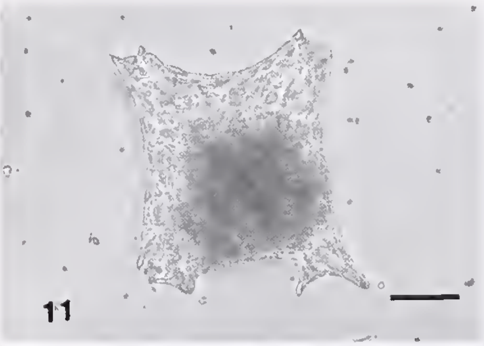

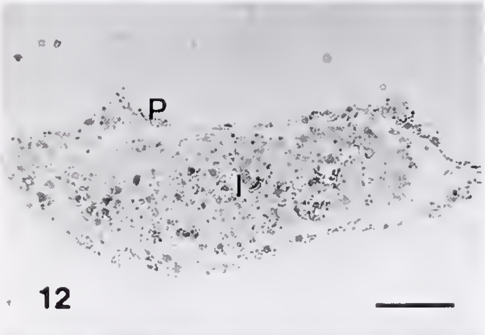

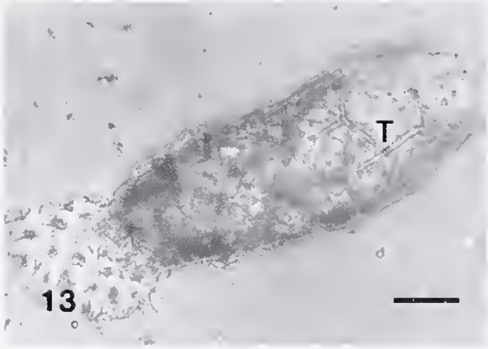

Figure 11. A live metamorphosing larva of *Leucosolenia laxa* about 18 h after settlement. Scale bar = 50 μm.

Figure 12. Section of the metamorphosing larva of *Leucosolenia laxa* about 18 h after settlement. I: inner cell mass, P: pinacoderm. Scale bar = 50 μm.

Figure 13. A live juvenile sponge of *Leucosolenia laxa* about 72 h after settlement. The basal end of this sponge spreads and attaches to the substratum. T: triradiate spicule. Scale bar = 50 μm.

not yet very thin. The cells of an inner cell mass are in the midst of dedifferentiation, and they usually have large autophagosomes in which we found glutinous granules (Fig. 15) and basal rootlets under digestion (Fig. 16). As metamorphosis progresses the pinacocytes become thinner except at their nuclear region; the gap or space between the pinacocytes becomes wider (Fig. 17); and a number of small holes open, piercing through the thin cytoplasm of the pinacocytes (Fig. 18).

Choanocytes. Choanocytes derive from the cells of an inner cell mass. Figure 17 shows immature choanocytes that have been arranged in a cell layer but as yet have no flagellum and no collar. They have glutinous granules and autophagosomes in the cytoplasm.

Figure 18 shows the choanoderm of a juvenile sponge. Choanocytes are flattened, but their central part projects into a gastral cavity. From the center of the projection one flagellum emerges, and from the margin of the projection a row of microvilli, or a collar, emerges. One collar consists of a row of 30–45 microvilli. The nucleolated nucleus, with scattered heterochromatin masses, is always located away from the center of the cell. In the cytoplasm are mitochondria and autophagosomes whose contents have been almost entirely digested.

Although the structure of the choanocyte flagellum is similar to that of larval flagellated cells, the flagellar basal apparatus is quite different. Figure 19 shows that the basal body of choanocytes lacks rootlets and a foot. A Golgi apparatus is located adjacent to the basal body, but perpendicular to it. On the cell membrane is a fuzzy coat encircled by a collar (Fig. 20).

Scleroblasts. Cells beneath a pinacoderm differentiate to scleroblasts in the mesohyl. Figure 21 shows a scleroblast with a large space that had been occupied by a spicule. The fine calcareous spicules, formed in the space surrounded by a membrane, were dissolved in the fixative. We found a small amount of spicule remnants in the space, but no axial filament. These cells have a nucleolated nucleus and glutinous granules in the cytoplasm.

Scleroblasts characteristically have multivesicular bodies. Figure 22 shows that the multivesicular body fuses with a membrane around a spicule and opens into a space for a spicule. The small vesicles of the multivesicular bodies probably contain calcium for spicule formation. Evidence that triradiates are formed by multiple cells is seen in Figure 22, where the spicule is surrounded by two (or more) cells. Although spicules are formed in a space surrounded by a membrane, finished spicules are surrounded by discontinuous cytoplasm or by spongin microfilaments only (Fig. 23).

Vacuolar cells and others. The mesohyl of metamorphosing larvae contains vacuolar cells (Fig. 24), but bottle cells and free cells in a central cavity are never found in the settled larvae. Spongin formation begins soon after the appearance of the mesohyl, about 24 h after settlement. The spongin microfilaments are scattered rather evenly in the mesohyl, but around the spicules they are concentrated.

Discussion

Cell lineages during metamorphosis

The coeloblastulae of *Leucosolenia laxa* consist of four kinds of cells: flagellated cells, bottle cells, vesicular cells, and free cells in a central cavity. Neither bottle cells nor vesicular cells have been described in the coeloblastulae of other calcinean sponges (Minchin, 1896; Borojevic, 1969). The flagellated cells are the principal cell type of the coe-

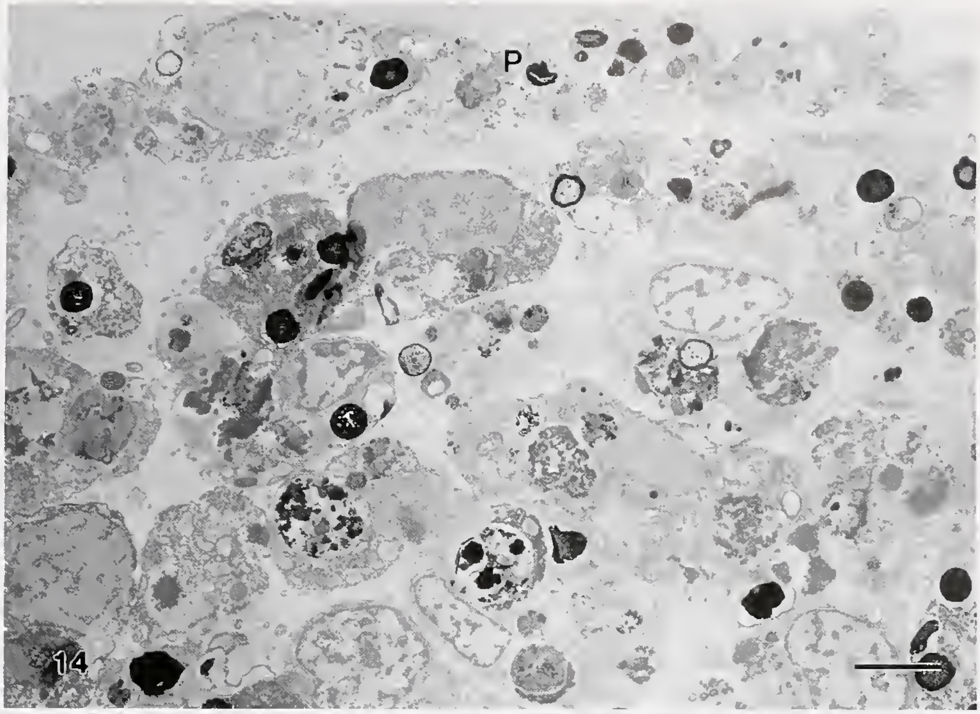

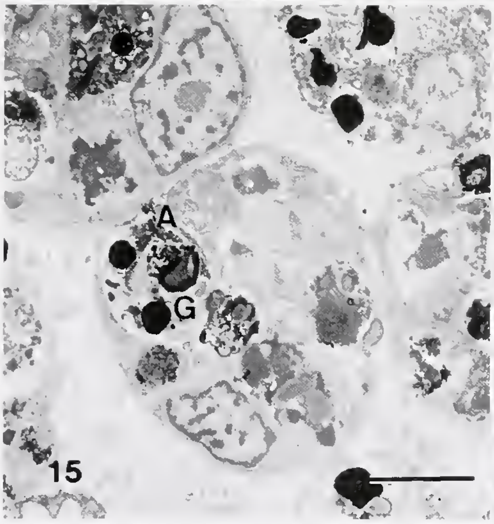

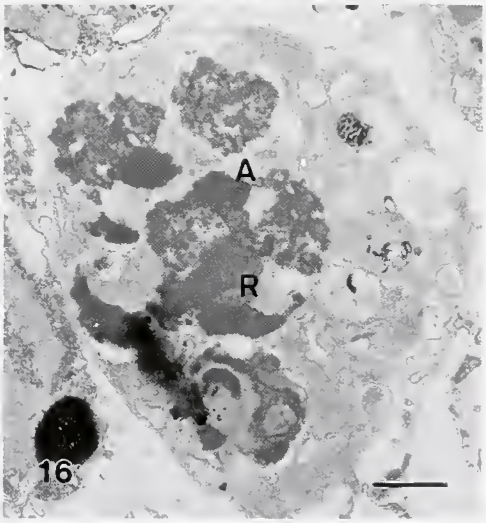

Figure 14. Section of the settled larva of *Leucosolenia laxa*, consisting of a pinacoderm (P) and an inner cell mass about 18 h after settlement. Scale bar = 2 μm.

Figure 15. Autophagosome (A) with glutinous granules (G) in the inner cell mass of the settled larva of *Leucosolenia laxa* about 18 h after settlement. Scale bar = 2 μm.

Figure 16. Autophagosome (A) with a degenerative rootlet (R) in the inner cell mass of the settled larva of *Leucosolenia laxa* about 18 h after settlement. Scale bar = 1 μm.

loblastulae; therefore, we thoroughly studied the fate of these cells during metamorphosis. Examination of a large number of electron micrographs revealed that the flagellated cells become the three principal cell types of juvenile sponges—that is, pinacocytes, scleroblasts, and choanocytes. This conclusion is supported by the fact that these three cell types contain glutinous granules, which only the flagellated cells have in the free-swimming larva. This fact shows clearly that the flagellated cells of the coeloblastulae hold multipotency, although they have been specialized for swimming. Experimental approaches in future research will indisputably demonstrate the developmental potency of the larval cells.

The flagellated cells of coeloblastulae pass through the intermediate stage of dedifferentiation in a settled larva before they differentiate to the cells of a juvenile sponge.

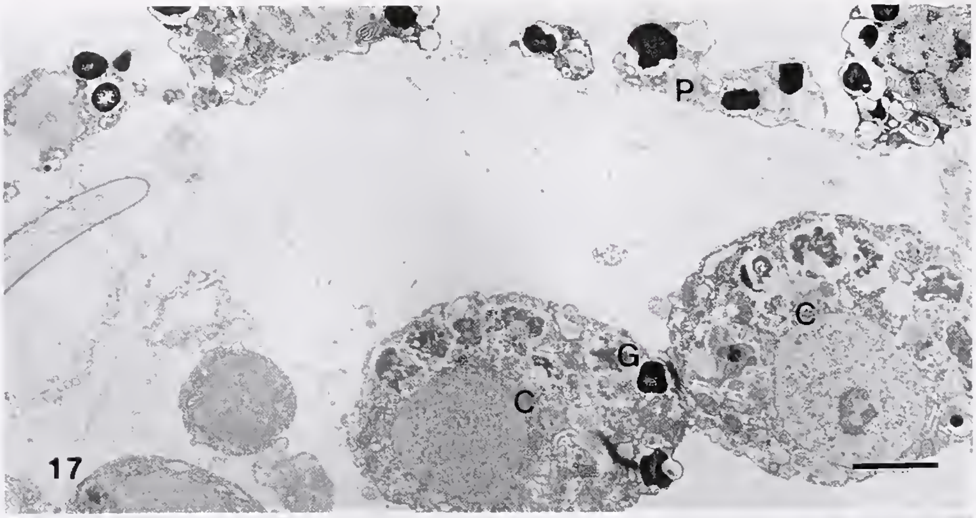

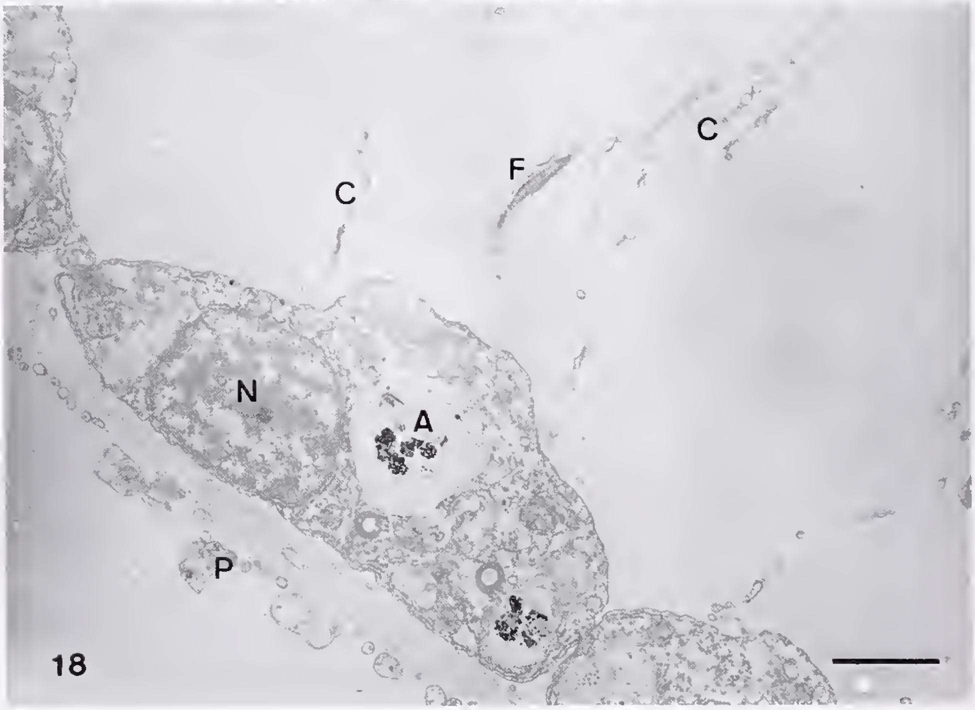

Figure 17. Immature choanocytes (C) of the juvenile sponge of *Leucosolenia laxa* about 36 h after settlement. G: glutinous granule, P: pinacoderm. Scale bar = 2 μm.

Figure 18. Choanoderm of the juvenile sponge of *Leucosolenia laxa* about 72 h after settlement. A: autophagosome, C: collar, F: flagellum of a choanocyte, N: nucleus, P: pinacoderm. Scale bar = 2 μm.

The flagellated cells are arranged in a pseudostratified layer in a swimming larva. This cell layer is not a true epithelium because—like similar layers in other sponges—it lacks a basal lamina (Gaino *et al.*, 1985; Woollacott and Pinto, 1995). One flagellum emerges from the flat outer surface of the cell. In most sponges, however, larval flagella emerge from a pit at an outer surface (Amano and Hori, 1992, 1994; Woollacott, 1993; Woollacott and Pinto, 1995). After settlement, the flagellated cells soon loose their flagellum and dedifferentiate. The dedifferentiation is apparently triggered by the settlement of the larva. Autophagosomes play a central role in the intracellular processes of dedifferentiation. These autophagosomes are different in origin and structure from the phagosome-like granules in the basal cytoplasm of the larval flagellated cells: the latter were probably formed to take in nutritive materials by phagocytosis during ovogenesis (Fell, 1969); the former are formed *de novo* after settlement and are usually larger than the latter. Glutinous granules, fibrous yolk granules, and basal rootlets in various stages of digestion are observed in the

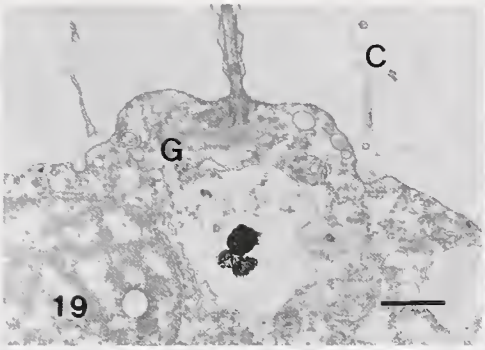

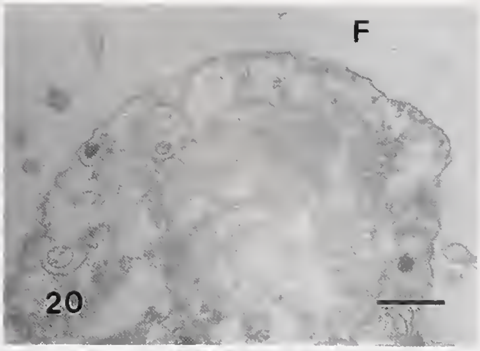

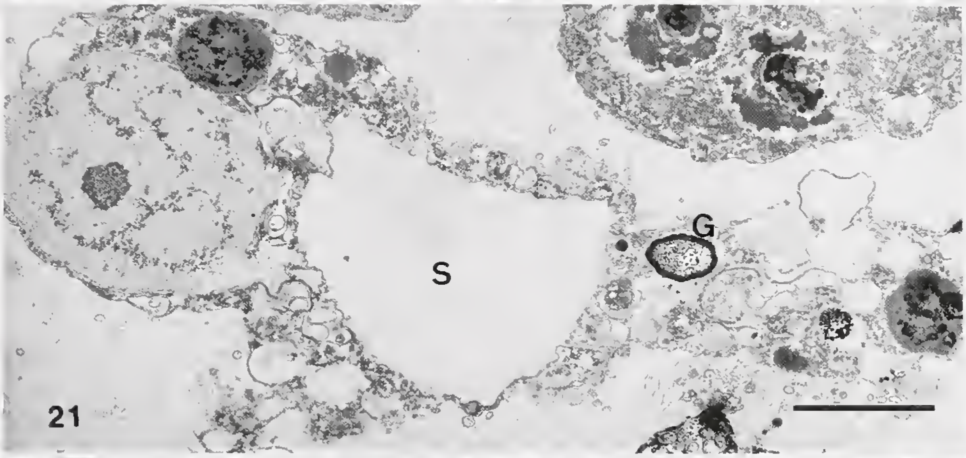

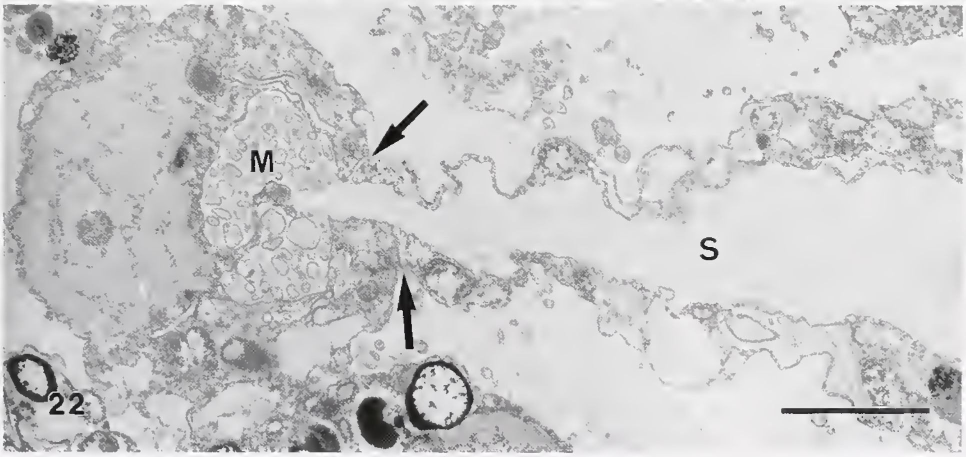

Figure 19. Basal apparatus of a choanocyte in the juvenile sponge of *Leucosolenia laxa* about 72 h after settlement. C: collar. G: Golgi apparatus. Scale bar = 1 μm.

Figure 20. Fuzzy coat (F) of a choanocyte in the juvenile sponge of *Leucosolenia laxa* about 72 h after settlement. Scale bar = 0.5 μm.

Figure 21. Scleroblast in the juvenile sponge of *Leucosolenia laxa* about 72 h after settlement. G: glutinous granule. S: space occupied by a triradiate spicule. Scale bar = 2 μm.

Figure 22. Two scleroblasts forming a triradiate spicule in the juvenile sponge of *Leucosolenia laxa* about 72 h after settlement. A multivesicular body (M) opens into the space occupied by a spicule (S). Arrow: cell junction between scleroblasts. Scale bar = 2 μm.

autophagosomes of the inner cell mass of settled larvae. The choanocytes of juvenile sponges contain autophagosomes whose contents have been almost entirely digested.

Bottle cells are described for the first time in this report. These large cells, like the cruciform cells of amphiblastulae (Duboscq and Tuzet, 1937; Amano and Hori, 1992), are located among the flagellated cells. The function of the bottle cells is not known; they apparently do not contribute to the development of the juvenile sponge and disappear during metamorphosis, as do the cruciform cells. Both cell

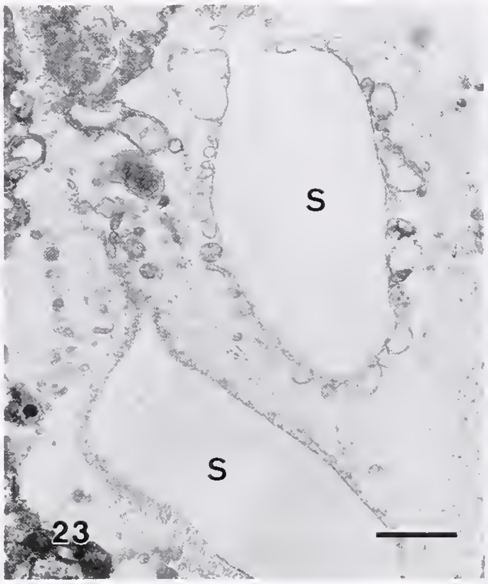

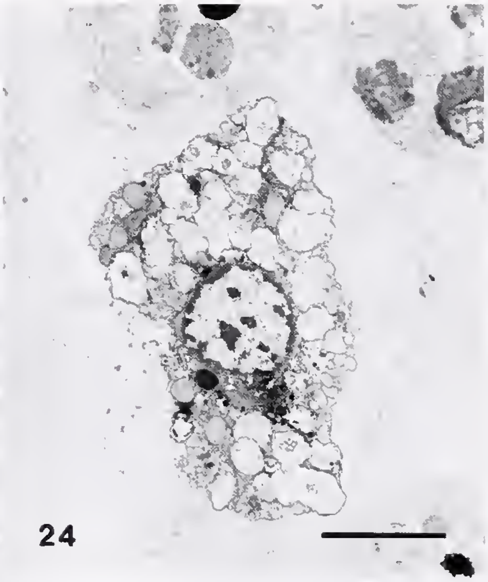

Figure 23. Spicules surrounded by spongin fibers and by discontinuous cytoplasm in the juvenile sponge of *Leucosolenia laxa* about 72 h after settlement. S: space occupied by a triradiate spicule. Scale bar = 1 μm.

Figure 24. A vacuolar cell in the mesohyl of the juvenile sponge of *Leucosolenia laxa* about 72 h after settlement. Scale bar = 2 μm.

types may have similar functions, but the bottle cells cannot be named cruciform cells because the former cells are not arranged in each quadrant in a horizontal plane. Vesicular cells in the coeloblastula are also described for the first time. Their function is not known, but we know that they participate in metamorphosis, because they are found in the mesohyl of juvenile sponges. Free cells in a central cavity are probably somatic cells derived from the mother sponge. Similar maternally derived nutritive cells are found in the larvae of other sponges (Warburton, 1961; Gallissian and Vacelet, 1992). These cells disappear during metamorphosis.

Juvenile sponge formation

After settlement, a coeloblastula becomes a mass of dedifferentiated cells on the substratum. The first cells to differentiate are pinacocytes, which are apparently formed from cells at the surface of the cell mass. The pinacocytes are flattened, except at their nuclear region. As a juvenile sponge becomes larger, the cytoplasm of the pinacocytes becomes thinner. We found no ostia in the juvenile sponge; however, after osculum formation, seawater can flow into the gastral cavity through the spaces between the cells and the small holes of the thin cytoplasm.

Scleroblasts are the next cells to differentiate in the cell mass settled on the substratum. Cells beneath the pinacoderm become scleroblasts. These cells form triradiates, a characteristic spicule of calcareous sponges, in the mesohyl of juvenile sponges. The scleroblasts always enclose a large space delimited by a membrane. This space had been occupied by a calcareous spicule that was dissolved in the fixative. Similarly, siliceous spicules are formed in a space surrounded by a membrane called the silicalemma (Simpson and Vaccaro, 1974). An axial filament is essential for siliceous spicule formation (Garrone, 1969; Cha *et al.*, 1999), but the calcareous triradiate is formed without the aid of an axial filament (Ilan *et al.*, 1966; Jones, 1967; Amano and Hori, 1993). Here—as in other calcareous spicules—no axial filament was found in the space formerly occupied by a spicule. The scleroblasts usually have a small number of multivesicular bodies. We showed that the multivesicular bodies fuse with the membrane around the space and open into it. The multivesicular bodies probably supply calcium and membrane components for spicule formation. Similarly, in the metamorphosis of amphiblastulae, a number of small vesicles open into the space for spicule formation (Amano and Hori, 1993). Scleroblasts that form siliceous spicules also have a number of vesicles in the cytoplasm (Simpson and Vaccaro, 1974). Although the spicules are formed within the scleroblasts, the finished spicules free of cells are usually covered by spongin filaments (Jones, 1967; Garrone, 1985).

Lastly, the cells of an inner cell mass differentiate to choanocytes. In the inner cell mass, a space develops *de novo* among the cells and becomes larger as metamorphosis progresses. A layer of immature choanocytes, not yet possessing a flagellum or collar, encircles the large space, which is a gastral cavity. The gastral cavity is different in origin and structure from the central cavity of coeloblastulae, which is a retained blastocoel (Borojevic, 1969). As the gastral cavity develops, the choanocytes are flattened except at their thick central region. Then one flagellum emerges from the center of the central region and a collar of microvilli develops around the thick central region. The basal body of the flagellum lacks rootlets and a foot; other sponges also lack these structures (Amano and Hori, 1993, 1996). On the cell membrane we found a fuzzy coat encircled by a collar; a similar fuzzy coat is found in demosponges (Bergquist and Green, 1977; Lethias *et al.*, 1983). About 72 h after settlement, an osculum opens at the uppermost part of the metamorph and water flow begins. Thus an asconoid juvenile sponge, an olynthus, is formed.

Coeloblastulae of other calcinean sponges

While the coeloblastulae of *L. laxa* are swimming, the flagellated cells do not migrate into a central cavity and the cells do not lose their flagellum. When the larvae adhere to the substratum for settlement, their flagella still continue active beating. In the coeloblastulae of other calcinean sponges, however, the larval flagellated cells have been reported to migrate into a central cavity while the larvae are swimming (Minchin, 1896; Borojevic, 1969). The reason for this discrepancy is not known. Time to initiate the dedifferentiation of larval flagellated cells may differ among calcinean sponges. A more likely explanation is that bottle cells and vesicular cells were erroneously judged to be the flagellated cells under migration into the central cavity. We showed that the bottle cells and vesicular cells of *L. laxa* protrude extensively into the central cavity. Indeed, Borojevic (1969) noted that larval cells migrate into the blastocoel firstly from the posterior region of the coeloblastula, where vesicular cells are concentrated. If the resolution of larval images is not high enough, it seems to be difficult to know which is the case.

In the calcinean sponge *Clathrina reticulum*, Borojevic (1969) described pigment granules in larval flagellated cells; however, these are apparently glutinous granules. Although the granules in question are indeed very electrondense, they cannot be pigment granules, because coeloblastulae are colorless. We showed that the granules can be released from the cells and that their content is a sticky substance, so they may participate in larval settlement. We know that some of them are, however, digested intracellularly, because they were found in autophagosomes in the inner cell mass of settled larvae.

Fates of larval flagellated cells

After settlement, flagella and basal apparatus meet different fates of degeneration depending on the types of larvae. In the parenchymellae of demosponges, flagella are withdrawn into the cell and decomposed in the cytoplasm after they are severed at the transitional region between a basal body and the proximal end of an axoneme (Boury-Esnault, 1976; Amano and Hori, 1996). In the coeloblastulae and amphiblastulae of calcareous sponges, however, the axonemes are probably shed soon after settlement (Amano and Hori, 1993). The basal bodies and rootlets, severed from the axoneme, are decomposed in the cytoplasm in the amphiblastulae and parenchymellae (Amano and Hori, 1993, 1996). In the coeloblastula of *L. laxa*, however, they are digested in autophagosomes.

The developmental potency of larval flagellated cells differs greatly among the types of sponge larvae. In the coeloblastula of *L. laxa*, the flagellated cells apparently become all three principal cell types of juvenile sponges. In amphiblastulae, another larval type of calcareous sponges, the flagellated cells become scleroblasts and choanocytes but not pinacocytes (Amano and Hori, 1993). The pinacocytes are derived from larval granular cells. In the parenchymellae of demosponges, the flagellated cells are not multipotential and become only choanocytes (Borojevic, 1966; Amano and Hori, 1996). The parenchymellae usually consist of many more cell types than do coeloblastulae or amphiblastulae, and in such complex larvae, juvenile sponge cells are derived from distinctive larval cells. During the geologic eras after the Vendian age, each type of sponge larva evolved to metamorphose in different ways (Li *et al.*, 1998).

Acknowledgments

We thank Mr. S. Tamura and Mr. M. Washio of the Asamushi Marine Biological Station for help in collecting sponges.

Literature Cited

Amano, S. 1986. Larval release in response to a light signal by the intertidal sponge *Halichondria panicea*. *Biol. Bull.* **171:** 371–378.

Amano, S. 1988. Morning release of larvae controlled by the light in an intertidal sponge, *Callyspongia ramosa*. *Biol. Bull.* **175:** 181–184.

Amano, S., and I. Hori. 1992. Metamorphosis of calcareous sponges I. Ultrastructure of free-swimming larvae. *Invertebr. Reprod. Dev.* **21:** 81–90.

Amano, S., and I. Hori. 1993. Metamorphosis of calcareous sponges II. Cell rearrangement and differentiation in metamorphosis. *Invertebr. Reprod. Dev.* **24:** 13–26.

Amano, S., and I. Hori. 1994. Metamorphosis of a demosponge I. Cells and structure of swimming larva. *Invertebr. Reprod. Dev.* **25:** 193–204.

Amano, S., and I. Hori. 1996. Transdifferentiation of larval flagellated cells to choanocytes in the metamorphosis of the demosponge *Haliclona permollis*. *Biol. Bull.* **190:** 161–172.

Bergquist, P. R., and K. Glasgow. 1986. Developmental potential of ciliated cells of ceractinomorph sponge larvae. *Exp. Biol.* **45:** 111–122.

Bergquist, P. R., and C. R. Green. 1977. An ultrastructural study of settlement and metamorphosis in sponge larvae. *Cah. Biol. Mar.* **18:** 289–302.

Borojevic, R. 1966. Étude expérimentale de la différenciation des cellules de l'éponge au cours de son développement. *Dev. Biol.* **14:** 130–154.

Borojevic, R. 1969. Étude du développement et de la différenciation cellulaire d'éponges calcaires calcinéennes (generes *Clathrina* et *Ascandra*). *Ann. Embryol. Morphog.* **2:** 15–36.

Borojevic, R., and C. Levi. 1965. Morphogenèse expérimentale d'une éponge à partir de cellules de la larve nageante dissociée. *Z. Zellforsch. Mikrosk. Anat.* **68:** 57–69.

Boury-Esnault, N. 1976. Ultrastructure de la larve parenchymella d'*Hamigera hamigera* (Schmidt) (Démosponge, Poecilosclerida). Origine des cellules grises. *Cah. Biol. Mar.* **17:** 9–20.

Brusca, R. C., and G. J. Brusca. 1990. *Invertebrates.* Sinauer Associates, Sunderland, MA.

Cha, J. N., K. Shimizu, Y. Zhou, S. C. Christiansen, B. F. Chmelka, G. D. Stucky, and D. E. Morse. 1999. Silicatein filaments and subunits from a marine sponge direct the polymerization of silica and silicones *in vitro. Proc. Natl. Acad. Sci.* **96:** 361–365.

Duboscq, O., and O. Tuzet. 1937. L'ovogénèse, la fécondation et les premiers stades du développement des eponges calcaires. *Arch. Zool. Exp. Gen.* **79:** 157–316.

Fell, P. E. 1969. The involvement of nurse cells in oogenesis and embryonic development in the marine sponge, *Haliclona ecbasis. J. Morphol.* **127:** 133–150.

Gaino, E., B. Burlando, M. A. Sabatini, and P. Buffa. 1985. Cytoskeleton and morphology of dissociated sponge cells. A whole-mount and scanning electron microscopic study. *Eur. J. Cell Biol.* **39:** 328–332.

Gallissian, M.-F., and J. Vacelet. 1992. Ultrastructure of the oocyte and embryo of the calcified sponge, *Petrobiona massiliana* (Porifera, Calcarea). *Zoomorphology* **112:** 133–141.

Garrone, R. 1969. Collagène, spongine et squelette Minéral chez l'éponge *Haliclona rosea* (O.S.) (Démosponge, Haploscléride). *J. Microsc.* **8:** 581–598.

Garrone, R. 1985. The collagen of the Porifera. Pp. 157–175 in *Biology of Invertebrate and Lower Vertebrate Collagens*, A. Bairati and R. Garrone, eds. Plenum Press, New York.

Ilan, M., J. Aizenberg, and O. Gilor. 1966. Dynamics and growth patterns of calcareous sponge spicules. *Proc. R. Soc. Lond. B* **263:** 133–139.

Jones, W. C. 1967. Sheath and axial filament of calcareous sponge spicules. *Nature* **214:** 365–368.

Kaye, H. R., and H. M. Reiswig. 1991. Sexual reproduction in four Caribbean commercial sponges. III. Larval behaviour, settlement and metamorphosis. *Invertebr. Reprod. Dev.* **19:** 25–35.

Lethias, C., R. Garrone, and M. Mazzorana. 1983. Fine structure of sponge cell membranes: comparative study with freeze-fracture and conventional thin section methods. *Tissue Cell* **15:** 523–535.

Li, C.-W., J.-Y. Chen, and T.-E. Hua. 1998. Precambrian sponges with cellular structures. *Science* **279:** 879–882.

Maldonado, M., and C. M. Young. 1996. Effects of physical factors on larval behavior, settlement and recruitment of four tropical demosponges. *Mar. Ecol. Prog. Ser.* **138:** 169–180.

Minchin, M. A. 1896. Note on the larva and the postlarval development of *Leucosolenia variabilis,* H. sp., with remarks on the development of other Asconidae. *Proc. R. Soc. Lond.* **60:** 42–52.

Misevic, G. N., V. Schlup, and M. M. Burger. 1990. Larval metamorphosis of *Microciona prolifera:* evidence against the reversal of layers. Pp. 182–187 in *New Perspectives in Sponge Biology*, K. Rützler, ed. Smithonian Institution Press, Washington, DC.

Müller, W. E. G. 1997. Origin of metazoan adhesion molecules and adhesion receptors as deduced from cDNA analysis in the marine sponge *Geodia cydonium:* a review. *Cell Tissue Res.* **289:** 383–395.

Simpson, T. L. 1984. *The Cell Biology of Sponges.* Springer-Verlag, New York.

Simpson, T. L., and C. A. Vaccaro. 1974. An ultrastructural study of silica deposition in the freshwater sponge *Spongilla lacustris. J. Ultrastruct. Res.* **47:** 296–309.

Spurr, A. R. 1969. A low-viscosity epoxy resin embedding medium for electron microscopy. *J. Ultrastruct. Res.* **26:** 31–43.

Tuzet, O. 1947. L'ovogenése et la fécondation de l'éponge calcaire *Leucosolenia (Clathrina) coriacea* Mont. et de l'éponge siliceuse *Reniera elegans* Bow. *Arch. Zool. Exp. Gen.* **85:** 127–148.

Warburton, F. E. 1961. Inclusion of parental somatic cells in sponge larvae. *Nature* **191:** 1317.

Woollacott, R. M. 1993. Structure and swimming behavior of the larva of *Haliclona tubifera* (Porifera: Demospongiae). *J. Morphol.* **218:** 301–321.

Woollacott, R. M., and R. L. Pinto. 1995. Flagellar basal apparatus and its utility in phylogenetic analysis of the Porifera. *J. Morphol.* **226:** 247–265.

Reference: *Biol. Bull.* **200:** 33–50. (February 2001)

Interspecific Relationships Between Egg Size and the Level of Parental Investment per Offspring in Echinoderms

L. R. McEDWARD* AND K. H. MORGAN

Department of Zoology, University of Florida, Gainesville, Florida 32611

Abstract. The relationship between the size of an egg and its energy content was analyzed using published data for 47 species of echinoderms. Scaling relationships were evaluated for all species, as well as for subsets of the species, based on mode of development. Regressions were calculated using linear, power function, full allometric, and second-order polynomial models. The full allometric model is preferred because it is relatively simple and the most general. Among these species of echinoderms, larger eggs contain more energy. Egg energy content scales isometrically across a wide range of egg sizes both among and within different modes of development. The only exception is among species with feeding larval development, where there does not seem to be a clear scaling relationship. In most cases, the regressions were statistically significant and explained a very large proportion of the variance in energy content. However, there were wide confidence intervals around the estimated regression parameters. In all cases, the predictive power of the regression was poor, requiring large differences in egg size to yield significantly different predictions of energy content. Consequently, egg size is of limited value for the quantitative prediction of egg energy content and should be used with caution in life-history studies.

Introduction

A major goal of ecological research is to explain the evolution of life histories, *i.e.*, how natural selection modifies reproduction and development to yield the patterns that are observed in nature. Quantitative, theoretical models have been the primary tool used to explore hypotheses on the effects of selection on life-history traits. As a result, theoretical developments became fairly sophisticated and are now considerably ahead of the empirical database. In addition to the emphasis on modeling, the difficulty of obtaining the appropriate data is also responsible for the discrepancy between theory and data. Pianka (1976, p. 782) argued that "A great deal of ingenuity and effort will be required to design and execute research to test this elegant body of theory." Beyond that, Stearns (1977) contended that there might well be fundamental limitations on the kinds of information that ecologists can obtain about life-history evolution.

The relationship between parental investment per offspring and offspring fitness is one of the central tenets of life-history theory that has been particularly difficult to evaluate empirically. Given that the total resources that the parent devotes to reproduction are limited, there should be an inverse relationship between the investment made in each offspring and the number of offspring that can be produced. Further, it has been assumed that as parents allocate more material and energy to each individual offspring, the fitness of the offspring increases because of an increase in the quality of the young (*e.g.*, Smith and Fretwell, 1974). This is a seemingly straightforward and intuitively reasonable assumption. Why has it been so difficult to test empirically?

An important obstacle to the critical evaluation of the relationship between parental investment and offspring fitness is the difficulty in defining parental investment in precise and measurable terms. What exactly are the resources that a parent devotes to its offspring? How can we effectively measure the variation in the level of investment that exists among offspring of a given parent or among the offspring of different parents? Parental care is common

Received 27 December 1999; accepted 27 October 2000.

*To whom correspondence should be addressed. E-mail: mcedward@zoo.ufl.edu

among animals, and it is extremely difficult to identify components of care that represent quantifiable resources. Time and energy budgets of parents are particularly difficult to measure precisely and even more difficult to quantify in terms of the actual resources that were spent on the offspring.

The problem of parental care can be avoided by studying free-spawning benthic marine organisms. Although some marine organisms do provide protection and care for their young, a very large number are free-spawners, and do not. The latter simply release gametes into the surrounding seawater; fertilization and development occur independently of the parents. In this case, parental investment can reasonably be defined as the material and energy contained in the egg, because that is the only contribution that the mother makes to the young. The paternal contribution consists of the sperm pronucleus and functional centrioles, but this is quantitatively insignificant relative to the contents of the egg.

Given the suitability of free-spawning organisms for measurement and analysis of parental investment, have marine ecologists succeeded in evaluating the relationship between investment and offspring fitness? Unfortunately, no. We have been remarkably unsuccessful in our attempts to acquire data necessary to test and further develop this aspect of life-history theory. This is in spite of a tremendous increase in the interest and research effort in "larval ecology" in recent years.

The failure is due in large part to the fact that marine ecologists have not measured parental investment (as egg energy content) directly; rather they have relied on measurements of egg size as an index of investment. In fact, this is a central assumption of the theory that underlies most of the quantitative models of life-history evolution in marine benthic invertebrates (*e.g.*, Vance, 1973; Christensen and Fenchel, 1979; Pechenik, 1979; Perron and Carrier, 1981; Grant, 1983; Emlet *et al.*, 1987; Strathmann, 1985; Havenhand, 1995; Levitan, 1996; McEdward, 1997). These models attempt to describe the effects of natural selection on egg size, given some reasonable assumptions about the reproductive and developmental correlates of differing parental investment per offspring. "Egg size" is explicitly defined in energetic, rather than geometric, units in these models (*e.g.*, Vance, 1973), to indicate that the quantity of theoretical interest is parental investment per offspring. Unfortunately, use of the term "size" has contributed to the mistaken perception that either geometric size is the primary object of the models or egg dimensions provide a reliable index of energetic size. Nonetheless, given constant reproductive effort, there is an important trade-off between fecundity and energy content per egg. The logical extremes are the production of very many "small" eggs with minimal material or production of very few "large" yolky eggs. The models then predict the direction of evolution of egg size (and related life-history traits) under different environmental conditions.

There are many reasons why it has been convenient, and in fact necessary, to assume that egg size (*i.e.*, egg dimensions) reliably reflects egg energy content. First, it is biologically reasonable that large eggs contain more material than small eggs. Egg sizes span a considerable range in many taxa. For example, in free-spawning asteroid echinoderms (starfish), the egg size range is 2000-fold, from $5\text{–}7 \times 10^{-4}$ μl ($\approx$100 μm diameter; *e.g., Asterias vulgaris, Astropecten irregularis, Ophidiaster guildingii, Pentaceraster mammilatus;* Emlet *et al.*, 1987) to about 0.9–1.0 μl (1200 μm diameter; *Perknaster fuscus, Henricia* sp. *(leviuscula?), Pteraster tesselatus*; McClintock and Pearse, 1986; McEdward and Coulter, 1987; McEdward and Chia, 1991). It is clear that very large eggs will contain more energy than very small eggs, regardless of differences in biochemical composition. Given the wide range of egg sizes, obvious questions arise concerning the existence of discernible patterns within this diversity, especially patterns that might reflect taxonomy, adult ecology, biogeography, or mode of development.

Second, for more than 50 years, descriptive and comparative studies have provided much information on what life-history patterns exist, what traits characterize each pattern, and in which taxa and in which environments these patterns occur (reviewed by Levin and Bridges, 1995). There exists a large body of literature showing that egg size is strikingly correlated with important life-history traits such as fecundity, duration of the larval period, larval size, and mode of larval nutrition (see Levin and Bridges, 1995). These studies provide the empirical database from which the theoretical models were developed and within which their assumptions and predictions have been evaluated. Since biologists routinely measure and report egg size, but have not measured egg energy content, the assumption that egg size reflects the level of parental investment is necessary for the integration of life-history theory with the information on reproduction and development of marine invertebrates.

Third, egg sizes (*i.e.*, dimensions) are easily measured, requiring relatively few eggs and no specialized skills or equipment. In contrast, direct measurements of energy content traditionally involve large numbers of eggs and specialized equipment and procedures (*e.g.*, biochemical analyses or bomb calorimetry). However, even when measurements of energy content have been feasible, there remains a serious drawback. Measurement of energy content destroys the egg, making it impossible to know both the level of parental investment and the consequence of that level of investment for the success of the offspring. This is a fundamental limitation on our ability to evaluate the relationship between parental investment and offspring fitness in all groups of organisms. In contrast, measurement of egg size does not harm the egg, but it also does not measure the quantity of theoretical interest. We must, at the very least, assume that eggs of the same size contain the same amount of energy and materials, if we are to relate parental investment to offspring success using correlations with egg size.

From the reasons given above, it is understandable why egg size has been used as an index of the level of parental investment per offspring. Egg size can be measured simply and nondestructively, it is correlated with many of the life-history features that characterize the patterns we want to explain, and it is reasonable to assume that larger eggs contain more energy and material than small eggs. But, the question remains, is it a valid assumption? Does the measurement of egg dimensions provide a reliable prediction of egg energy content?

Background

Only a few studies have analyzed the relationship between egg size and energy content. Nearly all of the relevant data are from echinoderms, and this is the only group of marine invertebrates for which there is information on egg size, energy content, biochemical composition, and relationships between size and content at different intraspecific levels. In addition, echinoderms exhibit several distinct patterns of development: planktotrophy, pelagic development with feeding larvae; pelagic lecithotrophy, pelagic development with nonfeeding larvae; and brooding, benthic development with nonfeeding offspring that are associated with the parent until they become juveniles.

Strathmann and Vedder (1977) reported that organic matter content was significantly and positively correlated with egg volume among eight species of echinoderms, all with relatively small eggs ($\approx 2 \times 10^{-4}$–36×10^{-4} μl volume, $\approx$80–200 μm diameter) and planktotrophic larval development. Egg content was not proportional to egg volume; rather it was proportional to a fractional power (0.753) of volume. A regression of organic matter concentration (content per unit volume) against egg size had a significant, but negative slope (see Strathmann and Vedder, 1977; fig. 2). They concluded that their results confirmed the assumption that larger eggs contain more organic matter, but they could not explain why smaller eggs had more concentrated organic matter than larger eggs.

Soon after, Turner and Lawrence (1979) examined the biochemical composition of eggs from seven species of echinoderms in order to address a different, but related, question. Are eggs of different sizes and from different species qualitatively alike? They examined species with planktotrophic, pelagic lecithotrophic, and brooding modes of development. Egg sizes ranged from $\approx 2 \times 10^{-4}$–2.4×10^{-1} μl ($\approx$80–750 μm). They reported that both egg size and percentage biochemical composition (protein, lipid, carbohydrate) were variable among species. There was not a relationship between volume and composition. In spite of the variability in size and composition, organic matter content generally increased with increasing egg volume. In addition, they found considerable intraspecific variation in size and composition, especially among individuals from different geographic regions and in different years.

These studies provided empirical support for the assumption that size reflects the organic content of the egg. No one had expected a perfect correspondence between content and size, so the lack of direct proportionality or the variability in composition was of little concern. At the least, there seemed to be a reliable rank correlation between size and energy content that would allow measurements of egg size to be used to infer differences in the level of parental investment among species.

Subsequent research did little to alter the emerging picture of a species trend in egg size and energy content. Lawrence *et al.* (1984) and McClintock and Pearse (1986) reported sizes, biochemical composition (protein, lipid, carbohydrate), and energy content of eggs from nine species of echinoderms. All of the species were from Antarctic or sub-Antarctic regions, had very large eggs ($\approx$1–23 μl volume, $\approx$1200–3500 μm diameter), and all, except for one species, were brooders. McEdward and Carson (1987), McEdward and Coulter (1987), and McEdward and Chia (1991) reported egg size and energy content from nine species of echinoderms with large yolky eggs ($\approx$0.06–1 μl volume, 500–1250 mm diameter) and pelagic lecithotrophic development. Collectively, these species had eggs with very high energy content, and the data confirmed the general trend relating egg size and content.

Several other studies provided new data on egg sizes and energy content or biochemical composition but did not analyze the relationship across species. Jaeckle (1995) reviewed the literature on echinoderm eggs and analyzed the scaling relationship across all species by using linear regression on log-transformed egg volume and log-transformed content (either dry organic weight [DOW] or energy content [*J*]). The striking result from Jaeckle's analysis was that in spite of methodological differences among studies or different measures of egg content (DOW or J), egg content scaled very nearly in proportion to egg volume (scaling exponent 1.06–1.07 ± 0.05) across the entire range of egg sizes, taxa (classes), and modes of development.

Studies by McEdward and Carson (1987) and McEdward and Coulter (1987) focused on the intraspecific relationship between egg size and energy content. They demonstrated that within species, even within the spawns of individual females, there was considerable variation in size and content. Although statistically significant correlations were found, a very large fraction (61%–88%) of the variation in egg energy content was not explained by the relationship with egg size. Confidence belts were used to evaluate the predictive power of the regression of egg energy content on egg volume (see explanation below). Surprisingly, in most cases, egg size could not be used reliably to predict content.

It is now clear that in general, and on some scales, larger eggs contain more energy and material than small eggs. But the question remains: do egg dimensions provide a reliable and useful prediction of egg energy content? In this paper, we will present an analysis of the relationship between egg volume and egg energy content among species of echinoderms. Our objectives are to identify patterns (scaling relationships) and to evaluate the usefulness of egg size as a predictor of the level of egg provisioning. What is the scaling relationship between egg volume and energy content across species and developmental modes? What is the scaling relationship within developmental modes? What statistical models should be used to describe scaling relationships, and how should those models be evaluated? What is the predictive power of these relationships?

Materials and Methods

Sources of data

To evaluate the relationship between egg size and energy content in echinoderms, we analyzed data obtained from the literature on 47 species, including 22 asteroids, 1 crinoid, 20 echinoids, and 4 holothuroids. Of these, 9 species brood their young, 16 have pelagic nonfeeding development, 21 have planktotrophic larvae, and 1 has larvae that are facultatively planktotrophic. A complete list of the species, with egg volume, egg energy content, class, developmental mode, and literature source, is given in Table 1.

Various authors used different methods to measure egg size and content and reported the results in a variety of units. To facilitate comparison among species from different studies, all of these data have been converted to a standard format and units. Egg volume is reported as microliters (μl) and energy content is given in units of ($J \cdot egg^{-1}$). Volumes were calculated from diameters (d_1, d_2, d_3) using Eq. 1.

$$V = \frac{\pi}{6} d_1 d_2 d_3 \tag{1}$$

In cases where original data on egg size and content for a given species were obtained and reported independently in more than one study, we calculated the arithmetic mean of the published values and reported a single (overall mean) value for the species. Data for egg energy content were incomplete in some studies because the carbohydrate fraction was not reported (*e.g.*, Shilling and Manahan, 1994; George *et al.*, 1997; see Table 1). We calculated the average percentage of carbohydrate (3.54%) for all species in which lipid, protein, and carbohydrate were measured. This average value was used to estimate the carbohydrate fraction for all species in which only protein and lipid had been reported. This calculation made the estimates of total energy more consistent across species and studies; however, because the fraction of carbohydrate is very low, this had a negligible effect on total energy content.

After correcting for missing data on the carbohydrate fraction, we calculated the average "remainder" fraction for all species in which protein, lipid, carbohydrate, and dry organic weight were reported or could be calculated or extracted from figures. The remainder fraction is the difference between the summed biochemical components (protein, lipid, and carbohydrate) and total dry organic (ash-free) weight (DOW). Lawrence *et al.* (1984) and McClintock and Pearse (1986) reported the remainder as an insoluble protein fraction. In other cases (*e.g.*, Turner and Lawrence, 1979; Shilling and Manahan, 1994), the remainder fraction was not reported, but we could calculate it as the difference between DOW and the sum of protein, lipid, and carbohydrate. Turner and Lawrence (1979) did not report specific values for DOW, but, they plotted DOW and summed biochemical fractions in their figure 3. We extracted values from a scanned image of their plot using the Experimental Data Analyst package in Mathematica (version 4; Wolfram Research, Inc.) Using the calculated average % remainder fraction, we then estimated the remainder fraction (R, $\mu g \cdot egg^{-1}$) for those cases where biochemical fractions were reported but DOW was not (George *et al.*, 1997) using Eq. 2, where P, L, C are the protein, lipid, and carbohydrate fractions ($\mu g \cdot egg^{-1}$) and r is the average % (of DOW) remainder fraction. The quotient represents the estimated DOW, including the remainder.

$$R = \frac{\Sigma P, L, C}{1 - r}(r) \tag{2}$$

The remainder fraction has been assumed to be composed of insoluble protein (2.40×10^{-2} J $\cdot \mu g^{-1}$) or a uniform mixture of protein, lipid, and carbohydrate (2.70×10^{-2} J $\cdot \mu g^{-1}$) by different authors. We calculated total energy content using each of these assumptions, but because the total energy values were so similar, we report only the results from calculation based on the latter assumption. Studies that measured energy content using the dichromate oxidation method were not adjusted for a remainder fraction because all organic material is oxidized and measured in that method. It does not rely on summing separately measured components. No adjustment was made to results from the dichromate oxidation studies compared to results from measurements of individual biochemical fractions. Where both methods were used on the same species (*e.g.*, *Arbacia punctulata*), independently by different authors, the results are remarkably consistent (summed biochemical fractions = 1.416 $J \cdot egg^{-1}$; summed biochemical fractions = 1.285 $J \cdot egg^{-1}$; dichromate oxidation = 1.254 $J \cdot egg^{-1}$). Furthermore, Jaeckle's (1995) analyses explicitly evaluated the scaling relationships as a function of the methods of

Table I

Egg volume (μl), egg energy content ($J\ egg^{-1}$), mode of development (P = planktotrophic; L = pelagic lecithotrophic; B = brooded lecithotrophic), and taxonomic class (A = Asteroidea; C = Crinoidea; E = Echinoidea; H = Holothuroidea) for all 47 species of echinoderms

Species	Volume	Energy	Dev	Class	Reference
Arbacia punctulata	0.00022	0.00132*	P	E	Strathmann and Vedder, 1977; Turner and Lawrence, 1979[r]; George, Young, and Fenaus, 1997[cr]
Arbacia lixula	0.00024	0.00281*	P	E	George, Young, and Fenaux, 1997[cr]
Strongylocentrotus purpuratus	0.00027	0.00165	P	E	Strathmann and Vedder, 1977
Paracentrotus lividus	0.00041	0.00284*	P	E	George, Young, and Fenaux, 1997[cr]
Aspidodiadema jacobyi	0.00049	0.00295*	P	E	George, Young, and Fenaux, 1997[cr]
Lytechinus variegatus	0.00061	0.00528*	P	E	Turner and Lawrence, 1979[r]
Echinometra lucunter	0.00063	0.00224*	P	E	George, Young, and Fenaux, 1997[cr]
Stylocidaris lineata	0.00070	0.00317*	P	E	George, Young, and Fenaux, 1997[cr]
Coelopleurus floridanus	0.00080	0.00784*	P	E	George, Young, and Fenaux, 1997[cr]
Dendraster excentricus	0.00090	0.00328	P	E	Strathmann and Vedder, 1977
Asterias forbesi	0.00124	0.00796*	P	A	Turner and Lawrence, 1979[r]
Archaeopneustes histrix	0.00129	0.00654*	P	E	George, Young, and Fenaux, 1997[cr]
Strongylocentrotus franciscanus	0.00144	0.00577	P	E	Strathmann and Vedder, 1977
Pisaster ochraceus	0.00195	0.00783	P	A	Strathmann and Vedder, 1977
Strongylocentrotus droebachiensis	0.00206	0.01218*	P	E	Strathmann and Vedder, 1977; Turner and Lawrence, 1979[r]
Strongylocentrotus pallidus	0.00235	0.00904	P	E	Strathmann and Vedder, 1977
Luidia clathrata	0.00245	0.01986*	P	A	Turner and Lawrence, 1979[r]
Odontaster validus	0.00257	0.01955*	P	A	Shilling and Manahan, 1994[c]
Parastichopus californicus	0.00359	0.00951	P	H	Strathmann and Vedder, 1977
Encope aberrans	0.00359	0.00401	P	E	Herrera, McWeeney, and McEdward, 1996
Encope michelini	0.00510	0.04639*	P	E	George, Young, and Fenaux, 1997[cr]
Florometra serratissima	0.00742	0.04555	L	C	McEdward, Carson, and Chia, 1988
Clypeaster rosaceus	0.01149	0.02060	P/L	E	Emlet, 1986
Cucumaria miniata	0.06398	0.82539	L	H	McEdward and Chia, 1991
Acodontaster hodgsoni	0.08711	0.97715*	L	A	Shilling and Manahan, 1994[c]
Psolus chitinoides	0.09828	1.04957	L	H	McEdward and Chia, 1991
Echinaster sp. 1	0.19912	2.88073*	L	A	Turner and Lawrence, 1979[r]
Echinaster sp. 2	0.23916	4.69026*	L	A	Turner and Lawrence, 1979[r]
Solaster endeca	0.28510	3.55631	L	A	McEdward and Chia, 1991
Echinaster spinulosus	0.31000	3.51600*	L	A	George, Young, and Fenaux, 1997[cr]
Solaster dawsoni	0.37250	4.00467	L	A	McEdward and Chia, 1991
Solaster stimpsoni	0.40600	4.52640	L	A	McEdward and Carson, 1987
Psilaster charcoti	0.44892	2.57138*	L	A	Shilling and Manahan, 1994[c]
Mediaster aequalis	0.45990	5.78792	L	A	McEdward and Chia, 1991
Cucumaria curata	0.52360	4.58365*	B	H	Turner and Rutherford, 1976[r]
Pteraster tesselatus	0.87000	8.26919	L	A	McEdward and Coulter, 1987, McEdward and Chia, 1991
Perknaster fuscus	0.90478	3.1990*	L	A	Shilling and Manahan, 1994[c]
Pteraster militaris	0.90478	10.2000	L	A	McClary and Mladenov, 1990
Henricia leviuscula	1.01000	13.7157	L	A	McEdward and Chia, 1991
Abatus shakeltoni	1.09807	18.1273*	B	E	McClintock and Pearse, 1986[r]
Abatus cordatus	1.25983	16.4600*	B	E	Lawrence, McClintock, and Guille, 1984[r]
Anasterias rupicola	1.34636	18.5340*	B	A	Lawrence, McClintock, and Guille, 1984[r]
Anasterias perrieri	2.80616	39.3162*	B	A	Lawrence, McClintock, and Guille, 1984[r]
Abatus nimrodi	4.00310	45.3448*	B	E	McClintock and Pearse, 1986[r]
Diplasterias meridionalis	11.3713	155.504*	B	A	Lawrence, McClintock, and Guille, 1984[r]
Diplasterias brucei	11.4940	161.297*	B	A	McClintock and Pearse, 1986[r]
Notasterias armata	23.2278	143.019*	B	A	McClintock and Pearse, 1986[r]

* Indicates that values for egg energy content were adjusted as indicated in the Reference column (see text for details).

[c] Values for egg energy content were adjusted for the absence of measured carbohydrate.

[r] Values for egg energy content were adjusted for remainder fractions or by recalculation of the energy value of the remainder fraction.

measurement and found that biochemical fraction data and dichromate data yielded the same scaling relationships.

A complete analysis of the scaling relationships was then conducted for each of the three data sets: the data as originally reported; data adjusted for the absence of the carbohydrate fraction; and data adjusted for carbohydrates and the remainder fraction. The results of these analyses were very similar for all three data sets, so we have reported results only for the "best" or "most fully adjusted" data set in this paper. The fact that adjusting the data did not have a substantial effect on the scaling relationships indicates that the analyses of scaling are robust to details of the data and differences among studies.

Egg diameters and energy contents for the asteroid *Pisaster ochraceus*, the echinoids *Arbacia punctulata*, *Strongylocentrotus droebachiensis*, *S. pallidus*, *S. franciscanus*, *S. purpuratus*, and *Dendraster excentricus*, and the holothuroid *Parastichopus californicus* were measured by Strathmann and Vedder (1977), but were not reported directly. Mean values for each of these species were calculated from the original data and reported by Emlet *et al.* (1987, p. 76) as egg diameter and energy density (=concentration). We calculated egg volume from the reported diameter by assuming that the eggs were spherical (*i.e.*, $d_1 = d_2 = d_3$). We calculated energy content as the product of volume and concentration, using the mean value for energy concentration reported by Emlet *et al.* (1987, p. 76).

Turner and Lawrence (1979, p. 34) reported the organic components of eggs from the asteroids *Asterias forbesi*, *Luidia clathrata*, two species of *Echinaster*, the echinoids *Arbacia punctulata*, *Lytechinus variegatus*, *Strongylocentrotus droebachiensis*, and the holothuroid *Cucumaria curata* (see also Turner and Rutherford, 1976) as lipid, protein, and carbohydrate content ($\mu g \cdot egg^{-1}$). We calculated the energy content of the eggs by summing the energy equivalents of the three organic components and the estimated remainder fraction: lipid = 3.95×10^{-2} J $\cdot \mu g^{-1}$, protein = 2.40×10^{-2} J $\cdot \mu g^{-1}$, carbohydrate = 1.75×10^{-2} J $\cdot \mu g^{-1}$ (Gnaiger, 1983), remainder = 2.70×10^{-2} J $\cdot \mu g^{-1}$ (Jaeckle, 1995). Egg sizes were reported as volumes (Turner and Lawrence, 1979, p. 30) but did not correspond to the egg samples that were analyzed in all cases. Egg diameters were reported by Lawrence *et al.* (1984, p. 253) for the study by Turner and Lawrence (1979), calculated from the appropriate original egg size data. Their calculated diameters represent the diameter of a sphere of equivalent volume; therefore, we calculated egg volumes from the diameters reported by Lawrence *et al.* (1984) using Eq. 1, setting $d_1 = d_2 = d_3$.

Lawrence *et al.* (1984, p. 253) reported diameters and caloric content (cal $\cdot$ egg^{-1}) of eggs from the asteroids *Anasterias perrieri*, *Anasterias rupicola*, and *Diplasterias meridionalis*, and the echinoid *Abatus cordatus*. We converted calories to J using the conversion factor of 4.187 J $\cdot$ cal^{-1} and recalculated the insoluble protein fraction as a remainder fraction. McClintock and Pearse (1986, p. 342) reported egg diameters and energy contents (J $\cdot$ egg^{-1}) from the asteroids *Diplasterias brucei*, *Notasterias armata*, and *Perknaster fuscus*, and the echinoids *Abatus shackletoni* and *Abatus nimrodi*. The energy content values for *Perknaster* were anomalously high and were replaced with the values reported by Shilling and Manahan (1994). We used the average of the two values reported for *Diplasterias brucei* as the mean value for that species. Insoluble protein was recalculated as a remainder fraction. Emlet (1986, p. 186) reported the diameter and organic matter content (μg glucose equivalent $\cdot$ egg^{-1}) from the echinoid *Clypeaster rosaceus*. Egg energy concentration was calculated from organic matter content and size and reported as J $\cdot$ mm^{-3} by Emlet *et al.* (1987, p. 76). We calculated egg volumes from the diameters using Eq. 1, setting $d_1 = d_2 = d_3$, for all of the species in these three studies.

McEdward and Carson (1987, p. 162) reported volume and organic (carbon) content (μg C $\cdot$ egg^{-1}) of eggs from the asteroid *Solaster stimpsoni*. Using the original data, we converted organic content (expressed as glucose equivalents) to energy content (J $\cdot$ egg^{-1}), using a conversion factor of 3.90×10^{-2} J $\cdot \mu g$ C^{-1} based on constants given by Parsons *et al.* (1984). McEdward and Coulter (1987) reported egg volume and egg energy content (J $\cdot$ egg^{-1}) from the asteroid *Pteraster tesselatus*. McEdward *et al.* (1988) reported egg volume and energy content (J $\cdot$ egg^{-1}) from the crinoid *Florometra serratissima*. McEdward and Chia (1991) reported volume and energy content (J $\cdot$ egg^{-1}) for eggs from the asteroids *Solaster endeca*, *S. dawsoni*, *Mediaster aequalis*, *Pteraster tesselatus*, and *Henricia* sp. (*leviuscula?*), and the holothuroids *Cucumaria miniata* and *Psolus chitinoides*.

Herrera *et al.* (1996) reported the egg diameter and energy content (J $\cdot$ egg^{-1}) of the eggs of the echinoid *Encope aberrans*. McClary and Mladenov (1990) measured the egg diameter and energy content (J $\cdot$ egg^{-1}) of the asteroid *Pteraster militaris*. For both species, egg volume was calculated using Eq. 1, by assuming that the eggs were spherical.

Shilling and Manahan (1994) reported egg volume and the protein and lipid content ($\mu g \cdot egg^{-1}$) of the eggs of the asteroids *Odontaster validus*, *Acondontaster hodgsoni*, and *Psilaster charcoti*. Data for *Perknaster fuscus* were not reported directly but were extracted from their figure 2. We calculated estimates for the carbohydrate and remainder fractions. George *et al.* (1997) reported egg volume and biochemical content (protein and lipid, $\mu g \cdot egg^{-1}$) for the eggs of the asteroid *Echinaster spinulosus* and the echinoids *Arbacia lixula*, *Arbacia punctulata*, *Paracentrotus lividus*, *Aspidodidema jacobyi*, *Echinometra lucunter*, *Stylocidaris lineata*, *Coelopleurus floridanus*, *Archaeopneustes histrix*, and *Encope michelini*. We calculated energy content from the measured energy equivalents (Gnaiger, 1983) for the lipid and protein fractions and the estimated carbohydrate and remainder fractions.

Scaling relationships

Any attempt to describe the scaling of egg energy content *versus* egg size involves a search for a pattern in the data. A scaling relationship is a trend whereby the response variable (energy content) changes in some predictable way as a function of the explanatory variable (egg volume). Two factors influence the description of scaling relationships. The first important factor is the relationship between the variables of interest. This determines the underlying pattern (*i.e.*, the existence and nature of a trend) and accounts for the variance in the variables that is independent of the pattern. The second important factor is the statistical model that is used to characterize the pattern. What is sought is a simple model for which there is a good fit with the data. This involves two steps: selecting the model and then evaluating the fit. The choice of the statistical model imposes on the data the investigator's assumptions about the basic nature of the pattern. Statistical models are selected on the basis of multiple considerations: patterns that are evident when data are visualized graphically, *a priori* assumptions about pattern inferred from the biology of the system, goodness of fit to the data when several competing models are compared, simplicity (biological interpretation) of the model, and ease of calculation. Often, especially with messy biological data, there is no single unambiguously best model. There will generally be a trade-off between simplicity (understandable, but possibly a poor fit) and complexity (nearly perfect fit, but uninterpretable). Very complex models (*e.g.*, higher order polynomials) defeat the purpose of the exercise by describing the data exactly without capturing any aspect of a pattern.

Statistical models

We evaluated four regression models in our analysis of scaling relationships in echinoderm eggs: (1) linear regression; (2) power function regression; (3) full allometric regression; and (4) polynomial (second-order) regression (Table 2). All of the models were fitted by the least-squares criterion as model I regressions (egg size assumed to be measured without error). Although egg size is not measured without error and reduced major axis (model II) regressions would be appropriate, only model I regressions permit calculation of prediction intervals.

Properties of various linear and nonlinear regression models have been examined in detail by Albrecht *et al.* (1993). The linear model has the advantage of simplicity and ease of calculation; it is also biologically reasonable; that is, energy is packaged into eggs in direct proportion to egg volume. The power function model is the traditional form of the allometric equation (Huxley, 1932). It is often approximated using a linear model on log-transformed data. A log-log model $\ln(Y) = \ln(b) + k\ln(X)$ is algebraically equivalent to the power function, but logarithmic transformation of the variables changes the distribution of the data and therefore influences the fitting of the model and the estimation of the regression parameters. An advantage of the log-log regression is that the model is recast in linear form and therefore can be readily calculated. However, with modern software, direct methods of fitting nonlinear models are widely available. Since logarithmic versions of the full allometric and the polynomial models are not possible, the power function was fit directly on untransformed data for consistency with the other models. The three nonlinear models were used to cover the situation in which egg energy scales allometrically (*i.e.*, not in direct proportion) with egg volume. There are many examples of such scaling in biology, and it is easy to imagine reasons why it might apply to egg provisioning, such as changes in biochemical composition with size. The full allometric model, like the power function, can capture nonproportional scaling relationships, but has the advantage of not being constrained to pass through the origin. It is therefore a more general model. The second-order polynomial model captures nonlinearity differently from the power function and allometric model. Whereas the latter models describe nonlinear, continuously increasing or decreasing trends (but not both), a second-order polynomial model is the simplest model that allows for an intermediate maximum or minimum in the response variable. Higher order polynomials can provide exceptionally good fits to virtually any relationship between two variables, including data generated randomly. However, the model parameters do not have any clear biological interpretation.

Table 2

Regression models used in analysis of egg size and energy scaling relationships

Model	Regression equation
Linear	$Y = a + bX$
Power	$Y = bX^k$
Allometric	$Y = a + bX^k$
Polynomial	$Y = a + bX + cX^2$

Analysis of fit

Two criteria were used to evaluate the fit between the models and the data. The first is the proportion of the variance in egg energy content that is explained by its relationship with egg volume. This is calculated as the quotient of the regression sum of squares over the total sum of squares (r^2 in linear regression and an analogous measure in nonlinear regression; hereafter referred to as fit). The second criteria are the confidence intervals around the estimated regression parameters. All regression calculations were carried out using Mathematica (version 4; Wolfram Research, Inc.) by means of the Regress (LinearRegression) or the NonlinearRegress (NonlinearFit) function in the Statistics standard add-on package. Regression analyses provided parameters of the best-fit model, 95% confidence intervals around the fitted parameters, and the regression ANOVA.

Identification of influential data

Influential data are those values that exert much greater than average influence on the estimation of the regression parameters. The existence of such data can be problematic because then the best-fit regression is based on a small, possibly atypical, subset of the data, and does not reflect any overall trend. Whether such data are outliers that reduce our ability to detect and describe pattern or are particularly information-rich data essential to the detection and description of pattern is a biological, not a statistical, question. We used a regression diagnostic called the Hat Diagonal to identify strongly influential data (Belsley *et al.*, 1980). Once identified, strongly influential data were eliminated from the data set, and the regressions were recalculated to evaluate the effect of these data on the estimation of the scaling relationship and model fit.

Evaluation of predictive power

After quantifying the scaling relationship between egg volume and energy content, we evaluated the statistical significance of that relationship. In addition, we evaluated the predictive power of the relationship, using the approach described by McEdward and Carson (1987). If a regression is statistically significant, then some of the variance in egg energy content is explained by its relationship with egg volume. In that case, it is possible to measure the size of an additional egg and predict its content. Unless the regression explains all of the variance in content, there will be some scatter around the regression line and some error associated with the calculated prediction of content. That error can be estimated by calculating the confidence interval around the predicted value (Neter *et al.*, 1990, pp: 81–84) (Eq. 3).

$$\hat{Y}_h \pm \sqrt{\mathrm{MSE}\left[1 + \frac{1}{n} + \frac{(X_h - \bar{X})^2}{\Sigma\,(X_i - \bar{X})^2}\right]} \cdot t_{(1-\alpha)/(2,n-2)} \qquad (3)$$

Where $\hat{Y}_h$ represents the $1 - \alpha$ confidence limits for the prediction generated from the new measurement of the explanatory variable (X_h). MSE is the residual mean square from the regression ANOVA, and t is the Student's t statistic with $n - 2$ degrees of freedom.

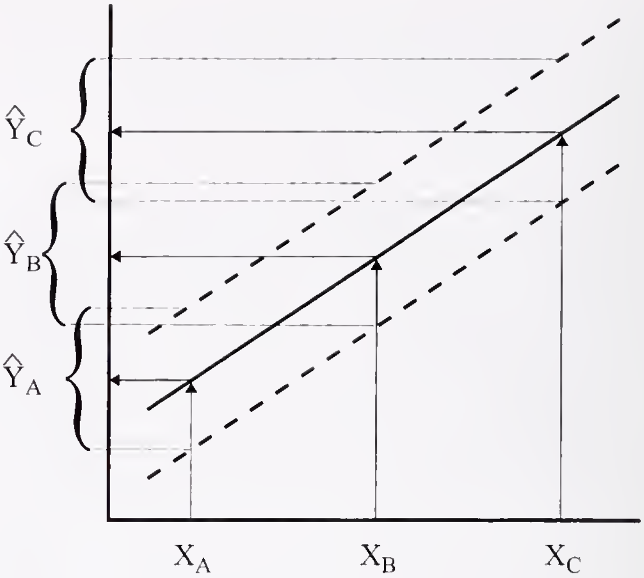

Figure 1. Evaluation of predictive power of a regression using overlap of 95% confidence intervals. Bold, solid diagonal line = least squares regression; bold, dashed diagonal lines = 95% confidence belts for regression. X_A, X_B, X_C = additional measurements of egg size for which predicted energy contents ($\hat{Y}_A$, $\hat{Y}_B$, $\hat{Y}_C$) are calculated using the regression equation (solid vertical and horizontal lines). The 95% confidence intervals for predicted energy contents are obtained from the 95% confidence belts around the regression (dashed horizontal lines). Overlap of the 95% confidence intervals indicates that two predicted egg energy contents are not significantly different. In this example, $\hat{Y}_A$ and $\hat{Y}_C$ are significantly different ($\hat{Y}_A + \mathrm{CI} < \hat{Y}_C - CI$), but neither is significantly different from $\hat{Y}_B$.

To evaluate the predictive power of a regression, we asked: what is the minimum difference in egg size that yields significantly different predictions of egg content? Two predictions of egg energy content were considered to be significantly different (*i.e.*, statistically distinguishable) only if the confidence intervals around them did not overlap (Fig. 1). Starting at the midpoint of the observed range of egg volumes, predictions were calculated for pairs of egg sizes, each pair progressively farther apart, until the confidence intervals around the two predictions did not overlap, or until the entire range of egg sizes had been evaluated. The resolution of this analysis was 0.1% of the observed egg volume range.

The 95% confidence belts around the regression represent the confidence intervals around the predicted egg energy content for all values of the explanatory variable and are needed for our evaluation of predictive power. Both the linear and nonlinear regression analyses generated a table of the single-prediction confidence limits for the actual egg volumes in the data set. From these, we generated equations for the upper and lower confidence belts by fitting the same regression model to the upper and lower (respectively) values of the prediction confidence limits. Given confidence belt equations, it was possible to calculate the confidence limits around predicted egg energy content for any egg volume between the minimum and maximum observed values for linear and allometric regression models.

The predictive power of a regression depends on the width of the confidence belts around the regression and the slope of the regression. Narrow confidence belts result in greater predictive power because nonoverlapping predictions occur with smaller differences in egg volume (Fig. 1). Likewise, steeper slopes yield greater predictive power because the absolute difference between predicted values is greater for a given difference in egg size than with a regression that has a shallow slope. Hence, predictive power does not have a simple relationship with other regression statistics, such as the fit (proportion of variance in the egg energy that is explained by egg size).

This approach was not feasible with the power function regression model. The reason for this is that the power function regression must pass through the origin, which influences the way that predictive power is estimated. Likewise, the estimation of predictive power with the polynomial model can be misleading because of strong curvature in the regressions (*e.g.*, Fig. 2D). The problem with using overlap of confidence belts with strongly nonlinear relationships is that as the slope of the relationship changes, the overlap of confidence belts changes, and therefore the predictive power changes across the range of egg sizes. Evaluations of predictive power would be valid only over small regions of the egg size range. Rather than report what would seem to be anomalous values for predictions by the power and polynomial functions, we report predictive values only for the linear and full allometric models.

Comparison of means

ANOVAs and Student-Newman-Kuels multiple range tests were used to evaluate differences among taxonomic classes or among developmental modes in mean egg volume or mean egg energy content. All tests were conducted at the 5% significance level.

Results

Brooders make eggs (6.348 μl) that are significantly larger than the eggs of species with planktotrophic (0.0016 μl) or pelagic lecithotrophic development (0.417 μl). Brooders also provision eggs with significantly more energy (66.910 J) than do planktotrophs (0.0087 J) or pelagic lecithotrophs (4.363 J). However, there are no significant differences among the taxonomic classes (excluding Crinoidea with only a single species) in egg size ($P = 0.165$) or energy content ($P = 0.124$).

Scaling relationships for all species

Among these 47 species of echinoderms, both egg size and energy content vary across five orders of magnitude.

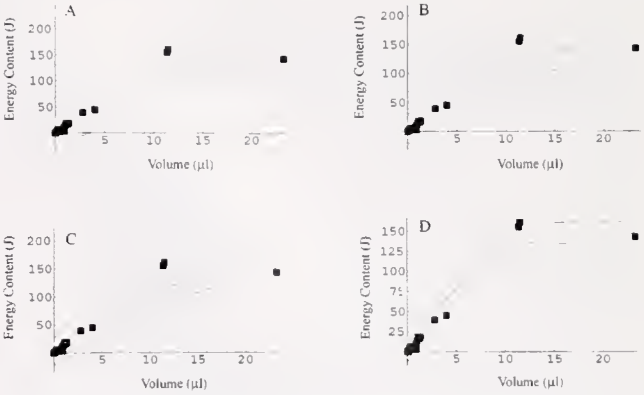

Figure 2. Plots of egg volume and energy content for all 47 species of echinoderms. Panels show different regression models fit to the data and the 95% confidence belts around the regression line. A, linear regression; B, power function; C, full allometric model; D, polynomial model.

There is a strong trend for larger eggs to contain more energy (Fig. 2A). The linear model indicates that the intercept is not significantly different from zero and that egg energy (J) is approximately 8.6-fold greater than the egg volume (μl) (see Table 3 for parameter estimates and regression statistics for all models). The linear regression explains most of the variation in egg content (fit = 84%), but eggs must differ by more than 8 μl in volume (≈35% of the egg size range) to allow the confident prediction that they contain different amounts of energy. This does not provide a useful means of predicting content from measurements of volume. The power function (Fig. 2B) yields a better fit to the data than the linear model, explaining 91% of the variance in egg energy content. The exponent of the power function (0.70) indicates that egg energy content scales with negative allometry relative to egg volume. This means that energy content does not change in proportion to egg volume and that a linear model is inappropriate for

Figure 3. Standardized residual plots for all 47 species of echinoderms. Panels show residuals for different regression models fit to the data. A, linear regression; B, power function; C, full allometric model; D, polynomial model.

Table 3

Regression parameters for all 47 species of echinoderms

Model	*a*	*b*	*c*	*k*	Fit	Δ*X* predict *Y*
Linear	2.607 [−2.179–7.393]	8.610 [7.474–9.746]	—	—	0.838	8.11 μl [35%]
Power	—	20.381 [14.331–26.432]	—	0.702 [0.592–0.812]	0.907	—
Allometric	−3.141 [−8.194–1.912]	23.128 [14.925–31.331]	—	0.666 [0.543–0.789]	0.911	8.36 μl [36%]
Polynomial	−2.201 [−3.922–−0.481]	19.478 [18.229–20.727]	−0.561 [−0.622–−0.500]	—	0.984	—

Regression parameters are illustrated for each model in Table 2. Fit is the proportion of the total variance in egg energy content that is explained by the regression against egg volume. Δ*X* predict *Y* gives the minimum difference in egg volume needed to yield significantly different predictions of egg energy content.

these data. The full allometric model (Fig. 2C) yields a negligibly better fit than the power function, with nearly the same parameter values. The allometric model has weak predictive power; the minimum difference in egg size necessary to yield significantly different predictions is more than 8 μl. The polynomial regression provides the best fit to the data among the four models tested, with a fit of 98%. It shows that the data are strongly curvilinear (Fig. 2D).

Do any of these models fit well enough to justify concluding that we have described the pattern of scaling between egg size and content? In one sense, yes, using all of the data with fairly simple, general models that were explicitly chosen beforehand yields an objective analysis. Besides, the fit in terms of the explained variance is quite good for all models tested (84%–98%). However, the confidence intervals for the regression parameters are broad in all cases, and this cautions against putting too much confidence in the described scaling relationship. Can the fit of any of the models be improved substantially? Examination of the data (Fig. 2), the standardized residuals (Fig. 3), and especially the Hat Diagonals shows that there is one point which strongly influences the estimated regression parameters. On the basis of this finding, the asteroid *Notasterias armata* was removed from the data set, and the regressions were recalculated.

The most striking result of removing this species is that the relationship between egg size and energy content becomes linear (Fig. 4). With the modified data set, the fits (% variance explained) are exceptionally high (99%), the confidence intervals for all of the regression parameters are quite narrow, and the four models generate very similar parameter values (*e.g.*, the intercept is zero; the slope is in the low teens; and the allometric exponent is only slightly greater than one, indicating nearly proportional or isometric scaling of energy content with volume) (Table 4). In addition, the standardized residuals are more evenly distributed (Fig. 5), and the 95% confidence belts are much narrower. This suggests that *Notasterias armata* is an anomalous

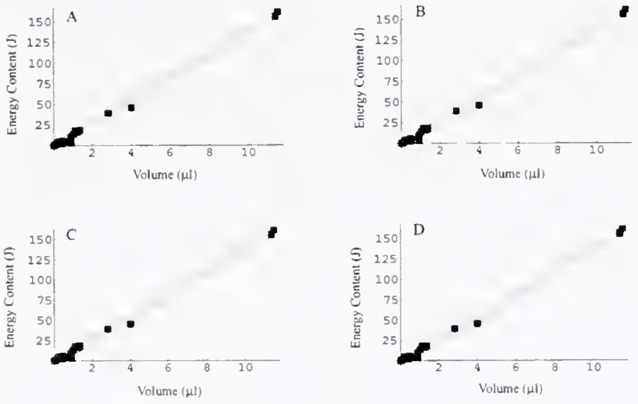

Figure 4. Plots of egg volume and energy content for 46 species of echinoderms, excluding *Notasterias armata*. Panels show different regression models fit to the data and the 95% confidence belts around the regression line. A, linear regression; B, power function; C, full allometric model; D, polynomial model.

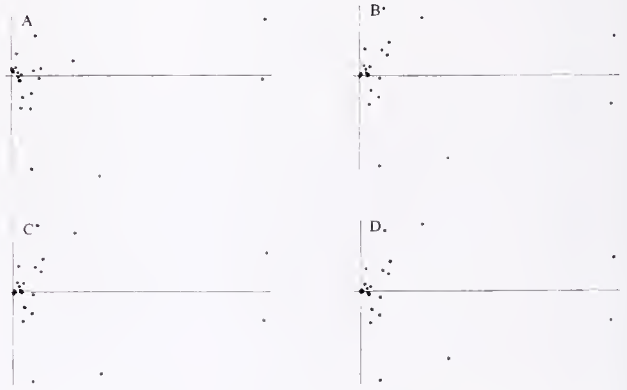

Figure 5. Standardized residual plots for 46 species of echinoderms, excluding *Notasterias armata*. Panels show residuals for different regression models fit to the data. A, linear regression; B, power function; C, full allometric model; D, polynomial model.

Table 4

Regression parameters for 46 species of echinoderms, excluding Notasterias armata

Model	a	b	c	k	Fit	ΔX predict Y
Linear	−0.640 [−1.360–0.080]	13.755 [13.470–14.039]	—	—	0.995	0.75 μl [7%]
Power	—	11.582 [10.594–12.570]	—	1.073 [1.036–1.109]	0.997	—
Allometric	0.094 [−0.646–0.833]	11.494 [10.283–12.705]	—	1.076 [1.032–1.119]	0.997	0.69 μl [6%]
Polynomial	−0.038 [−0.728–0.652]	11.721 [10.673–12.769]	0.186 [0.093–0.280]	—	0.997	—

Regression parameters are illustrated for each model in Table 2. Fit is the proportion of the total variance in egg energy content that is explained by the regression against egg volume. ΔX predict Y gives the minimum difference in egg volume needed to yield significantly different predictions of egg energy content.

species, in terms of egg size, energy content, or both. All subsequent analyses were conducted excluding this species. The biological basis of the anomalous egg characteristics is not known (see below).

How good is the predictive power of these regressions? Both the linear and the allometric models indicate that significantly different predictions of content require differences in egg volume of 0.69–0.75 μl, which comprise only about 6%–7% of the egg size range. This is substantially less than in the previous analyses, but just how useful is it? Given that the 35 species with the smallest eggs all lie within a range of volumes that spans only 0.52 μl, then it is clear that we are only able to conclude with confidence that very large eggs of species with lecithotrophic larval development (benthic brooding or pelagic) contain more energy than very small eggs of species with planktotrophic (feeding) larval development. These regressions, even given extremely good fit with the data, have poor predictive power.

Scaling relationships within developmental patterns

Is the predictive power of the relationship improved by restricting the analysis to just those species with particular modes of development? In general, egg size and content of planktotrophic and lecithotrophic species are very different (Fig. 2). All species with planktotrophic larval development produce eggs that contain less energy ($\leq 4.64 \times 10^{-2}$ J · egg^{-1}) than eggs from all species with pelagic or benthic (brooded) lecithotrophic development ($\geq 82.5 \times 10^{-2}$ J · egg^{-1}), except for the crinoid *Florometra serratissima* (4.55×10^{-2} J · egg^{-1}) (Table 1). There is overlap in size or content among a few species that represent the extremes within planktotrophy and lecithotrophy. The echinoid *Clypeaster rosaceus* has larvae that are lecithotrophic, in that they do not require exogenous food for larval development and metamorphosis (Emlet, 1986). However, unlike all other lecithotrophic larvae, they have functional feeding structures and can acquire and utilize exogenous, particulate food. This species, being a facultative feeder, has a mixture of traits characteristic of planktotrophic and nonfeeding lecithotrophic larvae. It has a larger egg (1.15×10^{-2} μl) than any obligately planktotrophic species and, with only a single exception, it has greater egg energy (2.06×10^{-2} J · egg^{-1}) than any obligate planktotroph. Only the echinoid *Encope michelini* (4.64×10^{-2} J · egg^{-1}) has greater egg energy than *C. rosaceus*. *Encope michelini* is an obligate planktotroph, but it can complete most of larval development using endogenous reserves and has only a minimal need for exogenous food (Eckert, 1995).

Clypeaster rosaceus produces eggs that are larger than one of the pelagic lecithotrophs, the crinoid *Florometra serratissima*. The eggs of *Florometra* are unusually small (7.42×10^{-3} μl, 4.55×10^{-2} J · egg^{-1}) for nonfeeding lecithotrophs, containing 8.6-fold less volume and 18.1-fold less energy than the next largest egg (*Cucumaria miniata*, 6.40×10^{-2} μl, 8.25×10^{-1} J · egg^{-1}). If *Clypeaster* and *Florometra* are discounted, then the distinction between the eggs of planktotrophs and lecithotrophs is very striking: there is an 12.5-fold difference in egg volume and an 17.8-fold difference in energy content between the largest egg from planktotrophic species (*Encope michelini*) compared to the smallest egg found among lecithotrophs (*Cucumaria miniata*) (Table 1). This difference in egg characteristics is consistent with the nutritional strategies of planktotrophy and lecithotrophy. Obligately planktotrophic larvae must supplement the material provided in the egg by feeding on planktonic particles. Nonfeeding lecithotrophs cannot capture or ingest particles and must rely on nutritional reserves provided in the egg by the parent, possibly supplemented by uptake of dissolved organic matter from the surrounding seawater. The eggs of nearly all brooders are larger and contain more energy than the eggs of pelagic lecithotrophs (Table 1). This is surprising because, whereas pelagic lecithotrophic larvae are independent of the parent throughout development and are incapable of utilizing

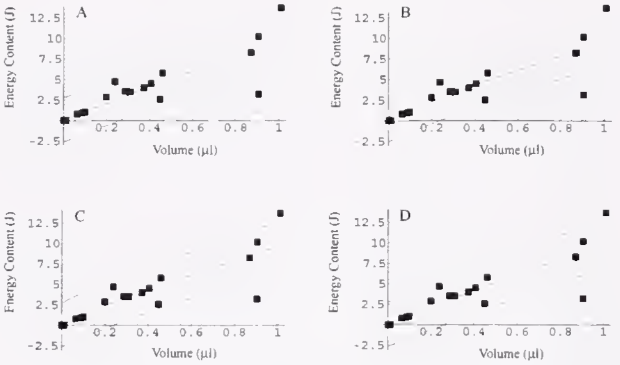

Figure 6. Plots of egg volume and energy content for the 38 species of echinoderms with planktotrophic or lecithotrophic development. Panels show different regression models fit to the data and the 95% confidence belts around the regression line. A, linear regression; B, power function; C, full allometric model; D. polynomial model.

planktonic food particles, brooders retain the offspring on or in the body of the parent and therefore have the potential to provide nutrition to the developing young.

Scaling relationships among free-spawners

Among free-spawning species, linear regression explains 84% of the variance in egg energy content in this sample of 38 species (Fig. 6). The best-fit linear regression passes through the origin (the intercept confidence interval includes zero) and has a slope of 9.87 (Table 5). The power function and the allometric models each explain 88% of the variance. Their slopes (9.64) are not different from the slope of the linear regression, and their scaling exponents (0.87) are not significantly different from 1. This indicates that energy content increases roughly in proportion to egg volume.

The predictive power of these scaling relationships does not improve substantially by restricting the analysis to development modes without offspring retention. Eggs that differ by 0.56–0.62 µl in volume have different predicted energy contents. Note that this is still more than half of the entire range of egg sizes in these two modes of development. How good is this? Volume is the most useful measure of egg size for comparison with content, but it is not easy to visualize. Biologists routinely report egg size as diameter because it is easy to measure and it is what one sees in an optical section under the microscope. Obviously, the diameter difference required to generate a difference of 0.56 µl in volume will depend on the size range of eggs considered. To illustrate the point, consider an egg with a diameter of 1000 µm; it has a volume of 0.52 µl. Eggs must be larger than 1250 µm in diameter in order to yield different predictions of content. However the egg of 1000 µm has a predicted content that is indistinguishable from the contents of all eggs that are smaller. In effect, all that can be concluded from the regression of size and content is that most lecithotrophs produce eggs with more energy in them than do planktotrophs.

Scaling relationships among species with nonfeeding development

The pelagic lecithotrophs and brooders together comprise the species with nonfeeding modes of development. Among these 24 species, all four regression models yield excellent fit, narrow parameter confidence intervals, and reasonably good predictive power (Fig. 7, Table 6). All of the models account for more than 99% of the variance in energy content. Both the power function (1.07) and allometric (1.08) model exponents are only slightly different from 1, indicating nearly proportional scaling of content with volume. The predictive power is good in that the minimum difference in egg volume needed for significantly different predictions of content is only 1.0 µl, 9% of the egg volume range in this sample. But as can be seen from the plot (Fig. 7), this difference allows predictions only between the lecithotrophs

Table 5

Regression parameters for the 38 species of echinoderms with planktotrophic or lecithotrophic development

Model	*a*	*b*	*c*	*k*	Fit	ΔX predict Y
Linear	0.099 [−0.400–0.599]	9.870 [8.407–11.333]	—	—	0.839	0.56 µl [55%]
Power	—	9.636 [8.167–11.105]	—	0.871 [0.610–1.132]	0.882	—
Allometric	−0.012 [−0.592–0.567]	9.644 [8.097–11.190]	—	0.868 [0.569–1.167]	0.882	0.62 µl [61%]
Polynomial	0.066 [−0.476–0.609]	10.688 [5.620–15.756]	−0.957 [−6.627–4.712]	—	0.880	—

Regression parameters are illustrated for each model in Table 2. Fit is the proportion of the total variance in egg energy content that is explained by the regression against egg volume. ΔX predict Y gives the minimum difference in egg volume needed to yield significantly different predictions of egg energy content.

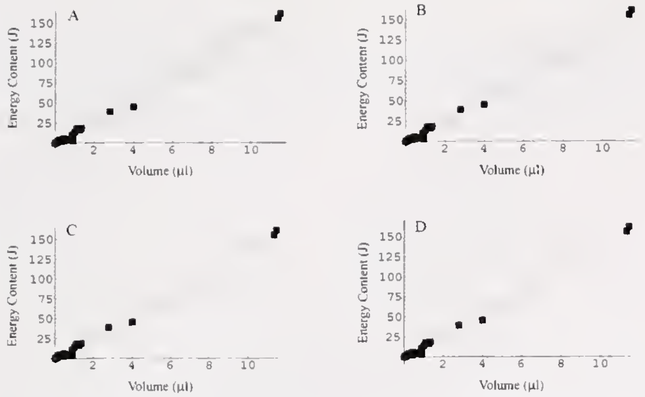

Figure 7. Plots of egg volume and energy content for the 24 species of echinoderms with lecithotropic or brooded development, excluding *Notasterias armata*. Panels show different regression models fit to the data and the 95% confidence belts around the regression line. A, linear regression; B, power function; C, full allometric model; D, polynomial model.

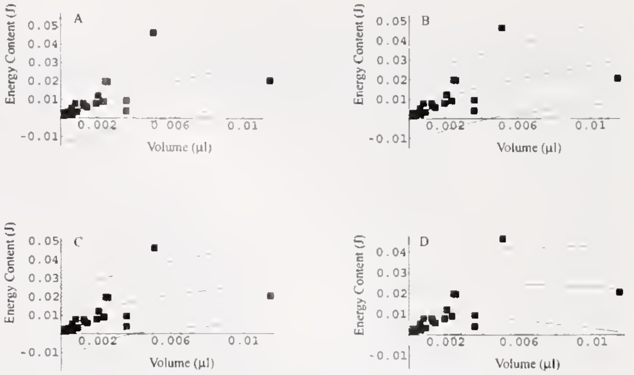

Figure 8. Plots of egg volume and energy content for the 22 species of echinoderms with feeding larvae, including *Clypeaster roseaceus*. Panels show different regression models fit to the data and the 95% confidence belts around the regression line. A, linear regression; B, power function; C, full allometric model; D, polynomial model.

as a group and between the four brooders with the largest eggs.

Scaling relationships for species with planktotrophic larval development

Planktotrophic species produce small eggs that develop into feeding larvae. The echinoid *Clypeaster rosaecus* has, for all previous analyses, been considered to be lecithotrophic because the energy content of the egg is sufficient to support complete larval development to metamorphosis (Emlet, 1986). However, since it has feeding larvae, it could be considered a facultative planktotroph. We analyzed the scaling relationships among planktotrophs with *C. rosaceus* included and excluded from the data. When *Clypeaster* is included there are 22 species with feeding larvae (Table 1). The linear regression model yields a relatively poor fit to the data, explaining only 37% of the variance in content (Fig. 8, Table 7). The power function and the allometric models explain 70%–72% of the variance, and the polynomial regression generates the best fit (77%). For all of these models the parameter confidence intervals are very broad, and none of the models have any predictive power (Table 7). Even the extremes in the range of egg sizes do not yield significantly different predictions of content. Excluding *Clypeaster* improves the fit of the regressions, but the parameter confidence intervals remain very large. Based on Hat Diagonals and residuals, we removed three additional species (*Encope aberrans, Encope michelini, Parastichopus californicus*) and then two more species from the planktotrophic dataset (*Luidia clathrata, Odontaster validus*). These changes did not result in better estimates of the regression parameters (CIs). Furthermore, the nonlinear models were drastically different for each subset of the data. The allometric model exponent varied from 0.335 (negative allometry) to 1.97 (positive allometry) as species were included or excluded from the analysis. However, the allometric exponent was not significantly different from isometric (1.0) for any of the

Table 6

Regression parameters for the 24 species of echinoderms with lecithotrophic or brooded development, excluding Notasterias armata

Model	a	b	c	k	Fit	ΔX predict Y
Linear	−1.318 [−2.735–0.098]	13.848 [13.435–14.261]	—	—	0.995	1.00 µl [9%]
Power	—	11.582 [10.180–12.985]	—	1.073 [1.021–1.124]	0.997	—
Allometric	0.326 [−1.614–2.265]	11.279 [8.998–13.560]	—	1.083 [1.002–1.164]	0.997	1.03 µl [9%]
Polynomial	−0.088 [−1.745–1.568]	11.759 [9.951–13.568]	0.183 [0.028–0.339]	—	0.997	—

Regression parameters are illustrated for each model in Table 2. Fit is the proportion of the total variance in egg energy content that is explained by the regression against egg volume. ΔX predict Y gives the minimum difference in egg volume needed to yield significantly different predictions of egg energy content.

Table 7

Regression parameters for the 22 species of echinoderms with feeding larvae, including Clypeaster roseaceus

Model	*a*	*b*	*c*	*k*	Fit	Δ*X* predict *Y*
Linear	0.004 [0.000–0.009]	2.482 [0.960–4.004]	—	—	0.367	— [>100%]
Power	—	0.403 [−0.340–1.145]	—	0.583 [0.256–0.910]	0.703	—
Allometric	−0.013 [−0.079–0.052]	0.151 [−0.200–0.502]	—	0.289 [−0.510–1.089]	0.717	— [>100%]
Polynomial	−0.001 [−0.007–0.004]	7.600 [3.719–11.480]	−481.456 [−825.424–−137.488]	—	0.765	—

Regression parameters are illustrated for each model in Table 2. Fit is the proportion of the total variance in egg energy content that is explained by the regression against egg volume. Δ*X* predict *Y* gives the minimum difference in egg volume needed to yield significantly different predictions of egg energy content.

subsets of planktotrophic species that we analyzed. Likewise, the coefficient of the second-order term of the polynomial regression varied from positive (upward curvature) to negative (downward curvature), but the 95% confidence interval for that parameter ranged from positive to negative for most analyses. The behavior of these models indicates that there is not a clear scaling trend among species with feeding larvae. This is consistent with the growing appreciation that planktotrophic species utilize a wide range of nutritional strategies and are characterized by different life history trade-offs across those strategies (Herrera *et al.*, 1996; McEdward and Janies, 1997; McEdward, 1997). At this point, with existing data, it is not possible to characterize the scaling relationships between egg size and energy content, and it is certainly impossible to use regression analysis to predict energy content from measurements of egg volume. Data on additional planktotrophic species might provide a clear picture of how egg energy scales with volume. However, it is also possible that energetic diversity among planktotrophs is considerable and clear trends for the entire suite of species with feeding larvae do not exist.

Scaling relationships among species with pelagic lecithotrophic development

There are data for 17 species (*Clypeaster* included) of echinoderms that have pelagic lecithotrophic development (Table 1). Egg volumes range from 0.007 to 1.01 μl, and energy contents range between 0.021 and 13.7 J · egg^{-1} (Fig. 9). The linear model explains 73% of the variance in egg energy content and the nonlinear models explain 88% (Table 8). The scaling exponents are 0.87 and 0.90 respectively for the power and allometric models, suggesting negative allometry, but neither is statistically different from isometry. The predictive power of all of the models is low, requiring differences in egg size on the order of the entire observed range of sizes (Table 8).

Scaling relationships among brooders

The eggs of nearly all brooders are larger and contain more energy than the eggs of pelagic lecithotrophs (Table 1). The only exception to this generalization is the brooding holothuroid *Cucumaria curata,* which has small eggs (0.52 μl, 4.58 J, Table 1). This is surprising because brooders have the potential to provide nutrition to the developing young (*e.g.*, Sewell and Chia, 1994; Byrne, 1996), whereas pelagic nonfeeding larvae are independent of the parent throughout development and are incapable of utilizing planktonic food particles. Is this a general result? Emlet *et al.* (1987) reported egg sizes, but not energy content, for nearly 200 species of asteroids and echinoids. They found that there was very little, if any, overlap in the egg size ranges of planktotrophs and lecithotrophs, but there was considerable overlap in the egg sizes produced by pelagic lecithotrophs and brooders (Emlet *et al.*, 1987, p. 108). In spite of the overlap, the largest eggs produced by both asteroids and echinoids occurred in brooding species. These observations

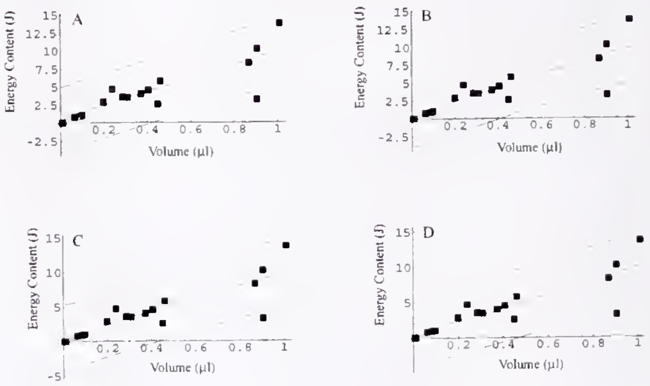

Figure 9. Plots of egg volume and energy content for the 17 species of echinoderms with lecithotrophic development, including *Clypeaster roseaceus.* Panels show different regression models fit to the data and the 95% confidence belts around the regression line. A, linear regression; B, power function; C, full allometric model; D, polynomial model.

Table 8

Regression parameters for the 17 species of echinoderms with lecithotrophic development, including Clypeaster roseaceus

Model	*a*	*b*	*c*	*k*	Fit	ΔX predict Y
Linear	0.421 [−1.196–2.038]	9.385 [6.217–12.554]	—	—	0.727	0.97 μl [97%]
Power	—	9.631 [7.237–12.025]	—	0.869 [0.443–1.296]	0.882	—
Allometric	0.137 [−2.937–3.212]	9.524 [9.580–13.091]	—	0.900 [0.087–1.714]	0.882	— [>100%]
Polynomial	0.510 [−1.857–2.877]	8.722 [−4.122–21.567]	0.659 [−11.680–12.998]	—	0.882	—

Regression parameters are illustrated for each model in Table 2. Fit is the proportion of the total variance in egg energy content that is explained by the regression against egg volume. ΔX predict Y gives the minimum difference in egg volume needed to yield significantly different predictions of egg energy content.

suggest that brooding, with its potential for post-spawning parental investment, does not necessarily result in lower levels of parental investment by means of the egg. Rather, it seems to provide the opportunity to increase levels of parental investment per offspring over those found in pelagic lecithotrophs. Possibly the functional requirements of pelagic life (*e.g.*, buoyancy control, swimming, settlement) preclude very large eggs and offspring. Alternatively, parental protection of brooded young could reduce the risk of offspring mortality sufficiently to allow allocation of more resources to individual young.

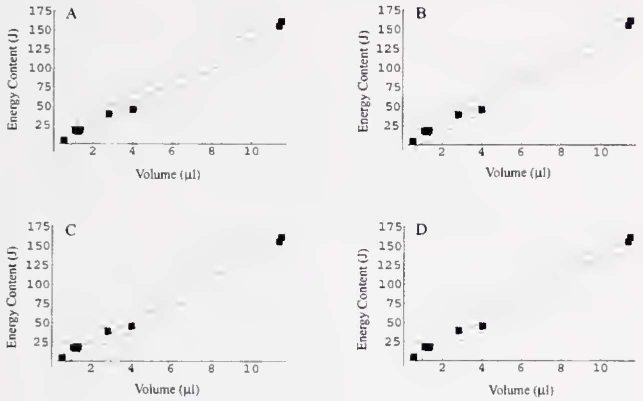

Figure 10. Plots of egg volume and energy content for the 8 species of echinoderms with brooded development, excluding *Notasterias armata*. Panels show different regression models fit to the data and the 95% confidence belts around the regression line. A, linear regression; B, power function; C, full allometric model; D, polynomial model.

The eight species of brooders (*Notasterias* excluded) are fit well by both the linear and nonlinear models (Fig. 10, Table 9). More than 99% of the variance in content is explained by each regression model. However, parameter confidence intervals are still quite wide; for example, the scaling exponent of the allometric model (1.15) is not significantly different from 1. The predictive power is reasonably good for both models, requiring egg size differences of 16%–17% of the observed range.

Discussion

Among echinoderms, larger eggs do contain more energy. The general pattern that is suggested by this study is

Table 9

Regression parameters for the 8 species of echinoderms with brooded development, without Notasterias armata

Model	*a*	*b*	*c*	*k*	Fit	ΔX predict Y
Linear	−1.495 [−6.788–3.798]	13.897 [13.018–14.775]	—	—	0.996	1.74 μl [16%]
Power	—	12.152 [9.111–15.192]	—	1.053 [0.946–1.159]	0.998	—
Allometric	4.414 [−6.389–15.218]	9.277 [2.102–16.453]	—	1.153 [0.858–1.447]	0.998	1.86 μl [17%]
Polynomial	3.056 [−5.483–11.595]	10.566 [5.376–15.757]	0.264 [−0.142–0.669]	—	0.999	—

Regression parameters are illustrated for each model in Table 2. Fit is the proportion of the total variance in egg energy content that is explained by the regression against egg volume. ΔX predict Y gives the minimum difference in egg volume needed to yield significantly different predictions of egg energy content.

that egg energy scales very nearly in direct proportion to egg volume across a remarkable range of egg sizes both within and among different modes of development. This seems to be a robust result that emerges from different analyses using different regression models and different methods and assumptions for calculating egg energy (see Jaeckle, 1995).

Statistically significant linear and nonlinear regressions were obtained in nearly all of these interspecific analyses. This demonstrates that some, and often a large proportion, of the variance in content is related to egg size. However, in many cases there were wide confidence intervals around the estimated regression parameters, suggesting caution in interpretation of the parameters. Whether the precision of regression parameter estimates will improve with new data for additional species or whether new data will confirm an underlying diversity in the egg size-content relationship is not clear. We believe that the latter possibility is likely, especially for moderate increases in the number of species analyzed. Once a substantial number of new species are added to the dataset and the underlying diversity is adequately sampled, then additional data should lead to more precise estimates of scaling patterns.

A statistically significant regression provides a means to predict content from a measurement of size. But a significant regression, even with a very good fit (% variance explained), does not ensure that predictions based on it will be useful or reliable. Although we have tried to bias the outcome by excluding some species or restricting the analysis to subsets of the data, in all of the cases examined here the predictive power of the regressions was poor. We strongly advocate explicit tests of regression results, whether the regression is used to describe scaling patterns or to make predictions from future measurements. At a minimum, we advocate evaluation of parameter confidence intervals and some test of the predictive power of the regression.

The analyses presented here clearly show how poor the predictive power of regressions can be, even when there is a good fit to the data. In some cases, the predictive power is poor because many of the data points are clustered at the low end of the egg size range. So that even if the minimum difference in egg size needed to yield significant predictions of content is a small percentage of the egg size range, the difference is quite large relative to the egg size differences among many of the species (*e.g.*, nonfeeding development, Fig. 7, Table 6). In other cases, the predictive power is low because the regression slope is shallow relative to the width of the confidence bands and the range of egg sizes (*e.g.*, lecithotrophs, Fig. 9, Table 8). In still other cases, the poor predictive power is the result of a poor fit between the regression and the data (*e.g.*, linear model for planktotrophs, Fig. 8A, Table 7) or a strongly curvilinear regression (*e.g.*, allometric model for planktotrophs, Fig. 8C, Table 7).

On the basis of our results in this study, we advocate use of the full allometric model for studies of scaling relationships. This model has the advantage of being simple and general (see also Emlet, 1989; Albrecht *et al.*, 1993; Ebert and Russell, 1994). It can capture linear and nonlinear patterns, can handle nonzero intercepts, and is reasonably easy to interpret. The most obvious disadvantages do not present serious problems. First, the allometric model cannot be converted to linear form (for ease of calculation) using logarithms, but log transformations are objectionable because they can strongly influence the fitting of model to data and the estimation of the regression parameters. Use of the allometric model requires nonlinear fitting algorithms, which are now available in many statistical and mathematical programs. Alternatively, effective iterative fitting methods can be easily programmed (see Manaster and Manaster, 1975; Albrecht *et al.*, 1993, or contact the authors for documented source code). The second disadvantage is that the allometric model cannot capture complex nonlinear patterns. There are relatively few cases in which scaling patterns have been convincingly shown to be complex. Furthermore, the parameters of complex regression models are often difficult to interpret biologically, in spite of providing very good fit to the data. The alternatives to the allometric model that we analyzed in this study all suffer from serious drawbacks. The linear model is too limited, since it cannot capture nonproportional (allometric) scaling, which is a common pattern in biology. The power function is simply a limited version of the allometric model that forces the regression to pass through the origin, an unnecessary and often erroneous assumption in biology, which also precludes evaluating the predictive power of the regression. The polynomial regression sometimes yielded a slightly better fit to the data, but there was no case in which the data were characterized by nonlinearity that could be fit with the polynomial but not the allometric model. Polynomial models, even low-order models such as the quadratic that we used in this study, are hard to interpret biologically.

One asteroid species, *Notasterias armata* (a brooder), is strikingly different in egg size or energy content relative to all other species. It potentially exerts extraordinary influence on the regression analyses. Given that these data are not the result of serious measurement error, it become an interesting problem to explain the basis for such different levels of egg provisioning in this Antarctic species. It has exceptionally large eggs (23.2 μl^{-1}), but the energy content is the same as that of *Diplasterias meridionalis* and *Diplasterias brucei* (Table 1). These two species are also Antarctic asteroids that brood their young. Their eggs are 3 times greater in volume than those of any other species in our data set, but their eggs are only half the size of *Notasterias* eggs. It is not obvious what selection pressures would favor substantially increased egg volume without increased egg energy content, especially in an organism that broods its offspring.

Our conclusion from this study is that egg size is of limited value for fine-scale quantitative predictions of egg energy content and should be used with caution. This conclusion challenges a fundamental assumption in reproductive ecology and, as a result, increases the difficulty of understanding life-history patterns in marine invertebrates.

Acknowledgments

We thank G. Albrecht for kindly providing advice and source code for the iterative method for fitting the full allometric model. The assistance of B. Bolker, D. Brazeau, A. Kohn, C. Lanciani, C. Osenberg, D. Padilla, R. Strathmann, and especially C. Solari with data analysis is greatly appreciated. L. McEdward and M. McEdward assisted with proofreading the manuscript. This work was supported by grants from the University of Florida and the National Science Foundation (OCE-9818593) to L. McEdward.

Literature Cited

Albrecht, G. H., B. R. Gelvin, and S. E. Hartman. 1993. Ratios as a size adjustment in morphometrics. *J. Physiol. Anthropol.* **39:** 441–468.

Belsley, D. A., E. Kuh, and R. E. Welsch. 1980. *Regression Diagnostics: Identifying Influential Data and Sources of Collinearity.* John Wiley, New York.

Byrne, M. 1996. Viviparity and intragonadal cannibalism in the diminutive sea stars *Patiriella vivipara* and *P. parvivipara* (family Asterinidae). *Mar. Biol.* **125:** 551–567.

Christiansen, F. B., and T. M. Fenchel. 1979. Evolution of marine invertebrate reproductive patterns. *Theor. Popul. Biol.* **16:** 267–282.

Ebert, T. A., and M. P. Russell. 1994. Allometry and model-II nonlinear regression. *J. Theor. Biol.* **168:** 367–372.

Eckert, G. L. 1995. A novel larval feeding strategy of the tropical sand dollar, *Encope michelini* (Agassiz): adaptation to food limitation and an evolutionary link between planktotrophy and lecithotrophy. *J. Exp. Mar. Biol. Ecol.* **187:** 103–128.

Emlet, R. B. 1986. Facultative planktotrophy in the tropical echinoid *Clypeaster rosaceus* (Linnaeus) and a comparison with obligate planktotrophy in *Clypeaster subdepressus* (Gray) (Clypeasteroidea: Echinoidea). *J. Exp. Mar. Biol. Ecol.* **95:** 183–202.

Emlet, R. B. 1989. Apical skeletons of sea urchins (Echinodermata: Echinoidea): two methods for inferring mode of larval development. *Paleobiology* **15:** 223–254.

Emlet, R. B., L. R. McEdward, and R. R. Strathmann. 1987. Echinoderm larval ecology viewed from the egg. *Echinoderm Stud.* **2:** 55–136.

George, S. B., C. M. Young, and L. Fenaux. 1997. Proximate composition of eggs and larvae of the sand dollar *Encope michelini* (Agassiz): the advantage of higher investment in planktotrophic eggs. *Invertebr. Reprod. Dev.* **32:** 11–19.

Gnaiger, E. 1983. Calculation of energetic and biochemical equivalents of respiratory oxygen consumption. Pp. 337–345 in *Polarographic Oxygen Sensors,* E. Gnaiger and H. Forstner, eds. Springer-Verlag, Berlin.

Grant, A. 1983. On the evolution of brood protection in marine benthic invertebrates. *Am. Nat.* **122:** 549–555.

Havenhand, J. N. 1995. Evolutionary ecology of larval types. Pp. 79–122 in *Ecology of Marine Invertebrate Larvae,* L. R. McEdward, ed. CRC Press, Boca Raton, FL.

Herrera, J., S. McWeeney, and L. R. McEdward. 1996. Diversity of energetic strategies among echinoid larvae and the transition from feeding to nonfeeding development. *Oceanol. Acta* **19:** 313–321.

Huxley, J. 1932. *Problems of Relative Growth.* Dover Publications, New York.

Jaeckle, W. B. 1995. Variation in the size, energy content, and biochemical composition of invertebrate eggs: correlates to the mode of larval development. Pp. 49–78 in *Ecology of Marine Invertebrate Larvae,* L. R. McEdward, ed. CRC Press, Boca Raton, FL.

Lawrence, J. M., J. B. McClintock, and A. Guille. 1984. Organic level and caloric content of eggs of brooding asteroids and an echinoid (Echinodermata) from Kerguelen (South Indian Ocean). *Int. J. Invertebr. Reprod. Dev.* **7:** 249–257.

Levin, L. A., and T. S. Bridges. 1995. Pattern and diversity in reproduction and development. Pp. 1–48 in *Ecology of Marine Invertebrate Larvae,* L. R. McEdward, ed. CRC Press, Boca Raton, FL.

Levitan, D. R. 1996. Predicting optimal and unique egg sizes in free-spawning marine invertebrates. *Am. Nat.* **148:** 174–188.

Manaster, B. J., and S. Manaster. 1975. Techniques for estimating allometric equations. *J. Morphol.* **147:** 299–308.

McClary, D. J., and P. V. Mladenov. 1990. Brooding biology of the sea star *Pteraster militaris* (O. F. Muller): energetic and histological evidence for nutrient translocation to brooded juveniles. *J. Exp. Mar. Biol. Ecol.* **142:** 183–199.

McClintock, J. B., and J. S. Pearse. 1986. Organic and energetic content of eggs and juveniles of Antarctic echinoids and asteroids with lecithotrophic development. *Comp. Biochem. Physiol.* **85A:** 341–345.

McEdward, L. R. 1997. Reproductive strategies of marine benthic invertebrates revisited: facultative feeding by planktotrophic larvae. *Am. Nat.* **150:** 48–72.

McEdward, L. R., and S. F. Carson. 1987. Variation in egg organic content and its relationship with egg size in the starfish *Solaster stimpsoni. Mar. Ecol. Prog. Ser.* **37:** 159–168.

McEdward, L. R., and F. S. Chia. 1991. Size and energy content of eggs from echinoderms with pelagic lecithotrophic development. *J. Exp. Mar. Biol. Ecol.* **147:** 95–102.

McEdward, L. R., and L. K. Coulter. 1987. Egg volume and energetic content are not correlated among sibling offspring of starfish: implications for life-history theory. *Evolution* **41:** 914–917.

McEdward, L. R., and D. A. Janies. 1997. Relationships among development, ecology, and morphology in the evolution of Echinoderm larvae and life cycles. *Biol. J. Linn. Soc.* **60:** 381–400.

McEdward, L. R., S. F. Carson, and F. S. Chia. 1988. Energetic content of eggs, larvae, and juveniles of *Florometra serratissima* and the implications for the evolution of crinoid life histories. *Int. J. Invertebr. Reprod. Dev.* **13:** 9–22.

Neter, J., W. Wasserman, and M. H. Kutner. 1990. *Applied Linear Statistical Models.* Irwin, Burr Ridge, IL.

Parsons, T. R., M. Takahashi, and B. Hargrave. 1984. *Biological Oceanographic Processes.* Pergamon, New York.

Pechenik, J. A. 1979. Role of encapsulation in invertebrate life histories. *Am. Nat.* **114:** 859–870.

Perron, F. E., and R. H. Carrier. 1981. Egg size distributions among closely related marine invertebrate species: Are they bimodal or unimodal? *Am. Nat.* **118:** 749–755.

Pianka, E. R. 1976. Natural selection of optimal reproductive tactics. *Am. Zool.* **16:** 775–784.

Sewell, M. A., and F. S. Chia. 1994. Reproduction of the intraovarian brooding apodid *Leptosynapta clarki* (Echinodermata; Holothuroidea) in British Columbia. *Mar. Biol.* **121:** 285–300.

Shilling, F. M., and D. T. Manahan. 1994. Energy metabolism and amino acid transport during early development of Antarctic and temperate echinoderms. *Biol. Bull.* **187:** 398–407.

Smith, C. C., and S. D. Fretwell. 1974. The optimal balance between size and number of offspring. *Am. Nat.* **108:** 499–506.

Stearns, S. C. 1977. The evolution of life history traits: a critique of the theory and a review of the data. *Annu. Rev. Ecol. Syst.* **8:** 145–171.

Strathmann, R. R. 1985. Feeding and nonfeeding larval development and life-history evolution in marine invertebrates. *Annu. Rev. Ecol. Syst.* **16:** 339–361.

Strathmann, R. R., and K. Vedder. 1977. Size and organic content of eggs of echinoderms and other invertebrates as related to developmental strategies and egg eating. *Mar. Biol.* **39:** 305–309.

Turner, R. L., and J. M. Lawrence. 1979. Volume and composition of echinoderm eggs: implications for the use of egg size in life-history models. Pp. 25–40 in *Reproductive Ecology of Marine Invertebrates,* S. E. Stancyk, ed. University of South Carolina Press, Columbia, SC.

Turner, R. L., and J. C. Rutherford. 1976. Organic, inorganic, and caloric composition of eggs, pentaculae, and adults of the brooding sea cucumber *Cucumaria curata* Cowles (Echinodermata: Holothuroidea). *J. Exp. Mar. Biol. Ecol.* **24:** 49–60.

Vance, R. R. 1973. On reproductive strategies in marine benthic invertebrates. *Am. Nat.* **107:** 339–352.

Reference: *Biol. Bull.* **200:** 51–58. (February 2001)

The Adaptive Bleaching Hypothesis: Experimental Tests of Critical Assumptions

ROBERT A. KINZIE III[1,*], MICHELLE TAKAYAMA[2], SCOTT R. SANTOS[3], AND MARY ALICE COFFROTH[3]

[1]*Zoology Department and Hawaii Institute of Marine Biology, University of Hawaii, Honolulu, Hawaii 96822;* [2]*Claremont McKenna College, Claremont, California 91711-6400; and* [3]*Department of Biological Sciences, The University at Buffalo, Buffalo, New York 14260-1300*

Abstract. Coral bleaching, the loss of color due to loss of symbiotic zooxanthellae or their pigment, appears to be increasing in intensity and geographic extent, perhaps related to increasing sea surface temperatures. The adaptive bleaching hypothesis (ABH) posits that when environmental circumstances change, the loss of one or more kinds of zooxanthellae is rapidly, sometimes unnoticeably, followed by formation of a new symbiotic consortium with different zooxanthellae that are more suited to the new conditions in the host's habitat. Fundamental assumptions of the ABH include (1) different types of zooxanthellae respond differently to environmental conditions, specifically temperature, and (2) bleached adults can secondarily acquire zooxanthellae from the environment. We present simple tests of these assumptions and show that (1) genetically different strains of zooxanthellae exhibit different responses to elevated temperature, (2) bleached adult hosts can acquire algal symbionts with an apparently dose-dependent relationship between the concentration of zooxanthellae and the rate of establishment of the symbiosis, (3) and finally, bleached adult hosts can acquire symbionts from the water column.

Introduction

Coral bleaching has increased in frequency, intensity, and geographical extent over the last two decades (Huppert and Stone, 1998). Concern is being expressed both by reef scientists (Brown, 1990, 1997; Goreau and Hayes, 1994) and the general public (Brown and Ogden, 1993; Wilson, 1999) about the future of the planet's reefs. Bleaching is a general term describing the loss of color in corals and other symbiotic reef invertebrates, usually due to the loss of their intracellular dinoflagellate symbionts, colloquially termed zooxanthellae. A reduction in the density or pigment content of symbiotic algae can be elicited by a variety of environmental factors including low (Goreau, 1964) and high (Nakano *et al.*, 1997) salinity, low and high levels of illumination—especially ultraviolet radiation (Banaszak and Trench, 1995; Lesser and Shick, 1989), disease (Kushmaro *et al.*, 1996; Rosenberg and Loya, 1999), and high (Iglesias-Prieto *et al.*, 1992; Warner *et al.*, 1996) and low (Steen and Muscatine, 1987; Kobluk and Lysenko, 1994) temperatures, as well as combinations of these factors. Although any of these may act on a local scale, widespread bleaching has generally been linked to high water temperatures at larger geographic scales, particularly those associated with El Niño-Southern Oscillation (ENSO) events (Glynn, 1984, 1991; Coffroth *et al.*, 1988). Most recently, the high sea surface temperatures (SSTs) of the summer of 1998 resulted in massive mortality of reefs in Okinawa, Tahiti, and Belau (ISRS, 1998; Hoegh-Guldberg, 1999; Tsuchiya, 1999). Such events may be becoming more frequent, and it has been suggested that they will become even more common if global warming persists and summer SSTs increase (Glynn, 1991). The loss, in association with such events, of zooxanthellae from a host may be partial or essentially complete. In the latter case recovery frequently does not occur, and the subsequent death of large numbers of symbiotic reef invertebrates can drastically alter the composition of the reef community (Goreau, 1992). Thus, the potential for increased incidence of bleaching may have negative effects on these ecosystems. Here we present results from experiments

Received 12 April 2000; accepted 14 November 2000.

* To whom correspondence should be addressed. E-mail: kinzie@hawaii.edu

relating zooxanthellar diversity to potential recovery from loss of symbionts.

Our original view of the symbiotic system of reef invertebrates and their algal symbionts was based on the idea that, at least in cnidarians, there was a single algal partner, *Symbiodinium microadriaticum* (Freudenthal) (Taylor, 1974). The elucidation of the complexities of coral and zooxanthellar systematics and taxonomy has made the picture more complex (Rowan and Powers 1991a; Knowlton *et al.*, 1992; Rowan, 1998). About a dozen named dinoflagellate taxa are currently known to associate with temperate and tropical invertebrates (Blank and Trench, 1985; Banaszak *et al.*, 1993; McNally *et al.*, 1994), but the diversity of the algae is probably much higher than this (Rowan, 1998; Darius *et al.*, 1998; Carlos *et al.*, 1999; Baillie *et al.*, 2000). A broad classification of zooxanthellae, based on sequence differences in the small subunit of the ribosomal nuclear genes (ssrDNA) has been proposed (Rowan and Powers, 1991a). This region of the genome contains a range of domains that have evolved at different rates; these domains are useful in characterizing phylogenetic relationships and have been used to characterize populations of zooxanthellae (Rowan, 1991; Rowan and Powers, 1991a, b; Sadler *et al.*, 1992; McNally *et al.*, 1994; Zardoya *et al.*, 1995; Carlos *et al.*, 1999). Analysis of restriction fragment length polymorphism (RFLP) of the ssrDNA has shown that zooxanthellae can be divided into at least four clades (Rowan and Powers, 1991a, b; Rowan, 1998), each probably including many species (Rowan, 1998). In addition, we now know that although some invertebrates may host a single algal clade, others can harbor at least three distinctly different types of zooxanthellae (Rowan and Knowlton, 1995). When more than one clade occurs, the balance among the population densities and the location of the clades within a host coral colony can be altered by changes in microscale environmental conditions (Rowan and Powers, 1991a; Rowan and Knowlton, 1995; Rowan *et al.*, 1997; Buddemeier, 1997). Furthermore, evidence suggests that the consortium may readily alter membership (Davy *et al.*, 1997; Hill and Wilcox, 1998; Belda-Baillie *et al.*, 1999; Bates, 2000). Thus, this symbiosis, which—at least in scleractinians—has persisted since the late Triassic (Stanley and Swart, 1995), appears to be both complex and mutable.

This combination of persistence over geological time scales (Kinzie and Buddemeier, 1996; Buddemeier *et al.*, 1997) and the apparently multifaceted array of symbiotic partnerships that may occur in some hosts (Rowan and Powers, 1991a; Baker and Rowan, 1997; Rowan, 1998) has given rise to the "adaptive bleaching hypothesis" (ABH) (Buddemeier and Fautin, 1993). This hypothesis posits that different algal partners within hosts shift in space—over a range of scales—and time, resulting in a symbiotic complex with many potential combinations, some being more functional under certain environmental conditions than others. According to the ABH, as environmental conditions change, the makeup of the symbiotic unit responds, tracking environmental changes by shuffling the algal membership of the symbiotic consortium. This hypothesis, presented 7 years ago, was explicitly stated so as to be experimentally testable, but despite substantial work both in the field and in laboratories around the world on causes and mechanisms of coral bleaching, surprisingly little effort has been devoted to such tests. Here we present the results of experimental tests of some fundamental assumptions underlying the ABH.

One assumption of the ABH is that the various algal types have physiological differences that are related to the etiology of bleaching. High temperatures are known to negatively affect zooxanthellae through degradation of photosystem II (Iglesias-Prieto *et al.*, 1992), but there has been little study of temperature effects on different zooxanthellar types. It has been known for some time that different zooxanthellae differ in their ability to grow in different hosts (Schoenberg and Trench, 1980) and to support growth and reproduction of the animal hosts (Kinzie and Chee, 1979; Fitt, 1985). Additionally, algae differ in their photosynthetic abilities (Chang *et al.*, 1983) and in their production of mycosporine-like amino acids in response to ultraviolet irradiance (Banaszak *et al.*, 2000).

A second assumption of the ABH is that bleached adult hosts can obtain new symbionts from the reef habitat and reestablish a symbiosis; that is, secondary acquisition of algae is possible. Many studies have demonstrated initial acquisition of newly settled aposymbiotic juveniles (Kinzie, 1974; Fitt and Trench, 1981; Muller-Parker and D'Elia, 1996; Benayahu *et al.*, 1989) or freely swimming planulae (Schwarz *et al.*, 1999). Numerous symbiotic reef invertebrates utilize horizontal transmission (i.e., each generation obtains its algal symbionts from the environment rather than maternally), showing that there must be substantial populations of potential zooxanthellae partners in reef waters (Goulet and Coffroth, 1997). These potential symbiotic partners exist outside of hosts and may occur in fish feces (Muller-Parker, 1984), be released from corals (Stimson and Kinzie, 1991; Hoegh-Guldberg *et al.*, 1987), or occur free living (Carlos *et al.*, 1999). Direct study of free-living zooxanthellae on reefs is difficult because we currently have very little data on their density, spatial distribution, or temporal behavior. We wished to determine whether bleached hosts could acquire symbiotic algae from populations of zooxanthellae in more natural situations. Although bleached adults have been shown to take up zooxanthellae under laboratory conditions, these experiments either used extremely high concentrations of zooxanthellae or the algae were injected into the coelenteron. The ability of adult cnidarians, once they have become bleached, to re-acquire symbionts from populations at concentrations likely to occur *in situ* is less studied (Franzisket, 1970).

Because understanding of the symbiotic unit is based on knowledge about the individual partners (Iglesias-Prieto *et al.*, 1992), we examined the algal partner under culture conditions to test the first assumption of the ABH. Although certain physiological traits of zooxanthellae can change in culture, (Stochaj and Grossman, 1997), use of well-characterized and controlled partners in isolation provides strong experimental control. In testing the other assumptions we used bleached hosts and naturally occurring populations of zooxanthellae.

Materials and Methods

Algal cultures

We refer to the zooxanthellae used in our experiments as "isolates," referencing the host from which they were isolated rather than a dinoflagellate species because the systematics and nomenclature of the entire group are in formative stages (Lee *et al.*, 1995). The isolates used are from a range of hosts (Table 1) and have been in culture for 4 to 20 years. Each culture was initiated with zooxanthellae from a single host. Because some hosts may harbor more than a single zooxanthellar genotype (Rowan and Powers, 1991a; Rowan and Knowlton, 1995; Rowan *et al.*, 1997; Buddemeier, 1997; Goulet and Coffroth, 1997; Carlos *et al.*, 2000), the isolates could have been initiated from more than a single genetic strain of zooxanthellae. In addition, the culturing process itself may exert strong selection on which genotypes thrive. To determine the number and types of clades present in the isolates as well as those that colonized bleached hosts, zooxanthellar genotypes were characterized using RFLP analysis of zooxanthellar ssrDNA (Rowan and Powers, 1991a). Cladal membership of the stock cultures was determined before the start of the experiment and one month after the experiments were terminated. The experimental cultures were analyzed at the end of the experiment. The resultant RFLP groups were classified by comparison with known zooxanthellae (*i.e., Symbiodinium* clades A, B, and C, Rowan and Powers, 1991b). Each stock culture contained a single algal clade (*sensu* Rowan and Powers, 1991a; Table 1). In the analysis, algal DNA extraction followed the protocols of Coffroth *et al.* (1992) and Goulet and Coffroth (1997), and RFLP analysis followed the protocols of Rowan and Powers (1991b).

Table 1

Isolates used in temperature tolerance experiments

Isolate designation	Clade	Host	Source
Cassiopea xamachana	A	Scyphozoan	Caribbean (*Symbiodinium microadriaticum*)
Montipora verrucosa	C	Scleractinian	Hawaii (*Symbiodinium kawagutii*)
Pocillopora damicornis	B	Scleractinian	Hawaii
Cassiopea KB8	A	Scyphozoan	Hawaii
Zoanthus sociatus	A	Zoanthid	Caribbean (*Symbiodinium pilosum*)
Tridacna gigas	A	Giant clam	Central Pacific
Aiptasia pulchella	B	Anemone	Hawaii (*Symbiodinium pulchrorum*)

Specific names in parentheses are species names given to zooxanthellae from these species (Blank and Trench, 1985, and Banaszak *et al.*, 1993).

Stock cultures were grown in f/2 medium (Guillard and Ryther, 1962) held at 25°C under $160\ \mu E\ m^{-2}\ s^{-1}$ ($160\ \mu mol\ m^{-2}\ s^{-1}$) on a 12:12 light-dark cycle. Cultures were transferred to new medium monthly. Periodically, cultures were treated with antibiotics (Polne-Fuller, 1991) but were not axenic. As discussed below, even though some isolates have been in culture for more than two decades, they retain their ability to infect their normal host.

Temperature sensitivity of different algal isolates

Aliquots from each cultured isolate were diluted to 1×10^4 cells ml^{-1} with sterile f/2 medium and put into twelve 150-ml culture tubes. Four tubes for each isolate were randomly assigned to one of the three temperature treatments. Zooxanthellae were exposed to temperatures of 27, 29, and 31°C over a 2-week period during which growth rates of the cultures were determined fluorometrically. Temperature treatments consisted of 28 tubes (4 per isolate and 7 isolates) in a test tube rack immersed in a 10-l water bath with an aquarium heater; an aquarium pump kept the water mixed. The three water baths were placed by an east-facing window that provided natural light. Solar radiation within the culture tubes (measured with a BioSpherical quantum meter, model QS100 with a 4π sensor inserted into a tube) ranged from $800\ \mu E\ m^{-2}\ s^{-1}$ in the morning to $100\ \mu E\ m^{-2}\ s^{-1}$ ($100\ \mu mol\ m^{-2}\ s^{-1}$) in the afternoon. Variability within a tube, from the top of the culture medium to the bottom of the tube, was about 30%. Each day, when tubes were read, the positions of the three water baths were rotated, and the positions of the tubes in the racks within each bath were shuffled. Aside from the temperature effects, growth was probably light-limited (unpubl. data) because we wished to reduce the potential for interaction between radiation stress and the experimental treatment. Growth was followed using *in vivo* fluorescence with a Turner Designs model 10 fluorometer. Fluorescence was measured daily starting at 0830. Racks were held in the dark at the experimental temperature for 30 min before fluorescence was read. Just before the reading, cultures in the tubes were dispersed with a vortex mixer to ensure even suspensions. Readings were taken from day 0, when inoculation took place, until day 13, when several of the cultures became difficult to disperse. At the termination of the experiment, 1-ml samples were preserved in Lugol's solution for cell enumeration with a Spiers-Levi eosinophil hemacytometer. Growth was measured as daily increase in fluorescence. We used growth rate as a measure of each strain's ability to tolerate high temperatures because faster growing zooxanthellae would directly correlate with a coral's recovery from bleaching. Population growth rate is generally considered to be a primary measure of fitness (Cole, 1954). At the end of the experiment, the cell counts were used to convert fluorescence to cell density. Specific growth rate (cell cell^{-1} d^{-1}) was determined from regressions of cell density over time. Growth rate was determined as the slope of the natural log of fluorescence over time. Subsequent analysis indicated that growth was logarithmic over this time period.

Ability of bleached hosts to acquire new symbionts

To demonstrate that secondary acquisition of algal symbionts by bleached adults can occur at low concentrations of zooxanthellae, we used the anemone *Aiptasia pulchella* as a model organism. This symbiotic anthozoan can be bleached completely and maintained indefinitely in this condition, making it particularly useful for reinfection studies. *Aiptasia* polyps were held individually in 50-ml beakers with 0.45-μm-filtered seawater (FSW) in the dark and fed *Artemia* nauplii once a week. After at least one year in the dark, bleached *Aiptasia* were moved to the light (natural sunlight through north-facing windows), and held in 0.22-μm FSW with weekly feeding of *Artemia* nauplii. No anemones were used in experiments unless they remained aposymbiotic in the light for at least 5 months. We have kept bleached *Aiptasia* for more than a year with no signs of zooxanthellae.

Bleached *Aiptasia* polyps were exposed to algal symbionts isolated from *A. pulchella* at concentrations that ranged from 10^5 to 10^0 cells ml^{-1}. Stock culture of the *A. pulchella* isolate (in culture for >20 years) was diluted to 1×10^5 cells ml^{-1} (verified by direct hemacytometer counts), then diluted to the different experimental concentrations with 0.22-μm FSW. The seawater in the beakers with the *Aiptasia* was replaced with the algal suspensions ($n = 3$ per treatment). Anemones remained in the suspension for 48 h, after which the suspension was removed and replaced with 0.22-μm FSW. Anemones were maintained in 0.22-μm FSW with the same light and feeding conditions, and were checked daily. We measured the time required for the zooxanthellae to proliferate to the point that the first brown color was visible. We termed this "visible infection." None of the controls ever showed signs of establishment of symbiosis with algae.

Existence of suitable strains of zooxanthellae in natural waters

Table 2

Exposure and infection of bleached Aiptasia pulchella *polyps*

Treatment	Number of *Aiptasia*	Number reinfected	Time to infection (days)	
			Mean	Range
Water table	9	6	41.2	5–76
Lagoon	3	3	54	41–61
Coral reef	10	3	28	18–46

To test the possibility that bleached adult hosts can acquire algal symbionts from natural waters, we exposed bleached *Aiptasia* to unfiltered seawater in three situations: on a seawater table in the laboratory, in the lagoon, and on the coral reef (Table 2). The anemones used in these treatments were randomly selected from the set of bleached *Aiptasia* described above. In the laboratory, 9 anemones were placed in individual uncovered 50-ml beakers that were then immersed in running unfiltered seawater (from the laboratory's system) on a water table that had a population of naturally occurring symbiotic *Aiptasia* polyps. For the field exposures, *Aiptasia* were placed in plastic tubes (*ca.* 50 ml) with coarse (5-mm-mesh) netting over the ends. A tube with 3 anemones was suspended at a depth of 0.5 m in the lagoon at a site that had moderate densities of symbiotic *Aiptasia*. A tube with 10 anemones was suspended 1 m above the reef at a site where no *Aiptasia* were visible. The anemones were held in these treatment conditions for 1 to 7 days, then returned to 0.22-μm FSW and kept in the conditions described in the previous section.

Results

Temperature sensitivity of different algal isolates

All seven isolates showed positive growth at all three temperatures, even at 31°C, which is often associated with bleaching events (Hoegh-Guldberg and Salvat, 1995; Davies *et al.*, 1997; Drollet *et al.*, 1995) (Fig. 1). Although all the zooxanthellae were able to grow at these three temperatures, there were significant differences among the isolates (Table 3). Clade B zooxanthellae showed decreasing growth at higher temperatures, whereas the single clade C isolate showed increasing growth rates at higher temperatures. Among the clade A isolates tested, the response to temperature was variable. Clade A isolates included the fastest growing isolate, which showed increasing growth rates with increasing temperatures, and the slowest growing isolate, which showed decreased growth rates at the higher temperatures. RFLP analysis of ssrDNA of the stock cultures both before and after the experiments verified that each stock culture contained a single algal clade. RFLP analysis of the experimental cultures at the termination of the experiment revealed that several of the treatments showed low levels of contamination with a second clade. Because the cladal type of the stock cultures did not change during this time and the growth rates of replicate isolates were similar, we conclude

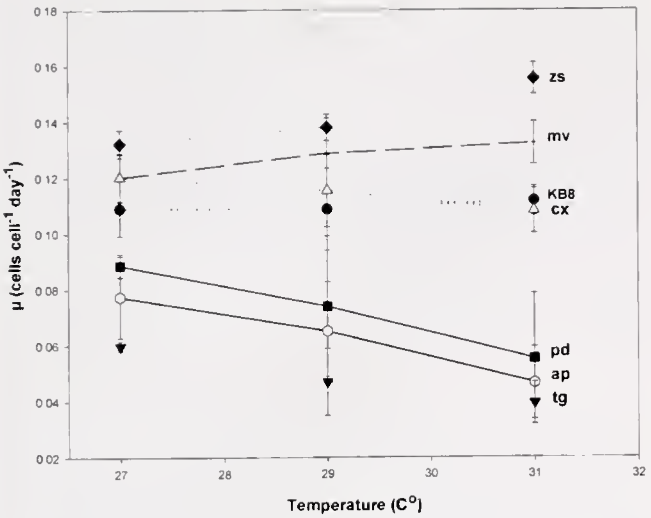

Figure 1. Growth rates of zooxanthellae isolated from 7 hosts at three temperatures. Points represent means; error bars represent ±1 SD ($n = 4$). Data were obtained as increase in fluorescence over the 13-day growth period. Growth was logarithmic during this time. Fluorescence units were converted to cell density at the end of the growth period. Host: zs—*Zoanthus sociatus*, mv—*Montipora verrucosa*, cx—*Cassiopea xamachana*, KB8—*Cassiopea* KB8, pd—*Pocillopora damicornis*, ap—*Aiptasia pulchella*, tg—*Tridacna gigas*. The dotted lines represent algae in clade A, the solid lines algae in clade B, and the dashed line the alga in strain C.

that the contamination was introduced at the termination of the experiments when samples were being processed for chlorophyll *a* measurements, cell counts, and photosynthetic rate studies, which was also when samples were taken for cladal identification of the experimental cultures.

Ability of bleached hosts to acquire new symbionts at low zooxanthellae concentrations

Symbiosis was successfully established at concentrations as low as 10 cells ml^{-1} (Fig. 2). Anemones exposed to higher concentrations became visibly infected sooner than those exposed to lower concentrations, suggesting that repopulation was due to multiple infection events during the 48-h exposure period and that the time to visible infection is dose-dependent. Although it is not known whether recovery following natural bleaching events comes from a residual population within the host or from free-living populations in reef waters, the minimum effective dose we demonstrated of 10 cells ml^{-1} implies that the concentrations of zooxanthellae repopulating bleached hosts could be almost undetectably low, yet still be sufficient for the bleached host to recover.

Table 3

Analysis of variance of growth rates by temperature for the seven zooxanthella isolates

Source	DF	SS	MS	*F*	*P*
Isolate	6	0.089	0.015	101.03	<0.0001
Temperature	2	0.001	0.000	3.32	0.043
Isolate × Temperature	12	0.006	0.000	3.31	0.0009

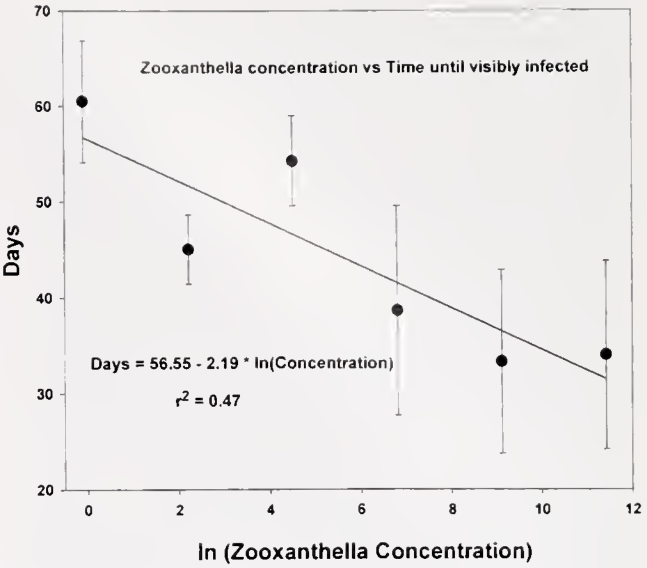

Figure 2. Time to infection of bleached *Aiptasia pulchella* polyps *vs.* concentration of zooxanthellae isolated from *Aiptasia pulchella.*

Existence of infective forms of zooxanthellae in natural waters

Two-thirds of the bleached anemones exposed to unfiltered seawater in the water table became infected, as did one-third of the bleached anemones suspended above the reef and all of the bleached anemones suspended in the lagoon (Table 2). All *Aiptasia* that became infected when exposed to natural seawater were found to harbor clade B zooxanthellae, which is the zooxanthellar clade normally found in this anemone. We emphasize that in both experiments, in which *Aiptasia* did regain zooxanthellae, none of the control anemones showed any sign of infection at the termination of the experiments, and the same polyps remain aposymbiotic 10 months later. There was no correlation between the time in the treatment and the time to infection.

Discussion

Temperature sensitivity of different algal isolates

The algal isolates we studied responded differently to the different temperatures. Some showed lowered growth rate with increasing temperature, some showed the same growth rate at all three temperatures, and two showed higher growth rates with increasing temperatures. Given that temperatures of 30°C, even when applied for short periods (2 days), can cause breakdown in the photosynthetic machinery of some zooxanthellae (Iglesias-Prieto *et al.*, 1992; Iglesias-Prieto, 1997; Warner *et al.*, 1996, 1999), the ability of these isolates to grow at 31°C, and for some to apparently show their highest growth rate at this temperature, is surprising. Also unexpected is the apparent lack of relationship between the habitat of the host and the temperature tolerance of the zooxanthellae. For example, algae from *Montipora verrucosa*, isolated from a coral from Hawaii, from relatively cool waters, showed increased growth rates at higher temperatures, whereas an isolate from the giant clam *Tridacna gigas*, typically found in shallow, more equatorial waters, was one of the most sensitive to high temperatures.

When the data are examined in terms of zooxanthellar clade, several trends are apparent. First, clade A zooxanthellae, for which we tested the largest number of isolates, had the widest range of growth rates. This is consistent with previous characterizations of clade A zooxanthellae as "weedy" (Rowan, 1998). Some clade A zooxanthellae showed increased growth with increasing temperatures (*e.g., Zoanthus sociatus*), others showed decreasing growth (*Tridacna gigas*), and isolates from the two species of *Cassiopea* showed little change in growth rate over the experimental temperature range. Clade B zooxanthellae, for which we tested only two isolates, showed less variability in response to temperature, with both isolates growing slower at higher temperatures. Growth rates in the single clade C isolate tested showed a slightly higher growth rate at higher temperatures and was the second fastest growing of all the isolates we tested. The results from clade A zooxanthellae demonstrate that, at least in some algal groups, the variability in physiological response within a clade may be as great as or greater than between clades. Further, these data suggest that the potential for selection for the most ecologically suitable taxon or genotype could occur within a clade. If this proves to be generally true, it might be impossible to detect ecologically significant shifts in the algal complement of an animal host by using the identification techniques we employed in this study.

Ability of bleached hosts to reestablish symbiosis at low zooxanthellae concentrations

Even though the isolate used in these experiments has been in culture for more than two decades, it retained the ability to successfully reestablish a symbiosis with its normal host, even when at exceedingly low densities. Thus, although some physiological changes may occur in the course of the culturing process (Stochaj and Grossman, 1997), the basic mechanisms of recognition and entry to host cells appear to remain intact. The dose-response relationship demonstrated here is ecologically important because it suggests that the chances of secondary acquisition, such as may occur during recovery from bleaching, will be greater at sites where zooxanthellae are abundant in the waters overlying the reef (and presumably their hosts). This implies an effect of spatial scale and community composition in the probability of recovery from different sorts of bleaching events. The experiments described here were done in closed containers, so the concentration at which a 48-h exposure results in infection may not easily translate to concentrations in the water overlying the reef.

Existence of infective forms of zooxanthellae in natural waters

On the reef, water motion is an important factor in ameliorating the effects of low concentration of nutrients on algal growth (Larned and Atkinson, 1997). The same phenomenon is likely to be important in exposing bleached animals to free-living zooxanthellae, potentially resulting in reestablishing the symbiosis even when zooxanthellae are at very low concentrations. It is noteworthy that on the reef at the Hawaii Institute of Marine Biology pier where water motion is greatest, the density of *Aiptasia* is much lower than in the calm lagoon, and yet the mean time to establishment of the symbiosis was the shortest in this location. However, the percentage of polyps that secondarily acquired zooxanthellae was lowest at the reef site. These apparently conflicting results could mean that in open waters, free-living zooxanthellae are sometimes at very low densities and perhaps patchily distributed. Because all 10 anemones were within the same tube, it is also possible that only one took up algae from the water column and the rest somehow obtained their zooxanthellae from this individual.

Conclusion

In summary, we have provided experimental tests of fundamental assumptions of the ABH. The differential growth rates of the isolates in response to increasing temperatures suggest that different responses to a factor suspected as a cause of recent large-scale bleaching events do exist among zooxanthellae. Furthermore, the variability in this response can be as great within a clade as between zooxanthellae from different clades. The uptake of zooxanthellae *in situ* by bleached hosts demonstrates that secondary acquisition can occur, and the results of the laboratory studies show that new symbionts can be acquired when the alga concentrations are very low. These findings address important aspects of the ABH. The assumptions tested here are necessary but not sufficient conditions of the ABH. In addition, the lack of clear cladal patterns in the temperature response demonstrates that the ability to withstand high temperatures is not correlated with membership in a specific clade and implies that finer genetic differentiation will be required to understand the dynamics of these symbionts. A clearer understanding of the significance of the different temperature responses and the bearing these differences have on the ABH will require studies of intact symbioses.

Acknowledgments

We thank H. Lasker and E. F. Cox for comments on the manuscript. This study was partly supported by Grants-in-Aid for Scientific Research from the Ministry of Education, Science, Sports and Culture of Japan, and the A. Y. Yoshinaga foundation (to RAKIII); REU support from NSF OCE-96-22782 (to MT); an NSF minority fellowship (to SRS); and NSF OCE-95-30057 (to MAC). Heather Reed assisted with both laboratory and field aspects of the study.

Literature Cited

Baillie, B. K., C. A. Belda-Baillie, V. Silvestre, M. Sisin, A. V. Gomez, E. D. Gomez, V. Monje. 2000. Genetic variation in *Symbiodinium* isolates from giant clams based on random-amplified-polymorphic DNA (RAPID) patterns. *Mar. Biol.* **136:** 829–836.

Baker, A. C., and R. Rowan. 1997. Diversity of symbiotic dinoflagellates (zooxanthellae) in scleractinian corals of the Caribbean and eastern Pacific. *Proceedings of the Eighth International Coral Reef Symp. (Panama)* **2:** 1301–1306.

Banaszak, A. T., and R. K. Trench. 1995. Effects of ultraviolet (UV) radiation on marine microalgal-invertebrate symbioses. I. Response of the algal symbionts in culture and *in hospite*. *J. Exp. Mar. Biol. Ecol.* **194:** 213–232.

Banaszak, A. T., T. R. Iglesias-Prieto, and R. K. Trench. 1993. *Scrippsiella velellae* sp. nov. (Peridiniales) and *Gloeodinium viscum* sp. nov. (Phytodiniales), dinoflagellate symbionts of two hydrozoans (Cnidaria). *J. Phycol.* **29:** 517–528.

Banaszak, A. T., T. C. LaJeunesse, and R. K. Trench. 2000. The synthesis of mycosporine-like amino acids (MAAs) by cultured, symbiotic dinoflagellates. *J. Exp. Mar. Biol. Ecol.* **249:** 219–233.

Bates, A. 2000. The intertidal distribution of two algal symbionts hosted by *Anthopleura xanthogrammica* (Brandt 1935). *J. Exp. Mar. Biol. Ecol.* **249:** 249–262.

Belda-Baillie, C. A., M. Sison, V. Silvestre, K. Villamor, V. Monje, E. D. Gomez, and B. K. Baillie. 1999. Evidence for changing symbiotic algae in juvenile tridacnids. *J. Exp. Mar. Biol. Ecol.* **241:** 207–221.

Benayahu, Y., Y. Achituv, and T. Berner. 1989. Metamorphosis of an octocoral primary polyp and its infection by algal symbiosis. *Symbiosis* **7:** 159–169.

Blank, R. J., and R. K. Trench. 1985. Speciation and symbiotic dinoflagellates. *Science* **229:** 656–658.

Brown, B. E. (Ed). 1990. Coral bleaching: special issue. *Coral Reefs* **8:** 153–232.

Brown, B. E. 1997. Coral bleaching: causes and consequences. *Coral Reefs* **16** Suppl.: S129–S138.

Brown, B. E., and J. C. Ogden. 1993. Coral bleaching. *Sci. Am.* **268:** 64–70.

Buddemeier, R. W. 1997. Making light work of adaptation. *Nature* **388:** 65–73.

Buddemeier, R. W., and D. G. Fautin. 1993. Coral bleaching as an adaptive mechanism. *BioScience* **43:** 320–326.

Buddemeier, R. W., D. G. Fautin, and J. R. Ware. 1997. Acclimation, adaptation and algal symbiosis in reef-building scleractinian corals. *Proceedings of the Sixth International Conference on Coelenterate Biology*, Noordwijkerhout, The Netherlands, 1995 **1:** 3–10.

Carlos, A. A., B. K. Baillie, M. Kawachi, and T. Maruyama. 1999. Phylogenetic position of *Symbiodinium* (Dinophyceae) isolates from Tridacnids (Bivalvia), Cardids (Bivalvia), a sponge (Porifera), a soft coral (Anthozoa), and a free-living strain. *J. Phycol.* **35:** 1054–1062.

Carlos, A. A., B. K. Baillie, and T. Maruyama. 2000. Diversity of dinoflagellate symbionts (zooxanthellae) in a host individual. *Mar. Ecol. Prog. Ser.* **195:** 93–100.

Chang, S. S., B. B. Prézelin, and R. K. Trench. 1983. Mechanisms of photoadaptation in three strains of the symbiotic dinoflagellate *Symbiodinium microadriaticum*. *Mar. Biol.* **76:** 219–229.

Coffroth, M. A., H. R. Lasker, and J. Oliver. 1988. Coral mortality outside of the Eastern Pacific during 1982–83: Relationship to El Niño. Pp. 141–182 in *Some Ecological Consequences of the 1982/1983 El Niño Event to Marine Life*. P. W. Glynn, ed. Elsevier, Amsterdam.

Coffroth, M. A., H. R. Lasker, M. E. Diamond, J. A. Bruenn, and E. Bermingham. 1992. DNA fingerprints of a gorgonian coral: a method for detecting clonal structure in a vegetative species. *Mar. Biol.* **114:** 317–325.

Cole, L. C. 1954. The population consequences of life history phenomena. *Q. Rev. Biol.* **29:** 103–135.

Darius, H. T., C. Dauga, P. A. D. Grimont, E. Chungue, and P. V. Martin. 1998. Diversity in symbiotic dinoflagellates (Pyrrophyta) from seven scleractinian coral species: Restriction enzyme analysis of small subunit ribosomal RNA genes. *J. Eukaryot. Microbiol.* **45:** 619–627.

Davies, J. M., R. P. Dunne, and B. E. Brown. 1997. Coral bleaching and elevated sea-water temperature in Milne Bay Province, Papua New Guinea, 1996. *Mar. Freshw. Res.* **48:** 513–516.

Davy, S. K., I. A. N. Lucas, and J. R. Turner. 1997. Uptake and persistance of homologous and heterologous zooxanthellae in the temperate sea anemone *Cereus pedunculatus* (Pennant). *Biol. Bull.* **192:** 208–216.

Drollet, J., H. M. Faucon, and P. M. V. Martin. 1995. Elevated sea-water temperature and solar UV-B flux associated with two successive coral mass bleaching events in Tahiti. *Mar. Freshw. Res.* **46:** 1153–1157.

Fitt, W. K. 1985. Effect of different strains of the zooxanthella *Symbiodinium microadriaticum* on growth and survival of their coelenterate and molluscan hosts. *Proceedings of the Fifth International Coral Reef Congress* (Tahiti) **6:** 131–136.

Fitt, W. K., and R. K. Trench. 1981. Spawning, development, and acquisition of zooxanthellae by *Tridacna squamosa* (Mollusca, Bivalvia). *Biol. Bull.* **161:** 213–235.

Franzisket, L. 1970. The atrophy of hermatypic reef corals maintained in darkness and their subsequent regeneration in light. *Int. Rev. Gesamten Hydrobiol.* **55:** 1–12.

Glynn, P. W. 1984. Widespread coral mortality and the 1982–1983 El Niño warming event. *Environ. Conserv.* **11:** 133–146.

Glynn, P. W. 1991. Coral reef bleaching in the 1980's and possible connections with global warming. *Trends Ecol. Evol.* **6:** 175–179.

Goreau, T. F. 1964. Mass expulsion of zooxanthellae from Jamaican reef communities after Hurricane Flora. *Science* **145:** 383–386.

Goreau, T. J. 1992. Bleaching and reef community change in Jamaica: 1951–1991. *Am. Zool.* **32:** 683–695.

Goreau, T. J., and R. L. Hayes. 1994. Coral bleaching and ocean "hot spots." *Ambio* **23:** 176–180.

Goulet, T. L., and M. A. Coffroth. 1997. A within colony comparison of zooxanthella genotypes in the Caribbean gorgonian *Plexaura kuna*. *Proceedings of the Eighth International Coral Reef Symposium (Panama)* **2:** 1331–1334.

Guillard, R. R. L., and J. H. Ryther. 1962. Studies of marine planktonic diatoms. I: *Cyclotella nana* Hustedt and *Detonula confervacea* (Cleve) Gran. *Can. J. Microbiol.* **8:** 229–239.

Hill, M., and T. Wilcox. 1998. Unusual mode of symbiont repopulation

FEB 26 2001

after bleaching in *Anthosigmella varians:* acquisition of different zooxanthellae strains. *Symbiosis* **25:** 279–289.

Hoegh-Guldberg, O. 1999. *Climate Change, Coral Bleaching and the Future of the World's Coral Reefs.* Greenpeace, Washington DC.

Hoegh-Guldberg, O., and B. Salvat. 1995. Periodic mass-bleaching and elevated sea temperatures: bleaching of outer reef slope communities in Moorea, French Polynesia. *Mar. Ecol. Prog. Ser.* **121:** 181–190.

Hoegh-Guldberg, O., L. R. McCloskey, and L. Muscatine. 1987. Expulsion of zooxanthellae by symbiotic cnidarians from the Red Sea. *Coral Reefs* **5:** 201–204.

Huppert, A., and L. Stone. 1998. Chaos in the Pacific's coral reef bleaching cycle. *Am. Nat.* **152:** 447–459.

Iglesias-Prieto, R. 1997. Temperature-dependent inactivation of photosystem II in symbiotic dinoflagellates. *Proceedings of the Eighth International Coral Reef Symposium (Panama)* **2:** 1313–1318.

Iglesias-Prieto, R., J. L. Matta, W. A. Robis, and R. K. Trench. 1992. Photosynthetic response to elevated temperature in the symbiotic dinoflagellate *Symbiodinium microadriaticum* in culture. *Proc. Nat. Acad. Sci. USA* **89:** 10302–10305.

ISRS (International Society for Reef Studies). 1998. Statement on bleaching. *Reef Encounter* **24:** 19–20.

Kinzie, R. A. 1974. Experimental infection of aposymbiotic gorgonian polyps with zooxanthellae. *J. Exp. Mar. Biol. Ecol.* **15:** 335–345.

Kinzie, R. A. III, and R. W. Buddemeier. 1996. Reefs Happen. *Global Change Biol.* **2:** 479–494.

Kinzie, R. A. III, and G. S. Chee. 1979. The effect of different zooxanthellae on the growth of experimentally reinfected hosts. *Biol. Bull.* **156:** 315–327.

Knowlton, N., E. Weil, L. A. Weight, and H. M. Guzmán. 1992. Sibling species in *Montastrea annularis,* coral bleaching, and the coral climate record. *Science* **255:** 330–333.

Kobluk, D. R., and M. A. Lysenko. 1994. "Ring" bleaching in southern Caribbean *Agaricia agaricites* during rapid water cooling. *Bull. Mar. Sci.* **54:** 142–150.

Kushmaro, A., Y. Loya, M. Fine, and E. Rosenberg. 1996. Bacterial infection and coral bleaching. *Nature* **380:** 396.

Larned, S. T., and M. J. Atkinson. 1997. Effects of water velocity on NH_4 and PO_4 uptake and nutrient-limited growth in the macroalga *Dictyosphaeria cavernosa. Mar. Ecol. Prog. Ser.* **157:** 295–302.

Lee, J. J., C. G. Wray, and C. Lawrence. 1995. Could foraminiferal zooxanthellae be derived from environmental pools contributed by different coelenterate hosts? *Acta Protozool.* **34:** 75–85.

Lesser, M. P., and J. M. Shick. 1989. Effects of irradiance and ultraviolet radiation on photoadaptation in the zooxanthellae of *Aiptasia pallida:* primary production, photo-inhibition, and enzymic defenses against oxygen toxicity. *Mar. Biol.* **102:** 243–255.

McNally, K. L., N. S. Govind, P. E. Thomé, and R. K. Trench. 1994. Small-subunit ribosomal DNA sequence analysis and a reconstruction of the inferred phylogeny among symbiotic dinoflagellates (Pyrrophyta). *J. Phycol.* **30:** 316–329.

Muller-Parker, G. 1984. Dispersal of zooxanthellae on coral reefs by predators on cnidarians. *Biol. Bull.* **167:** 159–167.

Muller-Parker, G., and C. F. D'Elia. 1996. Interactions between corals and their symbiotic algae. Pp. 96–113 in *Life and Death of Coral Reefs,* C. Birkland, ed. Chapman and Hall, New York.

Nakano, Y., K. Yamazato, H. Masuhara, and S. Ito. 1997. Responses of Okinawan reef-building corals to artificial high salinity. *Galaxia* **13:** 181–195.

Polne-Fuller, M. 1991. A novel technique for preparation of axenic cultures of *Symbiodinium* (Pyrrophyta) through selective digestion by amoebae. *J. Phycol.* **27:** 552–554.

Rosenberg, E., and Y. Loya. 1999. *Vibrio shiloi* is the etiological (causative) agent of *Oculina patagonica* bleaching: General implications. *Reef Encounter* **25:** 8–10.

Rowan, R. 1991. Molecular systematics of symbiotic algae. *J. Phycol.* **27:** 661–666.

Rowan, R. 1998. Diversity and ecology of zooxanthellae on coral reefs. *J. Phycol.* **34:** 407–417.

Rowan, R., and N. Knowlton. 1995. Intraspecific diversity and ecological zonation in coral-algal symbiosis. *Proc. Nat. Acad. Sci.* **92:** 2850–2853.

Rowan, R., and J. D. Powers. 1991a. A molecular genetic classification of zooxanthellae and the evolution of animal-algal symbioses. *Science* **251:** 1348–1351.

Rowan, R., and J. D. Powers. 1991b. Molecular genetic identification of symbiotic dinoflagellates (zooxanthellae). *Mar. Ecol. Prog. Ser.* **71:** 65–73.

Rowan, R., N. Knowlton, A. Baker, and J. Jara. 1997. Landscape ecology of algal symbionts creates variation in episodes of coral bleaching. *Nature* **388:** 265–269.

Sadler, L. A., K. L. McNally, N. S. Govind, C. F. Brunk, and R. K. Trench. 1992. The nucleotide sequence of the small subunit ribosomal RNA gene from *Symbiodinium pilosum,* a symbiotic dinoflagellate. *Curr. Genet.* **21:** 409–416.

Schoenberg, D. A., and R. K. Trench. 1980. Genetic variation in *Symbiodinium (=Gymnodinium) microadriaticum* Freudenthal, and specificity in its symbiosis with marine invertebrates. III. Specificity and infectivity of *Symbiodinium microadriaticum. Proc. R. Soc. Lond. B* **207:** 445–460.

Schwarz, J. A., D. A. Krupp, and V. M. Weis. 1999. Late larval development and onset of symbiosis in the scleractinian coral *Fungia scutaria. Biol. Bull.* **196:** 70–79.

Stanley, G. D. Jr., and P. K. Swart. 1995. Evolution of the coral-zooxanthellae symbiosis during the Triassic: A geochemical approach. *Paleobiology* **21:** 179–199.

Steen, R. G., and L. Muscatine. 1987. Low temperature evokes rapid exocytosis of symbiotic algae by a sea anemone. *Biol. Bull.* **172:** 246–263.

Stimson, J., and R. A. Kinzie III. 1991. The temporal pattern and rate of release of zooxanthellae from the reef coral *Pocillopora damicornis* (Linnaeus) under nitrogen-enrichment and control conditions. *J. Exp. Mar. Biol. Ecol.* **153:** 63–74.

Stochaj, W. R., and A. R. Grossman. 1997. Differences in the protein profiles of cultured and endosymbiotic *Symbiodinium* sp. (Pyrrophyta) from the anemone *Aiptasia pallida* (Anthozoa). *J. Phycol.* **33:** 44–58.

Taylor, D. L. 1974. Symbiotic marine algae: taxonomy and biological fitness. Pp. 245–262 in *Symbiosis in the Sea,* W. B. Vernberg, ed. University of South Carolina Press, Columbia, SC.

Tsuchiya, M. 1999. Warning from the coral reefs. *Galaxia* **1:** 27–29 (in Japanese and English).

Warner, M. E., W. K. Fitt, and G. W. Schmidt. 1996. The effects of elevated temperature on the photosynthetic efficiency of zooxanthellae *in hospite* from four different species of reef coral: a novel approach. *Plant Cell Environ.* **19:** 291–299.

Warner, M. E., W. K. Fitt, and G. W. Schmidt. 1999. Damage to photosystem II in symbiotic dinoflagellates: A determinant of coral bleaching. *Proc. Nat. Acad. Sci.* **96:** 8007–8012.

Wilson, A. D. 1999. Coral reefs: A threatened resource. *Sea Technol.* **40:** 10–15.

Zardoya, R., E. Costas, V. Lopez-Rodas, A. Garrido-Pertierra, and J. M. Bautisa. 1995. Revised dinoflagellate phylogeny inferred from molecular analysis of large-subunit ribosomal RNA gene sequences. *J. Mol. Evol.* **41:** 637–645.

Reference: *Biol. Bull.* **200:** 59–66. (February 2001)

Role of Aerobic and Anaerobic Circular Mantle Muscle Fibers in Swimming Squid: Electromyography

IAN K. BARTOL

Department of Organismic Biology, Ecology, and Evolution, University of California, Los Angeles, 621 Charles E. Young Drive South, Los Angeles, California 90095-1606

Abstract. Circular mantle muscle of squids and cuttlefishes consists of distinct zones of aerobic and anaerobic muscle fibers that are thought to have functional roles analogous to red and white muscle in fishes. To test predictions of the functional role of the circular muscle zones during swimming, electromyograms (EMGs) in conjunction with video footage were recorded from brief squid *Lolliguncula brevis* (5.0–6.8 cm dorsal mantle length, 10.9–18.3 g) swimming in a flume at speeds of 3–27 cm s^{-1}. In one set of experiments, in which EMGs were recorded from electrodes intersecting both the central anaerobic and peripheral aerobic circular mantle muscles, electrical activity was detected during each mantle contraction at all swimming speeds, and the amplitude and frequency of responses increased with speed. In another set of experiments, in which EMGs were recorded from electrodes placed in the central anaerobic circular muscle fibers alone, electrical activity was not detected during mantle contraction until speeds of about 15 cm s^{-1}, when EMG activity was sporadic. At speeds greater than 15 cm s^{-1}, the frequency of central circular muscle activity subsequently increased with swimming speed until maximum speeds of 21–27 cm s^{-1}, when muscular activity coincided with the majority of mantle contractions. These results indicate that peripheral aerobic circular muscle is used for low, intermediate, and probably high speeds, whereas central anaerobic circular muscle is recruited at intermediate speeds and used progressively more with speed for powerful, unsteady jetting. This is significant because it suggests that there is specialization and efficient use of locomotive muscle in squids.

Received 16 June 2000; accepted 10 October 2000. E-mail: ikbartol@lifesci.ucla.edu

Introduction

Fishes have three myotomal muscle types, that is, red, pink, and white fibers, that are structurally, metabolically, and functionally distinct. The red muscle is characterized by a high myoglobin content, extensive capillary beds, a high density of mitochondria, and high levels of oxidative enzymes (Bone, 1966; 1978). It operates aerobically, fatigues slowly, has low rates of activation and relaxation, and has low shortening velocities (Johnston *et al.*, 1977). White muscle is characterized by a high myofibrillar density, a low content of mitochondria, poor blood supply, and high levels of glycolytic enzymes (Flitney and Johnston, 1979). It operates anaerobically, fatigues rapidly, has high rates of activation and relaxation, and has high shortening velocities (Curtin and Woledge, 1988). Pink muscle is intermediate in structure, metabolism, and contractile properties between red and white muscle (Johnston *et al.*, 1977; Coughlin *et al.*, 1996). Generally, red muscle is recruited for the lowest, steady, undulatory swimming speeds (Rome *et al.*, 1984); pink muscle is recruited at intermediate swimming speeds (Johnston *et al.*, 1977); both red and pink muscle are recruited at maximum steady swimming speeds (Coughlin *et al.*, 1996); and white muscle is recruited at higher swimming speeds when swimming becomes unsteady (Rome *et al.*, 1984; Jayne and Lauder, 1996).

Squids and cuttlefishes have muscle types in the mantle musculature similar to red and white muscle. The mantle musculature of cephalopods functions as a constant volume system with a three-dimensional array of tightly bundled muscles commonly called a muscular-hydrostat (Kier and Smith, 1985; Smith and Kier, 1989). During jet propulsion, circular muscles within the mantle contract, which consequently decreases mantle diameter and forces intramantle water out of the funnel. Because changes in mantle length during contraction are negligible and the mantle musculature is constant in volume, contraction of circular muscle results in concomitant thickening of the mantle wall. Obliquely oriented collagen fibers traversing the thickness of the mantle wall are strained and store energy. This energy together with contraction of radially oriented muscle fibers, which extend from the inner to outer surface of the mantle, power mantle refilling (Gosline and Shadwick, 1983; Gosline et al., 1983; Kier, 1988). The circular muscle responsible for mantle contraction within this system consists of three anatomically and metabolically distinct muscle layers when viewed in cross section: an inner, outer, and middle layer (Bone *et al.*, 1981; Mommsen *et al.*, 1981). The inner and outer (peripheral) layers are thin and rich in mitochondria; they have high succinic dehydrogenase (SDH) activity, a high ratio of oxidative to glycolytic enzyme activity, and heavy vascularization. The middle (central) layer is thick and poor in mitochondria; it has low SDH activity, a high ratio of glycolytic to oxidative enzyme activity, and sparse vascularization. Because of these structural and biochemical differences, Bone *et al.* (1981) and Mommsen *et al.* (1981) suggested that the inner and outer layers are analogous to aerobic red muscle in fish and are used for slow, steady swimming and rhythmic, respiratory contractions, while the central layer is analogous to anaerobic white muscle and is used during burst swimming, escape, and capture events. This is consistent with the classic view (Wilson, 1960) that squid switch between quiet "respiratory" jetting and giant fiber escape responses. However, O'Dor (1982, 1988a) and Bartol (1999) have reported fully graded swimming in squid swim-tunnel studies, and Otis and Gilly (1990) and Preuss and Gilly (2000) have shown that interplay between giant and non-giant axon systems, which innervate the circular mantle musculature of squid, allow for considerable flexibility in jetting behavior and may facilitate smooth speed transitions.

Although peripheral and central circular muscle have several structural and biochemical similarities to red and white muscle in fishes, the functional roles of circular muscle types during swimming in squids and cuttlefishes remain unresolved. Bone *et al.* (1994) found large-amplitude electromyographic activity in the mantle of cuttlefish *Sepia officinalis* during escape jetting and concluded that both the central anaerobic and peripheral aerobic circular muscles were active. However, since electrodes were not inserted exclusively in either muscle layer, the functional role of the circular muscle types is still uncertain. Accumulations of metabolic end products within mantle musculature of squids during routine behavior, exercise, and after exercise have been the focus of many studies (Hochachka *et al.*, 1975; Grieshaber and Gade, 1976; Storey and Storey, 1978; Fields and Quinn, 1981; Pörtner *et al.*, 1991, 1993; Finke *et al.*, 1996), but no distinctions were made in those studies between end products found within the various layers of circular muscle. On the basis of mantle pressure measurements, O'Dor (1988b) concluded that both types of circular muscle fiber must be active in *Illex illecebrosus* at subcritical swimming speeds to generate the necessary swimming power. Furthermore, Finke *et al.* (1996) suggested that *Lolliguncula brevis*, which tends to oscillate between high and low muscular activity at increased swimming velocities, relies on both types of circular muscle fiber at high speeds. However, once again, direct documentation of the functional roles of the two circular mantle muscle fibers is lacking.

In this study electromyograms (EMGs) were collected in conjunction with video footage to determine the role of the peripheral aerobic and central anaerobic circular muscle layers in brief squid *Lolliguncula brevis* swimming over a range of speeds. Two experiments are reported: in one, EMG activity was recorded from electrodes traversing both peripheral and central circular muscle layers; in the other, EMG activity was recorded from electrodes embedded exclusively in the central circular muscle layer. It was not possible to embed electrodes solely in peripheral circular muscle because the muscle layer was too thin (~0.1 mm) for reliable placement. However, by comparing results from the two experiments, it was possible to postulate the functional roles of the circular muscle zones.

Materials and Methods

Experimental animals

In August–October 1998, brief squid *Lolliguncula brevis* (Blainville) were captured by trawl within embayments along the seaside of Virginia's Eastern Shore and within the York River, Virginia. Squid captured along the Eastern Shore of Virginia were transported to the Virginia Institute of Marine Science (VIMS) Eastern Shore Laboratory in Wachapreague, Virginia; squid captured in the York River were transported to the VIMS main campus in Gloucester Point, Virginia. Squid were kept alive in the field using 120-quart coolers equipped with filtration and aeration systems, which were powered by 12-V, sealed, gel-cell batteries. At Wachapreague and Gloucester Point, squid were kept in flow-through raceway tanks for at least one week prior to experimentation and fed a diet of grass shrimp *Palaemonetes pugio*. Experiments on 12 squid (3.5–7.8 cm dorsal mantle length [DML], 4.3–27.6 g) were performed, but results from only 5 squid (5.0–6.8 cm DML, 10.9–18.3 g) are reported here. Some squid were eliminated from consideration because of one or more of the following: (1) the location of the electrodes in the muscle was somewhat uncertain, (2) ambient electrical noise was excessive, (3) the squid was not cooperative in swim tunnels.

Electromyogram (EMG) recordings

Disposable, paired hook-wire electrodes (150-μm-gauge insulated nickel alloy, Nicolet Biomedical, Madison, WI) were used for EMG recordings. The hook portions of the manufactured electrode wires were too large for recording EMGs from the peripheral and central circular muscle layers, which were about 0.1 mm and 1.0 mm thick, respectively. Therefore, the hook portions of the electrodes were modified so that they were 1.0 mm in total length with 0.5 mm of insulation removed at the tip. The squid were anesthetized (~2 min) in an isotonic solution of $MgCl_2$ (7.5% $MgCl_2 \cdot 6H_2O$) and seawater (Messenger *et al.*, 1985), and each pair of electrodes was inserted obliquely, using a hypodermic needle, into the lateral mantle wall at a point 60% of the mantle length from posterior. Electrode spacing within the muscle was about 2–6 mm. Insertion of two pairs of electrodes for simultaneous recording from different muscle groups was attempted on several occasions, but these attempts were unsuccessful because dissections revealed that at least one pair of electrodes was not in target muscle fibers or the two sets of electrodes interfered with swimming. Thus, recordings from only one pair of electrodes during each experiment are reported.

The electrode pair from which EMGs were recorded was embedded in either the central circular muscle layer or both the central circular muscle layer and the peripheral circular muscle layer adjacent to the skin. It was not possible to embed electrodes exclusively in the peripheral layer of circular muscle because it was too thin (~0.1 mm) for hook-wire electrodes. Fine wire needle electrodes like those described in Kier *et al.* (1989), which allow for very precise electrode placement, were not used because of difficulties associated with anchoring the electrodes to the mantle of *L. brevis* and the high probability that anchoring tools (*e.g.*, clamping blocks) would disrupt swimming. During electrode placement, no attempt was made to avoid radial muscles, which extend from the inner to outer mantle surface and partition the circular muscle into 0.1-mm sections. Electrical activity of radial muscles, however, did not obscure electrical activity from the circular muscle layers, because radial muscles are active during mantle expansion, whereas circular muscles are active during mantle contraction (Gosline and Shadwick, 1983; Gosline *et al.*, 1983). To help ensure reliable placement of electrodes, many practice insertions were performed on preserved squid prior to the experiments, and depth references were marked on hypodermic needles used for implantation. Sufficient slack in the electrode wires was provided so that anchoring electrodes at other locations along the body was not necessary to prevent dislodgment.

After successful implantation, squid were placed in a 20 × 10 × 10 cm holding section within a 16-l recirculating water tunnel (Vogel and LaBarbera, 1978) filled with aerated seawater (24‰, 22 °C) and allowed to recover from surgery at low flow velocity (1 cm s^{-1}). Flow velocity in the tunnel was controlled using two propellers arranged in a rotor-stator configuration and a ¼ hp variable-speed motor, which was shielded using aluminum sheeting to reduce radiated electromagnetic noise. A ground electrode was attached to a downstream collimator within the flume. The ground electrode together with the embedded bipolar hook-wire electrodes, which were attached to insulated Nicolet micrograbbers, were plugged into a two-channel differential amplifier using Nicolet DIN 42 802 connectors. The differential amplifier was part of a Nicolet Compass II PortaBook system, which is designed to record electromyograms and somatosensory, auditory, and visual evoked potentials from human patients. The PortaBook was used to record, amplify, and filter electromyograms collected at various frequencies. For this study, EMGs were collected in the free-run mode using a bandpass filter of 20–10,000 Hz, which was the most effective Nicolet filter available for electromyographic recordings, and all EMG traces were recorded on the hard drive.

After the squid became active in the holding section, flow velocity within the flume was increased to 6 cm s^{-1} and the animal was allowed to acclimate to flow, which generally occurred within 15 min. After the acclimation period, squid were exposed to a flow velocity of 3 cm s^{-1} for 10 min. Speed was subsequently increased by 3 cm s^{-1} every 10 min until the squid could no longer keep pace with free-stream flow. During each of the 10-min speed increments, EMGs were collected. Because of limitations of the PortaBook, it was not possible to record EMG signals on a channel of a video recorder or precisely timelock video and EMG recordings. Therefore, to provide a synchronized record of EMG responses and swimming behavior, the computer screen of the PortaBook was positioned below the holding section of the flume, and both Nicolet display output and swimming behavior of the squid were videotaped simultaneously from a lateral perspective using a Sony Hi-8 video camera. After squid were exhausted and could no longer maintain free-stream velocity, they were removed from the flume and over-anesthetized in an isotonic solution of $MgCl_2$ (7.5% $MgCl_2 \cdot 6H_2O$) and seawater. The squid then were transferred to 10% buffered formalin for later dissection to determine precise electrode location. Some cooperative squid were not euthanized after the initial recording session. Instead, the electrode wires were cut, leaving the embedded section undisturbed within the mantle so that it could be examined later to determine placement, and the squid were returned to the raceway tanks. After several hours these squid were retrieved, electrodes were embedded in a different circular muscle layer, and EMGs were recorded during another swimming session. Following the completion of the second swimming session, these animals were over-anesthetized, fixed, and dissected as described above to determine electrode placement.

Kinematic analysis

Video footage of trials in which squid were cooperative at all swimming speeds, ambient electrical noise was low, and electrode placement was unambiguous was analyzed using a

Sony EVO-9700 editing deck and a Peak Motus video and computer motion measurement system (Peak Performance Technologies, Englewood, CO). At each speed several video sequences with clear mantle profiles and representative EMG recordings were selected. Mantle diameter at the location of electrode placement, swimming velocity, and acceleration of the squid were measured for each frame of video (30 frames s^{-1}) within the sequences, and frames where EMG responses began and ended were marked using the event feature in the Peak Motus system. Mantle diameter, velocity, and acceleration data were smoothed using a fourth-order Butterworth filter to account for video jitter and digitization error. Peak video data and Nicolet EMG data were imported into Microsoft Excel and aligned using event markers from the Peak file and timebase frequencies from both files. Synchronization of the data was reliable only to within 33.3 ms because the video camera records at 30 frames s^{-1}. Since the objective of this study was simply to determine the presence or absence of EMG activity within the circular muscle layers during mantle contractions, more precise analysis of the timing of EMG activity was unnecessary.

Results

The five specimens of *Lolliguncula brevis* (5.0–6.8 cm DML) considered in this study matched free-stream flow well at speeds less than 21 cm s^{-1}, but at higher speeds they had some difficulty matching flow velocity and eventually collapsed against the downstream weir. Prior to collapse, the squid accelerated and decelerated erratically, and the contraction frequencies were more irregular than those observed at lower velocities. At low (3–9 cm s^{-1}) and intermediate (12–18 cm s^{-1}) swimming velocities, squid relied on both fin and jet propulsion, whereas at high subcritical speeds (21–27 cm s^{-1}), they relied exclusively on jet propulsion and, like *Loligo opalescens* and *Illex illecebrosus* (O'Dor, 1988a), wrapped their fins against the mantle. The electrodes did not appear to impede swimming in the five squid considered; however, some squid, which were excluded from this analysis, were visibly agitated after surgery, swam inconsistently at most swimming speeds, and frequently swam forcibly into the flume sides.

The amplitude and frequency of electrical activity varied from animal to animal, but the basic patterns of activity presented in this paper are representative of all the squid considered. Results from a squid with electrodes inserted into the central and peripheral circular muscle layers (Fig. 1) show significant EMG activity at low (6 cm s^{-1}), intermediate (15 cm s^{-1}), and high speeds (24 cm^{-1}); this activity was correlated with mantle contraction. The amplitude of EMG activity increased with speed and, as was typical of other squid examined, frequency of mantle contraction was greater at the highest speed tested (24 cm s^{-1}) than at low speed (6 cm s^{-1}). Moreover, maximum accelerations throughout the jet cycle were closely coupled with high-magnitude EMG bursts recorded during mantle contraction. At high speeds (24 cm s^{-1}), lower amplitude electrical activity sometimes occurred during mantle expansion.

Electromyographic recordings from a squid with electrodes embedded in only central circular muscle (Fig. 2), but with settings for bandpass filter, sensitivity, timebase, etc., identical to those used for recordings from both central and peripheral layers, show no EMG activity during mantle expansion and contraction at 6 cm s^{-1}. At an intermediate speed of 15 cm s^{-1}, occasional EMG activity was detected. (The mean central circular muscle recruitment speed for all squid considered was 15.3 ± 3.7 [SD] cm s^{-1}.) Most of the large-amplitude electrical activity at intermediate speeds occurred during the contraction phase of the jet cycle, but sometimes smaller amplitude activity occurred during mantle expansion (Fig. 2). Furthermore, the large-amplitude EMGs at intermediate speeds were coupled with large changes in mantle diameter and high peaks of acceleration. Generally, the frequency of EMG bursts increased with speed up to maximum speeds of 21–27 cm s^{-1}, when muscular activity coincided with the majority of mantle contractions. Again large-amplitude signals correlated with mantle contraction, whereas less frequent low-amplitude signals correlated with mantle expansion. Contraction amplitude and frequency were more irregular at 24 cm s^{-1} than at lower velocities, and high-amplitude EMG peaks were strongly coupled with high accelerations.

Discussion

The results of this study indicate that the peripheral aerobic and the central anaerobic circular muscle fibers in squid probably have distinct functional roles during swimming. Electrodes implanted in both peripheral and central circular muscle fibers recorded EMG activity with each mantle contraction at all swimming speeds (3–27 cm s^{-1}). However, electrodes implanted exclusively in central (anaerobic) muscle did not record EMG activity during mantle contraction until speeds of about 15 cm s^{-1}, when activity was sporadic. At speeds above 15 cm s^{-1}, the frequency of electrical activity increased with swimming speed up to maximum speeds of 21–27 cm s^{-1}, when anaerobic muscular activity coincided with the majority of mantle contractions and with high accelerations. These results indicate that peripheral aerobic circular muscle is used for slow, intermediate, and probably high speeds, whereas central anaerobic muscle is recruited at intermediate speeds and used progressively more with increasing speed for powerful, unsteady jetting typical of higher speed swimming.

The observed periodic detection of central anaerobic circular muscle activity at intermediate speeds is interesting given that anaerobic muscle is often associated only with

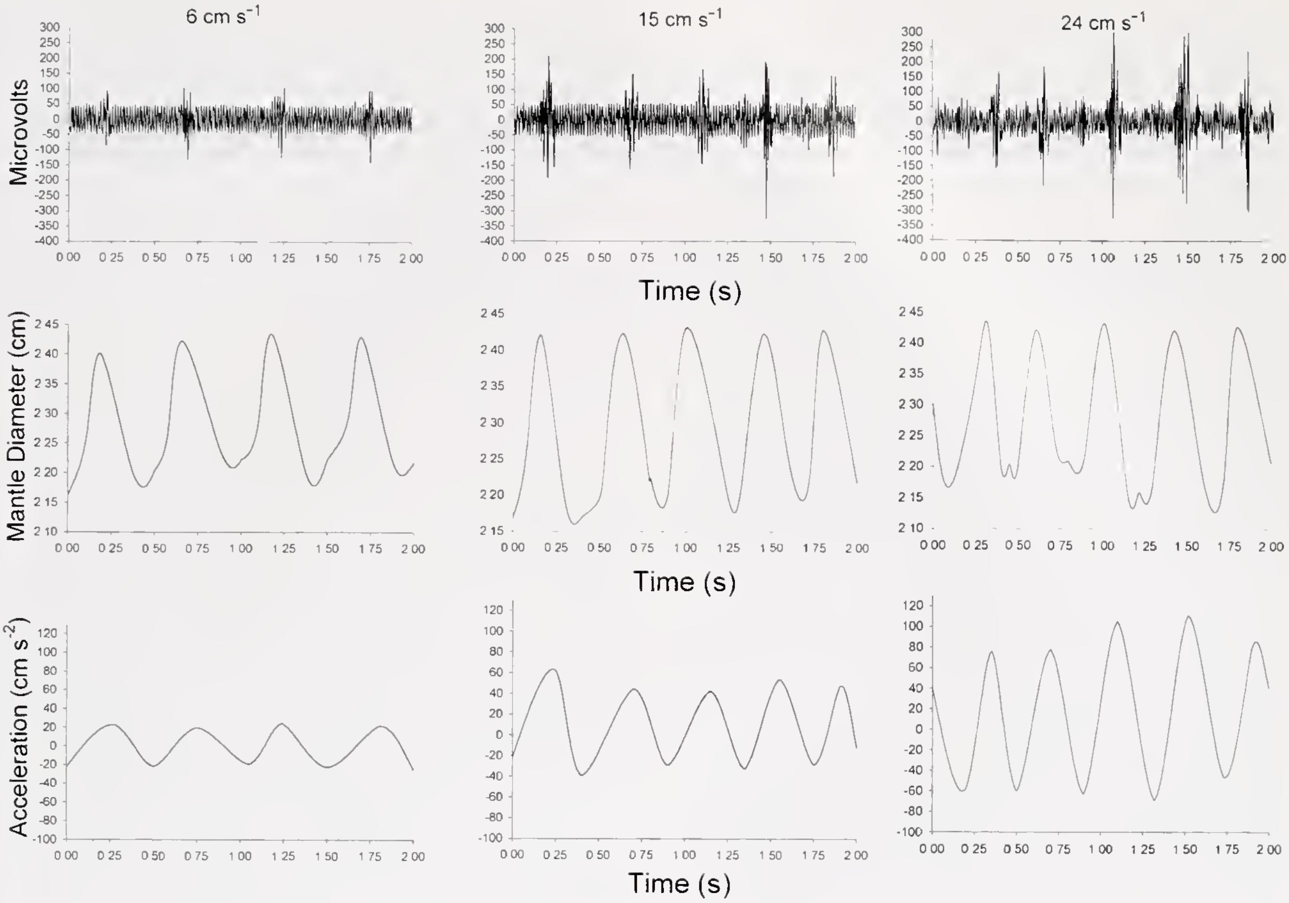

Figure 1. Electromyograms recorded from electrodes embedded in both peripheral aerobic circular muscle and central anaerobic circular muscle of a brief squid (5.5 cm dorsal mantle length) while swimming at 6, 15, and 24 cm s^{-1}. Mantle diameter and acceleration are plotted underneath each recording. Electrical activity occurs during each mantle contraction, and at high speeds electrical activity is sometimes present during mantle expansion.

burst swimming in fishes (Rome *et al.*, 1984; Jayne and Lauder, 1996) and escape jets in cephalopods (Bone *et al.*, 1981, 1994; Mommsen *et al.*, 1981). Finke *et al.* (1996) determined that anaerobic end products, such as α-glycerophosphate, succinate, and octopine, begin to accumulate in *Lolliguncula brevis* at speeds of 1.5–2.0 mantle lengths s^{-1} (8.3–11.0 cm s^{-1} for a specimen of 5.5-cm DML), suggesting that anaerobic metabolism may occur in the mantle at low intermediate speeds. Moreover, intramantle pressure records revealed that at speeds of 3.2 mantle lengths s^{-1} (17.6 cm s^{-1} for a specimen of 5.5-cm DML) high mantle pressures comparable to those recorded at speeds of 4.3 mantle lengths s^{-1} (23.7 cm s^{-1} for a specimen of 5.5-cm DML) are periodically generated (Finke *et al.*, 1996). Accumulation of anaerobic end products and the occasional detection of high intramantle pressures at intermediate speeds are consistent with the activity of anaerobic circular muscle observed at intermediate speeds in this study. Periodic anaerobic circular mantle activity at intermediate speeds boosted power production, which helped squid keep pace with free-stream flow in the tunnels. Periodic anaerobic activity was probably not energetically deleterious since anaerobic metabolic changes can be rapidly reversed in squid (Pörtner *et al.*, 1993). At higher speeds, central anaerobic circular muscle activity was more frequent, but there was still some oscillation between aerobic and anaerobic muscular activity. Finke *et al.* (1996) suggest that oscillating between aerobic and anaerobic circular muscle recruitment rather than simply relying exclusively on anaerobic muscle at a critical speed allows for an extended net use of anaerobic resources before fatigue sets in.

One limitation of this study was the level of background noise (±40 μV at between 60 and 120 Hz) in EMG recordings despite attempts to reduce such interference by shielding the variable-speed flume motor and performing trials in laboratories with minimal electrical equipment. The noise probably came from interference produced by the flume motor and other electrical laboratory equipment (*e.g.*, fluorescent lights, proportional controllers, and rheostats) and was allowed through the 20–10,000-Hz bandpass filter. A

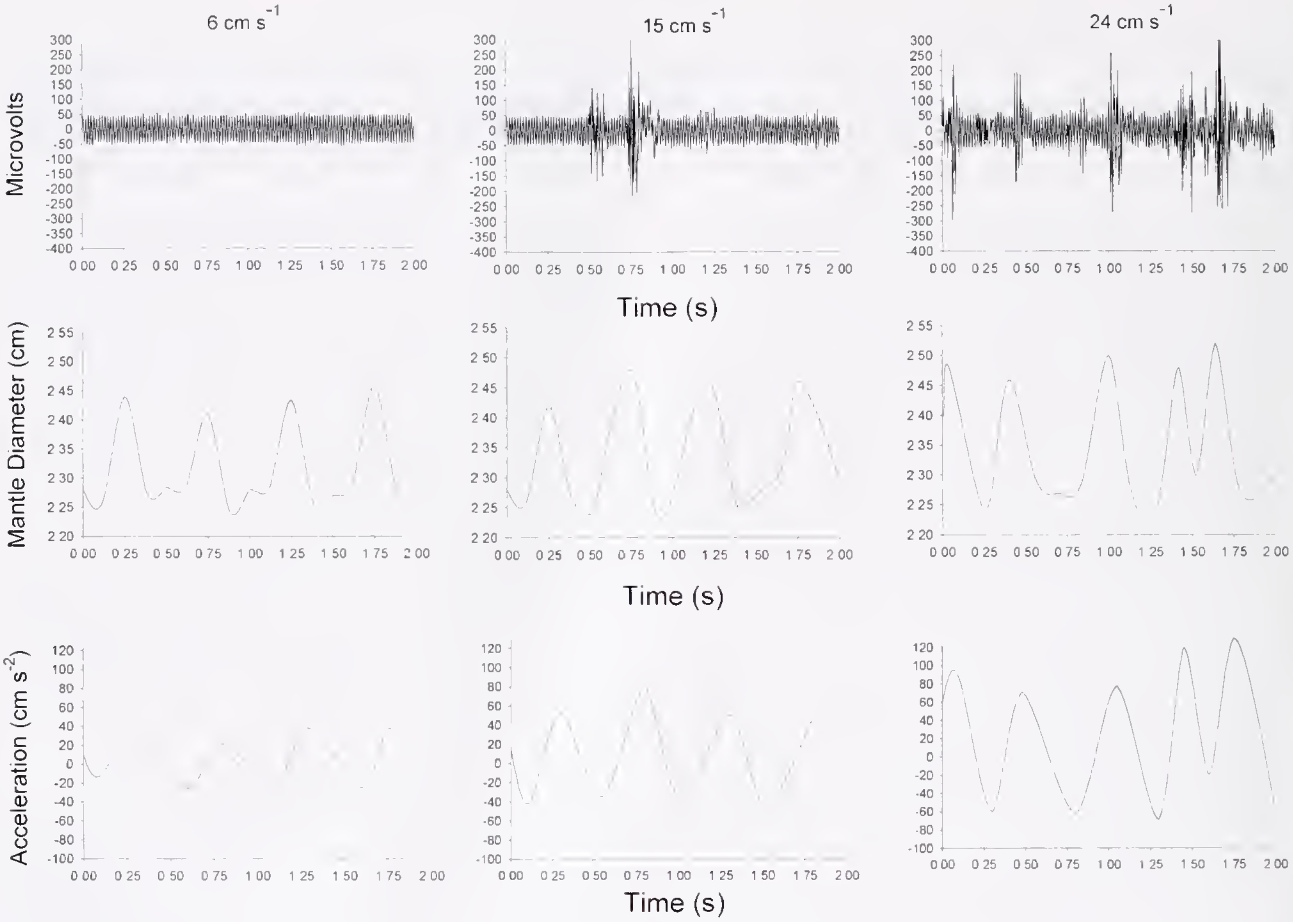

Figure 2. Electromyograms recorded from electrodes embedded in central anaerobic circular muscle of a brief squid (5.7 cm dorsal mantle length) while swimming at 6, 15, and 24 cm s^{-1}. Mantle diameter and acceleration are plotted underneath each recording. There are no obvious waveforms at 6 cm s^{-1}, occasional waveforms at 15 cm s^{-1}, and frequent waveforms at high speeds (24 cm s^{-1}). At high speeds, high-amplitude electrical activity occurs during each mantle contraction, and lower amplitude electrical activity sometimes occurs during mantle expansion. Furthermore, mantle contractions are more erratic at 24 cm s^{-1} than at 6 cm s^{-1}.

significant proportion of the noise might have been removed with a 60-Hz notch filter (Loeb and Gans, 1986), but unfortunately the electromyographic system used could not be configured with a notch filter. Considering the high level of background noise, it is possible that some low-level EMG activity was undetected. However, it is unlikely that anaerobic EMG activity was absent at low speeds because it was concealed in the noise. EMG activity from the thin peripheral (aerobic) muscle zones was easily distinguishable and consistently recorded at low speeds when muscular activity was lowest in spite of the electrical noise, and thus EMG activity from the thick, powerful central (anaerobic) muscle zone should have been visible if those fibers were active.

Although electrical noise probably did not mask circular muscle activity, which was the focus of this study, it interfered with detection of EMG activity from the smaller radial muscles. Dissections revealed that electrodes crossed radial muscle bands, which are active during mantle expansion and hyperinflation (*i.e.*, a sharp increase in mantle diameter just prior to contraction) (Gosline *et al.*, 1983; Bone *et al.*, 1994). However, no radial EMG activity was detected at low speeds. This is not surprising given that Wilson (1960) and Ward (1972), who were the first to record electrical activity in the squid mantle musculature, were unable to detect radial muscle activity, and Gosline *et al.* (1983) and Bone *et al.* (1994) were able to detect consistent radial muscle activity in squid and cuttlefish only when using a 60-Hz notch filter and a Faraday cage, respectively. Radial muscle activity at low speeds detected by Gosline *et al.* (1983) and Bone *et al.* (1994), who examined squid and cuttlefish in dissecting pans and small aquaria and consequently did not have to contend with a motor-driven swim tunnel, was often less than 40 μV. Therefore, low-speed radial muscle activity presumably was hidden by the electrical noise. From squid engaged in escape jets, Gosline *et al.* (1983), without using a 60-Hz notch filter, recorded radial muscle activity during refilling and hyperinflation. At high speeds, EMG activity frequently was observed in the present study during mantle expansion. Since circular muscle is not active during mantle expansion (Gosline *et al.*, 1983), radial muscles—the only other muscle into which electrodes were imbedded—were probably responsible for the EMG activity observed during mantle refilling. The detection of radial muscle activity at high speeds when anaerobic circular muscle was active suggests that significant radial muscle activity is used to expand the mantle during vigorous jetting. Elastic energy stored within the connective tissue of the mantle also probably plays an important role during mantle expansion (Gosline and Shadwick, 1983; Gosline *et al.*, 1983; Pabst, 1996).

Using electromyography, Kier *et al.* (1989) demonstrated that anaerobic and aerobic zones of muscle in cuttlefish *Sepia officinalis* fins have distinct functional roles, with aerobic fibers responsible for gentle fin movements and anaerobic muscles responsible for vigorous fin movements and support for that movement. The results of the present study indicate that peripheral aerobic circular muscle and central anaerobic circular muscle in brief squid *Lolliguncula brevis* also have distinct functional roles that are analogous to red and white myotomal fibers in fishes. Contrary to the situation in many fishes, however, in squids the anaerobic muscle appears to be used at subcritical speeds. The discovery of functional "gears" in squids, which is yet another instance of convergent evolution in fishes and cephalopods, is significant because it suggests that there is specialization and efficient use of locomotive muscle in squids. Future study on the innervation and neural control of these different muscle fibers during unrestrained swimming should provide further insight into the locomotive system of cephalopods.

Acknowledgments

I gratefully acknowledge intellectual input from R. Mann and M. R. Patterson and electromyographic advice from S. L. Sanderson and W. M. Kier. I thank M. Vecchione and M. Luckenbach for constructive criticisms of earlier drafts, and I am especially appreciative of the generosity of M. Lenhardt, who allowed me to use his Nicolet Compass PortaBook II. This study was supported in part by the VIMS/SMS Minor Research Grants, the Eastern Shore Seaside Corporate Scholarship, and Newport News Shipbuilding. Financial support during the writing phase of this project was provided by the Office of Naval Research under contract N00014-96-0607.

Literature Cited

Bartol, I. K. 1999. *Distribution, Swimming Physiology, and Swimming Mechanics of the Brief Squid* Lolliguncula brevis. Ph.D. dissertation, College of William and Mary, Virginia Institute of Marine Science, Gloucester Point, VA. 215 pp.

Bone, Q. 1966. On the function of the two types of myotomal muscle fibers in elasmobranch fish. *J. Mar. Biol. Assoc. UK* **46:** 321–349.

Bone, Q. 1978. Locomotor muscle. Pp. 361–424 in *Fish Physiology*, vol. 7, W. S. Hoar and D. J. Randall, eds. Academic Press, New York.

Bone, Q., A. Pulsford, and A. D. Chubb. 1981. Squid mantle muscle. *J. Mar. Biol.* **61:** 327–342.

Bone, Q., E. R. Brown, and G. Travers. 1994. On the respiratory flow in the cuttlefish *Sepia officinalis*. *J. Exp. Biol.* **194:** 153–165.

Coughlin, D. J., L. Valdes, and L. C. Rome. 1996. Contraction dynamics and power production of pink muscle of scup (*Stenotomus chrysops*). *J. Exp. Biol.* **199:** 2703–2712.

Curtin, N. A., and R. C. Woledge. 1988. Power output and force-velocity relationships of live fibers from white myotomal muscle of the dogfish, *Scyliorhinus canicula*. *J. Exp. Biol.* **140:** 187–197.

Fields, J. H. A., and J. F. Quinn. 1981. Some theoretical considerations on cytosolic redox balance during anaerobiosis in marine invertebrates. *J. Theor. Biol.* **88:** 35–45.

Finke, E., H. O. Pörtner, P. G. Lee, and D. M. Webbher. 1996. Squid (*Lolliguncula brevis*) life in shallow waters: oxygen limitation of metabolism and swimming performance. *J. Exp. Biol.* **199:** 911–921.

Flitney, F. W., and I. A. Johnston. 1979. Mechanical properties of isolated fish red and white muscle fibers. *J. Physiol.* **295:** 49–50.

Gosline, J. M., and R. E. Shadwick. 1983. The role of elastic energy storage mechanisms in swimming: an analysis of mantle elasticity in escape jetting in the squid, *Loligo opalescens*. *Can. J. Zool.* **61:** 1421–1431.

Gosline, J. M., J. D. Steeves, A. D. Harman, and E. DeMont. 1983. Patterns of circular and radial mantle muscle activity in respiration and jetting of the squid *Loligo opalescens*. *J. Exp. Biol.* **104:** 97–109.

Grieshaber, M. E., and G. Gade. 1976. The biological role of octopine in the squid, *Loligo vulgaris* (Lamarck). *J. Comp. Physiol.* **108:** 225–232.

Hochachka, P. W., T. W. Moon, T. Mustafa, and K. B. Storey. 1975. Metabolic sources of power for mantle muscle of a fast swimming squid. *Comp. Biochem. Physiol.* **52B:** 151–158.

Jayne, B. C., and G. V. Lauder. 1996. New data on axial locomotion in fishes: how speed affects diversity of kinematics and motor patterns. *Am. Zool.* **36:** 642–655.

Johnston, I. A., W. Davison, and G. Goldspink. 1977. Energy metabolism of carp swimming muscles. *J. Comp. Physiol.* **114:** 203–216.

Kier, W. M. 1988. The arrangement and function of molluscan muscle. Pp. 211–252 in *The Mollusca, Form and Function*, vol. 11, E. R. Trueman and M. R. Clarke, eds. Academic Press, New York.

Kier, W. M., and K. K. Smith. 1985. Tongues, tentacles and trunks: the biomechanics of movement in muscular hydrostats. *Zool. J. Linn. Soc.* **83:** 307–324.

Kier, W. M., K. K. Smith, and J. A. Miyan. 1989. Electromyography of the fin musculature of the cuttlefish *Sepia officinalis*. *J. Exp. Biol.* **143:** 17–31.

Loeb, G. E., and C. Gans. 1986. *Electromyography for Experimentalists*. University of Chicago Press, Chicago.

Messenger, J. B., M. Nixon, and K. P. Ryan. 1985. Magnesium chloride as an anaesthetic for cephalopods. *Comp. Biochem. Physiol.* **82C:** 203–205.

Mommsen, T. P., J. Ballantyne, D. MacDonald, J. Gosline, and P. W. Hochachka. 1981. Analogues of red and white muscle in squid mantle. *Proc. Natl. Acad. Sci. USA* **78:** 3274–3278.

O'Dor, R. K. 1982. The respiratory metabolism and swimming performance of the squid, *Loligo opalescens*. *Can. J. Fish. Aquat. Sci.* **39:** 580–587.

O'Dor, R. K. 1988a. The forces acting on swimming squid. *J. Exp. Biol.* **137:** 421–442.

O'Dor, R. K. 1988b. Limitations on locomotor performance in squid. *J. Appl. Physiol.* **64:** 128–134.

Otis, T. S., and W. F. Gilly. 1990. Jet-propelled escape in the squid *Loligo opalescens:* concerted control by giant and non-giant motor axon pathways. *Proc. Natl. Acad. Sci. USA* **87:** 2911–2915.

Pabst, D. A. 1996. Springs in swimming animals. *Am. Zool.* **36:** 723–735.

Pörtner, H. O., D. M. Webber, R. G. Boutilier, and R. K. O'Dor. 1991. Acid-base regulation in exercising squid (*Illex illecebrosus, Loligo pealei*). *Am. J. Physiol.* **261:** R239–R246.

Pörtner, H. O., D. M. Webber, R. K. O'Dor, and R. G. Boutilier. 1993. Metabolism and energetics in squid (*Illex illecebrosus, Loligo pealei*) during muscular fatigue and recovery. *Am J. Physiol.* **265:** R157–R165.

Preuss, T., and W. F. Gilly. 2000. Role of prey-capture experience in the development of the escape response in the squid *Loligo opalescens:* a physiological correlate in an identified neuron. *J. Exp. Biol.* **203:** 559–565.

Rome, L. C., P. T. Loughna, and G. Goldspink. 1984. Muscle fiber activity of carp as a function of swimming speed and muscle temperature. *Am. J. Physiol.* **247:** R272–R279.

Smith, K. K., and W. M. Kier. 1989. Trunks, tongues and tentacles: moving with skeletons of muscle. *Am. Sci.* **77:** 28–35.

Storey, K. B., and J. M. Storey. 1978. Energy metabolism in the mantle muscle of the squid, *Loligo pealeii. J. Comp. Physiol.* **123:** 169–175.

Vogel, S., and M. LaBarbera. 1978. Simple flow tanks for research and teaching. *BioScience* **10:** 638–643.

Ward, D. V. 1972. Locomotory function of the squid mantle. *J. Zool. (Lond).* **167:** 487–499.

Wilson, D. M. 1960. Nervous control of movement in cephalopods. *J. Exp. Biol.* **37:** 57–72.

Reference: *Biol. Bull.* **200:** 67–76. (February 2001)

Temperature Effects on Hemocyanin Oxygen Binding in an Antarctic Cephalopod

S. ZIELINSKI, F. J. SARTORIS, AND H. O. PÖRTNER*

Alfred-Wegener-Institute for Marine and Polar Research, Ecophysiology and Ecotoxicology, Columbusstrasse, 27568 Bremerhaven, Germany

Abstract. The functional relevance of oxygen transport by hemocyanin of the Antarctic octopod *Megaleledone senoi* and of the eurythermal cuttlefish *Sepia officinalis* was analyzed by continuous and simultaneous recordings of changes in pH and hemocyanin oxygen saturation in whole blood at various temperatures. These data were compared to literature data on other temperate and cold-water cephalopods (octopods and giant squid).

In *S. officinalis,* the oxygen affinity of hemocyanin changed at ΔP_{50}/°C = 0.12 kPa (pH 7.4) with increasing temperatures; this is similar to observations in temperate octopods. In *M. senoi,* thermal sensitivity was much smaller (<0.01 kPa, pH 7.2). Furthermore, *M. senoi* hemocyanin displayed one of the highest levels of oxygen affinity ($P_{50} < 1$ kPa, pH 7.6, 0 °C) found so far in cephalopods and a rather low cooperativity ($n_{50} = 1.4$ at 0 °C). The pH sensitivity of oxygen binding ($\Delta \log P_{50}/\Delta$ pH) increased with increasing temperature in both the cuttlefish and the Antarctic octopod. At low $P\text{O}_2$ (1.0 kPa) and pH (7.2), the presence of a large venous oxygen reserve (43% saturation) insensitive to pH reflects reduced pH sensitivity and high oxygen affinity in *M. senoi* hemocyanin at 0 °C. In *S. officinalis,* this reserve was 19% at pH 7.4, 20 °C, and 1.7 kPa O_2, a level still higher than in squid.

These findings suggest that the lower metabolic rate of octopods and cuttlefish compared to squid is reflected in less pH-dependent oxygen transport. Results of the hemocyanin analysis for the Antarctic octopod were similar to those reported for *Vampyroteuthis*—an extremely high oxygen affinity supporting a very low metabolic rate. In contrast to findings in cold-adapted giant squid, the minimized thermal sensitivity of oxygen transport in Antarctic octopods will reduce metabolic scope and thereby contribute to their stenothermality.

Introduction

Cephalopods are found throughout the seas of the world, from warm tropical waters to polar oceans (Roper *et al.,* 1984). Representatives of this group, especially squids, usually display the highest metabolic rates among marine invertebrates, even higher than those of fishes of similar size and mode of life (Webber and O'Dor, 1985; O'Dor and Webber, 1986). Oxygen delivery *via* the blood is maximized to cover metabolic requirements (Pörtner, 1994). However, the capacity of their blood pigment, hemocyanin, for carrying oxygen is constrained by the low concentration of an extracellular pigment. This limitation is due to the unfavorable increase in colloidal osmotic pressure and blood viscosity at high pigment concentrations (Mangum, 1983, 1990). Although cephalopods, in accordance with their high rate of oxygen consumption, display the highest hemocyanin concentrations in the animal kingdom, the level of bound oxygen in squid (up to 3 mmol l^{-1}; Brix *et al.,* 1989) remains below the 4–5 mmol l^{-1} of active fishes (Urich, 1990). Therefore, the hearts of squids pump large volumes of blood (Wells *et al.,* 1988; Shadwick *et al.,* 1990) and the tissues extract most of the oxygen (Pörtner, 1994). Compared to that of squids, the oxygen-binding capacity of octopod blood is somewhat reduced, ranging between 0.6 and 1.6 mmol l^{-1}, depending on hemocyanin levels (Senozan *et al.,* 1988; Brix *et al.,* 1989).

In most cephalopods, cooperativity and temperature- and pH-dependent changes in affinity are the only means of modulating hemocyanin function and adjusting oxygen transport (*e.g.,* Brix *et al.,* 1989; Mangum, 1990; Pörtner, 1990). Low-molecular-weight organic substances that contribute to blood pigment function in vertebrates or crusta-

---

Received 3 July 1999; accepted 10 October 2000.

* To whom correspondence should be addressed. E-mail: hpoertner@awi-bremerhaven.de

ceans are not found in this group. In consequence, extremely large Bohr shifts ($\Delta \log P_{50}/\Delta \mathrm{pH} < -1$; Bridges, 1994) and very high levels of pH-dependent cooperativity are common (Miller, 1985; Pörtner, 1990). Binding of CO_2 together with O_2 in arterial blood has been suggested to support pigment function on the venous side in sepioid species (Brix *et al.*, 1981), where both O_2 and CO_2 are released, and this CO_2 helps to exploit the large Bohr effect. In squid, supplementary oxygen uptake *via* the skin supports the excessive oxygen demand and provides the excess CO_2 required for the Bohr effect to function (Pörtner, 1994).

In some cephalopods, an increase in ambient temperature has a large effect on oxygen transport by hemocyanin; this effect is reflected by an increase in cooperativity and a fall in oxygen affinity (Brix *et al.*, 1989, 1994; Mangum, 1990). If a rise in metabolic rate with temperature is supported by an adequate rise in P_{50}, the species should be able to live at a broader range of temperatures than a species in which P_{50} remains constant or in which the change in P_{50} is too large. For example, the high thermal sensitivity of the oxygen affinity of hemocyanin in the giant squid *Architeuthis monachus* suggests that arterial saturation becomes impossible at high temperatures (Brix, 1983). This question has gained general importance since comparative studies in Antarctic and temperate fish and invertebrates (including cephalopods; Pörtner and Zielinski, 1998) revealed that the limits of thermal tolerance are characterized by oxygen limitation, owing to the inability of circulation or ventilation to provide sufficient oxygen at extreme temperatures (for review, see Pörtner *et al.*, 2000). Comparison of hemocyanin oxygen binding in cephalopods of different metabolic rates and from various latitudes should show how hemocyanin oxygen transport has adapted to different temperature regimes at various levels of metabolic activity and how blood pigment function contributes to the oxygen limitation of thermal tolerance.

These questions are especially interesting for an understanding of physiological adaptations to life in Antarctica. Here the marine environment is characterized by very stable water temperatures that are close to freezing (Clarke, 1988). Under these conditions more oxygen is physically dissolved, thereby facilitating oxygen uptake and supply to tissues. At the same time metabolic rate is reduced at lower temperatures, with the consequence that in some species blood pigments may be less important (for hemocyanin, see Mauro and Mangum, 1982b; Burnett *et al.*, 1988). Some Antarctic fishes, the icefishes (Channichtyidae) have even lost their respiratory pigments (Ruud, 1954). The question arises as to whether the importance of blood pigment function is also reduced in Antarctic cephalopods.

Live specimens of the octopod *Megaleledone senoi* became available during a recent expedition to Antarctica with the RV *Polarstern*. This species is found in the indo-atlantic sector of the Antarctic Ocean (Taki, 1961; Kubodera and Okutani, 1986, 1994). In our study we investigated oxygen binding to the hemocyanin of this stenothermal Antarctic octopod by using a technique that allows continuous and simultaneous recordings of blood pH and oxygenation and the construction of diagrams depicting changes in oxygen saturation with pH (pH/saturation diagrams; Pörtner, 1990). Such an approach is most suitable for cephalopod blood owing to the extremely large pH dependence of oxygen binding (see above). It avoids the use of artificial buffers that may lead to a change in oxygen-binding properties (Pörtner, 1990; Brix *et al.*, 1994). At the same time, the amount of blood required is reduced such that more sophisticated data can be collected from the very few animals accessible in remote environments like the Antarctic. The oxygen-binding properties of *M. senoi* hemocyanin were compared with those from other eurythermal and stenothermal cephalopods. For eurythermal octopods some literature data were available. Temperature effects on oxygen binding were studied experimentally in the cuttlefish *Sepia officinalis* to complement the data set available in the literature (Lykkeboe *et al.*, 1980; Johansen *et al.*, 1982a). To some extent, cuttlefish display a mode of life similar to that of octopods. Like octopods, they live close to the bottom of the sea (von Boletzky, 1983), but they have a larger scope for activity and metabolism, which might influence the thermal adaptation of hemocyanin function.

Materials and Methods

Animals

Antarctic octopods (*Megaleledone senoi*, up to 9 kg body weight) were caught in November 1996 north of Elephant Island, Antarctica, during expedition ANT XIV/2 of the RV *Polarstern*. The animals were collected from bottom trawls. Samples were taken immediately after capture.

Cuttlefish (*Sepia officinalis*, 470 to 960 g body weight) were obtained from the Marine Biomedical Institute of the University of Texas, Galveston, Texas, where this species has been bred and grown for several consecutive generations. They were kept at a salinity of 35‰ at temperatures of 20 to 22 °C.

Sampling procedure

Animals were anesthetized by transferring them into seawater containing 2% ethanol (v/v). The animals were then removed from the seawater and the mantle was opened by a ventral incision. Blood was collected from the vena cava, the systemic heart, and the gill hearts. Blood samples from all animals were pooled, frozen, and stored for up to one year at close to −20 °C until utilized for *in vitro* studies of oxygen binding.

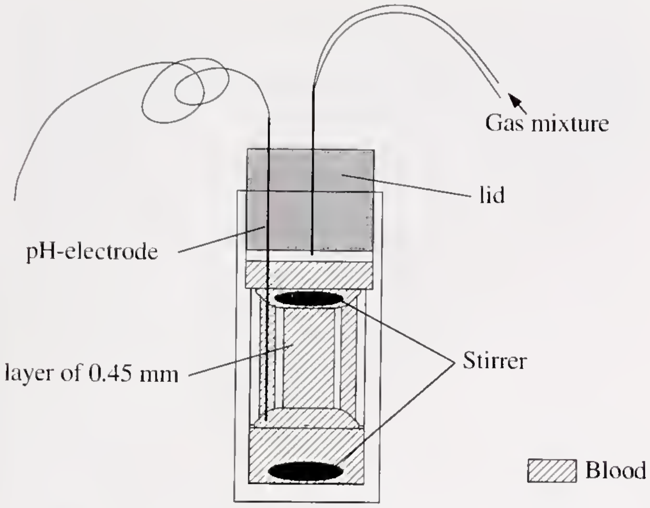

Figure 1. Cuvette used for the measurement of oxygen-binding properties. Dashed areas show the compartments of the cuvette filled with blood. Absorbance was measured through a thin layer, 0.45-mm thick, in the center part of the cuvette.

Analysis of oxygen binding

Oxygen-binding characteristics of cephalopod hemocyanin were studied using a specially constructed cuvette, built by Hellma GmbH & Co. (Mülheim, Germany; Fig. 1). The cuvette consisted of an upper and a lower compartment connected by two shafts (1.5 and 2 mm in diameter) in the left and right periphery of the cuvette, as well as a central compartment between the shafts, where blood formed a thin layer of only 0.45 mm. Stirring bars operating in the upper and lower compartments ensured continuous exchange of blood between all compartments and thus uniform mixture of the blood. Oxygen saturation was monitored continuously by using a diode array spectrophotometer with fiber optics (X-dap, IKS Optoelektronik Meßgeräte GmbH, Waldbronn, Germany) to measure absorbance at 345 nm through the thin layer. Blood samples were equilibrated by introducing humidified gas mixtures through a hole in the lid of the cuvette. Gas mixtures of variable $P\text{O}_2$ (between 1.0 and 20.0 kPa) were prepared from pure O_2, CO_2, and N_2 by gas-mixing pumps (type 2M303/a-F, Wösthoff, Bochum, Germany); complete deoxygenation occurred under pure N_2. Blood pH was varied by changing $P\text{CO}_2$ (between 0.09 and 1.01 kPa) or by replacing small volumes (<10 μl per 2 ml of blood) of supernatant plasma after ultracentrifugation (1 h at 120,000 × *g*; Beckman Airfuge, Beckman Instruments, Inc., Fullerton, CA) with fixed acid (1 mol l^{-1} HCl) or base (2 mol l^{-1} NaOH; Morris *et al.*, 1985; Pörtner, 1990). Changes in blood pH during oxygenation and deoxygenation of hemocyanin were measured continuously by using a needle pH electrode (long micro needle electrode #811, Diamond General Corp., Ann Arbor, MI) that was introduced into one of the shafts *via* a second hole in the lid.

Total CO_2 was analyzed at 0 °C in 50-μl blood samples of *M. senoi;* the gas chromatography method of Lenfant and Aucutt (1966) modified after Boutilier *et al.* (1985) was used. Measurements of oxygen-binding properties were carried out at 0, 5, and 10 °C for samples of *M. senoi* and at 0, 10, and 20 °C for samples of *S. officinalis;* 10 °C was chosen since this temperature can be reached in the northern part of *Sepia's* distribution range (Isemer and Hasse, 1985).

Graphical analysis and calculations

Hemocyanin concentrations were measured photometrically and calculated using the extinction coefficients of Nickerson and van Holde (1971). Oxygen capacity was estimated using the molecular weights for octopods and *Sepia* as compiled by Miller (1994) and the assumption that there are 70 O_2-binding sites per hemocyanin molecule in octopods and 80 in *Sepia.* For the evaluation of hemocyanin oxygen saturation, constant absorbance levels in the range of the highest values of $P\text{O}_2$ and pH were set to 100% saturation. Changes in hemocyanin oxygenation and pH were plotted in a pH/saturation diagram according to Pörtner (1990). The resulting oxygen-binding curves represent isobars delineating the change in oxygenation with pH at constant $P\text{O}_2$. The points of intersection of the oxygen isobars with the line of half saturation quantify P_{50}, because it depends on pH. These P_{50} and pH values were used to evaluate the Bohr coefficient, $\Delta \log P_{50}/\Delta\text{pH}$ by linear regression analysis. For comparison, and owing to the presence of a large pH-insensitive oxygen reserve at low temperatures, the coefficient $\Delta \log P_{80}/\Delta\text{pH}$ was evaluated following the same procedure. The Haldane coefficient ($\Delta\text{HCO}_3^-/\Delta\text{HcyO}_2$) was evaluated from the vertical distance between buffer lines in a pH/bicarbonate diagram (as used by Brix *et al.*, 1981). To assess whether oxygen-linked CO_2 binding to the hemocyanin occurs (Lykkeboe *et al.*, 1980), "measured" and calculated apparent bicarbonate levels were compared. Apparent "bicarbonate" (the sum of HCO_3^- and CO_3^{2-} levels) was calculated from measured CO_2 concentrations ($C\text{CO}_2$) using the applied $P\text{CO}_2$ and the measured pH according to the formula

$$[\text{HCO}_3^-] = C\text{CO}_2 - \alpha P\text{CO}_2 \qquad (1)$$

where α is the solubility of CO_2. For comparison, bicarbonate levels were also calculated according to equation (1) with $C\text{CO}_2$ values derived from the Henderson-Hasselbalch equation:

$$C\text{CO}_2 = P\text{CO}_2 \cdot (\alpha \cdot 10^{\text{pH}-\text{pK}'''} + \alpha) \qquad (2)$$

α and pK‴ were calculated according to Heisler (1986).

Along each isobar in the pH/saturation diagram, values of saturation S depend on pH values and the $P\text{O}_2$ of the isobar. The pH/saturation diagram allows comparison of S and log $P\text{O}_2$ with P_{50} at the same pH ($=\text{pH}_{50}$). This leads to an analysis of cooperativity at a specific pH. If this is done in the range of saturation S between 0.4 and 0.6, the analysis leads to an estimate of Hill coefficients (n_{50}) according to

$$\log(S/1 - S) = n_{50}(\log Po_2 - \log P_{50}) \qquad (3)$$

where Po_2 is the Po_2 of the isobar, S results from Po_2 at a specific pH (pH_{50}), and P_{50} is the Po_2 for $S = 0.5$ at the same pH (Pörtner, 1990).

Results

The concentration of hemocyanin in native blood (hemolymph) was 93 g l^{-1} for *Megaleledone senoi* and 142 g l^{-1} for *Sepia officinalis*. This is equivalent to a maximum level of hemocyanin-bound oxygen of 1.86 mmol O_2 l^{-1} in the octopod and of 2.84 mmol l^{-1} in *Sepia*. For *M. senoi* hemocyanin, the highest pH sensitivity of oxygen binding was found at 10 °C, as indicated by maximum slopes $\Delta S/\Delta pH$ (Fig. 2). Lower temperatures resulted in a somewhat decreased pH sensitivity of oxygen affinity, with a maximum of $\Delta S/\Delta pH = 13\%$ per pH unit at 10 °C, compared to a maximum of 10% per pH unit at 0 °C. Saturation at 0 °C did not fall below 43% even at low pH (6.4 and 6.6) and low Po_2 (1 kPa). At 10 °C, saturation dropped to a minimum of 32% at the same

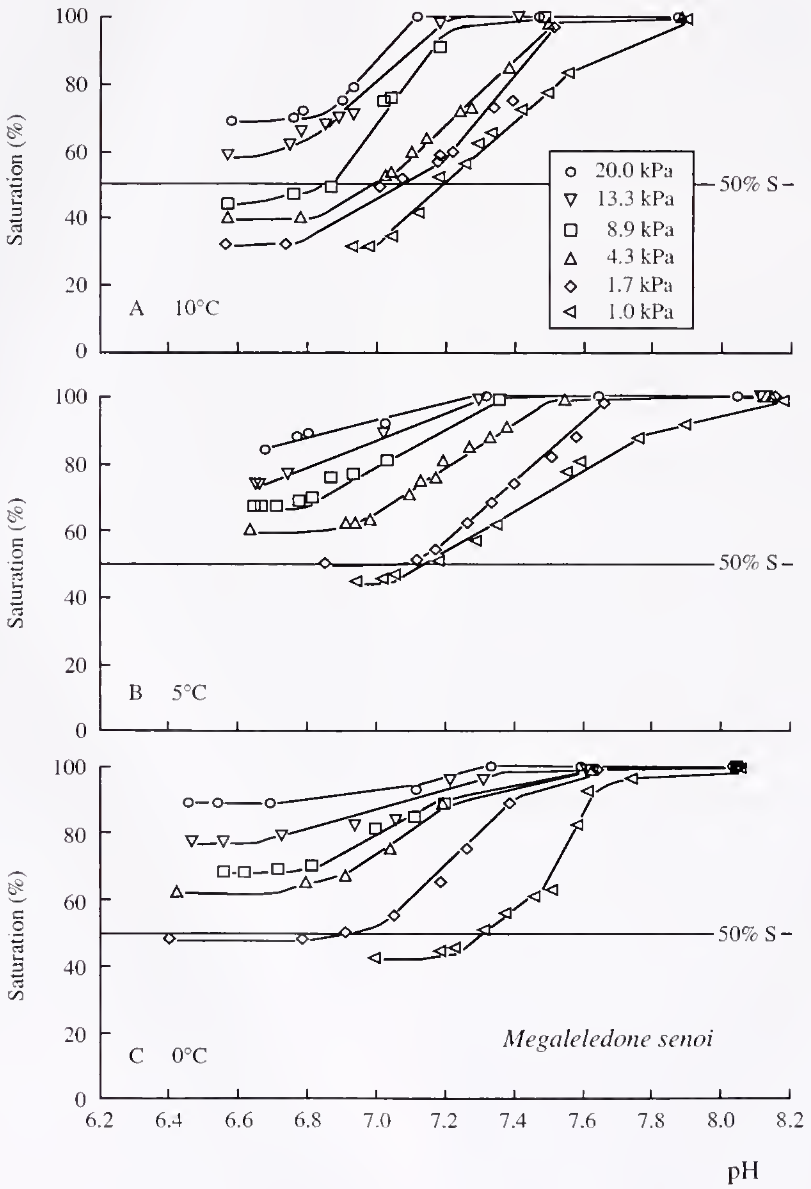

Figure 2. Continuous analysis of the relationships between oxygen binding, pH, and Po_2 in whole blood of the Antarctic octopod *Megaleledone senoi* at temperatures between 0 and 10 °C (S = saturation; points were chosen at regular intervals from the continuous recordings).

Table 1

Oxygen affinity (P_{50}), Bohr, Haldane, and Hill coefficients evaluated for the hemocyanins of the Antarctic octopod Megaleledone senoi *and of the cuttlefish* Sepia officinalis *at different temperatures*

Temperature (°C)	P_{50} (kPa)	Bohr coefficient (Δ log P_{50}/ΔpH)	(Δ log P_{80}/ΔpH)	Haldane coefficient ($\Delta HCO_3^-/\Delta HcyO_2$)	Hill coefficient (n_{50})
Megaleledone senoi					
0	0.98 (pH 7.2)	≈ −0.9	−1.51	0.66 (pH 6.2) 0.50 (pH 6.8) 0.39 (pH 7.2)	1.4 (pH 7.43)
5		ND	−1.46	ND	1.5 (pH 7.24) 1.0 (pH 7.31)
10	1.10 (pH 7.2)	−2.33	−2.13	ND	1.2 ± 0.1 (pH 6.83–7.31; n = 6)
Sepia officinalis					
10	5.3 (pH 7.4)	−0.99	−1.44		4.6 (pH 7.29)
20	6.5 (pH 7.4)	−1.33	−1.94		5.9 (pH 7.48)

P_{50}, Haldane, and Hill coefficients are valid for the pH values given in brackets. ND, not determined; $HcyO_2$, concentration of oxygenated hemocyanin.

Po_2. Intermediate values of pH sensitivity and maximum unloading were found at 5 °C.

A large Bohr coefficient of −2.33 was found at 10 °C, similar to the coefficient Δ log P_{80}/Δ pH (Table 1). The experimental evaluation of the Bohr coefficient was not possible at lower temperatures due to the fact that pH-dependent saturation did not drop below 50% at most partial pressures of oxygen. An extrapolation of binding data to very low partial pressures of oxygen revealed a Bohr coefficient of approximately −0.9 at 0 °C, below the level of Δ log P_{80}/ΔpH. Furthermore, oxygen affinity (P_{50}) at pH 7.2 changed only at ΔP_{50}/°C < 0.01 kPa, from 0.98 kPa at 0 °C to 1.10 kPa at 10 °C (Table 1).

For *S. officinalis* hemocyanin, pH sensitivity was high at 20 °C, reaching a maximum $\Delta S/\Delta$pH of 41% per pH unit (Fig. 3). Especially in the pH range between 7.4 and 7.8, very small pH changes were sufficient to cause maximal unloading of oxygen, down to 19% saturation. The pH sensitivity at 20 °C was higher than found for *M. senoi* at all temperatures. As in *M. senoi*, lower temperatures decreased the pH sensitivity of oxygen binding with a decreased Bohr factor and level of Δ log P_{80}/ΔpH (Table 1) and an increase in the pH-insensitive reserve at the same Po_2. At 0 °C, $\Delta S/\Delta$pH reached a maximal value of only 7% per pH unit. Oxygen saturation remained above 50% at all investigated partial pressures of oxygen and values of pH. At pH 7.4, oxygen affinity fell from P_{50} = 5.3 kPa at 10 °C to P_{50} = 6.5 kPa at 20 °C (ΔP_{50}/°C = 0.12 kPa, Table 1).

The change in cooperativity with pH and temperature for *S. officinalis* is shown in Figure 4. At 20 °C, the largest Hill coefficient (n_{50}) of 5.9 was found at a pH (7.48) where pH sensitivity ($\Delta S/\Delta$pH) was also high. A decrease in temperature to 10 °C resulted in a decrease of the maximal Hill coefficient to n_{50} = 4.6 (pH 7.29). The maximum was shifted to lower pH. In contrast to cuttlefish, *M. sensoi* had much lower Hill coefficients (Table 1). At 0 °C, n_{50} was 1.4 (pH 7.43), and it varied between 1.0 (pH 6.83) and 1.4 (pH 7.31) at 10 °C. No clear maximum could be found.

Analysis of total CO_2 in *M. senoi* blood during variations of Po_2 and Pco_2 yields the buffer lines depicted in the pH/bicarbonate diagram (Fig. 5). The position of the buffer line shifts between oxygenated and deoxygenated blood according to the quantity of H^+ bound by the pigment. The vertical distance between the buffer lines yields the Haldane coefficient ($\Delta HCO_3^-/\Delta HcyO_2$). For *M. senoi* hemocyanin at 0 °C, the Haldane coefficient rose with falling pH (Table 1). The calculated apparent bicarbonate levels for oxygenated and deoxygenated blood diverge only slightly from the measured values, suggesting that O_2-linked CO_2 binding does not exist (Fig. 5). The non-bicarbonate buffer value (β_{NB}) of 4.25 mmol l^{-1} pH $units^{-1}$ of *M. senoi* blood at 0 °C is in the same range as in the squids *Illex illecebrosus* and *Loligo pealei* (5.0 and 5.8 mmol l^{-1} pH $units^{-1}$, respectively; Pörtner, 1990).

Discussion

At the low temperatures of Antarctica icefishes rely exclusively on the transport of oxygen that is physically dissolved in the blood (see Introduction). The presence of hemocyanin-bound oxygen in *Megaleledone senoi* blood at levels similar to those seen in squids and temperate octopods (*cf.* Brix *et al.*, 1989) suggests that oxygen transport *via* hemocyanin is as important in this Antarctic species as in temperate and warm-water cephalopods. In contrast to Antarctic fishes, the unchanged requirement for blood oxygen transport in Antarctic cephalopods may be related to the

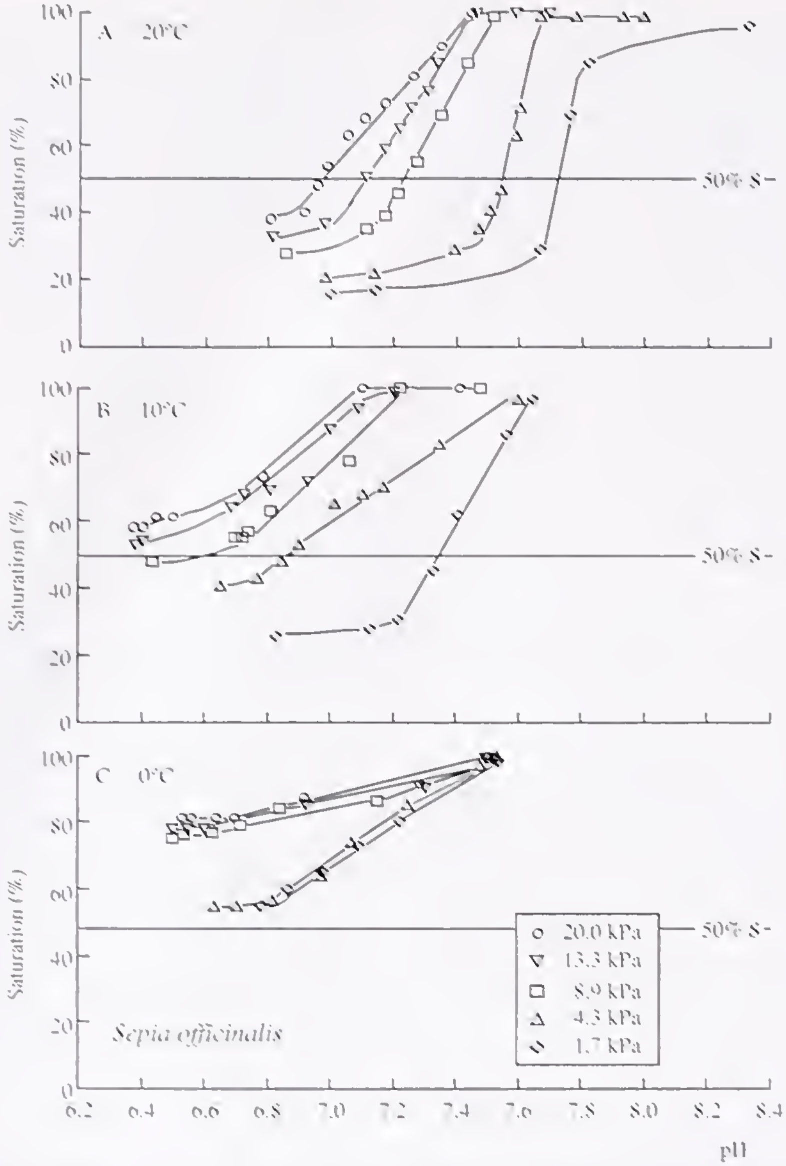

Figure 3. Depiction of oxygen-binding properties of *Sepia officinalis* hemocyanin at temperatures between 0 and 20 °C in a pH saturation diagram. Each line indicates an oxygen isobar and shows the changes in oxygen binding depending on pH (S = saturation; points were chosen at regular intervals from the continuous recordings).

low level of capillarization of cephalopod musculature compared to fish muscles (Bone *et al.*, 1981).

In cephalopods, pH and temperature are most important factors in the regulation of hemocyanin oxygen transport (Brix *et al.*, 1989; Bridges, 1994; Pörtner, 1994). The temperature dependence of P_{50} varies greatly between species. For example, the oxygen affinity of the hemocyanin of giant squid (*Architeuthis monachus*) decreases at $\Delta P_{50}/\Delta T$ = 1.89 kPa per degree Celsius (pH 7.4), while a value of only 0.20 kPa/°C (pH 7.4) was found for the octopod *Octopus vulgaris* (calculated after Brix *et al.*, 1989). A lower value of $\Delta P_{50}/\Delta T$ = 0.10 kPa/°C (pH 7.4) was found for the octopod *Eledone cirrhosa* (calculated after Bridges, 1994); this was similar to the value of 0.12 kPa/°C (pH 7.4) calculated for *Sepia officinalis* hemocyanin in the present study. In eurythermal cephalopods like *Sepia officinalis*, *Octopus vulgaris*, or *Eledone cirrhosa* and in some squids, a moderate rise in P_{50} with temperature occurs (*cf.* Brix *et al.*, 1994). In this way capillary P_{O_2} is maintained ("buffered") at progressively higher levels, which are required for elevated diffusive oxygen flux to mitochondria during increased rates of oxygen consumption. Such changes in P_{50} with temperature allow *S. officinalis* to be distributed over a wide range, from the Mediterranean to the North Sea (von

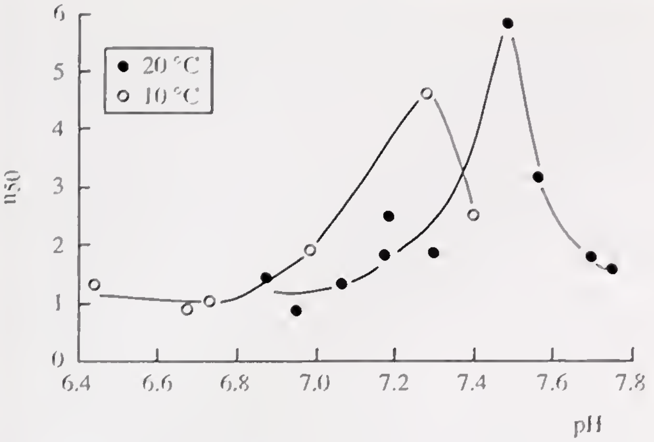

Figure 4. Hill coefficients (n_{50}) of *Sepia officinalis* hemocyanin depending on pH and temperature.

Boletzky, 1983). In contrast, the extreme thermal sensitivity of P_{50} seen in giant squid may eliminate oxygen transport by hemocyanin and contribute to the heat intolerance of these animals (Brix, 1983). The very small adjustments of P_{50} found in *M. senoi* hemocyanin ($\Delta P_{50}/\Delta T$ = 0.01 kPa/°C, pH 7.2) may also be detrimental, because when temperature rises, blood Po_2 will be held at levels too low to adequately support an increase in metabolic rate. In consequence, Antarctic octopods like *M. senoi* are very stenothermal (Pörtner and Zielinski, 1998).

For *S. officinalis* the greatest pH sensitivity (Fig. 3) at 20 °C was found in the range of *in vivo* blood pH (7.4–7.8 at 17–19 °C; Johansen *et al.*, 1982a). The same phenomenon occurs in squid (Pörtner, 1990). The fact that the oxygen transport system responds to even small changes in extracellular acid-base status is consistent with the pH-dependent Po_2 buffer function of the hemocyanin (Pörtner, 1994). This is not surprising, because cephalopods regulate primarily extracellular, not intracellular, acid-base balance (Pörtner, 1994).

The blood pH of the Antarctic octopod is not known. Assuming that blood pH follows α-stat predictions (Reeves, 1972) and is high in the cold, as seen in *Loligo pealei* blood *in vitro* (Howell and Gilbert, 1976), the *in vivo* pH range for *M. senoi* is between pH 7.7 and 7.9 at 0 °C. With the highest pH sensitivity in this pH range, oxygen unloading would occur at very low oxygen tensions ($<$1 kPa), supporting only very low metabolic rates (Fig. 2). A P_{50} below 1 kPa (pH 7.6; 0 °C) reflects one of the highest oxygen affinities reported so far for cephalopods. This value is close to the P_{50} of 0.47 to 0.55 kPa evaluated for the cold-water vampire squid *Vampyroteuthis infernalis* (5 °C; Seibel *et al.*, 1999). These findings suggest that *M. senoi* displays a low metabolic rate similar to that of the Antarctic octopod *Pareledone charcoti* (0.3 μmol g^{-1} h^{-1} at 0 °C and about 50 g body weight; H. O. Pörtner, T. Hirse, V. Wegewitz, unpubl. data, 15 times lower than similar sized *S. officinalis* at 17 °C, 4.4 μmol g^{-1} h^{-1}, Johansen *et al.*, 1982b) or even lower and close to the 0.1 μmol g^{-1} h^{-1} measured at 5 °C in the deep-sea squid *Vampyroteuthis infernalis* (Seibel *et al.*, 1997).

The Bohr coefficient evaluated for both investigated cephalopod species dropped when temperature decreased. This result is similar to findings in the crustaceans *Cancer magister* and *Cancer anthonyi* (Burnett *et al.*, 1988) and in the octopod *Eledone cirrhosa* (Bridges, 1994). In *S. officinalis*, Δ log P_{50}/ΔpH decreased moderately, from −1.33 at 20 °C to −0.99 at 10 °C (Table 1). In *M. senoi*, the Bohr coefficient fell drastically, from an extremely high value of −2.33 at 10 °C to a much smaller value evaluated by extrapolation to be −0.9 at 0 °C (Table 1). The Bohr factor in the vampire squid was found to be even lower (−0.22; Seibel *et al.*, 1999). These results indicate that the Bohr effect becomes less important at low temperature and low metabolic rate.

A mechanism of oxygen-linked CO_2 binding has been proposed for *Sepia* hemocyanin, which transports both O_2 and CO_2 to the tissues. The CO_2 produced in metabolism and the CO_2 released during deoxygenation would elicit a drop in pH, as required for the large Bohr effect ($<$ −1.0) to function normally (Lykkeboe *et al.*, 1980; Brix *et al.*, 1981). No oxygen-linked CO_2 transport was found in *M. senoi* (Fig. 5). At 0 °C, the estimated Bohr coefficient of Δ log P_{50}/ΔpH ≈ −0.9 would reflect normal function of the Bohr effect, whereas the extremely high Bohr coefficient at 10 °C would be counterproductive for oxygen transport.

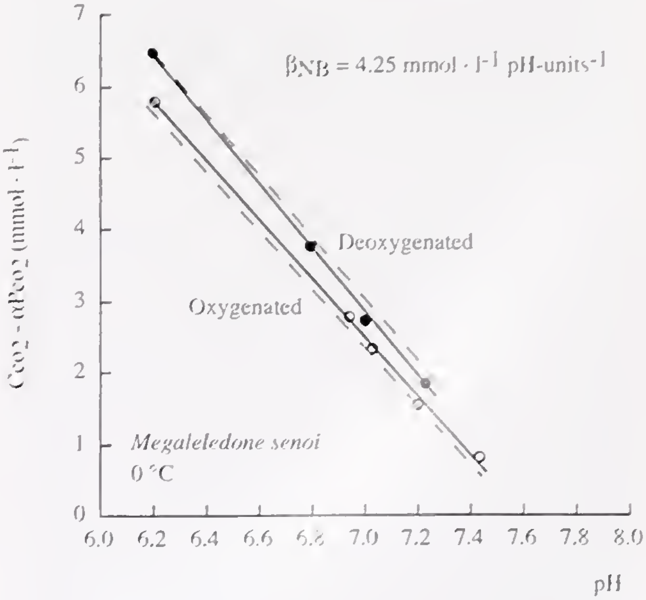

Figure 5. pH/bicarbonate diagram for whole blood of *Megaleledone senoi*. Experimental buffer lines of oxygenated and deoxygenated blood match those derived from calculated apparent bicarbonate levels (broken lines; see text).

a finding consistent with the stenothermality of Antarctic animals.

A reduced pH sensitivity of hemocyanin oxygen binding in *M. senoi* and other octopods compared to *S. officinalis* and squids is reflected in the magnitude of the pH-independent venous reserve, which rises as temperature falls (Figs. 2, 3). This reserve represents the amount of oxygen that remains bound to the respiratory pigment at constant Po_2, even when pH falls to very low values. Comparison of this venous reserve for several cephalopod species at normal environmental temperatures and low Po_2 shows that it is below 5% (at 1.7 kPa) for the squid *Illex illecebrosus* (15 °C; Pörtner, 1990), 19% (at 1.7 kPa) for *S. officinalis* (20 °C; this study), and 43% (at 1 kPa) for the Antarctic octopod *M. senoi* (0 °C; this study). A value of below 10% results for the hemocyanin of the octopod *Octopus dofleini* (at 1.7 kPa and 20 °C; Pörtner, 1990; calculated after Miller and Mangum, 1988); however, the *in vivo* value may be higher for this species because it lives at lower temperatures. The high pH sensitivity of squid hemocyanins maximizes the release of oxygen in the tissues and supports their high metabolic rate (Pörtner, 1990, 1994). Sepioids and, even more so, octopods display a less active life style with lower metabolic rates (for example: Houlihan *et al.*, 1982; Webber and O'Dor, 1985, 1986; Finke *et al.*, 1996; Seibel *et al.*, 1997). A low-activity mode of life may eliminate the necessity to maximize pH-dependent oxygen transport to the extent seen in squids.

With falling pH, the pH-independent venous reserve increased and was reached at higher Po_2 (88% at pH 6.8, 20 kPa O_2, and 0 °C in *M. senoi*, or 40% at pH 6.8, 20 kPa O_2, and 20 °C in *S. officinalis*). At normoxic Po_2 (20 kPa O_2) and low pH, this resembles a Root effect (Bridges, 1994) but at the same time, further pH sensitivity (the Bohr effect) is eliminated and deoxygenation depends exclusively on Po_2 (Figs. 2 and 3).

The cooperativity of respiratory pigments is characterized by the Hill coefficient (n_{50}). In *S. officinalis* at 20 °C (Fig. 4) and in the squids *Illex illecebrosus* and *Loligo vulgaris*, the highest cooperativity correlates with the highest pH sensitivity of oxygen binding ($\Delta S/\Delta$pH) in the range of *in vivo* pH (Pörtner, 1990). Here maximal deoxygenation occurs at minimal pH change (Pörtner, 1990, 1994). A decrease in temperature caused the maximal Hill coefficient of *S. officinalis* hemocyanin to drop from n_{50} = 5.9 at 20 °C to n_{50} = 4.6 at 10 °C. At the same time, maximum cooperativity was shifted to lower pH values, when *in vivo* pH should rise according to α-stat predictions (Reeves, 1972). A similar temperature dependence of the Hill coefficient was found for several crustaceans (Mauro and Mangum, 1982a,b). As with the Bohr effect, the progressive mismatch between the pH range of maximum cooperativity and the actual blood pH suggests that cooperativity becomes less important in oxygen transport at lower temperatures. Accordingly, a low cooperativity of n_{50} = 1.4 was found for *M. senoi*, at 0 °C (Table 1) and of n_{50} = 2.2 for the vampire squid (Seibel *et al.*, 1999). Surprisingly, cooperativity did not increase with temperature in *M. senoi* hemocyanin.

The question arises as to why thermal sensitivity is so low in *M. senoi* hemocyanin but so high in the blood pigment of cold-adapted giant squid (*cf.* Brix, 1983). A high value of ΔP_{50} $°C^{-1}$ reflects a high heat of oxygenation (*cf.* Brix *et al.*, 1994) or Arrhenius activation energy. Giant squid probably display higher metabolic rates and thus must maintain P_{50} levels higher than those of *M. senoi*. A high heat of oxygenation may be required for setting P_{50} values high at low temperature as in giant squid. In that respect the low thermal sensitivity of hemocyanin in the Antarctic octopod is again in accordance with the low metabolic rate of this group.

In summary, the pH sensitivity of oxygen binding in cephalopod hemocyanins is adjusted to metabolic rate. The pH-insensitive oxygen reserve in hemocyanin was largest in *M. senoi* and intermediate in *S. officinalis*, if compared to squids (this study and Pörtner, 1990). Furthermore, the Bohr effect is reduced and the pH-insensitive oxygen reserve rises during cooling, suggesting that pH sensitivity falls in the cold. The temperature dependence of the Bohr factor is less pronounced in the eurythermal *S. officinalis*, which would, together with an appropriate change in P_{50}, ensure a supply of oxygen at changing temperatures. In *M. senoi*, a high oxygen affinity of hemocyanin, a moderately high Bohr coefficient, and a low cooperativity at 0 °C cause blood Po_2 to be maintained ("buffered") at low values matching a low rate of oxygen consumption. In this species the low thermal sensitivity of oxygen affinity prevents an upward shift of the buffered Po_2 at higher temperatures, suggesting that oxygen transfer to tissues may become limiting when oxygen demand rises. This observation is in contrast to the findings in giant squid, where arterial oxygen uptake is hampered by an excessive drop in oxygen affinity, thereby limiting heat tolerance (Brix, 1983). Accordingly, hemocyanin function probably contributes to an oxygen limitation of heat tolerance that sets in early and characterizes thermal tolerance in Antarctic octopods (Pörtner and Zielinski, 1998) and probably also in giant squid.

Acknowledgments

The authors thank Iris Hardewig and Boris Klein for sampling hemolymph from *Megaleledone senoi* during the expedition with RV *Polarstern*. The technical and logistical help by the staff of the Marine Biomedical Institute is gratefully acknowledged. Supported by grants of the Deutsche Forschungsgemeinschaft to H.O. Pörtner (Po 278).

Literature Cited

Bone, Q., A. Pulsford, and A. D. Chubb. 1981. Squid mantle muscle. *J. Mar. Biol. Assoc. UK* **61:** 327–342.

Boutilier, R. G., G. K. Iwama, T. A. Heming, and D. J. Randall. 1985. The apparent pK of carbonic acid in rainbow trout blood plasma between 5 and 15 °C. *Respir. Physiol.* **61:** 237–254.

Bridges, C. R. 1994. Bohr and Root effects in cephalopod haemocyanins—paradox or pressure in *Sepia officinalis?* Pp. 121–130 in *Physiology of Cephalopod Molluscs—Lifestyle and Performance Adaptations*, H. O. Pörtner, R. K. O'Dor, and D. MacMillan, eds. Gordon and Breach, Basel.

Brix, O. 1983. Giant squids may die when exposed to warm water currents. *Nature* **303:** 422–423.

Brix, O., G. Lykkeboe, and K. Johansen. 1981. The significance of the linkage between the Bohr and Haldane effects in cephalopod bloods. *Respir. Physiol.* **44:** 177–186.

Brix, O., A. Bardgard, A. Cau, A. Colosimo, S. G. Condò, and B. Giardina. 1989. Oxygen-binding properties of cephalopod blood with special reference to environmental temperatures and ecological distribution. *J. Exp. Zool.* **252:** 34–42.

Brix, O., A. Colosimo, and B. Giardina. 1994. Temperature dependence of oxygen binding to cephalopod haemocyanins: ecological implications. Pp. 149–162 in *Physiology of Cephalopod Molluscs—Lifestyle and Performance Adaptations*, H. O. Pörtner, R. K. O'Dor, and D. MacMillan, eds. Gordon and Breach, Basel.

Burnett, L. E., D. A. Scholnick, and C. P. Mangum. 1988. Temperature sensitivity of molluscan and arthropod hemocyanins. *Biol. Bull.* **174:** 153–162.

Clarke, A. 1988. Seasonality in the Antarctic marine environment. *Comp. Biochem. Physiol.* **90B:** 461–473.

Finke, E., H. O. Pörtner, P. G. Lee, and D. M. Webber. 1996. Squid (*Lolliguncula brevis*) life in shallow waters: oxygen limitation of metabolism and swimming performance. *J. Exp. Biol.* **199:** 911–921.

Heisler, N. 1986. Buffering and transmembrane ion transfer processes. Pp. 3–47 in *Acid-Base Regulation in Animals*, N. Heisler, ed. Elsevier, Amsterdam.

Houlihan, D. G., A. J. Innes, M. J. Wells, and J. Wells. 1982. Oxygen consumption and blood gases of *Octopus vulgaris* in hypoxic conditions. *J. Comp. Physiol.* **148:** 35–40.

Howell, B. J., and D. L. Gilbert. 1976. pH-temperature dependence of the hemolymph of the squid, *Loligo pealei. Comp. Biochem. Physiol.* **55A:** 287–289.

Isemer, H. J., and L. Hasse. 1985. *The Bunker Climate Atlas of the North Atlantic Ocean. Vol I: Observations.* Springer Verlag, Berlin. 218 pp.

Johansen, K., O. Brix, and G. Lykkeboe. 1982a. Blood gas transport in the cephalopod, *Sepia officinalis. J. Exp. Biol.* **99:** 331–338.

Johansen, K., O. Brix, S. Kornerup, and G. Lykkeboe. 1982b. Factors affecting O_2 uptake in the cuttlefish, *Sepia officinalis. J. Mar. Biol. Assoc. UK* **62:** 187–191.

Kubodera, T., and T. Okutani. 1986. New and rare cephalopods from the Antarctic waters. *Mem. Natl. Inst. Polar Res., Spec. Issue* **44:** 129–143.

Kubodera, T., and T. Okutani. 1994. Eledonine octopods from the Southern Ocean: systematics and distribution. In *Southern Ocean Cephalopods: Life Cycles and Populations*, P. G. Rodhouse, U. Piatkowski and C. C. Lu, eds. *Antarct. Sci.* **6:** 205–214.

Lenfant, C., and C. Aucutt. 1966. Measurement of blood gases by gas chromatography. *Respir. Physiol.* **1:** 398–407.

Lykkeboe, G., O. Brix, and K. Johansen. 1980. Oxygen-linked CO_2 binding independent of pH in cephalopod blood. *Nature* **287:** 330–331.

Mangum, C. P. 1983. Oxygen transport in the blood. Pp. 373–429 in *The Biology of Crustacea*, Vol. 3, L. H. Mantel, ed. Academic Press, New York.

Mangum, C. P. 1990. Gas transport in the blood. Pp. 443–468 in *Squid as Experimental Animals*, D. L. Gilbert, E. J. Adelman, Jr., and J. M. Arnold, eds. Plenum, New York.

Mauro, N. A., and C. P. Mangum. 1982a. The role of the blood in the temperature dependence of oxidative metabolism in decapod crustaceans. I. Intraspecific responses to seasonal differences in temperature. *J. Exp. Zool.* **219:** 179–188.

Mauro, N. A., and C. P. Mangum. 1982b. The role of the blood in the temperature dependence of oxidative metabolism in decapod crustaceans. II. Interspecific adaptations to latitudinal changes. *J. Exp. Zool.* **219:** 189–195.

Miller, K. I. 1985. Oxygen equilibria of *Octopus dofleini* hemocyanin. *Biochemistry* **24:** 4582–4586.

Miller, K. I. 1994. Cephalopod hemocyanins. A review of structure and function. Pp. 101–120 in *Physiology of Cephalopod Molluscs—Lifestyle and Performance Adaptations*, H. O. Pörtner, R. K. O'Dor, and D. MacMillan, eds. Gordon and Breach, Basel.

Miller, K., and C. P. Mangum. 1988. An investigation of the nature of Bohr, Root, and Haldane effects in *Octopus dofleini* hemocyanin. *J. Comp. Physiol.* **158B:** 547–552.

Morris, S., A. C. Taylor, C. R. Bridges, and M. K. Grieshaber. 1985. Respiratory properties of the haemolymph of the intertidal prawn *Palaemon elegans* (Rathke). *J. Exp. Zool.* **233:** 175–186.

Nickerson, K. W., and K. E. van Holde. 1971. A comparison of molluscan and arthropod hemocyanin. I. Circular dichroism and absorption spectra. *Comp. Biochem. Physiol.* **39B:** 855–872.

O'Dor, R. K., and D. M. Webber. 1986. The constraints on cephalopods: why squid aren't fish. *Can. J. Zool.* **64:** 1591–1605.

Pörtner, H. O. 1990. An analysis of the effects of pH on oxygen binding by squid (*Illex illecebrosus, Loligo pealei*) haemocyanin. *J. Exp. Biol.* **150:** 407–424.

Pörtner, H. O. 1994. Coordination of metabolism, acid-base regulation and haemocyanin function in cephalopods. Pp. 131–148 in *Physiology of Cephalopod Molluscs—Lifestyle and Performance Adaptations*, H. O. Pörtner, R. K. O'Dor, and D. MacMillan, eds. Gordon and Breach, Basel.

Pörtner, H. O., and S. Zielinski. 1998. Environmental constraints and the physiology of performance in squids. In *Cephalopod Biodiversity, Ecology and Evolution*, A. I. L. Payne, M. R. Lipinski, M. R. Clarke, and M. A. C. Roeleveld, eds. *S. Afr. J. Mar. Sci.* **20:** 207–221.

Pörtner, H. O., P. L. M. van Dijk, I. Hardewig, and A. Sommer. 2000. Levels of metabolic cold adaptation: tradeoffs in eurythermal and stenothermal ectotherms. Pp. 109–122 in *Antarctic Ecosystems: Models for Wider Ecological Understanding*. W. Davison and C. Howard Williams, eds. Caxton Press, Christchurch, New Zealand.

Reeves, R. B. 1972. An imidazole alphastat hypothesis for vertebrate acid-base-regulation: tissue carbon dioxide content and body temperature in bullfrogs. *Respir. Physiol.* **81:** 255–274.

Roper, C. F. E., M. J. Sweeney, and C. E. Nauen. 1984. *FAO Species Catalogue. Vol. 3: Cephalopods of the World. An Annotated and Illustrated Catalogue of Species of Interest to Fisheries. FAO Fisheries Synopses 125*, FAO/UNDP, Rome. 277 pp.

Ruud, J. T. 1954. Vertebrates without erythrocytes and blood pigment. *Nature* **173:** 848–850.

Seibel, B. A., E. V. Thuesen, J. J. Childress, and L. A. Gorodezky. 1997. Decline in pelagic cephalopod metabolism with habitat depth reflects differences in locomotory efficiency. *Biol. Bull.* **192:** 262–278.

Seibel, B. A., F. Chausson, F. H. Lallier, F. Zal, and J. J. Childress. 1999. Vampire blood: respiratory physiology of the vampire squid (Cephalopoda: Vampyromorpha) in relation to the oxygen minimum layer. *Exp. Biol. Online* **4:** 1.

Senozan, N. M., A. Avinc, and Z. Unver. 1988. Hemocyanin levels in *Octopus vulgaris* and the cuttlefish *Sepia officinalis* from the Aegean sea. *Comp. Biochem. Physiol.* **91A:** 581–585.

Shadwick, R. E., R. K. O'Dor, and J. M. Gosline. 1990. Respiratory and cardiac function during exercise in squid. *Can. J. Zool.* **68:** 192–198.

Urich, K. 1990. *Vergleichende Biochemie der Tiere.* Gustav Fischer, Stuttgart. 708 pp.

Taki, I. 1961. On two new eledonid octopods from the Antarctic sea. *J. Fac. Fish. Anim. Husb. Hiroshima Univ.* **3:** 297–316.

von Boletzky, S. 1983. *Sepia officinalis.* Pp. 31–52 in *Cephalopod Life Cycles,* Vol. I. P. R. Boyle, ed. Academic Press, London.

Webber, D. M., and R. K. O'Dor. 1985. Respiration and swimming performance of short-finned squid (*Illex illecebrosus*). *Northwest Atl. Fish. Organ. Sci. Counc. Stud.* **9:** 133–138.

Webber, D. M., and R. K. O'Dor. 1986. Monitoring the metabolic rate and activity of free-swimming squid with telemetered jet pressure. *J. Exp. Biol.* **126:** 203–224.

Wells, M. J., R. T. Hanlon, P. G. Lee, and F. P. Dimarco. 1988. Respiratory and cardiac performance in *Lolliguncula brevis* (Cephalopoda, Myopsida): the effects of activity, temperature and hypoxia. *J. Exp. Biol.* **138:** 17–36.

Reference: *Biol. Bull.* **200:** 77–86. (February 2001)

Muscular Alteration of Gill Geometry *in vitro*: Implications for Bivalve Pumping Processes

SCOTT MEDLER* AND HAROLD SILVERMAN

Louisiana State University, Baton Rouge, Louisiana 70803

Abstract. In bivalves, water-pumping potential is determined both by ciliary activity and by the geometry of the system of passageways that acts as a conduit for water flow. Smooth muscles intrinsic to the gills of eulamellibranch bivalves possess the anatomical organization needed to regulate the dimensions of these water passageways. The tone of these muscles can be controlled experimentally using excitatory neurotransmitters to elicit muscle contraction and by removing Ca^{++} from the Ringer's solution to induce muscular relaxation. These experimental methods were used to investigate the effects of smooth muscle tone on the gill dimensions of two freshwater bivalves, *Dreissena polymorpha* and *Corbicula fluminea*, and one marine bivalve, *Mercenaria mercenaria*. In addition, endoscopic observations were made from the suprabranchial chamber of a freshwater unionid, *Lampsilis anodontoides*. Contraction of gill muscles led to a significant reduction in interfilament width, internal ostial area, and the cross-sectional area of the water tubes. Endoscopic observation from minimally disturbed *L. anodontoides* revealed rapid constriction of the water tubes upon contraction of the muscles of the gill and gill axis. Taken together, these data support the idea that alteration of smooth muscle tone in the gill provides a mechanism for controlling water-pumping activities.

Introduction

Filter-feeding is a complex process, employed by a diverse assemblage of aquatic animals, in which small particles are separated from the water suspending these food items (reviewed by Jørgensen, 1990; Riisgård and Larsen, 1995). Filter-feeding animals exhibit a variety of convergent designs for pumping water, shaped both by the intrinsic limitations of biological systems and by extrinsic constraints such as those arising from the physical nature of the environment (LaBarbera, 1990; Vogel, 1994). Bivalves, brachiopods, ascidians, and other distinct phyla all use the same type of low-velocity ciliary pump in their filter-feeding processes (LaBarbera, 1990; Vogel, 1994; Riisgård and Larsen, 1995). Most biological pumps consist of a pump and a system, where the pump represents the pressure-generating component and the series of vessels or "pipes" acting as conduits for water flow constitute the system (Jørgensen, 1989; LaBarbera, 1990; Riisgård and Larsen, 1995; Grünbaum *et al.*, 1998). In animals that use low-velocity ciliary pumps, the beating cilia collectively represent the pump, and the system consists of an incurrent region, a transfer region, and an excurrent region (LaBarbera, 1990; Riisgård and Larsen, 1995). The term "bivalve pump" is used to describe the water-pumping processes of filter-feeding bivalves, independent of other events such as particle capture and feeding (Jørgensen *et al.*, 1986).

Extensive research has been carried out to better understand bivalve pumping processes, and data on the rate of water pumping by various bivalves provide an important component needed to develop general models of the pumping process (Foster-Smith, 1976; Møhlenberg and Riisgård, 1979; Silvester and Sleigh, 1984; Meyhöfer, 1985; Jørgensen *et al.*, 1986, 1990; Jørgensen and Riisgård, 1988; Kryger and Riisgård, 1988; Silvester, 1988; Jørgensen, 1989; Jones *et al.*, 1992; Nielsen *et al.*, 1993). There is general agreement that the lateral ciliated cells provide the driving force for water flow and that changes in valve gape and siphon dimension contribute to adjustments in pumping rate. However, little work has addressed the potential role of other system components in regulating pumping processes, and a detailed understanding of the overall control of pumping remains elusive. Debate continues as to whether pump-

Received 23 March 2000; accepted 19 October 2000.

* Author to whom correspondence should be addressed. Current address: Department of Biology, Colorado State University, Ft. Collins, CO 80523. E-mail: Skmedler@aol.com

ing and feeding are regulated only in an on/off mode (Jørgensen *et al.*, 1988; Jørgensen, 1996) or whether a more sophisticated physiological regulation of these processes is possible (Ward and Targett, 1989; Wildish and Saulnier, 1993; Navarro *et al.*, 1994; Ward *et al.*, 1997). Further refinement of bivalve pumping models requires more detailed knowledge of the gill itself.

Models of the bivalve pump have relied heavily on the principles of fluid mechanics to develop mathematical descriptions of pumping processes (Foster-Smith, 1976; Silvester and Sleigh, 1984; Jørgensen *et al.*, 1986, 1988; Silvester, 1988; Grünbaum *et al.*, 1998). This type of analysis requires a thorough knowledge of the animal's morphology to accurately estimate pumping properties. For example, the length and width of water passageways are used to estimate pressure losses stemming from the frictional resistance to flow. These system components are generally approached as rigid structures, with models applying fixed estimates of gill geometry to calculate system characteristics (Foster-Smith, 1976; Silvester and Sleigh, 1984; Jørgensen *et al.*, 1986, 1988; Silvester, 1988). Although this is a logical simplification for modeling purposes, a body of evidence indicates that smooth muscles are important in affecting the geometry of the passages that constitute the system (Setna, 1930; Elsey, 1935; Atkins, 1943; Gardiner *et al.*, 1991; Medler and Silverman, 1997, 1998). Poiseuille's law describes fluid flow in a circular pipe as: $Q = \pi \Delta P r^4 / 8 L \mu$, where Q is flow rate, ΔP is pressure difference, r is pipe radius, L is pipe length, and μ is dynamic viscosity of the fluid (LaBarbera, 1990). One of the implications of Poiseuille's law is that relatively small changes in vessel radius result in significant alteration of fluid flow. Many organisms take advantage of this principle to regulate flow by contracting or relaxing smooth muscles or muscle-like cells that line the vessels. For example, vertebrates modify arteriole diameter to regulate blood flow into capillary beds (Eckert *et al.*, 1988), sponges change water flow by contracting or relaxing porocytes and myocytes as water enters the animal (Bagby, 1964; Pearse *et al.*, 1987), and bivalves adjust flow through the alteration of siphon dimensions (Foster-Smith, 1976; Jørgensen *et al.*, 1986, 1988). In this study, we focus on the ability of the eulamellibranch gill to change the dimensions of water passageways by altering the tone of integral smooth muscles.

Bivalves possess several muscles that have the potential to affect water flow. The most widely recognized of these are the adductor muscles and muscles of the mantle edges and siphons that are important for controlling valve gape and siphon dimensions. The integral gill muscles are not as widely appreciated, but are also likely to play a role in basic pumping processes. Each of the individual conduits for water flow is closely associated with smooth muscle fibers that can alter the dimensions of these passageways (Setna, 1930; Elsey, 1935; Atkins, 1943; Gardiner *et al.*, 1991; Medler and Silverman, 1997, 1998). In addition, extensive muscles in the gill axis lying dorsal to the suprabranchial chamber are important in shortening the gill (Setna, 1930; Atkins, 1943). Previous endoscopic studies have documented changes in interfilament width, ostial dimension, and water-tube dimension in living animals (Tankersley and Dimock, 1993; Ward *et al.*, 1994; Tankersley, 1996). Although the exact mechanism of such movements has not been clearly defined, these are consistent with the types of movements observed after the contraction of smooth muscles in the gill (Setna, 1930; Elsey, 1935; Atkins, 1943; Gardiner *et al.*, 1991; Medler and Silverman, 1997). Examination of gills in their fully relaxed and contracted states is useful for defining the extremes in a continuum of gill dimensions. We report here 2- to 6-fold differences between the dimensions of the water passages in fully relaxed and fully contracted gills.

Materials and Methods

Animals

Two freshwater bivalves, *Dreissena polymorpha* and *Corbicula fluminea*, and one marine species, *Mercenaria mercenaria*, were used for gill measurements. Large specimens (shell length about 10 cm) of the freshwater unionid *Lampsilis anodontoides* were used for endoscopic observations. *C. fluminea* and *L. anodontoides* were collected locally from ponds in Baton Rouge, Louisiana. *D. polymorpha* was collected from the Huron River in Michigan, and *M. mercenaria* was purchased from the Marine Biological Laboratory in Woods Hole, Massachusetts.

Solutions

Freshwater animals were maintained in aerated aquaria with artificial pondwater (APW) at 22–24°C as described in Dietz *et al.* (1994). Specimens of *M. mercenaria* were held in aerated aquaria with artificial seawater (ASW) at 4°C as specified in Chambers and De Armendi (1979). Ringer's solutions for the freshwater bivalves were prepared as described for *D. polymorpha* in Dietz *et al.* (1994), with differences in hemolymph osmolality between species being corrected by adding NaCl to the solutions as needed. For *M. mercenaria*, ASW was used in place of Ringer's solution. Calcium-free solutions were prepared by omitting Ca^{++} from the solutions and adding 4 m*M* EDTA in its place (Medler *et al.*, 1999). Neurotransmitters were added to Ringer's solution or ASW at a concentration of 1 m*M*, a pharmacological dose that has been shown to elicit maximal contraction of these muscles (Medler and Silverman, 1997; Gainey *et al.*, 1998). Acetylcholine is effective as an excitatory neurotransmitter in the gills of *D. polymorpha* (Medler and Silverman, 1997) and *C. fluminea* (Medler, unpub. obs.) and was used to stimulate contraction in these species.

Serotonin acts as an excitatory neurotransmitter in the gill muscles of *M. mercenaria* (Gainey *et al.*, 1998) and was used to stimulate contraction in this species.

Gill preparation

Gills were removed from animals by cutting along the dorsal connection to the body with surgical scissors and were placed in the appropriate Ringer's solution or ASW. The gills from one side of an animal were placed in a solution containing Ca^{++} before exposing them to an excitatory neurotransmitter; those of the opposite side were placed in a Ca^{++}-free solution. Interfilament width and internal ostial area were measured from live gills as described below.

Gills normally exhibit severe muscular contraction upon exposure to fixatives such as glutaraldehyde. This was not the case in the present study, since the gills with Ca^{++} available to trigger contraction were already contracted through exposure to excitatory neurotransmitter. In fact, any further contraction that occurred helped to ensure that the gill was in a fully contracted state. We have recently demonstrated that the removal of extracellular Ca^{++} blocks muscle contraction in the gills of *D. polymorpha* (Medler *et al.*, 1999), and this effect is also evident for *C. fluminea* and *M. mercenaria.* Exposure of these relaxed gills to glutaraldehyde failed to initiate any muscular contraction during the fixation process.

Water-tube measurements were made from gill sections. Excised gills were fixed with a 2% glutaraldehyde solution in isosmotic phosphate buffer for the freshwater species and a 2% glutaraldehyde solution in ASW for *M. mercenaria.* Tissues were fixed for 1 h in glutaraldehyde, rinsed twice in either buffer or ASW, and postfixed for 1 h in 1% OsO_4. After fixation, the gills were rinsed twice in deionized water and dehydrated in a graded ethanol series. Whole gills were embedded in LR White (London Resin Co.) medium-grade resin by first placing them in a 1:1 mixture of ethanol and resin for 24 h. They were then transferred to 100% resin for 12 h and embedded flat in fresh resin at 60°C for 24–48 h.

Water-tube dimension

A small portion of the central region of relaxed and contracted gills (approximate midpoint along both the dorsoventral and anterioposterior axes) was cut from embedded, fixed gills and cross-sectioned. Sections were cut using a Reichert-Jung ultracut E ultramicrotome at 1–2 μm thickness and stained with toluidine blue. The sections were viewed with a Nikon Microphot FXA using bright field optics, and the cross-sectional area of the water tube was measured from digitized video images using Image-1 computer software (Universal Imaging Corp.). Because muscle contraction causes a shortening of the gill in an anterioposterior direction, it was necessary to account for this change in our water-tube measurements. This adjustment was made by standardizing water-tube area per unit length of gill (number of filaments spanning the anterioposterior direction). Thus, water-tube area is given as (μm^2/filaments). This correction would be unnecessary if the total cross-sectional area of the gill were measured, but measurements were made from only a portion of the gill. Failing to correct for the shortening would overestimate the cross-sectional area in contracted gills. Water-tube dimensions from relaxed and contracted gills from individuals of each species were compared with paired t tests ($n = 5$).

Studies using fixed and dehydrated tissues are sometimes criticized for introducing artifacts due to shrinkage. Indeed, these procedures do lead to changes in gill dimensions that should be noted when an accurate measure of absolute dimensions is critical (Silverman *et al.*, 1995). In the present study, we were interested only in comparing the relative differences between important dimensions in the fully relaxed and fully contracted states. When the gills were fixed for measurement of water-tube area, each gill pair came from an individual animal and was processed with the same fixatives, dehydration steps, and embedding. Thus, any shrinkage is expected to be proportional in the relaxed and contracted gills, leaving the relative change unaffected.

Interfilament width

Live gills were placed on microscopic slides in the appropriate solution and covered by coverslips elevated on posts of petroleum jelly to prevent the gills from being compressed. Gills were examined with differential interference contrast (DIC) optics on a Nikon Microphot FXA. Interfilament distances from digitized video images were measured as described above, and distances were calibrated with a stage micrometer. Interfilament widths from relaxed and contracted gills from individuals of each species were compared by paired t tests ($n = 5$).

Internal ostial area

Live gills were split into single lamellae and placed in an irrigation chamber as described in a previous study (Medler and Silverman, 1997). Gill lamellae were placed in Ca^{++}-free solutions to completely relax their musculature before any measurements were made and remained in this solution when placed into the chamber. The internal water-channel epithelium was placed toward the bottom of the chamber so that the internal ostia could be observed using an inverted Nikon microscope with Hoffman modulation optics. After the relaxed gill ostia were measured, the chamber was irrigated with Ringer's or ASW containing an excitatory neurotransmitter. The gill was observed and videotaped as it contracted; the ostia were remeasured once contraction was complete (about 1 min later). Ostial areas (μm^2) were measured from digitized video images as described above and were calibrated with a stage micrometer in the experimental set-up. Ostial areas from relaxed and contracted gills from individuals of each species were compared with paired *t* tests ($n = 5$).

Scanning electron microscopy

Gills in contracted and relaxed states were fixed as described above. After dehydration, the gills were wrapped in lens paper, critical-point dried, and mounted on stubs. Dehydrated gills were either sectioned or split apart to reveal relevant regions of the gills. Specimens were sputter coated with a mixture of gold and palladium (20 nm) and viewed with a Cambridge S-260 scanning electron microscope. Digitized video images were enhanced for optimal brightness and contrast using Adobe Photoshop 5.0 software (Adobe Systems, Inc.).

Video endoscopy of live gills

An optical insertion tube (OIT) was inserted into the suprabranchial chamber of large specimens of *L. anodontoides* using the general approach described by Tankersley (1996). This species was selected because individuals tend to gape widely, allowing observations to be made without wedging the valves open. Animals were placed in an aerated container of APW (about 4 l) and fixed in position by means of a nylon bolt cemented to one valve. The OIT (1.7 mm diam. × 101 mm long; AEI North America) was attached to a 150 W halogen fiberoptic light source and inserted through the exhalent aperture into the suprabranchial chamber. A mirror sleeve was attached to the OIT to provide the 90° view needed for direct observation of the water tubes. The OIT was attached to a zoom adapter that provided a maximal magnification of about 150×. Maximum resolution was estimated to be approximately 5 μm at maximum magnification. The OIT and zoom adapter were coupled to a Costar color video camera (0.85 cm CCD model CV-730) mounted on a microscope stage. The microscope stage served as a micromanipulator, allowing movements in the *X*, *Y*, and *Z* planes. Observations were recorded on VHS videotape, and digitized video images of portions of these recordings were captured using Image-1 computer software. Images were adjusted for brightness and contrast using Adobe Photoshop 5.0 software.

No pharmacological agents were used during endoscopy. Animals were held in a darkened room, and once the endoscope was positioned, there was minimal disturbance to the animals. Changes in the geometry of the gills and suprabranchial chamber were spontaneous, not resulting from any discernible stimulus.

Results

Water flow through the eulamellibranch gill begins as water moves between parallel filaments and into the external ostia that lead into the water canals of the gill (Fig. 1). These canals empty through internal ostia into the central water channel that separates the ascending and descending gill lamellae. For clarification, some studies use the term "interfilament canal" to mean the space between filaments leading all the way into the central water channel of the gill (Jørgensen *et al.*, 1986), whereas others use the term "ostia" for the same canal system (Foster-Smith, 1976). We use the term "interfilament space" more strictly, as defining the region between filaments on the frontal face of the gill, and the term "ostia" to mean the openings of the water canals that lead from the interfilament space to the central water channel. The central water channel is partitioned into water tubes by septae that connect the two opposing gill lamellae. Water moves dorsally through the water tubes before emptying into the suprabranchial chamber and then out of the excurrent siphon.

Each of the dimensions from gills with relaxed muscles was significantly larger than those with muscles contracted. Interfilament width was approximately 20 μm in relaxed gills from each species and decreased to less than 10 μm after muscle contraction (Fig. 2). Contracted gills had significantly narrower interfilament widths than relaxed gills for each of the three species examined (mean ± SE): *Corbicula fluminea* (23.3 ± 0.7 *vs.* 8.7 ± 1.1 μm; $P < 0.002$), *Dreissena polymorpha* (19.2 ± 2.1 *vs.* 3.3 ± 0.3 μm; $P < 0.001$), *Mercenaria mercenaria* (22.7 ± 1.7 *vs.* 6.5 ± 0.6 μm; $P < 0.001$) (Fig. 2). In fully contracted gills, filaments viewed from the frontal surface appear to abut one another, often producing a zig-zag pattern along the length of the filaments (Fig. 2c). At the level of the lateral ciliated cells, even these gills have about 5 μm between the apical cell surfaces. This apparent discrepancy results from the fact that extended cilia project from the apical cell surfaces and obscure the small gap remaining between filaments.

Internal ostial dimension (per ostium) was quite variable between species, with *C. fluminea* and *M. mercenaria* having larger ostia than *D. polymorpha* (Fig. 3a). After muscular contraction, gills had significantly smaller individual ostial areas for each of the three species examined (mean ± SE): *C. fluminea* (9052 ± 701 *vs.* 3674 ± 404 μm^2; $P < 0.002$), *D. polymorpha* (3175 ± 436 *vs.* 1123 ± 393 μm^2; $P < 0.022$), *M. mercenaria* (16082 ± 1283 *vs.* 9949 ± 1186 μm^2; $P < 0.002$) (Fig. 3).

Water-tube dimension was also variable between species, with larger species having larger gills and water tubes (Fig. 4a). As the muscles of the gill contracted, the cross-sectional area of the water tubes significantly decreased in each species (mean ± SE): *C. fluminea* (8191 ± 727 *vs.* 4164 ± 364 μm^2/filament; $P < 0.002$), *D. polymorpha* (3486 ± 545 *vs.* 502 ± 161 μm^2/filament; $P < 0.005$), *M. mercenaria* (142982 ± 31212 *vs.* 22156 ± 5084 μm^2/filament; $P < 0.001$) (Fig. 4).

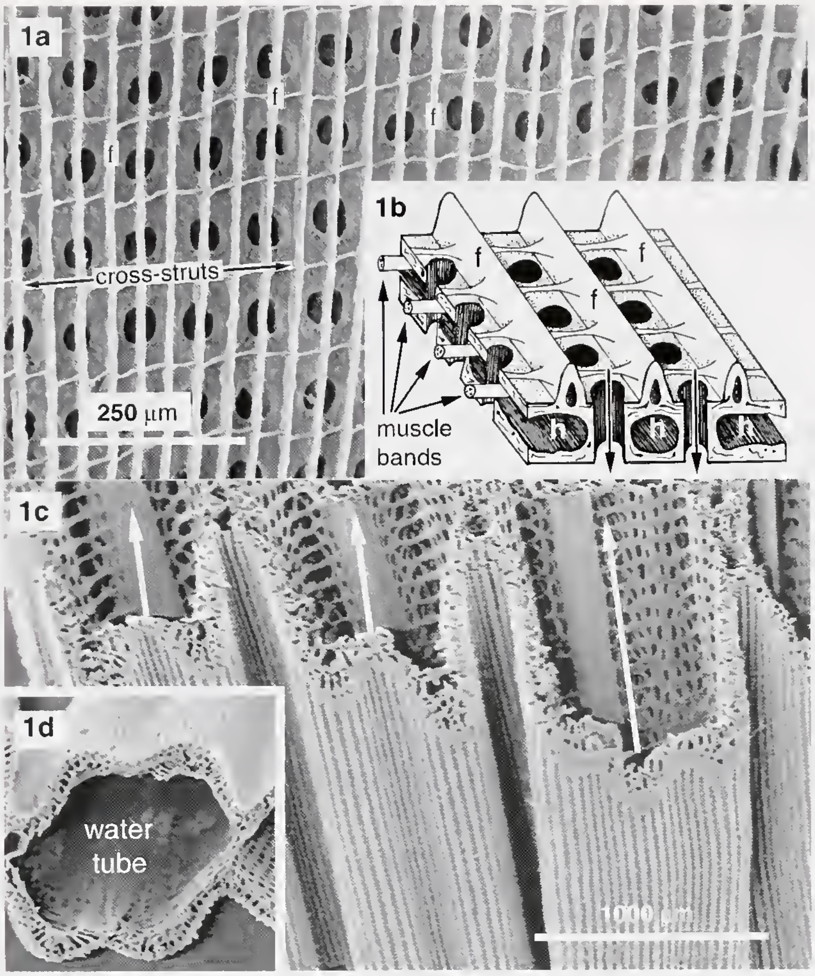

Figure 1. Eulamellibranch gill organization and water flow. (a, b) General organization of a single gill lamella with epithelial tissue removed to reveal the organization of the supporting structures (modified from Medler and Silverman, 1998, with permission from *Invertebrate Biology*). (a) *Dreissena polymorpha* gill (SEM) showing parallel filaments (*f*) held apart by connective tissue cross-struts. Bands of smooth muscles are found below the cross-struts (b); during muscle contraction, the cross-struts bend inwardly and the filaments are drawn closer to one another. In addition to these muscle bands, more diffuse smooth muscle fibers (depicted as thin wavy lines) are found in the connective tissue sheets that enclose the hemocoel (*h*) at the base of the filaments (b). Water is drawn into the central water channel of the gill through water canals (indicated by arrows in b). Ostia (dark openings perforating the gill lamellae) represent the ends of the water canals and provide a route for water to flow into the central region of the gill. (c, d) Frontal (c) and cross-sectional (d) views (SEM) of *Mercenaria mercenaria* gill, demonstrating the movement of water (indicated by arrows in c) through the water tubes of the gill after entering the gill through the water canals. The route of water flow through the gill is between the gill filaments and then through the gill ostia and associated water canals. Water moves to the suprabranchial chamber (not shown) though the water tubes of the central water channel. The suprabranchial chamber at the top of each gill is connected directly to the excurrent aperture where the water leaves the animal.

Endoscopic observations from the suprabranchial chamber of *Lampsilis anodontoides* revealed distinct changes in the geometry of the chamber and water tubes after spontaneous muscle contractions that caused obvious shortening of the gill and suprabranchial chamber. One such change was a rapid reduction in the cross-sectional area of the water tubes, which occurred during a time period of less than 5 s (Fig. 5). Part of the reduction in water-tube area resulted from a shortening of the gill axis, caused by contraction of a large bundle of muscle fibers located dorsal to the suprabranchial chamber and running in the anterioposterior direction. These muscle bundles were described for a number of species by Atkins (1943) and were identified in transverse sections of the dorsal gill region of *L. anodontoides* (data not shown). Many of the observed gill responses were not accompanied by any other obvious changes, such as valve closure. In fact, the valves usually continued to gape widely throughout the observational period.

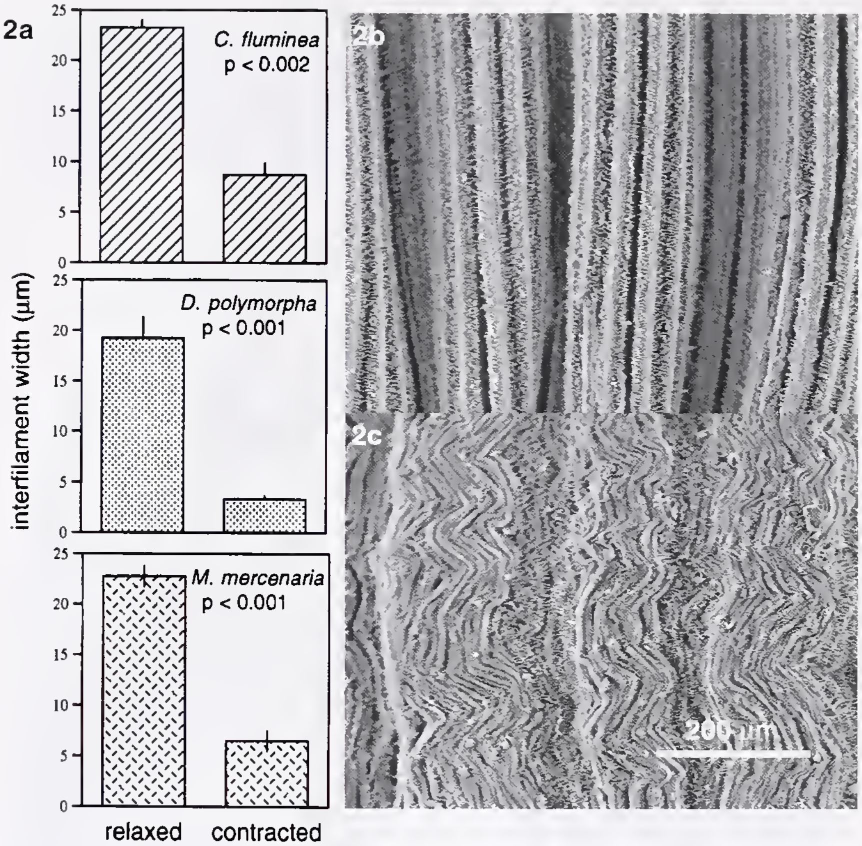

Figure 2. Interfilament distance. (a) Relaxed gills from each of the species (*Corbicula fluminea, Dreissena polymorpha,* and *Mercenaria mercenaria*) had an interfilament distance of about 20 μm, but this distance was significantly reduced to less than 10 μm upon muscle contraction (mean ± SE; $n = 5$). (b, c) Frontal face (SEM) of a *C. fluminea* gill: (b) relaxed gill; (c) gill from the same animal following muscle contraction.

Discussion

Two of the most important factors affecting bivalve pumping potential are the dimensions of the interfilament passages and the exit loss (derived from the kinetic energy carried by the water jet leaving the excurrent siphon) (Foster-Smith, 1976; Jørgensen *et al.*, 1986, 1988; Jørgensen and Riisgård, 1988; Jørgensen, 1989; Riisgård and Larsen, 1995). Both of these factors are ultimately controlled by muscle tone, since integral gill muscles control gill dimensions and exit loss is controlled by the muscles affecting siphon dimensions. It is reasonable to expect higher pumping rates when the gill muscles are fully relaxed, because in this condition the passageways for water flow are significantly more open than when the muscles contract. Jørgensen and colleagues have long held that pumping activities are correlated with the degree of valve gape and the associated changes of the gill (Jørgensen *et al.*, 1986, 1988; Jørgensen and Riisgård, 1988; Jørgensen, 1989, 1990). Their interpretation is that gill dimensions are controlled secondarily to the contraction of muscles within the gill axis and that the muscles of the gill axis contract when the adductor muscles reduce valve gape (Jorgensen *et al.*, 1988; Jørgensen, 1989, 1990). We agree with this general description, but would refine it by stipulating that interfilament distance and other gill dimensions are controlled directly by integral smooth muscles. Part of this distinction relates to the fact that Jorgensen's model is based on animals that possess filibranch gills, rather than the eulamellibranch organization described here. In filibranch gills, there is no direct connection between adjacent filaments aside from that made through the ciliary discs. Nevertheless, these discs clearly cause changes in interfilament distance even in excised gill fragments independent of the gill axis (Jørgensen, 1976; Jones *et al.*, 1992; Medler, unpub. obs.). In addition, such movements are probably aided by the muscles that attach at the base of the ciliary discs in many filibranch species (Atkins, 1943).

Jorgensen and colleagues have highlighted alteration of interfilament distance as a central control mechanism for regulating pumping activities (Jørgensen *et al.*, 1986, 1988; Jørgensen and Riisgård, 1988; Jørgensen, 1989, 1990). There are several possible consequences of changes in

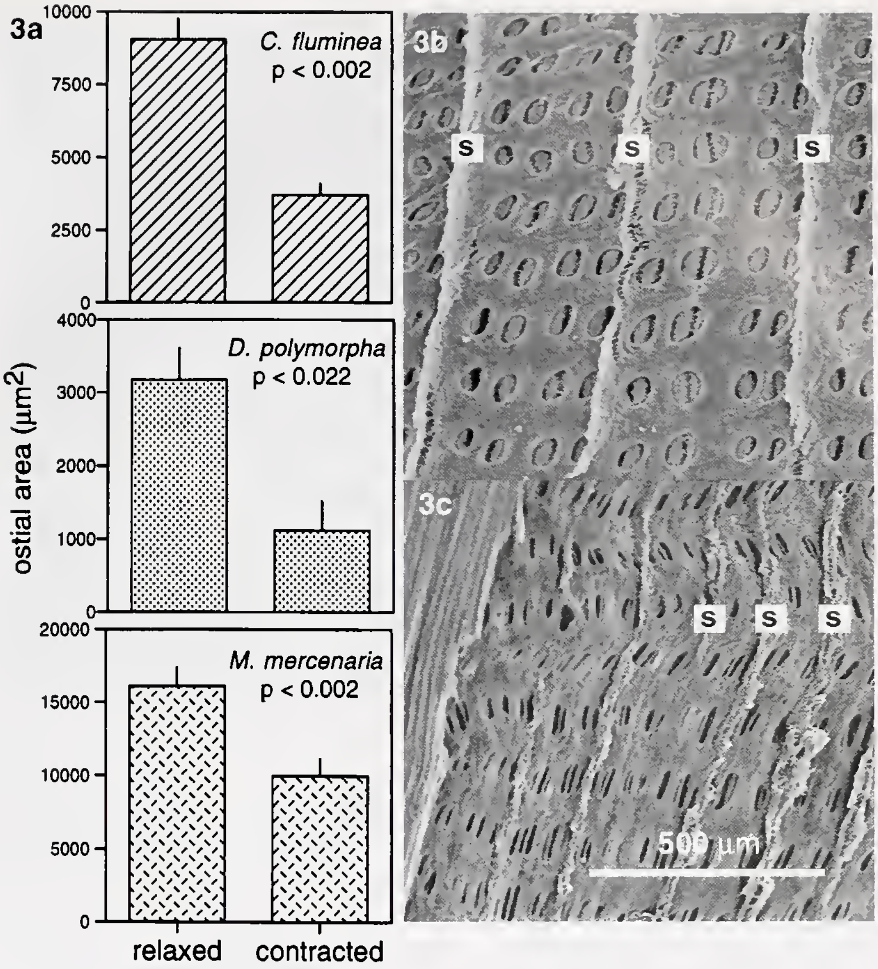

Figure 3. Ostial area. (a) Area of the internal ostia of relaxed gills from each of the species (*Corbicula fluminea, Dreissena polymorpha,* and *Mercenaria mercenaria*) was significantly reduced upon muscular contraction (mean ± SE; $n = 5$). (b, c) Internal face (SEM) of a *D. polymorpha* gill: (b) relaxed gill; (c) gill from the same animal following muscle contraction. The relative position of septa (*s*) that connect opposing lamellae and form the water tubes give an indication of shortening in the anterior to posterior axis.

interfilament distance, with the most obvious being that a change in distance will affect the resistance to water flow (Foster-Smith, 1976; Jorgensen *et al.*, 1986). In addition, it has been suggested that as the filaments move toward one another, the lateral ciliated cells responsible for establishing water flow begin to interfere with one another (Jørgensen *et al.*, 1988; Jørgensen, 1989, 1990). Recent mathematical modeling of gill dimensions has provided further insight into the specific consequences of a particular interfilament distance (Grünbaum *et al.*, 1998). One of the predictions of this model is that the optimal interfilament width for maximizing water flow depends upon the pressure gradient producing the flow. At low pressure differences, a ciliary gap of near 20 µm is optimal; as pressure differences increase, the optimal gap decreases toward 5–10 µm (Grünbaum *et al.*, 1998). This range corresponds well with the distances observed for each of the species in this study (Fig. 2a). When the gill muscles are relaxed, the interfilament width is close to 20 µm, but can quickly change to 10 µm or less as the muscles contract (Medler and Silverman, 1997; Fig. 2a). An environmental variable that may dictate adjustments of pump properties is water temperature, since water viscosity changes inversely with temperature and has direct effects on pumping activities (Jørgensen *et al.*, 1990). It has also been suggested that changes in interfilament width may provide a mechanism to adjust feeding rate and efficiency (Ward *et al.*, 1998). The data in this and previous studies provide evidence that interfilament distance is controlled directly by the activity of smooth muscles, allowing these animals to adjust interfilament distance as needed (Gardiner *et al.*, 1991; Medler and Silverman, 1997).

Connecting the interfilament spaces with the suprabranchial chamber are the passages that constitute the "pipes" of the gill. As indicated by Grünbaum *et al.* (1998),

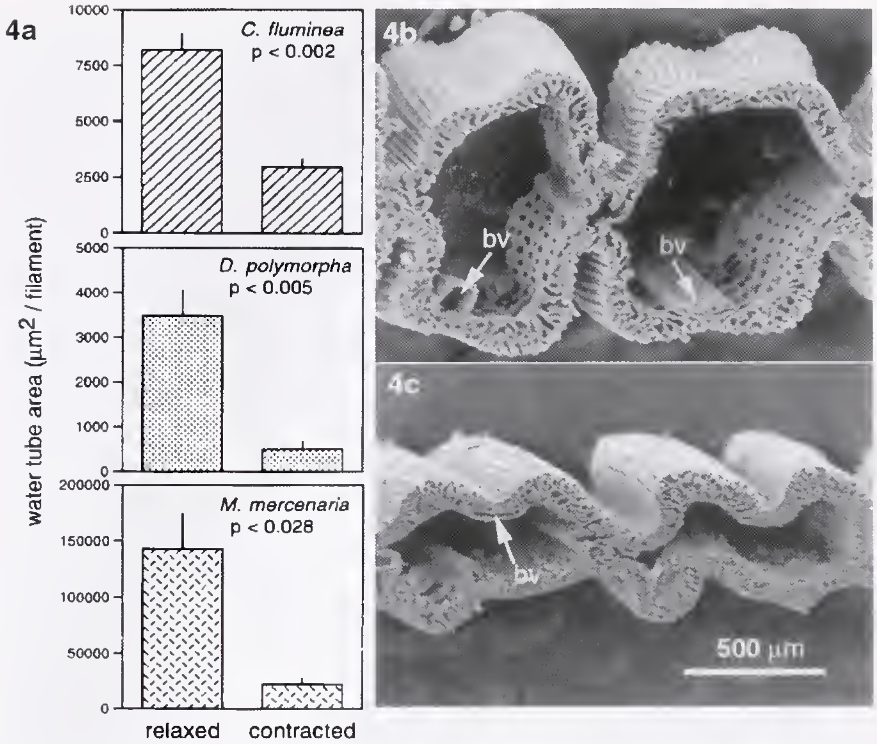

Figure 4. Water-tube dimension. (a) Cross-sectional area of the water tubes per unit gill length significantly decreased upon muscular contraction for each of the species (*Corbicula fluminea, Dreissena polymorpha,* and *Mercenaria mercenaria*) examined (mean ± SE; $n = 5$). (b, c) *M. mercenaria* gill (SEM) in cross-section: (b) relaxed gill; (c) gill from the same animal after the gill muscles contracted. Blood vessels (*bv*) are visible, with only the vessel at the top left appearing to be open.

the pressure drop across the gill filaments is dependent on filament geometry and upon the type of "piping system" to which the filaments are attached. In the eulamellibranch gill, these pipes include the water canals that lead to the central water channel (beginning with external ostia and emptying into the water channel *via* internal ostia) and the water tubes

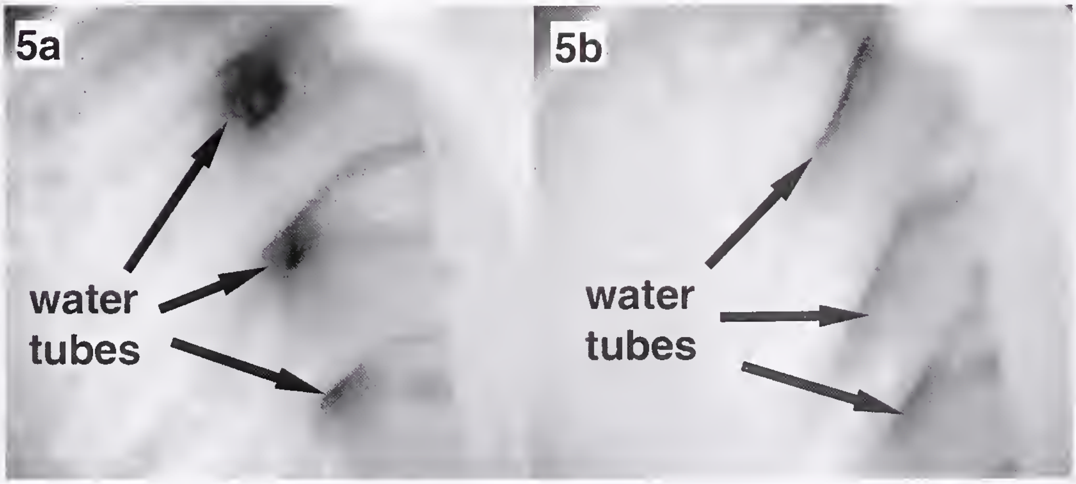

Figure 5. Endoscopic observations. Water tubes are seen at the position where they empty into the suprabranchial chamber of *Lampsilis anodontoides.* During active pumping, the tubes are open (a); when the muscles of the gill and gill axis contract, the water tubes are drawn together and largely close the tubes (b). This type of contraction takes about 1–5 s.

that lead to the suprabranchial chamber. Previous *in vivo* studies from several bivalve species indicate that the ostia are more open during active pumping (Foster-Smith, 1976; Tankersley, 1996), and Jørgensen and colleagues have emphasized a correlation between valve gape, ostial dimension, and rate of water pumping (Jørgensen *et al.*, 1986, 1988; Jorgensen, 1990). Foster-Smith (1976) noted that changes in ostial dimension affect pumping activities, indicating that reductions in ostial size produce pressure losses across the gill. In this and a previous study, we have observed rapid and dramatic changes in internal ostial dimension in live gills (Fig. 3; Medler and Silverman, 1997). In addition, muscle contraction clearly leads to a reduction in the dimension of the water tubes (Figs. 4 and 5). Tankersley (1996) documented similar changes in water-tube dimension in another unionid bivalve, *Pyganodon cataracta*. Although no previous work has addressed the potential effects of such changes in water-tube dimension on pumping processes, Poiseuille's law predicts that as the internal diameter is halved, the flow rate decreases by a factor of 16. Other endoscopic studies have reported a rhythmic expansion and contraction of the gills that was believed to augment water flow through the water tubes (Tankersley and Dimock, 1993; Ward *et al.*, 1994).

Bivalve pumping is a complex process that is dependent on ciliary motors as well as on the muscles that control valve gape, mantle and siphon posture, and gill dimension. The values provided by this study represent the extremes of a range of dimensions that the gills can adopt. It is likely that a continuum of ciliary activity and muscular tone are coordinated through the branchial nerves. Although it is well established that the nerves of the gill have control over ciliary activity (reviewed by Paparo, 1988), almost nothing is understood about the nervous control of the gill muscles. What is known is that the muscles respond to various neurotransmitters *in vitro* (Jørgensen, 1976; Gardiner *et al.*, 1991; Medler and Silverman, 1997; Gainey *et al.*, 1998), and that in a unionid bivalve, the neurotransmitter serotonin induces the gill muscles to relax while increasing the activity of the lateral ciliated cells (Gardiner *et al.*, 1991). The apparent effect of serotonin in this species is to increase pumping rate by enhancing motor activity while simultaneously decreasing the resistance to water flow, but whether these processes are controlled by serotonergic neurons *in vivo* is unknown. Recent work by Gainey *et al.* (1999) reveals that peptides found in nerves in the gills of *Mercenaria mercenaria* have modulatory effects on ciliary activity and that these nerves are closely associated with the muscles of the gills. One of the conclusions drawn from that study is that the peptides are important for modulating both the ciliary and muscular activity involved in feeding activities (Gainey *et al.*, 1999). Understanding the neural control over the muscles of the gill should be a productive focus of future research.

Acknowledgments

Thanks to Julie Cherry and Dr. Thomas H. Dietz for editorial assistance and suggestions. Thanks to Dr. John W. Lynn for assistance with endoscopic techniques and to Ron Bouchard for assistance with imagery. This work was supported by Louisiana Sea Grant NA46RG0096 R/ZMM-5.

Literature Cited

Atkins, D. 1943. On the ciliary mechanisms and interrelationships of the lamellibranchs. Part VIII. Notes on gill musculature in Microciliobranchia. *Q. J. Microsc. Sci.* **84:** 187–256.

Bagby, R. M. 1964. The fine structure of myocytes in the sponges *Microciona prolifera* (Ellis and Solander) and *Tedania ignis* (Duchassaing and Michelotti). *J. Morphol.* **118:** 167–182.

Chambers, E. L., and J. De Armendi. 1979. Membrane potential, action potential and activation potential of eggs of the sea urchin *Lytechinus variegatus*. *Exp. Cell Res.* **122:** 203–218.

Dietz, T. H., D. Lessard, H. Silverman, and J. W. Lynn. 1994. Osmoregulation in *Dreissena polymorpha:* the importance of Na, Cl, K, and particularly Mg. *Biol. Bull.* **187:** 76–83.

Eckert, R., D. Randall, and G. Augustine. 1988. *Animal Physiology. Mechanisms and Adaptations*, 3rd ed. Freeman, New York.

Elsey, C. R. 1935. On the structure and function of the mantle and gill of *Ostrea gigas* (Thunberg) and *O. lurida* (Carpenter). *Trans. R. Soc. Can.* sec. **5:** 131–158.

Foster-Smith, R. L. 1976. Some mechanisms for the control of pumping activity in bivalves. *Mar. Behav. Physiol.* **4:** 41–60.

Gainey, L. F., Jr., K. J. Vining, and M. J. Greenberg. 1998. Pharmacology of gill muscle fibers of *Mercenaria mercenaria*. *Am. Zool.* **38:** 122A.

Gainey, L. F., Jr., K. J. Vining, K. E. Doble, J. M. Waldo, A. Candelario-Martinez, and M. J. Greenberg. 1999. An endogenous SCP-related peptide modulates ciliary beating in the gills of a venerid clam, *Mercenaria mercenaria*. *Biol. Bull.* **197:** 159–173.

Gardiner, D. B., H. Silverman, and T. H. Dietz. 1991. Musculature associated with the water canals in freshwater mussels and response to monoamines *in vitro*. *Biol. Bull.* **180:** 453–465.

Grünbaum, D., D Eyre, and A. Fogelson. 1998. Functional geometry of ciliated tentacular arrays in active suspension feeders. *J. Exp. Biol.* **201:** 2575–2589.

Jones, H. D., O. G. Richards, and T. A. Southern. 1992. Gill dimensions, water pumping rate, and body size in the mussel *Mytilus edulis* L. *J. Exp. Mar. Biol. Ecol.* **155:** 213–237.

Jorgensen, C. B. 1976. Comparative studies on the function of gills in suspension feeding bivalves, with special reference to effects of serotonin. *Biol. Bull.* **151:** 331–343.

Jorgensen, C. B. 1989. Water processing in ciliary feeders, with special reference to the bivalve filter pump. *Comp. Biochem. Physiol.* **94A:** 383–394.

Jorgensen, C. B. 1990. *Bivalve Filter Feeding: Hydrodynamics, Bioenergetics, Physiology and Ecology*. Olsen and Olsen, Fredensborg, Denmark.

Jørgensen, C. B. 1996. Bivalve filter feeding revisited. *Mar. Ecol. Prog. Ser.* **142:** 287–302.

Jorgensen, C. B., and H. U. Riisgård. 1988. Gill pump characteristics of the soft clam *Mya arenaria*. *Mar. Biol.* **99:** 107–109.

Jørgensen, C. B., P. Famme, H. S. Kristensen, P. S. Larsen, F. Møhlenberg, and H. U. Riisgård. 1986. The bivalve pump. *Mar. Ecol. Prog. Ser.* **34:** 69–77.

Jorgensen, C. B., P. S. Larsen, F. Mohlenberg, and H. U. Riisgård. 1988. The mussel pump: properties and modelling. *Mar. Ecol. Prog. Ser.* **45:** 205–216.

Jørgensen, C. B., P. S. Larsen, and H. U. Riisgård. 1990. Effects of temperature on the mussel pump. *Mar. Ecol. Prog. Ser.* **64:** 89–97.

Kryger, J., and H. U. Riisgård. 1988. Filtration rate capacities in 6 species of European freshwater bivalves. *Oecologia* **77:** 34–38.

LaBarbera, M. 1990. Principles of design of fluid transport systems in zoology. *Science* **249:** 992–1000.

Medler, S., and H. Silverman. 1997. Functional organization of intrinsic gill muscles in zebra mussels, *Dreissena polymorpha* (Mollusca: Bivalvia), and response to transmitters *in vitro*. *Invertebr. Biol.* **116:** 200–212.

Medler, S., and H. Silverman. 1998. Extracellular matrix and muscle fibers in the gills of freshwater bivalves. *Invertebr. Biol.* **117:** 288–298.

Medler, S., C. C. Thompson, T. H. Dietz, and H. Silverman. 1999. Ionic effects on intrinsic gill muscles in the freshwater bivalve, *Dreissena polymorpha*. *Comp. Biochem. Physiol.* **122A:** 163–172.

Meyhöfer, E. 1985. Comparative pumping rates in suspension-feeding bivalves. *Mar. Biol.* **85:** 137–142.

Møhlenberg, F., and H. U. Riisgård. 1979. Filtration rate, using a new indirect technique, in thirteen species of suspension-feeding bivalves. *Mar. Biol.* **54:** 143–147.

Navarro, E., J. I. P. Iglesias, M. M. Ortega, and X. Larretxea. 1994. The basis for a functional response to variable food quantity and quality in cockles *Cerastoderma edule* (Bivalvia, Cardiidae). *Physiol. Zool.* **67:** 468–496.

Nielsen, N. F., P. S. Larsen, H. U. Riisgård, and C. B. Jørgensen. 1993. Fluid motion and particle retention in the gill of *Mytilus edulis:* video recordings and numerical modeling. *Mar. Biol.* **116:** 61–71.

Paparo, A. A. 1988. Ciliary activity on the ctenidium of bivalve molluscs. *Comp. Biochem. Physiol.* **91C:** 99–110.

Pearse, V., J. Pearse, M. Buchsbaum, and R. Buchsbaum. 1987. *Living Invertebrates.* Boxwood Press, Pacific Grove, CA.

Riisgård, H. U., and P. S. Larsen. 1995. Filter-feeding in marine macro-invertebrates: pump characteristics, modelling, and energy cost. *Biol. Rev. Camb. Philos. Soc.* **70:** 67–106.

Setna, S. B. 1930. The neuro-muscular mechanism of the gill of *Pecten*. *Q. J. Microsc. Sci.* **73:** 365–392.

Silverman, H., E. C. Achberger, J. W. Lynn, and T. H. Dietz. 1995. Filtration and utilization of laboratory-cultured bacteria by *Dreissena polymorpha*, *Corbicula fluminea*, and *Carunculina texasensis*. *Biol. Bull.* **189:** 308–319.

Silvester, N. R. 1988. Hydrodynamics of flow in *Mytilus* gills. *J. Exp. Mar. Biol. Ecol.* **120:** 171–182.

Silvester, N. R., and M. A. Sleigh. 1984. Hydrodynamic aspects of particle capture by *Mytilus*. *J. Mar. Biol. Assoc. UK* **64:** 859–879.

Tankersley, R. A. 1996. Multipurpose gills: effects of larval brooding on the feeding physiology of freshwater unionid mussels. *Invertebr. Biol.* **115:** 243–255.

Tankersley, R. A., and R. V. Dimock. 1993. Endoscopic visualization of the functional morphology of the ctenidia of the unionid mussel *Pyganodon cataracta*. *Can. J. Zool.* **71:** 811–819.

Vogel, S. 1994. Nature's pumps. *Am. Sci.* **82:** 464–471.

Ward, J. E., and N. M. Targett. 1989. Influence of marine microalgal metabolites on the feeding behavior of the blue mussel *Mytilus edulis*. *Mar. Biol.* **101:** 313–321.

Ward, J. E., R. I. E. Newell, R. J. Thompson, and B. A. MacDonald. 1994. *In vivo* studies of suspension-feeding processes in the eastern oyster, *Crassostrea virginica* (Gmelin). *Biol. Bull.* **186:** 221–240.

Ward, J. E., J. S. Levinton, and S. E. Shumway. 1997. Site of particle selection in a bivalve mollusc. *Nature* **390:** 131–132.

Ward, J. E., L. P. Sanford, R. I. E. Newell, R. J. Thompson, and B. A. MacDonald. 1998. A new explanation of particle capture in suspension-feeding bivalve molluscs. *Limnol. Oceanogr.* **43:** 741–752.

Wildish, D. J., and A. M. Saulnier. 1993. Hydrodynamic control of filtration in *Placopecten magellanicus*. *J. Exp. Mar. Biol. Ecol.* **174:** 65–82.

Reference: *Biol. Bull.* **200:** 87–91. (February 2001)

Controlled Field Release of a Waterborne Chemical Signal Stimulates Planktonic Larvae to Settle

KENNETH A. BROWNE AND RICHARD K. ZIMMER*

Department of Biology, University of California, Los Angeles, California 90095-1606

Settlement rates and distributions of planktonic larvae are critical determinants of population dynamics in marine and freshwater benthic communities. On the basis of the principles of solute diffusion from a porous material, chemical-releasing collectors (CRCs) were engineered and tested in an estuary. Significantly more barnacle larvae (Balanus amphitrite) *were found to colonize collectors emitting trace amounts of the synthetic peptide analog, glycyl-glycyl-L-arginine* (5×10^{-8} M)*, than those emitting either seawater or an organic enrichment (glycyl-glycyl-L-histidine) control. The inductive compound is similar in structure to peptide signal molecules that have been shown to elicit settlement under laboratory conditions and are naturally released by adult barnacles and oysters. The potent effects of subtle changes in seawater chemistry may thus warrant careful attention as putative agents mediating habitat colonization.*

For a half-century or more, the pervasive perception that small planktonic organisms are passively transported by flow has fostered the notion that active larval behaviors can be important only at the time of settlement and in response only to surface-adsorbed chemical cues (1, 2, 3, 4, 5). Circumstances exist, however, where larval responses to dissolved chemical cues in the water column could indeed enhance or determine settlement. The numerical model of Gross *et al.* (6), for example, indicates that hydrodynamic processes directly control larval encounter rate with the seabed and, indirectly, control settlement rate, assuming there is a high probability of larvae accepting the encountered substratum. That is, if larvae move downward (sinking or swimming) in response to a waterborne cue, their vertical distribution will become bottom-skewed, and thus more larvae can be swept into contact with the seabed by fluid flow. Settlement rate may increase dramatically (7).

Whereas settlement is presumed mediated through substratum-adsorbed compounds, induction by dissolved substances is typically regarded as a novelty demonstrated only under strictly controlled laboratory conditions (but see 8, 9, 10). Field studies of the effects of waterborne chemical agents on settlement are needed to evaluate the potencies and performances of these molecules. Although considerable efforts have been made to identify the natural cues that stimulate settlement, no waterborne inducer has been isolated and fully characterized (11, 12). In the absence of purified natural inducers, synthetic analogs are valuable tools for quantitative field studies.

Recently, experiments involving chemical isolations of seawater indicated that low-molecular-mass peptides with carboxy-terminal arginine or lysine residues were released by adult conspecifics and elicited settlement of barnacle (*Balanus amphitrite*) and oyster (*Crassostrea virginica*) larvae in the laboratory (13, 14). Synthetic peptides were screened; whereas glycyl-glycyl-L-arginine (GGR) was identified as a particularly potent analog for the natural inducers in these two species, glycyl-glycyl-L-histidine (GGH) was without effect (15, 16).

We used the mathematical principles of solute diffusion from a porous material to design a gel for the controlled release of peptides from larval collectors in the field (17, 18, 19). Acrylamide was chosen over agar for its relative lack of microbial intrusion, its ease of use, and its small pore sizes; this latter point is particularly important with small solutes. Free-radical crosslinking of an 8.0% acrylamide solution in ASW (artificial seawater made from Forty Fathoms Marinemix salts in deionized water [dH_2O]; pH = 8.0, salinity = 30‰, 0.45-μm filtered) with N,N'-methylene-bis(acrylamide) (bis; 2.4% of the total acrylamide concentration) was

---

Received 27 September 2000; accepted 16 November 2000.

* To whom correspondence should be addressed. E-mail: z@biology.ucla.edu

Abbreviations: ASW, artificial seawater; CRC, chemical-releasing collector; GGH, glycyl-glycyl-L-histidine; GGR, glycyl-glycyl-L-arginine.

initiated with 0.05% ammonium persulfate (APS; w/v, final) and catalyzed with 0.05% tetramethylenediamine (TEMED; v/v, final). These methods resulted in polymerization within 30 min and pore diameters of about 39 Å (20).

$$\frac{C_t}{C_0} = \frac{4}{\pi^2} \sum_{N=0}^{\infty} \frac{1}{(2N+1)^2} e^{[-\pi^2(2N+1)^2(D_p t/L^2)]} \tag{1}$$

Eq. 1 indicates that the fraction of solute remaining in a cylindrical gel (C_t/C_0) with a single open end is a nonlinear function of time (t), the gel length (L), and the diffusion coefficient (D_p) for a particular acrylamide concentration summated in a Bessel series of N terms. D_p was estimated from Eq. 2 and a rearranged version of the Wilke-Chang formula (Eq. 3):

$$D_p = D_0 e^{[-(0.05+10^{-6}M)P]} \tag{2}$$

$$D_0 = \frac{7.4 \times 10^{-8}(\Phi M)^{0.5} K}{\mu V^{0.6}} \tag{3}$$

where D_0 is the diffusion coefficient of a solute in H_2O; M is molecular mass (g mol^{-1}) of the solute and H_2O in Eq. 2 and Eq. 3, respectively; P is the percent (w/v) of polyacrylamide; μ is the dynamic viscosity of H_2O (=1.002 centipose); K is the temperature in Kelvin; Φ is the "association" parameter of H_2O (=2.6); and V is the molal volume of the solute at its normal boiling point (370 cm^3 g mol^{-1} for disodium fluorescein).

Through computer simulations, the rates of solute release from acrylamide were determined by applying Eq. 1 to cylindrical gels with lengths ranging from 0.1 to 10 cm for up to 5 days of field exposure. Fluorescein was chosen as a tracer because its molecular mass (and, hence, diffusion coefficient) is close to that of the small peptides used in the settlement assays (330 g mol^{-1} *versus* 269 and 288 g mol^{-1} for GGH and GGR, respectively). The diffusion coefficients for fluorescein in 8.0% acrylamide (D_p) and H_2O (D_0) were calculated from Eq. 2 and Eq. 3, respectively, to be 2.9 × 10^{-6} and 4.4 × 10^{-6} cm^2 s^{-1} at 27 °C. From these simulations, it was clear that at lengths greater than 4–5 cm, gels release very little (≤50%) of their included organic compounds in 3–5 d (Figs. 1 and 2). If the gel is too thin (<0.8 cm), however, more than 90% of the solute is lost within 0.5 d.

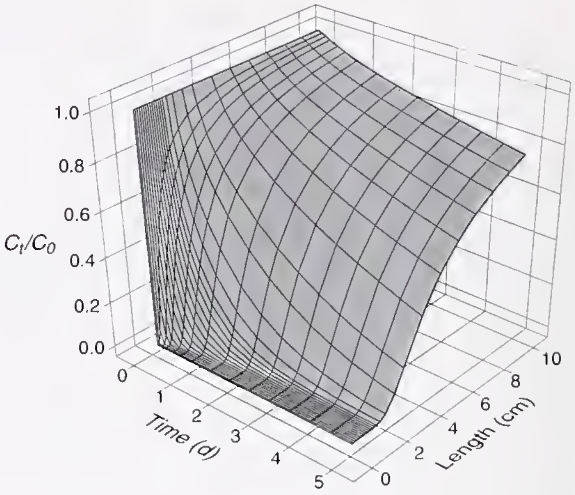

Figure 1. Fluorescein remaining in an 8.0% polyacrylamide gel as a function of time and gel length. These data were generated from Eq. 1 using $D_p = 2.9 \times 10^{-6}$ cm^2 s^{-1} and four terms (0–3) in the Bessel series. The fraction of dye in the gel has been non-dimensionalized by division with the $t = 0$ values (C_t/C_0).

Chemical-releasing collectors (CRCs) were engineered to test the effects of waterborne cues on larval settlement in natural habitats. Each CRC was built of a 4.0-cm-long polyvinyl chloride (PVC) cylinder, 9.5-cm i.d., sealed at one end with a flat sheet of PVC. Three 12-cm-long eyebolts were fastened symmetrically around the cylinder, 2 cm from either end. A 1.0-cm layer of acrylamide (71 ml) in ASW, with or without added stimulant, was polymerized nearest the PVC sheet. One centimeter of crushed, cleaned oyster shell hash (pieces 0.5–1.0 mm in diam) was layered over the acrylamide to form a diffusional dampener. The remaining 2 cm of the CRC were filled with six large, flat oyster shells (surface area *ca.* 240 cm^2) set flush with the collector opening to provide settlement substrata. Oyster shells (sun bleached ≥6 months) from the local estuary

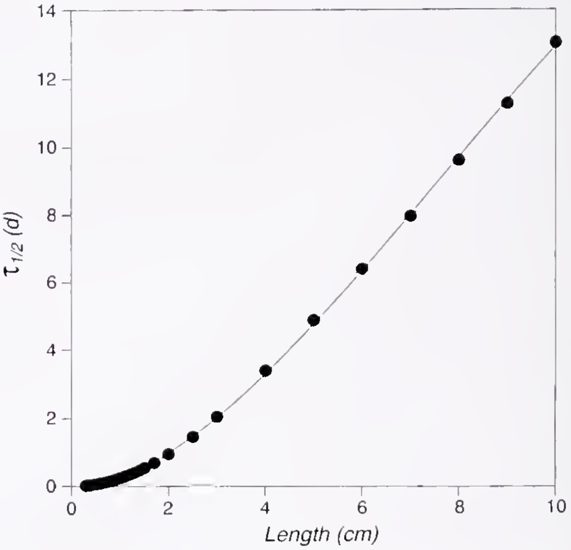

Figure 2. Plot of $\tau_{1/2}$ *versus* gel length. The nonlinear curve has been fitted to a third-order expression relating the variation in the residency time (τ) of a small solute within a gel to the gel length ($\tau_{1/2} = -0.00911 \times \text{Length}^3 + 0.202 \times \text{Length}^2 + 0.196 \times \text{Length} - 0.127$; $R^2 > 0.999$, $n = 24$). The slope of the polynomial regression of log C_t/C_0 *versus* time is inversely proportional to the half-life, or chemical residency time, in the gel matrix ($\tau_{1/2}$ = 0.3/slope).

were prepared for use as settlement substrata by scrubbing free all sediment, flora and fauna, bathing for 5 min in 2%–3% NaOCl, rinsing ≥12 h in continuously running H_2O; and autoclaving to sterilize. These shells were found to be superior to preliminary systems containing scoured glass or PVC substrata (data not shown). Monofilament mesh (0.6-cm pore size) was secured over the shells with cable ties tightened around the cylinder portion of each CRC.

The field experiments were conducted in the North Inlet Estuary (Town Creek; 33° 19.5′ N, 79° 11.5′ W) near Georgetown, South Carolina. This tidal creek is shallow and rapidly flushed, with flow speeds up to 35 cm s^{-1} (and shear velocities to 3.8 cm s^{-1}) about 2200 m from the mouth of the inlet. The creek bank falls steeply, 2–3 m, to a mud bottom. Deployments occurred during August, when the mean (±SEM) water temperature and salinity were 28.3 ± 0.2 °C and 30.3 ± 0.6‰, respectively (P. Kenny and D. Allen, unpubl. data). The CRCs were held above the creek bed, at least 20 cm below mean low tide level, by harnesses constructed of 0.6-cm-diam. nylon rope and brass fittings attached to wooden posts embedded into the sediment.

Concentrations of diffused solute from acrylamide gel were measured using disodium fluorescein and GGR as chemical tracers in the field. The experiment employing fluorescein was performed to elucidate the effects of tracer release rate. GGR determinations were subsequently made for seawater sampled during tests of larval settlement. Three replicate 1-ml aliquots of seawater were removed *via* sterile syringes from 0.5, 1.1, and 3.5 cm above the gels. The samples were filtered on site with 0.45-μm syringe filter cartridges, stored in sterile vials, and placed on ice in the dark until analysis was performed (GGR samples were maintained at −80 °C upon return to the laboratory). The sampling was repeated for 12 or 4 replicate collectors at 12-h and 24-h intervals in the fluorescein and GGR experiments, respectively, for a total of 72 h. Fluorescein concentrations were determined from fluorescent output (Turner Designs field fluorometer, model 10-AU-005, excitation wavelengths 455–500 nm, emission wavelengths 510–700 nm) by comparison to a standard concentration curve. GGR was quantified by high-performance liquid chromatography (HPLC) with a Beckman System Gold 126 binary solvent module/507 autosampler and a Jasco FP-920 fluorescence detector. Briefly, the guanidinium group of the arginine on GGR reacted with benzoin under basic conditions to quantitatively form a highly fluorescent derivative (21, 22). Separation through a silica-based bonded phenyl column (Waters Corp.) was induced by increasing the concentration of ethyl alcohol in the 75 m*M* Tris-HCl (pH 8.1) mobile phase from 25% to 85% in a series of gradients over 23 min at 0.8 ml min^{-1}. HPLC peaks (excitation $\lambda = 325$ nm, emission $\lambda = 435$ nm) were identified by their retention times relative to previously run standards (guanidinium, arginine, glycyl-L-arginine, and GGR), and concentrations were calculated from the areas under the peaks (23).

Previous laboratory investigations with barnacle and oyster larvae indicated maximum settlement in response to peptides at 10^{-7} to 10^{-8} *M* (15, 16). Concentrations greater or less than two orders of magnitude from these target doses substantially diminished the effectiveness of GGR to stimulate settlement. A gel concentration of 1 mg ml^{-1} fluorescein produced mean levels that were nearly constant through 72-h field deployments. These values were as follows: for shell-hash pore waters: 1.1 (±0.1 SEM) × 10^{-2} mg ml^{-1}; for settlement (shell) substrata: 2.1 (±0.1 SEM) × 10^{-4} mg ml^{-1}; and, for the water column at 0.5 cm above the collector: 1.0 (±0.1 SEM) × 10^{-6} mg ml^{-1}. On the basis of this information, a concentration of 2 × 10^{-4} *M* peptide was established for the gels. A 3700-fold dilution led to a mean GGR concentration of 5.4 (±0.5 SEM) × 10^{-8} *M* in the settlement substrata during the field trials, in good agreement with our measurements of fluorescein release. The inclusion of the shell-hash layer above the gel resulted in near steady-state concentrations of fluorescein and GGR. Solute concentrations in shell-hash, settlement substrata, and water at 0.5 cm above the collector did not significantly change as a function of time since placing the CRCs in the field (Table 1, and one-way ANOVAs: $F \leq 1.23$, $P \geq 0.37$, all comparisons).

This field study was intended to determine the settlement responses of barnacle and oyster larvae to a waterborne chemical cue. The densities of larvae in the water column were estimated at the beginning and end of the deployment from the number of larvae collected at the study site in paired 3–6 min oblique tows (≥4 m^3 filtered seawater) taken with 30-cm-diam., 153-μm-mesh Nitex plankton nets. The results indicated that oyster larvae in the water column were rare (≤2.1 individuals m^{-3}) during the course of the investigation, so only data for barnacle larvae (mean concentration: 40.4 larvae m^{-3}) are presented here.

The effects of ASW, glycyl-glycyl-L-arginine in ASW (GGR; settlement stimulant), and glycyl-glycyl-L-histidine in ASW (GGH; organic enrichment control) were determined by assaying eight CRCs of each chemical treatment. The exact position of each CRC was established according to a randomized block design in which eight sets of three collectors (one collector of each treatment) were placed along a 120-m transect parallel to and 4 m from shore. The CRCs were incubated in the field with the open ends oriented upward for 72 h. At the end of the incubation time, the chambers were removed from the estuary and the number of newly metamorphosed barnacle (*Balanus amphitrite*) juveniles on the settlement (shell) substrates were counted under a dissecting microscope.

GGR was found to stimulate substrate colonization by sig-

Table 1

Mean (±SEM) concentrations of disodium fluorescein (μg/ml) and glycyl-glycyl-L-arginine (GGR; nM) in waters sampled from among the shell substrata of larval collectors

	Time (h) since collector was placed in the field					
Compound	12	24	36	48	60	72
Disodium fluorescein	0.18 ± 0.05	0.22 ± 0.06	0.21 ± 0.04	0.25 ± 0.08	0.22 ± 0.07	0.20 ± 0.04
GGR	—	58 ± 13	—	59 ± 16	—	45 ± 18

Time = 0 is defined as the point at which collectors were first submerged in field habitats and for which neither fluorescein nor GGR had yet been released from polyacrylamide gels. Separate experiments were performed for fluorescein and GGR. Initial concentrations of the compounds in acrylamide gels were 1 mg/ml (fluorescein) and 2×10^{-4} *M* (GGR). Seawater samples of fluorescein and GGR were collected at 12-h and 24-h intervals, respectively.

nificantly more barnacle larvae than did either ASW or GGH (Fig. 3). Because GGR and GGH are basic peptides with nearly identical molecular weights and chemical functionalities, settlement induction cannot be attributed to stimulation by organic compounds in general but is due, specifically, to the arginine moiety at the carboxy terminus of the peptide.

These results show that even weakly swimming larvae like barnacle cyprids (mean speed: 2.9 mm s^{-1}; 24) can select their settlement sites upon receipt of an appropriate chemical stimulus in turbulent flow. After being released from a benthic source, such as patches of the conspecific target organism, a peptide signal molecule can be transported a considerable distance above the bottom by turbulent eddies (25). Larval delivery to the seabed may thus result from hydrodynamic transport of larvae that also may swim down in response to dissolved signal molecules. The latter process tends to concentrate larvae near the bed, enhancing settlement rate (26). In this manner, water-soluble cues might remotely entrain larvae to settle in suitable adult habitat, and therefore warrant careful attention as putative agents mediating supply and delivery of planktonic larvae to benthic environments.

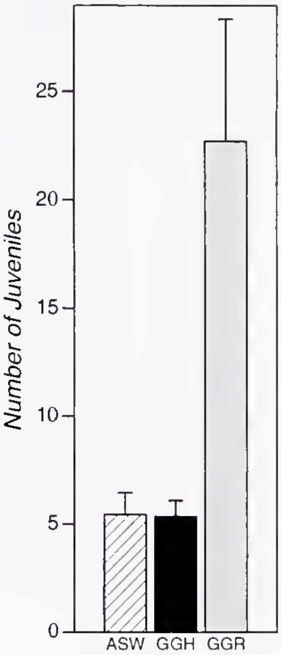

Figure 3. The numbers (mean ± SEM; *n* = 8) of newly metamorphosed barnacle juveniles (*Balanus amphitrite*) on clean oyster shells, provided as settlement substrata, were counted for chemical-releasing collectors (CRCs) with either no organic enrichment (ASW, control) or with 2×10^{-4} *M* GGR or GGH. Significantly more barnacle juveniles were found in response to GGR than to the control or GGH ($P < 0.001$, one-way ANOVA followed by multiple, paired comparisons using Bonferroni's correction; 27). All CRCs were oriented with their openings facing upward with an 8.0% acrylamide gel (2.4% crosslinking) prepared using sterile ASW. ASW, artificial seawater; GGH, glycyl-glycyl-L-histidine; GGR, glycyl-glycyl-L-arginine.

Acknowledgments

This study was supported by an award from the NOAA Sea Grant College program (R/CZ-152) through the National Marine Biotechnology Initiative. D. Allen and P. Kenny generously provided unpublished data on temperature, salinity, and plankton counts for North Inlet waters. Earlier drafts of this manuscript were greatly improved by comments from M. S. Gordon, and especially from C. A. Zimmer.

Literature Cited

1. **Crisp, D. J. 1974.** Factors influencing settlement of marine invertebrate larvae. Pp. 177–265 in *Chemoreception in Marine Organisms*, P. T. Grant and A. M. Mackie, eds. Academic Press, London.
2. **Morse, A. N. C., and D. E. Morse. 1984.** Recruitment and metamorphosis of *Haliotis* larvae induced by molecules uniquely available at surfaces of crustose red algae. *J. Exp. Mar. Biol. Ecol.* **75:** 191–215.
3. **Butman, C. A. 1987.** Larval settlement of soft-bottom invertebrates: the spatial scales of pattern explained by active habitat selection and the emerging role of hydrodynamical processes. *Oceanogr. Mar. Biol. Annu. Rev.* **25:** 113–165.
4. **Gaines, S. D., and M. D. Bertness. 1992.** Dispersal of juveniles and variable recruitment in sessile marine species. *Nature* **360:** 579–580.
5. **Pawlik, J. R., and C. A. Butman. 1993.** Settlement of a marine tube worm as a function of current velocity: interacting effects of hydrodynamics and behavior. *Limnol. Oceanogr.* **38:** 1730–1740.

6. **Gross, T. F., F. E. Werner, and J. E. Eckman. 1992.** Numerical modeling of larval settlement in turbulent bottom boundary layers. *J. Mar. Res.* **50:** 611–642.
7. **Eckman, J. E., F. E. Werner, and T. F. Gross. 1994.** Modelling some effects of behavior on larval settlement in a turbulent boundary layer. *Deep-Sea Res. II—Top. Stud. Oceanogr.* **41:** 185–208.
8. **Hadfield, M. G., and D. Scheuer. 1985.** Evidence for a soluble metamorphic inducer in *Phestilla:* ecological, chemical and biological data. *Bull. Mar. Sci.* **37:** 556–566.
9. **Forward, R. B., Jr., R. A. Tankersley, D. Blondel, and D. Rittschof. 1997.** Metamorphosis of the blue crab *Callinectes sapidus:* effects of humic acid and ammonium. *Mar. Ecol. Prog. Ser.* **157:** 277–286.
10. **Fleck, J., and W. K. Fitt. 1999.** Degrading mangrove leaves of *Rhizophora mangle* Linne provide a natural cue for settlement and metamorphosis of the upside down jellyfish *Cassiopea xamachana* Bigelow. *J. Exp. Mar. Biol. Ecol.* **234:** 83–94.
11. **Pawlik, J. R. 1992.** Chemical ecology of the settlement of benthic marine invertebrates. *Oceanogr. Mar. Biol. Annu. Rev.* **30:** 273–335.
12. **Steinberg, P. D., R. de Nys, and S. Kjelleberg. 2001.** Chemical mediation of surface colonisation. In *Marine Chemical Ecology,* J. B. McClintock and B. J. Baker, eds. CRC Press, St. Petersberg, FL. (In press).
13. **Rittschof, D. 1985.** Oyster drills and the frontiers of chemical ecology: unsettling ideas. *Am. Malacol. Bull. Special Edition No.* **1:** 111–116.
14. **Zimmer-Faust, R. K., and M. N. Tamburri. 1994.** Chemical identity and ecological implications of a waterborne, larval settlement cue. *Limnol. Oceanogr.* **39:** 1075–1087.
15. **Tegtmeyer, K., and D. Rittschof. 1989.** Synthetic peptide analogs to barnacle settlement pheromone. *Peptides* **9:** 1403–1406.
16. **Browne, K. A., M. N. Tamburri, and R. K. Zimmer-Faust. 1998.** Modelling quantitative structure-activity relationships between animal behaviour and environmental signal molecules. *J. Exp. Biol.* **201:** 245–258.
17. **Ogston, A. G. 1958.** The spaces in a uniform random suspension of fibres. *Trans. Faraday Soc.* **54:** 1754–1757.
18. **White, M. L., and G. H. Dorion. 1961.** Diffusion in a crosslinked acrylamide polymer gel. *J. Polymer Sci.* **55:** 731–740.
19. **Davis, B. K. 1974.** Diffusion in polymer gel implants. *Proc. Natl. Acad. Sci. USA* **71:** 3120–3123.
20. **Fawcett, J. S., and C. J. O. R. Morris. 1966.** Molecular-sieve chromatography of proteins on granulated polyacrylamide gels. *Sep. Sci.* **1:** 9–26.
21. **Ohkura, Y., and M. Kai. 1979.** Fluorometric determination of monosubstituted guanidino compounds with benzoin-dimethylformamide reagent. *Anal. Chim. Acta* **196:** 89–94.
22. **Kai, M., T. Miyazaki, M. Yamaguchi, and Y. Ohkura. 1983.** High-performance liquid chromatography of guanidino compounds using benzoin as a pre-column fluorescent derivitization reagent. *J. Chromatogr.* **268:** 417–424.
23. **Decho, A. W., K. A. Browne, and R. K. Zimmer-Faust. 1998.** Chemical cues: why basic peptides are signal molecules in marine environments. *Limnol. Oceanogr.* **43:** 1410–1417.
24. **Tamburri, M. N., and R. K. Zimmer-Faust. 1996.** Suspension feeding: basic mechanisms controlling recognition and ingestion of larvae. *Limnol. Oceanogr.* **41:** 1188–1197.
25. **Zimmer-Faust, R. K., M. N. Tamburri, and A. W. Decho. 1997.** Chemosensory ecology of oyster larvae: benthic-pelagic coupling. Pp. 37–50 in *Sensory Ecology and Physiology of Zooplankton,* D. L. Hartline, P. Lenz, and J. E. Purcell, eds. Gordon and Breach, Toronto.
26. **Tamburri, M. N., C. M. Finelli, D. S. Wethey, and R. K. Zimmer-Faust. 1996.** Chemical induction of larval settlement behavior in flow. *Biol. Bull.* **191:** 367–373.
27. **Sokal, R. R., and F. J. Rohlf. 1981.** *Biometry.* 2nd ed. W. H. Freeman, San Francisco, CA.

Reference: *Biol. Bull.* **200:** 92–96. (February 2001)

Molecular Evidence for Cryptic Species of *Aurelia aurita* (Cnidaria, Scyphozoa)

MICHAEL N. DAWSON[1,2]* AND DAVID K. JACOBS[1]

[1]*Organismic Biology, Ecology, and Evolution, University of California, 621 Charles E. Young Drive South, Los Angeles, California 90095-1606; and* [2]*Coral Reef Research Foundation, Koror, Palau*

Morphological taxonomy suggests that marine faunas are species poor compared to terrestrial and freshwater faunas (1). This dichotomy has been attributed to the unique potential of marine plankters for distant dispersal across homogenous oceans with few barriers to gene flow (2). The relative scarcity of opportunities for allopatric divergence has resulted in depauperate marine faunas characterized by a high proportion of widespread or cosmopolitan species. Aurelia aurita *(Linnaeus) has been considered a good example of such a cosmopolite (3, 4, 5, 6). However, recent molecular studies have revealed cryptic species in many marine taxa (7), suggesting that marine biodiversity is higher and opportunities for speciation have been more frequent than generally recognized. Here, we present nuclear and mitochondrial DNA sequence evidence of seven sibling species of* Aurelia aurita *and two additional species,* A. limbata *Brandt and* A. labiata *Chamisso & Eysenhardt. These sequence data indicate speciation events as early as the late Cretaceous or early Tertiary, consistent with the formation of well-recognized biogeographic barriers to gene flow in the seas.*

Traditionally, the genus *Aurelia* comprises two species: *A. limbata*, a polar species, and *A. aurita*, a common inhabitant of nearshore waters circumglobally between about 50 °N and 55 °S (3, 4, 5; Fig. 1). Perhaps due to its ubiquity, *A. aurita* has become a popular research organism for studies as diverse as protein chemistry, development, ecology, ethology, and hydrodynamics (6). *A. aurita* also is economically important because worldwide it preys on or competes with larvae of commercial fisheries and because swarms of medusae may impede trawling or block power-plant intakes (8). Furthermore, this "pest" has been introduced at least into San Francisco Bay (9) and possibly many other places (10). *A. aurita* is also familiar to nonspecialists because it is the most commonly displayed medusa in public aquaria. The systematics of *A. aurita* therefore is of considerable scientific, economic, and general interest.

Aurelia has a typical bipartite scyphozoan life history in which benthic scyphopolyps asexually strobilate ephyrae that grow into sexual medusae, the females of which brood larvae that settle into the shallow coastal benthos within a few days of being released. Of these life stages, the medusa probably is the principal dispersal phase because only the medusa is both long-lived (several months to more than one year; 11) and planktonic (6). The potential of medusae for distant dispersal is consistent with the current classification of *A. aurita* as a circumglobal, almost cosmopolitan, species (4, 5). However, *A. aurita* medusae in Saanich Inlet, British Columbia, and perhaps elsewhere, migrate directionally (12), maintaining breeding aggregations within isolated inlets and probably limiting gene flow among populations. Consistent with limited gene flow, allozyme differences have been found between populations of *A. aurita* in the eastern and western Atlantic Ocean, the Gulf of Mexico, and the eastern and western Pacific Ocean (9, 13). In addition, one species, *A. labiata*, was recently recognized as native to Pacific North America and distinct from *A. aurita* (10).

Novel DNA sequence data from nuclear internal transcribed spacer one (ITS-1) and mitochondrial cytochrome oxidase *c* subunit I (COI) reveal highly structured gene genealogies and at least nine distinct clades of *Aurelia* (Figs. 1, 2). Several lines of argument suggest that these clades warrant recognition as distinct species. First, the length of ITS-1 varies from 240 nucleotides (Charlestown, RI) to 360 nucleotides (Cananéia, Brazil). Such length variation is comparable to that found among congeneric species of

---

Received 7 August 2000; accepted 19 October 2000.

* To whom correspondence should be addressed at Coral Reef Research Foundation, Box 1765, Koror, PW 96940, Palau.

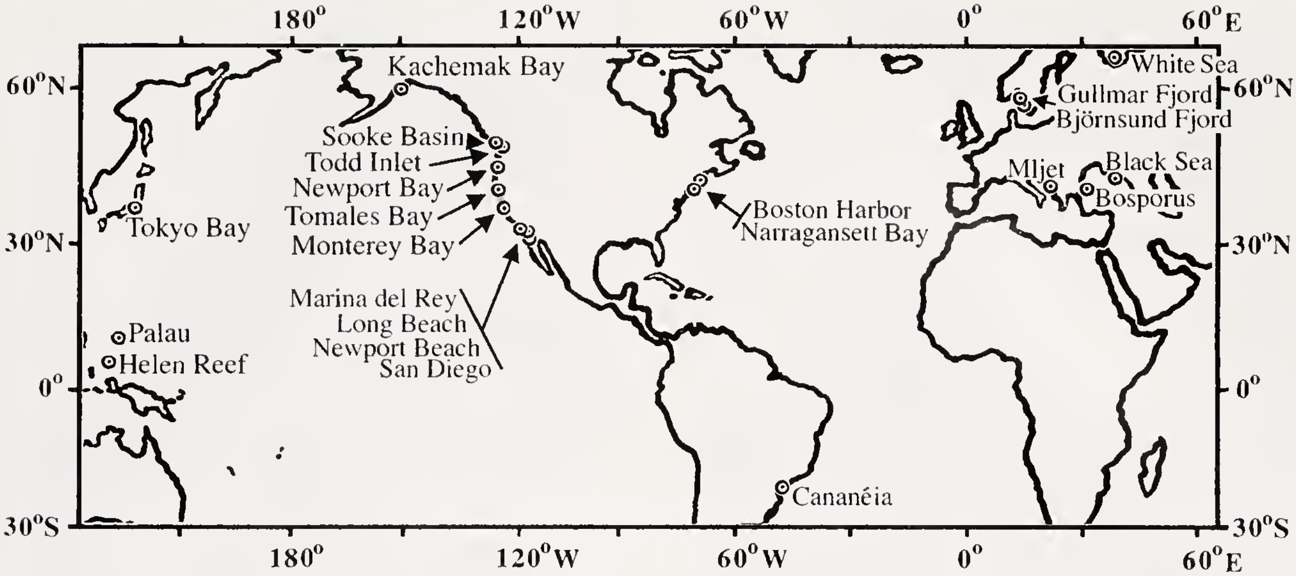

Figure 1. Sample locations of *Aurelia* in this study include sites within the ranges of the three currently recognized morphospecies: *A. labiata* (Pacific North America), *A. limbata* (polar seas below 70 °N from western Greenland to Siberia), and *A. aurita* (Europe [the type locality], northern Atlantic, and all remaining regions). Samples from Narragansett Bay comprise two sites: the semi-enclosed Charlestown Salt Pond and the open Greenwich Cove. Samples from Palau comprise several sites from three different habitats: land-locked, generally meromictic, marine lakes (Big Jellyfish Lake, Ongael Lake, Ongeim'l Tketau, Hotwater Lake); semi-enclosed holomictic 'coves' or similar waters (Tab Kukau, Malakal, Tketau); and the lagoon, which is open to the ocean (Ngell Channel) [see refs. 29, 31]. The population in Mljet inhabits a semi-enclosed meromictic "cove." Gut, bell margin, or oral arm tissues were cleaned, biopsied, and preserved in DMSO + NaCl (29). Total DNA was extracted using a CTAB extraction protocol. PCRs were set up according to the guidelines issued with *Taq* polymerase (Perkin Elmer) in MJ Research MiniCyclers and amplification products cloned using Invitrogen's Topo TA Cloning Kit. Cloned DNA was purified with Pharmacia's Flexiprep kit and sequenced on Applied Biosystems 373 autosequencers according to protocols in the ABI PRISM manual. Sequencing employed the PCR primers (HCO [32], AaCOIi-L = 5′-gcccgtyytaataggrgggtttgg, jfITS1-5f = 5′-ggtttccgtaggtgaacctgcggaaggatc, and jfITS1-3r = 5′-cgcacgagccgagtgatccaccttagaag [29]) and Invitrogen's M13Reverse and M13 Forward primers.

Corallimorpharia (286 to 350 nucleotides; 14) and between genera within the Scleractinia (214 to 297 nucleotides; 15) and Octocorallia (216 to 336 nucleotides; 15). Second, inter-clade percent sequence differences in ITS-1 (excluding regions containing microsatellites), which range from 10% (*A. labiata* [Kachemak, AK] *vs. Aurelia* sp. 1 [Newport Beach, CA]) to 40% (*Aurelia* sp. 2 [Cananéia] *vs. Aurelia* sp. 4 [Ongeim'l Tketau]), also are more similar to inter-specific and inter-generic than intra-specific differences in other taxa. For example, percent sequence difference in ITS-1 among congeneric species ranges from 4.5% to 14.9% in the Corallimorpharia (14) and from 5.8% to 19.5% in mosquitoes (16), and is less than 29% in the scleractinian *Acropora* (17). Inter-generic sequence differences in ITS-1 range from 27% to 79% in the Anthozoa (14, 15). Thus, if a difference of from 5% to 15% between ITS-1 sequences indicates species-level divergence, the sequences reported here are evidence of at least nine species of *Aurelia: A. limbata, A. labiata,* and *A. aurita,* plus six cryptic species previously identified as *A. aurita* (Fig. 2A).

Sequence variation in COI in *Aurelia,* which ranges from 13% (*A. limbata vs. Aurelia* sp. 1 [Marina del Rey, CA]) to 24% (*Aurelia* sp. 3 [Tab Kukau Cove, Palau] *vs. Aurelia* sp. 2 [Cananéia]) also is comparable to inter-specific differences in other metazoans. For example, 18% sequence difference in COI distinguishes congeneric species of copepods (18), 4% to 19% distinguishes species of the snapping shrimp *Alpheus* (19), about 7.5% indicates species of deep-sea clam (Vesicomyidae; 20), and 11.5% to 30.8% characterizes congeneric species of the amphipod *Gammarus* (21). Thus, if 10% to 20% sequence difference is taken as a benchmark of distinct species, these COI data also support recognition of *A. limbata, A. labiata,* and seven sibling species of *A. aurita* (Fig. 2B).

Several other observations suggest that the nine clades of *Aurelia* distinguished by sequence data represent distinct species. For example, *A. labiata* and *A. limbata* are sympatric in Kachemak Bay, providing strong evidence that their molecular differences reflect reproductive isolation. Similarly, Palau cove *Aurelia* occasionally are advected into the lagoon, but have not, according to the molecular data, interbred with lagoon *Aurelia* for millions of years, again implying reproductive isolation. Reproduction by *Aurelia* in Palau coves, lagoon, and lakes is also ecologically, usually geographically, and often temporally isolated (pers. obs.), and brackish, marine lake *Aurelia* may be physiologically inhibited from encountering congeners in seawater (5). For similar reasons, *Aurelia* in the fjord-like Mljet "lake" are probably reproductively isolated from *Aurelia* that occur elsewhere in Europe, including the Black Sea and probably

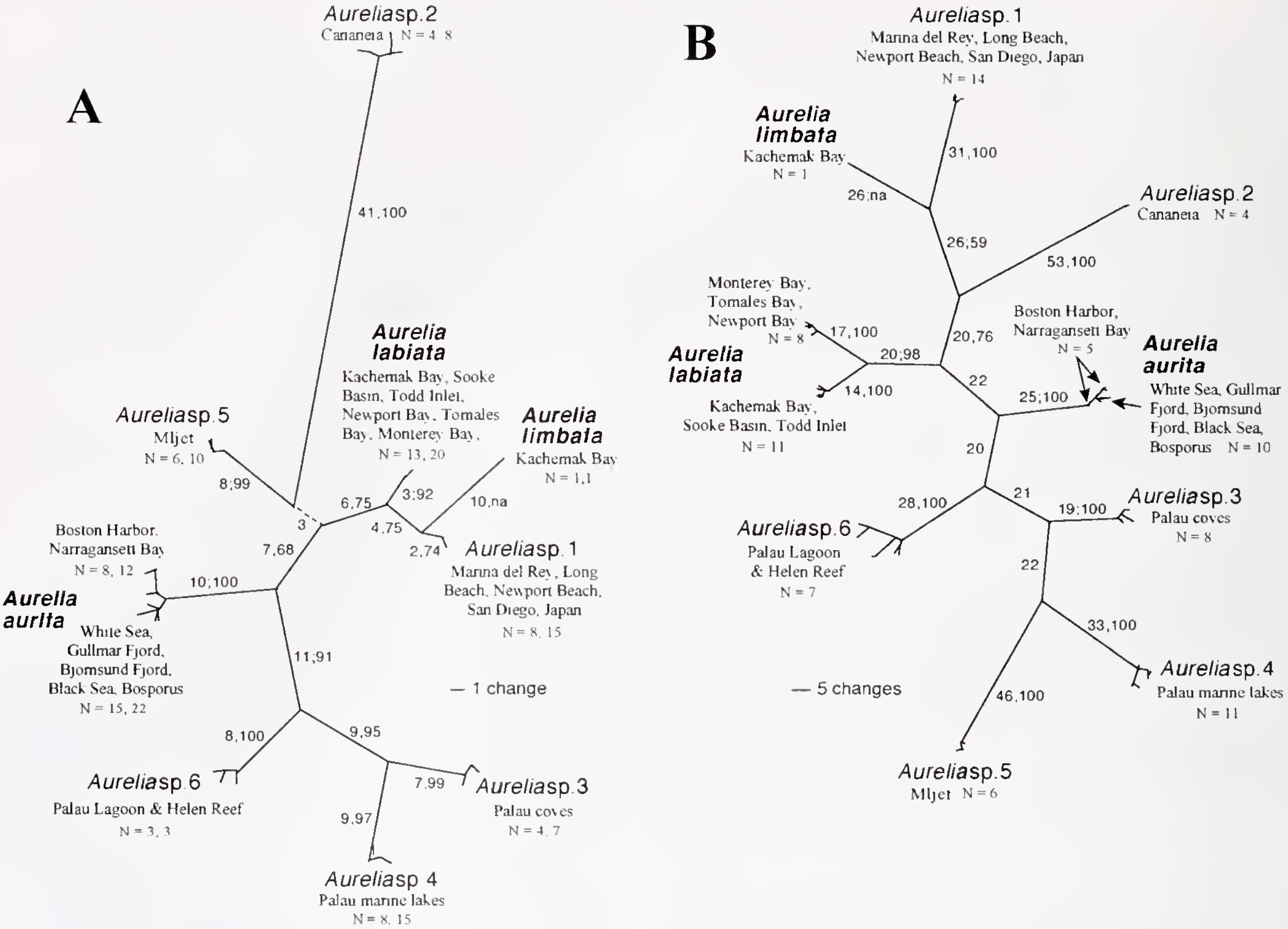
A
Aureliasp.2
Cananeia N = 4 8
41,100
Aurelia labiata
Kachemak Bay, Sooke Basin, Todd Inlet, Newport Bay, Tomales Bay, Monterey Bay,
N = 13, 20
Aurelia limbata
Kachemak Bay
N = 1,1
Aureliasp.5
Mljet
N = 6, 10
8;99
3
6,75
3;92
4,75
10,na
2,74
Aureliasp.1
Marina del Rey, Long Beach, Newport Beach, San Diego, Japan
N = 8, 15
7,68
Boston Harbor, Narragansett Bay
N = 8, 12
10;100
Aurelia aurita
White Sea, Gullmar Fjord, Bjomsund Fjord, Black Sea, Bosporus
N = 15, 22
11;91
— 1 change
8,100
9,95
Aureliasp.6
Palau Lagoon & Helen Reef
N = 3, 3
7.99
Aureliasp.3
Palau coves
N = 4, 7
9,97
Aureliasp 4
Palau marine lakes
N = 8, 15
B
Aureliasp.1
Marina del Rey, Long Beach, Newport Beach, San Diego, Japan
N = 14
Aurelia limbata
Kachemak Bay
N = 1
31,100
26;na
Aureliasp.2
Cananeia N = 4
26;59
53,100
Monterey Bay, Tomales Bay, Newport Bay
N = 8
17,100
Aurelia labiata
20;98
14,100
Kachemak Bay, Sooke Basin, Todd Inlet
N = 11
20,76
Boston Harbor, Narragansett Bay
N = 5
Aurelia aurita
22
25;100
White Sea, Gullmar Fjord, Bjomsund Fjord, Black Sea, Bosporus N = 10
20
28,100
21
19;100
Aureliasp.3
Palau coves
N = 8
Aureliasp.6
Palau Lagoon & Helen Reef
N = 7
22
33,100
Aureliasp.4
Palau marine lakes
N = 11
— 5 changes
46,100
Aureliasp.5
Mljet N = 6

Figure 2. DNA sequence analyses of ITS-1 and COI are consistent with previous allozyme studies and morphological descriptions of *Aurelia* (3, 9, 10, 13) that indicated European and northeastern Atlantic clades within *A. aurita*, northeastern Pacific (*A. labiata*), polar (*A. limbata*), and Japanese or southern California lineages. DNA sequence analyses of ITS-1 and COI also indicate an additional six cryptic species of *A. aurita*. (A) Unrooted ITS-1 gene tree. One of 571 shortest trees (length = 168 steps; CI = 0.7738) recovered by unweighted maximum parsimony analysis (PAUP ver. 4.0b4a; 33) of sequences aligned in CLUSTALW (34; gap opening:extension penalty = 5:1) and amended by eye; gapped positions were excluded from the parsimony analysis, therefore emphasizing the better aligned portions of sequences (*i.e.*, 164 characters of which 83 were parsimony informative). Major branches present in the strict consensus tree are annotated with branch-length and bootstrap support (if >50%); the dashed branch was not present in the strict consensus. Parsimony analyses employed the tree-bisection-reconnection and accelerated transformation options, searching on 5000 trees ≤5 steps longer than the shortest tree encountered during each of 1000 heuristic searches. The same topology was recovered when transitions were downweighted 1:2 cf. transversions, which reflected the relative frequency of these changes in the aligned sequences. Bootstrap analyses (1000 replicates) of unweighted data were completed in PAUP ver. 4.0b4a using the options described above for parsimony analyses (50 heuristic searches per bootstrap replicate). The number of medusae and ITS-1 sequences analyzed (*N* = medusae, sequences) are stated for each region. (B) Unrooted COI gene tree constructed using unweighted maximum parsimony analysis of a 466-bp region in PAUP ver. 4.0b4a (search options as described above). The tree is topologically consistent with the strict consensus of 667 shortest trees (length = 844 steps; CI = 0.5616) recovered by weighted maximum parsimony analyses (1^{st}:2^{nd}:3^{rd} positions were weighted 3:11:1, reflecting the distribution of parsimony informative sites among these positions; weighting transitions:transversions 1:2 did not affect tree topology). Major branches present in the strict consensus tree are annotated with branch-length and bootstrap support. Bootstrap analyses (1000 replicates) of weighted data were completed in PAUP ver. 4.0b4a using the options described above for parsimony analyses (50 heuristic searches per bootstrap replicate). The number of medusae analyzed (*N*) is stated for each region.

the Mediterranean. Finally, at least seven species of *Aurelia*—those from coves, lagoon, and lakes in Palau, the one from Southern California (pers. obs.), and *A. aurita*, *A. labiata*, and *A. limbata* (3, 4, 5, 10)—are discernible from each other by their morphologies. Unfortunately, however, phylogenetically robust morphological characters are rare in *Aurelia* (4, 9), so new molecular phylogenies may be difficult to reconcile with antiquated morphological varieties or nominal species (*e.g.*, *A. coerulea* Lendenfeld, *A. colpota* Brandt, *A. hyalina* Brandt, *A. japonica* Kishinouye, and *A. maldivensis* Bigelow). Despite this, species of *Aurelia* do conform, at least in part, to biological (isolation), evolutionary, phylogenetic, and recognition species concepts, as well as to the flawed but historically invaluable morphological species concept (22). Considering that many regions of the world remain unsampled—including Africa, Australia, the Caribbean, much of the Pacific, most of South America, and the Indian Ocean—nine is probably a modest estimate of the number of species of *Aurelia*.

Assuming a rule-of-thumb evolutionary rate of 0.5% to 1.4% sequence divergence per million years for COI (19), sequence differences between these nine species (13% to 24% [see above]) suggest divergences on the order of 10 to 50 million years before present (My BP). Similarly, based on the mean evolutionary rate of introns (3.3×10^{-9} substitutions year^{-1} site^{-1}; 23), ITS-1 sequence differences (10% to 40% [see above]) suggest species divergences between 30 and 120 My BP. These divergence times must be treated with caution for several reasons. First, they may be underestimates due to saturation of mutation ("multiple hits") at effectively neutral nucleotide positions. Alternatively, ITS-1 sequence differences may be slightly inflated by difficulties in aligning such highly variable sequences. Third, the clock calibrations are not based on cnidarian sequences and, as in other cnidarians (7, 24), the rates of molecular evolution in *Aurelia* may be slower than those in most other taxa. These factors considered, however, it still seems likely that these species of *Aurelia* diverged tens of millions of years before present.

The modern biogeography of *Aurelia*, therefore, has probably been influenced by ancient vicariant events that have contributed to modern species distributions that are consistent with modern patterns of marine zoogeography (25, 26). Vicariant events that affected the evolution of *Aurelia* may have included the formation of modern temperate faunas approximately 40 My BP (27); segregation of eastern and western Pacific faunas around the Mesozoic-Cenozoic boundary by formation of the East Pacific Barrier (25, 28); formation of the Tethys Sea approximately 95 My BP and subsequent isolation of the Mediterranean Basin from the Indo-Pacific during the Miocene, approximately 18 My BP (26); or possibly earlier events, including species radiations following the breakup of Pangea and the dispersion of continents during and after the late Jurassic, or radiations following the K-T mass extinction (22).

Later dispersal events probably also influenced the modern zoogeography of *Aurelia*. For example, the highly divergent Mljet *Aurelia* may be a relict of the primitive Tethys fauna that survived depletion of the Mediterranean Sea during the Messinian Salinity Crisis and which was subsequently contacted secondarily by *A. aurita* from Northern Europe during the early Pliocene (~5 MyBP) when the Strait of Gibraltar breached (26). Alternatively, both the Mljet *Aurelia* and *A. aurita* may have recolonized the Mediterranean, probably from the Indian and Atlantic oceans respectively, after the Messinian. More recent dispersal events are indicated by the occurrence of two species of *Aurelia* in Palau in habitats that were unavailable 10,000 years ago (29), although the geographic origins and earlier evolutionary histories of these species are as yet unknown. Such dispersal events, new records of *Aurelia* from Pacific islands (*e.g.*, Chuuk; 30), and common haplotypes in Palau and Helen Reef suggest that, although *Aurelia* has generally been considered a neritic genus (3, 5, 6), the medusae of some wider-ranging *Aurelia* species may be largely oceanic.

Aurelia is the best studied of all scyphozoans, yet its taxonomy, biogeography, phylogeography, and evolution are poorly known. This lack of knowledge is attributable largely to the morphological simplicity of *Aurelia* and to homoplasy that, as in other marine taxa, has contributed to drastic underestimation of species diversity (4, 7, 9). The underestimation of marine species diversity seriously compromises our ability to understand the evolution and ecology of marine environments. For example, morphological similarity superficially suggests widespread species, high gene flow, few barriers to dispersal, a dearth of allopatric speciation and, therefore, greater probability that other modes of speciation have contributed significantly to marine biodiversity (2). However, these novel DNA sequence data describing multiple cryptic species in an *Aurelia aurita* species complex suggest that barriers to gene flow—both geographic and ecological—are important sources of diversity in marine taxa. For *Aurelia*, as for other marine organisms including other scyphozoans (7), new morphological studies, more molecular analyses, and better distributional data are required to establish a robust evolutionary framework in which ecological, applied, and other scientific or educational endeavors can be placed in their correct contexts.

Acknowledgments

This work would have been impossible without specimens provided generously by A. Benovic (Mljet), the Birch Aquarium (San Diego), O. Chaga (White Sea), the Coral Reef Research Foundation (Helen Reef), J. Costello (Boston), H. Ishii and M. Omori (Japan), A. Kideys (Bosporus), A. Knowlton (Kachemak), O. Lindahl (Sweden), A. C. Morandini (Brazil), P. Rankin (Newport Bay, Oregon), K. Raskoff (Tomales Bay), T. Shiganova (Black Sea), B. Sullivan (Narragansett Bay), West Wind Sealab Supplies (Vancouver Island), and D. Wrobel (Monterey); information about other sites was provided by L. Gershwin. The early development of this project was contributed to by K. Raskoff, L. Martin, W. Hamner, and L. Gershwin. D. Swofford kindly provided access to invaluable β-versions of PAUP. This work was made possible and enjoyable by the generosity of many people in Palau, particularly all at Coral Reef Research Foundation, Palau Conservation Society, and Fish 'n Fins. The national Division of Marine Resources and Koror State Government kindly granted research permits for work in Palau. M. N. Arai, L. E. Martin, and an anonymous reviewer provided valuable comments on draft manuscripts. This project was funded by grants to MND from the University of California (UCLA); the Department of Organismic Biology, Ecology, and Evolution at UCLA; the International Women's Fishing Association; the American Museum of Natural History (Lerner-Grey Award); and the British Schools and Universities Foundation.

Literature Cited

1. **May, R. M. 1994.** Biological diversity: differences between land and sea. *Philos. Trans. R. Soc. Lond. B* **343:** 105–111.
2. **Palumbi, S. R. 1992.** Marine speciation on a small planet. *Trends Ecol. Evol.* **7:** 114–118.
3. **Mayer, A. G. 1910.** *Medusae of the World, III: the Scyphomedusae.* Carnegie Institute, Washington, DC.
4. **Kramp, P. L. 1968.** The scyphomedusae collected by the Galathea expedition 1950–52. *Vidensk. Medd. Dan. Naturhist. Foren.* **131:** 67–98.
5. **Russell, F. S. 1970.** *The Medusae of the British Isles. II Pelagic Scyphozoa with a Supplement to the First Volume on Hydromedusae.* Cambridge University Press, Cambridge.
6. **Arai, M. N. 1997.** *A Functional Biology of Scyphozoa.* Chapman & Hall, London.
7. **Knowlton, N. 2000.** Molecular genetic analyses of species boundaries in the sea. *Hydrobiologia* **420:** 73–90.
8. **Möller, H. 1980.** Scyphomedusae as predators and food competitors of larval fish. *Meeresforschung* **28:** 90–100.
9. **Greenberg, N., R. L. Garthwaite, and D. C. Potts. 1996.** Allozyme and morphological evidence for a newly introduced species of *Aurelia* in San Francisco Bay, California. *Mar. Biol.* **125:** 401–410.
10. **Wrobel, D., and C. Mills. 1998.** *Pacific Coast Pelagic Invertebrates: a Guide to the Common Gelatinous Animals.* Sea Challengers and Monterey Bay Aquarium, Monterey, CA.
11. **Hamner, W. M., and R. M. Jenssen. 1974.** Growth, degrowth, and irreversible cell differentiation in *Aurelia aurita. Am. Zool.* **14:** 833–849.
12. **Hamner, W. M., P. P. Hamner, and S. W. Strand. 1994.** Sun-compass migration by *Aurelia aurita* (Scyphozoa): population retention and reproduction in Saanich Inlet, British Columbia. *Mar. Biol.* **119:** 347–356.
13. **Zubkoff, P. L., and A. L. Linn. 1975.** Isozymes of *Aurelia aurita* scyphistomae obtained from different geographical locations. Pp. 915–930 in *Isozymes IV, Genetics and Evolution*, C. L. Markert, ed. Academic Press, New York.
14. **Chen, C. A., B. L. Willis, and D. J. Miller. 1996.** Systematic relationships between tropical corallimorpharians (Cnidaria: Anthozoa: Corallimorpharia): utility of the 5.8s and internal transcribed spacer (ITS) regions of the rRNA transcription unit. *Bull. Mar. Sci.* **59:** 196–208.
15. **Beauchamp, K. A., and D. A. Powers. 1996.** Sequence variation of the first internal spacer (ITS-1) of ribosomal DNA in ahermatypic corals from California. *Mol. Mar. Biol. Biotechnol.* **5:** 357–362.
16. **Wesson, D. M., C. H. Porter, and F. H. Collins. 1992.** Sequence and secondary structure comparisons of ITS rDNA in mosquitoes (Diptera:Culicidae). *Mol. Phylogenet. Evol.* **1:** 253–269.
17. **Odorico, D. M., and D. J. Miller. 1997.** Variation in the ribosomal internal transcribed spacers and 5.8s rDNA among five species of *Acropora* (Cnidaria: Scleractinia): patterns of variation consistent with reticulate evolution. *Mol. Biol. Evol.* **14:** 465–473.
18. **Bucklin, A., A. M. Bentley, and S. P. Franzen. 1998.** Distribution and relative abundance of *Pseudocalanus moultoni* and *P. newmani* (Copepoda: Calanoida) on Georges Bank using molecular identification of sibling species. *Mar. Biol.* **132:** 97–106.
19. **Knowlton, N., and L. A. Weigt. 1998.** New dates and new rates for divergence across the Isthmus of Panama. *Proc. R. Soc. Lond. B.* **265:** 2257–2263.
20. **Peek, A. S., R. G. Gustafson, R. A. Lutz, and R. C. Vrijenhoek. 1997.** Evolutionary relationships of deep-sea hydrothermal vent and cold-water seep clams (Bivalvia: Vesicomyidae): results from mitochondrial cytochrome oxidase subunit I. *Mar. Biol.* **130:** 151–161.
21. **Meyran, J.-C., M. Monnerot, and P. Taberlet. 1997.** Taxonomic status and phylogenetic relationships of some species of the genus *Gammarus* (Crustacea, Amphipoda) deduced from mitochondrial DNA sequences. *Mol. Phylogenet. Evol.* **8:** 1–10.
22. **Futuyma, D. J. 1998.** *Evolutionary Biology*, 3rd ed. Sinauer, Sunderland, MA.
23. **Li, W.-H., and D. Graur. 1991.** *Fundamentals of Molecular Evolution.* Sinauer, Sunderland, MA.
24. **Romano, S. L., and S. R. Palumbi. 1997.** Molecular evolution of a portion of the mitochondrial 16S ribosomal gene region in scleractinian corals. *J. Mol. Evol.* **45:** 397–411.
25. **Briggs, J. C. 1974.** *Marine Zoogeography.* McGraw-Hill, New York.
26. **Gili, J.-M., J. Bouillon, F. Pagès, A. Palanques, P. Puig, and S. Heussner. 1996.** Origin and biogeography of the deep-water Mediterranean hydromedusae including the description of two new species collected in submarine canyons of Northwestern Mediterranean. *Sci. Mar.* **62:** 113–134.
27. **Kafanov, A. I. 1982.** The Cenozoic history of the molluscan faunas of the North Pacific Shelf. Pp. 134–176 in *Morskaya Biogeografiya: Predmet, Metody, Printsipy Raionirovaniya.* Nauka Press, Moscow. (Translated from Russian by *Can. Transl. Fish. Aquat Sci.* #5052, 1984).
28. **Grigg, R. W., and R. Hey. 1992.** Paleoceanography of the tropical Eastern Pacific Ocean. *Science* **255:** 172–178.
29. **Dawson, M. 2000.** Molecular variation and evolution in coastal marine taxa. Ph.D. dissertation, University of California, Los Angeles. 244 pp.
30. **Colin, P. L., and C. Arneson. 1995.** *Tropical Pacific Invertebrates.* Coral Reef Press, Beverly Hills, CA.
31. **Hamner, W. M., and P. P. Hamner. 1998.** Stratified marine lakes of Palau (Western Caroline Islands). *Phys. Geogr.* **19:** 175–220.
32. **Folmer, O., M. Black, W. Hoeh, R. Lutz, and R. Vrijenhoek. 1994.** DNA primers for amplification of mitochondrial cytochrome c oxidase subunit I from diverse metazoan invertebrates. *Mol. Mar. Biol. Biotechnol.* **3:** 294–299.
33. **Swofford, D. L. 2000.** *PAUP: Phylogenetic Analysis Using Parsimony, v. 4.0b4a.* Smithsonian Institution and Sinauer Associates, Sunderland, MA.
34. **Thompson, J. D., D. G. Higgins, and T. J. Gibson. 1994.** CLUSTAL W: improving the sensitivity of progressive multiple sequence alignment through sequence weighting, position specific gap penalties and weight matrix choice. *Nucl. Acids Res.* **22:** 4673–4680.

It's Time To Make A New Discovery
Axiovert 200. The New Standard In Inverted Microscopy.
Carl Zeiss, Inc., Microscopy & Imaging Systems
One Zeiss Drive, Thornwood, NY 10594 micro@zeiss.com, www.zeiss.com/micro

Being a scientist, you're more than familiar with the rigorous demands of your research. Discover the Axiovert 200, a new standard in inverted microscopy from Zeiss. Superior performance, brilliant fluorescence, greater stability, flexibility and reliability set it apart from the pack. Uncompromising quality guarantees you the edge you need for success. A powerful tool with impact, you'll see more and achieve more with the new Axiovert 200. **For further details call 800.233.2343.**

ZEISS

Volume 200

Number 2

THE BIOLOGICAL BULLETIN

APRIL 2001

Published by the Marine Biological Laboratory

Thanks Galileo, Hooke and Leeuwenhoek for the incentive.

We walk in the footsteps of visionaries. And see with the eyes of disciples.

Galileo up close: astronomer, physicist, mathematician, dethroner of Aristotle, defender of Copernicus and, yes, credited with making double convex lenses and the first biological observations with a microscope. A compound microscope. In 1624.

Hooke: 43 years later, the compound microscope reveals living things are composed of cells.

Leeuwenhoek: invents the first practical microscope and discovers bacteria.

Armed with the knowledge and inspiration of these and other Olympians, secure in the history of our own accomplishments and aware that the mind's eye should always focus on challenging the enigmatic as well as the undeniable, Olympus has created the BX2 series of clinical and research microscopes, noteworthy for their enhancements in optics, imaging and ergonomics.

And each so individual, it deserves the nomenclature My Microscope.

From possibility to actuality, it is wonderful to behold.
A posse ad esse est mirabile visu.

Welcome to the next golden age of microsopy.

BX2
Microscope Series

The BX41

The new standard in laboratory microscopy vis-a-vis performance, versatility, operation.

Uncanny digitized imaging: enhanced with the **DP11 digital camera**, delivering high-resolution image recording beyond the norm.

Unusually insightfu optics: observe magnifications fron **1.25x to 100x without changing the condenser.** Choice of condenser includes Abbe, swing out, phase-contrast and darkfield.

Unerringly precise-motion stage: selectable for right/ left hand. Discover speed, ease, touch, comfort, and clinica accuracy.

Uncommonly easy-to-operate controls: extended fine-focus knob; forwarded-positioned illumination intensity dial; tactile X-Y control.

The BX45

The new standard in ergonomic microscopy. A dramatic metamorphosis: innovative, intelligent, insightful design improvements specifically addressing the needs of those spending hours looking through a microscope.

The **lowest low-position stage: three inches lower** than standard microscopes, offering the promise of minimum effort and hand movement when changing specimens.

The **tilting, telescoping observation tube:** a marvel of adjustability, it can be changed to accommodate any observation position. 80mm higher and 70mm closer to the operator than a conventional tilting tube. And the eyepoint can be moved forward by 45mm and inclined from 0–25 degrees.

The BX51

The new standard in research microscopy. The words "new" and "standard" really don't do it justice. How about "ingenious" or "original," "paragon" or "prototypical." Prepare yourself for a higher power.

The **6-position filter cube turret:** Not 4, not 5, but 6, so single and multiband imaging of new fluorochromes and fluorescent proteins is faster, simpler and exclusively tailored.

5
6
2
4
5
6
WU
IG
WIY

The **rectangular field stop: ours alone**. By cleverly matching the camera's field of view, only the area requiring fluorescence excitation is exposed. Which means that the surrounding areas are protected from photo bleaching.

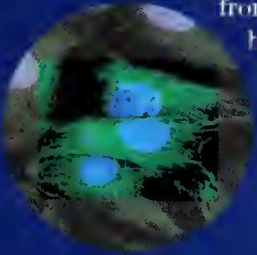

The **fluorescence excitation balancers:** another **Olympus exclusive**. A continuously variable excitation bandwidth. Visualization is enhanced, differentiation of multi-labels is immeasurably improved, capturing of images is at an unheard-of level.

Triple Labeled Specimen (l to r):

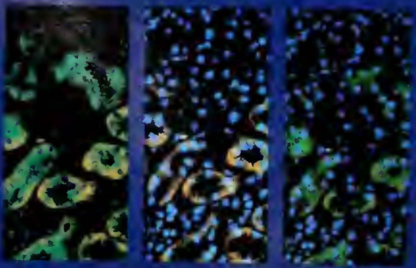

- with prevalent FITC and Cy3
- with prevalent DAPI and Cy3
- with balanced fluorescence emission

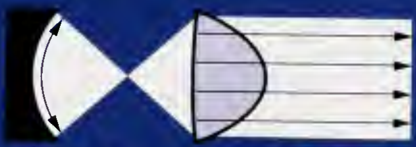

wider mirror aspherical lens

The **aspherical collector lens:** *sui generis*, in a class by itself. Specimens appear **brighter** and **more evenly illuminated**; and achromatic performance now incorporates wavelengths from UV to IR.

The **universal condenser: with 8 positions**, it can accept optical inserts for DIC, phase, brightfield and darkfield illumination. And the advanced Nomarski DIC system has been expanded and optimized to encompass prisms for enhanced contrast and image resolution.

OLYMPUS®

FOCUS ON LIFE

Visit us at www.olympusamerica.com
or call 1-800-455-8236

©Olympus America Inc.

Wait until you see what 12 million pixels of capture resolution gets you. The DXM1200, designed exclusively for photomicrography, provides ultra high fidelity color reproduction and resolution virtually equal to film.

In addition, the DXM1200 comes complete with Nikon's highly intuitive ACT-1™ software with:

- 12 frames per second data transfer for faster image capture than you ever thought possible.
- Image archiving and retrieval that's faster and simpler than ever before.

To find out more about the surprisingly affordable DXM1200 digital camera, call **1-800-52-NIKON ext. 380**.

For complete tutorials of the ACT-1 software and a gallery of DXM1200 images, visit MicroscopyU at our newly designed website **www.nikonusa.com**

NOW YOU'RE TALKING HIGH RESOLUTION

GET LARGER, MORE VIVID MICROSCOPY IMAGES FROM NIKON'S DXM1200 ULTRA-HIGH RESOLUTION DIGITAL CAMERA.

Nikon

© 2001 Nikon Instruments Inc.

KODAK MDS 290

Section One: Analogies

1) Film is to the KODAK MDS 290 as

A) Typewriter is to Word Processor
B) Magnifying Glass is to Microscope
C) Abacus is to Calculator
D) Pony Express is to E-Mail
E) All of the Above

see answer below

DIGITAL IMAGING 101

faster

better

cheaper

The above statement refers to comparison to film

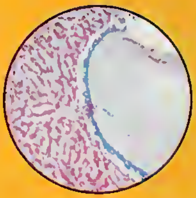

The New Microscopy Documentation System 290

The revolutionary digital imaging tool for microscopy documentation is both versatile and easy to use. With 2.1 mega-pixel clarity, accurate color fidelity, and USB connection, the KODAK MDS 290 produces film-quality images of your brightfield, darkfield, and bright fluorescence specimens. The included software module operates seamlessly with ADOBE PHOTOSHOP Software and allows you to control the camera (exposure, preview, optical zoom, and compression) direct from your MACINTOSH Computer or PC. Off of the microscope, the DC290 can be used as a point and shoot digital camera for routine laboratory photography. Now you can access, adjust, print, or share your image files instantly from your computer, and completely eliminate film costs and processing delays. With its low price tag and unmatched performance, your lab can't afford to be without one.

To learn more, visit www.kodak.com/go/mds290e
or call 1-877-SIS-HELP express code 7. In the US,
the MDS 290 is also available from Fisher Scientific.

**Please visit us at
the ASM Meeting
May 21-23
Booth # 317**

Correct Answer: E) All of the Above

KODAK SCIENTIFIC IMAGING SYSTEMS

Kodak

THE BIOLOGICAL BULLETIN

APRIL 2001

Editor	MICHAEL J. GREENBERG	The Whitney Laboratory, University of Florida
Associate Editors	LOUIS E. BURNETT	Grice Marine Biological Laboratory, College of Charleston
	R. ANDREW CAMERON	California Institute of Technology
	CHARLES D. DERBY	Georgia State University
	MICHAEL LABARBERA	University of Chicago
Section Editor	SHINYA INOUÉ, *Imaging and Microscopy*	Marine Biological Laboratory
Online Editors	JAMES A. BLAKE, *Keys to Marine Invertebrates of the Woods Hole Region*	ENSR Marine & Coastal Center, Woods Hole
	WILLIAM D. COHEN, *Marine Models Electronic Record and Compendia*	Hunter College, City University of New York
Editorial Board	PETER B. ARMSTRONG	University of California, Davis
	ERNEST S. CHANG	Bodega Marine Lab., University of California, Davis
	THOMAS H. DIETZ	Louisiana State University
	RICHARD B. EMLET	Oregon Institute of Marine Biology, Univ. of Oregon
	DAVID EPEL	Hopkins Marine Station, Stanford University
	GREGORY HINKLE	Cereon Genomics, Cambridge, Massachusetts
	MAKOTO KOBAYASHI	Hiroshima University of Economics, Japan
	ESTHER M. LEISE	University of North Carolina Greensboro
	DONAL T. MANAHAN	University of Southern California
	MARGARET MCFALL-NGAI	Kewalo Marine Laboratory, University of Hawaii
	MARK W. MILLER	Institute of Neurobiology, University of Puerto Rico
	TATSUO MOTOKAWA	Tokyo Institute of Technology, Japan
	YOSHITAKA NAGAHAMA	National Institute for Basic Biology, Japan
	SHERRY D. PAINTER	Marine Biomed. Inst., Univ. of Texas Medical Branch
	J. HERBERT WAITE	University of California, Santa Barbara
	RICHARD K. ZIMMER	University of California, Los Angeles
Editorial Office	PAMELA CLAPP HINKLE	Managing Editor
	VICTORIA R. GIBSON	Staff Editor
	CAROL SCHACHINGER	Editorial Associate
	WENDY CHILD	Subscription & Advertising Secretary

Published by
MARINE BIOLOGICAL LABORATORY
WOODS HOLE, MASSACHUSETTS

Marine Biological Laboratory /
Woods Hole Oceanographic Institution
Library
APR 27 2001
Woods Hole, MA 02543

Cover

The six-legged walking machine on the cover is similar to the walking stick watching nearby, in that both can traverse an irregular, unstable terrain with a relatively undisturbed gait. More to the point, the gait in both "organisms" is generated by a control system that is remarkably decentralized; that is, each leg has its own controller, and the gait is an emergent property of interactions between them and the physical properties of the legs and the environment. The characteristics of the control system for the robot (named TARRY2) were inspired by investigations of the walking stick *Carausius morosus* by Josef Schmitz and his colleagues at the University of Bielefeld (Germany); these studies are described in this issue (pp. 195-200).

The paper by Schmitz *et al.* is part of the proceedings of a workshop entitled *Invertebrate Sensory Information Processing: Implications for Biologically Inspired Autonomous Systems* (see p. 145). The workshop was sponsored by the Center for Advanced Studies in the Space Life Sciences and held in April 2000 at the Marine Biological Laboratory (MBL), Woods Hole, Massachusetts. The participants included scientists from the fields of invertebrate sensory biology, sensory guided behavior, and biologically inspired robotics. They asked how complex invertebrates process sensory data and use it to cope with dynamic environments, and they also evaluated the performance of automatons built to emulate those animals and their behaviors.

The photograph of TARRY2 was taken by Martin Guddat (University of Duisburg, Germany). In real life, this biomimetic robot is 50 cm long, spans 50 cm, and weighs 3 kg. The stick insect, in contrast, was only 8 cm long (without its 2-cm antennae), spanned 5 cm, and weighed 1 g; its photographer was Josef Schmitz. The composite image on the cover was produced by Beth Liles at the MBL.

Marine Biological Laboratory /
Woods Hole Oceanographic Institution
Library

APR 27 2001

Woods Hole, MA 02543

CONTENTS

Volume 200, No. 2: April 2001

DEVELOPMENT AND REPRODUCTION

Rahman, M. Aminur, Tsuyoshi Uehara, and John S. Pearse
Hybrids of two closely related tropical sea urchins (Genus *Echinometra*): evidence against postzygotic isolating mechanisms 97

Pernet, Bruno
Escape hatches for the clonal offspring of serpulid polychaetes 107

PHYSIOLOGY

Levy, O., L. Mizrahi, N. E. Chadwick-Furman, and Y. Achituv
Factors controlling the expansion behavior of *Favia favus* (Cnidaria: Scleractinia): effects of light, flow, and planktonic prey 118

SYMBIOSIS

Wakefield, Timothy S., and Stephen C. Kempf
Development of host- and symbiont-specific monoclonal antibodies and confirmation of the origin of the symbiosome membrane in a cnidarian–dinoflagellate symbiosis 127

INVERTEBRATE SENSORY INFORMATION PROCESSING: IMPLICATIONS FOR BIOLOGICALLY INSPIRED AUTONOMOUS SYSTEMS

Blazis, Diana E. J., and Frank W. Grasso
Introduction 147

Breithaupt, Thomas
Fan organs of crayfish enhance chemical information flow 150

Fraser, Peter J.
Statocysts in crabs: short-term control of locomotion and long-term monitoring of hydrostatic pressure . . 155

Grasso, Frank W.
Invertebrate-inspired sensory-motor systems and autonomous, olfactory-guided exploration 160

Barlow, Robert B., James M. Hitt, and Frederick A. Dodge
Limulus vision in the marine environment 169

Cronin, Thomas W., and Justin Marshall
Parallel processing and image analysis in the eyes of mantis shrimps 177

Webb, Barbara
View from the boundary 184

Robert, Daniel
Innovative biomechanics for directional hearing in small flies 190

Schmitz, Josef, Jeffrey Dean, Thomas Kindermann, Michael Schumm, and Holk Cruse
A biologically inspired controller for hexapod walking: simple solutions by exploiting physical properties 195

Macmillan, David L., and Blair W. Patullo
Insights for robotic design from studies of the control of abdominal position in crayfish 201

Birmingham, J. T.
Increasing sensor flexibility through neuromodulation 206

Derby, Charles D., and Pascal Steullet
Why do animals have so many receptors? The role of multiple chemosensors in animal perception 211

Srinivasan, Mandyam V., Shaowu Zhang, and Javaan S. Chahl
Landing strategies in honeybees and possible applications to autonomous airborne vehicles 216

Ishida, H., T. Nakamoto, T. Moriizumi, T. Kikas, and J. Janata
Plume-tracking robots: a new application of chemical sensors 222

Mountain, David C., and Allyn E. Hubbard
Sensing scenes with silicon 227

Higgins, Charles M.
Sensory architectures for biologically inspired autonomous robotics 235

List of Participants 243

THE BIOLOGICAL BULLETIN

THE BIOLOGICAL BULLETIN is published six times a year by the Marine Biological Laboratory, 7 MBL Street, Woods Hole, Massachusetts 02543.

Subscriptions and similar matter should be addressed to Subscription Manager, THE BIOLOGICAL BULLETIN, Marine Biological Laboratory, 7 MBL Street, Woods Hole, Massachusetts 02543. Subscription per year (six issues, two volumes): $235 for libraries; $95 for individuals. Subscription per volume (three issues): $117.50 for libraries; $47.50 for individuals. Back and single issues (subject to availability): $40 for libraries; $20 for individuals.

Communications relative to manuscripts should be sent to Michael J. Greenberg, Editor-in-Chief, or Pamela Clapp Hinkle, Managing Editor, at the Marine Biological Laboratory, 7 MBL Street, Woods Hole, Massachusetts 02543. Telephone: (508) 289-7428. FAX: 508-289-7922. E-mail: pclapp@mbl.edu.

http://www.mbl.edu/BiologicalBulletin/

The home page for the electronic companion to THE BIOLOGICAL BULLETIN—*the Marine Models Electronic Record*—and other BIOLOGICAL BULLETIN publications is available on the World Wide Web at the address shown above.

THE BIOLOGICAL BULLETIN is indexed in bibliographic services including *Index Medicus* and MEDLINE, *Chemical Abstracts, Current Contents, Elsevier BIOBASE/Current Awareness in Biological Sciences,* and *Geo Abstracts.*

Printed on acid free paper,
effective with Volume 180, Issue 1, 1991.

POSTMASTER: Send address changes to THE BIOLOGICAL BULLETIN, Marine Biological Laboratory,
7 MBL Street, Woods Hole, MA 02543.

Copyright © 2001, by the Marine Biological Laboratory

Periodicals postage paid at Woods Hole, MA, and additional mailing offices.
ISSN 0006-3185

INSTRUCTIONS TO AUTHORS

The Biological Bulletin accepts outstanding original research reports of general interest to biologists throughout the world. Papers are usually of intermediate length (10–40 manuscript pages). A limited number of solicited review papers may be accepted after formal review. A paper will usually appear within four months after its acceptance.

Very short, especially topical papers (less than 9 manuscript pages including tables, figures, and bibliography) will be published in a separate section entitled "Research Notes." A Research Note in *The Biological Bulletin* follows the format of similar notes in *Nature.* It should open with a summary paragraph of 150 to 200 words comprising the introduction and the conclusions. The rest of the text should continue on without subheadings, and there should be no more than 30 references. References should be referred to in the text by number, and listed in the Literature Cited section in the order that they appear in the text. Unlike references in *Nature,* references in the Research Notes section should conform in punctuation and arrangement to the style of recent issues of *The Biological Bulletin.* Materials and Methods should be incorporated into appropriate figure legends. See the article by Lohmann *et al.* (October 1990, Vol. **179:** 214–218) for sample style. A Research Note will usually appear within two months after its acceptance.

The Editorial Board requests that regular manuscripts conform to the requirements set below; those manuscripts that do not conform will be returned to authors for correction before review.

1. ***Manuscripts.*** Manuscripts, including figures, should be submitted in quadruplicate, with the originals clearly marked. (Xerox copies of photographs are not acceptable for review purposes.) The submission letter accompanying the manuscript should include a telephone number, a FAX number, and (if possible) an E-mail address for the corresponding author. The original manuscript must be typed in no smaller than 12 pitch or 10 point, using double spacing (*including* figure legends, footnotes, bibliography, etc.) on one side of 16- or 20-lb. bond paper, 8 by 11 inches. Please, no right justification. Manuscripts should be proofread carefully and errors corrected legibly in black ink. Pages should be numbered consecutively. Margins on all sides should be at least 1 inch (2.5 cm). Manuscripts should conform to the *Council of Biology Editors Style Manual,* 5th Edition (Council of Biology Editors, 1983) and to American spelling. Unusual abbreviations should be kept to a minimum and should be spelled out on first reference as well as defined in a footnote on the title page. Manuscripts should be divided into the following components: Title page, Abstract (of no more than 200 words), Introduction, Materials and Methods, Results, Discussion, Acknowledgments, Literature Cited, Tables, and Figure Legends. In addition, authors should supply a list of words and phrases under which the article should be indexed.

2. ***Title page.*** The title page consists of a condensed title or running head of no more than 35 letters and spaces, the manuscript title, authors' names and appropriate addresses, and footnotes listing present addresses, acknowledgments or contribution numbers, and explanation of unusual abbreviations.

3. ***Figures.*** The dimensions of the printed page, 7 by 9 inches, should be kept in mind in preparing figures for publication. We recommend that figures be about 1 times the linear dimensions of the final printing desired, and that the ratio of the largest to the smallest letter or number and of the thickest to the thinnest line not exceed 1:1.5. Explanatory matter generally should be included in legends, although axes should always be identified on the illustration itself. Figures should be prepared for reproduction as either line cuts or halftones. Figures to be reproduced as line cuts should be unmounted glossy photographic reproductions or drawn in black ink on white paper, good-quality tracing cloth or plastic, or blue-lined coordinate paper. Those to be reproduced as halftones should be mounted on board, with both designating numbers or letters and scale bars affixed directly to the figures. All figures should be numbered in consecutive order, with no distinction between text and plate figures and cited, in order, in the text. The author's name and an arrow indicating orientation should appear on the reverse side of all figures.

Digital art: The Biological Bulletin will accept figures submitted in electronic form; however, digital art must conform to the following guidelines. Authors who create digital images are wholly responsible for the quality of their material, including color and halftone accuracy.

Format. Acceptable graphic formats are TIFF and EPS. Color submissions must be in EPS format, saved in CMKY mode.

Software. Preferred software is Adobe Illustrator or Adobe Photoshop for the Mac and Adobe Photoshop for Windows. Specific instructions for artwork created with various software programs are available on the Web at the Digital Art Information Site maintained by Cadmus Professional Communications at http://cjs.cadmus.com/da/home.html

Resolution. The minimum requirements for resolution are 1200 DPI for line art and 300 for halftones.

Size. All digital artwork must be submitted at its actual printed size so that no scaling is necessary.

Multipanel figures. Figures consisting of individual parts (*e.g.*, panels A, B, C) must be assembled into final format and submitted as one file.

Hard copy. Files must be accompanied by hard copy for use in case the electronic version is unusable.

Disk identification. Disks must be clearly labeled with the following information: author name and manuscript number; format (PC or Macintosh); name and version of software used.

Color: The Biological Bulletin will publish color figures and plates, but must bill authors for the actual additional cost of printing in color. The process is expensive, so authors with more than one color image should—consistent with editorial concerns, especially citation of figures in order—combine them into a single plate to reduce the expense. On request, when supplied with a copy of a color illustration, the editorial staff will provide a pre-publication estimate of the printing cost.

4. ***Tables, footnotes, figure legends, etc.*** Authors should follow the style in a recent issue of *The Biological Bulletin* in preparing table headings, figure legends, and the like. Because of the high cost of setting tabular material in type, authors are asked to limit such material as much as possible. Tables, with their headings and footnotes, should be typed on separate sheets, numbered with consecutive Roman numerals, and placed after the Literature Cited. Figure legends should contain enough information to make the figure intelligible separate from the text. Legends should be typed double spaced, with consecutive Arabic numbers, on a separate sheet at the end of the paper. Footnotes should be limited to authors' current addresses, acknowledgments or contribution numbers, and explanation of unusual abbreviations. All such footnotes should appear on the title page. Footnotes are not normally permitted in the body of the text.

5. ***Literature cited.*** In the text, literature should be cited by the Harvard system, with papers by more than two authors cited as Jones *et al.*, 1980. Personal communications and material in preparation or in press should be cited in the text only, with author's initials and institutions, unless the material has been formally accepted and a volume number can be supplied. The list of references following the text should be headed Literature Cited, and must be typed double spaced on separate pages, conforming in punctuation and arrangement to the style of recent issues of *The Biological Bulletin*. Citations should include complete titles and inclusive pagination. Journal abbreviations should normally follow those of the U. S. A. Standards Institute (USASI), as adopted by Biological Abstracts and Chemical Abstracts, with the minor differences set out below. The most generally useful list of biological journal titles is that published each year by Biological Abstracts (biosis List of Serials; the most recent issue). Foreign authors, and others who are accustomed to using The World List of Scientific Periodicals, may find a booklet published by the Biological Council of the U.K. (obtainable from the Institute of Biology, 41 Queen's Gate, London, S.W.7, England, U.K.) useful, since it sets out the World List abbreviations for most biological journals with notes of the USASI abbreviations where these differ. Chemical Abstracts publishes quarterly supplements of additional abbreviations. The following points of reference style for The Biological Bulletin differ from USASI (or modified World List) usage:

A. Journal abbreviations, and book titles, all underlined (for *italics*)

B. All components of abbreviations with initial capitals (not as European usage in World List *e.g., J. Cell. Comp. Physiol.* NOT *J. cell. comp. Physiol.*)

C. *All* abbreviated components must be followed by a period, whole word components *must not* (*i.e., J. Cancer Res.*)

D. Space between all components (*e.g., J. Cell. Comp. Physiol.*, not *J.Cell.Comp.Physiol.*)

E. Unusual words in journal titles should be spelled out in full, rather than employing new abbreviations invented by the author. For example, use *Rit Vísindafjélags Islendinga* without abbreviation.

F. All single word journal titles in full (*e.g., Veliger, Ecology, Brain*).

G. The order of abbreviated components should be the same as the word order of the complete title (*i.e., Proc.* and *Trans.* placed where they appear, not transposed as in some BIOLOGICAL ABSTRACTS listings).

H. A few well-known international journals in their preferred forms rather than WORLD LIST or USASI usage (*e.g., Nature, Science, Evolution* NOT *Nature, Lond., Science, N.Y.; Evolution, Lancaster, Pa.*)

6. ***Reprints, page proofs, and charges.*** Authors may purchase reprints in lots of 100. Forms for placing reprint orders are sent with page proofs. Reprints normally will be delivered about 2 to 3 months after the issue date. Authors (or delegates for foreign authors) will receive page proofs of articles shortly before publication. They will be charged the current cost of printers' time for corrections to these (other than corrections of printers' or editors' errors). Other than these charges for authors' alterations, *The Biological Bulletin* does not have page charges.

Reference: *Biol. Bull.* **200:** 97–106. (April 2001)

Hybrids of Two Closely Related Tropical Sea Urchins (Genus *Echinometra*): Evidence Against Postzygotic Isolating Mechanisms

M. AMINUR RAHMAN[1], TSUYOSHI UEHARA[1,*], AND JOHN S. PEARSE[2]

[1]*Department of Marine and Environmental Sciences, Graduate School of Engineering and Science, University of the Ryukyus, 1 Senbaru, Nishihara-cho, Okinawa 903-0213, Japan; and*
[2]*Long Marine Laboratory, University of California, Santa Cruz, California 95064*

Abstract. A series of cross-fertilization experiments were conducted with two unnamed, sympatric species of sea urchins in the *Echinometra mathaei* species complex, *Echinometra* sp. A (Ea) and *Echinometra* sp. C (Ec). Heterogametic fertilization success was high when eggs of Ec and sperm of Ea were involved, and low with eggs of Ea and sperm of Ec. Hybrids produced from crosses in either direction developed normally to sexually mature adults; Ea × Ea were largest in test size, followed by Ec (ova) × Ea (sperm), Ea (ova) × Ec (sperm), and Ec × Ec, respectively. Color patterns of the hybrids were closer to the maternal coloration, whereas other characters such as relative test dimensions and spine lengths, morphology of tubefoot and gonad spicules, and gamete sizes were intermediate. Fertilization rates in F_1 backcrosses were high, minimizing the possibility that hybrid infertility is a postzygotic mechanism of reproductive isolation. On the other hand, intensive surveys failed to find individuals with hybrid characteristics in the field, suggesting that natural hybridization between the two species is rare. Prezygotic isolating mechanisms, such as microhabitat separation and gamete incompatibility, at least between Ea eggs and Ec sperm, most likely maintain the genetic integrity of these two closely related species.

Introduction

Recent morphological, biochemical, ecological, and reproductive studies have revealed the presence of four sympatric biological species of sea urchins within the *Echinometra mathaei, sensu lato,* species complex at Okinawa, Japan. These species have been referred to as *Echinometra* species A, B, C, and D (*e.g.*, Uehara and Shingaki, 1985; Uehara *et al.*, 1990, 1991; Arakaki and Uehara, 1991; Matsuoka and Hatanaka, 1991; Nishihira *et al.*, 1991; Palumbi and Metz, 1991; Palumbi, 1996, 1998; Aslan and Uehara, 1997; Palumbi *et al.*, 1997). *E.* sp. B is now recognized as *E. mathaei* (de Blainville, 1825), *sensu stricto,* (Arakaki *et al.*, 1998), while *E.* sp. D belongs in the *E. oblonga* (de Blainville, 1825) species complex, which may include at least three species (Arakaki and Uehara, 1999).

In sympatric echinoids like these species on Okinawa, interspecific reproductive isolation can result from different reproductive characteristics, such as timing and sites of spawning or gametic incompatibility (Lessios and Cunningham, 1990; Uehara *et al.*, 1990; Palumbi and Metz, 1991; Metz *et al.*, 1994; Palumbi, 1994, 1998; Vacquier *et al.*, 1995; Aslan and Uehara, 1997; Lessios, 1998; McCartney *et al.*, 2000). Of these factors, gamete incompatibility, preventing gametes of different species from fertilizing, may be particularly important for maintaining reproductive isolation of many animals (Dobzhansky *et al.*, 1977), including echinoderms (Palumbi and Metz, 1991; Byrne and Anderson, 1994; Vacquier *et al.*, 1995; Palumbi, 1998). On the other hand, postzygotic mechanisms such as the production of nonviable or infertile hybrids also could lead to and maintain reproductive isolation in various species (Coyne, 1992; Knowlton, 1993), including those of sea urchins (Chen and Baltzer, 1975; Lessios and Cunningham, 1990; Lessios, 1998; McCartney *et al.*, 2000).

Of the four species on Okinawa, two, Ea and Eb, appear to be reproductively isolated by gametic incompatibility,

---

Received 4 May 2000; accepted 15 December 2000.

* To whom correspondence should be addressed. E-mail: ueharago@sci.u-ryukyu.ac.jp, or k988562@sci.u-ryukyu.ac.jp

Table 1

Echinometra *sp. A and* Echinometra *sp. C: summary of characters relevant to identification and reproductive isolation*

Character	*Echinometra* sp. A	*Echinometra* sp. C	Sources*
Habitat	Moat and tide pools	Burrows in reef margin	1, 2, 6
Bathymetric range	Intertidal, below mean low water	Intertidal, above mean low water	1, 2, 6
Salinity and thermotolerance	Lower tolerance to sudden temperature and salinity changes	Higher tolerance to sudden temperature and salinity changes	4, 5
Body size	Biggest among Okinawan *Echinometra*	Moderate among Okinawan *Echinometra*	3
Wet weight (g)	50.8 ± 12.8	39.2 ± 8.7	7
Test length (mm)	47.4 ± 4.6	43.3 ± 0.1	7
Spine length (mm)	22.5 ± 1.1	16.6 ± 0.9	7
Spine color	Entirely white to greenish, or brownish-black, with white tip; distinct basal white ring	Entirely green, brown, or greenish-brown, without white tip; basal translucent, white ring.	3
Tubefoot spicules	Bihamate (C-like)	Triradiate	3
Gonadal spicules	Spindle shaped	Triradiate, curved triradiate, and bihamate	3
Breeding season	April–December (max. around late September)	April–December (max. around late September)	4, 5
Egg diameter (μm)	66.9 ± 1.3	71.8 ± 1.4	7
Sperm head length (μm)	3.9 ± 0.6	6.4 ± 0.7	7
Jelly layer thickness (μm)	23.9 ± 3.2	18.1 ± 3.5	7

* Data sources: 1, Tsuchiya and Nishihira (1984); 2, Tsuchiya and Nishihira (1985); 3, Uehara and Shingaki (1985); 4, Arakaki (1989); 5, Arakaki and Uehara (1991); 6, Nishihira *et al.* (1991); 7, this study; measurements from 25 adult individuals of each species examined for each character, mean ± standard deviation.

because hybrids are not formed when their gametes are mixed (Uehara *et al.,* 1990; Metz *et al.*, 1994). On the other hand, two other species, Ec and Ed, readily form hybrids when their gametes are mixed, while all other combinations between the species show high asymmetries in fertilization (*i.e.*, ova of one species are readily fertilized by sperm of another species, but not *vice versa*) (Uehara *et al.*, 1990). Fertilization asymmetry also has been noted for the species of *Echinometra* in the Caribbean and eastern Pacific (Lessios and Cunningham, 1990). Although fertilization asymmetry indicates gamete incompatibility in one direction, there may be little or no gamete incompatibility in the other direction, allowing for ready hybridization. Because of such a possibility for hybridization, Lessios (1998) and McCartney *et al.* (2000) suggested that postzygotic mechanisms are important in maintaining the genetic integrity of these species in the field.

Sequence data of the cytochrome oxidase I gene indicates that the four species of *Echinometra* on Okinawa are of recent origin, considerably less than 3 million years old (Palumbi, 1996), and similar to the time of divergence between the Atlantic and eastern Pacific species of *Echinometra* (McCartney *et al.*, 2000). Moreover, allozyme evidence indicates that among the four species on Okinawa, Ea and Ec are the most closely related to each other, while Ea and Ed are the most divergent (Matsuoka and Hatanaka, 1991). Experimental hybridization and rearing experiments by Aslan and Uehara (1997) reported that Ed ova were readily fertilized by Ea sperm, but Ea ova were much less able to be fertilized by Ed sperm. Hybrids resulting from crosses in both directions developed normally into fertile adults, and Aslan and Uehara (1997) suggested that introgression between Ea and Ed was probably minimized by prezygotic mechanisms, particularly separation of their respective microhabitats. Rahman *et al.* (2000) also reported asymmetrical fertilization in Ea × Ec crosses, with Ec ova being more readily fertilized by Ea sperm than Ea ova were fertilized by Ec sperm. Moreover, they found that the viability and growth of Ec (ova) × Ea (sperm) hybrids was similar to that of conspecifics, while that of Ea (ova) × Ec (sperm) hybrids was significantly lower. We report here further details of hybrids between these two species. In spite of their close relationship, individuals of Ea and Ec can be readily distinguished from each other by differences in adult morphology, as well as microhabitat preference (Table 1). On the other hand, their breeding seasons overlap extensively (Arakaki and Uehara, 1991) and because of the proximity of their microhabitats (Nishihira *et al.*, 1991), they are likely to have opportunities to hybridize in the field.

Materials and Methods

Mature adults of Ea (identified by their brownish dark test and white-tipped spines), and Ec (greenish test, spines without white tips, but with white basal ring distinguishing it from Eb) (Uehara, 1990; Arakaki *et al.*, 1998) were collected from the Sunabe coast of Okinawa Island (26°07′ N; 127°46′ E) at low tide within their natural breeding season from early May to late October, 1996 and 1997. Specimens were immediately transported to the laboratory, where they were maintained in closed aquaria until spawned. Cross-fertilization of the two species of *Echinometra* was con-

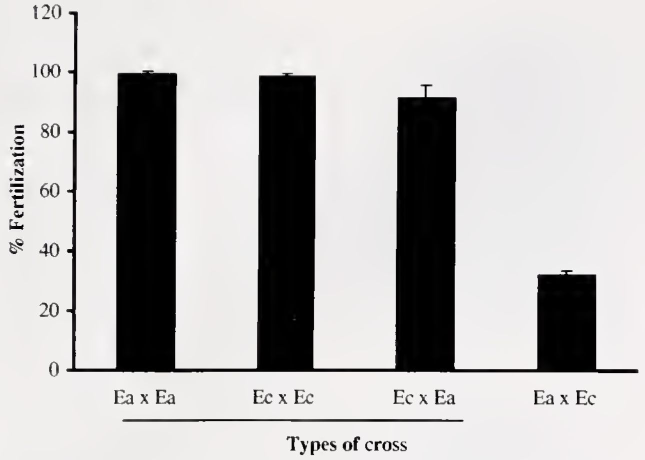

Figure 1. Mean percentage of eggs fertilized in conspecific and heterospecific crosses of *Echinometra* sp. A (Ea) and *Echinometra* sp. C (Ec); maternal species named first. Calculated from number of embryos in the 2- to 4-cell stage counted in 100 eggs 1.5 hours after gamete mixing. A total of 13 replicate crosses were done using gametes from new individuals each time; error bars indicate 1 standard deviation. Fertilization rate of Ea × Ec significantly different from those of Ea × Ea, Ec × Ec, and Ec × Ea (ANOVA, $P < 0.01$), as indicated by the horizontal bar. Data from Rahman *et al.* (2000).

ducted using all possible combinations of ova and sperm at room temperatures (26–28°C) (Rahman *et al.*, 2000). For consistency, when referring to heterospecific crosses, the maternal species is named first. As found earlier by Uehara *et al.* (1990), fertilization was high for the conspecific and Ec × Ea crosses, but significantly lower for the Ea × Ec crosses (Fig. 1). The juveniles produced from these crosses were used in the work reported here.

The embryos and larvae were reared through metamorphosis, as described by Rahman *et al.* (2000). Larval survival was 68%–73% for the conspecific and Ec × Ea crosses, and 50% for the Ea × Ec crosses. Larval body form and development of both conspecific controls and reciprocal hybrids were similar to each other, and no particular abnormalities were observed. After 20–24 days, larvae were placed in small (25 × 20 × 10 cm) aquaria with aerated, filtered seawater, and pieces of coralline algal skeletons were added to induce settlement and metamorphosis. Metamorphosis rate was high (84%–89%) and not significantly different for the conspecific and Ec × Ea larvae, and lower (67%) for the Ea × Ec hybrids (Rahman *et al.*, 2000). Seawater was partially changed once a week with fresh, filtered seawater, and coralline-algal-encrusted pieces of coral skeletons were provided as food. By 3 months, 65%–69% of the conspecific and Ec × Ea juveniles, and 57% of the Ec × Ea juveniles remained; they were all 6.0–7.0 mm in test diameter.

The cultures were continued for one year, by which time the animals were sexually mature; survival at one year was 78%–84% for the conspecifics and Ec × Ea hybrids, and 70% for the Ea × Ec hybrids (Rahman *et al.*, 2000). Then they were spawned, and their gametes were used for reciprocal back crosses to determine fertility among both hybrids and conspecifics. After the animals were spawned, data on animal weight, test dimensions, spine lengths, spicule characteristics, body and spine coloration, gamete sizes, and other specific characters of all the animals were recorded and compared among the treatments. The tests of echinoids in the family Echinometridae are oblong, so both length and width, as well as height, were measured. Spicule types in both the tube feet and gonads were counted in 10 replicate samples from 20 different individuals of each cross (80 animals; 800 counts). Gametes were measured using a phase contrast microscope following Amy (1983) (eggs at 400× in a slide well; sperm at 1000× on a flat slide).

Percentages were arcsine transformed to normalize the data and reduce heterogeneity in variances. Homogeneity of variances was analyzed by a Bartlett test (Bartlett, 1937); when variances were not significantly heterogeneous and showed no major departure from normality, a one-way analysis of variance (ANOVA) was done, followed by Duncan's multiple range test (Duncan, 1955). The level for statistical significance was set at 0.05. Untransformed values are presented in the tables and figures.

To examine the occurrence of hybridization between Ea and Ec in the field, searches for specimens with hybrid morphology were conducted along the Sunabe coast of Okinawa and the coast of Sesoko Island, where both species occur close together (within 1–2 m) in adjacent, interdigitating microhabitats.

Results

Comparisons of laboratory-reared adult Echinometra *sp. A,* Echinometra *sp. C, and their reciprocal hybrids*

Test length of animals 1 year after metamorphosis (Table 2) was less than for field-collected animals (Table 1), which were probably several years old. On the other hand, spine lengths of the experimental animals were greater than those of the field-collected animals, which live in rock depressions under turbulent conditions and experience considerable spine-tip abrasion.

Mean values for wet weight, test length, width, height, and spine length were greatest in Ea × Ea progeny and smallest in Ec × Ec progeny (Table 2). All these parameters were significantly different between Ea × Ea and Ec × Ec, and between each of these and the hybrids. On the other hand, there were no significant differences ($P > 0.05$) between Ea × Ec and Ec × Ea. Measurements in both of the reciprocal hybrids were closer to those of Ea × Ea than to Ec × Ec. These measurements mirror the different growth rates found for these animals by Rahman *et al.* (2000).

The aboral body coloration differed between conspecifics and hybrids (Fig. 2, upper). In Ea × Ea specimens, test

Table 2

Weight, test size, and spine length comparison of Echinometra *sp. A (Ea × Ea),* Echinometra *sp. C (Ec × Ec), and their reciprocal hybrids 1 year after metamorphosis*

Character	Ea × Ea	Ea × Ec	Ec × Ea	Ec × Ec
Wet weight (gm)	14.7 ± 0.7^{a} (14.6–14.8)	13.6 ± 0.2^{b} (13.6–13.7)	13.9 ± 0.5^{b} (13.8–14.0)	9.2 ± 0.5^{c} (9.1–9.3)
Test length (mm)	29.4 ± 0.8^{a}* (28.2–31.0)	28.4 ± 0.9^{b} (27.0–30.0)	28.7 ± 0.8^{b} (27.5–30.5)	24.2 ± 1.1^{c} (23.0–26.0)
Test width (mm)	27.3 ± 0.8^{a} (26.1–29.0)	26.3 ± 0.9^{b} (25.0–28.1)	26.5 ± 0.8^{b} (25.3–28.5)	22.2 ± 1.0^{c} (21.0–23.9)
Test height (mm)	14.2 ± 0.4^{a} (13.6–15.0)	13.5 ± 0.4^{b} (12.8–13.9)	13.6 ± 0.3^{b} (13.1–14.2)	12.0 ± 0.5^{c} (11.2–13.0)
Spine length (mm)	26.8 ± 1.0^{a} (24.4–28.2)	23.4 ± 0.7^{b} (22.3–24.9)	24.3 ± 0.6^{b} (23.4–25.5)	20.7 ± 0.7^{c} (19.3–21.9)

* Thirty adult specimens were measured for each treatment; mean ± SD, ranges in parentheses. Wet weight data from Rahman *et al.* (2000). Numbers in the same row having the same superscripts are not significantly different ($P > 0.05$).

color was dark brownish, and each spine had a white tip and a translucent white ring at its base. Ec × Ec specimens were uniformly greenish, and each spine was uniformly colored except for a faded basal white ring. Ea × Ec hybrids were more similar to Ea × Ea conspecifics, having dark brownish tests and white-tipped spines with a translucent white, basal ring. On the other hand, Ec × Ea hybrids were more similar to Ec × Ec conspecifics; the tests were uniformly deep greenish, and the spines had barely detectable white tips and basal white rings.

Orally (Fig. 2, lower), Ea × Ea conspecifics had white-tipped spines around the mouth and brownish dark tests, whereas Ec × Ec conspecifics had yellowish green spines around the mouth and a greenish test color. Ea × Ec hybrids were more similar to Ea × Ea, whereas Ec × Ea hybrids were more similar to Ec × Ec; that is, hybrid coloration was most similar to maternal coloration.

Tubefoot spicules in Ea × Ea were always bihamate (C-shaped), whereas those in Ec × Ec were always triradiate (Fig. 3). Tubefoot spicules of Ea × Ec hybrids were bihamate (58%), bihamate-like (17%), triradiate-bihamate (20%), and triradiate (5%), whereas those of Ec × Ea were bihamate (32%), bihamate-like (12%), triradiate-bihamate (44%), and triradiate (13%). Therefore, the tubefoot spicule morphologies of the hybrids were intermediate and tended toward maternal affinities.

There was little intraspecific variation in gonadal spicule morphology (Fig. 4). The spicules in Ea gonads were almost all spindle-shaped (98%; other spicules seen: bihamate, <1%; irregular, 1%; no triradiates were found). In contrast, those in Ec gonads were nearly all triradiate (94%; other spicules seen: spindle, 5%; bihamate, 1%). Gonads in both Ea × Ec and Ec × Ea had high proportions of spindle-shaped spicules (62% and 46%, respectively), with spindle-like (16% and 11%), triradiate-spindle (13% and 25%), triradiate (7% and 15%), bihamate (1% in both), and irregular (1% in both) spicules in smaller proportions.

Gamete sizes of conspecific and hybrid individuals were different. Egg diameters of Ea × Ea were smallest among the four treatments, whereas the Ec × Ec eggs were largest (Table 3). Hybrids contained intermediate-sized eggs that were significantly different from the eggs of either of the conspecifics. The sizes of sperm heads were also smallest in Ea × Ea, and were significantly different among all the crosses, including between the hybrids.

Existence of natural hybrids

The characteristics of reproductively mature hybrids are summarized in Table 4. Two hundred individuals with coloration more-or-less intermediate between the two species were collected from the field. However, detailed comparisons of spicule shapes and gamete sizes revealed that none actually had character combinations common to the experimentally obtained hybrids; that is, all could be assigned to either Ea or Ec on the basis of both spicule shapes and gamete sizes.

Similarly, Aslan and Uehara (1997) did not find any natural hybrids between Ea and Ed in the field, even though they were able to rear hybrids of these species in the laboratory.

Backcrosses

There was no indication that the hybrids were any less fertile than either of their conspecific half-siblings (Table 5). Eggs from both Ea × Ec and Ec × Ea yielded higher percentages of fertilization with Ea × Ea sperm (93% and 98%), than with Ec × Ec sperm (82.2% and 89.2%), similar to the findings with the parental crosses in which Ea sperm more readily fertilized Ec eggs than Ec sperm fertilized Ea eggs (Fig. 1). Moreover, backcrosses by sperm from males of Ea × Ec and Ec × Ea yielded higher percentages of fertilization with Ec × Ec ova (99.3% and 99.7%) than with Ea × Ea ova (84% and 86.5%); Ea ova appear to be more discriminating than Ec ova. The higher fertilization rates between the same types of hybrids *versus* the different types of hybrids (99.5% and 99% *versus* 95% and 86%) indicate the presence of a complex sorting of gamete compatibility genes.

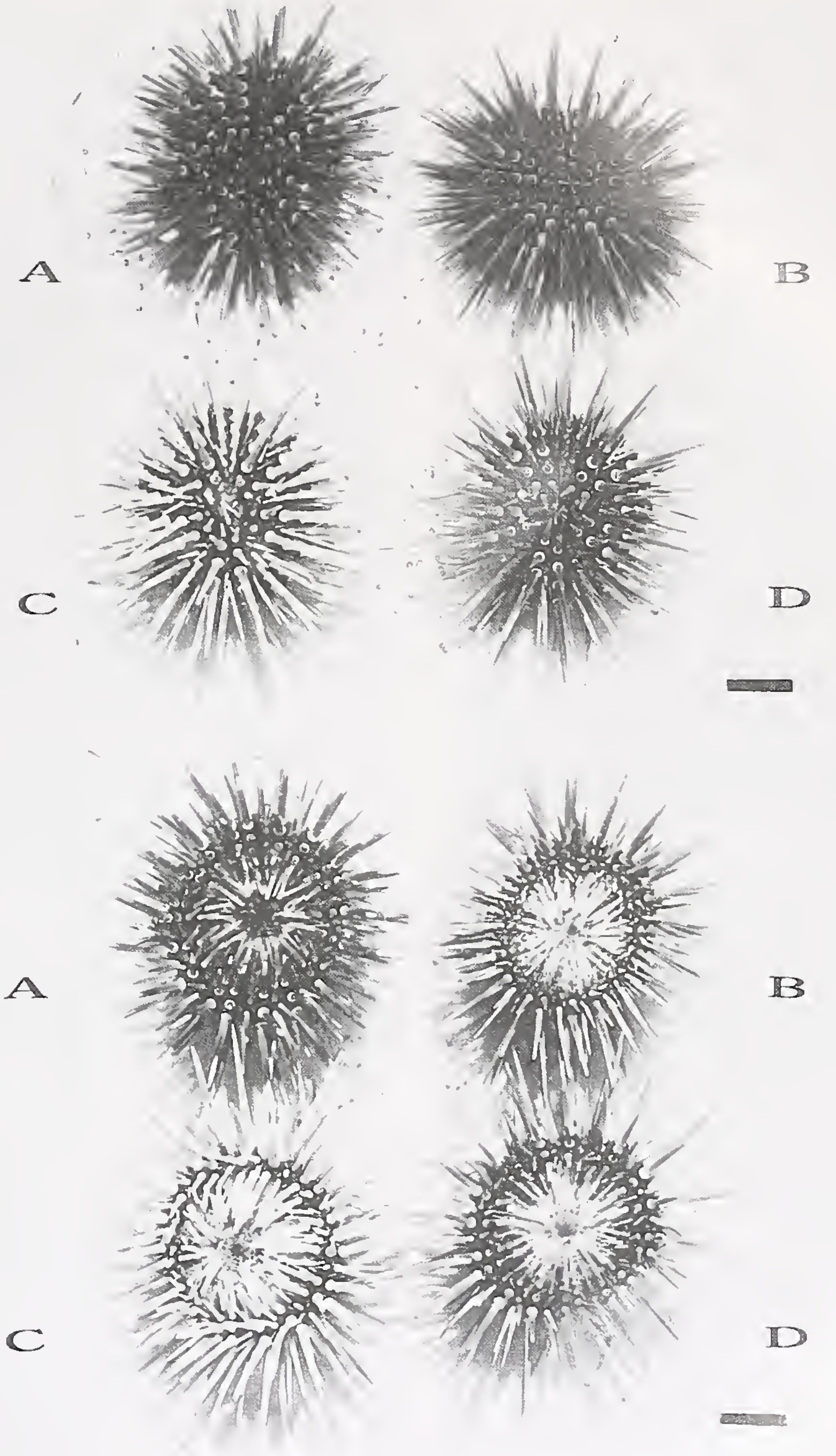

Figure 2. Aboral (upper) and oral (lower) color patterns of *Echinometra* sp. A and *E.* sp. C, and their reciprocal hybrids, 1 year after metamorphosis; maternal species named first. (A) Ea × Ea; (B) Ec × Ec; (C) Ea × Ec; (D) Ec × Ea.

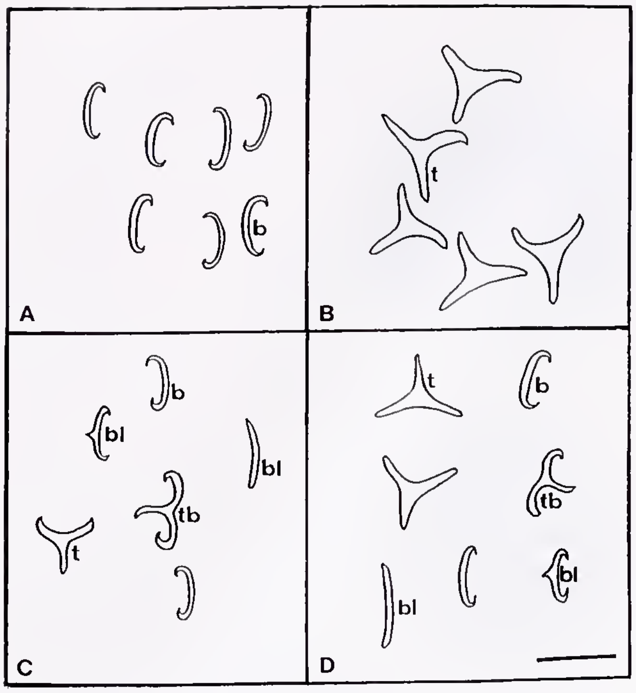

Figure 3. Morphology of tubefoot spicules of *Echinometra* sp. A and *Echinometra* sp. C and their reciprocal hybrids, 1 year after metamorphosis; maternal species named first. (A) Ea × Ea; (B) Ec × Ec; (C) Ea × Ec; (D) Ec × Ea. b, bihamate; bl, bihamate-like; t, triradiate; tb, triradiate-bihamate. Scale bar, 50 μm.

Discussion

The crosses between Ea-Ec showed a distinct asymmetry in fertilization success, as reported previously by Uehara *et al.* (1990) and Rahman *et al.* (2000). Heterogamic fertilization rate was high when eggs of Ec were mixed with sperm of Ea, but much lower when eggs of Ea were mixed with sperm of Ec. The reduction in fertilization with the Ea egg × Ec sperm crosses indicates the presence of a protein-binding system for gamete recognition, as reported by Metz *et al.* (1994), and Metz and Palumbi (1996). Such a system might eventually lead to gamete incompatibility and reproductive isolation, and thus provide a mechanism for maintaining species integrity, as proposed by Metz *et al.* (1994), Vacquier *et al.* (1995), Metz and Palumbi (1996), and Palumbi (1998). However, with the high fertilization of Ec eggs by Ea sperm, prezygotic isolation by gamete incompatibility hardly appears to be present between these two species, or among most of the other species of *Echinometra* on Okinawa, most of which, like the two sympatric species of Caribbean *Echinometra,* also show high asymmetry in fertilization among hybrid crosses (Uehara *et al.,* 1990; Lessios and Cunningham, 1990). Consequently, it seems unlikely that gamete incompatibility, by itself, provides a mechanism for reproductive isolation in *Echinometra.* Reproductive isolation and speciation apparently occurred before gametic incompatibility closed off the possibility of gene flow, and as in two sympatic species of asteroids in the genus *Patiriella* that do not have gamete incompatibility (Byrne and Anderson, 1994), other mechanisms need to be found to explain how species integrity is maintained in these closely related, interfertile species.

Furthermore, the Ea-Ec crosses had higher fertilization rates in the F_1 backcrosses than Aslan and Uehara (1997) found for Ea-Ed F_1 backcrosses. The higher fertilization rate may be due to the higher genetic similarity between Ea and Ec than between Ea and Ed, as proposed by Matsuoka and Hatanaka (1991). If this is true, it provides evidence for the eventual evolution of complete gamete incompatibility in these species. Supporting the idea of a transition of gamete compatibility to incompatibility after speciation, Uehara *et al.* (1990) reported that fertilization between Ec and Ed was high in both directions, while crosses between Ea and Eb were completely infertile; other combinations among the four species were asymmetrical. Whether these differences reflect evolutionary distances among the species, or indicate that other factors—such as some sort of reinforcement selection coupled to microhabitat proximity—are involved, or

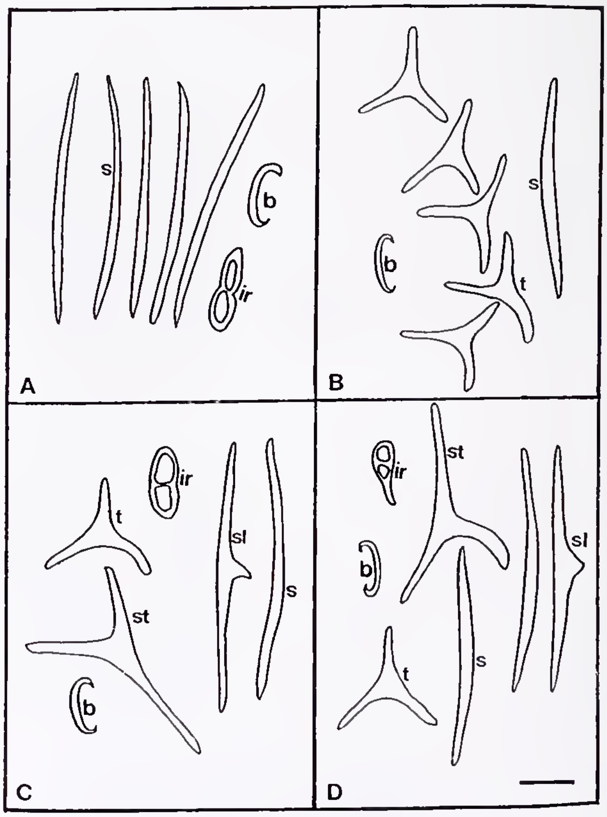

Figure 4. Morphology of gonadal spicules of *Echinometra* sp. A and *Echinometra* sp. C and their reciprocal hybrids, 1 year after metamorphosis; maternal species named first. (A) Ea × Ea; (B) Ec × Ec; (C) Ea × Ec; (D) Ec × Ea. b, bihamate, ir, irregular, s, spindle; sl, spindle-like; st, spindle-triradiate; t, triradiate. Scale bar, 100 μm.

Table 3

Gamete sizes of Echinometra *sp. A (Ea × Ea),* Echinometra *sp. C (Ec × Ec), and their reciprocal hybrids 1 year after metamorphosis*

Measurement	Ea × Ea	Ea × Ec	Ec × Ea	Ec × Ec
Egg diameter	66.9 ± 1.0^{a}* (65.0–67.5)	71.0 ± 1.2^{b} (70.0–73.8)	70.2 ± 1.1^{b} (67.5–72.5)	72.6 ± 1.3^{c} (71.3–75.0)
Sperm head length	4.1 ± 0.5^{a} (3.1–5.0)	5.7 ± 0.7^{b} (4.3–6.8)	5.2 ± 0.8^{c} (4.3–6.8)	6.5 ± 0.8^{d} (5.0–7.4)

* Twenty individuals were examined from each cross with 25 eggs and 25 sperm from each individual; mean ± SD in μm, ranges in parentheses. Figures in the same row having the same superscripts are not significantly different ($P < 0.05$).

suggest that gametic incompatibility in one or the other species "simply happened by accident" (Lessios and Cunningham, 1990, p. 938) remains to be determined.

The successful culturing of hybrids to fertile adults in laboratory conditions suggests that postzygotic isolating mechanisms, such as hybrid inviability or sterility, are not involved in maintaining species integrity. However, Rahman *et al.* (2000) found that Ea × Ec hybrids had lower larval survival, metamorphosis success, and juvenile survival than either Ec × Ea hybrids or conspecific half-siblings. Consequently, not only gamete incompatibility but postzygotic fitness parameters act against Ea × Ec hybrids. Nevertheless, the surviving Ea × Ec hybrids grow at the same rate as conspecifics (Rahman *et al.*, 2000), and as shown in the present study, are as fertile as the conspecifics in backcrosses. Moreover, Ec × Ea hybrids are as viable and fertile as the conspecifics, indicating that there are neither gametic nor postzygotic blocks to introgression for at least half of the possible hybrid events.

Table 4

Characterization of hybrids produced experimentally through cross fertilization between Echinometra *sp. A (Ea) and* Echinometra *sp. C (Ec)*

Distinctive features	Ea × Ec	Ec × Ea
Body color		
a. Oral	Ea-like	Ec-like
b. Aboral	Ea-like	Ec-like
Test sizes		
a. Length	Intermediate	Intermediate or Ea-like
b. Width	Intermediate	Intermediate or Ea-like
c. Height	Intermediate	Intermediate or Ea-like
Spines		
a. Length	Intermediate	Intermediate or Ea-like
b. Color	Ea-like with white tip or intermediate	Ec-like or intermediate with faint white spine tip
c. Milled ring color	Ea-like	Ea-like
Spicules		
a. Tubefoot	Intermediate and Ea-like	Intermediate and Ec-like
b. Gonad	Intermediate and Ea-like	Intermediate and Ea-like
Gametes		
a. Sperm sizes/form	Intermediate	Intermediate
b. Egg sizes	Intermediate	Intermediate

Besides gamete incompatibility, potential prezygotic mechanisms that may occur between these two species include ecological separation and asynchronous reproductive cycles (Mayr, 1970; Palumbi, 1994). The two species of sea urchins in this study, Ea and Ec, live relatively close to each other but occupy different microhabitats; Ea inhabits the calmer moat and tidepools of the reef-flat, generally below the mean low water level, whereas Ec inhabits burrows or crevices in the wave-swept intertidal of the reef margin (Table 1). These differences in microhabitats may be enough to prevent most chances of cross fertilization. In broadcast spawning invertebrates such as echinoids, for example, fertilization success drops dramatically with distance between spawning individuals (Pennington, 1985; Levitan, 1998a, b). However, individuals of Ea are occasionally found near and within the reef margin where Ec predominates, and it remains unclear, whether microhabitat separation, by itself, is sufficient to prevent introgression between the two species, or at least through Ec ova and Ea sperm where there is little or no gamete incompatibility, hybrid viability, or hybrid fertility.

In addition to the problem of being separated enough in adjacent microhabitat to prevent gamete mixing after spawning, there is the problem of maintaining microhabitat differentiation that could assure reproductive isolation. This problem is especially acute for species with long-lived, widely dispersing larvae, such as species of *Echinometra*. The different larvae would have to have exquisite settling cues that assured that they would be established in their exact microhabitats or suffer highly selective postsettlement mortality outside their particular microhabitats. There is little evidence of highly selective habitat selection in sea urchin larvae (Pearse and Cameron, 1991). Indeed, Rahman and Uehara (2001) found no discrimination in settling preferences by competent larvae of the four species of *Echinometra* on Okinawa; all showed settlement rates of 86%–89% on coralline red algae, and much lower rates on other algae. The mechanism resulting in and maintaining microhabitat differentiation among broadcast spawning species such as those of *Echinometra* in the tropical west Pacific remain unknown and unexplored.

Echinoid sperm are active for only a short time after spawning, much less than an hour in temperate species

Table 5

Percentage of eggs fertilized in backcrosses among laboratory-reared F_1 generation of conspecifics and hybrids of Echinometra *sp. A (Ea) and* Echinometra *sp. C (Ec)*

	Eggs from			
Sperm from	Ea × Ea	Ea × Ec	Ec × Ea	Ec × Ec
Ea × Ea	99.7 ± 0.5 (99–100)	93.0 ± 1.4 (91–95)	98.0 ± 1.4 (96–100)	86.8 ± 1.7 (84–88)
Ea × Ec	84.0 ± 1.6 (82–86)	99.0 ± 0.9 (98–100)	95.0 ± 1.4 (93–97)	99.3 ± 0.8 (98–100)
Ec × Ea	86.5 ± 1.9 (84–88)	86.0 ± 1.8 (83–88)	99.5 ± 0.8 (98–100)	99.7 ± 0.5 (99–100)
Ec × Ec	30.7 ± 2.0 (28–33)	82.2 ± 1.8 (80–84)	89.2 ± 2.1 (87–93)	99.8 ± 0.4 (99–100)

Each value represents six replicate crosses with gametes from different individuals in each replicate; mean ± SD, ranges in parentheses.

(Hinegardner, 1975; Levitan *et al.*, 1991), and probably even less in tropical species. Asynchrony in spawning, therefore, would ensure that these two species could exist in sympatry as separate species whether or not their gametes are capable of fertilization (Lessios, 1984). However, Ea and Ec mature at the same time and their spawning periods overlap extensively (Arakaki and Uehara, 1991; Table 1). Consequently, seasonal separation of spawning is not a mechanism of reproductive isolation. On the other hand, gametes may be released at different times of the day or specific pheromonal spawning cues may differ between the species, and these factors may prevent near simultaneous spawning that could lead to hybridization. Natural spawning in the field has not yet been observed.

The sperm concentration used in this study was probably much higher than would be encountered under usual natural conditions, especially considering the dilution that would occur if individuals were separated by 1 m or more (Pennington, 1985; Levitan, 1998b). However, Uehara *et al.* (1990) provide data showing that fertilization rates of eggs of both Ea and Ec mixed with sperm from Ea were similar over a wide range of sperm concentrations, whereas the sperm of Ec had very low fertilization success with Ea eggs, even at high concentrations, up to 10^{-2}. Consequently, it is equivocal whether inappropriate sperm concentrations were used in this study, and Ea sperm, at least, appear as likely to fertilize Ec eggs as Ea eggs over concentrations found in the field.

In addition, the eggs in this study were exposed to sperm at relatively high concentrations for 1.5 h, much longer than they would likely be so exposed in the field. Levitan *et al.* (1991) found that fertilization increases in sea urchins with time of exposure of eggs to sperm over a range of 10–60 s. It is possible, therefore, that fertilization rates would be lower in the Ec × Ea crosses if the gametes had been kept together for shorter times. Preliminary experiments indicate that fertilization reaches the asymptote in less than 2 min in conspecific crosses of Ea and Ec, within 4 min in Ec × Ea crosses, and by about 6 min in Ea × Ec crosses (Rahman, unpubl. data). Therefore, more extended exposure times, like those used in the study, would not increase the fertilization rates. However, if gametes are spawned in the field at the same time by equal numbers of adjacent individuals of both sexes of both species, most conspecific gametes would probably be fertilized before much hybridization could occur. On the other hand, where the populations intermingle it seems as likely that a spawning Ec female could be closer to a spawning Ea male than to spawning Ec males, so that hybrids could be expected to occur.

To date there have been no experiments with mixed populations of gametes. Palumbi (1998) showed that at low concentrations where less than near 100% fertilization is achieved, sperm from different males of the same species of sea urchins fertilized different proportions of eggs from the same female, and eggs from different females were fertilized in different proportions by sperm from the same male. These differences were further related to differences in the sequence of the bindin alleles. This opens the possibility of some sort of interlocus antagonistic coevolution between gametes, as was proposed by Rice (1998) and which was demonstrated to be occurring in multiple-mating, internally fertilizing species such as crickets (Howard *et al.*, 1998). How such sperm competition could be achieved in broadcast spawning, externally fertilizing species such as sea urchins, if it occurs at all, remains to be determined. However, if it does occur, and if conspecific sperm are always at an advantage when mixed at low concentrations with sperm from another species because of more compatible gametes, a mechanism for maintaining species integrity in sympatric species may be present.

Some characteristics of the hybrid progeny found in the present study were mainly maternal. Color patterns of both hybrids, for instance, tended to be maternally inherited. Maternal inheritance of color pattern also was observed in hybrids between *Strongylocentrotus nudus* and *S. intermedius* (Osanai 1974). On the other hand, other characteristics, such as spine length and spicule shapes, especially those from the gonads, showed intermediate features, and can be used to distinguish the hybrids from either parent. Such distinct hybrid phenotypes are important for finding hybrids in the field (*e.g.*, Hagström and Lønning, 1961; Menge, 1986; Palumbi and Metz, 1991; Lessios and Pearse, 1996). We searched for distinctive intermediate phenotypes in the field, and although suggestive color morphs were found, examination of the spicules revealed no hybrids. Similarly, although hybrids with distinguishing characteristics can be formed in the laboratory between Ea and Ed, Aslan and Uehara (1997) were unable to find such hybrids in the field. Moreover, although two species of the tropical long-spined sea urchins, *Diadama savignyi* and *D. setosum*, readily hybridize in the laboratory (Uehara *et al.*, 1990) and often occur in mixed populations in the field (Pearse, 1998), genetic analyses, using allozyme analyses, showed that hybrids only occur rarely in the field and there is limited introgression (Lessios and Pearse, 1996). Genetic analyses using allozyme or DNA markers should now be done with sympatric species of *Echinometra* to determine whether some introgression is occurring that has not been detectable by morphological characters.

The adult hybrids of these two species were completely fertile, indicating that genetic differences between them are not large enough to cause developmental or gamete incompatibility, in spite of their morphological differences and microhabitat segregation. The high fertilization rates in backcrossing further suggests that they are genetically very close to each other. Similar results were obtained from crosses that produced fertile hybrids between Ea and the putatively more distantly related Ed (Aslan and Uehara, 1997). There is no reason to believe that fertile hybrids could not be produced in crosses between most other species of *Echinometra* on Okinawa, including between Ec and Ed, which show high fertilization with each other in both directions (Uehara *et al.*, 1990). Only Ea and Eb (=*Echinometra mathaei*) showed very low fertilization with each other in either direction, and may be isolated by gamete incompatibility (Uehara *et al.*, 1990; Metz *et al.*, 1994). These latter two species co-occur in pools and channels below mean low water on the reef flats of Okinawa, and they may have the greatest opportunity for gamete mixing in the field. Consequently, for these two species, gamete incompatibility may be necessary to maintain species integrity. Reproductive isolation of the other species, however, probably depends on additional prezygotic isolating mechanisms, such as microhabitat separation.

New biological species are formed when populations become reproductively isolated from other, previously conspecific populations. How and when reproductive isolation develops has yet to be established for broadcast spawning marine invertebrates such as sea urchins (Lessios, 1984; Knowlton, 1993; Palumbi, 1994). Although not isolated by full gamete incompatibility, or by hybrid inviability or infertility, Ea and Ec are both morphologically and genetically distinct, and hybridization between them appears to be either very low or nonexistent—that is, they appear to be effectively reproductively isolated. The morphological distinctness and apparent genetic integrity maintained between them warrants their recognition as distinct biological species despite their ability to produce viable and fertile hybrids in the laboratory. They should be given taxonomic descriptions and appropriate species names that are distinct from *Echinometra mathaei, sensu stricto* (=Eb; Arakaki *et al.*, 1998) and Ed (=the Okinawan component of the *Echinometra oblonga* species complex; Arakaki and Uehara, 1999).

Acknowledgments

We are greatly indebted to L. M. Aslan, H. A. Lessios, H. Ota, and two anonymous reviewers for their critical and valuable suggestions on this manuscript. We also extend our appreciation and grateful thanks to the Director and staff of the Sesoko Station of the Tropical Biosphere Research Center, University of the Ryukyus, who provided space and facilities for culturing sea urchins; and to Motobu Fisheries Research Center for providing samples of *Chaetoceros gracilis* and instructions for culturing it. The first author is also grateful to the Rotary Yoneyama Memorial Foundation, Japan, for scholarship grants, and especially to Dr. Tomio Iha, Naha Rotary Club, Okinawa, for his continuous cooperation and encouragement during the period of the grants.

Literature Cited

Amy, R. L. 1983. Gamete sizes and developmental time tables of five tropical sea urchins. *Bull. Mar. Sci.* **33:** 173–176.

Arakaki, Y. 1989. A comparative ecological and reproductive study on the four types of sea urchin *Echinometra mathaei* (Blainville) on Okinawan reef flats. Master's thesis, University of the Ryukyus, Japan.

Arakaki, Y., and T. Uehara. 1991. Physiological adaptation and reproduction of the four types of *Echinometra mathaei* (Blainville). Pp. 105–111 in *Biology of Echinodermata*, T. Yanagisawa, I. Yasumasu, C. Oguro, N. Suzuki, and T. Motokawa, eds. A. A. Balkema, Rotterdam.

Arakaki, Y., and T. Uehara. 1999. Morphological comparison of black *Echinometra* individuals among those in the Indo-west Pacific. *Zool. Sci. Japan* **16:** 551–558.

Arakaki, Y., T. Uehara, and I. Fagoone. 1998. Comparative studies of the genus *Echinometra* from Okinawa and Mauritius. *Zool. Sci. (Tokyo)* **15:** 159–168.

Aslan, L. M., and T. Uehara. 1997. Hybridization and F_1 backcrosses between two closely related tropical species of sea urchins (genus *Echinometra*) in Okinawa. *Invertebr. Reprod. Dev.* **31:** 319–324.

Bartlett, M. S. 1937. Some examples of statistical methods of research in agriculture and applied biology. *J. Roy. Stat. Soc., Suppl.* **4:** 137–170.

Byrne, M., and M. J. Anderson. 1994. Hybridization of sympatric *Patiriella* species (Echinodermata: Asteroidea) in New South Wales. *Evolution* **48:** 564–576.

Chen, P. S., and F. Baltzer. 1975. Morphology and biochemistry of diploid and androgenetic haploid (merogonic hybrids). Pp. 424–445 in *The Sea Urchin Embryo—Biochemistry and Morphogenesis*, G. Czihak, ed. Springer-Verlag, Berlin.

Coyne, J. A. 1992. Genetics and speciation. *Nature* **355:** 511–515.

Dobzhansky, T., F. J. Ayala, G. L. Stebbins, and J. W. Valentine. 1977. *Evolution*. W. H. Freeman, San Francisco.

Duncan, D. B. 1955. Multiple range and multiple F-tests. *Biometrics* **11:** 1–42.

Hagström, B. E., and S. Lønning. 1961. Morphological and experimental studies on the genus *Echinus. Sarsia* **4:** 21–31.

Hinegardner, R. 1975. Care and handling of sea urchin eggs, embryos, and adults (principally North American species). Pp. 10–25 in *The Sea Urchin Embryo—Biochemistry and Morphogenesis,* G. Czihak, ed. Springer-Verlag, Berlin.

Howard, D. J., M. Reece, P. G. Gregory, V. Chu, and M. L. Cain. 1998. The evolution of barriers to fertilization between closely related organisms. Pp. 279–288 in *Endless Forms: Species and Speciation,* D. J. Howard and S. H. Berlocher, eds. Oxford University Press, New York.

Knowlton, N. 1993. Sibling species in the sea. *Annu. Rev. Ecol. Syst.* **24:** 189–216.

Lessios, H. A. 1984. Possible prezygotic reproductive isolation in sea urchins separated by the Isthmus of Panama. *Evolution* **38:** 1144–1148.

Lessios, H. A. 1998. The first stage of speciation as seen in organisms separated by the Isthmus of Panama. Pp. 186–201 in *Endless Forms: Species and Speciation,* D. J. Howard and S. H. Berlocher, eds. Oxford University Press, New York.

Lessios, H. A., and C. W. Cunningham. 1990. Gametic incompatibility between species of the sea urchin genus *Echinometra* on the two sides of the Isthmus of Panama. *Evolution* **44:** 933–941.

Lessios, H. A., and J. S. Pearse. 1996. Hybridization and introgression between Indo-Pacific species of *Diadema. Mar. Biol.* **126:** 715–723.

Levitan, D. 1998a. Does Bateman's principle apply to broadcast-spawning organisms? Egg traits influence *in situ* fertilization rates among congeneric sea urchins. *Evolution* **52:** 1043–1056.

Levitan, D. R. 1998b. Sperm limitation, gamete competition, and sexual selection in external fertilizers. Pp. 175–217 in *Sperm Competition and Sexual Selection,* T. R. Birkhead and A. P. Møller, eds. Academic Press, San Diego, CA.

Levitan, D. R., M. A. Sewell, and F.-S. Chia. 1991. Kinetics of fertilization in the sea urchin *Strongylocentrotus franciscanus:* interaction of gamete dilution, age, and contact time. *Biol. Bull.* **181:** 371–378.

Matsuoka, N., and T. Hatanaka. 1991. Molecular evidence for the existence of four sibling species within the sea urchin, *Echinometra mathaei* in Japanese waters and their evolutionary relationships. *Zool. Sci. (Tokyo)* **8:** 121–133.

Mayr, E. 1970. *Populations, Species, and Evolution.* Harvard University Press, Cambridge, MA.

McCartney, M. A., G. Keller, and H. A. Lessios. 2000. Dispersal barriers in tropical oceans and speciation in Atlantic and eastern Pacific sea urchins of the genus *Echinometra. Mol. Ecol.* **9:** 1391–1400.

Menge, B. A. 1986. A preliminary study of the reproductive ecology of the sea stars *Asterias vulgaris* and *A. forbesi* in New England. *Bull. Mar. Sci.* **39:** 467–476.

Metz, E. C., and S. R. Palumbi. 1996. Positive selection and sequence rearrangements generate extensive polymorphism in the gamete recognition protein binding. *Mol. Biol. Evol.* **13:** 397–406.

Metz, E. C., R. E. Kane, H. Yanagimachi, and S. R. Palumbi. 1994. Fertilization between closely related sea urchins is blocked by incompatibilities during sperm-egg attachment and early stages of fusion. *Biol. Bull.* **187:** 23–34

Nishihira, M., Y. Sato, Y. Arakaki, and M. Tsuchiya. 1991. Ecological distribution and habitat preference of four types of *Echinometra mathaei* on Okinawan coral reef. Pp. 91–104 in *Biology of Echinodermata,* T. Yanagisawa, I. Yasumasu, C. Oguro, N. Suzuki, and T. Motokawa, eds. A. A. Balkema, Rotterdam.

Osanai, K. 1974. Interspecific hybridization of sea urchins, *Strongylocentrotus nudus* and *Strongylocentrotus intermedius. Bull. Mar. Biol. Stn. Asamushi* **15:** 37–45.

Palumbi, S. R. 1994. Genetic divergence, reproductive isolation, and marine speciation. *Annu. Rev. Ecol. Syst.* **25:** 547–572.

Palumbi, S. R. 1996. What can molecular genetics contribute to marine biogeography? An urchin's tale. *J. Exp. Mar. Biol. Ecol.* **203:** 75–92.

Palumbi, S. R. 1998. Species formation and the evolution of gamete recognition loci. Pp. 271–278 in *Endless Forms: Species and Speciation,* D. J. Howard and S. H. Berlocher, eds. Oxford University Press, New York.

Palumbi, S. R., and E. C. Metz. 1991. Strong reproductive isolation between closely related tropical sea urchins (genus *Echinometra*). *Mol. Biol. Evol.* **8:** 227–239.

Palumbi, S. R., G. Grabowsky, T. Duda, L. Geyer, and N. Tachino. 1997. Speciation and population genetic structure in tropical Pacific sea urchins. *Evolution* **51:** 1506–1517.

Pearse, J. S. 1998. Distribution of *Diadema savignyi* and *D. setosum* in the tropical Pacific. Pp. 777–782 in *Echinoderms: San Francisco,* R. Mooi and M. Telford, eds. A. A. Balkema, Rotterdam.

Pearse, J. S., and R. A. Cameron. 1991. Echinodermata: Echinoidea. Pp. 513–662 in *Reproduction of Marine Invertebrates, Vol. VI, Echinoderms and Lophophorates,* A. C. Giese, J. S. Pearse, and V. B. Pearse, eds. Boxwood Press, Pacific Grove, CA.

Pennington, J. T. 1985. The ecology of fertilization of echinoid eggs: the consequences of sperm dilution, adult aggregation, and synchronous spawning. *Biol. Bull.* **169:** 417–430.

Rahman, M. A., and T. Uehara. 2001. Induction of metamorphosis and substratum preference in four sympatric and closely related species of sea urchins (Genus *Echinometra*) in Okinawa. *Zool. Stud.* **40:** 29–43.

Rahman, M. A., T. Uehara, and L. M. Aslan. 2000. Comparative viability and growth of hybrids between two sympatric species of sea urchins (genus *Echinometra*) in Okinawa. *Aquaculture* **183:** 45–56.

Rice, W. R. 1998. Intergenomic conflict, interlocus antagonistic coevolution, and the evolution of reproductive isolation. Pp. 261–270 in *Endless Forms: Species and Speciation,* D. J. Howard and S. H. Berlocher, eds. Oxford University Press, New York.

Tsuchiya, M., and M. Nishihira. 1984. Ecological distribution of two types of sea-urchin, *Echinometra mathaei* (Blainville). *Galaxea* **3:** 131–143.

Tsuchiya, M., and M. Nishihira. 1985. Agonistic behavior and its effect on the distribution pattern in two types of the sea urchin *Echinometra mathaei* (Blainville). *Galaxea* **4:** 37–48.

Uehara, T. 1990. Speciation in *Echinometra mathaei. Iden* **44:** 47–53 (in Japanese).

Uehara, T., and M. Shingaki. 1985. Taxonomic studies in the four types of sea urchin, *Echinometra mathaei* from Okinawa. *Zool. Sci. (Tokyo)* **2:** 1109.

Uehara, T., H. Asakura, and Y. Arakaki. 1990. Fertilization blockage and hybridization among species of sea urchins. Pp. 305–310 in *Advances in Invertebrate Reproduction,* M. Hoshi and O. Yamashita, eds. Elsevier, Amsterdam.

Uehara, T., M. Shingaki, K. Taira, Y. Arakaki, and H. Nakatomi. 1991. Chromosome studies in eleven Okinawan species of sea urchins, with special reference to four species of the Indo-Pacific *Echinometra.* Pp. 119–129 in *Biology of Echinodermata,* T. Yanagisawa, I. Yasumasu, C. Oguro, N. Suzuki, and T. Motokawa, eds., A. A. Balkema, Rotterdam.

Vacquier, V. D., W. J. Swanson, and M. E. Hellberg. 1995. What have we learned about sea urchin sperm binding? *Dev. Growth Differ.* **37:** 1–10.

Reference: *Biol. Bull.* **200:** 107–117. (April 2001)

Escape Hatches for the Clonal Offspring of Serpulid Polychaetes

BRUNO PERNET

Smithsonian Marine Station at Fort Pierce, 701 Seaway Drive, Fort Pierce, Florida 34949

Abstract. Serpulid polychaetes in the genera *Filograna* and *Salmacina* reproduce asexually by releasing a single bud at a time from their posterior ends into their calcareous tubes. Here I show that buds of *Salmacina amphidentata* gain access to the exterior of these tubes *via* escape hatches built into the tubes by the parent worms. Each escape hatch consists of a hole in the tube blocked by a calcareous disc that is supported in place by an organic membrane. After buds detach from their parents, the calcareous discs are dislodged, and buds begin to form their own tubes from the resulting openings. Repeated bouts of asexual reproduction result in the formation of aggregations of branched tubes. A survey of *Filograna* and *Salmacina* spp. from the Atlantic, Indian, and Pacific oceans suggests that the formation of escape hatches for clonal offspring is common to many members of these genera.

Introduction

Serpulid polychaete worms are common members of hard substratum communities in all of the world's oceans, and are usually easily recognized by their white calcareous tubes. Construction of these tubes begins when planktonic serpulid larvae arrive at benthic settlement sites and undergo metamorphosis. During metamorphosis each juvenile secretes a primary tube of organic material which attaches it to the substratum (*e.g.*, Nott and Parkes, 1975; Carpizo-Ituarte and Hadfield, 1998). It then adds to one end of this primary tube by precipitating calcium carbonate in a pair of anterior glands, suspending the resulting crystals in a fluid organic matrix, and molding this slurry onto the anterior tube margin, where it hardens (Hedley, 1956; Neff, 1971; Nott and Parkes, 1975; Clark, 1976). By continuing this process of marginal accretion as it grows, each worm forms a simple calcareous tube attached to the substratum and open only at one end, from which the worm extends its suspension-feeding and respiratory tentacles. Though serpulids are not physically attached to their tubes, under normal circumstances they do not leave them, and worms removed from their tubes are unable to build new ones (*e.g.*, Faouzi, 1931). Tube growth requires a pre-existing tube onto which new material can be added, and apparently only newly metamorphosed juveniles are capable of secreting such a structure *de novo*, in the form of the primary tube.

This pattern of tube growth creates two problems for the few species of serpulids that, in addition to producing larvae by sexual reproduction, reproduce asexually. Asexual reproduction is best known in members of the widely distributed genera *Filograna* and *Salmacina* (see Materials and Methods for comments on the systematics of these taxa), though it occurs in members of at least five other genera as well (*Filogranella, Filogranula, Josephella, Rhodopsis,* and *Spiraserpula:* H. ten Hove, Zoological Museum, Amsterdam, The Netherlands, pers. comm.; ten Hove, 1979; Nishi and Yamasu, 1992; Pillai and ten Hove, 1994). Adults of *Filograna* and *Salmacina* spp. reproduce asexually by paratomous fission, releasing a single budded offspring at a time from the posterior end (Malaquin, 1895; Faulkner, 1930; Cresp, 1964). A newly released bud is thus effectively sealed in a tube whose only opening is blocked by the parent worm. How do these asexually derived individuals gain access to the exterior environment to feed, grow, and reproduce? Once they have gained access to the exterior, how do they build their own tubes?

An important clue is that adults of *Filograna* and *Salmacina* spp. occur in conspecific aggregations of branching tubes. Though individual adults of these species are small, rarely exceeding 500 μm in diameter and a few millimeters

Received 14 September 2000; accepted 18 January 2001.

Current address: Oregon Institute of Marine Biology, P.O. Box 5389, 63466 Boat Basin Drive, Charleston, OR 97420. E-mail: pernet@oregon.uoregon.edu.

in length, aggregations may be composed of hundreds or thousands of individuals and reach dimensions of tens of centimeters (ten Hove, 1979; Nishi and Nishihira, 1997). Observations of aggregation growth and form suggest that asexually derived individuals somehow form tubes that branch off from the tubes of their parents (Benham, 1927; Hanson, 1948). Benham (1927) suggested that new tubes branch from the mouths of parental tubes. This might obtain, for example, if a parent shared its tube opening with a bud while the latter began to build a new tube. In contrast, Hanson (1948) concluded that newly released buds bore holes in the parental tubes to gain access to the exterior and then build their own tubes starting from these newly created openings. Either of these hypotheses would account for both the escape of clonal offspring from the parental tubes and the formation of aggregations of branching tubes. Determining which, if either, is correct requires more detailed observations of the processes of asexual reproduction and tube growth.

In this paper I report the results of such observations on the serpulid *Salmacina amphidentata*. I show that each bud gains access to the exterior of the parental tube *via* an escape hatch built into the tube for it by the parent worm. It then uses the parental tube as a starting point for building its own tube. A survey of *Filograna* and *Salmacina* spp. from the Atlantic, Indian, and Pacific oceans suggests that this pattern of tube growth, among the most complex known in the serpulids, is widespread among members of these genera. These observations raise novel questions concerning the evolution of both asexual reproduction and tube formation in serpulids, as well as the signals that coordinate these two processes.

Materials and Methods

During the spring and summer of 2000, I collected aggregations of *Salmacina amphidentata* consisting of tens to hundreds of individuals from the intertidal and shallow subtidal zones of the Indian River Lagoon in the vicinity of Fort Pierce Inlet, Florida. Aggregations were very common at these sites, on the undersides of stones and the shells of dead bivalves.

Systematics of Filograna *and* Salmacina

I identify the Floridian specimens studied here as *Salmacina amphidentata*, but both the generic and specific names applied are tentative. Members of *Filograna* and *Salmacina* have been distinguished by the presence or absence, respectively, of opercula; because this trait may be variable even within species, Zibrowius (1968) transferred *Salmacina* spp. to the older genus *Filograna*. Despite this, some systematists continue to refer to operculate forms as *Filograna* spp. and inoperculate forms as *Salmacina* spp. (*e.g.*, ten Hove and Wolf, 1984), a practice I continue here. The species-level systematics of these genera are also uncertain (Zibrowius, 1973; ten Hove and Wolf, 1984). Nine species of *Salmacina* have been described (ten Hove, pers. comm.), but most descriptions are based on only a few specimens from single localities, and the degree of variation in what are considered distinguishing traits has usually not been assessed (but see Gee, 1963; Nishi, 1992). Confident identification to species will only be possible following a revision of these taxa. The specimens I studied closely resembled *Salmacina amphidentata* from Jamaica (Jones, 1962). They differed from the description of that species only in their greater maximum number of chaetigers (33 *vs.* 25), greater variation in number of thoracic chaetigers (seven or eight, rarely six, *vs.* seven, rarely six), and larger size of thoracic and abdominal uncini. Voucher specimens have been deposited in the U.S. National Museum of Natural History (#186807).

Observations of asexual reproduction and tube growth

Aggregations of living worms were examined with a dissecting microscope soon after collection to study tube morphology and branching patterns. Detailed observations of asexual reproduction and tube growth were made on worms cultured in the laboratory. Cultures were initiated by chipping individual worms in their tubes from the substrates on which they were collected. I blotted tubes dry and attached them to numbered glass microscope slides with cyanoacrylate glue. Slides were held in open plastic slide boxes submerged in containers of vigorously aerated seawater (salinity 34 ppt) at 25°C. I changed the water in containers every other day, and after each water change added enough cells of *Isochrysis* and *Nannochloris* to color the water slightly. Worms grew rapidly under these conditions, adding new tube material at the anterior end and producing clonal offspring. I examined them daily with a dissecting microscope to study tube growth. New sections of tube typically grew prostrate, attached directly to the glass slides. Because these tubes were incomplete in cross-section, I could follow the events of asexual reproduction in individual worms by looking into tubes through the glass slides. Asexual reproductive stages were observed at higher magnifications by dissecting worms from their tubes and examining them with a compound microscope. I also used time-lapse video to observe tube growth more continuously in two individuals. The growing margins of tubes viewed through a dissecting microscope equipped with a color CCD video camera were recorded on a time-lapse recorder set to record one frame every 0.2 s.

Views of the external morphology of tubes and worms were obtained by scanning electron microscopy (SEM). Tubes recently collected from the field were prepared for SEM by first chipping portions of interest from the substratum. They were fixed for 10 min in 5% formalin in seawater, rinsed in distilled water, dehydrated in several changes of 100% ethanol, and air-dried. Worms to be prepared for SEM were removed from their tubes and relaxed in a mixture of 7.5% $MgCl_2$ and seawater, then fixed in 5% formalin in seawater for 30 min, rinsed in seawater, and post-fixed in 1% osmium in seawater for 2–4 h. They were rinsed several times in distilled water, dehydrated in an ascending concentration series of ethanol solutions, and critical-point dried with CO_2 as the transitional fluid. Specimens were mounted on stubs with adhesive carbon tabs (Ted Pella, Inc.) and sputter-coated with gold before being viewed with a JEOL 6400V microscope.

I sectioned several tubes in order to examine their internal structure, using modifications of methods suggested by K. Fauchald (National Museum of Natural History, Smithsonian Institution, Washington, DC) and K. Fitzhugh (Los Angeles County Museum of Natural History, Los Angeles, CA). Pieces of tubes recently collected from the field were prepared as for SEM, except that once dehydrated they were transferred through several changes of propylene oxide and embedded in PolyBed 812 resin (Polysciences Inc.). Excess polymerized resin was removed with a Buehler Isomet low-speed saw equipped with a diamond wafering blade, and trimmed blocks were glued to glass petrographic slides with five-minute epoxy resin. Blocks were then sectioned with the low-speed saw and polished to the desired level with a Buehler Ecomet 2 grinder-polisher. Finally, I stained the sectioned surface in a solution of hot azure II and methylene blue (each 0.5%, in 0.5% sodium borate: Richardson *et al.*, 1960) for 1 min, rinsed with distilled water, air-dried, and covered the cut surface with immersion oil and a coverslip for photography.

Tube growth in Filograna *and* Salmacina *spp. from other regions*

I examined patterns of tube growth in aggregations of *Filograna* and *Salmacina* spp. from localities in the Atlantic, Indian, and Pacific oceans. Sources of material included the U.S. National Museum of Natural History and specimens in my own collections.

Results

Morphology of Salmacina amphidentata *from the Indian River Lagoon*

Knowledge of the morphology of both aggregations and individual worms is needed to understand patterns of asexual reproduction and tube growth. Small aggregations (10–1000 individuals) of *Salmacina amphidentata* are common in the shallow waters of the Indian River Lagoon on the undersides of hard objects like empty bivalve shells and small stones (Fig. 1A). Tubes are white, 250–400 μm in outside diameter, with walls 20–50 μm thick. They are generally attached to the substratum along most of their lengths. Individual tubes can be up to several centimeters long, but older regions are usually eroded away or covered with other encrusting organisms, including sponges, hydrozoans, and bryozoans. Though the overall form of aggregations is often obscured by these other organisms, with careful examination it is possible to see that the tubes of *S. amphidentata* branch periodically. Branching is more easily seen in aggregations of worms raised in the laboratory (Fig. 1B).

Tubes are built and inhabited by worms 1.5–4 mm in length and 200–350 μm in diameter. Their bodies are divided into three regions—an anterior thorax, a median achaetigerous region, and a posterior abdomen (Fig. 1C). The anterior end of the thorax bears eight main feeding tentacles, or radioles, each of which bears side branches (pinnules) arranged in alternating rows. The tips of the radioles are not at all or sometimes very slightly inflated, but never bear structures resembling the opercula of *Filograna* spp. Behind the radioles the thorax is encircled by a collar of tissue. The collar is divided by deep incisions into one ventral and two lateral lobes. The lateral lobes of the collar are continuous with two dorsal flaps of tissue, the thoracic membranes, that extend the entire length of the thorax. The thorax is composed of seven or eight (rarely six) chaetigerous segments, of which the first is associated with the collar and bears elongate chaetae (capillary or fin-and-blade) dorsally. The remaining thoracic segments bear elongate chaetae of several kinds dorsally, and uncini (short, hooked chaetae) ventrally.

Posterior to the thorax is a short achaetigerous body region, and behind this is the abdomen. In the abdomen the positions of the chaetae are reversed relative to those of the thorax—here, the uncini are dorsal and elongate chaetae are ventral. This pattern of chaetal inversion is found in all serpulids, as well as in the related sabellariids and sabellids (Fitzhugh, 1989). The abdomen is variable in length, and is composed of from 5 to 25 chaetigerous segments. Finally, the terminal end of the abdomen is capped by the pygidium, which bears the anus.

Asexual reproduction and tube growth

Worms raised in the laboratory grew rapidly, adding to their tubes at rates of up to several millimeters a day. The process of normal tube growth in *Salmacina amphidentata* was similar to that described in other serpulids (*e.g.*, Hedley, 1956, 1958; Neff, 1971). Worms added to the anterior margins of their tubes while they were actively feeding, with the radioles extended out of the tube opening and the three lobes of the collar folded back over the tube margin. The ventral collar lobe bore two lateral pores on the surface that was in contact with the tube margin (not shown); I assumed that these were the openings of the calcium-secret-

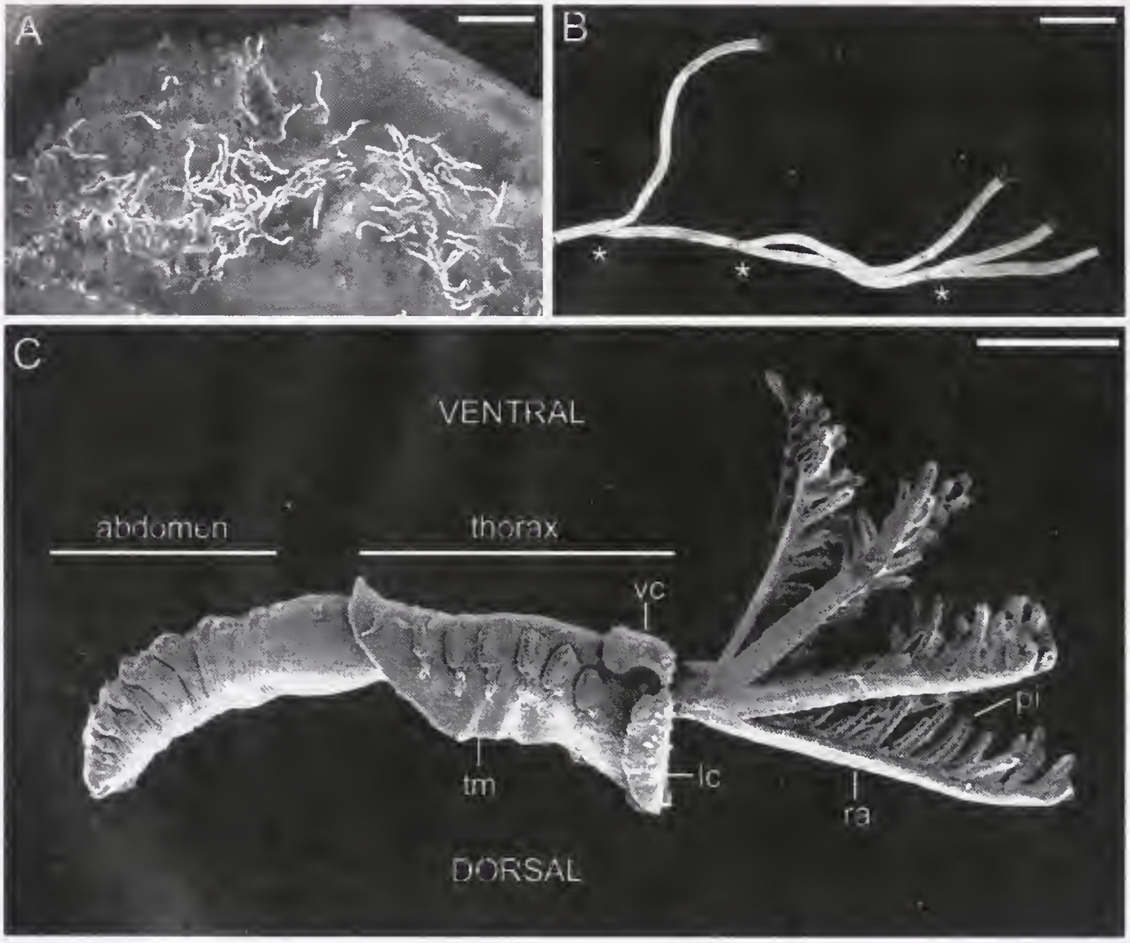

Figure 1. Morphology of aggregations and individuals of *Salmacina amphidentata.* (A) Aggregation of tubes growing attached to the shell of a dead bivalve. Scale bar = 6 mm. (B) Detail of an aggregation cultured in the laboratory on a glass microscope slide, showing periodic branching of the tubes (asterisks). The feeding tentacles (radioles) of three individuals are extended from their tube openings. Scale bar = 2.5 mm. (C) An adult *S. amphidentata* in lateral view. Between the anterior thorax and the posterior abdomen is a short achaetigerous region. The elongate chaetae of the first thoracic chaetiger (the "collar chaetae") are obscured by the lateral lobe of the collar. Scale bar = 250 μm. lc = lateral lobe of the collar, pi = pinnules, ra = radioles, tm = thoracic membrane, vc = ventral lobe of the collar.

ing glands, as in other serpulids (Hedley, 1956). Time-lapse video sequences revealed that calcareous material was slowly added to the tube margin underneath the collar flaps, resulting in an increase in tube length. Growth was not continuous, but resulted from bouts of feeding and tube deposition that lasted for a few minutes and were interrupted by retraction of the worms into their tubes for variable lengths of time.

In addition to adding to their tubes, worms raised in the laboratory reproduced asexually, with most adults releasing from one to four buds per month. (They did not reproduce sexually during this 6-month study, though a few aggregations collected from the field during this period contained sexually mature adults and larvae brooded in the parental tubes.) The events of asexual reproduction in *Salmacina amphidentata* were very similar to those described in other species of *Filograna* and *Salmacina* (*e.g.*, Malaquin, 1895; Faulkner, 1930; Cresp, 1964). Briefly, the first overt sign of asexual reproduction in an adult worm was the appearance of a dense accumulation of bright orange granules in the coelomic cavities of a variable number (5–15) of its posteriormost abdominal segments. Soon after this accumulation of granules appeared, two dorsolateral groups of rudimentary radioles, four on each side, developed on the anteriormost abdominal segment that contained orange granules; these radioles marked the anterior end of the new bud (Fig. 2A, B). At this stage, radioles were simple unciliated cylinders and bore no pinnules. The rudiments of the thoracic membranes appeared at this time as well, as two small dorsolateral flaps of tissue posterior to the radioles (Fig. 2B). The demarcation between the body regions of the bud became evident soon after with the shedding of the origi-

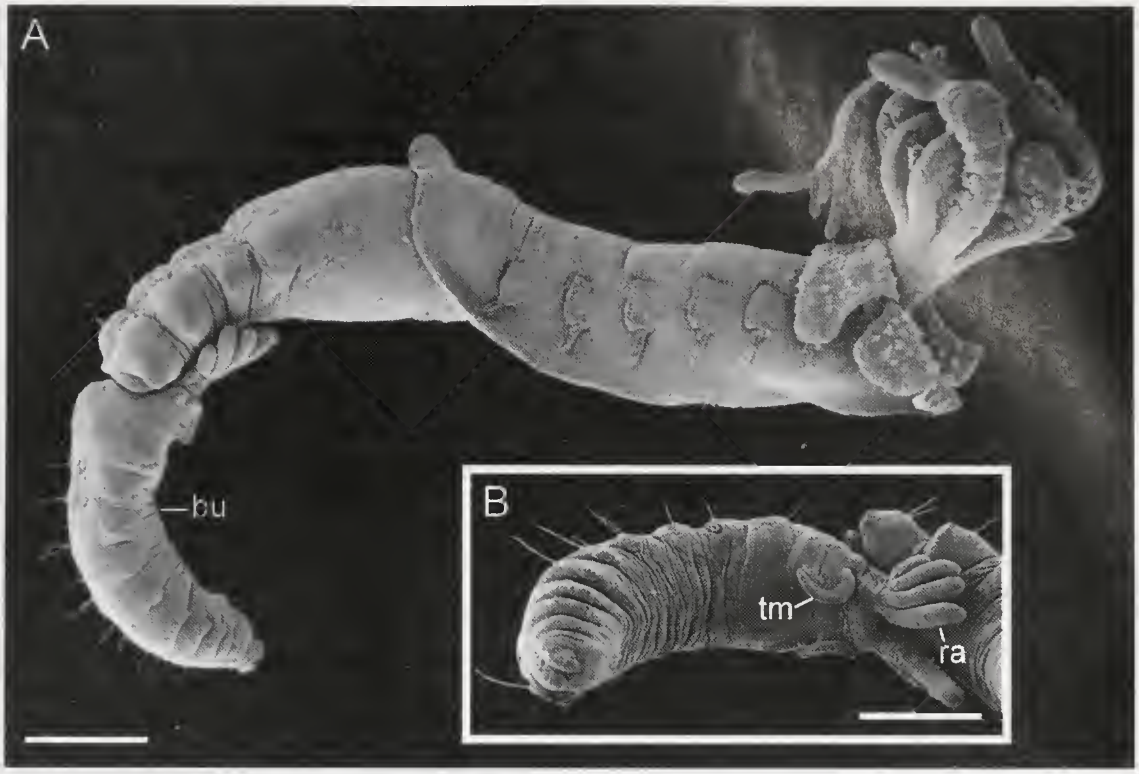

Figure 2. Asexual reproduction by posterior budding in *Salmacina amphidentata.* (A) Lateral view of an individual with developing bud fixed on the day that it built an escape hatch in the tube. Scale bar = 200 μm. (B) Dorsal view of the developing bud. The bud's thoracic chaetae have not yet appeared. Note the rudimentary radioles and thoracic membranes. Scale bar = 250 μm. bu = bud, ra = radioles, tm = thoracic membrane.

nally adult abdominal chaetae in the first segment of the bud, and the sequential development (anterior to posterior) of three thoracic chaetigers from this segment. The first thoracic chaetiger bore only elongate chaetae dorsally. The next two thoracic chaetigers, which developed soon after the first, bore both dorsal elongate chaetae and ventral uncini. Posterior to these new thoracic chaetigers, the segments retained the abdominal configuration of chaetae present when the segments belonged to the adult (*i.e.,* uncini were dorsal). During this time, the gut of the bud remained continuous with that of the adult, and algal cells ingested by the adult passed through the developing bud. Though I did not follow the timing of early events of asexual reproduction in detail, the period from the initial appearance of orange granules in the posterior of an adult to the stage illustrated in Figure 2 took no more than 4 days.

At this stage in development—when the bud had formed eight radioles, the rudiments of the thoracic membrane, and from zero to three thoracic chaetigers—the parent worm altered its pattern of tube growth in a striking way. Instead of continuing to form a normal cylindrical tube, it built a small trumpet-shaped flare, or peristome, in the tube opening. Immediately distal to the peristome, the adult continued to form a cylindrical tube, but built into its uppermost surface a circular or ovoid hole of about the adult worm's diameter. The hole was almost completely blocked with a calcareous disc slightly smaller than the hole in diameter (Fig. 3A–D). The disc was supported in the hole by a very thin layer of organic material (~1–3 μm: Fig. 3E) that lined the entire inner surface of the tube.

Time-lapse video sequences of the construction of these escape hatches showed that they were formed directly as the adult was laying down new tube material, not indirectly by the selective removal of material (by chemical dissolution or mechanical abrasion) from a previously built section of complete tube. It appeared that adults were building cylindrical tubes in the normal fashion, but not depositing calcareous material in the narrow gap between the disc and the rest of the tube. In many cases the edges of both the hole and disc were somewhat jagged (Fig. 3B, D). These jagged edges were formed because bouts of tube deposition, as noted above, were frequently interrupted by retraction into the tube for short periods. When tube deposition was resumed, worms frequently failed to lay down new material that was continuous with the last-deposited material, creating jagged edges.

Once the escape hatch was complete (12–18 h after it was started), the adult continued producing a normal

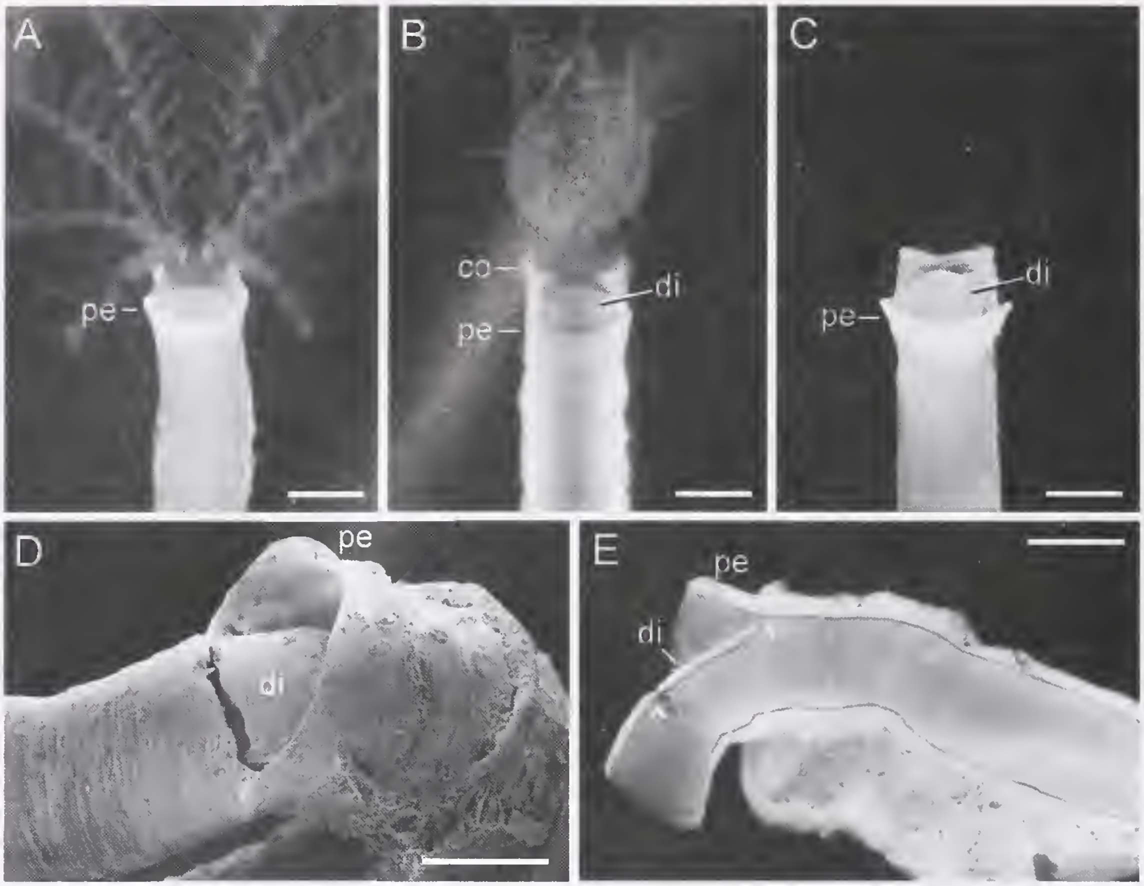

Figure 3. Formation of escape hatches in the tubes of *Salmacina amphidentata.* (A) This worm has finished building a peristome in the tube opening and is beginning to form an escape hatch. Scale bar = 250 μm. (B) Another worm at a later stage in formation of an escape hatch. Scale bar = 250 μm. (C) The tube opening of a worm that has just completed an escape hatch. Scale bar = 250 μm. (D) A recently finished escape hatch. Direction of growth to the left. Scale bar = 200 μm. (E) A recently finished escape hatch in section. Richardson's stain has marked a thin organic membrane that lines the entire tube and supports the disc in the hole (arrowheads). Direction of growth to the left. Scale bar = 250 μm. co = collar, di = calcareous disc, pe = peristome.

cylindrical tube (Fig. 3C–E). During this time, the bud continued to develop. It added additional thoracic segments by transformation of the anteriormost abdominal segments, and added abdominal segments by typical annelid teloblastic growth (Malaquin, 1895; Faulkner, 1930; Cresp, 1964). The radioles elongated, developed pinnules, and became ciliated. In 18 budding events whose timing I followed carefully, the bud detached from the parent worm from 2 to 10 days (mean = 3.3) after formation of the escape hatch. The detached bud could move forward and backward in the parent's tube, but it was unable to approach the main tube opening, which was blocked by the parent's body. By this time, however, the parent had typically added 3–8 mm of new tube beyond the escape hatch, so this structure was accessible to the bud. From 1 to 7 days (mean = 2.5) after the bud had detached from the parent, the calcareous disc was pushed out of the escape hatch. I did not observe this process as it happened, so I do not know which worm (parent or bud) actually dislodged the disc. Soon after the disc was dislodged, the bud began to feed from the resulting opening. The disc often remained precariously attached to the hole for several weeks, presumably by the organic membrane that had originally held it in place (Fig. 4A).

On two occasions, during routine handling, I accidentally partially crushed the escape hatches prior to escape of the buds. In both cases, the buds were unable to exit through the damaged structures. The buds gradually got smaller over the course of 2 weeks trapped in the parental tubes, and they eventually died.

Once a bud had gained access to the exterior *via* the escape hatch, it constructed its own tube using the parental tube as a starting point (Fig. 4A, B). As the new tube emerged from the hole, it was initially directed upward at an angle of about 45 degrees from the parent's tube, continuous

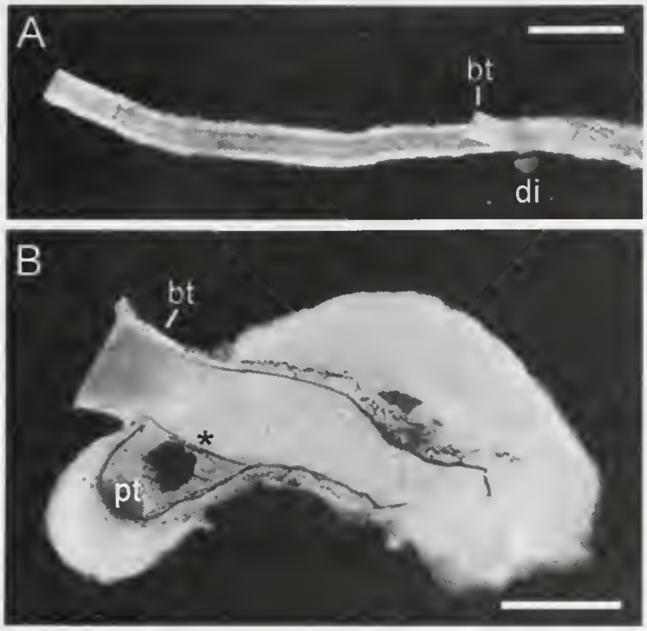

Figure 4. Growth beyond the escape hatch in tubes of *Salmacina amphidentata.* (A) A recently opened hatch, with the calcareous disc still precariously attached to the parent's tube. The bud that opened the hatch has started to build its own tube from the opening. Scale bar = 750 μm. (B) A recently opened escape hatch in section. The parent's tube is growing towards the lower left. Note that the bud has completely blocked off the parent's tube with its own tube material (asterisk) and that the bud's tube is continuous with the peristome secreted by the parent prior to the formation of the escape hatch. The black material in the parent's tube is organic debris. Scale bar = 250 μm. bt = new tube formed by bud, di = calcareous disc, pt = parental tube.

with the peristome formed by the parent immediately prior to constructing the escape hatch (Fig. 4B), but it usually curved back down to the substratum rapidly. A new bud would often build a peristome and escape hatch in its new tube just a few hundred micrometers beyond its point of emergence from the parent's tube. This new escape hatch was eventually used by the bud's own asexually produced offspring 1 to 2 weeks later.

This growth pattern was seen several hundred times in laboratory-raised aggregations. In field-collected aggregations, events of asexual reproduction and tube growth were more difficult to follow, because the substrate was opaque, the aggregations were composed of dense masses of tubes, and tubes were partly covered with other encrusting organisms. Nevertheless, all stages of skeletal growth described above were seen regularly in aggregations collected from the field. Peristomes in tubes were almost always immediately followed by either escape hatches or tubes branching off. The junction between a parental tube and the tube of a bud was always located immediately distal to a peristome in the parental tube. On a few occasions, recently dislodged calcareous discs were seen at the junction between bud and parental tubes.

Tube growth in Filograna *and* Salmacina *spp. from other regions*

I examined aggregations of *Filograna* and *Salmacina* spp. from the Atlantic, Indian, and Pacific oceans in the collections of the U.S. National Museum of Natural History, and in my own collections (Table 1). In all of the aggregations I examined that had clearly visible branching tubes, branching patterns were as described above for *Salmacina amphidentata.* Side tubes always branched from parental tubes immediately distal to peristomes in the parental tube. Further, in three lots of preserved material from the Pacific ocean, I observed escape hatches identical in form to those described above.

Discussion

These observations bear on two questions about asexual reproduction in *Filograna* and *Salmacina* spp.: how do clonal offspring gain access to the exterior of the parental tube, and how do they begin to form their own tubes? The answers to these questions center on the escape hatches built into tubes by parent worms. Buds or parents open these escape hatches, which allows buds to reach the outside of the parental tubes. Buds also use the resulting openings as starting points for their own new tubes. This has been most carefully documented in *Salmacina amphidentata* cultured in the laboratory, but clear evidence of escape hatch formation can also be seen regularly in tubes of that species collected from the field, and in preserved material of other species of *Filograna* and *Salmacina* from geographically widespread localities (Table 1). Alternative hypotheses on how buds escape parental tubes (*e.g.*, briefly sharing the main opening of the tube with the parent, or boring a hole through the parent's tube: Benham, 1927; Hanson, 1948) are not supported by the results of this study, nor by any other data that I am aware of.

It is remarkable that escape hatches in the tubes of *Filograna* and *Salmacina* spp. have not been described before, since asexual reproduction in these two genera has been the focus of detailed studies for well over a century (*e.g.*, Huxley, 1855; Malaquin, 1895; Faulkner, 1930; Vannini and Ranzoli, 1954; Cresp, 1964; Nishi and Nishihira, 1994). In part, this may be because most of these workers focused their attention specifically on the morphology of developing buds, and not on the consequences of posterior budding for clonal offspring. Still, the questions of how buds might escape parental tubes and subsequently form their own tubes have been asked regularly over the past 75 years (Benham, 1927; Hanson, 1948; ten Hove, 1979; Nishi, 1992; ten Hove and van den Hurk, 1993).

The observations reported here also show clearly how the clonal offspring of *Salmacina amphidentata,* and at least some other *Filograna* and *Salmacina* spp., are retained near parent worms and contribute to the growth of aggregations

Table 1

Evidence of the formation of escape hatches for clonal offspring in tubes of Filograna *and* Salmacina *spp.*

Species*	Collection locality	Evidence of escape hatch formation	Year collected
Filograna implexa (NMNH #4462)	Atlantic Ocean: Martha's Vineyard, Massachusetts, USA, 55 m	Tubes branch distal to peristomes	1893
Filograna sp. (NMNH #79634)	Atlantic Ocean: Tangier Harbor, Morocco, 5 m	Tubes branch distal to peristomes	1982
Filograna sp. (NMNH #79633)	Indian Ocean: Mauritius, 18 m	Tubes branch distal to peristomes	1974
Filograna sp. (NMNH #81507)	Pacific Ocean: South Pacific (43°48 S, 147°34 E), 146 m	Escape hatches present; tubes branch distal to peristomes	1968
Filograna sp. (NMNH #98500)	Pacific Ocean: Galapagos Islands, 0–15 m	Tubes branch distal to peristomes	1966
Salmacina amphidentata (author's collection)	Atlantic Ocean: Fort Pierce, Florida, USA, 0–1 m	Escape hatches present; tubes branch distal to peristomes	2000
Salmacina dysteri (NMNH #67631)	Atlantic Ocean: Charleston, South Carolina, USA, 32 m	Tubes branch distal to peristomes	1978
Salmacina dysteri (author's collection)	Pacific Ocean: Pearl Harbor, Hawai'i, USA, 0–1 m	Escape hatches present; tubes branch distal to peristomes	2000
Salmacina incrustans (NMNH #50436)	Atlantic Ocean: La Parguera, Puerto Rico, 1 m	Tubes branch distal to peristomes	1963
Salmacina tribranchiata (author's collection)	Pacific Ocean: Santa Cruz, California, USA, 0–1 m	Escape hatches present; tubes branch distal to peristomes	2000

* Names listed are those used in the collections of the U.S. National Museum of Natural History (NMNH), or, for specimens in the author's collection, those used in regional guides (California: Blake, 1975; Hawai'i: Bailey-Brock and Hartman, 1987). Both generic and specific identifications should be viewed with skepticism. See Materials and Methods for additional comments on systematics.

of branching tubes. It should be noted that aggregations of *Filograna* and *Salmacina* spp. are not necessarily composed only of the genetically identical offspring of a single founder individual. Recruitment of planktonic larvae may contribute substantially to their growth (Nishi *et al.*, 1996; Nishi and Nishihira, 1997). The branching tubes characteristic of aggregations of *Filograna* and *Salmacina* spp., however, are undoubtedly the consequence of repeated bouts of asexual reproduction. Many species of serpulids that do not reproduce asexually also form aggregations (ten Hove and van den Hurk, 1993), but these do not contain branching tubes.

Mechanisms and timing of escape hatch formation in Salmacina amphidentata

Though the escape hatches formed by *Salmacina amphidentata* are among the most complex tube structures known from the serpulids, the actual mechanism of their formation does not seem to have required great modifications of the routine processes of tube growth. The ability to carefully control where calcareous tube material is deposited around the margin of the tube, which permits *S. amphidentata* to build escape hatches, is widespread in serpulids. Many species, for example, deposit more material at some locations around the tube margin than at others, resulting in the formation of sculptural elements like keels or spines (*e.g.*, *Pomatoceros triqueter:* Hedley, 1958; *Filogranula gracilis* (as *Omphalopoma*): Zibrowius, 1968; *Spiraserpula* spp.: Pillai and ten Hove, 1994). A few species form even more complex structures such as brood chambers for developing embryos (Ben-Eliahu and ten Hove, 1989; Nishi, 1993). Adults of *S. amphidentata* avoid depositing any calcareous tube material at all in the narrow gaps between the calcareous disc and the rest of the tube, while depositing it elsewhere along the tube margin. Such precise control over the location of deposition may be mediated by two processes. First, the slurry of calcareous crystals in a fluid organic matrix may be deposited directly at the correct sites on the tube margin by the pair of calcium-secreting glands on the ventral lobe of the collar, with the adult rotating in the tube to position the gland openings correctly. However, in each of the two episodes of escape hatch formation I observed in detail by time-lapse video, the adult worm rotated in its tube infrequently. Further, for most of the time spent building hatches, the openings of calcium-secreting glands were approximately adjacent to the gaps between the calcareous disc and the rest of the tube, exactly where no calcareous tube material was deposited. A more plausible possibility is that muscular movements of the collar mold the slurry of tube material into the correct positions on the tube margin. I did not observe such movements, but would expect them to be subtle and difficult to see at the low magnifications used in this study. The slurry of tube material is not molded onto the tube margin by the action of cilia on the collar, as its relevant surfaces lack cilia (not shown).

In *Salmacina amphidentata,* the calcareous discs of the escape hatches were supported in place by a thin organic membrane (Fig. 3E). This organic layer lined the inner surface of the entire tube. Though it is rarely mentioned in accounts of tube structure or growth, a similar "coating membrane" has been found lining the tubes of at least five other species of serpulids (Muzii, 1968; Pernet, pers. obs.), and is probably an integral component of the tube in all species of serpulids. This is presumably the material that the chaetae of serpulids interact with during routine movement up and down the tube, and also during anchoring when a predator attempts to pull the worm from the tube (*e.g.*, Merz and Woodin, 2000). Two observations suggest that the coating membrane is deposited prior to or at the same time as the calcareous tube material. First, during the process of escape hatch formation, *Filograna* and *Salmacina* spp. construct a calcareous disc that is discontinuous with the rest of the calcareous tube. As noted earlier, however, it appears that the growth of calcareous tubes in all serpulids requires a pre-existing tube margin onto which new calcareous material can be added. During the deposition of calcareous discs, it seems likely that such a pre-existing tube margin is present in the form of a coating membrane. Second, the calcareous disc is supported in place by the coating membrane; it seems likely that this is true throughout its construction. That the coating membrane has been found in all serpulids that have been carefully examined (Muzii, 1968; Pernet, pers. obs.) and that it appears to be deposited prior to or simultaneously with the calcareous portion of the tube suggest that it plays an important and rarely considered role in tube formation. It may also be important in considerations of the evolution of the calcareous tube, a defining feature of the serpulids (Rouse, 2000).

The close temporal coordination of events in asexual reproduction and tube growth in *Salmacina amphidentata* suggests the possibility of signaling pathways between buds and parents. Only after a developing bud had reached a certain stage (with unbranched radioles, 0–3 thoracic segments, and rudimentary thoracic membranes) did the parent worm begin to form an escape hatch. Adults never built escape hatches unless they were in the midst of a budding cycle. What stimulates the parent worm to alter its pattern of tube deposition at this particular stage in bud development? It is possible that bud and escape hatch formation are part of a single developmental pathway in adult worms, such that once asexual reproduction is initiated, escape hatch formation several days later is inevitable. Alternatively, once a bud reaches a certain stage, it may somehow signal to the adult that it is an appropriate time to form an escape hatch. For example, buds at the stage shown in Figure 2 may already be producing their own hormonal products, perhaps involved in controlling such processes as the transformation of former adult abdominal segments into thoracic segments for the bud. Adult worms, which are still attached to the buds at this stage, might use such signals as a cue to alter their patterns of tube deposition. Endocrine substances produced in the prostomium (or in other parts of the anterior end) are well known as signals controlling the timing of asexual reproduction and changes in chaetal morphology in other polychaetes (*e.g.*, Schroeder, 1967; Franke and Pfannenstiel, 1984). A test of this hypothesis might involve implanting the prostomium of a developing bud into the body of a non-budding adult, and examining the effects on tube growth.

Once buds have detached from the parent, they are free to move forward and backward in the parental tube. Within a few days, however, they must gain access to the outside *via* the escape hatch. I did not determine which worm actually dislodged the calcareous disc from the escape hatch, though it seems likely that the bud does this rather than the parent, which has usually grown well beyond the escape hatch by this time. Buds may identify the site of the escape hatch by simply moving around and testing the tube walls until they find a weak spot. Dislodging the calcareous disc presumably does not require much force, as it is held in place only by a very thin coating membrane.

I did not measure rates of asexual reproduction, or how these might be related to rates of tube growth. In laboratory cultures, both the frequency of asexual reproduction and the rate of tube growth appeared to vary within and among clones, resulting in great variation in the distance between side branches from parental tubes. Many factors, both environmental (food levels, temperature, water flow) and genetic, might affect these parameters, as has been described in other clonal organisms (*e.g.*, Sebens, 1980; Keen and Gong, 1989). Understanding the determinants of rates of asexual reproduction and tube growth in *Filograna* and *Salmacina* spp. is of particular interest since these parameters should strongly affect the eventual form of clonal aggregations. In nature, aggregations are quite variable in form.

Distribution and evolution of escape hatches in asexually reproducing serpulids

Some *Filograna* and *Salmacina* spp. from the Atlantic, Indian, and Pacific oceans form escape hatches for their clonal offspring (Table 1). In three lots of relatively recently preserved material, escape hatches identical in form to those described above in *Salmacina amphidentata* were present. In the remaining six lots of material I examined, which had been in preservative for 18–107 years, branching patterns of tubes were identical to those described above, but no intact escape hatches were found. The absence of intact escape hatches in this older material is not too surprising, even if escape hatches were present at the time of collection. The tubes of these species are delicate and are often damaged during collection and handling. It is also likely that they are gradually dissolved during storage, unless preservatives are well buffered. Escape hatches in particular are prone to damage or dislodgement, as the organic membrane that supports calcareous discs in the tube is extremely thin (Fig. 3E). These comparative data suggest that the formation of escape hatches for clonal offspring is widespread in members of *Filograna* and *Salmacina*.

Asexual reproduction is also known from several other genera of serpulids (*Filogranella, Filogranula, Josephella, Rhodopsis,* and *Spiraserpula*). Members of these genera that reproduce asexually do so by posterior budding, as in *Filograna* and *Salmacina* spp. (ten Hove, 1979; Ben-Eliahu and ten Hove, 1989; Nishi, 1992; Pillai and ten Hove, 1994). Their clonal offspring should also face the dual problems of escaping from the parental tubes and starting to build their own tubes. How they solve these problems is not known. Aggregations of branching tubes similar to those of *Filograna* and *Salmacina* spp., suggesting some mechanism of reaching the exterior of the parental tube but not dispersing from it, are reported in members of three of these genera (*Filogranella, Josephella,* and *Spiraserpula:* ten Hove, pers. comm.; George, 1974; Pillai and ten Hove, 1994).

A few members of a closely related family of tube-dwelling polychaetes, the Sabellidae, also reproduce asexually by posterior budding (Knight-Jones and Bowden, 1984). Sabellid tubes are typically constructed of secreted organic compounds and sediment particles, and are not calcified. How the clonal offspring of sabellids escape the parental tubes is not known. Adults of several species are apparently capable of boring holes in their own tubes (Fitzsimmons, 1965), and it is possible that buds are able to do this as well. Once buds have gained access to the exterior of parental tubes, they may be free to disperse far from their parents before building new tubes, as many sabellids are able to build tubes *de novo* throughout their lives (Fitzsimmons, 1965; Lewis, 1968).

In serpulids, asexual reproduction by posterior budding is only profitable if buds have some way of gaining access to the exterior of the parent's tube (such as escape hatches), but it is difficult to imagine how escape hatches might have evolved in the absence of asexual reproduction. One scenario for the evolution of both of these traits (which seem to be tightly correlated in extant species of *Filograna* and *Salmacina*, at least) involves the initial evolution of posterior budding. Tubes of serpulids—especially the very thin tubes characteristic of species that have small maximum body sizes (Nishi, 1993)—are easily damaged by chance biological or physical insults, and buds may have originally used such fortuitous openings to gain access to the exterior of parental tubes. Adult worms that secreted generally weaker skeletons, or skeletons with weak points, would have had more consistent success in fledging clonal offspring, though this might have been balanced by greater vulnerability to predators. Selection might then eventually lead to adults that built extremely weak points—escape hatches—into their tubes to ensure that buds would find exits. This is obviously speculative. However, this scenario might be tested with comparative data on living clonal serpulids examined in the context of a well-supported phylogeny. Neither sort of data is yet available. Such an analysis might reveal persistent and informative variation in the mechanisms buds use to gain access to the exterior of parental tubes.

Acknowledgments

I thank the director and staff of the Smithsonian Marine Station at Fort Pierce for support during this study, especially S. Reed for guidance in the field and J. Piraino for operating the electron microscope. K. Fauchald, E. Kupriyanova, and especially H. ten Hove provided advice on taxonomic problems. K. Fauchald and L. Ward made museum collections available, and K. del Carmen and B. Nedved (Hawaii) and K. Wasson (California) kindly collected worms for me. I thank R. Brodie, K. Fauchald, H. ten Hove, A. J. Kohn, E. Kupriyanova, E. Nishi, S. Woodin, and a reviewer for discussion or comments on the manuscript. Smithsonian Marine Station at Fort Pierce Contribution #510.

Literature Cited

Bailey-Brock, J. H., and O. Hartman. 1987. Polychaeta. Pp. 216–454 in *Reef and Shore Fauna of Hawai'i. Section 2: Platyhelminthes through Phoronida* and *Section 3: Sipuncula through Annelida.* D. M. Devaney and L. G. Eldredge, eds. Bishop Museum Press, Honolulu, Hawai'i.

Ben-Eliahu, M. N., and H. A. ten Hove. 1989. Redescription of *Rhodopsis pusilla* Bush, a little known but widely-distributed species of Serpulidae. *Zool. Scr.* **18:** 381–395.

Benham, W. B. 1927. Polychaeta. British Antarctic ("Terra Nova") Expedition, 1910. *Nat. Hist. Rep. Zool., Br. Mus. Nat. Hist.* **7:** 47–182.

Blake, J. A. 1975. Phylum Annelida: Class Polychaeta. Pp. 151–243 in *Light's Manual: Intertidal Invertebrates of the Central California Coast,* 3rd ed. R. I. Smith and J. T. Carlton, eds. University of California Press, Berkeley.

Carpizo-Ituarte, E., and M. G. Hadfield. 1998. Stimulation of metamorphosis in the polychaete *Hydroides elegans* Haswell (Serpulidae). *Biol. Bull.* **194:** 14–24.

Clark, G. R., Jr. 1976. Shell growth in the marine environment: approaches to the problem of marginal calcification. *Am. Zool.* **16:** 617–626.

Cresp, J. 1964. Études expérimentales et histologiques sur la régénération et le bourgeonnement chez les Serpulides *Hydroides norvegica* et *Salmacina incrustans. Bull. Biol. Fr. Belg.* **98:** 3–152.

Faouzi, H. 1931. Tube formation in *Pomatoceros triqueter. J. Mar. Biol. Assoc. UK* **17:** 379–384.

Faulkner, G. H. 1930. The anatomy and histology of bud-formation in the serpulid *Filograna implexa,* together with some cytological observations on the nuclei of the neoblasts. *J. Linn. Soc. Lond. Zool.* **37:** 109–190.

Fitzhugh, K. 1989. A systematic revision of the Sabellidae-Caobangidae-Sabellongidae complex (Annelida: Polychaeta). *Bull. Am. Mus. Nat. Hist.* **192:** 1–104.

Fitzsimmons, G. 1965. Feeding and tube-building in *Sabellastarte magnifica. Bull. Mar. Sci.* **15:** 642–671.

Franke, H.-D., and H.-D. Pfannenstiel. 1984. Some aspects of endocrine control of polychaete reproduction. Pp. 53–72 in *Polychaete Reproduction: Progress in Comparative Reproductive Biology*, A. Fischer and H.-D. Pfannenstiel, eds. Gustav Fischer Verlag, Stuttgart.

Gee, J. M. 1963. On the taxonomy and distribution in South Wales of *Filograna, Hydroides* and *Mercierella. Ann. Mag. Nat. Hist.* **13:** 705–715.

George, J. D. 1974. The marine fauna of Lundy. Polychaeta (marine bristleworms). *Reports of the Lundy Field Society* **25:** 33–48.

Hanson, J. 1948. Formation and breakdown of serpulid tubes. *Nature* **161:** 610–611.

Hedley, R. H. 1956. Studies of serpulid tube formation. II. The calcium secreting glands in the peristomium of *Spirorbis, Hydroides,* and *Serpula. Q. J. Microsc. Sci.* **97:** 421–427.

Hedley, R. H. 1958. Tube formation by *Pomatoceros triqueter. J. Mar. Biol. Assoc. UK* **37:** 315–322.

Hove, H. A. ten. 1979. Different causes of mass occurrence in serpulids. Pp. 281–298 in *Biology and Systematics of Colonial Organisms,* G. Larwood and B. R. Rosen, eds. Academic Press, London.

Hove, H. A. ten, and P. van den Hurk. 1993. A review of Recent and fossil serpulid 'reefs': actuopalaentology and the 'Upper Malm' serpulid limestones in NW Germany. *Geol. Mijnbouw* **72:** 23–67.

Hove, H. A. ten, and P. S. Wolf. 1984. Serpulidae. Chapter 55, pp. 1–34 in *Taxonomic Guide to the Polychaetes of the Northern Gulf of Mexico,* J. M. Uebelacker and P. G. Johnson, eds. Barry A. Vittor and Associates, Mobile, AL.

Huxley, T. H. 1855. On a hermaphrodite and fissiparous species of tubicolar annelid *Protula dysteri. Edinburgh Phil. J. New Series* **1:** 113–129.

Jones, M. L. 1962. On some polychaetous annelids from Jamaica, the West Indies. *Bull. Am. Mus. Nat. Hist.* **124:** 169–212.

Keen, S. L., and A. J. Gong. 1989. Genotype and feeding frequency affect clone formation in a marine cnidarian (*Aurelia aurita* Lamarck 1816). *Funct. Ecol.* **3:** 735–745.

Knight-Jones, P., and N. Bowden. 1984. Incubation and scissiparity in Sabellidae. *J. Mar. Biol. Assoc. UK* **64:** 809–818.

Lewis, D. B. 1968. Feeding and tube-building in the Fabriciinae. *Proc. Linn. Soc. Lond.* **179:** 37–49.

Malaquin, A. 1895. La formation du schizozoïte dans la scissiparité chez les Filigranes et les Salmacynes. *C. R. Hebd. Seances Acad. Sci.* **121:** 953–955.

Merz, R. A., and S. A. Woodin. 2000. Hooked setae: tests of the anchor hypothesis. *Invertebr. Biol.* **119:** 67–82.

Muzii, E. O. 1968. A coating membrane in the calcareous tubes of serpulids. *Pubbl. Staz. Zool. Napoli* **36:** 135–137.

Neff, J. M. 1971. Ultrastructural studies of the secretion of calcium carbonate by the serpulid polychaete worm, *Pomatoceros caerulus. Z. Zellforsch. Mikrosk. Anat.* **120:** 160–186.

Nishi, E. 1992. Notes on the reproductive biology of some serpulid polychaetes at Sesoko Island, Okinawa, with brief accounts of setal morphology of three species of *Salmacina* and *Filograna implexa. Mar. Foul.* **10:** 11–16.

Nishi, E. 1993. On the origin of brooding characteristics in spirorbids with the phylogeny of sabellids and serpulids. *Proc. Jpn. Soc. Syst. Zool.* **49:** 6–12.

Nishi, E., and M. Nishihira. 1994. Colony formation via sexual and asexual reproduction in *Salmacina dysteri. Zool. Sci.* **11:** 589–595.

Nishi, E., and M. Nishihira. 1997. Multi-clonal pseudo-colony formation in the calcareous tube worm *Salmacina dysteri. Nat. Hist. Res.* **4:** 93–100.

Nishi, E., and T. Yamasu. 1992. Brooding and development of a serpulid tube worm *Salmacina dysteri. Bull. Coll. Sci., Univ. Ryukyus* **54:** 107–121.

Nishi, E., T. Yamasu, and T. Kikuchi. 1996. Intra-colonial allozyme variation in the serpulid polychaete *Salmacina dysteri. Publ. Amakusa Mar. Biol. Lab., Kyushu University* **12:** 55–62.

Nott, J. A., and K. R. Parkes. 1975. Calcium accumulation and secretion in the serpulid polychaete *Spirorbis spirorbis* at settlement. *J. Mar. Biol. Assoc. UK* **55:** 911–923.

Pillai, T. G., and H. A. ten Hove. 1994. On Recent species of *Spiraserpula* Regenhardt, 1961, a serpulid polychaete genus hitherto known only from Cretaceous and Tertiary fossils. *Bull. Nat. Hist. Mus. Lond.* **60:** 39–104.

Richardson, K. C., L. Jarett, and E. H. Finke. 1960. Embedding in epoxy resins for ultrathin sectioning in electron microscopy. *Stain Technol.* **35:** 313–323.

Rouse, G. W. 2000. Family Serpulidae. Pp. 184–189 in *Polychaetes and Allies: The Southern Synthesis. Volume 4A Polychaeta, Myzostomida, Pogonophora, Echiura, Sipuncula.* P. L. Beesley, G. J. B. Ross, and C. J. Glasby, eds. CSIRO Publishing, Melbourne.

Schroeder, P. C. 1967. Morphogenesis of epitokous setae during normal and induced metamorphosis in the polychaete annelid *Nereis grubei. Biol. Bull.* **133:** 426–437.

Sebens, K. P. 1980. The regulation of asexual reproduction and indeterminate body size in the sea anemone, *Anthopleura elegantissima* (Brandt). *Biol. Bull.* **158:** 370–382.

Vannini, E., and F. Ranzoli. 1954. Rigenerazione, schizogonia e maturazione sessulae nel polichete *Salmacina incrustans. Boll. Zool.* **21:** 467–479.

Zibrowius, H. 1968. Étude morphologique, systématique et écologique, des Serpulidae de la région de Marseille. *Recl. Trav. Sta. Mar. Endoume Bull.* **43:** 81–252.

Zibrowius, H. 1973. Serpulidae des côtes ouest de l'Afrique et des archipels voisins. *Ann. Mus. R. Afr. Cent. Ser. Quarto Zool.* **207:** 1–93.

Reference: *Biol. Bull.* **200:** 118–126. (April 2001)

Factors Controlling the Expansion Behavior of *Favia favus* (Cnidaria: Scleractinia): Effects of Light, Flow, and Planktonic Prey

O. LEVY*, L. MIZRAHI, N. E. CHADWICK-FURMAN, AND Y. ACHITUV

Faculty of Life Sciences, Bar-Ilan University, Ramat Gan 52900, Israel

Abstract. Colonies of the massive stony coral *Favia favus* were exposed to different flow speeds and levels of light, and to the addition of zooplankton prey. The relative importance of each factor in controlling polyp expansion behavior was tested. The coral polyps fully expanded when they were exposed to low light intensity (0–40 μmol m^{-2} s^{-1}) and high flow speed (15 cm s^{-1}), regardless of prey presence. They also partially expanded under low and medium light (40–80 μmol m^{-2} s^{-1}) at medium flow speed (10 cm s^{-1}). The corals expanded their polyps only when they were exposed to light levels below compensation irradiance (I_{com}: light level at which photosynthesis = respiration), which was determined to be about 107 ± 24 μmol m^{-2} s^{-1}.

The results presented here indicate that high flow, low light, and the presence of planktonic prey induce coral expansion. There is a hierarchy of response to these stimuli, in which light level and flow speed are dominant over prey presence. Coral response to these three factors is probably due to the relative importance of gas exchange and zooplankton prey.

Introduction

Diel patterns of polyp expansion and contraction vary between species of anthozoans, including reef-building corals (Kawaguti, 1954; Porter, 1974; Lasker, 1979), gorgonians (Wainwright, 1967), and sea anemones (Pearse, 1974; Sebens and DeRiemer, 1977). Most reef corals expand their tentacles nocturnally, but some expand continuously or only during the day (Abe, 1939; Porter, 1974; Lasker, 1979). Corals that expand tentacles at night remain open until dawn, but a beam of light or mechanical stimulation may cause them to contract immediately (Abe, 1939). Sea anemones show a similar range of behavior. Structures containing high densities of zooxanthellae (such as pseudotentacles and column vesicles) may expand under conditions favorable for photosynthesis, whereas structures that contain few or no zooxanthellae (such as feeding tentacles) contract under these conditions (Sebens and DeRiemer, 1977). In the stony coral *Plerogyra sinuosa*, vesicles with high zooxanthellae density expand only during daytime, and feeding tentacles expand at night (Vareschi and Fricke, 1986). Likewise, polyps of the encrusting gorgonian *Erythropodium caribbaeorum* have pinnate tentacles with dense populations of zooxanthellae that do not function in nocturnal feeding and are expanded during the day (Sebens and Miles, 1988). It is assumed that, since such structures contract when their main function is impeded, their expansion involves some form of energy cost. When feeding tentacles themselves contain dense populations of zooxanthellae, they serve both functions of prey capture and photosynthesis, and generally are expanded continuously.

Zooplankton prey are most abundant at night on coral reefs (Sorokin, 1990), so it has been assumed that most corals expand their tentacles nocturnally in order to capture prey (Porter, 1974; Lewis and Price, 1975). Tentacular expansion also is affected by water flow, which reduces the thickness of the boundary layer over tissues and enhances gas exchange (Shashar *et al.*, 1993). Increases in water flow result in higher (approximately doubled) rates of respiration by sea anemones, stony corals, and soft corals (Patterson and Sebens, 1989; Patterson *et al.*, 1991).

The effect of flow on respiration is likely to be magnified when the exposed tissue surface area is increased by extension of either tentacles or specialized column structures.

Received 25 April 2000; accepted 14 December 2000.

* To whom correspondence should be addressed. E-mail: levysher@netvision.net.il.

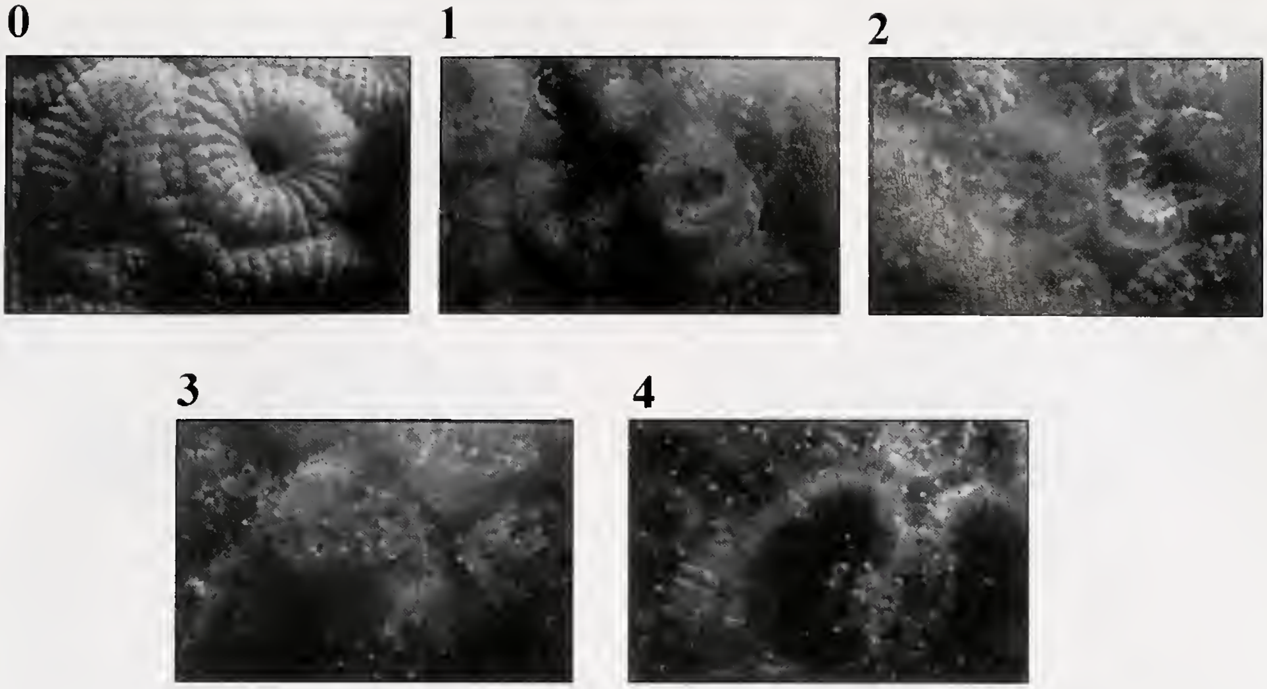

Figure 1. Levels of tentacle expansion in colonies of the stony coral *Favia favus*. Five levels were arbitrarily designated as follows: 0 = full contraction, 1 = 25% expansion, 2 = 50% expansion, 3 = 75% expansion, 4 = 100% expansion. Each score refers to a whole coral colony.

Low flow rate limits the diffusion of materials in the water column to and from coral tissues, thereby regulating and reducing metabolic rates (Patterson and Sebens, 1989; Patterson *et al.*, 1991), zooxanthellae productivity (Dennison and Barnes, 1988; Shick, 1990; Patterson *et al.*, 1991), and nutrient uptake (Atkinson and Bilger, 1992). Oxygen builds up to high levels within and above coral tissue surfaces during the day as a result of photosynthesis, and is extremely depleted near those surfaces at night due to respiration; both gradients are reduced, improving delivery of dissolved substances to and from tissues, with even small increases of flow speed (Shashar and Stambler, 1992; Kuhl *et al.*, 1995; Shashar *et al.*, 1996).

Polyp size, tentacle morphology, and tissue surface area vary widely among coral species, and all three factors contribute to prey encounter and capture rate. Porter (1976) suggested that large polyps with elongate tentacles specialize in zooplankton capture, at the expense of high surface area conducive to photosynthesis. However, more recent evidence shows that certain small-polyped corals are able to capture almost the same size range of prey as do those with larger polyps, and actually have much higher rates of prey capture per unit biomass because of the high surface area of the tentacles that they expose to moving water (Sebens, 1987a). The small-polyped coral *Madracis mirabilis* captures 30 times more zooplankton per coral biomass than does the much larger-polyped *Montastrea cavernosa* (Sebens *et al.*, 1996). The biomass of polyps of *M. mirabilis* is only 1/90th of the biomass of *M. cavernosa* polyps, but an equal biomass of *M. mirabilis* colony has 12 times the tentacular surface area of a *M. cavernosa* colony.

A primary cost associated with expansion in corals is increased respiration, facilitated by a larger surface area of tissue in contact with the overlying water, including water inside the coelenteron, than in contracted corals. Polyp expansion is energy consuming, in that it is achieved by pressurization of the coelenteron. Pressurization is brought about by ciliary pumping of water into the coelenteron, which acts on the viscoelastic material of the polyp wall (Barnes, 1987).

Rates of respiration are known to be significantly reduced in contracted corals (Brafield and Chapman, 1965; Pearse, 1974; Robbins, and Shick, 1980; Lasker, 1981). The magnitude of this difference depends on ambient oxygen concentration (Beattie, 1971; Sassaman and Mangum, 1972, 1973, 1974; Shumway, 1978) and on the ratio of expanded to contracted tissue area, rather than being a simple response to low external oxygen concentration alone. Contraction may be a means of producing a low oxygen concentration in the coelenteron, resulting in lower metabolic rates and in savings of energy or carbon regardless of the external oxygen level (Sebens, 1987b). In contrast, expansion may aid in the diffusion of excess oxygen away from photosynthesizing coral tissues, thus reducing local hyperoxia and its negative effect on metabolic rates or damage due to superoxide radicals (Lesser and Shick, 1989; Shick, 1991). On the other hand, contraction could result in anaerobic metabolism and oxygen debt.

The effects of polyp expansion and contraction on gas exchange and on the key metabolic processes of photosynthesis and respiration are unknown in stony corals. In some cases, photosynthesis contributes all of the required carbon for corals, as in the shallow-water, high-light-adapted *Stylophora pistillata* (Falkowski *et al.*, 1984), whereas in low-light-adapted *S. pistillata* (Falkowski *et al.*, 1984) and in other coral species that depend mostly on predation, photosynthesis supplies only a small fraction of energy demand. Since, in the course of photosynthesis, oxygen is evolved while carbon dioxide is consumed, it is possible that in some corals and other zooxanthellate organisms, the extension and contraction of tentacles is tightly coupled to photosynthetic rates. Tentacle expansion status in corals affects the amount of light absorbed by the zooxanthellae, and in turn photosynthetic rates determine O_2 and CO_2 concentrations in the coral tissue and surrounding waters.

Predation on coral tentacles may cause their retraction at times when predators are active. However, a considerable number of coral species with zooxanthellate tentacles expand during the daytime when many coral predators (*e.g.*, chaetodontid fish) are active, suggesting that predation on tentacles is not a currently active selective force on these behavioral patterns.

On coral reefs at Eilat (Gulf of Aqaba, northern Red Sea), colonies of the massive stony coral *Favia favus* expand their tentacles only after sunset and remain open until sunrise (O. Levy, unpub. obs.). In the present study, we determined the relative importance of flow speed, photosynthetically active radiation (PAR), and planktonic prey availability in controlling tentacle expansion behavior in *Favia favus*.

Materials and Methods

Coral collection and flow tank setup

Colonies of the common coral *Favia favus* were collected from the reef adjacent to the Interuniversity Institute for Marine Science at Eilat, Israel, northern Red Sea, from depths of 5–7 m. Individuals of this species were chosen for study because they are abundant on coral reefs at Eilat, their polyps are large (about 1 cm diameter) and easy to observe, and they exhibit regular diel behavior under laboratory conditions. The collected coral colonies, each up to 10 cm diameter, were transferred to the laboratory and placed in shallow tanks supplied with running seawater for 10 h of acclimation before experiments were begun. New corals were collected for each combination of experimental treatments.

Experiments on tentacle expansion behavior were performed in two 25-l recirculating flow tanks; procedures were based on those described by Vogel and LaBarbera

Low flow speed

A. low light

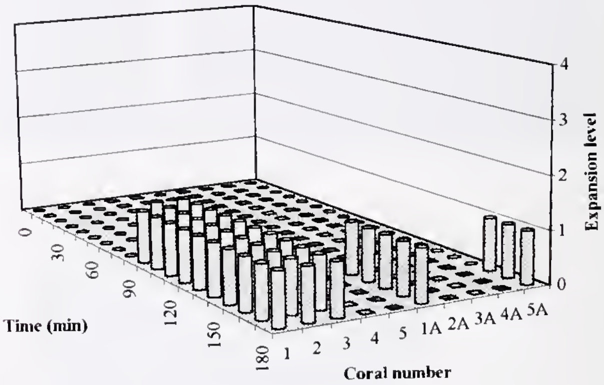

B. medium light

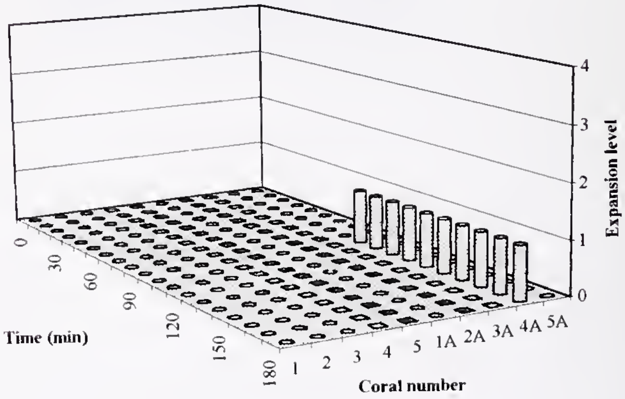

C. high light

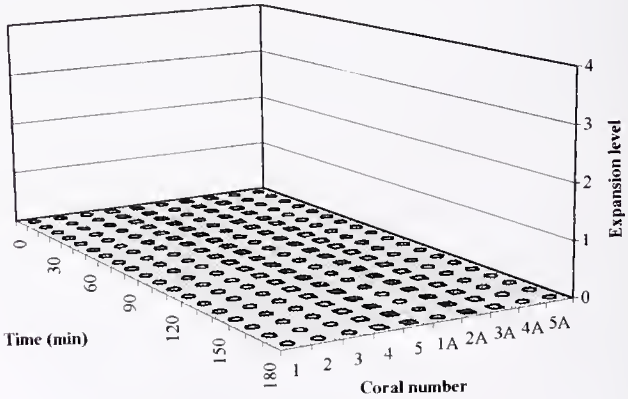

Figure 2. Tentacle expansion behavior of the stony coral *Favia favus* at low flow (5 cm s^{-1}), with variation in light intensity and prey presence (*Artemia* nauplii). Corals marked with A were fed *Artemia* after 90 min. (A) Light intensity 40 μmol m^{-2} s^{-1}. (B) Light intensity 80 μmol m^{-2} s^{-1}. (C) Light intensity 120 μmol m^{-2} s^{-1}.

(1978). Each tank was 100 cm long × 10 cm wide × 25 cm high, and seawater was circulated with a 12-V DC motor. Electronic function generators, consisting of computer programs that were interfaced through a digital-to-analog circuit, controlled the motor speed. Flow speed was measured by following the movement of brightly illuminated particles that were added to the water. Particle movements were recorded using a video camera (Sony CCD 2000E, Hi8 PAL system) with a close-up lens. Flow velocity was measured as described by Trager *et al.* (1990), using a videocassette recorder (Sony EVO-9800P) for frame-to-frame tracking of the movement of the back-lit particles suspended in the flowing water.

Coral expansion experiments

Colonies of *F. favus* were tested at three flow speeds: 5, 10, and 15 cm s^{-1}. These speeds were selected as similar to natural flow speeds on coral reefs at Eilat, which range between about 5 and 20 cm s^{-1} (Genin *et al.*, 1994). For each set of experiments, 20 colonies were used; five corals were placed in each of four tanks. Two of the tanks served as controls with no flow, while in the other two tanks flow was generated as described above. Halogen lamps coupled to fiber optics were set above all four tanks within each experiment, and three light irradiance levels were tested—40, 80, and 120 μmol m^{-2} s^{-1} (equivalent to 40, 80, and 120 μE m^{-2} s^{-1}). Irradiance was measured as photon flux, with a QSI-140 quantum scalar irradiance meter. Temperature was maintained at 24 ± 0.1°C. Each experiment lasted 180 min, and coral expansion behavior was recorded every 10 min. The tanks were rinsed between experiments. In feeding experiments, freshly hatched *Artemia* nauplii were added *ad libidum.* Tentacle expansion of *F. favus* was scored on a scale based on Lasker (1979), ranging from 0 to 4, where 0 represents 0% expansion (full contraction), 1 is 25% expansion, 2 is 50% expansion, 3 is 75% expansion, and 4 is 100% expansion (Fig. 1). Each score refers to a whole coral colony (Fig. 1).

The first set of three experiments was conducted at a flow speed of 5 cm s^{-1}, with three levels of irradiance (40, 80, 120 μmol m^{-2} s^{-1}). In one of the two tanks with water flow, and in one of the control tanks without flow, *Artemia* nauplii serving as zooplankton prey were added after 90 min. In the second set of three experiments, the flow speed was set to 10 cm s^{-1}, and the last set of three experiments was run with new colonies of *F. favus* at a flow speed of 15 cm s^{-1}. Thus, in the three sets of experiments, corals were exposed to all possible combinations of water flow, light intensity, and prey presence. The corals were replaced with new colonies in each experiment to avoid changes in behavior with experience. At the beginning of all experiments, the tentacles of the *F. favus* colonies were contracted (Fig. 1).

Medium flow speed

A. low light

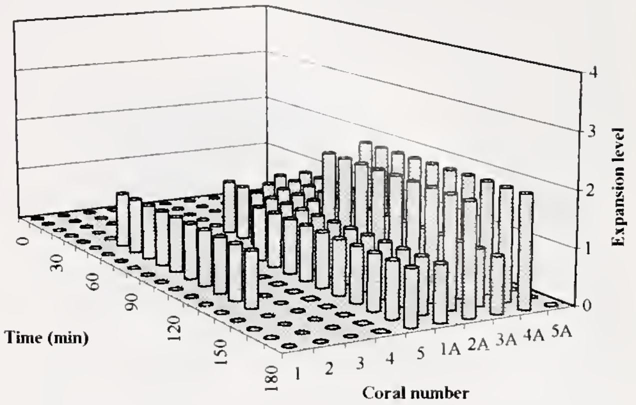

B. medium light

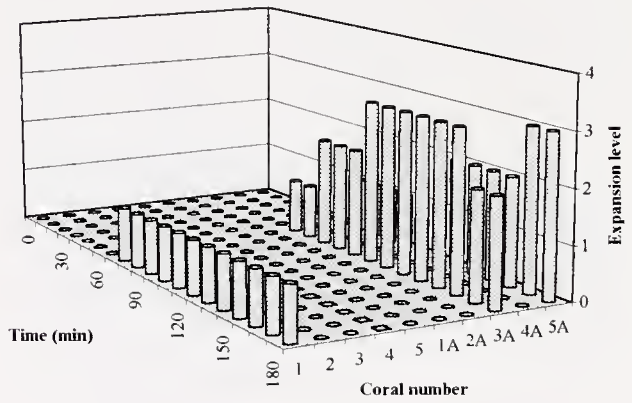

C. high light

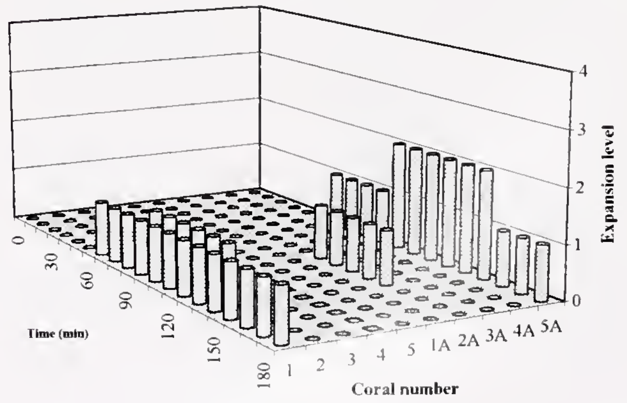

Figure 3. Tentacle expansion behavior of the stony coral *Favia favus* at medium flow (10 cm s^{-1}), with variation in light intensity and prey presence (*Artemia* nauplii). Corals marked with A were fed *Artemia* after 90 min. (A) Light intensity 40 μmol m^{-2} s^{-1}. (B) Light intensity 80 μmol m^{-2} s^{-1}. (C) Light intensity 120 μmol m^{-2} s^{-1}.

High flow speed

A. low light

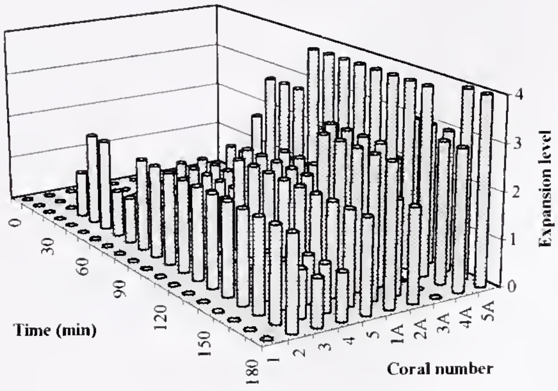

B. medium light

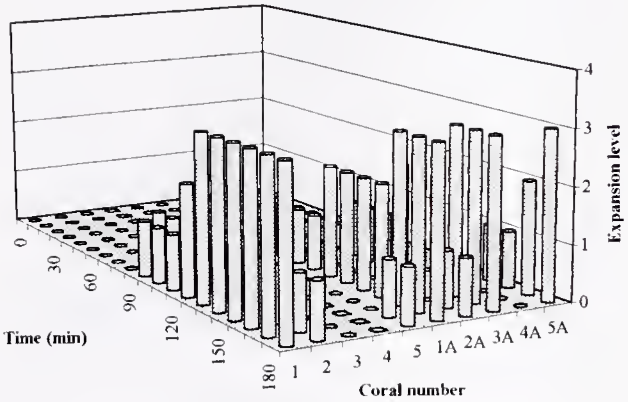

C. high light

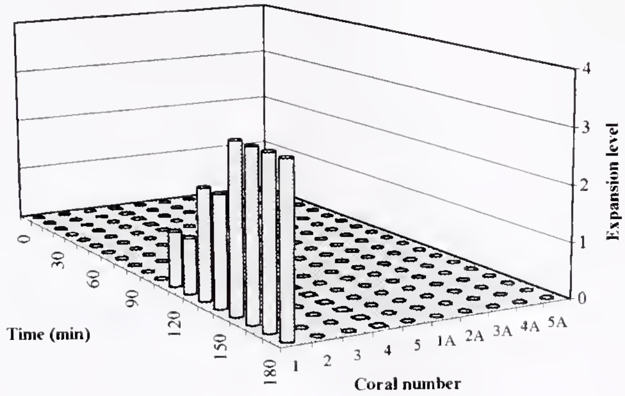

Figure 4. Tentacle expansion behavior of the stony coral *Favia favus* at high flow (15 cm s^{-1}), with variation in light intensity and prey presence (*Artemia* nauplii). Corals marked with A were fed *Artemia* after 90 min. (A) Light intensity 40 μmol m^{-2} s^{-1}. (B) Light intensity 80 μmol m^{-2} s^{-1}. (C) Light intensity 120 μmol m^{-2} s^{-1}.

We assessed possible interaction effects between light intensity, prey presence, and flow speed on tentacle expansion behavior in *F. favus* by performing three-way ANOVA tests on the results.

Determination of light compensation point (I_{com})

The light compensation point for *F. favus* was determined by measuring coral respiration in a closed system (Haramaty *et al.*, 1997). Photosynthesis (under different light intensities) and dark respiration were measured as changes in oxygen concentration, using a Clark-type O_2 electrode (YSI 5331) (Dubinsky *et al.*, 1987). Measurements were made in a double-walled, cylindrical 230-ml chamber filled with filtered seawater (GF/C 0.45 μm). Temperature was maintained at 24 ± 0.1°C. The water in each respirometry chamber was stirred by a magnetic bar beneath a perforated plate supporting the coral. An oxygen electrode detected the rate of oxygen decline in the chamber with an amplifier, which was connected to a data logger (Furier, Israel), coupled to an oxygen meter. Oxygen uptake was measured in the dark for 30 min, and then light intensity was increased, in steps of 30 min, to 10, 40, 80, 120, and 200 μmol m^{-2} s^{-1}.

Colony surface area was measured by covering each coral colony with plasticene, then removing the cover and spreading it flat. The outline of the plasticene sheet was then copied onto aluminum foil and cut; surface area was determined by the weight of the foil in relation to the weight of a piece of foil of known surface area (Marsh, 1970). For calculation of light compensation point (I_{com}), we used computer software attached to the data logger, and the inverse quadratic equation for unit surface area, as described by Ben-Zion and Dubinsky (1988).

Results

Coral expansion behavior

The expansion behavior of *F. favus* colonies varied with each combination of stimuli. In the first set of experiments at low flow speed (5 cm s^{-1}) under low irradiance levels (40 μmol m^{-2} s^{-1}), the coral tentacles expanded only partially with or without the addition of *Artemia* nauplii (Fig. 2A), up to level 1 (25%) (Fig. 1). Most tentacles remained fully contracted under medium irradiance level (Fig. 2B); when prey were added, only one coral responded and expanded up to level 1 (25%). In the control tanks with no water flow, the corals remained contracted during the entire 180 min of the experiment. When corals were exposed to higher irradiance (120 μmol m^{-2} s^{-1}), tentacle expansion did not occur at all, and the corals remained contracted during the entire experiment (180 min) (Fig. 2C). The same response occurred in the two control tanks in which corals were exposed to no flow at 120 μmol m^{-2} s^{-1}.

Table 1

Three-way ANOVA, with interactions among the variables of light intensity, prey presence, and flow speed on the behavior of tentacle expansion in the stony coral Favia favus *after 180 min*

Source of variation	DF	Mean square	*F*	*P*
Light	2	3298.61	6.55	<0.01
Prey	1	2777.77	5.52	<0.05
Light × Prey	2	1173.61	2.33	Not significant
Flow	2	5361.11	10.65	0.001
Light × Flow	4	1027.77	2.04	Not significant
Prey × Flow	2	694.44	1.38	Not significant
Light × Prey × Flow	4	590.27	1.17	Not significant

$P < 0.0001$, $F_{(17,89)} = 3.54$.

Table 2

Three-way ANOVA, without interaction among the variables of light intensity, prey presence, and flow speed on the behavior of tentacle expansion in the stony coral Favia favus *after 180 min*

Source of variation	DF	Mean square	*F*	*P*
Light	2	3298.61	5.96	<0.01
Prey	1	2777.77	5.02	<0.005
Flow	2	5361.11	9.69	<0.001

$P < 0.0001$, $F_{(5,84)} = 7.27$.

In the second set of experiments at intermediate water flow rate (10 cm s^{-1}), at a low light intensity of 40 μmol m^{-2} s^{-1}, and in the absence of *Artemia* nauplii, two corals expanded up to level 1 (25%). When *Artemia* nauplii were added, four corals expanded their tentacles—two to level 1 (25%) and two up to level 2 (50%) (Fig. 3A). In the control tanks with no flow, all corals remained contracted during the entire experiment, even when prey was added. When light intensity was increased to 80 μmol m^{-2} s^{-1}, only three corals responded. Two colonies out of the group fed with *Artemia* expanded to level 3 (75%); the third colony from the unfed group expanded only to level 1 (25%) (Fig. 3B). No expansion responses occurred in the two control groups at 80 μmol m^{-2} s^{-1}. At high light intensity (120 μmol m^{-2} s^{-1}) and intermediate flow speed, only four corals expanded their tentacles slightly, two in the *Artemia*-fed group and two in the non-fed group (Fig. 3C). Again, there was no expansion response by the control corals.

In the third set of experiments run at high flow speed (15 cm s^{-1}), with low irradiance (40 μmol m^{-2} s^{-1}), most of the corals showed positive response and expanded their tentacles. In the group fed with *Artemia*, four corals responded: two fully expanded to level 4 (100%), and two opened to level 3 (75%).

In the non-fed group, four corals responded: two expanded to level 1 (25%), and the other two expanded up to level 2 (50%) (Fig. 4A). In the two control groups, with no flow, the corals remained contracted during the entire experiment. Similar responses occurred at medium light intensity 80 μmol m^{-2} s^{-1} (Fig. 4B), but no expansion response occurred in the two (no-flow) control groups. Only one coral expanded its tentacles to level 3 (75%) when light irradiance was increased to 120 μmol m^{-2} s^{-1}, and all the corals, including those in the other control groups, remained contracted during the entire 180 min (Fig. 4C).

A three-way ANOVA of expansion behavior with the three variables tested (light, flow, and prey) revealed no significant interactions between the variables ($P < 0.0001$, $F_{(17,89)} = 3.54$) (Table 1). A three-way ANOVA without interactions showed significant variation in expansion with each variable ($P < 0.0001$, $F_{(5,84)} = 7.27$) (Table 2). Duncan's test (Table 3) showed significantly higher frequencies of coral expansion at high flow (15 cm s^{-1}) than at low (5 cm s^{-1}) and medium flow (10 cm s^{-1}). Expansion rates also were significantly higher at low-to-medium irradiance levels (40 and 80 μmol m^{-2} s^{-1}) than at high irradiance (120 μmol m^{-2} s^{-1}). When prey (*Artemia*) was present, expansion rates were significantly higher than for corals not fed with prey (Table 3).

Light compensation point (I_{com})

Calculation of the P/I curve revealed that the irradiance level needed to achieve compensation in *F. favus* was 107 ± 24 μmol m^{-2} s^{-1} ($n = 5$ corals tested). We calculated only the I_{com}, therefore the maximum light intensity that the corals were exposed to was only 200 μmol m^{-2} s^{-1}.

Table 3

Duncan's test on the effect of three types of stimuli (light intensity, prey presence, and flow speed) on the tentacle expansion behavior of the stony coral Favia favus

Stimulus	Tentacle expansion (mean %)	Duncan grouping
Light intensity (μmol m^{-2} s^{-1})		
40	27.5	A
80	19.16	A
120	6.66	B
Prey (*Artemia* nauplii)		
Present	23.33	A
Absent	12.22	B
Flow speed (cm s^{-1})		
5	5	B
10	16.66	B
15	31.66	A

Maximum coral expansion occurred when light intensity was low (40 μmol m^{-2} s^{-1}), prey were present, and water flow speed was high (15 cm s^{-1}). See Fig. 1 for description of % tentacle expansion. Means with the same letter are not significantly different at $P = 0.05$.

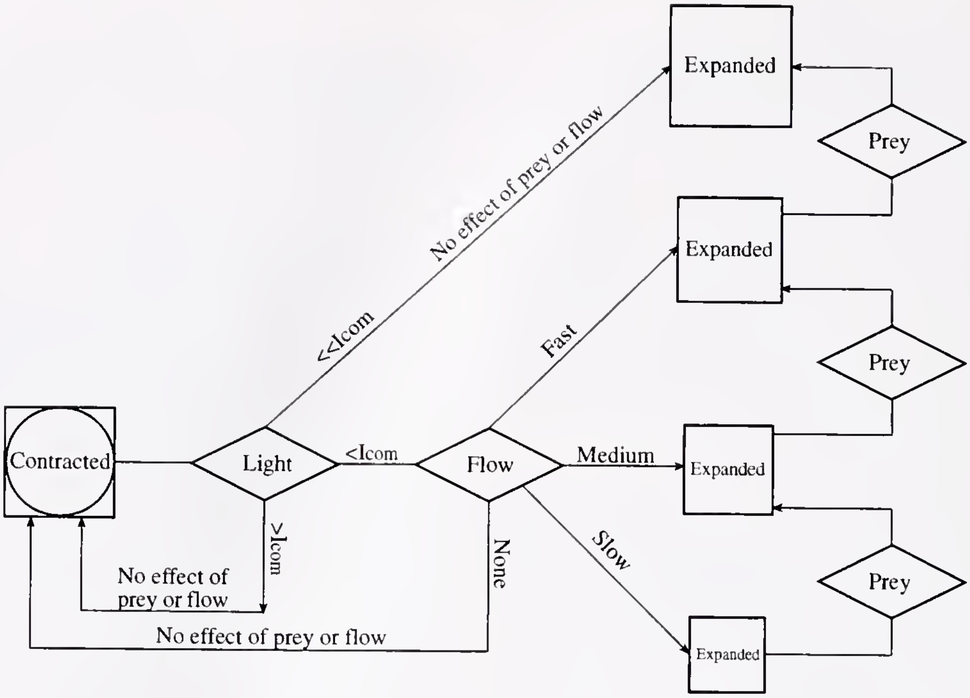

Figure 5. A conceptual diagram of tentacle expansion behavior in the stony coral *Favia favus* in response to different levels of light intensity, flow speed, and the addition of prey (*Artemia* nauplii). Maximum tentacle expansion occurred at dark. At low irradiance, under the compensation point (I_{com}), corals will expand with correlation to the flow rate. Furthermore, the addition of prey can enlarge tentacle expansion response in those conditions. At high irradiance level, above I_{com} the tentacles remain contracted regardless of the presence of neither flow nor prey. In still water the corals remain contracted.

Discussion

We demonstrate here the relative importance of light, flow, and zooplankton prey in controlling the expansion behavior of a stony coral. Although previous studies have examined these factors separately, the present study is the first to test all three factors simultaneously and to elucidate that prey presence is of secondary importance to light and flow in inducing the expansion of coral tissue.

Several reports have demonstrated that stony corals and sea anemones expand their tentacles in the presence of food (Mariscal and Lenhoff, 1968; Reimer, 1970, 1971; Lewis and Price, 1975). Electrophysiological studies using suction electrodes in the coral *Meandrina meandrites* have shown that repeated stimulation of the nerve net evokes oral disk expansion and tentacle extension, similar to the expansion behavior that normally occurs at night when the corals feed (McFarlane, 1978). It is assumed that the nervous responses occur due to prey stimulation of chemoreceptors, as described for the mushroom coral *Heliofungia actiniformis* by McFarlane and Lawn (1991). Flow also is known to cause expansion by corals; high flow speed increases both the potential for encountering plantonic prey and the mass transfer rate of dissolved gases and nutrients (Sebens *et al.*, 1997).

Our analysis of three variables simultaneously shows that each factor has an impact on the expansion behavior of *F. favus*, but that flow and light are the main triggers. Maximum tentacle expansion in *F. favus* corals occurred with high flow, low irradiance, and the addition of prey (Fig. 4A). When there was no addition of prey, but light intensity remained low and flow velocity high, the corals responded and expanded their tentacles up to 75%. Positive responses also occurred in medium flow, with medium light (Fig. 3A, B), but there was almost no response at all when light intensity was maximal (120 μmol m^{-2} s^{-1}), regardless of flow speed or prey presence.

At high flow, the benefits of flow to photosynthesis are greater than the costs associated with increased respiration, thus energy available to the coral for growth and reproduction is greater, up to some asymptote, with increasing flow speed (Patterson *et al.*, 1991; Patterson, 1992). Coral energetics depend upon tissue expansion state, which alters both the surface area exposed to flow and the thickness of the tissue layers through which materials diffuse. In high-speed flow environments, flow modulation of coral energetics is minimal. When water flow is low, dense branches or other morphologies that increase the total volume and thickness of a colony's diffusional boundary layer may negatively affect the coral's energy balance. In low-flow environments, the diffusional boundary layer may become severely limiting to metabolic processes; corals in these environments show morphologies that maximize the exposure of their tissue surfaces to flow (Lesser *et al.*, 1994; Sebens *et al.*, 1997).

We suggest that expansion behavior in zooxanthellate corals relates to their energy equilibrium between heterotrophy and autotrophy. The expanded tentacles of *F. favus* corals have low densities of zooxanthellae and may produce a self-shadow on the rest of the coral tissue that contains dense algae (O. Levy, unpub. obs.). Thus, under conditions of high light, expansion may lead to a decrease in overall photosynthetic rate and an increase in coral metabolic rate, resulting in a net loss of energy.

The expansion responses that we observed here lead us to propose a hierarchy of response to the three variables examined. According to our results, in still water, corals will not expand their tentacles even if light and prey levels vary (Fig. 5). When the light level is too high (over I_{com}), they also will not expand, even when flow and prey vary. When light levels are low ($<I_{com}$), the expansion behavior depends on conditions of flow and prey (Fig. 5). Finally, if no prey is present, the corals will still expand, but only if light is low and flow speed is medium to high. Therefore, the coral's response to prey presence is secondary to its response to light and flow.

This relative importance of different environmental factors in controlling tentacular expansion (Fig. 5) may apply to many coral species, which, like the colonies of *F. favus* tested here, have low densities of algae in their tentacles and are known for their nocturnal expansion behavior. However, these results probably do not apply to corals that contain high algal densities in their tentacles and thus would benefit from expansion when light levels are high.

Acknowledgments

We thank the staff of the Interuniversity Institute for Marine Science in Eilat for hospitality and diving facilities. We acknowledge the assistance of S. Karko, D. Zakai, N. Stambler, and N. Simon-Blecher in conducting the experiments. We thank K. Tarnaruder for help with graphical design; we also appreciate the help of R. Levy with the statistical analysis.

Literature Cited

Abe, N. 1939. On the expansion and contraction of the polyp of a reef coral *Caulastrea furcata* Dana. *Palao Tropical Biological Station Studies* **1:** 651–670.

Atkinson, M. J., and R. W. Bilger. 1992. Effects of water velocity on phosphate uptake in coral reef-flat communities. *Limnol. Oceanogr.* **37:** 273–279.

Barnes, R. D. 1987. *Invertebrate Zoology,* 5th ed. Saunders, Philadelphia. 893 pp.

Beattie, C. W. 1971. Respiratory adjustments of an estuarine coelenterate to abnormal levels of environmental phosphate and oxygen. *Comp. Biochem. Physiol. B* **40B:** 721–728.

Ben-Zion, M., and Z. Dubinsky. 1988. An on-line system for measuring the rate and characteristics of photosynthesis in phytoplankton via an oxygen electrode. *J. Plankton Res.* **10:** 555–558.

Brafield, A. E., and G. Chapman. 1965. The oxygen consumption of *Pennatulata rubra* Ellis and some other anthozoans. *Z. Vgl. Physiol.* **50:** 363–370.

Dennison, W. C., and D. J. Barnes. 1988. Effect of water motion on coral photosynthesis and calcification. *J Exp. Mar. Biol. Ecol.* **115:** 67–77.

Dubinsky, Z., P. G. Falkowski, A. F. Post, and U. M. van Nes. 1987. A system for measuring phytoplankton photosynthesis in a defined light field with an oxygen electrode. *Plankton Res.* **9:** 607–612.

Falkowski, P. G., Z. Dubinsky, L. Muscatine, and J. W. Porter. 1984. A system for measuring phytoplankton photosynthesis in a defined light field with an oxygen electrode. *Bioscience* **34:** 705–709.

Genin, A., L. Karp, and A. Miroz. 1994. Effects of flow on competitive superiority in scleractinian corals. *Limnol. Oceanogr.* **39:** 913–924.

Haramaty, L., Y. Achituv, and Z. Dubinsky. 1997. Morphology, photoadaptation and autotrophy in hermatypic corals. *Proc. 8th Int. Coral Reef Symp. Panama* **1:** 855–860.

Kawaguti, S. 1954. Effects of light and ammonium on the expansion of polyps in reef corals. *Biol. J. Okayama Univ.* **2:** 45–50.

Kuhl, M., Y. Cohen, T. Dalsgaard, B. B. Jorgensen, and N. P. Revsbech. 1995. Microenvironment and photosynthesis of zooxanthellae in scleractinian corals studied with microsensors for O_2 pH and light. *Mar. Ecol. Prog. Ser.* **117:** 159–172.

Lasker, H. R. 1979. Light dependent activity patterns among reef corals: *Montastrea cavernosa. Biol. Bull.* **156:** 196–211.

Lasker, H. R. 1981. Phenotypic variation in the coral *Montastrea cavernosa* and its effects on coral energetics. *Biol. Bull.* **160:** 292–302.

Lesser, M. P., and J. M. Shick. 1989. Effects of irradiance and ultraviolet radiation on photoadaptation in the zooxanthellae of *Aiptasia pallida:* primary production, photoinhibition, and enzymic defenses against toxicity. *Mar. Biol.* **102:** 243–255.

Lesser, M. P., V. M. Weiss, M. R. Patterson, and P. L. Jokiel. 1994. Effects of morphology and water motion on carbon delivery and productivity in the reef coral *Pocillopora damicornis* (Linnaeus): Diffusion barriers, inorganic carbon limitation, and biochemical plasticity. *J. Exp. Mar. Biol. Ecol.* **198:** 143–179.

Lewis, J. B., and W. S. Price. 1975. Feeding mechanisms and feeding strategies of Atlantic reef corals. *J. Zool. (Lond.)* **176:** 527–544.

Mariscal, R. N., and H. M. Lenhoff. 1968. The chemical control of feeding behavior in *Cyphastrea ocellina* and in some other Hawaiian corals. *J. Exp. Biol.* **49:** 689–699.

Marsh, J. A. 1970. Primary productivity of reef-building calcareous red algae. *Ecology* **51:** 255–263.

McFarlane, I. D. 1978. Multiple conducting systems and the control of behaviour in the brain coral *Meandrina meandrites* (L.). *Proc. R. Soc. Lond. B* **200:** 193–216.

McFarlane, I. D., and I. D. Lawn. 1991. The senses of the sea anemones: responses of the SS1 nerve net to chemical and mechanical stimuli. *Hydrobiologia* **216:** 599–604.

Patterson, M. R. 1992. A chemical engineering view of cnidarian symbiosis. *Am. Zool.* **32:** 566–582.

Patterson, M. R., and K. P. Sebens. 1989. Forced convection modulates gas exchange in cnidarians. *Proc. Natl. Acad. Sci.* **86:** 8833–8836.

Patterson, M. R., R. R. Olson, and K. P. Sebens. 1991. *In situ* measurements of forced convection on primary production and dark respiration in reef corals. *Limnol. Oceanogr.* **36:** 936–948.

Pearse, V. B. 1974. Modification of sea anemone behavior by symbiotic zooxanthellae: expansion and contraction. *Biol. Bull.* **147:** 641–651.

Porter, J. 1974. Zooplankton feeding by the Caribbean reef-building coral *Montastrea cavernosa. Proc. 2nd Int. Coral Reef Symp.* **1:** 111–125.

Porter, J. W. 1976. Autotrophy, heterotrophy and resource partitioning in Caribbean reef building corals. *Am. Nat.* **110:** 731–742.

Reimer, A. A. 1970. Chemical control of feeding behaviour and role of glycine in nutrition of *Zoanthus* (Coelenterata, Zoanthidea). *Comp. Biochem. Physiol.* **39A:** 743–749.

Reimer, A. A. 1971. Feeding behaviour in the Hawaiian zoanthids *Palythoa* and *Zoanthus. Pac. Sci.* **25:** 512–520.

Robbins, R. E., and J. M. Shick. 1980. Expansion-contraction behavior in the sea anemone *Metridium senile:* environmental clues and energetic consequences. Pp. 101–116 in *Nutrition in the Lower Metazoa*, D. C. Smith and Y. Tiffon, eds. Pergamon, New York.

Sassaman, C., and C. P. Mangum. 1972. Adaptations to environmental oxygen levels in infaunal and epifaunal sea anemones. *Biol. Bull.* **143:** 657–678.

Sassaman, C., and C. P. Mangum. 1973. Relationship between aerobic and anaerobic metabolism in estuarine anemones. *Comp. Biochem. Physiol. A* **44A:** 1313–1319.

Sassaman, C., and C. P. Mangum. 1974. Gas exchange in a cerianthid. *J. Exp. Zool.* **188:** 297–306.

Sebens, K. P. 1987a. Coelenterata. Pp. 55–120 in *Animal Energetics*, F. J. Vernberg and T. J. Pandian, eds. Academic Press, New York.

Sebens, K. P. 1987b. The ecology of indeterminate growth in animals. *Annu. Rev. Ecol. Syst.* 371–407.

Sebens, K. P., and K. DeRiemer. 1977. Diel cycles of expansion and contraction in coral reef anthozoans. *Mar. Biol.* **43:** 247–256.

Sebens, K. P., and J. S. Miles. 1988. Sweeper tentacles in a gorgonian octocoral: morphological modifications for interference competition. *Biol. Bull.* **175:** 378–387.

Sebens, K. P., K. S. Vandersall, L. A. Savina, and K. R. Graham. 1996. Zooplankton capture by two scleractinian corals, *Madracis mirabilis* and *Montastrea cavernosa*, in a field enclosure. *Mar. Biol.* **127:** 303–317.

Sebens, K. P., J. Witting, and B. Helmuth. 1997. Effects of water flow and branch spacing on particle capture by the reef coral *Madracis mirabilis. J. Exp. Mar. Biol. Ecol.* **211:** 1–28.

Shashar, N., and N. Stambler. 1992. Endolithic algae within corals—life in an extreme environment. *J. Exp. Mar. Biol. Ecol.* **163:** 277–286.

Shashar, N., Y. Cohen, and Y. Loya. 1993. Extreme diel fluctuations of oxygen in diffusive boundary layers surrounding stony corals. *Biol. Bull.* **185:** 455–461.

Shashar, N., S. Kinane, P. L. Jokiel, and M. R. Patterson. 1996. Hydromechanical boundary layers over a coral reef. *J. Exp. Mar. Biol. Ecol.* **199:** 17–28.

Shick, J. M. 1990. Diffusion limitation and hyperoxic enhancement of oxygen consumption in zooxanthellate sea anemones, zoanthids, and corals. *Biol. Bull.* **179:** 148–158.

Shick, J. M. 1991. *A Functional Biology of Sea Anemones.* Chapman & Hall, New York.

Shumway, S. E. 1978. Activity and respiration in the anemone *Metridium senile* (L.) exposed to salinity fluctuations. *J. Exp. Mar. Biol. Ecol.* **33:** 85–92.

Sorokin, Y. U. I. 1990. Plankton in the reef ecosystems. Pp. 291–327 in *Ecosystems of the World: Coral Reefs*, Z. Dubinsky, ed. Elsevier, Amsterdam.

Trager, G., J. S. Hawang, and J. R. Strickler. 1990. Barnacle suspension feeding in variable flow. *Mar. Biol.* **105:** 117–127.

Vareschi, E., and H. Fricke. 1986. Light responses of a scleractinian coral (*Plerogyra sinuosa*). *Mar. Biol.* **90:** 395–402.

Vogel, S., and M. LaBarbera. 1978. Simple flow tanks for research and teaching. *Bioscience* **28:** 638–643.

Wainwright, S. A. 1967. Diurnal activity of hermatypic gorgonians. *Nature* **216:** 1941.

Reference: *Biol. Bull.* **200:** 127–143. (April 2001)

Development of Host- and Symbiont-Specific Monoclonal Antibodies and Confirmation of the Origin of the Symbiosome Membrane in a Cnidarian–Dinoflagellate Symbiosis

TIMOTHY S. WAKEFIELD[1,*] AND STEPHEN C. KEMPF[2]

[1]*Division of Natural Sciences, John Brown University, Siloam Springs, Arkansas 72761; and*
[2]*Department of Biological Sciences, Auburn University, Alabama 36849-5414*

Abstract. The "symbiosome membrane" as defined by Roth *et al.* (1988) is a single, host-derived membrane that surrounds an endosymbiotic organism, separating it from the cytoplasm of the host cell. However, in the case of cnidarian–dinoflagellate endosymbioses, clear identification of the symbiosome membrane is complicated by the fact that each algal symbiont is surrounded by multiple layers of apparent membrane. The origin and molecular nature of these membranes has been the subject of considerable debate in the literature. Here we report the development of host-specific (G12) and symbiont-specific (PC3) monoclonal antibodies that allow separation of the host and symbiont components of these multiple membranes. Using immunocytochemistry at both the light and the electron microscopic level, we present data supporting the conclusion that the definitive symbiosome membrane is a single, host-derived membrane, whereas the remainder of the underlying apparent membranes surrounding the algal cell are symbiont-derived. The potential for macromolecules associated with these membranes to act as cellular signals critical to recruiting symbionts and maintaining established symbioses is discussed.

Introduction

Endocytobiotic associations (symbioses in which one organism lives inside the cell cytoplasm of another organism) are fairly common in nature. They include many prokaryote–eukaryote associations (Jeon and Jeon, 1976; Lerouge *et al.*, 1990; Regensburg-Tuink and Hooykaas, 1993; Udvardi and Day, 1997; Ferrari *et al.*, 1999) as well as a wide variety of eukaryote–eukaryote associations including parasite–vertebrate (Sibley *et al.*, 1986; Hall *et al.*, 1991; Russell *et al.*, 1992; Sam-Yellowe, 1992; Collins *et al.*, 1997; Forero *et al.*, 1999) and microalgal–invertebrate (for reviews see Lee and Anderson, 1991; Trench, 1993). A common feature of many of these associations is the membranes that surround the microsymbiont, effectively separating it from the cytoplasm of the host cell. These membranes form the boundary across which all cell-to-cell communication between the symbiotic partners must occur; thus the membranes become the critical interface for communication and control between symbiont and host (Day and Udvardi, 1992). An understanding of how these membranes mediate interactions between the partners of a symbiotic association requires a knowledge of their origin and molecular nature.

In an attempt to consolidate endosymbiotic research so that homologies in all the systems could be investigated, Roth *et al.* (1988) introduced the terms "symbiosome" and "symbiosome membrane" to describe the intracellular symbiotic compartment in which symbionts reside. In zooxanthellae–cnidarian symbioses, the symbiosome is commonly recognized to include a continuous outer, or vacuole, membrane underlain by multiple layers of additional membrane that surround the "pellicle," or cell wall, of the internal symbiont (Battey, 1992). The origin and nature of these membranes have been debated since they were first described. Taylor (1968) stated that some of these membranes were formed from host tissue, but others were contributed by the symbiont itself; however, he also stated that deter-

---

Received 23 June 2000; accepted 21 December 2000.

* To whom correspondence should be addressed. E-mail: twakefie@jbu.edu.

mining which membranes came from which source was difficult. Dodge and Crawford (1970), in their investigation of the "periplast" of zooxanthellae, agreed with Taylor, stating that "it is impossible to tell whether these [membranes] belong to the host or alga." Undaunted by this proclamation, many papers have been published suggesting possible origins for these membranes. These suggestions have naturally centered on two possible origins: (1) the host cell (Colley and Trench, 1983; Palincsar *et al.*, 1988; Rands *et al.*, 1993; Tripodi and Santisi, 1982), and (2) the algal cell (Kevin *et al.*, 1969; Taylor, 1971; Trench and Winsor, 1987; Wakefield *et al.*, 1998, 2000). Unfortunately, in all cases, suggested origins are presented without any supporting experimental evidence.

In this study, immunocytochemical methods were employed to obtain evidence needed to support or dispute the claims of symbiont *versus* host origins of the multiple layers of apparent membrane surrounding the endosymbiont. The marine anthozoan *Aiptasia pallida* and its endosymbiont *Symbiodinium bermudense* (Banaszak *et al.*, 1993) were used in confocal and electron microscopic investigations that employed two monoclonal antibodies produced against antigens associated with the membranes surrounding the algal symbiont. The data obtained provide the experimental evidence needed to reject one of the proposed hypotheses for the origin of the multiple layers of membrane. The significance of these findings is discussed.

Materials and Methods

Animal collection and care

Specimens of *Aiptasia pallida* were collected in the Florida Keys and transported to Auburn University, Alabama. Collected animals ranged in length from about 4.0 to 8.0 cm, with an oral disc radius of about 2.5 to 5.0 cm. The animals were maintained in two sets of established 300-gallon aquarium systems with both external trickle and undergravel filtration. Artificial seawater for the aquaria was prepared with deionized water and Reef Crystals (Aquarium Systems) at a salinity of about 30 ppt. One aquarium system was maintained on a 12-h light/12-h dark cycle; the other was kept in total darkness. The constant dark condition causes a gradual loss of all photosynthetic symbionts within the host cells; these bleached animals are said to be aposymbiotic. Animals were fed with newly hatched brine shrimp nauplii every other day. Tank temperature ranged between 25 and 30 °C. Individual animals reproduce asexually by producing pedal lacerations: small pieces of tissue that pull away from the pedal disc and grow into a new individual. Thus, within the aquaria, animal sizes ranged from less than 0.5 to about 8 cm in length.

Monoclonal antibody production

Antigen preparation. Eight specimens of *Aiptasia pallida*, each about 5.0–8.0 cm long, were removed from the aquaria. Two specimens were placed in 6.0 ml of a homogenization solution consisting of 1.0 m*M* phenylmethylsulfonyl fluoride (PMSF) in 0.45-μm Millipore-filtered seasoned aquarium water (MFSAW) pre-cooled to 4 °C. The tissues of the specimens were fully dispersed using a Handishear (Virtis) tissue homogenizer; an ice bath was used to maintain the pre-cooled temperature. This process was repeated for all eight specimens, which were then combined and split into four samples. Each sample was poured into 15-ml glass centrifuge tubes and centrifuged at about 250 × *g* for 3 min to pellet the extracted symbiosomes. The supernatant was discarded, and the pelleted symbiosomes were resuspended in homogenization solution. This process was repeated three times until a firm pellet of extracted symbiosomes was obtained in each tube. Each symbiosome pellet was resuspended in 1.0 ml of nanopure filtered water (np-H_2O) and either remained untreated or was processed in one of the following ways: (1) fixed in 4% paraformaldehyde containing 0.2 *M* Millonigs phosphate buffer (MPB) for 10 min and then rinsed three times in 0.2 *M* MPB and finally resuspended in np-H_2O, (2) boiled for 1 min, or (3) repeatedly frozen and thawed by placing the sample in an Eppendorf tube, dropping it into liquid nitrogen, removing and warming until it thawed, and then repeating. All four types of samples were then combined to produce about 4.0 ml of "symbiosome slurry." This slurry was used as a source of antigen for the production of antibodies.

Antibody production. The production of monoclonal antibodies followed standard procedures (Kohler and Milstein, 1975). Briefly, BALB\C mice were injected subcutaneously with 0.1–0.2 ml of the symbiosome slurry in Freund's complete adjuvent. At 3 weeks and 6 weeks, symbiosome slurry in Freund's incomplete adjuvent was injected into the peritoneal cavity. Seven days after the last injection, blood was taken from the tail vein of the inoculated mice. Blood sera were titered 1:50 through 1:10,000 and placed in a 96-well plate coated with fixed symbiosomes to undergo an enzyme-linked immunosorbant assay (ELISA) for the presence of symbiosome antibodies.

Once levels of serum antibodies were sufficient, a mouse was selected and sacrificed. Lymphocytes were removed from the spleen, washed to remove red blood cells, and then suspended in RPMI 1640 tissue culture medium (RPMI). Throughout the fusion procedure, this suspension was maintained at 37 °C by using a dry heating block. A 4:1 mixture of lymphocytes and AG-8.653 myeloma cells was added to a sterile centrifuge tube and pelleted. The supernatant was removed, and a solution of 50% polyethylene glycol in 20 m*M* phosphate buffered saline (PEGM) was slowly added while the cell suspension was constantly stirred. Additional

RPMI was then added while stirring continued. After several minutes the suspension was again centrifuged to pellet the cells, and the PEGM + RPMI medium was removed and replaced with RPMI supplemented with BSA (15% bovine serum albumin), OPI (0.15% oxaloacetate, 0.05% pyruvate, 0.0082% bovine insulin), and HAT (5×10^{-5} *M* hypoxanthine, 2×10^{-7} *M* aminopterin, 8×10^{-6} *M* thymidine). The resulting fusion mixture of cells was aliquoted in 100-μl amounts into the wells of 96-well plates that were then incubated at 37 °C.

Developing cell cultures were periodically fed and checked as they increased in size. Once the 96-well plate cultures had reached one-third confluency they were screened by an immunofluorescent dot-spot test to identify culture wells that were producing antibodies against symbiosome antigens (see below).

Screening. Symbiosomes that had been extracted using the above-outlined procedure were fixed in 4% paraformaldehyde and 0.2 *M* MPB for 10 min. Fixed symbiosomes were rinsed three times in 0.2 *M* MPB and then resuspended and diluted in np-H_2O. Spots of fixed symbiosomes were dried onto spot slides. Each spot was incubated first in 30 μl of blocking media (BM) consisting of 5% heat-inactivated goat serum in 20 m*M* phosphate buffered saline solution containing 0.1% Triton X-100 (PBS+). Subsequently, spots were incubated in 30 μl each of RPMI supernatant from cell-culture wells for about 1 h. Spots were then washed three times in PBS+ and incubated in goat anti-mouse fluorescence isothiocyanate (FITC)-conjugated secondary antibody (1:100 in BM) for 1 h, followed by three more rinses in PBS+. Spots were then examined with a Zeiss epifluorescence microscope. Cells in culture wells producing symbiosome antibodies were suspended in RPMI and cloned by limiting dilution. Upon reaching one-third confluency, clone wells were screened and positive wells cloned again. This process of recloning was repeated until all of the clones in a freshly inoculated 96-well plate showed the same degree of antigen recognition. The final outcome was the isolation of two hybridoma cell lines (G12 and PC3) producing antibodies that recognized antigens associated with the symbiosome membranes. The two cell lines were then expanded, allowing collection of antibody containing spent culture medium for immunohistochemistry and providing cells for frozen storage in liquid nitrogen.

The two cell lines were isotyped using an ISO-1 isotyping kit purchased from SIGMA chemical company. The G12 antibody was found to be an IgG, and the PC3 antibody was an IgM.

Immunocytochemistry and confocal microscopy

Cultured symbionts. Axenic cultures of *Symbiodinium microadriaticum* (Freudenthal, 1962) extracted from *Cassiopea xamachana, S. pulchrorum* (Banaszak *et al.*, 1993) extracted from *Aiptasia pulchella*, and *S. bermudense* extracted from *A. tagetes* (= *A. pallida* Muller-Parker *et al.*, 1996) have been continuously maintained in incubation chambers within our laboratory for about 3 years (cultures were initially provided by Dr. William Fitt, University of Georgia). Incubation temperatures were maintained at 28.5 °C and illumination of the cultures was on a 12-h light/12-h dark cycle. Cultures were grown in 10 ml of ASP-8A culture medium (Blank, 1987) in sterile 15-ml culture tubes. New cultures were started from existing cultures roughly every 2 months, using sterile techniques.

Samples from each culture were removed and fixed in 4% paraformaldehyde in 0.2 *M* MPB. Fixed algal cell samples were rinsed three times in 0.2 *M* MPB and then incubated in the following solutions: BM for 1 h, PC3 primary antibody (1:100 in BM) or G12 primary antibody (1:100 in BM) for 3 h, rinsed 3 times in PBS+ for 10 min each, FITC-conjugated–IgM-specific secondary antibody (1:100 in BM) for PC3 antibody or FITC-conjugated–IgG-specific secondary antibody (1:1000 in BM) for G12 antibody for 1 h, followed by three rinses in PBS+ for 10 min each. Controls were also run using either BM only or a nonspecific antibody-producing hybridoma cell supernatant in place of the primary antibody solution.

Extracted symbiosomes. Symbiotic *Aiptasia pallida* specimens were homogenized, and the symbiosomes were extracted and fixed using the previously described procedures. Labeling of the fixed symbiosomes with the same controls was done using the procedures described above for cultured symbionts.

Cryostat samples. Small (0.5–1.0 cm) symbiotic and aposymbiotic specimens of *Aiptasia pallida* were fixed and rinsed following the same procedure as used on the extracted symbiosomes. After rinsing, these specimens were placed in a 1:1 mixture of 0.2 *M* MPB and Fisherbrand tissue freezing medium (TFM) and left overnight. Specimens were then removed from the 1:1 mixture and placed in 100% TFM. Specimens were frozen, and thin sections were cut using a Reichert-Jung 2800 Frigocut N cryostat. The sections were collected and placed on warm, 4% gelatin-coated slides. The tissues were labeled using the same procedures as those used to label extracted symbiosomes. Sections of symbiotic tissue and aposymbiotic tissue were tested for positive labeling using both PC3 and G12 primary antibodies. The same controls as those used on the extracted symbiosomes were used on the cryosectioned tissue.

Whole-tissue samples. Tentacles (2.0–3.0 cm long) from *A. pallida* were removed from symbiotic specimens. Small (0.5–1.0 cm) whole, aposymbiotic *A. pallida* specimens were also collected. Both types of tissue were fixed and rinsed following the same procedure as that used for extracted symbiosomes and sectioned tissue. After the final rinse, the aposymbiotic specimens were cut into small pieces (2.0–3.0 mm). Symbiotic tentacles were also cut into small pieces (2.0–3.0 mm), and additional cuts was made longitudinally through the tentacle so that the symbiotic endodermal layer was fully exposed to the incubating solutions. Single- and double-labeling experiments using G12 and PC3 primary antibody were performed using the same procedures and controls as described above for extracted symbiosomes and sections.

Imaging. Labeled symbiosomes, sections, and whole-tissue samples were placed on glass slides and infiltrated with either glycerol mounting medium containing 4% *n*-propyl gallate (pH 9.5, Giloh and Sadat, 1982) or Permafluor aqueous mounting medium (Beckman Coulter). Fluorescent images were captured using a BioRad MRC-1000 laser scanning confocal microscope equipped with a krypton-argon laser. For those tissues that were labeled only with FITC-conjugated antibodies, the FITC-labeled tissue was visualized first with 488-nm laser excitation and a 500-nm fluorescent emission filter. A second image was then acquired of the autofluorescence of the algal chloroplast by using 514-nm laser excitation and a 660-nm fluorescent emission filter. When the filter sets provided with the confocal microscope are used, autofluorescence due to chlorophyll is very dim; thus it was necessary to maximize the gain to capture images of chloroplast fluorescence. Each image was saved, pseudocolored (green for FITC; red for autofluorescence), and merged using BioRad's confocal assistant. For double-labeled tissues the same procedures were employed as for single-labeled tissues, except that maximizing the gain for the RITC-labeled tissue was unnecessary because its fluorescence was much brighter than the apparent autofluorescence of the chloroplast.

To ensure that the labeling could be compared accurately, the positively labeled tissue was imaged first. The laser intensity, iris diameter, gain, black level, and enhancement were all optimized for the FITC label. After switching the filter set, each parameter (*i.e.*, laser intensity, iris diameter, *etc.*) was again optimized to capture either the autofluorescent algal chloroplast or the RITC label. Once both sets of parameters were established (one for FITC and the other for either autofluorescence or RITC label), they were not changed during the image acquisition of other experimental tissues.

Electron microscopy

Standard fixation and embedding. Small pieces (2–4 mm) of symbiotic tentacle were removed from a live anemone and fixed in 0.5% glutaraldehyde + 4% paraformaldehyde + 0.2 *M* sucrose in 20 m*M* phosphate buffered saline (PBS) solution at 37 °C for 4 h. Tissues were rinsed in 20 m*M* PBS + 0.2 *M* sucrose three times for 15 min each time and dehydrated in an ethanol series (30%, 50%, 70%, 85%, 90%, 95%, 100%) for 30 min in each, at room temperature, with constant rotation. Tissues were then incubated in a 1:1 mixture of 100% ethanol and LR White and left overnight with constant rotation. The next day, tissues were placed in 100% LR White, incubated for 6 h with constant rotation, and then placed in fresh LR White in an aluminum pan; the pan was placed inside an acrylic plastic chamber and sealed. Intake and outflow valves were used to flood the chamber with N_2 and exclude oxygen. Finally, the sealed chamber was incubated at 70 °C overnight to polymerize the plastic.

Cryofixation and embedding. As above, small pieces (2–4 mm) of symbiotic tentacle were removed from a live anemone. Two or three pieces were placed in a brass planchet, inserted into a Balzers 010 HPM high pressure freezing machine, and quick-frozen. Frozen tissues were transferred to liquid N_2 and held there briefly before being transferred into a Leica EM AFS automatic freeze-substitution system. The tissues were placed in a freeze-substitution medium of methanol (MeOH) + 0.5% uranyl acetate. The freeze-substitution medium and tissues were maintained at −90 °C for 2 days before the temperature of the system was slowly ramped up 5 °C/h until it was stabilized at −45 °C. The freeze-substitution medium was removed and the tissues were rinsed twice, for 30 min each time, in pure MeOH. The tissues were then incubated at −45 °C in the following: a 1:1 mixture of MeOH:Lowicryl HM20 resin for 2 h, a 1:2 mixture of MeOH:HM20 for 2 h, pure HM20 for 2 h, and finally pure HM20 overnight. Tissues were placed into molds filled with fresh HM20 and polymerized at −45 °C by ultraviolet light over a 3-day period.

Sectioning, labeling, and staining. Blocks of the standard-fixed and cryofixed tissues were trimmed, and ultrathin sections were cut using a Reichert-Jung Ultracut E ultramicrotome. Sections were collected on carbon-coated, Formvar-covered slot and 100-mesh grids. Grid-mounted sections were incubated on drops of the following solutions: 0.05 *M* glycine in incubation buffer (10 m*M* phosphate buffer + 150 m*M* NaCl + 0.1–0.2% Aurion BSA-c [acetylated bovine serum albumin] + 20 m*M* NaN_3) for 15 min, blocking medium (incubation buffer + 5% BSA + 0.1% cold water fish skin gelatin + 5% heat inactivated goat serum) for 30 min, incubation buffer 3 × 5 min, diluted primary antibody (see below) in incubation buffer overnight, incubation buffer 6 × 5 min, immunogold-conjugated secondary antibodies (see below) diluted in incubation buffer for 2 h, incubation buffer 6 × 5 min, 10 m*M* PBS 3 × 5 min, postfixed in 2.5% glutaraldehyde in 10 m*M* PBS for 5 min and then rinsed in 10 m*M* PBS for 5 min, nanopure H_2O 5 × 2 min, Aurion silver enhancement for 20 min, nanopure H_2O (np-H_2O) 3 × 5 min, saturated uranyl acetate in 50% MeOH for 20 min, and nanopure H_2O 3 × 5 min. Grids were then carefully blotted by touching the edge of the grid to filter paper and allowing most of the water to be wicked away. Grids were then placed on filter paper and allowed to dry. Labeled tissues were viewed and photographed using a Zeiss EM-10 transmission electron microscope.

Primary antibody dilutions used in the procedure above were either PC3 1:100, G12 1:100, or both 1:100 in incubation buffer. Secondary antibodies used were goat anti-mouse (GAM) IgM-specific antibody conjugated to an ultrasmall (~1.0 nm) gold particle (Aurion), GAM IgG-specific antibody conjugated to an ultrasmall gold particle (Aurion), or a combination of the GAM IgM-specific antibody–ultrasmall gold with a GAM IgG-specific antibody conjugated to a 20-nm gold particle (ICN). Some sections were treated with protein A conjugated to a 15-nm gold particle (Aurion). Sections were incubated in both 1:10 or 1:100 dilutions of secondary antibody or protein A in incubation buffer.

Single-label controls included incubations in BM or nonspecific primary antibodies in place of PC3 or G12. Controls for nonspecific cross reaction of the secondary antibodies were also done. This included incubation in PC3 followed by the IgG-specific secondary antibody and incubation in G12 followed by the IgM-specific secondary antibody. Double-label controls included incubations in BM, in nonspecific primary antibodies, in PC3 only, or in G12 only; each was followed by incubations in both secondary antibodies.

Ultra-cryomicrotomy. Small pieces (2–4 mm) of symbiotic *A. pallida* tentacle were removed from a live specimen. Tentacle pieces were fixed using the same protocol as that used in the standard fixation and embedding procedure described above. However, after the tissue had been rinsed it was placed in an 80% sucrose solution at 4 °C and left overnight. The following day the tentacle pieces were removed and placed on small metal stubs. Care was taken to remove excess sucrose solution, and then the stub and tissue were plunged into liquid nitrogen (LN_2) until completely frozen. Following this initial freezing the tissues remained frozen at all times, either in LN_2 or in the cold chamber of the ultra-cryomicrotomy apparatus.

The frozen tissue was trimmed and sectioned on the Reichert-Jung Ultracut E ultramicrotome fitted with an FC4E ultra-cryomicrotomy unit. Trimming was done at −70 °C with glass knives; sections were cut at −100 °C with a Diatome 45° angle ultra-cryomicrotomy diamond knife. A Diatome Static Line I was also used to reduce the build-up of static charge on the knife surface, allowing a fine ribbon of 75- to 85-nm sections to be produced. Each ribbon was pulled from the knife's edge with an eyelash brush and picked up by using a tiny drop of 80% sucrose suspended in a wire loop. (The sucrose drop begins to freeze as it is brought near the knife surface, and the tissue was picked up just before the drop was completely frozen. Thus the tissue was frozen onto the sucrose drop and removed from the knife.)

The drop was removed from the cryo-chamber and allowed to thaw. The drop was then applied, tissue side down, to a 100-mesh, Formvar + carbon-coated nickel grid. The grid adhered to the drop so that it could be flipped over and floated off the wire loop onto a plate of 4 °C solidified 2% gelatin in np-H_2O. Grids could be stored on the gelatin for several days before being used in the immunogold labeling procedure.

In preparation for labeling the grids, a small amount of the solidified gelatin was removed from around and under each grid. The grids and gelatin were placed on a small piece of Parafilm attached to a glass petri dish and placed in a 37 °C oven for about 30 min. When the plate was removed, the grids could be easily picked out of the now-liquid gelatin with fine forceps. The grids were immediately placed into the 0.05% glycine solution and were incubated in all of the same solutions used on the plastic-embedded tissues. After the final rinse in np-H_2O, the grids were floated onto a solution of 2% methyl cellulose in np-H_2O + 2% uranyl acetate (MU). The grids were then picked up with a wire loop that was just slightly larger than the grid itself, and the excess MU was wicked away by touching the edge of the loop to a piece of filter paper. Care was taken to ensure that only a thin layer of MU was left over the tissue. The MU was then allowed to dry completely, and the grids were removed from the loops and stored in grid boxes until they were viewed and photographed using the Zeiss EM-10 transmission electron microscope.

Results

Immunofluorescence single label

Table 1 presents the overall results for the immunofluorescent labeling of the various tissues used in these experiments. The cultured symbionts of the two species of *Aiptasia* showed positive labeling with the PC3 antibody. In those cultures that did show positive labeling, only a few cells were actually labeled among a larger population of unlabeled algal cells (Fig. 1a). However, none of the cultured symbionts showed any positive labeling with the G12 antibody (Fig. 1b). The symbionts extracted from *Cassiopeia* also did not show positive labeling to the PC3 antibody and appeared the same as negative controls (Fig. 1c, d). Extracted symbiosomes from *Aiptasia* showed very strong positive labeling to the PC3 antibody (Fig. 1e), whereas most of the labeling with the G12 antibody appeared to be in the contaminating host tissues (Fig. 1f).

Cryosectioned aposymbiotic tissues and pieces of tentacle from aposymbiotic animals all showed strong positive labeling for the G12 antibody (Fig. 2a). Neither sections nor whole mounts of aposymbiotic *A. pallida* showed any positive labeling with the PC3 antibody, and they appeared the same as negative controls (Fig. 2b). Sections and whole mounts of symbiotic *A. pallida* showed positive labeling with both the G12 antibody (Fig. 2c) and the PC3 antibody (Fig. 2d). As seen in Figure 2c, the G12 antigen was found

Table 1

Results of immunofluorescence imaging of cultured symbionts, extracted symbiosome, and whole tissue using PC3 and G12 antibodies

Tissue or cell tested	PC3 antibody	G12 antibody	Secondary antibody only	Nonspecific primary antibody
Cultured symbionts				
Symbiodinium microadriaticum	–	–	–	–
S. pulchrorum	+	–	–	–
S. bermudense	+	–	–	–
Extracted symbiosomes from *Aiptasia pallida*	+	+	–	–
Cryosections				
Aposymbiotic tissue	–	+	–	–
Symbiotic tissue	+	+	–	–
Whole fixed tissue				
Aposymbiotic tissue	–	+	–	–
Symbiotic tissue	+	+	–	–

around the symbionts but was apparent in other portions of the host tissue as well. In contrast, as seen in Figure 2d, the PC3 antigen was found only directly around the symbionts and was not found throughout the host tissue.

Controls for cryosectioned symbiotic and aposymbiotic tissues and whole pieces of tissue that were incubated in either BM or a nonspecific primary antibody showed either no fluorescence in aposymbiotic tissues (Fig. 2b) or only the autofluorescence of symbiont chloroplasts (Fig. 2e).

Immunofluorescence double label

Double-labeled tissues (Fig. 2f) revealed the PC3 antibody labeling (green) to be confined to a very narrow band immediately surrounding the symbionts. Alternatively, G12 labeling (red) was distributed evenly throughout the entire endodermal layer of the host and also appeared as a thin yellow line (the overlap color of red and green) that was immediately adjacent and external to the PC3 label (Fig. 2f). [Note that since the autofluorescence of the algal cell chloroplast is emitted at the same wavelength as the much brighter RITC label used for G12 identification, it was not possible to boost the gain and capture it. This resulted in the symbionts appearing as "black holes" (*e.g.*, Fig. 2f), in contrast to what is seen in the single-labeling experiments (*e.g.*, Fig. 2c).]

Immunogold single label

Table 2 summarizes the results of the immunogold labeling in these experiments. Standard fixed tissue and rapid-

---

Figure 1. Cultured symbionts and extracted symbiosomes from *Aiptasia pallida*, labeled with monoclonal primary antibodies PC3 or G12 and fluorescent secondary antibodies. Every picture, including the negative control, is a false color merger of green FITC labeling and red autofluorescence of the algal chloroplast. (a) Specific peripheral labeling of a minority of cultured *Symbiodinium bermudense* treated with PC3 antibody. (b) Total lack of labeling in cultured *S. bermudense* treated with G12 antibody. (c) Total lack of labeling in cultured *S. microadriaticum* treated with PC3 antibody. (d) Total lack of labeling in the negative control of cultured *S. bermudense* treated with secondary antibody only (all negative controls appeared the same). (e) Specific peripheral labeling of extracted symbiosomes from tissues of *A. pallida*, treated with PC3 antibody. (f) Extracted symbiosomes and contaminating host tissue from *A. pallida*, labeled with G12 and FITC. Scale bars = 20 μm.

Figure 2. Cryosections and whole-tissue pieces of *Aiptasia pallida* labeled with PC3 antibody, G12 antibody, or both. Each picture, including the negative controls, is a merged image of green FITC labeling and red algal autofluorescence or RITC labeling. (a) General labeling of host tissue in a cryosection of aposymbiotic *A. pallida* treated with G12 antibody. (b) Total lack of labeling in a cryosection of aposymbiotic *A. pallida* treated with PC3 antibody. (c) General labeling of host tissue, as well as symbiosome membrane, in whole tissue from symbiotic *A. pallida* treated with G12 antibody. (d) Specific labeling of symbiosome-associated membranes without host tissue labeling in whole tissue from symbiotic *A. pallida* treated with PC3 antibody. (e) Total lack of labeling in a negative control of whole tissue from symbiotic *A. pallida* treated only with secondary FITC-conjugated antibody. (f) Double labeling of whole tissue from symbiotic *A. pallida* with PC3 (FITC—green) and G12 (RITC—red) antibodies; PC3 labeling is clearly limited to the symbiosome, whereas G12 labeling is mainly a characteristic of host tissue, but slightly overlaps the symbiosome, as represented by a thin yellow line surrounding the periphery of some symbiosomes. The black holes are the algal symbionts, the autofluorescence of which cannot be seen at the lower gain levels used to image the RITC signal. The bright orange spot in the center of many algal cells (c, d, e) is either the pyrenoid or the accumulation body of the cell. Data gathered using tissues labeled with acridine orange, a fluorescent nuclear stain, indicate that this structure is not the nucleus (Wakefield, unpubl. data). Scale bars: (a, b) = 50 μm; (c–f) = 10 μm.

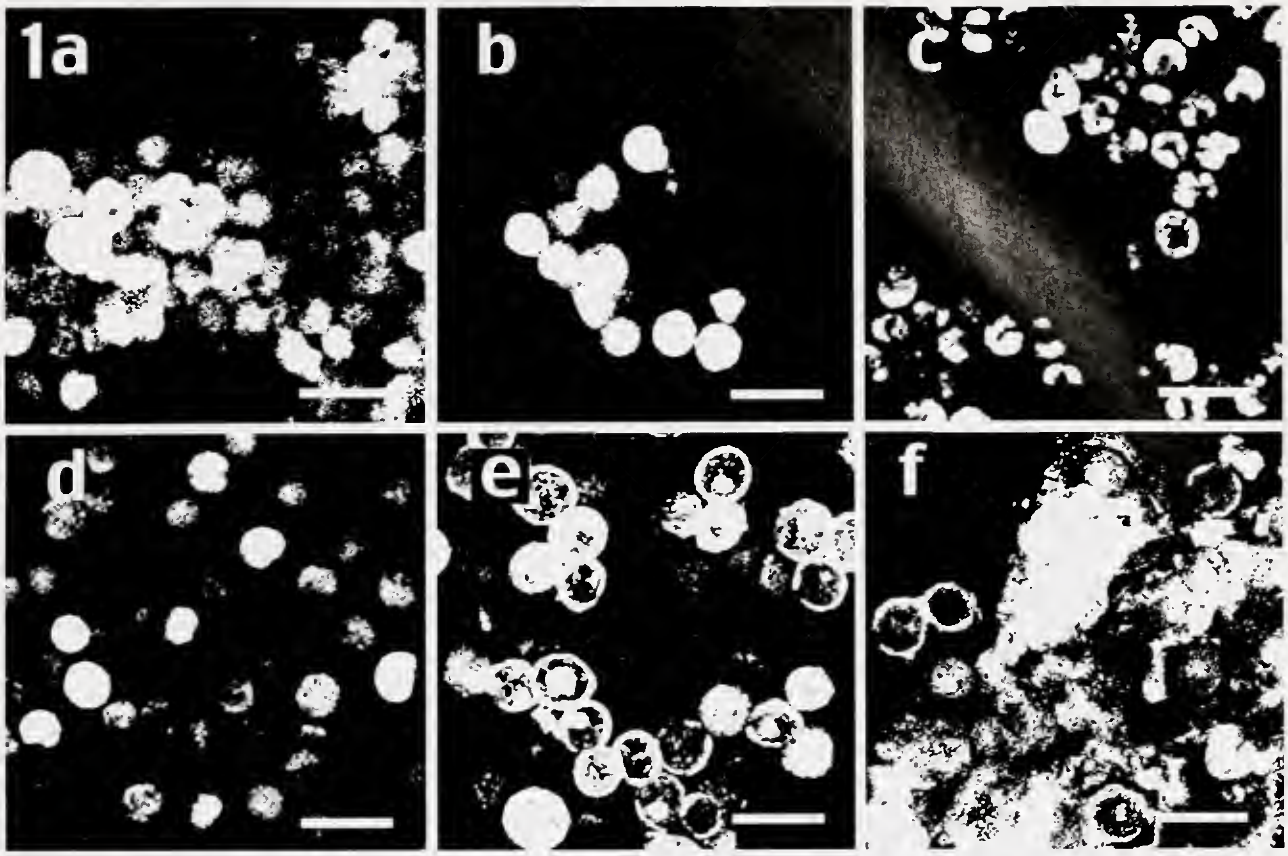
1a
b
c
d
e
f

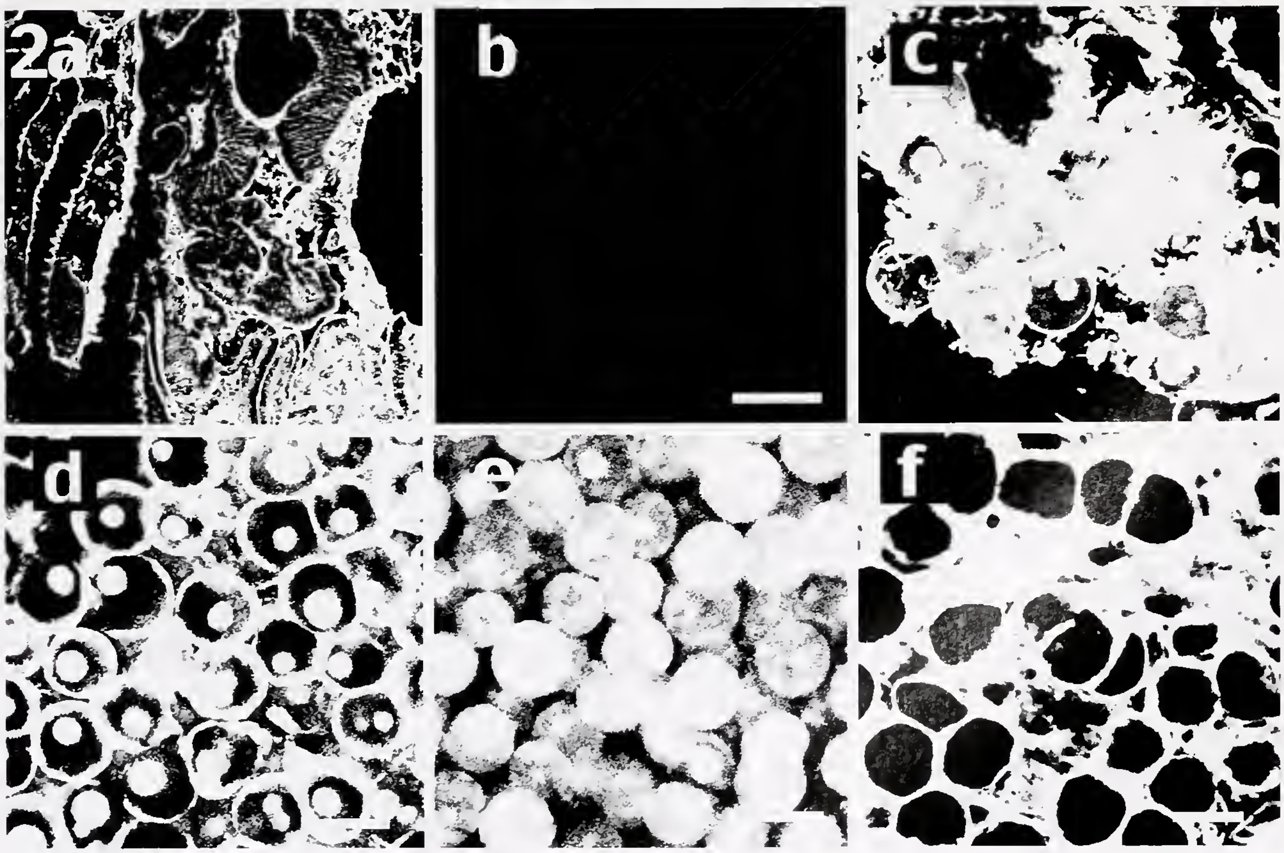
2a
b
c
d
e
f

Table 2

Results of immunogold labeling of in situ *symbionts using PC3 and G12 antibodies*

Tissue components	PC3 label	G12 label	2° ab. only	Nonspecific primary	PC3 + IgG 2°	G12 + IgM 2°
Host tissues						
Ectoderm	−	−	−	−	−	−
Mesoglea	−	+	−	−	−	+
Endoderm	−	+	−	−	−	+
Symbiosome/Symbiont components						
Outermost symbiosome membrane	−	+	−	−	−	−
Multiple layers of membrane	+	−	−	−	+	−
Cell wall	−	−	−	−	−	−
Thecal vesicles	−	−	−	−	−	−
Cytoplasm	+	−	−	−	+	−

freeze–freeze-substituted–low-temperature-embedded tissue labeled with G12 and examined with the electron microscope showed positive labeling of the host cell plasmalemma and internal membranes. In particular, the outermost symbiosome membrane was clearly labeled (Fig. 3a). There was also a strong labeling within the mesoglea of the host tissue (Fig. 3b). However, there was no labeling of the symbiont. A close examination revealed that the multiple layers of membrane that are immediately adjacent to the symbiont were not labeled by the G12 antibody (Fig. 3c); the ectodermal layer of the host tissue also lacked label. In fact, long extensions of the mesoglea could be traced into the ectodermal layer due to the strong label found therein and the absence of label within the ectodermal cells (Fig. 3b).

Controls that were incubated in either BM or a nonspecific primary antibody did not show positive labeling anywhere in the tissues (Fig. 3d).

The tissue sectioned by ultra-cryomicrotomy confirmed our findings that the G12 antigen indicated specific binding in the host membranes and mesoglea (Fig. 4a, b). It also revealed the specificity of the PC3 antibody to the algal symbiont (Fig. 4c, d). The labeling with the PC3 antibody was significant because our early attempts to label standard-fixed, LR-White-embedded tissue with PC3 had totally failed. Thus, the ultra-cryomicrotomy technique provided our first glimpse of the specificity of the PC3 antibody to the algal symbiont. Unfortunately, the preservation of ultrastructure in the ultra-cryomicrotomy technique was less than favorable, necessitating the use of the freeze-substituted–Lowicryl-embedding technique.

Labeling of the freeze-substituted–Lowicryl-embedded tissues with the PC3 antibody revealed strong labeling of the symbiont (Fig. 5a). Although there was a small amount of labeling present in the chloroplast and other cell organelles, the vast majority of label was found in the cytoplasm of the symbiont. Although the internal thecal vesicles and plates of the symbiont did not appear to be labeled, the PC3 antigen was concentrated around the periphery of the cell, between the chloroplast profiles (Fig. 5b). It was sometimes also seen in the cell wall directly adjacent to these peripheral cytoplasmic concentrations (Fig. 5b). Dense labeling was also present in the space between the symbiont and the outermost symbiosome membrane, including areas where multiple layers of membrane were present (Fig. 5b). Host cell cytoplasm and associated membranes surrounding the symbiosomes were essentially devoid of label (Fig. 5a). The minute amount of labeling in the host cell cytoplasm was similar to that of the negative controls (Fig. 5c) and was thus considered to be background labeling.

Immunogold double label

Tissues labeled with both primary antibodies and different-sized gold-conjugated secondary antibodies confirmed our single-labeled experiments. The outermost symbiosome membrane, host endodermal cell membranes, and mesoglea showed dense labeling with large gold particles, indicating the presence of the G12 antigen. Conversely, the multiple layers of membrane directly adjacent to the cell wall, the cytoplasm between the chloroplast profiles, and the cell wall adjacent to these cytoplasmic areas were heavily labeled with small gold particles, indicating the presence of the PC3 antigen (Fig. 6a, b). Negative controls in which the primary and secondary antibodies were switched did show a small amount of cross reactivity. This was most evident with PC3 and the IgG-specific antibody, perhaps due to its larger particle size. However, the cross reaction of the IgG-specific antibody to PC3 confirmed that the PC3 antibody was specific for the algal cell (Fig. 6c). There was some cross reactivity of the IgM antibody to G12, but this also confirmed that the G12 antibody was specific for host tissue and not for the algal cell.

Discussion

The results of both the immunofluorescent and immunogold labeling experiments clearly support the hypothesis

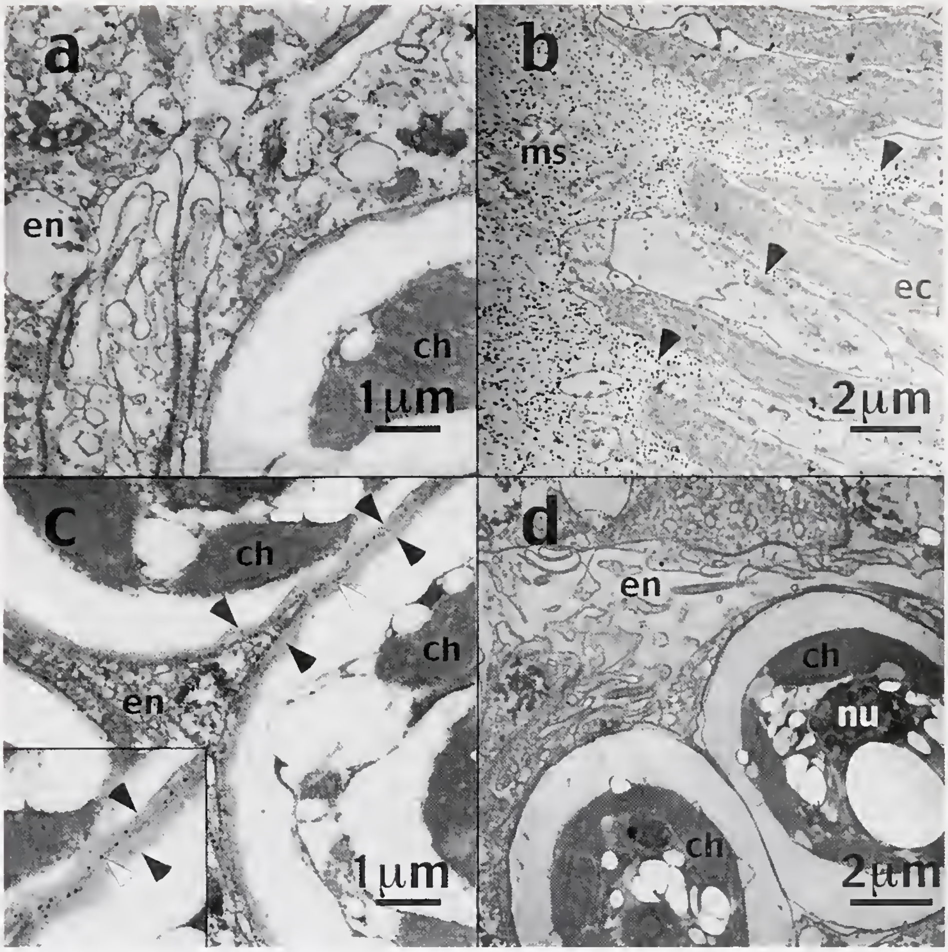

Figure 3. Labeling of host membranes in plastic-embedded tissues of symbiotic *Aiptasia pallida* treated with G12 antibody and visualized with immunogold particles. (a) General labeling of host cell membranes in standard aldehyde-fixed and dehydrated *A. pallida*, embedded in LR White (G12 visualized with protein A–15-nm gold particles). (b) Extension of labeled mesoglea (arrowheads) into unlabeled ectoderm in freeze-substituted *A. pallida*, embedded in Lowicryl (G12 localization visualized with silver-enhanced ultrasmall gold particles). (c) Labeling of the outermost symbiosome membrane in standard aldehyde-fixed and dehydrated *A. pallida*, embedded in LR White (G12 visualized with protein A–15-nm gold particles); insert shows labeling of the outermost membranes of two adjacent symbiosomes. Note that host membrane (white arrowhead) is labeled, but inner, symbiont-associated membranes (black arrowheads) are not. (d) Lack of specific labeling in a negative control section of standard aldehyde-fixed and dehydrated *A. pallida* tentacle embedded in LR White, incubated without G12 antibody followed with incubation with protein A–15-nm gold particles; all negative controls appeared the same with only minor background scattering of gold particles. ch = chloroplast, ec = ectodermal cells, en = endodermal cell cytoplasm, ms = mesoglea, nu = nucleus.

that the two monoclonal antibodies, G12 and PC3, are specific for the different partners in this symbiotic association. The fact that G12 shows positive labeling of host tissue in whole mounts and sections of *Aiptasia pallida* and no labeling of cultured symbionts demonstrates that it is binding to some antigen that is found exclusively in host tissue. Also, since it shows positive labeling of both symbiotic and aposymbiotic tissues, it is clear that this antigen is not symbiont-induced and is present in the host tissue regardless of its symbiotic condition. By contrast, PC3 labeling is apparent only in symbiotic tissues and is completely absent in the aposymbiotic condition. One possible explanation is that the PC3 antigen is induced in the host by the presence of the symbionts and then somehow transferred to them. However, since *in vitro* cultured *Symbiodinium bermudense* and *S. pulchrorum* also show positive (albeit reduced) labeling with the PC3 antibody, it is clear that this antigen is symbiont-derived.

The finding that cultured *S. microadriaticum* is not labeled by the PC3 antibody but both *S. pulchrorum* and *S. bermudense* are labeled may reflect phylogenetic differences between the three tested algal species. In past studies,

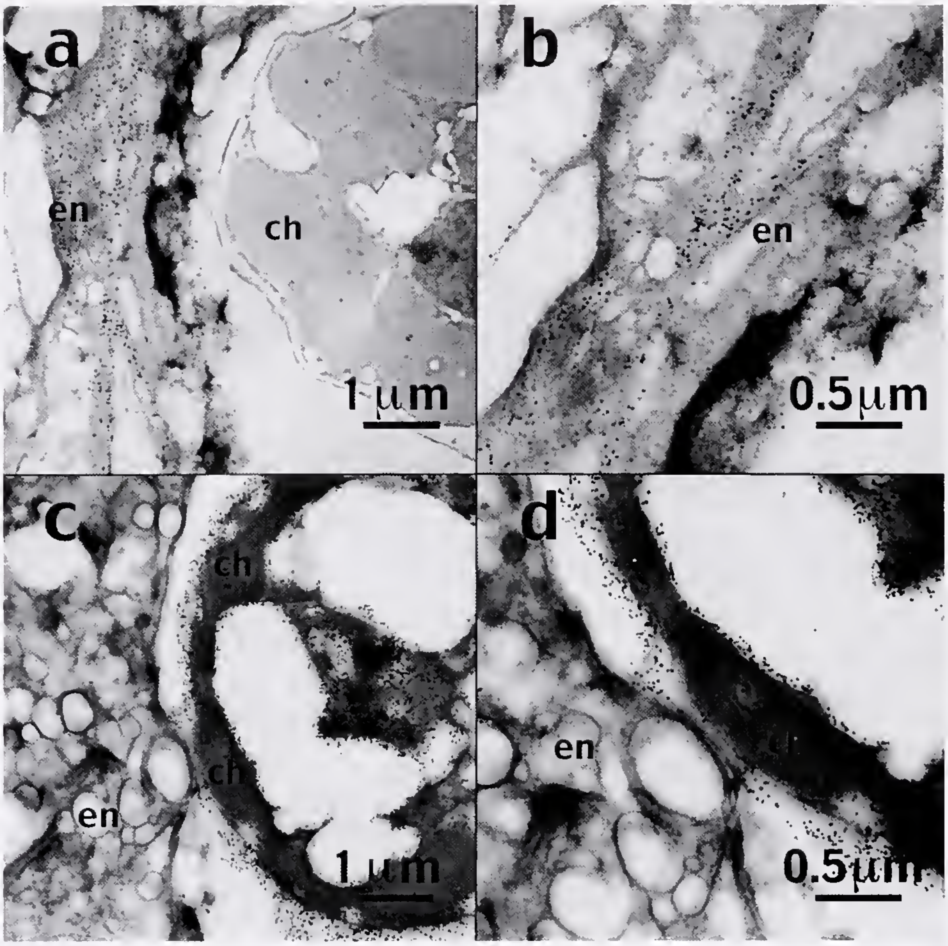

Figure 4. Ultra-cryomicrotomy-sectioned symbiotic *Aiptasia pallida* labeled with G12 or PC3 and immunogold particles indicating the specificity of the antibodies to their respective tissues. Fixation quality varied greatly, but cell morphology was adequate to distinguish host *versus* symbiont. (a) Host endodermal cell cytoplasm labeled in tentacle tissue of *A. pallida*, incubated with G12 and an IgG-specific secondary antibody conjugated to ultrasmall gold particles. Note that algal symbionts are not labeled. (b) Higher magnification of the ultra-cryomicrotomy-sectioned *A. pallida*, labeled with G12 and an IgG-specific secondary antibody conjugated to an ultrasmall gold particle (1:10). (c) Labeling of algal symbionts and associated material in tentacle tissue of *A. pallida* incubated with PC3 and an IgM-specific secondary antibody conjugated to an ultrasmall gold particle. Note the labeling of material between the symbiont and the host cytoplasm as well as internally within the algal symbiont. Label within the symbiont is localized in the cytoplasm surrounding the chloroplasts. Host cytoplasm is devoid of label. (d) Higher magnification of the ultra-cryomicrotomy-sectioned *A. pallida*, labeled with PC3 and an IgM-specific secondary antibody conjugated to an ultrasmall gold particle (1:10). ch = chloroplast, en = endoderm.

evidence based on karyotyping (Blank and Trench, 1985), morphology (Schoenberg and Trench, 1980b; Trench and Blank, 1987), isoenzyme patterns (Schoenberg and Trench, 1980a), physiology (Fitt and Trench, 1981; Chang *et al.*, 1983; Fitt and Trench, 1983), and biochemistry (Chang and Trench, 1982; Govind *et al.*, 1990) has indicated that the genus *Symbiodinium* consists of many different species. Also, an examination of similarities and differences in the genes that encode for the small ribosomal subunit of algal symbionts has revealed that *S. bermudense* and *S. pulchrorum* are closely related but different species, and both have been placed into clade B of the "zooxanthellae" phylogenetic tree (Rowan, 1998). *S. microadriaticum*, on the other hand, is more distantly related and has been identified as belonging to clade A (McNally *et al.*, 1994; Rowan, 1991, 1998; Rowan and Powers, 1991). The results of our immunofluorescent studies support the concept of phylogenetic diversity among the symbionts and may be added to the list of biochemical differences that exist among some *Symbiodinium* species.

The double-labeled immunofluorescent and immunogold results clearly demonstrate that the algal symbionts are surrounded by layers of material that originate from the different symbiotic partners. The narrow region of PC3

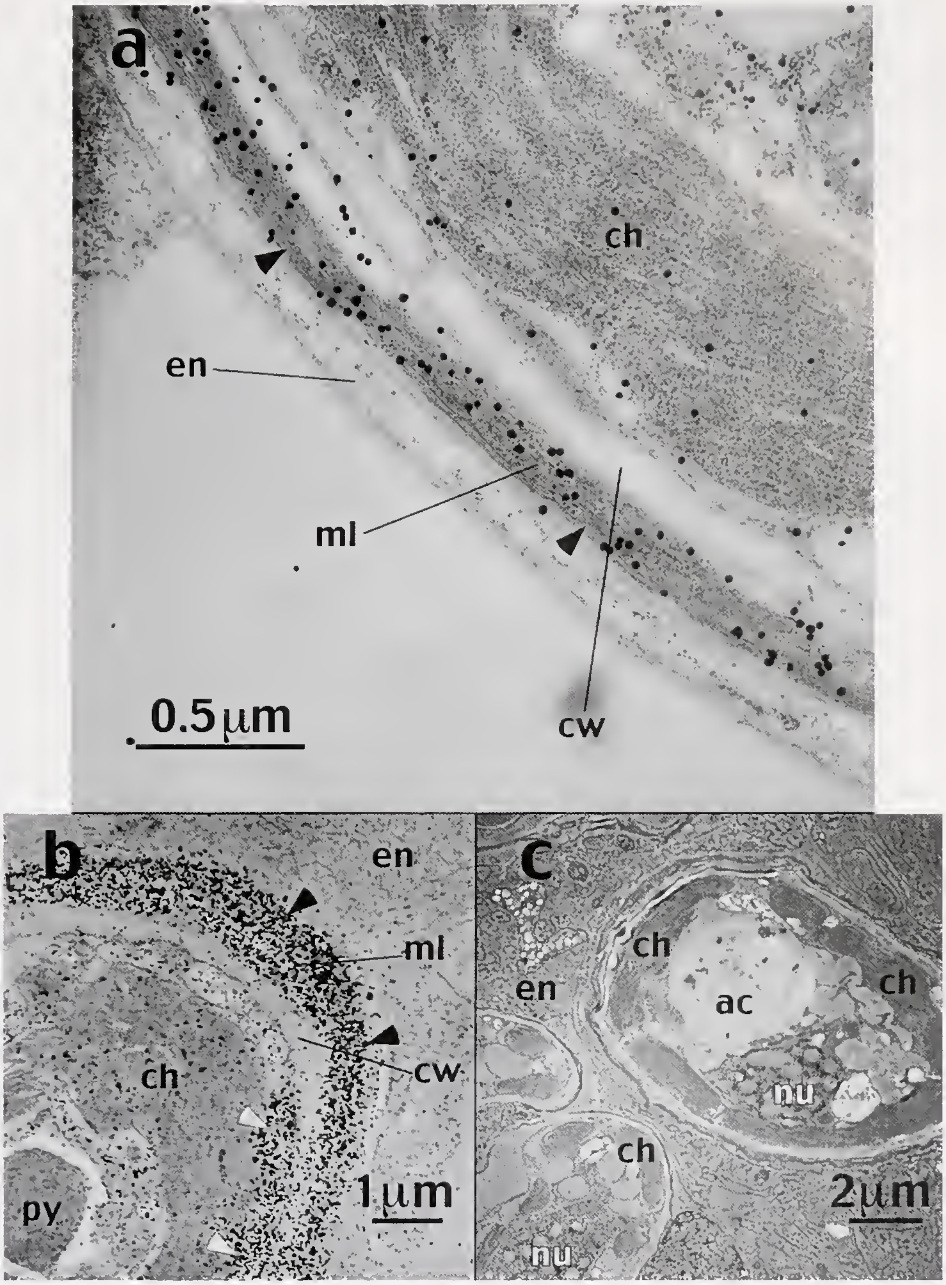

Figure 5. Freeze-substituted symbiotic *Aiptasia pallida* labeled with PC3 and an IgM-specific secondary antibody conjugated to an ultrasmall gold particle. The fixation of this tissue was extremely good for EM cytochemical studies. Both host and symbiont tissues were well preserved, and distinct morphological features were easily discernible. (a) Freeze-substituted symbiotic *A. pallida* tissue labeled with PC3 and ultrasmall gold antibody (1:100); arrowheads indicate label of multiple layers of membrane; note the absence of label in either the host endodermal layer or the symbiont's cell wall. (b) Specific labeling of symbiont membranes and no host-tissue labeling in freeze-substituted *A. pallida* labeled with PC3 and ultrasmall gold antibody (1:10); arrowheads indicate heavily labeled multiple layers of symbiont membranes; white arrowheads indicate abundance of PC3 antigen at the periphery of the algal cell. (c) Freeze-substituted *A. pallida* tissue negative control; blocking media followed by ultrasmall gold antibody (1:10); all negative controls appeared the same, with only minor background scattering of gold particles. ac = accumulation body, ch = chloroplast, cw = cell wall, en = host endodermal tissue, ml = multiple layer of symbiont membranes, nu = nucleus, py = pyrenoid.

labeling that is peripheral to the symbionts and is surrounded by a single, host-derived "symbiosome membrane" and also by a large ubiquitous area of G12 labeling illustrates that a limited layer of this symbiont-derived antigen is maintained within a vast amount of host tissue. The immunogold results indicate that the PC3 antigen is present in the

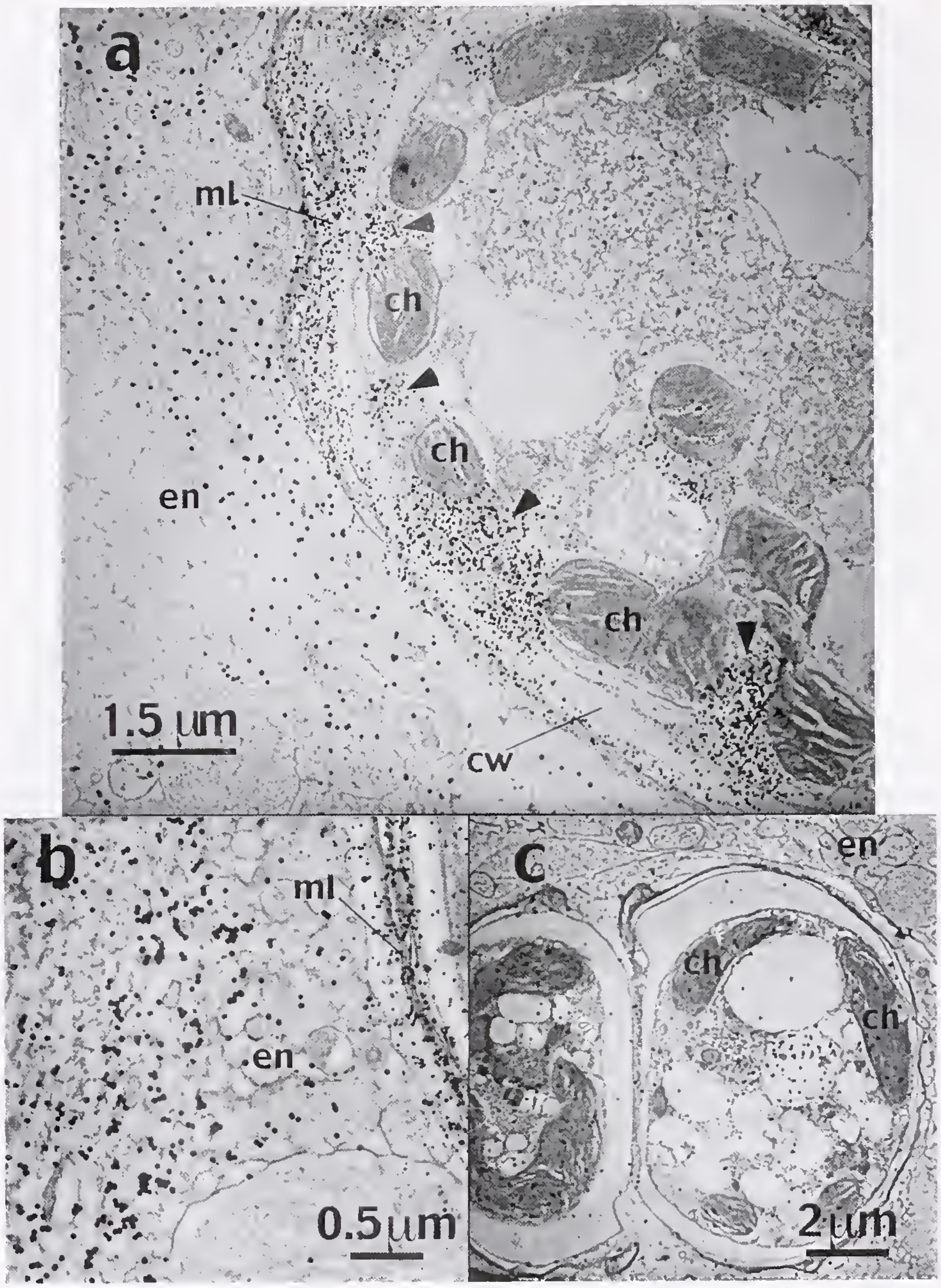

Figure 6. Freeze-substituted symbiotic *Aiptasia pallida* double labeled with both G12 and PC3 and with IgG-specific-antibody–20-nm gold particle and IgM-specific-antibody–ultrasmall gold particle. (a) Note the difference in particle size between the host membranes and the symbiont membranes and cytoplasm that clearly defines the distribution of the G12 (large particles) and PC3 (small particles) antigens; arrowheads indicate abundance of PC3 antigen at the periphery of the algal cell, particularly between the chloroplast profiles. (b) Higher magnification of the freeze-substituted symbiotic *A. pallida* double label, clearly showing the PC3-labeled symbiont membranes and the G12-labeled host membranes. (c) Freeze-substituted symbiotic *A. pallida* cross reactivity control in which PC3 was incubated with the IgG-specific secondary antibody; the slight cross reactivity of this nonspecific secondary antibody supports the assertion that PC3 is an algal-cell-specific antibody (note the lack of label in the host tissues). ch = chloroplast, cw = cell wall, en = host endodermal tissue, ml = multiple layer of symbiont membranes.

algal cell wall, but only in areas directly adjacent to high cytoplasmic levels of this antigen. This suggests that these may be areas of secretion for a molecule or molecules containing the PC3 antigen. The fact that the PC3 antigen is found both within the algal cell cytoplasm and also closely associated with the multiple layers of membrane, beneath the G12-labeled host symbiosome membrane, supports the hypothesis that these membranous layers are of symbiont rather than host origin.

The results of this research should help clarify some confusing terminology currently used in the field of cnidarian–dinoflagellate endosymbiosis. The term "symbiosome," as introduced by Roth *et al.* (1988), was defined as "a membrane-bound compartment containing one or more symbionts and certain metabolic components located in the cytoplasm of eukaryotic cells." They further describe the "symbiosome membrane" as being a host-derived membrane that surrounds the microsymbiont, creating a "symbiosome space" (Roth *et al.*, 1988). This terminology has been adopted by researchers in various fields of endosymbiotic research, including plant–bacteria interactions (Day and Udvardi, 1992; Udvardi and Day, 1997), protozoan–bacteria interactions (Choi and Jeon, 1992; Jeon, 1992), and invertebrate–algal interactions (Rands *et al.*, 1993; Wakefield *et al.*, 1998; Wakefield *et al.*, 2000). For plant–bacterial and protozoan–bacterial interactions, these terms are adequate and clearly define the endosymbiotic situation of these partners. However, for invertebrate–algal symbioses, particularly cnidarian–dinoflagellate symbioses, use of the term "symbiosome membrane" has been problematic.

In situ dinoflagellate symbionts have been identified as existing predominantly in a coccoid, or vegetative, state within the host cells (Trench and Blank, 1987). The coccoid state is defined by the presence of the spherical "pellicle," or cell wall. However, exterior to the cell wall exist multiple layers of apparent membranes. Historically, these layers have been referred to by a variety of terms, including the periplast (Dodge and Crawford, 1970; Kevin *et al.*, 1969; Palincsar *et al.*, 1988; Taylor, 1968; Trench and Blank, 1987), the amphiesma (Schoenberg and Trench, 1980a; Thinh *et al.*, 1986), the theca (Battey, 1992; Taylor, 1971), the vacuolar membranes (Colley and Trench, 1983), or simply the cell covering (Tripodi and Santisi, 1982). The origin of these membranes has also been debated for quite some time.

Tripodi and Santisi (1982), working with the symbiotic octocoral *Eunicella stricta*, assigned the multiple membranes to the host cell. They stated that the location of recognizable host organelles on the "inner side" of the membranes indicated that, in this host species, the membranes were composed of host plasmalemma. They also stated that the "many times folded" plasmalemma would have an increased surface area and thus could have a functional significance; however, they did not relate what this might be, nor did they indicate how the plasmalemma would accomplish this folding process (Tripodi and Santisi, 1982). Palinscar *et al.* (1988), working with *Aiptasia pallida*, also assigned the multiple membranes to the host but suggested that they were formed from internal host cell membranes rather than from the plasmalemma. They hypothesized that membrane-bound cytoplasmic extensions of host tissue could envelope the symbiont, followed by the extrusion of the cytoplasm. This would produce the multiple layers of membrane with no cytoplasmic separations (Palincsar *et al.*, 1988). Other authors, including Colley and Trench (1983) and Rands *et al.* (1993), have also assigned the origin of the multiple membranes to the host cell.

On the other hand, Kevin *et al.* (1969), Schoenberg and Trench (1980b), Trench and Blank (1987), and Muller-Parker *et al.* (1996) have identified a single host-derived membrane and assigned the origin of the multiple layers of membrane to the algal symbiont. Most do so without postulating a mechanism for how these membranes might be produced; however, Trench and Blank (1987) have suggested one possibility. They stated that the cell wall of symbionts is covered by an acidic polysaccharide or glycoprotein layer that resembles a membrane at the ultrastructural level, but in fact contains no lipids. They further suggested that this layer is occasionally sloughed off the outer surface of the cell wall. As these layers accumulate, they appear as multiple membranes exterior to the cell wall and produce the peripheral scroll-like layers of apparent membrane often seen in ultrastructural sections (Trench and Blank, 1987).

In earlier papers (Wakefield *et al.*, 1998, 2000), we also suggested that the membranes were derived from algal cells, but we proposed a very different mechanism for the production of these membranes than that put forth by Trench and Blank (1987). Briefly, we hypothesized that the algal symbionts were continuing through their normal ecdysis cycle within the host cell vacuole. By cycling through the coccoid-to-thecate stage and back again, a layer of apparent multiple membranes would accumulate between the host cell symbiosome membrane and the symbiont. The membranous layers would be composed of the sloughed plasma membrane, thecal vesicles, and plates from each ecdysis event. Therefore, we feel that any assignment of the multiple layers of membrane to the host (with the exception of the single outermost symbiosome membrane) is unsubstantiated and probably in error.

If the host-derived origin for the membranes were correct, then each and every membrane in the layer could be defined as the "symbiosome membrane," as defined by Roth *et al.* (1988). However, the results of labeling with our PC3 antibody indicate that the multiple layers of membrane lying between the host vacuole membrane and the symbiont cell wall originate from the algal symbiont and are held in place by the presence of a single host-derived membrane. Therefore, the host-derived membrane is the definitive symbiosome membrane, while the other apparent membranes could be defined as symbiont-derived "metabolic components" within the symbiosome space (see Roth's [1988] original definition of the symbiosome). However, designating these membranes as mere "metabolic components" may belie their potential importance to the symbiotic system. In subsequent text, the term "symbiont membranes" is used to describe these structures.

On the basis of the presence of the PC3 antigen within the symbiont membranes and the cytoplasm, it may be hypothesized that, during the ecdysis process, cytoplasmic material containing the PC3 antigen is also shed and becomes trapped between the layers of plasmalemma and thecal vesicles described by Wakefield *et al.* (2000). Another possibility is that the PC3 antigen is simply a substance exuded through the cell wall during the coccoid stage of the life cycle. This material could accumulate and become trapped between the layers of shed plasmalemma and thecal vesicles during ecdysis. Alternatively, if Trench and Blank (1987) are correct, exuded PC3 antigen would become trapped between the layers of polysaccharide or glycoprotein material that is occasionally sloughed from the outer cell wall.

Although the identification of the PC3 and G12 antigens is still under investigation in our laboratory, recent data indicate that the PC3 antigen is, in fact, an exuded material (Wakefield and Kempf, unpubl. data). Markell and Trench (1993) have demonstrated that cultured symbionts do exude large water-soluble glycoconjugates. If this exudate is produced *in situ* (in the symbiotic state), then these molecules could provide essential nutrients to the host (provided the host could digest them), and might also serve as molecular signals between the host and the symbiont (Markell and Trench, 1993).

The potential of the symbiont membranes (or trapped exudates) to act as molecular signals is suggested by the findings of Colley and Trench (1983). They performed a series of experiments in which freshly isolated symbiosomes from *Cassiopeia xamachana, Aiptasia pallida, A. pulchella, Anthopleura elegantissima,* and *Zoanthus* sp. were introduced into the gastrovascular cavity of aposymbiotic scyphistomae of *C. xamachana.* They also introduced cultured algae isolated from the cnidarian hosts *C. xamachana, A. pallida, A. tagetes,* and *Zoanthus sociatus.* They found that all cultured algae, even those that were specific for *C. xamachana,* were either completely rejected or phagocytosed at almost immeasurably low rates. By contrast, the freshly isolated symbiosomes from each host species were all phagocytosed at relatively rapid rates. When viewed with the transmission electron microscope, all of the freshly isolated symbionts were surrounded by multiple layers of apparent membrane. These membranes were completely absent from the cultured algal cells. After several experiments, the authors concluded that a recognition process must be occurring at the surface between the host endodermal cell and the specific membrane layers that surround the algal symbiont (Colley and Trench, 1983).

Believing that there were no algal cell membranes exterior to the cell wall, Colley and Trench (1983) assigned the origin of these membranes to the host and called them "vacuolar membranes." They hypothesized that the enhanced uptake of freshly isolated symbiosomes was a result of the presence of these host membranes, and that there must be a specific molecular factor involved. Since the host endodermal cell was making its initial contact with various "host membranes" of injected symbiosomes, they concluded that there was no actual intercellular (host–symbiont) recognition occurring, and that the uptake of symbiosomes might be indistinguishable from the phagocytosis of food particles.

As we have clearly demonstrated in this study, in *Aiptasia pallida* there are a multitude of symbiont-produced membranes or membrane-like layers that surround the algal cell wall and are associated with high concentrations of the symbiont-derived PC3 antigen. We postulate that the rapid uptake of isolated symbiosomes compared to the low uptake of cultured algae observed by Colley and Trench (1983) may have resulted from the absence of the correct molecular signal at the external surface of most cultured algal cells. Since our results reveal the PC3 antigen to be absent from most (but not all) suspended, cultured algal symbionts from *A. pallida* and *A. pulchella* and present in all symbiosomes *in situ,* it is possible that such an antigen may be the actual signal that stimulated rapid phagocytosis in the experiments of Colley and Trench (1983). Similarly, since cultured symbionts lack the multiple layers of symbiont membranes found *in situ,* it is also possible that these membranes may contain the molecular signal that stimulates phagocytosis. We feel that it would be useful to reexamine the question of host recognition of algal symbionts with attention to these possibilities.

It is unknown how aposymbiotic cnidarian offspring that must recruit their symbionts from the environment achieve an initial infection (Berner *et al.,* 1993; Davy *et al.,* 1997; Schwarz *et al.,* 1999); however, there is some support for the hypothesis that the motile thecate stage of the symbiont rather than the sessile coccoid stage is capable of infecting (Kinzie, 1974). If the plasmalemma of the thecate stage contains the appropriate molecular signal, these algal cells would be readily phagocytosed, thus resulting in the initial infection. If such signal molecules can stimulate phagocytosis, then other host- or symbiont-specific molecules must be involved in maintaining the symbiosis once it is established (Trench, 1993). Although Colley and Trench (1983) found that all of the freshly isolated symbionts were phagocytosed by *Cassiopeia xamachana* scyphistomae, only *Symbiodinium microadriaticum* and *S. bermudense* were ultimately maintained in the endodermal cells and could stimulate strobilation. Therefore, the signals that stimulate phagocytosis could not be the same as those that maintain the symbiosis.

Host–symbiont-specific signaling has been shown to occur in many other symbiotic associations such as the *Rhi-*

zobium–legume association (Lerouge *et al.*, 1990; Sanchez *et al.*, 1991), pathogenic-bacteria–plant interactions (Dixon and Lamb, 1990; Regensburg-Tuink and Hooykaas, 1993), *Mycobacterium*–macrophage invasions (Ferrari *et al.*, 1999), X-bacteria–amoeba symbiosis (Jeon, 1992, 1997), parasite–host infections (Sibley *et al.*, 1986; Sibley and Krahenbuhl, 1988; Perkins, 1989; Sam-Yellowe, 1992; Collins *et al.*, 1997), and diatom–foraminifera interactions (Lee *et al.*, 1988, 1997; Lee, 1998; Chai and Lee, 1999, 2000). In many of these associations, the specific signals leading to successful symbiotic interactions have been elucidated. *Agrobacterium tumefaciens,* a bacterium that induces tumors in many types of plants, is dependent upon the VirF protein for tumor formation (Regensburg-Tuink and Hooykaas, 1993). *Plasmodium falciparum* uses several proteins, including the 155-kDa ring-infected surface antigen and the 140/130/110/-kDa rhoptry complex, to bind to appropriate erythrocyte membranes (Sam-Yellowe, 1992). *Rhizobium meliloti* uses a β-1,4-tetrasaccharide of D-glucosamine to induce root nodules in alfalfa (Lerouge *et al.*, 1990). *Mycobacterium* species use the TACO protein to inhibit lysosomal fusion in macrophages (Ferrari *et al.*, 1999). The frustules of all endosymbiotic diatoms of large foraminifera display a 104-kDa polypeptide that prevents their digestion by the host (Chai and Lee, 1999).

Attempts to locate and characterize similar types of molecular signals required for establishing and maintaining zooxanthella–cnidarian symbioses have met with little success; however, the two reported attempts to identify these signals concentrated on the algal cell wall (Markell *et al.*, 1992) and on water-soluble glycoconjugates released by algal cells in culture (Markell and Trench, 1993). Because we have identified the symbiont membranes to be of algal-cell origin and intimately associated with a symbiont-derived antigen (PC3), and because an earlier investigation (Kinzie, 1974) supports the hypothesis that molecular signals associated with the thecate motile stage must stimulate phagocytosis, it may be hypothesized that these symbiont membranes are involved in this signal transduction event. It is likely that knowledge of the identity and function of such molecular signals will be critical to our understanding of the cellular mechanisms orchestrating events such as coral bleaching (Bunkley-Williams and Williams, 1990; Ghiold, 1990; Gleason and Wellington, 1993; Goreau and Hayes, 1994; Brown *et al.*, 1995), where such signaling capabilities have apparently been lost.

Acknowledgments

The authors thank David Werneke for many hours of hard work during the production of the two monoclonal antibodies. We also thank Dr. Hong Yi and Jan L. M. Leunissen for their aid, expertise, and generosity in supplying materials and advice concerning immunogold labeling. Dr. William Fitt and the Key Largo Marine Research Laboratory, and Dr. Mike Miller and the Auburn University Biological Electron Microscope Imaging Facility provided assistance with some aspects of this research. This work was supported by NSF #9018698 (SCK), NSF-BIR #9220230 (SCK), ONR #3231114 (SCK), and a grant from the Alabama Agricultural Experiment Station (SCK).

Literature Cited

Banaszak, A. T., R. Iglesias-Prieto, and R. K. Trench. 1993. *Scrippsiella velellae* sp. nov. (Peridiniales) and *Gloedodinium viscum* sp. nov. (Phytodiniales), dinoflagellate symbionts of two hydrozoans (Cnidaria). *J. Phycol.* **29:** 517–528.

Battey, J. F. 1992. Carbon metabolism in zooxanthellae–coelenterate symbiosis. Pp. 153–187 in *Algae and Symbioses,* W. Reiser, ed. Biopress, Bristol, England.

Berner, T., G. Baghdasarian, and L. Muscatine. 1993. Repopulation of a sea anemone with symbiotic dinoflagellates: analysis by *in vivo* fluorescence. *J. Exp. Mar. Biol. Ecol.* **170:** 145–158.

Blank, R. J. 1987. Cell architecture of the dinoflagellate *Symbiodinium* sp. inhabiting the Hawaiian stony coral *Montipora verrucosa. Mar. Biol.* **94:** 143–155.

Blank, R. J., and R. K. Trench. 1985. Speciation and symbiotic dinoflagellates. *Science* **229:** 656–658.

Brown, B. E., M. D. A. Letissier, and J. C. Bythell. 1995. Mechanisms of bleaching deduced from histological studies of reef corals sampled during a natural bleaching event. *Mar. Biol.* **122:** 655–663.

Bunkley-Williams, L., and E. H. Williams. 1990. Global assault on coral reefs. *Nat. Hist.* **99:** 46–54.

Chai, J., and J. J. Lee. 1999. Initial recognition of endosymbiotic diatom surface antigens by the larger foraminifer *Amphistegina lobifera. Symbiosis* **26:** 39–53.

Chai, J., and J. J. Lee. 2000. Recognition, establishment and maintenance of diatom endosymbiosis in foraminifera. *Micropaleontology* **46:** 182–195.

Chang, S. S., and R. K. Trench. 1982. Peridinin-chlorophyll *a*-proteins from the symbiotic dinoflagellate *Symbiodinium* (= *Gymnodinium*) *microadriaticum* Freudenthal. *Proc. R. Soc. Lond. B.* **215:** 191–210.

Chang, S. S., B. B. Prezelin, and R. K. Trench. 1983. Mechanisms of photoadaptation in three strains of the symbiotic dinoflagellate *Symbiodinium microadriaticum. Mar. Biol.* **76:** 219–231.

Choi, E. Y., and K. W. Jeon. 1992. Bacterial-endosymbiote-derived lipopolysaccharides on amoeba symbiosome membranes. *J. Protozool.* **39:** 205–210.

Colley, N. J., and R. K. Trench. 1983. Selectivity in phagocytosis and persistence of symbiotic algae by the scyphistoma stage of the jellyfish *Cassiopeia xamachana. Proc. R. Soc. Lond. B* **219:** 61–82.

Collins, H. L., U. E. Schaible, J. D. Ernst, and D. G. Russell. 1997. Transfer of phagocytosed particles to the parasitophorous vacuole of *Leishmania mexicana* is a transient phenomenon preceding the acquisition of annexin I by the phagosome. *J. Cell Sci.* **110:** 191–200.

Davy, S. K., I. A. N. Lucas, and J. R. Turner. 1997. Uptake and persistence of homologous and heterologous zooxanthellae in the temperate sea anemone *Cereus pedunculatus* (Pennant). *Biol. Bull.* **192:** 208–216.

Day, D. A., and M. K. Udvardi. 1992. Metabolite exchange across symbiosome membranes. *Symbiosis* **14:** 175–189.

Dixon, R. A., and C. J. Lamb. 1990. Molecular communication in interactions between plants and microbial pathogens. *Annu. Rev. Plant Physiol.* **41:** 339–367.

Dodge, J. D., and R. M. Crawford. 1970. A survey of thecal fine structure in the Dinophyceae. *Bot. J. Linn. Soc.* **63:** 53–67.

Ferrari, G., H. Langen, M. Naito, and J. Pieters. 1999. A coat protein on phagosomes involved in the intracellular survival of mycobacteria. *Cell* **97:** 435–447.

Fitt, W. K., and R. K. Trench. 1981. Spawning, development, and acquisition of zooxanthellae by *Tridacna squamosa* (Mollusca, Bivalvia). *Biol. Bull.* **161:** 213–235.

Fitt, W. K., and R. K. Trench. 1983. Endocytosis of the symbiotic dinoflagellate *Symbiodinium microadriaticum* Freudenthal by endodermal cells of the scyphistomae of *Cassiopeia xamachana* and resistance of the algae to host digestion. *J. Cell Sci.* **64:** 195–212.

Forero, M. E., M. Marin, A. Corrales, I. Llano, H. Moreno, and M. Camacho. 1999. *Leishmania amazonensis* infection induces changes in the electrophysiological properties of macrophage-like cells. *J. Membr. Biol.* **170:** 173–180.

Freudenthal, H. D. 1962. *Symbiodinium* gen. nov. and *Symbiodinium microadriaticum* sp. nov., a zooxanthella: taxonomy, life cycle and morphology. *J. Protozool.* **9:** 45–52.

Ghiold, J. 1990. White death: the fate of a deserted coral. *New Sci.* **126:** 46.

Giloh, H., and J. W. Sedat. 1982. Fluorescence microscopy: reduced photo-bleaching of rhodamine and fluorescein protein conjugates by *n*-propyl gallate. *Science* **217:** 1252–1255.

Gleason, D. F., and G. M. Wellington. 1993. Ultraviolet radiation and coral bleaching. *Nature* **365:** 836–838.

Goreau, T. J., and R. L. Hayes. 1994. Coral bleaching and ocean "hot spots." *Ambio* **23:** 176–180.

Govind, N. S., S. J. Roman, R. Iglesias-Prieto, R. K. Trench, E. L. Triplett, and B. B. Prezelin. 1990. An analysis of the light-harvesting peridinin–chlorophyll *a*-proteins from dinoflagellates by immunoblotting techniques. *Proc. R. Soc. Lond. B.* **240:** 187–195.

Hall, B. F., G. C. Furtado, and K. A. Joiner. 1991. Characterization of host cell-derived membrane proteins of the vacuole surrounding different intracellular forms of *Trypanosoma cruzi* in J774 cells. *J. Immunol.* **147:** 4313–4321.

Jeon, K. W. 1992. Macromolecules involved in the amoeba–bacteria symbiosis. *J. Protozool.* **39:** 199–204.

Jeon, K. W. 1997. Symbiosis and macromolecules. Pp. 359–366 in *Eukaryotism and Symbiosis,* H. E. A. Schenk, R. G. Herrman, K. W. Jeon, N. E. Muller, and W. Schwemmler, eds. Springer-Verlag, Heidelberg.

Jeon, K. W., and M. S. Jeon. 1976. Endosymbiosis in amoebae: recently established endosymbionts have become required cytoplasmic components. *J. Cell. Physiol.* **89:** 337–347.

Kevin, M. J., W. T. Hall, J. J. A. McLaughlin, and P. A. Zahl. 1969. *Symbiodinium microadriaticum* Freudenthal, a revised taxonomic description, ultrastructure. *J. Phycol.* **5:** 341–350.

Kinzie, R. A., III. 1974. Experimental infection of aposymbiotic gorgonian polyps with zooxanthellae. *J. Exp. Mar. Biol. Ecol.* **15:** 333–345.

Kohler, G., and C. Milstein. 1975. Continuous cultures of fused cells secreting antibody of predefined specificity. *Nature* **256:** 495–497.

Lee, J. J. 1998. "Living sands"—larger foraminifera and their endosymbiotic algae. *Symbiosis* **25:** 71–100.

Lee, J. J., and O. R. Anderson. 1991. Symbiosis in foraminifera. Pp. 157–220 in *Biology of Foraminifera,* J. J. Lee and O. R. Anderson, eds. Academic Press, London.

Lee, J. J., Y. Chan, and A. Lagziel. 1988. An immunofluorescence approach toward the identification of endosymbiotic diatoms in several species of larger formaminifera. Pp. 230–241 in *Immunochemical Approaches to Coastal, Estuarine, and Oceanographic Questions,* C. M. Yentsch, F. C. Mague, and P. K. Horan, eds. Springer-Verlag, New York.

Lee, J. J., J. Morales, J. Chai, C. Wray, and R. Rottger. 1997. Progress in the studies of endosymbiotic algae from larger foraminifera. Pp. 329–344 in *Eukaryotism and Symbiosis,* H. E. A. Schenk, R. G. Herrman, K. W. Jeon, N. E. Muller, and W. Schwemmler, eds. Springer-Verlag, Heidelberg.

Lerouge, P., P. Roche, C. Faucher, F. Maillet, G. Truchet, J. C. Prome, and J. Denaire. 1990. Symbiotic host-specificity of *Rhizobium meliloti* is determined by a sulfated and acylated glucosamine oligosaccharide signal. *Nature* **344:** 781–784.

Markell, D. A., and R. K. Trench. 1993. Macromolecules exuded by symbiotic dinoflagellates in culture: amino acid and sugar composition. *J. Phycol.* **29:** 64–68.

Markell, D. A., R. K. Trench, and R. Iglesias-Prieto. 1992. Macromolecules associated with the cell walls of symbiotic dinoflagellates. *Symbiosis* **12:** 19–31.

McNally, K. L., N. S. Govind, P. E. Thome, and R. K. Trench. 1994. Small-subunit ribosomal DNA sequence analyses and a reconstruction of the inferred phylogeny among symbiotic dinoflagellates (Pyrrophyta). *J. Phycol.* **30:** 316–329.

Muller-Parker, G., K. W. Lee, and C. B. Cook. 1996. Changes in the ultrastructure of symbiotic zooxanthellae (*Symbiodinium* sp., Dinophyceae) in fed and starved sea anemones maintained under high and low light. *J. Phycol.* **32:** 987–994.

Palincsar, J. S., W. R. Jones, and E. E. Palincsar. 1988. Effects of isolation of the endosymbiont *Symbiodinium microadriaticum* (Dinophyceae) from its host *Aiptasia pallida* (Anthozoa) on cell wall ultrastructure and mitotic rates. *Trans. Am. Microsc. Soc.* **107:** 53–66.

Perkins, M. 1989. Erythrocyte invasion by the malarial merozoite: recent advances. *Exp. Parasitol.* **69:** 94–99.

Rands, M. L., B. C. Loughman, and A. E. Douglas. 1993. The symbiotic interface in an alga–invertebrate symbiosis. *Proc. R. Soc. Lond. B* **253:** 161–165.

Regensburg-Tuink, A. J. G., and P. J. J. Hooykaas. 1993. Transgenic *N. glauca* plants expressing bacterial virulence gene *virF* are converted into hosts for nopaline strains of *A. tumefaciens*. *Nature* **363:** 69–71.

Roth, K. E., K. Jeon, and G. Stacey. 1988. Homology in endosymbiotic systems: the term "Symbiosome." Pp. 220–225 in *Molecular Genetics of Plant–Microbe Interactions,* R. Palacios and D. P. S. Verma, eds. APS Press, St. Paul, MN.

Rowan, R. 1991. Molecular systematics of symbiotic algae. *J. Phycol.* **27:** 661–666.

Rowan, R. 1998. Diversity and ecology of zooxanthellae on coral reefs. *J. Phycol.* **34:** 407–417.

Rowan, R., and D. A. Powers. 1991. A molecular genetic classification of zooxanthellae and the evolution of animal–algal symbioses. *Science* **251:** 1348–1351.

Russell, D. G., S. Xu, and P. Chakraborty. 1992. Intracellular trafficking and the parasitophorous vacuole of *Leishmania mexicana*-infected macrophages. *J. Cell Sci.* **103:** 1193–1210.

Sam-Yellowe, T. Y. 1992. Molecular factors responsible for host cell recognition and invasion in *Plasmodium falciparum*. *J. Protozool.* **39:** 181–189.

Sanchez, F., J. E. Padilla, H. Perez, and M. Lara. 1991. Control of nodulin genes in root-nodule development and metabolism. *Annu. Rev. Plant Physiol.* **42:** 507–528.

Schoenberg, D. A., and R. K. Trench. 1980a. Genetic variation in *Symbiodinium* (=*Gymnodinium*) *microadriaticum* Freudenthal, and specificity in its symbiosis with marine invertebrates. I. Isoenzyme and soluble protein patterns of axenic cultures of *Symbiodinium microadriaticum*. *Proc. R. Soc. Lond. B* **207:** 405–427.

Schoenberg, D. A., and R. K. Trench. 1980b. Genetic variation in *Symbiodinium* (=*Gymnodinium*) *microadriaticum* Freudenthal, and specificity in its symbiosis with marine invertebrates. II Morphological variation in *Symbiodinium microadriaticum*. *Proc. R. Soc. Lond. B* **207:** 429–444.

Schwarz, J. A., D. A. Krupp, and V. M. Weis. 1999. Late larval development and onset of symbiosis in the scleractinian coral *Fungia scutaria*. *Biol. Bull.* **196:** 70–79.

Sibley, L. D., and J. L. Krahenbuhl. 1988. Modification of host cell phagosomes by *Toxoplasma gondii* involves redistribution of surface proteins and secretion of a 32 kDa protein. *Eur. J. Cell Biol.* **47:** 81–87.

Sibley, L. D., J. L. Krahenbuhl, G. M. W. Adams, and E. Weidner. 1986. *Toxoplasma* modifies macrophage phagosomes by secretion of a vesicular network rich in surface proteins. *J. Cell Biol.* **103:** 867–874.

Taylor, D. L. 1968. *In situ* studies on the cytochemistry and ultrastructure of a symbiotic marine dinoflagellate. *J. Mar. Biol. Assoc. UK* **48:** 349–366.

Taylor, D. L. 1971. Ultrastructure of the 'zooxanthella' *Endodinium chattonii in situ*. *J. Mar. Biol. Assoc. UK* **51:** 227–234.

Thinh, L. V., D. J. Griffiths, and H. Winsor. 1986. Ultrastructure of *Symbiodinium microadriaticum* (Dinophyceae) symbiotic with *Zoanthus* sp. (Zoanthidea). *Phycologia* **25:** 178–184.

Trench, R. K. 1993. Microalgal–invertebrate symbioses: a review. *Endocytobiosis Cell Res.* **9:** 135–175.

Trench, R. K., and R. J. Blank. 1987. *Symbiodinium microadriaticum* Freudenthal, *S. goreauii*, sp. nov., *S. kawagutii*, sp. nov., and *S. pilosum*, sp. nov.: gymnodinioid dinoflagellate symbionts of marine invertebrates. *J. Phycol.* **23:** 469–481.

Trench, R. K., and H. Winsor. 1987. Symbiosis with dinoflagellates in two pelagic flat worms *Amphiscolops* sp. and *Haplodiscus* sp. *Symbiosis* **3:** 1–22.

Tripodi, G., and S. Santisi. 1982. A study on the cell covering of *Symbiodinium*, a symbiote of the octocoral *Eunicella*. *J. Submicrosc. Cytol.* **14:** 613–620.

Udvardi, M. K., and D. A. Day. 1997. Metabolite transport across symbiotic membranes of legume nodules. *Annu. Rev. Plant Physiol. Plant Mol. Biol.* **48:** 493–523.

Wakefield, T. S., S. C. Kempf, and M. A. Farmer. 1998. The contribution of *Symbiodinium microadriaticum* to the symbiosome membrane in the anthozoan host *Aiptasia pallida*. *Microsc. Microanal.* **4:** 1182–1183.

Wakefield, T. S., M. A. Farmer, and S. C. Kempf. 2000. Revised description of the fine structure of *in situ* "zooxanthellae" genus *Symbiodinium*. *Biol. Bull.* **199:** 76–84.

INVERTEBRATE SENSORY INFORMATION PROCESSING: Implications for Biologically Inspired Autonomous Systems

Proceedings
of a workshop
sponsored by
THE CENTER FOR ADVANCED STUDIES
IN THE SPACE LIFE SCIENCES
AT THE MBL

15 to 17 June 2000

J. Erik Jonsson Center
for the National Academy of Sciences,
Woods Hole, Massachusetts

Funded by THE NATIONAL AERONAUTICS AND SPACE ADMINISTRATION under Cooperative Agreement NCC 2-896. Reprints of this symposium can be obtained from the Center for Advanced Studies in the Space Life Sciences, 7 MBL Street, Woods Hole, MA 02543.

CONTENTS

Invertebrate Sensory Information Processing: Implications for Biologically Inspired Autonomous Systems

Blazis, Diana E. J., and Frank W. Grasso
Introduction 147

Breithaupt, Thomas
Fan organs of crayfish enhance chemical information flow 150

Fraser, Peter J.
Statocysts in crabs: short-term control of locomotion and long-term monitoring of hydrostatic pressure . . 155

Grasso, Frank W.
Invertebrate-inspired sensory-motor systems and autonomous, olfactory-guided exploration 160

Barlow, Robert B., James M. Hitt, and Frederick A. Dodge
Limulus vision in the marine environment 169

Cronin, Thomas W., and Justin Marshall
Parallel processing and image analysis in the eyes of mantis shrimps 177

Webb, Barbara
View from the boundary 184

Robert, Daniel
Innovative biomechanics for directional hearing in small flies. 190

Schmitz, Josef, Jeffrey Dean, Thomas Kindermann, Michael Schumm, and Holk Cruse
A biologically inspired controller for hexapod walking: simple solutions by exploiting physical properties. . . . 195

Macmillan, David L., and Blair W. Patullo
Insights for robotic design from studies of the control of abdominal position in crayfish. 201

Birmingham, J. T.
Increasing sensor flexibility through neuromodulation 206

Derby, Charles D., and Pascal Steullet
Why do animals have so many receptors? The role of multiple chemosensors in animal perception 211

Srinivasan, Mandyam V., Shaowu Zhang, and Javaan S. Chahl
Landing strategies in honeybees and possible applications to autonomous airborne vehicles 216

Ishida, H., T. Nakamoto, T. Moriizumi, T. Kikas, and J. Janata
Plume-tracking robots: a new application of chemical sensors. 222

Mountain, David C., and Allyn E. Hubbard
Sensing scenes with silicon 227

Higgins, Charles M.
Sensory architectures for biologically inspired autonomous robotics 235

List of Participants 243

Reference: *Biol. Bull.* **200:** 147–149. (April 2001)

Introduction

DIANA E. J. BLAZIS[1] AND FRANK W. GRASSO[2,*]

[1]*The Center for Advanced Studies in the Space Life Sciences, Marine Biological Laboratory, Woods Hole, Massachusetts; and* [2]*Boston University Marine Program, Marine Biological Laboratory, Woods Hole, Massachusetts 02453*

This workshop—entitled "Invertebrate Sensory Information Processing: Implications for Biologically Inspired Autonomous Systems"—was sponsored by the Center for Advanced Studies in the Space Life Sciences at the Marine Biological Laboratory. At this meeting, scientific leaders in the fields of invertebrate sensory biology and sensory-guided behavior were brought together with biologists and engineers who develop robotic systems that are based on biologically inspired algorithms and architectures. The participants discussed how moderately complex metazoan organisms (*e.g.*, insects, crustaceans, and cephalopods) process the sensory information that is required to perform natural tasks in a changeable, dynamic environment. They also critiqued the extant, man-made autonomous systems that were built to emulate various invertebrate abilities (*e.g.*, fly in-flight control of air-speed for landing or maintaining course; crustacean ability to track a turbulent odor plume to its source; sensory compensation for lost appendages in walking insects; cricket and parasitic fly recognition; and tracking of a specific acoustic signature in a noisy background). The participants considered the gaps in our knowledge about biological sensory information processing and the limitations in our present technology, both of which limit the transfer of biological competence to man-made autonomous systems. They also identified and debated established and speculative biological concepts and technologies that will facilitate the development of autonomous systems with invertebrate levels of capabilities.

The proceedings of this workshop comprise a substantial subset of the presentations delivered at the meeting, and thus reflect the major themes that emerged during those discussions. These themes are highlighted in the following summary of the papers making up the proceedings.

The variety of modalities of information processing that are used by invertebrates are well represented in the proceedings. In many cases, these modalities may be useful in the exploration of novel environments. For example, invertebrates use polarization and multi-spectral imaging (Cronin and Marshall, 2001). Invertebrate chemoreception includes examples of the identification and classification of complex odors *via* a range of bimodal sensors (Derby and Steullet, 2001). Tunable sensors are used in acoustic processing to expand the available range, while filtering out background noise and locking onto important or new signals (Mountain and Hubbard, 2001; Robert, 2001; Webb, 2001). Understanding these forms of information processing and their roles in certain environmental niches can illuminate our knowledge of sensory biology and expand our options for sensory processing in autonomous systems.

Many invertebrate systems are robust across a wide range of conditions and make efficient use of limited material and energy. This robustness results, in part, from close coupling between sensory and motor systems: vision (Srinivasan *et al.*, 2001; Barlow *et al.*, 2001); olfaction (Derby and Steullet, 2001; Grasso, 2001); audition (Mountain and Hubbard, 2001; Robert, 2001); vestibular senses (Fraser, 2001); rheosense (Breithaupt, 2001). Natural organisms seem not to calculate exact solutions to equations; rather they perform tasks only approximately—just exactly enough to survive—as stick insects do when they target the posterior leg onto the position of the anterior leg during walking (Schmitz *et al.*, 2001). Elegant studies of visual guidance for fly landing provide a powerful example of this coupling (Srinivasan *et al.*, 2001): simple mechanisms suffice because the motor systems provide a predictable sampling context. Examples like this clearly show that, as the functional origins of robust invertebrate behavior in dynamic environments are better understood, valuable insights about

---

[*] Current address: Department of Psychology, Brooklyn College, CUNY, 2900 Bedford Ave., Brooklyn, New York 11210.

the engineering of autonomous systems that can explore unfamiliar or variable environments will be provided.

Invertebrate sensory systems are flexible, and dynamism is built into every processing stage. Contrary to traditional neurobiological dogma, we find plasticity present in abundance in invertebrate systems. Sensory receptors are plastic and show adaptation (Barlow *et al.*, 2001; Fraser, 2001; Mountain and Hubbard, 2001; Robert, 2001); central processes, including learning and memory, augment sensory processing, and the animals themselves show behavioral plasticity (Macmillan and Patullo, 2001; Breithaupt, 2001). Changes in sensory networks have been interpreted as instances of a system adapting to ("discovering") causal relationships in the environment (Birmingham, 2001; Schmitz *et al.*, 2001). Sensory systems can adapt to the statistics of natural scenes, as noted by Breithaupt in crayfish. Indeed, the ability to express these levels of dynamic processing means that an animal is capable of engineering new circuits "on the fly."

Redundancy is a feature of biological sensory systems that assures the attainability of a particular goal. During olfactory learning in spiny lobsters, for example, discrimination, local searching, and distance orientation are carried out by two separate pathways, as described by Derby and Steullet (2001). But *apparent* redundancy can, in fact, disguise an organization that produces deeper computational and energetic savings (Higgins, 2001).

In general, invertebrates make greater use than vertebrates of multi-modal, multifunctional sensor arrays. Thus, statocysts are used for angular and linear acceleration, vibration, and hydrostatic pressure sensing (Fraser, 2001). Birmingham described the stretch receptor in the crustacean foregut that functions at different times, either as a strain gauge or a volume sensor. Crustacean antennules combine information from flow and chemical sensors located on the same anatomical structure, and can therefore make spatial and temporal correlations across these two modalities (Breithaupt, 2001; Grasso, 2001; Derby and Steullet, 2001). This ability to multitask sensory inputs has implications for the design and implementation of light, efficient systems.

Our understanding of sensory systems and our development of useful autonomous systems depend upon having the best information possible about the to-be-explored environment, as well as stimulus dynamics in those environments. Understanding the stimulus environment speaks to the "design" of sensory receptors and processors and clarifies the evolutionary pressures that shape both the sensory biology and the behavioral choices of an organism. Several investigators, particularly those examining chemosensory behaviors (*e.g.*, Breithaupt, 2001; Grasso, 2001; and Ishida *et al.*, 2001), described their work in stimulus dynamics (*e.g.*, the odor plume as viewed through a single stationary or moving sensor shows complex time series). Obviously, an unexplored environment is one for which limited information is available, but systems deployed in unfamiliar environments must be able to survive and function through interpretation of the sense data that are available to them.

Two strategies for robot building emerged at this workshop. First, ideas borrowed from biology can be used in the design and construction of robots that are meant to accomplish a particular task. Examples of this approach include the robots designed by Ishida *et al.* (2001). In the second strategy, followed for example by Grasso (2001) and Webb (2001), biomimetic robots were used as platforms for hypothesis testing. Both approaches involve common ground upon which biologists and engineers can collaborate and progress effectively.

Robert Barlow, in his presentation (Barlow *et al.*, 2001), noted that the field of invertebrate sensory biology began in 1926 at Woods Hole with the investigations of Haldan Keffer Hartline (co-recipient of the Nobel Prize in Medicine, 1967). It is thus appropriate that more than 70 years later, scientists and engineers gathered at Woods Hole to assess our present understanding of invertebrate information processing. From the theoretical and empirical insights of neuroscientists and neuroethologists like H. K. Hartline, we look toward a deeper, future understanding that will use physical models to implement theories of biological information processing in natural physical environments. These are the most rigorous and realistic of testing conditions for theories. They are also our best models for the complex historic environments that shaped the evolution of the invertebrate body, brain, and behavior.

The Center for Advanced Studies in the Space Life Sciences (CASSLS) was established in 1999 through a cooperative agreement between the Marine Biological Laboratory and the Life Sciences Division of the National Aeronautics and Space Administration. The Center acts as an interface between NASA and the basic science community, promoting interactions and discussion in areas of basic biology that are of mutual interest. This workshop is an example of the many ways in which the Center achieves these goals.

Literature Cited

Barlow, R. B., J. M. Hitt, and F. A. Dodge. 2001. *Limulus* vision in the marine environment. *Biol. Bull.* **200:** 169–176.

Birmingham, J. T. 2001. Increasing sensor flexibility through neuromodulation. *Biol. Bull.* **200:** 206–210.

Breithaupt, T. 2001. Fan organs of crayfish enhance chemical information flow. *Biol. Bull.* **200:** 150–154.

Cronin, T. W., and J. Marshall. 2001. Parallel processing and image analysis in the eyes of mantis shrimps. *Biol. Bull.* **200:** 177–183.

Derby, C. D., and P. Steullet. 2001. Why do animals have so many receptors? The role of multiple chemosensors in animal perception. *Biol. Bull.* **200:** 211–215.

Fraser, P. J. 2001. Statocysts in crabs: short-term control of locomotion and long-term monitoring of hydrostatic pressure. *Biol. Bull.* **200:** 155–159.

Grasso, F. W. 2001. Invertebrate-inspired sensory-motor systems and autonomous, olfactory-guided exploration. *Biol. Bull.* **200:** 160–168.

Higgins, C. M. 2001. Sensory architectures for biologically inspired autonomous robotics. *Biol. Bull.* **200:** 235–242.

Ishida, H., T. Nakamoto, T. Moriizumi, T. Kikas, and J. Janata. 2001. Plume-tracking robots: a new application of chemical sensors. *Biol. Bull.* **200:** 222–226.

Macmillan, D. L., and B. W. Patullo. 2001. Insights for robotic design from studies of the control of abdominal position in crayfish. *Biol. Bull.* **200:** 201–205.

Mountain, D. C., and A. E. Hubbard. 2001. Sensing scenes with silicon. *Biol. Bull.* **200:** 227–234.

Robert, D. 2001. Innovative biomechanics for directional hearing in small flies. *Biol. Bull.* **200:** 190–194.

Schmitz, J., J. Dean, T. Kindermann, M. Schumm, and H. Cruse. 2001. A biologically inspired controller for hexapod walking: simple solutions by exploiting physical properties. *Biol. Bull.* **200:** 195–200.

Srinivasan, M. V., S. Zhang, and J. S. Chahl. 2001. Landing strategies in honeybees and possible applications to autonomous airborne vehicles. *Biol. Bull.* **200:** 216–221.

Webb, B. 2001. View from the boundary. *Biol. Bull.* **200:** 184–189.

Reference: *Biol. Bull.* **200:** 150–154. (April 2001)

Fan Organs of Crayfish Enhance Chemical Information Flow

THOMAS BREITHAUPT

Fakultät für Biologie, Universität Konstanz, Postfach 5560, 78457 Konstanz, Germany

Abstract. Animals as well as autonomous robots need to acquire environmental signals in order to adjust their activity in time and space. Some information is accessible to the sensors only as a result of specific behaviors for stimulus acquisition. Due to the slow rate of molecular diffusion, dispersal of chemical stimuli depends on fluid flow. Aquatic crustaceans can generate directed water currents by specialized appendages. Here I describe the crayfish fan organs, which are feathered flagella of the mouthparts, and their activity in sending and receiving chemical signals in environments with stagnant flow conditions. During the power-stroke, the fan opens and displaces water; during the return stroke, it collapses and thereby minimizes drag. These organs can create a variety of flow fields including water jets, and in many different directions. Bilateral upward fanning draws water horizontally from all directions toward the anterior chemoreceptors. Unilateral upward fanning draws water from only one side towards the body. The versatility of the crayfish fan organ makes it a candidate for biomimetic reconstruction and use in autonomous robots that can search chemical sources.

Exchange of Chemical Information at Different Size Scales

A prerequisite of life is the exchange of matter and information between an organism and its environment. Whereas the exchange of (organic) matter is necessary for nutrient uptake by and waste removal from living organisms, the acquisition of information that serves to modify the behavior of organisms with respect to environmental resources (*e.g.*, water, food, mates) and threats (*e.g.*, predators, obstacles) is important for any living organism as well as for autonomous robots.

The oldest method of information exchange is by means of chemical stimuli. Microorganisms (*e.g.*, motile bacteria) need to search for micropatches of higher nutrient concentration and adjust their motility with respect to chemical stimuli (Blackburn *et al.*, 1998). Microorganisms also exchange chemical signals ("pheromones") with conspecifics to synchronize their mating activity (Agosta, 1992). The movement of chemicals from a source to a receiver at such small size scales (below 0.1 mm, Reynolds number below 10^{-2}) is driven by molecular diffusion, or random molecular motion. Cohesion among water molecules at that scale makes it almost impossible to influence the direction of chemical information flow except by locomotion of the whole organism.

With increasing size and velocity of organisms (increasing Reynolds number) molecular diffusion loses in importance for the dispersal of chemicals (Weissburg, 2000). In water, molecular diffusion is a very slow process that on average would displace a molecule by no more than 0.7 mm (70 mm in air) in 1 min and by only 5 mm (500 mm in air) in 1 h (Dusenbery, 1992). Water flow is much more effective in dispersing odor molecules, and animals can influence the flow in their immediate neighborhood by using undulating, beating, or fanning appendages. By modulating the nearby flow pattern, they can facilitate the exchange of chemical information with their environment. Insects as well as some vertebrates use wing-fanning for delivering pheromones to their mates (bees: Free, 1987; butterflies: Boppré, 1984; bats: Voigt and von Helversen, 1999). Wing-fanning may facilitate odor perception by drawing nearby

---

E-mail: Thomas.Breithaupt@uni-konstanz.de

This paper was originally presented at a workshop titled *Invertebrate Sensory Information Processing: Implications for Biologically Inspired Autonomous Systems.* The workshop, which was held at the J. Erik Jonsson Center for the National Academy of Sciences, Woods Hole, Massachusetts, from 15–17 April 2000, was sponsored by the Center for Advanced Studies in the Space Life Sciences at the Marine Biological Laboratory, and funded by the National Aeronautics and Space Administration under Cooperative Agreement NCC 2-896.

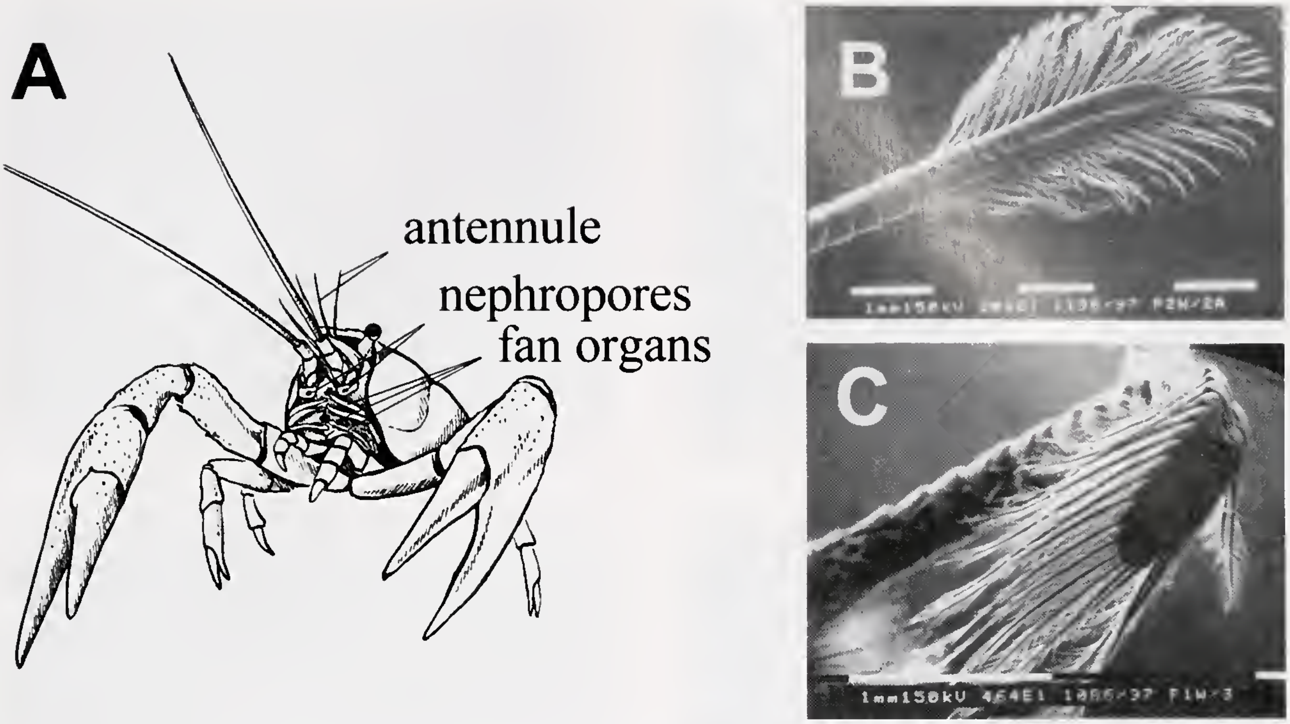

Figure 1. (A) Location of fan organs, urinary pores (nephropores), and major chemoreceptor organs (antennules) of crayfish. (B) The fan organs are multi-segmental flagella of the mouthparts (maxillipeds) with feathered setae on the distal part. During the power stroke (scanning electron microscopy "SEM" picture of *Procambarus clarkii*) the feathered hairs are extended. (C) During the recovery stroke (SEM picture of *Procambarus clarkii*) the feathered hairs are tilted downstream. White scale bars in SEM pictures represent 1 mm.

molecules towards the receptors. Wing-fanning of silkworm moths in response to pheromone (Agosta, 1992) may aid in stimulus acquisition (Ishida *et al.,* 1996). Crustaceans are well known for their ability to create directed water currents by pumping or fanning appendages (Brock, 1926; Burrows and Willows, 1969; Budd *et al.*, 1979; Koehl and Strickler, 1981; Atema, 1985; Lavalli and Factor, 1995). This behavior can be used for gill ventilation, locomotion, suspension feeding, and chemoreception or chemical signaling. Planktonic copepods, small crustaceans of 1 to 10 mm, generate water currents that are used for capturing food particles and that carry odor information from the food particles to the chemoreceptors (Yen, 2000). Here I describe the fanning behavior of crayfish, typical of larger crustaceans, that is used for both sending and receiving chemical signals in aquatic environments with stagnant flow conditions.

Maxilliped Flagella, the Fan Organs of Crayfish

One of the first reactions of many crustaceans to chemical stimulation is the onset of the rhythmic beating of three pairs of flagella of the maxillipeds (mouthparts). These so-called fan organs (Atema, 1985) in crayfish are distributed around the mouth opening below the major chemoreceptor organs ("antennules") and the urinary pore ("nephropore") (Fig. 1A). Each fan organ consists of a multi-segmental, flattened stem. It is feathered in one plane, with setae emerging laterally on both sides of the flattened stem (Fig. 1B). The setae are feathered themselves, and their rami overlap with those of adjacent setae to form a dense layer (Fig. 1B). During the power stroke, the fan—with stem erect and setae extended—acts like a paddle propelling fluid past the organism (Fig. 1B; Cheer and Koehl, 1987). During the recovery stroke, the setae are tilted downstream and the stem is flexed (Fig. 1C). This behavior reduces the area of the leading, water-displacing surface and therefore effectively reduces the drag during the return stroke. This fanning activity is similar to that of a rowing paddle and can generate unidirectional flow. All three flagella on one side usually beat simultaneously and with the same frequency (between 5 and 8 Hz in *Procambarus clarkii*). The rhythmic movements of the three flagella are metachronally phase-shifted by about 0.2 to 0.5 wavelengths (data from high-speed video-recordings; Breithaupt, unpubl. data). By changing the angle of the mouthparts, the flagella can modify the axis of fanning activity. By fanning only one side or

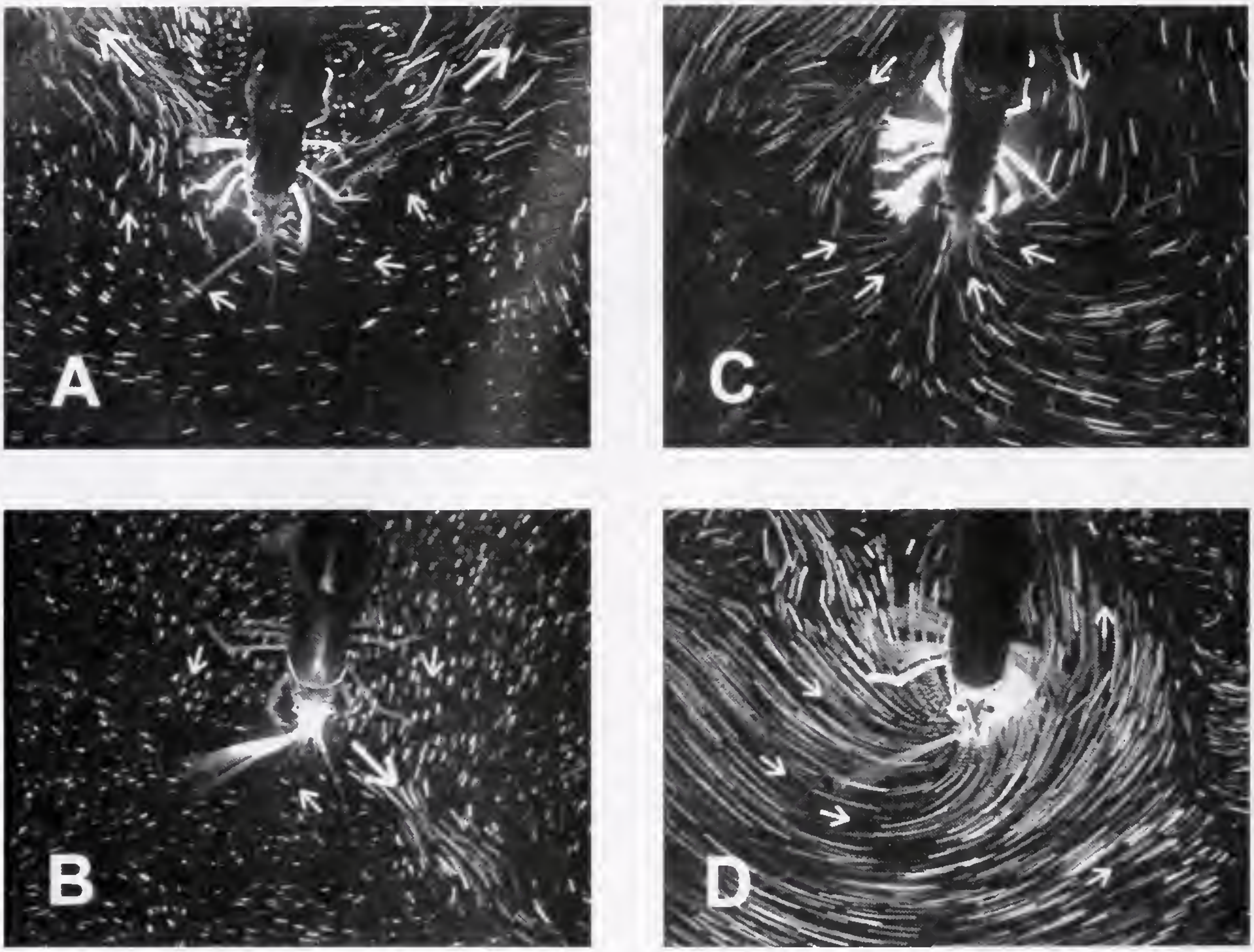

Figure 2. Examples of horizontal flow fields generated by the fan organs of an adult male crayfish (*Procambarus clarkii*) without claws. Flow pictures were generated by superimposing 25 video-frames (Breithaupt and Ayers, 1998) of neutrally buoyant particles moving in a 5-mm-thick horizontal light sheet, and tracing the flow lines. (A) Fans of both sides beat backward and generate bilateral backward-directed water jets (light sheet at 1 cm above ground lasting for 2 s). Large arrows indicate fluid velocities of 1 cm/s; small arrows represent velocities of 0.5 cm/s. (B) Fans of left side only are beating forward and produce a forward-directed jet (at 3.5 cm for 2 s; arrows as in A). (C) Fans of both sides beat upward and in the horizontal plane draw water from all directions towards the frontal mouthparts (at 1 cm for 10 s). Arrows denote fluid velocities of 0.1 cm/s. (D) Fans of right side only beat upward and draw water from right to left (at 2.5 cm for 12 s; arrows as in C).

both sides and by changing the direction of fanning activity, crayfish can generate a variety of flow fields.

Flow Fields Generated by the Fan Organs

Visualization of the flow fields using small (50 μm), neutrally buoyant particles illuminated within a horizontal and a vertical light sheet (Breithaupt and Ayers, 1998) revealed that crayfish can modulate the flow environment in their immediate vicinity in a variety of ways (Fig. 2). In the horizontal plane that is probably most significant for most of the crayfish's activities, the flow can be directed either away from (Fig. 2A, B) or toward (Fig. 2C, D) the head region. Flow velocity of the outgoing water jets can be up to 4 cm/s. Incoming water in the horizontal plane is usually much slower, with velocities between 0.1 and 0.5 cm/s depending on the distance to the fan organs. By beating the flagella on only one side, crayfish can draw in water exclusively from this side (Fig. 2D).

Biological Significance of Fanning Behavior

Many crayfish species live in environments with stagnant flow conditions. The flow velocity in a lake inhabited by the European narrow-clawed crayfish (*Astacus leptodactylus*) rarely exceeds 1 cm/s even on stormy days (T. Breithaupt and E. Ebert, unpubl. data). In such environments, flow fields created by the animals themselves help in getting access to distant odor stimuli and provide directional information. Fanning is a major activity of crayfish during food search in stagnant water. Blindfolded crayfish (*Astacus leptodactylus*) with restrained fan organs that could not generate water currents were not able to find the odor source (T. Breithaupt and E. Ebert, unpubl. data). This demonstrates the importance of the fan organs in actively scanning the environment and transporting the odor molecules towards the chemoreceptors on the antennules (Fig. 1). The crayfish may identify the direction of the odor source by comparing the arrival time of the moving odor patches at different receptor locations on the bilateral antennules. Recent studies suggested bilateral directional information as a critical element in chemical orientation of decapod crustaceans at turbulent flow conditions (Atema, 1996; Grasso *et al.*, 1998).

A second important function of the fan organs is to carry urine-borne pheromone from the nephropores to the chemoreceptors of nearby conspecifics. Visualization of urine release during fights of American lobsters and crayfish revealed that signaling with urine is an integral component of aggressive communication in these animals (Breithaupt and Atema, 2000; T. Breithaupt and P. Rohleder, unpubl. data). The crayfish *Procambarus clarkii* uses frontally projecting fan organ currents to carry urine signals toward the opponent (T. Breithaupt and P. Rohleder, unpubl. data). The currents are also used to direct urine signals in directions other than forward.

Lessons to Learn From the Fan Organs of Crayfish

Only by using such elaborate appendages can crustaceans acquire and send chemical information in environments with stagnant flow conditions. Fan organs are widely used in the animal kingdom to propel and direct chemical stimuli away from and toward organisms. Flow-generating devices can also greatly enhance the search success of autonomous robots orienting to chemical sources. The use of a rotating propeller fan has been shown to help terrestrial autonomous robots to locate chemical sources by actively drawing air to their chemical sensor and scanning different directions for the presence of chemicals (Nakamoto *et al.*, 1999; Ishida *et al.*, 2001). Recent progress in the development of aquatic robots has been inspired by research on crustaceans (Grasso, 2001). The versatility of the paddlelike fan design of the crayfish appendage goes beyond that of propeller fans by enabling the exchange of chemical information in three dimensions. A thorough analysis of the behavior and the mechanics of flow production as well as the underlying muscular and neural activity should further illuminate the functional organization of this beautiful system and may trigger biomimetic designs for artificial fans.

Acknowledgments

Thanks to Frank Grasso for organizing the inter-disciplinary symposium. I would also like to thank Myriam Schmid and Dr. Joachim Hentschel for assistance in the SEM study of fan organs, the graphics workshop of the University of Konstanz for the crayfish drawing in Fig. 1, Kirsten Pohlmann and two anonymous reviewers for helpful comments on the manuscript, and Prof. Dr. Axel Meyer for supporting the study. The research was funded by the Deutsche Forschungsgemeinschaft (Br 1321/3-1).

Literature Cited

Agosta, W. C. 1992. *Chemical Communication: the Language of Pheromones.* Scientific American Library, New York.

Atema, J. 1985. Chemoreception in the sea: adaptations of chemoreceptors and behaviour to aquatic stimulus conditions. *Soc. Exp. Biol. Symp.* **39:** 386–423.

Atema, J. 1996. Eddy chemotaxis and odor landscapes: exploration of nature with animal sensors. *Biol. Bull.* **191:** 129–138.

Blackburn, N., T. Fenchel, and J. Mitchell. 1998. Microscale nutrient patches in planktonic habitats shown by chemotactic bacteria. *Science* **282:** 2254–2256.

Boppré, M. 1984. Chemically mediated interactions between butterflies. Pp. 259–275 in *The Biology of Butterflies*, R. I. Vane-Wright and P. R. Ackery, eds. Academic Press, London.

Breithaupt, T., and J. Atema. 2000. The timing of chemical signaling with urine in dominance fights of male lobsters (*Homarus americanus*). *Behav. Ecol. Sociobiol.* **49:** 67–78.

Breithaupt, T., and J. Ayers. 1998. Visualization and quantification of biological flow fields through video-based digital motion-analysis techniques. *Mar. Freshw. Behav. Physiol.* **31:** 55–61.

Brock, F. 1926. Das Verhalten des Einsiedlerkrebses *Pagurus arrosor* Herbst während der Suche und Aufnahme der Nahrung. *Z. Morph. Oekol. Tiere* **6:** 415–552.

Budd, T. W., J. C. Lewis, and M. L. Tracey. 1979. Filtration feeding in *Orconectes propinquus* and *Cambarus robustus* (Decapoda, Cambaridae). *Crustaceana Suppl.* **5:** 131–134.

Burrows, M., and A. O. D. Willows. 1969. Neuronal co-ordination of rhythmic maxilliped beating in brachyuran and anomuran Crustacea. *Comp. Biochem. Physiol.* **31:** 121–135.

Cheer, A. Y. L., and M. A. R. Koehl. 1987. Paddles and rakes: fluid flow through bristled appendages of small organisms. *J. Theor. Biol.* **129:** 17–39.

Dusenbery, D. B. 1992. *Sensory Ecology: How Organisms Acquire and Respond to Information.* W. H. Freeman, New York.

Free, J. B. 1987. *Pheromones of Social Bees.* Chapman and Hall, London.

Grasso, Frank W. 2001. Invertebrate inspired sensory-motor systems and autonomous, olfactory-guided exploration. *Biol. Bull.* **200:** 160–168.

Grasso, F. W., J. A. Basil, and J. Atema. 1998. Toward the convergence: robot and lobster perspectives of tracking odors to their source in the turbulent marine environment. Pp. 259–263 in *Proceedings of the 1998 IEEE*, Gaithersburg, MD.

Ishida, H., Y. Kagawa, T. Nakamoto, and T. Moriizumi. 1996. Odor-source localization in the clean room by an autonomous mobile sensing system. *Sens. Actuators* **B 33:** 115–121.

Ishida, H., T. Nakamoto, T. Moriizumi, T. Kikas, and J. Janata. 2001. Chemical sensors for plume tracing robots. *Biol. Bull.* **200:** 222–226.

Koehl, M. A. R., and J. R. Strickler. 1981. Copepod feeding currents: food capture at low Reynolds number. *Limnol. Oceanogr.* **26:** 1062–1073.

Lavalli, K. L., and J. R. Factor. 1995. The feeding appendages. Pp. 349–393 in *Biology of the Lobster* Homarus americanus, J. R. Factor, ed. Academic Press, Orlando, FL.

Nakamoto, T., H. Ishida, and T. Moriizumi. 1999. A sensing system for odor plumes. *Anal. Chem.* **71:** 531A–537A.

Voigt, C. C., and O. von Helversen. 1999. Storage and display of odour by male *Saccopteryx bilineata* (Chiroptera, Emballonuridae). *Behav. Ecol. Sociobiol.* **47:** 29–40.

Weissburg, M. J. 2000. The fluid dynamical context of chemosensory behavior. *Biol. Bull.* **198:** 188–202.

Yen, J. 2000. Life in transition: balancing inertial and viscous forces by planktonic copepods. *Biol. Bull.* **198:** 213–224.

Reference: *Biol. Bull.* **200:** 155–159. (April 2001)

Statocysts in Crabs: Short-Term Control of Locomotion and Long-Term Monitoring of Hydrostatic Pressure

PETER J. FRASER

Zoology Department, Aberdeen University, Tillydrone Avenue, Aberdeen AB24 2TZ Scotland

Abstract. Crabs show well-coordinated locomotion. They have proprioceptors similar to those of lobsters, but they differ in terms of their balancing systems and their condensed nervous system, which allows rapid interganglionic conduction. Typically they exhibit dynamically stable locomotion with a highly developed semicircular canal system that codes angular acceleration in each of three orthogonal planes (horizontal and vertical at 45° and 135° to the pitching plane). Left and right interneurons each code one direction of angular acceleration, carrying information between the brain and the thoracic ganglia. Cell A codes head-up vertical plane angular accelerations. Cell B codes rotations in the horizontal plane. Interneurons C and D code head-down vertical plane information, carrying it ipsilaterally and contralaterally respectively. These interneurons have a central role in locomotion. They are activated and have their responsiveness to angular acceleration enhanced before and during locomotion. Such simple activation pathways point to how an angular-acceleration-controlled robot (CRABOT) could be constructed. Hydrostatic pressure information carried by the thread hairs, which also sense angular acceleration, is filtered out from direct pathways onto the interneurons, but spectral analysis shows that it still has an influence *via* central pathways. Long-term recordings from equilibrium interneurons in free-walking crabs taken from the wild into constant conditions show tidally changing frequencies of bouts of activity, with peaks that correspond to times of high tide.

Introduction

Brachyuran crabs are conspicuous animals that occupy a variety of habitats and show well-coordinated locomotor ability while walking, crawling, climbing, swimming, or burrowing under a variety of hydrostatic pressure conditions. Compared with the ladder-like nerve cord of macrurans (crayfish and lobsters), their nervous system shows condensation and fusion of thoracic ganglia, allowing rapid interganglionic conduction of impulses. The abdomen has been much reduced and, in contrast to that of macrurans, is little used in normal or escape swimming. These crabs can survive leg autotomy: 13%–43% of individual *Carcinus* sampled from the wild have missing legs (McVean, 1982). Typically they exhibit dynamically stable locomotion, with statocyst (or balancing organ) interneurons having a central role (Fig. 1; Fraser, 1982; Fraser *et al.*, 1987). Thread hair receptors, which respond to fluid displacements in the statocyst, have been shown to have their spontaneous activity and sensitivity to angular acceleration modulated by small changes in hydrostatic pressure (Fraser and Macdonald, 1994; Macdonald and Fraser, 1999). Clearly, elucidating the simplifying principles underlying such versatility and diversification of function is an important aim. One approach to dissecting such complexity is to concentrate on a fundamental difference between crabs and lobsters—that is, the elaboration in crabs of the statocyst and its central pathways.

Statocysts and Leg Proprioceptors Involved in Locomotion

The statocyst contains a statolith and angular acceleration receptors. In the crab, the crescent of statolith hairs (Sand-

---

E-mail: p.fraser@abdn.ac.uk

This paper was originally presented at a workshop titled *Invertebrate Sensory Information Processing: Implications for Biologically Inspired Autonomous Systems.* The workshop, which was held at the J. Erik Jonsson Center for the National Academy of Sciences, Woods Hole, Massachusetts, from 15–17 April 2000, was sponsored by the Center for Advanced Studies in the Space Life Sciences at the Marine Biological Laboratory, and funded by the National Aeronautics and Space Administration under Cooperative Agreement NCC 2-896.

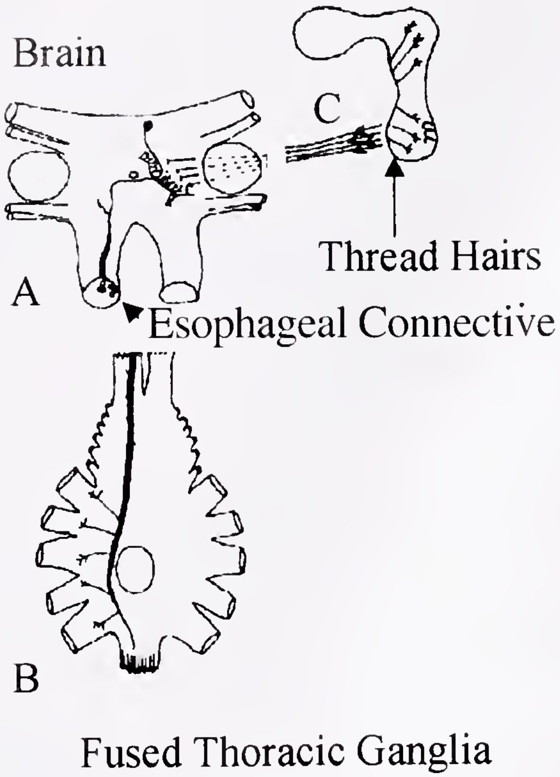

Figure 1. Equilibrium cell A in brain (A) and thoracic ganglia (B) of the crab *Carcinus maenas*. The large axon runs in the esophageal connective. Thread hair afferents (C), which are activated by angular acceleration in the plane of the vertical canal of the statocyst, contact the equilibrium interneurons directly. (Redrawn from Fraser, 1989).

eman and Okajima, 1972) is much smaller than the macruran crescent (see Lemmnitz and Wolff, 1990). The fluid-filled sac has been shaped from a simple cavity in the macruran statocyst into two orthogonal semicircular canals. Angular accelerations in the planes of the horizontal or vertical canals are monitored by a row of long, slender thread hairs (Fig. 1C; Sandeman and Okajima, 1972; Fraser and Takahata, 2001). Typically the response of thread hairs to an angular acceleration is unidirectional, with two oppositely responding directional classes. Analogous to those of vertebrates, the receptors integrate angular acceleration and code angular velocity in the horizontal plane or in vertical planes either at 45° or at 135° to the median line. Thread hairs are the main sensory component involved in a variety of statocyst-driven behaviors ranging from walking to eyestalk movement, with free hook hairs and statolith hairs playing a lesser role (Cohen and Dijkgraaf, 1961; Fraser, 1989; Fraser and Takahata, 2001). An inertial angular acceleration detector based on an orthogonal semicircular canal system could be easily added to a robot by using connectivity and coding principles derived from crab equilibrium interneurons, which are described below.

Crabs normally walk sideways. The leading legs pull and the trailing legs push to move the body (Clarac and Coulmance, 1971; Evoy and Ayers, 1982). Crabs do not exhibit regular gait patterns, but have a great variety of gaits and leg activation sequences. Hence Evoy and Ayers (1982) state that "changes in gait occur and conditions strictly satisfying the alternating tetrapod gait are rarely seen." During high-speed running, ghost crabs may even become bipedal, with only two legs alternating on the trailing side (Burrows and Hoyle, 1973). Statocyst ablation affects sideways walking and the rearing reflex (Cohen and Dijkgraaf, 1961; Fraser, 1974). Swimming activity is more stereotyped and again highly dependent on statocyst input (Fraser *et al.*, 1987). During swimming, all muscles in the fifth legs are active in a sequence that causes cyclical sculling. Only muscles that operate joints controlling dorsolateral movements are involved in sideways walking, and they are used in a different temporal pattern than in swimming (Fraser *et al.*, 1987).

Leg proprioceptors are used in the fine motor control to produce coordinated behavior, but during rhythmic behavior, sensory information does not vary much on each cycle unless a leg hits an obstacle. A variety of receptors include muscle receptor organs, which measure muscle stretch (Bush, 1977); chordotonal organs, which are articular (joint rotation) receptors measuring stretch around joints; and apodeme receptors and cuticular stress receptors, which record muscular tension *via* tendons and cuticle respectively (Wales *et al.*, 1971). The funnel canal organs at the ends of the dactylopodites must be silent for the animal to swim, whereas their rhythmic firing in walking is used for step regulation (Libersat *et al.*, 1987). Although it is not possible here to do justice to the complexity of information relayed by these proprioceptors, in general their role in locomotion in crabs is broadly similar to that in lobsters and crayfish.

Equilibrium Interneurons Involved in Locomotion

The angular acceleration sensors, the thread hairs, project onto a small set of eight large interneurons that link the brain to the fused thoracic and abdominal ganglia (Fig. 1; Fraser, 1974, 1990). These fire in the short term during angular accelerations caused by locomotion (Fig. 2A, B; Fraser, 1982). but are also activated centrally before and during bouts of walking or swimming (Fig. 2B; Fraser *et al.*, 1987; Fraser, 1975, 1989). Their activity long term consists of quiescent periods with short bouts of extremely elevated activity. Cells are not coupled and are more likely to act in anti-phase during short-term oscillations that form part of the locomotion. Over a longer time scale, on the order of minutes, their overall activity is well synchronized. Vector information is hence preserved (Fraser *et al.*, 1997, 2001). During these bouts of firing, the gain in the statocyst pathways alters greatly so that perturbations of angular acceleration have a large effect (Fig. 3).

In the context of discussing the role of the interneurons in

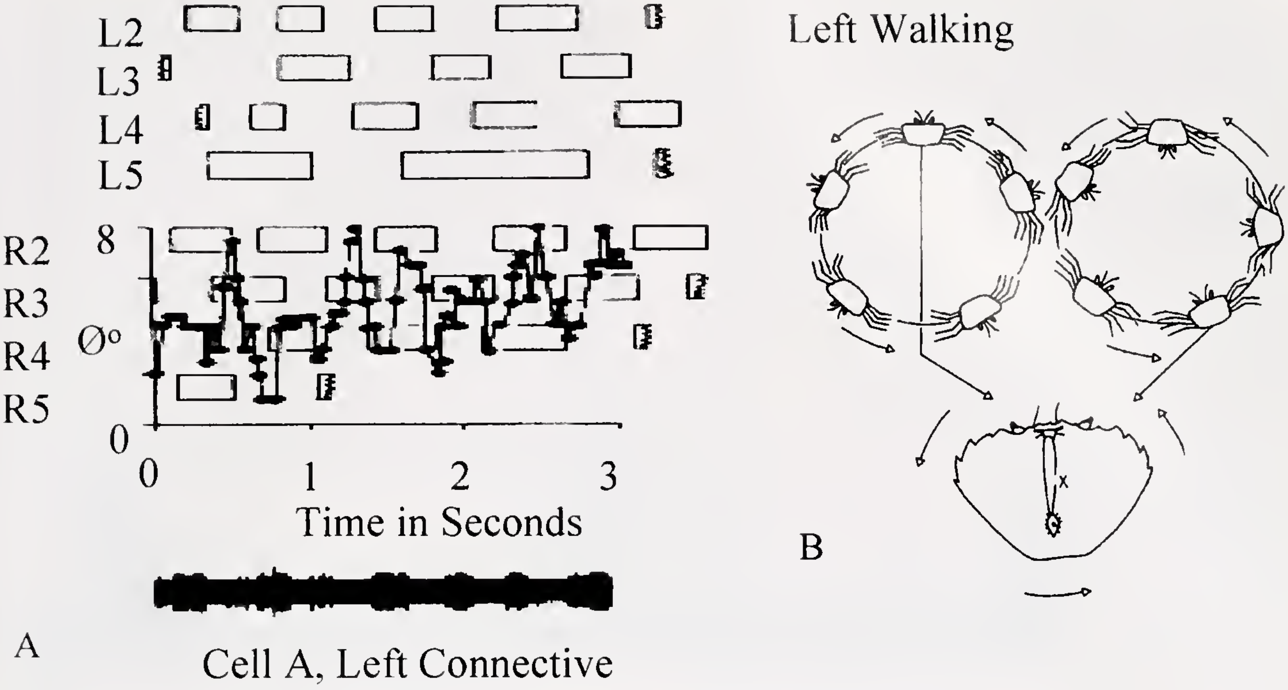

Figure 2. (A) Extension phases of left and right 2nd to 5th legs during a short sequence of walking to the left by a crab. The extracellular recording shows cell A in the left esophageal connective. The series of bursts of activity are more related to slight angular excursions of the body (ϕ) than to the gait pattern. ϕ is the clockwise angular displacement of the body of the crab around the horizontal longitudinal axis. (B) The effect of cutting the right esophageal connective on locomotion in the crab *Carcinus maenas.* Gait alters and the crab prefers walking left. Regardless of the direction of walking, the crab always turns counterclockwise (Bethe, 1897). This is the direction that optimally excites Cell B in the right connective. Electrical stimulation of the cut end of the connective will straighten or reverse the counterclockwise movement.

locomotion, Fraser (1982) points out that "where a behavior involves vectorial output in more than one dimension, or where feedback loops are involved, then the output measured by displacement of appendages or by muscle activity is no longer an adequate measure of the behavior . . . in terms of understanding the underlying neural activity, locomotion in crabs may be better described in terms of components of force and torque in the planes used by the equilibrium cells rather than in terms of the gaits employed." The angular displacements of crabs have been monitored in orthogonal planes with a miniature triaxial accelerometer.

Although proprioceptor input affects the activity of the interneurons, their outputs in free-walking animals are not particularly complicated (Fraser, unpubl. data; Fraser, 1995). Interestingly, Cruse *et al.* (1998) and Schmitz (2001) state that in the stick insect there is little evidence for a central pattern generator. Instead sensory information derived from leg position and ground contact, together with six different coupling mechanisms, allows selection between swing networks and stance networks. Lobster walking has been successfully modeled with five main classes of components: central pattern generators, command systems, coordinating systems, proprioceptive and exteroceptive sensors, and phase- and amplitude-modulating sensory feedback (Ayers *et al.*, 1998). Stepping rates for such models are low. It may be that the crab has more similarities to the stick insect model than to the lobster model in terms of its reliance on sensory control, and an orthogonal command set based on the equilibrium interneurons may be sufficient to control a large part of its locomotion.

The finding that the statocyst thread hair receptors alter their activity under the influence of hydrostatic pressure makes understanding of their role more complicated (Fraser and Macdonald, 1994; Fraser *et al.*, 1996; Macdonald and Fraser, 1999). Positive-going and negative-going modulation of thread hair spike frequency is thought to arise from activation of the two directional classes of mechanoreceptors *via* the linking chorda because of the slight volume changes associated with differential compressibility of the cuticle and other tissue components. Although thread hairs respond directly to alterations in hydrostatic pressure, thread hair interneurons do not seem to do so. Tidal period rhythms of firing pattern in equilibrium interneurons occur and match those found for general locomotor activity (Naylor and Atkinson, 1972; Fraser and Takahata, 2001). These are affected by hydrostatic pressure pulses or cycles, and spectral analyses of long sequences show that some of the

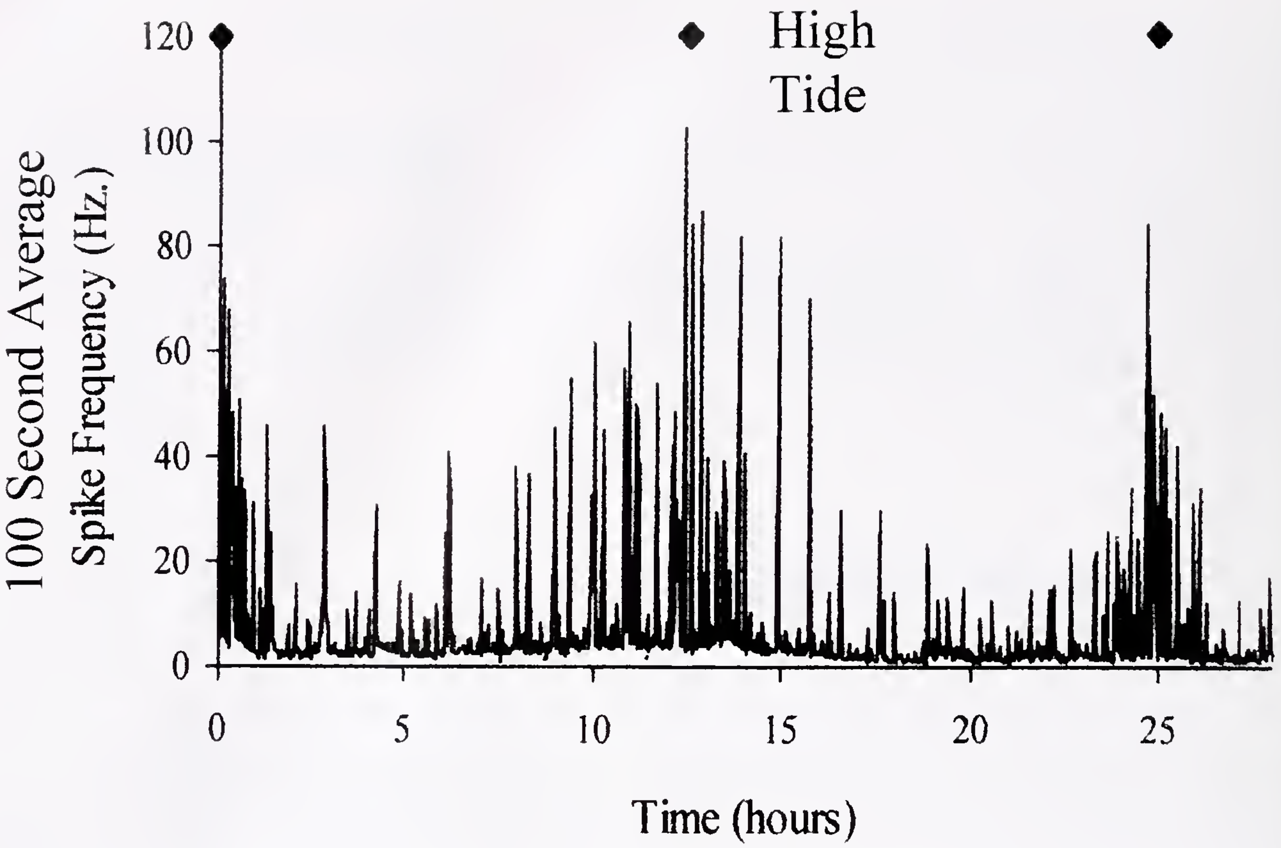

Figure 3. Long-term recording from equilibrium interneurons (spike frequency measured every 100 s) in a free-walking crab, *Carcinus maenas*, taken into constant conditions in an aquarium after capture at low tide. The recording starts 6 h after capture. Arrows mark the occurrence of high tides. High bouts of activity in the cells correspond to locomotor behavior in the crab, and there is clear tidal rhythmicity. (Redrawn from Fraser and Takahata, 2001).

pressure information is getting through, presumably *via* higher order inputs (Fraser *et al.*, 2001).

CRABOTS in the Future

Crabs show well-coordinated but highly variable walking patterns and easy transitions between walking and swimming. Activation patterns of equilibrium interneurons during such movement are simple and should be easily copied. This points the way to how an angular acceleration controlled walking robot (CRABOT) could be constructed, which would advance maneuverability of such robots and should save energy. Optimism for the success of this approach comes from early experiments showing circling movements in crabs when one esophageal connective was cut and reversal of this circling behavior with stimulation of the cut connective. This circling may be explained in terms of the effects on equilibrium cells (Fig. 2B; Bethe, 1897; Fraser, 1982). At present, a major limitation regarding realistic robotic modeling is the stepping frequency of artificial limbs and activators.

Literature Cited

Ayers, J., P. Zavracky, N. McGruer, D. P. Massa, W. S. Vorus, R. Mukherjee, and S. Currie. 1998. A modular behavioral-based architecture for biomimetic autonomous underwater robots. Pp. 15–21 in *Proceedings of the Autonomous Vehicles in Mine Countermeasures Symposium*, 5–9 April 1998. Naval Postgraduate School, Monterey, CA.

Bethe, A. 1897. Das Nervensystem von *Carcinus maenas*. Ein anatomisch-physiologischer Versuch. I. Theil, II. Mittheil. *Arch. Mikrosk. Anat. Entwicklungsmech.* **50:** 589–639.

Burrows, M., and G. Hoyle. 1973. The mechanism of rapid running in the ghost crab, *Ocypode ceratothalma*. *J. Exp. Biol.* **58:** 327–349.

Bush, B. M. H. 1977. Non-impulsive afferent coding and stretch reflexes in crabs. Pp. 439–460 in *Identified Neurons and Behavior of Arthropods*, G. Hoyle, ed. Plenum Press, New York.

Clarac, F., and M. Coulmance. 1971. La marche lateral du crabe (*Carcinus*): Coordination des movements articulaires et regulation proprioceptive. *Z. Vgl. Physiol.* **73:** 408–438.

Cohen, M. J., and S. Dijkgraaf. 1961. Pp. 65–108 in *The Physiology of Crustacea, Vol. II*, T. H. Waterman, ed. Academic Press, New York.

Cruse, H., T. Kindermann, M. Schumm, J. Dean, and J. Schmitz. 1998. Walknet—a biologically inspired network to control six-legged walking. *Neural Networks* **11:** 1435–1447.

Evoy, W. H., and J. Ayers. 1982. Locomotion and control of limb movements. Pp. 61–105 in *The Biology of Crustacea, Vol. 4: Neural Integration and Behavior,* D. C. Sandeman and H. L. Atwood, eds. Academic Press, New York.

Fraser, P. J. 1974. Interneurons in crab connectives (*Carcinus maenas* (L.)): directional statocyst fibres. *J. Exp. Biol.* **61:** 615–628.

Fraser, P. J. 1975. Three classes of input to a semicircular canal interneuron in the crab, *Scylla serrata* and a possible output. *J. Comp. Physiol.* **104:** 261–271.

Fraser, P. J. 1978. Vector coding and command fibres. In *The Command Neuron Concept,* I. Kupfermann and K. R. Weiss, eds. *Behav. Brain Sci.* **1:** 3–39.

Fraser, P. J. 1982. Views on the nervous control of complex behavior. Pp. 293–319 in *The Biology of Crustacea, Vol. 4: Neural Integration and Behavior,* D. C. Sandeman and H. L. Atwood, eds. Academic Press, New York.

Fraser, P. J. 1989. Vector coding and multiplicative gain control in the nervous system of the crab. Pp. 95–102 in *New Developments in Neural Computing,* J. G. Taylor and C. L. T. Mannion, eds. Adam Hiliger, New York.

Fraser, P. J. 1990. Equilibrium control by statocyst activated interneurons. Pp. 187–192 in *Frontiers in Crustacean Neurobiology,* K. Wiese, W. D. Krenz, J. Tautz, H. Reichert, and B. Mulloney, eds. Birkhäuser Verlag, Basel.

Fraser, P. J., and A. G. Macdonald. 1994. Crab hydrostatic pressure sensors. *Nature* **371:** 383–384.

Fraser, P. J., and M. Takahata. 2001. Statocysts and statocyst control of motor pathways in crayfish and crabs. In *The Crustacean Nervous System,* K. Wiese *et al.,* eds. Springer Verlag, Berlin. (In press).

Fraser, P. J., M. Bevengut, and F. Clarac. 1987. Swimming patterns and the activity of identified equilibrium interneurons in the shore crab, *Carcinus maenas. J. Exp. Biol.* **130:** 305–330.

Fraser, P. J., A. G. Macdonald, and R. N. Gibson. 1996. Low pressure hydrostatic pressure receptors in the crab *Carcinus maenas* (L.). In *Basic and Applied High Pressure Biology IV.* J. C. Rostain, A. G. Macdonald, and R. E. Marquis, eds. *Medsubhyp. Int.* **5:** 59–68.

Fraser, P. J., A. G. Macdonald, S. F. Cruickshank, and M. P. Schraner. 1997. Integration of hydrostatic pressure information by identified interneurons in the crab *Carcinus maenas* (L.); long term recordings. *Proc. R. Inst. Navigation RIN* **97:** 25.1–25.10.

Fraser, P. J., A. G. Macdonald, S. F. Cruickshank, and M. P. Schraner. 2001. Integration of hydrostatic pressure information by identified interneurons in the crab *Carcinus maenas* (L.); long term recordings. *J. Navigation* (In press).

Lemmnitz, G., and H. G. Wolff. 1990. Recording from sensory cells in the statocyst of *Astacus.* Pp. 97–105 in *Frontiers in Crustacean Neurobiology,* K. Wiese, W. D. Krenz, J. Tauz, H. Reichert, and B. Mulloney, eds. Birkhäuser Verlag, Basel.

Libersat, F., F. Clarac, and S. Zill. 1987. Force sensitive mechanoreceptors of the dactyl of the crab: single unit responses during walking and evaluation of function. *J. Neurophysiol.* **57:** 1618–1637.

Macdonald, A. C., and P. J. Fraser. 1999. The transduction of very small hydrostatic pressures. *Comp. Biochem. Physiol. A* **122:** 13–36.

McVean, A. 1982. Autotomy. Pp. 107–132 in *The Biology of Crustacea, Vol. 4: Neural Integration and Behavior,* D. C. Sandeman and H. L. Atwood, eds. Academic Press, New York.

Naylor, E., and R. J. W. Atkinson. 1972. Pressure and rhythmic behavior of inshore marine animals. *Symp. Soc. Exp. Biol.* **26:** 395–416.

Sandman, D. C., and A. Okajima. 1972. Statocyst-induced eye movements in the crab *Scylla serrata I.* The sensory input from the statocyst. *J. Exp. Biol.* **57:** 187–204.

Schmitz, J., J. Dean, T. Kinderman, M. Schumm, and H. Cruse. 2001. A biologically inspired controller for hexapod walking: simple solutions by exploiting physical properties. *Biol. Bull.* **200:** 195–200.

Wales, W., F. Clarac, and M. S. Laverack. 1971. Stress detection at the autotomy plane in the decapod crustacea. I. Comparative anatomy of the receptors of the basi-ischiopodite region. *Z. Vgl. Physiol.* **73:** 357–382.

Reference: *Biol. Bull.* **200:** 160–168. (April 2001)

Invertebrate-Inspired Sensory-Motor Systems and Autonomous, Olfactory-Guided Exploration

FRANK W. GRASSO*

Boston University Marine Program, Marine Biological Laboratory, Woods Hole, Massachusetts 02453

Abstract. The localization of resources in a natural environment is a multifaceted problem faced by both invertebrate animals and autonomous robots. At a first approximation, locomotion through natural environments must be guided by reliable sensory information. But natural environments can be unpredictable, so from time to time, information from any one sensory modality is likely to become temporarily unreliable. Fortunately, compensating mechanisms ensure that such signals are replaced or disambiguated by information from more reliable modalities. For invertebrates and robots to rely primarily on chemical senses has advantages and pitfalls, and these are discussed. The role of turbulence, which makes tracking a single odor to its source a complex problem, is contrasted with the high-fidelity identification of stimulus quality by the invertebrate chemoreceptor and by artificial sensors.

Chemical Senses in the Resource Localization Problem

The ability of an animal or an autonomous robot to secure resources (*e.g.*, a supply of energy, a source of water, a shelter from dangerous weather conditions or other hazards) is critical to its behavior and survival. In natural environments critical resources are rarely stable for long. As they are depleted, become inaccessible, or simply disappear, the problem of securing resources is one that autonomous agents must solve repeatedly. Whether all of the resources in a given region are mapped at once for future use or new resources are found sequentially by foraging as identified ones expire, the activity is exploration.

The first step in exploring for spatially distributed resources is localizing them with appropriate sensory equipment. That animals and robots rely on their senses to locate resources is a tautology: an entity without sensors cannot determine the location of anything. Simple, single-modality search mechanisms have been well studied in robots and invertebrates. If the resource is obvious and detectable from a unique cue, a simple scan with a ranged (distance) sensor from a single site will suffice to locate it. If the resource, and therefore the diagnostic cue, is hidden, a systematic probe of each location in the search region may be required. In the former case no locomotion is required of the animal or robot to localize the resource; in the latter the animal or robot must locomote everywhere. Robots and animals typically employ mechanisms that combine or lie between these two extremes, depending on the complexity of the sensory task.

Optical illusions are the result of a deceived visual sense (Gibson, 1982). Echoes from the substrate can confound auditory localization senses (Mountain and Hubbard, 2001; Robert, 2001). Though the mixing of odors from different sources may muddle olfactory recognition under some conditions, olfaction offers an advantage over vision and audition in sensing the nature of distant objects. By definition, a chemical sensor is detecting a sample that was a physical constituent of the resource. Once detected, therefore, the resource must certainly be in the vicinity, and the agent may then make inferences about the resource's quality. Thus, the chemical senses are advantageous when used in resource localization, because the rate of false positives is low.

Although invertebrates are much more effective than existing robots in chemical tracking, scientists and engineers face three formidable and interrelated challenges that

---

* Current address: Dept. of Psychology, Brooklyn College, CUNY, 2900 Bedford Ave., Brooklyn, NY 11210.

E-mail: fgrasso@biomimetics.mbl.edu

This paper was originally presented at a workshop titled *Invertebrate Sensory Information Processing: Implications for Biologically Inspired Autonomous Systems.* The workshop, which was held at the J. Erik Jonsson Center for the National Academy of Sciences, Woods Hole, Massachusetts, from 15–17 April 2000, was sponsored by the Center for Advanced Studies in the Space Life Sciences at the Marine Biological Laboratory, and funded by the National Aeronautics and Space Administration under Cooperative Agreement NCC 2-896.

must be surmounted before invertebrate solutions can be put to work for us in autonomous systems designed for exploration. First, we must thoroughly understand the sensory and behavioral repertoires of organisms that are proficient chemical trackers. Second, we must be able to transfer the principles abstracted from animals to implementation in autonomous systems. The principal pitfall, however, is turbulence, which governs spatial distributions of chemicals in most macroscopic environments. In this essay I discuss the advantages and the pitfalls of identifying the chemical sensing strategies employed in or inspired by invertebrate systems and using them to solve the resource localization problem. Natural fluid-dispersal processes are a two-edged sword: turbulence complicates the chemical tracking problem, but turbulence simultaneously provides a "dynamic similarity" that is invariant in its characteristics across environments.

The Physics of Tracking Chemicals to Their Source

Tracking an odor (a chemical or chemical cocktail perceived by an olfactory system) to its source might, naively, be imagined to involve the maintenance of the chemical sensors in continuous contact with the odor. The analogy to keeping the image of a visually tracked object fixated on the retina or the vibrations arising from an acoustically tracked object on the cochlea is tempting. However, given that the odor track can be stationary on a solid substrate or moving in the fluid medium above, the olfactory counterpart of the analogy is trail following, not plume tracking.

Among invertebrates, chemical trails are used by conspecifics for social purposes but also by predators or parasites to exploit the trail-leaving individual; and these are distinct behaviors demanding distinct strategies. Ants, for example, follow the pheromone trails left on the substrate by their nest mates (Wilson, 1962). Male snakes locate potential mates by following the chemical signatures left on the ground by females (Ford and Low, 1984; Ford, 1986). Snails (Wells and Buckley, 1972) track similarly, though they sometimes vary their search for mates by indulging in cannibalistic predation (Snyder and Snyder, 1971). Notwithstanding that the strategies underlying these activities are widely recognized for their effectiveness in autonomous systems, they may be of limited utility for exploration of an unknown chemical landscape. In all of these examples—and in the case of cooperative foraging by eusocial insects—salient trails are deliberately generated by one individual for another to follow. Therefore, localization strategies that draw on examples from foraging or hunting creatures hold more promise for autonomous exploration. Shrimp track the odor trail left in the wake of sinking pieces of food (Hamner and Hamner, 1977). For small organisms like bacteria (Alder, 1969) and copepods (Yen, 2000), which operate at spatial scales dominated by diffusion (rather than turbulent dispersal), odor forms a single, stationary patch contiguous with the source that these creatures exploit. Similarly, nematodes (*Caenorhabditis elegans*) may track the gradients of particles between sand grains to locate mates and sources of nourishment (Morse *et al.*, 1998; Pierce-Shimomura *et al.*, 1999). In any event, however, following a stationary odor trail is only a small part of the behavioral invertebrate repertoire.

Although tracking a stationary odor source may appear to be an easier task than tracking a moving one, the principles of fluid mechanics, upon which olfaction depends, make the problem of the moving trail more tractable. When a stationary object or resource donates portions of itself to the ambient medium through the release of volatile compounds or through surface erosion, that region of space containing the detached chemical from the source is termed a plume (Fig. 1).

Long-lasting odor plumes from a stationary source can leave traces that accumulate on the substrate. This precipitated odor creates onto the substrate a two-dimensional imprint resembling a time-average image of the plume (Fig. 1). Depending on the conditions, the image might resemble a trail or an annulus, with its highest concentrations near the source. Production of such an image would require stable release and environmental conditions for long periods relative to the dispersal process. Above the micro-scale of nematodes mentioned earlier, no studies of animals tracking such plume images appear in the literature. This is probably because conditions to permit such precipitated plume images are rarely realized physically in natural environments (terrestrial aquatic or marine). This method of inferring a plume from long-term time averages could find application in exploration for persistent resources under conditions favorable to such long-term deposition such as in the vicinity of deep-sea vents or in subterranean caverns.

Most animals that used chemo-orientation to locate resources do so by making use of plumes borne on the fluid medium rather than deposited on the substrate. Among invertebrates, plume tracking is a common olfactory-guided behavior. Because it depends on transport by a fluid, it is fundamentally different from acoustic tracking, visual tracking, or stationary trail-following. For an agent to locate sources of odor, the odor must be carried by the ambient fluid from the surface of the object to the surface of the chemical sensors of the robot or the animal.

The extent to which the continuity of the odor plume is maintained depends on the viscosity of the fluid (ν), the velocity of the fluid (U), and the length scale of interest (l). The relationship is summarized in the Reynolds number, Re:

$$\mathrm{Re} = lU/\nu$$

When the value of $\mathrm{Re} < 1$ viscous forces dominate, and the continuity of the odor in space will be preserved. This is the regime to which bacteria, copepods, and nematodes are

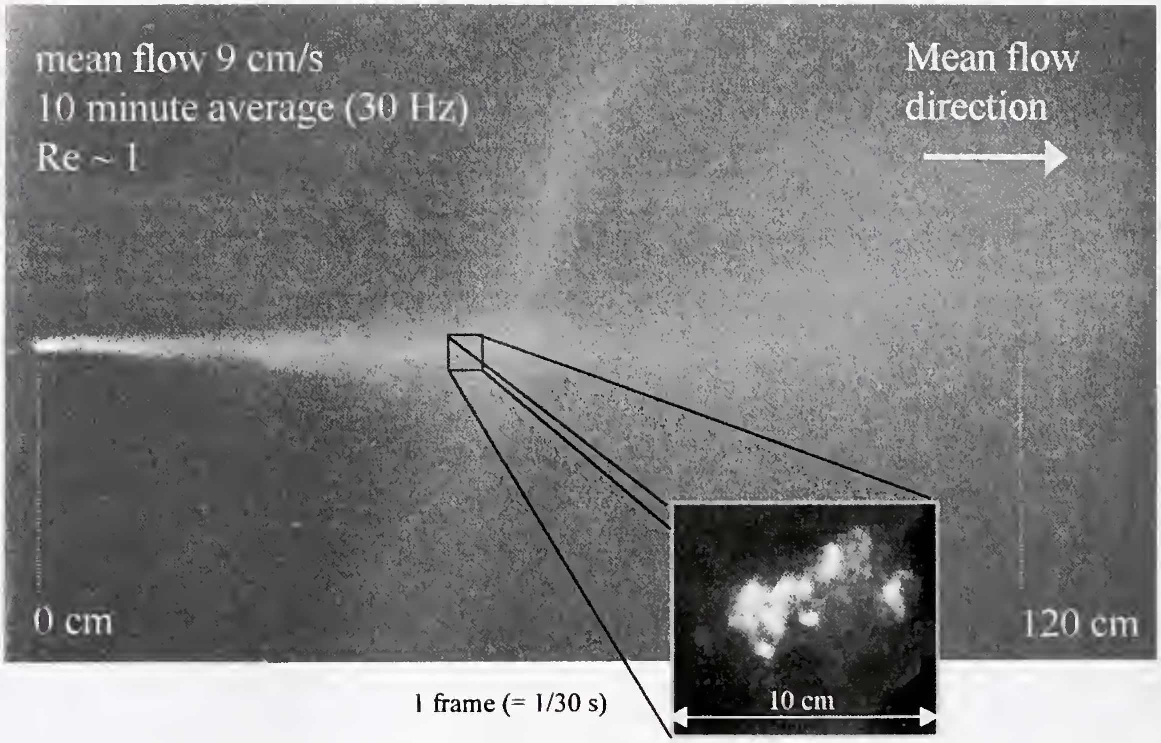

Figure 1. "Leaky" plume characterization in the laboratory. This plume models the odor from an immobile object on the bottom. It was generated in a flume that produced approximately laminar flow. The source, a narrow tube on the floor of the flume, released dye at an "isokinetic" rate matched to that of the ambient flow. We refer to such plumes as leaky to contrast them with jet plumes and wakes that add momentum coincident with the injection of tracer. This is thus a good model for a passive resource on the substrate of a fluid environment. This figure illustrates the spatial distribution of this plume as visualized from trace dye concentration averaged over 5 min at 30 Hz. It shows the plume as a very slow moving animal would experience it with its olfactory organs. This is contrasted with an inset instantaneous (<10 μs) section of the same plume as visualized with the laser-induced fluorescence (LIF) method (see text). The inset gives an indication of the intermittent nature of this plume as faster moving animals might experience it.

adapted. At Re $>$ 1 inertial forces dominate, and plume coherence begins to break down. The higher the value of Re, the greater the degree of turbulence. Most resource localization problems solved by macroscopic invertebrates and those that are of interest for human-scale exploration fall within fluid mechanical regimes that exceed Re $>$ 10.

Intermittent signaling results directly from the action on inertial forces of chemical distribution. When turbulence acts to fragment a continuous stream of chemicals released from an odor source, patches of ambient fluid are interposed between patches of odor (Murlis and Jones, 1981; Moore and Atema, 1991; Murlis *et al.*, 1992). From the perspective of a sensor in the plume, the patches of chemical in space are detected as pulses in time. The problem of tracking odors to their source is thus a temporal one, requiring the use of a time series of encounters with patches of odor for guidance to their source.

The temporal or spatial dispersal patterns produced by different Reynolds regimes are diverse. However, the Reynolds number points to a principle of similarity as well as diversity. Regardless of the specific length scale, viscosity, or velocity, conditions with Re within an order of magnitude are "dynamically similar." Put another way, any strategy that can lead an agent to the source of a chemical or odor at one combination of viscosity, velocity, and length scale is predicted to work for all combinations of these three variables that have similar Reynolds regimes.

A dramatic demonstration of this principle was the huge smoke plume generated by the recent fire at Los Alamos. Imaged from an orbiting remote sensing platform, the plume from the fire spread eastward over the Rocky Mountains and covered six states. The overall shape was reminiscent of many other plumes (Fig. 1). My colleagues and I could pick out features and characteristic structures that could as easily have been found in a plume from a campfire, in a bathtub, or in one of our laboratory flumes. It is not clear at this time whether animals can recognize the Reynolds regime in which they find themselves and adjust their behavior appropriately; indeed, the problem may be ill-posed. Yet, if this is possible it would be a powerful means for selection of appropriate strategies by biological or human fabricated autonomous agents.

Invertebrates and Chemical Plume-Tracking

Plume-tracking behavior

G. S. Fraenkel and D. L. Gunn defined a set of theoretical mechanisms and proposed that these could explain the orientation behavior of animals (Fraenkel and Gunn, 1961). The *kineses* are defined as undirected reactions to a stimulus: The animal may change direction or speed, systematically or randomly, to the cue or source, but this does not lead to systematic orientation of the animal's body. Kineses are characteristic of bacteria (Berg and Purcell, 1977; Alder, 1987). *Taxes* involve directed reactions to a stimulus. In *klino*taxis the animal takes sequential samples of a stimulus and estimates whether movement is with or against the spatial gradient of stimulus intensity. Insect maggots and *Euglena* are examples of creatures that use this mechanism (Mast, 1938). *Tropo*taxis is a mechanism by which the animal makes simultaneous comparisons with two or more sensors to yield an instantaneous estimate for guidance to move with or against a cue gradient. The use of two or more spatially separated sensors by odor-tracking decapod crustaceans (Reeder and Ache, 1980; Devine and Atema, 1982; Beglane *et al.*, 1997) and by adult flying insects (Srinivasan *et al.*, 1996, 2001) and walking insects (McCoy, 1984; Bell, 1986) has been interpreted as indicative of a tropotactic mechanism. These theories, already advanced in the 1940s, have had a long and productive influence on ideas of chemo-orientation in animals since. There is a growing understanding, however, that their intuitive appeal often exceeds their practical utility as explanations of specific tracking behavior in turbulent plumes.

Since the pioneering work of J. Murlis (Murlis and Jones, 1981), biologists have been aware of the problems posed by the intermittency caused by the natural odor dispersal and have proposed alternative mechanisms to single modality taxes and kineses. *Odor gated rheotaxis* (OGR) (Kennedy, 1986) combines the guidance provided by two sensory modalities. Thus, while the animal is sensing odor, it moves "upstream" against the ambient fluid flow. When contact with the odor is lost, the motion is directed cross-stream, perpendicular to the mean flow. This "casting," if in the correct direction, can recover contact with the plume and cause a new upstream surge. This mechanism is common among invertebrates; it is found in many species of moths (Kennedy, 1986; Baker *et al.*, 1988; Vickers and Baker, 1992; Mafra-Neto and Carde, 1994; Mafra-Neto and Carde, 1996) and in blue crabs (Weissburg and Zimmer-Faust, 1994; Zimmer-Faust *et al.*, 1995). In recognition of the costs associated with the degree of persistence involved in casting and surging upstream, a variant of OGR called *counter-turner*, which incorporates an internal oscillator, has also been advanced (Belanger and Willis, 1996). Atema has proposed *eddy-chemo-rheotaxis* (ECR) (Atema, 1996), a mechanism in which the microflow-associated eddies produced by turbulence (as contrasted with the mean flow used in OGR) are combined with the "flavor" of the eddy to provide guidance for movement. Eddies dissipate into the ambient flow (have births and deaths) as they move from the source. Thus, depending on the distance from the source at which the animal encounters them, they will possess different characteristics. This is a potentially rich source of information about the nature of the source and its distance from the agent. Speculations about other sources of information for guidance have also been advanced (Grasso *et al.*, 1996a).

As studies of chemo-orientation break away from the classical notions of taxes and kineses, work on OGR and ECR points to two major themes for the future. First is multi-modal research: that information from multiple sensory modalities must inform investigations of olfactory searching behavior. The second theme is the exploitation by searching agents of the structures produced by turbulence as it carries the odor from the source. Further research in these new areas is likely to find many other novel—and to judge from the data provided by animal studies—much more efficient strategies.

Switching between behaviors. Animals alter their behavior as they progress through a plume. In the course of a successful tracking episode an animal may show variations in speed or direction that are characteristic of a specific phase of tracking behavior. Lobsters show an initial increase in speed, followed by a steady speed phase, and a final decrease, as they progress toward the source (Moore *et al.*, 1991; Basil, 1994). Their headings also show systematic variation as they track certain types of plumes. Such shifts may be attributed to differences in the spatial organization of the plume (Grasso *et al.*, 1996b). As blue crabs and lobsters near the source, they shift from using their antennules, which are elevated above the substrate, to using the chemo-receptors on their dactyls (feet), which are in contact with the substrate (Moore *et al.*, 1991; Basil, 1994; Weissburg and Zimmer-Faust, 1994).

These behavioral observations, and the changes in the structure of the plume as it evolves on its way downstream, suggest that a critical problem in the design of artificial autonomous systems will be the need to match the tracking algorithm to the ambient conditions. To do this, the robot, like an animal, must be able to recognize a given condition, and particularly those conditions that require a change from one strategy to another. Solutions to the problem may entail (1) shifting modalities; (2) giving a different weight to the information coming from one sensory modality relative to another; or (3) identifying more subtle shifts in the information extracted by a given modality.

The spatial biomechanics of olfactory sampling

The use and integration of multiple sensors is a faculty at which invertebrates seem to excel. Invertebrates bristle with a diversity of chemosensors and fluid-mechanosensors. Indeed, this and similar observations have led some to speculate that invertebrates have pushed their neural processing peripherally to lighten the central processing load and thereby to increase response speed (Wehner, 1987). The preceding discussion of turbulent fluid dispersal underscores the complexity of the problems that animals face in placing and maintaining these sensor arrays in contact with a plume (Fig. 1, inset). To maintain that contact, many invertebrates have evolved modes of body locomotion that are expressed during searching. In particular, the sensors are moved through space (a principle they share with vertebrates) and moveable antennae that place some of the sensors away from the body occur (structures that are atypical of the vertebrate bauplan; though catfish, sea robins, *etc.*, possess chemical sensors at the ends of moveable appendages).

Antennae make the experience of odors very different from our own. Humans, and vertebrates in general, have internal nasal passages that homogenize and obliterate the natural spatial and temporal structure of odor signals before they contact the chemoreceptor. Invertebrates with chemical sensors on the ends of long thin stalks (arthropods, cephalopods, and certain gastropods being common examples) have more direct access to the temporal structure of odor signals produced by turbulence. Distal placement frees the sensors from the boundary layers and hydrodynamic shadow of the body, and movement of the appendages enables a search for contact with the plume in ways that are informed by recent experience. The motions of the whole body are also critical to determining the patterns of spatial sampling experienced by the receptor surface. To the extent that motions of an animal's body and sensory antennae may be important components of any active searching plume-tracking strategy, similar mechanisms would be of great importance in developing autonomous plume-tracking systems.

Neural processing of olfactory signals

That chemoreceptors reside on the ends of antennae, free from body boundary layers, is not evidence that invertebrates actually utilize data about the structure of the odor plume. The chemoreceptors must be fast enough, and sensitive enough, to capture the information and transfer it centrally. Recordings from peripheral chemoreceptors in lobsters (Gomez and Atema, 1996a; Gomez and Atema, 1996b; Gomez *et al.*, 1999) and cockroaches (Lemon and Getz, 1996, 1999) suggest that, to a first approximation, this is the case in both terrestrial and marine invertebrates. Modeling studies of both species, constrained by physiological data, indicate that dynamic information on the time scale of ambient turbulence can be passed centrally and is not filtered out by the chemoreceptors (Getz, 1999; Grasso, unpubl. data).

We know very little about how the natural dynamics of odor signals are processed centrally. Arthropod brains, like those of vertebrates, contain olfactory information-processing centers that are subdivided into glomeruli (Hildebrand and Shepherd, 1997; Derby and Steullet, 2001). These dense regions of neuropile are thought to be the sites of convergence for information about the quality or identity of an odor. Recent research (particularly that employing molecular techniques) has mapped the pathways that carry olfactory information to the glomeruli, and the results support the long-held notion that the coding of odor quality is somehow mirrored in the spatial arrangement of glomeruli (Hildebrand and Shepherd, 1997). A recent study in the three-toed box turtle suggests that concentration coding is independent of this level of anatomical organization in the olfactory bulb (Wachowiak *et al.*, 2000). Variation in odor concentration rather than information about odor quality is the stimulus dimension along which natural odor dynamics information is expected to be encoded in the central nervous system.

The central processing and representation of the dynamics of natural odor has received virtually no attention. Once an animal has solved the quality problem (*i.e.*, an odor has been recognized as worth tracking), information reflecting the temporal series of odor patch encounters must be received, interpreted, and translated into motor commands that lead to the source. An explanation of any piece of this process will aid our understanding of olfactory systems and not just plume tracking. The speed and efficiency with which certain invertebrates (notably arthropods) track a turbulent plume to its source demonstrates that the requisite temporal to spatial transformation can be carried out by the nervous system.

Autonomous Systems and Chemical Tracking

Many simulation studies of chemo-orientation behavior by man-made systems have confirmed that the classic taxes and kineses proposed by Fraenkel and Gunn (1961) can lead to localization of a source in a gradient and have quantitatively delineated the conditions under which taxes and kineses will succeed or fail (Rohlf and Davenport, 1969; Braitenberg, 1984; Beer *et al.*, 1991; Holland and Melhuish, 1996; Ferree *et al.*, 1997). A small number of laboratory robot implementations (Deveza *et al.*, 1994; Ishida *et al.*, 1996; Grasso *et al.*, 2000; Ishida *et al.*, 2001) designed to explain animal chemo-orientation behavior or to produce practical chemical tracking devices have explicitly or implicitly employed various single-modality taxes and kineses. The robot performance, however, has lagged far behind the expectations raised by successful simulations. The paths taken by robots that have successfully tracked a turbulent plume are very inefficient compared to the paths taken by animals under comparable conditions; and the algorithms used have been effective only in limited contexts (*i.e.*, they do not generalize). These performance discrepancies are not due to sloppy hardware or software implementations of the algorithms; they result from the failure of these mechanisms to account for the realistic fluid dynamics the robots encounter. The gradients present in naively simulated plumes (and tacitly assumed by the single-modality kineses and taxes by Fraenkel and Gunn) are absent from physical settings where turbulence dominates the patterns of odor dispersal at reasonable time-scales (Warhaft, 2000). The problem rests with our understanding and representation of the environment in simulation studies. The solution requires algorithms that are designed to operate in real plumes rather than smooth gradients.

Improved simulations of real environmental conditions is not a straightforward matter. Simulation of fluid dynamics, with sufficient accuracy, over the required range of temporal and spatial scales is not computationally feasible and perhaps impossible (Warhaft, 2000). An alternative is to capture the dispersal of a given plume in digital form and to use the resulting "digital movie" as the simulation environment. This method is achieved in practice by putting a fluorescent dye into the plume source and capturing the laser-induced fluorescence (LIF) of the dye with digital imaging techniques. From the digital movies, flow fields can simultaneously be obtained for the same plume (Cowen and Monismith, 1997). This "one plume at a time" approach does not lead to generality, but it does allow for the evaluation of many candidate plume-tracking algorithms and for exploring the parameter sensitivity of those algorithms under realistic fluid conditions. This simulation prescreening can be done on a scale that would be impracticable with robots.

These LIF methods, however, cannot include the agent's own influence on turbulent dispersal as it moves through the plume. For this, and to avoid the false sense of progress described in the first paragraph in this section, robots must provide the final test. Robotic studies of chemical plume tracking progress more slowly from simulation studies (but faster than animal studies!). Therefore, a combination of prescreening of algorithms in simulation to weed out patently unsuccessful strategies, followed by definitive testing with robots seems a sound approach.

Compared to the toy problems with which robots and experimental animals are challenged in the laboratory (where experimental control requires variables to be held to a minimum), resource localization problems in natural settings are vastly more complex at many levels. Physical hazards, obstacles, competitors, and predators require behavioral responses that interrupt the smooth application of a foraging strategy. The recognition of false cues, early abandonment of false trails, and maintenance of a stream of appropriate guidance information in unpredictable environments may also require real-world animals and robots to employ a hierarchy of behavioral responses that may deviate from the application of a single simple mechanism. A mechanism that switches between strategies when conditions change, or that varies the weighting of sensory modalities with their reliability, offers solutions to many of these difficulties. Such strategies—so essential for the success of autonomous systems—have scarcely been addressed in animal and biomimetic robotic studies.

Biomimetic Robots and Hypothesis Testing Methods

The preceding sections show that fluid mechanics, animal behavior, neuroscience, and cybernetics can each contribute to the understanding that will finally permit us to construct autonomous systems that can locate resources based on their chemical signature and under chaotic environmental conditions. Each field has reached a point where its methodology has provided tantalizing hints about the robust plume-tracking strategies of invertebrates; but each faces difficult technical and conceptual hurdles before it can advance further. Biomimetic robots offer a methodology that can answer some of the questions raised by each of these approaches.

In my own studies, conducted with colleagues in the laboratory of J. Atema at the Marine Biological Laboratory in Woods Hole, the behavior of a robot told us something unsuspected about the plume structure (Grasso *et al.*, 1996b). The behavior of this robot changed in different regions of the plume as it was executing a simple tropotactic tracking algorithm. This result indicated a qualitative difference in plume structure from the robot's perspective and serves notice that changes in animal behavior must be interpreted with caution. We have also explored spatial sampling issues by varying the separation between paired sensors (Grasso *et al.*, 1997). This work had an engineering aspect—finding an optimal sampling configuration—and a biological aspect—determining the information that animals obtain from the inter-sensor separations they possess. We have also studied tropotactic algorithms in one (jet) plume (Grasso *et al.*, 2000) and OGR in two (leaky) plumes (Grasso, unpubl. data) that American lobsters are known to track. As these robot experiments accumulate, they raise new biological questions and narrow the possible biological and physical explanations of plume tracking by lobsters.

The performance of the robots used in these studies was *quantitatively* evaluated against the performance of the American lobster. This unique comparison was possible because we tested the robot under physical conditions virtually identical to those under which animal experiments had previously been conducted (*i.e.*, the plume was composed of a natural food extract for the lobster and a synthetic tracer for the robot, but all other experimental conditions

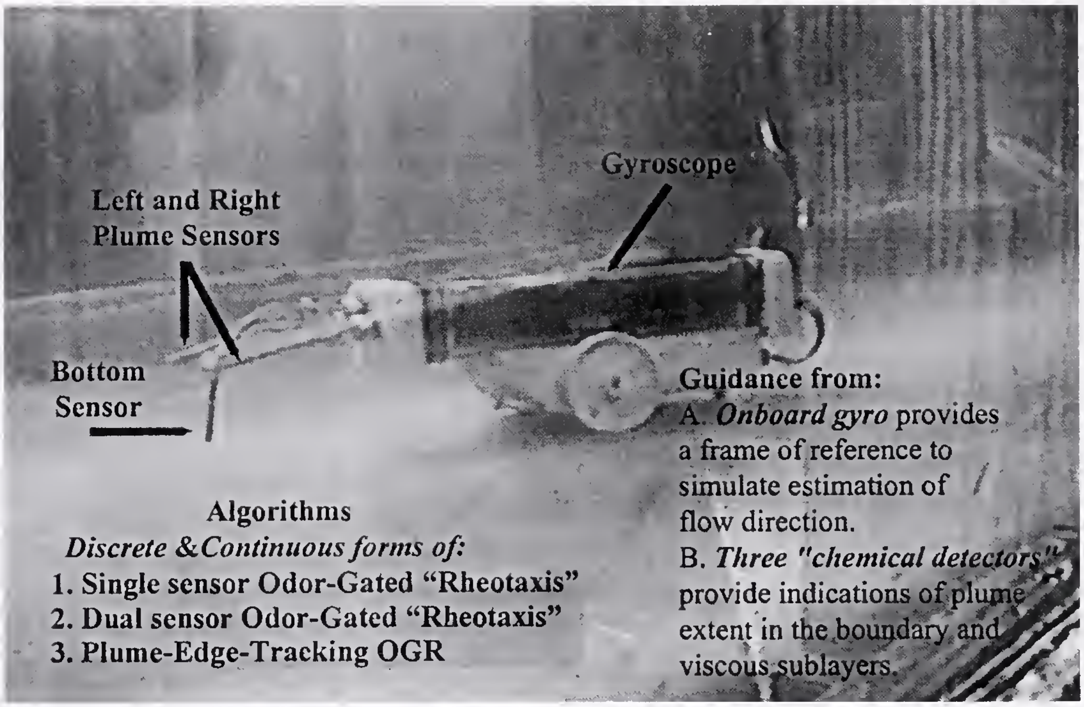
Gyroscope
Left and Right Plume Sensors
Bottom Sensor
Guidance from:
A. *Onboard gyro* provides a frame of reference to simulate estimation of flow direction.
B. *Three "chemical detectors"* provide indications of plume extent in the boundary and viscous sublayers.
Algorithms
Discrete & Continuous forms of:
1. Single sensor Odor-Gated "Rheotaxis"
2. Dual sensor Odor-Gated "Rheotaxis"
3. Plume-Edge-Tracking OGR

Figure 2. One of our biomimetic robots, in the large flume facility at the Marine Biological Laboratory, Woods Hole. The biologically inspired chemical sensing aquatic autonomous robots (BISAAR) are equipped with two antenna-like fluorescence sensors that detect fluorescein dye with the spatial (1 mm) and temporal (>5 Hz) resolution of the lobster lateral antennule. From this information, and an approximation of the mean flow in the tank provided by a gyroscope, the BICSAAR robots are a platform for exploring plume-tracking algorithms. The third chemical sensor, the "bottom sensor," pointed toward the flume floor is intended to fulfill part of the role of the chemical sensors on the legs of real lobsters. It is used in studies of behavioral switching between antennule and leg-guided chemo-orientation. The wheeled chassis is capable of propelling and turning faster than its biological counterparts, so to a first approximation it achieves locomotory biomimetic scaling.

were identical). The comparison was also possible because the critical factors of robot hardware and software required to implement the algorithms were matched to the corresponding biological characteristics of the lobster (Fig. 2). I refer to this as *biomimetic scaling.*

My use of the term biomimetic is not intended to denote a slavish mimicry of all the biological details. The mimicry is primarily conceptual and is structural only as needed to support the conception. The idea of biomimetic scaling is to reproduce only those points that are essential to test a given hypothesis. Thus, to test the power of OGR or tropotaxis as explanations of plume tracking by lobsters, we constrained the following critical features to known lobster values: body size and shape, sensor arrangement in space, speed and pattern of locomotion, and temporal and spatial resolution of the sensors in the robots' hardware and software to known lobster values (Grasso *et al.*, 2000).

These experiments were conducted to evaluate behavioral theories. The results, while germane to the plume-tracking problem, had broader implications for the study of fluid mechanics, cybernetics, and neuroscience, as noted above. Continued studies with more strenuous constraints—from implementation of a realistic neural architecture, to software or sensors configured to take advantage of fluid flow around the robot in ways that mimic antennal morphology—will lead to the evaluation of theories with ever-greater explanatory (or exclusionary) power. In future studies, biomimetic scaling will allow us to use robots to explore issues of neural processing and biomechanical strategies of spatial sampling.

Though space prohibits a detailed review, note that affordable technologies are available from commercial suppliers to make small processors and actuators as well as biologically scaled sensors that are suitable to meet the demands of biomimetic scaling (Ishida *et al.*, 2001; Robert, 2001).

Conclusions

With the methodology described in this paper, we cannot "prove" that the algorithms biomimetic robots implement are the exact analogs of biological mechanisms. Those mechanisms can only be determined from biological experiments. But in the application of the scientific method, we can exclude untenable biological explanations, simply stating that they fail to account for the biological behavior.

As this process of excluding the biologically implausible proceeds, something unrelated will occur in parallel. The ability of the robots to track chemical plumes to their source will improve as their performance approaches that of real animals. Thus, although there is no scientific guarantee that the robots will ever match their biological models, a realizable benchmark will be systematically approached. The algorithms gleaned from these biologically inspired studies can find practical application as components in autonomous systems intended for exploration.

Though the "one plume at a time" approach is a slow and inductive one, the principle of "dynamic similarity" indicates that strategies developed in one context may find general utility in autonomous systems that are designed to operate at a variety of scales with coincidental Reynolds numbers. This extends to regimes in fluids of different viscosity like water and air (or any fluid for that matter). Studies of behavioral switching by animals may help to demarcate these boundaries and may also suggest control hierarchies that will recognize strategies appropriate to particular fluid-dynamic contexts.

Finally, invertebrates offer excellent models for the study of plume tracking. Their external sensors, borne on movable antennae, provide access to dynamic information associated with plume structures that is simply not available to vertebrates with internal noses. This may mean a richer diversity of information, and by analogy to the significance of eye movements for visual information processing (Yarbus, 1967), the motions of the antennae provide an easily assayed indication of information-processing strategies.

Acknowledgments

This work was supported in part by a grant from the joint DARPA/ONR plume-tracing program administered by Keith Ward (ONR) and Regina Dugan (DARPA). I thank Jelle Atema, Jennifer Basil, David Mountain, and Rainer Voigt for stimulating and inspiring discussions; Lisa Borden, Todd Cowen, Jonathan Dale, Kevin Dittmer, and John Hanna, for technical assistance; Diana Blazis and Pam Oldham for making the ISIP-BIAS symposium possible and successful; and Todd Cowen, Jeff Kosseff, and Don Webster for discussions of fluid dynamics and for drawing my attention to the Los Alamos plume.

Literature Cited

Alder, J. 1969. Chemoreceptors in bacteria. *Science* **166:** 1588–1597.

Alder, J. 1987. How motile bacteria are attracted and repelled by chemicals: an approach to neurobiology. *Biol. Chem.* **386:** 163–173.

Atema, J. 1996. Eddy chemotaxis and odor landscapes: exploration of nature with animal sensors. *Biol. Bull.* **191:** 129–138.

Baker, T. C., B. S. Hansson, C. Lofstedt, and J. Lofqvist. 1988. Adaptation of antennal neurons in moth is associated with cessation of pheromone-mediated upwind flight. *Neurobiology* **85:** 9826–9830.

Basil, J., and J. Atema. 1994. Lobster orientation in turbulent odor plumes: simultaneous measurement of tracking behavior and temporal odor patterns. *Biol. Bull.* **187:** 272–273.

Beer, R. D., H. J. Chiel, and L. S. Sterling. 1991. An artificial insect: computer-simulated insects that adapt to their environment may be the next stage in evolution of artificial intelligence. *Am. Sci.* **79:** 444–452.

Beglane, P. F., F. W. Grasso, J. A. Basil, and J. Atema. 1997. Far field chemo-orientation in the American lobster, *Homarus americanus:* effects of unilateral ablation and lesioning of the lateral antennule. *Biol. Bull.* **193:** 214–215.

Belanger, J. H., and M. A. Willis. 1996. Adaptive control of odor-guided locomotion: behavioral flexibility as an antidote to environmental unpredictability. *Adapt. Behav.* **4:** 217–253.

Bell, W. J. 1986. Responses of arthropods to temporal chemical stimulus changes: simulation of a humidity differential and a pheromone plume. Pp. 139–148 in *Mechanisms in Insect Olfaction*, T. L. Payne, M. C. Birch, and C. E. J. Kennedy, eds. Clarendon Press, Oxford.

Berg, R. C., and E. M. Purcell. 1977. The physics of chemoreception. *Biophysics* **20:** 193–219.

Braitenberg, V. 1984. *Vehicles: Experiments in Synthetic Psychology.* Bradford Books, MIT Press, Cambridge, MA.

Cowen, E. A., and S. G. Monismith. 1997. A hybrid digital particle tracking velocimetry technique. *Exp. Fluids* **22:** 199–211.

Derby, C. D., and P. Steullet. 2001. Why do animals have so many receptors? The role of multiple chemosensors in animal perception. *Biol. Bull.* **200:** 211–215.

Deveza, R., D. Thiel, A. Russell, and A. Mackay-Sim. 1994. Odor sensing for robot guidance. *Int. J. Robot. Res.* **13:** 232–239.

Devine, D. V., and J. Atema. 1982. Function of chemoreceptor organs in spatial orientation of the lobster, *Homarus americanus:* differences and overlap. *Biol. Bull.* **163:** 144–153.

Ferree, T. C., T. M. Morse, and S. R. Lockery. 1997. Neural networks for chemotaxis in *C. elegans:* rule extraction and robotics. Society for Neuroscience: 27th Annual Meeting, New Orleans, 25–30 October 1997. Abstr. #527.10.

Ford, N. B. 1986. The role of pheromone trails in the sociobiology of snakes. Pp. 261–278 in *Chemical Signals in Vertebrates*, D. Duvall, D. Muller-Schwartze, and R. M. Silverstien, eds. Plenum, New York.

Ford, N. B., and J. R. Low. 1984. Sex pheromone source location by garter snakes: a mechanism of detection of direction in nonvolatile trails. *J. Chem. Ecol.* **10:** 1193–1199.

Fraenkel, G. S., and D. L. Gunn. 1961. *The Orientation of Animals: Kineses, Taxes and Compass Reactions.* Dover, New York.

Getz, W. 1999. A kinetic model of the transient phase in the response of olfactory receptor neurons. *Chem. Senses* **24:** 497–508.

Gibson, J. J. 1982. Ecological physics, magic and reality. Pp. 217–223 in *Reasons for Realism: Selected Essays of James J. Gibson*, R. Edward and R. Jones, eds. Lawrence Erlbaum Associates, London.

Gomez, G., and J. Atema. 1996a. Temporal resolution in olfaction: stimulus integration time of lobster chemoreceptor cells. *J. Exp. Biol.* **199:** 1771–1779.

Gomez, G., and J. Atema. 1996b. Temporal resolution in olfaction II: time course of recovery from adaptation in lobster chemoreceptor cells. *J. Neurophysiol.* **76:** 1340–1343.

Gomez, G., R. Voigt, and J. Atema. 1999. Temporal resolution in olfaction III: flicker fusion and concentration-dependent synchronization with stimulus pulse trains of antennular chemoreceptor cells in the American lobster. *J. Comp. Physiol.* **185:** 427–436.

Grasso, F. W., T. Consi, D. Mountain, and J. Atema. 1996a. Locating odor sources in turbulence with a lobster inspired robot. Pp. 104–112 in *From Animals to Animats 4: Proceedings of the Fourth International Conference on Simulation of Adaptive Behavior*, P. Maes, M. J. Mataric, J.-A. Meyer, J. Pollack, and S. W. Wilson, eds. MIT Press, Cambridge, MA.

Grasso, F. W., J. H. Dale, T. R. Consi, D. C. Mountain, and J. Atema. 1996b. Behavior of purely chemotactic robot lobster reveals different odor dispersal patterns in the jet region and the patch field of a turbulent plume. *Biol. Bull.* **191:** 312–313.

Grasso, F. W., J. H. Dale, T. R. Consi, D. C. Mountain, and J. Atema. 1997. Effectiveness of continuous bilateral sampling for robot chemotaxis in a turbulent odor plume: implications for lobster chemo-orientation. *Biol. Bull.* **193:** 215–216.

Grasso, F. W., T. R. Consi, D. C. Mountain, and J. Atema. 2000. Biomimetic robot lobster performs chemo-orientation in turbulence using a pair of spatially separated sensors: progress and challenges. *Robot. Aut. Sys.* **30:** 115–131.

Hamner, P., and W. M. Hamner. 1977. Chemosensory tracking of scent trails by the planktonic shrimp *Acetes sibogae australis. Science* **195:** 886–888.

Hildebrand, J. G., and G. M. Shepherd. 1997. Mechanisms of olfactory discrimination: converging evidence for common principles across phyla. *Annu. Rev. Neurosci.* **20:** 595–631.

Holland, O., and C. Melhuish. 1996. Some adaptive movements of animats with single symmetrical sensors. Pp. 53–64 in *From Animals to Animats: Proceedings of the Fourth International Conference on Simulation of Adaptive Behavior*, P. Maes, M. J. Mataric, J.-A. Meyer, J. Pollack, and S. W. Wilson, eds. MIT Press, Cambridge, MA.

Ishida, H., Y. Kagawa, T. Nakamoto, and T. Moriizumi. 1996. Odor-source localization in the clean room by an autonomous mobile sensing system. *Sensors and Activators B* **33:** 115–121.

Ishida, H., T. Nakamoto, T. Moriizumi, T. Kikas, and J. Janata. 2001. Plume-tracing robots: a new application of chemical sensors. *Biol. Bull.* **200:** 222–226.

Kennedy, J. S. 1986. Some current issues in orientation to odour sources. Pp. 11–25 in *Mechanisms in Insect Olfaction*, T. L. Payne, M. C. Birch, and C. E. J. Kennedy, eds. Clarendon Press, Oxford.

Lemon, W. C., and W. M. Getz. 1996. Temporal resolution of general odor pulses by olfactory sensory neurons in American cockroaches. *J. Exp. Biol.* **200:** 1809–1819.

Lemon, W. C., and W. M. Getz. 1999. Responses of cockroach antennal lobe projection neurons to pulsatile olfactory stimuli. *Ann. N. Y. Acad. Sci.* **855:** 517–520.

Mafra-Neto, A., and R. T. Carde. 1994. Fine-scale structure of pheromone plumes modulates upwind orientation of flying moths. *Nature* **369:** 142–144.

Mafra-Neto, A., and R. T. Carde. 1996. Dissection of the pheromone-modulated flight of moths using single-pulse response as a template. *Experientia* **52:** 373–379.

Mast, S. O. 1938. Factors involved in the orientation of lower organisms to light. *Biol. Rev.* **13:** 186–224.

McCoy, M. M. 1984. Antennal movements of the American cockroach *Periplaneta americana.* Ph.D. dissertation. University of Kansas, Lawrence.

Moore, P. A., and J. Atema. 1991. Spatial information in the three-dimensional fine structure of an aquatic odor plume. *Biol. Bull.* **181:** 408–418.

Moore, P. A., N. Scholz, and J. Atema. 1991. Chemical orientation of lobsters, *Homarus americanus,* in turbulent odor plumes. *J. Chem. Ecol.* **17:** 1293–1307.

Morse, T. M., T. C. Ferree, and S. R. Lockery. 1998. Robust spatial navigation in a robot inspired by chemotaxis in *Caenorhabditis elegans. Adapt. Behav.* **6:** 393–410.

Mountain, D. C., and A. E. Hubbard. 2001. Sensing scenes with silicon. *Biol. Bull.* **200:** 227–234.

Murlis, J., and C. D. Jones. 1981. Fine-scale structure of odour plumes in relation to insect orientation to distant pheromones and other attractant sources. *Physiol. Entomol.* **6:** 71–86.

Murlis, J., J. S. Elkinton, and R. T. Carde. 1992. Odor plumes and how insects use them. *Annu. Rev. Entomol.* **37:** 505–532.

Pierce-Shimomura, J. T., T. M. Morse, and S. R. Lockery. 1999. The fundamental role of pirouettes in *Caenorhabditis elegans* chemotaxis. *J. Neurosci.* **19:** 9557–9569.

Reeder, P. B., and B. W. Ache. 1980. Chemotaxis in the Florida spiny lobster, *Panulirus argus. Anim. Behav.* **28:** 831–839.

Robert, D. 2001. Innovative biomechanics for directional hearing in small flies. *Biol. Bull.* **200:** 190–194.

Rohlf, J. F., and D. Davenport. 1969. Simulation of simple models of animal behavior. *J. Theor. Biol.* **23:** 400–424.

Snyder, N. F. R., and H. A. Snyder. 1971. Pheromone-mediated behaviour of *Fasciolaria tulipa. Anim. Behav.* **19:** 257–268.

Srinivasan, M. V., S. Zhang, and J. S. Chahl. 2001. Landing strategies in honeybees and possible applications to autonomous airborne vehicles. *Biol. Bull.* **200:** 216–221.

Srinivasan, M. V., S. W. Zhang, M. Lehrer, and T. S. Collett. 1996. Honeybee navigation en route to the goal: visual flight control and odometry. *J. Exp. Biol.* **199:** 237–244.

Vickers, N. J., and T. C. Baker. 1992. Male *Heliothis virescens* maintain upwind flight in response to experimentally pulsed filaments of their sex pheromone (Lepidoptera: Noctuidae). *J. Insect Behav.* **5:** 669–687.

Wachowiak, M., M. Zochowski, L. B. Cohen, and C. X. Falk. 2000. The spatial representation of odors by olfactory receptor neuron input to the olfactory bulb is concentration invariant. *Biol. Bull.* **199:** 162–163.

Warhaft, Z. 2000. Passive scalars in turbulent flows. *Annu. Rev. Fluid Mech.* **32:** 203–240.

Wehner, R. 1987. Matched filters—neural models of the external world. *J. Comp. Physiol. A* **161:** 511–531.

Weissburg, M. J., and R. K. Zimmer-Faust. 1994. Odor plumes and how blue crabs use them in finding prey. *J. Exp. Biol.* **197:** 349–375.

Wells, M. J., and S. K. L. Buckley. 1972. Snails and trails. *Anim. Behav.* **20:** 345–355.

Wilson, E. O. 1962. Chemical communication among workers of the fire ant *Solenopsis saevissima* (Fr. Smith). 1. The organization of mass foraging. *Anim. Behav.* **10:** 134–147.

Yarbus, A. L. 1967. *Eye Movements and Vision.* Plenum Press, New York.

Yen, J. 2000. Life in transition: balancing inertial and viscous forces by planktonic copepods. *Biol. Bull.* **198:** 213–224.

Zimmer-Faust, R. K., C. M. Finelli, N. D. Pentcheff, and D. S. Wethey. 1995. Odor plumes and animal navigation in turbulent water flow: a field study. *Biol. Bull.* **188:** 111–116.

Reference: *Biol. Bull.* **200:** 169–176. (April 2001)

Limulus Vision in the Marine Environment

ROBERT B. BARLOW*, JAMES M. HITT, AND FREDERICK A. DODGE

Center for Vision Research, Department of Ophthalmology, Upstate Medical University, 750 Adams Street, Syracuse, New York 13210

Abstract. Horseshoe crabs use vision to find mates. They can reliably detect objects resembling potential mates under a variety of lighting conditions. To understand how they achieve this remarkable performance, we constructed a cell-based realistic model of the lateral eye to compute the ensembles of optic nerve activity ("neural images") it transmits to the brain. The neural images reveal a robust encoding of mate-like objects that move underwater during the day. The neural images are much less clear at night, even though the eyes undergo large circadian increases of sensitivity that nearly compensate for the millionfold decrease in underwater lighting after sundown. At night the neural images are noisy, dominated by bursts of nerve impulses from random photon events that occur at low nighttime levels of illumination. Deciphering the eye's input to the brain begins at the first synaptic level with lowpass temporal and spatial filtering. Both neural filtering mechanisms improve the signal-to-noise properties of the eye's input, yielding clearer neural images of potential mates, especially at night. Insights about visual processing by the relatively simple visual system of *Limulus* may aid in the design of robotic sensors for the marine environment.

Introduction

The world is rich with sensory information, and animals are highly efficient at extracting what is essential for their survival. The retina begins the processing of visual information by transforming patterns of incident light intensity into trains of impulses in optic nerve fibers (Dowling, 1987). The retina encodes information it receives in a reliable and efficient manner (Rieke *et al.*, 1997) but does not encode all of it. Rather, the retina extracts certain features in the visual scene at the expense of others (Lettvin *et al.*, 1959). An important first step for exploring the neural code the eye transmits to the brain when an animal sees is to understand what an animal can see in its natural habitat. The next step is to examine the retinal coding of natural scenes in activity of optic nerve fibers. Recordings from single nerve fibers have indeed yielded useful insights about retinal function; however, it is difficult to infer from them the information transmitted by arrays of optic nerve fibers to the brain about the complex patterns of illumination animals encounter in their natural habitat. Techniques such as multielectrode arrays (Meister *et al.*, 1994) and voltage-sensitive dyes (Wong *et al.*, 1995) can access patterns of activity generated by ensembles of retinal neurons, but they are not practical for recording from large numbers of optic nerve fibers in behaving animals.

A Computational Model of the *Limulus* Eye

An alternative approach is to construct a realistic computational model of the eye. The relative simplicity of the eyes of lower vertebrates and invertebrates offers the best opportunities (Werblin, 1991; Teeters *et al.*, 1997). The lateral eye of the horseshoe crab *Limulus polyphemus* is a particularly attractive model system for the following reasons: first, its visually guided behavior is well known (Barlow *et al.*, 1982; Powers *et al.*, 1991; Herzog *et al.*, 1996); second, it processes visual information with integrative mechanisms shared by more complex systems (Barlow, 1969; Ratliff, 1974); and third, its lateral eye contains the largest neural network (~1000 neurons) for which a quantitative cell-based model exists (Hartline and Ratliff, 1957, 1958; Barlow and Quarles, 1975; Barlow *et al.*, 1993b).

---

* To whom correspondence should be addressed. E-mail: barlowr@upstate.edu.

This paper was originally presented at a workshop titled *Invertebrate Sensory Information Processing: Implications for Biologically Inspired Autonomous Systems.* The workshop, which was held at the J. Erik Jonsson Center for the National Academy of Sciences, Woods Hole, Massachusetts, from 15–17 April 2000, was sponsored by the Center for Advanced Studies in the Space Life Sciences at the Marine Biological Laboratory, and funded by the National Aeronautics and Space Administration under Cooperative Agreement NCC 2-896.

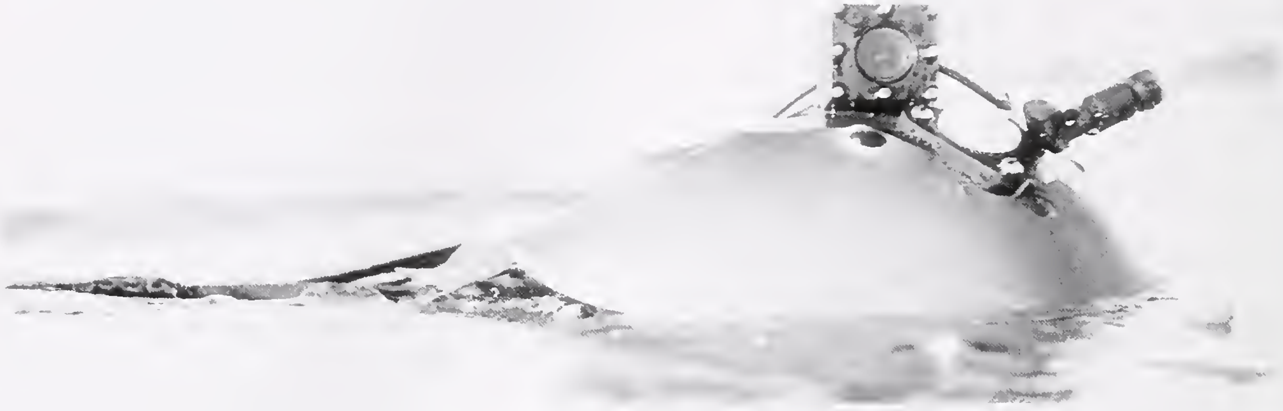

Figure 1. A horseshoe crab, *Limulus polyphemus*, mounted with a video camera, "CrabCam," for recording underwater movies and a microsuction electrode for recording responses from a single optic nerve fiber. A white Teflon cap (2.5 cm diameter) seals the recording chamber, which is attached to the carapace anterior to the right lateral eye. The barrel of the microsuction electrode protrudes from the recording chamber to the right. Tethers lead the video and optic nerve signals to recording electronics located on shore or in an overhead skiff as the animal moves about underwater at depths of 0.5 to 1 m. Experiments were carried out in an estuary near the Marine Biological Laboratory, Woods Hole, Massachusetts.

We have constructed a computational model of the lateral eye that predicts optic nerve responses with good accuracy (Passaglia *et al.*, 1998). In brief, the model treats the retina as an array of neurons that samples visual space as the compound eye does, incorporates the known excitatory and inhibitory integrative mechanisms of the retina, and adapts to changes in ambient illumination.

Our strategy for examining the retinal code underlying behavior is to first videotape the lateral eye's view of its underwater world with an animal-mounted camera ("CrabCam") while simultaneously recording from a single optic nerve fiber of an ommatidium viewing the central region of the videotaped scene (Passaglia *et al.*, 1997a). Figure 1 shows the CrabCam and the watertight recording chamber mounted on an animal before it enters the water and passes near submerged mate-like objects near the water's edge in Woods Hole, Massachusetts. Back in the laboratory we digitize the CrabCam recordings and feed them to the cell-based model, which then computes the arrays of optic nerve activities in response to the underwater scenes. The computed arrays of activities are converted to a grey scale and mapped to their appropriate retinal location, generating "neural images" of the eye's input to the brain (Fig. 2). Finally, we assess the accuracy of the model's predictions by comparing the response recorded from a single optic nerve fiber to that computed by the model for the corresponding receptor. Correlation coefficients between recorded and com-

Figure 2. Computed responses of the *Limulus* eye and brain to moving mate-like objects day and night. Top panel shows the results for a low-contrast object, and the bottom panel shows those for a high-contrast object. The two objects approximate the size (0.3 m diameter, 0.15 m high) and range of contrasts of adult female crabs. They move across the visual field at a distance of 0.6 m, where most visual detection occurs (Herzog *et al.*, 1996). The left column ("Visual stimulus") shows CrabCam images of the high- and low-contrast objects after sampling by the eye's optical apparatus. The arrays of pixels indicate the light intensities incident on the 16 × 16 array of ommatidia viewing the videotaped scene. The adjacent column ("Neural image") shows the ensembles of optic nerve activities computed by the retinal model in response to the visual stimuli on the left. The arrays of pixels in the neural images give the computed firing rates of optic nerve fibers mapped onto a gray scale with black set to 0 impulses/s and white set to twice the mean firing rate. Photon fluxes were reduced by $\sim 10^6$ in the model calculations to simulate the "Night" state of the eye. The neural images represent snapshots of the responses of the 16 × 16 array of ommatidia to the visual stimulus. The third column shows the computed neural images of synaptic activity in the brain after "temporal integration" of the retinal neural image with an integration time of 400 ms. The synaptic activities are mapped onto a gray scale with black set to 0 mv and white set to twice the mean amplitude of the synaptic potential. The fourth column displays the computed neural images of synaptic activity in the brain after "spatial summation" within the excitatory centers of the presumptive receptive fields of laminar cells. Note that at night, phototransduction noise obscures the neural images of the visual stimuli, but temporal and spatial integration partially recovers them.

puted responses are typically greater than 95% ($n = 5$) under controlled laboratory conditions but lower for field experiments because of the difficulty of precisely determining the stimulus to the recorded ommatidium. Once satisfied with the accuracy of the model's predictions, we analyze the neural images for information the eye sends to the brain when the animal sees.

The *Limulus* Eye Functions as a Global Feature Detector

The eye transmits to the brain robust "neural images" of objects having the size, contrast, and motion of potential mates (Passaglia *et al.*, 1997a). Inspection of the neural images computed for the daytime state of the eye in Figure 2 shows that the eye is highly sensitive to images of crab-

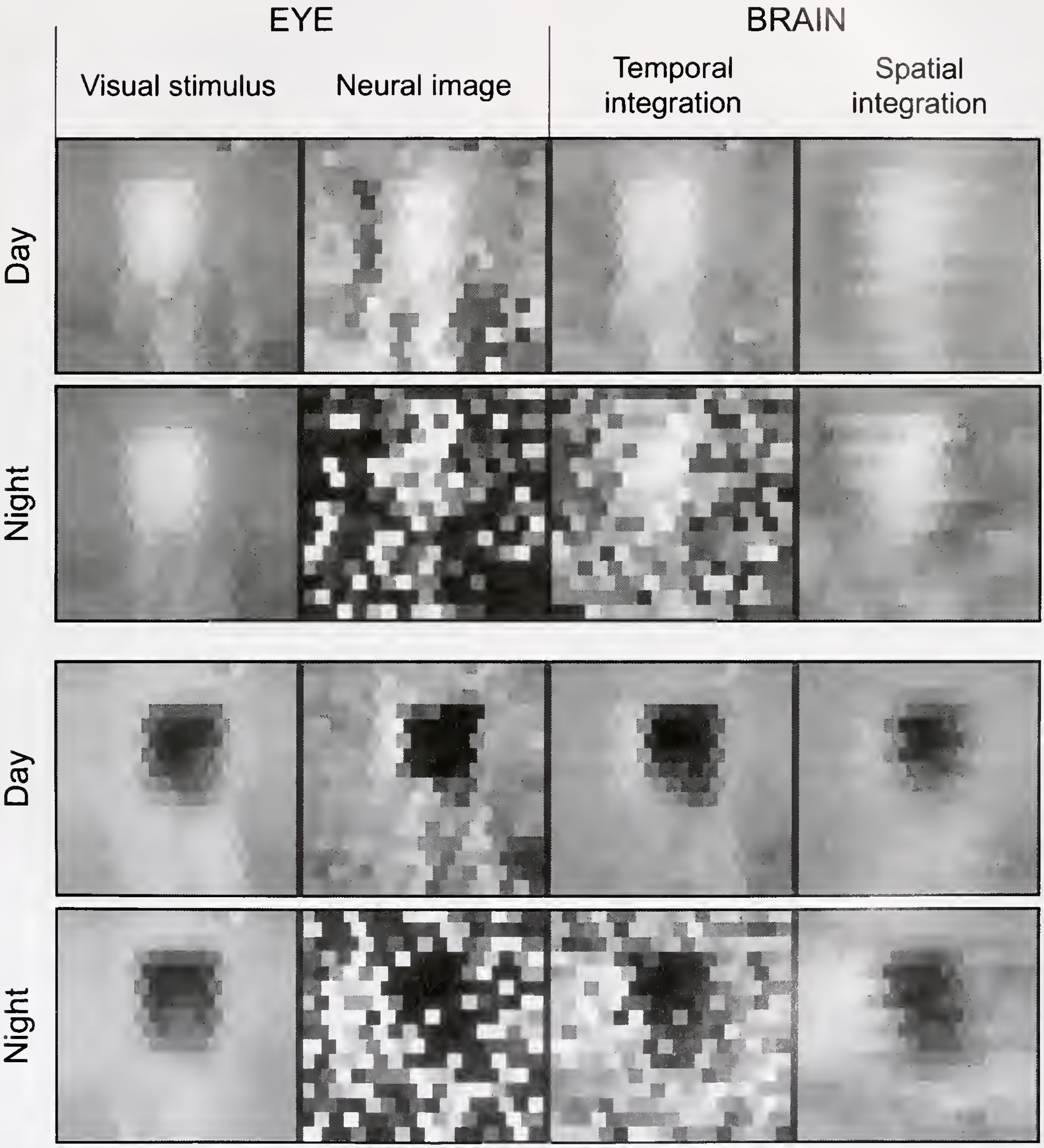
EYE
BRAIN
Visual stimulus
Neural image
Temporal integration
Spatial integration
Day
Night
Day
Night

Table 1

Circadian rhythms in the Limulus *lateral eye*

Retinal property	Day	Night	Reference
Efferent input	Absent	Present	Barlow *et al.*, 1977; Barlow, 1983
Gain	Low	High	Renninger *et al.*, 1984; Barlow *et al.*, 1987
Noise	High	Low	Barlow *et al.*, 1977; Kaplan and Barlow, 1980; Barlow *et al.*, 1993a
Quantum bumps	Short	Long	Kaplan *et al.*, 1990
Frequency response	Fast	Slow	Batra and Barlow, 1990
Dark adaptation	Fast	Slow	Kass and Berent, 1988
Lateral inhibition	Strong	Weak	Renninger and Barlow, 1979; Ruta *et al.*, 1999
Cell position	Proximal	Distal	Barlow and Chamberlain, 1980; Barlow *et al.*, 1980
Pigment granules	Clustered	Dispersed	Barlow and Chamberlain, 1980
Aperture	Constricted	Dilated	Chamberlain and Barlow, 1977, 1987
Acceptance angle	6°	13°	Barlow *et al.*, 1980
Photomechanical movements	Trigger	Prime	Chamberlain and Barlow, 1987
Photon catch	Low	High	Barlow *et al.*, 1980
Membrane shedding	Trigger	Prime	Chamberlain and Barlow, 1979, 1984
Arrestin mRNA level	High	Low	Battelle *et al.*, 2000
Intense light effects	Protected	Labile	Barlow *et al.*, 1989
Visual sensitivity	Low	High	Powers and Barlow, 1985; Herzog *et al.*, 1996

size objects moving within the animal's visual range at about the speed of a horseshoe crab (15 cm/s). Indeed, measurements of the spatial and temporal transfer functions of the eye using linear systems analysis show that it functions as a tuned spatiotemporal filter. These filtering properties can readily account for the animal's ability to see high-contrast objects but not low-contrast ones. Natural fluctuations of underwater lighting enhance the visibility of low-contrast objects. Beams of light created by overhead waves strobe the underwater scene in a range of frequencies (~2–6 Hz) for which the temporal transfer function shows the eye is maximally sensitive. Such wave-induced flicker increases the visibility of low-contrast, crab-sized objects during the day, as observed in field studies (Passaglia *et al.*, 1997b; Krutky *et al.*, 2000). The strobic light evokes coherent bursts of nerve impulses from clusters of neighboring ommatidia as the object moves across the visual field. These coherent bursts of activity are equal in amplitude to those evoked by moving, high-contrast objects, which is consistent with the animal's ability to detect mate-like objects regardless of their contrast. Stationary objects, either high or low contrast, are hardly recognizable in the computed neural images (not shown).

Limulus vision requires both stimulus motion and activities generated over ensembles of retinal receptors. The neural code for moving crab-like objects is not found in ambiguous messages of individual optic nerve fibers but in the coherent activity of small ensembles of nerve fibers. Such "distributed coding" has been detected in amphibian (Warland *et al.*, 1997; Brivanlou *et al.*, 1998) and mammalian visual systems (Field, 1994; Alonso *et al.*, 1996; Berry *et al.*, 1997; De Vries, 1999; Meister and Berry, 1999). In *Limulus*, stimulus motion binds these coherent activities together, sending a robust signal to the brain about potential mates. Endowed with spatiotemporal filtering properties, the eye is a sensitive detector of moving, crab-sized objects.

A Circadian Clock Modulates Lateral Eye Sensitivity

The *Limulus* eye operates in two distinct states: daytime and nighttime. It not only responds to changes in illumination, it anticipates them. At dusk a circadian oscillator in the brain transmits efferent optic-nerve signals to the lateral eye, influencing almost every physiological and anatomical property of the retina (Table 1).

The endogenous rhythms of the retina combine with mechanisms of light and dark adaptation to increase visual sensitivity by about 10^6 at night, nearly compensating for the decrease in the intensity of illumination in the animal's marine environment. In our initial theoretical analysis of retinal coding discussed above, we constructed a computational model to simulate the daytime state of the eye. To examine the retinal coding that underlies vision at night, we must modify our computational model so that it can account for the circadian changes in lateral eye function. We have developed a "nighttime" model that includes most of the circadian changes listed in Table 1.

Photon Noise Dominates Retinal Responses at Night

Neural images of mate-like objects are less clear at night. They are dominated by bursts of spikes triggered by random photon events that characterize low nighttime levels of illumination (Hitt *et al.*, 2000). The high-contrast object is detectable in the computed neural image in Figure 2, but the low-contrast object is almost completely obscured by random photon events. Computations require the setting of

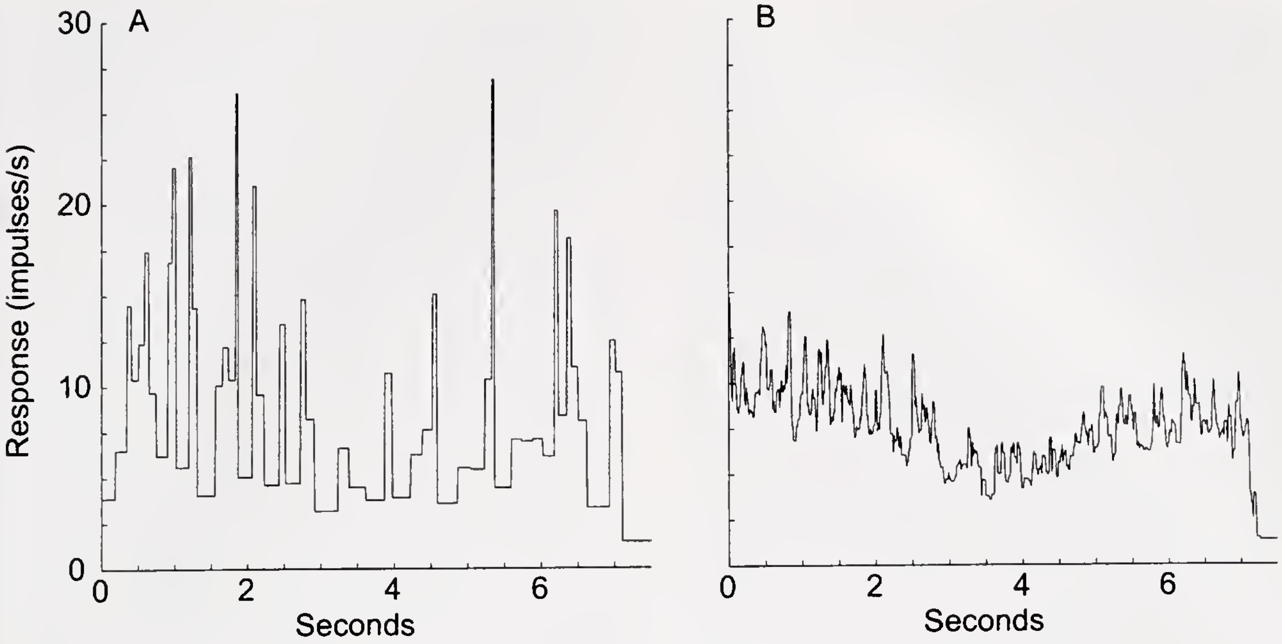

Figure 3. (A) Response of a single optic nerve fiber to a black mate-like object moving across the visual field. Plotted are the instantaneous frequencies, reciprocals of the intervals between nerve impulses, of the train of spikes over a 7-s period. The highly variable discharge reflects phototransduction noise caused by random photon events at low nighttime light levels. (B) Average of the responses of the single optic nerve fiber to 15 repetitions of the visual stimulus. Modulation by the moving black object is evident in the average response but not in the single one.

initial conditions, and an important initial condition is the mean light level of the visual scene. To simulate the nighttime state we reduce the mean light level by 10^6 relative to daytime levels. At such low light levels the Poisson nature of photon absorption events produces substantial phototransduction noise that can obscure signals generated by visual stimuli.

The response of a single optic nerve fiber in Figure 3A recorded under nighttime light levels is indeed variable. It shows no clear sign that a high-contrast crab-sized object had moved across the visual field. This experiment was performed in the laboratory because the Crabcam is insensitive to the low light levels in the animal's habitat at night. To overcome this problem we simulated nighttime conditions by aligning an animal in front of a monitor that played back CrabCam recordings made in the animal's habitat. The output of the monitor was attenuated by 10^6 with neutral density filters to approximate nighttime levels of illumination. The highly variable optic nerve response shown in Figure 3A is consistent with the noisy neural images in Figure 2 that were computed with the nighttime model of the eye.

Brain Processing Enhances Retinal Signals

How does the brain extract a reliable signal from such a noisy retinal input? Optic nerve fibers carrying the retinal signals synapse on neurons of the lamina of the brain. Single-cell recordings show that the laminar synapses integrate retinal signals with a time constant of about 400 ms (Passaglia *et al.*, 1997a). To assess the effect of these "slow" synapses we added a stage of temporal integration to the computational models. Figure 2 shows that synaptic integration with such a long time constant suppresses the high-frequency fluctuations in optic nerve activity both day and night. The effect is especially striking in the neural images computed for the daytime state where temporal integration nearly recovers the visual stimulus. It is interesting that in another invertebrate visual system, that of the fly *Lucilia cuprina*, temporal integration reliably recovered the stimulus-induced response component from noisy neuronal signals in the motion pathway (Warzecha and Egelhaaf, 1997). Returning to *Limulus*, temporal integration of the neural images generated by the retina in its nighttime state does not recover the visual stimulus. The burstiness evoked by random photon events (Fig. 2) remains prominent and obscures information about the visual stimulus.

Because horseshoe crabs can see potential mates nearly as well at night as during the day, the brain must possess additional neural mechanisms for processing the retinal input, although these mechanisms need not be located in the lamina. One such mechanism could be spatial integration within the receptive fields of laminar neurons (Hitt *et al.*, 2000). Although the dimensions of receptive fields in the lamina have not been mapped with precision, we assumed for preliminary calculations that each laminar neuron sums optic nerve inputs from a 3 × 3 matrix of retinal receptors. Figure 2 shows that adding such a stage of spatial integration significantly improves the signal-to-noise properties of the neural images in the brain computed for the nighttime state of the eye. Integrating the optic nerve responses from an array of retinal receptors viewing partially overlapping regions of visual space is nearly equivalent to averaging the responses from a single receptor. Indeed, Figure 3B shows that averaging responses of a single receptor to repeated visual stimuli yielded a clear modulation of optic nerve activity, whereas a single response exhibited no detectable modulation. We conclude that circadian increases in the sensitivity of the lateral eye in combination with lowpass spatial and temporal filtering in the brain can yield detectable visual signals in the presence of high phototransduction noise caused by low nighttime light levels. The circadian and neural integrative mechanisms may help explain how *Limulus* can see so well at night.

What Is the Neural Basis of Behavior?

How does the intricate circuitry of a nervous system receive sensory information, process it, and generate a behavioral response? Analyzing a relatively simple nervous system may yield important insights about the functioning of more complex ones. Indeed the visual system of *Limulus* has proven complex enough to be interesting, yet simple enough to be understood. Using a computational approach, we unraveled its coding properties and determined the neural image it sends to the brain about behaviorally relevant stimuli during the day. The *Limulus* eye, however, turned out not to be so "simple" after all. A circadian clock increases its sensitivity at night, enabling the animal to detect potential mates, a critical task that it performs equally well day and night. The clock does so by modulating almost every property of the retina, from stabilizing rhodopsin to weakening lateral inhibition and increasing photoreceptor gain (see Table 1). The challenge addressed in this paper is to understand how the eye efficiently encodes information about potential mates under the photon-limited conditions of the animal's marine environment at night. The answer in part appears to be that coding mechanisms in the eye together with integrative mechanisms in the brain overcome environmental noise to enhance the neural images of behaviorally important visual stimuli.

The neural basis of visually guided behavior has been studied extensively in another invertebrate, the fly. Particular attention has been paid to understanding how the fly visual system adapts to, encodes, and processes natural stimuli (Review: Rieke *et al.*, 1997). Adaptative mechanisms in the fly retina appear to enhance the efficiency of coding information about natural scenes (Review: Laughlin, 1994). In more central pathways, adaptive motion-sensitive mechanisms rescale the dynamic range of neural responses to match that of stimuli and thereby maximize information transmission (Brenner *et al.*, 2000). Adaptation of the motion-sensitive mechanisms decreases contrast sensitivity while preventing saturation of neural responses and preserving receptive field response properties (Harris *et al.*, 2000). Whether *Limulus* possesses such adaptive mechanisms is not known. However, as described above, retinal mechanisms endow the *Limulus* eye with high sensitivity to the motion of natural stimuli, and central mechanisms suppress noisy retinal signals to recover stimulus-induced responses.

This brings us to more complex systems such as the vertebrate retina. With tens of millions of cells, dendritic processes, and synaptic contacts, the task of deciphering its neural code is indeed daunting. Developing a cell-based, realistic computational model as we did for *Limulus* appears unrealistic. A different computational approach is needed; one that by necessity models ensembles of neurons. The danger is that such modeling may overlook essential details in the neural circuitry. As was the case for *Limulus*, important insights can come from understanding the function of a sensory organ and how it adapts to changing environmental conditions. Endogenous adaptation mechanisms, such as efferent inputs and circadian oscillators, can often reveal critical aspects of underlying neural mechanisms. Perhaps most important of all is first to understand the role of a sensory modality in an animal's life and then to investigate the underlying neural mechanisms.

Implications for Artificial Sensory Systems

Sensory systems, especially those of invertebrates, often serve primary functions. They are highly efficient at extracting from the physical world specific information for behaviors essential for survival: mating, finding food, and avoiding predators. In some animals, subsections of a sensory system may serve singular functions. For example, the *Limulus* brain segregates the processing of visual information, devoting a major locus in the medulla to the region of the visual field that views potential mates. Horizontal strips of ommatidia serving this region form a precise map onto an expanded locus in the medulla (Chamberlain and Barlow, 1982), suggesting that the primary task of this region is mate detection (Dodge *et al.*, 1999). Understanding the functions of such specialized regions of a sensory system and the underlying neural integrative mechanisms may aid in the design of artificial sensory systems useful for remote sensing and robotics.

Excitation and inhibition are universal mechanisms for processing the spatial and temporal features of sensory information. They "tune" sensory systems, selecting essential features from a world rich in information. Remarkably, the integrative mechanisms of the *Limulus* eye make it highly sensitive to moving, mate-like objects. Mechanisms of adaptation enable the eye to operate over wide ranges of environmental conditions. In sum, the neural mechanisms of this so-called "primitive" eye encode and analyze visual information and send a highly processed neural image to the brain both day and night.

The implications for artificial sensory systems are (1) a relatively simple neural circuit can encode and process sensory information, and (2) the same neural circuit can operate over a wide range of environmental conditions. Can an artificial system be designed and constructed with these properties? We implemented a software-based computational model that incorporates these properties, but with current hardware it cannot function in real time. Computations are an order of magnitude slower than real time; that is, computing the eye's response (neural images) to 6 s of visual input requires about 60 s. At this time a computational model appears unrealistic. An alternative approach is to construct a silicon retina having all the known properties of the *Limulus* eye. Such artificial retinas have been fabricated (Mahowald and Mead, 1991), but they are mostly hardwired and not readily adaptable to changing environmental conditions. However, techniques of microcircuitry are advancing at a rapid pace. Perhaps in the not-too-distant future it will be possible to fabricate a silicon retina with stimulus-dependent circuitry that can simulate an eye's numerous adaptative mechanisms. Such a dynamic "softwired eye" would find many uses, from remote sensing in hazardous environments to the navigational control of robots. Because *Limulus* incorporates many of the integrative mechanisms found in more complex vertebrate eyes, it is conceivable that a *Limulus*-inspired "softwired eye" may also prove useful as the first stage of a prosthetic visual system for humans.

Acknowledgments

Supported by NSF-IBN0077583, NIH-MH49741, NIH-EY00667, Research to Prevent Blindness, and the Lions of Central New York.

Literature Cited

Alonso, J-M., W. M. Usrey, and R. C. Reid. 1996. Precisely correlated firing in cells of the lateral geniculate nucleus. *Nature* **383:** 815–819.

Barlow, R. B. 1969. Inhibitory fields in the *Limulus* lateral eye. *J. Gen. Physiol.* **54:** 383–396.

Barlow, R. B., and D. A. Quarles. 1975. Mach bands in the lateral eye of *Limulus:* Comparison of theory and experiment. *J. Gen. Physiol.* **65:** 709–730.

Barlow, R. B., S. J. Bolanowski, and M. L. Brachman. 1977. Efferent optic nerve fibers mediate circadian rhythms in the *Limulus* eye. *Science* **197:** 86–89.

Barlow, R. B., S. C. Chamberlain, and J. Z. Levinson. 1980. The *Limulus* brain modulates the structure and function of the lateral eye. *Science* **210:** 1037–1039.

Barlow, R. B., R. R. Birge, E. Kaplan, and J. R. Tallent. 1993a. On the molecular origin of photoreceptor noise, retinas. *Nature* **366:** 64–66.

Barlow, R. B., R. Prakash, and E. Solessio. 1993b. The neural network of the *Limulus* retina: From computer to behavior. *Am. Zool.* **33:** 66–78.

Barlow, R. B., Jr. 1983. Circadian rhythms in the *Limulus* visual system. *J. Neurosci.* **3:** 856–870.

Barlow, R. B., Jr., and S. C. Chamberlain. 1980. Light and circadian clock modulate structure and function in *Limulus* photoreceptors. Pp. 247–269 in *The Effects of Constant Light on Visual Processes*, T. P. Williams and B. N. Baker, eds. Plenum Press, New York.

Barlow, R. B., Jr., L. C. Ireland, and L. Kass. 1982. Vision has a role in *Limulus* mating behavior. *Nature* **296:** 65–66.

Barlow, R. B., Jr., E. Kaplan, G. H. Renninger, and T. Saito. 1987. Circadian rhythms in *Limulus* photoreceptors. I. Intracellular recordings. *J. Gen. Physiol.* **89:** 353–378.

Barlow, R. B., Jr., S. C. Chamberlain, and H. K. Lehman. 1989. Circadian rhythms in invertebrate vision. Pp. 257–280 in *Facets of Vision*, D. C. Stavenga and R. C. Hardie, eds. Springer-Verlag, Berlin.

Batra, R., and R. B. Barlow, Jr. 1990. Circadian rhythms in the temporal response of the *Limulus* lateral eye. *J. Gen. Physiol.* **95:** 229–244.

Battelle, B. A., C. D. Williams, J. L. Schremser-Berlin, and C. Cacciatore. 2000. Regulation of arrestin mRNA levels in *Limulus* lateral eye: Separate and combined influences of circadian efferent input and light. *Visual Neurosci.* **17:** 217–227.

Berry, M. J., D. K. Warland, and M. Meister. 1997. The structure and precision of retinal spike trains. *Proc. Natl. Acad. Sci. USA* **94:** 5411–5416.

Brenner, N., W. Bialek, and R. R. de Ruyter van Steveninck. 2000. Adaptive rescaling maximizes information transmission. *Neuron* **26:** 695–702.

Brivanlou, I. H., D. K. Warland, and M. Meister. 1998. Mechanisms of concerted firing among retinal ganglion cells. *Neuron* **20:** 527–539.

Chamberlain, S. C., and R. B. Barlow, Jr. 1977. Morphological correlates of efferent circadian activity and light adaptation in the *Limulus* lateral eye. *Biol. Bull.* **153:** 418–419.

Chamberlain, S. C., and R. B. Barlow, Jr. 1979. Light and efferent activity control rhabdom turnover in *Limulus* photoreceptors. *Science* **206:** 361–363.

Chamberlain, S. C., and R. B. Barlow, Jr. 1982. Retinotopic organization of lateral eye input to the *Limulus* brain. *J. Neurophysiol.* **48:** 505–520.

Chamberlain, S. C., and R. B. Barlow, Jr. 1984. Transient membrane shedding in *Limulus* photoreceptors: Control mechanisms under natural lighting. *J. Neurosci.* **4:** 2792–2810.

Chamberlain, S. C., and R. B. Barlow, Jr. 1987. Controls of structural rhythms in the lateral eye of *Limulus:* Interactions of diurnal lighting and circadian efferent activity. *J. Neurosci.* **7:** 2135–2144.

DeVries, S. H. 1999. Correlated firing in rabbit retinal ganglion cells. *J. Neurophysiol.* **81:** 908–920.

Dodge, F. A., J. M. Hitt, and R. B. Barlow. 1999. Segregation of visual information processing in the *Limulus* brain. *Soc. Neurosci. Abstr.* **25:** 1429.

Dowling, J. E. 1987. *The Retina: An Approachable Part of the Brain.* Harvard University Press, Cambridge, MA.

Field, D. 1994. What is the goal of sensory coding? *Neural Comput.* **6:** 559–601.

Harris, R. A., D. C. O'Carroll, and S. B. Laughlin. 2000. Contrast gain reduction in fly motion adaptation. *Neuron* **28:** 595–606.

Hartline, H. K., and F. Ratliff. 1957. Inhibitory interactions of receptor units in the eye of *Limulus*. *J. Gen. Physiol.* **40:** 357–376.

Hartline, H. K., and F. Ratliff. 1958. Spatial summation of inhibitory influences in the eye of *Limulus*, and the mutual interactions of receptor units. *J. Gen. Physiol.* **41:** 1049–1066.

Herzog, E. H., M. K. Powers, and R. B. Barlow. 1996. *Limulus* vision in the ocean day and night: Effects of image size and contrast. *Visual Neurosci.* **13:** 31–41.

Hitt, J. M., V. Ruta, F. A. Dodge, and R. B. Barlow. 2000. Explaining night vision in *Limulus*. *Invest. Ophthalmol. Visual Sci.* **41:** S28.

Kaplan, E., and R. B. Barlow, Jr. 1980. Circadian clock in *Limulus* brain increases response and decreases noise of retinal photoreceptors. *Nature* **286:** 393–395.

Kaplan, E., R. B. Barlow, G. Renninger, and K. Purpura. 1990. Circadian rhythms in *Limulus* photoreceptors. II. Quantum bumps. *J. Gen. Physiol.* **96:** 665–685.

Kass, L., and M. Berent. 1988. Circadian rhythms in adaptation to light of *Limulus* photoreception. *Comp. Biochem. Physiol.* **91:** 229–239.

Krutky, M. A., J. L. Atherton, S. Smith, F. A. Dodge, and R. B. Barlow. 2000. Do the properties of underwater lighting influence the visually guided behavior of *Limulus? Biol. Bull.* **199:** 178–179.

Laughlin, S. B. 1994. Matching coding, circuits, cells, and molecules to signals: General principles of retinal design in the fly's eye. *Prog. Ret. Eye Res.* **13:** 165–196.

Lettvin, Y. L., H. R. Maturana, W. S. McColluch, and W. H. Pitts. 1959. What the frog's eye tells the frog's brain. *Proc. Inst. Radio Eng.* **47:** 1940–1951.

Mahowald, M. A., and C. Mead. 1991. The silicon retina. *Sci. Am.* **264:** 76–82.

Meister, M., and M. J. Berry, II. 1999. The neural code of the retina. *Neuron* **22:** 435–450.

Meister, M., J. Pine, and D. A. Baylor. 1994. Multi-neuronal signals from the retina: Acquisition and analysis. *J. Neurosci. Methods* **51:** 95–106.

Passaglia, C. L., F. A. Dodge, E. H. Herzog, S. Jackson, and R. B. Barlow. 1997a. Deciphering a neural code for vision. *Proc. Natl. Acad. Sci. USA* **94:** 12649–12654.

Passaglia, C. L., M. E. McSweeney, K. M. Stewart, E. Kim, E. J. Mole, M. K. Powers, and R. B. Barlow. 1997b. Visual performance of horseshoe crabs: Role of underwater lighting. *Biol. Bull.* **193:** 205–207.

Passaglia, C. L., F. A. Dodge, and R. B. Barlow. 1998. A cell-based model of the *Limulus* lateral eye. *J. Neurophysiol.* **80:** 1800–1815.

Powers, M. K., and R. B. Barlow, Jr. 1985. Behavioral correlates of circadian rhythms in the *Limulus* visual system. *Biol. Bull.* **169:** 578–591.

Powers, M. K., R. B. Barlow, and L. Kass. 1991. Visual performance of horseshoe crabs day and night. *Visual Neurosci.* **7:** 179–189.

Ratliff, F. 1974. Studies of excitation and inhibition in the retina. Rockefeller University Press, New York.

Renninger, G. H., and R. B. Barlow, Jr. 1979. Lateral inhibition, excitation, and the circadian rhythm of the *Limulus* compound eye. *Soc. Neurosci. Abstr.* **5:** 804.

Renninger, G. H., E. Kaplan, and R. B. Barlow, Jr. 1984. A circadian clock increases the gain of photoreceptor cells of the *Limulus* lateral eye. *Biol. Bull.* **167:** 532.

Rieke, F., D. Warland, R. R. DeRuyter van Steveninck, and W. Bialek. 1997. *Spikes: Exploring the Neural Code.* MIT Press, Cambridge, MA.

Ruta, V. J., F. A. Dodge, and R. B. Barlow. 1999. Evaluation of circadian rhythms in the *Limulus* eye. *Biol. Bull.* **197:** 233–234.

Teeters, J., A. Jacobs, and F. Werblin. 1997. How neural interactions form neural responses in the salamander retina. *J. Comp. Neurosci.* **4:** 5–27.

Warland, D. K., P. Reinagel, and M. Meister. 1997. Decoding visual information from a population of retinal ganglion cells. *J. Neurophysiol.* **78:** 2336–2350.

Warzecha, A. K., and M. Egelhaaf. 1997. How reliably does a neuron in the visual motion pathway of the fly encode behaviourally relevant information? *Eur. J. Neurosci.* **9:** 1365–1374.

Werblin, F. S. 1991. Synaptic connections, receptive fields, and patterns of activity in the tiger salamander retina. *Invest. Ophthalmol. Visual Sci.* **32:** 459–483.

Wong, R. O., A. Chernjavsky, S. J. Smith, and C. J. Shatz. 1995. Early functional networks in the developing retina. *Nature* **374:** 716–718.

Reference: *Biol. Bull.* **200:** 177–183. (April 2001)

Parallel Processing and Image Analysis in the Eyes of Mantis Shrimps

THOMAS W. CRONIN[1,*] AND JUSTIN MARSHALL[2]

[1]*Department of Biological Sciences, University of Maryland Baltimore County, Baltimore, Maryland 21250; and* [2]*VTHRC, University of Queensland, Brisbane, Queensland 4072, Australia*

Abstract. The compound eyes of mantis shrimps, a group of tropical marine crustaceans, incorporate principles of serial and parallel processing of visual information that may be applicable to artificial imaging systems. Their eyes include numerous specializations for analysis of the spectral and polarizational properties of light, and include more photoreceptor classes for analysis of ultraviolet light, color, and polarization than occur in any other known visual system. This is possible because receptors in different regions of the eye are anatomically diverse and incorporate unusual structural features, such as spectral filters, not seen in other compound eyes. Unlike eyes of most other animals, eyes of mantis shrimps must move to acquire some types of visual information and to integrate color and polarization with spatial vision. Information leaving the retina appears to be processed into numerous parallel data streams leading into the central nervous system, greatly reducing the analytical requirements at higher levels. Many of these unusual features of mantis shrimp vision may inspire new sensor designs for machine vision.

Introduction

Of all the senses, vision provides animals with the most precise spatial registration of the external world and of objects in it. Animal vision operates in the spectral range between 300 and 750 nm, but technology has extended the "visual" senses of artificial sensors to cover the spectrum from X-rays to microwaves. Nevertheless, engineers can learn much from the mechanisms that animals use to image the world; to map it to self-centered coordinates; to segment the physical properties of light transmitted, scattered, or reflected by objects; and finally to extract the critical features necessary for survival. Like autonomous vehicles, animals must distinguish and recognize items of interest (*e.g.*, landmarks, predators, prey, and conspecifics); they need to discriminate signals from noise; and they must find their way around a geometrically complicated and visually confusing world.

Biological systems are far more constrained than artificial ones in their choice of materials and in the means by which information is transduced and transmitted. More fundamentally, living visual systems are products both of evolution and development. Evolutionary history acts as a bottleneck, greatly limiting the options available in the design of a modern animal's eye. Also, the eye must pass through a biologically feasible developmental sequence. If the animal is one that undergoes metamorphosis (like many insects and crustaceans), the developing eye must also be functional for the larva's habitat and biological demands, which may affect the eye design available to the adult.

Here, we consider the highly evolved eyes of stomatopod crustaceans, commonly known as mantis shrimp. These marine invertebrates possess compound eyes both as adults and as larvae. Compound eyes are bulky, and they provide very poor spatial resolution for their size. These limits exist because each photoreceptor unit of a compound eye, termed a *rhabdom,* is paired with an individual optical system. Thus, the compound eye type demands an immense proliferation of optical units, increasing its size and complexity, and ultimately limiting the total number of receptors to a few thousand at best (compared to many millions in a

---

* E-mail: cronin@umbc.edu

This paper was originally presented at a workshop titled *Invertebrate Sensory Information Processing: Implications for Biologically Inspired Autonomous Systems.* The workshop, which was held at the J. Erik Jonsson Center for the National Academy of Sciences, Woods Hole, Massachusetts, from 15–17 April 2000, was sponsored by the Center for Advanced Studies in the Space Life Sciences at the Marine Biological Laboratory, and funded by the National Aeronautics and Space Administration under Cooperative Agreement NCC 2-896.

vertebrate-type eye). In compound eyes, the unitary structure composed of optics, photoreceptors, and associated pigment cells is called an *ommatidium.*

Compound eyes, nevertheless, do offer certain possibilities not available to the much more compact camera eye design. Normally, all photoreceptors in a single ommatidium view an identical receptive field, which may be imaged onto several photoreceptor types for spectral or polarizational analysis. Furthermore, the geometry of the compound eye is very flexible, and it is even possible for ommatidia in well-separated regions of the eye to view the same spatial location. These options provide for considerable flexibility in the analysis of an image, and greatly multiply the possibilities for parallel processing. Indeed, much of the image analysis performed in the visual systems of mantis shrimps occurs very early in the visual process (sometimes at the level of single photoreceptor cells), producing a well-analyzed and much-simplified data stream flowing into higher visual centers. The compound eye design serves as an excellent model for artificial sensors in its modularity and in its ability to analyze image features and characteristics independently in each unit.

In this paper, we consider some of the specializations found in mantis shrimp compound eyes that permit both serial and parallel analysis of visual stimuli. We also describe some other unusual features of these eyes that permit the decomposition of images into their polarizational, spectral, spatial, and depth-plane features. Wherever possible, we indicate potential applications of mantis shrimp visual design to the development of autonomous systems.

Mantis Shrimp Compound Eyes

As their common name implies, the stomatopods look much like other modern crustaceans. This appearance belies their distinctive evolutionary history, which has been separate from the crustacean mainline for about 400 million years. Unlike other crustaceans, they actively hunt prey and disable or kill it with a catapult-like blow of a specialized raptorial appendage. They also can severely injure other members of their own species, an ability that has encouraged the evolution of complicated signaling behavior, often involving color or polarization features. Among the most interesting adaptations are those involving the structure and function of their compound eyes.

Figure 1 shows the eyes of *Neogonodactylus oerstedii,* a mantis shrimp species from the Caribbean. Superficially, these ovoid eyes appear to be similar to those of other crustaceans, or even insects, but a closer inspection reveals some important differences. Although most of the eye consists of a standard hexagonal array of ommatidia, there is a band of six parallel rows of specialized ommatidia running around the equator of each eye, looking something like a tire tread in the figure. These divide the eye into two roughly equal groups of receptors, forming two approximately hemispherical halves (see also Manning *et al.,* 1984). Most ommatidia throughout each of these two hemispheres share visual fields with ommatidia in the other, providing the possibility of stereoscopic vision in a single eye (Marshall and Land, 1993). The various ommatidial rows of the midband are individually specialized for spectral and polarizational analysis. We describe these specializations in detail later in the paper.

Another unusual feature is that the eyes are mounted on stalks. Stalked compound eyes occur throughout the Crustacea, but in mantis shrimps the movement of the eye on the stalk is unusually free, with the eye being driven in all possible axes of movement by six functional groups of muscles (Jones, 1994). Thus, whereas eye movements in other crustaceans are used to stabilize the eye in the visual field, mantis shrimp eyes are impressively and spontaneously active, giving the animals an air of curiosity and intelligence. However, the movements of the two eyes seem entirely uncoordinated, which is disconcerting to watch.

Specializations for the analysis of polarized light

Even though it is not recognized by our visual systems, polarized light is abundant in nature, being produced by reflection or scattering from almost any object. Analysis of partially linearly polarized light, the most common form, can be used to infer the surface texture or orientation of an object, and many animals use natural polarized-light fields for navigation. Machine-vision systems are beginning to incorporate polarization-vision concepts for material identification, surface-orientation detection, and other applications (see Wolff, 1997). The combination of spatial, spectral, and polarizational analysis in sensors may be simplified by resorting to the compound eye design as a model, and the analytical synthesis of these independent visual modalities may substantially increase the information content of artificial images. Technically, the addition of polarization analytical ability to artificial imagers is rather simple (Wolff, 1997).

The structure of arthropod photoreceptors naturally makes them sensitive to the plane of polarization of incoming light, because the visual pigments that absorb light are dichroic and are oriented mostly parallel in small, tubular membranes called microvilli. Most crustaceans take advantage of this sensitivity by producing ommatidia that contain two photoreceptor classes. Each class has microvilli that are all parallel but are perpendicular to those of the other receptor class, together producing a system with two analyzers, each maximally sensitive at an *e*-vector orientation orthogonal to the other (see Waterman, 1981). Mantis shrimps are no exception here, and ommatidia throughout the eye (except in parts of the midband, as described later) are all polarization-sensitive.

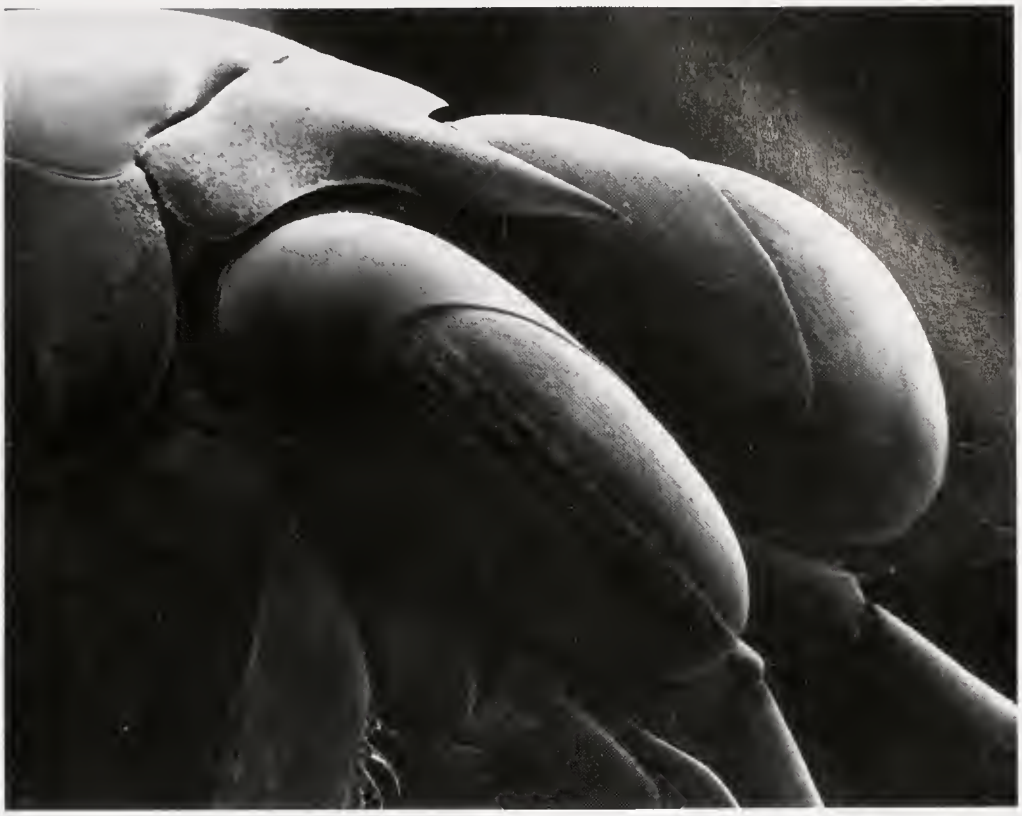

Figure 1. The anterior end of an adult mantis shrimp, *Neogonodactylus oerstedii*, imaged by scanning electron microscopy. This species is found throughout the Caribbean, living in coral rock and coralline algae. The visual regions of the compound eyes, revealed here by the densely packed facets (each of which represents the cornea of a single ommatidium), lie at the ends of stalks that pivot at their proximal ends. Each compound eye consists of two flattened hemispheres separated by six parallel rows of ommatidia, called the midband. Magnification: approx. 30×.

Figure 2 is a diagram of a typical ommatidium from the hemispherical regions of the eye outside the midband. The top half of this structure, including the refracting cornea and the underlying crystalline cone, is devoted to optics, focusing light on the top of the photosensitive structure, called the rhabdom. This rhabdom is constructed from eight receptor cells formed into a single light guide. It consists of a small upper tier, produced by receptor cell number 8 (R8), and a much longer underlying tier formed by contributions from receptor cells numbered 1 to 7 (R1–7). R8 is sensitive only to ultraviolet light (Cronin *et al.*, 1994b; Marshall and Oberwinkler, 1999), but the fused receptor produced by R1–7 is sensitive to middle-wavelength light, near 500 nm (see Cronin and Marshall, 1989a, b). The R8 receptor is polarization-insensitive, as its microvilli are not all parallel, but the two sets of receptors in the main rhabdom have orthogonal microvilli and are very sensitive to the plane of polarization (see also Marshall, 1988; Marshall *et al.*, 1991a). Axons from these two receptor sets converge onto higher order interneurons (Horwood and Marshall, unpubl. obs.), which could explain how polarization opponency arises in mantis shrimp vision (see Yamaguchi *et al.*, 1976). Thus, information leaving the outer regions of the retina has already undergone processing that emphasizes differences in the signals received by paired sets of receptors.

Ommatidia like those of Figure 2 are also typical of crabs and other "standard" crustaceans. In contrast, the ommatidia of the six rows of the midband are unique to the stomatopods. For convenience in discussing the function of midband ommatidia, we have grouped them into three types (Fig. 3), each of which normally appears in two of the six ommatidial rows of the midband. These types vary primarily in the construction of the rhabdom, so only this part of each ommatidium is diagrammed in Figure 3.

Type 1 (found in the two most ventral rows of the midband) is the simplest and is specialized for the analysis of polarized light, like the rhabdoms in ommatidia of the retinal hemispheres. Here, however, the R8 (ultraviolet) receptor is much enlarged and has microvilli that are all parallel and thus polarization-sensitive. The rest of the rhabdom, formed by receptors R1–7, is normal, providing two orthogonal receptor channels. Thus, the overall structure has a single ultraviolet-sensitive polarization analyzer on top and two orthogonal middle-wavelength (near 500 nm) ana-

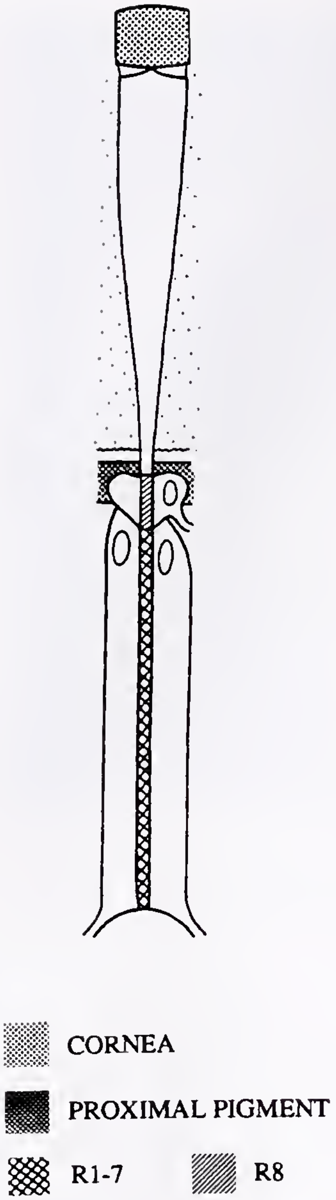

Figure 2. Diagram of a typical ommatidium from the hemispherical region of a mantis shrimp compound eye. Proceeding from surface of the ommatidium (at the top) inwards, it consists of a cornea, a crystalline cone (the long, tapered structure), the eighth receptor cell (R8), and a group of receptor cells numbered 1 through 7. The receptors form a rhabdom, which is diagonally hatched in the R8 region and crosshatched in the R1–7 region, and each receptor cell terminates in an axon that exits the ommatidium at the base. The receptor region is shielded from off-axis light by an overlying layer of proximal pigment.

lyzers in the main part of the rhabdom. A second ultraviolet system, perpendicular to the first, is available as well, because the two ommatidial rows with the Type I ommatidium are rotated 90° to each other. Together, these systems provide excellent polarization vision in two separate spectral regions.

The Type I ommatidium has an additional potential function. The overlying R8 receptor, with its parallel microvilli, may serve as a quarter-wavelength retarder. If so, it would convert circularly polarized light to linearly polarized light, which could then be analyzed by the polarization-sensitive cells of the main part of the rhabdom. Circular polarization may be produced naturally by reflection from metals or certain birefringent structures (such as crustacean cuticle), or by transmission through birefringent material or solutions of some complex molecules. The ability to detect and analyze circular polarization would add yet another information channel to the data stream flowing into the central nervous system. Note also that the geometrical arrangement of the receptors (*i.e.*, their segregation into tiers in a single rhabdom) permits each level both to operate on its own and also to affect the operation of receptors placed more deeply in the overall retina.

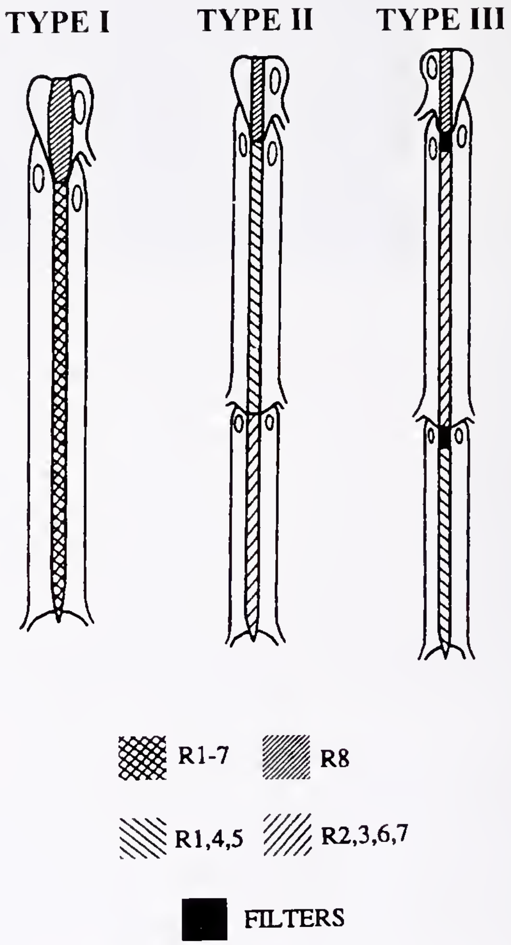

Figure 3. Diagrams of the rhabdomal portions of ommatidia located in the midband regions of compound eyes of most stomatopod species. Each rhabdom has an R8 receptor cell, which has its sensitivity maximum in the ultraviolet, on top. The main rhabdom (R1–7) exists in a single tier in Type I ommatidia (left), but is divided into two tiers by separating R1, 4, and 5 from R2, 3, 6, and 7 in Types II (center) and III (right). Type III also has colored, photostable filters at the junctions between tiers. See the text for further details.

Specializations for the spectral analysis of light

The spectrum of light reflected from an object gives rise to the psychophysical perception of color. Color is an inherent property of an object, useful for object recognition and identification. It also can be used to discriminate objects that have similar brightnesses but different reflectance spectra and to recognize borders. Many animals, including mantis shrimps, use colored markings to produce highly recognizable and unambiguous signals.

The two themes just discussed with reference to polarization vision—tiering of receptors to modify the responses of receptors at deeper levels and immediate processing of receptor output into opponent channels—continue with further elaborations in the spectral analysis systems of mantis shrimp compound eyes. These retinal specializations give mantis shrimps the potentially most complicated color vision systems of any animals. Ommatidia specialized for spectral analysis are those of Types II and III (Fig. 3; see also Marshall, 1988; Marshall *et al.*, 1991a, b).

Type II ommatidia are located in two of the four most dorsal ommatidial rows of the midband. In these, the main rhabdom that formed a single tier in ommatidia specialized for polarizational analysis is divided into two tiers. Therefore, light entering the rhabdom transits first the ultraviolet-sensitive R8 receptor, then the distal tier of the main rhabdom, and finally the main rhabdom's proximal tier.

Visual pigments, the molecules that absorb light and trigger the biochemical processes of vision, modify incoming light because they absorb within particular spectral regions. Rhabdoms of Type II ommatidia thus operate as a series of spectral filters, each of which affects all receptors beneath. Unlike the situation in other ommatidia, in Type II main rhabdoms (as well as those of Type III, to be described shortly), the distal tier and proximal tiers of main rhabdoms contain different visual pigments. In every case, the pigment of the distal tier absorbs at shorter wavelengths than that of the proximal tier, thereby acting as a long-pass filter. Each tier of Type II rhabdoms sharpens and tunes the spectral sensitivity of the receptors below, producing a set of spectrally specialized, narrow-band photoreceptors (see Cronin and Marshall, 1989a, b).

The serial filtering of Type II ommatidia is further elaborated in Type III (Fig. 3), found in the remaining two ommatidial rows of the midbands of most mantis shrimp species. Type III rhabdoms intercalate colored filters, made of tightly packed vesicles containing strongly absorbing, photostable pigments, at each successive junction between tiers (see Marshall, 1988; Cronin and Marshall, 1989a, b; Marshall *et al.*, 1991a, b; Cronin *et al.*, 1994a). Light entering each tier is therefore altered not only by absorption by visual pigments at all higher levels, but also by the colored filters that it has transited. Type III rhabdoms are particularly suitable for producing middle-to-long-wavelength receptor classes. Visual pigments tend to absorb poorly at these wavelengths (thus making weak filters), but the photostable filters are very effective for such tuning.

The tiers of the main rhabdoms in Type II and Type III ommatidia are formed from the same receptor sets that produce the orthogonal polarization channels in the remainder of the retina. Thus, of the seven receptor cells that contribute to the main rhabdom, those numbered 1, 4, and 5 produce one polarization channel, while 2, 3, 6, and 7 produce the other. These same groupings are retained in the tiers of Type II and Type III ommatidia (see Fig. 3), and this converts what was originally a polarization-opponent organization into chromatic-opponent channels (see Cronin and Marshall, 1989a, b; Marshall *et al.*, 1991a, b, 1996). To prevent confusion between polarization and spectral components, receptors in Type II and Type III rhabdoms are polarization-insensitive, having randomly oriented microvilli (Marshall *et al.*, 1991b).

Since four rows of the midband include ommatidial Types II and III, eight varieties of receptor tiers exist in their main rhabdoms. Each of these contains a different visual pigment (Cronin and Marshall, 1989a, b), producing eight distinct classes of spectral receptor. Together, these sharply tuned receptors span the visual spectrum to peak at wavelengths from about 400 nm to nearly 700 nm in some species. To these are added a diversity of ultraviolet receptor types (in the R8 cells) and also the polarization classes, for a grand total of perhaps 16 spectral receptor classes (see Cronin *et al.*, 1994c; Marshall and Oberwinkler, 1999).

With all these receptor types, one might conclude that no crustacean brain could possibly interpret such a complex, multivariate set of incoming data. Obviously, the polarization system would make things even worse. However, the actual situation is probably quite the opposite. By handling incoming information with a large number of individually specialized receptors (groups of which analyze the same location in visual space) and by processing receptor outputs immediately, sensory information leaving the retina is already streamed into a parallel series of data channels. Each of these may act as a single labeled line of visual information.

The division of the visual spectrum into a series of discrete channels has another, less obvious, advantage. It is difficult for most visual systems (and systems of artificial imaging) to achieve color constancy—the ability to recognize a given color unambiguously—underwater or in spectrally challenging environments. Different classes of color receptors normally respond to a broad spectrum of light, and this can cause them to adapt strongly to stimuli that are spectrally far from their wavelengths of peak sensitivity. By having narrow, sharply tuned spectral classes, a visual system reduces this adaptation to off-peak wavelengths, and thereby maintains excellent color constancy (Osorio *et al.*, 1997). Mantis shrimps use color flamboyantly in their signals (Caldwell and Dingle, 1975), more so than any other aquatic invertebrate. Their unique system of color vision (see also Marshall *et al.*, 1996; Chiao *et al.*, 2000) makes this possible. When color constancy is critical, artificial designs should use narrow, well-chosen spectral channels for accuracy.

Spatial and motion analysis, and the integration of visual information

Being active predators that incapacitate their prey using a ballistic strike, mantis shrimps require a very high-quality sense of space. Again, their eyes are uniquely specialized for this purpose as well. The overlapping fields of view shared by the two halves of each eye probably form the basis of a monocular rangefinder, whereby the distance to a particular object determines which particular receptor pair converges onto it. Since the stalked eyes of mantis shrimps (Fig. 1) move freely in pitch, roll, and yaw, binocular stereopsis is difficult or impossible for these animals to achieve. So monocular rangefinding is particularly suitable (Milne and Milne, 1961).

The very mobility of the eyes of mantis shrimps can confound their interpretation both of spatial location and of relative motion. Like most animals with mobile eyes, the mantis shrimps solve this problem by immobilizing their eyes most of the time relative to the overall visual field, and making rapid eye movements (saccades) to object of interest (Cronin *et al.*, 1991). They may also track individual objects moving within the visual background (Cronin *et al.*, 1988, 1992). These stabilizing mechanisms, necessary to any visual system, whether biological or artificial, permit mantis shrimps to recognize self-motion or motion of other objects in their vicinity.

Mantis shrimps move their eyes for far more unusual purposes. In many species, including *Neogonodactylus oerstedii*, the ommatidia of the compound eye are located at the end of a relatively long stalk, the pivot of which is far from the visual region of the eye (see Fig. 1). Consequently, as the eye swings, its motion produces a visual flow field in which more distant objects move slowly relative to nearby objects. This relative motion provides an additional depth cue, operating at substantially greater range than the monocular rangefinders, that could be used to distinguish foreground from background. The basic design principle is that the nodal point of the optics is removed from the geometrical center of rotation; some vertebrates (*e.g.*, the sandlance fish and chameleons) have hit on a similar solution to the problem of monocular rangefinding (Ott and Schaeffel, 1995; Pettigrew *et al.*, 1999).

Equally unusual are the small scanning movements that mantis shrimps use, apparently to map their spatially restricted senses of color and polarization onto the extended visual fields of the hemispheric regions of the compound eye. The problem that these animals must solve is a consequence of the geometry of the midband. Since its six rows of receptors all lie in a single plane, together they sample only a planar slice through visual space. Yet this slice contains the most highly analyzed chromatic, ultraviolet, and polarization information. To "paint" color, ultraviolet intensity, and polarization onto the extended visual field, mantis shrimps use small and slow scanning movements. These sweep the planar visual fields of midband ommatidia over the broad and extended visual fields of ommatidia in the hemispherical regions of the compound eye (Land *et al.*, 1990). Engineers often attempt to minimize sensor motion relative to the external world, but in mantis shrimps, motion is essential for visual function. As is also implied in the work of Srinivasan and his colleagues (2001), sensor motion can add information, and instrument design incorporating sensor movement deserves further study.

Summary and Conclusions

Mantis shrimps are among the most successful invertebrate predators in shallow, tropical waters. They are formidable hunters, either cruising about the bottom actively in search of prey or stealthily ambushing it from a concealed burrow. Their success is largely due to their extraordinary visual senses, which perform much of the required lower-level processing of incoming visual information before relaying it to higher visual centers. In doing so, they considerably reduce the computational overhead required in the central nervous system, permitting decisions to be made rapidly and accurately. Although the central nervous system of stomatopods is poorly studied at present, it seems likely that the extensive retinal pre-processing may guide appropriate motor output with relatively minor amounts of central processing. These principles should find excellent application in artificial autonomous constructs as well, and can serve as models for the design of systems of artificial vision.

Acknowledgments

We thank Christina King, Mike Land, Simon Laughlin, and Roger Hardie for discussions. Phil Rutledge and Tim Ford helped to prepare the figures. This work is based on research supported in the United States by the National Science Foundation under Grant Number IBN-9724028, in the United Kingdom by the BBSRC, and in Australia by the Australian Research Council.

Literature Cited

Caldwell, R. L., and H. Dingle. 1975. Ecology and evolution of agonistic behavior in stomatopods. *Naturwissenschaften* **62:** 214–222.

Chiao, C. C., T. W. Cronin, and N. J. Marshall. 2000. Eye design and color signaling in a stomatopod crustacean, *Gonodactylus smithii*. *Brain Behav. Evol.* **56:** 107–122.

Cronin, T. W., and N. J. Marshall. 1989a. A retina with at least ten spectral types of photoreceptors in a mantis shrimp. *Nature* **339:** 137–140.

Cronin, T. W., and N. J. Marshall. 1989b. Multiple spectral classes of photoreceptors in the retinas of gonodactyloid stomatopod crustaceans. *J. Comp. Physiol. A* **166:** 261–275.

Cronin, T. W., J. N. Nair, R. D. Doyle, and R. L. Caldwell. 1988. Ocular tracking of rapidly moving visual targets by stomatopod crustaceans. *J. Exp. Biol.* **138:** 155–179.

Cronin, T. W., N. J. Marshall, and M. F. Land. 1991. Optokinesis in gonodactyloid mantis shrimps (Crustacea; Stomatopoda: Gonodactylidae). *J. Comp. Physiol. A* **168:** 233–240.

Cronin, T. W., H. Y. Yan, and K. D. Bidle. 1992. Regional specialization for control of ocular movements in the compound eyes of a stomatopod crustacean. *J. Exp. Biol.* **171:** 373–393.

Cronin, T. W., N. J. Marshall, and R. L. Caldwell. 1994a. The intrarhabdomal filters in the retinas of mantis shrimps. *Vision Res.* **34:** 279–291.

Cronin, T. W., N. J. Marshall, C. A. Quinn, and C. A. King. 1994b. Ultraviolet photoreception in mantis shrimp. *Vision Res.* **34:** 1443–1452.

Cronin, T. W., N. J. Marshall, R. L. Caldwell, and N. Shashar. 1994c. Specialization of retinal function in the compound eyes of mantis shrimps. *Vision Res.* **34:** 2639–2656.

Jones, J. P. 1994. Architecture and composition of the muscles that drive stomatopod eye movements. *J. Exp. Biol.* **188:** 317–331.

Land, M. F., N. J. Marshall, D. Brownless, and T. W. Cronin. 1990. The eye-movements of the mantis shrimp *Odontodactylus scyllarus* (Crustacea: stomatopods). *J. Comp. Physiol. A* **167:** 155–166.

Manning, R. B., H. Schiff, and B. C. Abbott. 1984. Eye structure and classification of stomatopod crustaceans. *Zool. Scr.* **13:** 41–44.

Marshall, N. J. 1988. A unique colour and polarisation vision system in mantis shrimps. *Nature* **333:** 557–560.

Marshall, N. J., and M. F. Land. 1993. Some optical features of the eyes of stomatopods. I. Eye shape, optical axes and resolution. *J. Comp. Physiol. A* **173:** 565–582.

Marshall, J., and J. Oberwinkler. 1999. The colourful world of the mantis shrimp. *Nature* **401:** 873–874.

Marshall, N. J., M. F. Land, C. A. King, and T. W. Cronin. 1991a. The compound eyes of mantis shrimps (Crustacea, Hoplocarida, Stomatopoda). I. Compound eye structure: the detection of polarised light. *Phil. Trans. R. Soc. Ser. B* **334:** 33–56.

Marshall, N. J., M. F. Land, C. A. King, and T. W. Cronin. 1991b. The compound eyes of mantis shrimps (Crustacea, Hoplocarida, Stomatopoda). II. Colour pigments in the eyes of stomatopod crustaceans: polychromatic vision by serial and lateral filtering. *Phil. Trans. R. Soc. Ser. B* **334:** 57–84.

Marshall, N. J., J. P. Jones, and T. W. Cronin. 1996. Behavioural evidence for color vision in stomatopod crustaceans. *J. Comp. Physiol. A* **179:** 473–481.

Milne, L. J., and M. Milne. 1961. Scanning movements of the stalked compound eyes in crustaceans of the order Stomatopoda. Pp. 422–426 in *Progress in Photobiology*, B. C. Christensen and B. Buchmann, eds. *Proceedings of the Third International Congress on Photobiology*. Elsevier, New York.

Osorio, D., N. J. Marshall, and T. W. Cronin. 1997. Stomatopod photoreceptor spectral tuning as an adaptation for colour constancy in water. *Vision Res.* **37:** 3299–3309.

Ott, M., and F. Schaeffel. 1995. A negatively powered lens in the chameleon. *Nature* **373:** 692–694.

Pettigrew, J. D., S. P. Collin, and M. Ott. 1999. Convergence of specialised behaviour, eye movements and visual optics in sandlance (Teleostei) and the chameleon. *Curr. Biol.* **9:** 421–424.

Srinivasan, M. V., S. Zhang, and J. S. Chahl. 2001. Landing strategies in honeybees and possible applications to autonomous airborne vehicles. *Biol. Bull.* **200:** 216–221.

Waterman, T. H. 1981. Polarization sensitivity. Pp. 281–469 in *Handbook of Sensory Physiology, Vol. VII/6B*. H. Autrum, ed. Springer, New York.

Wolff, L. B. 1997. Polarization vision: a new sensory approach to image understanding. *Image Vision Comput.* **15:** 81–93.

Yamaguchi, T., Y. Katagiri, and K. Ochi. 1976. Polarized light responses from retinular cells and sustaining fibers of the mantis shrimp. *Biol. J. Okayama Univ.* **17:** 61–66.

Reference: *Biol. Bull.* **200:** 184–189. (April 2001)

View From the Boundary

BARBARA WEBB

Center for Cognitive and Computational Neuroscience, Department of Psychology, University of Stirling, Stirling FK9 4LA, Scotland, UK

Abstract. Re-implementing biological mechanisms on robots not only has technological application but can provide a unique perspective on the nature of sensory processing in animals. To make a robot work, we need to understand the function as part of an embodied, behaving system. I argue that this perspective suggests that the terms "representation" and "information processing" can be misleading when we seek to understand how neurobiological mechanisms carry out perceptual processes. This argument is presented here with reference to a robot model of cricket behavior, which has demonstrated competence comparable to that of the insect, but utilizes surprisingly simple central processing. Instead it depends on sensory interfaces that are well matched to the task, and on the link between environment, action, and perception.

Introduction

The intersection of biology and robotics—the position of my own research—is often characterized as taking information from neuroethological investigations of natural systems to implement as new technology for man-made systems. However, another aspect of work in this area is to use the robotic implementations as a means of exploring biological hypotheses (Webb, 2000). This approach can provide a perspective on fundamental issues that is complementary to the view of the biologist engaged in primary research on the animal. This includes ideas on the most promising routes by which biological understanding might inform technological developments.

My main thesis will be that examining invertebrate sensory systems from this perspective teaches us that they do not actually do much "information processing" or "representation"—depending, of course, on how you define these terms (see below). When we look at invertebrates, it appears that the function of the sensory systems is not to inform the animal generally but to control specific behaviors; that the means by which they do so is often determined as much by peripheral sensory physics as by central computation; and that appreciating the problem in terms of an embodied animal interacting with an environment is more appropriate than approaching it in terms of building an internal representation of the external stimuli. Wehner (1987) used the term "matched filters" to describe how animals may be faced with problems that apparently need sophisticated information processing solutions, but actually solve them by exploiting sensor mechanisms and behaviors that are uniquely matched to the required tasks. Further examples presented in this collection of symposium papers included the simple visual variables exploited by the bee to control flight (Srinivasan, 2001), and the use of "fanning" by crayfish (Breithaupt, 2001) or moth (Ishida, 2001) to improve chemical plume tracking.

Given that the terms "representation" and "information processing" are nevertheless commonly used by invertebrate neuroethologists (*e.g.*, during the symposium Thomas Cronin discussed the scanning movements of the mantis shrimp eye as implying a relatively sophisticated system for registering the information properly onto a subjective representation of space [Cronin and Marshall, 2001]), a distinction may need to be drawn between this usage and the kind of full-blown symbolic encoding and manipulation that characterizes the "information processing" view of perception and cognition in traditional Artificial Intelligence. The claim that a pattern of neural firing represents a stimulus is

---

E-mail: b.h.webb@stir.ac.uk

This paper was originally presented at a workshop titled *Invertebrate Sensory Information Processing: Implications for Biologically Inspired Autonomous Systems.* The workshop, which was held at the J. Erik Jonsson Center for the National Academy of Sciences, Woods Hole, Massachusetts, from 15–17 April 2000, was sponsored by the Center for Advanced Studies in the Space Life Sciences at the Marine Biological Laboratory, and funded by the National Aeronautics and Space Administration under Cooperative Agreement NCC 2-896.

often only a claim that the firing and the presence of the stimuli causally co-vary: in the same way the electric current in a wire might be said to represent the position of an on-off switch. However, some deplore this as a misuse of the term "representation." For example, Maze (1981; p. 87) says that "the connection between the brain state and the external fact the knowledge of which it subserves . . . is just that of cause and effect, not representation," and Clancey (1991; p. 110) argues that "structures in the brain that cannot be perceived [by the agent] have no representational status to the agent."

The background for this disagreement over appropriate usage reflects two distinguishable senses of the relationship of representation. The first I will call "intentional representation," defined in the theory of signs by Peirce (cited in Fetzer, 1988) as "something that stands in for something (else) in some respect or other for somebody" (p. 134)—for example, use of the term "LGN" by a scientist to represent a part of the brain. The second I will call "causal representation," which describes indirect or mediated presentation, for example, the activity of ganglion cells presenting retinal stimulation patterns to LGN. The critical distinction between these two is that the "intentional" case requires that the thing represented can be directly experienced by the representor: the scientist can hear the sound "LGN," or look at the brain part, and this is why he can use one to represent the other. In the "causal" case the LGN cannot access the retinal activity independently—for example, to confirm that the "representation" by the ganglion cells is correct. To illustrate the distinction another way: an ant may use a pattern of landmarks as a representation of a nest position, in which case it can know about the presence of the landmarks and the presence of the nest in the same way (*i.e.*, through its senses). If the ant is also said to use the response pattern of neurons in its brain to "represent" the presence of the landmarks, the ant's relationship to the neural firing and to the landmarks are not comparable. We are using different levels of description when we say it "recognizes" the landmarks or "recognizes" the pattern of neural firing. (A possible source of confusion here is that looking at the ant's behavior and its neural processes from our point of view, we may well find that one (the firing) seems to stand in for the other (the landmark): but this is "intentional representation" only to the experimenter; to the ant it is merely "causal representation.")

Similarly, there are distinctions to be drawn between usages of "information processing." There is the formal communication theory sense as defined by Shannon (1948); there is the everyday sense in which information is taken to be something containing meaning; and then there is the more recent identification of information processing with computation—that is, involving syntactic manipulation. None of these maps directly onto the usage whereby, for example, lateral inhibition in the retina is called information processing (there is no well-defined sender, receiver, or probability function; the meaning is opaque in the same way that the "representation" is non-intentional; and the processing is governed by physical rather than syntactic rules). The more apposite term here would seem to be *signal* processing, but "information processing" has become ubiquitous.

Do these distinctions matter, or are they mere semantics? I would argue they are important because the explanatory power of applying the terms is very different. It is an empirical, and somewhat controversial, hypothesis to say that invertebrate behavior is controlled by intentional internal representations, manipulated in meaningful information processing. Whereas to say that behavior is controlled by "causal" representations and involves "signal" processing is merely to say that the activity of the nervous system has a role in controlling the behavior, which was not in doubt. The same point has been expressed by Beer (2000, p. 97) with regard to cognitive science: "If any internal state is a representation and any systematic process is a computation then a computational theory of mind loses its force."

Moreover, it is not always clear that insect neuroethologists, in their usage, are not drawing conclusions that rest on conflating the meanings. An example is the tendency to start from the observation that an animal behaves differently in the presence of some stimulus, go on to describe the process involved as the animal internally "identifying" that stimulus before responding to it, and from this end up looking inside the brain for the neural mechanism that carries out the "identification." If the use of "identify" is only metaphorical, then it should not constrain the interpretation of findings, but it does. As an illustration, we can consider a classic piece of neuroethology in cricket phonotaxis research, the discovery of "recognition" neurons in the cricket brain whose firing rate response corresponds remarkably well to the likelihood of tracking by the cricket when it is presented with songs of different syllable rates (Schildberger, 1984a). Although this discovery is certainly of significance in trying to disentangle the neural wiring underlying the behavior, this "representation" of the "attractiveness" of syllable rates by the firing rate of an identified neuron is by no means an explanation of the behavior. First, it is not surprising, given that the animal behaves in different ways to different songs, that we find some neurons active under conditions when it does respond and not active when it does not—this is simply to say that its motor behavior is under some kind of neural control. Furthermore, the result does not in itself tell us how the neuron comes to have this property: understanding the mechanism of "recognition" requires understanding the neural connectivity leading to this property, which to date is still not fully resolved. Finally, in the neural model described below, we found highly comparable property of correlation of firing rate in certain neurons with syllable rate preference—yet the firing rate here had no functional role in the behavior but was simply a side-effect (Fig. 1). In fact,

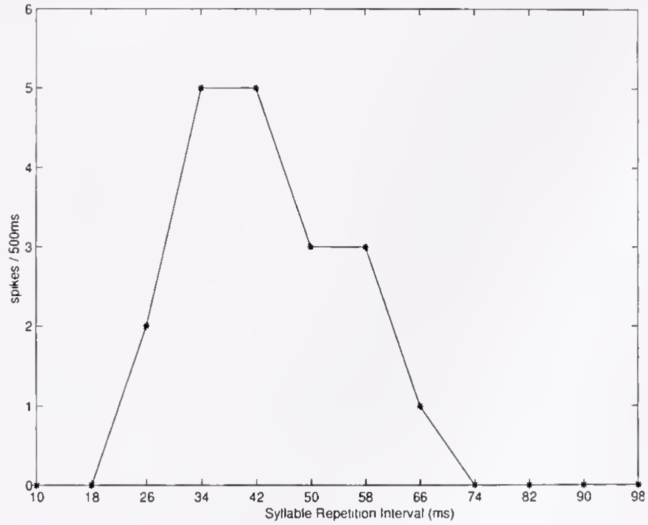

Figure 1. The "firing rate" of a neuron in the robot model matches the "phonotactic preference" displayed in behavior. This looks like the "recognition" neuron discovered in the cricket (Schildberger, 1984) but in fact plays no functional role in the behavior. (Adapted from Webb and Scutt, 2000.)

there need not be any explicit "identifier" in the brain for the animal to single out and approach a specific signal, as I will now describe in more detail.

Modeling Cricket Behavior

Cricket phonotaxis—the ability of females to track down male calling songs—includes a significant range of the problems of responding appropriately to specific sensory signals: identifying the signal against a noisy background; recognizing that it is the correct one; localizing its source; possibly choosing between rival signals. An information processing approach to this problem identifies the problems to be solved by the cricket's neural system as filtering for the right carrier frequency and filtering for the right repetition rate to recognize the signal (Popov and Shuvalov, 1977; Thorson *et al.*, 1982; Stout and McGhee, 1988); comparing the amplitude of the auditory signal between two sensors to determine the direction of the source or at least which way to turn (Schmitz *et al.*, 1982; Schildberger and Horner, 1988; Huber, 1992); and separating simultaneous sound sources sufficiently to assess and approach the more attractive one (Doherty, 1985; Simmons, 1988; Pollack, 1998).

However, closer examination of the peripheral sensing system in the animal suggests that it may solve at least some of these problems directly, without any explicit representation of the song. The pressure difference receiver mechanism that enables the animal to detect the sound direction (Michelsen *et al.*, 1994) is inherently dependent on that sound being within a particular range of wavelengths. The neural encoding of the subsequent intensity difference between the ears is potentially in the form of a temporal code (Schildberger, 1984b; Stumpner *et al.*, 1995) that could explain the pattern dependency of the response. Finally, the animal's behavior in response to sound will position it in the sound field in such a way that it is likely to end up at the most attractive source rather than confused between them (see below). In other words, the behavior does not require any internal representation of the nature or position of the sound source.

That this is indeed possible has been demonstrated in a robot implementation of this suggested mechanism for phonotaxis (Webb, 1995; Lund *et al.*, 1997; Webb and Scutt, 2000). The robot has an auditory system that, like the cricket's ears, uses cross-delay and summation of the two signals to produce a strongly directional response despite small receptor separation. Because the delay is fixed, the wavelength of the signal is a crucial determinant of the effectiveness of the device. Thus the robot will, for example, locate a 4.7-kHz signal better than one at higher or lower frequencies, and will preferentially approach a 4.7-kHz signal when a song of differing frequency is simultaneously presented, with no other form of frequency filtering.

The behavior of the robot is controlled by a spiking neural network consisting of only four units. Two input units integrate the auditory signal and initiate firing above a threshold (their behavior is closely modeled on the response properties of identified neurons [AN1] in the cricket). They respectively excite two output units, but cross inhibit each other's axons. Thus the unit that fires first effectively suppresses the effect of the other side. The input-output connection is further modulated by synaptic suppression—that is to say, successive spikes have progressively less effect on the postsynaptic membrane potential, unless there is a gap in which the synapse can recover. The result is that unless the input has an appropriate on-off pattern, it is not effective in generating an appropriate motor response as controlled by the output units. For example, the robot will show consistent tracking behavior only to songs that fall within a particular band of syllable repetition rates, the same as that preferred by the cricket (Fig. 2). Although this behavioral preference has a corresponding neural "representation" in the firing rates of the output units (Fig. 1), the actual explanation of the behavior lies in the interactions of the neural time courses of summation and decay, and indeed these generate the appropriate response much faster than the time that would be needed to get a reasonable estimate of the firing rate.

Having the model implemented in a physical device allowed us to test the behavior in realistic sound fields that would be difficult to simulate convincingly. Further characteristics of cricket behavior could thus be shown to emerge from the interaction of the controller, the physical interface, and the environment, without requiring further elaboration of the model. With sound from directly above (*i.e.,* lacking any horizontal directional difference), the

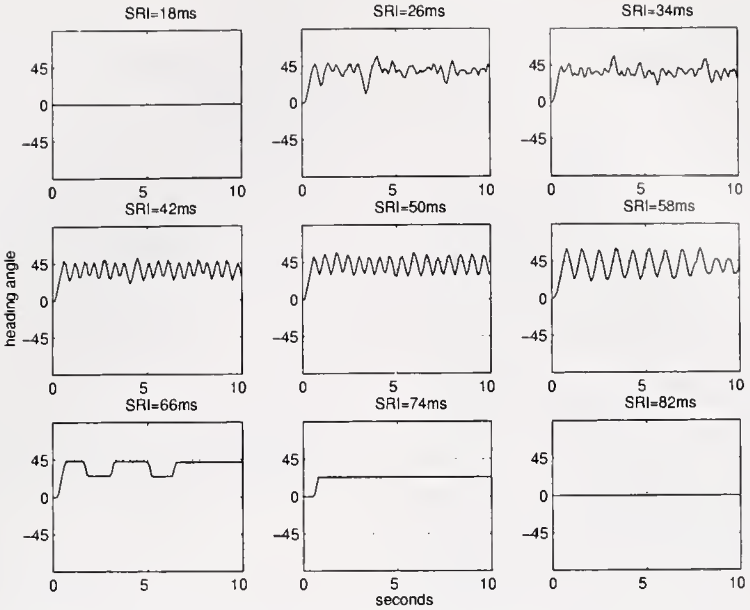

Figure 2. Tracking behavior of the robot in response to cricket songs at different syllable repetition intervals (SRI). The sound is at 45 degrees to the starting position of the robot. A SRI between 26 and 58 ms (comparable to the cricket) is needed for the robot to consistently turn and meander in the sound direction. (From Webb and Scutt, 2000.)

robot, like the cricket (Weber *et al.*, 1981), showed a tendency to perform tracking-like behavior without actually following one consistent direction. When the sound from above was paired with a continuous (*i.e.*, unattractive) stimulus from one side, the robot, like the cricket (Stabel *et al.*, 1989), tracked away from the lateral stimulus. When two similar sounds were played simultaneously, the robot could choose and track one of them because once it had turned slightly more to one side; the sound from that side captured the response. If the sounds differed slightly in temporal

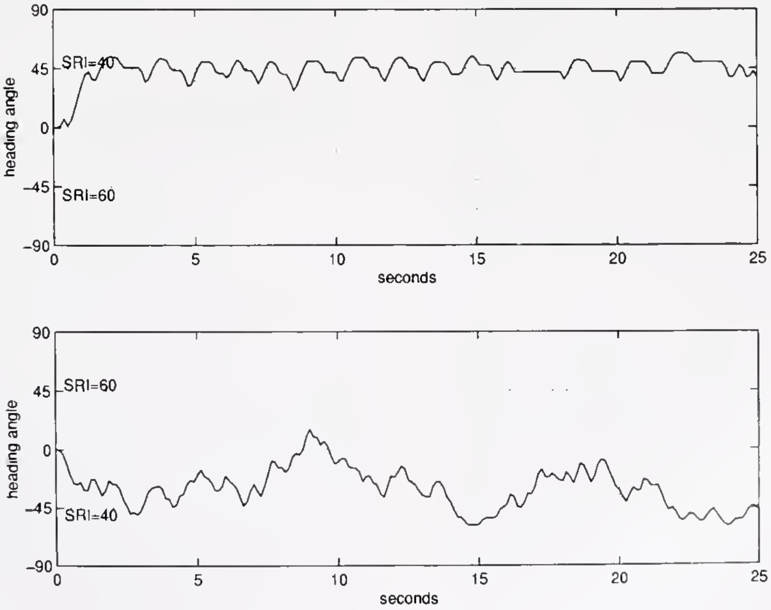

Figure 3. Tracking behavior of the robot to simultaneous cricket songs at different syllable rates. The robot (like the cricket) turns and tracks the faster repetition rate (SRI = 40) whether it is on the left (upper plot) or the right (lower plot). (Adapted from Webb and Scutt, 2000.)

pattern, the robot, like the cricket (Doherty, 1985), could consistently choose one as the more attractive signal (Fig. 3).

Integrating Sensory Systems

One argument advanced in favor of (real) information processing solutions is that they are more amenable to scaling up to explain more complex, flexible behaviors such as the integration of different sensory sources to control behavior. From an engineering or designer point of view, this might indeed be the case. Whether it is true of biology is another question: perhaps biological systems can offer us alternative schemes—perhaps more specialized to the animal's task niche, but on the other hand flexible and robust—for solving these kinds of problems. As a preliminary starting point for investigating these issues, I will describe some recent work done in collaboration with Reid Harrison (Webb and Harrison, 2000a,b) to look at the integration of the phonotaxis behavior on the robot with another fundamental sensorimotor reflex, the optomotor response.

Like many other insects, crickets will rotate in response to rotation of their visual surroundings. Normally this serves as a basic stabilization mechanism. The underlying sensor and neural circuitry for this response has been closely studied, particularly in the fly (Gotz, 1975; Reichardt and Poggio, 1976; Heisenberg and Wolf, 1988; Egelhaaf and Borst, 1993). It has been suggested that, in lit conditions, crickets will additively integrate their phonotaxis response and their optomotor response (Bohm *et al.*, 1991), which could improve the accuracy of their approach to sound (Weber *et al.*, 1981) by controlling for unintended course deviations.

A sensor that embodies the hypothesized mechanism of the optomotor response has been built in analog VLSI (very large scale integration) hardware (Harrison and Koch, 1998). This is a single chip that contains photoreceptors, temporal filters, comparison units, and widefield summation. The output can be used as a "torque" signal for the direction and approximate velocity of motion that would compensate for the visual rotation. We interfaced this chip to a robot that also had the sound-sensing circuit and neural model for phonotaxis described above. The two behaviors were initially combined in a directly additive way; that is, the motor output was a weighted sum of the signal given by the phonotactic turning decision and the signal given by the optomotor torque. However, this caused some problems, because turns in response to sound would generate strong visual rotation signals that the robot would attempt to correct, thus negating the initial turn. As a second approach, we used an inhibition scheme in which the robot would ignore the optomotor signal while turning in response to sound (other possible solutions are discussed in Webb and Harrison, 2000b).

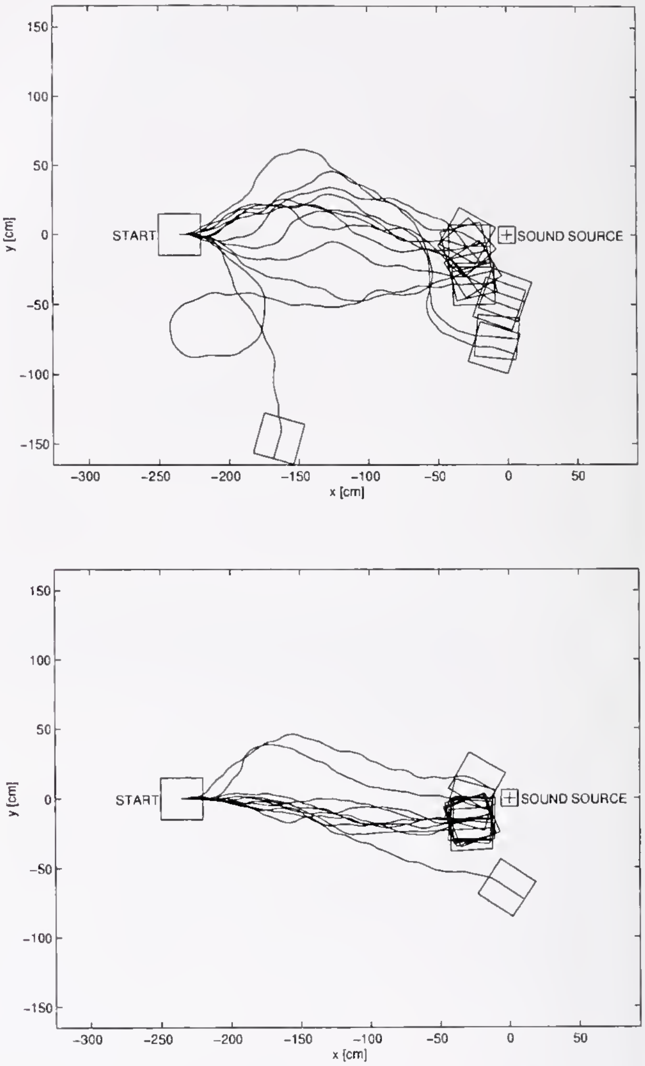

Figure 4. Tracks of a robot with a 20% motor bias. Top, using phonotaxis only. Bottom, with an optomotor response added. The optomotor behavior significantly improves the ability to go directly to the sound source. (From Webb and Harrison, 2000b.)

With this simple interaction scheme it was possible to show that the added optomotor capability could significantly improve phonotaxis, more obviously so under conditions where the motor capability was made less reliable. Thus Figure 4 shows the behavior of the robot when approaching a sound source with an induced bias in its motor output that makes the left wheel turn 20% faster than the right. Without the optomotor response the robot had some difficulty reaching the speaker; with the response added it successfully and directly reached the speaker on all but one trial. Because the two hardware sensor systems are well tuned to executing their specific tasks, it was relatively simple to combine the behaviors to produce a robust performance without any explicit representation of the "fused" auditory and visual information.

Conclusion

Robotics engineers already know a lot about information processing on representations. It is the standard computational paradigm, but it has proved difficult to employ to get robots to display behavioral competence comparable to even "mere" invertebrates. What they can learn from biology is how to build smart sensors that are matched to tasks; how to devise control systems that include patterns of behavior as part of the sensing process; and how to design internal nervous systems that exploit these factors. Calling these latter kinds of processes "representation" and "information processing" obscures the distinctive character of the mechanisms on offer. There is much yet to learn about the interplay of environments, behaviors, physics, and physiology. Biologists may have as much to learn from attempts to implement these mechanisms as do engineers.

Literature Cited

Beer, R. D. 2000. Dynamical approaches to cognitive science. *Trends Cognit. Sci.* **4:** 91–98.

Bohm, H., K. Schildberger, and F. Huber. 1991. Visual and acoustic course control in the cricket *Gryllus bimaculatus*. *J. Exp. Biol.* **159:** 235–248.

Breithaupt, T. 2001. Fan organs of crayfish: devices supporting chemical information exchange with the environment. *Biol. Bull.* **200:** 150–154.

Clancey, W. J. 1991. Situated cognition: stepping out of representational flatland. *Ai Commun.* **4:** 109–112.

Cronin, T. W., and J. Marshall. 2001. Parallel processing and image analysis in the eyes of mantis shrimps. *Biol. Bull.* **200:** 177–183.

Doherty, J. A. 1985. Phonotaxis in the cricket, *Gryllus bimaculatus* De Geer: comparisons of choice and no choice paradigms. *J. Comp. Physiol. A* **157:** 279–289.

Egelhaaf, M., and A. Borst. 1993. A look into the cockpit of the fly—visual orientation, algorithms, and identified neurons. *J. Neurosci.* **13:** 4563–4574.

Fetzer, J. H. 1988. Signs and minds: an introduction to the theory of semiotic systems. Pp. 133–161 in *Aspects of Artificial Intelligence*, J. H. Fetzer, ed., Kluwer, Berlin.

Gotz, K. G. 1975. The optomotor equilibrium of the *Drosophila* navigation system. *J. Comp. Physiol. A* **99:** 187–210.

Harrison, R. R., and C. Koch. 1998. An analog VLSI model of the fly elementary motion detector. Pp. 880–886 in *Advances in Neural Information Processing Systems 10*. M. I. Jordan, M. J. Kearns, and S. A. Solla, eds., MIT Press, Cambridge, MA.

Heisenberg, M., and R. Wolf. 1988. Reafferent control of optomotor yaw torque in *Drosophila melanogaster*. *J. Comp. Physiol. A* **163:** 373–388.

Huber, F. 1992. Behavior and neurobiology of acoustically oriented insects. *Naturwissenschaften* **79:** 393–406.

Ishida, H., T. Nakamoto, T. Moriizumi, T. Kikas, and J. Janata. 2001. Plume-tracking robots: a new application of chemical sensors. *Biol. Bull.* **200:** 222–226.

Lund, H. H., B. Webb, and J. Hallam. 1997. A robot attracted to the cricket species *Gryllus bimaculatus*. Pp. 246–255 in *Fourth European Conference on Artificial Life*. P. Husbands and I. Harvey, eds. MIT Press, Cambridge, MA.

Maze, J. 1981. *The Meaning of Behaviour*. Allen and Unwin, London.

Michelsen, A., A. V. Popov, and B. Lewis. 1994. Physics of directional hearing in the cricket *Gryllus bimaculatus*. *J. Comp. Physiol. A* **175:** 153–164.

Pollack, G. S. 1998. Neural processing of acoustic signals. Pp. 139–196 in *Comparative Hearing: Insects*, R. R. Hoy, A. N. Popper, and R. R. Fay, eds. Springer, Berlin.

Popov, A. V., and V. F. Shuvalov. 1977. Phonotactic behaviour of crickets. *J. Comp. Physiol. A* **119:** 111–126.

Reichardt, W., and T. Poggio. 1976. Visual control in the fly. A quantitative analysis. *Q. Rev. Biophys.* **9:** 311–375.

Schildberger, K. 1984a. Multimodal interneurons in the cricket brain: properties of identified extrinsic mushroom body cells. *J. Comp. Physiol. A* **154:** 71–79.

Schildberger, K. 1984b. Temporal selectivity of identified auditory interneurons in the cricket brain. *J. Comp. Physiol. A* **155:** 171–185.

Schildberger, K., and M. Horner. 1988. The function of auditory neurons in cricket phonotaxis. I. Influence of hyperpolarization of identified neurons on sound localization. *J. Comp. Physiol. A* **163:** 621–631.

Schmitz, B., H. Scharstein, and G. Wendler. 1982. Phonotaxis in *Gryllus campestris* L. (Orthoptera, Gryllidae). I. Mechanism of acoustic orientation in intact female crickets. *J. Comp. Physiol. A* **148:** 431–444.

Shannon, C. E. 1948. A mathematical theory of communication. *Bell System Tech. J.* **27:** 379–423.

Simmons, L. W. 1988. The calling song of the field cricket *Gryllus bimaculatus* (de Geer): constraints on transmission and its role in intermale competition and female choice. *Anim. Behav.* **36:** 380–394.

Srinivasan, M. V., S. Zhang, and J. S. Chahl. 2001. Landing strategies in honeybees and possible applications to autonomous airborne vehicles. *Biol. Bull.* **200:** 216–221.

Stabel, J., G. Wendler, and H. Scharstein. 1989. Cricket phonotaxis: localization depends on recognition of the calling song pattern. *J. Comp. Physiol. A* **165:** 165–177.

Stout, J. F., and R. McGhee. 1988. Attractiveness of the male *Acheta domestica* calling song to females. II. The relative importance of syllable period, intensity, and chirp rate. *J. Comp. Physiol. A* **164:** 277–287.

Stumpner, A., G. Atkins, and J. F. Stout. 1995. Processing of unilateral and bilateral auditory inputs by the ON1 and L1 interneurons of the cricket *Acheta domesticus* and comparison to other cricket species. *J. Comp. Physiol. A* **177:** 379–388.

Thorson, J., T. Weber, and F. Huber. 1982. Auditory behaviour of the cricket. II. Simplicity of calling-song recognition in *Gryllus* and anomalous phonotaxis at abnormal carrier frequencies. *J. Comp. Physiol. A* **146:** 361–378.

Webb, B. 1995. Using robots to model animals: a cricket test. *Robot. Auton. Syst.* **16:** 117–134.

Webb, B. 2000. What does robotics offer animal behaviour? *Anim. Behav.* **60:** 545–558.

Webb, B., and R. R. Harrison. 2000a. Eyes and ears: combining sensory motor systems modelled on insect physiology. Pp. 3913–3918 in *IEEE International Conference on Robotics and Automation*. San Francisco, 24–28 April 2000.

Webb, B., and R. R. Harrison. 2000b. Integrating sensorimotor systems in a robot model of cricket behavior. *Sensor Fusion and Decentralised Control in Robotic Systems III*. SPIE, Boston, 6–8 Nov. 2000.

Webb, B., and T. Scutt. 2000. A simple latency dependent spiking neuron model of cricket phonotaxis. *Biol. Cybern.* **82:** 247–269.

Weber, T., J. Thorson, and F. Huber. 1981. Auditory behaviour of the cricket. I. Dynamics of compensated walking and discrimination paradigms on the Kramer treadmill. *J. Comp. Physiol. A* **141:** 215–232.

Wehner, R. 1987. Matched filters—neural models of the external world. *J. Comp. Physiol. A* **161:** 511–531.

Reference: *Biol. Bull.* **200:** 190–194. (April 2001)

Innovative Biomechanics for Directional Hearing in Small Flies

DANIEL ROBERT

Laboratory of Bioacoustics, Institute of Zoology, University of Zürich,
Winterthurerstrasse 190, CH-8057 Zürich, Switzerland

Abstract. In humans and animals alike, the localization of sound constitutes a fundamental processing task of the auditory system. Directional hearing relies on acoustic cues such as the interaural amplitude and time differences and also, sometimes, the signal spectral composition. In small animals, such as insects, the auditory receptors are forcibly set close together, a design constraint imposing very short interaural distances. Due to the physics of sound propagation, the close proximity of the sound receivers results in vanishingly small amplitude and time cues. Yet, because of their directionality, small auditory systems embed original and innovative solutions that can be of inspirational value to some acute problems of technological miniaturization. Such ears are found in a parasitoid fly that acoustically locates its singing cricket host. Anatomically rather unconventional, the fly's auditory system is endowed with a directional sensitivity that is based on the mechanical coupling between its two hemilateral tympanal membranes. The functional principle permitting this directionality may be of particular relevance for technological applications necessitating sensors that are low cost, low weight, and low energy. Based on silicon-etching technology, early prototypes of sub-millimeter acoustic sensors provide evidence for directional mechanical responses. Further developments hold the promise of applications in hearing aid technology, vibration sensors, and miniature video-acoustic surveillance systems.

Introduction

In the sense of evolution, sensory systems constitute "adaptive packages" of biological engineering that have been proven sufficiently refined and efficient by the combined processes of natural and sexual selections. From this evolutionary vantage point, the considerable diversity of insect auditory systems (Hoy and Robert, 1996) can be regarded as an array of original and adapted solutions to the particular problems of acoustic detection using small sensors. Because they evolved under the particular constraints imposed by small body size, insects are likely to be of significant inspirational value for general problems of miniaturization. Our investigations are focused on questioning whether insects at the small end of the biometric range (millimeter and less) can be endowed with auditory organs, whether they can be directionally sensitive, and if so, what mechanisms are responsible for such directionality?

Design Constraints for a Miniature Auditory System

One such small insect is a parasitoid fly that acoustically locates and attacks singing field crickets (Cade, 1975). As part of their reproductive cycle, female parasitoid flies *Ormia ochracea* must find their cricket hosts as a source of food for their larval offspring. Remarkably, successful song localization can take place in complete darkness, that is, in the presence of acoustic information alone, but in the absence of visual and olfactory cues (Ramsauer and Robert, 1999, 2000). Hence, because of its crucial role in reproduction, audition is of great importance in the evolutionary history of these flies: promoting an increased reproductive success, efficient audition is likely to be under acute selective pressure.

Both detection and localization of the singing host are mediated by a pair of auditory sensory organs situated on

---

E-mail: drobert@zool.unizh.ch

This paper was originally presented at a workshop titled *Invertebrate Sensory Information Processing: Implications for Biologically Inspired Autonomous Systems*. The workshop, which was held at the J. Erik Jonsson Center for the National Academy of Sciences, Woods Hole, Massachusetts, from 15–17 April 2000, was sponsored by the Center for Advanced Studies in the Space Life Sciences at the Marine Biological Laboratory, and funded by the National Aeronautics and Space Administration under Cooperative Agreement NCC 2-896.

the anterior thorax just above the first pair of legs, which are directly below the fly's neck (Robert *et al.*, 1992) (Fig. 1A). The ears of the fly are endowed with two thin tympanal membranes, the eardrums, that are set very close together across the midline of the animal. In fact, while the tympanal membranes together span about 1.2 mm in width, the mechanoreceptive sensory organs are separated from each other by only 520 μm (Robert *et al.*, 1994) (Fig. 1A). As expected from the fly's small size and the resulting minute interaural distance, the largest interaural time difference (ITD) generated by a passing sound wave does not exceed 2 μs (Robert *et al.*, 1996). In the best possible case, for an azimuthal angle of incidence of 90° off the longitudinal axis of the animal, the ITD was measured with probe microphones to be 1.45 μs (SD: 0.49 μs, $n = 10$) (Fig. 1B). Such time difference is clearly much too small to be encoded by the nervous system of the fly. For humans, in comparison, ITDs at such an angle of incidence are much larger (Fig. 1B), varying from 500 μs to 700 μs, depending on head size, the sound path considered, and the frequency considered. It thus becomes apparent that microsecond-range ITDs, and possibly smaller ones, ought to constitute a major difficulty for the auditory system of the fly, both at the mechanical and neural coding levels. Another difficulty arises when the second directional cue, the interaural intensity difference (IID), is considered. The behaviorally relevant frequency range is that of the cricket's calling song, which spans from 4.6 to 5.2 kHz. Since at such frequencies the ratio of wavelength (66 mm at 5.2 kHz) to interaural distance (520 μm) is larger than 100, diffraction is very unlikely to occur around the fly's body, or at her ears (Morse and Ingard, 1968). Measurements made with custom probe microphones (100-μm acceptance diameter) and with ⅛-in microphones (Brüel & Kjaer type 4138, Naerum, Denmark) failed to indicate diffraction-elicited sound pressure differences around the fly that could constitute IID cues.

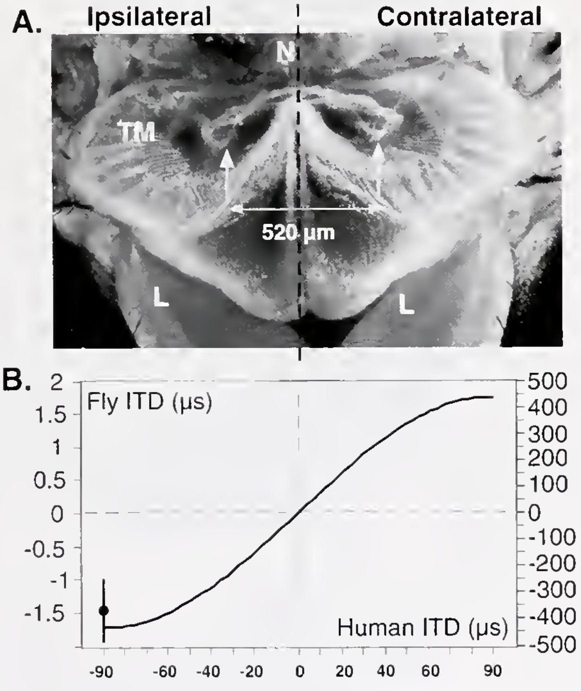

Figure 1. Auditory anatomy and temporal acoustic cues. (A) The auditory organs of the parasitoid fly *Ormia ochracea* are located on the anterior thorax, between the first pair of legs (L) and the neck (N). The tympanal membranes (TM) are adjacent to each other and set close together by the midline of the animal (vertical dashed line). Providing a connection between the two TMs across the midline, the intertympanal bridge is made of thicker cuticle than TMs and has the shape of a coat hanger. Two depressions at both ends of the intertympanal bridge indicate the insertion point of the sensory organs (arrows). Arrows also point to the interaural distance. (B) Interaural time difference (ITD) as a function of the angle of incidence of the sound stimulus. Right ordinate: ITDs calculated for humans (ear separation of 170 mm). Left ordinate: ITDs at the fly's ears calculated for an interaural distance of 0.6 mm. Data point (with standard deviation) shows ITD measurement made at −90° azimuth and 5 kHz tone, with two probe microphones located at the TMs.

Admittedly, the minuscule ITD (1.7 μs) and IID (<1 dB) generated from an incident sound wave constitute less than reliable acoustic cues for directional hearing. This finding, however, stands in sharp contrast to the behavioral capacity of this fly to localize the song of her host, as demonstrated in the field and laboratory (Robert *et al.*, 1992; Walker, 1993; Ramsauer and Robert, 2000).

Innovative Tympanal Mechanics

Taking place at the peripheral level of the tympanal membranes, the first step in the process of hearing pertains to the conversion of acoustic energy into mechanical energy. Thus, tympanal mechanics was examined in response to incident sound waves, either with pure tones mimicking cricket songs, or with band-limited white noise. Using microscanning laser vibrometry (Robert and Lewin, 1998), displacement velocities were assessed over several hundred measurement locations on both tympanal membranes and on the associated cuticular elements. In response to random noise as well as pure tone stimuli, the amplitude and phase responses of both tympanal membranes differ strongly from those expected for two independent pressure receivers set 0.5 mm apart (Fig. 2). Firstly, independent receivers would indicate immeasurably small differences in amplitude, whereas the fly's tympana undergo large differences in their vibrations above about 4.5 kHz (Fig. 2A). Secondly, independent receivers such as microphones indicate interaural time delays on the order of 2 μs (Fig. 1B), an ITD significantly smaller than the delays (also measured as the phase lag at maximal deflection) observed in the mechanical response of the tympanal membranes (on average: 55 μs; SD: 12

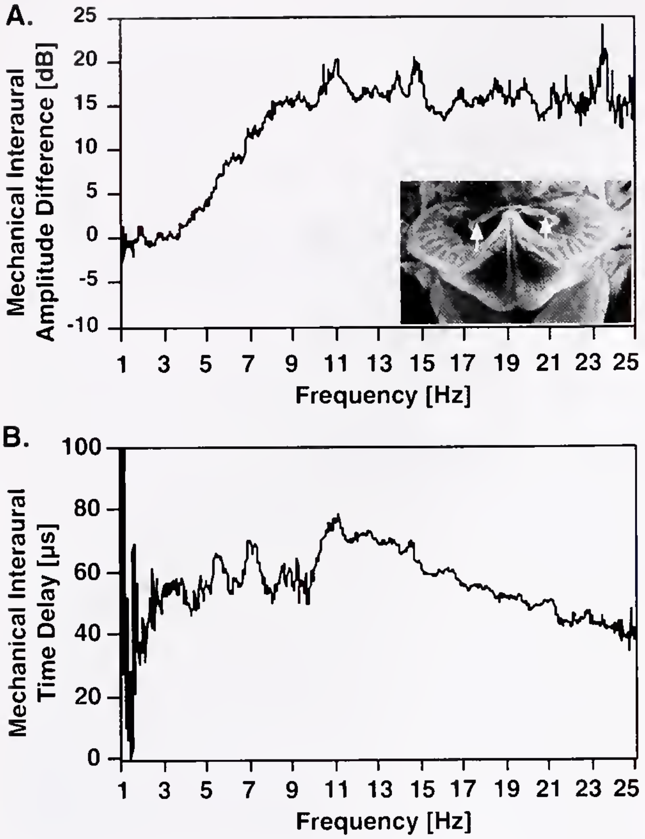

Figure 2. Mechanical response of the tympanal membranes in amplitude and time. (A) Difference amplitude spectrum of the mechanical response at the anatomical locations indicated in the inset (arrows). The contralateral mechanical response is subtracted from the ipsilateral one. (B) Time delay between the ipsilateral and contralateral mechanical responses, calculated from the difference phase spectrum. Sound stimulus at 45° incidence in azimuth, band-limited white noise (1–30 kHz).

μs, n = 769 frequency points) (Fig. 2B). In effect, these measurements indicate that the mechanical response of the tympanal membranes has a pronounced directionality. Interaural time and intensity differences in the mechanical response of the tympana are significantly larger than those available in the acoustic field. The analysis of tympanal deflection shapes (see Fig. 3A) provides evidence that such differences between the ipsilateral and contralateral responses are due to the particular mechanical properties of this small tympanal system. Reflecting the asymmetrical responses reported earlier (Fig. 2), deflection shapes at frequencies around 5 kHz indicate that while the ipsilateral tympanum undergoes an outward deflection, the contralateral tympanum experiences an inward deflection, but of much lesser amplitude (Fig. 3B). Such asymmetry in the response is due to the fact that the two hemilateral tympanal membranes are not vibrating independently. The tympana are in fact connected, across the midline, by a specialized cuticular structure (Robert *et al.*, 1994, 1996).

The Process of Intertympanal Coupling

In an effort to unite structure and function in a functional explanation, the reconstitution of actual tympanal deflections provides key information on the anatomical basis for the observed mechanical behavior. The particularity—and perhaps uniqueness—of these ears is that they are physically connected by an unpaired cuticular structure, the intertympanal bridge (Figs. 1A, 4A). This bridge is thicker (2–10 μm), and therefore stiffer, than the surrounding tympanal membranes (0.2–1 μm) to which it attaches. Thus, the tympana are mechanically linked by a relatively rigid cuticular bridge, a fact that can also be easily assessed by gently deflecting one tympanic membrane downwards with

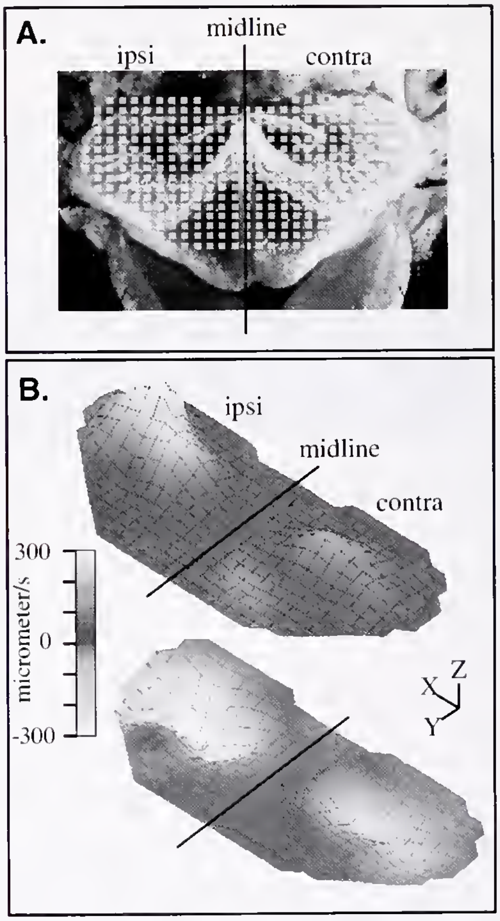

Figure 3. Tympanal deflection shapes. (A) Tympanal vibration velocity was monitored at 364 locations over tympanal and non-tympanal areas. Coherence values exceeded 0.95, indicating little contamination by uncorrelated noise. Stimulus: band-limited random noise (1 to 30 kHz; 94 dB SPL [sound pressure level]) at 90° azimuth to the longitudinal axis of the fly. Ipsilateral and contralateral conventions as indicated. (B) Upper panel shows maximum outward deflection of the ipsilateral tympanal membrane at 5 kHz excitation frequency. Lower panel depicts the maximum inward deflection reached half a period later, *e.g.*, 100 μs later. *X* axis: lateral; *Y*: ventral; *Z*: axis of measured tympanal deflections. For animation of deflection, please visit: www.unizh.ch/~ormia/research_flies.html

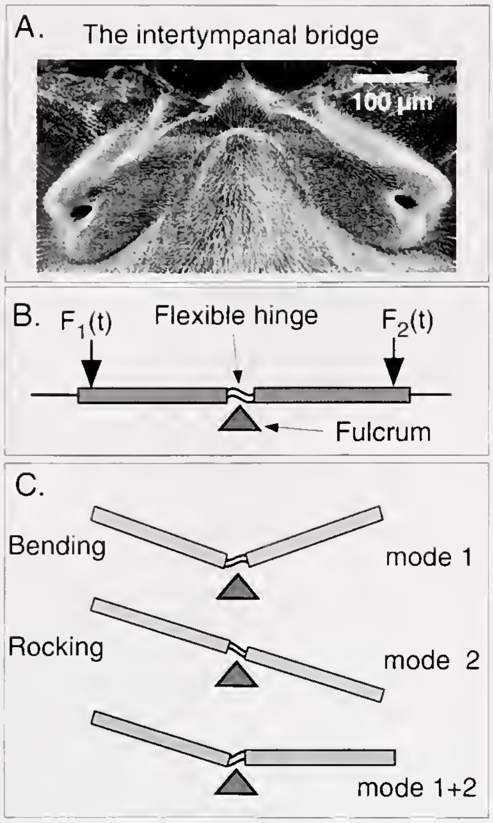

Figure 4. The anatomy of mechanical coupling, and vibrational modes of the flexible intertympanal bridge. (A) Close-up of the intertympanal bridge connecting the tympanal membranes. (B) Simple mechanical model of the bridge as a seesaw endowed with two rigid bars connected by a flexible central hinge (≈). (C) On the basis of the laser vibrometric micromechanical analysis, it is suggested that two basic modes can characterize the observed mechanical response. Bending occurred at low frequencies (mode 1; <4 kHz), whereas rocking was measured at intermediate frequencies (mode 2; 5–7 kHz). At higher frequencies (15 kHz and above), bending and rocking modes combine to elicit motion in one tympanum only (mode 1 + 2).

a human hair, and observing the other deflect upwards as a result.

Deflection shapes obtained by microscanning laser Doppler vibrometry for different stimulus frequencies (*e.g.*, 2, 5 or 15 kHz) reveal that this micromechanical system can produce several different patterns of deflection that are reminiscent of the movements of a flexible seesaw (Fig. 4B). The simple mechanical model shown in Figure 4B has been proposed as a reasonable functional, and intuitively accessible, approximation of this unconventional peripheral auditory system (Miles *et al.*, 1995; Robert *et al.*, 1996). The physical action of the intertympanal bridge is to convert small acoustic ITDs into larger time *and* amplitude differences at the mechanical level. The functional principle for this effect resides in the somewhat complex linear interaction between two coupled oscillators—the tympanal membranes. Very briefly, for low frequencies of stimulation (2 kHz), the deflections of the ipsilateral and contralateral membranes show little difference in amplitude and phase. In this case, the forces applied to the bridge (Fig. 4B) have a phase difference of only 1° and result in sympathetic deflections, owing to the bending of the bridge (Fig. 4C, mode 1). At this frequency of excitation, the first mode of deflection dominates the response. Excitation of this first mode results in little directionality—or asymmetry—in the mechanical response, as shown for frequencies lower than about 3 kHz (Fig. 2A). As stimulus frequency increases, a transition to the second mode of deflection is expressed by the rocking motion of the bridge (Fig. 4, mode 2). Noteworthy is the fact that for intermediate frequencies (*i.e.*, 5 kHz) and a given effective interaural distance, the phase difference in the driving forces increases. At 5 kHz, this phase is very small—2.6°—yet, it is sufficient to drive this system to its rocking mode (Fig. 3B). A combination of these two modes (rocking and bending) will take place at even higher frequencies (*e.g.*, 15 kHz) and result in the deflection of the ipsilateral tympanum, but in the silencing of the contralateral one (Fig. 4C, mode 1 + 2). Hence, the relative flexibility of the bridge, be it localized at the fulcrum point or distributed along the lateral arms, constitutes the key to the directionality of the observed mechanical response.

In addition, experiments of mechanical actuation in the absence of sound have demonstrated that mechanical coupling is mediated and can be explained by the action of the intertympanal bridge alone (Robert *et al.*, 1998). The mechanical actuation of one tympanum at amplitudes of about 10 nanometers—mimicking the displacement amplitudes observed during acoustic stimulation—elicits a correlated mechanical displacement of the other tympanum. The finite flexibility of the intertympanal bridge accounts for the IIDs and ITDs in the mechanical deflections, for which two modes dominate at different frequencies (Robert *et al.*, 1996). Hence, in summary, the mechanical structure of the hearing organs increases the minimal acoustic interaural time and amplitude difference cues into more substantial mechanical cues that can be processed by the nervous system (Robert *et al.*, 1996).

Intertympanal Coupling as an Evolutionary Novelty

As such, the process of mechanical coupling between tympanal membranes, and its amplification effect on interaural auditory cues, seems to be unique to flies. In essence, intertympanal coupling constitutes a novel mechanism for directional hearing, representing a third kind of directional receiver for terrestrial animals. One other kind of directional system is found in most vertebrates, and is based on two acoustically isolated pressure receivers set apart on the head of the animal. In other small animals, such as frogs (Narins *et al.*, 1988) and some birds (Calford and Piddington, 1988), the auditory receivers are acoustically coupled (pressure-difference receivers), a system that has been shown to result in the amplification of the perceivable ITDs and IIDs available in the sound field.

Conclusions

One of the outcomes of the research presented here has been to explore the possibility of transferring the mechanism of intertympanal coupling to microsensor technology. Abstracting the functional principle unraveled in the parasitoid fly may indeed contribute to the development of subminiature microphones. Besides the inherent directionality of the receiver's mechanics despite its small size, two other, definite and foreseeable, advantages of fly-inspired acoustic receivers would be their low cost and low energy consumption. Indeed, one of the possible attractive aspects of such a system is the fact that the first stage of acoustic processing is made on a mechanical basis, without the intervention of energy-consuming electronics. Using microelectromechanical systems technology (MEMS), our early prototypes etched on silicon wafers provide evidence that coupled pressure receivers no larger than 500 μm are directionally sensitive at about 5 kHz. Further optimization promises the development of subminiature microphones endowed with directionality in the range of human speech. Finally, possible applications can be envisaged that could contribute to the development of hearing aids or miniature personal communication devices endowed with improved receiver acoustics, or small surveillance systems capable of pinpointing a source of noise.

Acknowledgments

This work was supported by the Swiss National Science Foundation.

Literature Cited

Cade, W. H. 1975. Acoustically orienting parasitoid: fly phonotaxis to cricket song. *Science* **190:** 1312–1313.

Calford, M. B., and R. W. Piddington. 1988. Avian interaural canal enhances interaural delay. *J. Comp. Physiol. A* **162:** 503–510.

Hoy, R. R., and D. Robert. 1996. Tympanal hearing in insects. *Annu. Rev. Entomol.* **41:** 433–450.

Miles, R. N., D. Robert, and R. R. Hoy. 1995. Mechanically coupled ears for directional hearing in the parasitoid fly *O. ochracea. J. Acoust. Soc. Am.* **98**(6): 3059–3070.

Morse, P. M., and K. U. Ingard. 1968. *Theoretical Acoustics.* McGraw Hill, New York. Pp. 418–422.

Narins, P. M., G. Ehret, and J. Tautz. 1988. Accessory pathway for sound transfer in a neotropical frog. *Proc. Natl. Acad. Sci. USA* **85:** 1508–1512.

Ramsauer, N., and D. Robert. 1999. Acoustic attraction of the parasitoid fly *Ormia ochracea* to the song of its host. *J. Acoust. Soc. Am.* **105:** 1319.

Ramsauer, N., and D. Robert. 2000. Phonotactic orientation in a parasitoid fly. *Naturwissenschaften* **87:** 315–319.

Robert, D., and A. Lewin. 1998. Microscanning laser vibrometry applied to the biomechanical study of small auditory systems. Pp. 564–571 in *Third International Conference of Vibration Measurements by Laser Techniques.* Ancona, Italy. E. P. Tomasini, ed. *Proceedings of the International Society of Optical Engineers,* Vol. 3411. Bellingham, WA.

Robert, D., J. Amoroso, and R. R. Hoy. 1992. The evolutionary convergence of hearing in a parasitoid fly and its cricket host. *Science* **258:** 1135–1137.

Robert, D., M. P. Read, and R. R. Hoy. 1994. The tympanal hearing organ of the parasitoid fly *Ormia ochracea* (Diptera, Tachinidae, Ormiini). *Cell Tissue Res.* **275:** 63–78.

Robert, D., R. N. Miles, and R. R. Hoy. 1996. Directional hearing by mechanical coupling in the parasitoid fly *Ormia ochracea. J. Comp. Physiol. A* **179:** 29–44.

Robert, D., R. N. Miles, and R. R. Hoy. 1998. Tympanal mechanics in the parasitoid fly *Ormia ochracea:* intertympanal coupling during mechanical vibration. *J. Comp. Physiol. A* **183:** 443–452.

Walker, T. J. 1993. Phonotaxis in female *Ormia ochracea* (Diptera, Tachinidae), a parasitoid of field crickets. *J. Insect Behav.* **6:** 389–410.

Reference: *Biol. Bull.* **200:** 195–200. (April 2001)

A Biologically Inspired Controller for Hexapod Walking: Simple Solutions by Exploiting Physical Properties

JOSEF SCHMITZ*, JEFFREY DEAN, THOMAS KINDERMANN,
MICHAEL SCHUMM, AND HOLK CRUSE

*Department of Biological Cybernetics, University of Bielefeld,
P.O. Box 100131, D-33501 Bielefeld, FRG*

Abstract. The locomotor system of slowly walking insects is well suited for coping with highly irregular terrain and therefore might represent a paragon for an artificial six-legged walking machine. Our investigations of the stick insect *Carausius morosus* indicate that these animals gain their adaptivity and flexibility mainly from the extremely decentralized organization of the control system that generates the leg movements. Neither the movement of a single leg nor the coordination of all six legs (*i.e.*, the gait) appears to be centrally pre-programmed. Thus, instead of using a single, central controller with global knowledge, each leg appears to possess its own controller with only procedural knowledge for the generation of the leg's movement. This is possible because exploiting the physical properties avoids the need for complete information on the geometry of the system that would be a prerequisite for explicitly solving the problems. Hence, production of the gait is an emergent property of the whole system, in which each of the six single-leg controllers obeys a few simple and local rules in processing state-dependent information about its neighbors.

Introduction

The advantages of legged locomotion in contrast to wheel-driven locomotion are particularly obvious in rough terrain. A disadvantage, however, is that legs can provide only discontinuous support of the body. At a certain point within its posterior working range, each leg has to be lifted off the ground and swung forward to regain ground contact for the next step. Hence during each step cycle each leg has to go through two mutually exclusive phases: the stance, in which the leg supports the body and can exert propulsion forces; and the swing, in which the leg cannot contribute to the movement of the body.

The control system that generates the leg movements of an animal faces several problems. During the stance, the trajectories of all leg endpoints have to be coordinated in such a way that each leg with ground contact contributes efficiently to propel the central body in the desired direction and with the desired velocity. Thus, in a six-legged animal with 3 joints per leg (Fig. 1a), as many as 18 joints have to be controlled. (For simplicity, the tarsus is considered as a passive foothold only, and the tip of the tibia is considered as the leg endpoint throughout this paper.) Four factors further complicate this control task: (1) the number and combinations of legs in stance vary continuously, (2) during curve walking, the legs move at different speeds, (3) on compliant substrates the movement of a leg may vary unpredictably, and (4) the geometry of the system may vary due to nonrigid suspension of the joints or due to injuries of leg segments. For the swing movement, it appears to be easier to solve the problems because no mechanical couplings *via* the substrate have to be considered. However, for the stability of an animal, the timing of the switch from

---

[*] To whom correspondence should be addressed. E-mail: Josef.Schmitz@Biologie.Uni-Bielefeld.De

This paper was originally presented at a workshop titled *Invertebrate Sensory Information Processing: Implications for Biologically Inspired Autonomous Systems.* The workshop, which was held at the J. Erik Jonsson Center for the National Academy of Sciences, Woods Hole, Massachusetts, from 15–17 April 2000, was sponsored by the Center for Advanced Studies in the Space Life Sciences at the Marine Biological Laboratory, and funded by the National Aeronautics and Space Administration under Cooperative Agreement NCC 2-896.

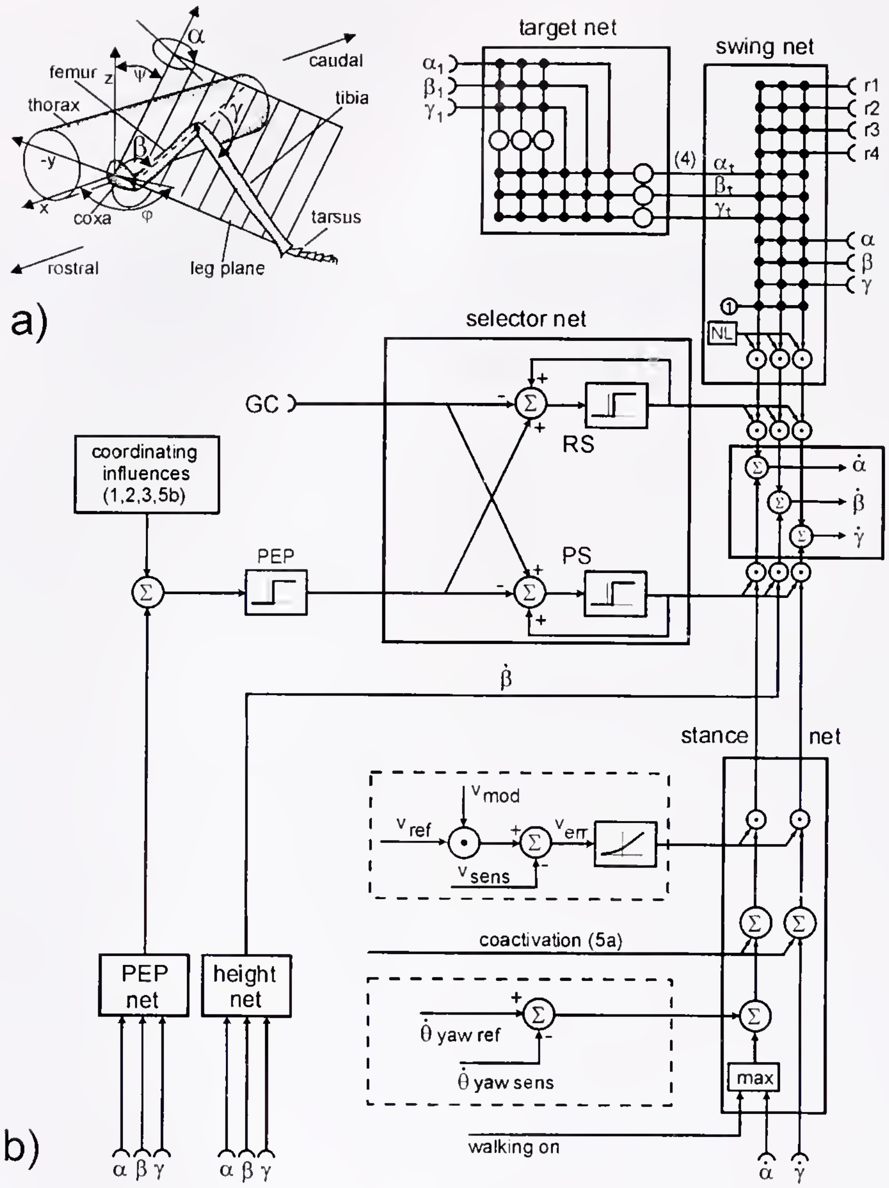
a)
femur
z
ψ
α
caudal
thorax
tibia
γ
β
-y
x
coxa
φ
tarsus
rostral
leg plane
b)
target net
swing net
α1
β1
γ1
r1
r2
r3
r4
(4)
αt
βt
γt
α
β
γ
1
NL
selector net
GC
RS
PS
PEP
coordinating influences (1,2,3,5b)
α̇
β̇
γ̇
β̇
stance
net
Vmod
Vref
Verr
Vsens
coactivation (5a)
θ̇ yaw ref
θ̇ yaw sens
max
walking on
PEP net
height net
α β γ
α β γ
α̇ γ̇

Figure 1. Summary of leg geometry and the single leg control network. (a) Schematic drawing of a stick insect leg showing the arrangement of the joints and their axes of rotation. (b) The leg controller consists of three parts: the swing net, which controls the leg movement during swing; the stance net, which controls the stance movement; and the selector net, which determines whether the swing or the stance net can control the motor output, *i.e.*, the velocity of the three joints α, β, and γ. The selector net contains four units: the PEP unit, which signals posterior extreme positions; the GC unit, which signals ground contact; the RS unit, which controls the return stroke (swing movement); and the PS unit, which controls the power stroke (stance movement). The target net transforms information on the configuration of the anterior target leg, given by the angles α_1, β_1, γ_1, into angular values for the next caudal leg (α_r, β_r, γ_r), which place the two tarsi close together. These desired final values and the current values of the leg angles, α, β, and γ, are input to the swing net together with bias inputs and sensory inputs (r1–r4) that are activated by an obstruction blocking the swing and thereby initiate appropriate avoidance movements. NL is a nonlinear compensation term. The stance net uses the β joint for height control *via* a negative-feedback system. Walking velocity is controlled by a negative-feedback system, which compares v_{ref} and v_{sens}, and influences the α and γ gains. The α channels are further subject to a yaw control (angle θ), which stabilizes straight and curve walking. The sign of this influence is opposite for the left and right legs. Walking is switched on by another central influence, which passes through a maximum detector and influences the α channels of all legs.

stance to swing is crucial. A control system therefore also has to ensure proper spatiotemporal coordination among all legs.

Each single problem mentioned above can be solved by means of classical control algorithms; this is, however, very costly in terms of computational time. In contrast, insects, like all other animals equipped with a slow-processing neuronal system, solve all these problems in real time and, beyond this, are able to react immediately even to such extreme changes as, for example, the loss of a whole leg. The solutions invented by nature are therefore not only interesting for the biologist, but could also be useful for solving problems in robotics.

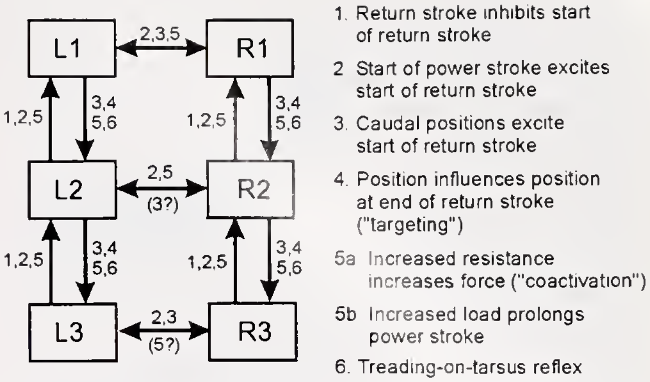
L1
R1
L2
R2
L3
R3
2,3,5
1,2,5
3,4
5,6
1,2,5
3,4
5,6
2,5
(3?)
1,2,5
3,4
5,6
1,2,5
3,4
5,6
2,3
(5?)
1. Return stroke inhibits start of return stroke
2 Start of power stroke excites start of return stroke
3. Caudal positions excite start of return stroke
4. Position influences position at end of return stroke ("targeting")
5a Increased resistance increases force ("coactivation")
5b Increased load prolongs power stroke
6. Treading-on-tarsus reflex

Figure 2. Summary of the main coordinating influences between adjacent legs during walking.

Control of the Gait

Results from biological investigations show that each leg is controlled by its own controller (*e.g.*, Cruse, 1990) and may indicate that even each leg controller consists of separate control networks (*e.g.*, Bässler, 1988). The relaxation oscillator making up the step pattern generator is assumed to consist of a swing net that controls the swing movement and a stance net that controls the movement of the leg during stance (Fig. 1b). The transition between swing and stance is controlled by the selector net. The swing net and the stance net are always active, but the selector net determines which of the two has access to the motor output at any given time. The decision of when to switch from one state into the other is completely determined by sensory input. The selector net consists of a two-layer feedforward net with positive feedback connections in the second layer. These positive-feedback connections serve to stabilize the ongoing activity, namely stance or swing. The three most important coordinating mechanisms used in our present model influence the selector net so as to modulate the beginning of a swing movement, and therefore the end-point of a stance movement (the posterior extreme position, PEP). These influences (numbers 1–3, summarized in Fig. 2) are described in detail elsewhere (*e.g.*, Cruse, 1990; Cruse *et al.*, 1998). The end of the swing movement in the animal is modulated by a single, caudally directed influence (number 4 in Fig. 2) that depends on the position of the next rostral leg. This mechanism is responsible for the targeting behavior—the placement of the tarsus at the end of a swing close to the tarsus of the adjacent rostral leg.

A computer simulation of this system showed proper temporal coordination of the legs when these are walking at different speeds on a horizontal plane (Cruse *et al.*, 1998). The steps of ipsilateral legs are organized in triplets forming "metachronal waves," which proceed from back to front, whereas the steps of the contralateral legs on each segment step approximately in alternation. With increasing walking speed, the typical change in coordination from the tetrapod to a tripod-like gait is found. The coordination pattern is very stable. For example, when the movement of one leg is interrupted briefly during the stance, the normal coordination is regained immediately after the perturbation. Note that in our approach, the temporal sequence of the activities of the legs is not explicitly produced by a master timer but is implicitly determined by the connections between the leg controllers. These coordinating mechanisms had been successfully tested on a variety of six-legged robots (*e.g.*, Espenschied *et al.*, 1993; Ferrell, 1995; Pfeiffer *et al.*, 1995; Flannigan *et al.*, 1998; Frik *et al.*, 1999).

Control of the Swing Movement

The geometry of the stick insect's leg is shown in Figure 1a. The coxa-trochanter (β) and femur-tibia (γ) joints, the two distal joints, are simple hinge joints with one degree of freedom corresponding to elevation and to extension of the tarsus, respectively. The subcoxal (α) joint is more complex, but during forward walking most of its movement is in a rostrocaudal direction around the nearly vertical axis. The leg can thus be considered as a manipulator with three degrees of freedom for movement in three dimensions, and the control network must have at least three output channels, one for each leg joint. As has been shown by Cruse *et al.* (1998), a simple, two-layer feedforward net with three output units and six input units can produce movements that closely resemble the swing movements observed in walking stick insects. In the simulation, the three outputs of this net, interpreted as the angular velocities $d\alpha/dt$, $d\beta/dt$, and $d\gamma/dt$, are fed into an integrator (not shown in Fig. 1b), which in the animal corresponds to the leg itself, to obtain the joint angles. The actual angles are measured and fed back into the net. *Via* this loop through the environment, the network becomes a recurrent system. In addition to the actual angles of the three leg joints, three other input units (α_t, β_t, γ_t) represent the target of the swing movement, *i.e.*, the leg position that should be achieved at the end of the return stroke (targeting influence, number 4 in Fig. 2).

This system with only eight or nine nonzero weights is able to generalize over a considerable range of untrained situations. Furthermore, the swing net is remarkably tolerant with respect to external disturbances (Fig. 3). The learned trajectories represent a kind of attractor to which the disturbed trajectory returns. This compensation for disturbances is possible because the system does not compute explicit trajectories but—using actual sensor data—calculates only the next movement increment. This ability to compensate for external disturbances permits simple extensions of the swing net in order to simulate avoidance behaviors observed in insects (additional inputs "r1–r4" in Fig. 1b).

Control of the Stance Movement

To control the stance movement, it is not enough simply to specify a movement for each leg on its own: the mechanical coupling through the substrate means that efficient locomotion requires coordinated movement of all the joints of all the legs in contact with the substrate—that is, a total of 18 joints when all legs of an insect are on the ground. However, the number and combination of mechanically coupled joints varies from one moment to the next, depending on which legs are lifted. A further complication occurs when the animal negotiates a curve, because then the different legs move at different speeds.

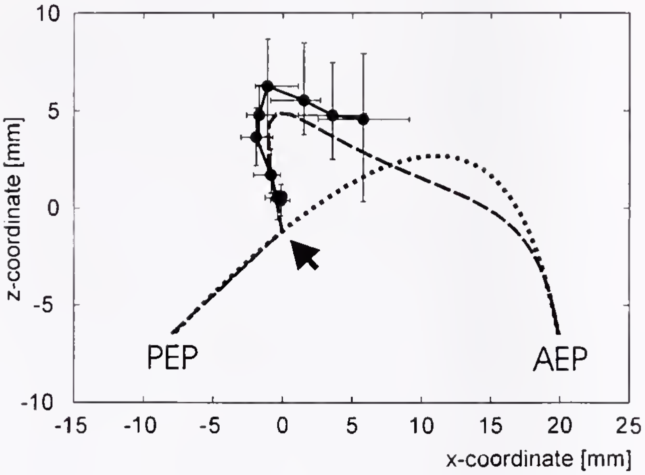

Figure 3. Behavior of the swing net. The fine stippled line represents a trajectory (in the x-z plane, *i.e.*, in a side view) of the tibia endpoint of a middle leg of an undisturbed swing movement. The leg lifts off at the posterior extreme position (PEP) and swings forward to the anterior extreme position (AEP). The dashed line represents a swing trajectory of the middle leg in which the movement of the tibia was obstructed (arrow). The swing net instantaneously generates a new trajectory, which avoids the obstruction by retracting and lifting the tibia and which then reaches the AEP on this new trajectory. The filled circles (with x-z error bars) connected by the continuous line show the reaction of a stick insect whose swing movement was obstructed at the same moment in swing as it was applied to the simulation.

In robots, these problems can be solved using traditional, though computationally costly, methods, because these approaches consider the ground-reaction forces of all legs in stance and seek to optimize some additional criteria, such as minimizing the tension or compression exerted by the legs on the substrate. Due to the nature of the mechanical interactions, and inherent in the search for a globally optimal control strategy, such algorithms require a single, central controller; they do not lend themselves to distributed processing. This makes real-time control difficult, even in the simple case of walking on a rigid substrate.

Despite the evident complexity of the task, it is mastered even by insects. Therefore, there must be a solution fast enough that on-line computation is possible even for slow-processing neuronal systems. How can this be done? To solve the particular problem at hand, we propose to replace a central controller by distributed control in the form of local positive feedback (Cruse *et al.*, 1995a). Positive feedback (or in other words, reflex reversals) had already been reported to occur during walking in the stick insect (*e.g.*, Bässler, 1988; Schmitz *et al.*, 1995). Compared to earlier versions of the leg controller (Cruse *et al.*, 1995b), this change permits the stance net to be radically simplified. The positive feedback occurs at the level of single joints: the position signal of each is fed back to control the motor output of the same joint (Fig. 1b, stance net). How does this system work? Let us assume that any one of the joints is moved actively. Then, because of the mechanical connections, all other joints begin to move passively, but in exactly the proper way. Thus, the movement direction and speed of each joint does not have to be computed, because this information is already provided by the physics. The positive feedback then transforms this passive movement into an active movement.

There are, however, several problems to be solved that are inherent in positive feedback systems. The first is that positive feedback using the raw position signal would lead to unpredictable changes in movement speed. This problem can be solved by introducing a kind of bandpass filter into the feedback loop. The effect is to make the feedback proportional to the angular velocity of joint movement, not the angular position. In the stick insect, the bandpass filter property can be attributed to the phasic response characteristic of the sense organs and the lowpass filter properties of the neuromuscular system. The second problem is that using positive feedback for all three leg joints leads to unpredictable changes in body height, even in a computer simulation neglecting gravity. A physical system would, of course, be pulled downward by gravity, and the positive feedback would accelerate this movement. In the stick insect, body height is controlled by a distributed system in which each leg acts like an independent, proportional controller (Cruse *et al.*, 1993). Thus, no master height controller is necessary; the only central information is the invariant reference value

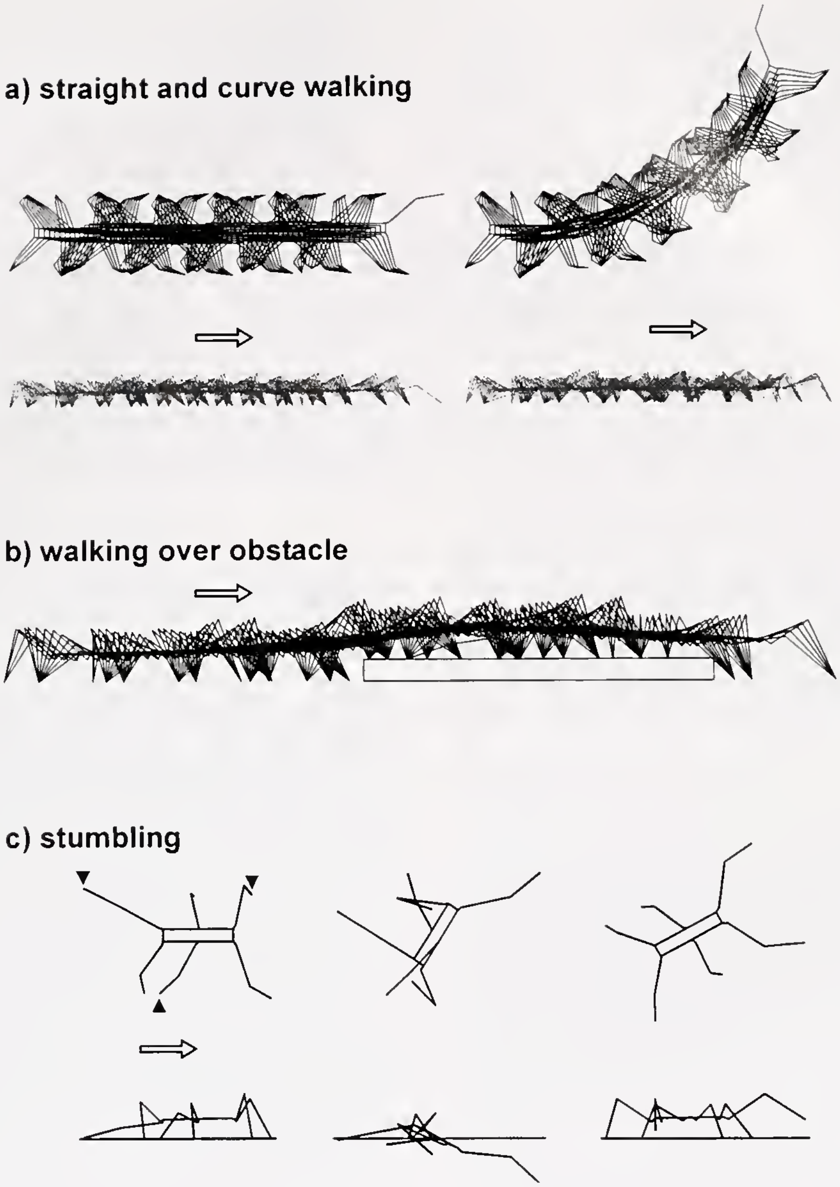

a) straight and curve walking

b) walking over obstacle

c) stumbling

Figure 4. Strobe-shot video of a simulation of the six-legged system with negative feedback applied to all six β joints and positive feedback to all α and γ joints. Leg positions are shown only during stance and only for each fifth time interval. In (a), straight (angle $\theta_{ref} = 0$) and curve walking (angle $\theta_{ref} \neq 0$) is shown from both a top and a side view. Walking direction is from left to right. In (b), a straight walk over an obstacle (obstacle height is 90% of the normal body-substrate clearance) is shown from a side view. In (c), three single frames (both top and side view each) of a situation in which the system was forced to fall to the ground are shown. The fall caused an extremely disordered arrangement of the legs, but within a few seconds the system stood up by itself and resumed proper coordinated walking.

for each leg. In the WalkNet we implemented this such that only the α and the γ joints are under positive feedback control, whereas the β joint remains under classical negative feedback as in the standing animal. In this way, it is possible to solve the problems mentioned above in an easy and computationally simple manner. This hypothesis is also compatible with biological results obtained from animals subject to disturbances during stance movements (Bartling and Schmitz, 2000).

Finally, we have to address the question of how walking speed is determined in such a positive feedback controller. We assume a central value that represents the desired walking speed v_{ref}. This is compared with the actual speed, which could be derived from the optical flow or by monitoring leg movement. An error signal, resulting from a deviation, modifies the gain of the positive feedback for all α and γ joints of all six legs accordingly (Fig. 1b, stance net). With our controller, curve walking is achieved in an easy way. Again we assume a central value that represents the intended angle of body yaw. A traditional negative feedback system controls the rate of yaw ($\dot{\theta}_{\text{yaw}}$, Fig. 1b). The error signal modifies the gain of the positive feedback of the legs. Keeping $\dot{\theta}_{\text{ref}}$ at zero results in straight walks; a bias to one or the other side results in curve walking with the curvature proportional to the amplitude of the bias (Fig. 4a).

Walking over irregularities in the terrain is performed sufficiently well due to the adaptive properties inherent in our control approach (Fig. 4b). Moreover, we found further emergent properties of the decentralized control structure. If the system was made to stumble and fall to the ground, it stood up by itself and resumed proper walking (Fig. 4c). This happened even when the fall placed the six legs in an extremely disordered arrangement. This means that the simple solution proposed here also eliminates the need for a special supervisory system to rearrange leg positions after such an emergency.

Summary

Considering the problems with which an adaptive control system for walking must cope, one could be inclined to propose a highly centralized system with global knowledge. Our biologically inspired model shows, however, that the most complex task (stance movement) can be handled by a rather simple system (local positive feedback). The simplification is possible because instead of explicit calculations, the physical properties of the system and its environment are exploited. This is shown in our model at several stages:

- The rhythmic movements of single legs are not produced by a top-down approach but emerge from the interaction of the neuromuscular system with the environment.
- For the swing movement, no explicit trajectory is precalculated and then spooled out; rather the trajectory is calculated on the basis of the actual sensor data of the ongoing swing.
- The discrepancy between the complexity of the task and the simplicity of the solution is most obvious for the control of the stance movement. Local rules for each single joint are sufficient to solve the given task in an adaptive way.

Furthermore, our simulation shows that at the systems level, complex behavior can emerge from the cooperation of local rules:

- The coordination mechanisms produce proper tripod or tetrapod gait. These gaits are robust against disturbances.
- The system, by combining local positive and negative feedback loops, can cope with a variety of disturbances such as restricting movement of a single leg or removal of leg segments.
- If the system was forced to stumble and fall to the ground, it stood up by itself and resumed proper walking.

These findings encourage us to propose a decentralized control scheme as a basis for legged robot locomotion. This basis can be extended to integrate further reflexes and behaviors, in order to achieve in the robot a level of agility similar to that found in insects.

Acknowledgments

Supported by Deutsche Forschungsgemeinschaft (Cr 58/9-2) and the Körber-Foundation.

Literature Cited

Bartling, C., and J. Schmitz. 2000. Reaction to disturbances of a walking leg during stance. *J. Exp. Biol.* **203:** 1211–1233.

Bässler, U. 1988. Functional principles of pattern generation for walking movements of stick insect forelegs: the role of the femoral chordotonal organ afferences. *J. Exp. Biol.* **136:** 125–147.

Cruse, H. 1990. What mechanisms coordinate leg movement in walking arthropods? *Trends Neurosci.* **13:** 15–21.

Cruse, H., J. Schmitz, U. Braun, and A. Schweins. 1993. Control of body height in a stick insect walking on a treadwheel. *J. Exp. Biol.* **181:** 141–155.

Cruse, H., C. Bartling, and T. Kindermann. 1995a. High-pass filtered positive feedback for decentralized control of cooperation. Pp. 668–678 in *Advances in Artificial Life*, F. Moran, A. Moreno, J. J. Merelo, and P. Chacon, eds. Springer, New York.

Cruse, H., C. Bartling, D. E. Brunn, J. Dean, M. Dreifert, T. Kindermann, and J. Schmitz. 1995b. Walking: a complex behavior controlled by simple systems. *Adapt. Behav.* **3:** 385–418.

Cruse, H., T. Kindermann, M. Schumm, J. Dean, and J. Schmitz. 1998. Walknet—a biologically inspired network to control six-legged walking. *Neural Networks* **11:** 1435–1447.

Espenschied, K. S., R. D. Quinn, H. J. Chiel, and R. D. Beer. 1993. Leg coordination mechanisms in the stick insect applied to hexapod robot locomotion. *Adapt. Behav.* **1:** 455–468.

Ferrell, C. 1995. A comparison of three insect-inspired locomotion controllers. *Robot. Auton. Syst.* **16:** 135–159.

Flannigan, W. C., G. M. Nelson, and R. D. Quinn. 1998. Locomotion controller for a crab-like robot. Pp. 152–162 in *IEEE Proc. Robotics and Automation 1998*, Leuven, Belgium.

Frik, M., M. Guddat, M. Karatas, and C. D. Losch. 1999. A novel approach to autonomous control of walking machines. Pp. 333–342 in *Proc. 2nd Conference on Climbing and Walking Robots*, CLAWAR 1999. Professional Engineering Publishing, Bury St. Edmunds, UK.

Pfeiffer, F., J. Eltze, and H. J. Weidemann. 1995. Six-legged technical walking considering biological principles. *Robot. Auton. Syst.* **14:** 223–232.

Schmitz, J., C. Bartling, D. E. Brunn, H. Cruse, J. Dean, T. Kindermann, M. Schumm, and H. Wagner. 1995. Adaptive properties of "hard-wired" neuronal systems. *Verh. Dtsch. Zool. Ges.* **88.2:** 165–179.

Reference: *Biol. Bull.* **200:** 201–205. (April 2001)

Insights for Robotic Design From Studies of the Control of Abdominal Position in Crayfish

DAVID L. MACMILLAN* AND BLAIR W. PATULLO

Department of Zoology, University of Melbourne, Parkville, Victoria 3052, Australia

Abstract. Studies of the control of position and movement of the abdomen of crayfish illustrate a number of features of invertebrate sensory-motor systems that have implications for their use to inform robotic design. We use the abdominal slow extensor motor system to illustrate three of them here: first, the way in which a behaviorally flexible length-servo device can be achieved with very few elements; second, the importance of knowledge of the biological and behavioral context in which the elements operate; third, that design solutions resulting from natural selection have been constrained by the previous evolutionary history of the animal, which can affect the outcomes in ways that may not be immediately apparent in a design context.

Introduction

Crayfish, and other crustaceans with tubular bodies, have proprioceptive structures called muscle receptor organs (MROs) spanning the articulations between the segments (Alexandrowicz, 1951). Each MRO signals the relative position and movement of the two segments to which it attaches. Since the discovery of MROs, many different aspects of their biology have attracted the interest of neurobiologists (Fields, 1976; Macmillan, 2001). In this paper we combine data from the literature with insights from our current work on crayfish to highlight three aspects of MRO biology with interesting implications for biologically inspired robots: that arthropods achieve complex behavioral outcomes with few neurons, that assumptions derived from reduced preparations or parts of animals need to be tested in biologically meaningful situations in intact animals, and that it is important to have an appreciation of the impact of natural selection when examining biological solutions to engineering design problems.

The abdomen, or tail, of the crayfish is composed of five similar, articulated tubes connected by simple lateral hinges that permit movement only in the pitch plane (Fig. 1A). The connection between the thorax and the first abdominal segment is different. It is surrounded by strong, flexible membranes enclosing stout muscles anchored deep within the thorax. In addition to movement above and below the horizontal line of the body, the joint allows limited rotation in the roll and yaw planes so that it acts as a limited-range universal joint. The functional outcome is flexibility of position and movement at the other end of the tail where the biramous appendages (uropods) of the sixth abdominal segment, together with the telson, form a tailfan (Fig. 1A). The tailfan elements elevate and depress and also slide over each other laterally so that the whole tailfan can vary in size and can change shape from paddle to scoop. This flexibility at the end of the hinged lever that is the tail permits the animal to modify the direction and magnitude of the forces generated when it flexes and extends its tail for swimming and balancing. The arrangement presents an interesting case study for biological solutions to problems associated with the dynamics and control of multi-jointed levers.

The muscles controlling the movement of the tail are divided into four matching sets: the slow and fast flexors and extensors. The fast flexors ventrally and fast extensors dorsally occupy most of the abdominal cavity (Fig. 1B) and are responsible for escape tail flip behavior and swimming. Although related developmentally to their segment of ori-

---

*Author to whom correspondence should be addressed. E-mail: dlmacm@unimelb.edu.au.

This paper was originally presented at a workshop titled *Invertebrate Sensory Information Processing: Implications for Biologically Inspired Autonomous Systems*. The workshop, which was held at the J. Erik Jonsson Center for the National Academy of Sciences, Woods Hole, Massachusetts, from 15–17 April 2000, was sponsored by the Center for Advanced Studies in the Space Life Sciences at the Marine Biological Laboratory, and funded by the National Aeronautics and Space Administration under Cooperative Agreement NCC 2-896.

Abbreviations: ACC, accessory motor neuron; MRO, muscle receptor organ; SEMN, slow extensor motor neuron; SR, stretch receptor.

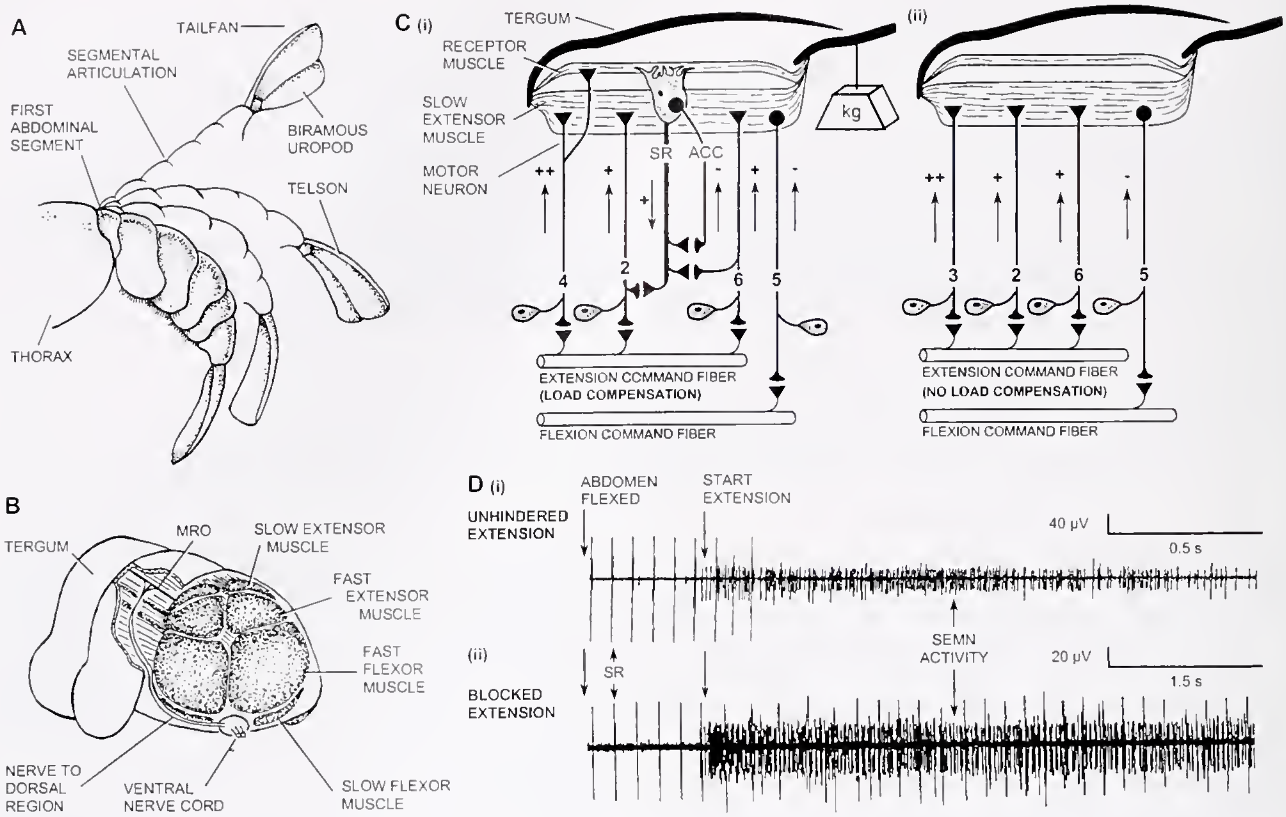
A
TAILFAN
SEGMENTAL ARTICULATION
FIRST ABDOMINAL SEGMENT
BIRAMOUS UROPOD
TELSON
THORAX
C (i)
TERGUM
RECEPTOR MUSCLE
SLOW EXTENSOR MUSCLE
MOTOR NEURON
SR
ACC
kg
++
+
-
4
2
6
5
EXTENSION COMMAND FIBER (LOAD COMPENSATION)
FLEXION COMMAND FIBER
(ii)
3
EXTENSION COMMAND FIBER (NO LOAD COMPENSATION)
FLEXION COMMAND FIBER
B
TERGUM
MRO
SLOW EXTENSOR MUSCLE
FAST EXTENSOR MUSCLE
FAST FLEXOR MUSCLE
NERVE TO DORSAL REGION
VENTRAL NERVE CORD
SLOW FLEXOR MUSCLE
D (i)
UNHINDERED EXTENSION
ABDOMEN FLEXED
START EXTENSION
40 µV
0.5 s
SEMN ACTIVITY
(ii)
BLOCKED EXTENSION
SR
20 µV
1.5 s

Figure 1. (A) Lateral view of the crayfish abdomen showing the changing position and shape of the segments and tailfan during a movement from a mid-flexed position to full extension. The joints between the abdominal segments permit movement only in the pitch plane, whereas that between the thorax and first abdominal segment permits movement in pitch, roll, and yaw planes. (B) Diagram of a section of the abdomen showing placement of the main muscle blocks in cross-section and the ventral nerve cord and its connection with the MRO in one segment. (C) Summary of the nerve-muscle connections operating when (i) the SEMN4 program is operating and the SR load-compensation loop can be recruited, and (ii) the SEMN3 program is operating and the SR load-compensation loop is not recruited. Triangles and circles represent excitatory and inhibitory synapses respectively. (D) Pattern of activity of the SEMNs and SRs recorded from the dorsal nerves during a platform drop extension (i) in abdominal segment 4 when the movement is unhindered, and (ii) in abdominal segment 2 when a rod and mechanical stop prevent straightening of the joint spanned by this MRO throughout the extension taking place at the other abdominal joints. Note that these recordings are displayed on different time and amplitude scales.

gin, they are organized into the overlapping muscle spirals familiar to lovers of lobster as a gourmet delicacy. Common connective tissue strands that run the length of the tail ensure that they act as a coordinated unit when delivering their power. The slow flexor and extensor muscles, which are responsible for slow movements and postural adjustments, lie ventrally and dorsally respectively, in thin sheets external to the bulk of the fast muscles and immediately beneath the surface of the exoskeleton (Fig. 1B).

The Remarkable Parsimony of Arthropod Neuromuscular Control

Vertebrates achieve fine control in muscles primarily by having large numbers of motor units that can be recruited sequentially and, to a lesser extent, by heterogeneity of their nerve and muscle. The pools of motor neurons employed by vertebrates to achieve fine control of their muscles need space that the small-bodied arthropods do not have. Arthropods achieve comparable levels of control with far fewer neurons (insects typically have only two or three motor neurons per muscle and crustaceans have up to five or six). They achieved this reduction in part by employing nerve-muscle combinations ranging in their contraction characteristics from slow and gradual to fast and twitching, and partly by evolving motor neurons that inhibit muscle contraction in parallel with the more familiar ones that cause contraction. These developments massively increase the possibilities for a continuously graded range of contraction outputs and for the integration of excitatory and inhibitory inputs throughout the control mechanism without a concomitant increase in the number of motor neurons. These ingenious and effective ways of reducing the number of neurons could well be of interest in robotic design. The fact that variations of these arrangements are found throughout the arthropods suggests that they evolved early. Comparative studies show that they have not necessarily been advantageous in all subsequent behavioral situations and provide interesting insights into ways in which design flexibility is achieved from a base model constrained by its evolutionary history to very few motor neurons (Paul, 1991).

Each of the segmental muscle groups in the crayfish is innervated by just six motor neurons per segment; these are conventionally numbered from 6 to 1 in descending order of axonal diameter (Fields and Kennedy, 1965; Fields, 1966; Drummond and Macmillan, 1998a,b). Each displays particular functional characteristics exemplified by the slow extensor sensory-motor system about which most is known and on which we will concentrate here. Slow extensor motor neuron 6 (SEMN6) is the largest motor neuron in the group. It innervates predominantly the fastest fibers in the slow extensor muscle. At low firing frequencies it produces large membrane responses that facilitate rapidly and sum when the frequency of stimulation is high to produce strong, twitch-type contractions. SEMN5 is slightly smaller in diameter than SEMN6. Its effect on the muscle potential is inhibitory—that is, it produces ionic permeability changes that hyperpolarize the muscle membrane and move its excitability away from the threshold for contraction, thereby modifying the nature of the contraction produced by exciter activity. SEMN4 and SEMN3 are almost indistinguishable in size and innervate almost the same population of slow extensor muscle fibers throughout all the slow extensor muscle bundles. They both evoke small to medium-sized responses that show modest facilitation and sum readily to produce smooth contractions at higher frequencies. SEMN2 is a small neuron that innervates almost all the slow extensor muscle fibers. Its activation produces small, non-facilitating muscle responses that sum to produce strong, slow muscle contractions at high frequencies. SEMN1 is a neuron of about the same size, but its muscle potentials and contractions are small, so its physiology is not well documented. From a design perspective, these elements provide for a full range of control options in the slow-fast and fine-coarse spectra while preserving remarkable component economy.

This brief outline of the innervation of this major muscle series shows that although the slow extensors in each segment are controlled by bilateral pairs of only six motor neurons, the flexibility inherent in their properties and patterns of innervation together with the trick of peripheral inhibition provide the same sort of flexibility available to multi-neuronal vertebrate equivalents. SEMN6 can be used for twitch or brief, strong contractions; SEMN4 and SEMN3 for rapidly developing and decaying smooth contractions; and SEMN2 for slowly developing, sustained smooth contractions. Activation of SEMN5 reduces the contractions evoked by any contemporaneous exciter activity and also returns the membrane potential of slower fibers to their resting level more rapidly following slow exciter activity, thereby increasing the rate of muscle relaxation.

What do we know about how the potential flexibility of this parsimonious arrangement is employed by the crayfish? To answer this question we have to make a brief side trip into the sensory biology of the MROs.

The Sensory Biology of the Muscle Receptor Organs

A pair of MROs span the articulations between adjacent abdominal segments on each side of the body (Fig. 1B). Each pair of MROs has two stretch receptor (SR) neurons, a large, high-threshold phasic neuron and a smaller, low-threshold, tonic one. These respond to changes in the tension of a small, innervated receptor muscle strand in which they are embedded. Because the muscle spans the articulation, the SRs monitor the position of the abdominal segments relative to one another, and because the strand is innervated, their level of activity, or set point, can be adjusted from the central nervous system. SR activity levels can also be adjusted by the axons of inhibitory cells called accessory motor neurons (ACC) that synapse directly onto the SR surface and inhibit or delay sensory spike activation (Fig. 1Ci). The receptor muscles lie in parallel with the slow extensor muscle but are not powerful enough to assist with joint movement. These elements and their arrangement suggest those an engineer might employ in designing a servo-controlled load-compensating device (Fig. 1Ci).

Analysis reveals that this sophisticated and economical arrangement of elements has the potential to deliver flexible abdominal control. Experiments on semi-intact and isolated abdominal preparations (mainly in *Procambarus clarkii* and *Cherax destructor*) reveal a number of connections and reflexes involving the tonic SRs and the motor neurons in the local and adjacent segments (Fields, 1976; Drummond and Macmillan, 1998a; summarized in Fig. 1C). Activation of the tonic SR excites ACC, which inhibits the sensory neuron itself (Eckert, 1961)—a negative feedback loop that radiates weakly to adjacent segments. Functionally, this loop provides a classic myotatic reflex: it damps small displacements of the joint by externally imposed force, and it may also damp SR reflex loops. The tonic SR also excites the ipsilateral SEMN2 in its own segment, the motor neuron that produces slow sustained contractions in most of the slow extensor muscle fibers. This is the basis of a "resistance reflex." If the joint is flexed so that the tonic SR is activated, it will excite SEMN2, which will fire and extend the joint until the receptor is unloaded and stops firing (Fields, 1966; Fields *et al.*, 1967).

Another important feature of the neuromuscular wiring is that SEMN4 innervates both the slow extensor muscle and the receptor muscle so that both could contract synchronously when it is activated. This relationship spawned a hypothesis about the way in which feedback could operate on the tonic sensor to produce different behavioral outputs. If central drive for extension included SEMN4, the tonic SR would not be activated during the extension because the MRO receptor muscle would contract with the main extensor muscle. If the movement met with resistance and the rate of extension slowed, the receptor muscle would continue to contract at the rate determined by the central drive onto SEMN4. Rising tension in the receptor muscle would activate the SR to recruit SEMN2 or increase its firing rate until the receptor was again unloaded. The circuitry is also configured to permit the same movement without activation of SR-mediated load compensation (Fig. 1Cii). If the central drive for extension were directed through SEMN3 rather than SEMN4, the same muscle fibers would be activated but the receptor muscle would not contract during the movement, and thus the length-servo loop would not be activated. This is how this sensory-motor cluster appears to operate in isolated *C. destructor* preparations. The SEMN3 and SEMN4 are not active together during spontaneous activity (Drummond and Macmillan, 1998a), and SEMN6 only fires at the peak of bursts of spontaneous activity in SEMN4 or SEMN3. SEMN2, on the other hand, can be recruited at any stage during ongoing activity in either unit. The pattern of firing in SEMN5, the inhibitor, suggests that it is used both to inhibit extensor contractions—for example, by firing during flexor muscle activity—and also to move the contractions due to repetitive activation of the intermediate fast-slow units SEMN3 and SEMN4 towards the more phasic end of their spectrum by suppressing their tendency to sum responses. In summary, there is ample potential for remarkable functional flexibility, notwithstanding the small number of neurons involved.

The Operation of the Receptors in Freely Behaving Animals

The finding that circuitry is capable of producing outputs predicted by a hypothesis and that it does so in non-behavioral, dissected preparations is a valuable step towards understanding how it might function, but from a robotics viewpoint, observation of its function and role in the biological and behavioral world of the animal is essential. We therefore set out to examine how the MROs and SRs operate in intact, freely behaving animals. Using surface markings to locate the position of the MROs, we implanted fine wire electrodes to make long-term recordings from the SRs and the SEMNs in *C. destructor* (McCarthy and Macmillan, 1999a,b). When an immersed crayfish loses contact with the substrate, it extends its abdomen so that it falls in a balanced, feet-down attitude, ready to walk as soon as it lands. This type of extension movement can be evoked by dropping a hinged platform on which the animal is standing (Larimer and Eggleston, 1971). The behavior was therefore dubbed "a platform-drop extension." The outcome of our platform-drop experiments provided a sharp reminder of the importance of evaluating hypotheses derived from reductionist analysis by testing them in the real world of the animal. This caution is particularly germane if the interpretations are to inform or lead robotic design.

In *C. destructor*, the tonic SR was invariably active when the animal was in the resting position with its abdomen curled beneath the body. The neuron fired very regularly, with a frequency around 16 Hz (Fig. 1D), the actual rate being slightly higher or lower depending on the whether the abdomen was more or less flexed. Activity was seen in the SEMNs as soon as the platform was dropped to initiate the extension, but by the time extension movement was apparent to an observer, the SR had ceased firing (Fig. 1Di). This result surprised us because previous results from other species suggested that the SR would fire throughout the extension (Sokolove, 1973). It could, however, be explained in system terms if the SR falls silent because the receptor muscle and the working extensor muscle are contracting at about the same rate but with the straightening of the joint just slightly leading the contraction of the receptor muscle. To test this possibility, we recorded from the SR in a segment that was prevented from straightening at all because of a small rod inserted between two acrylic plastic blocks glued either side of the joint. In this situation, the expected load compensation occurred, as evidenced by the increase in output by the motor neurons compared with their firing rates in the unblocked situation (Fig. 1Dii). It was not, however, due to recruitment of the local MRO, because the rate of firing in the SR remained constant throughout the extension movement (Fig. 1Dii). Some other receptors must have been responsible. This outcome was also unexpected because of earlier indications from other species that the MROs might be involved in load compensation (Sokolove, 1973). We hypothesized, however, that the reason the SR load-compensation pathway is not selected for platform-drop extensions is that, in this situation, the animal uses the SEMN3 mode rather than the SEMN4 one. Extension in this context is part of a stability or balancing behavior that gives the body a parachute-like profile. In the unlikely event that the animal encounters resistance during its fall through the water, it can then change posture to prepare for defense or other behaviors, some of which may involve the SR-SEMN4 load-compensation loop. To test this hypothesis, we used our ability to record from freely moving animals to study the activity of the SRs and SEMNs during a range of other behaviors, including some—such as the extension that accompanies the assumption of the defense posture—in which load compensation, possibly mediated by the SR loop, could be expected to occur. As yet, we have found no behavior in *C. destructor* in which the SR-SEMN4 loop is activated when SEMN output increases in response to increased load (Patullo *et al.*, 2001).

Behavioral Context—the Key to Design Insights

The message is clear. This elegant circuitry works in a dish and we can see ways in which it could be employed to control movement, but we do not yet know enough about the biology to understand completely how the animal uses the components. Such understanding is necessary if we are to exploit the full potential of this sensory-motor system to inform our design of fine movement control devices with component economies suitable for robotic applications. It may be that the capabilities of the circuitry are not primarily targeted at the control of slow, postural movements. We have evidence, for example, that the SRs are cyclically active during non-giant swimming and that interference with their function alters such movements (Daws, McCarthy and Macmillan, unpubl. data). It is also possible that the normal function of the local feedback loops is evident only when they are operating as part of a concatenated chain involving the whole of the jointed abdominal lever. In support of this possibility is evidence that the cord stretch receptors have different effects on motor output when they are activated in groups rather than singly (Drummond and Macmillan, 1997). The study of abdominal movement in these animals has already provided insights into the way in which fine control can be achieved with very few elements and the necessity of fully understanding the context in which control mechanisms are to function. It promises many more as we achieve a better understanding of the biology.

Acknowledgments

We gratefully acknowledge the support of NASA for underwriting the stimulating cross-disciplinary ISIP-BIAS meeting that generated this paper and Dr. Diana Blazis and Dr. Frank Grasso for their assistance and support in its conception and publication. Supported by a grant from the Australian Research Council to DLM and from NASA under Cooperative Agreement NCC 2-896.

Literature Cited

Alexandrowicz, J. S. 1951. Muscle receptor organs in the abdomen of *Homarus vulgaris* and *Panulirus vulgaris. Q. J. Microsc. Sci.* **92:** 163–199.

Drummond, J. M., and D. L. Macmillan. 1997. Cord stretch receptors of the Australian freshwater crayfish, *Cherax destructor. Soc. Neurosci. Abstr.* **23:** 1569.

Drummond, J. M., and D. L. Macmillan. 1998a. The abdominal motor system of the crayfish, *Cherax destructor.* I. Morphology and physiology of the superficial extensor motor neurons. *J. Comp. Physiol. A* **183:** 583–601.

Drummond, J. M., and D. L. Macmillan. 1998b. The abdominal motor system of the crayfish, *Cherax destructor.* II. Morphology and physiology of the deep extensor motor neurons. *J. Comp. Physiol. A* **183:** 603–619.

Eckert, 1961. Reflex relationships of the abdominal stretch receptors of the crayfish. I. Feedback inhibition of the receptors. *J. Cell. Comp. Physiol.* **57:** 149–162.

Fields, H. L. 1966. Proprioceptive control of posture in the crayfish abdomen. *J. Exp. Biol.* **44:** 455–468.

Fields, H. L. 1976. Crustacean abdominal and thoracic muscle receptor organs. Pp. 65–114 in *Structure and Function of Proprioceptors in the Invertebrates,* P. J. Mill, ed. Chapman and Hall, London.

Fields, H. L., and D. Kennedy. 1965. Functional role of the muscle receptor organs in crayfish. *Nature* **206:** 1235–1237.

Fields, H. L., W. H. Evoy, and D. Kennedy. 1967. Reflex role played by efferent control of an invertebrate receptor. *J. Neurophysiol.* **30:** 859–874.

Larimer, J. L., and A. C. Eggleston. 1971. Motor programs for abdominal positioning in crayfish. *Z. Vgl. Physiol.* **74:** 388–402.

Macmillan, D. L. 2001. The abdominal muscle receptor organ of crayfish and lobsters: old models new challenges. In *Frontiers in Crustacean Neurobiology.* Springer, Berlin. (In press).

McCarthy, B. J., and D. L. Macmillan. 1999a. Control of abdominal extension in the freely moving intact crayfish *Cherax destructor.* I. Activity of the tonic stretch receptor. *J. Exp. Biol.* **202:** 171–181.

McCarthy, B. J., and D. L. Macmillan. 1999b. Control of abdominal extension in the freely moving intact crayfish *Cherax destructor.* II. Activity of the superficial extensor motor neurones. *J. Exp. Biol.* **202:** 183–191.

Patullo, B., Z. Faulkes, and D. L. Macmillan. 2001. The muscle receptor organs do not mediate load compensation during body roll and defence. *J. Exp. Zool.* (in press).

Paul, D. H. 1991. Pedigrees of neurobehavioral circuits: tracing the evolution of novel behaviors by comparing motor patterns, muscles, and neurons in members of related taxa. *Brain Behav. Evol.* **38:** 226–239.

Sokolove, P. G. 1973. Crayfish stretch receptor and motor unit behaviour during abdominal extensions. *J. Comp. Physiol.* **84:** 251–266.

Reference: *Biol. Bull.* **200:** 206–210. (April 2001)

Increasing Sensor Flexibility Through Neuromodulation

J. T. BIRMINGHAM*

Volen Center and Biology Department, Brandeis University, Waltham, Massachusetts 02454-9110

Abstract. Both biological and man-made motor control networks require input from sensors to allow for modification of the motor program. Real sensory neurons are more flexible than typical robotic sensors because they are dynamic rather than static. The membrane properties of neurons and hence their excitability can be modified by the presence of neuromodulatory substances. In the case of a sensory neuron, this can change, in a functionally significant way, the code used to describe a stimulus. For instance, extension of the neuron's dynamic range or modification of its filtering characteristics can result. This flexibility has an apparent cost. The code used may be situation-dependent and hence difficult to interpret. To address this issue and to understand how neuromodulation is used effectively in a motor control network, I am studying the GPR2 stretch receptor in the crustacean stomatogastric nervous system. Several different neuromodulatory substances can modify its encoding properties. Comparisons of physiological and anatomical evidence suggest that neuromodulation can be effected both by GPR2 itself and by other neurons in the network. These results suggest that the analog of neuromodulation might be useful for improving sensor performance in an artificial motor control system.

Introduction

Many forms of locomotion in both invertebrates and vertebrates result from the activity of central pattern generator (CPG) networks of neurons (see review by Marder and Calabrese [1996]). CPGs produce rhythmic motor patterns by virtue of the intrinsic properties of the neurons and the connections between them, even when disconnected from sensory afferents (Wilson, 1961). Sensory feedback, however, is usually essential for modifying the details of the basic rhythm to shape a physiologically relevant output in response to particular environmental or body conditions (Grillner and Wallen, 1977; Foth and Graham, 1983a,b; Pearson *et al.*, 1983).

Man-made CPG networks are used to generate movement in biologically inspired robots, as reflected in the papers in this collection (CASSLS, 2001). An artificial CPG has both the power and limitations of a biological one: it has a built-in robustness, but if there is to be flexibility in its output, it too will require input from sensors. The sensors employed in many robots differ from biological sensory neurons in a fundamental way. A typical man-made sensor is static. It always gives the same unambiguous response to a particular stimulus. Real sensory neurons are dynamic. The spike trains they generate depend not solely on the stimulus but also can be influenced by other factors. One of these factors is the presence of neuromodulators, substances that modify a neuron's membrane properties and hence its excitability (Kaczmarek and Levitan, 1987). Neuromodulation affects neurons in the sensory, central, and motor systems. In the case of a sensory neuron, neuromodulation can modify the spike train generated in response to a particular sensory stimulus. This can have functional significance. For example, when primary olfactory receptors in the newt are exposed to micromolar concentrations of adrenaline, the receptor's threshold for and differential sensitivity to odor perception are affected (Kawai *et al.*, 1999). This modulation may very well be crucial for an animal trying to find a mate or avoid becoming a meal.

The fact that sensory neurons can be modulated prompts an interesting line of questioning. Two distinct stimuli pre-

---

* Present address: Department of Physics, Santa Clara University, 500 El Camino Real, Santa Clara, CA 95053.

This paper was originally presented at a workshop titled *Invertebrate Sensory Information Processing: Implications for Biologically Inspired Autonomous Systems*. The workshop, which was held at the J. Erik Jonsson Center for the National Academy of Sciences, Woods Hole, Massachusetts, from 15–17 April 2000, was sponsored by the Center for Advanced Studies in the Space Life Sciences at the Marine Biological Laboratory, and funded by the National Aeronautics and Space Administration under Cooperative Agreement NCC 2-896.

sented in two different neuromodulatory environments could quite conceivably result in very similar spike trains. Does that imply that the meaning of the spike train is ill-defined? How might what appears to be ambiguity in the code be removed? In particular, how can sensor modulation be used to advantage in a CPG network?

The crab stomatogastric nervous system (STNS) is an ideal preparation in which to address some of these questions. The STNS controls the movements of stomach muscles used to grind and filter food and is today probably the most carefully studied and best understood small CPG network. Gastropyloric receptor 2 (GPR2) is a stretch-sensitive neuron that monitors the movement of two stomach muscles (Katz *et al.*, 1989) and provides this information to the CPG. There are several reasons why GPR2 is an attractive candidate for studying the computational significance of neuromodulation. (1) The stimulus (muscle tension) is well defined and one-dimensional (Katz *et al.*, 1989). (2) The neuron's response to muscle stretch can be modulated in several different ways, as will be described below. (3) The synaptic targets of GPR2 are known and accessible (Katz and Harris-Warrick, 1989, 1990), and signal processing of the sensory information can be investigated directly. The results discussed below imply that neuromodulation of GPR2 may allow the neuron to interact both with the stimulus environment and the central nervous system so that it can remain sensitive to important stimuli. Our investigations suggest that incorporation of the analog of neuromodulation into a robotic nervous system might similarly be useful for introducing dynamics to sensors to increase their functionality.

All experiments were done using male *Cancer borealis* crabs purchased from local seafood suppliers in Boston, Massachusetts. From the gut of the crab, a preparation consisting of two muscles and the nerve containing the GPR2 cell body was removed, placed flat in 5-ml silicone elastomer-coated petri dishes and continuously superfused with cooled physiological saline. One side of the *cpv3a* muscle (nomenclature from Maynard and Dando [1974]) was pinned to the dish. The other side was attached to a force-displacement transducer. This transducer in turn was attached to the arm of a computer-controlled pen motor. The muscle was stretched using various waveforms (steps, sine waves, white noise). The resulting spikes generated by the sensory neuron were measured using an extracellular electrode on the nerve. Neuromodulatory substances were introduced to the preparation *via* switching ports in the superfusion system. A detailed description of the experimental setup and technique has previously been published (Birmingham *et al.*, 1999).

Modulation of a Stretch Receptor

I have discovered that the response of GPR2 to stretch can be modulated in two very different ways. In one case, the neuron's sensitivity can be continuously tuned through the application of several neuroactive substances. In the other case, an unknown internal mechanism drives the neuron between two qualitatively distinct modes of firing (Katz *et al.*, 1989; Birmingham *et al.*, 1999).

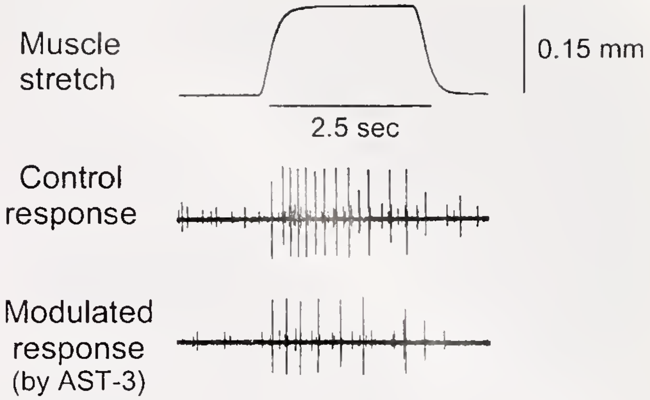

Figure 1. Stretch receptor response can be modulated by peptide application. Extracellular recordings of the activity of crab GPR2 neuron in control saline (middle) and in saline containing 10^{-8} *M* AST-3 (bottom) in response to stretch of the *cpv3a* muscle (top).

The sensitivity of the GPR2 response to muscle stretch can be modified by at least four distinct substances: serotonin, γ-aminobutyric acid (GABA), and the peptides TNRNFLRF-amide and allatostatin-3 (AST-3). I will focus on the effects of AST-3 in this paper. Figure 1 shows that the number of GPR2 spikes generated in response to muscle stretch is reduced in the presence of 10^{-8} *M* AST-3. The decrease in response is a continuous function of modulator concentration. The threshold for the AST-3 effect on firing rate is $10^{-9} - 10^{-8}$ *M*, and saturation occurs above 10^{-7} *M*. In most cases, the GPR2 stretch response is completely eliminated in 10^{-6} *M* AST-3.

Real sensory neurons have a maximum firing rate and thus a limited-amplitude dynamic range. Beyond the stretch amplitude corresponding to this rate, the neuron no longer is sensitive to additional stretch. One result of AST-3 application is to extend the dynamic range, as shown in Figure 2. Reduction in sensitivity causes the curve of rate *versus* stretch to be linearized. Large-amplitude stretches that were indistinguishable under control conditions can be differentiated in the modulator.

AST-3 application may also qualitatively change the feature detection capability of the GPR2 neuron. Figure 3 shows control and modulated responses to a *cpv3a* muscle stretch generated from filtered white noise. The corresponding muscle stretch velocity is shown beneath the spike trains. Under control conditions, the amplitude of the stretch is well described in the spike times (Birmingham *et al.*, 1999). In a high concentration (10^{-6} *M*) of AST-3, this is no longer the case. Many fewer spikes are generated, and it appears that those spikes might be correlated with large positive stretch velocities.

What is the effect of AST-3 application on the GPR2 code? More experiments are required to answer this question. One possibility is that AST-3 simply reduces the

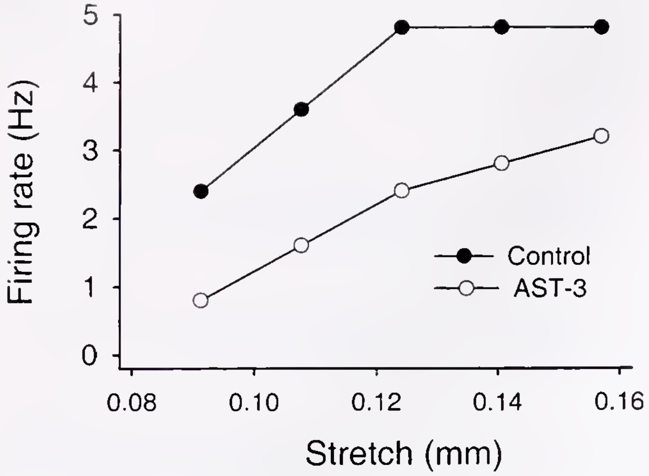

Figure 2. Neuromodulation can increase dynamic range. GPR2 firing rate as a function of *cpv3a* stretch amplitude in control saline and in saline containing 10^{-8} *M* AST-3.

sensitivity of GPR2 in a linear fashion, so that essentially the same features in the stimulus are being encoded as under control conditions. Far more interesting is the possibility that AST-3 changes the filtering properties of the neuron. The presence of the peptide might change GPR2 from what is basically a position detector into a sensor with a response that has a stronger dependence on muscle velocity.

GPR2 operates in two modes: the conventional "spiking" mode and a novel "bursting" mode (Katz *et al.*, 1989). In the spiking mode, which was the behavior shown in Figures 1–3, GPR2 generates spikes only during the stretch and is silent when not under tension. In contrast, in the bursting mode, GPR2 generates bursts of spikes (several seconds in duration) even when no stretch is imposed. In the initial description of the bursting mode, the average burst period was found to be ~17 s (Katz *et al.*, 1989). More recently, burst periods ranging between 12 and 101 s have been reported (Birmingham *et al.*, 1999). GPR2 can be driven from the spiking mode into the bursting mode though prolonged muscle activity (Birmingham *et al.*, 1999). The encoding properties of the neuron in the two modes are complementary. In the spiking mode, the neuron is best able to encode rapidly varying stretches, but not slower ones. In the bursting mode, fast stretches are ignored, while slower stretches (varying over minutes or hours) are encoded in the burst times (Birmingham *et al.*, 1999).

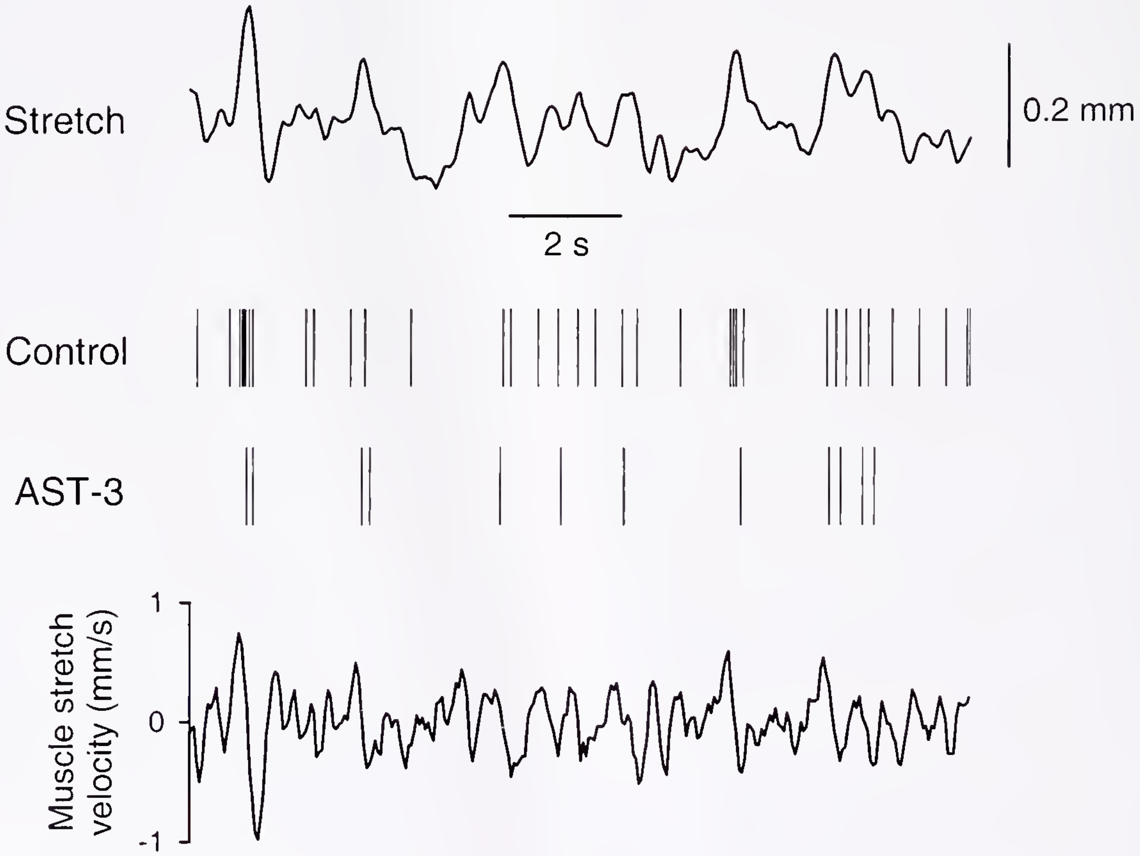

Figure 3. Neuromodulation may change a sensory neuron's filtering properties. GPR2 spikes in control saline and in 10^{-6} *M* AST-3 in response to *cpv3a* stretch generated from filtered white noise (top). Corresponding muscle stretch velocity is shown below the spike trains.

Pathways of Modulation of a Peripheral Sensor

At least three other neuromodulators, in addition to AST-3, affect GPR2 stretch response. Serotonin and GABA both decrease the response in a manner similar to that of AST-3. The peptide TNRNFLRF-amide, on the other hand, increases the neuron's spiking in response to a given stretch. Under what conditions GPR2 might be exposed to each of the various neuromodulatory substances remains unknown, but a hint is provided by immunohistochemical studies of the STNS. Both serotonin (Katz *et al.*, 1989) and an allatostatin-like peptide (Skiebe and Schneider, 1994) are contained within the GPR2 neuron itself. There have been no measurements yet made to determine whether either neuromodulator is released peripherally; however, since the stretch receptor both contains and responds to each substance, it is possible that GPR2 releases either or both to effect gain control through negative feedback. This would be similar to what has been observed in *Aplysia* bag cell neurons (Kauer *et al.*, 1987). The use of feedback to modify sensitivity in a crustacean stretch receptor has been previously reported for the lobster oval organ (Pasztor and Bush, 1989). They suggested that release of the peptide proctolin is used to activate a positive feedback loop that increased sensitivity to stretch. The activity-dependent switch from GPR2 spiking to bursting can likewise be viewed as feedback. We have confirmed that neither AST-3 nor serotonin can drive GPR2 into the bursting mode; the switching mechanism remains unknown and of great interest.

The GPR2 neuron does not contain GABA; however, there are GABA-containing neurons in the STNS whose axons project into the vicinity of GPR2 (Swensen *et al.*, 2000). Hence, GPR2 sensitivity might be modulated by instructions from another specific neuron in the nervous system. Peptides in the FLRFamide family have not been found in any of the cell bodies in the STNS but are known to circulate as hormones. Thus any GPR2 modulation by these substances would probably be accompanied by modifications of other elements in the nervous system.

Use of Adaptive Sensors in Robotic Applications

There are precedents for adaptive sensing in the field of artificial vision. "Active vision" schemes allow observer (robot) and sensor to interact continually (Blake and Yuille, 1992). The observer constantly changes its vantage point to allow the sensor to pick out the characteristics of images that are required to perform a task, while ignoring the rest. Strategies that allow economical data acquisition or handling are advantageous, especially with the development of high-resolution CCD cameras that generate huge amounts of data.

During the past decade, advances in chip design have resulted in the development of adaptive silicon photoreceptors (Delbruck and Mead, 1994). These sensors have high sensitivity and large dynamic range and were in part modeled after biological photoreceptors in the retina. They adjust their own sensitivities, without instructions from the central processor, in order to respond appropriately to changing environmental conditions. This is analogous to our model of how AST-3 and serotonin are used by GPR2. However, to the best of our knowledge, there are no robotic analogs to the GABA effect on GPR2, where the central processor sends instructions to a peripheral sensor to modify its response characteristics. This type of architecture might be useful in a smart robot. The sensor's performance could be adjusted for a given task in response to a command from the central processor or even from another sensor with a different modality.

Decoding the Signal From a Modulated Sensory Neuron

Modulation appears to give a sensory neuron the opportunity to be more flexible in its ability to encode different sorts of stimuli. However, the flip side of this flexibility, at least from the observer's point of view, is that there appears to be ambiguity in how a particular spike train should be interpreted. Two different sensory stimuli, encoded in two different neuromodulatory environments, could result in very similar neural signals. How is the apparent ambiguity in the "code" thus removed? This is a very general question that undoubtedly is an issue for most, if not all, sensory neurons, and the answer is not obvious. In the STNS this question is tractable because so many of the synaptic connections have been identified and characterized. GPR2 makes synapses onto many of the motor neurons in the CPG (Katz and Harris-Warrick, 1989, 1990), and so the postsynaptic responses to GPR2 spike trains can be directly measured using intracellular electrodes. It will be interesting to determine which features of the GPR2 spike train are important to the cells in the network, and if those are the same features we have identified in our mathematical decoding experiments.

We are well on our way to characterizing the encoding properties of the GPR2 neuron in its various modulated states. We are just beginning, however, to discover how GPR2 activity affects the output of the stomatogastric nervous system. Realistic GPR stimulation has been shown to initiate or modify specific motor programs (Katz and Harris-Warrick, 1989, 1990, 1991; Blitz and Nusbaum, 1996). In the STNS we can study how modulation of GPR2 affects the activity of individual targets as well as the output of the network, and we hope to discover how interactions between a CPG and a peripheral sensor can improve the performance of both sensor and network.

Acknowledgments

I thank Eve Marder for advice, encouragement, and support. Research supported by NIH Individual National Research Service Award NS-10564 and the W. M. Keck Foundation.

Literature Cited

Birmingham, J. T., Z. B. Szuts, L. F. Abbott, and E. Marder. 1999. Encoding of muscle movement on two time scales by a sensory neuron that switches between spiking and bursting modes. *J. Neurophysiol.* **82:** 2786–2797.

Blake, A., and A. Yuille, eds. 1992. *Active Vision.* MIT Press, Cambridge, MA.

Blitz, D. M., and M. P. Nusbaum. 1996. Sensory neuron activation of modulatory projection neurons. *Soc. Neurosci. Abstr.* **22:** 1375.

CASSLS (The Center for Advanced Studies in the Space Life Sciences). 2001. Invertebrate sensory information processing: implications for biologically inspired autonomous systems. *Biol. Bull.* **200:** 145–245.

Delbruck, T., and C. A. Mead. 1994. Analog VLSI phototransduction by continuous-time, adaptive, logarithmic photoreceptor circuits. *CNS Memo #30.* Computation and Neural Systems Department, California Institute of Technology, Pasadena, CA 91125.

Foth, E., and D. Graham. 1983a. Influence of loading parallel to the body axis on the walking coordination of an insect. I. Ipsilateral effects. *Biol. Cybern.* **47:** 17–23.

Foth, E., and D. Graham. 1983b. Influence of loading parallel to the body axis on the walking coordination of an insect. II. Contralateral effects. *Biol. Cybern.* **47:** 149–157.

Grillner, S., and P. Wallen. 1977. Is there a peripheral control of the central pattern generators for swimming in dogfish? *Brain Res.* **127:** 291–295.

Kaczmarek, L. K., and I. B. Levitan. 1987. *Neuromodulation: The Biochemical Control of Neuronal Excitability.* Oxford University Press, New York.

Katz, P. S., and R. M. Harris-Warrick. 1989. Serotonergic/cholinergic muscle receptor cells in the crab stomatogastric nervous system. II. Rapid nicotinic and prolonged modulatory effects on neurons in the stomatogastric ganglion. *J. Neurophysiol.* **62:** 571–581.

Katz, P. S., and R. M. Harris-Warrick. 1990. Neuromodulation of the crab pyloric central pattern generator by serotonergic/cholinergic proprioceptive afferents. *J. Neurosci.* **10:** 1495–1512.

Katz, P. S., and R. M. Harris-Warrick. 1991. Recruitment of crab gastric mill neurons into the pyloric motor pattern by mechanosensory afferent stimulation. *J. Neurophysiol.* **65:** 1442–1451.

Katz, P. S., M. H. Eigg, and R. M. Harris-Warrick. 1989. Serotonergic/cholinergic muscle receptor cells in the crab stomatogastric nervous system. I. Identification and characterization of the gastropyloric receptor cells. *J. Neurophysiol.* **62:** 558–570.

Kauer, J. A., T. E. Fisher, and L. K. Kaczmarek. 1987. Alpha bag cell peptide directly modulates the excitability of the neurons that release it. *J. Neurosci.* **7:** 3623–3632.

Kawai, F., T. Kurahashi, and A. Kaneko. 1999. Adrenaline enhances odorant contrast by modulating signal encoding in olfactory receptor cells. *Nat. Neurosci.* **2:** 133–138.

Marder, E., and R. L. Calabrese. 1996. Principles of rhythmic motor pattern generation. *Physiol. Rev.* **76:** 687–717.

Maynard, D. M., and M. R. Dando. 1974. The structure of the stomatogastric neuromuscular system in *Callinectes sapidus, Homarus americanus* and *Panulirus argus* (Decapoda Crustacea). *Philos. Trans. R. Soc. Lond. B.* **268:** 161–220.

Pasztor, V. M., and B. M. W. Bush. 1989. Primary afferent responses of a crustacean mechanoreceptor are modulated by proctolin, octopamine, and serotonin. *J. Neurobiol.* **20:** 234–254.

Pearson, K. G., D. N. Reye, and R. M. Robertson. 1983. Phase-dependent influences of wing stretch receptors on flight rhythm in the locust. *J. Neurophysiol.* **49:** 1168–1181.

Skiebe, P., and H. Schneider. 1994. Allatostatin peptides in the crab stomatogastric nervous system: inhibition of the pyloric motor pattern and distribution of allatostatin-like immunoreactivity. *J. Exp. Biol.* **194:** 195–208.

Swensen, A. M., J. Golowasch, A. E. Christie, M. J. Coleman, M. P. Nusbaum, and E. Marder. 2000. GABA and responses to GABA in the stomatogastric ganglion of the crab *Cancer borealis. J. Exp. Biol.* **203:** 2075–2092.

Wilson, D. M. 1961. The central nervous control of flight in a locust. *J. Exp. Biol.* **38:** 471–490.

Reference: *Biol. Bull.* **200:** 211–215. (April 2001)

Why Do Animals Have So Many Receptors? The Role of Multiple Chemosensors in Animal Perception

CHARLES D. DERBY* AND PASCAL STEULLET

Department of Biology and Center for Behavioral Neuroscience,
Georgia State University, Atlanta, Georgia

Abstract. Many animals have an abundance and diverse assortment of peripheral sensors, both across and within sensory modalities. Multiple sensors offer many functional advantages to an animal's ability to perceive and respond to environmental signals. Advantages include extending the ability to detect and determine the spatial distribution of stimuli, improving the range and accuracy of discrimination among stimuli of different types and intensities, increasing behavioral sensitivity to stimuli, ensuring continued sensory capabilities when the probability of damage or other loss of function to some sensors is high, maintaining sensory function over the entire sensory surface during development and growth, and increasing the richness of behavioral output to sensory stimulation. In this paper, we use the crustacean chemosensory system as the primary example to discuss these functions of multiple sensors. These principles may be applicable to the function of autonomous robots and should be considered in their design.

Introduction

Each animal has a plethora of peripheral sensors that enable the detection of different sensory stimuli, including light, chemicals, vibrations, and many others. The number of sensors that an animal possesses can be exceedingly high. In many animals, the complement of receptor cells far exceeds the number of central neurons that process sensory information. This is particularly true for the chemical senses. For example, decapod crustaceans have millions of chemosensory neurons in their cephalic and thoracic appendages (Derby and Atema, 1988; Laverack, 1988a, b; Derby, 1989; Cate and Derby, 2000), and mammals have tens of millions of olfactory receptor neurons (Hildebrand and Shepherd, 1997; Weiler and Farbman, 1997). Convergence ratios between peripheral and central olfactory neurons can be as high at 300:1 in invertebrates and vertebrates (Meisami, 1989; Ache, 1991; Schmidt and Ache, 1996b; Hildebrand and Shepherd, 1997). Within a sensory modality, an animal also typically has a diversity of sensor types.

What factors explain why animals have multiple sensors? One answer to this question is a general one: each animal has a rich diversity of behaviors that enable the acquisition of resources needed to survive and reproduce, and extensive sensory information is required to perform these behaviors. Thus, sensory systems have evolved to extract information about the quality and quantity of important environmental stimuli, such as the variety of wavelengths, intensities, and patterns that constitute each animal's sensory world.

In this paper, we offer explanations for the multiplicity of peripheral sensors. We argue that multiple sensors function in one or more of the following ways: (1) extend the range of spatial sampling by increasing the sensory surface area; (2) extend the range of types of stimuli that are discriminated by having a diversity of sensors, each of which is tuned to a subset of stimulus qualities, intensities, or temporal dynamics; (3) increase the sensitivity and accuracy of resolution through response summation; (4) maintain the function of the system in the face of damage to sensors; (5) compensate for non-functioning developmental stages of sensors; (6) enable formation of specialized central processing centers with different behavioral functions.

---

* To whom correspondence should be addressed. E-mail: cderby@gsu.edu.

This paper was originally presented at a workshop titled *Invertebrate Sensory Information Processing: Implications for Biologically Inspired Autonomous Systems.* The workshop, which was held at the J. Erik Jonsson Center for the National Academy of Sciences, Woods Hole, Massachusetts, from 15–17 April 2000, was sponsored by the Center for Advanced Studies in the Space Life Sciences at the Marine Biological Laboratory, and funded by the National Aeronautics and Space Administration under Cooperative Agreement NCC 2-896.

In developing the ideas in this paper, we draw heavily from the chemical senses of crustaceans, although some examples from other animals and sensory systems are included. Nonetheless, the principles are general. Additionally, we argue that these principles of multiple sensors may be applicable to autonomous robots and should be considered in their development.

Multiple Sensors Enhance the Probability of Detecting Stimuli by Enlarging the Sensory Surface Area

Having sensors distributed across an animal's entire body surface increases the chances that the animal will encounter environmental chemical signals. In fact, chemoreceptors are distributed across the body surface of many animals, including vertebrates (fish: Caprio, 1988) and invertebrates (insects: Dethier, 1976). In crustaceans, receptor neurons are packaged into cuticular extensions of the exoskeleton, called sensilla. Chemosensilla of crustaceans are present on most or all surfaces (Laverack, 1988a; Derby, 1989; Cate and Derby, 2000), enhancing the probability that chemical signals will be encountered.

A Diversity of Sensor Types Enhances the Ability to Discriminate Stimulus Attributes

Although chemosensors are found all over the body and appendages of crustaceans, there exists a diversity of chemosensors with a variety of properties. Having an extensive variety of sensors that extract different stimulus features should allow an animal to have a more accurate representation of its environment and aid in the discrimination of these stimuli. The sensors covering the body surface of an animal differ in structure, innervation, and distribution, reflecting different functions. In the case of insect chemosensilla, the diversity is immense: gustatory sensilla and olfactory sensilla differ in some fundamental features, but much of the diversity is within either the olfactory or gustatory modality (Dethier, 1976; Altner *et al.*, 1981; Shanbhag *et al.*, 1999). The diverse types of crustacean chemosensilla include unimodal sensilla—*e.g.*, aesthetasc sensilla (Grünert and Ache, 1988; Hallberg *et al.*, 1997), and bimodal (chemo-mechano) sensilla—*e.g.*, hair pegs, hedgehog and fringed sensilla, hooded sensilla, simple sensilla (Altner *et al.*, 1983; Schmidt and Gnatzy, 1984; Derby, 1989; Schmidt, 1989; Cate and Derby, 2000). The sensilla can be short (*e.g.*, hair pegs and hooded sensilla are *ca.* 50 μm) or long (aesthetascs can be >600 μm and guard setae can be >1200 μm) (Cate and Derby, 2000). These different sensillar types often have restricted distributions. For example, aesthetascs are only on the distal half of antennular lateral flagella, and hedgehog and fringed sensilla are only on the distal two segments of some legs.

The specific distributions, structure, and innervation of different sensilla undoubtedly have functional consequences. For example, the location of aesthetascs at the anterior end of the animal places them where odor-laden currents often first reach an animal and also where fan organs can direct odors toward or away from their own sensors (Breithaupt, 2001). In the same way, chemoreceptors on the tips of legs are more likely to encounter chemicals associated with the objects in the substrate, and chemoreceptors around the mouth will receive maximal stimulation when food is held in the mouthparts.

The fact that some sensilla are innervated by both chemoreceptor neurons and mechanoreceptor neurons makes these bimodal sensilla ideal for identifying the spatial location of chemotactile stimuli, especially if the axons of these neurons project topotopically into the central nervous system. There is evidence that mechanoreceptor neurons and chemoreceptor neurons from bimodal sensilla on the antennules project to the same central neuropils (Schmidt *et al.*, 1992; Schmidt and Ache, 1996a), but it is not known if their maps are overlapping as in some insects (Newland *et al.*, 2000), or what is the spatial relationship between projections from mechanoreceptor neurons and chemoreceptor neurons from the same sensillum.

A sensory appendage can have a variety of chemoreceptor neurons that differ in their sensitivities. Antennular chemoreceptor neurons of lobsters have diverse sensitivities to different types or qualities of odorants, thus broadening the range of chemical signals to which the entire organ is sensitive (Derby and Atema, 1988; Voigt and Atema, 1992; Derby, 2000). Antennular chemoreceptor neurons also differ from each other in their sensitivities to odor concentrations (Derby and Atema, 1988; Merrill *et al.*, 1994; Daniel *et al.*, 1996) and in their ability to follow high-frequency odor pulses (*e.g.*, flicker-fusion properties) (Gomez *et al.*, 1999). Thus, different neurons extract different stimulus features, together building an image of the chemical and mechanical features of the external world.

Multiple Sensors Increase Response Sensitivity Through Response Summation

Having multiple sensors allows animals to detect lower amplitude signals. This is because central neurons can sum responses from many sensory neurons, increasing signal capturing and the signal-to-noise ratio and thus allowing finer resolution between related signals (Van Drongelen *et al.*, 1978; Meisami, 1989). For example, olfactory systems typically have at least tens to hundreds of thousands of receptor cells (Chase, 1986; Ache, 1991; Farbman, 1992; Hildebrand and Shepherd, 1997). If each neuron responded to one chemical with one spike above spontaneous activity and to another chemical with two spikes, a summation involving all neurons would dramatically amplify the difference in the magnitude of the responses to the two stimuli, thus providing the multineuronal system with a resolving capacity far beyond that of one or a few neurons.

Multiple Sensors Ensure Functional Integrity of a Sense Organ Following Localized Damage

Multiple sensors may serve to compensate for local damage to sensory organs. Given that chemosensors are used to probe an animal's external environment for chemical signals, these sensors are often highly exposed and vulnerable to physical, chemical, and biological damage. Damage can affect sensory function (Hamilton and Case, 1983; Bauer, 1989), but multiple sensors minimize the impact of damage by increasing the probability that some sensors are undamaged and functional (Daniel *et al.*, 2000). As an example, aesthetascs are repeating functional units, each containing a broad complement of receptor neurons with different sensitivities (Spencer, 1986; Mellon and Alones, 1993; Steullet *et al.*, 2000b). This type of organization ensures that localized damage does not have significant impact on an animal's ability to respond to and discriminate different types of chemicals (Steullet *et al.*, 1999, 2000c; Horner *et al.*, 2000). In addition, many chemoreceptor systems, including the aesthetasc system, have mechanisms for self-renewal. Continuous turnover, including addition and loss, of chemoreceptors occurs in the vertebrates (Weiler and Farbman, 1997; Calof *et al.*, 1998) and invertebrates (Chase, 1986; Chase and Rieling, 1986; Sandeman and Sandeman, 1996; Steullet *et al.*, 2000a; Harrison *et al.*, 2001a, b). This turnover enables the renewal of neurons that have a finite life span, which helps to maintain function of a system over time in spite of damage. Similar turnover also occurs in crustacean mechanoreceptor sensilla (Macmillan *et al.*, 1998; Steullet *et al.*, 2000a).

Multiple Sensors Compensate for Nonfunctioning Developmental Stages of Sensors

As animals develop and grow, they must add new sensors to maintain sensitivity over their enlarging body surfaces. To ensure that the animals can detect chemicals that impinge anywhere on the body surface, the number of sensors must increase both during development (Schafer and Sanchez, 1973; Laverack, 1988b) and throughout the lives of those species with indeterminate growth (Mellon and Alones, 1993). The antennular receptors of crustaceans are added as units in two ways (Sandeman and Sandeman, 1996; Steullet *et al.*, 2000a). First, the antennule is composed of many segments called annuli, and new annuli are added at molting. Second, new sensilla are added to existing annuli. In some cases, such as aesthetascs and their associated chemo-mechanoreceptive sensilla, new sensilla are added in highly organized spatial arrays. In this way, the addition of annuli and sensilla creates a multiplicity of repeating, modular packages of sensors.

In addition, turnover of neurons in olfactory systems causes some neurons to be nonfunctional because they are either immature or senescing (Chase, 1986; Farbman, 1992; Steullet *et al.*, 2000a). Since the percentage of nonfunctional cells is high in the vertebrates and invertebrates, there could be compensation by maintaining large numbers of sensors (Chase, 1986).

Multiple Sensors Enable Formation of Specialized Central Processing Centers With Different Behavioral Functions

If different sensor types are differentially coupled to central processors and motor programs, then a greater richness in behavioral outputs should be possible. For example, it has been demonstrated that the function of a chemosensory neuron in *Caenorhabditis elegans* is determined by that neuron's central connections rather than by the receptor molecules that it expresses (Troemel *et al.*, 1997). Crustaceans have not only a diversity of antennular chemo- and mechanoreceptor types but also a diversity of sensory neuropils that receive their projections. These sensory neuropils include olfactory lobes (OLs), which receive input from aesthetasc chemoreceptors (Mellon and Munger, 1990; Sandeman *et al.*, 1992; Schmidt and Ache, 1996b); lateral antennular neuropils (LANs), which are thought to receive input from non-aesthetasc chemoreceptors and mechanoreceptors on both lateral and medial antennular flagella (Schmidt *et al.*, 1992; Schmidt and Ache, 1996a; Roye *et al.*, 2000); and median antennular neuropils (MANs), which receive projections from statocysts, equilibrium receptors, and receptors from the antennular proximal segments (Sandeman *et al.*, 1992; Schmidt *et al.*, 1992; Schmidt and Ache, 1993, 1996a; Cate and Roye, 1997). The organization of these neuropils gives hints about their function. The OLs have a glomerular neuropil, similar to the olfactory neuropils of insects (antennal neuropils) and vertebrates (olfactory bulbs), in which the glomeruli represent different but overlapping chemical sensitivities (Hildebrand and Shepherd, 1997). This suggests that OLs encode chemical quality and are involved in olfactory discrimination. The LANs have a bilobed organization, with each lobe receiving input from one of the two antennular flagella (Schmidt *et al.*, 1992). Additionally, the lobes have a stratified organization, reflecting regionalized sensory input and stratified motor output from antennular motor neurons (Schmidt *et al.*, 1992; Schmidt and Ache, 1996a). This organization suggests that LANs may function in the sensori-motor control of antennular behavior, including flicking (Maynard, 1966) or discriminating the location of chemo-mechanostimulation on the antennule. The MANs are involved in maintaining equilibrium (Sandeman *et al.*, 1992; Schmidt and Ache, 1993; Cate and Roye, 1997), but their function may be broader than this (Fraser, 2001).

Our analyses of the function of the different types of antennular sensors and antennular sensory neuropils in Caribbean spiny lobsters suggest that there is some overlap in chemosensory function of the aesthetasc/OL pathway and the non-aesthetasc/LAN pathway (Steullet *et al.*, 1999, 2000c; Horner *et al.*, 2000). Our working hypothesis is that antennular chemosensory neuropils have both unique and overlapping functions. Overlapping functions may include resolution of temporal characteristics of odors and mediation of discrimination of odors such as food-related chemicals. Functions unique to a neuropil may include, for the OLs, processing of pheromones (Gleeson, 1991), and for the LANs, determining location of chemotactile antennular stimulation and thus controlling local antennular reflexes (Maynard, 1966; Schmidt *et al.*, 1992; Schmidt and Ache, 1993, 1996a; Roye *et al.*, 2000).

Multiple Sensors and the Design of Autonomous Robots

Based on the assumption that the design of animals provides a guide for the principles to be used in constructing autonomous robots, we argue that such robots should have multiple sensors with the following characteristics. The sensors are sufficiently spatially distributed to sample stimulus space. They are sufficiently redundant to allow for signal summation and the resultant enhancement in sensitivity and resolving power. They are sufficiently diverse to sample the different stimulus qualities, intensities, and temporal profiles. Self-repair of sensors in autonomous robots may be too complicated to be feasible, but the functional equivalent could be achieved by having redundant sensors, only some of which are physically or functionally operational at any one time. Dysfunction of some sensors could be detected and automatically compensated by bringing back-up sensors of similar types on-line. Such a system could function as a self-repair mechanism while limiting the energy demands and processing requirements of having all sensors simultaneously and constantly functional. Sensors with different sensitivities should be connected to the integrative and motor systems related to their function, such as attraction or avoidance.

Acknowledgments

We thank Paul Harrison, Holly Cate, and Amy Horner for discussions and comments on the manuscript, and acknowledge the grant support of NIH (DC00312), NSF (IBN 0077474), and the Georgia Research Alliance.

Literature Cited

Ache, B. W. 1991. Phylogeny of smell and taste. Pp. 3–18 in *Smell and Taste in Health and Disease*, T. V. Getchell, R. L. Doty, L. M. Bartoshuk, and J. B. Snow, Jr., eds. Raven Press, New York.

Altner, H., C. Routil, and R. Loftus. 1981. The structure of bimodal chemo-, thermo-, and hygroreceptive sensilla on the antenna of *Locusta migratoria*. *Cell Tissue Res.* **215:** 289–308.

Altner, I., H. Hatt, and H. Altner. 1983. Structural properties of bimodal chemo- and mechanoreceptive setae on the pereiopods chelae of the crayfish, *Austropotamobius torrentium*. *Cell Tissue Res.* **228:** 357–374.

Bauer, R. T. 1989. Decapod crustacean grooming: functional morphology, adaptive value, and phylogenetic significance. Pp. 48–73 in *Functional Morphology of Feeding and Grooming in Crustacea*, B. E. Felgenhauer, L. Watling, and A. B. Thistle, eds. A. A. Balkema, Rotterdam.

Breithaupt, T. 2001. The fan organs of crayfish enhance chemical information flow. *Biol. Bull.* **200:** 150–154.

Calof, A. L., J. S. Mumm, P. C. Rim, and J. Shou. 1998. The neuronal stem cell of the olfactory epithelium. *J. Neurobiol.* **36:** 190–205.

Caprio, J. 1988. Peripheral filters and chemoreceptor cells in fishes. Pp. 313–338 in *Sensory Biology of Aquatic Animals*, J. Atema, R. R. Fay, A. N. Popper, and W. N. Tavolga, eds. Springer, New York.

Cate, H. S., and C. D. Derby. 2000. A novel chemo-/mechanosensillum that is widely distributed on the Caribbean spiny lobster and other lobsters. *Chem. Senses* **25:** 633–634 (abstract).

Cate, H. S., and D. B. Roye. 1997. Ultrastructure and physiology of the outer row statolith sensilla of the blue crab *Callinectes sapidus*. *J. Crustac. Biol.* **17:** 398–411.

Chase, R. 1986. Lessons from snail tentacles. *Chem. Senses* **11:** 411–426.

Chase, R., and J. Rieling. 1986. Autoradiographic evidence for receptor cell renewal in the olfactory epithelium of a snail. *Brain Res.* **384:** 232–239.

Daniel, P. C., M. F. Burgess, and C. D. Derby. 1996. Responses of olfactory receptor neurons in the spiny lobster to binary mixtures are predictable using a noncompetitive model that incorporates excitatory and inhibitory transduction pathways. *J. Comp. Physiol. A* **178:** 523–536.

Daniel, P. C., C. D. Derby, D. Naram, and S. Saul. 2000. Function of antennular grooming behaviour in Caribbean spiny lobsters. International Symposium on Olfaction and Taste XIII, 20–24 July, 2000, Brighton, UK. Int. Society for Neuroethology [Abstr].

Derby, C. D. 1989. Physiology of sensory neurons in morphologically identified cuticular sensilla of crustaceans. Pp. 27–47 in *Functional Morphology of Feeding and Grooming in Crustacea*, B. E. Felgenhauer, L. Watling, and A. B. Thistle, eds. A. A. Balkema, Rotterdam.

Derby, C. D. 2000. Learning from spiny lobsters about chemosensory coding of mixtures. *Physiol. Behav.* **69:** 203–209.

Derby, C. D., and J. Atema. 1988. Chemoreceptor cells in aquatic invertebrates: peripheral filtering mechanisms in decapod crustaceans. Pp. 365–388 in *Sensory Biology of Aquatic Animals*, J. Atema, R. R. Fay, A. N. Popper, and W. N. Tavolga, eds. Springer, New York.

Dethier, V. G. 1976. *The Hungry Fly. A Physiological Study of the Behavior Associated with Feeding*. Harvard University Press, Cambridge, MA.

Farbman, A. 1992. *Cell Biology of Olfaction*. Cambridge University Press, Cambridge.

Fraser, P. J. 2001. Statocysts in crabs: short-term control of locomotion and long-term monitoring of hydrostatic pressure. *Biol. Bull.* **200:** 155–159.

Gleeson, R. A. 1991. Intrinsic factors mediating pheromone communication in the blue crab, *Callinectes sapidus*. Pp. 17–32 in *Crustacean Sexual Biology*, R. T. Bauer and J. W. Martin, eds. Columbia University Press, New York.

Gomez, G., R. Voigt, and J. Atema. 1999. Temporal resolution in olfaction. III. Flicker fusion and concentration-dependent synchronization with stimulus pulse trains of antennular chemoreceptor cells in the American lobster. *J. Comp. Physiol. A* **185:** 427–436.

Grünert, U., and B. W. Ache. 1988. Ultrastructure of the aesthetasc (olfactory) sensilla of the spiny lobster, *Panulirus argus*. *Cell Tissue Res.* **251:** 95–103.

Hallberg, E., K. U. I. Johansson, and P. Wallén. 1997. Olfactory sensilla in crustaceans: morphology, sexual dimorphism and distribution patterns. *Int. J. Insect Morphol. Embryol.* **26:** 173–180.

Hamilton, K. A., and J. F. Case. 1983. Effects of abrasion and Na^+ on dactyl-mediated chemoreception in mature kelp crabs, *Pugettia producta* (Randall). *J. Exp. Zool.* **226:** 363–372.

Harrison, P. J. H., H. S. Cate, E. S. Swanson, and C. D. Derby. 2001a. Post-embryonic proliferation in the spiny lobster antennular epithelium: rate of genesis of olfactory receptor neurons is dependent on molt-stage. *J. Neurobiol.* (In press).

Harrison, P. J. H., H. S. Cate, P. Steullet, and C. D. Derby. 2001b. Continuous change in the olfactory system of the Caribbean spiny lobster *Panulirus argus:* multiple mechanisms exist for growth, turnover, and response to injury. *Mar. Freshw. Res.* **51.** (In press).

Hildebrand, J. G., and G. M. Shepherd. 1997. Mechanisms of olfactory discrimination: converging evidence for common principles across phyla. *Annu. Rev. Neurosci.* **20:** 595–631.

Horner, A. J., V. Ngo, P. Steullet, T. Keller, M. J. Weissburg, and C. D. Derby. 2000. The role of different types of antennular sensilla in orientation by Caribbean spiny lobsters to a natural odor stimulus under controlled flow conditions. *Chem. Senses* **25:** 670–671 (abstract).

Laverack, M. S. 1988a. The diversity of chemoreceptors. Pp. 287–312 in *Sensory Biology of Aquatic Animals*, J. Atema, R. R. Fay, A. N. Popper, and W. N. Tavolga, eds. Springer, New York.

Laverack, M. S. 1988b. The numbers of neurones in decapod Crustacea. *J. Crustac. Biol.* **8:** 1–11.

Macmillan, D. L., T. Stuart, and M. Thomas. 1998. Development of a proprioceptive organ on the walking legs of the rock lobster *Jasus edwardsii* (Decapoda: Palinuridae) by ordered addition and loss of receptor elements. *J. Crustac. Biol.* **18:** 1-9.

Maynard, D. M. 1966. Integration in crustacean ganglia. *Symp. Soc. Exp. Biol.* **20:** 111–149.

Meisami, E. 1989. A proposed relationship between increases in the number of olfactory receptor neurons, convergence ratio and sensitivity in the developing rat. *Dev. Brain Res.* **46:** 9–19.

Mellon, D., Jr., and V. Alones. 1993. Cellular organization and growth-related plasticity of the crayfish olfactory midbrain. *Microsc. Res. Tech.* **24:** 231–259.

Mellon, D., Jr., and S. D. Munger. 1990. Nontopographic projection of olfactory sensory neurons in the crayfish brain. *J. Comp. Neurol.* **296:** 253–262.

Merrill, C. L., R. Voigt, and J. Atema. 1994. Reliability of chemoreceptor cell response. I. Intensity coding by pattern and response magnitude with a comparison of analytical methods. *J. Comp. Physiol. A* **175:** 95–105.

Newland, P. L., S. M. Rogers, I. Goabouh, and T. Matheson. 2000. Parallel somatotopic maps of gustatory and mechanosensory neurons in the central nervous system of an insect. *J. Comp. Neurol.* **425:** 82–96.

Roye, D. B., C. M. Kilroy, J. M. Doyle, and L. E. Reuss. 2000. Decussating interneurons mediate antennular withdrawal in the blue crab, *Callinectes sapidus*. *J. Crustac. Biol.* **20:** 603–613.

Sandeman, D., R. Sandeman, C. Derby, and M. Schmidt. 1992. Morphology of the brain of crayfish, crabs, and spiny lobsters: a common nomenclature for homologous structures. *Biol. Bull.* **183:** 304–326.

Sandeman, R., and D. C. Sandeman. 1996. Pre- and postembryonic development, growth and turnover of olfactory receptor neurones in crayfish antennules. *J. Exp. Biol.* **199:** 2409–2418.

Schafer, R., and T. Sanchez. 1973. Antennal sensory system of the cockroach, *Periplaneta americana:* postembryonic development and morphology of the sense organs. *J. Comp. Neurol.* **149:** 335–354.

Schmidt, M. 1989. The hair-peg organs of the shore crab, *Carcinus maenas* (Crustacea, Decapoda): ultrastructure and functional properties of sensilla sensitive to changes in seawater concentration. *Cell Tissue Res.* **257:** 609–621.

Schmidt, M., and B. W. Ache. 1993. Antennular projections to the midbrain of the spiny lobster. III. Central arborizations of motoneurons. *J. Comp. Neurol.* **336:** 583–594.

Schmidt, M., and B. W. Ache. 1996a. Processing of antennular input in the brain of the spiny lobster, *Panulirus argus*. I. Non-olfactory chemosensory and mechanosensory pathway of the lateral and median antennular neuropils. *J. Comp. Physiol. A* **178:** 579–604.

Schmidt, M., and B. W. Ache. 1996b. Processing of antennular input in the brain of the spiny lobster, *Panulirus argus*. II. The olfactory pathway. *J. Comp. Physiol. A* **178:** 605–628.

Schmidt, M., and W. Gnatzy. 1984. Are the funnel-canal organs the "campaniform sensilla" of the shore crab, *Carcinus maenas* (Decapoda, Crustacea)? II. Ultrastructure. *Cell Tissue Res.* **237:** 81–93.

Schmidt, M., L. Van Ekeris, and B. W. Ache. 1992. Antennular projections to the midbrain of the spiny lobster. I. Sensory innervation of the lateral and medial antennular neuropils. *J. Comp. Neurol.* **318:** 277–290.

Shanbhag, S. R., B. Mueller, and R. A. Steinbrecht. 1999. Atlas of olfactory organs of *Drosophila melanogaster*. 1. Types, external organization, innervation and distribution of olfactory sensilla. *Int. J. Insect Morphol. Embryol.* **28:** 377–397.

Spencer, M. 1986. The innervation and chemical sensitivity of single aesthetasc hairs. *J. Comp. Physiol. A* **158:** 59–68.

Steullet, P., T. Flavus, D. Radman, G. Hamidani, M. Zhou, O. Dudar, R. Hill, and C. D. Derby. 1999. The aesthetasc-olfactory lobe pathway of spiny lobsters is not necessary for odor-activated searching behavior, odor-associative learning, and discrimination of complex odors. *Chem. Senses* **24:** 613 (abstract).

Steullet, P., H. S. Cate, and C. D. Derby. 2000a. A spatio-temporal wave of turnover and functional maturation of olfactory receptor neurons in the spiny lobster *Panulirus argus*. *J. Neurosci.* **20:** 3282–3294.

Steullet, P., H. S. Cate, W. C. Michel, and C. D. Derby. 2000b. Functional units of a compound nose: aesthetasc sensilla house similar populations of olfactory receptor neurons on the crustacean antennule. *J. Comp. Neurol.* **418:** 270–280.

Steullet, P., D. R. Krnetzfeldt, G. Hamidani, T. Flavus, and C. D. Derby. 2000c. Functional overlap of two antennular chemosensory pathways in food odor discrimination behavior of spiny lobsters. *Chem. Senses* **25:** 671 (abstract).

Troemel, E. R., B. E. Kimmel, and C. I. Bargmann. 1997. Reprogramming chemotaxis responses: sensory neurons define olfactory preferences in *C. elegans*. *Cell* **91:** 161–169.

Van Drongelen, W., A. Holley, and K. B. Doving. 1978. Convergence in the olfactory system: quantitative aspects of odour sensitivity. *J. Theor. Biol.* **71:** 39–48.

Voigt, R., and J. Atema. 1992. Tuning of chemoreceptor cells of the second antenna of the American lobster (*Homarus americanus*) with a comparison of four of its other chemoreceptor organs. *J. Comp. Physiol. A* **171:** 673–683.

Weiler, E., and A. I. Farbman. 1997. Proliferation in the rat olfactory epithelium: age-dependent changes. *J. Neurosci.* **17:** 3610–3622.

Reference: *Biol. Bull.* **200:** 216–221. (April 2001)

Landing Strategies in Honeybees, and Possible Applications to Autonomous Airborne Vehicles

MANDYAM V. SRINIVASAN*, SHAOWU ZHANG, AND JAVAAN S. CHAHL

Centre for Visual Science, Research School of Biological Sciences, Australian National University, P.O. Box 475, Canberra, A.C.T. 2601, Australia

Abstract. Insects, being perhaps more reliant on image motion cues than mammals or higher vertebrates, are proving to be an excellent organism in which to investigate how information on optic flow is exploited to guide locomotion and navigation. This paper describes one example, illustrating how bees perform grazing landings on a flat surface. A smooth landing is achieved by a surprisingly simple and elegant strategy: image velocity is held constant as the surface is approached, thus automatically ensuring that flight speed is close to zero at touchdown. No explicit knowledge of flight speed or height above the ground is necessary. The feasibility of this landing strategy is tested by implementation in a robotic gantry, and its applicability to autonomous airborne vehicles is discussed.

Introduction

Unlike vertebrates, insects have immobile eyes with fixed-focus optics. Therefore, they cannot infer the distances to objects or surfaces from the extent to which the directions of gaze must converge to view the object, or by monitoring the refractive power that is required to bring the image of the object into focus on the retina. Furthermore, compared with human eyes, the eyes of insects are positioned much closer together and have inferior spatial acuity (Horridge, 1977). Therefore, the precision with which insects could estimate range through binocular stereopsis would be much poorer and restricted to relatively small distances, even if they possessed the requisite neural apparatus (Srinivasan, 1993). Not surprisingly, then, insects have evolved alternative strategies for dealing with the problems of visually guided flight. Many of these strategies rely on using image motion, generated by the insect's own motion, to infer the distances to obstacles and to control various maneuvers (Horridge, 1987; Srinivasan, 1993, 1998).

Here we describe how honeybees use image motion cues to perform smooth landings on a flat surface.

How Bees Perform Smooth Landings

The seminal work of Gibson (1950) highlighted the optic-flow cues that can be brought to bear in controlling the landing of an aircraft. Studies of landing behavior in flies have revealed that, as a surface is approached, the expansion of the image of the surface provides strong cues that are used to control deceleration and trigger extension of the legs in preparation for contact (Goodman, 1960; Eckert and Hamdorf, 1980; Wagner, 1982; Borst and Bahde, 1988). There is also evidence that the rate of expansion of the image is used to infer the time to contact the surface, even if the insect does not possess explicit information about the speed of its flight or the distance to the surface (Wagner, 1982).

However, when an insect makes a grazing landing on a flat surface, cues derived from image expansion are relatively weak. This is because the dominant pattern of image motion is then a translatory flow in the front-to-back direction. Given that flying insects often make grazing landings on flat surfaces, what are the processes by which such landings are orchestrated?

Recently, this question was investigated by Srinivasan *et*

---

* To whom correspondence should be addressed. E-mail: M.Srinivasan@anu.edu.au.

This paper was originally presented at a workshop titled *Invertebrate Sensory Information Processing: Implications for Biologically Inspired Autonomous Systems.* The workshop, which was held at the J. Erik Jonsson Center for the National Academy of Sciences, Woods Hole, Massachusetts, from 15–17 April 2000, was sponsored by the Center for Advanced Studies in the Space Life Sciences at the Marine Biological Laboratory, and funded by the National Aeronautics and Space Administration under Cooperative Agreement NCC 2-896.

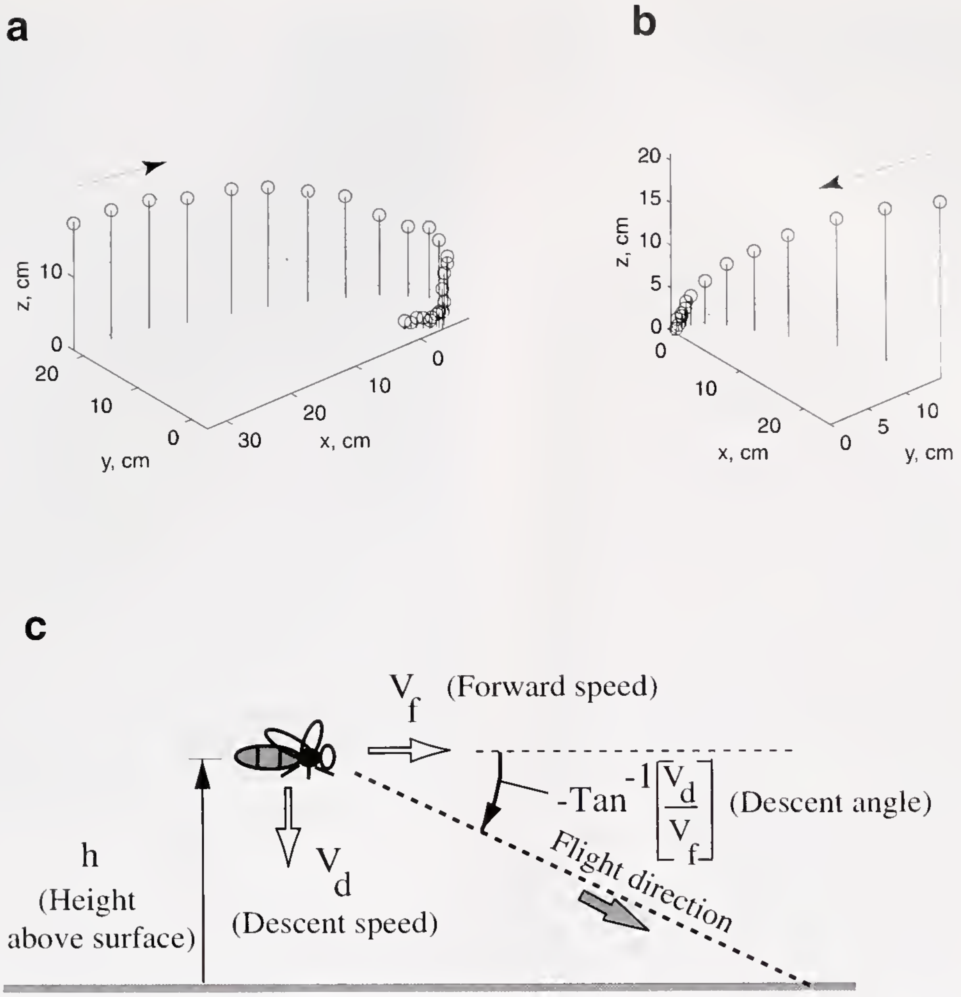

Figure 1. (a, b) Three-dimensional reconstruction of two typical landing trajectories, from video films. Vertical lines depict height above surface. (c) Illustration of some of the variables analyzed to investigate the control of landing. *h* (cm): height above surface; V_f (cm/s): horizontal (forward) flight speed; V_d (cm/s): vertical (descent) speed; $\mathrm{Tan}^{-1}(V_d/V_f)$ (deg or rad): descent angle. Adapted from Srinivasan *et al.* (2000).

al. (2000), who video-filmed trajectories, in three dimensions, of bees landing on a flat, horizontal surface.

Two examples of landing trajectories, reconstructed from the data, are shown in Figure 1a, b. A number of such landing trajectories were analyzed to examine the variation of the instantaneous height above the surface (h), instantaneous horizontal (forward) flight speed (V_f), instantaneous descent speed (V_d) and descent angle (α). These variables are illustrated in Figure 1c.

Analysis of the landing trajectories revealed that the descent angles were indeed quite shallow. The average value measured in 26 trajectories was about 28° (Srinivasan *et al.*, 2000).

Figure 2a, b shows the variation of flight speed with height above the surface, analyzed for two landing trajectories. These data reveal one of the most striking and consistent observations with regard to landing bees: Horizontal speed is roughly proportional to height, as indicated by the linear regression on the data. When a bee flies at a horizontal speed of V_f cm/s at a height of h cm, the angular velocity ω of the image of the surface directly beneath the eye is given by $\omega = V_f/h$ rad/s. From this relationship it is clear that, if the bee's horizontal flight speed is proportional to her height above the surface (as shown by the data), then the angular velocity of the image of the surface, as seen by the eye, must be constant as the bee approaches it. This angular velocity is given by the slope of the regression line. The angular velocity of the image varies from one trajectory to another, but is maintained at an approximately constant value in any given landing. An analysis of 26 landing trajectories revealed a mean image angular velocity of about 500°/s (Srinivasan *et al.*, 2000).

These results reveal two important characteristics. First, bees landing on a horizontal surface tend to approach the

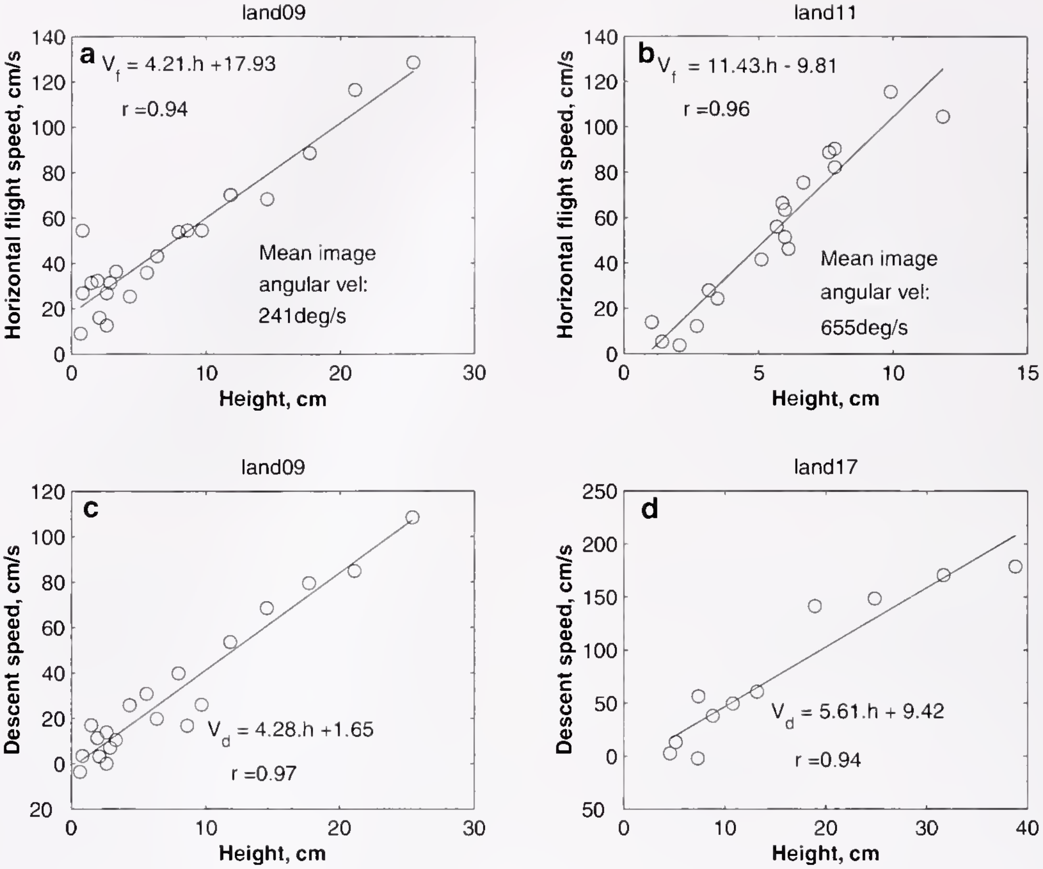

Figure 2. (a, b) Variation of horizontal flight speed (V_f) with height (h) above the surface, for two landing trajectories. (c, d) Variation of descent speed (V_d) with height (h) above the surface, for two landing trajectories. The straight lines are linear regressions through the data, as represented by the equations; r denotes the regression coefficient. Adapted from Srinivasan *et al.* (2000).

surface at a relatively shallow descent angle. Second, landing bees tend to hold the angular velocity of the image of the ground constant as they approach it.

What is the significance of holding the angular velocity of the image of the ground constant during landing? One important consequence is that the horizontal speed of flight is automatically reduced as the height decreases. In fact, by holding the image velocity constant, the horizontal speed is regulated to be proportional to the height above the ground, so that when the bee finally touches down (at zero height), her horizontal speed is zero, thus ensuring a smooth landing. The attractive feature of this simple strategy is that it does not require explicit measurement or knowledge of the speed of flight, or the height above the ground. Thus, stereoscopic methods of measuring the distance of the surface (which many insects probably do not possess) are not required. What is required, however, is that the insect be constantly in motion, because the image motion resulting from the insect's own motion is crucial in controlling the landing.

The above strategy ensures that the bee's horizontal speed is zero at touchdown, but it does not regulate the descent speed. How is the descent speed controlled? Plots of descent speed *versus* height reveal a linear relationship between these two variables, as well. Two examples are shown in Figure 2c, d. This finding implies that landing bees (a) control their forward flight speed to hold the image velocity of the ground constant and (b) control the descent speed to be proportional to the forward speed, so that the descent speed decreases with the forward speed and also becomes zero at touchdown. (In flying *Drosophila*, for example, there is good evidence that lift and thrust co-vary [Götz and Wandel, 1984].) The ratio of descent speed to forward speed, V_d/V_f, determines the descent angle. The two rules described above, operating together, ensure a smooth landing.

Tests on a Robotic Gantry

The feasibility of the landing strategy described above has been tested by implementation in a computer-controlled gantry robot carrying a visual system (Srinivasan *et al.*, 2000). Vision is provided by a video camera mounted on the

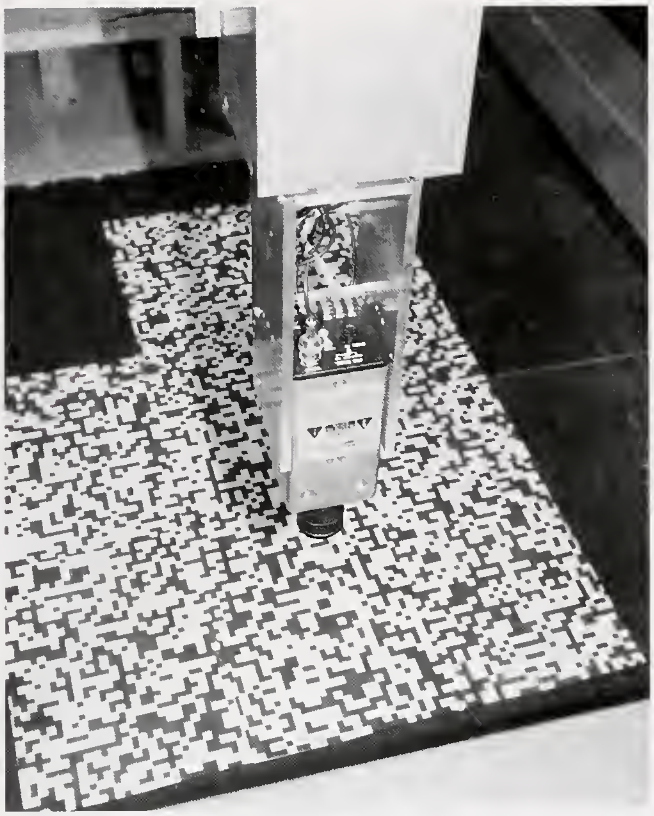

Figure 3. View of robotic gantry, showing camera head and visual texture on the floor. Adapted from Srinivasan *et al.* (2000).

gantry head, which can be translated in three dimensions (x, y, and z). For the purpose of implementing the landing strategy, translatory motion of the camera is restricted to the forward (x) and downward ($-z$) directions. There is no rotary motion about the z axis.

The system is placed under closed-loop control by using a computer to analyze the motion in the image sequence captured by the camera, and to control the motion of the gantry. A view of the gantry and camera is shown in Figure 3. The floor, defined to be the landing surface, is covered with a spatially random, black-and-white visual texture. The camera faces downwards and views the floor. The velocity of image motion is measured by using an image interpolation algorithm, details of which are given in Srinivasan (1994).

Landing is controlled as follows. The system is required to maintain a constant descent angle ($\tan^{-1}(V_d/V_f)$) and a constant image angular velocity, ω_{set}, as it descends. In the first time step, the gantry moves the camera head along the direction of descent at an arbitrarily chosen initial speed. The image velocity is measured during this step, using the image interpolation algorithm. Let us denote the measured image velocity by ω_{meas}. In the next step, the speed of motion of the head is increased or decreased, depending upon whether the measured image velocity is lower or higher than the set image velocity. Specifically, the forward speed $V_f(i + 1)$ of the camera during the next step is related to the current speed $V_f(i)$ by

$$V_f(i + 1) = V_f(i) \cdot \frac{\omega_{set}}{\omega_{meas}} \qquad (1)$$

The speed of descent is also corrected by the same factor, since the forward and descent speeds are proportional to each other and linked by the desired angle of descent. This speed correction ensures that the image velocity during the next step will have the desired value ω_{set}, provided the camera maintains its present altitude. However, since the camera continues to descend during the new step, the forward speed in the following step would have to be reduced further. Thus, both the forward and descent speeds decrease continuously as the camera descends, reaching very low values when the camera is close to the ground.

Landing trajectories generated, using this procedure, by the gantry are shown in Figure 4a for three descent angles. The image velocities maintained during these three landings are shown in Figure 4b. It is clear that the image velocity, though somewhat noisy, is held approximately constant. The height of the camera decreases exponentially with time (Fig. 4c), as do the forward speed and the speed of descent. These behaviors are as expected: a quantitative model of the landing strategy predicts and verifies that these variables do indeed vary exponentially with time (Srinivasan *et al.*, 2000).

The results with the robotic gantry suggest that the strategy proposed is a feasible one for landing on flat surfaces, provided the surface carries visual texture that will enable the measurement of image motion. In undulating terrain, the system reduces the forward and descent speeds when the ground rises toward the camera, and increases them when the ground falls away. This is obviously a desirable feature, but has limitations in that the system cannot cope with a situation in which the ground in front rises abruptly to a level above the camera's current height.

A little reflection will reveal that the landing strategy described here can be used by an aerial vehicle to dock with any flat surface, regardless of its orientation: horizontal, vertical, or oblique. All that is required is that the vehicle approach the surface in a straight line and hold the image velocity constant during the approach. This will automatically ensure that the vehicle's speed decreases as the surface is approached, ensuring smooth docking. In the special case in which the surface is approached perpendicularly, the image velocity will be zero in the "straight ahead" direction: the flow field has a pole there. However, the strategy can still be implemented by holding constant the image speed in an annular region surrounding the pole, or in a large region

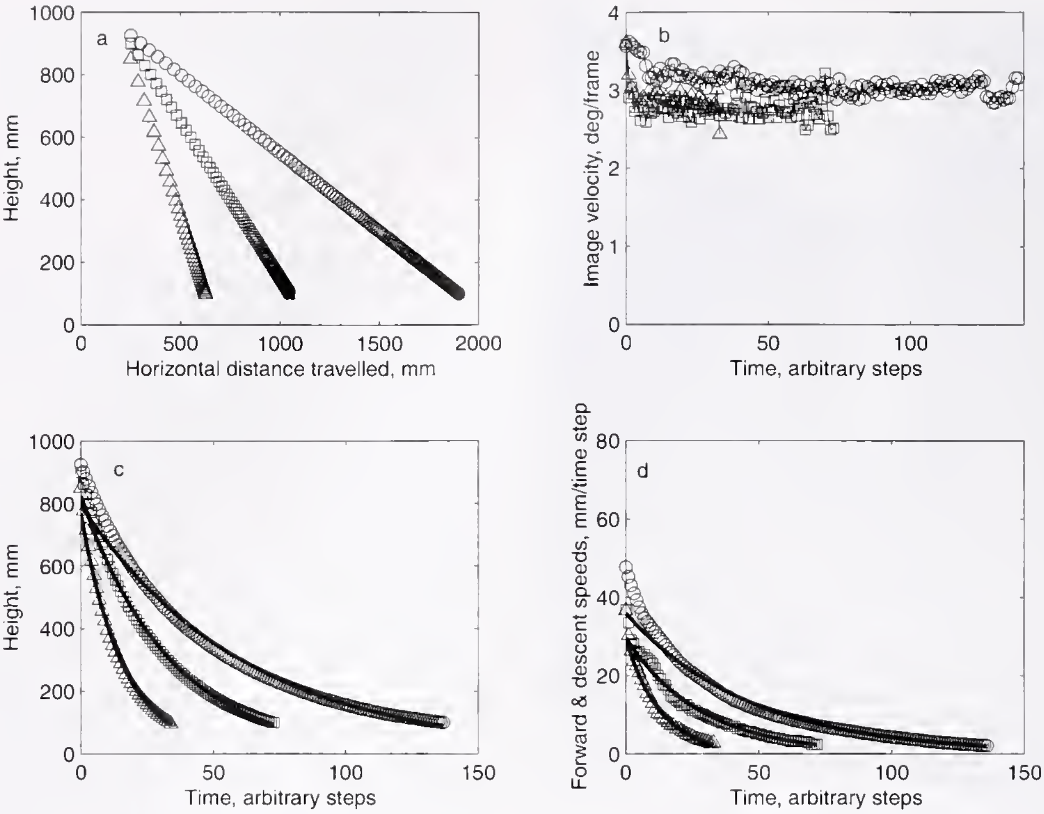

Figure 4. Landing trajectories generated by the robotic gantry. (a) Height *versus* distance traveled for three descent angles: −26.5° (circles), −45° (squares), and −63.5° (triangles). (b) Variation of image angular velocity as a function of time. The symbols in this and other panels refer to the three different descent angles, as in (a). (c) Variation of height with time. (d) Variation of forward speed with time. The line curves in (c) and (d) depict least-squares fits of exponential functions to the data. Descent speed also declines exponentially (data not shown). Adapted from Srinivasan *et al.* (2000).

centered on the pole. Although the present study does not reveal whether bees are actually "aware" of the orientation of the surface in relation to the direction of their approach, it is clear from the above discussion that this information is not necessary for executing the landing process.

Conclusions

Analysis of vision in simple natural systems, such as those found in insects, can often point to novel ways of tackling tenacious problems in autonomous navigation. This is probably because insects, with their "stripped down" nervous systems, have been forced to evolve ingenious strategies to cope with visual challenges within their environment. This article has outlined a surprisingly simple way in which insects use motion cues to perform smooth landings on flat surfaces. The next step is to investigate whether this principle can be used to advantage in the design of visually based control systems for autonomously flying vehicles.

Acknowledgments

We thank the anonymous referees for their assistance in improving the manuscript. This research was supported partly by a grant from the Australian Defence Science and Technology Organisation, Salisbury, Grant RG 84/97 from the Human Frontiers in Science Program, and Grant N00014-99-1-0506 from the U.S. Defense Advanced Research Projects Agency and the Office of Naval Research.

Literature Cited

Borst, A., and S. Bahde. 1988. Visual information processing in the fly's landing system. *J. Comp. Physiol. A* **163:** 167–173.

Eckert, H., and K. Hamdorf. 1980. Excitatory and inhibitory response components in the landing response of the blowfly, *Calliphora erythrocephala*. *J. Comp. Physiol.* **138:** 253–264.

Gibson, J. J. 1950. *The Perception of the Visual World.* Houghton Mifflin, Boston.

Goodman, L. J. 1960. The landing responses of insects. I. The landing response of the fly, *Lucilia sericata*, and other Calliphoridae. *J. Exp. Biol.* **37:** 854–878.

Götz, K. G., and U. Wandel. 1984. Optomotor control of the force of flight in *Drosophila* and *Musca*. II. Covariance of lift and thrust in still air. *Biol. Cybern.* **51:** 135–139.

Horridge, G. A. 1977. Insects which turn and look. *Endeavour* **1:** 7–17.

Horridge, G. A. 1987. The evolution of visual processing and the construction of seeing systems. *Proc. R. Soc. Lond. B* **230:** 279–292.

Srinivasan, M. V. 1993. How insects infer range from visual motion. Pp. 139–156 in *Visual Motion and Its Role in the Stabilization of Gaze*, F. A. Miles and J. Wallman, eds. Elsevier, Amsterdam.

Srinivasan, M. V. 1994. An image-interpolation technique for the computation of optic flow and egomotion. *Biol. Cybern.* **71:** 401–416.

Srinivasan, M. V. 1998. Insects as Gibsonian animals. *Ecol. Psychol.* **10:** 251–270.

Srinivasan, M. V., S. W. Zhang, J. S. Chahl, E. Barth, and S. Venkatesh. 2000. How honeybees make grazing landings on flat surfaces. *Biol. Cybern.* **83:** 171–183.

Wagner, H. 1982. Flow-field variables trigger landing flies. *Nature* **297:** 147–148.

Reference: *Biol. Bull.* **200:** 222–226. (April 2001)

Plume-Tracking Robots: A New Application of Chemical Sensors

HIROSHI ISHIDA*[,1], TAKAMICHI NAKAMOTO[2], TOYOSAKA MORIIZUMI[2], TIMO KIKAS[1], AND JIRI JANATA[1]

[1]*School of Chemistry and Biochemistry, Georgia Institute of Technology, Atlanta, GA 30332-0400; and*
[2]*Department of Physical Electronics, Tokyo Institute of Technology, 2-12-1 Ookayama, Meguro-ku, Tokyo 152-8552, Japan*

Abstract. Many animals have the ability to search for odor sources by tracking their plumes. Some of the key features of this search behavior have been successfully transferred to robot platforms, although the capabilities of animals are still beyond the current level of sensor technologies. The examples described in this paper are (1) incorporating into a wheeled robot the upwind surges and casting used by moths in tracking pheromone plumes, (2) extracting useful information from the response patterns of a chemical sensor array patterned after the spatially distributed chemoreceptors of some animals, and (3) mimicking the fanning behavior of silkworm moths to enhance the reception of chemical signals by drawing molecules from one direction. The achievements so far and current efforts are reviewed to illustrate the steps to be taken toward future development of this technology.

Introduction

Many species of animals rely for their survival on their ability to track odor plumes. Male moths follow sexual pheromones to find their mates (Willis and Arbas, 1991) and marine crustaceans track smells to search for food (Weissburg and Zimmer-Faust, 1993; Atema, 1996; Grasso, 2001). Although their mechanisms are not yet fully revealed, these examples suggest that, if the underlying mechanisms are successfully transferred to robotic platforms, the chemical senses can be as effective as the visual (Viollet and Franceschini, 1999) or auditory senses (Webb and Scutt, 2000) in directing navigation of autonomous robots. The purpose of this paper is to give a general idea of the current state of development of robots that track chemical plumes. The potential applications for such robots include searching for hazardous chemicals and pollutant sources.

Signals Available in Chemical Plumes

The most fundamental characteristics of a chemical plume are concentration of the target chemical and flow direction. Since molecular diffusion is almost always slower than convection, a chemical plume trails downstream from its source, as shown in Figure 1A. There is no smooth concentration gradient in this instantaneous image since the eddies in the turbulent flow stretch and twist the plume. If an array of eight chemical sensors is immersed into the plume, it is exposed to the intermittent stimuli shown in Figure 2. The importance of flow direction is also seen in Figure 1A. When a searcher is in the plume, the source is always in the upstream direction. This is why many species of animals perform anemotaxis in air and rheotaxis in water (Willis and Arbas, 1991; Dusenbery, 1992; Arbas *et al.*, 1993; Weissburg and Zimmer-Faust, 1994).

Whereas animals have keen senses for detecting chemical and flow stimuli (Dusenbery, 1992), sensors for a robot to detect those signals with capabilities similar to those of animals are not yet available. In the case of chemical

---

Received 23 August 2000; accepted 11 January 2001.

* To whom correspondence should be addressed. Current address: Department of Physical Electronics, Tokyo Institute of Technology, 2-12-1 Ookayama, Meguro-ku, Tokyo 152-8552, Japan. E-mail: ishida@ee.titech.ac.jp

This paper was originally presented at a workshop titled *Invertebrate Sensory Information Processing: Implications for Biologically Inspired Autonomous Systems.* The workshop, which was held at the J. Erik Jonsson Center for the National Academy of Sciences, Woods Hole, Massachusetts, from 15–17 April 2000, was sponsored by the Center for Advanced Studies in the Space Life Sciences at the Marine Biological Laboratory, and funded by the National Aeronautics and Space Administration under Cooperative Agreement NCC 2-896.

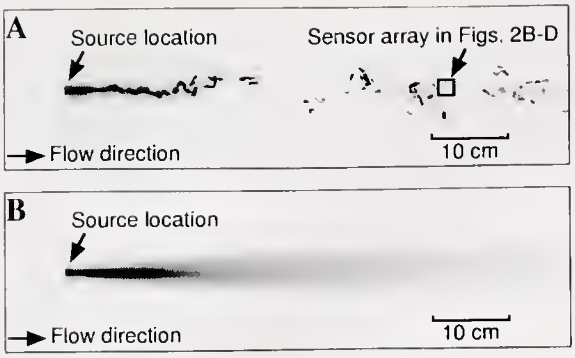

Figure 1. Images of a chemical plume in a turbulent flow. A fluorescent dye, rhodamine 6G, was released from a nozzle into a fully developed open-channel water flow. The effluent velocity of the dye matched the channel flow velocity, thus creating a passive source and avoiding the production of additional turbulence by the effluent itself. The images of the dye plume were captured using the planar laser-induced fluorescence (PLIF) measurement technique (Webster *et al.*, 1999). (A) is an instantaneous image, and (B) is the average of 6000 images measured at 10 frames/s.

sensors, a compromise has been made on the times of response onset and recovery, which can affect the performance of robots. For example, for our wheeled robot we chose semiconductor gas sensors that are commonly used for gas alarms to detect flammable gases and organic solvent vapors. Although these sensors have high sensitivity and fast response, it takes more than 30 s for their responses to return to the initial levels after gas is removed. Therefore, the crawling speed of the robot had to be slowed down to a few centimeters per second (Ishida *et al.*, 1996). Such slow sensors can be beneficial when time is not a critical issue. When averaged over long enough times (typically several minutes), chemical plumes have continuous concentration gradients, as shown in Figure 1B. By smoothing the fluctuating signals, slow sensors make it easier to acquire this gradient information.

Iterative measurements of time-averaged gradients until a robot reaches an odor source may need hours, however, and most applications do not permit such long search. Attempts have been made to extract rapidly changing signals from dull sensor responses by filtering or differentiation of sensor outputs (Nakamoto *et al.*, 1996b; Webb, 1998). Another option is to use faster sensors, such as quartz crystal microbalance sensors, although their sensitivities tend to be lower than those of semiconductor gas sensors. For underwater plume tracking, amperometric microelectrode sensors are promising. In the amperometric mode of sensing, a constant voltage is applied between a microelectrode and a counter electrode so that electrochemical reaction of a target chemical substance takes place on the electrodes. The signal measured is a current proportional to the concentration. A short response time comparable to that of animals' chemoreceptors (100 ms) can be easily achieved (Moore and Atema, 1991; Kikas *et al.*, 2000).

The direction of airflow can be detected by an array of hot wire sensors (Ishida *et al.*, 1994). However, wind slower than 5 cm/s is hard to detect (Lomas, 1986), and detection limits lower than this are required in some indoor environments. If a robot is used to detect gas leaks in industrial or domestic buildings with moderate air-conditioning, it often

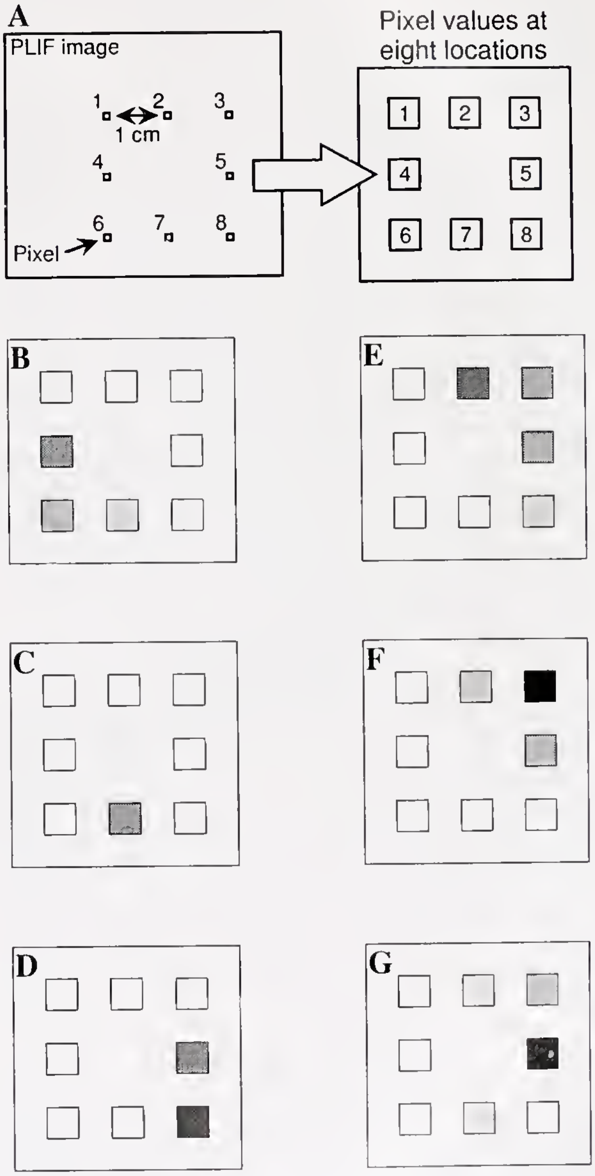

Figure 2. Concentration change in a plume represented by stimulus patterns exposed to chemical sensors. Eight pixels are chosen from PLIF images representing an array of eight sensors. The gray-scale value of each pixel is then drawn in a blown-up picture as shown in (A). Darker pixels represent higher concentrations. (B)-(D) are a series of stimulus patterns when the array position is 50 cm downstream from the source (Fig. 1A), and (E)-(G) are the patterns when the eight pixels surrounding the source are observed in successive 0.2-s intervals. The size and the location of the array shown in (B)-(D) are depicted in Figure 1A.

encounters wind fields with velocities less than 5 cm/s (Pluijm *et al.*, 1986). Search strategies that do not require flow sensors should be considered in this case. Chemical sensor arrays and the odor compass described later have been developed to address this issue (Nakamoto *et al.*, 1996a; Ishida *et al.*, 2000). The detection limits of various types of flow sensors are lowered in water because of the higher viscosity, heat capacity, and density of water compared to air (Lomas, 1986; Roberson and Crowe, 1997).

Realization of Various Aspects of Plume Tracking

Multiphase search algorithm

Animals show different types of behaviors in different situations (Dusenbery, 1992). Our multiphase algorithm for a wheeled robot was divided into anemotactic and chemotactic strategies (Ishida *et al.*, 1996). Although this combination was devised after many experiments using robots, each of those two is a fundamental search strategy seen in many animal species (Dusenbery, 1992; Arbas *et al.*, 1993). The anemotactic strategy is based on moths tracking pheromone plumes. The key feature implemented into the robot is to track a chemical plume by using wind direction, as a moth shows upwind surges when it perceives a pheromone (Willis and Arbas, 1991). When the robot by chance leaves the plume, it tries to relocate the lost plume by moving back and forth across the wind. This fail-safe mechanism, known in moths as casting flight (Willis and Arbas, 1991), is extremely important for successful plume tracking because of the random nature of a turbulent plume.

Another important feature of the multiphase algorithm is chemotactic search. It was added to the multiphase algorithm to cope with winds coming from multiple directions simultaneously (Ishida *et al.*, 1996). In a domestic or industrial building, the main source of wind is an air conditioner, and a robot often encounters winds from multiple air-supply openings. However, the anemotactic strategy described above failed in a clean room with two air-supply openings (Ishida *et al.*, 1996). In the experiments, an ethanol vapor source was placed near one of the openings. A plume extended from it approximately 1 m until the wind from another opening merged into a side of the plume. In such a case, care should be taken to employ the anemotactic strategy. When the detected concentration is low, the robot might be in the merging area where unstable winds often direct an anemotactic robot to wrong directions. Anemotaxis should be activated only when a high concentration is detected, thus only the wind from the source direction is considered to exist.

In the multiphase algorithm, the robot is programmed to employ the chemotactic strategy first, and anemotaxis is activated only when a concentration above a predefined threshold is detected. This change in strategies helps to prevent the robot from being trapped in the area where the wind direction is not stable (Ishida *et al.*, 1996). The robot is also programmed to change its strategies from anemotaxis to chemotaxis, or *vice versa*, when one strategy makes no significant progress for 60 s (Ishida *et al.*, 1996). This ensures timely changes in strategies even when the predefined threshold is inappropriate.

To accomplish fully autonomous search, there still remain many questions, including how to locate a plume for the first time in the absence of any chemical signals, and how to decide when the odor source has been located so as to terminate the search. These issues have been more fully discussed by Dusenbery (1989) and Ishida *et al.* (1998).

Array mode of information acquisition

Use of an array of sensors should provide more information than a pair or a limited number of chemical sensors, thus enhancing simple gradient detection. Extensive and spatially distributed arrays of chemoreceptors are used by many animals, including arthropods (Keller and Weissburg, 2000). Various array configurations and signal processing algorithms are being investigated in simulations (Ishida *et al.*, 2000), and they are being evaluated by their ability to acquire flow vector and source location. For example, consider an array of amperometric sensors with fast and linear response. Since their outputs faithfully trace the input stimuli, the stimulus pattern shown in Figure 2 can be regarded as the output pattern of the sensors. Keller and Weissburg (2000) showed that blue crabs use not only their antennules but also chemoreceptors on other appendages for tracking odor plumes. A crab of 1 cm in size would experience similar response patterns. As mentioned in the previous section, amperometric microelectrode sensors have response fast enough to yield such output patterns, and an array of this size can be easily fabricated and mounted on an underwater vehicle.

As seen in Figure 2, the observed responses are highly intermittent since they show instantaneous concentrations with no integration over time. This intermittency enables tracking of patches of the plume. When a patch passes over the sensor array from sensor 6 through 7 to 8, the flow direction and speed can be determined from this change in the response pattern (Fig. 2B–D).

Figure 2E–G shows the response pattern when the array is placed over the source location. From the responses of sensors 2 and 3, the flow can be determined to move from left to right. However, sensors 1, 4, and 6 at the upstream edge of the array do not show any response. Considering the fact that the plume always trails in the downstream direction, this response pattern indicates that the source is located within the array.

Modulation of chemical signals

Marine crustaceans flick their antennules, and terrestrial vertebrates show sniffing behavior. These actions modulate the dynamics of chemical signals at the animals' sensors. An interesting example of this signal modulation is the wing fanning of a male silkworm moth tracking a pheromone plume. Attempts are also being made to understand the fanning behavior of other animals (Breithaupt and Ayers, 1998; Breithaupt, 2001). Mimicking this mechanism, a sensing probe, termed an "odor compass," consisting of two gas sensors and a small fan to draw air to the sensors was fabricated (Nakamoto *et al.*, 1996a). Experiments showed that the effect of the fan is significant in obtaining directional cues. When an odor source is in front of the compass, odor molecules are carried towards both the left and right sensors by airflow produced by the fan. On the other hand, they are repelled by the airflow when a source is behind the compass. The obtained sensor outputs thus change according to the direction of the compass with respect to an odor source. Fanning was also found to enhance differences between the outputs of the left and right sensors. When a source is to the right of the compass, turning on the fan increases the output of the right sensor and decreases that of the left sensor. Therefore, the direction of an odor source is determined by rotating the compass and finding the direction where the sensors show the largest and matched response (Nakamoto *et al.*, 1996a).

Simulations

Simulation is a useful way to accelerate the development of plume-tracking systems, since it takes a long time to develop a new system by trial and error. There are several levels of simulations. The most common way is to simulate all the dynamics of fluid and the kinetics of sensors and robots in a computer. However, this is impractical because the simulation of turbulent flow with fine resolution requires massive computer power. Visualization techniques are more realistic methods of obtaining concentration data on a fine scale (Ferrier *et al.*, 1993; Webster *et al.*, 1999). If computer models for the kinetics of sensors or robots (or animals) are used, the simulation can be based on visualized plume data (Ishida *et al.*, 2000). This level of simulation is effective in testing algorithms and determining the specifications for robots. The next level of simulation can be performed with a "virtual plume (VP)," which is a test bench for an array of real chemical sensors (Kikas *et al.*, 2000). This system is based on the principles of multichannel flow injection analysis (FIA)/sequential injection analysis (SIA) (Ruzicka and Hansen, 1988) and the array of amperometric microelectrode sensors. A plug of chemical solution is introduced into a flow of carrier solution in tubing, divided into eight channels, and delivered to the sensors after passing through delay and dispersion elements. The delay element is a coil of tube that adjusts the timing with which a divided plug reaches the sensor at the end of the channel. The dispersion element is a small mixing chamber that adjusts the onset slope of the plug. By using those elements, VP can create various stimulus patterns that the sensor array would experience in real plumes.

Discussion

Research on plume tracking is still at its initial stages of development. Animals show a variety of behaviors, each of which is optimized for the habitat of that species. There seems to be no single search algorithm that is effective in every environment. Considering the variety of situations in which plume-tracking robots will be used, future work should use diverse algorithms and situations. Various aspects of the mechanisms underlying animal behavior have been transferred to robots through the interaction between biology and engineering. Although we should continue such efforts, we are now at a point where we can begin a synthesis of the data to develop a unified strategy for the design of plume-tracking systems. The first step toward this goal would be to evaluate the applicability of each algorithm in various situations. The limit of that algorithm will, then, be clarified, and quantitative comparison between different algorithms will be possible. The simulation techniques are expected to facilitate this progress by providing a way to compare a variety of situations quickly.

Acknowledgments

We thank Drs. Frank Grasso and Diana Blazis for inviting us for the insightful interdisciplinary workshop. We are grateful to Drs. Philip Roberts and Donald Webster for providing access to their LIF plume data sets. Enlightening discussions with Drs. Marc Weissburg, David Dusenbery, and Troy Keller are also gratefully acknowledged. We also thank two anonymous reviewers for valuable suggestions and fruitful criticisms. This work was partially supported by a grant from DARPA/ONR, Project Number N00014-98-1-0776.

Literature Cited

Arbas, E. A., M. A. Willis, and R. Kanzaki. 1993. Organization of goal-oriented locomotion: pheromone-modulated flight behavior of moths. Pp. 159–198 in *Biological Neural Networks in Invertebrate Neuroethology and Robotics*, R. D. Beer, R. E. Ritzmann, and T. McKenna, eds. Academic Press, San Diego.

Atema, J. 1996. Eddy chemotaxis and odor landscapes: exploration of nature with animal sensors. *Biol. Bull.* **191:** 129–138.

Breithaupt, Thomas. 2001. Fan organs of crayfish enhance chemical information flow. *Biol. Bull.* **200:** 150–154.

Breithaupt, T., and J. Ayers. 1998. Visualization and quantification of biological flow fields through video-based digital motion-analysis techniques. *Mar. Freshw. Behav. Physiol.* **31:** 55–61.

Dusenbery, D. B. 1989. Optimal search direction for an animal flying or swimming in a wind or current. *J. Chem. Ecol.* **15:** 2511–2519.

Dusenbery, D. B. 1992. *Sensory Ecology: How Organisms Acquire and Respond to Information.* W. H. Freeman, New York.

Ferrier, A. J., D. R. Funk, and P. J. W. Roberts. 1993. Application of optical techniques to the study of plumes in stratified fluids. *Dyn. Atmos. Oceans* **20:** 155–183.

Grasso, Frank W. 2001. Invertebrate-inspired sensory-motor systems and autonomous, olfactory-guided exploration. *Biol. Bull.* **200:** 160–168.

Ishida, H., K. Suetsugu, T. Nakamoto, and T. Moriizumi. 1994. Study of autonomous mobile sensing system for localization of odor source using gas sensors and anemometric sensors. *Sens. Actuators A* **45:** 153–157.

Ishida, H., Y. Kagawa, T. Nakamoto, and T. Moriizumi. 1996. Odor-source localization in the clean room by an autonomous mobile sensing system. *Sens. Actuators B* **33:** 115–121.

Ishida, H., T. Nakamoto, and T. Moriizumi. 1998. Remote sensing of gas/odor source location and concentration distribution using mobile system. *Sens. Actuators B* **49:** 52–57.

Ishida, H., T. Yamanaka, N. Kushida, T. Nakamoto, and T. Moriizumi. 2000. Study of real-time visualization of gas/odor flow image using gas sensor array. *Sens. Actuators B* **65:** 14–16.

Keller, T. A., and M. J. Weissburg. 2000. Chemically-mediated search strategies: elucidating the nature of stimulus dynamics for searching blue crabs (*Callinectes sapidus*). [Abstr.] *Aquatic Science Meeting,* Copenhagen, 5–9 June 2000. Am. Soc. Limnol. Oceanogr.

Kikas, T., H. Ishida, P. J. W. Roberts, D. R. Webster, and J. Janata. 2000. Virtual plume. *Electroanalysis* **12:** 974–979.

Lomas, C. G. 1986. *Fundamentals of Hot Wire Anemometry.* Cambridge University Press, Cambridge.

Moore, P. A., and J. Atema. 1991. Spatial information in the three-dimensional fine structure of an aquatic odor plume. *Biol. Bull.* **181:** 408–418.

Nakamoto, T., H. Ishida, and T. Moriizumi. 1996a. An odor compass for localizing an odor source. *Sens. Actuators B* **35:** 32–36.

Nakamoto, T., T. Yamanaka, H. Ishida, and T. Moriizumi. 1996b. Speed up of odor-source localization system using Kalman-filter sensor signal processing method. [Abstr.] *Annual Meeting,* San Antonio, TX, Fall 1996. *Electrochem. Soc.* **96–2:** 1163.

Pluijm, M. J. F. P., G. J. A. Sars, and C. H. Massen. 1986. Calibration unit for micro-anemometers at very low air velocities. *Appl. Sci. Res.* **43:** 227–234.

Roberson, J. A., and C. T. Crowe. 1997. *Engineering Fluid Mechanics,* 6th ed. John Wiley, New York.

Ruzicka, J., and E. H. Hansen. 1988. *Flow Injection Analysis,* 2nd ed. John Wiley, New York.

Viollet, S., and N. Franceschini. 1999. Visual servo system based on a biologically-inspired scanning sensor. Pp. 144–155 in *Sensor Fusion and Decentralized Control in Robotic Systems II,* G. T. McKee and P. S. Schenker, eds. *Proc. SPIE Int. Soc. Opt. Eng.* **3839.**

Webb, B. 1998. Robots, crickets and ants: models of neural control of chemotaxis and phonotaxis. *Neural Networks* **11:** 1479–1496.

Webb, B., and T. Scutt. 2000. A simple latency-dependent spiking-neuron model of cricket phonotaxis. *Biol. Cybern.* **82:** 247–269.

Webster, D. R., P. J. W. Roberts, S. Rahman, and L. P. Dasi. 1999. Simultaneous PIV/PLIF measurements of a turbulent chemical plume. [Abstr.] *ASCE Int. Water Resources Eng. Conf.,* Seattle, WA, August 1999. Am. Soc. Civil Engineers.

Weissburg, M. J., and R. K. Zimmer-Faust. 1993. Life and death in moving fluids: hydrodynamic effects on chemosensory-mediated predation. *Ecology* **74:** 1428–1443.

Weissburg, M. J., and R. K. Zimmer-Faust. 1994. Odor plumes and how blue crabs use them in finding prey. *J. Exp. Biol.* **197:** 349–375.

Willis, M. A., and E. A. Arbas. 1991. Odor-modulated upwind flight of the sphinx moth, *Manduca sexta* L. *J. Comp. Physiol. A* **169:** 427–440.

Reference: *Biol. Bull.* **200:** 227–234. (April 2001)

Sensing Scenes With Silicon

DAVID C. MOUNTAIN[1,*] AND ALLYN E. HUBBARD[2]

[1]*Boston University Hearing Research Center and Department of Biomedical Engineering,*
44 Cummington St., Boston, Massachusetts 02215; and [2]*Boston University Hearing Research Center*
and Department of Electrical and Systems Engineering and Department of Biomedical Engineering,
8 St. Mary's Street, Boston University, Boston, Massachusetts 02215

Abstract. Scene analysis, the process of converting sensory information from peripheral receptors into a representation of objects in the external world, is central to our human experience of perception. Through our efforts to design systems for object recognition and for robot navigation, we have come to appreciate that a number of common themes apply across the sensory modalities of vision, audition, and olfaction; and many apply across species ranging from invertebrates to mammals. These themes include the need for adaptation in the periphery and trade-offs between selectivity for frequency or molecular structure with resolution in time or space. In addition, neural mechanisms involving coincidence detection are found in many different subsystems that appear to implement cross-correlation or autocorrelation computations.

Introduction

As we walk in a busy city or even a pristine forest, our senses are bombarded by signals from many sources. The acoustic signals entering our ears are a mixture of sounds produced by many sources as well as innumerable echoes. The photons reaching our retina have been reflected off a complicated montage of clothing, faces, automobiles, and buildings or perhaps off a mixture of leaves, stems, insects, birds, soil, and flowers. Likewise, the molecules reaching our olfactory epithelium may be a mixture of burnt hydrocarbons, perfume, and the smell of decaying trash or a combination of fragrances from flowers, musk from animals, and byproducts of the breakdown of leaves. We refer to the problem of interpreting this jumble of sensory input and relating it to the physical world as *scene analysis.*

Many of the current ideas about scene analysis in general started with experimental and theoretical work on vertebrate vision. David Marr (1982) introduced a conceptual framework that spanned the entire range of issues from perception down through the physiological mechanisms to the actual underlying computations. The core idea is that sensory systems carry out specific computations that can be described mathematically, and that if these computations are understood, then they can be implemented as computer programs or in electronic hardware.

Our own approach to designing artificial systems for scene analysis follows Marr's lead. We start with physiologically based models that replicate the responses of the sensory receptors and neural structures that appear to be involved with the early stages of sensory processing. These models are then further abstracted to a form in which they can be used as the starting point for the design of very large-scale integrated circuits (VLSI). The VLSI circuits, after fabrication, are then integrated with appropriate sensors, and the outputs are fed to a microprocessor for tasks such as grouping, object localization, and object classification.

Visual Scene Analysis

Visual scene analysis in mammals is believed to take place through a series of parallel pathways (Fig. 1). The image projected by the lens onto the retina is transduced by photoreceptors, and then contrast is enhanced by neural processing before the visual information is split into specialized pathways that appear to extract important features

---

*To whom correspondence should be addressed. E-mail: dcm@bu.edu.

This paper was originally presented at a workshop titled *Invertebrate Sensory Information Processing: Implications for Biologically Inspired Autonomous Systems.* The workshop, which was held at the J. Erik Jonsson Center for the National Academy of Sciences, Woods Hole, Massachusetts, from 15–17 April 2000, was sponsored by the Center for Advanced Studies in the Space Life Sciences at the Marine Biological Laboratory, and funded by the National Aeronautics and Space Administration under Cooperative Agreement NCC 2-896.

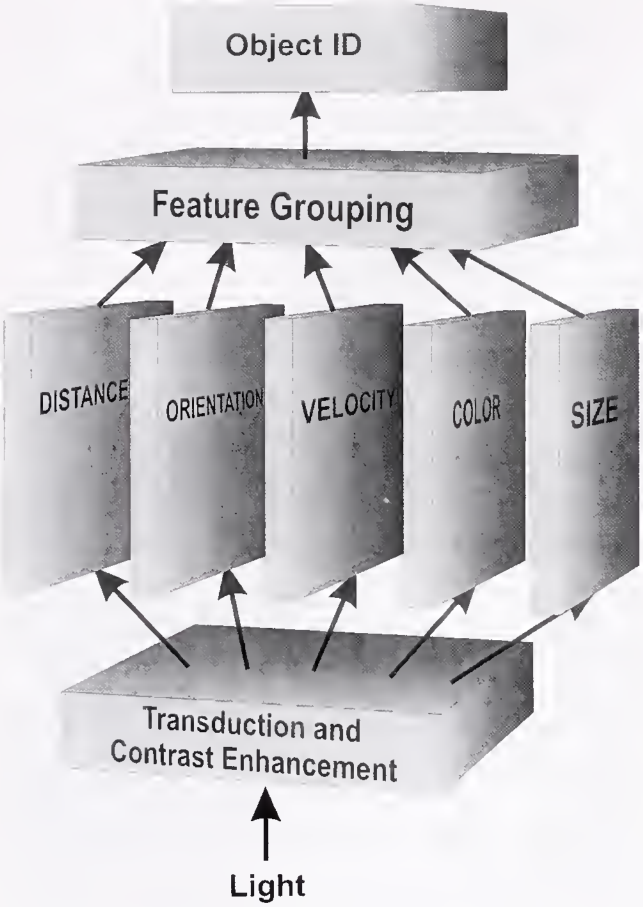

Figure 1. Visual feature analysis consists of first transducing the light projected onto the photoreceptor array and enhancing the contrast of the projected image. This is followed by parallel pathways of feature extraction, the outputs of which are then processed to group related elements to form visual objects.

such as distance, orientation, velocity, color, and size (Marr, 1982). Individual regions of the visual image are analyzed for these different features, and then selected portions are grouped together through selective attention to form visual objects that can be identified.

Similar processes may also be taking place in invertebrates. For example, cells from the third optic ganglion of dragonflies respond selectively to different target classes with properties that are remarkably similar to those of cells from the mammalian visual cortex (O'Carroll, 1993). Also, bees—like mammals—can recognize a familiar shape under a variety of viewing conditions regardless of whether it is initially sensed by color contrast, luminance contrast, or motion contrast (Zhang *et al.*, 1995).

The visual system must be able to cope with the large changes in ambient light level that take place due to time of day, presence or absence of clouds, and moving in and out of the shade. Even with fixed lighting conditions, some parts of the visual scene may be brightly lit while others may be in the shade. The image projected onto a receptor array is the product of the illumination falling upon the objects within the visual scene, multiplied by the reflectivities of these objects. Since it is the reflectivity (both overall magnitude and spectrum) that provides the useful information about object identity, the visual system needs a method to minimize the effects of varying illumination.

These illumination problems must be dealt with in the first stages of processing, before object formation can take place. The large changes in ambient light level appear to be handled at the receptor level through adaptation. Adaptation is a process whereby the sensitivity of the photoreceptor depends on the time-averaged light level. In biological photoreceptors, biochemical processes provide the needed automatic gain control. The outputs of small groups of photoreceptors are then combined so as to enhance the differences in reflectivity of objects within the scene by using a "center-surround" organization (Fig. 2, column 1). This is done by combining an excitatory input from a receptor or small cluster of receptors with inhibitory inputs from the surrounding neighbors (on-center receptive field) or by combining an inhibitory input from a receptor or cluster with excitatory inputs from the surrounding neighbors (off-center receptive field). Mathematically, the combination of adaptation and center-surround organization is equivalent to performing the combination of local normalization and a two-dimensional second spatial derivative on the output of the receptor array. This process has the effect of emphasizing contrast boundaries in the image. The spatial extent of the receptors contributing to the receptive field can be varied at the design stage to achieve different degrees of resolution (image smoothing). Alternatively, the scene can be processed by parallel pathways each with a different resolution. If appropriate weights are used for the excitation and inhibition, then the center-surround spatial filters can be approximated mathematically as Gabor functions (Weldon and Higgins, 1999). The multi-resolution approach can be thought of as taking a two-dimensional wavelet transform of the image (Porat and Zeevi, 1989).

Distance information is not available to the visual system directly, because the external three-dimensional world is mapped onto a two-dimensional array of receptors. If a three-dimensional internal representation is needed, say for navigational purposes, then the third dimension must be synthesized from the information available from the receptors. If the system has two eyes with overlapping visual fields, then differences due to parallax between the images from the two eyes can be exploited (binocular disparity) to estimate distance; otherwise, vergence or more subtle cues must be used. To estimate binocular disparity, the visual system appears to perform a spatial cross-correlation between corresponding regions of the two retinas (Marr, 1982).

Spatial cross-correlation is also used to detect motion.

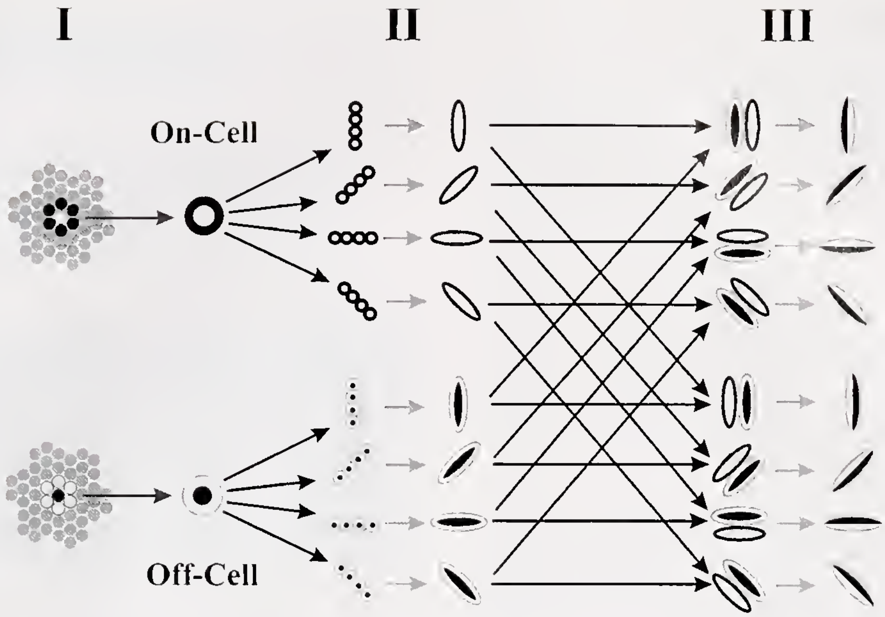

Figure 2. Orientation processing consists of combining the outputs of cells with center-surround organization (column I) to create oriented receptive fields (column II). These oriented receptive fields are then combined to form oriented edge detectors (column III).

Coincidence detection between the output of a cell and the delayed outputs of other cells with nearby receptive fields is mathematically equivalent to computing the spatial cross-correlation between the current visual frame and a previous visual frame on a region-by-region basis.

Orientation processing involves detecting lines and edges and estimating their angular orientation. Hubel and Wiesel (1962), working with cat visual cortex, showed that detection of oriented edges can be accomplished by a sequence of processing stages that combine the outputs of groups of cells with similar center-surround characteristics. By using groups of cells arranged as short linear arrays, short linear segments of light or dark can be detected (Fig. 2, column II). Different arrays have different orientations (orientation tuning), so that all possible edge segments within a region can be detected. If we then combine the output of pairs of these arrays that are slightly offset from each other and have the same orientation but with one array being of the "on" type and the other being of the "off" type, we have a system that detects edge segments between areas of different reflectivities (Fig. 2, column III). This process can be performed a second time to detect line segments. Higher-level processing can then be used to group the edge or line segments into longer lines and arcs (Pasupathy and Connor, 1999).

We have implemented this type of processing in silicon by designing a set of integrated circuits that implement the processing illustrated in Figure 2 (Hinck and Hubbard, 1999). We do not have space here to go into the details of the silicon implementation, but one significant difference between the biological and silicon system must be mentioned. In biological systems, the information between processing units (cells) is carried by axons that are self routing; in other words, they can work their way through the nervous tissue and find their targets. With silicon processing systems, the wiring problem becomes serious. The processing described within a single column of Figure 2 only requires communication between nearby elements on the chip. However, when we need to move information from one processing level or chip to another (from one column to another in Fig. 2), then we run into problems due to the sheer number of wires involved. To reduce this bottleneck, a technique known as address event representation (AER) is used (Boahen, 2000). When a silicon cell is "excited," it broadcasts its address (identity) to all listeners, which may be a one-to-one or a one-to-many mapping. Each broadcast event is equivalent to the production of a single action potential (spike) in the biological system, and given the bandwidth (speed) of the circuitry we have the ability to transmit the identity of all the spikes from all the cells on a chip. Because the processing is taking place in real time, there is no need to record a time stamp for the events. For simulations that do not run in real time, each event may need both a time stamp and an address.

With AER, signaling takes place only if a spike is generated; this minimizes power consumption because, for a single cell, spikes are relatively rare events. This minimization of power consumption is important, especially for small robots (as well as for biological systems), since low power consumption allows operation for longer periods of time without replenishment of energy stores.

Auditory Scene Analysis

A major challenge in auditory scene analysis is that acoustic signals from different sources can overlap in direction, frequency, and time. We believe that biological systems meet this challenge by dividing up the received signals in frequency and time and—through the use of appropriate grouping principles—enhance the signal-to-noise ratio for individual sources to the point where the bearing and identification of the source can be determined. In many applications, both transient and long-duration signals are of interest. In auditory scene analysis, each frequency band can be analyzed for the presence of specific features, and then the grouping rules can be used to combine information from selected frequency bands to produce the features vector that represents an auditory object.

Audition, unlike vision, has no method by which even two of the three physical dimensions of the external acoustic world can be projected directly onto the receptor array. To determine the direction of a sound source, one either needs to compare signals acquired by directional ears (microphones) with different orientations or compare measurements of pressure taken at different locations in space. In the latter case, the ears or microphones must be spaced sufficiently that the time delay due to the speed of sound is large enough to be sensed or measured. If only two ears or microphones are used, then directional ambiguities are present, but these can generally be resolved through rotation of the head or microphone array. The third dimension (source distance) is much more difficult to estimate in audition. Experiments with human listeners suggest that the ratio of direct to reverberant sound energy may be an important distance cue. How this ratio might be estimated is not clear.

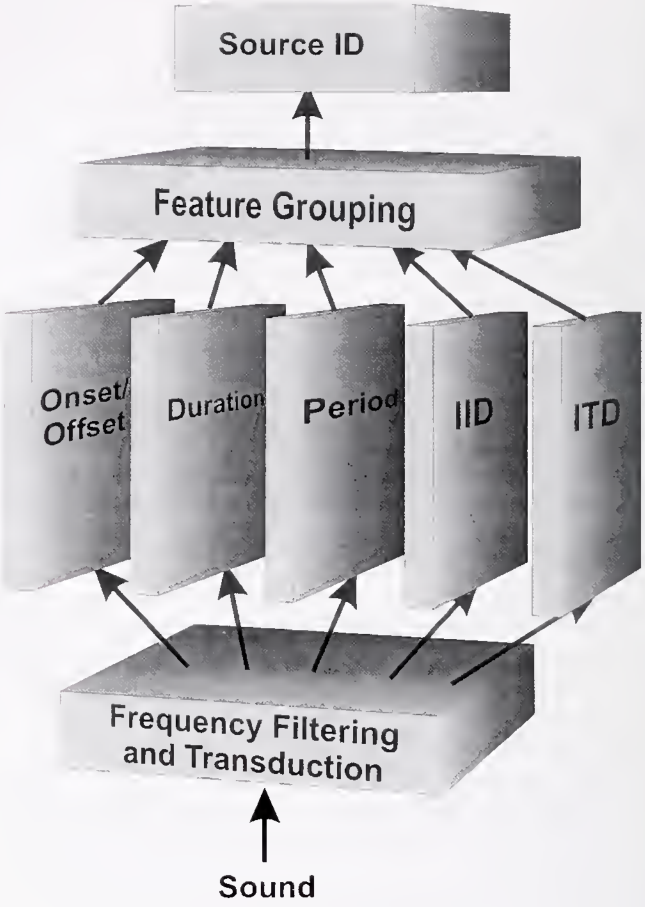

Figure 3. Auditory feature analysis consists of first filtering and transducing the sound received by the peripheral organs. This is followed by parallel pathways of feature extraction, the outputs of which are then processed to group related elements to form auditory objects.

Each frequency channel is analyzed in parallel through the computation of multiple features (Fig. 3). These features are likely to be similar for frequency channels that contain signals from the same sound source and are likely to differ for signals from different sound sources. For example, the differences in time delay between the arrival of the signals (interaural time differences, ITD) as well as differences in intensity (interaural intensity differences, IID) at two sensors will be similar across frequency channels for a single source because these features depend on source direction. Frequency components with similar onsets, offsets, duration, and envelope period are also most likely to be from a single sound source.

For many vertebrates, the head size is sufficient to create significant time delays (ITD) between the ears that can be used for localization; at higher frequencies the head shadow effect is large, producing a significant IID. For very small animals, especially insects, the ears are very close together, making ITD estimation *via* neural circuits impractical, and the animal's size precludes creating a sound shadow. These animals appear to use mechanical or acoustic means, or both, to detect the subtle pressure differences between the two sides of their body (Michelsen, 1998).

As was the case for visual processing, the final step before auditory source identification is the grouping process (Bregman, 1990). In each of the features maps described above, timing information is preserved. This enables the grouping process to use common bearing, as determined by the ITD and IID maps, and synchrony across maps as the major cues for grouping specific components together. This grouping process results in a simplified set of features that includes target direction, the major peaks in the target signal spectrum, and temporal features such as the period of the signal envelope. This set of features can then be compared to stored signatures to complete the identification process. Signatures in this context can be hardwired (acquired through evolution at the species level), learned through experience at the individual level, or derived from a combination of the two methods.

If the system is hardwired, then it is possible to implement the entire analysis/tracking system with simple circuits. For example, the Webb and Scutt (2000) model of cricket phonotaxis implements pattern recognition and source localization with a system comprising two receptors followed by four neurons. The pattern of interest in this case is the mating call of the male, which is characterized by a limited range of carrier frequencies and a limited range of syllable repetition intervals (SRI) (modulation periods). Filtering for the appropriate carrier frequencies takes place in the hearing organ, and subsequent filtering for SRI takes place using a pair (one for each ear) of output neurons that act as lowpass filters, followed by another pair of neurons that act as a highpass filters. Source localization is accomplished by using directional ears and a combination of excitation and inhibition in the same neurons that perform the highpass filtering.

For auditory scene analysis, it is essential that the filters that perform the frequency separation be designed to have impulse responses that are compact both in frequency and time. The performance measure commonly used to describe this feature is the time-bandwidth product. Simple, single mode resonances, although narrow in frequency, do not have good temporal performance and hence do not have good time-bandwidth products. The impulse response that achieves the theoretical time-bandwidth product limit is a sinusoid with a Gaussian envelope (Gabor function). Such an impulse response is physically unrealizable, but it is possible to combine multiple resonances to create a response that comes close to the ideal. Also, for a general purpose signal processing system, it is generally better to use filters with a constant ratio of bandwidth to center frequency (constant Q) rather than a constant bandwidth like that obtained with a Fourier transform. The widespread use of approximately constant-Q filtering across the ears of many species ranging from bush crickets (Hoy, 1992) to mammals (Javel, 1986) suggests that this approach offers significant survival value. The use of a constant-Q filter bank is very similar mathematically to taking a wavelet transform of the acoustic time signal. It should be noted that most of the acoustic frequencies of biological significance are higher than what most cells can follow, so the filtering is generally done mechanically before detection by the receptor cells. The number of frequency channels may vary from very few in insects (Michelsen, 1992) to hundreds in many vertebrates (Echteler *et al.*, 1994).

Typically this filtering process is implemented in silicon using a cascade of second-order filters with progressively lower resonant frequencies. This cascade is intended to simulate the traveling wave of the mammalian cochlea, which starts in the basal (high-frequency) end of the cochlea and propagates towards the apical (low-frequency) end. For this purpose, subthreshold circuits have been most commonly used (Mead, 1989; Fragniere *et al.*, 1997; Sarpeshkar *et al.*, 1998).

Like the visual system, the auditory system must also deal with a wide range of signal levels. Here again, adaptation (automatic gain control) plays an important role. In mammalian auditory systems the adaptation is specific to each frequency channel (Javel, 1986). In insects, responses of neurons in the central nervous system can also exhibit adaptation (*e.g.*, see Lewis, 1992).

Unlike the visual system, however, the auditory system is processing a very rapidly changing signal, one that often changes much faster than the biological hardware can follow. To circumvent the problem of following high-frequency signals, the receptor cells (hair cells) act as soft half-wave rectifiers (Mountain and Hubbard, 1996) so that at high frequencies they respond to the envelope of the acoustic signal rather than to the fine structure of the signal.

In the auditory system, temporal cross-correlation and autocorrelation-like processing is believed to play an important role (Colburn, 1996; Lyon and Shamma, 1996). In vertebrates, the time delay between the two ears (IID) is an important cue for localization. The combination of neural delay lines and coincidence detection is used to cross-correlate the signals from the two ears for each frequency channel. Periodicity analysis is believed to take place also using delays and coincidence detection. Periodicity analysis no doubt plays an important role for many species from insects to man, because so many communication sounds involve periodic amplitude modulation (AM). Figure 4 illustrates time waveforms in which AM is a prominent feature for a cricket call (panel A) and for a human vowel (panel C). Panels B and D show the results of spectral analysis using a constant-Q filter bank, and except for center frequency and modulation rate, the AM signals are remarkably similar.

Olfactory Scene Analysis

By analogy to the visual and auditory systems, we refer to the problem of identifying and localizing odor sources in complex environments as *olfactory scene analysis.* Unlike vision and hearing, in which the signal propagates *via* wave phenomena, olfaction is characterized by mass transport by currents in water or air and the associated turbulence found in these media (Grasso, 2001). No direct information about source location is present in the received signal, but approximate direction can be estimated by sensing wind or water-flow direction. The only way a source can be located with any certainty is to trace the odor plume back to its source.

In general, individual odor sources release mixtures of compounds into the environment, and the signal at the sensory organ is the result of the mixing of turbulent plumes from multiple sources. Due to the nature of turbulent transport, the plume produced by a single odor source is made up of a series of patches or filaments distributed within the plume; these move past the olfactory organ, creating a series

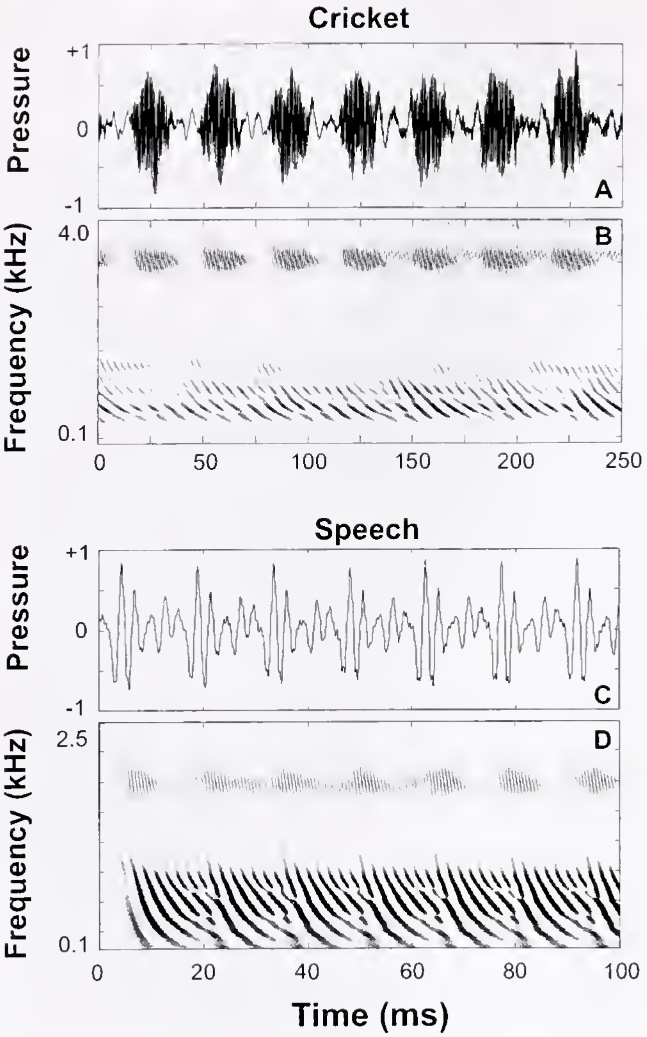

Figure 4. Spectral analysis of animal communication sounds. Time waveforms for a cricket call (panel A) and for a human vowel (panel C) are plotted along with the results of spectral analysis using a constant-Q filter bank (panels B and D).

of odor pulses at the receptors with random arrival times, durations, and amplitudes (Moore and Atema, 1991). The patchy nature of odor concentration signals can be seen in the two concentration signals shown in Figure 5. In a multi-source environment, the odor pulses from one source will be intermixed with pulses from other sources. In such an environment, the average concentration of a compound is not a useful feature for olfactory scene analysis. Even if only one odor source is present, the statistical nature of the plume is such that several minutes of signal averaging are necessary to get an accurate estimate of average concentration. However, behavioral experiments in plumes of this sort indicate that animals make olfactory decisions on the order of a few seconds (Basil and Atema, 1994).

Like the visual and auditory systems, the olfactory system must be able to cope with wide ranges in signal (concentration) level. Olfactory receptors, like their counterparts in the other sensory systems, also exhibit adaptation that adjusts the sensitivity of individual receptors on the basis of background concentration levels. Olfactory systems have many different receptor types, ranging from a few dozen in insects to approximately 1000 receptor types in mammals. Some receptors, mainly those that have evolved to detect pheromones, are extremely selective, but most will respond to a number of different compounds. The higher the selectivity of a receptor, the higher the affinity for the odor molecule and the slower the release of the odor molecule after it has bound to the receptor (Lauffenburger and Linderman, 1993). The relationship between high affinity and slow release comes about because affinity depends on the ratio of the binding to unbinding rates. The rate of binding is limited by the rate at which the odorant can access the binding site, a rate that is similar for all receptors. Affinity, therefore, varies from receptor to receptor, largely due to differences in the unbinding rate. This relationship means

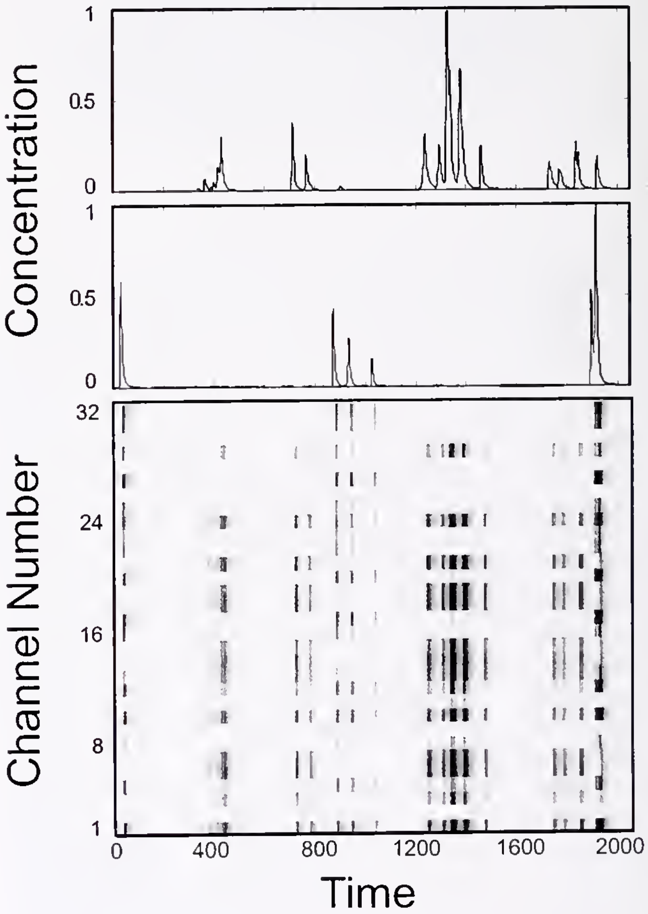

Figure 5. Simulation of how an array of olfactory receptor cells might respond to the mingling of odor plumes from two different sources. The top two panels show the concentration signals from the two sources, and the bottom panel is the response from a simulation of 32 receptors that vary in their sensitivity to the two odorants.

that high molecular selectivity leads to poor temporal resolution—not unlike the trade-off between frequency selectivity and temporal resolution in auditory filters.

Olfactory receptors have been shown to respond rapidly enough that the temporal characteristics of the concentration signals could be available to the central nervous system (Gomez and Atema, 1996). Since most odors are mixtures and a single olfactory receptor cell can be stimulated by more than one compound, the odor from a single source will excite a number of different receptor cells, with the pattern of excitation varying from one odor mixture to another. In Figure 5 we simulate how an array of olfactory receptor cells might respond to the mingling of odor plumes from two different sources. The top two panels show the concentration signals from the two sources, and the bottom panel is the response from a simulation of 32 receptors that vary in their sensitivity to the two odorants. One can see from Figure 5 that, as in the auditory system, grouping can be done using temporal cues. In other words, receptors whose activities co-vary in time are likely to be responding to the same odor source.

Hardware models of olfactory scene analysis have not progressed very far due to the lack of sensors with the combination of appropriate chemical selectivity and fast temporal responses. Most current experiments are being done with surrogate odor sources for which fast sensors are available. The systems used in these experiments are generally designed to locate the odor source and not to classify the odor type. Due to the difficulty of accurately simulating chemical plumes in software, artificial systems for olfactory scene analysis often involve the use of robots. For example, we have used an aquatic robot (RoboLobster) that uses conductivity sensors to locate sources of salt in a freshwater flume (Grasso *et al.*, 2000).

Summary and Conclusions

The comparisons of strategies for scene analysis across the three sensory modalities—visual, auditory, and olfactory—described above illustrate several common themes that operate across modalities. For example, we see the dissection of the sensory signal, its processing in parallel pathways to extract key features, and then the grouping of portions of the signal to form perceptual objects. In all three of these senses, adaptation plays an important role in the first stages of processing. Fundamental trade-offs such as spectral *versus* temporal resolution or molecular selectivity *versus* temporal resolution shape peripheral processing. The mathematical concept of cross-correlation and its neural counterpart, coincidence detection, show up over and over again. We believe that by comparing strategies for sensory processing across sensory modalities as well as across many different species we can derive fundamental principles of sensory information processing that can be used to design artificial systems capable of analyzing complex environments.

Acknowledgments

This work was funded in part by the Office of Naval Research.

Literature Cited

Basil, J., and J. Atema. 1994. Lobster orientation in turbulent odor plumes: simultaneous measurement of tracking behavior and temporal odor patterns. *Biol. Bull.* **187:** 272–273.

Boahen, K. A. 2000. Point-to-point connectivity between neuromorphic chips using address events. *IEEE Trans. Circuits Syst. II* **47:** 416–434.

Bregman, A. S. 1990. *Auditory Scene Analysis.* MIT Press, Cambridge, MA.

Colburn, H. S. 1996. Computational models of binaural processing. Pp. 332–400 in *Auditory Computation, Springer Handbook of Auditory Research*, H. L. Hawkins, T. A. McMullen, A. N. Popper, and R. R. Fay, eds. Springer Verlag, New York.

Echteler, S. M., R. R. Fay, and A. N. Popper. 1994. Structure of the mammalian cochlea. Pp. 134–171 in *Comparative Hearing. Mammals, Springer Handbook of Auditory Research*, R. R. Fay and A. N. Popper, eds. Springer Verlag, New York.

Fragniere, E., A. VanSchaik, and E. A. Vittoz. 1997. Design of an analogue VLSI model of an active cochlea. *Analog Integr. Circuits Signal Processing* **13:** 19–35.

Gomez, G., and J. Atema. 1996. Temporal resolution in olfaction: stimulus integration time of lobster chemoreceptor cells. *J. Neurophysiol.* **76:** 1340–1343.

Grasso, F. W. 2001. Invertebrate-inspired sensory-motor systems and autonomous, olfactory-guided exploration. *Biol. Bull.* **200:** 160–168.

Grasso, F. W., T. R. Consi, D. C. Mountain, and J. Atema. 2000. Biomimetic robot lobster performs chemo-orientation in turbulence using a pair of spatially separated sensors: progress and challenges. *Robot. Auton. Syst.* **30:** 115–131.

Hinck, T., and A. E. Hubbard. 1999. An analog VLSI image processing filter bank for enhancing oriented edge gradients. Pp. 897–902 in *Proc. 33rd Annual Conference on Information Sciences and Systems*, J. L. Prince and T. D. Tran, eds. Johns Hopkins University, Baltimore, MD.

Hoy, R. R. 1992. The evolution of hearing in insects as an adaptation to predation from bats. Pp. 115–139 in *The Evolutionary Biology of Hearing*, D. B. Webster, R. R. Fary, and A. N. Popper, eds. Springer Verlag, New York.

Hubel, D. H., and T. N. Wiesel. 1962. Receptive fields, binocular interaction and functional architecture in the cat's visual cortex. *J. Physiol. (Lond.)* **160:** 106–154.

Javel, E. 1986. Basic response properties of auditory nerve fibers. Pp. 213–245 in *Neurobiology of Hearing*, R. Altschuler and R. Bobbin, eds. Raven Press, New York.

Lauffenburger, D. A., and J. J. Linderman. 1993. *Receptors—Models for Binding, Trafficking, and Signalling.* Oxford University Press, Oxford.

Lewis, B. 1992. The processing of auditory signals in the CNS of Orthoptera. Pp. 95–114 in *The Evolutionary Biology of Hearing*, D. B. Webster, R. R. Fary, and A. N. Popper, eds. Springer Verlag, New York.

Lyon, R., and S. Shamma. 1996. Auditory representations of timbre and pitch. Pp. 221–270 in *Auditory Computation, Springer Handbook of Auditory Research*, H. L. Hawkins, T. A. McMullen, A. N. Popper, and R. R. Fay, eds. Springer Verlag, New York.

Marr, D. 1982. *Vision: A Computational Investigation into the Human Representation and Processing of Visual Information.* W. H. Freeman, San Francisco.

Mead, C. 1989. *Analog VLSI and Neural Systems.* Addison Wesley, Reading, MA.

Michelsen, A. 1992. Hearing and sound communication in small animals: evolutionary adaptations to the laws of physics. Pp. 61–77 in *The Evolutionary Biology of Hearing,* D. B. Webster, R. R. Fay, and A. N. Popper, eds. Springer Verlag, New York.

Michelsen, A. 1998. Biophysics of sound localization in insects. Pp. 18–62 in *Comparative Hearing: Insects, Springer Handbook of Auditory Research,* R. R. Hoy, A. N. Popper, and R. R. Fay, eds. Springer Verlag, New York.

Moore, P. A., and J. Atema. 1991. Spatial information in the three-dimensional fine structure of an aquatic odor plume. *Biol. Bull.* **181:** 408–418.

Mountain, D. C., and A. E. Hubbard. 1996. Computational analysis of hair cell and auditory nerve processes. Pp. 121–156 in *Auditory Computation, Springer Handbook of Auditory Research,* H. L. Hawkins, T. A. McMullen, A. N. Popper, and R. R. Fay, eds. Springer Verlag, New York.

O'Carroll, D. 1993. Feature-detecting neurons in dragonflies. *Nature* **362:** 541–543.

Pasupathy, A., and C. E. Connor. 1999. Responses to contour features in macaque area V4. *J. Neurophysiol.* **82:** 2490–2502.

Porat, M., and Y. Y. Zeevi. 1989. Localized texture processing in vision: analysis and synthesis in the Gaborian space. *IEEE Trans Biomed. Eng.* **36:** 115–129.

Sarpeshkar, R., R. F. Lyon, and C. Mead. 1998. A low-power wide-dynamic-range analog VLSI cochlea. *Analog Integrated Circuits Signal Processing* **16:** 245–274.

Webb, B., and T. Scutt. 2000. A simple latency-dependent spiking-neuron model of cricket phonotaxis. *Biol. Cybern.* **82:** 247–269.

Weldon, T., and W. E. Higgins. 1999. Designing multiple Gabor filters for multitexture image segmentation. *Optical Eng.* **38:** 1478–1489.

Zhang, S. W., M. V. Srinivasan, and T. Collett. 1995. Convergent processing in honeybee vision: multiple channels for the recognition of shape. *Proc. Natl. Acad. Sci. USA* **92:** 3029–3031.

Reference: *Biol. Bull.* **200:** 235–242. (April 2001)

Sensory Architectures for Biologically Inspired Autonomous Robotics

CHARLES M. HIGGINS

Neuromorphic Vision and Robotic Systems Laboratory, Department of Electrical and Computer Engineering, The University of Arizona, 1230 E. Speedway Blvd., Tucson, Arizona 85721

Abstract. Engineers have a lot to gain from studying biology. The study of biological neural systems alone provides numerous examples of computational systems that are far more complex than any man-made system and perform real-time sensory and motor tasks in a manner that humbles the most advanced artificial systems. Despite the evolutionary genesis of these systems and the vast apparent differences between species, there are common design strategies employed by biological systems that span taxa, and engineers would do well to emulate these strategies. However, biologically-inspired computational architectures, which are continuous-time and parallel in nature, do not map well onto conventional processors, which are discrete-time and serial in operation. Rather, an implementation technology that is capable of directly realizing the layered parallel structure and nonlinear elements employed by neurobiology is required for power- and space-efficient implementation. Custom neuromorphic hardware meets these criteria and yields low-power dedicated sensory systems that are small, light, and ideal for autonomous robot applications. As examples of how this technology is applied, this article describes both a low-level neuromorphic hardware emulation of an elementary visual motion detector, and a large-scale, system-level spatial motion integration system.

Engineers Have a Lot to Gain From Studying Biology

The architecture of biological sensory systems has something to teach conventional engineering about system-level design. Neurobiological representations of visual modalities including depth, motion, color, and form are quite unlike those employed by conventional computer vision systems. Neurobiological computational architectures are not modular, linear, or feedforward. And yet biological organisms routinely accomplish complex visual tasks such as object recognition, obstacle avoidance, and target tracking, which continue to challenge artificial systems.

Dealing with the complexity posed by the availability of a multitude of parallel sensors and a large number of redundant actuators is a major unsolved problem in modern computational systems. As we become more ambitious in our inclusion of computational systems into every possible device, more sensory inputs are available; more actuators are controlled by the computing system; more possible conditions must be recognized and appropriately dealt with. Engineers in fields from space-bound robotics and guided missile design to automotive navigation and prosthetics are beginning to realize the value of paying attention to biological solutions. The biological literature is replete with detailed analyses of systems that deal with complex sensory and motor control tasks and still manage to outperform, by any metric, anything created by mankind. In the papers in this collection (CASSLS, 2001), for example, Robert Barlow and colleagues describe a finely elaborated model of horseshoe crab visual processing, revealing how the crab manages to navigate and find mates in a highly variable and noisy underwater environment (Barlow *et al.*, 2001); Thomas Cronin and Justin Marshall give us insight into the marvelously complex mantis shrimp visual system, a

---

E-mail: higgins@ece.arizona.edu

This paper was originally presented at a workshop titled *Invertebrate Sensory Information Processing: Implications for Biologically Inspired Autonomous Systems.* The workshop, which was held at the J. Erik Jonsson Center for the National Academy of Sciences, Woods Hole, Massachusetts, from 15–17 April 2000, was sponsored by the Center for Advanced Studies in the Space Life Sciences at the Marine Biological Laboratory, and funded by the National Aeronautics and Space Administration under Cooperative Agreement NCC 2-896.

unique and highly specialized tool for predation (Cronin and Marshall, 2001); Mandyam Srinivasan and co-workers introduce us to the secrets of insect vision (Srinivasan *et al.*, 2001).

The daunting task for engineers is to produce—by abstraction from the specific organism—a set of general design principles to replace the top-down, linear, functional-block oriented strategies that characterize conventional design. These principles may include layered massively parallel processing, population coding, probabilistic information transmission, a mix of analog and digital coding strategies, connection-oriented architectures, removal of redundant information at every processing stage, positive as well as negative feedback, and the use of nonlinear computational elements (such as voltage-dependent conductances and neurons with adaptive properties), even though these elements make the system more difficult to describe analytically in closed form. Although the mathematical principles underlying conventional design are well known, it is not clear that we have the mathematical tools to analyze and design systems such as those suggested by neurobiology. However, these tools are being developed in the theory of nonlinear dynamical systems, as well as in the study of neurobiological systems themselves.

By building artificial sensory systems true to the representations and computational architectures used by neurobiology, we will be able to produce novel, highly capable autonomous robots, while at the same time suggesting testable hypotheses as to how biological systems accomplish sensory and motor tasks.

Efficient Implementation of Biological Computational Architectures

Because the primary computational strategy used by neurobiology is layered, massively parallel processing, an efficient parallel implementation is essential to make effective use of such computational architectures. Biological computational architectures, which are continuous-time parallel algorithms, map very badly onto conventional discrete-time serial processors. The conventional real-time implementation of a biological vision computation involves an imager providing discrete-time frames to a high-speed signal processor that *serially* performs a large number of operations that could be performed in *parallel*. In contrast, true parallel architectures may be straightforwardly implemented in neuromorphic VLSI (very large scale integration) hardware (Mead, 1989). This type of special-purpose hardware implements biological algorithms directly and efficiently in patterns of transistors, resistors, and capacitors. By making use of the physical primitives provided by electronic devices, highly efficient computations can be performed on signals represented by currents and voltages. Neuromorphic technology focuses on analog computation for efficiency, but in general mixes both analog and digital transistor circuitry. The implementation can be at a level of abstraction from the biophysical (Hahnloser *et al.*, 2000) to the neural (Boahen, 1999) to the mathematical (Higgins and Korrapati, 2000). The individual physical components in such a design are on the scale of micrometers and are fabricated together on a single piece of silicon measuring millimeters on a side, resulting in a physically robust compact package.

While general-purpose digital processors grow ever more powerful, special-purpose hardware will always be more efficient in power consumption and size for specific problems. This is because the former, by its nature, is not optimized for any specific computation, whereas the latter includes only the circuitry that is necessary for the problem at hand. The efficiency of a task-specific analog implementation comes at the price of precision and flexibility. The analog implementation of a computation is subject to inevitable noise that limits the possible precision, whereas a digital implementation can (potentially but usually not practically) be performed with virtually unlimited precision. The software implementation of a computation clearly has flexibility to change at the programmer's whim, whereas a dedicated hardware implementation is fixed at fabrication time. With awareness of these trade-offs, a designer will choose a special-purpose hardware solution where the power and size constraints are most important. This is often an appropriate choice in real-time vision applications on autonomous robots.

An Example of Neuromorphic Implementation: Low-Level Motion Detection

The neurobiological representation of visual motion in organisms from insects to primates is in terms of oriented spatiotemporal-frequency-tuned cells. The conventional *optical flow* representation is mathematically a vector field, allowing only one velocity of motion in every local area of the visual scene. The biological representation of visual motion is more powerful in that it allows multiple simultaneous directions of motion as long as they are distinguished in spatial or temporal frequency, making possible our perception of transparent motion and occlusion boundaries. However, the biological representation of motion requires a range of spatial- and temporal-frequency tunings to cover all stimuli of interest. Primates have a tremendous number of neurons (on the order of 10^{11}) and thus can afford to populate the whole spatiotemporal frequency space with a large bank of tuned neurons for each spatial location. Insects, with a much smaller set of neurons (on the order of 10^5), are forced to use a much smaller set of tunings, yet they operate very effectively in the same environment. Thus insects may provide engineers with a more neuron-efficient example of a visual motion system.

In a seminal 1985 paper, Adelson and Bergen proposed a model of the motion response of primate complex cells and showed it to be equivalent to the Reichardt (1961) model of elementary motion detection in the fly. We have implemented this *motion energy* model in neuromorphic VLSI hardware (Higgins and Korrapati, 2000), both to allow system-level hardware modeling of biological motion systems, addressed in the next section, and to provide a sensitive, real-time visual motion detector for robotic applications. Because of the lack of any digital thresholding step in the algorithm, motion energy sensors (like the motion-sensitive cells they model) are limited in contrast response only by signal-to-noise ratio, allowing them to perceive the direction of motion even for very low contrasts by integrating over time. The original algorithm, shown in Figure 1A, combines the response of four simple cells with a rectifying nonlinearity (a square) to create a spatiotemporal-frequency-tuned estimate of motion direction. Figure 1B shows how this model was implemented in hardware: several simplifications were made in the pursuit of a compact implementation, but the algorithm still performs a highly sensitive directional motion computation, as shown in Figure 2. This sensor was implemented with only 41 transistors, allowing hundreds or thousands of parallel sensors on a reasonably sized silicon substrate. Because of the analog implementation, each sensor consumes less than 40 microwatts of power, allowing large-scale parallel implementation without problematic power consumption or special cooling needs.

System-Level Neuromorphic Design: Spatial Motion Integration

As mentioned earlier, the spatiotemporal filter representation of motion common to a wide variety of organisms requires a range of spatial- and temporal-frequency tunings to cover all stimuli of interest and thus, unlike the conventional representation, must be implemented with a bank of filters for each spatial location. Once this bank of filters is computed, the information must be spatially integrated to be of use to the organism; in other words, information about spatial *patterns* of visual motion is more useful to the animal than the low-level motion information itself. This integration occurs in insect tangential neurons (Krapp and Hengstenberg, 1996) and in the medial superior temporal area (MST) of primate visual cortex (Perrone and Stone, 1998). This strategy suggests a computational architecture like that shown in Figure 3A, which includes a first-stage photosensitive array, a second stage of multiple parallel motion-processor arrays computing different spatial frequencies, orientations, and temporal frequencies, and a third integration stage that can synthesize units sensitive to wide-field spatial patterns of motion by combining spatial regions of low-level motion detectors.

We have implemented a preliminary version of such an architecture in neuromorphic VLSI hardware (Higgins and Shams, unpubl. data), as shown in Figure 3B. Each two-dimensional processing unit is implemented as a separate VLSI chip; chips communicate using trains of spikes modeling action potentials. This multi-chip neuromorphic VLSI system is capable of synthesizing units sensitive to complex arbitrary patterns of visual motion, including expansion, contraction, rotation, and translation, as shown in Figure 4. These patterns, along with more elaborate ones, allow determination of imager self-motion through the world for postural stability and navigation (Zemel and Sejnowski, 1998), tracking of objects (Gronenberg and Strausfeld, 1991), and obstacle avoidance (Gabbiani *et al.*, 1999). Despite the multi-chip nature of the system, it is still a compact, robust, low-power special-purpose computing system ideal for robotic applications.

Summary

This article contends that biological representations and computational architectures are useful in a wide range of engineering problems. However, in practice, it is difficult to separate biological algorithms from their implementation, and so we also present an implementation technology, neuromorphic VLSI, which is well suited for physical realization of these algorithms. A low-level motion processor based on the Adelson-Bergen model was described to illustrate how a biological model may be directly mapped onto an analog VLSI transistor circuit for highly efficient implementation. From an engineer's perspective, this sensor benefits not only from the biological representation, but also from the analog nature of the biological model computation. A multi-stage motion-processing system was also described, exemplifying a biologically inspired computing architecture that also uses representations inspired by biology. This architecture is very well matched to the vision problem and allows a specific useful computation to be done with very low requirements for power consumption and size. It is the author's contention that systems of this type are the best hope for future highly capable small autonomous robotic systems.

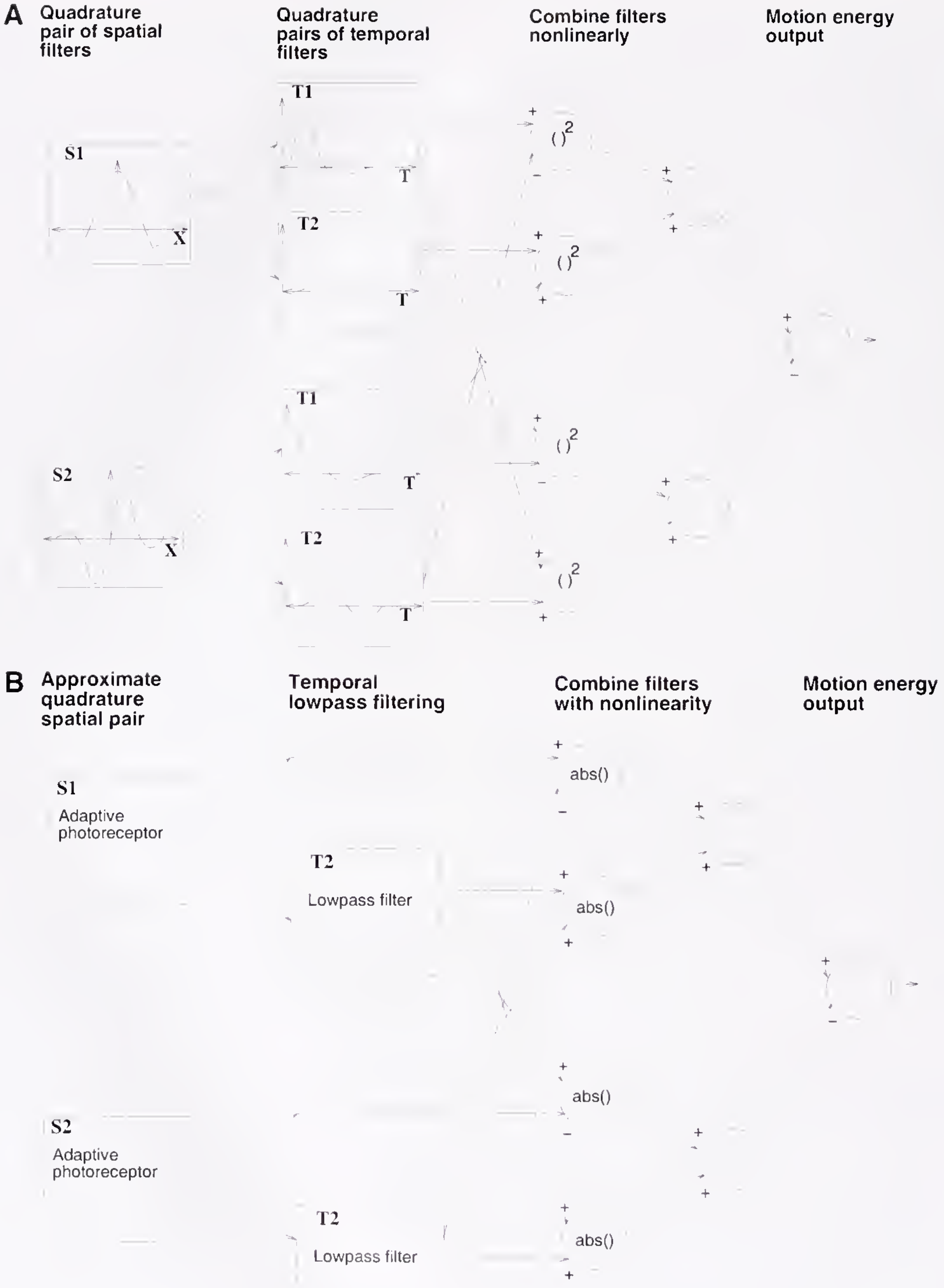
A
Quadrature pair of spatial filters
Quadrature pairs of temporal filters
Combine filters nonlinearly
Motion energy output
S1
X
S2
X
T1
T
T2
T
T1
T
T2
T
$()^2$
$()^2$
$()^2$
$()^2$
+
−
B
Approximate quadrature spatial pair
Temporal lowpass filtering
Combine filters with nonlinearity
Motion energy output
S1
Adaptive photoreceptor
S2
Adaptive photoreceptor
T2
Lowpass filter
T2
Lowpass filter
abs()
abs()
abs()
abs()
+
−

Figure 1. Low-level motion detection. (A) The canonical Adelson-Bergen motion energy model combines each of an even and odd spatial Gabor filter with two temporal bandpass filters to create the output of four linear simple cells. The output of these simple cells is combined nonlinearly in quadrature pairs to create a phase-independent motion direction estimate, which models a primate complex cell. (B) For hardware implementation, the spatial filters were implemented with a center-surround diffusive network, and the temporal filters by using a single lowpass filter. Rather than using a squaring operation, a simpler rectifying nonlinearity (the absolute value) was employed. The output of the implementation is quite comparable to the original model.

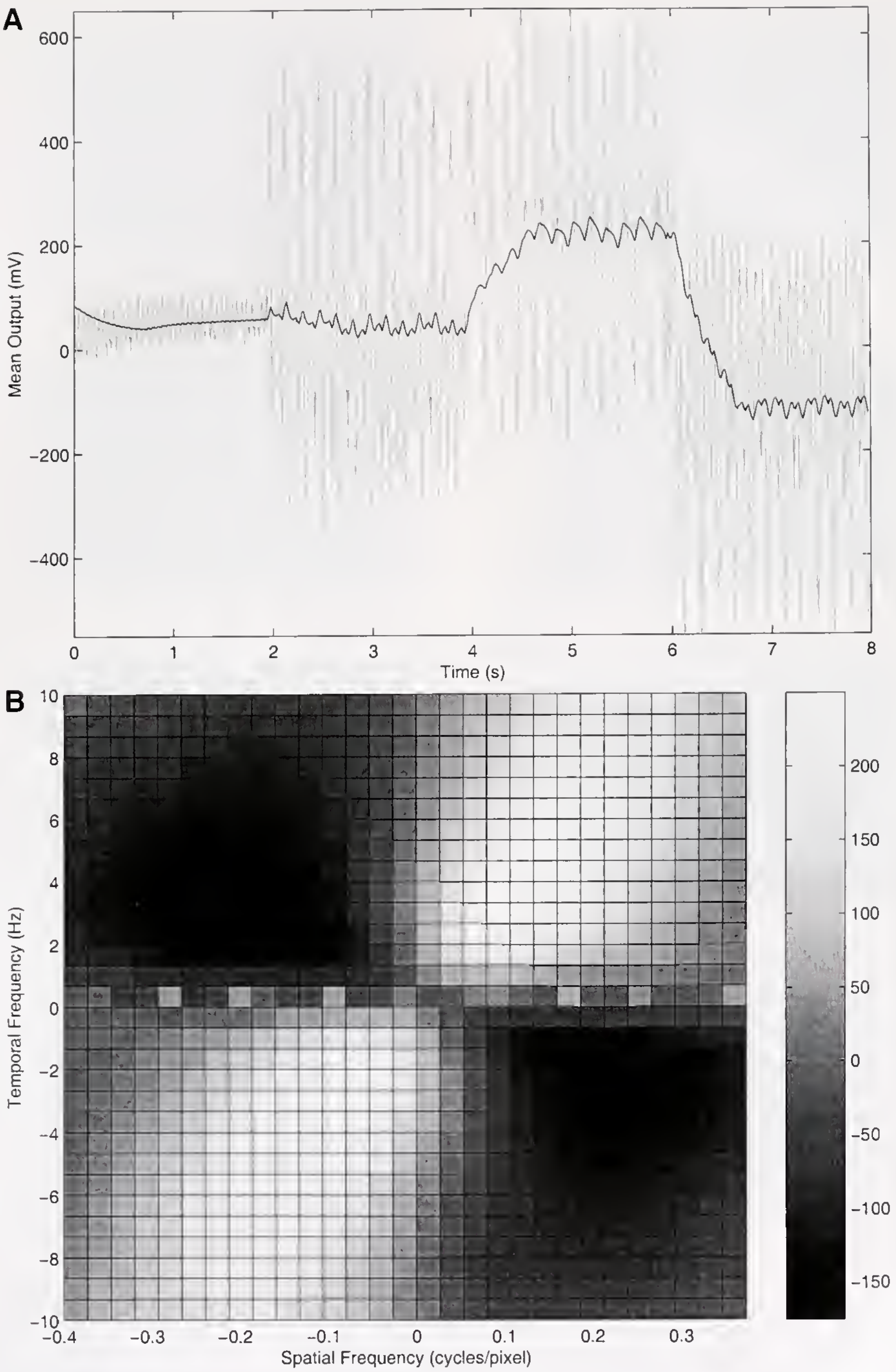

Figure 2. Output of the low-level motion detector. (A) The output of the hardware motion sensor is shown in response to no stimulus (under fluorescent lighting), an orthogonal, preferred and null direction sinusoid grating. The lighter traces represent raw output; darker lines are averaged output. (B) As the spatial and temporal frequency of a moving sinusoidal stimulus is varied, the sensor shows a strong preference in a certain band of frequencies.

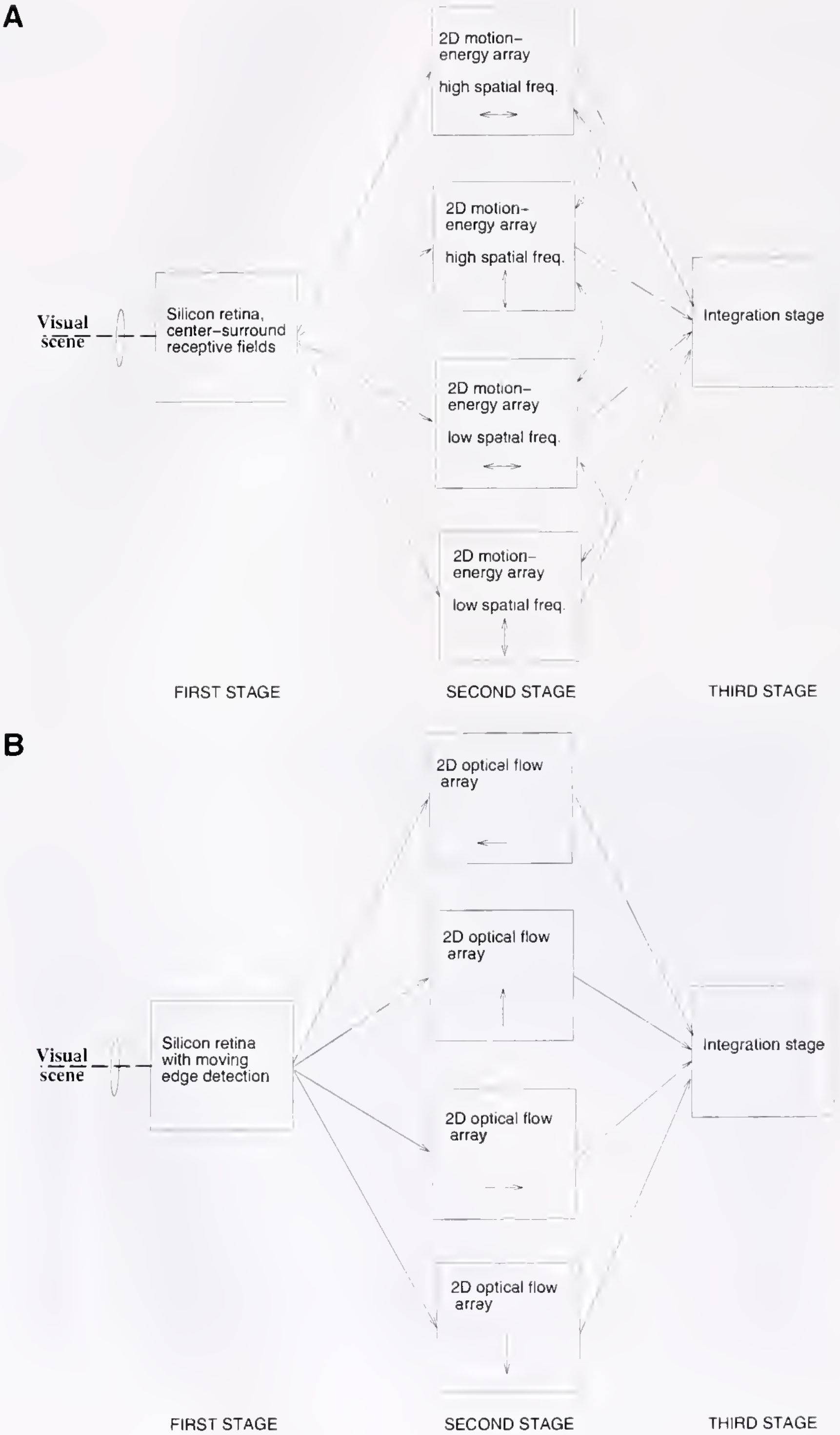
A
2D motion–energy array
high spatial freq.
2D motion–energy array
high spatial freq.
Visual scene
Silicon retina, center–surround receptive fields
Integration stage
2D motion–energy array
low spatial freq.
2D motion–energy array
low spatial freq.
FIRST STAGE
SECOND STAGE
THIRD STAGE
B
2D optical flow array
2D optical flow array
Visual scene
Silicon retina with moving edge detection
Integration stage
2D optical flow array
2D optical flow array
FIRST STAGE
SECOND STAGE
THIRD STAGE

Figure 3. Architecture for spatial motion integration. (A) In the idealized system, a first-stage silicon retina is followed by multiple second-stage motion processors tuned for different orientations and spatial and temporal frequencies. Interaction is allowed between second-stage motion processors. The final stage integrates over space to synthesize sensitivity to patterns of visual motion. (B) In the current system, the silicon retina detects moving edges and transmits this information to the next stage. The second-stage motion processors use the moving edge information to compute the direction of edge motion, with each of four processors tuned for a different direction of motion. The final stage synthesizes spatial motion sensitivity.

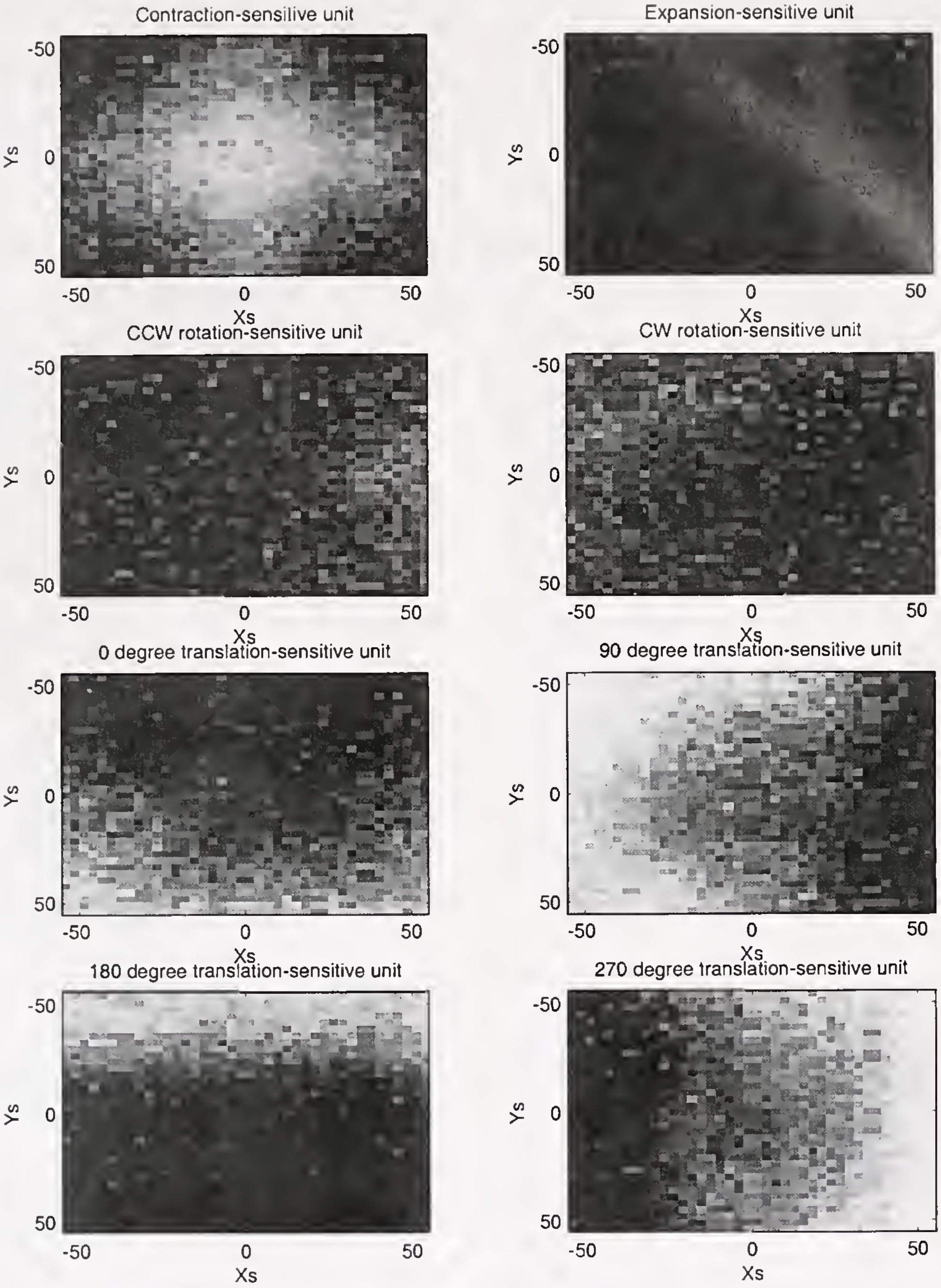

Figure 4. Performance of the spatial motion integration system. This figure shows the response of eight simultaneously synthesized units to a wide-field stimulus—a periodically contracting circle—as the focus of contraction is moved around the visual field. Lighter shading indicate stronger responses. The upper left unit is tuned for contraction at the center of the visual field and thus shows a strong response there. The upper right unit is tuned for expansion and thus shows no response. In the second row from the top, units tuned for clockwise and counterclockwise rotation likewise show little or no response. However, units shown at the bottom tuned for translation in four different directions show a strong response when the focus of contraction nears the appropriate edge of the visual field, because the farther the contracting pattern gets from the center, the more similar it becomes to a simple translating pattern.

Acknowledgments

The author gratefully acknowledges support for this research by the National Science Foundation through the California Institute of Technology Center for Neuromorphic Systems Engineering as part of the Engineering Research Centers program, by the Office of Naval Research under grant number N00014-97-1-0970, and by the National Science Foundation's State/Industry/University Cooperative Research Center for Low Power Electronics (CLPE). CLPE is supported by NSF (Grant #EEC-9523338), the State of Arizona, and the following companies and foundations: Burr-Brown, Inc., Conexant, Gain Technology, Intel Corporation, Medtronic Microelectronics Center, Microchip Technology, Motorola, Inc., The Motorola Foundation, Raytheon, Texas Instruments, and Western Design Center. The author also thanks the anonymous reviewers for their assistance in clarifying this manuscript.

Literature Cited

Adelson, E. H., and J. R. Bergen. 1985. Spatiotemporal energy models for the perception of motion. *J. Opt. Soc. Am. A* 2(2): 284–299.

Barlow, R. B., J. M. Hitt, and F. Dodge. 2001. *Limulus* vision in the marine environment. *Biol. Bull.* **200:** 169–176.

Boahen, K. 1999. Retinomorphic chips that see quadruple images. In *Proceedings of the 7th International Conference on Microelectronics for Neural, Fuzzy and Bio-inspired Systems,* University of Granada, Spain, 7–9 April 1999.

CASSLS (The Center for Advanced Studies in the Space Life Sciences). 2001. Invertebrate sensory information processing: implications for biologically inspired autonomous systems. *Biol. Bull.* **200:** 145–245.

Cronin, T., and J. Marshall. 2001. Parallel processing and image analysis in the eyes of mantis shrimps. *Biol. Bull.* **200:** 177–183.

Gabbiani, F., H. Krapp, and G. Laurent. 1999. Computation of object approach by a wide-field, visual neuron. *J. Neurosci.* **19:** 1122–1141.

Gronenberg, W., and N. J. Strausfeld. 1991. Descending pathways connecting the male-specific visual system of flies to the neck and flight motor. *J. Comp. Physiol. A* **169:** 413–426.

Hahnloser, R. H. R., R. Sarpeshkar, M. A. Mahowald, R. J. Douglas, and H. S. Seung. 2000. Digital selection and analogue amplification coexist in a cortex-inspired silicon circuit. *Nature* **405:** 947–951.

Higgins, C. M., and S. K. Korrapati. 2000. An analog VLSI motion energy sensor based on the Adelson-Bergen algorithm. In *Proceedings of the International ICSC Symposium on Biologically-Inspired Systems,* Wollongong, Australia, 12–15 December 2000.

Krapp, H. G., and R. Hengstenberg. 1996. Estimation of self-motion by optic flow processing in single visual interneurons. *Nature* **384:** 463–466.

Mead, C. A. 1989. *Analog VLSI and Neural Systems.* Addison-Wesley, Reading, MA.

Perrone, J. A., and L. S. Stone. 1998. Emulating the visual receptive-field properties of MST neurons with a template model of heading estimation. *J. Neurosci.* **18**(15): 5958–5975.

Reichardt, W. 1961. Autocorrelation, a principle for the evaluation of sensory information by the central nervous system. Pp. 303–317 in *Sensory Communication,* W. A. Rosenblith, ed. MIT Press, Cambridge, MA.

Srinivasan, M., S. Zhang, and J. S. Chahl. 2001. Landing strategies in honeybees, and possible applications to autonomous airborne vehicles *Biol. Bull.* **200:** 216–221.

Zemel, R. S., and T. J. Sejnowski. 1998. A model for encoding multiple object motions and self-motion in area MST of primate visual cortex. *J. Neurosci.* **18**(1): 531–547.

Reference: *Biol. Bull.* **200:** 243–245. (April 2001)

Participants

Barry W. Ache
University of Florida
Whitney Laboratory
9505 Ocean Shore Blvd.
St. Augustine, FL 32086

Raymond Arvidson
Washington University in St. Louis
McDonnell Hall
One Brookings Drive, Box 1169
St. Louis, MO 63130

Jelle Atema
Boston University Marine Program
7 MBL Street
Woods Hole, MA 02543

Joseph Ayers
Northeastern University
Marine Science Center
Nahant, MA 01908

Robert Barlow
SUNY Upstate Medical University at Syracuse
Center for Vision Research
750 E. Adams Street, 3258 Weiskotten Hall
Syracuse, NY 13210

Jennifer Basil
Brooklyn College
Department of Biology
2900 Bedford Avenue
Brooklyn, NY 11210

Jim Belanger
Tufts University
Department of Biology
Dana Lab
Medford, MA 02155

John Birmingham
Brandeis University
Volen Center for Complex Systems
MS-013
Waltham, MA 02454

Diana Blazis
Center for Advanced Studies in the Space Life Sciences
7 MBL Street
Woods Hole, MA 02543

Thomas Breithaupt
University of Konstanz
Faculty of Biology
D-78457 Konstanz, Germany

Chuan-Chin Chiao
University of Maryland, Baltimore County
Department of Biological Sciences
Baltimore, MD 21250

Thomas Consi
Massachusetts Institute of Technology
Department of Ocean Engineering
77 Massachusetts Avenue, Room 5-221
Cambridge, MA 02139

Thomas Cronin
University of Maryland, Baltimore County
Department of Biological Sciences
100 Hilltop Circle
Baltimore, MD 21250

Jonathan Dale
Boston University Marine Program
Marine Biological Laboratory
7 MBL Street
Woods Hole, MA 02543

Charles Derby
Georgia State University
Biology Department
P.O. Box 4010
Atlanta, GA 30302-4010

Frederick Dodge
SUNY Upstate Medical University at Syracuse
Center for Vision Research
Department of Physiology, 3260 Weiskotten Hall
Syracuse, NY 13210

NICOLAS FRANCESCHINI
CNRS / LNB3
Neurocybernetics Research Group
31, Chemin J. Aiguier
J. Aiguier Avenue 31
Marseille, France 13009

PETER FRASER
University of Aberdeen, UK
Department of Zoology
Tillydrone Avenue
Aberdeen, AB24 2TZ United Kingdom

CATHERINE GOLDEN
Fundamental Biology Research Program
NASA Ames Research Center
MS 19-20
Moffett Field, CA 94035

FRANK GRASSO
Visiting Assistant Professor
Department of Psychology
Brooklyn College
Brooklyn, NY 11210

ROGER HANLON
Marine Biological Laboratory
Marine Resources Center (MRC)
7 MBL Street
Woods Hole, MA 02543

ADAM HAYES
California Institute of Technology (136-93)
Microsystems Lab
Pasadena, CA 91125

CHARLES HIGGINS
University of Arizona
Department of Electrical & Computer Engineering
1230 E. Speedway Blvd.
Tucson, AZ 85721-0104

JOHN HINES
Fundamental Biology Research Program
NASA Ames Research Center
MS 19-20
Moffett Field, CA 94035

OWEN HOLLAND
California Institute of Technology (136-93)
Microsystems Lab
Pasadena, CA 91125

ALLYN E. HUBBARD
Boston University
Electrical & Computer Engineering
Boston, MA 02215

HIROSHI ISHIDA
Georgia Institute of Technology
School of Chemistry and Biochemistry
Atlanta, GA 30332-0400

ELLIS LOEW
Cornell University
Department of Biomedical Sciences
S1-086 Schurman Hall
Ithaca, NY 14853

DAVID MACMILLAN
The University of Melbourne
Dept. of Zoology
Parkville Victoria 3052 Australia

MEGAN MAHAFFY
Montana State University
Center for Computational Biology
30 AJM Johnson Hall
Bozeman, MT 59717

JOHN P. MILLER
Montana State University
Center for Computational Biology
30 AJM Johnson Hall
Bozeman, MT 59717

DAVID MOUNTAIN
Boston University
Department of Biomedical Engineering
44 Cummington Street
Boston, MA 02215

LESLIE OSBORNE
University of California - San Francisco
Dept. of Physiology - Sloan Center for Theoretical Neurobiology
513 Parnassus Ave., Room 0444
San Francisco, CA 94143-0444

DANIEL ROBERT
Laboratory of Bioacoustics
Institute for Zoology, Universität Zuerich
CH-8057 Zurich, Switzerland

JOSEF SCHMITZ
University of Bielefeld
Department of Biological Cybernetics
D-33501 Bielefeld, Germany

NADAV SHASAR
The Interuniversity Inst. of Eilat
Eilat, 88103, Israel

BRIAN SMITH
Ohio State University
Department of Entomology
1735 Neil Avenue
Columbus, OH 43210

MANDYAM SRINIVASAN
Australian National University
Centre for Visual Science – Research School
P.O. Box 475
Canberra, ACT 2601 Australia

PASCAL STEULLET
Georgia State University
Biology Department
P.O. Box 4010
Atlanta, GA 30302-4010

MARK A. STOPFER
California Institute of Technology
Pasadena, CA 91125

BARBARA WEBB
University of Stirling
Department of Psychology
Scotland, UK

WILLIAM "RED" WHITTAKER
Carnegie Mellon University
Robotics Institute
5000 Forbes Avenue
Pittsburg, PA 15213

JAN WITTING
Marine Science Center
East Point
Nahant, MA 01908

MARK WILLIS
University of Arizona
Hildebrand Lab - ARL Division of Neurobiology
P.O. Box 210077
Tucson, AZ 85721-0077

GERALDINE WRIGHT
Ohio State University
Department of Entomology
1735 Neil Avenue
Columbus, OH 43210

MARINE BIOLOGICAL LABORATORY

MBL EDUCATIONAL OPPORTUNITIES

Educational Programs at the Marine Biological Laboratory (MBL) provide opportunities for intensive academic inquiry under the guidance of expert and distinguished faculty The teaching staff of each MBL course is drawn from a variety of reseach institutions and frequently outnumbers the student enrollment.

Summer Courses have been a central part of the Laboratory's mission since its founding more than a century ago. The opportunity for exchange with members of the summer research community, as well as for intensive individual research, makes these programs unique in science education Summer courses last from six to nine weeks, and consist of formal lectures integrated with laboratory instruction and research. Laboratories emphasize application of the most current techniques. Summer courses are designed for graduate students, postdocs and independent investigators actively engaged in research Summer course topics include:

Biology of Parasitism ~ Embryology ~ Microbial Diversity ~ Neural Systems & Behavior ~ Neurobiology ~ Physiology

Special Topics Courses are intensive educational programs, one to five weeks long, providing experience in specialized research techniques, or are lecture and laboratory courses in topics of current interest. Generally, these courses are designed for graduate students, postdoctoral fellows, and other professionals actively engaged in research

MBL courses are supported by a wide range of donors The overall MBL educational program has been underwritten by gifts from the Howard Hughes Medical Institute and the Burroughs Wellcome Fund.

Visit our website to learn more about courses offered
at the Marine Biological Laboratory.
http://courses.mbl.edu

Marine Biological Laboratory ~ 7 MBL Street ~ Woods Hole, MA 02543 ~ (508) 548-3705

AxioCam
ZEISS
Achromatiu...
eg

Digital Imaging Platform

Meet the challenges of the digital age with **Axioplan 2 Imaging**. Not just a new microscope but a flexible system designed for the future – the digital imaging platform. A system that is set up and controlled by computer, with images captured and stored by computer, that communicates with other computers – truly digital from start to finish.

Combine with **AxioVision** software, with its built-in microscope control, and the new **AxioCam** ultra-high resolution digital camera and you have pure synergy – microscopy and more. Make yours the future-proof choice for high resolution image capture, image processing, archiving – even tele-microscopy. The digital age is with us. Are you?

Carl Zeiss, Inc.
Microscopy & Imaging Systems
One Zeiss Drive
Thornwood, NY 10594

800.233.2343, ext. 7858
micro@zeiss.com
www.zeiss.com/micro

ZEISS

Volume 200

Number 3

THE BIOLOGICAL BULLETIN

JUNE 2001

Published by the Marine Biological Laboratory

Thanks Galileo, Hooke and Leeuwenhoek for the incentive.

We walk in the footsteps of visionaries. And see with the eyes of disciples.

Galileo up close: astronomer, physicist, mathematician, dethroner of Aristotle, defender of Copernicus and, yes, credited with making double convex lenses and the first biological observations with a microscope. A compound microscope. In 1624.

Hooke: 43 years later, the compound microscope reveals living things are composed of cells.

Leeuwenhoek: invents the first practical microscope and discovers bacteria.

Armed with the knowledge and inspiration of these and other Olympians, secure in the history of our own accomplishments and aware that the mind's eye should always focus on challenging the enigmatic as well as the undeniable, Olympus has created the BX2 series of clinical and research microscopes, noteworthy for their enhancements in optics, imaging and ergonomics.

And each so individual, it deserves the nomenclature My Microscope.

From possibility to actuality, it is wonderful to behold. *A posse ad esse est mirabile visu.*

Welcome to the next golden age of microsopy.

BX2 Microscope Series

The BX41

The new standard in laboratory microscopy vis-a-vis performance, versatility, operation.

Uncanny digitized imaging: enhanced with the **DP11 digital camera**, delivering high-resolution image recording beyond the norm.

Unusually insightful optics: observe magnifications from **1.25x to 100x without changing the condenser.** Choice of condensers includes Abbe, swing-out, phase-contrast and darkfield.

Unerringly precise-motion stage: selectable for right/left hand. Discover speed, ease, touch, comfort, and clinical accuracy.

Uncommonly easy-to-operate controls: extended fine-focus knob; forwarded-positioned illumination intensity dial; tactile X-Y control.

The BX45

The new standard in ergonomic microscopy. A dramatic metamorphosis: innovative, intelligent, insightful design improvements specifically addressing the needs of those spending hours looking through a microscope.

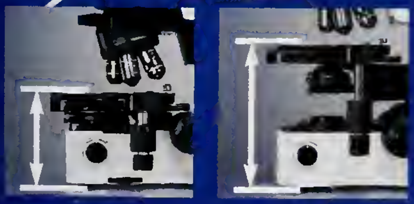

The **lowest low-position stage: three inches lower** than standard microscopes, offering the promise of minimum effort and hand movement when changing specimens.

The **tilting, telescoping observation tube:** a marvel of adjustability, it can be changed to accommodate any observation position. 80mm higher and 70mm closer to the operator than a conventional tilting tube. And the eyepoint can be moved forward by 45mm and inclined from 0–25 degrees.

The BX51

The new standard in research microscopy. The words "new" and "standard" really don't do it justice. How about "ingenious" or "original," "paragon" or "prototypical." Prepare yourself for a higher power.

The **6-position filter cube turret:** Not 4, not 5, but 6, so single and multiband imaging of new fluorochromes and fluorescent proteins is faster, simpler and exclusively tailored.

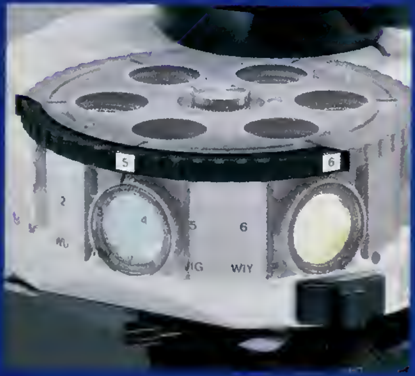

The **rectangular field stop: ours alone.** By cleverly matching the camera's field of view, only the area requiring fluorescence excitation is exposed. Which means that the surrounding areas are protected from photo bleaching.

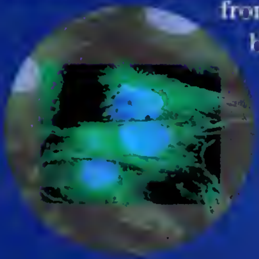

The **fluorescence excitation balancers:** another **Olympus exclusive.** A continuously variable excitation bandwidth. Visualization is enhanced, differentiation of multi-labels is immeasurably improved, capturing of images is at an unheard-of level.

Triple Labeled Specimen (l to r):

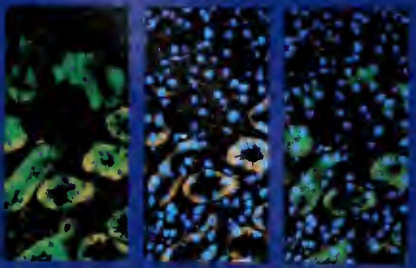

- with prevalent FITC and Cy3
- with prevalent DAPI and Cy3
- with balanced fluorescence emission

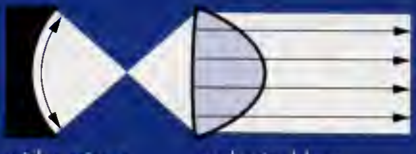

The **aspherical collector lens:** *sui generis*, in a class by itself. Specimens appear **brighter** and **more evenly illuminated**; and achromatic performance now incorporates wavelengths from UV to IR.

The **universal condenser: with 8 positions**, it can accept optical inserts for DIC, phase, brightfield and darkfield illumination. And the advanced Nomarski DIC system has been expanded and optimized to encompass prisms for enhanced contrast and image resolution.

OLYMPUS®

FOCUS ON LIFE

Visit us at www.olympusamerica.com
or call 1-800-455-8236

© Olympus America Inc.

MARINE RESOURCES CENTER

MARINE BIOLOGICAL LABORATORY • WOODS HOLE, MA 02543 • (508)289-7700
WWW.MBL.EDU/SERVICES/MRC/INDEX.HTML

zebrafish facilities

Animal and Tissue Supply for Education & Research

- 150 aquatic species available for shipment via online catalog: <http://www.mbl.edu/animals/index.html>; phone: (508)289-7375; or e-mail: specimens@mbl.edu
- zebrafish colony containing limited mutant strains
- custom dissection and furnishing of specific organ and tissue samples

MRC Services Available

- basic water quality analysis
- veterinary services (clinical, histopathologic, microbial services, health certificates, etc.)
- aquatic systems design (mechanical, biological, engineering, etc.)
- educational tours and collecting trips aboard the R/V Gemma

Using the MRC for Your Research

- capability for advanced animal husbandry (temperature, light control, etc.)
- availability of year-round, developmental life stages
- adaptability of tank system design for live marine animal experimentation

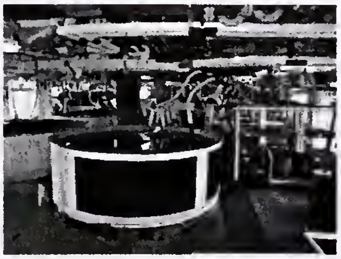

Wait until you see what 12 million pixels of capture resolution gets you. The DXM1200, designed exclusively for photomicrography, provides ultra high fidelity color reproduction and resolution virtually equal to film.

In addition, the DXM1200 comes complete with Nikon's highly intuitive ACT-1™ software with:

- 12 frames per second data transfer for faster image capture than you ever thought possible.
- Image archiving and retrieval that's faster and simpler than ever before.

To find out more about the surprisingly affordable DXM1200 digital camera, call **1-800-52-NIKON ext. 380**.

For complete tutorials of the ACT-1 software and a gallery of DXM1200 images, visit MicroscopyU at our newly designed website **www.nikonusa.com**

Nikon
Nikon PHOTO HEAD V TP
CAMERA POSITION
Nikon

NOW YOU'RE TALKING HIGH RESOLUTION

GET LARGER, MORE VIVID MICROSCOPY IMAGES FROM NIKON'S DXM1200 ULTRA-HIGH RESOLUTION DIGITAL CAMERA.

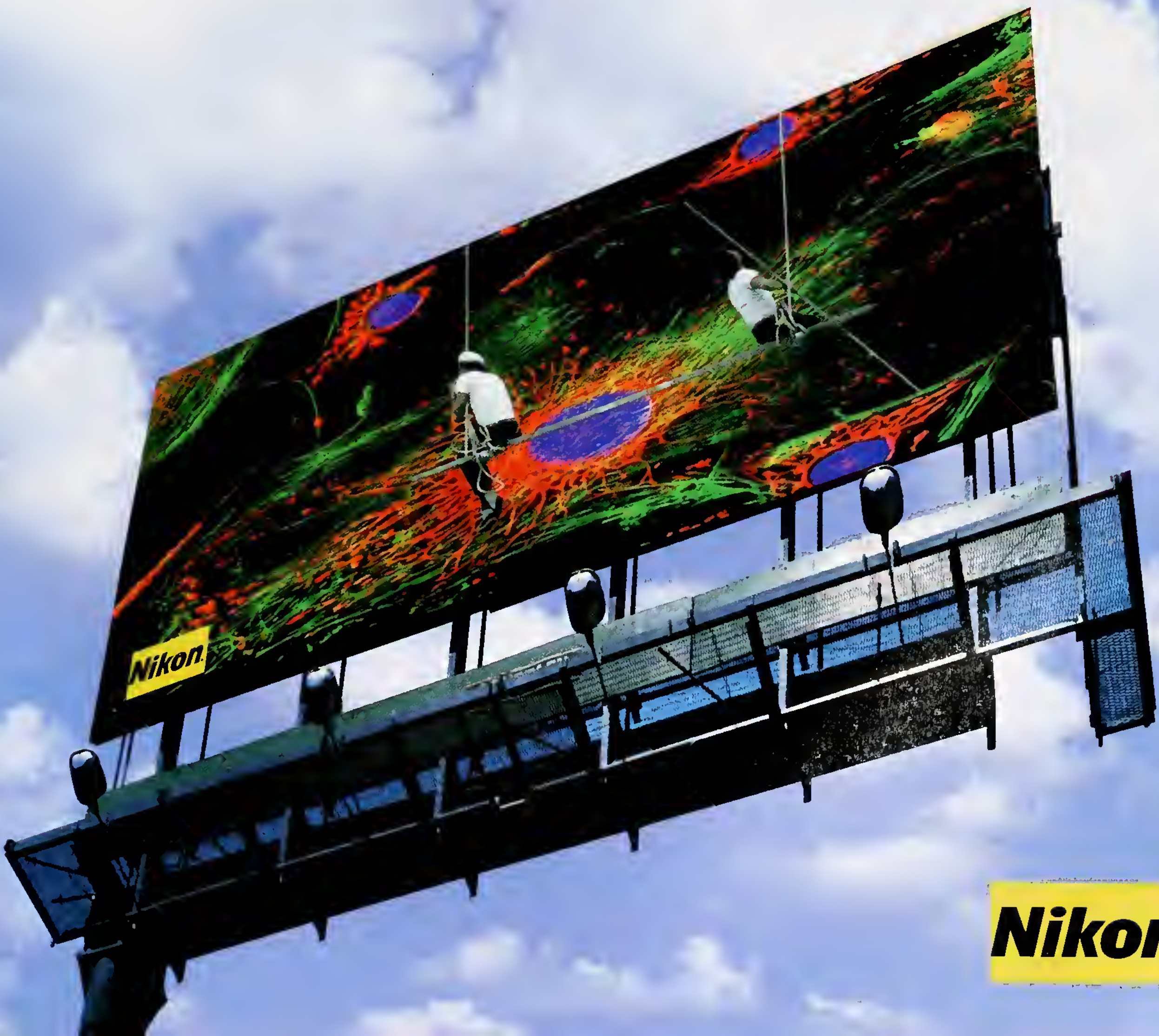

Nikon

© 2001 Nikon Instruments Inc.

THE
BIOLOGICAL BULLETIN

JUNE 2001

Marine Biological Laboratory
Woods Hole Oceanographic Institution
Library

JUN 26 2001

Woods Hole, MA 02543

Editor	Michael J. Greenberg	The Whitney Laboratory, University of Florida
Associate Editors	Louis E. Burnett	Grice Marine Biological Laboratory, College of Charleston
	R. Andrew Cameron	California Institute of Technology
	Charles D. Derby	Georgia State University
	Michael LaBarbera	University of Chicago
Section Editor	Shinya Inoué, *Imaging and Microscopy*	Marine Biological Laboratory
Online Editors	James A. Blake, *Keys to Marine Invertebrates of the Woods Hole Region*	ENSR Marine & Coastal Center, Woods Hole
	William D. Cohen, *Marine Models Electronic Record and Compendia*	Hunter College, City University of New York
Editorial Board	Peter B. Armstrong	University of California, Davis
	Ernest S. Chang	Bodega Marine Lab., University of California, Davis
	Thomas H. Dietz	Louisiana State University
	Richard B. Emlet	Oregon Institute of Marine Biology, Univ. of Oregon
	David Epel	Hopkins Marine Station, Stanford University
	Gregory Hinkle	Cereon Genomics, Cambridge, Massachusetts
	Makoto Kobayashi	Hiroshima University of Economics, Japan
	Esther M. Leise	University of North Carolina Greensboro
	Donal T. Manahan	University of Southern California
	Margaret McFall-Ngai	Kewalo Marine Laboratory, University of Hawaii
	Mark W. Miller	Institute of Neurobiology, University of Puerto Rico
	Tatsuo Motokawa	Tokyo Institute of Technology, Japan
	Yoshitaka Nagahama	National Institute for Basic Biology, Japan
	Sherry D. Painter	Marine Biomed. Inst., Univ. of Texas Medical Branch
	J. Herbert Waite	University of California, Santa Barbara
	Richard K. Zimmer	University of California, Los Angeles
Editorial Office	Pamela Clapp Hinkle	Managing Editor
	Victoria R. Gibson	Staff Editor
	Carol Schachinger	Editorial Associate
	Wendy Child	Subscription & Advertising Secretary

Published by
Marine Biological Laboratory
Woods Hole, Massachusetts

Cover

Christmas Island, a territory of Australia in the Indian Ocean south of Java, is the summit of a submarine mountain that rises 361 m above sea level to a central plateau. Twenty-three species of air breathing crabs are endemic to Christmas Island, but the red crab *Gecarcoidea natalis*, with an adult population estimated at about 50 million, is the most numerous. For most of the year, the red crabs inhabit burrows in the floor of the rainforests that grow on the island's plateau. Thus, this species is fully terrestrial, except for a three-week marine larval stage—a feature of the reproductive biology that necessitates the spectacular annual mass migration, from the forest down to the coast. The red crab migration is initiated by the start of the monsoonal rains, but spawning is synchronized with the lunar cycle, and all of the female crabs release their eggs into the sea on just one or two nights of the year. As the front cover shows, the morning after the females spawn, the rocks and cliffs lining the entire shoreline of Christmas Island are packed shoulder to shoulder with red crabs.

Although the mass migration of *G. natalis* is a well-documented phenomenon—indeed a tourist attraction—the descriptions are primarily anecdotal, and quantitative data are very limited. In this issue (pp. 305-320), A. M. Adamczewska and S. Morris establish, for the first time, such fundamental ethological details as the routes taken by the migrating red crabs, their direction and speed of walking, and their destinations.

The red crab breeding season, which can last from 3 to 6 weeks, is the most active period of the year for these animals; their activities include the unusually long migration, intense courtship behaviors, mating, and spawning. Moreover, these activities follow an extended period of relative inactivity during the dry season. Such varied activity levels impose quite different physiological demands on the red crabs. In a companion paper (pp. 321-335), Adamczewska and Morris have assessed the physiological demands of migratory locomotion and of activities related to breeding. They measured key metabolites, metabolic fuel stores, metabolic status, and thus the capacity of the red crabs to maintain their varied activities.

(The photograph on the cover was taken by Agnieszka Adamczewska.)

CONTENTS

VOLUME 200, NO. 3: JUNE 2001

RESEARCH NOTES

Rees, Bernard B., John A. L. Bowman, and Patricia M. Schulte
Structure and sequence conservation of a putative hypoxia response element in the lactate dehydrogenase-B gene of *Fundulus* 247

Okada, T., S. Stanley MacIsaac, Y. Katsuyama, Y. Okamura, and I. A. Meinertzhagen
Neuronal form in the central nervous system of the tadpole larva of the ascidian *Ciona intestinalis*. 252

Hickman, Carole S., and Michael G. Hadfield
Larval muscle contraction fails to produce torsion in a trochoidean gastropod 257

DEVELOPMENT AND REPRODUCTION

Paterson, Ian G., Vanessa Partridge, and John Buckland-Nicks
Multiple paternity in *Littorina obtusata* (Gastropoda, Littorinidae) revealed by microsatellite analyses. . . . 261

Beer, Amy-Jane, Claire Moss, and Michael Thorndyke
Development of serotonin-like and SALMFamide-like immunoreactivity in the nervous system of the sea urchin *Psammechinus miliaris* 268

NEUROBIOLOGY AND BEHAVIOR

Garm, A., and J. T. Høeg
Function and functional groupings of the complex mouth apparatus of the squat lobsters *Munida sarsi* Huus and *M. tenuimana* G. O. Sars (Crustacea: Decapoda) 281

ECOLOGY AND EVOLUTION

Kojima, S., R. Segawa, Y. Fijiwara, K. Fujikura, S. Ohta, and J. Hashimoto
Phylogeny of hydrothermal-vent–endemic gastropods, *Alviniconcha* spp., from the Western Pacific revealed by mitochondrial DNA sequences 298

Adamczewska, Agnieszka M., and Stephen Morris
Ecology and behavior of *Gecarcoidea natalis*, the Christmas Island red crab, during the annual breeding migration. 305

PHYSIOLOGY

Adamczewska, Agnieszka M., and Stephen Morris
Metabolic status and respiratory physiology of *Gecarcoidea natalis*, the Christmas Island red crab, during the annual breeding migration 321

Farmer, Mark A., William K. Fitt, and Robert K. Trench
Morphology of the symbiosis between *Corculum cardissa* (Mollusca: Bivalvia) and *Symbiodinium corculorum* (Dinophyceae). 336

Devlin, C. Leah
5-Hydroxytryptamine stimulates net Ca^{2+} flux in the ventricular muscle of a mollusc (*Busycon canaliculatum*) during cardioexcitation. 344

* * *

Index for Volume 200 351

THE BIOLOGICAL BULLETIN

THE BIOLOGICAL BULLETIN is published six times a year by the Marine Biological Laboratory, 7 MBL Street, Woods Hole, Massachusetts 02543.

Subscriptions and similar matter should be addressed to Subscription Manager, THE BIOLOGICAL BULLETIN, Marine Biological Laboratory, 7 MBL Street, Woods Hole, Massachusetts 02543. Subscription per year (six issues, two volumes): $235 for libraries; $95 for individuals. Subscription per volume (three issues): $117.50 for libraries; $47.50 for individuals. Back and single issues (subject to availability): $40 for libraries; $20 for individuals.

Communications relative to manuscripts should be sent to Michael J. Greenberg, Editor-in-Chief, or Pamela Clapp Hinkle, Managing Editor, at the Marine Biological Laboratory, 7 MBL Street, Woods Hole, Massachusetts 02543. Telephone: (508) 289-7428. FAX: 508-289-7922. E-mail: pclapp@mbl.edu.

http://www.mbl.edu/BiologicalBulletin/

The home page for the electronic companion to THE BIOLOGICAL BULLETIN—*the Marine Models Electronic Record*—and other BIOLOGICAL BULLETIN publications is available on the World Wide Web at the address shown above.

THE BIOLOGICAL BULLETIN is indexed in bibliographic services including *Index Medicus* and MEDLINE, *Chemical Abstracts, Current Contents, Elsevier BIOBASE/Current Awareness in Biological Sciences,* and *Geo Abstracts.*

Printed on acid free paper,
effective with Volume 180, Issue 1, 1991.

POSTMASTER: Send address changes to THE BIOLOGICAL BULLETIN, Marine Biological Laboratory,
7 MBL Street, Woods Hole, MA 02543.

Copyright © 2001, by the Marine Biological Laboratory

Periodicals postage paid at Woods Hole, MA, and additional mailing offices.
ISSN 0006-3185

INSTRUCTIONS TO AUTHORS

The Biological Bulletin accepts outstanding original research reports of general interest to biologists throughout the world. Papers are usually of intermediate length (10–40 manuscript pages). A limited number of solicited review papers may be accepted after formal review. A paper will usually appear within four months after its acceptance.

Very short, especially topical papers (less than 9 manuscript pages including tables, figures, and bibliography) will be published in a separate section entitled "Research Notes." A Research Note in *The Biological Bulletin* follows the format of similar notes in *Nature.* It should open with a summary paragraph of 150 to 200 words comprising the introduction and the conclusions. The rest of the text should continue on without subheadings, and there should be no more than 30 references. References should be referred to in the text by number, and listed in the Literature Cited section in the order that they appear in the text. Unlike references in *Nature,* references in the Research Notes section should conform in punctuation and arrangement to the style of recent issues of *The Biological Bulletin.* Materials and Methods should be incorporated into appropriate figure legends. See the article by Lohmann *et al.* (October 1990, Vol. **179:** 214–218) for sample style. A Research Note will usually appear within two months after its acceptance.

The Editorial Board requests that regular manuscripts conform to the requirements set below; those manuscripts that do not conform will be returned to authors for correction before review.

1. ***Manuscripts.*** Manuscripts, including figures, should be submitted in quadruplicate, with the originals clearly marked. (Xerox copies of photographs are not acceptable for review purposes.) The submission letter accompanying the manuscript should include a telephone number, a FAX number, and (if possible) an E-mail address for the corresponding author. The original manuscript must be typed in no smaller than 12 pitch or 10 point, using double spacing (*including* figure legends, footnotes, bibliography, etc.) on one side of 16- or 20-lb. bond paper, 8 by 11 inches. Please, no right justification. Manuscripts should be proofread carefully and errors corrected legibly in black ink. Pages should be numbered consecutively. Margins on all sides should be at least 1 inch (2.5 cm). Manuscripts should conform to the *Council of Biology Editors Style Manual,* 5th Edition (Council of Biology Editors, 1983) and to American spelling. Unusual abbreviations should be kept to a minimum and should be spelled out on first reference as well as defined in a footnote on the title page. Manuscripts should be divided into the following components: Title page, Abstract (of no more than 200 words), Introduction, Materials and Methods, Results, Discussion, Acknowledgments, Literature Cited, Tables, and Figure Legends. In addition, authors should supply a list of words and phrases under which the article should be indexed.

2. ***Title page.*** The title page consists of a condensed title or running head of no more than 35 letters and spaces, the manuscript title, authors' names and appropriate addresses, and footnotes listing present addresses, acknowledgments or contribution numbers, and explanation of unusual abbreviations.

3. ***Figures.*** The dimensions of the printed page, 7 by 9 inches, should be kept in mind in preparing figures for publication. We recommend that figures be about 1 times the linear dimensions of the final printing desired, and that the ratio of the largest to the smallest letter or number and of the thickest to the thinnest line not exceed 1:1.5. Explanatory matter generally should be included in legends, although axes should always be identified on the illustration itself. Figures should be prepared for reproduction as either line cuts or halftones. Figures to be reproduced as line cuts should be unmounted glossy photographic reproductions or drawn in black ink on white paper, good-quality tracing cloth or plastic, or blue-lined coordinate paper. Those to be reproduced as halftones should be mounted on board, with both designating numbers or letters and scale bars affixed directly to the figures. All figures should be numbered in consecutive order, with no distinction between text and plate figures and cited, in order, in the text. The author's name and an arrow indicating orientation should appear on the reverse side of all figures.

Digital art: The Biological Bulletin will accept figures submitted in electronic form; however, digital art must conform to the following guidelines. Authors who create digital images are wholly responsible for the quality of their material, including color and halftone accuracy.

Format. Acceptable graphic formats are TIFF and EPS. Color submissions must be in EPS format, saved in CMKY mode.

Software. Preferred software is Adobe Illustrator or Adobe Photoshop for the Mac and Adobe Photoshop for Windows. Specific instructions for artwork created with various software programs are available on the Web at the Digital Art Information Site maintained by Cadmus Professional Communications at http://cjs.cadmus.com/da/home.html

Resolution. The minimum requirements for resolution are 1200 DPI for line art and 300 for halftones.

Size. All digital artwork must be submitted at its actual printed size so that no scaling is necessary.

Multipanel figures. Figures consisting of individual parts (*e.g.*, panels A, B, C) must be assembled into final format and submitted as one file.

Hard copy. Files must be accompanied by hard copy for use in case the electronic version is unusable.

Disk identification. Disks must be clearly labeled with the following information: author name and manuscript number; format (PC or Macintosh); name and version of software used.

Color: The Biological Bulletin will publish color figures and plates, but must bill authors for the actual additional cost of printing in color. The process is expensive, so authors with more than one color image should—consistent with editorial concerns, especially citation of figures in order—combine them into a single plate to reduce the expense. On request, when supplied with a copy of a color illustration, the editorial staff will provide a pre-publication estimate of the printing cost.

4. ***Tables, footnotes, figure legends, etc.*** Authors should follow the style in a recent issue of *The Biological Bulletin* in preparing table headings, figure legends, and the like. Because of the high cost of setting tabular material in type, authors are asked to limit such material as much as possible. Tables, with their headings and footnotes, should be typed on separate sheets, numbered with consecutive Roman numerals, and placed after the Literature Cited. Figure legends should contain enough information to make the figure intelligible separate from the text. Legends should be typed double spaced, with consecutive Arabic numbers, on a separate sheet at the end of the paper. Footnotes should be limited to authors' current addresses, acknowledgments or contribution numbers, and explanation of unusual abbreviations. All such footnotes should appear on the title page. Footnotes are not normally permitted in the body of the text.

5. ***Literature cited.*** In the text, literature should be cited by the Harvard system, with papers by more than two authors cited as Jones *et al.*, 1980. Personal communications and material in preparation or in press should be cited in the text only, with author's initials and institutions, unless the material has been formally accepted and a volume number can be supplied. The list of references following the text should be headed Literature Cited, and must be typed double spaced on separate pages, conforming in punctuation and arrangement to the style of recent issues of *The Biological Bulletin*. Citations should include complete titles and inclusive pagination. Journal abbreviations should normally follow those of the U. S. A. Standards Institute (USASI), as adopted by Biological Abstracts and Chemical Abstracts, with the minor differences set out below. The most generally useful list of biological journal titles is that published each year by Biological Abstracts (biosis List of Serials; the most recent issue). Foreign authors, and others who are accustomed to using The World List of Scientific Periodicals, may find a booklet published by the Biological Council of the U.K. (obtainable from the Institute of Biology, 41 Queen's Gate, London, S.W.7, England, U.K.) useful, since it sets out the World List abbreviations for most biological journals with notes of the USASI abbreviations where these differ. Chemical Abstracts publishes quarterly supplements of additional abbreviations. The following points of reference style for The Biological Bulletin differ from USASI (or modified World List) usage:

A. Journal abbreviations, and book titles, all underlined (for *italics*)

B. All components of abbreviations with initial capitals (not as European usage in World List *e.g.*, *J. Cell. Comp. Physiol.* NOT *J. cell. comp. Physiol.*)

C. *All* abbreviated components must be followed by a period, whole word components *must not* (*i.e.*, *J. Cancer Res.*)

D. Space between all components (*e.g.*, *J. Cell. Comp. Physiol.*, not *J.Cell.Comp.Physiol.*)

E. Unusual words in journal titles should be spelled out in full, rather than employing new abbreviations invented by the author. For example, use *Rit Vísindafjélags Islendinga* without abbreviation.

F. All single word journal titles in full (*e.g.*, *Veliger*, *Ecology*, *Brain*).

G. The order of abbreviated components should be the same as the word order of the complete title (*i.e., Proc.* and *Trans.* placed where they appear, not transposed as in some BIOLOGICAL ABSTRACTS listings).

H. A few well-known international journals in their preferred forms rather than WORLD LIST or USASI usage (*e.g., Nature, Science, Evolution* NOT *Nature, Lond., Science, N.Y.; Evolution, Lancaster, Pa.*)

6. ***Reprints, page proofs, and charges.*** Authors may purchase reprints in lots of 100. Forms for placing reprint orders are sent with page proofs. Reprints normally will be delivered about 2 to 3 months after the issue date. Authors (or delegates for foreign authors) will receive page proofs of articles shortly before publication. They will be charged the current cost of printers' time for corrections to these (other than corrections of printers' or editors' errors). Other than these charges for authors' alterations, *The Biological Bulletin* does not have page charges.

CONTENTS
for Volume 200

No. 1: February 2001

BIOMECHANICS

Etnier, Shelley
Flexural and torsional stiffness in multi-jointed biological beams 1

Nauen, Jennifer C., and George V. Lauder
Three-dimensional analysis of finlet kinematics in the chub mackerel (*Scomber japonicus*) 9

DEVELOPMENT AND REPRODUCTION

Amano, Shigetoyo, and Isao Hori
Metamorphosis of coeloblastula performed by multipotential larval flagellated cells in the calcareous sponge *Leucosolenia laxa* 20

ECOLOGY AND EVOLUTION

McEdward, L. R., and K. H. Morgan
Interspecific relationships between egg size and the level of parental investment per offspring in echinoderms 33

Kinzie, Robert A., III, Michelle Takayama, Scott R. Santos, and Mary Alice Coffroth
The adaptive bleaching hypothesis: experimental tests of critical assumptions 51

PHYSIOLOGY

Bartol, Ian K.
Role of aerobic and anaerobic circular mantle muscle fibers in swimming squid: electromyography . . . 59

Zielinski, S., F. J. Sartoris, and H. O. Pörtner
Temperature effects on hemocyanin oxygen binding in an Antarctic cephalopod 67

Medler, Scott, and Harold Silverman
Muscular alteration of gill geometry *in vitro*: implications for bivalve pumping processes 77

RESEARCH NOTES

Browne, Kenneth A., and Richard K. Zimmer
Controlled field release of a waterborne chemical signal stimulates planktonic larvae to settle 87

Dawson, Michael N., and David K. Jacobs
Molecular evidence for cryptic species of *Aurelia aurita* (Cnidaria, Scyphozoa) 92

No. 2: April 2001

DEVELOPMENT AND REPRODUCTION

Rahman, M. Aminur, Tsuyoshi Uehara, and John S. Pearse
Hybrids of two closely related tropical sea urchins (Genus *Echinometra*): evidence against postzygotic isolating mechanisms 97

Pernet, Bruno
Escape hatches for the clonal offspring of serpulid polychaetes 107

PHYSIOLOGY

Levy, O., L. Mizrahi, N. E. Chadwick-Furman, and Y. Achituv
Factors controlling the expansion behavior of *Favia favus* (Cnidaria: Scleractinia): effects of light, flow, and planktonic prey 118

SYMBIOSIS

Wakefield, Timothy S., and Stephen C. Kempf
Development of host- and symbiont-specific monoclonal antibodies and confirmation of the origin of the symbiosome membrane in a cnidarian–dinoflagellate symbiosis 127

INVERTEBRATE SENSORY INFORMATION PROCESSING: IMPLICATIONS FOR BIOLOGICALLY INSPIRED AUTONOMOUS SYSTEMS

Blazis, Diana E. J., and Frank W. Grasso
Introduction 147

Breithaupt, Thomas
Fan organs of crayfish enhance chemical information flow 150

Fraser, Peter J.
Statocysts in crabs: short-term control of locomotion and long-term monitoring of hydrostatic pressure . . 155

Grasso, Frank W.
Invertebrate-inspired sensory-motor systems and autonomous, olfactory-guided exploration 160
Barlow, Robert B., James M. Hitt, and Frederick A. Dodge
Limulus vision in the marine environment 169
Cronin, Thomas W., and Justin Marshall
Parallel processing and image analysis in the eyes of mantis shrimps 177
Webb, Barbara
View from the boundary 184
Robert, Daniel
Innovative biomechanics for directional hearing in small flies 190
Schmitz, Josef, Jeffrey Dean, Thomas Kindermann, Michael Schumm, and Holk Cruse
A biologically inspired controller for hexapod walking: simple solutions by exploiting physical properties 195
Macmillan, David L., and Blair W. Patullo
Insights for robotic design from studies of the control of abdominal position in crayfish 201
Birmingham, J. T.
Increasing sensor flexibility through neuromodulation 206
Derby, Charles D., and Pascal Steullet
Why do animals have so many receptors? The role of multiple chemosensors in animal perception 211
Srinivasan, Mandyam V., Shaowu Zhang, and Javaan S. Chahl
Landing strategies in honeybees and possible applications to autonomous airborne vehicles 216
Ishida, H., T. Nakamoto, T. Moriizumi, T. Kikas, and J. Janata
Plume-tracking robots: a new application of chemical sensors 222
Mountain, David C., and Allyn E. Hubbard
Sensing scenes with silicon 227
Higgins, Charles M.
Sensory architectures for biologically inspired autonomous robotics 235

List of Participants 243

No. 3: June 2001

RESEARCH NOTES

Rees, Bernard B., John A. L. Bowman, and Patricia M. Schulte
Structure and sequence conservation of a putative hypoxia response element in the lactate dehydrogenase-B gene of *Fundulus* 247
Okada, T., S. Stanley MacIsaac, Y. Katsuyama, Y. Okamura, and I. A. Meinertzhagen
Neuronal form in the central nervous system of the tadpole larva of the ascidian *Ciona intestinalis*. 252
Hickman, Carole S., and Michael G. Hadfield
Larval muscle contraction fails to produce torsion in a trochoidean gastropod 257

DEVELOPMENT AND REPRODUCTION

Paterson, Ian G., Vanessa Partridge, and John Buckland-Nicks
Multiple paternity in *Littorina obtusata* (Gastropoda, Littorinidae) revealed by microsatellite analyses. . . . 261
Beer, Amy-Jane, Claire Moss, and Michael Thorndyke
Development of serotonin-like and SALMFamide-like immunoreactivity in the nervous system of the sea urchin *Psammechinus miliaris* 268

NEUROBIOLOGY AND BEHAVIOR

Garm, A., and J. T. Høeg
Function and functional groupings of the complex mouth apparatus of the squat lobsters *Munida sarsi* Huus and *M. tenuimana* G. O. Sars (Crustacea: Decapoda) 281

ECOLOGY AND EVOLUTION

Kojima, S., R. Segawa, Y. Fijiwara, K. Fujikura, S. Ohta, and J. Hashimoto
Phylogeny of hydrothermal-vent–endemic gastropods, *Alviniconcha* spp., from the Western Pacific revealed by mitochondrial DNA sequences 298
Adamczewska, Agnieszka M., and Stephen Morris
Ecology and behavior of *Gecarcoidea natalis*, the Christmas Island red crab, during the annual breeding migration. 305

PHYSIOLOGY

Adamczewska, Agnieszka M., and Stephen Morris
Metabolic status and respiratory physiology of *Gecarcoidea natalis*, the Christmas Island red crab, during the annual breeding migration 321
Farmer, Mark A., William K. Fitt, and Robert K. Trench
Morphology of the symbiosis between *Corculum cardissa* (Mollusca: Bivalvia) and *Symbiodinium corculorum* (Dinophyceae). 336
Devlin, C. Leah
5-Hydroxytryptamine stimulates net Ca^{2+} flux in the ventricular muscle of a mollusc (*Busycon canaliculatum*) during cardioexcitation. 344

* * *

Index for Volume 200 351

Reference: *Biol. Bull.* **200:** 247–251. (June 2001)

Structure and Sequence Conservation of a Putative Hypoxia Response Element in the Lactate Dehydrogenase-B Gene of *Fundulus*

BERNARD B. REES[1,*], JOHN A. L. BOWMAN[2], AND PATRICIA M. SCHULTE[2]

[1]*Department of Biological Sciences, University of New Orleans, New Orleans, Louisiana 70148; and*
[2]*Department of Biology, University of Waterloo, Waterloo, Ontario N2L 3G1, Canada*

Many aquatic habitats are characterized by periodic or sustained episodes of low oxygen concentration, or hypoxia, and organisms that survive in these habitats do so by utilizing a suite of behavioral, physiological and biochemical adjustments to low oxygen (1–3). In the killifish Fundulus heteroclitus, *one response to prolonged exposure to hypoxia is an increase in the activity of lactate dehydrogenase-B (LDH-B), the terminal enzyme of anaerobic glycolysis, in liver tissue (4). An increase in glycolytic enzyme activity also occurs in mammalian cells during hypoxia, a process due, in part, to increased rates of gene transcription mediated by the hypoxia-inducible transcription factor, HIF-1 (5). Given that a homolog of HIF-1 has been identified in fish (6), we hypothesized that HIF might be involved in the observed up-regulation of LDH-B in* F. heteroclitus. *Herein, we describe the presence of DNA elements in intron 2 of the* Ldh-B *gene from* F. heteroclitus *that resemble hypoxia response elements (HRE) described for mammalian genes (7–10). Specifically, over a region of approximately 50 base pairs we identified two consensus HIF-1 binding sites, as well as DNA elements that may bind other transcription factors (e.g., cyclic AMP response elements; CRE). We found that these sites were perfectly conserved among geographically diverse populations of* F. heteroclitus, *as well as being highly conserved among multiple species in the genus* Fundulus. *The spacing, orientation, and sequence conservation of these putative regulatory elements suggest that they may be functionally involved in the hypoxic regulation of* Ldh-B *in these fish.*

Hypoxia is common in a variety of biological settings, and one area of great current interest is the role of hypoxia in regulating gene expression. In mammals, the hypoxia-inducible factor 1 (HIF-1) has been shown to play a key role in many cases of hypoxia-dependent gene expression (5). HIF-1 is a heterodimeric transcription factor, composed of subunits HIF-1α and HIF-1β. Hypoxia leads to the accumulation of HIF-1α, dimerization with HIF-1β, and binding of the dimer to specific nucleotide sequences (hypoxia response elements, HRE) of target genes. Upon binding DNA, HIF-1 interacts with other transcription factors and accessory proteins to stimulate rates of gene transcription (10–12). Originally described as a mediator of increased rates of transcription of the glycoprotein hormone erythropoietin (*Epo*) during hypoxia (7), HIF-1 has subsequently been implicated in the hypoxia-dependent transcription of a variety of mammalian genes, including vascular endothelial growth factor, glucose transporters, and several glycolytic enzymes (5).

Whether HIF-1 (or the related proteins, HIF-2 or HIF-3; ref. 5) is involved in gene expression in organisms that face fluctuations in oxygen availability in their natural environment has received less attention. Because aquatic habitats frequently show spatial and temporal variation in oxygen (13, 14), fish and other aquatic organisms represent ideal systems in which to study gene regulation during ecologically relevant hypoxia. Evidence is emerging that fish have functional analogs or homologs of HIF that may be involved in hypoxic regulation of gene expression. For example, when nuclear proteins were extracted from liver tissue of gulf killifish, *Fundulus grandis,* that had been subjected to hypoxia, one or more nuclear proteins that bound to mam-

---

Received 28 November 2000; accepted 27 February 2001.

* To whom correspondence should be addressed. E-mail: brees@uno.edu.

Abbreviations: CRE, cyclic AMP response element; Epo, erythropoietin; HIF-1, hypoxia-inducible factor 1; HRE, hypoxia response element; LDH, lactate dehydrogenase.

malian HIF-1 binding sequences were found (B.B. Rees, unpub. obs.). Furthermore, a putative HIF-1α homolog has recently been cloned and sequenced from rainbow trout (6). However, the genes that may be subject to regulation by this transcription factor in fish remain largely uncharacterized (although see ref. 15).

We are interested in describing targets of hypoxia-dependent gene regulation in the killifish, *F. heteroclitus.* This species occurs in estuaries along the eastern seaboard of North America, habitats in which oxygen levels vary with depth, salinity, temperature, and degree of eutrophication (13, 16). We focused on the *Ldh-B* gene in *F. heteroclitus* because previous research had shown that the activity of LDH-B increased about 2-fold during exposure of this fish to hypoxia (4). Furthermore, much of the *F. heteroclitus Ldh-B* gene sequence is known from the studies by Powers and his colleagues on the thermal evolution of LDH-B isozymes in this species (17–20). In addition to the complete coding sequence, about 5 kb of promoter and 5′ flanking sequence (18–20) and up to 300 bp on each end of all seven introns (P.M. Schulte, unpub. obs.) have been sequenced. Finally, there is evidence of HIF homologs in this and closely related species (B.B. Rees, unpub. obs.; W. Powell and M. Hahn, Woods Hole Oceanographic Institution, pers. comm.; D. Crawford, University of Missouri, pers. comm.).

In the present study, we asked whether the *F. heteroclitus Ldh-B* gene contains conserved DNA regions that could serve as putative HIF-1 binding sites. We searched the available gene sequence for a hexanucleotide element (5′-ACGTGC-3′) representing the consensus HIF-1 binding site (21). In about 7 kb of DNA sequence, we found a single match to this sequence, located in the latter half of intron 2. We subsequently sequenced this intron in individuals from populations distributed across the geographic range of *F. heteroclitus* and found an intriguing pattern of sequence conservation in this intron (Fig. 1A). The 5′ half of the intron displayed a degree of variation consistent with the level of geographic variation noted in noncoding sequence from the 5′ flanking region and promoter of the same gene (19, 20). The 3′ half of the intron, however, was highly conserved among these individuals, and the putative HIF-binding site was perfectly conserved. To determine the degree of sequence conservation at greater phylogenetic distances, we sequenced *Ldh-B* intron 2 from 12 additional species within the genus *Fundulus* (Fig. 1B). Again, the 5′ half was found to be quite variable, whereas the 3′ half of the intron was highly conserved. The putative HIF-binding site, while not perfectly conserved among species, was present in 10 of the 13 species examined.

Closer examination of the 3′ half of *Fundulus Ldh-B* intron 2 revealed that this putative HIF-binding site was followed by DNA elements that may represent additional transcription factor binding sites. Immediately downstream of the HIF-binding site was the sequence 5′-AACAG-3′. Similar or identical sequences are present in the HREs of certain mammalian genes, and these sequences are required for hypoxic induction of those genes (7, 8, 22). The next downstream DNA element in the *Fundulus Ldh-B* intron 2 was 5′-CGTG-3′, which corresponds to the core DNA sequence of a second potential HIF-binding site (5). Finally, intron 2 ended with a DNA element that differed by only one nucleotide from the consensus CRE, 5′-(T/G)(T/A)CGTCA-3′ (23). Each of these sites was perfectly conserved among geographically diverse populations of *F. heteroclitus* (Fig. 1A), as well being remarkably well conserved among several species of *Fundulus* (Fig. 1B).

The HREs that have been characterized in mammalian genes typically have a di- or tripartite structure, in which HIF-binding sites are located close to other DNA elements necessary for hypoxic regulation of transcription. Figure 2 shows the arrangement of these elements in the mammalian *Epo* (7, 8) and *Ldh-A* (9, 10) genes and compares this arrangement with the consensus sequence we determined for the 3′-half of intron 2 from *F. heteroclitus Ldh-B.* This comparison shows that the occurrence and spacing of multiple putative binding sites in the *F. heteroclitus Ldh-B* intron 2 conform to the general structure of HREs defined for other genes. Indeed, there is a striking similarity among DNA elements identified to be important in hypoxic induction of mammalian *Ldh-A* (two HIF-binding sites and a CRE) and the putative binding sites we identified in the *F. heteroclitus Ldh-B* intron 2. The high degree of sequence conservation of these DNA elements within and among species of *Fundulus* (Fig. 1), combined with the similarity in spacing and orientation of these elements with known HREs (Fig. 2), suggests that the 3′-half of intron 2 from *F. heteroclitus Ldh-B* may act as an HRE and contribute to the regulation of this gene during hypoxia.

Previous research on the promoter and 5′ flanking region of *F. heteroclitus* indicated that sequence variation in noncoding regions of the *Ldh-B* gene can be quite high among populations, approaching 15 nucleotide changes per 100 bp across the geographic range of this species (19, 20). In light of this level of variation, the very low variability (one change in 50 bp, Fig. 1A) in the 3′ half of intron 2 of the *F. heteroclitus Ldh-B* gene was surprising. The observed degree of sequence conservation in this intron could be explained if the putative binding sites we described are functionally important and are maintained by selection. Although the location of this putative HRE within an intron is somewhat unusual, intronic locations for enhancers are not unprecedented. Binding sites for HIF-1 have been found within the introns of the mammalian glycolytic genes phosphofructokinase and aldolase (21), although in the case of aldolase the intronic site may not contribute to hypoxic regulation of this gene (22). Among fish, functional enhancers occur in introns of the immunoglobulin gene of the channel catfish (24) and the sonic hedgehog gene in ze-

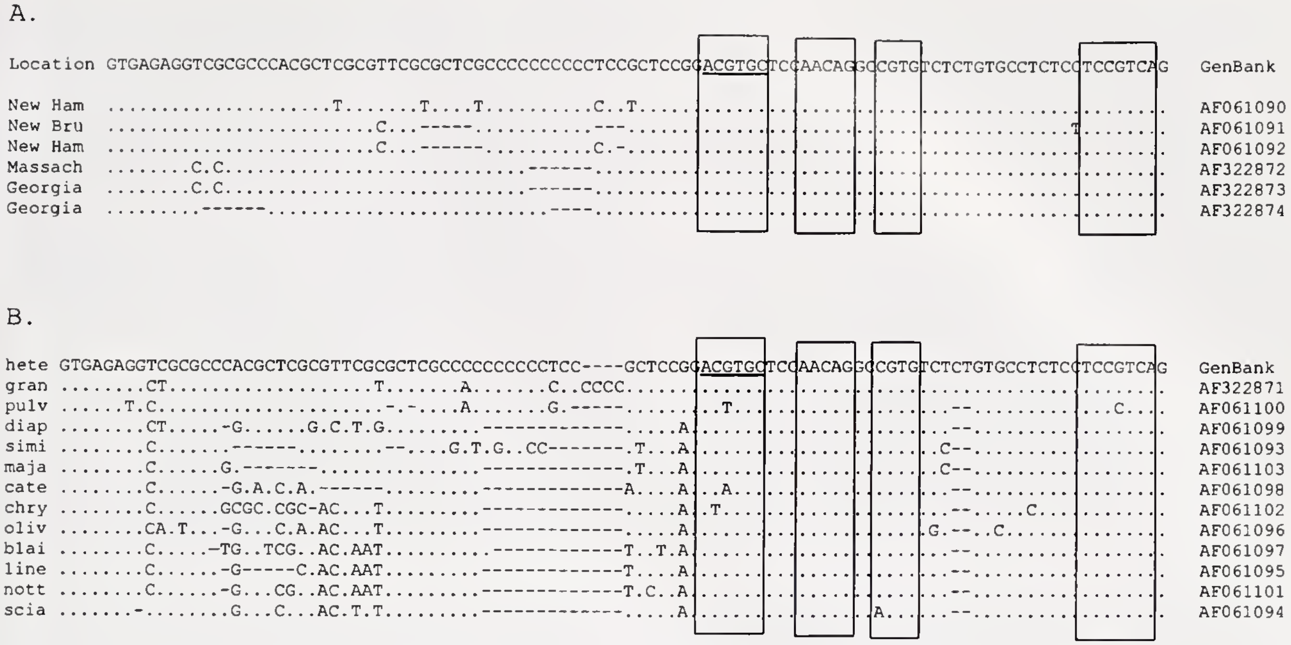
A.
Location GTGAGAGGTCGCGCCCACGCTCGCGTTCGCGCTCGCCCCCCCCCCTCCGCTCCGGACGTGCTCCAACAGGCCGTGTCTCTGTGCCTCTCCTCCGTCAG
GenBank
New Ham AF061090
New Bru AF061091
New Ham AF061092
Massach AF322872
Georgia AF322873
Georgia AF322874
B.
hete GTGAGAGGTCGCGCCCACGCTCGCGTTCGCGCTCGCCCCCCCCCCTCC----GCTCCGGACGTGCTCCAACAGGCCGTGTCTCTGTGCCTCTCCTCCGTCAG
GenBank
gran AF322871
pulv AF061100
diap AF061099
simi AF061093
maja AF061103
cate AF061098
chry AF061102
oliv AF061096
blai AF061097
line AF061095
nott AF061101
scia AF061094

Figure 1. (A) Sequence variation in intron 2 of *Ldh-B* from *Fundulus heteroclitus* representing populations from the geographic distribution of this species. Locations were New Brunswick, Canada (New Bru); Hampton, New Hampshire (New Ham); Woods Hole, Massachusetts (Massach): and Sapelo Island, Georgia (Georgia). (B) Sequence variation in intron 2 of *Ldh-B* from various species within the genus *Fundulus*. Species were *F. heteroclitus* (hete); *F. grandis* (gran); *F. pulvereus* (pulv); *F. diaphanus* (diap); *F. similis* (simi); *F. majalis* (maja); *F. catenatus* (cate); *F. chrysotus* (chry); *F. olivaceous* (oliv); *F. blairae* (blai); *F. lineolatus* (line); *F. notti* (nott); *F. sciadicus* (scia). In A and B, the consensus sequence for *F. heteroclitus* is given on the first line; dots indicate a nucleotide identical to that in the *F. heteroclitus* consensus, and dashes indicate a deletion. The boxed underlined letters indicate the consensus hexanucleotide HIF-1 binding site (21). Other boxed areas indicate other DNA regions of interest (see text). GenBank accession numbers are given at the end of each line. *Methods:* Genomic DNA was isolated by proteinase K digestion followed by high salt extraction (26). Spleen tissue was used as a source of genomic DNA for *F. heteroclitus* and *F. grandis,* and muscle tissue, kindly provided by Dr. Kate Shaw (University of Kansas), was used for *F. similis, F. lineolatus, F. sciadicus, F. notti, F. chrysotus, F. olivaceus, F. blairae, F. pulvereus,* and *F. catenatus.* Genomic DNA from *F. diaphanus* and *F. majalis* was kindly provided by Dr. Douglas L. Crawford (University of Missouri). PCR primers to amplify intron 2 of the *Fundulus Ldh-B* gene were designed based on an alignment of *Ldh-B* sequences from *Rattus norvegicus, Sus domesticus, Sceloporus undulatus, Xenopus laevis, F. heteroclitus,* and *F. parvipinnis* (27). One of two forward primers was used, either 139F (5′-GACGAGCTCGCTCTGGTGGA-3′) or 148F (5′-GCTCTGGTGGACGTGATGGA-3′), in combination with the reverse primer 368R (5′-GGGATGATGCACTTGAAGAC-3′). The position of the primers is indicated relative to the *Ldh-B* coding sequence, starting with +1 for the A of the methionine start-codon. PCR conditions were as follows: 40 cycles (1 min at 94°C, 1 min at 57°C, and 1 min 15 s at 72°C) in 50-μl reaction mixtures containing 10 m*M* Tris (pH 8.3), 1.5 m*M* $MgCl_2$, 5 m*M* KCl, 0.01% Nonidet P-40, and 0.01% Triton X-100, 0.6 μM of each primer, 200 μM of each dNTP, and 1 U of *Taq* polymerase. Genomic DNA concentrations were optimized for each sample. PCR fragments were cloned with no further purification into the EcoRV site of either the Bluescript II KS (−) T-vector (Stratagene, La Jolla, CA) or the pGEM-5Zf (−) T-vector (Promega, Madison, WI). All clones were completely sequenced at least once in each direction, and all reported sequences represent the consensus from at least two independent clones.

brafish (25). Therefore, the location of the putative HRE we describe is not inconsistent with a role in transcriptional regulation.

To our knowledge, this is the first description of a putative HRE in a gene from a non-mammalian vertebrate. In combination with the previously observed increase in LDH-B activity during hypoxia in this species (4), this result is significant insofar as it suggests that HIF or its homologs, heretofore described as regulators of gene expression in mammalian development, physiology, and pathology (5), may play a role in mediating effects of environmental hypoxia in other animals. Future functional studies will be required to assess the role of this putative HRE in regulating *Ldh-B* gene expression in *F. heteroclitus*. Although the 3′ half of this intron was highly conserved among the other members of the genus we examined, the observed nucleotide differences within putative binding sites (Fig. 1B) could impact the ability of this region to

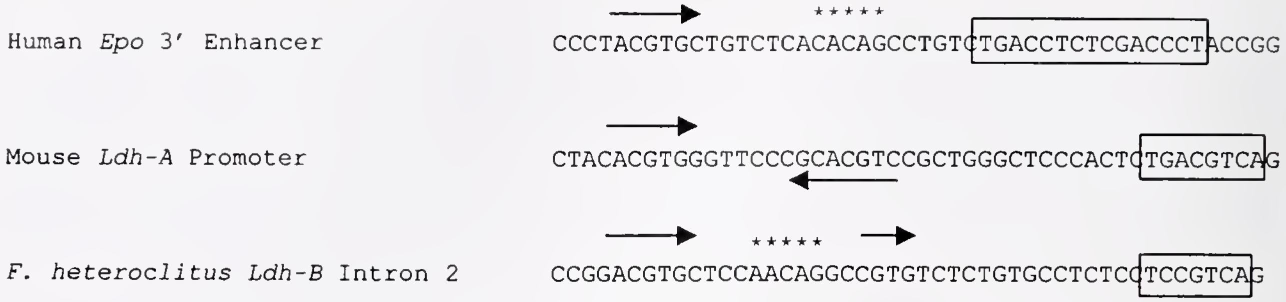
Human *Epo* 3′ Enhancer
CCCTACGTGCTGTCTCACACAGCCTGTCTGACCTCTCGACCCTACCGG
Mouse *Ldh-A* Promoter
CTACACGTGGGTTCCCGCACGTCCGCTGGGCTCCCACTCTGACGTCAG
F. heteroclitus Ldh-B Intron 2
CCGGACGTGCTCCAACAGGCCGTGTCTCTGTGCCTCTCCTCCGTCAG

Figure 2. Diagrammatic representation of the orientation and spacing of functional DNA elements in hypoxia response elements of the human erythropoietin 3′ enhancer (7, 8) and mouse *Ldh-A* promoter (9, 10). Arrows represent HIF binding sites (forward or reverse orientation). For human *Epo*, the asterisks indicate a DNA element necessary for hypoxic induction, and the boxed nucleotides represent a direct repeat of a steroid response element. For mouse *Ldh-A*, the boxed nucleotides represent a CRE. The location of similar DNA elements in the 3′ half of *Ldh-B* intron 2 from *F. heteroclitus* (consensus) are indicated using the same symbols (the boxed nucleotides form an imperfect CRE). The human *Epo* sequence is from (8) and begins at nucleotide + 3455; the mouse *Ldh-A* sequence is from (10) and begins at − 88 (nucleotide +1 is the transcription start site).

serve as an HRE in other species of *Fundulus*. Accordingly, this group of fish may provide a "natural experiment" on the role of these DNA elements in hypoxic regulation of gene expression.

Acknowledgments

We thank D.A. Powers (Stanford University) for calling our attention to the increase in LDH-B activity in *Fundulus heteroclitus* during hypoxia and for his encouragement during early phases of this work. We are grateful to D. Crawford (University of Missouri, Kansas City), W. Powell (Kenyon College, Ohio), and M. Hahn (Woods Hole Oceanographic Institution) for sharing unpublished sequence data of potential HIF homologs in *F. heteroclitus*. We thank K. Shaw (Collections manager; Natural History Museum, University of Kansas) for providing tissue samples, and T. Lallier (Louisiana State University) and D. Hurley (Tulane University) for their assistance in sequencing the *Ldh-B* intron 2 from *F. grandis*. This work was supported by grant number IBN 9723050 from the National Science Foundation (USA) to B.B. Rees and by an NSERC operating grant to P.M. Schulte.

Literature Cited

1. **Kramer, D. L. 1987.** Dissolved oxygen and fish behavior. *Environ. Biol. Fishes* **18:** 81–92.
2. **Jensen, F. B., M. Nikinmaa, and R. E. Weber. 1993.** Environmental perturbations of oxygen transport in teleost fishes: causes, consequences and compensations. Pp. 161–179 in *Fish Ecophysiology*, J.C. Rankin and F. B. Jensen, eds. Chapman and Hall, London.
3. **Van den Thillart, G., and J. Van Waarde. 1985.** Teleosts in hypoxia: aspects of anaerobic metabolism. *Mol. Physiol.* **8:** 393–409.
4. **Greaney, G. S., A. R. Place, R. E. Cashon, G. Smith, and D. A. Powers. 1980.** Time course of changes in enzyme activities and blood respiratory properties of killifish during long-term acclimation to hypoxia. *Physiol. Zool.* **53:** 136–144.
5. **Semenza, G. L. 1999.** Regulation of mammalian O_2 homeostasis by hypoxia-inducible factor 1. *Annu. Rev. Cell Dev. Biol.* **15:** 551–578.
6. **Soitamo, A. J., C. M. I. Rabergh, M. Gassman, L. Sistonen, and M. Nikinmaa. 2001.** Characterization of a hypoxia-inducible factor (HIF-1α) from rainbow trout: accumulation of protein occurs at normal venous oxygen tensions. *J. Biol. Chem.* Papers in Press, Mar 9, 2001: 10.1074/jbc. M908890199.
7. **Semenza, G. L., and G. L. Wang. 1992.** A nuclear factor induced by hypoxia via *de novo* protein synthesis binds to the human erythropoietin gene enhancer at a site required for transcriptional activation. *Mol. Cell. Biol.* **12:** 5447–5454.
8. **Blanchard, K. L., A. M. Acquaviva, D. L. Galson, and H. F. Bunn. 1992.** Hypoxic induction of the human erythropoietin gene: cooperation between the promoter and enhancer, each of which contains steroid receptor response elements. *Mol. Cell. Biol.* **12:** 5373–5385.
9. **Firth, J. D., B. L. Ebert, and P. J. Ratcliffe. 1995.** Hypoxic regulation of lactate dehydrogenase A: interaction between hypoxia-inducible factor 1 and cAMP response elements. *J. Biol. Chem.* **270:** 21021–21027.
10. **Ebert, B. L., and H. F. Bunn. 1998.** Regulation of transcription by hypoxia requires a multiprotein complex that includes hypoxia-inducible factor 1, an adjacent transcription factor, and p300/CREB binding proteins. *Mol. Cell. Biol.* **18:** 4089–4096.
11. **Arany, Z., L. E. Huang, R. Eckner, S. Bhattacharya, C. Jiang, M. A. Goldberg, H. F. Bunn, and D. M. Livingston. 1996.** An essential role for p300/CBP in the cellular response to hypoxia. *Proc. Natl. Acad. Sci. USA* **93:** 12969–12973.
12. **Carrero, P., K. Okamoto, P. Coumailleau, S. O'Brien, H. Tanaka, and L. Poellinger. 2000.** Redox-regulated recruitment of the transcriptional coactivators CREB-binding protein and SRC-1 to hypoxia-inducible factor 1α. *Mol. Cell. Biol.* **20:** 402–415.
13. **Breitburg, D. L. 1990.** Near-shore hypoxia in the Chesapeake Bay: patterns and relationships among physical factors. *Estuarine Coastal Shelf Sci.* **30:** 593–609.
14. **Diaz, R. J., and R. Rozenberg. 1995.** Marine benthic hypoxia: a review of its ecological effects and the behavioural responses of benthic macrofauna. *Oceanogr. Mar. Biol. Annu. Rev.* **33:** 245–303.
15. **Gracey, A. Y., J. V. Troll, and G. N. Somero. 2001.** Hypoxia-induced gene expression profiling in the euryoxic fish *Gillichthys mirabilis*. *Proc. Natl. Acad. Sci. USA* **98:** 1993–1998.
16. **Kuo, A. Y., and B. J. Neilson. 1987.** Hypoxia and salinity in Virginia estuaries. *Estuaries* **10:** 277–283.

17. **Powers, D. A., M. Smith, I. Gonzalez-Villasenor, L. DiMichele, D. Crawford, G. Bernardi, and T. Lauerman. 1993.** A multidisciplinary approach to the selectionist/neutralist controversy using the model teleost, *Fundulus heteroclitus.* Pp. 43–107 in *Oxford Surveys in Evolutionary Biology,* vol. 8., D. Futuyama and J. Antonovics, eds. Oxford University Press, Oxford.
18. **Segal, J. A., P. M. Schulte, D. A. Powers, and D. L. Crawford. 1996.** Descriptive and functional characterization of variation in the *Fundulus heteroclitus Ldh-B* proximal promoter. *J. Exp. Zool.* **275:** 355–364.
19. **Schulte, P. M., M. Gomez-Chiarri, and D. A. Powers. 1997.** Structural and functional differences in the promoter and 5′ flanking region of *Ldh-B* within and between populations of the teleost *Fundulus heteroclitus. Genetics* **145:** 759–769.
20. **Crawford, D. L., J. A. Segal, and J. L. Barnett. 1999.** Evolutionary analysis of TATA-less proximal promoter function. *Mol. Biol. Evol.* **16:** 194–207.
21. **Semenza, G. L., P. H. Roth, H. M. Fang, and G. L. Wang. 1994.** Transcriptional regulation of genes encoding glycoytic enzymes by hypoxia-inducible factor 1. *J. Biol. Chem.* **269:** 23757–23763.
22. **Semenza, G. L., B. H. Jiang, S. W. Leung, R. Passantino, J. P. Concordet, P. Marie, and A. Giallongo. 1996.** Hypoxia response elements in the aldolase A, enolase 1, and lactate dehydrogenase A gene promoters contain essential binding sites for hypoxia-inducible factor 1. *J. Biol. Chem.* **271:** 32529–32537.
23. **Latchman, D. S. 1995.** *Eukaryotic Transcription Factors.* Academic Press, London.
24. **Magor, B. G., D. A. Ross, D. L. Middleton, and G. W. Warr. 1997.** Functional motifs in the IgH enhancer of the channel catfish. *Immunogenetics* **46:** 192–198.
25. **Muller, F., B. Chang, S. Albert, N. Fischer, L. Tora, and U. Strahle. 1999.** Intronic enhancers control expression of zebrafish sonic hedgehog in floor plate and notochord. *Development* **126:** 2103–2106.
26. **Medrano, J. F., E. Aasen, and L. Sharrow. 1990.** DNA extraction from nucleated red blood cells. *Biotechniques* **8:** 43.
27. **Bernardi, G., P. Sordino, and D. A. Powers. 1993.** Concordant mitochondrial and nuclear DNA phylogenies for populations of the teleost fish *Fundulus heteroclitus. Proc. Natl. Acad. Sci. USA* **90:** 9271–9274.

Reference: *Biol. Bull.* **200:** 252–256. (June 2001)

Neuronal Form in the Central Nervous System of the Tadpole Larva of the Ascidian *Ciona intestinalis*

T. OKADA[1,*], S. STANLEY MacISAAC†, Y. KATSUYAMA[2], Y. OKAMURA‡, AND I. A. MEINERTZHAGEN[1,§]

[1]*Neuroscience Institute, Life Sciences Centre, Dalhousie University, Halifax, Nova Scotia, Canada B3H 4J1; and* [2]*Department of Developmental and Cell Biology, Developmental Biology Center, BioScience II, University of California Irvine, Irvine, California 92697*

The dorsal tubular central nervous system (CNS) of the ascidian tadpole larva is a diagnostic feature by which the chordate affinities of this group, as a whole, are recognized. We have used two methods to identify larval neurons of Ciona intestinalis. *The first is serial electron microscopy (EM), as part of a dedicated study of the visceral ganglion (1), and the second is the transient transfection of neural plate progeny with green fluorescent protein (GFP) (2), to visualize the soma and its neurites of individual neurons in whole-mounted larvae of* C. intestinalis. *Our observations reveal that ascidian larval neurons are simple in form, with a single axonal neurite arising from a soma that is either monopolar or has only very few, relatively simple neurites arising from it, as part of a presumed dendritic arbor. Somata in the visceral ganglion giving rise to axons descending in the caudal nerve cord are presumed to be those of motor neurons.*

Regardless of whether ancestral tunicates more closely resembled the adult than its larva (3, 4), or *vice versa* (5), urochordates form a sister group to chordates (*e.g.*, ref. 6). Yet, possibly because of their small size and transient life, the neurobiology of ascidian larvae has not received sufficient attention, even though they may be better known than other urochordates (7). This is not only a taxonomic omission but is also an opportunity missed, given that these simple nervous systems contain relatively few cells, only about 340 in the larva of *C. intestinalis,* an estimated 100 of which are neurons in that species (8). The criteria by which cells are recognized are, however, weak. Although cell maps exist for the entire larval CNS (8, 9), few studies identify these cells in any way. Markers identify a number of cell types (10), and the number of these has increased in recent years, but reports on the morphology of individual neurons are either lacking or are limited to partial studies on the receptor cells of the sensory vesicle (11, 12). Of particular interest are the motor neuron outputs of the CNS, because these generate undulations of the tail, rhythmical and otherwise (13), that underlie the larva's swimming behavior. The motor neurons have been widely presumed to lie in the visceral ganglion, the middle division of the CNS, between the rostral swelling of the sensory vesicle and the caudal nerve cord (8, 14).

To visualize neurons in their entirety, in whole-mounted larvae, we used a modification of the GFP transfection method of Corbo *et al.* (2). Alternatively, neurons in the visceral ganglion were reconstructed in three dimensions from serial-section EM. For GFP observations, using fluorescence microscopy we first selected those with intense GFP fluorescence from among several hundred transfected, fixed larvae. About 70% of

---

Received 3 November 2000; accepted 15 March 2001.

* Present address: Howard Hughes Medical Institute, Department of Neurobiology and Behavior, State University of New York, Stony Brook, NY 11794-5230.

† Present address: 405 Penn Circle, Apt. H, Allentown, PA 18102.

‡ Present address: Biomolecular Engineering Dept. (Ion Channel Group), National Institute of Bioscience and Human Technology, Agency of Industrial Science and Technology, Higashi 1-1, Tsukuba-shi, Ibaraki 305-8566, Japan.

§ To whom correspondence should be addressed. E-mail: IAM@IS.DAL.CA.

the larvae had such a positive signal, and we then observed about 50 of these by confocal microscopy. Those that were finally selected had either a single neuronal transfection or transfected neurons that were well separated, so that we could observe the entire morphology of the individual neurons, without the possibility of confusion with other GFP profiles. Some larvae had multiple transfections, but the number of cells simultaneously transfected was always restricted and never included all the neurons of a region in the CNS, possibly because of the low concentration of DNA we used.

Various forms of cell outline were visualized after GFP transfection (Fig. 1A-D). Confirming the neuron-specific promoter for the GFP, the cytological profiles were identified as those of neurons on the basis of the defining feature of a long slender neurite, the presumed axon. The terminals of these were rarely conspicuous. In addition, we saw few presumed dendritic neurites arising from the soma. Most somata therefore appeared to be monopolar, with a shape approximating a simple prolate spheroid, although two neurons were bipolar (data not shown).

Soma size in GFP transfected neurons varied between about 5.5 and 8 μm for the long axis and 2.5 and 5 μm for the minor axis (Fig. 1A-D); motor neurons reconstructed in three dimensions by computer were somewhat larger than this, with minor axis diameters about 5 μm (Fig. 1E). Neuron size in the ascidian larva is thus quite small, similar to the sizes of motor neurons in, for example, the salp ganglion (15) or the arthropod brain. For the latter, an average density of 4.6×10^6 per cubic millimeter in the housefly *Musca domestica* (16) corresponds to a mean cell diameter of 7.5 μm; and neuronal diameters in the *Drosophila* optic lobe fall between 3.6 and 5.0 μm for lamina monopolar cells and 2.8 and 4.2 μm for medulla cells (measurements from ref. 17). In the vertebrate brain, the density of the cerebellar granule cell layer is, for reference, $3\text{-}7 \times 10^6$ (18). The small size of ascidian larval neurons is compatible with the restricted extent of their arborizations, which are among the smallest examples of deuterostome neuron.

Different forms of neurons were identified with respect to the location of their somata and the direction of their axons (Fig. 1). Most neurons were descending with axons passing either from the sensory vesicle to the visceral ganglion region or from the visceral ganglion to the caudal nerve cord. For some reason, transfection of cells in the anterior region of the sensory vesicle occurred much less frequently than in either the posterior region of the sensory vesicle or the smaller visceral ganglion, even though there are many more cells in the anterior sensory vesicle.

To confirm that the morphological picture of ascidian neurons was correct, we compared images of GFP transfected neurons with three-dimensional reconstructions of motor neurons obtained from serial EM (Fig. 1E). The two neurons illustrated are one of five bilaterally symmetrical pairs of motor neurons in the visceral ganglion that have been reconstructed from one individual (1). Observations from two other serially sectioned larvae confirm the number of cells and their general morphology but were not analyzed in detail (Stanley MacIsaac, unpub.). The EM series contained images from only every third section, insufficient for fully tracing the finest neurites but sufficient to have seen coarse basal dendrites; the absence of the latter supports the picture, of simple somata lacking an extensive dendritic arbor, seen from GFP transfection. Neuromuscular terminals traced out to sites of presynaptic contact with the tail muscle do, however, indicate that these cells have bulbous terminals (Fig. 1E), in at least two sites each, that were not clearly seen after GFP transfection (Fig. 1A). Thus, GFP expression in a neuron may not always reveal the axon terminals, perhaps because there is insufficient GFP protein transported down the axon. On the other hand, the trajectory of the axon is clearly revealed.

Compared with the typical multipolar neuron of the vertebrate CNS, the form of neurons in the ascidian larval nervous system seems to be remarkably simple. All examples of neurons have somata with few slender neurites, or sometimes none, and a single axon with simple terminals. Although it is possible that GFP protein does not transport completely into the finest dendrites, serial EM of the motor neurons bears out the general impression that most neurons lack well-developed dendrites. In addition to monopolar neurons, at least two transfected cells each had two neurites, an axon and perhaps a stout dendrite, and thus appeared bipolar.

In the general level of their complexity, the transfected neurons resemble motor neurons in the salp ganglion (15) or in the amphioxus larva (19). By comparison, neurons in another deuterostome group, echinoderms (20, 21), seem morphologically more like vertebrate neurons. Thus neuron form does not relate closely to phylogenetic position. It does, however, correlate in general with neuron number, the simplest morphological types of neuron correlating with the least populous nervous systems. Indeed, one view of the dendritic tree is that it provides a structure to segregate different inputs to different dendritic limbs (22), the size and complexity of neuronal branching in a parasympathetic neuron, for example, increasing with the body size of a particular species (23, 24) and with the number of inputs on the neuron (25).

One distinction between vertebrate and invertebrate nervous systems lies in the placement of the soma with respect to its neurites. The monopolar cells of invertebrates can be seen as the product of segregating somata

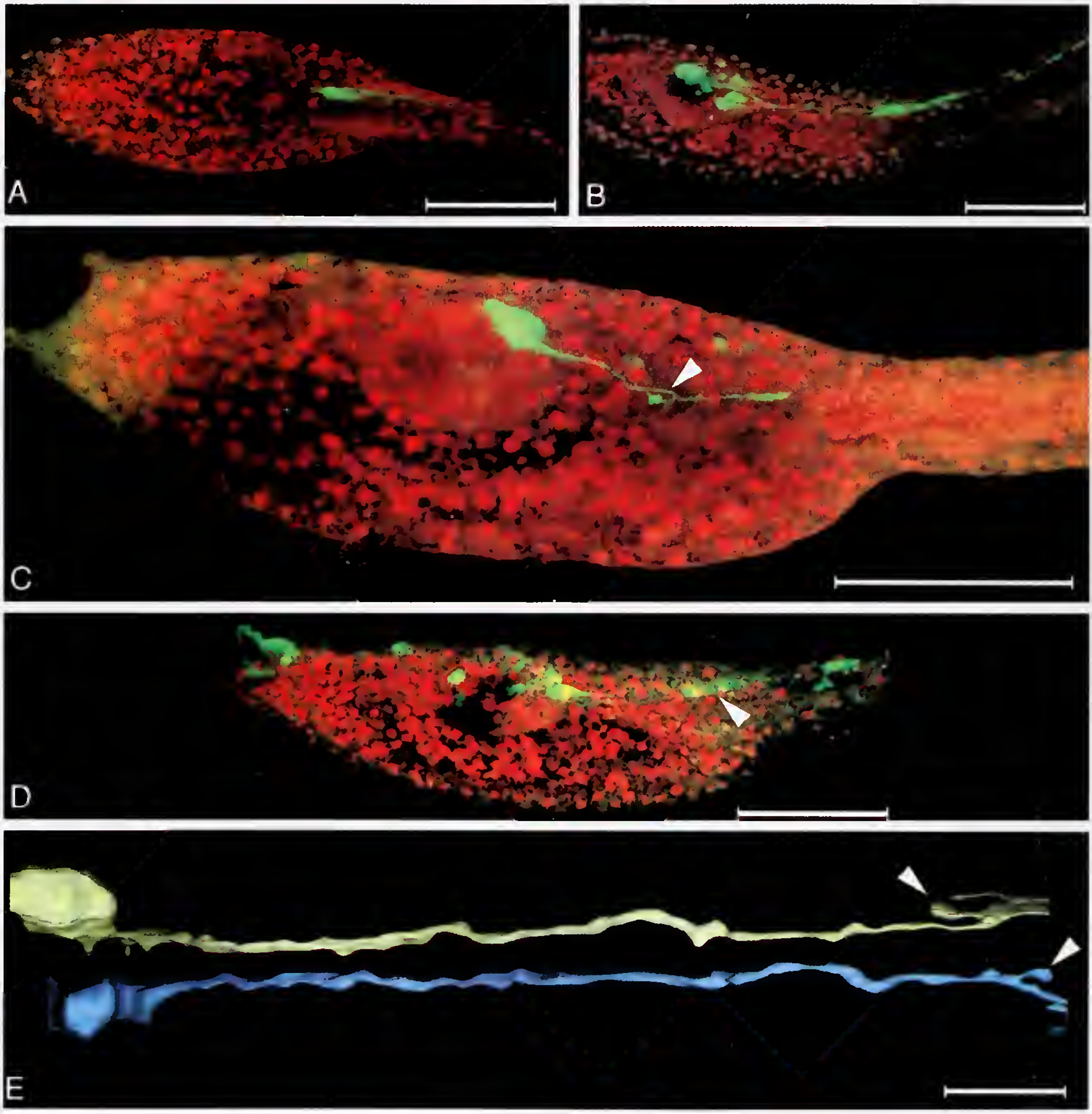

Figure 1. Neurons in newly hatched larvae of *Ciona*. The rostral tip of the trunk lies to the left in each figure. (A-D) Left lateral views of wholemount larvae of *C. intestinalis* expressing green fluorescent protein (GFP) in selected neurons of the larval CNS and stained with BOBO-3, viewed as collapsed stacks of confocal images. Scale bars: 25 μm. GFP transfection was achieved with a plasmid containing a 3.7-kb sequence upstream of ascidian synaptotagmin cDNA (Katsuyama *et al.*, unpublished), fused to a mutated bright form of GFP, pEGFP-N1 (Clontech) in pBluescript. Synaptotagmin is a protein essential for synaptic function, and in the larva is exclusively expressed in neurons, so that we used the synaptotagmin promoter to drive GFP expression in neurons. To obtain transfections, fertilized eggs were cultured in dechorionation solution, comprising 1% Na thioglycorate and 0.05% actinase E in filtered seawater to 10 ml of which 20 drops of 1 *N* NaOH were initially added, for 3–10 min at 18–20°C. Then eggs were dechorionated by repeated pipetting. After being washed several times, eggs were concentrated in a low-speed centrifuge and finally resuspended in 300 μl of filtered seawater and subjected to electroporation in the cuvette of a BioRad gene pulser II in a mixture of 250 μl each of DNA (100–200 μg/ml) and 1.54 *M* mannitol. Successful electroporation was attained with a time constant of *ca* 15 ms. Surviving eggs were then incubated, at 15–18°C in an agar-coated petri dish, spread out in a layer so that they did not touch each other. Emerging larvae were fixed in 2% paraformaldehyde in PBS, mounted in 70%

into a cortex of cell bodies surrounding the neuropile formed by their neurites. Because the neuropile region is very thin in the ascidian larval CNS (1, 26), in practice this distinction is hard to make in our case. A corollary of the arrangement in invertebrates is that the axonal and dendritic regions of the neuron are not strictly segregated at different regions of the neuronal arbor (27). In contrast, inputs in vertebrate neurons generally are exclusively received over the soma and its dendritic tree, quite separate from the output region at the axon terminal (28, 29). Our evidence does not yet allow us to examine whether this distinction is upheld by all neurons in the ascidian larval CNS. Available evidence does, however, indicate the presence of synaptic inputs at the soma (1, 11, 12) and outputs at neuromuscular terminals (1, 30). Our GFP evidence also does not allow us to determine whether axons arise from the apical or basal region of the soma (15), with respect to the neural canal, because this feature is not resolved in wholemount preparations.

The cells of the visceral ganglion are the subject of a recent study (1). Further documentation of the cells in the nervous system of the ascidian tadpole larva will, however, require a dedicated study of the sensory vesicle, where at least 60% of the cells in the CNS reside (8). Application of the GFP method we report here is a first step towards a systematic cataloging of cell types, and their correlation with cell maps derived either from histological methods (8) or from nuclear stains (31) will be a first step toward the analysis of the neural circuits these form and the behavior for which these are a substrate. Likewise, if expression turns on sufficiently early in the embryo and persists sufficiently long in the larva, the GFP method may be a way to examine the growth of neurites and their possible later regression during larval metamorphosis. We currently lack evidence on these points.

Acknowledgments

We thank Ms. Alison Cole for sharing unpublished work on BOBO-3 staining, Ms. Grazyna Tokarczyk for help with confocal imaging of larvae, and Ms. Jane Anne Horne for support with computer 3-D reconstructions. Supported by NSERC grant 0000065 (to I.A.M.).

Literature Cited

1. **Stanley MacIsaac, S. 1999.** Ultrastructure of the visceral ganglion in the ascidian larva *Ciona intestinalis:* cell circuitry and synaptic distribution. Master's thesis, Dalhousie University, Halifax, NS, Canada.
2. **Corbo, J. C., M. Levine, and R. W. Zeller. 1997.** Characterization of a notochord-specific enhancer from the *Brachyury* promoter region of the ascidian, *Ciona intestinalis. Development* **124:** 589–602.
3. **Garstang, W. 1928.** The morphology of the Tunicata, and its bearings on the phylogeny of the Chordata. *Q. J. Microsc. Sci.* **72:** 51–187.
4. **Berrill, N. J. 1950.** *The Tunicata with an Account of the British Species.* The Ray Society, London.
5. **Wada, H., and N. Satoh. 1994.** Details of the evolutionary history from invertebrates to vertebrates, as deduced from the sequences of 18S rDNA. *Proc. Natl. Acad. Sci. USA* **91:** 1801–1804.
6. **Cameron, C. B., J. R. Garey, and B. K. Swalla. 2000.** Evolution of the chordate body plan: new insights from phylogenetic analyses of deuterostome phyla. *Proc. Natl. Acad. Sci. USA* **97:** 4469–4474.
7. **Bone, Q., and G. O. Mackie. 1982.** Urochordata. Pp. 473–535 in *Electrical Conduction and Behaviour in 'Simple' Invertebrates,* G. A. B. Shelton, ed. Clarendon Press, Oxford.
8. **Nicol, D., and I. A. Meinertzhagen. 1991.** Cell counts and maps in the larval central nervous system of the ascidian *Ciona intestinalis* (L.). *J. Comp. Neurol.* **309:** 415–429.
9. **Cole, A. G. 2000.** Cell-lineage of the larval nervous system in the ascidian *Ciona intestinalis:* neurula stage through to hatched larva. Master's thesis, Dalhousie University, Halifax, NS, Canada.
10. **Chiba, S., and T. Nishikata. 1998.** Genes of the ascidian: an annotated list as of 1997. *Zool. Sci.* **15:** 625–643.
11. **Barnes, S. N. 1971.** Fine structure of the photoreceptor and cerebral ganglion of the tadpole larva of *Amaroucium constellatum* (Verrill) (Subphylum: Urochordata; Class: Ascidiacea). *Z. Zellforsch.* **117:** 1–16.

---

glycerin in PBS beneath a #00 coverglass raised up from the slide by spacers of #1.5 coverglass, and visualized using laser scanning confocal microscopy (Zeiss LSM512) with a 63×/1.4 Plan Neofluar objective. To confirm that GFP labeling was cellular, and to localize such labeling with respect to the cellular features of the CNS, larvae were counterstained with a nuclear stain (9). For this, larvae were permeabilized for 30 min in 4% Triton X-100 in PBS, washed in PBS, and incubated for *ca* 60 min in a 500-μg/ml solution of RNAse in PBS. They were then incubated overnight in the dark in 0.01% BOBO-3 (Cat # B-3586, Molecular Probes) in PBS at 4°C. (A) Motor neuron in the region of the visceral ganglion with an axon extending into the caudal nerve cord. (B) Several cells in the posterior sensory vesicle extend their axons towards the visceral ganglion. Other cells anterior to these in the sensory vesicle have axons that may remain locally. (C) Neuron in the posterior region of the sensory vesicle with an axon that appears to branch (arrowhead). (D) GFP-labeled cells in the visceral ganglion (arrowhead) and, anterior to this, in the sensory vesicle, with axons extending towards the visceral ganglion. In the rostral region of the tail, an irregular GFP outline is too large for a neuromuscular terminal, and so appears to be a cell in the caudal nerve cord. In the rostral tip of the trunk, a papilla exhibits GFP labeling, which could be neuronal except that no axon is visible. (E) Dorsal view of a pair of motor neurons in the visceral ganglion of *C. intestinalis* reconstructed in three dimensions from their profiles in the visceral ganglion, from a series of more than 2000 electron micrograph montages of 70-nm sections. The sections were cut from a fully hatched, 2-h-old larva of *C. intestinalis* fixed in osmium tetroxide and glutaraldehyde (8). Each motor neuron pair forms neuromuscular terminals (arrowhead) on both the dorsal and median muscle bands. Scale bar: 10 μm.

12. **Eakin, R. M., and A. Kuda. 1971.** Ultrastructure of sensory receptors in ascidian tadpoles. *Z. Zellforsch.* **112:** 287–312.
13. **Bone, Q. 1992.** On the locomotion of ascidian tadpole larvae. *J. Mar. Biol. Assoc. UK* **72:** 161–186.
14. **Katz, M. J. 1983.** Comparative anatomy of the tunicate tadpole, *Ciona intestinalis. Biol. Bull.* **164:** 1–27.
15. **Lacalli, T. C., and L. Z. Holland. 1998.** The developing dorsal ganglion of the salp *Thalia democratica,* and the nature of the ancestral chordate brain. *Philos. Trans. R. Soc. Lond. B* **353:** 1943–1967.
16. **Strausfeld, N. J. 1976.** *Atlas of an Insect Brain.* Springer-Verlag, Berlin.
17. **Fischbach, K.-F., and A. P. M. Dittrich. 1989.** The optic lobe of *Drosophila melanogaster.* I. A golgi analysis of wild-type structure. *Cell Tissue Res.* **258:** 441–475.
18. **Braitenberg, V., and R. P. Atwood. 1958.** Morphological observations on the cerebellar cortex. *J. Comp. Neurol.* **109:** 2–27.
19. **Lacalli, T. C., and S. J. Kelly. 1999.** Somatic motoneurones in amphioxus larvae: cell types, cell position and innervation patterns. *Acta Zool. (Stockh.)* **80:** 113–124.
20. **Lacalli, T. C., T. H. J. Gilmour, and J. E. West. 1990.** Ciliary band innervation in the bipinnaria larva of *Pisaster ochraceus. Philos. Trans. R. Soc. Lond. B* **330:** 371–390.
21. **Ghyoot, M., J. L. S. Cobb, and M. C. Thorndyke. 1994.** Localization of neuropeptides in the nervous system of the brittle star *Ophiura ophiura. Philos. Trans. R. Soc. Lond. B* **346:** 433–444.
22. **Purves, D. 1988.** *Body and Brain. A Trophic Theory of Neural Connections.* Harvard University Press, Cambridge.
23. **Purves, D., and J. W. Lichtman. 1985.** Geometrical differences among homologous neurons in mammals. *Science* **228:** 298–302.
24. **Snider, W. D. 1987.** The dendritic complexity and innervation of submandibular neurons in five species of mammals. *J. Neurosci.* **7:** 1760–1768.
25. **Purves, D., E. Rubin, W. D. Snider, and J. Lichtman. 1986.** Relation of animal size to convergence, divergence, and neuronal number in peripheral sympathetic pathways. *J. Neurosci.* **6:** 158–163.
26. **Torrence, S. A. 1983.** Ascidian larval nervous system: anatomy, ultrastructure and metamorphosis. Ph.D. dissertation, University of Washington, Seattle. 178 pp.
27. **Bullock, T. H., and G. A. Horridge. 1965.** *Structure and Function in the Nervous Systems of Invertebrates,* Vol. 2. W. H. Freeman, San Francisco.
28. **Bodian, D. 1962.** The generalized vertebrate neuron. *Science* **137:** 323–326.
29. **Bullock, T. H. 1974.** Comparisons between vertebrates and invertebrates in nervous organization. Pp. 343–431 in *The Neurosciences: Third Study Program,* F. O. Schmitt and F. G. Worden, eds. MIT Press, Cambridge, MA.
30. **Tannenbaum, A. S., and J. Rosenbluth. 1972.** Myoneural junctions in larval ascidian tail. *Experientia* **28:** 1210–1212.
31. **Meinertzhagen, I. A., A. G. Cole, and S. Stanley. 2000.** The central nervous system, its cellular organisation and development, in the tadpole larva of the ascidian *Ciona intestinalis. Acta Biol. Hung.* **51:** 417–431.

Reference: *Biol. Bull.* **200:** 257–260. (June 2001)

Larval Muscle Contraction Fails to Produce Torsion in a Trochoidean Gastropod

CAROLE S. HICKMAN[1,*] AND MICHAEL G. HADFIELD[2]

[1]*Department of Integrative Biology and Museum of Paleontology, University of California, Berkeley, California 94720; and* [2]*Kewalo Marine Laboratory, University of Hawaii, 41 Ahui Street, Honolulu, Hawaii 96813, and Department of Zoology, University of Hawaii at Manoa, Honolulu, Hawaii 96822*

The causes and effects of ontogenetic torsion in gastropods have been debated intensely for more than a century (1–19). Occurring rapidly and very early in development, torsion figures prominently in shaping both the larval and adult body plans. We show that mechanical explanations of the ontogenetic event that invoke contraction of larval retractor muscles are inadequate to explain the observed consequences in some gastropods. The classic mechanical explanation of Crofts (4, 5) and subsequent refinements of her explanation have been based on species with rigid larval shell properties (18, 19) that cannot be extrapolated to all gastropods. We present visual evidence of the lack of rigidity of the uncalcified larval shell in a basal trochid gastropod, Margarites pupillus *(Gould), and provide photographic confirmation of our prediction that larval retractor muscle contraction is insufficient to produce more than local deformation or dimpling at the site of muscle insertion. These findings do not refute muscular contraction as a primary cause of ontogenetic torsion in gastropods that calcify their larval shells prior to the onset of torsion, nor do they refute the monophyly of torsion. They do, however, suggest that torsion may be a loosely constrained developmental process with multiple pathways to the more constrained end result (20, 21).*

Torsion is defined as an ontogenetic process that twists the gastropod larval head and foot counterclockwise by 180° relative to the underlying (in the swimming larva) shell with its mantle epithelium and visceral mass. The process is recognized morphologically by its developmental consequence: a new anatomical configuration in which the mantle cavity, anus, and gill rudiment are positioned over the head. Torsion has been regarded as the hallmark of the Gastropoda (8), the evolutionary novelty or shared derived character defining this class of molluscs. When treated as a homologous feature throughout Gastropoda, torsion tends to take on a structural definition synonymous with the torted anatomical condition.

As an ontogenetic event, torsion occurs early in larval development and may be completed in as little as 2 min (22). Crofts' explanation (4, 5) of the mechanism initiating developmental rotation in the trochid gastropod *Calliostoma zizyphinum,* the abalone *Haliotis tuberculata,* and the patellid limpet *Patella vulgata* involved contraction of a larval retractor muscle and assumed that the larval shell on which the muscle is inserted is calcified or at least rigid. Crofts (5) constructed wax models of gastropod larvae that were designed to illustrate the rotation by pulling on a string that was attached to the foot and threaded through a hole in the shell at the point of insertion of the larval retractor muscle. The use of working models of torsion appears to have been widespread in Britain. Eales (7) referred to a working model constructed much earlier by Ray Lancaster, and she borrowed Crofts' models and made a set that she used in her presidential address to the Malacological Society of London (7). Physical models used "to illustrate the torsion process" (5) did not accurately simulate muscle contraction; but because they replicated the observed twist, they supported the theory of muscle contraction over differential growth as an explanation of torsion.

Although the onset of torsion and its completion are readily observed in populations of developing larvae of many species (pers. obs.), the underlying mechanism and details of the morphogenetic movements cannot be resolved (18). Debates over both the morphological changes and the underlying mechanisms have been based more on conjec-

---

Received 21 July 2000; accepted 12 February 2001.

[*] To whom correspondence should be addressed. E-mail: caroleh@socrates.berkeley.edu.

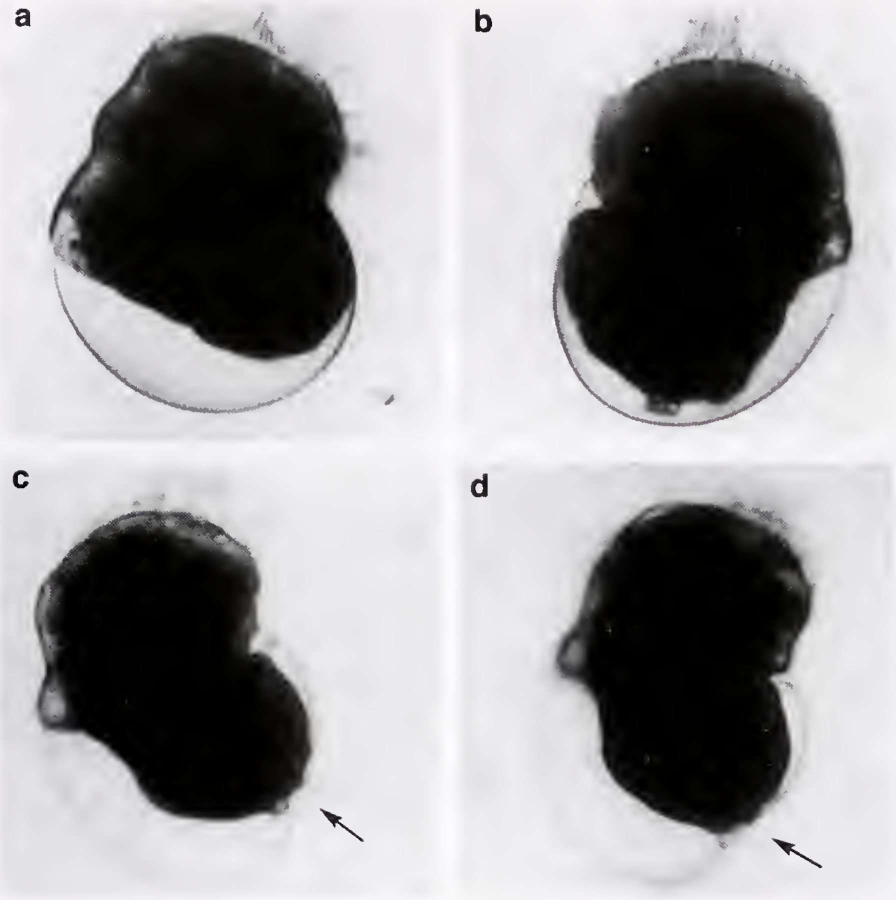

Figure 1. Individual frames from a videotape of the developing pre-torsional veliger larvae of the trochoidean gastropod *Margarites pupillus*. (a, b) Typical appearance of the larvae in most orientations, with the shell appearing evenly rounded. (c, d) Frames in which the larval retractor muscle is rotated into view while contracting to produce a temporary local dimpling (arrow) of the shell at the site of muscle attachment.

ture than on actual observation. Bandel (23) hypothesized that torsion in trochoidean gastropods was solely a consequence of differential growth, in contrast to the mechanism Wanninger *et al.* (19) described in patelloidean gastropods, which involved an alternation of muscle contractions and hydraulic swelling of the larval foot. Page (18), in a careful study of sectioned larvae of the haliotid gastropod *Haliotis kamtschatkana* Jonas, presented evidence that is consistent with potential roles for both muscle contraction and differential growth. In both *Haliotis* and *Patella* the larval shell is calcified at the onset of torsion (18, 19).

Can larval muscle contraction provide a global explanation of ontogenetic torsion? Our observations of early larval development in trochoidean gastropods led us to hypothesize that the thin organic larval shell was insufficiently calcified at the onset of torsion and lacked the mechanical rigidity to antagonize contraction of the larval retractor muscles. Contraction of a muscle inserted on a thin organic shell should produce, instead, only a local deformation.

During the late spring and early summer of 1994, representatives of the major clades of primitive marine gastropods (informally known as archaeogastropods) were spawned at the Friday Harbor Laboratories for comparative observations of larval development and changes in shell secretion at metamorphosis. Larvae of the margaritine trochid *Margarites pupillus* Dall were videotaped as trochophores and pre- and post-torsional veligers; further observations were made using a combination of standard brightfield light microscopy, polarizing microscopy, and differential interference contrast microscopy.

Larvae developed rapidly (at 12°C) to the pre-torsional veliger stage within the egg envelope prior to hatching, and had secreted a cap-shaped, transparent organic shell by 48 h post-fertilization (Fig. 1a). Although the initial shell was weakly birefringent, it collapsed and crumpled at this stage (between 48 and 72 h) when attempts were made to make preparations for scanning electron microscopy. We inferred that the primordial shell was not rigid at this stage, even if weakly calcified.

Immediately prior to hatching and torsion, the active veligers were rotating and constantly changing position within the egg envelope so that it was impossible to make continuous observations in a standard orientation. Two larval retractor muscles appeared to be well-developed, but only one was visible at a time in the rotating veliger, and for only a fraction of a second. Five different observers of larvae during this period were unable to agree on the number of muscles and the position of their insertion on the primordial shell.

Only by videotaping larvae and examining individual frames was it possible to identify sites of apparent muscle attachment (Fig. 1b). The central observation of this paper is that the normally rounded larval shells (Fig. 1a, b) show a periodic transitory dimpling at the site of attachment of a larval retractor muscle (Fig. 1b, c). We argue that the dimpling refutes a mechanical explanation of torsion in this species. Because the dimpling is not permanent, because the active larva is constantly and rapidly changing its orientation, and because the entire shell cannot be kept in focus, the dimple is visible only periodically and for a fraction of a second at a time.

We originally intended to address the further question of whether larval muscle contraction could explain the putative mechanical deformation of the larval shell first proposed by Bandel (24). Subsequently formalized by Morita (25) as "Bandel's Rule," the idea of mechanical deformation has been linked both with torsion and with the initiation of shell coiling. It is based on the observation that the larval shells of many "archaeogastropods" have protuberant lobes bordered by lateral grooves, giving the shell a coiled appearance. Our observations of transitory dimpling of the larval shell in response to muscle contraction suggest that much more powerful forces are required to permanently deform the symmetrical larval shell as a means of giving rise to the initial coil. At least in *Margarites pupillus*, shell morphogenesis is not explained by Bandel's Rule.

Two other studies now provide a more direct critique of Bandel's Rule (18, 26). Collin and Voltzow (26) have shown that mechanical deformation cannot explain the initiation of shell coiling in the abalone *Haliotis kamtschatkana*, because the larval shell is fully calcified and rigid when the alleged deformation occurs. Page (18) provides an elegant alternative explanation of the underlying observations through detailed histological investigation of development in *H. kamtschatkana*. The creases in the lateral flank of the protoconch correspond precisely with deep visceral clefts (indentations of the shell field epithelium) in the developing larva. Her observations show that the topography of the larval shell is superimposed on the indented topography of the visceral lobe of the larva.

Our observations of transitory dimpling at the site of muscle insertion on the flexible larval shell in a phylogenetically basal trochid gastropod clade (27) immediately prior to torsion show that muscle contraction is inadequate to explain the 180° rotation of the larval head and foot (cephalopodium) relative to the shell, primordial mantle complex, and visceral mass (visceropallium). However, extrapolation of these results to all gastropods is unwarranted. In patellid and haliotid gastropods the shell is calcified and rigid at the onset of torsion and may facilitate the process in an immediate mechanical sense (18, 19). In *Calliostoma ligatum*, a member of a more derived trochid clade (27), the larval shell is not completely calcified at the time of torsion (26), and we suspect that it also may lack the rigidity required to produce torsion by muscle contraction.

Further investigations of torsion, both as a developmental event and as a key evolutionary innovation, require a phylogenetic context in which comparative morphogenesis is pursued at a much higher level of resolution. The phenomenon of torsion becomes more interesting if loose constraints on the evolution of development have indeed permitted the emergence of multiple morphogenetic pathways to a single, more tightly constrained body plan of the torted larva and adult gastropod.

Acknowledgments

We thank R. and M. Strathmann for space and facilities at the Friday Harbor Laboratories and for their ideas and suggestions during the course of this study. Two anonymous reviewers provided helpful suggestions for improvement of the manuscript.

Literature Cited

1. **Spengel, J. W. 1881.** Die Geruchsorgane und das Nervensystem der Mollusken. *Zeitschrift für senschaftliche Zoologie* **35:** 333–383.
2. **Amaudrut, A. 1898.** La partie antérieure du tube digestive et la torsion chez les mollusques gastéropodes. *Ann. Sci. Nat. Zool.* **7:** 1–391.
3. **Garstang, W. 1928.** Origin and evolution of larval forms. *Nature* **122:** 366.
4. **Crofts, D. 1937.** The development of *Haliotis tuberculata* with special reference to organogenesis during torsion. *Philos. Trans. R. Soc. Lond. B* **228:** 219–268.
5. **Crofts, D. 1955.** Muscle morphogenesis and torsion. *Proc. Zool. Soc. Lond.* **125:** 711–750.
6. **Yonge, C. M. 1947.** The pallial organs in the aspidobranch Gastropoda, and their evolution throughout the Mollusca. *Philos. Trans. R. Soc. Lond. B* **232:** 443–518.
7. **Eales, N. B. 1949.** Torsion in the Gastropoda. *Proc. Malac. Soc. Lond.* **28:** 53–61.
8. **Morton, J. E. 1958.** Torsion and the adult snail; a re-evaluation. *Proc. Malac. Soc. Lond.* **33:** 2–10.
9. **Ghiselin, M. T. 1966.** The adaptive significance of gastropod torsion. *Evolution* **20:** 337–348.
10. **Batten, R., H. B. Rollins, and S. J. Gould. 1967.** Comments on "the adaptive significance of gastropod torsion." *Evolution* **21:** 405–406.
11. **Thompson, T. E. 1972.** Adaptive significance of gastropod torsion. *Malacologia* **5:** 423–430.
12. **Underwood, A. J. 1972.** Spawning, larval development and settle-

ment behaviour of *Gibbula cineraria* (Gastropoda: Prosobranchia) with a reappraisal of torsion in gastropods. *Mar. Biol.* **17:** 341–349.

13. **Stanley, S. M. 1982.** Opercula and predators: The evolutionary significance of gastropod torsion. *Neues Jahrb. Geol. Palaontol. Abh.* **164:** 95–107.
14. **Pennington, J. T., and F.-S. Chia. 1985.** Gastropod torsion: a test of Garstang's hypothesis. *Biol. Bull.* **169:** 391–396.
15. **Goodhart, C. B. 1987.** Garstang's hypothesis and gastropod torsion. *J. Molluscan Stud.* **53:** 33–36.
16. **Edlinger, K. 1988.** Torsion in gastropods: a phylogenetic model. *Malacol. Rev. Suppl.* **4:** 211–250.
17. **Haszprunar, G. 1988.** On the origin and evolution of major gastropod groups, with special reference to the Streptoneura. *J. Molluscan Stud.* **54:** 367–411.
18. **Page, L. R. 1997.** Ontogenetic torsion and protoconch form in the archaeogastropod *Haliotis kamtschatkana:* evolutionary implications. *Acta Zool.* **78:** 227–245.
19. **Wanninger, A., B. Ruthensteiner, and G. Haszprunar. 1999.** Torsion in *Patella caerulea* (Mollusca, Patellogastropoda): ontogenetic process, timing, and mechanisms. *Invertebr. Biol.* **119:** 177–187.
20. **Wagner, G. 1994.** Homology and the mechanisms of development. Pp. 273–200 in *Homology: The Hierarchical Basis of Comparative Biology.* B. K. Hall, ed. Academic Press, San Diego, CA.
21. **Hickman, C. S. 1999.** Larvae in invertebrate development and evolution. Pp. 21–59 in *The Origin and Evolution of Larval Forms,* B. K. Hall and M. H. Wake, eds. Academic Press, San Diego, CA.
22. **Boutan, L. 1898.** Sur le développement de l'*Acmaea virginea. C. R. Hebd. Seances Acad. Sci. Paris* **126:** 1882–1889.
23. **Bandel, K. 1982.** Morphologie und Bildung der frühontogenetischen Gehäuse bei conchiferin Mollusken. *Facies* **7:** 1–198.
24. **Bandel, K. 1986.** The ammonitella: a model of formation with the aid of the embryonic shell of archaeogastropods. *Lethaia* **19:** 171–180.
25. **Morita, R. 1993.** Development mechanics of retractor muscles and the "Dead Spiral Model" in gastropod shell morphogenesis. *Neues Jahrb. Geol. Palaontol. Abh.* **190:** 191–217.
26. **Collin, R., and J. Voltzow. 1998.** Initiation, calcification, and form of larval "archaeogastropod" shells. *J. Morphol.* **235:** 77–89.
27. **Hickman, C. S. 1996.** Phylogeny and patterns of evolutionary radiation in trochoidean gastropods. Pp. 177–198 in *Origin and Evolutionary Radiation of the Mollusca,* J. D. Taylor, ed. Oxford University Press, Oxford.

Reference: *Biol. Bull.* **200:** 261–267. (June 2001)

Multiple Paternity in *Littorina obtusata* (Gastropoda, Littorinidae) Revealed by Microsatellite Analyses

IAN G. PATERSON[1,*], VANESSA PARTRIDGE[2], AND JOHN BUCKLAND-NICKS[2]

[1]*Department of Biology, Acadia University, Wolfville, Nova Scotia, Canada B0P 1X0; and* [2]*Department of Biology, St. Francis Xavier University, Antigonish, Nova Scotia, Canada B2G 2W5*

Abstract. Parental identity for juvenile *Littorina obtusata* was determined from three egg masses by means of microsatellite DNA markers. Results confirm that the attendant adult female in each case was the dam of the offspring and that at least 4–6 males contributed to each brood. This correlates with our behavioral observations that indicated multiple copulations between the female and several males in each experimental aquarium. A significant number of offspring from each brood were sired by non-sampled males (males that had copulated with females before capture) whose sperm had been stored by the female. This is the first direct evidence of multiple paternity in the Littorinidae. Results are discussed in reference to current theories of sperm competition, male precedence, and cryptic female choice.

Introduction

Littorinids, as well as most other gastropods, fertilize internally. Sperm are stored temporarily in the bursa copulatrix and for longer periods (3 months or more) in a second storage organ, the seminal receptacle, which usually is located deep within the oviduct (Buckland-Nicks *et al.*, 1999). In other animals where multiple paternity occurs, this scenario of two sperm storage organs may be correlated with cryptic female choice, in which the female selects among the sperm of several rival males (see review by Birkhead and Møeller, 1998). Some gastropods are capable of using stored sperm for more than one year (Trüb, 1990; Baur, 1998). Furthermore, in pulmonates, one copulation per reproductive season is sufficient to fertilize all the eggs produced by an individual in one year, which suggests that females control sperm release from the seminal receptacle, using only a fraction of stored sperm for each batch of eggs (Chen and Baur, 1993; Haase and Baur, 1995).

Molecular genetic markers have been used very effectively in the past to create DNA "fingerprints" that can genetically determine paternity. Previous studies of gastropod relationships have suggested that starch gel electrophoresis is inadequate to "elucidate the ecological dynamics of fertilization and paternity" (Gaffney and McGee, 1992), whereas the high variability at microsatellite DNA loci enables a more powerful analysis of parental relationships.

The intertidal snail *Littorina obtusata* is gonochoric. Females lay benthic egg masses containing 50–150 eggs (Bandel, 1974) in which embryos undergo direct development and emerge as crawling juveniles. In the present study, single locus microsatellite DNA markers were used to determine paternity of *L. obtusata* juveniles hatched from three egg masses kept in isolation in aquaria with several potential sires and the attendant dam in each case.

Materials and Methods

Samples

Adult specimens of *Littorina obtusata* were collected in early May 1999 from sites along the northeastern shore of Nova Scotia, Canada. Each shell was marked for gender and site number with nail varnish. All female snails used in the breeding experiment were collected from the same site (Port Bickerton) to ensure that all were in a relatively synchronous breeding cycle. Males were collected from five sites (Table 1) to increase the chance of genetic variability among the competing sires and thus increase the ability to assign paternity to the resulting offspring.

Individual females were isolated with 4–5 males and kept in 20-l aquaria at 8°C with a 12-h light/dark cycle. Mating

---

Received 2 November 2000; accepted 14 February 2001.

* To whom correspondence should be addressed. E-mail: ian.paterson@acadiau.ca.

Table 1

Collection sites in Nova Scotia of male Littorina obtusata *used in breeding and paternity analysis*

Location	Male ID code	Position
Port Bickerton	PB	45° 06′N, 61° 43′W
Fisherman's Harbour Wharf	FH	45° 07′N, 61° 40′W
Isaacs Harbour	IH	45° 12′N, 61° 39′W
Seal Harbour Wharf	SH	45° 09′N, 61° 34′W
Tor Bay Provincial Park	TB	45° 14′N, 61° 19′W

behavior was observed opportunistically throughout the experiment. Males that were observed in a stationary position, forward, and on the right side of the female's shell with the shell-lip and mantle touching, were recorded as "copulating." Males that were observed similarly positioned but slightly distal and without contact between the male mantle and female shell-lip were recorded as "possible mate-guarding" (see Discussion). Once egg masses were laid, the water temperature was increased to 10°C, which was reported to be a suitable temperature for egg development in the congener *Littorina sitkana* (Buckland-Nicks, 1974). Three additional males were included in the analyses for one brood (brood C). These males had escaped into the study tank and were then considered as potential sires.

When the juveniles reached about 1.4 mg in weight, they were frozen in a physiological buffer (10 m*M* Tris, pH 6.8) at −86°C. Adults were removed from their shells and frozen at −86°C in buffer following successful oviposition by the female.

DNA extraction

For each adult snail, a section of the foot was excised, rinsed with double-distilled H_2O and chopped, using a fresh razor blade, on a clean glass plate. This tissue was placed in 100 μl of TE (10 m*M* Tris-HCl pH 8, 1 m*M* EDTA) plus 0.5% Tween 20, and incubated at 60°C with 3 μl proteinase K (20 mg/ml). Following complete digestion, the DNA was isolated using a standard phenol:chloroform method (Sambrook *et al.*, 1989). The DNA was further purified by passing it through polyvinylpolypyrrolidone spin columns (Berthelet *et al.*, 1996; Paterson and Snyder, 1999) to ensure the removal of compounds that are known to co-purify with molluscan DNA and inhibit the polymerase chain reaction (Winnepenninckx *et al.*, 1993; Mikhailova and Johannesson, 1998). DNA concentration was estimated for each individual against Lambda HindIII molecular weight marker using agarose gel electrophoresis (Maniatis *et al.*, 1982).

DNA from individual juveniles (~1.4 mg wet weight) was isolated using the following protocol. Each juvenile was rinsed with double-distilled H_2O and placed in an Eppendorf tube with 40 μl of TE plus 0.5% Tween 20, then crushed against the side of the tube with a micropipetter tip. Two microlitres of proteinase K (20 mg/ml) was added, and the tube was incubated at 60°C for 20 min, followed by a 5-min incubation at 95°C to denature the proteinase K. The tubes were spun briefly to pellet the shell debris. To avoid any loss of DNA during subsequent purification steps, no further purification was conducted.

DNA amplification

DNA was screened for microsatellite repeats at 12 loci using primers designed on the congener *Littorina subrotundata* (Tie *et al.*, 2000). Of the 12 primer pairs, 8 did not produce scorable amplifications, and one locus was invariant (Lsub 6). Three loci were used for the analyses (Table 2). Approximately one-third of the offspring of each brood was typed at these three loci (40–46 juveniles per brood).

Amplifications were carried out by polymerase chain reaction (PCR) in 5-μl volumes containing ~0.2 ng DNA, 0.08 μ*M* γ33P-ATP end-labeled forward primer, 0.42 μ*M* forward primer, 0.5 μ*M* reverse primer, 20 μ*M* each dNTP, 0.2–0.5 units Taq polymerase, and 1× buffer containing 20 m*M* Tris pH 8, 50 m*M* KCl, 1.5 m*M* $MgCl_2$, and 0.1% Tween 20. Reactions were performed in an MJ Research PTC 100 thermocycler using an initial denaturation of 3 min at 94°C, followed by 25 cycles of denaturing at 93°C for 30 s per cycle, followed by optimal annealing (Lsub 8: 60°C; Lsub 32: stepdown from 55°C to 48°C; Lsub 62:

Table 2

Microsatellite loci used for paternity assessment in Littorina obtusata

Locus	Repeat motif*	PCR product size range (bp)	Number of alleles	Primer sequence (5′–3′)
Lsub 8	$(ATA)_{29}$	178–211	10	ccagtgaccagatcatagcg ggaattgtaaagtgcttggagc
Lsub 32	$(CAA)_{13}TG(AAC)_5$ $TG(AAC)_{10}$	210–343	14	atcacatcgcacacgcttac acggtgtgtcatcatcaacg
Lsub 62	$(AAC)_{14}$	160–187	8	cgctttcccgttataccaac caccgtaaaaccttgtgagc

* From Tie *et al.* 2000.

64°C) for 40 s + 1 s per cycle. Products were separated using 6% denaturing polyacrylamide gel electrophoresis and visualized using autoradiography (Hillis *et al.*, 1996).

All individuals were scored at each locus except for one offspring of female A which did not amplify and was discarded, and two offspring of female B which were not typed at one locus each. Maternity was confirmed by direct comparison to the maternal genotype.

Statistical analyses

Paternity was initially assessed using exclusion, wherein putative fathers were excluded if there were any mismatches between their alleles and those of the offspring. Subsequently, paternity inference was conducted using CERVUS software (Marshall *et al.*, 1998; Slate *et al.*, 2000), which is a Windows-based maximum likelihood program designed for use with co-dominant markers. Paternity assignment using likelihood techniques was determined at an 80% confidence threshold. Marshall *et al.* (1998) suggested that 80% confidence in paternity is more accurate than can be achieved using direct observation, and better than can be achieved using exclusionary approaches because the degree of confidence in non-excluded males is unknown in the exclusion technique. Paternity is inferred from the log-likelihood ratios (LOD score) based on the genotypes of the offspring, candidate sire, and dam. Confidence levels are determined through simulation (10,000 iterations) and defined by the statistic delta (Δ) where Δ is the difference between the LOD scores of the two most likely candidates.

Input parameters for the CERVUS software have important effects on the resulting paternity assignments. The "error rate" parameter of the simulation program allows an estimate of scoring error to be included in the calculations. Allowing for error prevents exclusion of true paternal candidates due to errors causing single locus mismatches, while potentially including (erroneously) sires that would otherwise be excluded. As the number of loci sampled increases, this error estimator becomes more important due to the increased probability of mis-scoring or mutation (Slate *et al.*, 2000). Our data set is small and all scores were double-checked for accuracy, so the error rate is probably lower than the 1% adopted by Marshall *et al.* (1998). Another important simulation parameter for this data set is the proportion of males sampled. We assumed a minimum number of non-sampled males (9, see Discussion).

Results

Behavioral observations

Mating behavior in *Littorina obtusata* involves pursuit of a female by a male during which he crawls over the right side of her shell and inserts the penis, engorged with hemolymph, into her gonopore, which opens into the oviduct and bursa copulatrix. A series of ventral mammiliform penial glands are brought into contact with the shell and mantle during this process. Male ejaculate exits the prostate gland in a dorsal penial groove and passes along the groove with the aid of ciliary action. On several occasions when copulating pairs were separated, ejaculate was seen moving along the penial groove toward the tip of the penis.

A total of 19 copulatory pairings and 8 incidences of suspected mate-guarding were observed. Males remained in copulatory position with females for 1–4.5 h and occasionally remained on the female, without genital contact, for up to 2.5 h after copulation. Each female was observed copulating with more than one male, and repeat copulations by individual males occurred in a number of cases. Eggs were laid from 7 to 21 days after introduction of females to the aquaria.

Microsatellite analyses

Paternity of each brood involved not only sampled males from aquaria but also non-sampled males that had copulated with females prior to capture. Assessment of paternity through exclusion (putative parents are excluded as true parents if a mismatch occurs at any allele that is present in the offspring) suggested that a minimum of 2 of the sampled males contributed to each brood. Additionally, the presence and distribution of the alleles that were not contributed by the sampled males requires a minimum of 2 non-sampled sires of brood A, 4 non-sampled sires of brood B, and 3 non-sampled sires of brood C to explain the genotypes found in the offspring. Based on exclusion, these non-sampled males contributed from 22.5% (9 of 40, family C) to 70.7% (29 of 41, family A) of the offspring per brood. Thus, the alleles present in the offspring are accounted for by a minimum of 4 sires of brood A, a minimum of 6 sires of brood B, and a minimum of 5 sires of brood C.

Determination of paternity based solely on exclusionary methods is simplistic and, in this case, inadequate to accurately resolve paternity. Paternity assessment was therefore conducted using CERVUS software to enable paternity assignments with 80% confidence based on maximum likelihood calculations. An important aspect of the CERVUS likelihood analyses is the estimate of scoring error (Marshall *et al.*, 1998). We determined paternity assignment for a range of scoring-error estimates (from 0% to 1.0%); however, results were similar and only 0.5% assignments are presented here (Table 3). Paternity was assigned with 80% confidence in 19.5% of the offspring of brood A, 40.8% of brood B, and 20.0% of brood C. Paternity assignment was recalculated for each brood by using a modified data set that included the two most likely non-sampled male genotypes inferred from the genotypes of the non-assigned offspring. With inclusion of the inferred male genotypes,

Table 3

Summary of paternity inference at 80% confidence computed using the CERVUS program

Female	Candidate sire (number of obs. matings)	Known paternal genotypes		Including inferred paternal genotypes	
		Offspring sired	Percent sired	Offspring sired	Percent sired
A	PB1 (1)	2	4.9	2	4.9
	FH1 (1)	0	—	0	—
	IH1 (0)	0	—	0	—
	SH1 (0)	6	14.6	0	—
	TB1 (3)	0	0	3	7.3
	No assignation	33	80.5	6	14.6
	Unknown A1	n/a	n/a	25	61.0
	Unknown A2	n/a	n/a	5	12.2
B	PB2 (3)	11	23.9	17	37.0
	FH2 (2)	8	17.4	14	30.4
	SH2 (2)	0	0	0	0
	No assignation	27	58.7	8	17.4
	Unknown B1	n/a	n/a	2	4.3
	Unknown B2	n/a	n/a	5	10.9
C	PB4 (2)	7	17.5	7	17.5
	FH4 (1)	0	0	1	2.5
	SH4 (0)	0	0	0	0
	TB4 (5)	0	0	0	0
	IH3 (0)	1	2.5	1	2.5
	SH3 (0)	0	0	0	0
	PB3 (0)	0	0	3	7.5
	No assignation	32	80.0	24	60.0
	Unknown C1	n/a	n/a	1	2.5
	Unknown C2	n/a	n/a	3	7.5
	Total assigned	36	28.0	89	70.0

Paternity assignment is indicated for a scoring-error estimate of 0.5%. Unknowns indicate the two most likely non-sampled sires inferred from the observed genotypes.

paternity was assigned for 85.4%, 82.6%, and 40.0% of the offspring in the three respective broods (Table 3).

Multiple mating was observed in all three females. Multiple paternity is clearly evident within the three broods, but the degree of paternal success varies throughout. Results produced using the modified data set (inferred male genotypes included) indicate that brood A was dominated by a single sire (61.0%, unknown A1); brood B had two relatively equally successful sires (37% for PB2, 30.4% for FH2) with at least four other sires contributing less than 11% each; and brood C was sired by at least five males, with no clearly dominant contributors.

Discussion

Duration of copulation and mate guarding

The duration of copulations we observed for *Littorina obtusata* in the laboratory varied from 1 to 4.5 h, which is in agreement with Ankel's (1936, cited in Baur, 1998) observations for this species and similar to times reported from some other prosobranchs (Martel *et al.*, 1986). In contrast, Struhsaker (1966) reported copulatory pairing to last 30–45 min in *L. picta* and only 5–10 min in *L. pintado*. These differences in duration of mating may reflect real differences in reproductive behavior or morphology among different littorinids, including the presence or absence of penial glands, which are thought to secure the penis in place during copulation (Reid, 1989; Buckland-Nicks and Worthen, 1992). Parker (1970a) suggested that in some animal species, such prolonged copulations could be the male's way of reducing the probability of female remating by acting as a mechanical plug. Males of many animal species exhibit "passive phase behavior" in which they guard reproductive females after copulating (*e.g.*, Parker and Smith, 1975; Parker, 1984). The males in this study exhibited such behavior, remaining on the right side of the female's shell without genital contact for up to 2.5 h after copulation. An extended mating time plus guarding behavior may allow sufficient time for sperm to be transferred from the bursa copulatrix to the seminal receptacle, thereby increasing the male's chance of paternity. The time taken to transfer sperm between storage organs is not known for the Littorinidae, but Martel *et al.* (1986) reported that sperm are transferred quickly from the bursa to the seminal receptacle in *Buccinum undatum,* taking at the most 3 days.

Multiple paternity

Multiple paternity has been demonstrated in a number of molluscan species. Among gastropods, studies of multiple paternity have been largely restricted to pulmonates (*e.g.*, Mulvey and Vrijenhoek, 1981; Rollinson *et al.*, 1989; Wethington and Dillon, 1991; Baur, 1994), with fewer investigations conducted on marine prosobranchs (*e.g.*, Gaffney and McGee, 1992). However, multiple copulations by females with different males have been reported in a wide range of gastropod families, suggesting that multiple paternity is common (see Martel *et al.*, 1986). Evidence of multiple paternity in *L. obtusata* was expected from both field and laboratory observations of multiple copulations by individual females. In this study, the number of males contributing to each brood is relatively high, with an absolute minimum of 4–6 sires per brood. This may be an underestimate of the number of true sires since only a fraction of each brood was tested, and a number of the alleles examined were fairly common.

The candidate sire that had immediate access to the females prior to spawning (*i.e.*, sampled males) sired fewer offspring (average of 37.8%) than the previously mated males (non-sampled), providing no evidence of last-male precedence. This is in agreement with a study of pseudoscorpions by Zeh and Zeh (1994), who found last-male precedence to be typical of two male systems (see also Parker, 1970b; Parker and Smith, 1975; Gwynne, 1984), but found no evidence of last-male precedence in broods from more promiscuous females.

The success rate of individual males appears highly variable—the dominant sire contributed from 61% (non-sampled A1, brood A) to 17.5% (PB4, brood C) of the offspring. Although the dominance of brood A by a single male is suggestive of first-male precedence, this is not upheld in the other broods. Indeed, brood B had greater than half of the offspring sired by "later" males (67.4%), and no previously mated males contributed to more than 11% of the offspring (Table 3). Thus, first-male precedence is not the prevalent reproductive mode in *L. obtusata.*

Copulation does not necessarily indicate successful sperm transfer to the female, because the male may not have inserted his penis or may not have delivered ejaculate (Gibson, 1964). However, when Buckland-Nicks *et al.* (1999) examined sperm transfer in the penis of *Littorina littorea* specimens that had been flash-frozen during confirmed copulation, they determined that sperm transfer often had been occurring at the time of disruption. In the present study, incidence of copulation was inferred based on male position and duration of coupling. Pairs invariably separated when picked up and, as in observations made by Gibson (1964) on *L. planaxis,* ejaculate was observed moving along the penis in some instances. It is probable that sperm transfer was not occurring during some observations of "copulation"; for example, male TB4 was observed mating 5 times and male SH2 observed 2 times (Table 3), yet neither was successful in siring offspring.

In *L. obtusata* the high degree of multiple paternity in the resulting offspring indicates that sperm must be mixing within the female's reproductive tract. Although release of sperm from the seminal receptacle may merely be the result of the female contracting the muscle layer surrounding the seminal receptacle (Buckland-Nicks and Chia, 1990), post-copulatory selection is also a possibility. This could occur either through sperm competition within the seminal receptacle or bursa copulatrix, or through post-copulatory female choice. Post-copulatory female choice may be accomplished in a number of ways, such as by dumping unwanted sperm, as observed in *L. scabra* (reported in Buckland-Nicks, 1998), by sperm digestion in the bursa copulatrix (see reviews by Buckland-Nicks, 1974; Fretter and Graham, 1994), or by sperm sorting and differential use within the reproductive tract (Haase and Baur, 1995).

On sperm storage organs

How does such short-term mate guarding increase the male's chances of successful paternity? Species with a single blind-ended sperm storage organ usually show a pattern of last-male precedence in siring offspring, because rival males have the opportunity to actively disrupt or remove any sperm already stored there (*e.g.*, Waage, 1979, 1984) or to passively displace the sperm deeper, rendering it ineffectual (*e.g.*, Lefevre and Jonsson, 1962; Parker, 1970b). However, last-male precedence is not prevalent in species with two sperm storage organs, like littorinid snails, where there is an opportunity for the first male's sperm to be transferred to the second storage organ before physical interference is possible by a subsequent male.

Besides the number of storage organs present, the shape of the sperm storage organs also has an effect on sperm precedence. Species which exhibit last-male precedence often have a relatively long, tubular, blind-ended storage organ, which is thought to promote stratification of sperm, with older sperm being overlaid by sperm from successive matings (*e.g.*, Walker, 1980; Briskie and Montgomerie, 1993). However, Zeh and Zeh (1994) suggest that though tubular morphology may favor sperm stratification, this relationship breaks down if the storage organ becomes completely filled, which causes increased pressure and induces sperm mixing.

Spherical storage organs are thought to promote sperm mixing (Walker, 1980). In *L. obtusata,* the bursa copulatrix is the primary sperm storage organ. The bursa is a blind-ended sac, providing the potential for sperm stored there to be disturbed by the penial filaments of rival males. Although there is no evidence of physical sperm displacement from the bursa copulatrix in *Littorina*, this remains a possibility because penial filaments are extensible and very mobile (Buckland-Nicks, 1974; Buckland-Nicks *et al.*, 1999). The secondary sperm storage organ, the seminal receptacle, is much smaller than the bursa and is situated deep within the pallial oviduct, beyond the reach of the penial filament (Buckland-Nicks and Chia, 1990). The longer a male guards a female, preventing her from participating in further mating, the greater the likelihood of his sperm leaving the bursa copulatrix and becoming stored in the seminal receptacle, to which male genitalia have no access.

Whether female littorinids can selectively store and use sperm from the seminal receptacle is not known. Our results for two of the three broods (A and C) indicate that the males that mated prior to capture had more success than the last males to mate, even though these later males were isolated with the female for up to 3 weeks. Moreover, males from places other than the home locale of the females (Port Bickerton) had little to no success. It is thus possible that females have some ability to stratify sperm in the seminal receptacle or to dump sperm from the bursa copulatrix. In this context, Haase and Baur (1995) suggested that females may be able to manipulate fertilization of eggs by storing sperm in different areas of the seminal receptacle. In *L. obtusata*, one might expect that the first sperm to reach the seminal receptacle would be stored close to its exit, favoring first-male precedence. However, our results support neither first nor last-sperm precedence and suggest there is mixing of sperm within the female's reproductive tract.

The results of paternity from the three egg masses of *L. obtusata* raise some intriguing questions about sperm selection. To fully understand the occurrence of sperm competition or cryptic female choice in these snails, experiments must be designed that track the sperm of individual males inside the female, as well as in the resulting offspring. This might be accomplished by using sperm-specific fluorophores, genetic markers, or the tried and tested method of radioautography (Beeman, 1970).

Acknowledgments

This study would not have been possible without the generous contribution of primers by E. Boulding. Thanks are also due to M. Snyder and D. Stewart for helpful advice and the use of lab space and equipment. We are grateful to G. Gibson for comments that improved the manuscript. This study was supported by a NSERC of Canada research grant to J.B-N.

Literature Cited

Ankel, W. E. 1936. Prosobranchia. Pp. 1–240 in *Die Tierwelt der Nord- und Ostsee*. G. Grimpe and E. Wagler, eds. Akademische Verlagsgemeinschaft, Leipzig.

Bandel, K. 1974. Studies on Littorinidae from the Atlantic. *Veliger* **17:** 92–114.

Baur, B. 1994. Multiple paternity and individual variation in sperm precedence in the simultaneously hermaphroditic land snail *Arianta arbustorum*. *Behav. Ecol. Sociobiol.* **35:** 413–421.

Baur, B. 1998. Sperm competition in molluscs. Pp. 255–305 in *Sperm Competition and Sexual Selection*, T. R. Birkhead and A. P. Møeller, eds. Academic Press, New York.

Beeman, R. D. 1970. The anatomy and functional morphology of the reproductive system in the opisthobranch mollusk *Phyllaplysia taylori* Dall, 1950. *Veliger* **13:** 1–31.

Berthelet, M., L. G. Whyte, and C. W. Greer. 1996. Rapid, direct extraction of DNA from soils for PCR analysis using polyvinylpolypyrrolidone spin columns. *FEMS Microbiol. Lett.* **138:** 17–22.

Birkhead, T. R., and A. P. Moeller. 1998. *Sperm Competition and Sexual Selection*. Academic Press, London. 826 pp.

Briskie, J. V., and R. Montgomerie. 1993. Patterns of sperm storage in relation to sperm competition in passerine birds. *Condor* **95:** 442–454.

Buckland-Nicks, J. 1974. The functional morphology of the reproductive systems and the larval development of two intertidal snails, *Littorina sitkana* (Philippi 1845) and *Littorina scutulata* (Gould 1849) with special reference to the spermatozoa. Ph.D. thesis, University of Alberta, Canada. 258 pp.

Buckland-Nicks, J. 1998. Prosobranch parasperm: sterile germ cells that promote paternity? *Micron* **29:** 267–280.

Buckland-Nicks, J., and F. S. Chia. 1990. Egg capsule formation and hatching in the marine snail *Littorina sitkana*. *Philos. Trans. R. Soc. Lond. B* **326:** 159–176.

Buckland-Nicks, J., and G. T. Worthen. 1992. Functional morphology of the mammiliform penial glands of *Littorina saxatilis* (Gastropoda). *Zoomorphology* **112:** 217–225.

Buckland-Nicks, J., I. Bryson, L. Hart, and V. Partridge. 1999. Sex and a snail's sperm: on the transport, storage and fate of dimorphic sperm in Littorinidae. *Int. J. Invertebr. Reprod. Dev.* **36:** 145–152.

Chen, X., and B. Baur. 1993. The effect of multiple mating on female reproductive success in the simultaneously hermaphroditic land snail *Arianta arbustorum*. *Can. J. Zool.* **71:** 2431–2436.

Fretter, V., and A. Graham. 1994. *British Prosobranch Molluscs, Their Functional Anatomy and Ecology*, vol. 161. The Ray Society of London, London. 820 pp.

Gaffney, P. M., and B. McGee. 1992. Multiple paternity in *Crepidula fornicata*. *Veliger* **35:** 12–15.

Gibson, D. G. 1964. Mating behaviour in *Littorina planaxis* Philippi (Gastropoda: Prosobranchia). *Veliger* **7:** 134–139.

Gwynne, D. T. 1984. Male mating effort, confidence of paternity, and insect sperm competition. Pp. 117–149 in *Sperm Competition and the Evolution of Animal Mating Systems*. R. L. Smith, ed. Academic Press, New York.

Haase, M., and B. Baur. 1995. Variation in spermathecal morphology and storage of spermatozoa in the simultaneously hermaphroditic land snail *Arianta arbustorum* (Gastropoda: Pulmonata: Stylommatophora). *Invertebr. Reprod. Dev.* **28:** 33–41.

Hillis, D. M., B. K. Mable, A. Larson, S. K. Davis, and E. A. Zimmer. 1996. Nucleic acids IV: sequencing and cloning. Pp. 321–384 in *Molecular Systematics*, 2nd ed. D. M. Hillis, C. Moritz, and B. K. Mable, eds. Sinauer, Sunderland, MA.

Lefevre, G., and U. B. Jonsson. 1962. Sperm transfer, storage, displacement and utilization in *Drosophila melanogaster*. *Genetics* **47:** 1719–1736.

Maniatis, T., E. F. Fritsch, and J. Sambrook. 1982. *Molecular Clon-*

ing, a Laboratory Manual. Cold Spring Harbor Laboratory Press, Cold Spring Harbor, NY. 545 pp.

Marshall, T. C., J. Slate, L. E. B. Kruuk, and J. Pemberton. 1998. Statistical confidence for likelihood-based paternity inference in natural populations. *Mol. Ecol.* **7:** 639–655.

Martel, A., D. H. Larrivée, and J. H. Himmelman. 1986. Behaviour and timing of copulation and egg-laying in the neogastropod *Buccinum undatum* L. *J. Exp. Mar. Biol. Ecol.* **96:** 27–42.

Mikhailova, N., and K. Johannesson. 1998. A comparison of different protocols for RAPD analysis of *Littorina. Hydrobiologia* **378:** 33–42.

Mulvey, M., and R. C. Vrijenhoek. 1981. Multiple paternity in the hermaphroditic snail *Biomphalaria obstructa. J. Hered.* **72:** 308–312.

Parker, G. A. 1970a. Sperm competition and its evolutionary consequences in insects. *Biol. Rev. Camb. Philos. Soc.* **45:** 525–567.

Parker, G. A. 1970b. Sperm competition and its evolutionary effect on copula duration in the fly *Scatophaga stercoraria. J. Insect Physiol.* **16:** 1301–1328.

Parker, G. A. 1984. Sperm competition and the evolution of animal mating strategies. Pp. 2–60 in *Sperm Competition and Sexual Selection,* T. R. Birkhead and A. P. Møeller, eds. Academic Press, New York.

Parker, G. A., and J. L. Smith. 1975. Sperm competition and the evolution of the precopulatory passive phase behaviour in *Locusta migratoria migratorioides. J. Entomol. Ser. A* **49:** 155–171.

Paterson, I. G., and M. Snyder. 1999. Genetic evidence supporting the taxonomy of *Geum peckii* (Rosaceae) and *G. radiatum* as separate species. *Rhodora* **101:** 325–340.

Reid, D. G. 1989. The comparative morphology, phylogeny and evolution of the gastropod family Littorinidae. *Philos. Trans. R. Soc. Lond. B* **324:** 1–110.

Rollinson, D., R. A. Kane, and J. R. L. Linnes. 1989. An analysis of fertilization in *Bulinus cernicus* (Gastropoda: Planorbidae). *J. Zool. Lond.* **217:** 295–310.

Sambrook, J., E. F. Fritsch, and T. Maniatis. 1989. *Molecular Cloning, a Laboratory Manual.* Cold Spring Harbor Laboratory Press, Cold Spring Harbor, NY.

Slate, J., T. Marshall, and J. Pemberton. 2000. A retrospective assessment of the accuracy of the paternity inference program CERVUS. *Mol. Ecol.* **9:** 801–808.

Struhsaker, J. W. 1966. Breeding, spawning periodicity and early development in the Hawaiian *Littorina: L. pintado* (Wood), *L. picta* (Philippi) and *L. scabra* (Linné). *Proc. Malacol. Soc. Lond.* **37:** 137–166.

Tie, A. D., E. G. Boulding, and K. A. Naish. 2000. Polymorphic microsatellite markers for the marine gastropod *Littorina subrotundata. Mol. Ecol.* **9:** 108–110.

Trüb, H. 1990. Züchtung von Hybriden zwischen *Viviparus ater* und *V. contectus* (Mollusca: Prosobranchia) im Zürichsee und ökologische Untersuchungen in einer gemischten Population im Gardasee. Ph.D. Thesis, University of Zurich, Switzerland. 88 pp.

Waage, J. K. 1979. Dual function of the damselfly penis: sperm removal and transfer. *Science* **203:** 916–918.

Waage, J. K. 1984. Sperm competition and the evolution of odonate mating systems. Pp. 251–290 in *Sperm Competition and the Evolution of Animal Mating Systems,* R. L. Smith, ed. Academic Press, New York.

Walker, W. F. 1980. Sperm utilization strategies in nonsocial insects. *Am. Nat.* **115:** 780–799.

Wethington, A. R., and R. T. Dillon, Jr. 1991. Sperm storage and evidence for multiple paternity in a natural population of the freshwater snail *Physa americana. Am. Malacol. Bull.* **9:** 99–102.

Winnepenninckx, B., T. Backeljau, and R. De Wachter. 1993. Extraction of high molecular weight DNA from molluscs. *Trends Genet.* **9:** 407.

Zeh, J. A., and D. Zeh. 1994. Last-male sperm precedence breaks down when females mate with three males. *Proc. R. Soc. Lond. B* **257:** 287–292.

Reference: *Biol. Bull.* **200:** 268–280. (June 2001)

Development of Serotonin-like and SALMFamide-like Immunoreactivity in the Nervous System of the Sea Urchin *Psammechinus miliaris*

AMY-JANE BEER, CLAIRE MOSS*, AND MICHAEL THORNDYKE†

School of Biological Sciences, Royal Holloway, University of London, Egham, Surrey TW20 0EX, UK

Abstract. The present immunocytochemical study utilizes serotonin and SALMFamide antisera, together with confocal laser scanning microscopy, to provide new information about the development of the nervous system in the sea urchin *Psammechinus miliaris* (Echinodermata: Echinoidea). Special attention is paid to the extent of the nervous system in later larval stages (6-armed pluteus to metamorphic competency), a characteristic that has not been well described in this and other species of sea urchin. An extensive apical ganglion appears by the 6-armed pluteus stage, forming a complex of 10-20 cells and fibers, including discrete populations of both serotonin-like and SALMFamide-like immunoreactive cells. At metamorphosis this complex is large, comprising at least 40 cells in distinct arrays. Serotonin-like immunoreactivity is also particularly apparent in the lower lip ganglion of 6- to 8-armed plutei; this ganglion consists of 15-18 cells that are distributed around the mouth. The ciliary nerves that lie beneath the ciliary bands in the larval arms, the esophagus, and a hitherto undescribed network associated with the pylorus all show SALMFamide-like immunoreactivity. The network of cells and fibers in the pyloric area develops later in larval life. It first appears as one cell body and fiber, then increases in size and complexity through the 8-armed pluteus stage to form a complex of cells that encircles the pylorus. SALMFamide-like, but not serotonin-like, immunoreactivity is seen in the vestibule wall, tube feet, and developing radial nerve fibers of the sea urchin adult rudiment as the larva gains metamorphic competency.

Introduction

The presence of a nervous system in echinoid larvae was first suggested by observations of a putative thickening in the apical area (MacBride, 1914) and the presence of neuron-like cells in the adoral ciliary band (Mortensen, 1921). Further evidence for such a system was circumstantial, derived from observations of feeding, locomotion, settlement, and orientation behavior. These behaviors, although relatively simple, suggested the coordinating influence of a nervous system, an idea finally confirmed by studies on ciliary activity (Mackie *et al.*, 1969). More recent histological and histochemical studies have provided greater details of the arrangement and fine structure of neurons in the ciliated bands and esophageal musculature of echinoderms (Burke, 1978; Nakajima, 1986, 1988; Lacalli *et al.*, 1990).

A rich quota of neurochemicals is associated with the larval nervous system, including acetylcholine, serotonin, γ-aminobutyric acid (GABA), noradrenaline, and dopamine (Bisgrove and Burke, 1987; Nakajima, 1988). Such a variety of agents hints at the organizational complexity of this system. Histochemical and immunocytochemical methods have been especially productive in revealing previously unknown neural structures in larvae (Nakajima, 1986; Kroll and Voronezhskaya, 1996). The discovery of the native echinoderm neuropeptides, S1 (GFNSALMFamide – amino acid notation) and S2 (SGPYSFNSGLTFamide), and the subsequent availability of highly specific antibody probes have provided a further means to investigate the larval and adult echinoderm nervous system.

S1 was originally isolated from starfish and shown to have a ubiquitous distribution in the nervous system of *Asterias rubens* (Elphick *et al.*, 1991a; Newman *et al.*, 1995a, b). Similar peptides that seem to be members of the same family were also identified in holothurians (Diaz-

---

Received 21 March 2000; accepted 9 March 2001.

* Current address: Scottish Association for Marine Science, Oban, Argyll, PA34 4AD, UK.

† To whom correspondence should be addressed. E-mail: m.thorndyke@rhbnc.ac.uk.

Miranda *et al.*, 1992), and S1-like molecules are also present in crinoids and ophiuroids (Ghyoot *et al.*, 1994; Candia Carnevali *et al.*, 1998). This family of peptides has also been localized in the larval nervous systems of starfish (Moss *et al.*, 1994; Byrne *et al.*, 1999) and sand dollars (Thorndyke *et al.*, 1992), revealing subsets of neurons not previously identified with other probes.

Novel neurochemical markers (such as peptide antisera) can help us complete our picture of the larval and adult nervous systems and, perhaps, add supporting data to other studies of the physiological function of the molecules. That is, information about the location of neurochemicals within a cell, within a cell type, or within a tissue type can sometimes help to indicate whether these molecules may be involved in motor or sensory activities or may be neurotransmitters or neuromodulators. In echinoderms, neurochemical markers, when expressed at various developmental stages, can help us visualize the origin, growth, and fate of particular neural structures.

The aim of the present study was to map the development of the larval echinoid nervous system using immunocytochemical techniques, with established commercial (serotonin) and novel (SALMFamide) antisera serving as probes. We used *Psammechinus miliaris*, a small regular sea urchin of the class Echinoidea, which is common along the northeast Atlantic and North Sea coasts of the United Kingdom and Scandinavia. The development of *P. miliaris* has never been fully described in the literature, although we and other researchers (*e.g.*, Kelly *et al.*, 2000) have found it to be similar to that of other species of indirect developing sea urchins, passing through embryo, prism, and 4-, 6-, and 8-armed plutei stages to metamorphic competency (MacBride, 1913, 1914, 1918). In the current work, emphasis has been placed on the later larval stages, which are less well described by immunocytochemical studies. Confocal microscopy has been used to facilitate the accurate localization of larval neurons, to identify previously unknown components of the nervous system, and to improve the resolution of the cells and fibers.

Materials and Methods

Animal maintenance and larval culture

Specimens of *Psammechinus miliaris* were obtained from the University Marine Biological Laboratory at Millport, Isle of Cumbrae, and from Dunstaffnage Marine Laboratory, Oban, on the west coast of Scotland. They were maintained in circulating seawater systems at Royal Holloway or in Oban and fed on *Ulva lactuca*, *Mytilus edulis*, and an artificial food consisting of soya meal, fish oil, and spinach. Males and females could generally be distinguished by slight differences in the appearance of their gonopores. Animals were spawned by the injection of 0.5 *M* KCl in filtered seawater (FSW) into the area of the gonads, with the needle inserted through the peristomial membrane (Iwate and Fukase, 1964). Animals were placed in glass beakers for about 30 min, or until they spawned. Gametes were collected and eggs fertilized by standard methods (Strathmann, 1987). After hatching, larvae were maintained in autoclaved seawater in glass jars and gently stirred to prevent them from gathering at the bottom of the vessel. Once the gut had developed, the larvae were fed *Dunaliella tertiolecta* so that algae could always be seen in the gut. The larval cultures were kept clean by replacing one-third of the water three times a week. Cultured algae were separated from the growth medium and resuspended in FSW before being fed to the larvae. To prevent overcrowding, the concentration of larvae in each jar was kept at about 1 per 5 milliliters of FSW. Animals were thus maintained throughout larval development, until competency. Competent larvae with a large, well-developed rudiment were induced to settle by the introduction of algal-fouled glass plates from the aquarium. Similarly, larvae would also often settle and metamorphose on the bottom of the culture vessels, if these were allowed to become fouled with algal debris.

Fixation

Samples of larvae were removed from culture and fixed at regular intervals, ensuring that each stage (4-armed, 6-armed, and 8-armed plutei) was adequately represented. At least 100 larvae per sample were fixed at earlier stages. This reduced to 20 per sample for 8-armed animals with developed rudiments. Larvae were anesthetized in 4% $MgCl_2$ in FSW or killed by the addition of a few drops of 4% paraformaldehyde (PFA) in FSW. Excess seawater was then pipetted off, and the samples were fixed in 4% PFA in FSW for 2 h. For storage, animals were rinsed in FSW and stored in FSW containing 0.01% NaN_3 at 4°C.

Immunocytochemistry

Whole-mount incubations were carried out in 2-ml glass tubes at room temperature. Larvae were rinsed in phosphate buffered saline (PBS) and permeabilized by a 30-min incubation in 0.5% Triton-X 100 in PBS, followed by 30 min in 5% normal goat serum in PBS. To improve antiserum penetration, and thus the staining of the rudiment in older larvae, a further permeabilization step was carried out. After fixation, larvae were rapidly dehydrated to 70% ethanol, rehydrated, and incubated in 0.5% Triton-X 100 in PBS for 1-2 h. Primary antibodies were diluted in PBS, and the larvae were incubated in this solution for 16-18 h. The serotonin antiserum (SeraLabs, UK) was raised in rabbit against synthetic serotonin and used at 1:200 in PBS. All results with this antibody are referred to as serotonin-like immunoreactivity (5HT-Li IR). The peptide antisera were raised in rabbits and produced in this laboratory; they are all polyclonals. Anti-S1 (BL1V/anti-KYSALMFa) or anti-S1

(BLIIIa/anti-KYSALMFa) (Elphick *et al.*, 1991a, b) were used at 1:200 in PBS, which gave clear staining with low background. These antisera are two consecutive bleeds from one animal and will be referred to as S1-like immunoreactivity (S1-Li IR). Some 6-armed plutei were also stained for S2 with a new polyclonal raised in this laboratory (N1/anti-KYSGLTFa) (Potton, 1997), which produced preparations of high specificity and low background levels. Results with this antiserum are referred to as S2-like immunoreactivity (S2-Li IR).

After overnight incubation in primary antisera, larvae were washed in PBS, three times each for 5 min. Visualization was by a 1-h incubation in biotinylated anti-rabbit IgG (1:200 in PBS) (Vector Labs, Peterborough, UK), rinsing in PBS, and then a final incubation for 1 h in avidin-conjugated FITC or Texas red (1:100 in PBS) (Vector Labs). Larvae were rinsed in PBS and mounted in Vectashield antifade mountant (Vector Labs) and viewed on a Zeiss Axioplan with fluorescent attachments, or on a Leica TCS-4D confocal laser scanning microscope (CLSM).

Controls were produced by preabsorption of twice the working concentration of primary antiserum with an equal volume of 2 × 10 μM KYSALMFa, KYSGLTFa, or 5HT (Polak and Van Noorden, 1986). This reduced staining to background levels in all cases, although it was not completely removed. Preadsorption controls revealed weak cross-reactivity between the peptide antisera where preadsorption of anti-S1 with S2 did not affect staining as much as did preadsorption of anti-S2 with S1. Further controls for secondary antibodies were carried out by replacing the primary with PBS, or by using direct visualization with FITC- or Texas red-conjugated secondary antibodies, which controlled for reactions with endogenous biotins.

Results

For the purposes of this study, the development of *Psammechinus miliaris* was divided into five stages: prism (2 to 3 days post-fertilization), 4-armed, 6-armed, and 8-armed plutei (from 3 to 20 days), and competent plutei (from 20 to 30 days). The adult rudiment began to form at the 6-armed stage, and was well developed in the late 8-armed pluteus. In cultures of *P. miliaris* the total development period, from egg to new juvenile, was between 20 and 30 days. Figure 1 shows the key features of the pluteus nervous system and summary diagrams of the results. Figure 1A depicts the extent of the larval nervous system as it is known from previous immunocytochemical studies. Figure 1B shows the more extensive system revealed by the present immunocytochemical study.

Observations of living larvae revealed distinctive cell types associated with the sea urchin larval nervous system. These observations, together with previous descriptions of neuronal cell types in these areas (Burke, 1978; Nakajima, 1986; Lacalli *et al.*, 1990), assisted us in identifying those cells in *P. miliaris* that were stained by immunocytochemical methods. In late prism larvae (2-3 days post-fertilization), the ciliated band could be clearly observed. The cells of the blastocoelar network were also visible (Fig. 2A). These cells were previously thought to be part of the nervous system, but subsequent work has shown that they are not neural but have some other function, possibly associated with muscle activity (Burke, 1978). Neuron-like cells within the ciliary bands were visible; their characteristic shape, with a thick apical process, suggested they might be sensory cells (Fig. 2B, C). Fine basal processes contribute to a tract of fibers beneath the ciliary band, forming part of the ciliary nerve (Fig. 2C), which then putatively connects to other larval structures. The ciliary band and its associated neurons and fibers elongates as the larval arms develop and form the main neural pathways of the larva. Along with the apical ganglion, lower lip ganglion, and neural components of the gut, these structures constitute the main neuronal elements of the sea urchin larval nervous system (Fig. 1).

The immunocytochemical studies focused on later pluteal stages, which have been less thoroughly described in previous investigations (Bisgrove and Burke, 1987; Thorndyke *et al.*, 1992). These studies enabled a detailed examination of the fully developed apical ganglion and adult rudiment.

Development of immunoreactivity in plutei to the 8-armed stage

The earliest cellular labeling observed in young plutei was a single cell within the thickened lower lip of the stomatodeum, which was strongly immunoreactive to the serotonin antibody (Fig. 3A). This cell was seen in the most precocious larvae at about 72 h post-fertilization. The cell has a basal unlabeled nucleus and faintly immunoreactive basal processes that extended beneath the lip. There was also a suggestion of labeled cells in the ciliated band of the anterolateral arm buds. There was no comparable labeling with the other antisera in larvae of the same age or in control specimens that received only primary antibody or an inappropriate secondary antibody. At the fully developed 4-armed stage (4 or 5 days post-fertilization) the lower lip contains several cells with 5HT-Li IR in a symmetrical arrangement (Fig. 3B). A similar pattern of labeled lower lip cells is also apparent in 4-armed specimens stained with anti-S1, although these cells are comparatively large (15 μm), and less numerous. At this stage, no S1-Li IR cells were seen in the apical thickening. The larval stomach contains algae and is autofluorescent.

By the 6- to 8-armed pluteus stage, the number of labeled cells in the lower lip complex is increased, with up to 18 neurons showing 5HT- and S1-Li IR. When viewed from the side, these cells have a characteristic shape, with broad bases against the esophageal epithelium and narrower api-

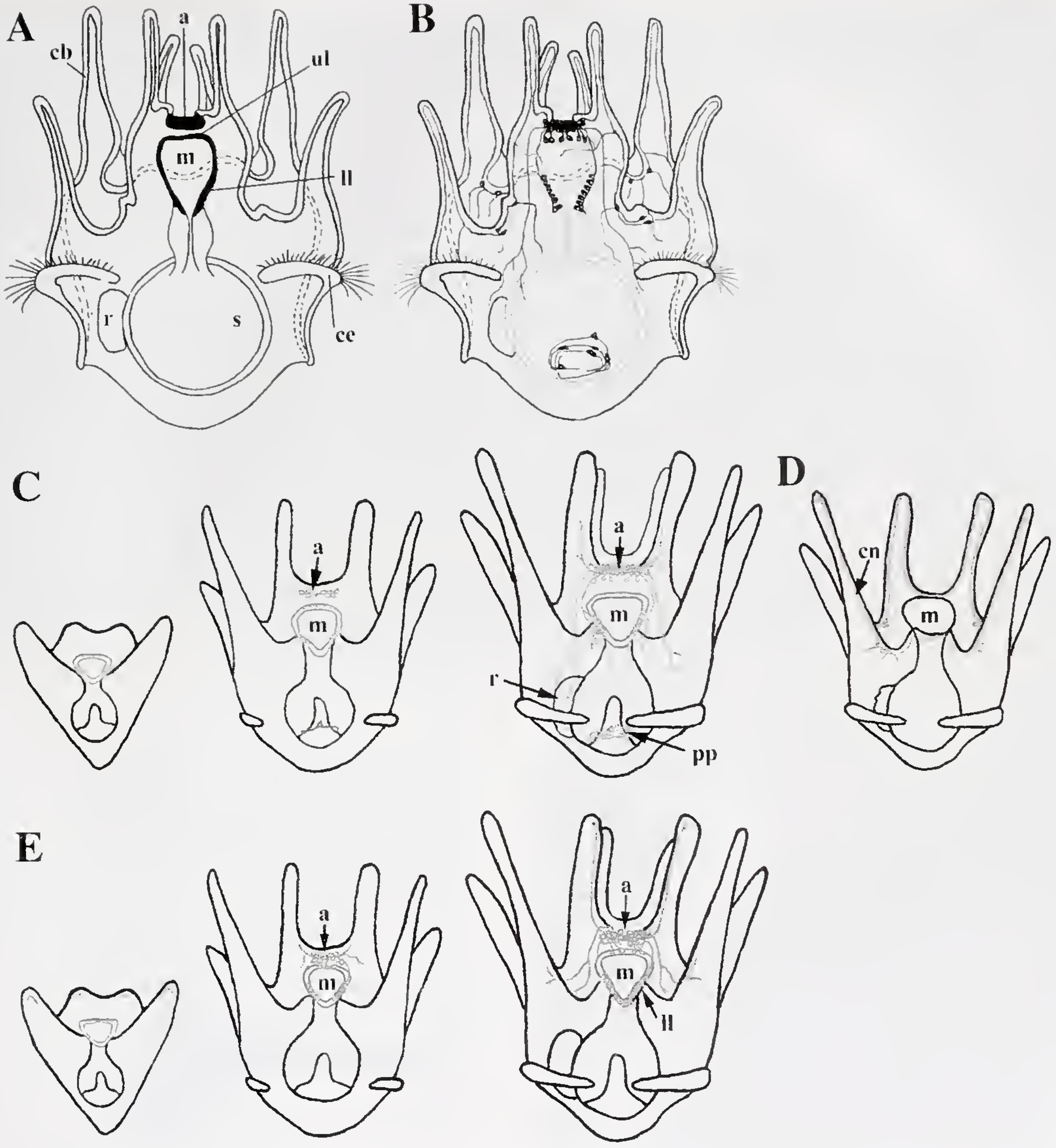

Figure 1. Diagrams of pluteus larvae. (A) Previously demonstrated sites of innervation (solid fill) in a sea urchin larva (Nakajima, 1986; Bisgrove and Burke, 1987; Thorndyke *et al.*, 1992). (B) The extent of the nervous system, as revealed in this study. (C) The main areas of S1-Li IR (gray) in the early 4-armed, early 6-armed, and 8-armed pluteus. (D) The main areas of S2-Li IR (gray) in the 6-armed pluteus. (E) The main areas of 5HT-Li IR (gray) in the early 4-armed, early 6-armed, and 8-armed pluteus, clearly showing its predominantly ventral distribution. a-apical ganglion, cb-ciliary band, ce-ciliary epaulette, cn-ciliary nerve, ll-lower lip, m-mouth, pp-pyloric plexus, r-rudiment, s-stomach, ul-upper lip. Not to scale.

ces at the ectoderm of the inner edge of the oral hood. From the 6-armed stage onwards the apical complex begins to increase dramatically in both size and complexity, whereas the lower lip complex expands no further. Indeed, the 5HT-Li IR appears to weaken at later stages. The row of small cells first seen in the upper lip at the 4-armed stage alters little during subsequent development.

In later plutei, 5HT-Li IR cells in the upper lip could be seen contributing processes to the expanding apical ganglion (Fig. 4A-D). This association is close enough at this stage for the apical and upper lip complexes to be considered part of the same ganglion. The apical complex becomes the predominant site of both 5HT and S1-Li IR neurons, as the 4- and 6-armed plutei progresses to a full 8-armed stage,

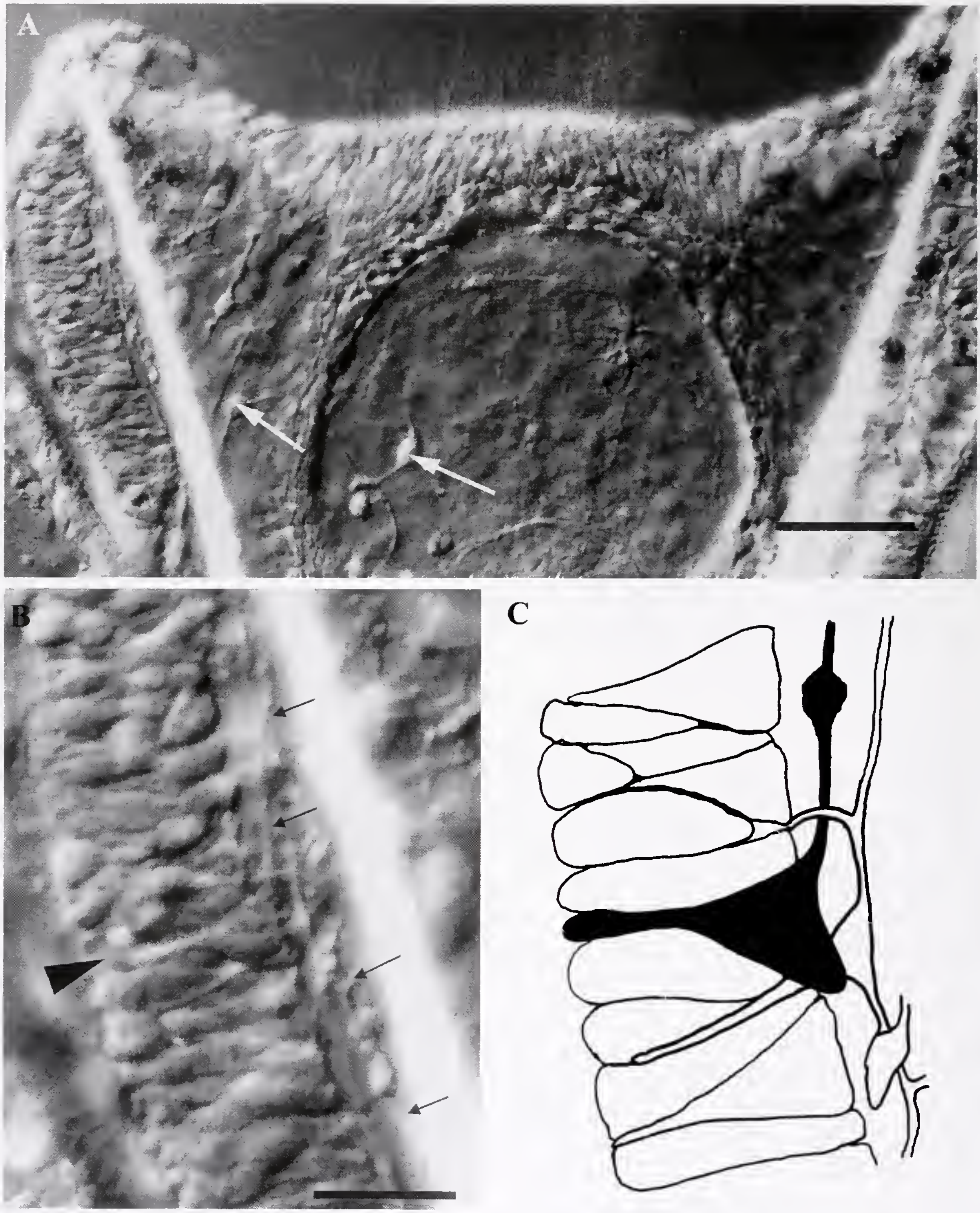

Figure 2. Observations of live larvae. (A) Multipolar cells of the blastocoelar network in the oral hood of an early 4-armed pluteus (arrows). (B) Higher magnification of (A) showing a flask-shaped bipolar neuron with a tapering apical process (arrowhead) and basal varicose axon contributing to the ciliary nerve (arrows). (C) Diagram of (B) with the neuron shown in black (not to scale). Bars: A = 25 μm, B = 10 μm.

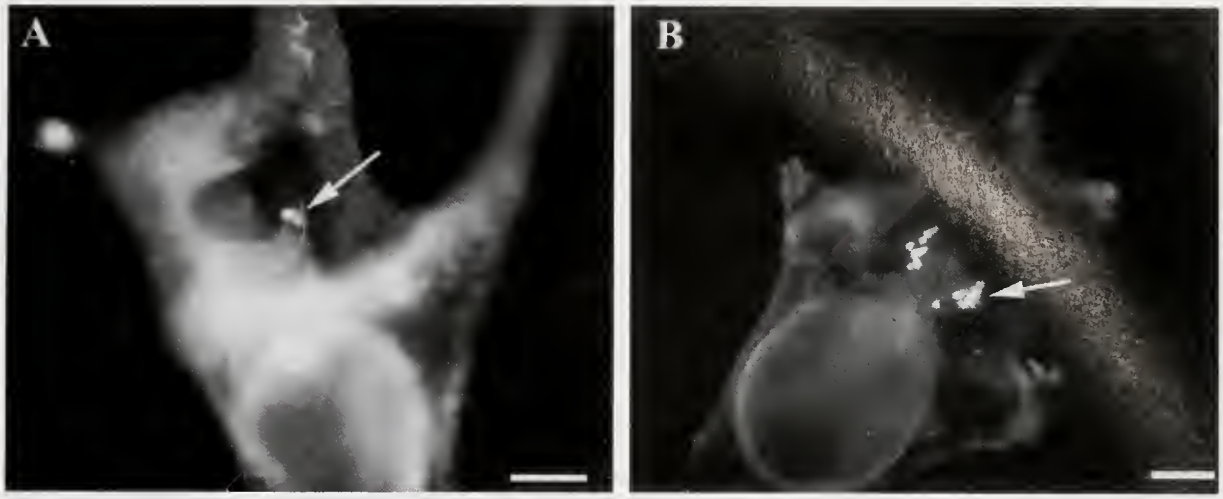

Figure 3. Immunoreactivity in the lower lip ganglion. (A) Late prism larva with a single serotonergic cell in the lower lip (arrow). (B) Lower lip ganglion with 10-12 cells showing 5HT-Li IR (arrow). Bars = 50 μm.

with cells being added rapidly through this period (Fig. 4A, B, D).

In fully developed 6- and 8-armed plutei, the differences in distribution between peptide and serotonin immunoreactivity become more apparent. The ciliary nerves show S2-Li IR, rather than S1-Li or 5HT-Li IR (Fig. 5A). These axons possess varicosities and some immunoreactive cell bodies associated with the descending loops of the ciliary bands (Fig. 5B, C). The neuronal cell bodies are generally multipolar, rounded or elliptical, and with large nuclei (Fig. 5B). Unlike the cells of the apical ganglion, these cells have no obvious sensory processes or contacts with ectodermal surfaces. No 5HT-Li IR was found in these areas.

Development of immunoreactivity in late plutei (8-armed stage to metamorphosis)

As the plutei grow and the rudiment forms, changes in the nervous system or in the distribution of neurotransmitters become more difficult to observe with traditional epifluorescence microscopy. However, scanning confocal laser microscopy allowed us to examine these changes in detail, especially in relation to the apical ganglion complex, which became very large and convoluted in older larvae.

The apical ganglion continues to increase in size and complexity until the mature 8-armed stage. In these older larvae, it is as much as 80 μm in length (left to right side of the larva) and 60 μm deep, extending from the thickened apical ciliated band down to the upper lip. To resolve this cluster of perikarya and dense neuropile, rotations were calculated for three-dimensional confocal images (Fig. 6). Some double-labeling studies were attempted, but due to the large size of the specimens and the large number of cells in the ganglion, the results obtained were not clear and have therefore not been presented here. However, confocal images of separately stained preparations were informative and suggested that the distributions of S1 and 5HT-Li IR within the apical ganglion differed significantly. Some cells may have expressed both substances, and there may have been other cell types present that expressed neither, but overall the rotational images provided the most comprehensive view of this structure to date.

In mature larvae, about 24 cell bodies in the apical ganglion show 5HT-Li IR. These are arranged symmetrically on either side of a dense central plexus, with all perikarya appearing to contribute fibers to the plexus or the subciliary axon tract (Fig. 6A-C). Specific pairs of cells are distinct and therefore can be recognized from one larva to the next. Three major nerves emerge on each side of the plexus. The first forms a descending loop beneath the ciliated band before leading up into the antero-lateral arm, the second extends around the larval mouth, and the third appears to extend into the larval body on either side of the esophagus (Fig. 4D). The smaller 5HT-Li IR nerves in the larval arms may also feed into the apical ganglion, although the precise termination of these fibers was not determined. The overall shape of the serotonergic elements in the apical ganglion was characterized by cell bodies arranged anterior and posterior to the central plexus, but never very far ventral or dorsal to it (Fig. 6A-C). Therefore, it appears as a rather two-dimensional structure in confocal rotations.

The bilateral symmetry of the S1-Li IR components of the apical ganglion is less pronounced than that of the 5HT-Li IR components. Cell bodies are arranged along the length of the ganglion, rather than in clusters at either end (Fig. 6D-F). All views of the ganglion appear to show a variety of cell shapes. Some are flask-shaped, with tapering apical processes typical of sensory cells, whereas others are more rounded. Upon rotation, the rounded cells appear as

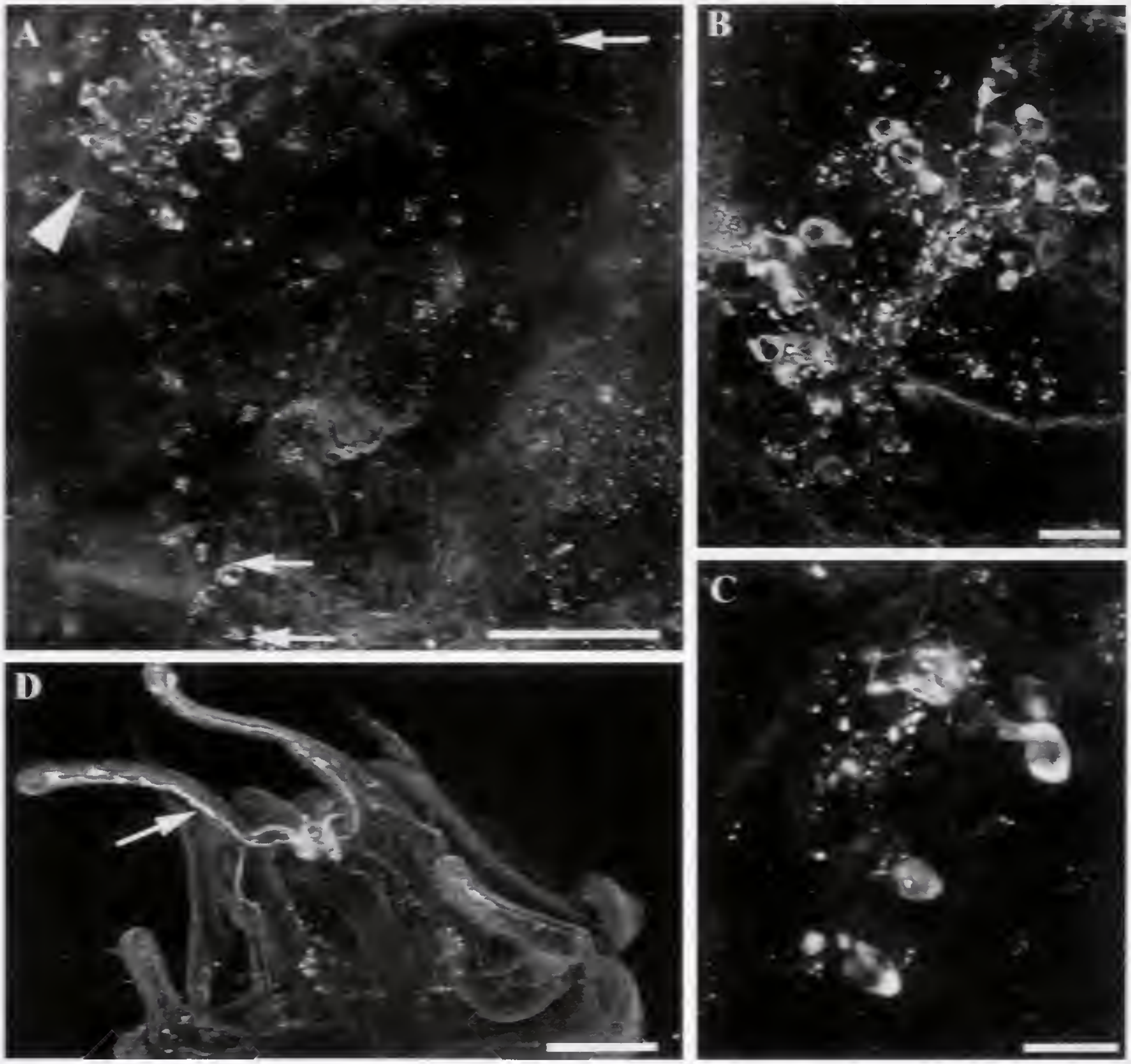

Figure 4. The serotonergic apical ganglion and circumoral complexes viewed by confocal laser scanning microscopy. (A) View of both the apical ganglion (arrowhead) and oral complexes and connecting fibers (arrows) in an 8-armed larva. (B and C) The apical ganglion and upper lip complexes are connected, but occupy different planes. The stack of confocal images used to construct (A) has been split to separate the cells of the apical ganglion (B) from those in the upper lip (C). (D) A 6-armed larva showing the limited ventral distribution of 5HT-Li IR. Major serotonergic nerve tracts can be seen exiting from the apical ganglion (arrow), passing into the anterolateral arms, around the mouth to the lower lip, and down into the larval body. Bars: A and D = 50 µm, B and C = 10 µm.

cross sections of flask-shaped cells, arranged at right angles to the others (Fig. 6D-F). Several major S1-Li IR axon tracts emerge from either side of the apical ganglion, projecting towards the larval arms and rudiment.

The larval pyloric neural complex

A new site of S1-Li IR was first detected in 10- to 11-day-old larvae (4- to 6-armed). A single fiber encircles the posterior end of the stomach at the pylorus (Fig. 7A) and is associated with a distinctive elongate cell body (Fig. 7B). The fiber is about 1 μm in diameter with 3 μm varicosities, and the bipolar cell body is 10-15 μm long. An optical section through the pylorus shows S1-Li IR on either side, although the fiber does not appear to be a ring. This circumpyloric nerve proves to be the origin of a nerve complex that increases in size throughout the rest of larval life.

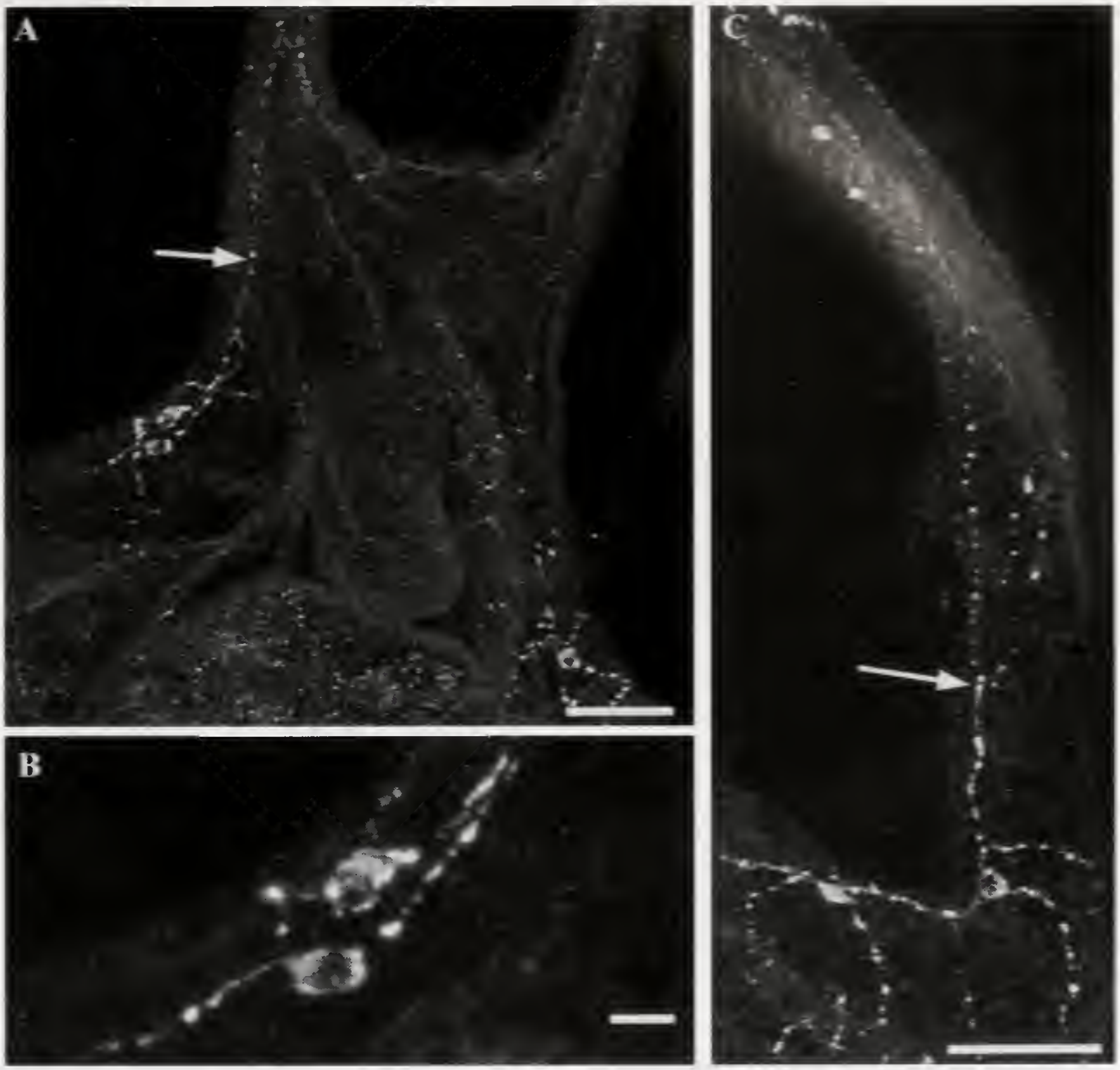

Figure 5. S2-Li IR associated with the ciliary band in a 6-armed larva viewed with confocal laser scanning microscopy. (A) S2-Li IR varicose axons underlying the ciliated band (arrow) and connecting to large immunoreactive neuronal cell bodies. (B) High power of the cell bodies shown in (A), lying between the anterolateral and posterodorsal arms. (C) S2-Li IR fibers extend into the larval body from neurons between the arms, as well as into the ciliary nerve (arrow) of the post-oral arms. Bars, A and C = 50 μm, B = 10 μm.

forming a loose web of fibers around much of the distal end of the stomach. Several days after the appearance of the first pyloric nerve, a second S1-Li IR neuron appears with a similar form to the first (Fig. 7C). More neurons are gradually added throughout development, and this complex continued to grow even in mature larvae where metamorphosis was delayed, apparently due to nutritional limitations. For example, in 50-day-old larvae, the pyloric neural complex consists of numerous cells and a plexus of fibers (Fig. 7D). No 5HT-Li IR was observed in this area.

The adult rudiment and metamorphosis

In early attempts to label the adult rudiment, the larval complexes were clearly immunoreactive, but nothing could be seen in the rudiment itself. Initial interpretations were that neurons in the rudiment either had not differentiated or did not express neuropeptide. However, semithin toluidine blue sections demonstrated the presence of developing radial nerve cords and the circumoral nerve ring. Therefore, the permeabilization procedure was modified in an attempt

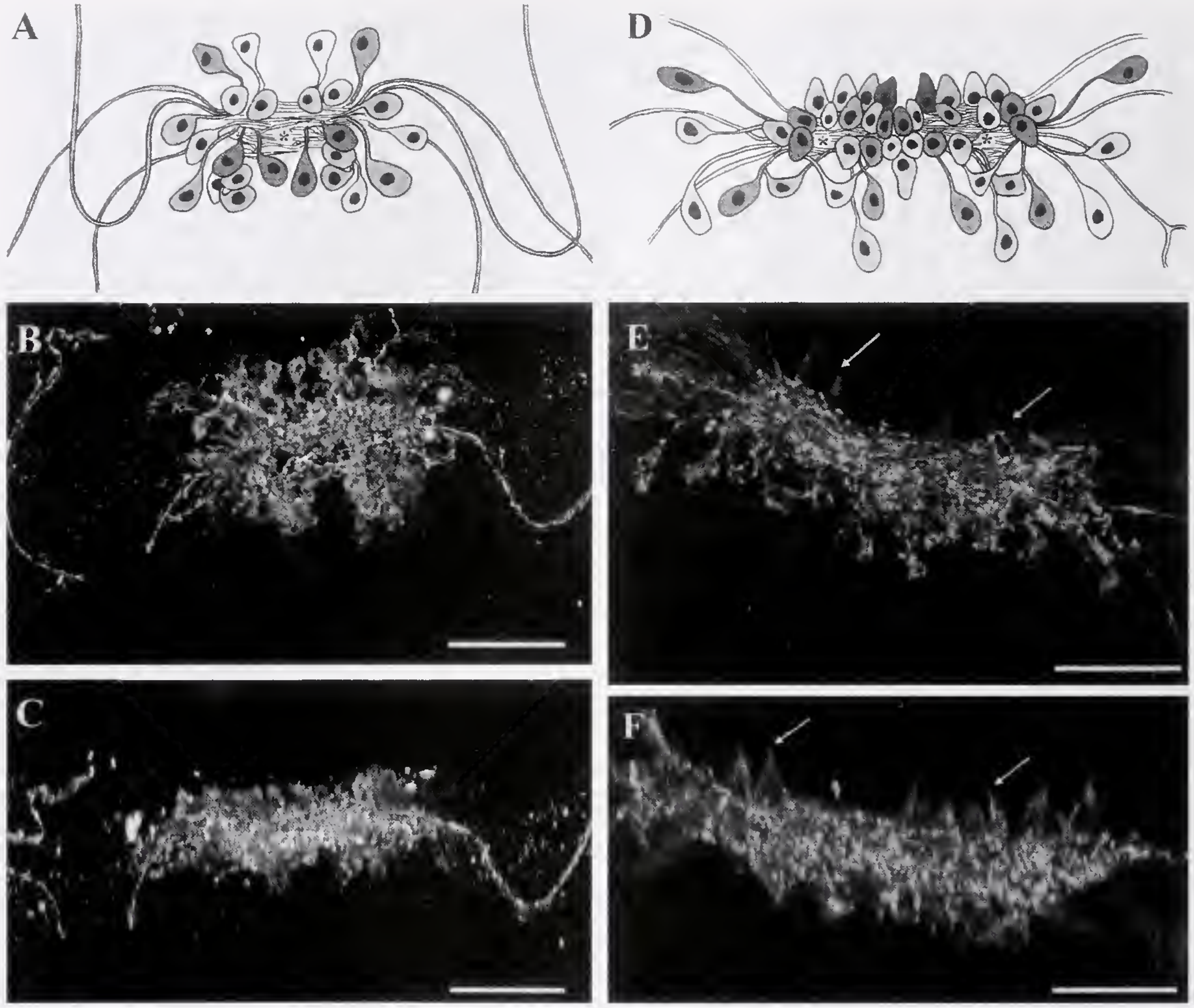

Figure 6. Representative drawings of 5HT and S1-Li IR neurons in the apical complex, and confocal images of the apical ganglion showing selected rotations from a full 360° series. (A) to (C) show the serotonergic cells of the apical ganglion. (A) Diagram of the apical ganglion viewed from the anterior/ventral surface of the larva, as deduced from the three-dimensional rotations. Not to scale. (B) 0° rotation. (C) 65° rotation. (D) to (F) show the SALMFamidergic cells of the apical ganglion. (D) Diagram of the SALMFamidergic cells of the apical ganglion as deduced from three-dimensional rotations. Not to scale. The ganglion is bilaterally symmetrical, apparently with pairs of cells (arrows). (E) 0° rotation. (F) 50° rotation; *indicates the nerve plexus. Bars = 25 μm.

to confirm unequivocally that the absence of immunoreactivity is due to the lack of antigen. This test still revealed positive labeling in several structures of the rudiment.

The first appearance of SALMFamide-like immunoreactivity in the rudiment of the larvae was in the ectodermally derived lining of the vestibular cavity (Fig. 8A). Some S1-Li IR appeared in the covering of the primary podia, which is also ectodermal in origin. The earliest S1-Li IR in the circumoral and radial nerve cords was rather diffuse. In later specimens competent to metamorphose (the primary podia were observed to move independently), the immunoreactivity was more concentrated, occurring in well-defined fiber tracts in the rays of the water vascular system, with the nerve ring in the tube feet clearly visible (Fig. 8B, C). No 5HT-Li IR was observed in the rudiment.

Discussion

The larval nervous system

This study describes the neural development of *Psammechinus miliaris,* from the 4-armed pluteus stage through to a metamorphically competent larvae with 8 arms and a developed adult rudiment. Most important, it extends the previously available descriptions of the echinoid larval nervous system to the late pluteus, and includes such previously unknown fea-

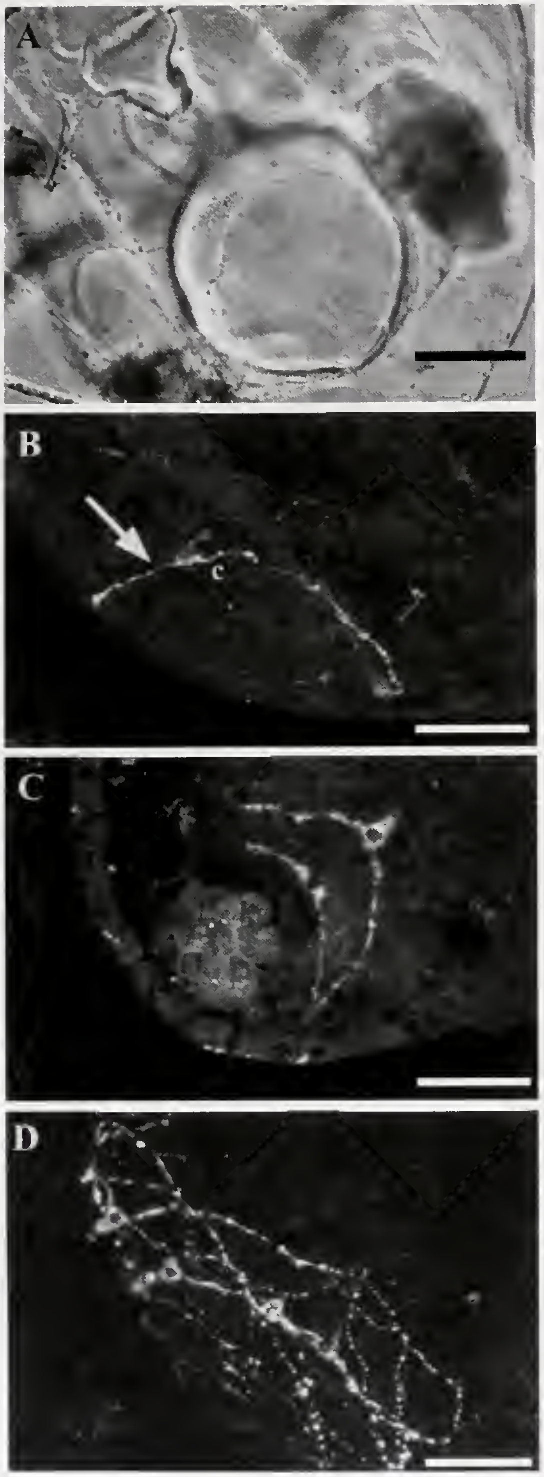

Figure 7. S1-Li IR in the pyloric neural complex. (A) 8-armed larva showing the pylorus. (B) Confocal image of the first immunoreactive cell (c) and fiber (arrow) in the complex in a 6-armed larva (10 days post-fertilization). (C) Two immunoreactive cells are present in the pyloric area by 16 days post-fertilization. (D) A plexus of cells develops in mature larvae, especially those which have delayed metamorphosis. Bars: A = 100 μm, B to D = 50 μm.

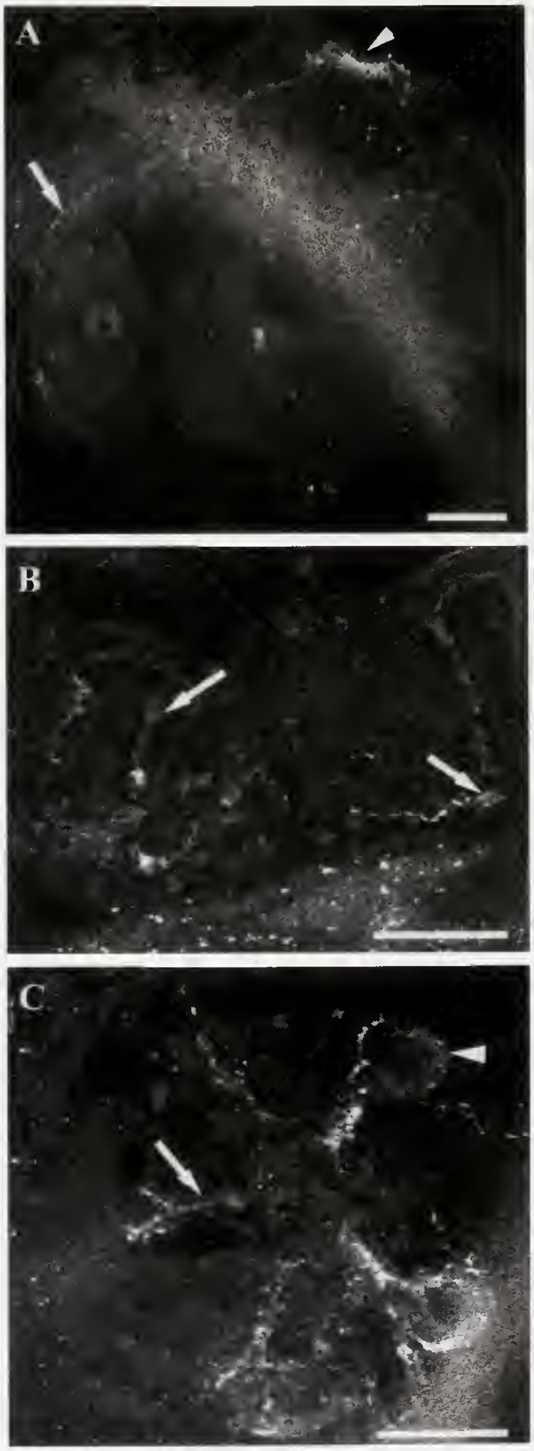

Figure 8. S1-Li IR in the adult rudiment. (A) Immunoreactivity can be seen in the apical ganglion of the larva (arrowhead) and in the vestibule wall of the rudiment (arrow) of a 27-day-old larva. (B) The earliest evidence of S1-Li IR in the developing radial nerves. Fibers in the neuroepithelium underlying the epineural space lead into the primary podia (arrows). (C) S1-Li IR shows the radial nerve cords (arrow) terminate in the podial rings of the primary tube feet (arrowhead). Bars = 100 μm.

tures as the pyloric plexus and details of the nervous system within the adult rudiment. It also provides the fullest description to date of the apical ganglion in mature larvae. This ganglion is a complex structure containing numerous cell types, with connecting fibers to other organs within the larval body, including the adult rudiment.

The structure of certain elements of the echinoderm larval nervous system has been previously determined by ultrastructural, histological, and histochemical studies, revealing a network of cell bodies and fibers that are regionally concentrated to form ganglia (Burke, 1978; Nakajima, 1986; Bisgrove and Burke, 1987; Lacalli *et al.*, 1990; Moss *et al.*, 1994; Byrne *et al.*, 1999; Chee and Byrne, 1999). The ciliary bands are a major component of the larval nervous system and contain numerous nerve cells of several types. Other components include localized specializations such as in the lower lip, the apical (or dorsal) ganglion, and an underlying major nerve tract, the ciliary nerve. Immunocytochemical studies have been especially useful in providing details of the overall structure of this system; in the absence of a single unambiguous marker, previous authors have combined information from several immunological markers to construct a neural map. Our latest neural map of echinoid larvae is one further step towards a better understanding of the structure and function of the echinoderm nervous system.

The development of the nervous system of *P. miliaris* correlates with changes in larval form, function, and behavior. Additional neurons often appear in association with newly formed or enlarged larval organs. For example, the ciliated band continues to grow in length until the fourth and final pair of arms, the pre-oral arms, are formed. According to Nakajima (1986), this band also increases in width, the number of rows of ciliated cells increasing with age, especially in the epaulettes. The nerves underlying the ciliated band elongate as it grows, and additional immunoreactive cell bodies appear. The apical ganglion continues to grow as larvae approach competency, with the addition of immunoreactive neurons and an associated increase in complexity in the neuropile and ciliary nerves surrounding the area. We show that neural structures associated with the pylorus continue to develop, even in advanced larvae. This continual addition to the larval nervous system for the greater part of larval life suggests an increased behavioral repertoire, possibly specifically in association with the development of the adult rudiment and the timing of metamorphosis.

The development of 5HT and SALMFamide immunoreactivity

The early development of 5HT-Li IR in *P. miliaris* follows a pattern seen in other studies on echinoids (Bisgrove and Burke, 1987). Immunoreactive cells appear, and the number of stained cells increases as the larva begins to swim and feed. 5HT-Li IR is restricted to those components of the nervous system in the ventral half of the larva that are considered to be sensory—in particular, the apical ganglion and flask-shaped cells in the ciliary bands. The suggestion of a predominantly sensory function for 5HT in *P. miliaris* is in keeping with other studies on larval echinoderms (Bisgrove and Burke, 1987; Nakajima, 1988; Moss *et al.*, 1994), molluscs (Kempf *et al.*, 1997; Marois and Carew, 1997), and phoronids (Hay-Schmidt, 1990). The role of 5HT may be associated with the detection of chemical cues, possibly those required to induce feeding or settlement and metamorphosis. However, the absence of 5HT in the rudiment and juvenile may also be significant. The podia of the rudiment have been implicated in substrate choice by metamorphosing sea urchins (Cameron and Hinegarder, 1978), and no 5HT was detected in these structures in the current study. This suggests that if 5HT is involved in settlement behavior, it may be as part of a pathway that integrates both the larval and juvenile nervous systems.

The development of S1-Li IR follows a pattern similar to that of 5HT, and its temporal appearance can also be seen to coincide with increased locomotory activity and feeding. Its final distribution is wider than that observed for 5HT, with numerous cells and fibers throughout the larval body, as well as in the newly described pyloric plexus. The shape and location of cells in the pyloric plexus and subciliary complexes is highly suggestive of a motor function, whereas the tapering apical processes that bristle around the apical ganglion may represent sensory receptors. This mixed function has also been suggested by other studies in which S1 has been localized (Thorndyke *et al.*, 1992; Moss *et al.*, 1994), and it is possibly an early indicator of their ubiquitous distribution in adult echinoderms (Newman, 1995a, b). It is interesting that the preliminary studies with anti-S2 revealed staining only in the ciliary bands and a few neuronal cell bodies, but none in the ganglia or gut. This may suggest a purely motor function for S2 in coordinating ciliary activity and is again in keeping with the more limited distribution of this peptide in adult echinoderms (Newman, 1995a, b). As the work on S2 was only carried out on one developmental stage, we cannot draw definitive conclusions about its overall distribution. However, it does provide a clear comparison to the S1 distribution and reinforces the likelihood that these two related peptides have very distinct functions in both larvae and adults.

Co-localization of SALMFamide peptides and 5HT was not examined. The distributions revealed in this study clearly point towards discrete populations of cells expressing a single neurotransmitter. However, comparison of the two staining patterns also suggests that co-localization within specific cells of the ganglia is possible. Indeed, S1 has an extensive distribution in larval echinoderms and is probably of equal importance to larval function as 5HT. Equivalent patterns of neuropeptide localization in other marine larvae have been reported for the molluscan neuropeptide FMRFamide, which is also found in central larval ganglia and peripheral nerves in larval phoronids (Hay-Schmidt, 1990). Otherwise the reporting of neuropeptide localization in the ganglia of marine invertebrate larvae is rare, and we are not yet able to draw any conclusions about their putative roles.

The apical ganglion

The apical ganglion is the major neural complex in the pluteus and probably has a central coordinating role. An apical neural structure, with varying degrees of complexity, has been implicated in the coordination of swimming, feeding, and settlement behavior in many marine invertebrate larvae, including molluscs (Chia and Koss, 1984; Marois and Carew, 1997; Kempf *et al.*, 1997), polychaetes (Lacalli, 1981), and echinoderms (Burke, 1983; Chia *et al.*, 1986; Nakajima *et al.*, 1993). This structure appears to be conserved in these larvae, and a consistent feature is the presence of 5HT-Li IR neurons, usually in a bilaterally symmetrical arrangement.

In the present study, CSLM has been used to trace the development of the apical ganglion and to analyze its structural complexity. At the 8-armed larvae stage it is by far the most complex neural structure in the larva, with an array of immunopositive cells and possibly other as yet undetected neurons. Although it appears highly developed, it presumably degenerates completely at metamorphosis, as it appears to coordinate only larval functions. In sea urchins, therefore, the entire larva seems to be under the control of a necessarily complex apical ganglion, which supports its functions in totality. In other words, the larval and juvenile nervous systems have been thought of as being almost totally distinct.

The apical ganglion may have a wider significance as a precursor of the chordate nervous system (Lacalli, 1994). Cell types within the larval nervous system have been compared with those in other phyla in an attempt to find homologous structures, implicating the larval nervous system, and especially the apical ganglion, as phylogenetically significant structures. The extensive ganglion revealed in 8-armed *P. miliaris* larvae may help shed further light on this possibility. Echinoderms, as deuterostome invertebrates, are useful for tracing such cells in chordates to their putative invertebrate ancestors. For example, Lacalli and West (1993) propose that the distinctive multipolar cells of echinoderm circumoral ciliary bands are homologous with similar neurons in the ciliary bands of the hemichordate tornaria, as well as with those in the dorsal nerve cord of ammocoete larvae of the lancelet *Branchiostoma*.

Development of immunoreactivity in the rudiment, and the fate of the larval nervous system

SALMFamide probes have revealed the presence of neuropeptides in the rudiment of the *P. miliaris* pluteus, indicating that adult neural development and differentiation is well under way during larval stages. This is the first immunocytochemical visualization of nerve cells in the developing rudiment and shows the clear separation of the larval and juvenile systems.

The discovery of the pyloric plexus in the older larvae is of particular interest since it has not been previously described. The structure continues to grow in mature larvae (and may continue to grow after metamorphosis), whereas other larval neural components have stopped growing, or may even be diminishing. These observations suggest that the pyloric plexus neurons may be incorporated into the adult basi-epithelial gut plexus. This is perhaps not surprising, since this area of the gut is incorporated into the rudiment along with associated nerves. Such a finding would indicate that some larval neural tissue is carried into the juvenile, with the major part of this system being resorbed at metamorphosis. However, the larval pyloric plexus and that of the juvenile may also be distinct structures that simply show expression of the same neuropeptide. Further studies focusing on this specific area may reveal more details of the metamorphic process and the relationship between larval and adult forms.

Acknowledgments

This work was supported by a BBSRC studentship No. 93309321 to A.-J.B. Thanks to Zyg Podhorodecki and Anton Page for photographic and confocal microscopy assistance. Also thanks to Maeve Kelly, Scottish Association for Marine Science, for help with culturing larvae.

Literature Cited

Bisgrove, B. W., and R. D. Burke. 1987. Development of the nervous system of the pluteus larva of *Strongylocentrotus droebachiensis. Cell Tissue Res.* **248:** 335–343.

Burke, R. D. 1978. The structure of the larval nervous system of the pluteus larva of *Strongylocentrotus purpuratus. Cell Tissue Res.* **191:** 233–247.

Burke, R. D. 1983. Neural control of metamorphosis in *Dendraster excentricus. Biol. Bull.* **164:** 176–188.

Byrne, M., F. Chee, P. Cisternas, and M. C. Thorndyke. 1999. Localisation of the neuropeptide S1 in the larval and adult nervous system of the sea star *Patiriella regularis.* Pp. 187–191 in *Echinoderm Research 1998,* M. D. Candia Carnevali and F. Bonasoro, eds. Balkema, Rotterdam.

Cameron, R. A., and R. T. Hinegarder. 1978. Early events in sea urchin metamorphosis, description and analysis. *J. Morphol.* **157:** 21–31.

Candia Carnevali, M. D., F. Bonasoro, U. Welsch, and M. C. Thorndyke. 1998. Arm regeneration and growth factors in crinoids.

Pp. 145–150 in *Echinoderms: San Francisco*, R. Mooi and M. Telford, eds. Balkema, Rotterdam.

Chee, F., and M. Byrne. 1999. Development of the larval serotonergic nervous system in the sea star *Patiriella regularis* as revealed by confocal imaging. *Biol. Bull.* **197:** 123–131.

Chia, F.-S., and R. Koss. 1984. Fine structure of the cephalic sensory organ in the larva of the nudibranch *Rostanga pulchra. Zoomorphology* **104:** 131–139.

Chia, F.-S., R. D. Burke, R. Koss, P. V. Mladenov, and S. S. Rumrill. 1986. Fine structure of the doliolaria larva of feather star, *Florometra serratissima*, with special emphasis on the nervous system. *J. Morphol.* **189:** 99–120.

Díaz-Miranda, L., D. A. Price, M. J. Greenberg, T. D. Lee, K. E. Doble, and J. E. García-Arrarás. 1992. Characterization of two novel neuropeptides from the sea cucumber, *Holothuria glaberrina. Biol. Bull.* **182:** 241–247.

Elphick, M. R., R. H. Emson, and M. C. Thorndyke. 1991a. Isolation of the neuropeptide SALMFamide-1 from starfish using a new antiserum. *Peptides* **12:** 455–459.

Elphick, M. R., D. A. Price, T. D. Lee, and M. C. Thorndyke. 1991b. The SALMFamides: a new family of neuropeptides isolated from an echinoderm. *Proc. R. Soc. Lond. B* **243:** 121–127.

Ghyoot, M., J. L. Cobb, and M. C. Thorndyke. 1994. Localisation of neuropeptides in the nervous system of the brittlestar *Ophiura ophiura. Philos. Trans. R. Soc. Lond. B* **346:** 433–444.

Hay-Schmidt, A. 1990. Distribution of catecholamine-containing, 5HT-like and FMRFamide-like IR neurons and processes in the nervous system of the actinotroch larvae of *Phoronis muelleri. Cell Tissue Res.* **259:** 105–118.

Iwata, K. S., and H. Fukase. 1964. Comparison of discharge of the gametes by three artificial means in sea urchins. *Biol. J. Okayama Univ.* **10:** 57–64.

Kelly, M. S., A. J. Hunter, C. L. Scholfield, and J. D. McKenzie. 2000. Morphology and survivorship of larval *Psammechinus miliaris* (Gmelin) (Echinodermata: Echinoidea) in response to varying food quantity and quality. *Aquaculture* **183:** 223–240.

Kempf, S. C., L. R. Page, and A. Pires. 1997. Development of serotonin-like immunoreactivity in the embryos and larvae of nudibranch molluscs with emphasis on the structure and possible function of the apical sensory organ. *J. Comp. Neurol.* **386:** 507–528.

Kroll, R. P., and E. E. Voronezhskaya. 1996. Early elements in gastropod neurogenesis. *Dev. Biol.* **173:** 344–347.

Lacalli, T. C. 1981. Structure and development of the apical organ in trochophores of *Spirobranchus polycerus, Phyllodoce maculata* and *Phyllodoce mucosa* (Polychaeta). *Proc. R. Soc. Lond. B* **212:** 381–402.

Lacalli, T. C. 1994. Apical organs, epithelial domains and the origins of the chordate central nervous system. *Am. Zool.* **34:** 533–541.

Lacalli, T. C., and J. E. West. 1993. A distinctive nerve cell type common to diverse deuterostome larvae: comparative data from echinoderms, hemichordates and amphioxus. *Acta Zool.* **74:** 1–8.

Lacalli, T. C., T. H. Gilmour, and J. E. West. 1990. Ciliary band innervation in the bipinnarian larva of *Pisaster ochraceus. Philos. Trans. R. Soc. Lond. B* **330:** 371–390.

MacBride, E. W. 1913. The development of *Echinocardium cordatum* I. External features of development. *Q. J. Microsc. Sci.* **59.**

MacBride, E. W. 1914. *A Textbook of Embryology.* Macmillan Press, London.

MacBride, E. W. 1918. The development of *Echinocardium cordatum* II. *Q. J. Microsc. Sci.* **63.**

Mackie, G. O., A. N. Spencer, and R. Strathmann. 1969. Electrical activity associated with ciliary reversal in an echinoderm larva. *Nature* **223:** 1384–1385.

Marois, R., and T. J. Carew. 1997. Fine structure of the apical ganglion and its serotonergic cells in the larva of *Aplysia californica. Biol. Bull.* **192:** 388–398.

Mortensen, T. H. 1921. Studies on the development and larval forms of echinoderms. G.E.C. Gad, Copenhagen.

Moss, C., R. D. Burke, and M. C. Thorndyke. 1994. Immunocytochemical localisation of the neuropeptides S1 and serotonin in larvae of the starfish *Pisaster ochraceus* and *Asterias rubens. J. Mar. Biol. Assoc. UK* **74:** 61–71.

Nakajima, Y. 1986. Development of the nervous system of sea urchin embryos: Formation of the ciliary bands and the appearance of two types of ectoneural cells in the pluteus. *Dev. Growth Differ.* **28:** 531–542.

Nakajima, Y. 1988. Serotonergic nerve cells of starfish larvae. Pp. 235–239 in *Echinoderm Biology*, R. D. Burke, P. V. Mladenov, P. Lambert, and R. L. Parsley, eds. Balkema, Rotterdam.

Nakajima, Y., R. D. Burke, and Y. Nnda. 1993. The structure and development of the apical ganglion in the sea urchin pluteus larvae of *Strongylocentrotus droebachiensis* and *Mespilia globulus. Dev. Growth Differ.* **35:** 531–538.

Newman, S. J., M. R. Elphick, and M. C. Thorndyke. 1995a. Tissue distribution of the SALMFamide neuropeptides S1 and S2 in the starfish *Asterias rubens* using novel monoclonal and polyclonal antibodies. I. Nervous and locomotory systems. *Proc. R. Soc. Lond. B* **261:** 139–145.

Newman, S. J., M. R. Elphick, and M. C. Thorndyke. 1995b. Tissue distribution of the SALMFamide neuropeptides S1 and S2 in the starfish *Asterias rubens* using novel monoclonal and polyclonal antibodies. II. Digestive system. *Proc. R. Soc. Lond. B* **261:** 187–192.

Polak, J. M., and S. Van Noorden. 1986. *Immunocytochemistry. Modern Methods and Applications.* John Wright and Sons, Bristol, United Kingdom.

Potton, D. 1997. Neuroendocrine control of feeding in the European starfish, *Asterias rubens*. Ph.D. thesis, University of London, United Kingdom.

Strathmann, M. F. 1987. Reproduction and development of marine invertebrates from the northern Pacific coast: data and methods for the study of eggs, embryos and larvae. University of Washington Press, Seattle.

Thorndyke, M. C., B. D. Crawford, and R. D. Burke. 1992. Localisation of a SALMFamide neuropeptide in the larval nervous system of the sand dollar, *Dendraster excentricus. Acta Zool.* **73:** 207–212.

Reference: *Biol. Bull.* **200:** 281–297. (June 2001)

Function and Functional Groupings of the Complex Mouth Apparatus of the Squat Lobsters *Munida sarsi* Huus and *M. tenuimana* G.O. Sars (Crustacea: Decapoda)

A. GARM* AND J. T. HØEG

Department of Zoomorphology, Zoological Institute, University of Copenhagen, Universitetsparken 15, 2100 Copenhagen, Denmark

Abstract. Like all other decapods, the anomuran squat lobsters *Munida sarsi* and *M. tenuimana* have a mouth apparatus composed of six pairs of mouthparts plus labrum and paragnaths (upper and lower lips). To study the functional significance of this complexity, we examined the mouthparts with scanning electron microscopy and also observed their function directly, under laboratory conditions, using macro-video equipment. No differences were found between the two species. The movement patterns of the mouthparts are described in detail and illustrated as serial drawings. Proceeding from maxillipeds 3 towards the mandibles, the movement pattern gets increasingly stereotypical, with the mandibles performing but a single movement in a medio-lateral plane. From morphology, the mouthparts are subdivided into 20 parts, but from the functional analyses the 20 parts form 8 functional groups: *1, transporting mouthparts* (maxilliped 2 endopod and maxilliped 3 endopod); *2, transporting–aligning mouthparts* (maxilliped 1 basis); *3, sorting–aligning mouthparts* (maxilla 1 basis and maxilla 2 basis); *4, current–generating mouthparts* (flagella of maxilliped 2 and maxilliped 3 exopods); *5, cutting–crushing mouthparts* (incisor and molar processes, labium, and mandibular palp); *6, ingesting mouthparts* (maxilla 1 coxa, maxilla 2 coxa, and maxilliped 1 coxa); *7, respiratory mouthparts* (scaphognathite, maxilliped 1 epipod, and maxilliped 2 and maxilliped 3 exopods); and *8, dorso-ventral mouthparts* (maxilla 1 endopod, maxilla 2 endopod, maxilliped 1 endopod, and maxilliped 1 exopod). These groupings apply mostly to the processes of food handling and have little significance with respect to grooming. When comparing our results to the literature on other decapods, we found much resemblance to conditions in other anomurans.

Introduction

One of the most interesting features among crustaceans is their very complex mouth apparatus. The basic limb-pattern for Eucrustacea (the condition in the stem species to all recent Crustacea) was a labrum, paired paragnaths, and two pairs of mouthparts (mandibles and maxillae 1), followed by a large number of more-or-less similar limbs (Walossek, 1998). Extant members of the Cephalocarida retain this system, but almost all other recent species have at least three pairs of mouthparts, *i.e.*, mandibles (Md), maxillae 1 (Mx1), and maxillae 2 (Mx2). Further specialization of the mouth apparatus is a very significant event in most crustacean lineages and often involves the specialization of thoracic limbs for food manipulation. This is especially so in the Decapoda, which has the first three pairs of thoracic appendages, the maxillipeds (Mxp1-3), specialized into feeding appendages. In many of these decapods, the feeding apparatus is even more advanced since one or more of the pairs of pereiopods, especially if chelate, take part in food manipulation. This complexity has without doubt played an important role in the success of the Decapoda, since it enables the members of the order to feed on such a great diversity of food objects (Schembri, 1982c; Cartes, 1993).

Received 2 February 2000; accepted 12 January 2001.

* To whom correspondence should be addressed. E-mail: Algarm@zi.ku.dk

Abbreviations: Lb, labrum; Inc, incisor process, Mp, molar process; Mdp, mandibular palp; Mx1 cox, maxilla 1 coxa; Mx1 bas, maxilla 1 basis; Mx1 endo, maxilla 1 endopod; Mx2 cox, maxilla 2 coxa; Mx2 bas, maxilla 2 basis; Mx2 endo, maxilla 2 endopod; Scapho, scaphognathite; Mxp1 cox, maxilliped 1 coxa; Mxp1 bas, maxilliped 1 basis; Mxp1 endo, maxilliped 1 endopod; Mxp1 exo, maxilliped 1 exopod; Mxp1 epi, maxilliped 1 epipod; Mxp2 endo, maxilliped 2 endopod; Mxp2 exo, maxilliped 2 exopod; Mxp3 endo, maxilliped 3 endopod; Mxp3 exo, maxilliped 3 exopod.

Unfortunately, we have but little understanding of the functional significance of this very complex feeding apparatus found in decapods, which on each side consists of at least 20 parts, each with their separate functions. Earlier functional studies of the decapod mouth apparatus have resulted in a division into inner mouthparts (Md, Mx1, Mx2, and Mxp1) and outer mouthparts (Mxp2 and Mxp3) (Nicol, 1932; Kunze and Anderson, 1979; Schembri, 1982a). This division is based on morphology, but is often used in ways that indicate similar functions within the groupings. Many of the studies have concentrated mostly on Mxp3, the largest of the mouthparts, but again many of the functional interpretations are based on morphology alone (*e.g.*, Greenwood, 1972; Farmer, 1974; Suthers and Anderson, 1981; Suthers, 1984; Lavalli and Factor, 1992). Grooming of the anterior part of the body using Mxp3 is well documented, and functional similarities are found throughout the Decapoda (Bauer, 1981, 1989). We know much less about the functions of Mx1, Mx2, and Mxp1. The small size and fast movements of these appendages impede any detailed observation, and in many decapods they are also hidden behind the larger Mxp2 and Mxp3. Recording mouthpart movements with macro-video equipment overcomes the first two problems (Stamhuis *et al.*, 1998); studying anomurans solves the last, since most are bottom dwellers with a rather open mouth apparatus, and pagurids in particular have received a lot of attention. At the gross level, anumurans have quite similar mouthparts, and the similarity with respect to Md, Mx1, Mx2, and Mxp1 is particularly striking (Pike, 1947; Roberts, 1968; Kunze and Anderson, 1979; Schembri, 1982a). The Anomura is accordingly an especially suitable taxon for studying mouthpart function, both from an experimental point of view and because it offers a chance to evaluate to what extent similar morphology implies similar function.

In a scanning electron microscopy (SEM) study of the morphology of mouthparts in the anomuran species *Munida sarsi*, we offered some provisional interpretations of their function (Garm and Høeg, 2000). In the present study we present detailed video-based evidence of mouthpart functions in this species and in *M. tenuimana*, with particular attention to the roles of Mx1, Mx2, and Mxp1.

Materials and Methods

Video-recordings

Seventy specimens of *Munida sarsi* with carapace lengths between 7 mm and 28 mm were caught with a Sneli dredge at the Faeroe Bank (08°44′08″ E, 61°24′46″ N) at depths between 330 and 345 m in water with a temperature of 7°C. Six specimens of *M. tenuimana* were caught with a triangular dredge northeast of the Faeroe Bank (09°28′95″ E, 61°25′52″ N) at depths between 690 and 715 m in water with a temperature of 4°C. Both species were caught in August 1998. The animals were kept alive at the Kaldbak Laboratory in 1000-l tanks with running natural seawater, keeping the temperature at 10°C. The animals were fed with other animals from the catch areas, but also with animal and algal tissue from shallow waters.

Video-recording took place in 50-l tanks under the same conditions with four kinds of sediment: two kinds of mud-gravel from the areas of the catches (many foraminiferans at 330-345 m); mud from shallow water (very rich in organic material); and shell-gravel (low in organic material). The recordings were made from outside the tank by a color (Y/C) CCD camera with a Micronikkor 105-mm lens, which enabled us to record structures 5 μm wide. Recordings were made on super VHS, and light was obtained from a 120-W spotlight. Comparison of our videos with *in situ* recordings of *M. sarsi* made by a submersible shows that *M. sarsi* behaved naturally in the tanks. To trace the movement patterns of the mouthparts, we analyzed video sequences on computer using the MS DOS version of Sigmascan. Representative shots of the mouthpart movements were grabbed with a time resolution of 0.02 s (50 fields/s) and imported into Corel PhotoPaint 8.0, with a resolution of 786×564 pixels (Fig. 1). We outlined the involved mouthparts and used the outlines for serial drawings. These drawings therefore accurately reflect the positions of mouthparts in the video sequences. For the analyses of the respiratory movements, the right branchiostegite of four individuals was dissected to get a clear view of the structures involved. All four animals behaved normally afterwards, although they only survived for a further 3-4 days.

Light and scanning electron microscopy

Specimens of *Munida sarsi* and *M. tenuimana* that had been fixed in 2% formalin were obtained from The BIOFAR 1 project at the Faeroe Islands (Station 070, 61°24′69″ N, 08°43′97″ E and Station 314, 60°51′8X″ N, 10°14′0X″ E, Norrevang *et al.*, 1994). Adult males and females with a carapace length between 17 mm and 28 mm were used. The mouthparts were cleaned by ultrasound and manually with a beaverhair brush. A standard dissection microscope was used for the drawings (Fig. 2). SEM preparation followed Felgenhauer (1987), except that osmium was not used. The photographs were taken on a JEOL 840 scanning electron microscope and were stored electronically using the JEOL program SemAfore 3.0. They were processed and manipulated in CorelDraw 8.0.

Abbreviations of mouthpart subdivisions

Labrum (Lb), mandibular incisor (Inc) and molar process (Mp), mandibular palp (Mdp), maxilla 1 coxa (Mx1 cox), maxilla 1 basis (Mx1 bas), maxilla 1 endopod (Mx1 endo), maxilla 2 coxa (Mx2 cox), maxilla 2 basis (Mx2 bas), maxilla 2 endopod (Mx2 endo), scaphognathite (Scapho),

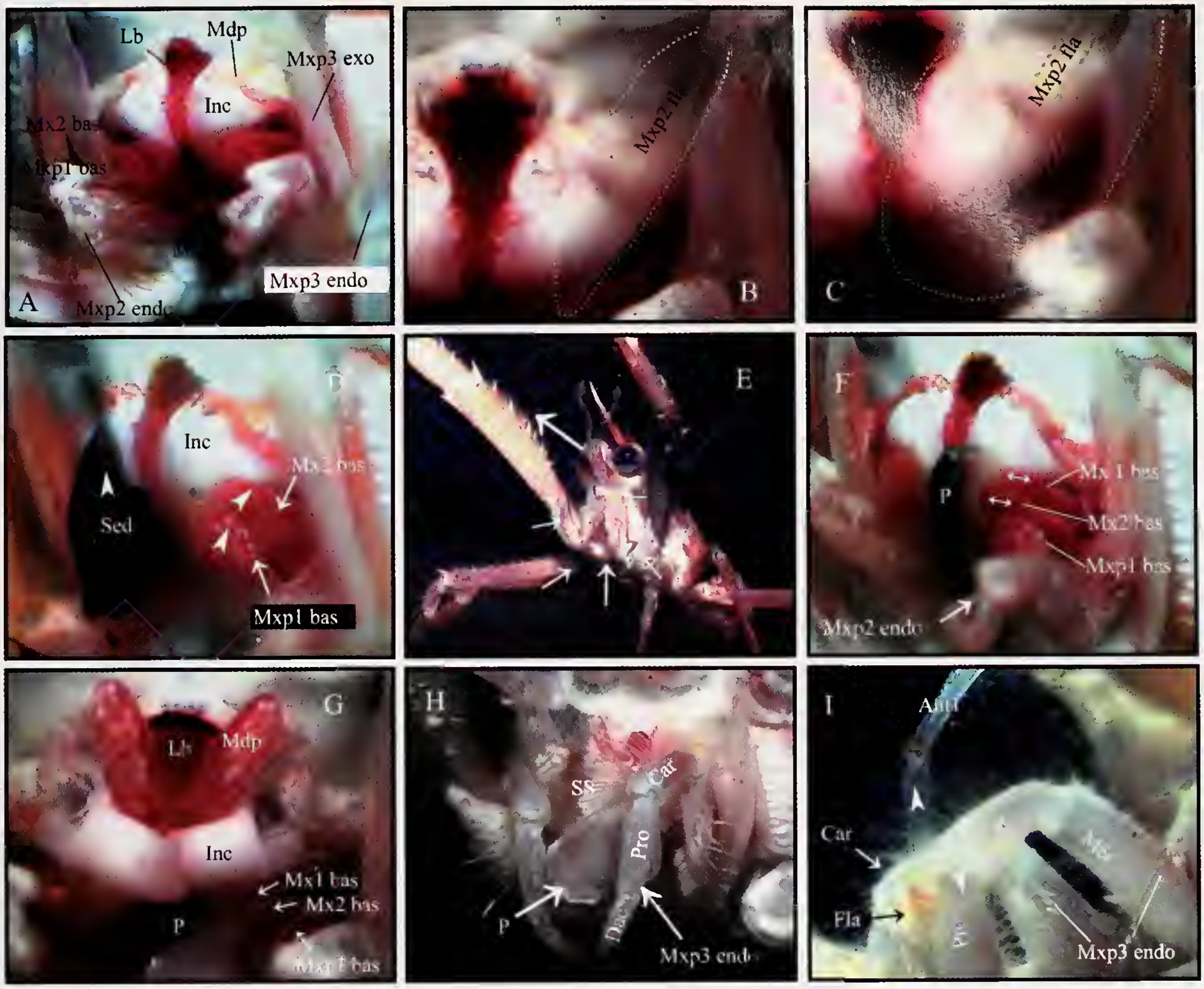

Figure 1. Frame-grabbed video images of *Munida sarsi*. (A) Overview of buccal area in resting position. (B) Flagellum of Mxp2 exopod in resting position. Dotted line outlines flagellum. (C) Flagellum from B spread out when moving anterio-dorsally. Dotted line outlines flagellum. (D) Sediment sorting by Mx2 basis and Mxp1 basis. (E) *M. sarsi* on muddy sediment. Arrows indicate flagella currents. Size of arrows indicate strength of current measured as relative velocity of suspended particles. (F) Holding a small prey item with Mx1 basis and Mx2 basis. (G) Biting by incisor processes. Mandibular palps and Lb are raised and incisor processes overlap with left on dorsal side. (H) Mxp3 endopods hold large prey; setal screen prevents prey items from escaping anteriorly. (I) Flagellum of Ant1 is groomed by setae distally on carpus of Mxp3 endopod. Arrowheads indicate direction of movements. Ant1 = antenna 1, Bas = basis, Car = carpus, Dac = dactylus, Endo = endopod, Exo = exopod, Fla = flagellum, Inc = incisor process, Lb = labrum, Mer = merus, Mdp = mandibular palp, Mx1 = maxilla 1, Mx2 = maxilla 2, Mxp1 = maxilliped 1, Mxp2 = maxilliped 2, Mxp3 = maxilliped 3, P = prey item, Pro = propodus, Sed = sediment, SS = setal screen.

maxilliped 1 coxa (Mxp1 cox), maxilliped 1 basis (Mxp1 bas), maxilliped 1 endopod (Mxp1 endo), maxilliped 1 exopod (Mxp1 exo), maxilliped 1 epipod (Mxp1 epi), maxilliped 2 endopod (Mxp2 endo), maxilliped 2 exopod (Mxp2 exo), maxilliped 3 endopod (Mxp3 endo), maxilliped 3 exopod (Mxp3 exo).

Results

Munida sarsi and *M. tenuimana* have very similar mouthparts, which differ only in details of setation (unpubl. results). Similarly, from the video-recordings we found no differences in feeding behavior between the two species, and the results presented below therefore apply to both species referred to hereafter as *Munida*.

The mouthparts have a wide variety of functions, including food manipulation, ingestion, water current generation, and grooming (Table 1), and the patterns of movement are often complex. When the endopods of Mxp2 and Mxp3 handle large prey items, the movements and structures involved largely depend on the size and shape of the prey. This changes with every situation, though some generalizations can still be made. Other movement patterns are much more stereotypical, especially those performed by Md, Mx1, Mx2, and Mxp1 when handling small prey items, and we will principally focus on these latter functions. Duration or frequency for the stereotypical movements are listed in Table 1 and illustrated in Figures 3 to 13.

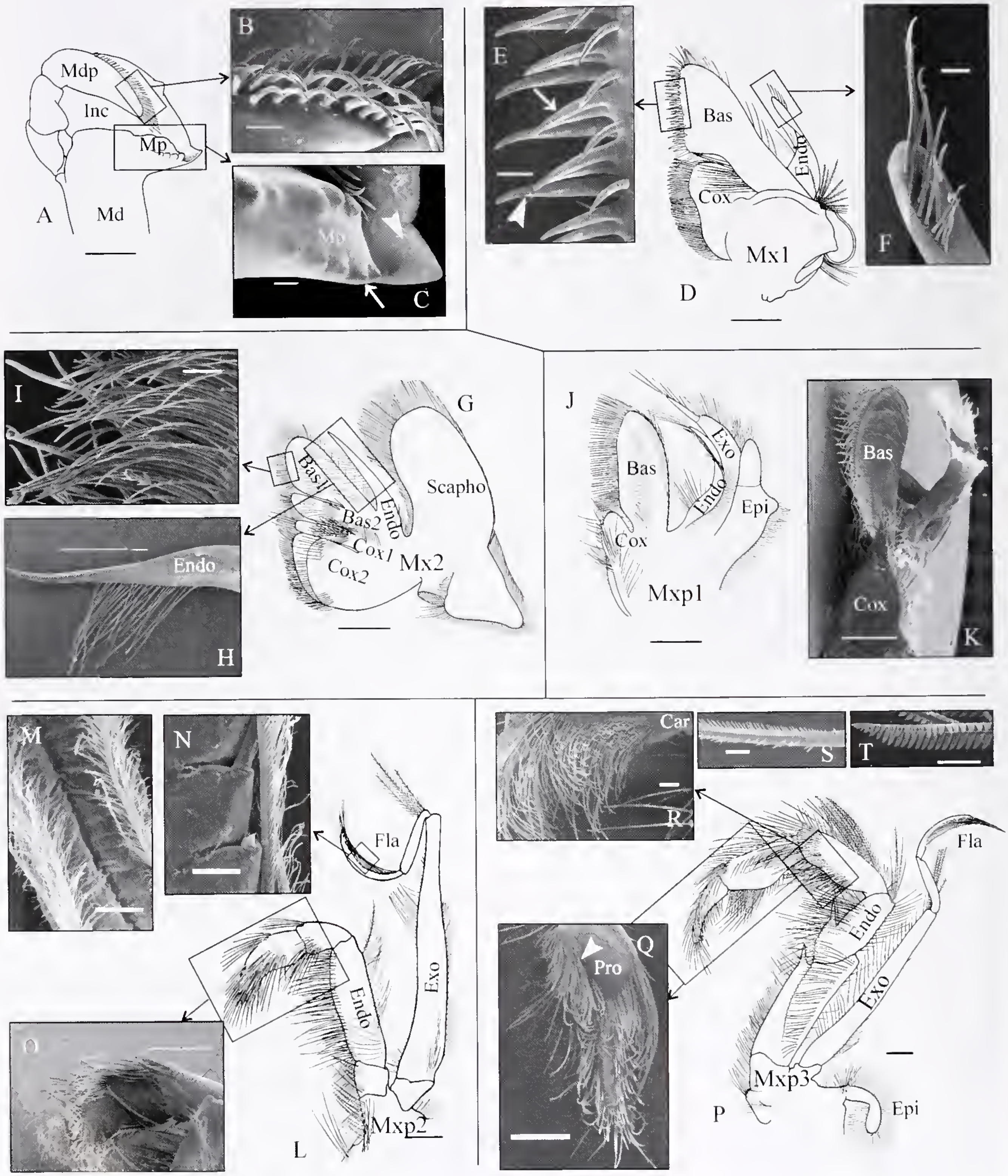
Mdp
Inc
Mp
A
Md
B
Mp
C
E
Bas
Endo
Cox
Mx1
D
F
I
H
Endo
G
Bas1
Bas2
Endo
Scapho
Cox1
Cox2
Mx2
J
Bas
Exo
Endo
Epi
Cox
Mxp1
Bas
Cox
K
M
N
Fla
Endo
Exo
O
L
Mxp2
Car
R
S
T
Fla
Q
Pro
Endo
Exo
Mxp3
P
Epi

Table 1

Behavioral processes and the structures involved

Behavioral process	Structures involved[1]	Duration (s)[2]	Frequency (Hz)[2]
1. Current generation	Mxp2 fla, Mxp3 fla		15.2 ± 1.6
2. Prey gathering	Mxp3 endo, P1	Variable	
3. Sediment gathering	Mxp3 endo, P1-P4	Variable	
4. Transfer sediment to inner mouthparts	Mxp2 endo, Mxp3 endo	Variable	
5. Sediment sorting/Particle rejection[3]	Mx1 bas, Mx2 bas, Mxp1 bas		3.26 ± 0.28
6. Rejection of large prey	Mxp2 endo, Mxp3 endo	Variable	
7. Rotating particle (transverse plan)[3]	Mx1 bas, Mx2 bas (Mxp1 bas[4])		3.21 ± 0.08
8. Rotating particle (medial plan)[3]	Mx1 bas, Mx2 bas (Mxp1 bas[4])		3.18 ± 0.27
9. Put prey between mandibles	Mxp1 bas, Mxp2 endo[5]	Variable	
10. Biting soft prey	Inc, Mx1 bas	1.20 ± 0.15	
11. Biting calcified prey	Inc, Mx1 bas	Variable	
12. Crushing very calcified prey	Mp	Variable	
13. Transfer prey to mouth	Lb, Mdp	Variable	
14. Ingestion[6]	Mx1 cox, Mx2 cox, Mxp1 cox	Not observed	
15. Grooming of Ant1	Mxp3 endo (car)	1.77 ± 0.48	
16. Grooming of Ant2	Mxp3 endo (pro)	2.28 ± 0.34	
17. Respiration[7]	Mx2 scapho		2.6 ± 0.1

[1] Bas = basis, Car = carpus, Cox = coxa, Endo = endopod, Fla = flagellum, Inc = incisor process, Lb = labrum, Mdp = mandibular palp, Mp = molar process, Mx1 = maxilla 1, Mx2 = maxilla 2, Mxp1 = maxilliped 1, Mxp2 = maxilliped 2, Mxp3 = maxilliped 3, P1-4 = pereiopod 1-4, Pro = propodus, Scapho = scaphognathite.

[2] Average ± standard deviation.

[3] The movements are circular, and the frequency is for one round of movements.

[4] Mxp1 bas are not directly involved, see text for details.

[5] Mxp2 endo are used only for large prey items.

[6] See Garm and Høeg (2000).

[7] When not handling any prey. When handling prey, the frequency is higher, see 6, 8, 9.

Resting position and current generation

Figure 1A shows the position of the mouthparts when they are not handling food. Lb and mandibular palps are in ventro-posterior positions, and Md, Mx2, and Mxp1 are opened to only about one-third of their maximum. Mxp2 and Mxp3 are held laterally, with their endopods bent into a U-shape and the flagella on their exopods (Mxp2 exo and Mxp3 exo) beating almost continuously in a dorso-ventral plane. This high-frequency beating generates a unidirectional current around the anterior end of the animal; the current proceeds from the sediment up through the mouthparts (Fig. 1E). During beating, the right Mxp2 flagellum is synchronized with the left Mxp3 flagellum and *vice versa.* The high frequency is correlated with the special morphol-

Figure 2. Morphology of the mouthparts. B, F, H, N, Q from *Munida tenuimana*, rest from *M. sarsi*. (A) Left Md seen posterio-medially. (B) Setae on mandibular palp bending ventrally. (C) Mp with tubercles (arrow). Note large posterior tooth on incisor process (arrowhead). (D) Dorsal view of right Mx1. (E) Closeup of spines (arrow) and robust setae (arrowhead) on medial edge of Mx1 basis. (F) Cluster of setae on tip of Mx1 endopod. (G) Dorsal view of right Mx2. Scapho inserts asymmetrically on rest of Mx2. (H) Dorsal view of dissected Mx2 endopod. Long slender setae project medially. (I) Medial edge of Mx2 basis1 composed of rather fragile setae. (J) Dorsal view of right Mxp1. Note close contact between endopod and exopod. (K) Medial view of Mxp1. Mxp1 basis is curved blade shaped. (L) Medial view of Mxp2. Fla is in resting position. (M) Dorsal view of Mxp2 fla cuticle in resting position. (N) Medial view of Mxp2 fla cuticle in resting position. (O) Posterior view of shovel-shaped distal end of Mxp2 endopod. (P) Medial view of Mxp3. Fla is in upper most position. (Q) Posterior view of shovel-shaped distal end of Mxp3 endopod. Arrowhead indicate setal cluster on Pro used for grooming antenna 2. (R) Setal cluster on Car used for grooming antenna 1. (S) Weakly serrate seta from cluster used for grooming antenna 1. (T) Strongly serrate setae from cluster used for grooming antenna 2. Scalebars: A, D, H, G, J, K, L, O, P, Q = 1 mm; B, C, E, F, I, M, T = 100 μm; N = 50 μm; R = 200 μm; S = 20 μm. Bas = basis, Car = carpus, Cox = Coxa, Endo = endopod, Epi = epipod, Exo = exopod, Fla = flagellum, Inc = incisor process, Md = mandible, Mdp = mandibular palp, Mp = molar process, Mx1 = maxilla 1, Mx2 = maxilla 2, Mxp1 = maxilliped 1, Mxp2 = maxilliped 2, Mxp3 = maxilliped 3, Pro = propodus, Scapho = scaphognathite.

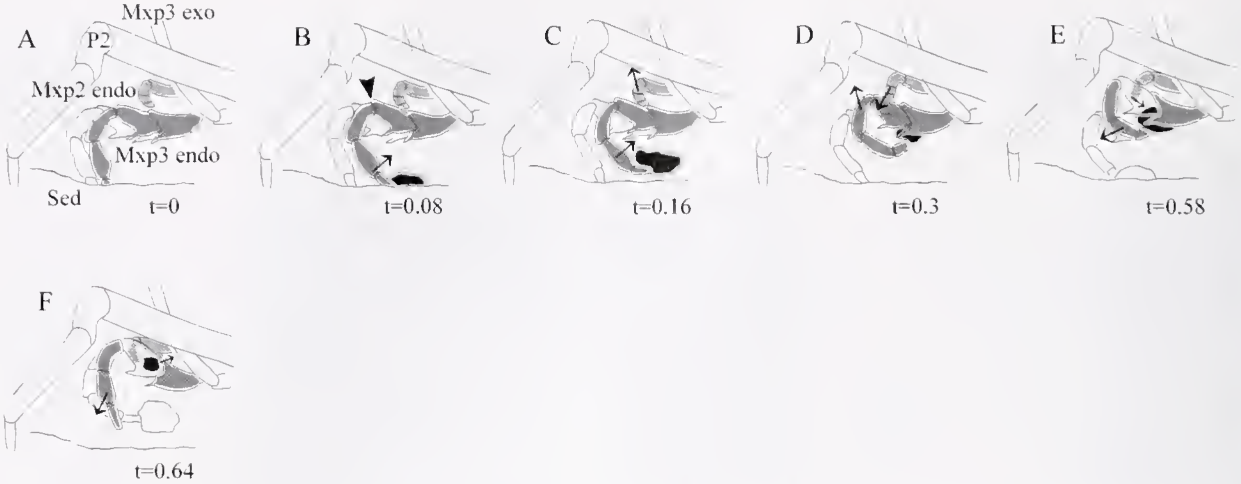

Figure 3. Sediment gathering by the endopods of Mxp3 (Mxp3 endo, dark gray), seen anterio-laterally. (A) Both dactyli of Mxp3 endopod are in the sediment (Sed). (B-D) Left Mxp3 endopod moves dorso-posterially, lifting up a lump of Sed sticking to the setae, and endopod of left maxilliped 2 (Mxp2 endo, light gray) moves dorso-anteriorly to get in front of the lump. Arrowhead in B indicates flexible merus-carpus joint. (E) Left Mxp2 endopod moves posteriorly, combing through setae of Mxp3 endopod, picking up Sed with distal segments. (F) Mxp2 endopod moves further posteriorly, transferring Sed to Mxp1 bas (see Fig. 4). Note that now right Mxp3 endopod has picked up a lump of Sed. Mxp3 exo = exopod of maxilliped 3, P2 = pereiopod 2, t = time in seconds (specific for series of pictures, not generalized).

ogy of the flagellar cuticle (Fig. 2M, N). When the flagellum is moving dorso-anteriorly, the water pressure causes the folded and flexible cuticle on the dorsal side of the flagellum to unfold. This raises the plumose setae into a fan, and this movement thus becomes the power stroke (Fig. 1C). During the ventro-posteriorly directed recovery stroke, the flagellar cuticle folds again, causing the setal fan to close (Fig. 1B). The flagellar current serves to reject small particles and gives the animal an opportunity to detect the composition of the sediment, since water is pumped up from close to the sediment and past the setae on the mouthparts (for details, see Garm and Høeg, 2000).

Food gathering

Most larger food particles are picked up by the long chelipeds and passed to the Mxp3 endopods, both of which extend to grasp the food between their dactyli and propodi. In some cases, the dactyli of the Mxp3 endopods can also pick up food objects directly from the sediment.

Sediment is gathered either with the dactyli of pereiopods 2-4 (P2-4), the chelipeds (P1), or the dactyli of the Mxp3 endopods. In the first two cases, the sediment is passed on to the dactyli of the Mxp3 endopods as they comb through the setae that hold the sediment on the cheliped or P2-4.

When the Mxp3 endopods collect sediment, they start by pressing the dactylus and sometimes also the propodus into it (Fig. 3A). Thereafter the distal end of the endopod bends posterio-dorso-medially (towards the mouth) and shovels up a lump of sediment (Fig. 3B-D). The great flexibility of the endopod, especially in the merus-carpus joint (Fig. 3B, arrowhead; Fig. 4), greatly facilitates this process. The efficacy of the Mxp3 endopods in handling sediment is improved by a rim of strong, serrate setae along the distal end (Fig. 2P, Q); this enlarges the shovel, and the setae serve as hooks. The Mxp3 endopods usually pick up sediment from the area right under the flagella. The two Mxp3 endopods may move synchronously when gathering sediment, but they are normally used one at a time, as seen in Figure 3.

Handling large prey items

With respect to larger food items, the animals were not at all choosy and ate all kinds of animal tissue presented to them, even sponges (Porifera) and gorgonians (Gorgonacea). Such large food objects are grasped by the endopods of Mxp2 and Mxp3 (Fig. 1H) and pushed directly towards the mandibles. The Mxp3 endopods are bent into a U-shape and hold the prey between the meri and the propodi. The dactyli are held under the prey if it is not too large. The bases of Mx1 and Mx2 are fairly inactive and mostly press against the prey, while possibly making fine adjustments of the food item for the mandibles. When the mandibles cut into a large food item, the bases of Mxp1 often scrape very actively along the object in circles, as shown in Figure 5. If the prey is soft, such as a lump of fish meat, the movements of the Mxp1 bases tend to squeeze it so it will fit more easily between the incisor processes of the mandibles (Inc). On a few occasions, the animals were also observed attempting to

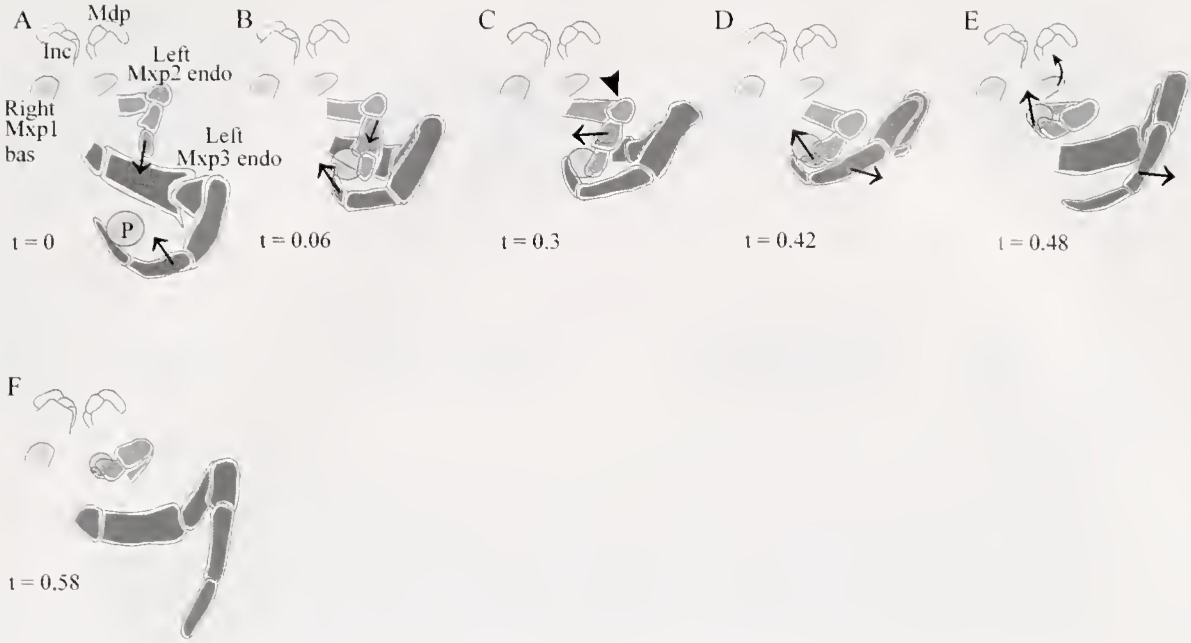

Figure 4. Transfer of particles (P) from endopod of maxilliped 3 (Mxp3 endo, dark gray) to the basis of maxilliped 1 (Mxp1 bas, light gray) seen ventro-anteriorly. Corresponds to D-F in Fig. 3. (A, B) Left Mxp3 endopod bends posterio-medially. Endopod of left maxilliped 2 (Mxp2 endo, middle gray) moves ventrally towards Mxp3 endopod. (C, D) Mxp2 endopod moves posteriorly, with the setae on dactylus combing through the setae on the distal part of Mxp3 endopod. Arrowhead in C indicates flexible merus-carpus joint. (E, F) Mxp3 endopod moves anterio-laterally; Mxp2 endopod moves posteriorly, with the distal part reaching the inner mouthparts. Left Mxp1 basis moves laterally to be able to collect P from Mxp2 endopod (see Fig. 5). Inc = incisor, Mdp = mandibular palp, t = time in seconds (specific for series of pictures, not generalized).

use the crista dentata on the ischium of Mxp3 endopods in a crablike manner. This would involve holding the prey between the incisor processes while both Mxp3 endopods move dorso-anteriorly, grasping the prey with the crista dentata while in the dorsal position, then lowering the Mxp3 endopods and thereby tearing the prey. However, this behavior was never observed to be successful in *Munida*, because the crista dentata never got hold of the prey items. Large objects are not rejected by the flagellar current, but are simply dropped or removed by Mxp2 endopods.

Handling small prey items

When carrying a small food item, the Mxp3 endopods bend posterio-medially to meet the endopod of maxilliped 2 (Mxp2 endo) (Figs. 3, 4), which passes sediment and particles further towards the mouth, that is, to the bases of Mxp1.

When the Mxp3 endopod approaches the mouth, the collateral Mxp2 endopod moves first dorso-anteriorly to get in front of the food item held distally on the Mxp3 endopod (Fig. 3C) and thereafter ventro-posteriorly to shovel up the item (Figs. 3D-F, 4A-D). Holding the food with its distal end, the Mxp2 endopod bends further towards the mouth and reaches the area of the bases of Mxp1. Meanwhile the collateral Mxp1 basis moves aside to make room for the food, and the Mxp3 endopod extends again (Fig. 4E, F). Most of the flexure of the Mxp2 endopod takes place in the merus-carpus joint (Fig. 4C, arrowhead), and the distal segments also form a shovel that enables them to carry the food (Fig. 2L, O). The serrate setae found distally on the Mxp2 endopod are less robust than those on the Mxp3 endopod, and therefore they can pass between the latter to collect the potential food. Like the Mxp3 endopods, the endopods of Mxp2 can be used at the same time—when one is moving anteriorly the other is moving posteriorly—but this is not the normal pattern.

The Mxp1 bases collect the particles from the Mxp2 endopod by making circular movements as shown in Figure 5, but in the opposite direction. Moving the curved and blade-shaped bases (Fig. 2J, K) medially when they reach the Mxp2 endopod and laterally when they meet the Mx2 bases ensures the direction of particle transport. Mx2 moves medially and grasps the prey.

Sediment sorting and particle rejection

Almost all collected particles eventually reach the Mx2 and Mx1 bases, which are the mouthparts responsible for rejecting or retaining food items. Figure 6 shows how the

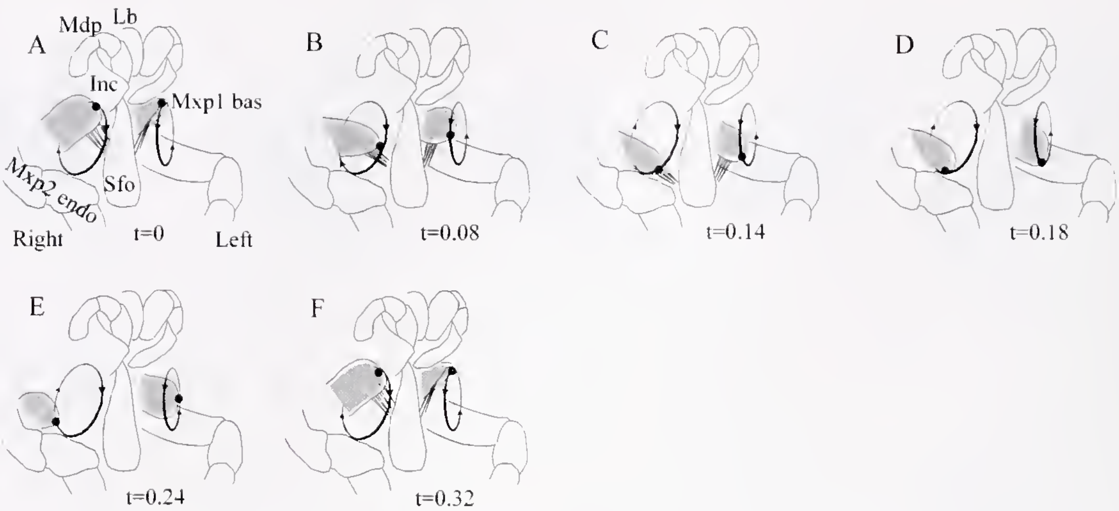

Figure 5. Movements of the bases of maxilliped 1 (Mxp1 bas, gray) seen anterio-laterally. To simplify drawings, maxilla 1 and maxilla 2 are left out and setae are shown only when in contact with prey. The appendages make circular movements in an angle to plane of view indicated by ellipse; thin part of ellipse is towards the animal. Black dots indicate the positions of the limbs in the movement. This movement can shred small and soft food objects (Sfo) held by mandibles or move particles away from mandibles. Movement can be reversed, which will move particles from endopod of maxilliped 2 (Mxp2 endo) towards basis of Mx2. Inc = incisor process, Lb = labrum, Mdp = mandibular palp, t = time in seconds (specific for series of pictures, not generalized).

Mx1 and Mx2 bases move in circles parallel to the mandibular incisor (Inc) when sorting sediment. The direction of movement is dorso-anteriorly when they are in the medial position and ventro-posteriorly when they are in the lateral position. Thus, from the animal's point of view, the distal tips of the right-side appendages rotate clockwise, while those on the left side rotate counterclockwise. This ensures that the cuspidate setae on their medial edges hit the particles from the ventro-posterior and push them in a dorso-anterior direction. The Mx1 bases and the Mx2 bases move out of phase, ensuring that one of these appendage pairs remains in contact with the particle most of the time. The circular movements continue until the particle enters the flagellar current and is rejected anteriorly (Figs. 1D, 6), or until the animal decides to retain the particle. The Mx1 bases are responsible for most of the particle movement. The medial rims of the Mx1 bases have much more robust cuspidate setae than the Mx2 bases (Fig. 2E, I), and this allows them to press harder against the particles, obtaining a more firm hold. Within a specific pair (Mx1 bases or Mx2 bases), left and right sides are synchronized so they are in the medial position at the same time. The Mxp1 bases move as described under "Handling small prey items," providing more particles, pushing them towards the Mx2 bases, and ensuring that nothing is lost ventro-anteriorly (Fig. 6). During the sorting process, the Mxp2 endopods are held medially where they form a setal screen which also prevents particles from escaping ventro-anteriorly. When the animal is handling large prey, the Mxp3 endopods provide a similar setal screen (Fig. 1H).

Particle rotation

When the animal finds a small particle worth eating, the Mx1 and Mx2 bases stop making circular movements and begin moving to and fro in the medio-lateral plane while keeping the particle in front of the incisor process (Fig. 1F). Again, the Mx1 and Mx2 bases move out of phase. If the particle is not orientated correctly for the Md, it will subsequently be rotated by the Mx1 and Mx2 bases (Figs. 7, 8).

During rotation of a particle in the transverse plane, the Mx2 and Mx1 bases again move out of phase and make circular movements parallel to the incisor process (Fig. 7). Unlike the situation during sediment sorting, all four mouthparts concerned (*i.e.*, both left- and right-side Mx2 bases and Mx1 bases) move either clockwise or counterclockwise. To turn a particle clockwise (as seen from the animal's point of view), the left-side Mx1 and Mx2 bases move dorso-anteriorly when in their medial position and ventro-posteriorly when in their lateral position, thereby pushing the left side of the particle dorso-anteriorly. In the medial position, the bases of the right-side Mx1 and Mx2 move in the opposite direction as the left-side bases; thus they push the right side of the particle ventro-posteriorly, and it is rotated in the transverse plane. The animal rotates the particle counterclockwise by reversing these movements.

Rotating a particle in the medial plane (Fig. 8) is always

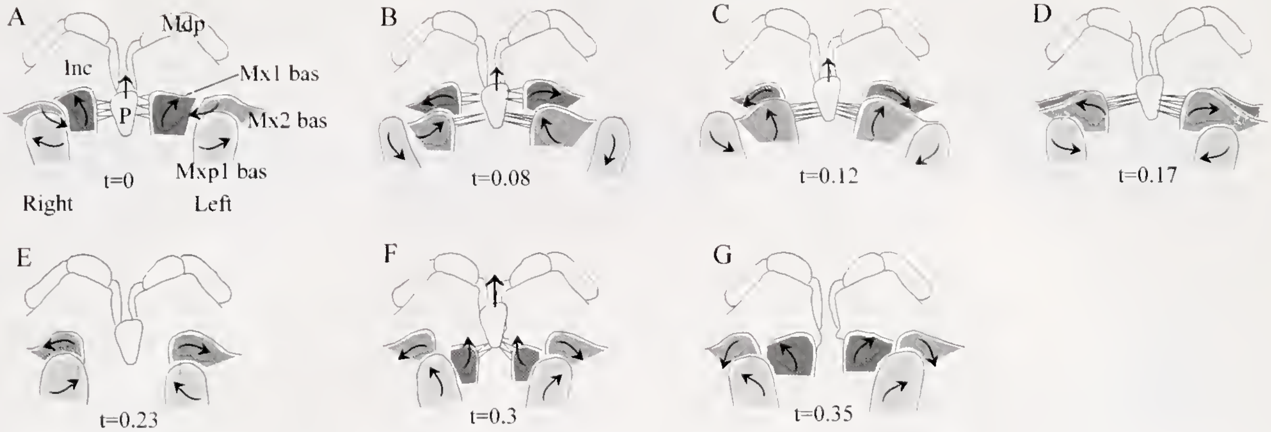

Figure 6. Rejection of unwanted particle (P) by bases of maxilla 1 (Mx1 bas, dark gray), maxilla 2 (Mx2 bas, middle gray), and maxilliped 1 (Mxp1 bas, light gray) seen ventro-anteriorly; setae are shown only when in contact with P. Arrows indicate direction of movements. (A) Mx1 basis in contact with P pushing dorso-anteriorly. (B, C) Mx2 basis gets in contact with P and pushes it dorso-anteriorly. Mx1 basis moves laterally and releases P. (D, E) Mx2 basis releases P. (F) P is pushed above mouthparts by Mx1 basis and enters the flagellar current. (G) P is rejected. During the rejection, Mxp1 basis is not in contact with P, but makes posterio-anteriorly circles (see Fig. 5), probably ensuring that P is not lost anteriorly. Inc = incisor process, Mdp = mandibular palp, t = time in seconds (specific for series of pictures, not generalized).

done in one direction, with the part of the particle closest to the animal moving dorso-anteriorly and the part away from the animal moving ventro-posteriorly, that is, clockwise when seen from the animal's right side. The mouthparts of the left and right sides move in synchrony, as when rotating particles in the transverse plane, but the distal tips of the Mx2 bases and the Mx1 bases now circle in opposite directions. The Mx1 bases move dorso-anteriorly when they are in the medial position and ventro-posteriorly when in the lateral position. They thereby hit the particle from a ventro-

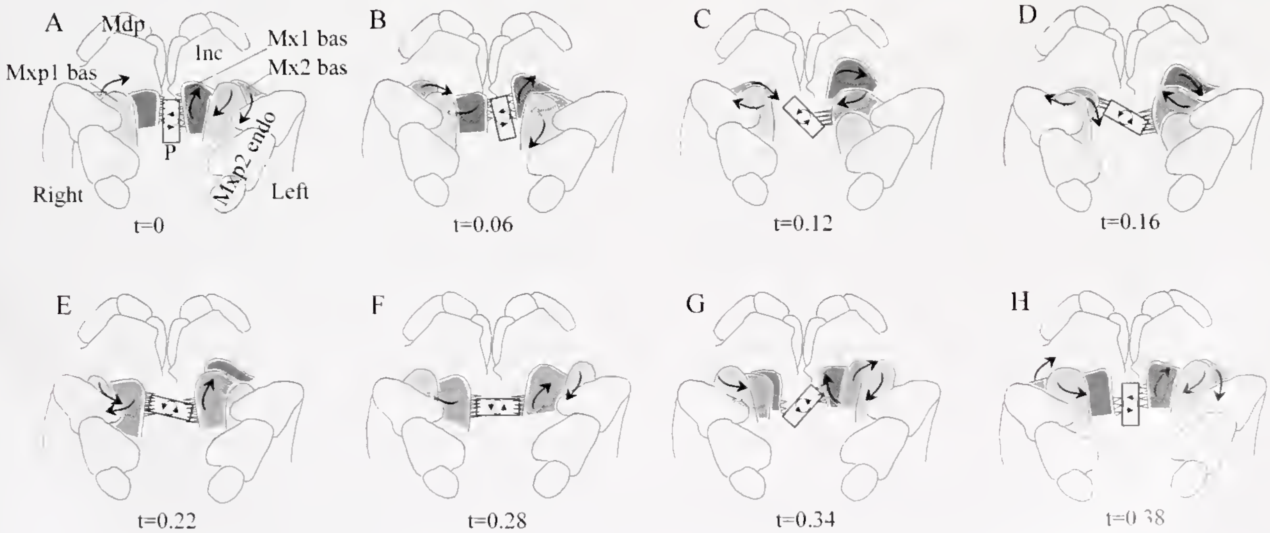

Figure 7. Rotation of a small particle (P) in a transverse plan by bases of maxilla 1 (Mx1 bas, dark gray) and maxilla 2 (Mx2 bas, middle gray). The view is ventro-anteriorly and setae are only shown when in contact with P. (A, B) P is held by Mx1 basis. Left Mx1 basis moves dorso-anteriorly; right Mx1 basis moves a little laterally. This starts the rotation. (C) Mx1 basis releases P; Mx2 basis gets in contact with P. (D-F) Mx2 basis in contact with P. Left moves dorso-anteriorly and right ventro-posteriorly, which rotates P further. (G) P is hit by left Mx1 basis from ventro-posterior and laterally by right Mx1. (H) Back in start position. During rotation the bases of maxilliped 1 (Mxp1 bas, light gray) are not in contact but tend to make anterio-posteriorly circles (see Fig. 5), probably ensuring P is not lost anteriorly. Inc = incisor process, Mdp = mandibular palp, Mxp2 endo = endopod of maxilliped 2, t = time in seconds (specific for series of pictures, not generalized).

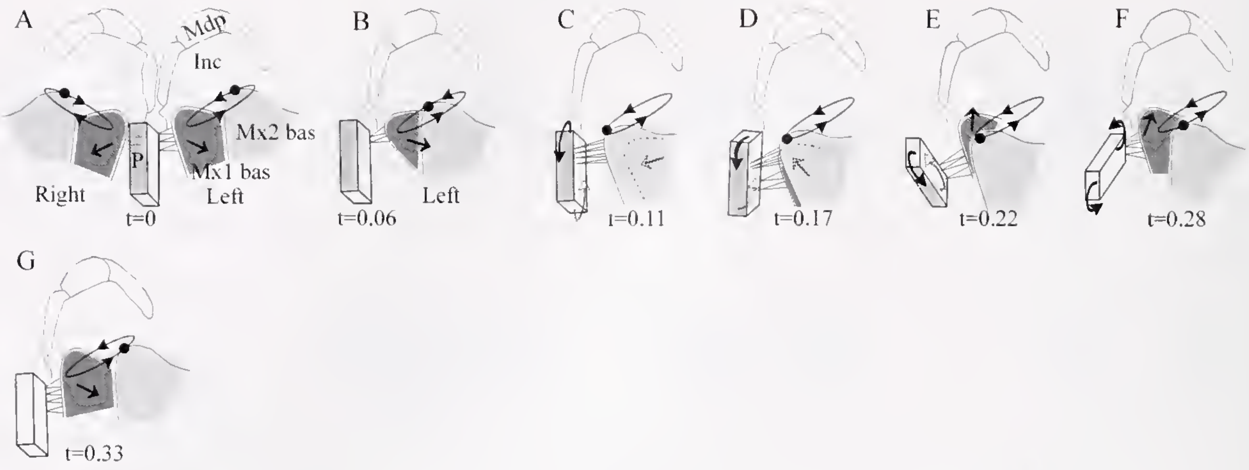

Figure 8. Rotation of a small particle (P) in a medial plan by the bases of maxilla 1 and maxilla 2 (Mx1 bas, dark gray and Mx2 bas, light gray). View is ventro-anterior. Only left side is shown in B-G, and setae are shown only when in contact with P. Right and left side move in synchrony and in phase. Arrows indicate direction of movements. Dotted line indicates hidden structure. Mx2 basis makes circular movements; black dots indicate the positions of the appendages in the circle. (A, B) Mx1 basis releases P. (C) Mx2 basis hits anterior edge of P from dorso-anterior, pushing it ventro-posteriorly. (D-F) Mx1 basis hits posterior edge of P from ventro-posterior, pushing it dorso-anteriorly. Mx2 basis releases P. (G) Mx2 basis moves laterally and up; Mx1 basis releases P. Process is ready to start again. Inc = incisorprocess, Mdp = mandibular palp, t = time in seconds (specific for series of pictures, not generalized).

posterior direction and push it dorso-anteriorly. When circling in the opposite direction, the Mx2 bases hit the particle from a dorso-anterior direction and push it ventro-posteriorly. This causes the particle to be rotated around a point between the bases of Mx1 and Mx2.

In both cases, the Mx1 bases are responsible for most of the rotation, and the animal has serrate and cuspidate setae in contact with the particle at all times. The Mxp1 bases tend to make circular movements that push the particle toward the Mx2 basis. Both during sediment sorting and when rotating a small particle, the Mx1, Mx2, and Mxp1 bases normally circle with the same frequency. The normal order of contact with the particle is Mx1 basis, Mx2 basis, Mxp1 basis, Mx1 basis, and so forth in a repeated way, as seen in Figure 6. However, the Mxp1 bases occasionally perform more complex movement patterns independent of the positions of the Mx1 and Mx2 bases, as indicated in Figure 7.

Cutting-crushing

Having orientated the particle correctly for maceration, the animal puts it between the mandibles (Fig. 9). At first, the mandibular incisors (Inc) move laterally while the labrum (Lb) and mandibular palps (Mdp) retract dorso-anteriorly to make room for the item (Fig. 9B). Subsequently, the Mxp1 bases (and possibly also the Mx1 and Mx2 bases) push the particle between the incisor processes, which move medially until they overlap about one-fifth, always with the right incisor process on the anterior side (Fig. 9C, D). A large posterior tooth on the left incisor process assures a good grip on the item (Fig. 2C, arrowhead). Meanwhile the food particle is held tight by the robust spines and cuspidate setae on the medial rim of the Mx1 bases (Fig. 2E). If the particle is slim, the incisor process will not move laterally first, but will move medially directly from resting position, thereby performing the cut. After the cut, the incisor processes move laterally and the mandibular palps and Lb move ventro-posteriorly (Fig. 9E, F), pushing the cut-off piece of food towards the mouth, an action facilitated by serrate setae on the mandibular palps (Fig. 2B) and setule-like outgrowths on Lb. The rest of the particle is pushed ventro-anteriorly to be further processed by the Mx1 and Mx2 bases. The ingestion is handled by the coxae of Mx1 and Mx2 and perhaps Mxp1. This is not seen on the videos but extrapolated from the organization of the mouth apparatus. The three pairs of coxae are situated just ventral to the mouth and, along with their setae, they curve into the mouth opening (for details, see Garm and Hoeg, 2000).

Prey too hard to cut with the incisor process, such as calciferous polychaete tubes, are instead crushed by the molar processes of the mandibles (Mp). The flattened shape and their rim of tubercles ensure that even very smooth objects such as mollusc shells will not easily slip away (Fig. 2C). The movements are identical to the cutting action (Fig. 9), except that the prey is placed between the molar processes posteriorly to the incisor processes and the process lasts longer.

Grooming the antennae

Grooming of both antenna 1 (Ant1) and antenna 2 (Ant2) is performed by the Mxp3 endopods, but by two different

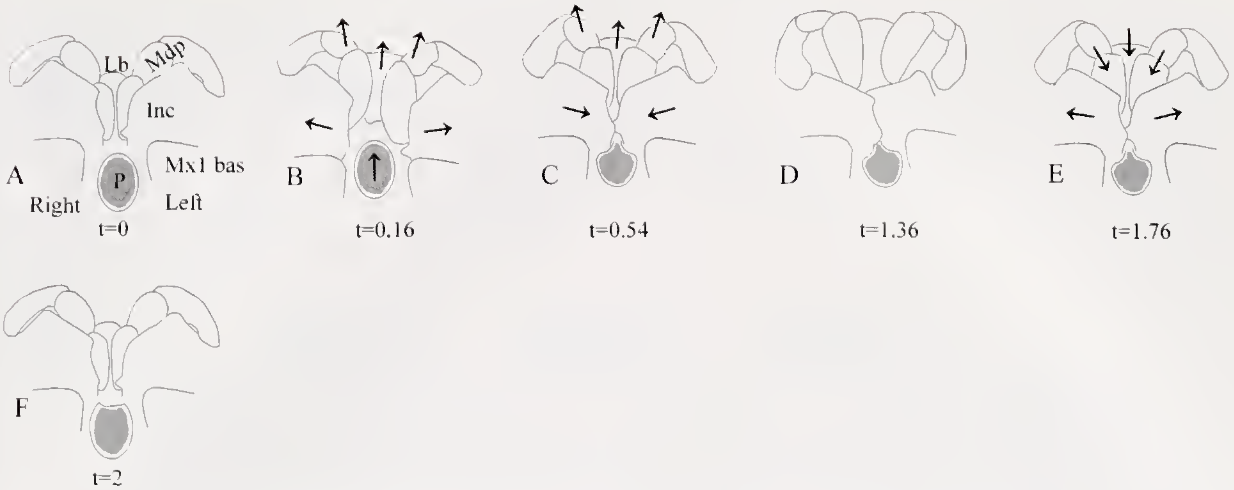

Figure 9. Cutting by mandibles seen ventro-anteriorly. (A) Resting position. Incisor processes (Inc) are a little opened; labrum (Lb) and mandibular palps (Mdp) are lowered. Prey (P) is held by bases of maxilla 1 (Mx1 bas). (B) Incisor processes move laterally; Lb and mandibular palps move anteriorly to make room for P. (C) Cut starts. Incisor processes move medially; Lb and mandibular palps move further anteriorly. (D) Incisor processes with maximum overlap, always left on dorsal side. Lb and mandibular palps in anteriormost position. (E) Cut ends. Incisor processes move laterally; Lb and mandibular palps move posteriorly and push the cut-off piece towards mouth. (F) Cut has ended; limbs back in resting position. During the cut, Mx1 are held medially to hold P. If P is small, stage B is skipped. t = time in seconds (specific for series of pictures, not generalized).

clusters of setae (Figs. 2P-R, 10, 11). The antennae are always groomed one at a time, and Ant1 are groomed much more frequently than Ant2. Grooming of an Ant1 starts with the appendage in question bending ventrally and both Mxp3 endopods moving dorsally (Fig. 10A). In the next step, Mxp3 endopods move medially and catch the peduncle of Ant1 with serrate setae on the carpi (Fig. 2R). With a loose grip, they move ventrally until they reach the flagellum of

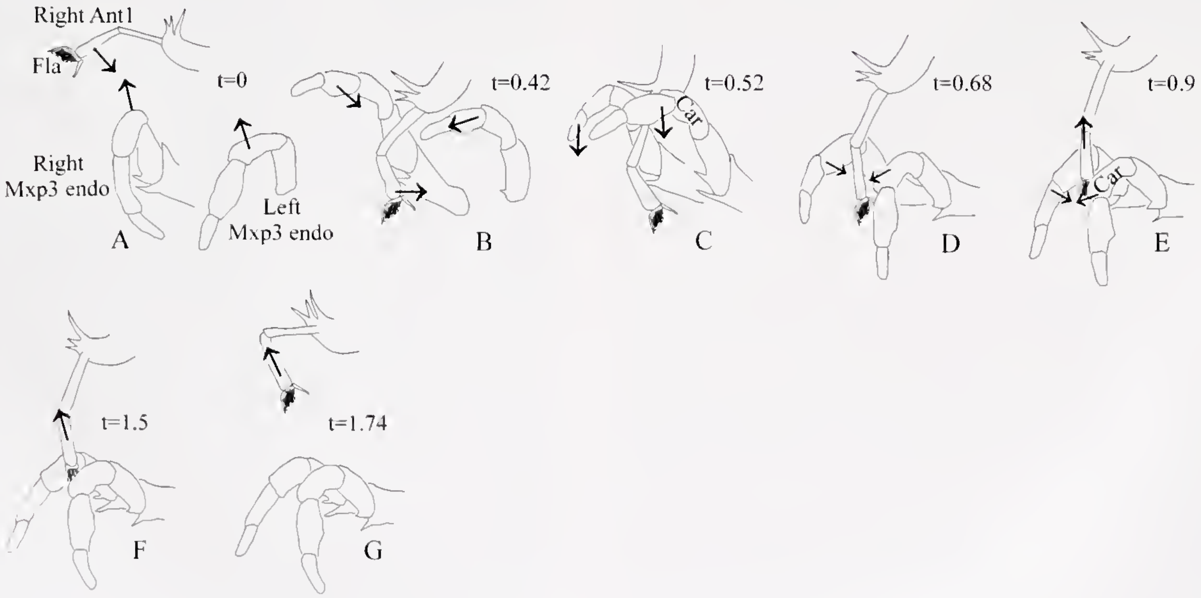

Figure 10. Grooming of antenna 1 (Ant 1) by endopods of maxilliped 3 (Mxp3 endo), seen anterio-laterally. (A) Mxp3 endopods reach up while Ant1 bends down. (B) Mxp3 endopods move ventro-medially and Ant1 bends posteriorly. (C) Ant1 is caught by long setae distally on carpus (Car), which move along shaft of Ant1. (D) When the flagellum (Fla) is reached, Mxp3 endopods move further medially. (E-G) Mxp3 squeeze tight around Fla and aesthetascs are pulled through setae on Car. t = time in seconds (specific for series of pictures, not generalized).

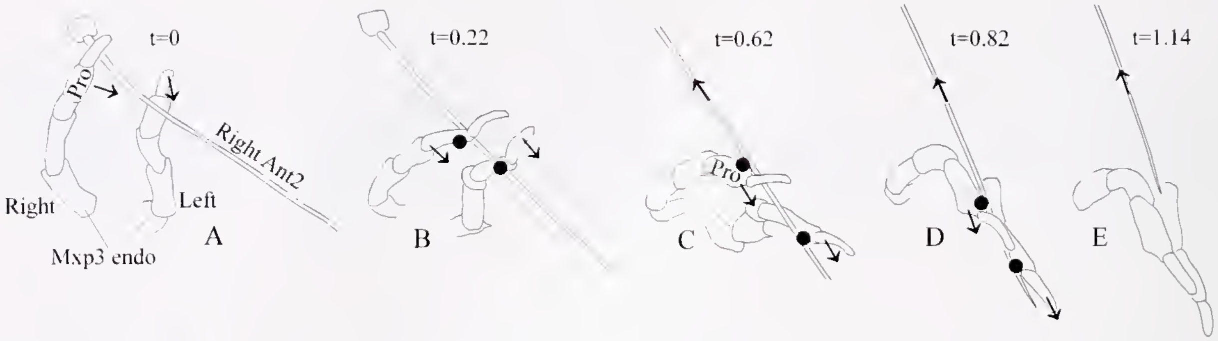

Figure 11. Grooming of right antenna 2 (Ant2) by endopod of maxilliped 3 (Mxp3 endo) seen ventro-anteriorly. The antenna is caught on right side and released on left. Arrows indicate direction of movements. Black dots indicate contact between Ant2 and propodus (Pro). (A) Mxp3 endopod has moved dorsally and right Ant2 has bent ventrally. Mxp3 endopod moves medially and catches Ant2 with long setae on distal part of Pro. (B) Mxp3 endopod moves downwards and Pro setae run along Ant2, grooming it. (C-E) Mxp3 endopod moves further down and Ant2 pulls itself up through setae distally on Pro. t = time in seconds (specific for series of pictures, not generalized).

Ant1 (Fig. 10B-D). Now the Mxp3 endopods move further medially, squeezing the Ant1 flagellum tightly between the carpi, and the flagellum is pulled through the serrate setae as the Ant1 moves dorsally (Figs. 11, 10E-G). Occasionally, the Mxp3 endopods move farther dorsally in the beginning of the process, reaching the eye situated just dorsal to Ant1. The eye is then groomed by setae on the dactyli and the propodi. The same setal clusters on the carpi also groom the Mxp2 and Mxp3 flagella, and the movements of the Mxp3 endopods are much the same.

Ant2 is also groomed by the Mxp3 endopods, but with setal clusters on the propodi instead of on the carpi (Figs. 2Q, T; 11). One of the Ant2 bends ventrally, and both Mxp3 endopods move dorsally and grasp the long flagellum of Ant2 between setal clusters distally on the propodi (Fig. 11A). When in contact with the flagellum, the Mxp3 endopods move ventro-anteriorly and Ant2 moves dorsally, pulling itself through the robust serrate setae (Fig. 11B-E). Ant2 grooming is an asymmetrical process: the appendage is grasped on the side of the animal where it is attached and subsequently released on the other side. Due to the twist of the movement, the two Mxp3 endopods move apart during the process and groom two different sites of Ant2 at a given time (Fig 11C, D). This means that Mxp3 endopods cannot squeeze the Ant2 flagellum as tightly as when grooming the Ant1 flagellum.

The setal clusters grooming Ant1 and Ant2 are situated differently on the Mxp3 endopod and are composed of different types of serrate setae (Fig. 2S, T). Those grooming Ant2 are more stout and have much more robust denticles.

One curious observation concerned a specimen of *M. sarsi* that had lost both Mxp3 during sampling. It neither ate nor groomed Ant1, but it did groom Ant2 with the chelae.

Respiration

Beating of the scaphognathites (Scapho), also called gill bailers, produces the respiratory currents. The Scapho are situated laterally on Mx2 (Fig. 2G), which places them in the anterior part of the gill chambers. When an Mx2 basis executes medio-lateral movements, its Scapho moves ventro-dorsally (Fig. 12). The movements of the Scapho are comparable to swimming with flippers. Because it inserts on the Mx2 coxa with the less flexible posteriormost part, the flexible anterior part moves with a delay when compared to the posterior part. When the posterior part starts moving dorsally, the anterior part initially remains at rest, but after a while it follows until the entire Scapho reaches its dorsalmost position (Fig. 12A-E). During the ventral stroke, the movement is again initiated by the posterior part, followed, with some delay, by the anterior part (Fig. 12F-I). The delayed movements of the anterior part ensure that the respiratory current is unidirectional, with water entering the posterior part of the gill chamber and exiting anteriorly. We never observed the reversal of the respiratory current that Bauer (1981) described for other decapods.

When moving ventrally, the anterior part of the Scapho sweeps across the epipod of Mxp1 and the exopods of Mxp2 and Mxp3, and these structures help direct the exhalant current (Fig. 12G-I). The posterior part sweeps the two anteriormost pairs of gills.

Dorsoventral mouthparts

Four structures of the mouth apparatus have not yet been dealt with, since their activities are not clear. These structures, which constitute the dorso-lateral part of the mouth apparatus, are the endopods of Mx1, Mx2, and Mxp1, and the exopod of Mxp1. When the Mx1 and Mx2 bases move

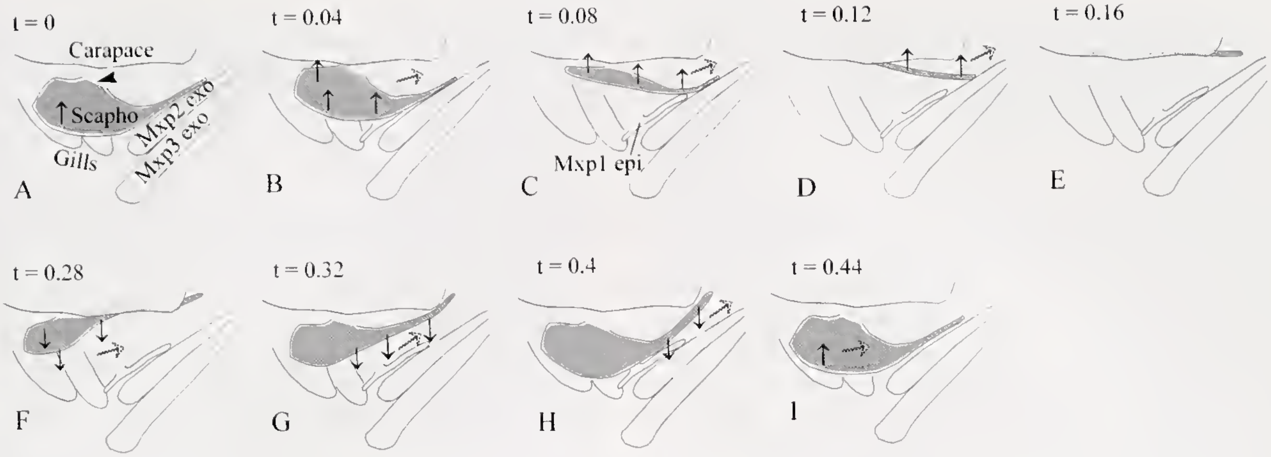

Figure 12. Respiratory movements of right scaphognathite (Scapho, gray) seen laterally; branchiostegite is removed. Arrows indicate moving part and direction of movement. Dotted arrows indicate respiratory current. Junction between Scapho and rest of maxilla 2 (arrowhead in A) is situated posteriorly on Scapho, which make posterior part follow movements of Mx2, dragging anterior part behind. Delayed movement of anterior part ensures that respiratory current is directed anteriorly. Note that Scapho sweeps across epipod of maxilliped 1 (Mxp1 epi). Mxp2 exo = exopod of maxilliped 2, Mxp3 exo = exopod of maxilliped 3, t = time in seconds (specific for series of pictures, not generalized).

in the medio-lateral plane, the endopods of Mx1 and Mx2 perform small semicircular movements (Fig. 13). This causes the distal tip of the Mx2 endopod to rub against the medial part of the base of the mandibular palp and the Mx1 endopod to sweep across a small part of the dorsal side of the Mx2 endopod. Both Mx1 and Mx2 endopods have a well-defined cluster of setae (Fig. 2F, H). The long serrulate setae of the Mx2 endopod lie in the space between the incisor process and the Mx1 basis and are in contact with the incisor process. The smaller serrate setae of the Mx1 endopod seem not to contact anything. The flagellum of the exopod of Mxp1 lies in the exhalant current and moves very little, even when the rest of the Mxp1 is actively processing food. Water from the flagellar current also passes the flagellum of the Mxp1 exopod. The Mxp1 endopod lies very close and dorso-ventral to the Mxp1 exopod (Fig. 2J, K), and is therefore also placed in the currents, but in Fig. 13 the Mxp1 exopod obscures it from view.

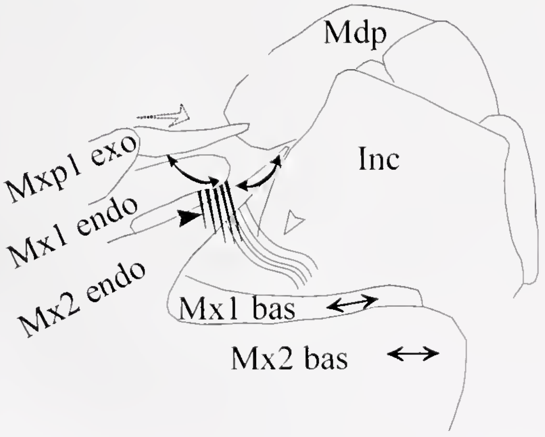

Figure 13. Placement and movements of dorso-ventral mouthparts (endopods of right maxilla 1 and maxilla 2 [Mx1 endo and Mx2 endo] and exopod of right maxilliped 1 [Mxp1 exo]), seen latero-anteriorly. Arrows indicate direction of movements. Dotted arrow indicates respiratory current. Open arrowhead indicates Mx2 setae lying in the space between Mx1 basis and incisor process (Inc) (see also Fig. 2H); black arrowhead indicates Mx1 setae (see also Fig. 2F). When Mx2 basis make medio-laterally movements, tip of Mx2 endopod rubs against base of the mandibular palp (Mdp). Setae on Mx1 endopod are apparently not in any contact. Flagellum of Mxp1 exopod is situated in respiratory current.

Discussion

Functional grouping of mouthparts

The six pairs of mouthparts (Md, Mx1, Mx2, and Mxp1-3) and the labrum are very different in both morphology (Fig. 2) and function (Figs. 3-13, Table 1). To some degree, their pronounced differences in size and shape correlate with function, since the large and pediform Mxp2 and Mxp3 handle large prey items, whereas the smaller and flattened Mx1, Mx2, and Mxp1 enable the animal to accurately manipulate even very small food objects. The dorso-ventrally flattened form of these small mouthparts enables several independently moving structures to operate close together, a prerequisite to accurate manipulation of small food. The freedom of movement decreases in the mouthparts that are nearer to the mouth and arranged very close together, and this explains why the Lb, Mx1, Mx2, and Md perform rather stereotypical movements in a two-dimensional plane. The maxillipeds have much more space in which to operate, and the Mxp2 and Mxp3 endopods can move in all directions anterior to the animal due to their flexible joints. They can therefore manipulate a great variety of food items.

Although morphology and organization could support the division of the mouth apparatus into inner and outer mouthparts, this is a much too simplified view when it comes to functions of the mouthparts. As mentioned earlier, each side of the mouth apparatus can be divided into at least 20 separate parts, but these parts seldom work independently; rather they operate in functional groups. The Mxp2 and Mxp3 endopods have fairly similar functions and often work jointly, at least when processing potential food objects. The Mx1 and Mx2 bases form another group with very high correlation of movements and functions when processing food particles. Both of these two groups relate to the Mxp1 bases, which do not clearly belong to a single functional group, but can work closely together with either the Mxp2 and Mxp3 endopods or with the Mx1 and Mx2 bases (Fig. 4 and Fig. 7, respectively). Therefore, the Mxp1 bases constitute a group of their own. The flagella of the Mxp2 and Mxp3 exopods form a well-defined functional group having exactly the same function, and they almost always work together. The labium, the incisor processes, the molar processes, and the mandibular palps form another functional group, where the elements rarely move independently. The functional group composed of the coxae of Mx1, Mx2, and Mxp1 cannot be seen in the videos, but their role in ingestion can be interpreted from their position and morphology (for details, see Garm and Høeg, 2000). The scaphognathite, the Mxp1 epipod, and the Mxp2-3 exopods form a functional group because they cooperate in creating and directing the respiratory currents. The Mx1, Mx2, and Mxp1 endopods and the Mxp1 exopod seem to form the last functional group. This follows solely from their position, since their functions are but poorly understood. The distal tip of the Mx2 endopod might groom the base of the mandibular palp, and the setae might groom the ventrolateral side of the incisor process. Situated in the respiratory current, sensory setae on the Mxp1 endopod and exopod could allow them to be used to sense the need for gill grooming. The Mxp1 endopod in the brachyuran crab *Ebalia tuberosa* forms an exhalant canal, as do the Mxp1 endopod and exopod in the hermit crab *Pagurus rubricatus* (Schembri, 1982a, b), but this is unlikely to be the case in *Munida* because those structures are so slender. We never observed any contact between the setal cluster on the distal tip of the Mx1 endopod and any other object or mouthpart, and this could imply that these may be remote chemosensory setae.

At least for *Munida*, our groupings seem to have more explanatory power than the conventional and superficial separation into inner and outer mouthparts. We suggest the following terms based on the observed functions:

1. *transporting mouthparts* for Mxp2 endopod and Mxp3 endopod;
2. *transporting–aligning mouthpart* for Mxp1 basis;
3. *sorting–aligning mouthparts* for Mx1 basis and Mx2 basis;
4. *current–generating mouthparts* for flagella of Mxp2 and Mxp3 exopods;
5. *cutting–crushing mouthparts* for incisor and molar processess, mandibular palp, and labrum;
6. *ingesting mouthparts* for Mx1 coxa, Mx2 coxa, and Mxp1 coxa;
7. *respiratory mouthparts* for scaphognathite, Mxp1 epipod, and Mxp2 and Mxp3 exopods;
8. *dorso–lateral mouthparts (with uncertain functions)* for Mx1 endopod, Mx2 endopod, Mxp1 endopod, and Mxp1 exopod.

These groupings are not entirely strict, as illustrated by the grooming behavior, in which each mouthpart (except Inc and Mp) partakes in grooming adjacent structures. The Mx2 bases can also move independently of the Mx1 bases, as evidenced by the respiratory movements, when the animal is not handling any food. Moreover, there is a slight division of functions between Mx1 and Mx2 when handling food items. The robust spines and serrate setae arming the Mx1 bases indicate their main function to be mechanoeffectory, whereas the several types of more delicate setae on the Mx2 basis suggest a mechanosensory function, a chemosensory function, or a combination of the two. If true, this gives the Mx2 bases a key role in sensing the quality of the potential food particles.

Comparison with other decapods

For most decapod taxa there is a lack of behavioral data, but a few earlier studies do describe some functional morphology accompanied by movement patterns (Anomura: Nicol, 1932; Roberts, 1968; Kunze and Anderson, 1979; Schembri, 1982a; Zainal, 1990. Thalassinidea: Stamhuis *et al.*, 1998. Palinura: Suthers and Anderson, 1981. Brachyura: Schembri, 1982b. Astacidea: Barker and Gibson, 1977; Lavalli and Factor, 1995. Caridea: Moore *et al.*, 1993. Penaeidea: Hunt *et al.*, 1992).

Most of these data concern anomurans, and it seems as if morphology and organization of the mouth apparatus are very similar for pagurids and most galatheids. One of the more detailed observations on mouthpart function comes from Schembri's (1982a) study on the shallow-water hermit crab *Pagurus rubricatus*, which grooms the anterior body (antennae, eyes, and mouthparts), gathers sediment and other prey items, and processes potential food by the Mxp2 and Mxp3 endopods in a way similar to that reported here for *Munida.* The resemblance is especially pronounced in the handling and maceration of large, soft prey items. The cutting–crunching process of the mandible and associated structures proceeds in much the same way, although *P. rubricatus* seems to hold the prey with the mandibular palp and the labium. The palp and labium were also observed to push the food directly into the mouth, but we find this unlikely, because their movements must be perpendicular to the mouth opening (Schembri, 1982a, fig. 8). From his figure 8 it seems more likely that these structures deliver the food to the coxae of Mx1, Mx2, and Mxp1, which control ingestion. We agree with Schembri (1982a) in grouping together the Mxp2 and Mxp3 exopods, and the functions are identical: creating currents around the buccal field. The pattern is a little dissimilar, since in *P. rubricatus* a flagellum on the Mxp1 exopod also contributes to the currents around the buccal field, and the flagella beat on one side at a time producing an asymmetrical flow, which shifts when the animal changes the side of beating. Schembri (1982a) also observed that the flagellar currents merely place the particles in the respiratory flow, which thereafter causes the rejection of unwanted particles. This is clearly not the case for *Munida*, since the flagellar currents are much stronger than the respiratory ones.

Schembri (1982a) made some very interesting observations on the function of the bases of Mx1 and Mx2. *P. rubricatus* sorts the sediment in a different way from what we observed for *Munida*. The Mx2 bases seemed to be the most active, collecting the sediment from the Mxp2 endopods (Mxp1 bases are not involved) and pressing it through cuspidate setae on the medial edge of the Mx1 bases, which then serve as a passive filter. We emphasize this because it could indicate that very similar structures (even at the setation level) can have different movement patterns and thereby serve very different functions. One should notice that Schembri (1982a) did not use video-recordings, without which 3-4 Hz movements (observed for *Munida*) can be difficult to follow. Similar movement patterns for Mx1 and Mx2 are not mentioned in other studies on pagurids (Roberts, 1968; Kunze and Anderson, 1979).

In general, hermit crabs possess additional feeding mechanisms that we did not observe in *Munida*. These mechanisms are antennulary filter feeding (Kunze and Anderson, 1979; Schembri, 1982c; Manjulatha and Babu, 1991), suspension feeding (Gerlach *et al.*, 1976; Schembri, 1982c), and gravel scrubbing (Orton, 1927; Roberts, 1968; Greenwood, 1972; Schembri, 1982a, c). The latter is the most significant and involves picking up pieces of gravel with the chelipeds and handing it over to the mouthparts, where the biofilm is scrubbed off. In *P. rubricatus*, the Mxp2 and Mxp3 endopods hold and turn the gravel, while the Mx2 and Mxp1 bases scrub it off with "vigorous" movements. Compared to *Munida*, where the chelae are primarily used in aggressive behavior (Berril, 1970; pers. obs.), pagurids generally seem to make more extensive use of their chelae and cristae dentatae to macerate food items.

Nicol (1932) studied feeding in five species of galatheids (*Galathea dispersa*, *G. squamifera*, *G. strigosa*, *Munida rondeletii* (=*rugosa*), and *Porcellana longicornis*). Her description of the gross morphology of the mouthparts closely resembles what we found for *Munida sarsi* and *M. tenuimana.* The functions she ascribed to the Mxp2 endopods, Mxp3 endopods, and mandibles are also very similar to those reported here. The Mxp3 endopods of *Porcellana longicornis* are somewhat different than those of other galatheids, since they have long plumose setae used to entrap particles in suspension. The general function, however, is the same—to collect prey and transfer it toward the mouth. Our observations also agree with those of Zainal (1990), who reports on both morphology and function of the mouthparts of *Munida rugosa*, but with limited detail.

Outside the Anomura, the most detailed data comes from mud shrimps, Thalassinidea. Stamhuis *et al.* (1998) give video-based information on most of the mouthpart functions of the thalassinid *Callianassa subterranea* during sediment sorting. The animal lives as a selective deposit feeder in mud burrows; due to this specialized way of living, the mouthparts of *C. subterranea* and especially their setation are somewhat different from that described for *Munida*. Still, Mxp3 endopod is used for collecting and transporting the food items, whereas the Mxp2 endopod is used for sorting the sediment by size. The sediment is not further sorted, and the bases of Mxp1 and Mx2 are merely used for transporting the particles towards the mouth. However, these appendages move with the same frequency as we report for *Munida*, 3-4 Hz. Very unlike *Munida, C. subterranea* does not use its Mx1 during deposit feeding and uses Md only to open or close the mouth (Stamhuis *et al.*, 1998). The movements of the maxillipeds of *C. subterranea* are also much more stereotypical than what we find for *Munida*. It has to be kept in mind that Stamhuis *et al.* analyzed only one type of feeding (deposit feeding), which of course will reduce the functional scheme of the mouthparts. There is morphological evidence (*e.g.*, well-developed mandibles, spines on maxilla 1, and crista dentata) that *C. subterranea* possesses other feeding strategies; it is most likely also carnivorous (Stamhuis *et al.*, 1998).

Hunt *et al.* (1992) studied the role of "the anterior mouthparts" (Md, Mx1, Mx2, Mxp1, Lb, and paragnaths) in the penaeid prawn *Penaeus merguiensis*. Much of the morphology is similar to *Munida*, but the mandibular palp is different and does not take part in feeding. When eating large prey items, Md, paragnaths, Mx2, and Mxp1 move laterally and Lb moves anteriorly to make room, while Mx1 basa put the prey between the incisor processes for cutting (Hunt *et al.*, 1992). Afterwards the Lb alone pushes the prey towards Mx1 coxae for ingesting. When feeding on small particles, *P. merguiensis* does not sort the sediment as *Munida* does, but filters them out of the water column by using pappose setae on Mxp1 and on the bases of Mx1 and Mx2 (Hunt *et al.*, 1992). The currents around the buccal area from which the particles are filtered are created by the respiratory beating of Mx2, since *P. merguiensis* lacks flagella on the maxillipeds.

What these comparisons show is that within hermit crabs and squat lobsters there are great similarities in mouthpart morphology, even at the setation level. Despite some differences, the functions reported for other squat lobsters and for hermit crabs are more or less comparable to our findings for *Munida*. Therefore, there is reason to believe that the functional groupings we suggest could apply to other anomurans; it goes without saying that more data are needed from other species before any final conclusions can be drawn. The additional feeding strategies described for some hermit crabs (*i.e.*, Schembri, 1982c) indicate that more functional groups must be added. It would be of major interest to gain information from the Lithodidae and Porcellanidae, the two other groups of anomurans that have either a different size range than the Galatheidae and Paguridae (most lithodid crabs are very large) or a different way of eating (porcellanid crabs are filter-feeders). Very little information is available for decapod taxa other than the Anomura. Not surprisingly, the two comparable studies (Hunt *et al.*, 1992; Stamhuis *et al.*, 1998) show a great diversity of mouthpart morphology and function within the Decapoda, and the functional groupings suggested here do not seem appropriate for all taxa.

Acknowledgments

We thank the Coast Guard of the Faeroe Islands for the use of their ship *Tjaldur*. We also thank Grethe Bruntse for assistance with the field work and the Kaldbak Laboratory for generously allowing us to use their facilities. We are grateful for the material and data supplied by the BIOFAR I collection and by Dr. André Freiwald, Bremen. We appreciate the financial support given by The Hede Nielsen Family Foundation and The Danish Society of Natural History (to AG). JTH also gratefully acknowledges grant nos. 94-01636 and 96-01405 from the Danish Natural Science Research Council and nos. 970381/40-1228 and 950260/40-1190 from The Carlsberg Foundation. We thank Nikolai Konow for never-ceasing interest in our study and Dr. G. Walker for some constructive comments.

Literature Cited

Barker, P. L., and R. Gibson. 1977. Observations on the feeding mechanism, structure of the gut, and digestive physiology of the European lobster *Homarus gammarus* (L.) (Decapoda: Nephropidae). *J. Exp. Mar. Biol. Ecol.* **26:** 297–324.

Bauer, R. 1981. Grooming behavior and morphology in the decapod Crustacea. *J. Crustacean Biol.* **1:** 153–174.

Bauer, R. 1989. Decapod crustacean grooming: functional morphology, adaptive value, and phylogenetic significance. Pp. 49–73 in *Crustacean Issues, Vol. 6*. B. E. Felgenhauer, L. Watling, and A. B. Thistle, eds. A. A. Balkema, Rotterdam.

Berril, M. 1970. The aggressive behavior of *Munida sarsi* (Crustacea: Galatheidae). *Sarsia* **43:** 1–11.

Cartes, J. E. 1993. Diets of two deep-sea decapods: *Nematocarcinus exilis* (Caridea: Nematocarcinidae) and *Munida tenuimana* (Anomura: Galatheidae) on the western Mediterranean slope. *Ophelia* **37:** 213–229.

Farmer, A. S. 1974. The functional morphology of the mouthparts and pereiopods of *Nephrops norvegicus* (L.) (Decapoda: Nephropidea). *J. Nat. Hist.* **8:** 121–142.

Felgenhauer, B. E. 1987. Techniques for preparing crustaceans for scanning electron microscopy. *J. Crustac. Biol.* **7:** 71–76.

Garm, A., and J. T. Høeg. 2000. Functional mouthpart morphology of the squat lobster *Munida sarsi* Huus with comparison to other anomurans. *Mar. Biol.* **137:** 123–138.

Gerlach, S. A., D. K. Ekstrøm, and P. B. Eckardt. 1976. Filter feeding in the hermit crab, *Pagurus bernhardus*. *Oecologia* **24:** 257–264.

Greenwood, J. G. 1972. The mouthparts and feeding behaviour of two species of hermit crabs. *J. Nat. Hist.* **6:** 325–337.

Hunt, M. J., H. Winsor, and C. G. Alexander. 1992. Feeding in penaeid prawns: the role of the anterior mouthparts. *J. Exp. Mar. Biol. Ecol.* **160:** 33–46.

Kunze, J., and D. T. Anderson. 1979. Functional morphology of the mouthparts and gastric mill in the hermit crabs *Clibanarius taeniatus*, *Clibanarius virescens*, *Paguristes squamosus* and *Dardanus setifer* (Anomura: Paguridae). *Aust. J. Mar. Freshwater Res.* **30:** 683–721.

Lavalli, K. L., and J. R. Factor. 1992. Functional morphology of the mouthparts of juvenile lobsters, *Homarus americanus* (Decapoda: Nephropidae), and comparison with the larval stages. *J. Crustac. Biol.* **12:** 467–510.

Lavalli, K. L., and J. R. Factor. 1995. The feeding appendages. Pp. 349–393 in *Biology of the Lobster* Homarus americanus, J. R. Factor, ed. Academic Press, San Diego, CA.

Manjulatha, C., and D. E. Babu. 1991. Functional organisation of mouth parts, and filter feeding, in *Clibanarius longitarsus* (Crustacea: Anomura). *Mar. Biol.* **109:** 121–127.

Moore, P. G., P. S. Rainbow, and R. J. Larson. 1993. The mesopelagic shrimp *Notostomus robustus* Smith (Decapoda: Oplophoridae) observed *in situ* feeding on the medusan *Atolla wyvillei* Haeckel in the Northwest Atlantic, with notes on gut contents and mouthpart morphology. *J. Crustac. Biol.* **13:** 690–696.

Nicol, E. A. T. 1932. The feeding habits of the Galatheidea. *J. Mar. Biol. Assoc. UK* **18:** 87–105.

Nørrevang, A., T. Brattegard, A. B. Josefson, J. A. Sneli, and O. S. Tendal. 1994. List of Biofar stations. *Sarsia* **79:** 165–180.

Orton, J. H. 1927. On the mode of feeding of the hermit crab *Eupagurus bernhardus*, and some other Decapoda. *J. Mar. Biol. Assoc. UK* **14:** 909–921.

Pike, R. B. 1947. Galathea. L. M. B. C. Memoirs XXXIV. *Proc. Trans. Liverpool Biol. Soc.* **55:** 1–179.

Roberts, M. H. 1968. Functional morphology of mouth parts of the hermit crabs, *Pagurus longicarpus* and *Pagurus pollicaris*. *Chesapeake Sci.* **9:** 9–20.

Schembri, P. J. 1982a. Functional morphology of the mouth parts and associated structures of *Pagurus rubricatus* (Crustacea: Decapoda: Anomura) with special reference to feeding and grooming. *Zoomorphology (Berlin)* **101**(1): 17–38.

Schembri, P. J. 1982b. The functional morphology of the feeding and grooming appendages of *Ebalia tuberosa* (Crustacea: Decapoda: Leucosiidae). *J. Nat. Hist.* **16:** 467–480.

Schembri, P. J. 1982c. Feeding behavior of 15 species of hermit crabs (Crustacea: Decapoda: Anomura) from the Otago region, southeastern New Zealand. *J. Nat. Hist.* **16:** 859–878.

Stamhuis, E. J., B. Dauwe, and J. J. Videler. 1998. How to bite the dust: morphology, motion pattern and function of the feeding appendages of the deposit-feeding thalassinid shrimp *Callianassa subterranea*. *Mar. Biol.* **132:** 43–58.

Suthers, I. M. 1984. Functional morphology of the mouthparts and gastric mill in *Penaeus plebejus* (Decapoda: Penaeidea). *Aust. J. Mar. Freshwater Res.* **35:** 785–792.

Suthers, I. M., and D. T. Anderson. 1981. Functional morphology of mouth parts and gastric mill of *Ibacus peronii* (Palinura: Scyllaridae). *Aust. J. Mar. Freshwater Res.* **32:** 931–944.

Walossek, D. 1998. On the Cambrian diversity of Crustacea. Pp. 3–29 in *Crustaceans and the Biodiversity Crisis, Vol. 1*, F. Schram and J. C. v. Vaupel Klein, eds. Brill, Leiden.

Zainal, K. A. Y. 1990. Aspects of the biology of the squat lobster, *Munida rugosa* (Fabricius, 1775). Ph.D. dissertation, University of Glasgow, 180 pp.

Reference: *Biol. Bull.* **200:** 298–304. (June 2001)

Phylogeny of Hydrothermal-Vent–Endemic Gastropods *Alviniconcha* spp. from the Western Pacific Revealed by Mitochondrial DNA Sequences

S. KOJIMA[1,*], R. SEGAWA[2], Y. FIJIWARA[3], K. FUJIKURA[3], S. OHTA[1],
AND J. HASHIMOTO[3]

[1] *Ocean Research Institute, University of Tokyo, 1-15-1 Minamidai, Nakano, Tokyo 164-8639, Japan;* [2] *Department of Biology, Faculty of Science, Tokyo Metropolitan University, 1-1 Minami-Osawa, Hachioji, Tokyo 192-0364, Japan; and* [3] *Japan Marine Science and Technology Center, 2-15 Natsushima, Yokosuka, Kanagawa 237-0061, Japan*

Abstract. Mitochondrial genes for cytochrome oxidase I (COI) from hydrothermal-vent–endemic gastropods of the genus *Alviniconcha* were sequenced to determine the phylogenetic relationships among specimens from three areas in the western Pacific. Individuals of *Alviniconcha hessleri* were collected at two vent fields (depths 1470 m and 3600 m) in the Mariana Trough. Specimens collected in the North Fiji Basin could be divided into two genetically distinct groups, both of which also differed from *A. hessleri* from the Mariana Trough. None of the specimens of the genus *Alviniconcha* collected in the Manus Basin differed genetically from the dominant group from the North Fiji Basin. We suggest that the specimens of the genus *Alviniconcha* analyzed in the present study can be tentatively classified into *A. hessleri* and two undescribed species.

Introduction

Since the late 1970s, various biological communities supported by chemosynthetic energy have been discovered in deep-sea reducing environments, such as hydrothermal vent fields and seep areas (Sibuet and Olu, 1998; Van Dover, 2000). The elucidation of dispersion, isolation, and speciation of endemic species is one of the most important issues of deep-sea biology (Vrijenhoek, 1997). Comparative studies of the genetic structure of their populations will provide useful information about such evolutionary processes.

The population structures of some dominant endemic species in deep-sea reducing environments have been analyzed by electrophoretic examination of allozymes (Vrijenhoek, 1997). Analyses based on DNA sequences would reveal more details of the structures of such populations. To date, population analyses using DNA markers have been reported for just a few species (for review, see Tyler and Young, 1999). In addition, most population genetic studies of organisms in deep-sea reducing environments have been performed on specimens collected in the eastern Pacific and the Atlantic. The accumulation of genetic information about endemic species in deep-sea reducing environments in the western Pacific, where the chemoautosynthesis-based communities have unique species composition (Tunnicliffe *et al.*, 1998), should provide more clues to the processes and mechanisms of evolution of fauna in deep-sea reducing environments.

Gastropods of the genus *Alviniconcha*, which live in symbiosis with chemosynthetic bacteria (Stein *et al.*, 1988; Endow and Ohta, 1989), are one of the most dominant groups in the chemoautosynthesis-based communities at some hydrothermal vent sites in the western Pacific back-arc basins, namely, the Mariana Trough (Craig *et al.*, 1987; Hessler and Lonsdale, 1991; Fujikura *et al.*, 1997), the Manus Basin (Both *et al.*, 1986; Tufer, 1990; Auzende *et al.*, 1997; Hashimoto *et al.*, 1999), the North Fiji Basin (KAIYO 87 Shipboard Party, 1988; Desbruyères *et al.*, 1994), and the Lau Basin (NAUTILAU Group, 1990; Desbruyères *et al.*, 1994) (Fig. 1).

Received 16 June 2000; accepted 12 February 2001.

[*] To whom correspondence should be addressed. E-mail: kojima@ori.u-tokyo.ac.jp.

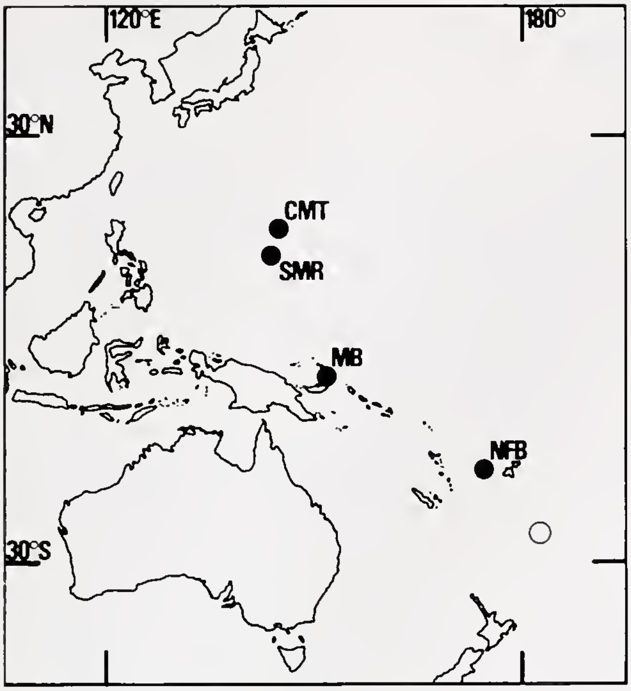

Figure 1. Collection sites: CMT, Central Mariana Trough; SMR, Southern Mariana Ridge; MB, Manus Basin; NFB, North Fiji Basin. An open circle denotes the location of the Lau Basin.

Okutani and Ohta (1988) described the species *Alviniconcha hessleri* on the basis of specimens collected in the hydrothermal fields along the spreading axis of the central Mariana Trough (3650 m depth). Further populations of *A. hessleri* were discovered in a vent area at a shallower site on the southern Mariana Ridge, at a depth of 1470 m (Johnson *et al.,* 1993). No distinct morphological differences were apparent in the specimens from these two vent sites (Hasegawa *et al.,* 1997).

Populations of *Alviniconcha* gastropods have also been discovered at the hydrothermal vents in the Manus Basin, the North Fiji Basin, and the Lau Basin. On the basis of slight differences in the radula and the shell, Beck (1991) proposed that *Alviniconcha* in the Manus Basin might be a subspecies of *A. hessleri.* Because distinctive morphological characteristics are scarce, information at the molecular level is necessary to establish exact taxonomic relationships among species of the genus *Alviniconcha.* To date, only one molecular analysis of this genus has been published (Denis *et al.,* 1993). In that study, an electrophoretic analysis of 12 enzymes showed that the populations of *Alviniconcha* gastropods in the North Fiji Basin and the Lau Basin are genetically distinct from one another. Molecular analysis of populations in the other hydrothermal vent sites will provide a useful basis for judgments about the taxonomic status of each population. In the present study, we used nucleotide sequences of mitochondrial DNA to analyze the phylogenetic relationships among populations of the genus *Alviniconcha* in the Mariana Trough, the North Fiji Basin, and the Manus Basin.

Materials and Methods

During dives of the submersibles *Shinkai 2000* and *Shinkai 6500* of the Japan Marine Science and Technology Center (JAMSTEC) and *Nautile* of Institut Français de Recherche pour l'Exploitation de la Mer (IFREMER), 40 specimens of *Alviniconcha hessleri* and 35 of the genus *Alviniconcha* were collected, as summarized in Table 1.

Mitochondrial DNA (mtDNA) was extracted from the deep-frozen head-foot region of each individual by a modified version of the method of Komm *et al.* (1982). In the case of some damaged samples, which had been collected in the North Fiji Basin in 1990 and stored at −20°C, total DNA was extracted by grinding the tissue, digestion with sodium dodecyl sulfate (SDS) and proteinase K, and extraction with phenol and chloroform.

A fragment (about 450 bp) of the mitochondrial gene for cytochrome oxidase I (COI) was amplified by the polymer-

Table 1

Summary of collection information for Alviniconcha *specimens*

Species	Sampling site	Depth (m)	Submersible	Dive #	Sample #
Alviniconcha hessleri	Alice Springs, Central Mariana Trough	3600	*Shinkai 6500*	D153	CMT-92-1–20
	Forecast Vent, Southern Mariana Ridge	1470	*Shinkai 6500*	D186	SMR-93-1–11
				D350	SMR-96-1–9
Alviniconcha spp.	PACMANUS site, Manus Basin	1630	*Shinkai 6500*	D914	MB-96-1–20
	White Lady site, North Fiji Basin	1970	*Nautile*	D12	NFB-90-1–4
			Shinkai 6500	D77	NFB-91-1–4
				D80	NFB-91-5, 6
	STARMER II site, North Fiji Basin	1980	*Nautile*	D15	NFB-90-5, 6
				D20	NFB-90-7–9

ase chain reaction (PCR) with universal metozoan primers, COI-3, 5′-GTNTGRGCNCAYCAYATRTTYACNGT-3′, and COI-6, 5′-GGRTARTCNSWRTANCGNCGNGGYAT-3′ (Shimayama *et al.*, 1990). The conditions for PCR were as follows: 94°C for 60 s; then 30 to 40 cycles at 92°C for 40 s, 40°C for 60 s, and 72°C for 90 s. Genereleaser (BioVenture Inc., Murfreesboro, TN) was used to sequester products of cell lysis that might have inhibited the polymerase. The nucleotide sequences (306 bp) were determined for both strands of PCR products by the dideoxynucleotide chain-termination method using a Sequenase PCR product sequencing kit (United States Biochemical Coop., Cleveland, OH) and primers COI-3 and COI-6.

A longer fragment (about 960 bp) of COI, which contains the region mentioned above, was amplified by PCR using Genereleaser and primers COI-B, 5′-GGATGAACNGTNTAYCCNCC-3′ (Hasegawa *et al.*, 1996) and COI-6. The conditions for PCR were as follows: 94°C for 60 s; then 30 to 40 cycles at 92°C for 40 s, 50°C for 60 s, and 72°C for 90 s. The nucleotide sequences within the upper region of this fragment were determined bidirectionally by a sequencer DSQ-2000L (Shimazu Corp., Kyoto, Japan) using primers Gastro-3, 5′-TTAGCTGGTGCTTCNTCNATYYTNGG-3′ (Kojima *et al.*, 2000) and TW-2, 5′-ACTACRTARTANGTRTCRTG-3 (Kojima *et al.*, 1997b). A nucleotide sequence of a single specimen of *A. hessleri* from the South Marina Ridge (No. CMT-92-1) was reported in a previous paper (Kojima *et al.*, 2000). Amino acid sequences of COI were deduced by reference to the modified genetic code of molluscan mtDNA (Shimayama *et al.*, 1990; Hoffmann *et al.*, 1992).

The genetic distances between haplotypes were calculated by Kimura's two-parameter method (Kimura, 1980). Phylogenetic trees were constructed by the neighbor-joining method (Saitoh and Nei, 1987) using MEGA (Kumar *et al.*, 1993) and the maximum parsimony method using the heuristic search approach of the computer program PARSIMONY, which was provided by Dr. K. Tamura of Tokyo Metropolitan University. *Ifremeria nautilei*, a hydrothermal-vent–endemic gastropod species closely related to *Alviniconcha* (Beck, 1991; Warén and Bouchet, 1993), was used as an outgroup for phylogenetic analysis (Kojima *et al.*, 2000).

Differences in frequencies of haplotypes between populations were examined by the exact test of population differentiation (Raymond and Rousset, 1995) using ARLEQUIN (Schnider *et al.*, 1996) and the randomized chi-squared test of independence (Raff and Bentzen, 1989). Chi-squared values were generated from 1000 simulated random samplings of the data. An unbiased fixation index, F_{ST} (Weir and Cockerham, 1984), was estimated, and the significance of the indices was tested by a nonparametric permutation approach using ARLEQUIN (Schnider *et al.*, 1996).

Results

Partial sequences (696 bp) of mitochondrial genes for COI were determined from 40 specimens of *Alviniconcha hessleri* and 35 specimens of *Alviniconcha* spp. Sequences of all individuals of the genus *Alviniconcha* collected in the North Fiji Basin and the Manus Basin were distinct from those of *A. hessleri* from the Mariana Trough. In addition, the sequences of three specimens of the genus *Alviniconcha* collected during a single dive (Dive 20 of *Nautile*) at the STARMER II site in the North Fiji Basin were very different from those of other specimens from the same area. These other North Fiji Basin specimens included two from the STARMER II site and 10 from the White Lady site. The STARMER II site is only 120 m southwest of the White Lady site in the North Fiji Basin. Individuals with mitochondrial DNA of the dominant type and those with DNA of the less frequent type are referred to hereafter as *Alviniconcha* spp. type 1 and *Alviniconcha* spp. type 2, respectively. Figure 2 shows nucleotide sequences from *Alviniconcha hessleri*, *Alviniconcha* spp. type 1, and *Alviniconcha* spp. type 2. A single amino acid substitution was detected between *Alviniconcha* spp. type 1 and the others (Fig. 2). Within the sequences from each of *A. hessleri*, *Alviniconcha* spp. type 1, and *Alviniconcha* spp. type 2, no amino acid substitutions were detected.

Twenty-seven, thirteen, and three haplotypes were obtained for *A. hessleri*, *Alviniconcha* spp. type 1, and *Alviniconcha* spp. type 2, respectively. Figure 3 shows the phylogenetic relationships among the specimens of the genus *Alviniconcha*. Specimens of *A. hessleri*, *Alviniconcha* spp. type 1, and *Alviniconcha* spp. type 2 formed separate monophyletic clusters. There were greater genetic variations among the three clusters of *Alviniconcha* than within each cluster. The monophyly of *A. hessleri*, *Alviniconcha* spp. type 1, and type 2 was supported by high bootstrap probabilities (93%, 100%, and 100%, respectively). *Alviniconcha hessleri*, *Alviniconcha* spp. type 1, and type 2 formed monophyletic groups in all maximum parsimony trees as well (data not shown).

Three of 27 haplotypes of *A. hessleri* were discovered in the specimens from both the central Mariana Trough and the southern Mariana Ridge (Fig. 3). Statistical analysis, by the exact test of population differentiation (Raymond and Rousset, 1995) and the randomized chi-squared test of independence (Raff and Bentzen, 1989), showed a genetic difference between the populations in the central Mariana Trough and on the southern Mariana Ridge ($P = 0.035$ and $P = 0.023$, respectively). In the case of *Alviniconcha* spp. type 1, four haplotypes were discovered among the specimens from both the North Fiji

```
Ah ATT ACT GCA GTA TTA TTA TTA CTT TCT TTA CCA GTT TTA GCA GGT GCT ATT ACA ATG CTT TTA ACA GAT CGA
A1 ... ... ... ..G ... ... ... ... ... ... ..R ... ... ... ... ... ... ... ... ... ... ... ... ...
A2 ... ... ... ..Y C.. ... ... ... ..C ... ..C ... C.. ... ... ... ... ... ... ... ... ... ... ...

Ah AAT TTY AAT ACT GCT TTC TTT GAC CCA GCT GGA GGT GGT GAT CCA ATT TTA TAY CAA CAT TTA TTT TGA TTC
A1 ... ..C ... ... ... ... ... ..T ..R ..Y ..R ... ... ... ... ... ... ..C ..G ... ... ... ... ...
A2 ... ..C ... ... ... ... ... ... ... ... ..G ... ... ..C ..T ... ... ..C ... ... C.. ... ... ...

Ah TTT GGG CAC CCA GAA GTT TAT ATT TTA ATT CTT CCT GGC TTT GGA ATG ATT TCT CAT ATT GTT AGA CAT TAT
A1 ..Y ... ... ... ... ... ... ... ... ... ... ... ... ... ... ..R ... ... ... ... ... ... ..C ...
A2 ... ... ..T ... ... ... ... ... ... ... ... ... ..T ... ... ..A ... ... ..C ... ... ... ..C ...

Ah TCA GCY AAG AAA GAA ACY TTT GGG ACA CTT GGA ATA ATY TAT GCA ATG ATA GCA ATT GGT TTA TTA GGT TTT
A1 ... ..T ... ... ... ..T ... ... ... ... ... ..G ..Y ... ... ..A ... ... ... ... C.. ... ... ...
A2 ... ..T ... ... ... ..T ... ..A ... ... ... ..G ..T ... ... ..A ..G ... ... ... ... C.. ... ...

Ah ATT GTA TGA GCT CAY CAT ATG TTT ACA GTA GGT ATG GAT GTA GAT ACT CGR GCT TAY TTT ACA GCA GCC ACT
A1 ... ... ... ... ..T ... ... ... ... ... ... ... ... ... ... ... ..A ... ..T ..C ... ... ..T ...
A2 ... ... ... ... ..C ... ... ... ... ... ... ... ... ... ... ... ..A ... ..T ... ... ... ... ...

Ah ATA ATT ATT GCY GTT CCA ACT GGA ATT AAG GTY TTC AGY TGA CTY GCC ACA ATT CAT GGS TCA AAA ATC AAG
A1 ... ... ... ..Y ... ... ... ... ... ... ..T ... ..T ... ..T ..Y ... ... ..C ..A ... ... ..T ..R
A2 ... ... ... ..T ... ... ... ... ... ... ..T ... ..T ... ..T ..T ... ..Y ... ..A ... ... ..T ...

Ah TAT GAA ACT CCT ATG CTT TGA GCT TTA GGR TTT ATT TTC TTG TTT ACT GTA GGG GGT TTA ACT GGA ATT GTT
A1 ... ... ... ... ... ... ... ... ... ..G ... ... ... ... ... ... ... ... ..Y C.. ... ... ... ...
A2 ... ... ... ... ... ... ... ... ... ..A ..C ... ... ..A ... ... ... ..A ..A ... ... ... ... ...

Ah CTT TCT AAT TGY TCY YTA GAT ATT ATG ATG CAY GAY ACT TAC TAT GTT GTA GCY CAT TTC CAT TAC GTR CTA
A1 ... ... ... ..C ..T C.. ... ... ... T.. ..C ..C ... ... ... ... ... ..T ..C ... ... ... ..G ..R
A2 ... ... ... ..T ..T T.. ... ... ... ... ..T ..T ... ..T ... ... ... ..C ... ... ... ..T ..T T..

Ah TCA ATR GGR GCA GTC TTY GCC YTA TTT GCA GCT TTT AAC TAT TGA TTY CCA TTA ATR AGA GGG GTA ACA CTT
A1 ... ..G ..A ... ... ..C ..Y T.. ... ... ... ... ... ..Y ... ..C ... ... ..G ..R ... ... ... ...
A2 ... ..A ..A ..G ... ..T ..T C.. ... ... ... ... ..T ..C ... ..C ... ..G ..G ... ... ... ... ...

Ah CAC TCT CGT TGA ACA AAA GCT CAT TTT TAT ATY ATR TTT ATY GGR GTA
A1 ... ... ... ... ... ... ... ... ... ... ..Y ..G ... ..T ..R ...
A2 ..T ... ..A ... ... ... ..C ... ... ... ..T ..G ... ..T ..A ...
```

Figure 2. Nucleotide sequences of mitochondrial genes for cytochrome oxidase I from *Alviniconcha hessleri* (Ah), *Alviniconcha* spp. type 1 (A1), and *Alviniconcha* spp. type 2 (A2). Dots indicate nucleotides identical to those in Ah. An underlined codon encodes an amino acid different from that in Ah. R denotes G or A; Y is T or C; S is G or C.

Basin and the Manus Basin (Fig. 3), and there was no genetic difference between the two populations (P = 0.793 for the exact test of population differentiation, and $P = 0.705$ for the randomized chi-squared test of independence). Although the F_{ST} value between the two populations of *A. hessleri* was significant ($P < 0.05$) and

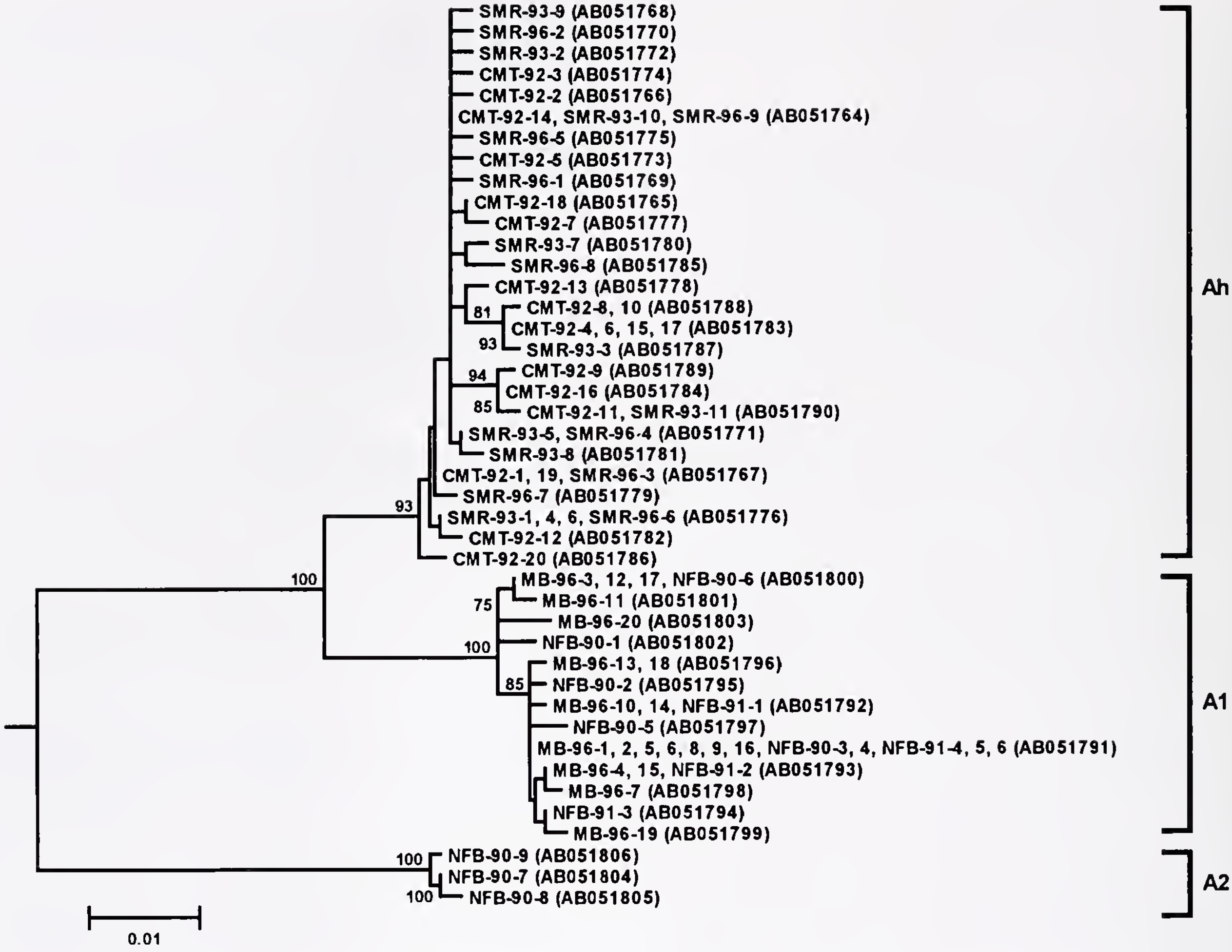
SMR-93-9 (AB051768)
SMR-96-2 (AB051770)
SMR-93-2 (AB051772)
CMT-92-3 (AB051774)
CMT-92-2 (AB051766)
CMT-92-14, SMR-93-10, SMR-96-9 (AB051764)
SMR-96-5 (AB051775)
CMT-92-5 (AB051773)
SMR-96-1 (AB051769)
CMT-92-18 (AB051765)
CMT-92-7 (AB051777)
SMR-93-7 (AB051780)
SMR-96-8 (AB051785)
CMT-92-13 (AB051778)
81
CMT-92-8, 10 (AB051788)
CMT-92-4, 6, 15, 17 (AB051783)
93
SMR-93-3 (AB051787)
94
CMT-92-9 (AB051789)
CMT-92-16 (AB051784)
85
CMT-92-11, SMR-93-11 (AB051790)
SMR-93-5, SMR-96-4 (AB051771)
SMR-93-8 (AB051781)
CMT-92-1, 19, SMR-96-3 (AB051767)
SMR-96-7 (AB051779)
93
SMR-93-1, 4, 6, SMR-96-6 (AB051776)
CMT-92-12 (AB051782)
CMT-92-20 (AB051786)
100
MB-96-3, 12, 17, NFB-90-6 (AB051800)
75
MB-96-11 (AB051801)
MB-96-20 (AB051803)
100
NFB-90-1 (AB051802)
MB-96-13, 18 (AB051796)
85
NFB-90-2 (AB051795)
MB-96-10, 14, NFB-91-1 (AB051792)
NFB-90-5 (AB051797)
MB-96-1, 2, 5, 6, 8, 9, 16, NFB-90-3, 4, NFB-91-4, 5, 6 (AB051791)
MB-96-4, 15, NFB-91-2 (AB051793)
MB-96-7 (AB051798)
NFB-91-3 (AB051794)
MB-96-19 (AB051799)
100
NFB-90-9 (AB051806)
NFB-90-7 (AB051804)
100
NFB-90-8 (AB051805)
0.01
Ah
A1
A2

Figure 3. Phylogenetic tree for specimens of *Alviniconcha* spp. The tree was constructed by the neighbor-joining method with *Ifremeria nautilei* (the most dominant haplotypes in the populations of the Manus Basin and the North Fiji Basin) as an outgroup. Numbers refer to specimens indicated in Table 1. Bootstrap values are shown above or below branches of clades that are supported by bootstrap values of more than 70%. Ah, A1, and A2 denote *Alviniconcha hessleri*, *Alviniconcha* spp. type 1, and *Alviniconcha* spp. type 2, respectively. The nucleotide sequence of each specimen will appear in the GSDB, DDBJ, EMBL, and NCBI nucleotide sequence databases under the accession number in parentheses.

estimated to be 0.047, that of *Alviniconcha* spp. type 1 was not significant ($P > 0.05$).

Discussion

In the present study, we analyzed the phylogenetic relationships among populations of the *Alviniconcha* gastropods in hydrothermal areas in the western Pacific. Both the neighbor-joining (NJ) method and the maximum parsimonious (MP) method showed that the 43 haplotypes identified among 80 specimens of the genus *Alviniconcha* formed three monophyletic clusters (Fig. 3). In the NJ tree, the monophyly of each of the three clusters was supported by a high bootstrap probability. The three clusters of *Alviniconcha* were distinct from one another, with a smaller range of sequence variations within clusters than among clusters. Therefore, we suggest tentatively that the specimens of the genus *Alviniconcha* analyzed in the present study should be classified as *A. hessleri* and two undescribed species.

Although the habitat on the southern Mariana Ridge is much shallower than the type locality of *A. hessleri* (the central Mariana Trough), all haplotypes identified from specimens collected at two vent sites formed a single cluster (Fig. 3). Although the exact test of population differentiation, a randomized chi-squared test, and the test of significance of the F_{ST} value showed that a genetic difference between the two populations was significant at the 5% level, they shared three haplotypes. From the pairwise F_{ST} value, the absolute number of migrants exchanged between these two populations was estimated to be 10.2. These results suggest that these two populations are conspecific and might be connected by significant gene flow. The present results are consistent with the absence of distinct morphological differences between these populations (Hasegawa *et al.*, 1997). The distribution of conspecific populations in the bathyal zone and the abyssal zone is in marked contrast with the strict depth zonation exhibited by endemic groups that inhabit the seep areas off central Japan, namely, bivalves of the genus *Calyptogena* (Kojima and Ohta, 1997) and vestimentiferans (Kojima *et al.*, 1997b). This difference might be due to environmental factors, such as water currents and the topography of the sea floor, or to differences in biological characteristics among groups.

The absence of genetic differences between the populations of *Alviniconcha* spp. type 1 in the Manus Basin and in the North Fiji Basin provides a typical example of the active interchange of fauna between western Pacific back-arc basins, which was first noted by Hessler and Lonsdale (1991). For *Ifremeria nautilei,* which is related to *Alviniconcha* spp., Kojima *et al.* (2000) reported that no haplotype was shared between the Manus Basin and the North Fiji Basin and concluded that the two populations should be considered to be conspecific populations that are isolated geographically from one another. The morphology of the larval shell of *Alviniconcha* is suggestive of planktonic development, whereas the larval type of *Ifremeria* remains unclear (Warén and Bouchet, 1993). The difference in degree of genetic differentiation between *I. nautilei* and *Alviniconcha* spp. type 1 might be attributed to differences in the larval type (Kojima *et al.*, 2000).

Denis *et al.* (1993) reported significant genetic differences between a population of *Alviniconcha* in the North Fiji Basin and one in the Lau Basin, and they proposed that individuals in these two populations should be treated as separate species. The North Fiji Basin is situated near the Lau Basin (Fig. 1); thus *Alviniconcha* spp. type 2 might be conspecific with the Lau Basin species proposed by Denis *et al.* (1993). Unfortunately, samples from the Lau Basin are not available, so we have been unable to test this hypothesis. To clarify the taxonomic status of these putative species, detailed morphological examination and further molecular analysis are required.

The dominance of gastropods of the family Provannidae offers one of the prominent features in some chemoautosynthesis-based communities in the back-arc basins in the western Pacific. This study and our previous ones (Kojima *et al.*, 2000) revealed the population structures of some species in the two representative genera of this family, namely *Alviniconcha* and *Ifremeria.* Although many other endemic taxa have been reported from the western Pacific (Desbruyères and Segonzac 1997; Miura *et al.*, 1997; Okutani *et al.*, 1999; Fujikura *et al.*, 2000), information about their population structures is still limited (Kojima *et al.*, 1997a, b). Information about the population structures of many endemic species in deep-sea reducing environments will be needed to reveal details of the evolution in such environments in the western Pacific and to compare them with those in other oceans.

Acknowledgments

The authors thank the shipboard parties of the STARMER cruises, the Y96-13 cruise, and the BIOACCESS-Manus '96 cruise, the operation teams of the submersibles *Shinkai 2000, Shinkai 6000,* and *Nautile,* and the officers and crew of the tender ships *Natsushima, Yokosuka,* and *Nadier* for their help in collecting samples. Dr. U. Tsunogai graciously provided specimens of *A. hessleri* collected during Dive 355 of the submersible *Shinkai 6500.* Dr. K. Tamura kindly provided the computer program PARSIMONY. Thanks are also extended to Dr. I. Hayashi and two anonymous reviewers for comments that improved manuscripts. Part of this study was supported by grants from the Science Technology Agency of Japan and from the Ministry of Education, Science, Sports and Culture of Japan (no. 12NP0201).

Literature Cited

Auzende, J.-M., J. Hashimoto, A. Fiala-Médioni, S. Ohta, and l'équipe Bioaccess. 1997. Étude géologique et biologique in situ de deux zones hydrothermales du bassin de Manus (Papouasie Nouvelle-Guinée). *C. R. Acad. Sci. Série II* **325:** 585–591 (in French with English abstract and abridgment).

Beck, L. A. 1991. *Olgaconcha tufari* n. gen. et n. sp.—a new mesogastropod (Gastropoda: Prosobranchia) from hydrothermal vents in the Manus back-arc basin (Bismarck Sea, Papua New Guinea). *Ann. Naturhist. Mus. Wien.* **92B:** 277–287.

Both, R., K. Crook, B. Taylor, S. Brogan, B. Chappell, E. Frankel, L. Lui, J. Sinton, and D. Tiffin. 1986. Hydrothermal chimneys and associated fauna in the Manus back-arc basin, Papua New Guinea. *EOS Trans. AGU* **67:** 489–490.

Craig, H., Y. Horibe, K. A. Farley, J. A. Welham, K.-R. Kim, and R. N. Hey. 1987. Hydrothermal vents in the Mariana Trough: results of the first *Alvin* dives. *EOS Trans. AGU* **68:** 1531.

Denis, F., D. Jollivet, and D. Moraga. 1993. Genetic separation of two allopatric populations of hydrothermal snail *Alviniconcha* spp. (Gastropoda) from two South Western Pacific back-arc basins. *Biochem. Syst. Ecol.* **21:** 431–440.

Desbruyères, D., and M. Segonzac (eds.). 1997. *Handbook of Deep-Sea Hydrothermal Vent Fauna.* IFREMER, Brest. 279 pp.

Desbruyères, D., A.-M. Alayse-Danet, S. Ohta, and Scientific parties of BIOLAU and STARMER Cruises. 1994. Deep-sea hydrothermal communities in Southwestern Pacific back-arc basins (the North Fiji and Lau Basins): composition, microdistribution and food web. *Mar. Geol.* **116:** 227–242.

Endow, K., and S. Ohta. 1989. The symbiotic relationship between bacteria and a mesogastropod snail, *Alviniconcha hessleri,* collected from hydrothermal vents of the Mariana back-arc Basin. *Bull. Jpn. Soc. Microb. Ecol.* **3:** 73–82.

Fujikura, K., T. Yamazaki, K. Hasegawa, U. Tsunogai, R. J. Stern, H. Ueno, H. Yamamoto, Y. Maki, S. Tsuchida, T. Kodera, H. Yamamoto, C. Sun, and T. Okutani. 1997. Biology and earth scientific investigation by the submersible "Shinkai 6500" system of deep-sea hydrothermalism and lithosphere in the Mariana back-arc Basin. *JAMSTEC J. Deep Sea Res.* **13:** 1–20 (in Japanese with English abstract).

Fujikura, K., S. Kojima, Y. Fujiwara, J. Hashimoto, and T. Okutani. 2000. New distribution records of vesicomyid bivalves from deep-sea chemosynthesis-based communities in Japanese waters. *Venus Jpn. J. Malacol.* **59:** 103–121.

Hasegawa, T., T. Yamaguchi, S. Kojima, and S. Ohta. 1996. Phylogenetic analysis among three species of intertidal barnacles of the genus *Tetraclita* (Cirripedia: Balanomorpha) by nucleotide sequences of a mitochondrial gene. *Benthos Res.* **51:** 33–39 (in Japanese with English abstract).

Hasegawa, K., K. Fujikura, and T. Okutani. 1997. Gastropod fauna associated with hydrothermal vents in the Mariana back-arc Basin: summary of the results of 1996 "Shinkai 6500" dives. *JAMSTEC J. Deep Sea Res.* **13:** 69–83.

Hashimoto, J., S. Ohta, A. Fiala-Médione, J.-M. Auzende, S. Kojima, M. Segonzac, Y. Fujiwara, J. C. Hunt, K. Gena, T. Miura, T. Kikuchi, T. Yamaguchi, T. Toda, H. Chiba, S. Tsuchida, J. Ishibashi, K. Henry, M. Zbinden, A. Pruski, A. Inoue, H. Kobayashi, J.-L. Birrien, J. Naka, T. Yamanaka, C. Laporte, K. Nishimura, C. Yeats, S. Malagun, P. Kia, M. Oyaizu, and T. Katayama. 1999. Hydrothermal vent communities in the Manus Basin, Papua New Guinea: Results of the BIOACCESS cruises '96 and '98. *InterRidge News* **8(2):** 12–18.

Hessler, R. R., and P. Lonsdale. 1991. Biogeography of Mariana Trough hydrothermal vent communities. *Deep-Sea Res.* **38:** 185–199.

Hoffmann, R. J., J. L. Boore, and W. M. Brown. 1992. A novel mitochondrial genome organization for the blue mussel, *Mytilus edulus. Genetics* **131:** 397–412.

Johnson, L., H. Fryer, H. Matsuda, T. Ishii, and T. Gamo. 1993. Hydrothermal deposits and two magma sources for volcanoes near 13°20′N in the Mariana backarc: a view from *Shinkai 6500. EOS Trans. AGU Fall Meet. Suppl.* **74:** 681.

KAIYO 87 Shipboard Party. 1988. Rift system in the North Fiji Basin: Results of Japan-France cooperative research on board KAIYO 87. *La Mer* **26:** 36–46 (in Japanese with English abstract).

Kimura, M. 1980. A simple method for estimating evolutionary rate of base substitutions through comparative studies of nucleotide sequence. *J. Mol. Evol.* **16:** 111–120.

Kojima, S., and S. Ohta. 1997. Bathymetrical distribution of the species of the genus *Calyptogena* in the Nankai Trough. *Venus Jpn. J. Malacol.* **56:** 293–297.

Kojima, S., K. Fujikura, J. Hashimoto, and S. Ohta. 1997a. Distribution and genetic structure of *Calyptogena soyoae* complex. *JAMSTEC J. Deep Sea Res.* **13:** 691–696 (in Japanese with English abstract).

Kojima, S., R. Segawa, J. Hashimoto, and S. Ohta. 1997b. Molecular phylogeny of vestimentiferans collected around Japan revealed by the nucleotide sequences of mitochondrial DNA. *Mar. Biol.* **127:** 505–513.

Kojima, S., R. Segawa, Y. Fujiwara, J. Hashimoto, and S. Ohta. 2000. Genetic differentiation of populations of a hydrothermal vent-endemic gastropod, *Ifremeria nautilei*, between the North Fiji Basin and the Manus Basin revealed by nucleotide sequences of mitochondrial DNA. *Zool. Sci.* **17:** 1167–1174.

Komm, B., A. Michaels, and J. Linton. 1982. Isolation and characterization of the mitochondrial DNA from the Florida spiny lobster, *Panulirus argus. Comp. Biochem. Physiol.* **73B:** 923–929.

Kumar, S., K. Tamura, and M. Nei. 1993. *MEGA: Molecular Evolutionary Genetics Analysis Ver. 1.0.* The Pennsylvania State University, University Park, PA.

Miura, T., J. Tsukahara, and J. Hashimoto. 1997. *Lamellibrachia satsuma*, a new species of vestimentiferan worms (Annelida: Pogonophora) from a shallow hydrothermal vent in Kagoshima Bay, Japan. *Proc. Biol. Soc. Wash.* **110:** 447–456.

NAUTILAU Group. 1990. Hydrothermal activity in the Lau Basin. First results from the NAUTILAU Cruise. *EOS Trans. AGU* **71:** 678–679.

Okutani, T., and S. Ohta. 1988. A new gastropod mollusk associated with hydrothermal vents in the Mariana back-arc basin, Western Pacific. *Venus Jpn. J. Malacol.* **47:** 1–9.

Okutani, T., K. Fujikura, and S. Kojima. 1999. Two new hadal bivalves of the family Thyasiridae from the plate convergent area of the Japan Trench. *Venus Jpn. J. Malacol.* **58:** 49–54.

Raff, D. A., and P. Bentzen. 1989. The statistical analysis of mitochondrial DNA polymorphisms and the problem of small samples. *Mol. Biol. Evol.* **6:** 539–545.

Raymond, M., and F. Rousset. 1995. An exact test for population differentiation. *Evolution* **49:** 1280–1283.

Saitoh, N., and M. Nei. 1987. The neighbour-joining method: a new method for reconstructing phylogenetic trees. *Mol. Biol. Evol.* **10:** 471–483.

Schnider, S., J.-M. Kueffer, D. Roessli, and L. Excoffer. 1996. *ARLEQUIN, a Software Package for Population Genetics.* Genetics and Biometry Lab., Dept. of Anthropology, University of Geneva, Geneva.

Shimayama, T., H. Himeno, J. Sasuga, S. Yokobori, T. Ueda, and K. Watanabe. 1990. The genetic code of a squid mitochondrial gene. *Nucleic Acids Symp. Ser.* **22:** 77–78.

Sibuet, M., and K. Olu. 1998. Biogeography, biodiversity and fluid dependence of deep-sea cold-seep communities at active and passive margins. *Deep-Sea Res. II* **45:** 517–567.

Stein, J. L., S. C. Cary, R. R. Hessler, S. Ohta, R. D. Vetter, J. J. Childress, and H. Felbeck. 1988. Chemoautotrophic symbiosis in a hydrothermal vent gastropod. *Biol. Bull.* **174:** 373–378.

Tufar, W. 1990. Modern hydrothermal activity, formation of complex massive sulfide deposits and associated vent communities in the Manus Back-Arc Basin (Bismarck Sea, Papua New Guinea). *Mitt. Osterr. Geol. Ges.* **82:** 183–210.

Tunnicliffe, V., A. G. McArthur, and D. McHugh. 1998. A biogeographical perspective of the deep-sea hydrothermal vent fauna. *Adv. Mar. Biol.* **34:** 351–442.

Tyler, P. A., and C. M. Young. 1999. Reproduction and dispersal at vents and cold seeps. *J. Mar. Biol. Assoc. UK* **79:** 193–208.

Van Dover, C. L. 2000. *The Ecology of Deep-Sea Hydrothermal Vents.* Princeton University Press, Princeton, NJ. 424 pp.

Vrijenhoek, R. C. 1997. Gene flow and genetic diversity in naturally fragmented metapopulations of deep-sea hydrothermal vent animals. *J. Hered.* **88:** 285–293.

Warén, A., and P. Bouchet. 1993. New records, species, genera, and a new family of gastropods from hydrothermal vents and hydrocarbon seeps. *Zool. Scr.* **22:** 1–90.

Weir, B. S., and C. C. Cockerham. 1984. Estimating *F*-statistics for the analysis of population structure. *Evolution* **38:** 1358–1370.

Reference: *Biol. Bull.* **200:** 305–320. (June 2001)

Ecology and Behavior of *Gecarcoidea natalis*, the Christmas Island Red Crab, During the Annual Breeding Migration

AGNIESZKA M. ADAMCZEWSKA[1,*] AND STEPHEN MORRIS[2]

[1]*Ocean Research Institute, University of Tokyo, 1-15-1 Minamidai, Nakano-ku, Tokyo 164-8639, Japan;*
and [2]*Morlab, School of Biological Sciences, Woodland Road, University of Bristol,*
Bristol BS8 1UG, UK

Abstract. The terrestrial crab *Gecarcoidea natalis* is endemic to the forests of Christmas Island but must migrate each year to the coast to breed. During 1993 and 1995, radio-tracking, mark and recapture, and counting methods were used to establish the routes, walking speeds, direction of travel, and destinations of migrating crabs, as well as crab numbers and distribution. The density of crabs ranged from 0.09 to 0.57 crabs per square meter, which gave a population estimate of 43.7 million adult crabs on the island. During the dry season the crabs were relatively inactive but on arrival of the wet season immediately began their migration. The crabs generally walked in straight lines, and most crabs from around the Island traveled toward the northwest shore instead of simply walking toward the nearest shore. The maximum recorded distance walked by a red crab in one day was 1460 m, but the mean was 680 m per day in 1993 and 330 m in 1995. Comparing the 1993 and 1995 study seasons, there was a 3-week difference in the timing of the start of the migration, but the spawning date was fixed by the lunar phase and took place 17 to 18 days after mating. In 1993, late rain prompted a "rushed" migration and crabs walked directly to their shore destinations; in contrast, in 1995 most crabs made stops of 1 to 7 days during the downward migration. By giving the crabs a chance to feed along the way and minimizing the time that the population was concentrated near the shore, these stops may be important in ensuring that the animals have enough food after the long dry season. Furthermore, this behavior implies that the crabs are able to judge how far away they are from the shore during the migration.

Introduction

The red crab *Gecarcoidea natalis* is endemic to Christmas Island and is distributed throughout the entire island (Hicks, 1985; O'Dowd and Lake, 1989; Hicks *et al.*, 1990; Green, 1993). For most of the year the red crabs are found within primary and mature regrowth forest (Hicks *et al.*, 1990; Green, 1997; pers. obs.), but each year these crabs must migrate to the coast to breed. The migration of red crabs is a well-documented phenomenon described by anecdotal observations (Andrews, 1900; Gibson-Hill, 1947) but by only limited quantitative data, including some information on crab densities and walking speeds across cleared areas (Hicks, 1985; O'Dowd and Lake, 1989; Green, 1993, 1997). There are no data on migratory routes, destinations or distances, nor on walking speeds of red crabs within the rainforest.

The arrival of the monsoonal rains allows increased activity of red crabs and stimulates the annual migration (Hicks, 1985; Green, 1993). During this breeding migration red crabs, like other terrestrial gecarcinids, must abandon their home ranges and travel down to the coast to mate and spawn (Garth, 1948; Gifford, 1962; Bliss *et al.*, 1978; Lake and O'Dowd, 1991; Pinder and Smits, 1993; Green, 1997). The downward migration normally requires at least a week, and the crabs migrate mainly during the first few hours of the morning and in the late afternoon (Hicks, 1985; Green, 1993). The males excavate burrows, which they must defend from other males, on the lowest shore terraces; mating occurs in or near the burrows. Soon after mating the males

Received 23 April 1999; accepted 21 February 2001.

* To whom correspondence should be addressed. E-mail: *ishka@ori.u.tokyo.ac.jp*

start the journey back inland to the forest, while the females lay their eggs and remain in the burrows for 2 weeks (Hicks, 1985; Hicks *et al.*, 1990). At the end of the incubation period the females vacate their burrows and make their way to the coastal cliffs, which almost completely surround the island, to cast their eggs into the ocean. The females then return to the forest while the crab larvae spend 3-4 weeks at sea before returning to land as juvenile crabs (Gibson-Hill, 1947; Hicks, 1985; Hicks *et al.*, 1990).

Since gecarcinid crabs must migrate to the shore to spawn, they must have well-developed navigational mechanisms. The means of navigation during the migrations are unknown, but visual cues, polarized light, magneto-reception, and learning are thought to be involved (Daumer *et al.*, 1963; Herrnkind, 1968; DeWilde, 1973; Bliss *et al.*, 1978; Lohmann *et al.*, 1995; Vannini and Cannicci, 1995; Deutschlander *et al.*, 1999).

Some data are available on the activity levels of terrestrial crustaceans in the natural environment (*e.g.*, Wolcott and Wolcott, 1985; Gherardi *et al.*, 1988; Gherardi and Vannini, 1989; Micheli *et al.*, 1990; Weinstein, 1995), but data comparing the activity patterns of gecarcinid crabs during normal foraging activities and during the migration are sparse (see DeWilde, 1973). The ecology of red crabs is characterized by a period of very low activity during the dry season, followed immediately by a breeding migration (Hicks, 1985; Green, 1997) that may require crabs to travel more than 4 km in less than a week. Such abrupt changes in activity levels impose specific demands on the physiology and metabolism patterns of red crabs.

The availability of food and water changes on a seasonal basis. Particularly during the migration, this could be a major determinant of the strategy, performance, and diel capacity for exercise. Limitations in food have implications for the importance and use of stored fuel reserves, both during the dry season and during the migratory activities. Thus, determining the distances traveled and the duration of the migration as well as the routes and destinations of the crabs was crucial in appreciating the physiological demands.

The aim of this study was to examine activity levels of red crabs in the field during the migration compared to the non-migratory season. The emphasis was to characterize the migration of *G. natalis* in detail, by determining the direction, speed, and distance traveled during the migration, as well the relationship between the point of origin of crabs in the forest and their shore destinations, thus providing a context for the physiological demands during their annual migration.

Materials and Methods

Christmas Island was formed by a series of geological uplifts. Thus, the structure of the island is reminiscent of a wedding cake, with a central plateau (>200 m above sea level) and a number of cliffs and terraces descending to a rugged shore line with few beaches (Fig. 1; Gray, 1995). Field studies on Christmas Island were carried out in two study areas. The primary study site (Study Area 1) was located on the central plateau, within the Christmas Island National Park (Fig. 1). This part of the Island is covered by primary rainforest and well-established secondary regrowth and has received minimum human disturbance over the past 20 years. Study Area 2, located in the northeast corner of the Island (Fig. 1), included the existing human settlement and airport, an area crisscrossed by many roads.

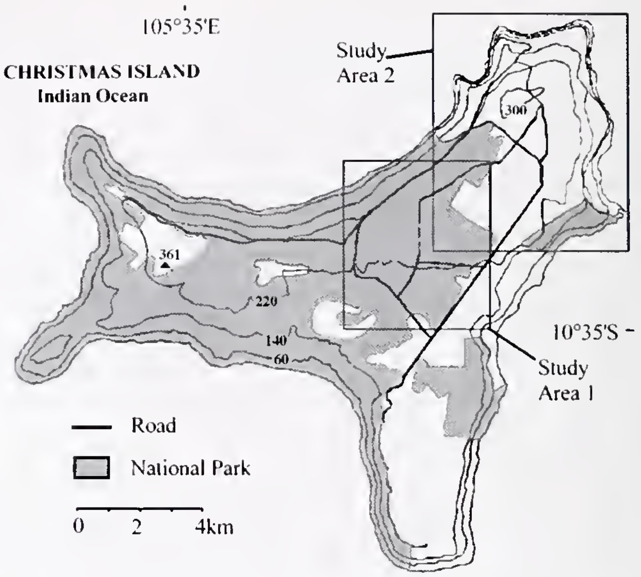

Figure 1. Christmas Island, Indian Ocean, showing areas of National Park and the location of the two study areas. Study Area 1 was located in the relatively undisturbed part of the island; Study Area 2 included the residential and industrial areas.

The annual activity cycle of red crabs was divided into a migratory and a non-migratory season. "The migratory season" (initiated by the arrival of the wet season, usually in November or December) is used in this study to collectively refer to the breeding behavior of the crabs, including the annual breeding migration, the related breeding activities, and the return journey from the shore terraces to the forest. The "non-migratory season" includes all other times of the year when the red crabs were not involved in breeding activities.

Non-migratory season

Population density. To obtain an index of density for red crabs, twelve stations (A to L) were selected; these included sites on the central plateau and on the upper terraces in both study areas (Fig. 2). All stations were located in primary or

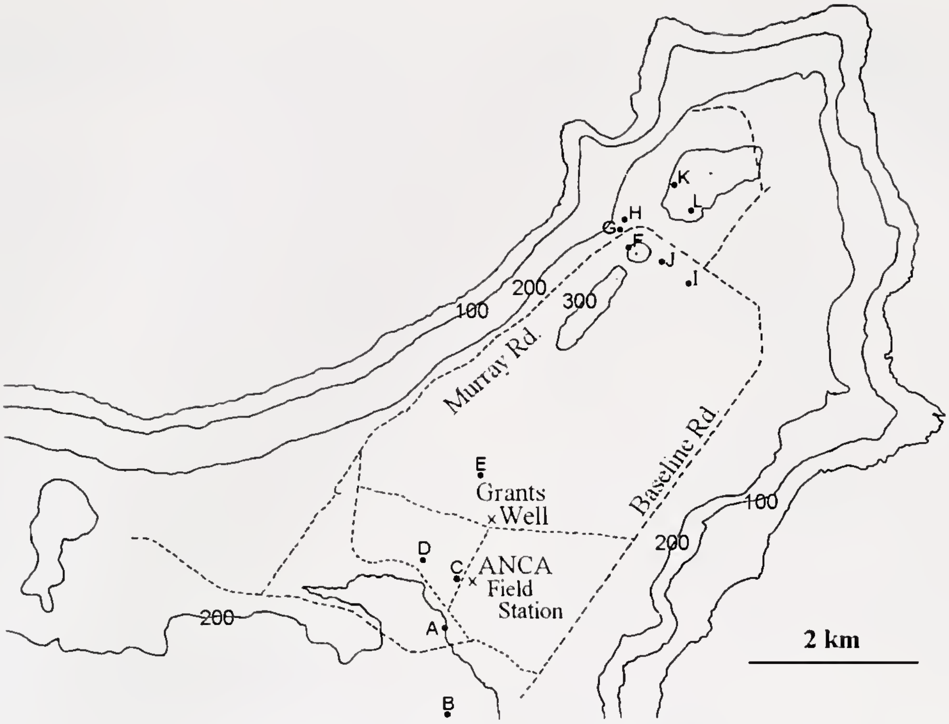

Figure 2. Locations of the sites for determining the density of red crabs during February and March 1995 (non-migratory season). Sites A-E were within Study area 1; sites F-L were in Study Area 2.

mature regrowth forest, but some were very close to cleared areas.

At each station the visible red crabs were counted in each of six grids (9 × 9 m). All counting was done either in the 2 hours after dawn, a period of foraging activity for red crabs, or during overcast conditions that normally stimulate a similar degree of activity (Hicks, 1985; Green, 1993, 1997). There is very little understory vegetation in the rainforest of Christmas Island, so foraging red crabs are easily visible and provide relatively accurate estimates of the crabs present in the area. Additionally, stations that were populated predominantly by large male crabs were discriminated from those with a more mixed population. These data were confirmed as having homogenous variance by using Bartlett's χ^2 test and were then analyzed by analysis of variance (ANOVA: Systat 5.03). *Post hoc* testing was by Tukey's HSD, and $P \leq 0.05$ was taken as significant in all cases.

Activity patterns. Two separate experiments were conducted to determine the activity patterns of red crabs during the non-migratory season (March 1993; wet season) at station B within Study Area 1 (for location, see Fig. 2). Firstly, crabs were selected at random and observed for a period of 2 min during their normal foraging activities. The distance that each crab walked during the 2 min was recorded (n = 15). During the second experiment, the actual walking speed of foraging crabs was recorded. A crab was chosen at random and observed until it started walking; the crab was then timed for as long as it continued to walk, and the distance it traveled was recorded (n = 14). All crabs used in these two experiments were subsequently captured, sexed, and measured (carapace width). These observations were made when the red crabs are most active, *i.e.*, when the humidity was over 85% (Green, 1993).

Migratory activities

Three methods were used to obtain information about the migration of red crabs: radio tracking to obtain precise speeds, routes, and direction of travel; spray-painting large numbers of crabs to gain information on *en masse* direction of travel; and counting of crabs at designated stations to provide quantitative snapshots of the numbers of crabs present in various parts of the island.

In Study Area 1, crabs were studied during the migratory season (November/December) of 1993 and 1995, but in Study Area 2 crabs were studied during the 1995 migration season only. The behavior of migrating red crabs in a relatively undisturbed area (Study Area 1) was compared to that of crabs in the inhabited part of the island (Study Area 2). Since red crabs have rather small home ranges during most of the year (Lake and O'Dowd, 1991; Green, 1993; pers obs.), the areas within the rainforest selected for color

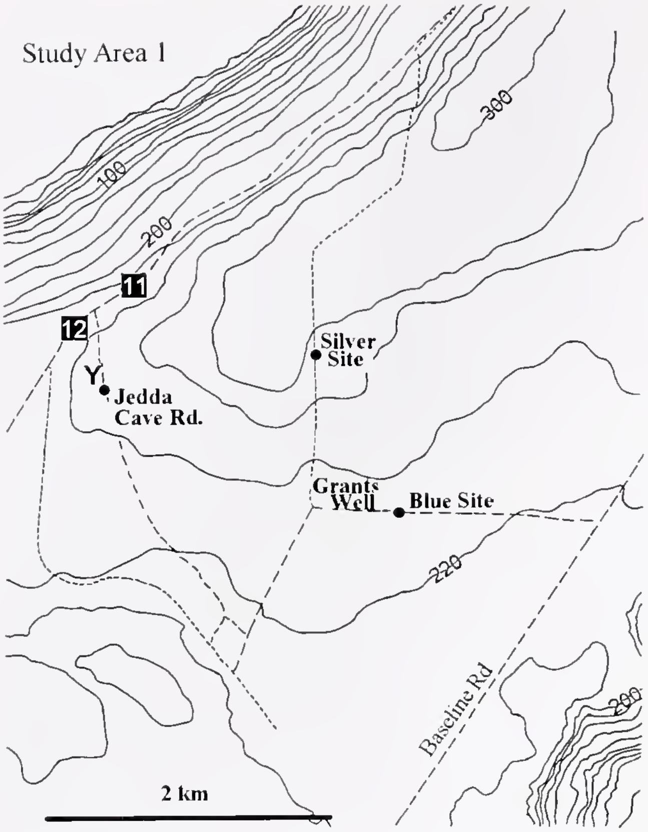

Figure 3. Study Area 1 showing locations of numbered grids (■) used for density counts during the migration and sites (●) of color coding crabs (where Y = yellow) and of radio-tracking "sites of origin" at Silver and Blue.

coding of the red crabs prior to the start of the migration were assumed to be the sites of origin for those crabs.

Radio-tracking of crabs. At the commencement of the migration in 1993, four large male red crabs (mass 400-503 g) were captured at each of two chosen study sites (Blue and Silver sites; for locations see Fig. 3) and fitted with radio transmitters (see below). During the 1995 migration this radio-tracking experiment was repeated by fitting male crabs (mass 415-480 g) originating at those same sites with radio transmitters on 8 and 9 November. Additionally, in 1995, radio transmitters were attached to three large male crabs (mass 460-570 g) at each of two more sites of origin (Yellow and Orange sites; Fig. 4) within Study Area 2, on 9 and 10 November respectively.

To attach the radio transmitters to the crabs a plastic sawn-off 20-ml syringe was first glued with an epoxy glue to the top of the carapace of each crab and allowed to set for a minimum of 6 hours. The radio transmitters (Microlite transmitters, model GP1; Titley Electronic, Ballina, NSW, Australia) were then inserted into the syringes with the antennae trailing behind the animals. The transmitter and the plastic syringe housing weighed 20–30 g. The posteriodorsal surface of each crab was spray-painted with acrylic paint corresponding to the color associated with its site of origin. Each crab was released in exactly the same spot where it was collected.

The crabs were tracked daily with a collapsible, directional antenna (A. H. Systems, Chatsworth, CA) connected to a Regal 2000 telemetry receiver (Titley Electronics). Crabs were firstly located by triangulation and, where possible, the location of each crab was confirmed visually. The triangulation technique proved quite reliable, pinpointing the location to within 30 m. The position and time of location for each crab fitted with a radio transmitter was recorded on a topographical map every day.

Color-coding of crabs. The posteriodorsal part of the carapace of crabs was spray-painted with nontoxic acrylic spray-paint, avoiding the eyes and mouthparts. In Study Area 1, at the commencement of the migration in 1993 (on the 17 Nov.), 530 crabs (male and female) were spray-painted yellow and 285 crabs were spray-painted blue (for location of sites, see Fig. 3). During the 1995 migration, 684 crabs were spray-painted blue and 750 were spray-painted silver at their respective sites of origin within Study Area 1 (Fig. 3).

In Study Area 2 (1995), 5622 red crabs were spray-painted different colors at eight locations within primary and mature regrowth forest in the plateau area (see Fig. 4 and Table 1 for location and the number of crabs painted at

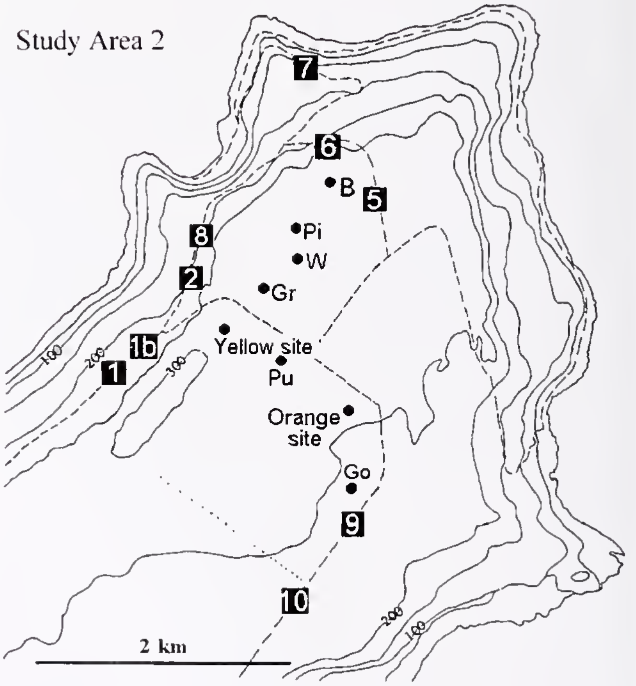

Figure 4. Study Area 2 showing locations of numbered grids (■) used for density counts during the migration and sites (●) of color coding crabs (where Pu = Purple, Gr = Green, W = White, Pi = Pink, B = Brown, Go = Gold) and of radio-tracking "sites of origin" at Orange and Yellow.

Table 1

Summary of 1995 color-coding experiment in Study Area 2

		Crabs		
			Sighted†	
Site code	Date painted*	Painted (no.)	(no.)	(%)
Purple (Pu)	5	556	70	13
Green (Gr)	5–8	999	310	31
Yellow (Y)	5–8	886	236	27
White (W)	5–8	701	269	38
Pink (Pi)	5–8	611	164	27
Brown (B)	7	169	15	9
Orange (O)	6–8	621	204	33
Gold (Go)	6–8	1079	70	6
TOTAL		5622	1338	23

* Day or range of days in November 1995.

† Between 8 November and 18 December 1995.

each site of origin). In Study Area 2, volunteers searched for painted crabs from 0630 to 1100 hours and from 1500 to 1730 between 8 November and 18 December 1995. To maximize sightings, the surveying took place mainly on and alongside roads and tracks, where color-coded crabs could be easily spotted as they crossed. All sightings reported by ANCA (Parks Australia) staff and local residents were also recorded.

Walking speed and density of crabs during the migration

Walking speeds of red crabs were measured for crabs crossing Murray Road (a limestone surface about 10 m wide; Fig. 2), during the downward and return male and female migrations. Observations on the migration patterns, mating activities, and spawning of the red crabs were recorded daily.

During the 1995 migration season, counting stations were set up on roads in Study Area 1 (2 stations; Fig. 3) and in Study Area 2 (9 stations; Fig. 4). At each counting station three counting grids (each 5 × 5 m) were spray-painted on the road. Counts were carried out at each station at 0800 and 1700 hours every day between 5 November and 18 December (a total of 87 counts at each station). The density of red crabs per square meter ± SEM was calculated from the mean of the three grids at each site. The data were analyzed by analysis of variance (ANOVA), using Systat for Windows version 5.03.

Results

Non-migratory season

Population density. The density of crabs ranged from 0.09 to 0.57/m^2. Sites located at the central plateau were occupied predominantly by large male crabs at a mean density of 0.14 ± 0.03/m^2. This density was significantly lower than that of mixed populations located mostly at lower altitudes (Fig. 5). The exception was station K, which was on the plateau but inhabited by a mixed population. However, at that part of the plateau the island falls almost directly to the ocean, making it the first accessible habitat for the smaller and juvenile crabs in this part of the island. There was evidence of decreasing crab density with increasing elevation in both study areas (Fig. 5); the relationship could be described as follows: crab density (number/m^2) = 1.047 − 0.003 (elevation in m); r^2 = 0.47, simple linear regression).

Activity patterns. In March 1993, red crabs had finished their migratory activities for the season but, with relative humidity over 90%, were still actively foraging above ground. Foraging red crabs walked intermittently, traversing an average distance of only 0.52 m in 2 min. During locomotion, the walking speeds ranged from 0.62 to 2.0 m · min^{-1} (mean = 1.11 ± 0.50 m · min^{-1}). The average carapace width of these crabs was 8.25 cm (range 6.5 – 11.5 cm).

Migratory activities

The monsoonal rains arrived at different times in the two study seasons, resulting in very different migratory behavior of red crabs. In 1993, the rains were late, migration on the plateau was initiated by heavy local rainfall at noon on 17 November. Within an hour, large numbers of red crabs began accumulating on vehicle tracks and open areas within Study Area 1 and commenced their annual migration. The migration started 1 week after the optimal date predicted on the basis of the lunar cycle, and it lasted only about 6 days (Fig. 6).

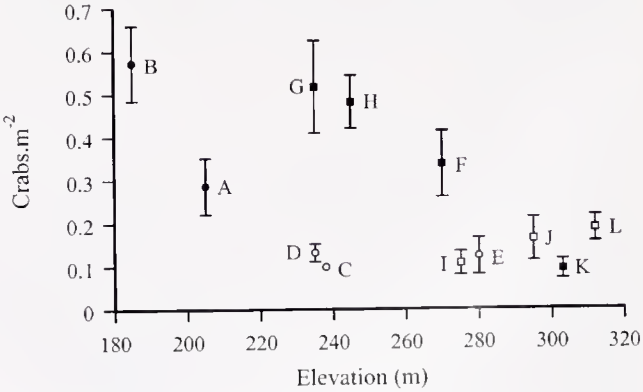

Figure 5. Density/elevation distribution of red crab population, mean number of crabs per m^2 ± SEM. Letters designate counting site (see Fig. 2 for location map). Closed symbols indicate a crab population of mixed sexes and different sizes. Open symbols indicate crab populations composed mostly of large male crabs. Sites from Study Area 1 are shown as circles (○, ●); sites from Study Area 2 are shown as squares (□, ■).

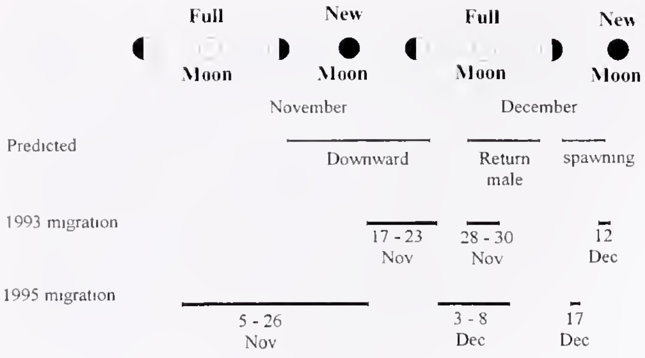

Figure 6. Graphical representation of the synchronization of breeding activities of *Gecarcoidea natalis* with the lunar phase. Predicted migratory activities were based on the descriptions presented by Hicks (1985) and Hicks *et al.* (1990). The actual timing of the downward migration, the return migration of male crabs, and the spawning recorded in 1993 and 1995 are also presented.

The migration of 1995 did not start abruptly on the plateau. A few light showers in October increased the humidity, and the red crabs became more active. A small percentage of red crabs were seen on their downward migration during the first week of November, before the main migration. The main migration on the plateau started 12 days before the date predicted by the lunar phase (Fig. 6), and consequently the red crabs were engaged in the downward migration for up to 3 weeks during the 1995 season.

Migration activity occurred almost exclusively during daylight. On rainy, overcast days the crabs were seen crossing roads throughout the day, although the numbers decreased during the middle of the day. However, on sunny days there was a distinct period of low activity during the middle of the day (1130–1500). During this time large numbers of red crabs accumulated in the bushes by the sides of the roads and resumed their migration later in the afternoon. A few individuals persisted in migrating for several hours after sunset on some days, but there was no migratory activity at night.

Migratory routes (Study Area 1)

Radio-tracking data showed that red crabs do not necessarily migrate to the nearest coast (Fig. 7a, b; Fig. 8a, b). All crabs with radio transmitters released in the Blue site in 1993 covered about 4.13 km to the northwestern shoreline within 6 days (Fig. 7), rather than walking only 1.8 km to the southeastern shore. Furthermore, the crabs did not need to follow contour lines to direct themselves towards the shoreline. Importantly, crabs radio-tracked from the same point of origin followed remarkably similar routes in both study seasons, and they traveled in surprisingly straight lines (Fig. 7a, b; Fig. 8a, b). The silver-coded crabs from the center of the Island also headed northwest, traveling approximately 2.4 km in as little as 3–4 days (Fig. 8a, b). The Jedda Cave road, where 500 crabs were painted yellow in 1993 (Fig. 3), was used as a travel route by some individuals. Yellow-colored crabs were noted on the road up to 3 days after being painted (Fig. 9a). Other crabs simply crossed the road without taking advantage of easier routes along cleared areas. Sightings of color-coded red crabs (Fig. 9a–c) provided a larger data set confirming that crabs originating from a particular area on the island tend to migrate to similar areas on the shore to carry out their breeding activities.

The distances traveled by the red crabs with radio transmitters in Study Area 1 varied greatly, from 120 to 1460 m/day. During the "rushed" migration in 1993, seven of the radio-tracked crabs traveled more than 900 m/day, and the average distance traveled in a day was 680 m (Fig. 7a, b). During the 1995 migration, the longest distance traveled in a day was 1000 m, and the average daily distance was 330 m—less than half that recorded during the 1993 migration.

During the 1993 migration season, the crabs made progress towards their shore destinations each day (Fig. 7a, b). In contrast, during the 1995 season, 5 of the 7 radio-tracked crabs in Study Area 1 paused in their downward migration to the ocean and remained in one place (within ~ 20 m diameter) for 2 to 5 days before they resumed their journey to the coast (Fig. 8a, b).

Using the 1993 data and assuming that red crabs walk continuously for 12 h per day (*i.e.*, during the daylight hours), the calculated average walking speed during the migration of the crabs with radio transmitters was 1.1 $m \cdot min^{-1}$. This was considerably slower than the speed of 4.7 ± 0.4 $m \cdot min^{-1}$ ($n = 17$) recorded for red crabs crossing Murray Road (10 m wide) during both of the study seasons. During the return migration, walking speeds for returning males (5.1 ± 0.3 $m \cdot min^{-1}$; $n = 13$) and returning females (6.2 ± 0.5 $m \cdot min^{-1}$; $n = 7$) crossing Murray Road were significantly faster than those of crabs on their downward migration ($P = 0.016$).

Migratory routes (Study Area 2)

In Study Area 2 the crabs also traveled predominantly northwest (Fig. 10a, b). Radio-tracking showed that crabs traveled along the sides of a road (thus becoming temporarily diverted from their course towards the shore) before eventually crossing the road to reach the terraces (Fig. 10a, b).

The crabs with radio transmitters from the Yellow site took between 10 and 13 days to travel 1.2 km to the shore terraces (Fig. 10b). The shore closest to the Orange site was 2.1 km due east, but most of the orange-coded crabs traveled more than 3.4 km in the northwest direction, walking for 17–21 days to reach the shore terraces at a point very close to the crabs from the Yellow site (Fig. 10a, b, Fig. 11).

Three crabs traveled over 1 km in a day, but the average

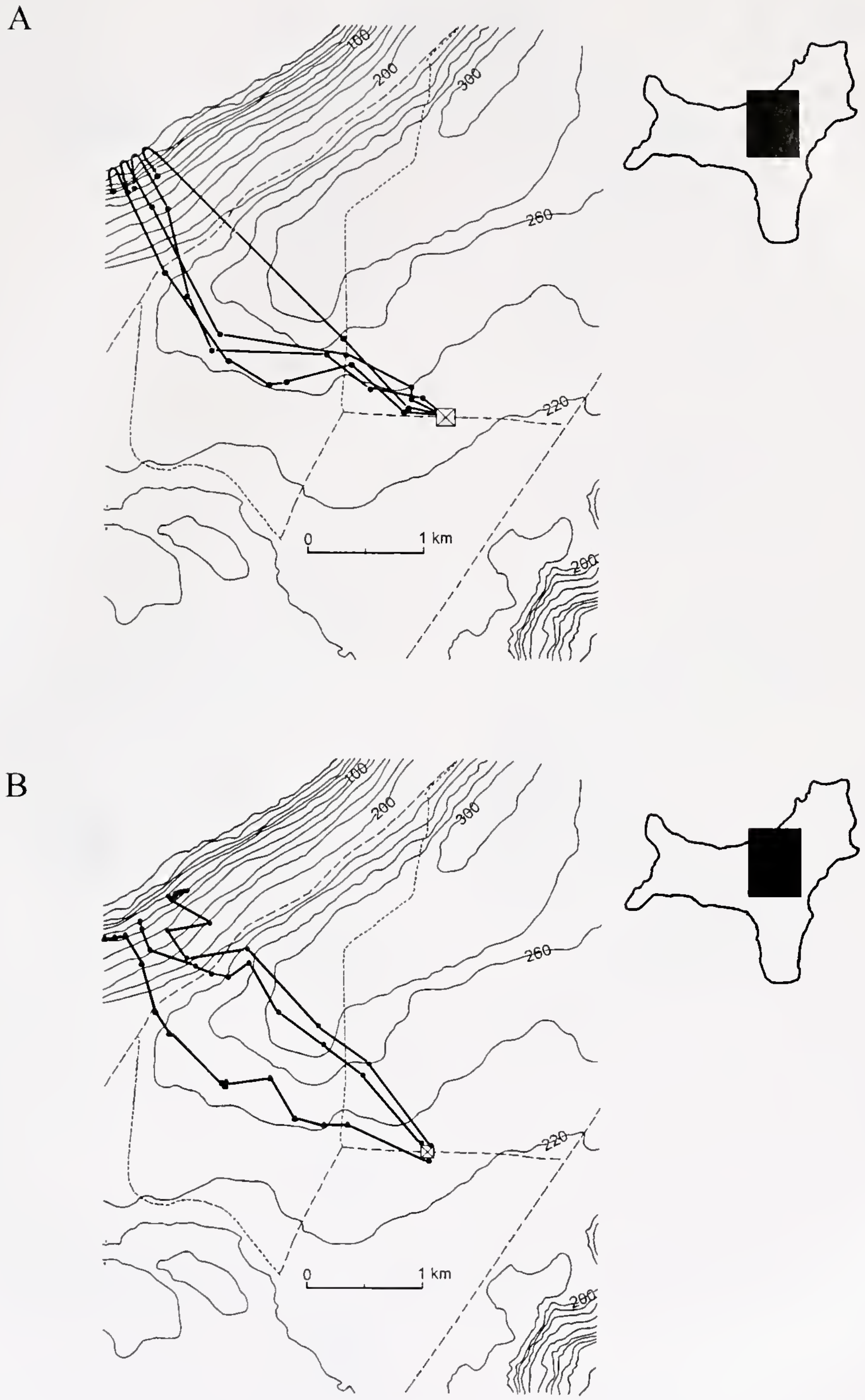
A
100
200
300
260
220
0
1 km
200
B
100
200
300
260
220
0
1 km
200

Figure 7. Migratory paths determined for radio-tracked crabs originating from the Blue site in Study Area 1 in 1993 (A) and in 1995 (B). The ⊠ symbol shows site of origin. The location of the enlarged section is indicated by the black rectangle.

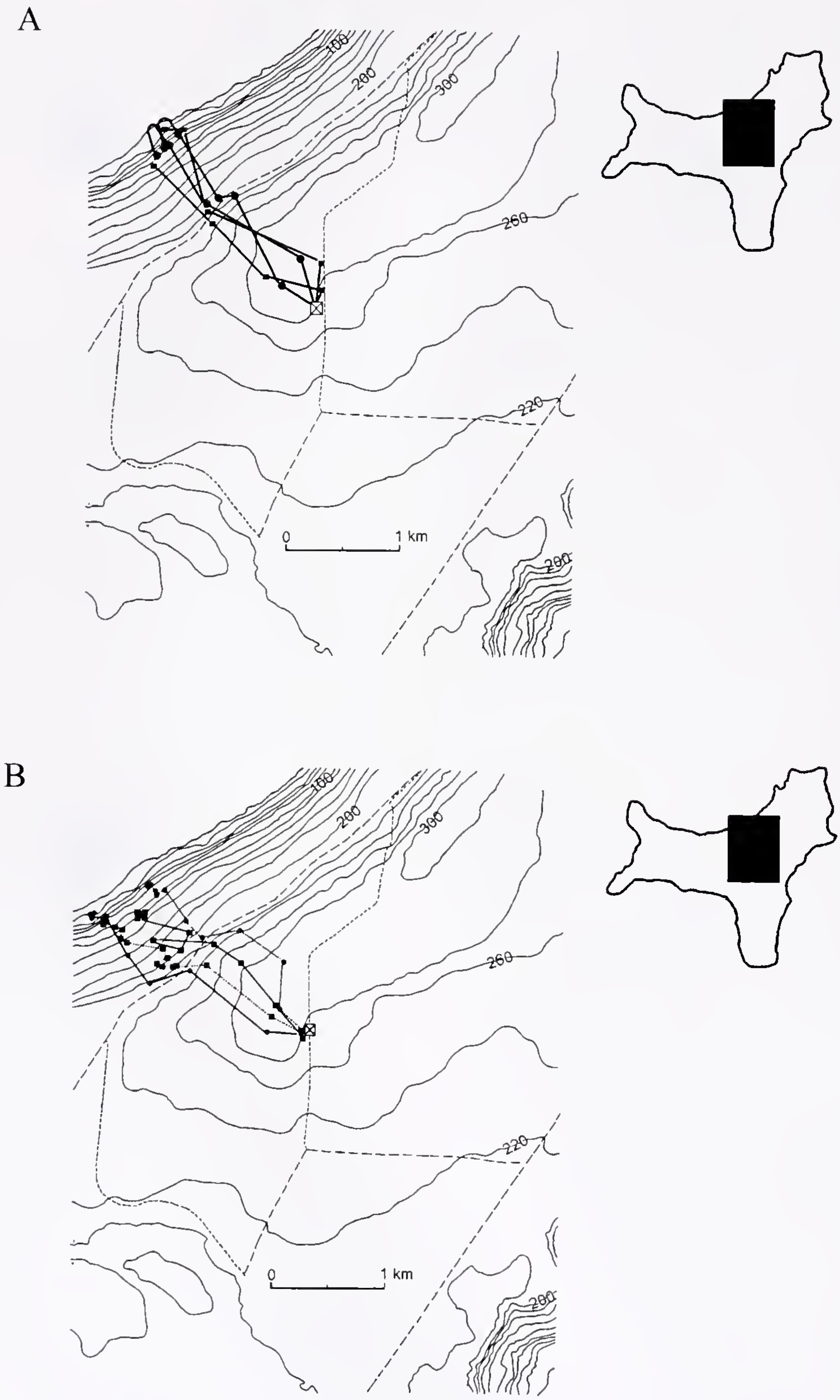
A
100
200
300
260
220
0
1 km
200
B
100
200
300
260
220
0
1 km
200

Figure 8. Migratory paths determined for radio-tracked crabs originating from the Silver site in Study Area 1 in 1993 (A) and in 1995 (B). The ☒ symbol shows site of origin. The location of the enlarged section is indicated by the black rectangle.

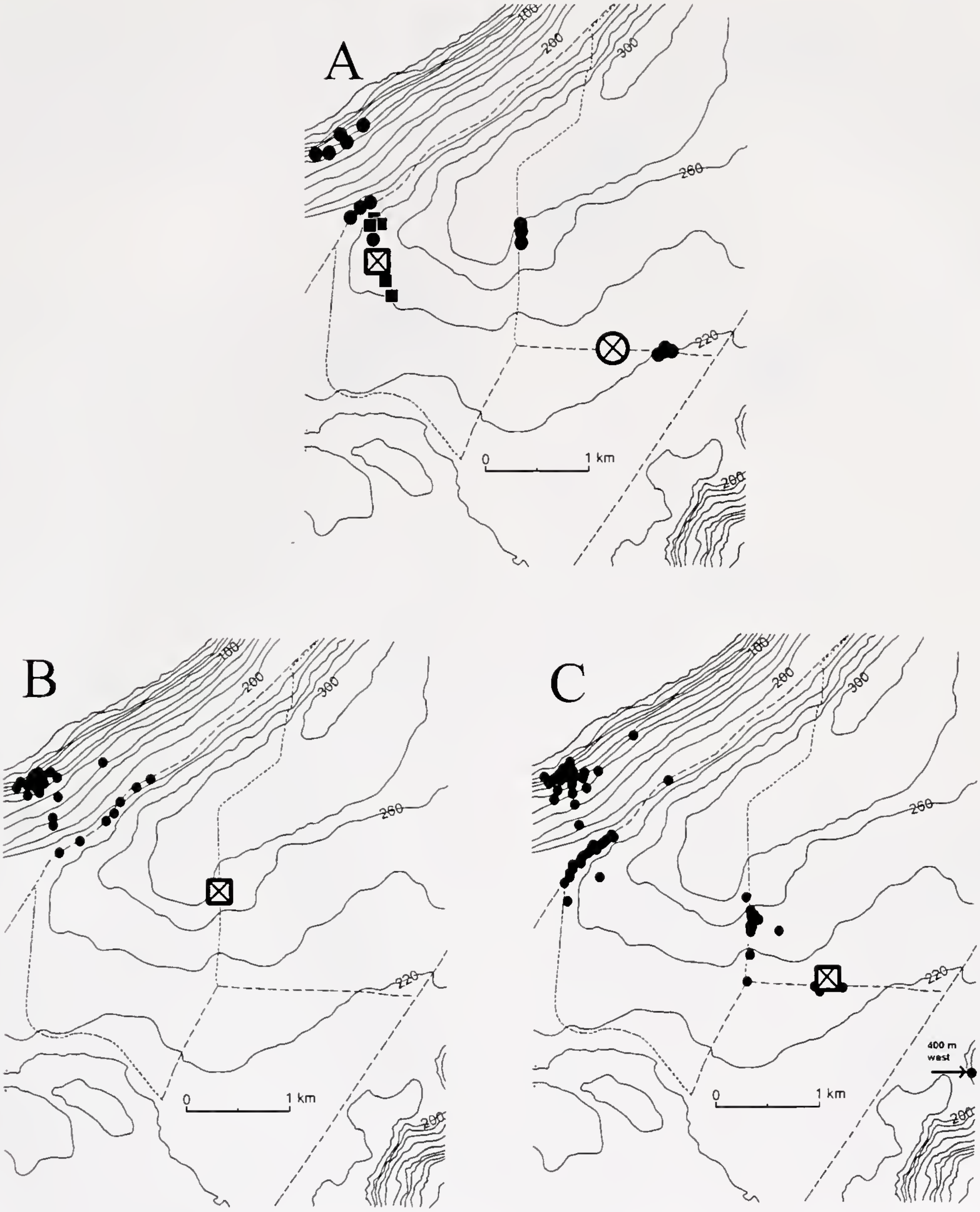

Figure 9. Locations of sightings of spray-painted crabs. (A) Yellow-painted crabs (■) and blue-painted crabs (●) during the 1993 migration. Yellow-coded crabs were seen for 3 days after painting on the Jeda Cave Road, and thus individual sightings are not shown. (B) Silver-painted crabs (●) during the 1995 migration. (C) Blue-painted crabs (●) during the 1995 migration. Open symbols show site of origin.

distance covered per day was only 200 m. In Study Area 2, 5 of the 6 radio-tracked crabs also made stops and remained within a small area (5-30 m diameter) for periods ranging from 1 to 7 days before continuing towards the coastal terraces (Fig. 10a, b).

Of the 5622 red crabs color-coded in eight sites within Study Area 2, 1338 sightings of color-coded crabs, on their downward or return migrations, were recorded. For every 100 color-coded crabs released, the subsequent sightings ranged from 38% for the white-coded crabs to only 6% for

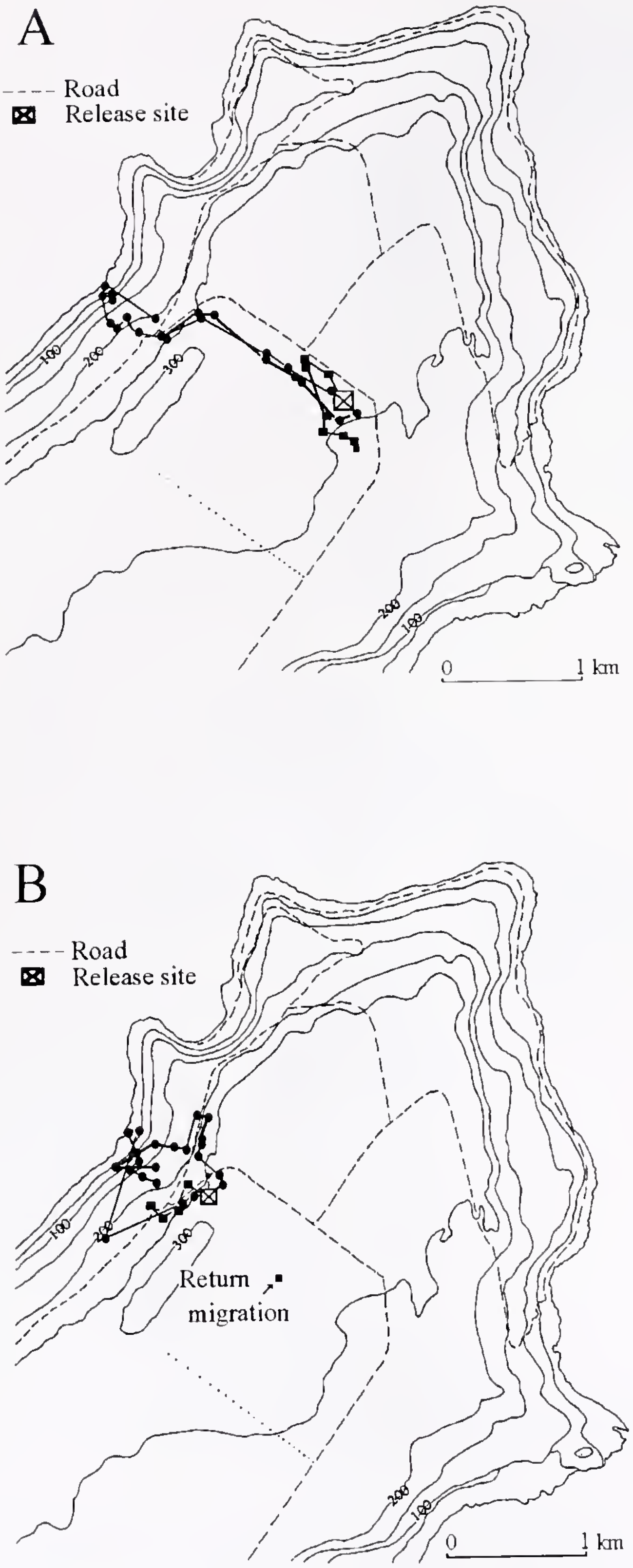

Figure 10. Migratory paths as determined by radio-tracking in Study Area 2 during the 1995 migration. (A) Three crabs from the Orange site. (B) Three crabs from the Yellow site. Open symbols show site of origin.

the gold-coded crabs (Table 1). The sightings indicated that painted crabs traveled predominantly towards the northwestern coast regardless of their site of origin (Fig. 11). In 4 of the 8 color-coded groups the greatest number of sightings were on Murray Road between grid 1 and grid 8 (for location, see Fig. 4). Crabs originating from the Brown site were an exception as the majority of crabs from this site headed due north.

Terrace activities

At least half of the crabs fitted with radio transmitters descended to the lowest shore terrace, immediately above the ocean. Males on the shore terraces were engaged in digging burrows; in places, burrow density was $3/m^2$.

In the 1993 season, the first matings were sighted on 25 November, and the return migration of the males began on 28 November and lasted 3 days (Fig. 6). The female red crabs spawned pre-dawn (0300–0400 hours) on 12 and 13 December, and their return migration lasted only 2 days. During the return migration very small individuals (~2 cm carapace width) that had not been observed on the downward migration were seen traveling inland with the returning females.

In 1995, the first matings were sighted on 29 November, and the return migration of the males began in earnest on 3 December (Fig. 6). The main return migration of male crabs lasted 5 days, with a few late crabs still walking for 2 more days. The female red crabs spawned pre-dawn on 17 December, with two small-scale spawnings occurring in a few places on the Island on 16 and 18 December. The returning females reached Murray Road on 19 and 20 December in very large numbers.

Density of crabs during the migration

The downward migration (in 1995) lasted from 5 to 26 of November. Prior to 9 November, only a few crabs were seen crossing through the counting grids (see Fig. 4 for locations) and only in certain areas (Fig. 12). The main downward migration showed a wavelike increase and decrease in the number of crabs moving across roads on different days—for example, grid 1b (Fig. 12a), grid 6 (Fig. 12e), and grid 8 (Fig. 12d).

The density of crabs was greatest on Murray Road, in Study Area 2, between grids 1 and 8 (Fig. 12a-d). The maximum density of crabs recorded was $1.35/m^2$ on grid 2 during the downward migration (Fig. 12c), but in Study Area 1, the maximum densities reached only $0.4–0.5/m^2$ (Fig. 12i, j; see Fig. 3 for locations).

The lowest densities of crabs, $<0.2/m^2$, were recorded on Phosphate Hill (grids 5, 6, and 7; Fig. 12e, f) and on the Base Line Road (grids 9 and 10; Fig. 12g, h respectively). No crabs were ever recorded in grid 5 (Fig. 4). The number of days during which at least one crab was present in the

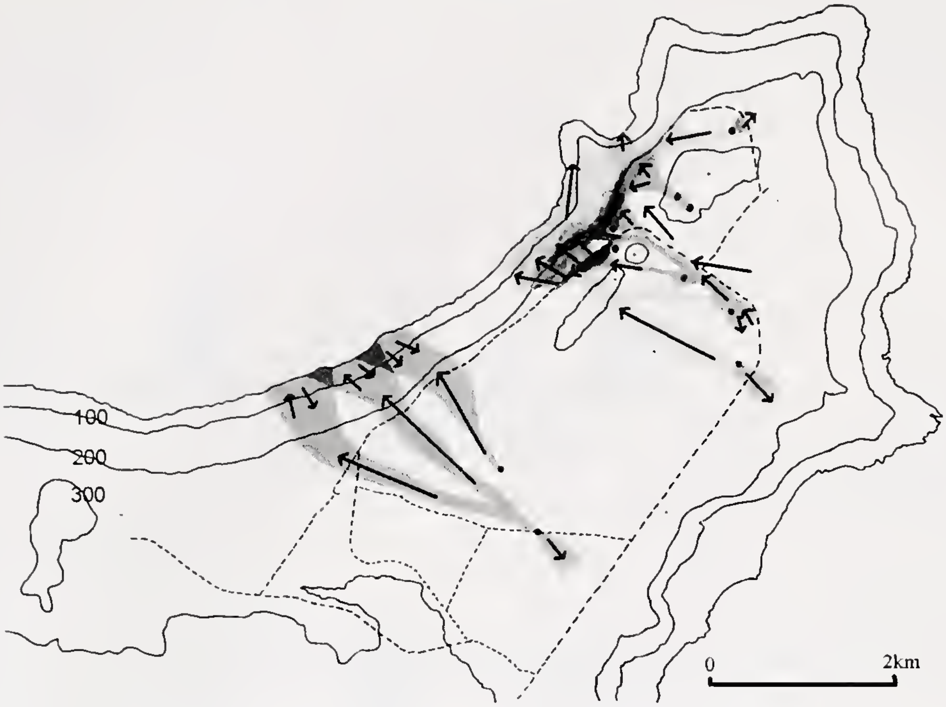

Figure 11. Composite showing general migration routes, directions, and destinations for the red crab migration. Derived from color-coding and radio-tracking data. Density of stipples indicates frequency of marked crab recaptures.

counting grids ranged from 2 at grid 7 to 11 at grid 6. In contrast, in the grids located on Murray Road, the crab migration lasted from 26 to 34 days.

Discussion

The distribution of *Gecarcoidea natalis* is not homogeneous throughout Christmas Island, and the activity levels and behavior of the crabs show extreme seasonal dichotomy. The largest male crabs live farthest from the coast; because they have the greatest distance to travel, they must start their migration before other crabs if they are to reach the shore together. Crabs from all locations walked in surprisingly straight lines to definite shore destinations to which they navigated together with their neighbors. Radio-tracking revealed that given adequate time to complete the migration, the male red crabs paused for several days *en route* to feed instead of crowding early into the limited terrace area adjacent to the shore. The migratory behavior, strategy, and potential stress (Adamczewska and Morris, 2001) are influenced by the distance an individual crab must travel. However, since the breeding migration is triggered by the arrival of the monsoonal rains and is synchronized with the lunar cycle (Hicks, 1985; Grey, 1995), the timing of the arrival of the seasonal rains will be fundamental in determining the speed of migration and the time spent walking each day.

The red crab population

The population of red crabs on Christmas Island was estimated by subdividing the area of the entire Island into three sections: (i) the terraces, with an area of 57.7 km^2 and an average density of 0.6 crabs per square meter; (ii) the plateau, with an area of 59.6 km^2 and a crab density of 0.15/m^2; and (iii) mined or cleared areas, with an area of 16.7 km^2 and a density of 0.01/m^2 (Lake and O'Dowd, 1991). The estimated population of adult red crabs on Christmas Island was 43.7 million, substantially less than the 120–157 million crabs suggested previously (Hicks, 1985; Hicks *et al.*, 1990). Importantly, the density of red crabs was similar in the mature regrowth forest within Study Area 2 and the relatively undisturbed forest of the terraces in Study Area 1.

The densities of red crabs recorded in this study were very similar to the values of 0.04 to 0.4/m^2 obtained by Lake and O'Dowd (1991) in transects. The population density of red crabs is very high; although several studies report the densities of other terrestrial gecarcinids in the range of 0.4 to 6/m^2 (Green, 1993, and references therein), these are generally the maximum densities recorded. The densities of red crabs can reach up to 40/m^2 on the ocean cliffs and beaches during spawning (Hicks, 1985; pers. obs.). As a consequence of the high biomass, these crabs have a very

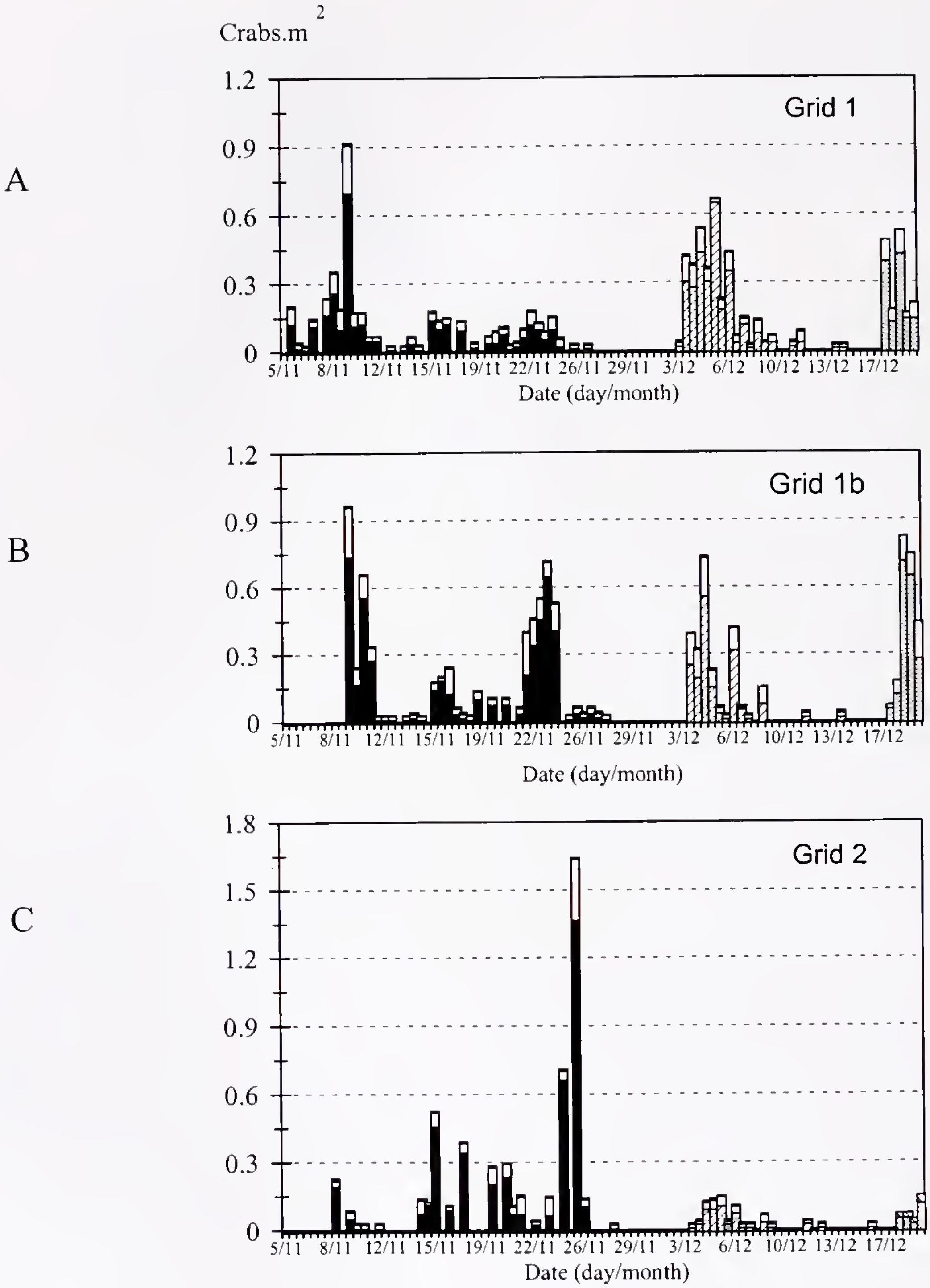

Figure 12. Density of crabs crossing roads during the downward migration (solid bars) and during the return migration of male crabs (bars with diagonal fill) and female crabs (bars with stippled fill) during the 1995 migratory season. Grids 1–10 were in Study Area 2; grids 11 and 12 were in Study Area 1. For location of grids, see Figures 3 and 4.

large impact on forest dynamics (Lake and O'Dowd, 1991; Green, 1993).

The density of red crabs on Christmas Island was related to population structure and altitude. The top plateau is populated predominantly by large males and, progressing towards the shore, the coastal terraces are

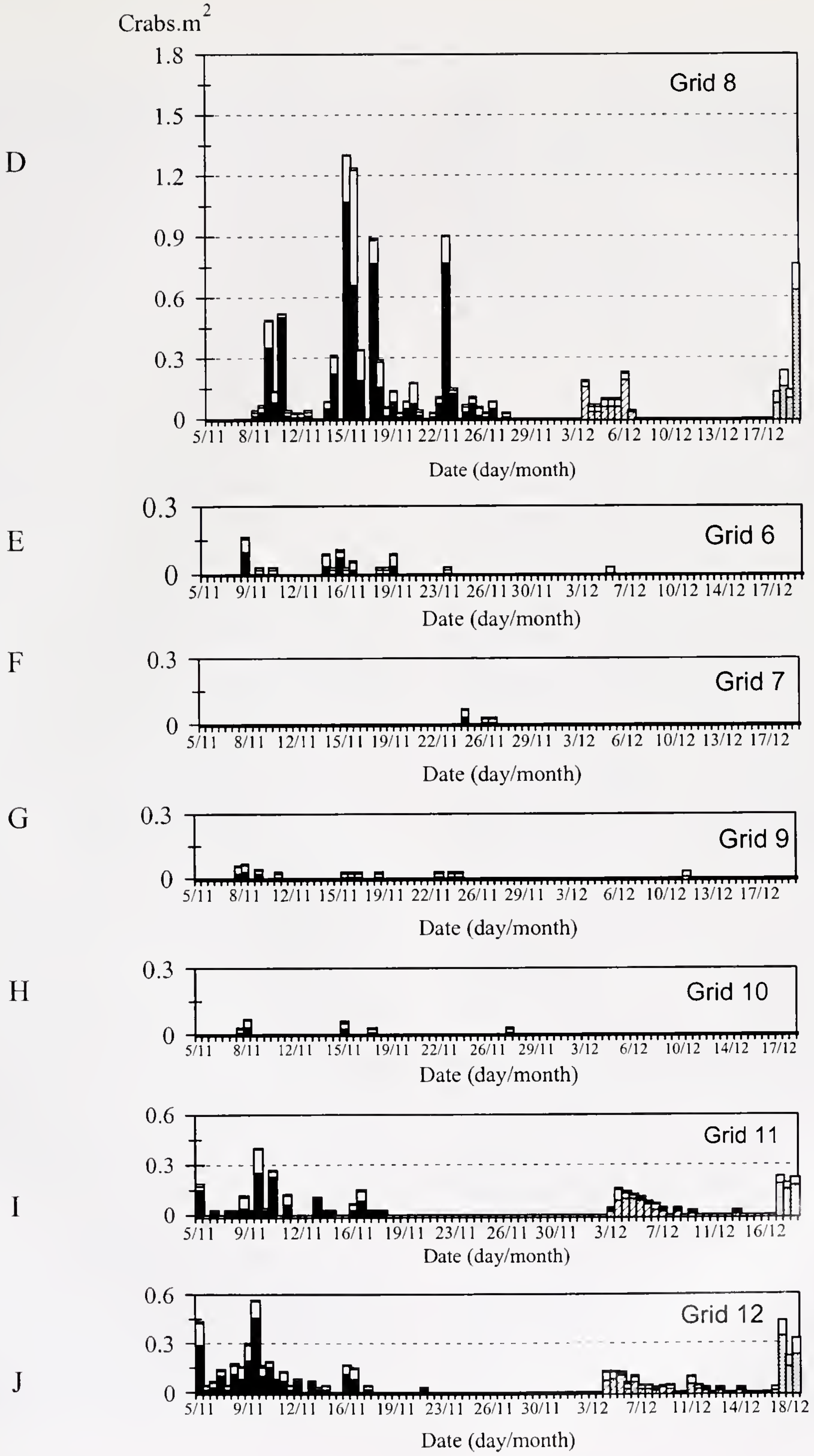

Figure 12. Continued.

populated by smaller individuals of both sexes (Fig. 5; Green, 1993, 1997). Crab densities decrease sharply in just 8–10 m when moving from the forest into cleared areas (Lake and O'Dowd, 1991). Walking speeds are slow, and the crabs seem quite sedentary during the non-migratory season; one marked crab was sighted within 15 m of where it was released 8 months earlier. Red crabs appear to be unaffected in their distribution and activities by conditions or events only a few meters removed (Lake and O'Dowd, 1991; pers. obs.), and they tend to have small foraging ranges during the non-migratory phase of the year.

Routes and destinations of migrating crabs

A combination of radio-tracking, color-coding, and counting stations located in various places around the island has revealed valuable information about the migratory patterns of red crabs. Three points have became apparent: firstly, crabs traveled predominantly towards the northwestern shore, which for some of the crabs was twice as far away as the southeastern shore; secondly, the crabs have specific shore destinations to which they apparently return each year; and thirdly, crabs originating from any one area on the plateau tend to travel in a similar direction and thereby reach the shore terraces in proximity to one another. The northwestern shore is much calmer, so the larvae probably have a better chance of landing ashore there after 3 weeks in the ocean. If the chances of recruitment on the northwestern shore are indeed substantially higher then elsewhere, then selective pressure would act in favor of the crabs that return to breed to the same shore where they emerged as larvae, as proposed by Gibson-Hill (1947) and DeWilde (1973).

The mode of navigation used by the red crabs during their migration remains speculative, but this study clearly shows that the crabs do not simply walk "down" toward the ocean as was suggested by Gibson-Hill (1947). Magnetic orientation could certainly account for straight paths taken by the red crabs (Vannini and Chelazzi, 1981; Lohmann *et al.*, 1995). Some gecarcinid crabs are thought to orient themselves towards the bright horizon (Klaassen, 1975; Bliss *et al.*, 1978; Wolcott and Wolcott, 1982); however, although red crabs in the jungle are unable to see the horizon, they do nonetheless avoid entering darkened areas.

If the young crabs can benefit from, or even need to, follow the older crabs to find their way to the shore to breed, then the idea of the "inexperienced" crabs following the "older, more experienced" crabs, proposed by DeWilde (1973), would certainly increase the breeding success of the young individuals. Additionally, traveling in groups would be advantageous in synchronizing the breeding activities. Crabs originating from the Green site and from the Gold site had very similar degrees of dispersal at the coast despite having walked different distances (1.4 km and nearly 3 km respectively); such similarity could only be expected if they traveled as cohorts. Experiments to relocate crabs before and during the migration would provide useful information about the navigation mechanisms used by the red crabs.

A comparison of the two study seasons of 1993 and 1995 in Study Area 1 reveals a 3-week difference in the timing of the start of the downward migration in relation to the lunar phase. In contrast, the spawning date appeared to be very consistent and most predictable from the lunar phase (Fig. 6). The synchronization of the spawning activities of red crabs may be important in maximizing the chances of survival for the newly hatched larvae (Morgan and Christy, 1995). In 1995, the wavelike patterns in densities of crabs crossing through the density estimation grids may be partially attributed to the different distances that crabs may have to travel to reach any given point, but they were at least partially the result of different timing of the initial rainfall in the different parts of the Island (pers. obs.). The counting grids provide snapshot images of the numbers of crabs moving through various parts of the island and further support the conclusion, which was based on sightings of color-coded crabs, that red crabs preferentially migrate towards the northwestern shore.

The radio-tracking data revealed an important difference in the behavior of migrating crabs between the two study seasons. In 1993, the red crabs walked towards their shore destinations every day and walked relatively longer daily distances. In 1995, however, 10 out of 13 radio-tracked crabs made stops of 1 to 7 days duration at various locations before eventually arriving at the shore terraces. A consequence of this behavior is to minimize the duration of time that the entire island's red crab population is crowded on the shore terraces and the subsequent depletion of local food resources. Since the red crabs embark on their annual breeding migration immediately after the end of the dry season during which their feeding opportunities were greatly reduced (Green, 1993), early arrival of the monsoonal rains provides an opportunity for these animals to stop and feed during their downward migration. Furthermore, if the red crabs were "avoiding" reaching the terraces too early, this implies they "know" how long it will take to reach the shore and do not need to actually come in contact with the seawater to know when they have reached the coast (Hicks, 1985; Hicks *et al.*, 1990; Greenaway, 1994).

The red crabs quite clearly avoid open areas: most crabs would travel for some distance along the side of the road under the cover of vegetation before eventually crossing the road. This observation could explain the more erratic migratory routes of red crabs in the more disturbed part of the island (Fig. 10a, b). Although the red crabs do not have any predators that might take advantage of their exposure in the open, desiccation and elevation in body temperature can reduce endurance and maximum speed of travel (Weinstein and Full, 1994; Weinstein *et al.*, 1994); this behavior minimizes exposure to lower humidity and higher temperatures in the clearings. The walking speed of red crabs crossing the road in this study was very similar to the 5.4 $m \cdot min^{-1}$ reported previously (Hicks, 1985), but was about 4 times faster than the overall migration speed estimated from the radio-tracking data.

After *G. natalis* completes its annual breeding activities, most crabs leave the lowest shore terraces and return to the upper terraces and the plateau. At least some crabs appear to follow a route similar to the one they took during their downward migration and to move farther inland than their place of origin (*e.g.*, Fig. 10b).

The environmental conditions restricting activity, coupled to the breeding biology of *G. natalis*, require the crabs to undertake a long migration after an extended period of relative inactivity. The breeding season, which can last from 3 to 6 weeks, represents the most active period of the year for the red crabs. Such varied activity levels impose quite different physiological demands on the animals. To assess the demands of the migration, we have also examined metabolic fuel stores, metabolic status, and capacity to maintain locomotion in red crabs during their migratory activities (Adamczewska and Morris, 2001).

Acknowledgments

This work is dedicated to the memory of Dr. Holger Rumpff, without whose enthusiasm, energy, and friendship these studies would not have been possible. We would like to thank the Government Conservator, Grahame Beech, as well as the staff of ANCA (Parks Australia) for their assistance and hospitality. Special thanks go to Max Orchard and Roger Hart. Part of this work was carried out and reported as an ANCA consultancy. We are especially indebted to all the volunteer "crab painters and spotters" for their assistance. We also thank Prospectors Supplies Pty. Ltd. for the donation of compasses, King Gee Clothing Pty. Ltd for work clothes, and Zeus Chemical Products Pty. Ltd for the nontoxic marking paints.

Literature Cited

Adamczewska, A. M., and S. Morris. 2001. Metabolic status and respiratory physiology of *Gecarcoidea natalis*, the Christmas Island red crab, during the annual breeding migration. *Biol. Bull.* **200:** 321–335.

Andrews, C. W. 1900. *Monograph of Christmas Island (Indian Ocean).* British Museum (Natural History), London.

Bliss, D. E., J. Van Montfrans, M. Van Montfrans, and J. R. Boyer. 1978. Behavior and growth of the land crab *Gecarcinus lateralis* (Fréminville) in southern Florida. *Bull. Am. Mus. Nat. Hist.* **160:** 111–152.

Daumer, K., R. Jander, and T. H. Waterman. 1963. Orientation of the ghost-crab *Ocypode* in polarized light. *Z. Vgl. Physiol.* **47:** 56–76.

Deutschlander, M. E., J. B. Phillips, and S. C. Borland. 1999. The case for light-dependent magnetic orientation in animals. *J. Exp. Biol.* **202:** 891–908.

DeWilde, P. A. W. J. 1973. On the ecology of *Coenobita clypeatus* in Curaçao. *Stud. Fauna Curaçao Other Caribb. Isl.* **144:** 1–138.

Garth, J. S. 1948. The brachyura of the "Askoy" expedition. *Bull. Am. Mus. Nat. Hist.* **92:** 1–66.

Gherardi, F., and M. Vannini. 1989. Spatial behaviour of the freshwater crab, *Potamon fluviatile*: a radio-telemetric study. *Biol. Behav.* **14:** 28–45.

Gherardi, F., F. Tarducci, and M. Vannini. 1988. Locomotor activity in the freshwater crab *Potamon fluviatile*: The analysis of temporal patterns by radio-telemetry. *Ethology* **77:** 300–316.

Gibson-Hill, C. A. 1947. Field notes on the terrestrial crabs. *Bull. Raffles Mus.* **18:** 43–52.

Gifford, C. A. 1962. Some observations on the general biology of the land crab, *Cardisioma guanhumi* (Latreille) in South Florida. *Biol. Bull.* **123:** 207–223.

Gray, H. S. 1995. *Christmas Island Naturally.* Scott Four Colour Print, Perth, Western Australia. Pp. 11–145.

Green, P. T. 1993. The role of Red Land Crabs in structuring rain forest on Christmas Island, Indian Ocean. Ph.D. thesis, Monash University, Clayton, Victoria.

Green, P. T. 1997. Red crabs in rain forest on Christmas Island, Indian Ocean: activity patterns, density and biomass. *J. Trop. Ecol.* **13:** 17–38.

Greenaway, P. 1994. Salt and water balance in field populations of the terrestrial crab *Gecarcoidea natalis*. *J. Crustac. Biol.* **14:** 435–453.

Herrnkind, W. F. 1968. Adaptive visually-directed orientation in *Uca pugilator*. *Am. Zool.* **8:** 585–598.

Hicks, J. W. 1985. The breeding behaviour and migrations of the terrestrial crab *Gecarcoidea natalis*. (Decapoda: Brachyura). *Aust. J. Zool.* **33:** 127–142.

Hicks, J., H. Rumpff, and H. Yorkston. 1990. *Christmas Crabs.* Golden Earth Design and Printing, Singapore.

Klassen, F. 1975. Ecological and ethological studies on the reproductive biology of *Gecarcinus lateralis* (Decapoda, Brachyura). *Forma Functio* **8:** 101–174.

Lake, P. S., and D. J. O'Dowd. 1991. Red crabs in rain forest, Christmas Island: biotic resistance to invasion by an exotic snail. *Oikos* **62:** 25–29.

Lohmann, K. J., N. D. Pentucheff, G. A. Newitt, G. D. Stetten, R. K. Zimmer-Faust, H. E. Jarrard, and L. C. Boles. 1995. Magnetic orientation of spiny lobsters in the ocean: Experiments with undersea coil systems. *J. Exp. Biol.* **198:** 2041–2048.

Micheli, F., F. Gherardi, and M. Vannini. 1990. Growth and reproduction in the freshwater crab, *Potamon fluviatile* (Decapoda, Brachyura). *Freshwater Biol.* **23:** 491–503.

Morgan, S. G., and J. H. Christy. 1995. Adaptive significance of the timing of larval release by crabs. *Am. Nat.* **145:** 457–479.

O'Dowd, D. J., and P. S. Lake. 1989. Red crabs in rain forest, Christmas Island: Removal and relocation of leaf-fall. *J. Trop. Ecol.* **5:** 337–348.

Pinder, A. W., and A. W. Smits. 1993. The burrow microhabitat of the land crab *Cardisoma guanhumi*: Respiratory/ionic conditions and physiological responses of crabs to hypercapnia. *Physiol. Zool.* **66:** 216–236.

Vannini, M., and S. Cannicci. 1995. Homing behaviour and possible congitive maps in crustacean decapods. *J. Exp. Mar. Biol. Ecol.* **193:** 67–91.

Vannini, M., and G. Chelazzi. 1981. Orientation of *Coenobita rugosus* (Crustacea: Anomura): A field study on Aldabra. *Mar. Biol.* **64:** 135–140.

Weinstein, R. B. 1995. Locomotor behaviour of nocturnal ghost crabs on the beach: Focal animal sampling and instantaneous velocity from three-dimensional motion analysis. *J. Exp. Biol.* **198:** 989–999.

Weinstein R. B., and R. J. Full. 1994. Thermal dependence of locomotor energetics and endurance capacity in the ghost crab, *Ocypode quadrata. Physiol. Zool.* **67:** 855–872.

Weinstein R. B., R. J. Full, and A. N. Ahn. 1994. Moderate dehydration decreases locomotor performance of the ghost crab *Ocypode quadrata. Physiol. Zool.* **67:** 873–891.

Wolcott, T. G., and D. L. Wolcott. 1982. Larval loss and spawning behavior in the landcrab *Gecarcinus lateralis* (Freminville). *J. Crustac. Biol.* **24:** 477–485.

Wolcott, T. G., and D. L. Wolcott. 1985. Factors influencing the limits of migratory movements in terrestrial crustaceans. *Contrib. Mar. Sci. Suppl.* **27:** 257–273.

Reference: *Biol. Bull.* **200**: 321–335. (June 2001)

Metabolic Status and Respiratory Physiology of *Gecarcoidea natalis*, the Christmas Island Red Crab, During the Annual Breeding Migration

AGNIESZKA M. ADAMCZEWSKA[1,*] AND STEPHEN MORRIS[2]

[1]*Ocean Research Institute, University of Tokyo, 1-15-1 Minamidai, Nakano-ku, Tokyo 164-8639, Japan;*
and [2]*Morlab, School of Biological Sciences, Woodland Road, University of Bristol,*
Bristol BS8 1UG, UK

Abstract. With the arrival of the monsoonal rains and after months of inactivity during the dry season, the terrestrial crab *Gecarcoidea natalis* embarks on its annual breeding migration to the coast. The physiological demands of the migration were assessed by determining respiratory gases in the hemolymph, key metabolites, and energy stores in *G. natalis* during two migratory seasons. At the end of each day of migration the pulmonary hemolymph P_{O_2} decreased by 1-2.5 kPa, but the hemocyanin remained saturated with O_2 and the venous reserve was largely unchanged ($O_2 > 0.4$ mmol · l^{-1}). The breeding migration of red crabs was accomplished without recourse to anaerobiosis, even though at times walking speeds (up to 6.2 ± 0.5 m · min^{-1}) exceeded those that promoted anaerobiosis in non-migrating crabs and in crabs exercised in the laboratory. In contrast to all previous studies, at the end of each day of migrating, red crabs experienced an alkalosis (up to 0.1 pH units) rather than any acidosis. This alkalosis was removed overnight when the crabs were inactive.

Although there were seasonal fluctuations in the glycogen, glucose, and triglyceride stores, crabs engaging in the migration did not draw on these stores and must have fed along the way. In contrast, crabs returning from breeding activities on the shore terraces had significantly depleted glycogen stores. Additionally, in 1993, the male crabs returning from the breeding activities on the terraces were dehydrated and experienced a decrease in muscle tissue water of 11%. In contrast to the breeding migration *per se*, fighting for burrows in which breeding occurs produced severe anaerobiosis in males, especially the victors: after 135 s of combat, the maximum L-lactate concentration in the hemolymph was 35 mmol · l^{-1}. It appears that burrowing, courtship, and mating are more demanding than the migration itself. Furthermore, the data provide evidence that the metabolic responses of migrating individuals of *G. natalis* might be different from those at other times of the year.

Introduction

All terrestrial gecarcinid crabs must migrate to the coast to release their eggs into the ocean (Gibson-Hill, 1947; Gifford, 1962; Klaassen, 1975; Wolcott, 1988; Adamczewska and Morris, 2001). However, the annual breeding migration of *Gecarcoidea natalis*, the Christmas Island red crab, is unique among the gecarcinid crabs for a number of reasons. Red crabs live further inland than most other gecarcinids (*e.g.*, Bliss *et al.*, 1978; Wolcott and Wolcott, 1985) and must thus travel farther to reach the coast. Furthermore, the red crabs undertake their migration during daytime, immediately after the arrival of the monsoonal rains and following extended periods of inactivity during the dry season. Since the migration is closely synchronized with the lunar cycle, when the rains in some years arrive late, the red crabs may have to make their downward migration in a relatively short period of time if they are to complete their burrowing and courtship activities. The red crabs may have to travel more than 4–5 km in 5–6 days during "rushed migrations" (Adamczewska and Morris, 2001).

The severity of exercise is often determined by measurements of metabolic rate as well as acid-base status and key metabolites in the hemolymph and muscle tissue. An exten-

Received 23 April 1999; accepted 20 February 2001.

[*] To whom correspondence should be addressed. E-mail: ishka@ori.u.tokyo.ac.jp

sive body of literature demonstrates that most crustaceans, including red crabs, tend to have low aerobic scope and rely on anaerobiosis to partially support locomotor activity (*e.g.*, review: McMahon, 1981; Booth and McMahon, 1985; Head and Baldwin, 1986; Herreid and Full, 1988; Greenaway *et al.*, 1988; Forster *et al.*, 1989; van Aardt, 1990; Henry *et al.*, 1994; Adamczewska and Morris, 1994b, 1998a). During their migration, red crabs must sustain locomotion for up to 6 consecutive days to reach the shore terraces where the males construct and defend burrows and engage in mating activities (Hicks *et al.*, 1990; Green, 1993, 1997; Adamczewska and Morris, 2001).

Laboratory studies of exhausting locomotion revealed information about the respiratory physiology of the crabs and indicated that they have no exceptional exercise ability (Adamczewska and Morris, 1994a, b). The gills and lungs of *G. natalis* are involved in gas exchange to different degrees, depending on the severity of exercise (Adamczewska and Morris, 1994a, 1998a; Farrelly and Greenaway, 1994). During exercise, *G. natalis* experienced the classical respiratory and metabolic perturbations found in other crustaceans during exercise; that is, hemolymph acidosis, increased ventilation and heart rate, and elevated glucose and L-lactate concentrations (Wood and Randall, 1981b; Booth *et al.*, 1984; Herreid and Full, 1988; van Aardt 1990; Henry *et al.*, 1994; Thorpe *et al.*, 1995). The aerobic scope of red crabs was surprisingly poor, implying little scope for increased locomotion; despite the fact that the hemocyanin remains saturated with O_2 when leaving the gas exchange surfaces, *G. natalis* accumulated very high levels of lactate during exercise in the laboratory (Adamczewska and Morris, 1994b).

Intermittent locomotion can increase the total distance walked before the onset of fatigue in ghost crabs (Weinstein and Full, 1992) and thus could present an important locomotor strategy for migrating crabs. However, red crabs in the laboratory incurred greater respiratory and metabolic perturbations during enforced intermittent locomotion than during continuous exercise (Adamczewska and Morris, 1998a). The crabs became anaerobic even though their walking speeds were within the range recorded for red crabs during the migration (Adamczewska and Morris, 2001).

On Christmas Island, seasonal differences in respiratory status and metabolite concentrations in free-ranging red crabs were related primarily to a higher level of basal activity in the crabs during the wet season (Adamczewska and Morris, 2000). When required to walk for 5 min, non-migrating crabs responded to exercise in essentially the same way during both the wet and the dry seasons. The responses of the crabs to non-exhausting exercise in the field during either season were comparable to those in the laboratory studies (Adamczewska and Morris, 1998a; 2000) and did not help explain how this species completes the annual breeding migration. The conditions and circumstances of the migration cannot be simulated in the laboratory nor replicated outside of the migration season. Thus, understanding the physiological processes involved and the consequences for migrating red crabs could only be addressed by making determinations *in situ* as the crabs journeyed to the ocean to breed.

The migration is the most intense period of activity during the year. Its physical demands immediately follow prolonged periods of inactivity during the dry season, when the crabs may spend up to 2 months in their burrows (Green, 1993). This abrupt change in activity levels demands a sudden change in energy metabolism and is compounded by the fact that the red crabs have reduced foraging opportunities because of the unfavorable environmental conditions during the dry season. Because the migratory activities are energetically demanding, they may require the use of stored metabolic fuels. Indeed, crustaceans are known to have substantial lipid and glycogen reserves in the midgut gland and in muscle tissues, which are utilized during starvation (*e.g.*, Parvathy, 1971; Pillay and Nair, 1973; Gibson and Barker, 1979; review: Chang and O'Connor, 1983; Nishida *et al.*, 1995).

G. natalis appears to have no superior locomotor abilities compared to other crabs, and this raises a number of questions. Primarily, is there a significant change in the respiratory physiology and metabolism at the onset of the migration, such that a different exercise regime can be supported? This could include, for example, tolerating an exceptional diurnal anaerobiosis and O_2 debt. Is prolonged locomotion facilitated by a reliance on stored fuels? Do the migrating crabs tolerate physiological perturbations such as dehydration and acidosis that limit their behavior at other times? These factors could circumscribe the potential migratory strategy of this species. Do the male crabs attempt to reach the terraces as fast as possible to obtain the best places for burrowing, arriving in less than peak condition? Alternatively, do they take more time to complete the downward migration—thus arriving at the shore terraces fit for combat, with ample energy stores—and then attempt to displace already resident crabs from their burrows?

The comprehensive description of the red crab migration (Adamczewska and Morris, 2001) provided a context for the first field investigation of the respiratory physiology and metabolism of migrating terrestrial crabs. The field investigations were carried out on Christmas Island during two migrations as well as in the inter-migratory period to assess annual as well as seasonal differences. Metabolites were measured in the hemolymph and muscle of migrating crabs during breeding activities and after the migration. The function and functioning of the respiratory and circulatory systems in gas exchange and transport were also determined. Stores of metabolic energy were quantified at various stages of the migration, and their importance in facilitating the migration and the associated breeding activities was as-

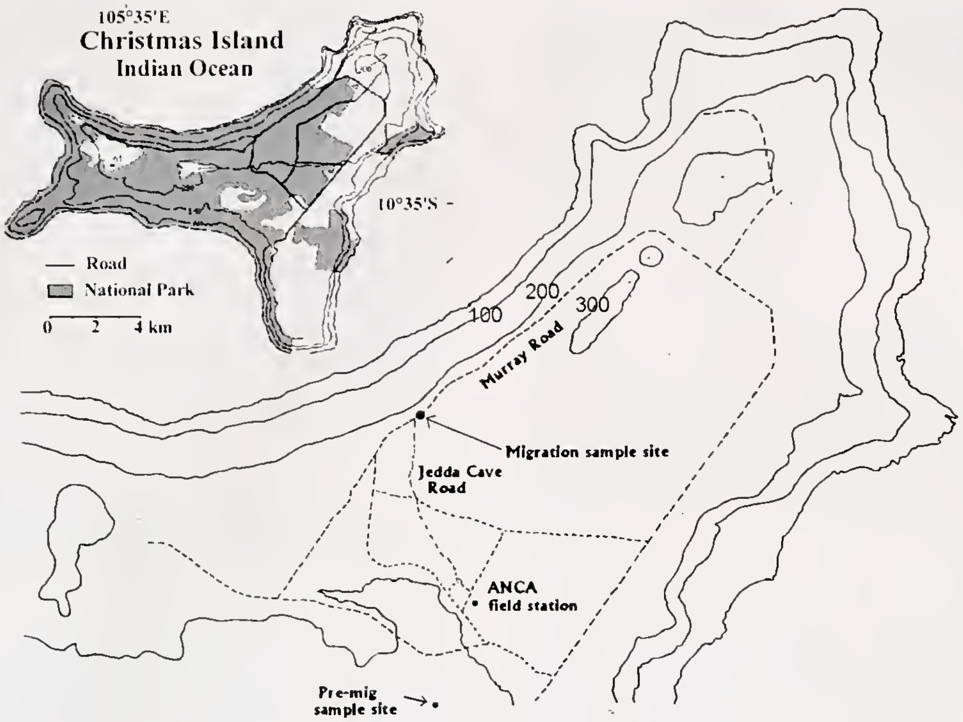

Figure 1. Map of Christmas Island showing the location of the ANCA (Parks Australia) field station and the locations of sampling sites prior to the start of the migration and during the migration.

sessed. The data were interpreted together with the behavioral and ecological information to provide a model for migrating individuals of *G. natalis.*

Materials and Methods

Respiratory gas and acid-base status in the hemolymph

Red crabs (*Gecarcoidea natalis*) were sampled in the field during two migration seasons (November and December) of 1993 and 1995. To assess the functioning of the respiratory surfaces and the circulatory system in gas exchange and transport to and from the tissues, hemolymph was sampled at various times and analyzed for respiratory gases and pH. Hemolymph was sampled from three groups of crabs in 1993 and from two groups in 1995. In 1993 the first group of crabs was sampled at the end of the dry season prior to the start of the migration, during the limited amount of time when they were found outside of their burrows (n = 12: 6 males and 6 females). The study site for this group was a 5-min drive from the ANCA (Parks Australia) Field Station ('Pre-mig study site': Fig. 1). In 1995 the migration of the red crabs commenced earlier than expected (Adamczewska and Morris, 2001), and thus it was not possible to obtain samples from resident red crabs in the immediately pre-migratory condition.

The remaining sample groups were composed of crabs migrating down to the coast. Two groups were sampled during both the 1993 and 1995 downward migration at the same site located on Murray Road near the junction of Jedda Cave Road (Fig. 1). Crabs sampled before sunrise, after "sleeping" the whole night, were designated as the morning, or "AM", group. Red crabs become immobile and unresponsive at night and "sleep" with their eyestalks folded down. The second group, referred to as the "PM" group, consisted of crabs sampled in the afternoon, at about 1630, after they had been walking for most of the day (Adamczewska and Morris, 2001) and had crossed Murray Road towards the shore terraces and the coast. In 1993 the AM and PM samples were taken on each of 5 days, and thus $n = 5$ for each group; in the slower migration of 1995, $n = 9$ for each of AM and PM sample groups. Hemolymph was sampled from large individuals of both sexes, but most often from male crabs (Adamczewska and Morris, 2001).

Three types of hemolymph were sampled from each crab: pulmonary (300 μl from the post-pulmonary vessel, hemolymph leaving the lungs); arterial (500 μl from the pericardial cavity, a mixture of post-pulmonary and post-branchial hemolymph); and venous hemolymph (700 μl from the venous sinus at the base of the last walking leg). The samples were analyzed for O_2 content ($[O_2]$) and partial pressure (Po_2), CO_2 content ($[CO_2]$), and pH at the ANCA Field Station as described previously by Adamczewska and Morris (1996). An aliquot of the remaining hemolymph was deproteinized with $HClO_4$ (0.6 mol $\cdot$ l^{-1}, ratio 1:1) and neutralized with 2.5 mol · l^{-1} K_2CO_3 for analysis of L-lactate. The deproteinized sample and the remainder of whole hemolymph were stored frozen until further analysis of metabolites, calcium, and osmotic pressure (see below). The percentage of Hc-O_2 saturation was determined as described previously by Adamczewska and Morris (1996).

Metabolites, metabolic fuels, and hydration state of the hemolymph and tissues

Glucose, L-lactate, and urate were measured in the hemolymph and leg muscle tissue to assess the extent of anaerobiosis and accelerated glycolysis in the crabs during the migration. Additionally, glycogen and lipids (triglycerides) were measured in the midgut gland (MGG) and the leg muscle as indices of metabolic fuel reserves. Hemolymph [Ca] was measured as an index of exoskeleton decalcification, which can be important in providing HCO_3^- base from $CaCO_3$ in response to acidosis (*e.g.*, Henry *et al.*, 1981).

Sampling protocol. Samples of leg muscle, MGG, and venous hemolymph were collected from free-ranging male and female red crabs prior to the start of the migration (n = 6 males and 6 females) during the 1993 migration season. Leg muscle tissue and venous hemolymph were collected each day of the downward migration in both 1993 and 1995: in the morning before sunrise (AM, n = 4) and in the afternoon at about 1630 (PM, n = 4). To minimize the number of sacrificed animals, samples of the MGG were taken only from the PM group.

During the 1995 season, no samples could be taken from crabs prior to the start of the migration; however, to provide a comparison, samples were taken from non-migrating crabs on the 10th day of the downward migration (color-coded crabs that did not leave their home ranges: Adamczewska and Morris, 2001).

Muscle, MGG, and hemolymph samples were also taken from crabs that had arrived at the lowest shore terraces but had not yet begun breeding activities (terrace: n = 8). Male (n = 8) and female (n = 8) red crabs were sampled during their respective return migrations from the shore terraces to the plateau, during both migration seasons. The site of sampling for the crabs returning from the terraces was the same as for the downward migration (Fig. 1).

Samples of the MGG and leg muscle were also taken from crabs during the times of the year when the crabs were not involved in breeding activities: in June 1994 (the middle of the dry season) and in February 1995 (the wet season—2 months after breeding activities ended). These samples were analyzed for energy stores in the form of glycogen and triglycerides (see below).

Hemolymph analysis. In the laboratory, hemolymph samples were analyzed for L-lactate (Boehringer Mannheim test kit #138 084), glucose (Sigma Diagnostics test-kit #510), and urate (Sigma Diagnostics test kit #685). Osmotic pressure was determined using a vapor-pressure osmometer (Wescor 5100C) calibrated with two precision standards, 290 and 1000 mOsm, containing NaCl. The concentration of Ca in the hemolymph was measured with an atomic absorption spectrophotometer (GBC 906, Melbourne). To suppress interference, samples and standards were diluted with 7.2 mmol · l^{-1} $LaCl_3$.

Tissue extraction and analysis. Leg muscle tissue was obtained by encouraging a crab to autotomize the second walking leg. The muscle tissue from the leg was immediately removed (~0.3 g) and deposited into a preweighed tube with 2 ml of ice-cold $HClO_4$ (0.6 mol · l^{-1}) to deproteinize the sample. The vials with the muscle tissue were weighed and then homogenized with an OMNI 1000 homogenizer (6-mm generator) and frozen until further processing and analysis (see below). Muscle tissue was also removed from another leg, weighed, and dried in an oven at 60 °C; the dry weight was recorded and the percentage of tissue water calculated.

Crabs were weighed and anesthetized by cold narcosis before removal of the MGG. The carapace was lifted and all of the MGG removed and weighed. One portion of the MGG was deproteinized in a preweighed tube with 2 ml of ice-cold $HClO_4$ (0.6 mol · l^{-1}) and homogenized in the field for later analysis. A second portion of MGG was set aside for triglyceride analysis. The remainder of the MGG was weighed and dried in an oven at 60 °C; the dry weight was recorded and the percentage of tissue water calculated. All samples to be analyzed for metabolites, lipids, and ions were kept frozen and transported on dry ice.

In the laboratory, muscle and MGG samples previously deproteinized with $HClO_4$ were homogenized with a glass homogenizer (Wheaton type) to obtain a finer homogenate. The homogenates were centrifuged in a refrigerated centrifuge for 15 min at 5300 × g, the supernatant was removed, and the pellet was resuspended in 0.7 ml of 0.4 mol · l^{-1} $HClO_4$ and centrifuged again. The second supernatant was removed and pooled with the first; the combined supernatant was neutralized with 0.8 ml of K_2CO_3 (3.75 mol · l^{-1}) and kept in an ice bath for 1 h. After another centrifugation, the final supernatant was removed and used for analysis. The concentrations of metabolites in the muscle tissue were expressed as millimoles per kilogram of wet tissue mass.

The deproteinized and neutralized leg muscle samples were analyzed for L-lactate (Boehringer Mannheim test kit #138 084). Additionally, the samples from both leg muscle and MGG samples were analyzed for glucose and glycogen by using a modified method described in Bergmeyer (1985). Briefly, amyloglucosidase (Boehringer Mannheim Cat. #208 469) made up to ≥ 10 kU · l^{-1} in an acetic acid buffer at pH 4.8 was used to hydrolyze glycogen into glucose during a 2-h incubation, with shaking, at 40 °C. At the end of the incubation the enzyme was denatured by addition of 0.6 mol · l^{-1} $HClO_4$. The solution was centrifuged at

10,000 × g for 10 min and the supernatant used for glucose analysis. For each sample, free glucose was also measured and subtracted from the glucose content obtained from the glycogen digestion.

Frozen MGG samples were analyzed for triglycerides by first homogenizing a sample with an equal mass of gum arabic (Sigma Catalog #G-9752) and 15 parts of bovine serum albumin (6% w/v Boehringer Mannheim Catalog #100-030) in a fine glass homogenizer (Wheaton type) at 55 °C. This homogenate was then diluted 1:10 with 6% w/v bovine serum albumin and used for triglyceride analysis (Sigma test kit #334-A). Triglyceride levels in the muscle tissue of red crabs were not detectable by this method.

Terrace activities

During the 1995 migration, concentrations of lactate, glucose, and urate were measured in the hemolymph as indicators of anaerobiosis and the intensity of male combat. Only male-male interactions involving physical contact were considered. Male crabs on the shore terraces were observed and if a fight was noticed, its duration was recorded. Fights lasting less than 10 s were not considered. The fight was considered to have ended when the victor remained in possession of the burrow and the loser retreated or was chased away by the other opponent. At this point both crabs were promptly captured (within 5 s) and hemolymph was withdrawn from the venous sinus by puncturing the arthrodial membrane. The design of the experiment dictated that fights could be used only if they occurred near the observer and only if they were observed from start to finish. A total of 14 fighting pairs were sampled over 4 days of breeding activities on the terraces. Hemolymph samples were also taken from six male crabs resting at the entrance of their burrows; these were used to determine the basal metabolite status of male crabs on the terraces during the breeding activities. The hemolymph samples were treated and stored as described above and analyzed in Sydney for glucose, L-lactate, and urate.

Statistical analysis

The data were tested for homogeneity of variances using Bartlett's χ^2 test, and any heterogenous data were log- or square-root transformed. Respiratory gas data were analyzed using two-factor ANOVA for the three hemolymph types (pulmonary, arterial, and venous) and the different sampling groups in each season. Seasonal differences between the AM and PM groups were also examined by ANOVA.

Statistical analyses on tissue and hemolymph metabolites and on water and ion measurements between the AM and PM samples for the days of downward migration were carried out by two-factor ANOVA. If no difference between the AM and PM groups was detected, then the data were pooled for each day for further analysis by ANOVA. Analyses between tissue types and between the two sampling seasons were also carried out where appropriate. *Post hoc* testing was done using the Tukey HSD multiple comparison test. All analyses were performed using the Systat for Windows 5.0 statistical package. The samples from fighting males were analyzed by analysis of co-variance (ANCOVA). Significance level was taken as $P = 0.05$ in all cases. All data are presented as mean ± SEM.

Results

There were no differences in hemolymph respiratory gases, acid-base balance, metabolite concentrations, or energy stores of male compared with female crabs at the end of the dry season in 1993. Therefore, these data were pooled and from here on are referred to as the "resident pre-mig" group.

Oxygen in the hemolymph

The $P_{\mathrm{p}}\mathrm{o}_2$ [efferent pulmonary oxygen partial pressure ($P\mathrm{o}_2$)] was consistently higher than the $P_{\mathrm{a}}\mathrm{o}_2$ (arterial $P\mathrm{o}_2$) in both 1993 and 1995 (Fig. 2). The $P_{\mathrm{v}}\mathrm{o}_2$ (venous $P\mathrm{o}_2$) was always lower than the $P_{\mathrm{a}}\mathrm{o}_2$ and the $P_{\mathrm{p}}\mathrm{o}_2$. During the 1995 migration, the hemolymph $P\mathrm{o}_2$ of the PM group was statistically lower than in the AM group (Fig. 2). In 1993, although the $P\mathrm{o}_2$ in the pulmonary hemolymph (8.26 ± 2.20 kPa) of the AM group was 3.5 kPa higher than in the PM group (Fig. 2), there was no overall statistical difference between the crabs in these two groups.

The O_2 content ($[O_2]$) of the hemolymph was similar in both migration seasons (Fig. 3). The O_2 content of pulmonary hemolymph ($[O_2]_p = 1.13$ and 0.96 mmol $\cdot\, l^{-1}$ in 1993 and 1995 respectively) was very similar to the arterial values, but $[O_2]$ in venous hemolymph decreased significantly, to about 0.50 mmol $\cdot\, l^{-1}$, in both seasons. The AM group sampled during the 1993 migration season was an exception because the arterial $[O_2]$ was significantly lower than the pulmonary hemolymph concentration. Additionally, in 1993, the $[O_2]_v$ in the AM group was significantly greater than in the pre-mig group (Fig. 3).

The saturation of hemocyanin (Hc) with O_2 varied between samples in a manner similar to that of the $[O_2]$. The O_2 saturation of the pulmonary hemolymph was high (mean = 102 ± 6%) and similar to the Hc saturation of arterial hemolymph except in the AM group of 1993, in which the arterial hemolymph was only 74% saturated. In comparison, the mean Hc-O_2 saturation of venous hemolymph decreased significantly in both seasons, to 43% in 1993 and 63% in 1995 ($P < 0.001$).

Carbon dioxide content and pH of the hemolymph

The pH of pulmonary, arterial, and venous hemolymph was similar within each group of red crabs sampled (Fig. 4);

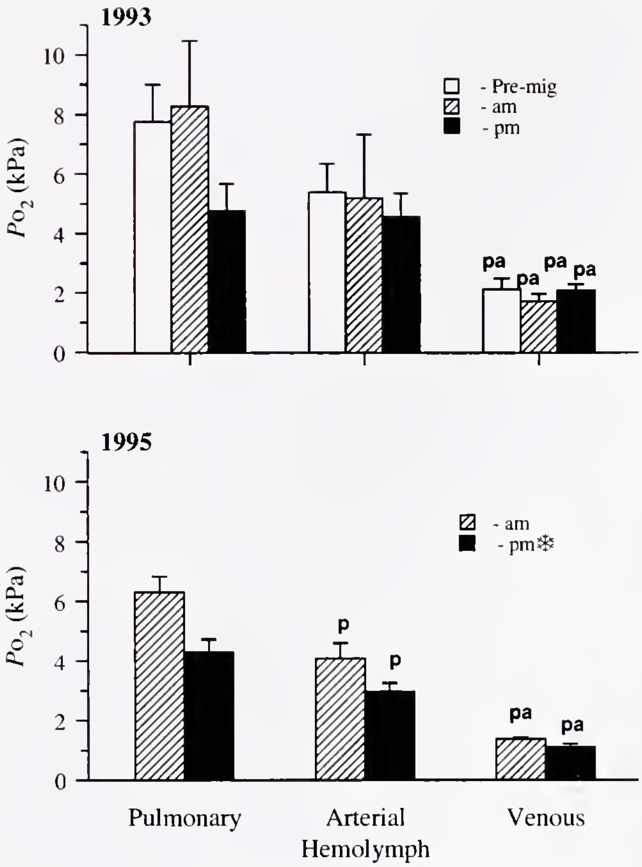

Figure 2. Oxygen partial pressure (Po_2, kPa) in the pulmonary, arterial, and venous hemolymph of *Gecarcoidea natalis* during two migration seasons, 1993 (top panel) and 1995 (bottom panel). Morning and afternoon groups were sampled during both migration seasons ($n = 5$ in 1993; $n = 9$ in 1995). Top panel (1993 season) includes measurements of Po_2 in crabs sampled 1 week prior to the start of the migration (pre-mig $n = 12$). The letters "p" and "a" indicate that the mean is significantly different from that of pulmonary or arterial hemolymph respectively, within a sample group. The ❄ symbol next to the legend indicates a significant difference between the AM and the PM groups.

thus, for further analysis between groups, the pH for the three hemolymph types was pooled for each sample group. The resident pre-mig red crabs in 1993 had a mean hemolymph pH of 7.61 ± 0.03, which decreased significantly after the onset of the migration to near 7.4 (Fig. 4). Most interestingly, the hemolymph was more acidic in crabs sampled in the morning (AM pH = 7.35 ± 0.07) than in crabs sampled in the afternoon (PM pH = 7.46 ± 0.06, $P < 0.001$). A similar alkalosis at the end of the day of migration was seen in 1995 (AM-PM difference of 0.042 pH units) but was less significant than during 1993 ($P = 0.068$; Fig. 4).

There was no difference in hemolymph CO_2 content ($[CO_2]$) between pulmonary, arterial, and venous samples within any one group of red crabs sampled (Fig. 5). During 1993, the $[CO_2]$ in the hemolymph of migrating crabs was significantly greater than in the resident pre-mig crabs (mean $[CO_2] = 9.8 \pm 0.8$ mmol · l^{-1}). In addition, the $[CO_2]$ in the hemolymph of the PM group was significantly greater than that of the AM group; the concentration was 3.3 mmol · l^{-1} higher in 1993 and 1.7 mmol · l^{-1} higher in 1995 (Fig. 5).

Hydration state of red crabs during migratory activities

There were no differences in the hydration state of crabs at the start and the end of a day walking; the AM and PM samples were thus pooled for each day. In the 1993 season the percentage of water in crab leg muscle was very stable during the entire downward migration (range 77.2%–78.3%) and, importantly, did not differ from that of the pre-migratory crabs (76.1% ± 0.4%). However, the male crabs returning from the shore terraces were dehydrated: the percentage of water in their muscle tissue was 11% lower

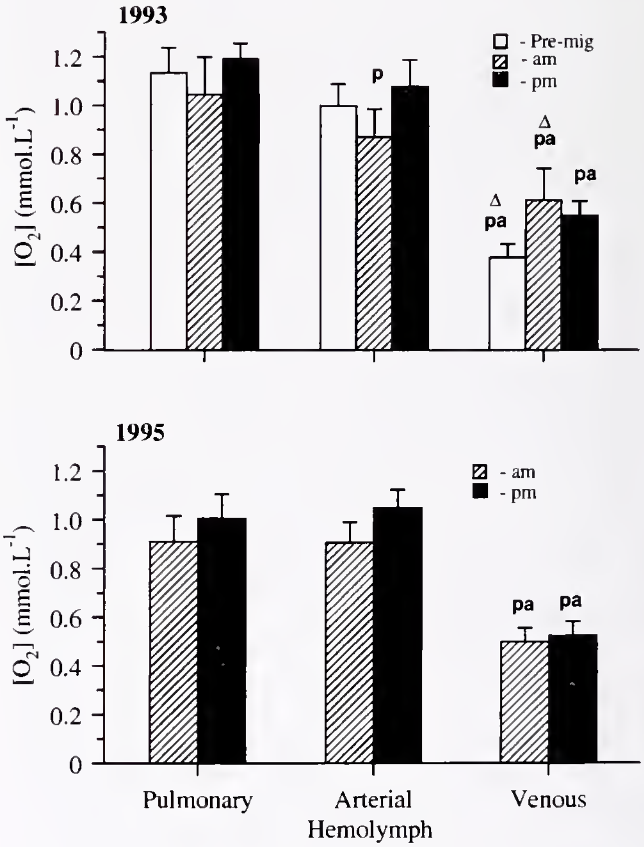

Figure 3. Oxygen content ($[O_2]$, mmol · l^{-1}) in the pulmonary, arterial, and venous hemolymph of *Gecarcoidea natalis* during two migration seasons, 1993 (top panel) and 1995 (bottom panel). Morning and afternoon groups were sampled during both migration seasons ($n = 5$ in 1993; $n = 9$ in 1995). Top panel (1993 season) also includes measurements of $[O_2]$ in crabs sampled 1 week prior to the start of the migration (pre-mig $n = 12$). The letters "p" and "a" indicate that the mean is significantly different from that of pulmonary or arterial hemolymph within a sample group. The pair of Δ symbols denote a significant difference in venous O_2 between the resident pre-mig and AM crabs.

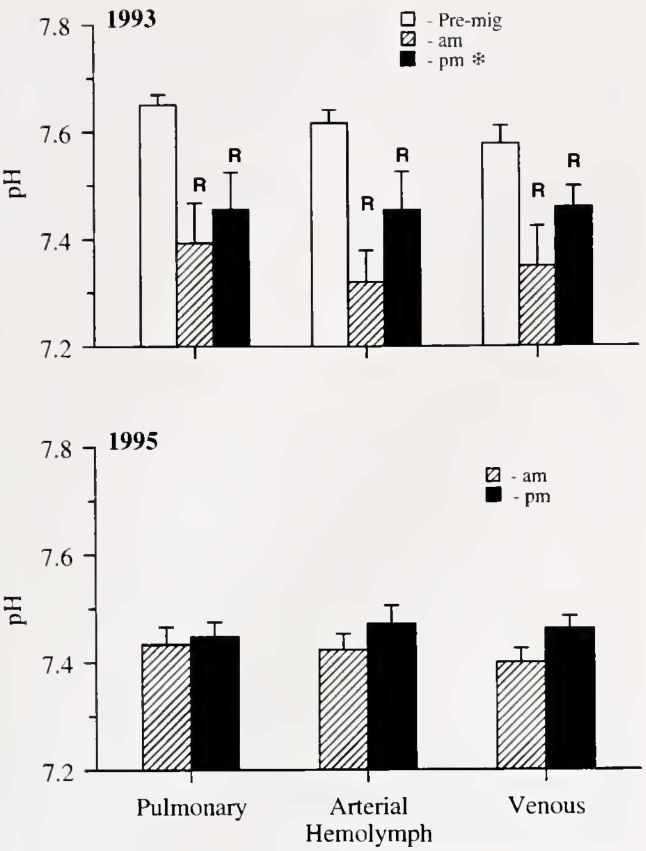

Figure 4. The hemolymph pH of pulmonary, arterial, and venous samples taken from *Gecarcoidea natalis* during two migration seasons, 1993 (top panel) and 1995 (bottom panel). Morning and afternoon groups were sampled during both migration seasons (n = 5 in 1993; n = 9 in 1995). Top panel (1993 season) also includes measurements of hemolymph pH in crabs sampled 1 week prior to the start of the migration (pre-mig n = 12). The ❄ symbol next to the legend indicates a significant difference between the AM and the PM groups. The "R" denotes a significant difference from the crabs at rest—that is, from the resident pre-mig crabs.

than in all the other groups sampled in that season. In contrast, during the 1995 migration season, both the returning male and female crabs had a significantly higher amount of water in muscle tissue (79.1%) than the crabs sampled during the downward migration (days 5–7; range 75.2%–76.9%).

The percentage of water in the MGG was more variable and significantly lower than in the muscle tissues, with a mean of 57.0% ± 1.5% during the 1993 migration and 61.7% ± 2.4% in 1995. Crabs that did not participate in the 1995 migration were unusual in that water constituted only 45.4% ± 1.8% of their midgut gland.

The osmotic pressure of the hemolymph was more variable than the percentage of water in the muscle tissue. The osmotic pressure in the hemolymph of the AM and PM groups on any one day was the same, and thus the data for each day were pooled for further analysis. The hemolymph osmotic pressure was largely constant during the downward migration of both the 1993 (771 ± 3 mOsm) and 1995 (803 ± 4) seasons; but in 1993 the osmotic pressure of crabs during the downward migration was significantly lower than that of the pre-mig crabs (815 ±7 mOsm) and the returning females (869 ± 14 mOsm). Additionally, in both 1993 and 1995 the returning males had lower osmotic pressure (mean 699 ± 16 mOsm) than did the crabs sampled during their downward migration.

Calcium and urate concentration in the hemolymph

The calcium concentration in hemolymph of resident pre-mig crabs (13.74 ± 0.42 mmol · l^{-1}) was significantly higher than in all the other groups sampled in 1993 (mean [Ca] = 9.29 ± 0.87 mmol · l^{-1}). During the 1995 migration

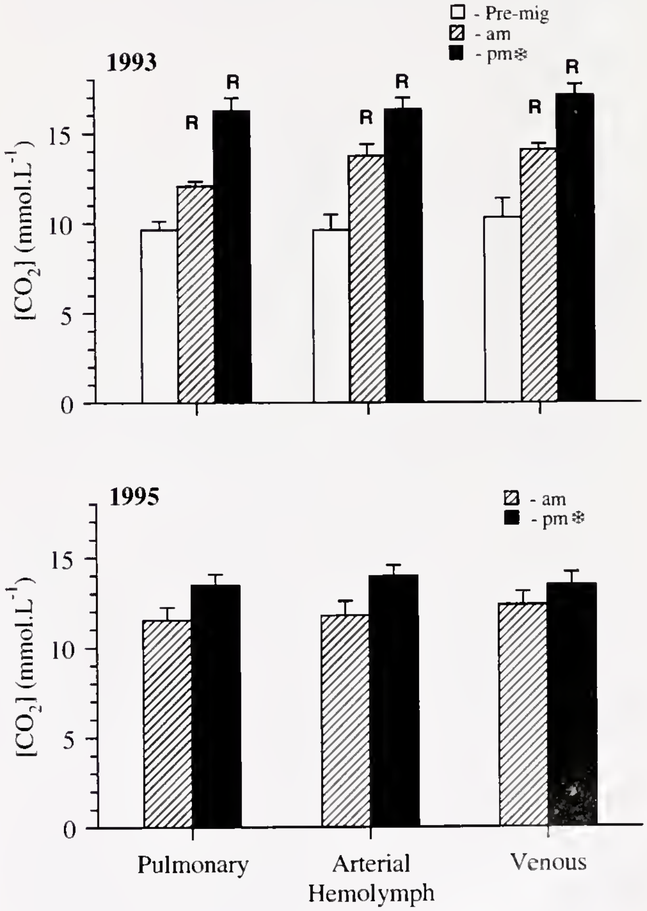

Figure 5. Carbon dioxide content ([CO_2], mmol · l^{-1}) in the pulmonary, arterial, and venous haemolymph of *Gecarcoidea natalis* during two migration seasons, 1993 (top panel) and 1995 (bottom panel). Morning and afternoon groups were sampled during both migration seasons (n = 5 in 1993; n = 9 in 1995). Top panel (1993 season) also includes measurements of [CO_2] in crabs 1 week prior to the start of the migration (pre-mig n = 12). The ❄ symbol next to the legend indicates a significant difference between the AM and the PM groups. The "R" denotes a significant difference of a sample group from the crabs at rest—that is, from the resident pre-mig crabs.

Table 1

L-lactate and glucose in the hemolymph and leg muscle tissue of Gecarcoidea natalis *during two migratory seasons, 1993 and 1995 (values given as mean ± SEM; sample size provided in parenthesis)*

	L-lactate				Glucose			
	1993		1995		1993		1995	
	Hemolymph	Leg muscle	Hemolymph	Leg muscle	Hemolymph	Leg muscle	Hemolymph	Leg muscle
pre-mig	1.8 ± 0.31 (12)	6.35 ± 1.22 (12)^{D}	—	—	0.44 ± 0.03 (12)	0.83 ± 0.09 (12)	—	—
AM	0.97 ± 0.34 (15)	1.00 ± 0.14 (15)	0.34 ± 0.17 (40)	2.83 ± 0.60 (20)	0.48 ± 0.04 (15)	0.26 ± 0.06 (15)	0.47 ± 0.08 (40)	0.24 ± 0.02 (20)
PM	1.10 ± 0.31 (25)	3.26^{I} ± 0.80 (25)	0.64 ± 0.18 (45)	3.11 ± 1.16 (25)	0.53 ± 0.07 (25)	0.28 ± 0.07 (25)	0.60 ± 0.11 (45)	0.35 ± 0.06 (25)
Terrace	0.91 ± 0.08 (8)	3.86 ± 0.55 (8)	0.14 ± 0.06 (8)	2.86 ± 0.45 (8)	0.85 ± 0.12 (8)^{R}♀♂	0.42 ± 0.06 (8)^{R}♀♂	0.42 ± 0.05 (8)	0.55 ± 0.20 (8)
Return male	1.26 ± 0.34 (8)♀	1.34 ± 0.56 (8)^{D}♀	0.35 ± 0.09 (8)	2.43 ± 0.88 (8)	0.38 ± 0.02 (8)	0.14 ± 0.03 (8)^{D}♀	0.35 ± 0.04 (8)	0.22 ± 0.04 (8)
Return female	1.69 ± 0.33 (8)♂	6.34 ± 1.30 (8)^{D}♂	0.30 ± 0.05 (8)	3.26 ± 0.88 (8)	0.48 ± 0.04 (8)	0.52 ± 0.12 (8)^{D}♂	0.32 ± 0.02 (8)	0.20 ± 0.04 (8)

^{R} Different from the crabs at rest—*i.e*, the resident pre-mig crabs.

^{D} Different from crabs engaged in the downward migration.

^{I} Increase in PM compared to AM.

♀ Different from the returning females.

♂ Different from the returning males.

season, the mean hemolymph [Ca] varied by up to 4.5 mmol · l^{-1} between the sample groups—that is, the AM and PM groups, males engaged in combat and breeding, and male crabs returning from the terraces—but these differences were not statistically significant.

Hemolymph urate was similar in both seasons, with an average concentration of 0.037 ± 0.005 mmol · l^{-1} in 1993 and 0.041 ± 0.006 mmol · l^{-1} in 1995. There were no statistical differences between any of the groups of red crabs sampled.

L-lactate and glucose in the hemolymph and muscle tissue

The concentration of L-lactate in the hemolymph generally remained low, less than 2 mmol · l^{-1} in 1993 and less than 1 mmol · l^{-1} in the 1995 season (Table 1), except in fighting males (see below).

The L-lactate concentration in the muscle tissue of migrating red crabs in 1993 was significantly lower than the 6.3 ± 1.2 mmol · kg^{-1} in the muscle of the pre-mig crabs (Table 1). Furthermore, in that year migrating crabs had a mean muscle L-lactate concentration that was low (1.0 ± 0.1 mmol · kg^{-1}) in the morning but increased slightly (to 3.3 ± 0.8 mmol · kg^{-1}) in the afternoon ($P < 0.001$). No such diel differences occurred in the 1995 migration season: the AM and PM crabs both contained lactate at close to 3 mmol · kg^{-1} (Table 1).

The glucose concentration in the hemolymph was below 1 mmol · l^{-1} in both seasons (Table 1). Red crabs descending to the terraces in 1993 had higher hemolymph glucose levels (0.85 ± 0.12 mmol · l^{-1}) than both the pre-migratory crabs (0.44 ± 0.04 mmol · l^{-1}) and the crabs sampled during their return migration (0.51 ± 0.06 mmol · l^{-1}, $P < 0.001$; Table 1). During the 1995 migration (mean [glucose] = 0.80 ± 0.09 mmol · l^{-1}) the variances of the data were severely heterogenous, and no significant differences could be detected between any of the sample groups (Table 1).

In the muscle tissue, the concentration of glucose was also less than 1 mmol · kg^{-1} during both seasons (Table 1). However, during 1993, the concentration in the leg muscle of the crabs engaged in the downward migration (0.29 ± 0.06 mmol · kg^{-1}) was lower ($P < 0.001$) than that in the resident pre-mig crabs (0.83 ± 0.09 mmol · kg^{-1}). The variances of the data collected during the 1995 migration were heterogenous, and it was not possible to detect any differences in glucose levels (Table 1).

Energy stores in the midgut gland and muscle tissues

Glycogen stores were measured as glucose units and expressed as concentration per wet weight of tissue. During the downward migration of 1995, leg muscle glycogen concentrations (69 mmol glucose · kg^{-1}) were about twice those of the crabs in 1993. The concentration of glycogen in the muscle of pre-migratory crabs in 1993 (31.6 ± 2.4

Table 2

Glucose and glycogen in the midgut gland of Gecarcoidea natalis *(values given as mean ± SEM; sample size provided in parenthesis)*

Day in relation to migration	1993 migration†		1995 migration		Non-migrating	
	Glucose†* ($\text{mmol} \cdot \text{kg}^{-1}$)	Glycogen† ($\text{mmol} \cdot \text{kg}^{-1}$)	Glucose* ($\text{mmol} \cdot \text{kg}^{-1}$)	Glycogen ($\text{mmol} \cdot \text{kg}^{-3}$)	Glucose ($\text{mmol} \cdot \text{kg}^{-1}$)	Glycogen ($\text{mmol} \cdot \text{kg}^{-1}$)
Non-mig Jun. 1994	—	—	—	—	9.65 ± 1.48 (8)#	0.95 ± 0.21 (8)‡
Non-mig Feb. 1995	—	—	—	—	3.83 ± 1.01 (8)#	12.14 ± 3.4 (8)‡
Pre-mig	17.81 ± 2.18 (12)	1.58 ± 0.35 (12)	—	—	—	—
5th day of mig	—	—	32.13 ± 7.11 (4)	18.36 ± 3.51 (4)	—	—
Non-mig (10th)	—	—	19.03 ± 1.82 (8)[D]	4.31 ± 0.34 (8)	—	—
11th day of mig	—	—	29.18 ± 7.95 (4)	19.02 ± 5.78 (4)	—	—
12th day of mig	—	—	25.68 ± 1.64 (4)	14.81 ± 2.55 (4)	—	—
Return male	8.92 ± 1.14 (8)	3.55 ± 0.99 (8)	13.44 ± 2.53 (8)	5.49 ± 0.96 (8)[D]	—	—
Return female	5.74 ± 0.88 (8)	0.55 ± 0.21 (8)	6.14 ± 0.84 (8)	8.22 ± 1.50 (8)[D]	—	—

[D] Different from crabs engaged in the downward migration.

† Difference between the two migration seasons.

* Difference between glucose and glycogen within a season.

# Two like symbols indicate a difference between the two groups.

‡ Two like symbols indicate a difference between the two groups.

mmol glucose · kg^{-1}) was significantly lower than that of red crabs during the downward migration (41.6 ± 5.7 mmol glucose · kg^{-1}). In both years, glycogen concentration in the muscle of both males and females had decreased significantly (to 14.2 ± 2.5 mmol glucose · kg^{-1} in 1993 and 24.9 ± 5.5 mmol glucose · kg^{-1} in 1995) by the time the crabs were sampled during their return migration.

The mean muscle glycogen concentration in crabs sampled during the dry season of June 1994 (17.6 ± mmol glucose · kg^{-1}) was just one-third of that measured in crabs during the wet season of February 1995.

The concentration of glycogen in the MGG was much lower than in the leg muscle, whereas the concentration of free glucose in the MGG was greater at all times (Table 2). The "total glucose" stores ([glucose] + [glycogen]) in the MGG during the 1995 migration season were consistently greater than in 1993 (Table 2).

The concentration of total glucose in the MGG of returning males (12.5 mmol · kg^{-1}) and returning females (5.7 ± 0.9 mmol · kg^{-1}) in 1993 was lower than that of crabs before the migration (19.4 mmol · kg^{-1}; Table 2). Similarly, in 1995 the returning males (19 ± 3 mmol · kg^{-1}) and females (14 ± 2 mmol · kg^{-1}) also had greatly reduced total glucose stores in the MGG compared with the crabs sampled during the downward migration (Table 2). There were otherwise no obvious seasonal trends in the total glucose stores in the MGG (Table 2).

The triglyceride content in the MGG of red crabs, measured as glycerol, did not change during the course of the migratory activities, and the mean concentration of triglycerides in the MGG was similar in both of the migration seasons (1993 mean = 247.3 ± 38.7 mmol glycerol · kg^{-1}, $n = 52$; 1995 mean = 234.8 ± 36.7 mmol glycerol · kg^{-1}, $n = 44$). There were seasonal differences in the triglyceride concentration of the MGG. The lowest levels were in samples collected in February 1995 (mean = 71.4 ± 6.6 mmol glycerol · kg^{-1}, $n = 8$), but triglycerides were considerably higher during the dry season in June 1994 (mean = 162.09 ± 22.6 mmol glycerol · kg^{-1}, $n = 8$). Nonetheless, the MGG triglycerides were lower during both of these seasons than during the actual migration.

Metabolite status in the hemolymph of male crabs after combat

Fights on the terraces occurred only between male crabs and were always for the possession of a burrow. Most of the fights on the terraces were very brief, less than 10 s, and thus were not used in this study. The duration of recorded fights varied between 18 and 135 s, with the majority lasting between 40 and 60 s.

The mean concentration of urate in the hemolymph was 0.043 mmol · l^{-1} and it did not increase in fighting crabs (Fig. 6A). Similarly, there was no difference in the hemolymph glucose concentration in crabs sampled at burrow entrances and immediately after a fight (Fig. 6B).

The mean concentration of L-lactate in the hemolymph of male crabs sampled at burrow entrances was high (7.4 ± 3.9 mmol · l^{-1}; Fig. 6C). Importantly, there was a significant increase in L-lactate in the hemolymph ($P < 0.01$) with increase in fight time, but only for the victorious crabs (Fig. 6C; ANCOVA and regression analysis). This increase can be described by the following equation [Lac] = time (s) × 0.25 − 3.20 ($r^2 = 0.71$). The maximum [L-lactate] in the

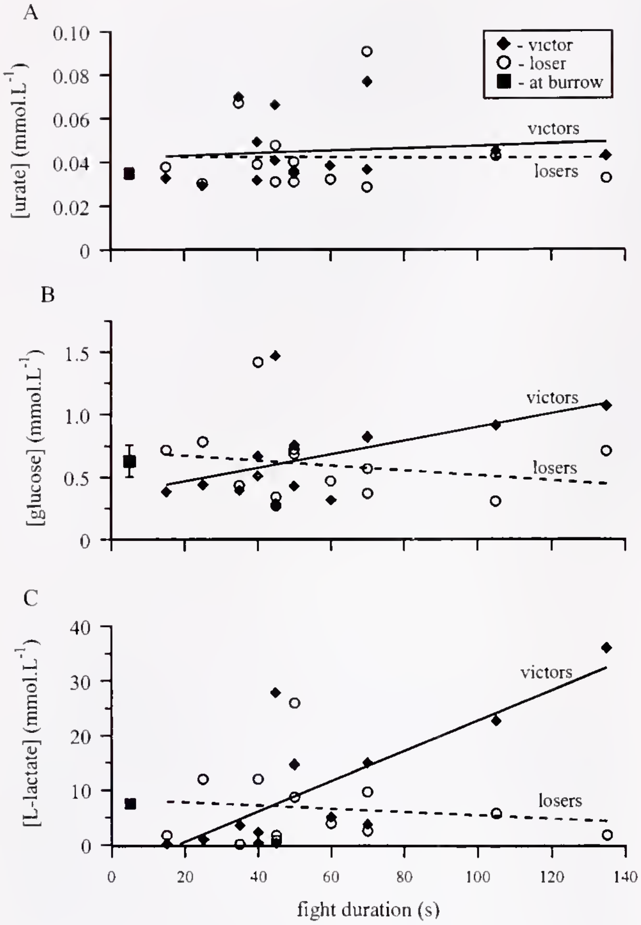

Figure 6. The concentration of (A) uric acid, (B) glucose, and (C) L-lactate (mmol · l^{-1}) in the hemolymph of male *Gecarcoidea natalis* guarding burrows during the breeding season (■) and immediately after combat, for losers (○) and victors (◆). Samples were taken from crabs engaged in physical fighting for possession of the burrows, and hemolymph metabolite concentration was plotted against the duration of the fight. The [L-lactate] was statistically dependent on fight duration in the victors but not the losers.

hemolymph of 35 mmol · l^{-1} was recorded after 135 s of combat for the crab that won.

Discussion

Christmas Island is composed largely of highly porous coral limestone with very little surface water outside of the wet season. Like other terrestrial crustaceans, the Christmas Island red crabs are prone to dessication and retreat into their burrows when humidity falls below 85% (Bliss *et al.*, 1978; Wolcott, 1992; Green, 1993, 1997). Dehydration has been shown to decrease locomotor capacity of some crustaceans (Weinstein *et al.*, 1994) and to interfere with respiratory gas transport in the hemolymph (Burggren and McMahon, 1981). The arrival of the monsoonal rains increases humidity, thereby creating more suitable conditions for activity above ground, and provides a cue for the start of the annual breeding migration of *Gecarcoidea natalis* (Hicks, 1985; Green, 1997; Adamczewska and Morris, 2001). During some years, when the monsoonal rains are late and an isolated shower triggers the migration, hemolymph osmolarity of 1100 mOsm has been recorded and the red crabs experience high mortality rates (Greenaway, 1994). The maintenance of hydration may be very important in determining the ability of the red crabs to undertake the breeding migration.

During the two migrations studied, the red crabs remained well hydrated. Although hemolymph osmolarity varied by up to 150 mOsm, the hydration state of leg muscle tissue generally varied by only 1%. The only sign of dehydration (11% decrease in muscle tissue water) was in the males during their return migration of 1993. These crabs had engaged in the strenuous activities of digging and defending their burrows during a 4-day period with no rain. The return migration of male crabs coincided with heavy rainfall, and although the male crabs were clearly drinking rain water, as seen by the hemodilution, they did not appear to rehydrate their muscle tissue before leaving the coastal terraces. A preferential defense of the extracellular over the intracellular fluid volume, previously reported for two gecarcinid species (Harris and Kormanik, 1981), may be a strategy limited to true land crabs (Taylor and Greenaway, 1994). Field studies using markers of extracellular fluid volume will be necessary to determine exact changes in hemolymph volume in migrating crabs (Harris and Andrews, 1982; Taylor and Greenaway, 1994).

Respiratory gas exchange in migrating crabs

The different durations of the migration in the two study years (5 days in 1993 *vs.* 21 days in 1995; Adamczewska and Morris, 2001) imposed very different physiological demands on the red crabs, but the respiratory changes the crabs experienced were remarkably similar. Previous inferences of the relative contribution of the gills and lungs in O_2 uptake by *G. natalis* have suggested both that the lungs are more important (Adamczewska and Morris, 1994a) and conversely that the gills and lungs play a comparable role (Adamczewska and Morris, 1998a; Farrelly and Greenaway, 1994). In both years studied here, the $P_{\mathrm{P}}\mathrm{O}_2$ of red crabs was consistently higher than the $P_{\mathrm{a}}\mathrm{O}_2$ but the pulmonary-arterial $P\mathrm{O}_2$ difference decreased at the end of each day of walking. This decrease was brought about by the lower $P_{\mathrm{P}}\mathrm{O}_2$ (by 1- 2.5 kPa) after each day walking and indicates some diffusion limitation across the lungs. Crabs forced to exercise in the field outside of the migration season showed no such loss of pulmonary oxygenation (Adamczewska and Morris, 2000). Thus, although the lungs routinely play an important role in O_2 uptake, the gills are nonetheless recruited to a greater extent during the migration. It is clear

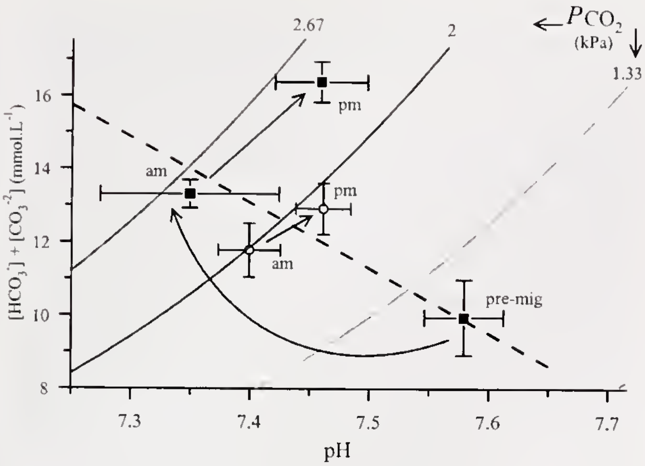

Figure 7. The pH/Bicarbonate relationship for *Gecarcoidea natalis* during two migration seasons, (■) 1993 and (○) 1995. The pre-migratory values in 1993 were assumed to be applicable to the 1995 season. The $P\text{co}_2$ isopleths were constructed using the Henderson-Hasselbalch equation using $\alpha\text{CO}_2 = 0.03962$ and $\text{p}K = 6.1$. The non-bicarbonate buffer line was adopted from Adamczewska and Morris (1994a).

that hemolymph shunting occurs between the gills and lungs during locomotion in red crabs. Investigation of hemolymph flow is now essential to determine the role of these two gas exchange structures in O_2 uptake.

During the migration, the $P\text{o}_2$ of hemolymph leaving the gas exchange surfaces varied between the groups of crabs sampled (mean 3-7.7 kPa) but was within the range of values recorded previously for this species (3.7-10.7 kPa: Farrelly and Greenaway, 1994; Adamczewska and Morris, 1994a). Despite the differences in $P\text{o}_2$, the high affinity of the Hc for O_2 in red crabs ($P_{50} = 1.77$ kPa: Adamczewska and Morris, 1998b) ensured Hc saturation with O_2 at the gas exchange surfaces.

Excretion of CO_2 was also maintained by walking crabs during the migration, but without any internal hypercapnia. Red crabs exercised in the field either before or after the migration season exhibited significantly decreased hemolymph CO_2 content due to a metabolic acidosis imposed on a respiratory acidosis (Adamczewska and Morris, 2000). Conversely, each day of migration resulted in an increase in hemolymph CO_2 of 2–3 mmol · l^{-1}, which was of metabolic rather than respiratory origin. Since the $P\text{co}_2$ remained constant and the diffusion gradient across the respiratory surfaces was unchanged, the increase in CO_2 did not indicate impairment of CO_2 excretion.

Acid-base perturbations

More detailed analysis using the Henderson-Hasselbalch plot showed that the AM crabs experienced a relative respiratory acidosis compared with the pre-mig crabs (Fig. 7). This acidosis (~0.2 pH units) persists during the wet season even after the migration is completed and appears to be a simple consequence of the higher activity levels made possible by high relative humidity. (Adamczewska and Morris, 2000). Active red crabs must increase O_2 uptake, and consequently CO_2 excretion is facilitated by an internal hypercapnic acidosis that improves the outward $P\text{co}_2$ gradient (*e.g.*, O'Mahoney and Full, 1984). Thus, the daily alkalosis observed in migrating red crabs in both 1993 and 1995 was superimposed on a seasonal acidosis brought about by increased basal activity. Importantly, there was no evidence of any additional respiratory acidosis as a result of walking each day during the migration (Fig. 7).

The obvious metabolic alkalosis experienced by the red crabs at the end of each day of migration contradicts all previous studies of acid-base perturbations during locomotion in crustaceans (*e.g.*, McMahon *et al.*, 1979; Smatresk *et al.*, 1979; Wood and Randall, 1981b; review: McMahon, 1981; Booth *et al.*, 1984; Greenaway *et al.*, 1988), including exercising red crabs (Adamczewska and Morris, 1998a, 2000). The alkalosis, which must originate either from the removal of H^+ from the hemolymph or the addition of metabolic base, was removed overnight, only to reappear at the end of the next day of migration. A diel de-calcification of the exoskeleton to supply metabolic base in the form of HCO_3^- seems unlikely because since there was no evidence of any change in hemolymph [Ca] between AM and PM crabs; such a change would normally accompany this process (*e.g.*, Henry *et al.*, 1981). A small increase in lactate concentration in the muscle of PM crabs in 1993 was not reflected in any increase the hemolymph. Similarly, a large increase in muscle lactate (values routinely near 6 mmol · kg^{-1}) seen in relatively inactive free-ranging crabs in the dry season of June 1994 was not reflected in the hemolymph (values only 0.72 mmol · l^{-1}). Furthermore, the muscle L-lactate concentrations of the relatively inactive dry-season crabs were nearly 4 mmol · kg^{-1} greater than those of more active wet-season crabs (Adamczewska and Morris, 2000). Clearly there are some aspects of the dynamics of lactate and possibly H^+ distribution that are different in *G. natalis* and require further investigation. The daily alkalosis experienced by red crabs during their downward migration would partially offset the wet-season acidosis and assist O_2 loading by increasing the oxygen affinity of the hemocyanin (Adamczewska and Morris, 1998b).

Metabolism during breeding activities

Crabs generally do not possess high aerobic capacity and tend to become anaerobic during enforced exercise (Smatresk and Cameron, 1981; Booth *et al.*, 1982; Herreid and Full, 1988; Forster *et al.*, 1989; Henry *et al.*, 1994). Hemolymph and tissue L-lactate levels may increase in excess of 30 mmol · l^{-1} in exercising crabs (*e.g.*, Greenaway *et al.*, 1988; Milligan *et al.*, 1989; Adamczewska and

Morris, 1994b). Since anaerobiosis accumulates acid and an O_2 debt that must be repaid later (Wood and Randall, 1981a; Ellington, 1983; Herreid, 1980), prolonged locomotion cannot depend on the anaerobic provision of energy. In migrating red crabs the L-lactate concentrations in the hemolymph and muscle tissue were generally low and comparable to those measured in free-ranging crabs during the non-migratory seasons (Adamczewska and Morris, 2000). Furthermore, L-lactate levels were similar during both of the migratory seasons, despite the fact that red crabs migrating in 1993 walked twice as far each day as those migrating in 1995 (Adamczewska and Morris, 2001). If the small diel change in muscle concentration of lactate during the 1993 migration represented anaerobiosis, this would be equivalent to only approximately 0.4 mmol ATP, or to 3–4 min of resting O_2 uptake (Adamczewska and Morris, 1994b).

Laboratory studies indicated that to cover a set distance in a fixed amount of time, red crabs are better suited to continuous travel than to periods of rapid walking interrupted by periodic rests (Adamczewska and Morris, 1998a). The mean daily walking speeds of red crabs (1.1 $m \cdot min^{-1}$, estimated from radio-tracking during the 1993 migration) are within the range that this species is capable of supporting aerobically (Adamczewska and Morris, 1994b; 2001). However, walking speeds measured for red crabs crossing roads (*e.g.*, 6.2 $m \cdot min^{-1}$ for returning females: Adamczewska and Morris, 2001) show that sometimes during the migration the crabs walk more than 4 times faster than can be sustained aerobically under laboratory conditions. There was an approximate doubling of muscle lactate in the returning female crabs in 1993, to 6.34 $mmol \cdot kg^{-1}$, but this was again confined to the muscle, and lactate concentrations remained low in the hemolymph (Table 1). This change in muscle lactate represents only about 5 min of resting oxygen uptake.

The possession of a burrow has direct consequences for the breeding success of a male red crab. For male crabs, defending a burrow was more strenuous than prolonged locomotion during the downward migration. The basal hemolymph [L-lactate] of crabs guarding their burrows was elevated by more than 6 $mmol \cdot l^{-1}$ compared with migrating crabs. Winning fights is energetically demanding, and the levels of L-lactate (up to 35 $mmol \cdot l^{-1}$) measured after combat were comparable to the concentrations recorded after 45 min of intense exercise (Adamczewska and Morris, 1994b) or after many hours of hypoxia (Gäde, 1984; Albert and Ellington, 1985; van Aardt, 1988). *G. natalis* expends much more energy in defending burrows than the aquatic crab *Necora puber* expends in a fight under laboratory conditions (Thorpe *et al.*, 1995). The high levels of L-lactate in red crabs either indicate an extreme effort put into winning a fight or represent an accumulated sum of attempting to win many fights. Since the losers of conflicts did not show the same accumulation of L-lactate as the winners, the decision to give up the fight is apparently determined early on, so that the eventual loser minimizes his investment in the conflict.

The metabolism of red crabs appears fundamentally altered during the migration. The crabs exhibit a unique metabolic alkalosis of the hemolymph that occurs only during the migration: crabs exercised under field conditions (Adamczewska and Morris, 2000) and in the laboratory (Adamczewska and Morris, 1994b) show the classical mixed respiratory/metabolic acidosis. The walking speed of red crabs crossing roads and clearings was estimated to be 380% of the speed that can be sustained aerobically (Adamczewska and Morris, 1994b, 2001), yet no significant anaerobic metabolism was detected during the downward migration. One possible conclusion is that the aerobic scope of red crabs, which is otherwise unusually low (Adamczewska and Morris, 1994b), is specifically increased for the purpose of the migration. If so, the signals and processes by which this is achieved are yet to be elucidated.

Storage and usage of metabolic fuels

The midgut gland and muscle tissue compose a large portion of the body mass in crustaceans and are considered to be major organs for the storage of metabolic fuel (Vonk, 1960; Chang and O'Connor, 1983; England and Baldwin, 1983; Tsai *et al.*, 1984; Schirf *et al.*, 1987). In *G. natalis*, the muscle tissue stores glycogen, whereas the MGG is a major site of lipid storage (Adamczewska and Morris, 1994b; Morris, unpub. data). In animals, fatty acids are primarily stored in the form of triglycerides, and in *G. natalis* triglycerides were estimated to constitute about 70% of total lipids in the MGG (380 mg lipid $\cdot g^{-1}$ dry tissue mass: S. Morris, unpub. data). The lipid stores in brachyuran crustaceans vary considerably between species, but total lipid stores in the MGG can reach 900 $mg \cdot g^{-1}$ dry mass (Giese, 1966; Heath and Barnes, 1970; Parvathy, 1971; Kucharski and DaSilva, 1991).

The glycogen stores in the muscle tissue of *G. natalis* sampled in the field (11-64 mg glucose $\cdot g^{-1}$ dry mass) were only a fraction of what this species is capable of storing (250 mg glucose $\cdot g^{-1}$ dry mass, Adamczewska and Morris, 1994b) but were within the range found in other brachyuran species (8-71 $mg \cdot g^{-1}$ dry tissue mass: Giese, 1966; Pillay and Nair, 1973; Hilmy *et al.*, 1986; Kucharski and Da Silva, 1991). Since the stores of metabolic fuels in red crabs in the field were not exceptional, red crabs either lack special requirements for large energy stores under natural conditions or have no opportunity to accumulate such stores (Greenaway and Linton, 1995; Greenaway and Raghaven, 1998).

Leaf litter is the major component of the diet of red crabs. During the dry season, when the red crabs are largely confined to burrows, a thick layer of leaf litter accumulates on the forest floor (Greenaway and Raghaven, 1998; Green *et al.*, 1999). Although glycogen stores in the muscle tissue of red crabs appeared to decrease during the dry seasons (June 1994 and pre-mig 1993), there was no corresponding decrease in triglyceride levels nor in muscle protein (S. Morris, unpub. data). More frequent sampling throughout the year is now required to determine the seasonal importance of energy storage in this species.

During the two migratory seasons red crabs apparently utilized neither triglycerides nor stores of muscle glycogen during the downward migration. However, both male and female crabs sampled on their return migration had substantially reduced glycogen reserves in both the muscle and the MGG. Interestingly, although the females stayed on the terraces 2 weeks longer than the male crabs (Hicks *et al.*, 1990; Adamczewska and Morris, 2001), the glycogen reserves were depleted to a similar extent in both sexes.

Assuming that 20% of the body mass is muscle tissue (Giese, 1966; Cameron and Wood, 1985) and using published values of $\dot{M}O_2$ (212 μmol $O_2 \cdot kg^{-1} \cdot min^{-1}$: Adamczewska and Morris, 1994b), the rate of glucose utilization in red crabs during walking would be 0.636 mmol of glucose per hour. The glycogen used by the red crabs during either the breeding activities on the terraces or the return migration was 26 and 53 mmol glucose $\cdot$ kg^{-1} in the two seasons and would be sufficient to provide fuel for about 2.5 h and 5 h of activity in 1993 and 1995 respectively. The glucose and glycogen stores utilized from the MGG would provide metabolic fuel for a further 0.5-2 h of walking. Therefore, considering that the red crabs spend a week or more engaged in breeding activities on the terraces, the glycogen stores used would only be sufficient to fuel a small portion of the active metabolism; the remainder must be supported by food intake (Greenaway and Linton, 1995; Green, 1997).

Sampling of *G. natalis* during the migration has provided unique information about the energy metabolism of these crabs and their capacity to undertake the annual migration. Perhaps surprisingly, it has become clear that the red crabs undertake the annual migration with minimal reliance on energy stores and support prolonged locomotion aerobically. In contrast, the recruitment of anaerobiosis by male red crabs while defending and maintaining their burrows indicates that these breeding activities are more energetically demanding than the actual migration. Above all, it seems clear that migrating red crabs possess a physiological capacity and exhibit physiological responses different from those of the crabs held in the laboratory and from those of non-migrating crabs in the field. Laboratory and further field-based investigations of the regulation of their metabolism are now required, especially of possible seasonal hormonal signals that might alter metabolic state.

Acknowledgments

This work is dedicated to the memory of Dr. Holger Rumpff, without whose commitment, enthusiasm, and especially friendship these studies would not have been possible. We thank the Government Conservators and staff of Parks Australia, Christmas Island, for their assistance and hospitality. We also express our appreciation to the two anonymous reviewers who put so much time into helping us to improve the manuscript. Thanks also to Ansett Airlines for provision and shipment of the dry ice and samples.

Literature Cited

Adamczewska, A. M., and S. Morris. 1994a. Exercise in the terrestrial Christmas Island red crab *Gecarcoidea natalis*. I. Blood gas transport. *J. Exp. Biol.* **188:** 235–256.

Adamczewska, A. M., and S. Morris. 1994b. Exercise in the terrestrial Christmas Island red crab *Gecarcoidea natalis*. II. Energetics of locomotion. *J. Exp. Biol.* **188:** 257–274.

Adamczewska, A. M., and S. Morris. 1996. The respiratory gas transport, acid-base state, ion and metabolite status of the Christmas Island blue crab. *Cardisoma hirtipes* (Dana) assessed *in situ* with respect to immersion. *Physiol. Zool.* **69:** 67–92.

Adamczewska, A. M., and S. Morris. 1998a. Strategies for migration in the terrestrial Christmas Island red crab *Gecarcoidea natalis*: intermittent *versus* continuous locomotion. *J. Exp. Biol.* **201:** 3221–3231.

Adamczewska, A. M., and S. Morris. 1998b. The functioning of the haemocyanin of the terrestrial Christmas Island red crab *Gecarcoidea natalis* and roles for organic modulators. *J. Exp. Biol.* **201:** 3233–3244.

Adamczewska, A. M., and S. Morris. 2000. Respiratory gas transport, metabolic status and locomotor capacity of the Christmas Island red crab *Gecarcoidea natalis* assessed in the field with respect to dichotomous seasonal activity levels. *J. Exp. Zool.* **286:** 552–562.

Adamczewska, A. M., and S. Morris. 2001. Ecology and behavior of *Gecarcoidea natalis*, the Christmas Island red crab, during the annual breeding migration *Biol. Bull.* **200:** 305–320.

Albert, J. L., and W. R. Ellington. 1985. Patterns of energy metabolism in the shore crab, *Menippe mercenaria*, during severe hypoxia and subsequent recovery. *J. Exp. Zool.* **234:** 175–183.

Bergmeyer, H. U. 1985. *Methods of Enzymatic Analysis.* 3rd ed. Vol. VI. Metabolites 1: Carbohydrates. VCH, Weinheim, Germany.

Bliss, D. E., J. Van Montfrans, M. Van Montfrans, and J. R. Boyer. 1978. Behavior and growth of the land crab *Gecarcinus lateralis* (Fréminville) in southern Florida. *Bull. Am. Mus. Nat. Hist.* **160:** 111–152.

Booth, C. E., and B. R. McMahon. 1985. Short communications. Lactate dynamics during locomotor activity in the blue crab, *Callinectes sapidus*. *J. Exp. Biol.* **118:** 461–465.

Booth, C. E., B. R. McMahon, and A. W. Pinder. 1982. Oxygen uptake and the potentiating effects of increased hemolymph lactate on oxygen transport during exercise in the blue crab, *Callinectes sapidus*. *J. Comp. Physiol.* **148:** 111–121.

Booth, C. E., B. R. McMahon, P. L. DeFur, and P. R. H. Wilkes. 1984. Acid-base regulation during exercise and recovery in the blue crab, *Callinectes sapidus*. *Respir. Physiol.* **58:** 395–376.

Burggren, W. W., and B. R. McMahon. 1981. Hemolymph oxygen transport, acid-base status, and hydromineral regulation during dehydration in three terrestrial crabs, *Cardisoma*, *Birgus* and *Coenobita*. *J. Exp. Zool.* **218:** 53–64.

Cameron, J. N., and C. M. Wood. 1985. Apparent H^+ excretion and CO_2 dynamics accompanying carapace mineralization in the blue crab (*Callinectes sapidus*) following moulting. *J. Exp. Biol.* **114:** 181–196.

Chang, E. S., and J. D. O'Connor. 1983. Metabolism and transport of carbohydrates and lipids. Pp. 263–287 in *The Biology of the Crustacea*, Vol. 5. L. H. Mantel, ed.. Academic Press, New York.

Ellington, W. R. 1983. The recovery from anaerobic metabolism in invertebrates. *J. Exp. Zool.* **228:** 431–444.

England, W. R., and J. Baldwin. 1983. Anaerobic energy metabolism in the tail musculature of the Australian yabby *Cherax destructor* (Crustacea, Decapoda, Parastacidae): role of phosphagens and anaerobic glycolysis during escape behavior. *Physiol. Zool.* **56:** 614–622.

Farrelly C. A., and P. Greenaway. 1994. Gas exchange through the lungs and gills in air breathing crabs. *J. Exp. Biol.* **187:** 113–130.

Forster, M. E., F. M. Waldron, and H. H. Taylor. 1989. Recovery from exhausting exercise in a bimodally breathing crab, *Leptograpsus variegatus* (Decapoda: Grapsidae). *J. Exp. Mar. Biol. Ecol.* **127:** 165–173.

Gäde, G. 1984. Effects of oxygen deprivation during anoxia and muscular work on the energy metabolism of the crayfish, *Orconectes limosus. Comp. Biochem. Physiol.* **77A:** 495–502.

Gibson, R., and P. L. Barker. 1979. The decapod hepatopancreas. *Oceanogr. Mar. Biol. Annu. Rev.* **17:** 285–346.

Gibson-Hill, C. A. 1947. Field notes on the terrestrial crabs. *Bull. Raffles Mus.* **18:** 43–52.

Giese, A. C. 1966. Lipids in the economy of marine invertebrates. *Physiol. Rev.* **46:** 244–298.

Gifford, C. A. 1962. Some observations on the general biology of the land crab, *Cardisoma guanhumi* (Latreille) in south Florida. *Biol. Bull.* **123:** 207–223.

Green, P. T. 1993. The role of Red Land Crabs in structuring rain forest on Christmas Island, Indian Ocean. Ph.D. thesis, Monash University, Clayton, Victoria, Australia.

Green, P. T. 1997. Red crabs in rain forest on Christmas Island, Indian Ocean: activity patterns, density and biomass. *J. Trop. Ecol.* **13:** 17–38.

Green P. T., P. S. Lake, and D. J. O'Dowd. 1999 Monopolization of litter processing by a dominant land crab on a tropical oceanic island. *Oecologia.* **119:** 435–444.

Greenaway, P. 1994. Salt and water balance in field populations of the terrestrial crab *Gecarcoidea natalis. J. Crustac. Biol.* **14:** 435–453.

Greenaway, P., and S. M. Linton. 1995. Dietary assimilation and food retention time in the herbivorous terrestrial crab *Gecarcoidea natalis. Physiol. Zool.* **68(6):** 1006–1028.

Greenaway, P., and S. Raghaven, 1998. Digestive strategies in two species of leaf-eating land crabs (Brachyura: Gecarcinidae) in a rain forest. *Physiol. Zool.* **71:** 36–44.

Greenaway P., S. Morris, and B. R. McMahon. 1998. Adaptations to a terrestrial existence by the Robber Crab *Birgus latro.* II. *In vivo* respiratory gas exchange and transport. *J. Exp. Biol.* **140:** 493–509.

Harris, R. R., and M. B. Andrews. 1982. Extracellular fluid volume changes in *Carcinus maenas* during acclimation to high and low environmental salinities. *J. Exp. Biol.* **99:** 161–173.

Harris, R. R., and G. A. Kormanik. 1981. Salt and water balance and antennal gland function in three Pacific species of terrestrial crab (*Gecarcoidea lalandii, Cardisoma carnifex, Birgus latro*). II. The effects of desiccation. *J. Exp. Zool.* **218:** 107–116.

Head, G., and J. Baldwin. 1986. Energy metabolism and the fate of lactate during recovery from exercise in the Australian freshwater crayfish *Cherax destructor. Aust. J. Mar. Freshw. Res.* **37:** 641–646.

Heath, J. R., and H. Barnes. 1970. Some changes in biochemical composition with season and during the moulting cycle of the common crab *Carcinus maenas* (L.). *J. Exp. Mar. Biol. Ecol.* **5:** 199–233.

Henry, R. P., G. A. Kormanik, N. J. Smatresk, and J. N. Cameron. 1981. The role of shell dissolution as a source of HCO_3^- for buffering hypercapnic acidosis in aquatic and terrestrial decapod crustaceans. *J. Exp. Biol.* **94:** 269–274.

Henry, R. P., C. E. Booth, F. H. Lallier, and P. J. Walsh. 1994. Post-exercise lactate production and metabolism in three species of aquatic and terrestrial decapod crustaceans. *J. Exp. Biol.* **186:** 215–234.

Herreid, C. F. 1980. Review: Hypoxia in invertebrates. *Comp. Biochem. Physiol.* **67A:** 311–320.

Herreid, C. F., and R. J. Full. 1988. Energetics and locomotion. Pp. 333–377 in *Biology of the Land Crabs*, W. W. Burggren and B. R. McMahon, eds. Cambridge University Press, New York.

Hicks, J. W. 1985. The breeding behaviour and migrations of the terrestrial crab *Gecarcoidea natalis.* (Decapoda: Brachyura). *Aust. J. Zool.* **33:** 127–142.

Hicks, J., H. Rumpff, and H. Yorkston. 1990. *Christmas Crabs.* Golden Earth Design and Printing, Singapore.

Hilmy, A. M., N. F. Abd El-Hamid, and K. H. G. Adham. 1986. Glycogen content of some organs of two marine crustaceans. *Bull. Inst. Oceanogr. Fish.* **12:** 215–229.

Klaassen, F. 1975. Ecological and ethological studies on the reproductive biology of *Gecarcinus lateralis* (Decapoda, Brachyura). *Forma Function* **8:** 101–174.

Kucharski, L. C. R., and R. S. M. Da Silva. 1991. Effect of diet composition on the carbohydrate and lipid metabolism in an estuarine crab, *Chasmagnathus granulata* (Dana, 1851). *Comp. Biochem. Physiol.* **99A:** 215–218.

McMahon, B. R. 1981. Oxygen uptake and acid-base balance during activity in decapod crustaceans. Pp. 299–335 in *Locomotion and Energetics in Arthropods*, C. F. Herreid and C. R. Fourtner, eds.. Plenum Press, New York.

McMahon, B. R., D. G. McDonald, and C. M. Wood. 1979. Ventilation, oxygen uptake and haemolymph oxygen transport, following enforced exhausting activity in the Dungeness crab *Cancer magister. J. Exp. Biol.* **80:** 271–285.

Milligan, C. L., P. J. Walsh, C. E. Booth, and D. G. McDonald. 1989. Intracellular acid-base regulation during recovery from locomotor activity in the blue crab *Callinectes sapidus. Physiol. Zool.* **62:** 621–638.

Nishida, S., Y. Takahashi, and J. Kittaka. 1995. Structural changes in the hepatopancreas of the rock lobster, *Jasus edwardsii* (Crustacea, Palinudidae) during development from the puerulus to post-puerulus. *Mar. Biol.* **123:** 837–844.

O'Mahoney, P. M., and R. J. Full. 1984. Respiration of crabs in air and water. *Comp. Biochem. Physiol.* **79A:** 275–282.

Parvathy, K. 1971. Glycogen storage in relation to the moult cycle in two crustaceans *Emerita asiatica* and *Ligia exotica. Mar. Biol.* **10:** 82–86.

Pillay, K. K., and N. B. Nair. 1973. Observations on the biochemical changes in gonads and other organs of *Uca annulipes, Portunus pelagicus* and *Metapenaeus affinis* (Decapoda: Crustacea) during the reproductive cycle. *Mar. Biol.* **18:** 167–198.

Schirf, V. R., T. Turner, L. Selby, C. Hannapel, P. Dela Cruz, and P. F. Dehn. 1987. Nutritional status and energy metabolism of crayfish (*Procambarus clarkii*, Girard) muscle and hepatopancreas. *Comp. Biochem. Physiol.* **88A:** 383–386.

Smatresk, N. J., and J. N. Cameron. 1981. Post-exercise acid-base balance and ventilatory control in *Birgus latro*, the coconut crab. *J. Exp. Zool.* **218:** 75–82.

Smatresk, N. J., A. J. Preslar, and J. N. Cameron. 1979. Post-exercise acid-base disturbance in *Gecarcinus lateralis*, a terrestrial crab. *J. Exp. Zool.* **210:** 205–210.

Taylor, H. H., and P. Greenaway. 1994. The partitioning of water and solutes during evaporative water loss in three terrestrial crabs. *Physiol. Zool.* **67:** 539–565.

Thorpe, E., A. C. Taylor, and F. A. Huntingford. 1995. How costly is fighting? Physiological effects of sustained exercise and fighting in swimming crabs, *Necora puber* (L.) (Brachyura, Portunidae). *Anim. Behav.* **50:** 1657–1666.

Tsai, D. E., H. Chen, and C. Tsai. 1984. Total lipid and cholesterol content in the blue crab, *Callinectes sapidus* Rathbun. *Comp. Biochem. Physiol.* **78B:** 27–31.

van Aardt, W. J. 1988. Lactate metabolism and glucose patterns in the river crab, *Potamonautes warreni* Calman, during anoxia and subsequent recovery. *Comp. Biochem. Physiol.* **91A:** 299–304.

van Aardt, W. J. 1990. Oxygen uptake and haemocyanin oxygen affinity of *Potamonautes warreni* Caman after exercise. *S. Afr. J. Zool.* **25:** 11–17.

Vonk, H. J. 1960. Digestion and metabolism. Pp. 291–316 in *Physiology of Crustacea,* Vol. 1. T. H. Waterman, ed. Academic Press, New York.

Weinstein, R. B., and R. J. Full. 1992. Intermittent exercise alters endurance in an eight-legged ectotherm. *Am. J. Physiol.* **262:** R852–R859.

Weinstein R. B., R. J. Full, and A. N. Ahn. 1994. Moderate dehydration decreases locomotor performance of the ghost crab *Ocypode quadrata. Physiol. Zool.* **67:** 873–891.

Wolcott, T. G. 1998. Ecology. Pp. 55–96 in *Biology of the Land Crabs.* W. W. Burggren and B. R. McMahon, eds. Cambridge University Press, Cambridge.

Wolcott, T. G. 1992. Water and solute balance in the transition to land. *Am. Zool.* **32:** 428–437.

Wolcott, T. G., and D. L. Wolcott. 1985. Factors influencing the limits of migratory movements in terrestrial crustaceans. *Contrib. Mar. Sci. Suppl.* **27:** 257–273.

Wood, C. M., and D. J. Randall. 1981a. Oxygen and carbon dioxide exchange during exercise in the land crab *Cardisoma carnifex. J. Exp. Zool.* **218:** 7–22.

Wood, C. M., and D. J. Randall. 1981b. Haemolymph gas transport, acid-base regulation, and anaerobic metabolism during exercise in the land crab *Cardisoma carnifex. J. Exp. Zool.* **218:** 23–35.

Reference: *Biol. Bull.* **200:** 336–343. (June 2001)

Morphology of the Symbiosis Between *Corculum cardissa* (Mollusca: Bivalvia) and *Symbiodinium corculorum* (Dinophyceae)

MARK A. FARMER,[1] WILLIAM K. FITT[2,*], AND ROBERT K. TRENCH[3]

[1]*Department of Cellular Biology, and* [2]*Institute of Ecology, University of Georgia, Athens, GA 30602 USA,* [3]*Department of Ecology, Evolution and Marine Biology, University of California at Santa Barbara, Santa Barbara, CA 93106 USA*

Abstract. Light and transmission electron microscopy of tissues of the symbiotic clam *Corculum cardissa* (L) showed that a symbiotic dinoflagellate, *Symbiodinium corculorum* (Trench), is found predominantly in the mantle and the gills. The data suggest that in *C. cardissa* the algae are located in a zooxanthellal tubular system that is associated with the hemocoel and is similar to that seen in tridacnine ("giant") clams. The algae occur within the lumen of the tertiary tubules and are thus separated from the hemolymph by a tissue that is one cell layer thick. Under a light microscope the tertiary tubules appear as rows of symbionts originating from the digestive diverticulum, presumably branching from the primary tubules that are also seen in symbiotic tridacnine clams. This morphological arrangement is discussed with regard to the ontogeny and the evolution of the tubular system within symbiotic bivalves.

Introduction

Several species of marine bivalves in the family Cardiidae harbor symbiotic dinoflagellates that belong to the genus *Symbiodinium*. These bivalves include all of the species in the subfamily Tridacninae, including the well-known genera of larger clams, *Tridacna* and *Hippopus*, as well as less well-known genera of much smaller clams in the subfamily Fraginae, such as *Corculum* and *Fragum* (Kawaguti, 1950, 1983; Schneider, 1998). For many years, the symbiotic algae in tridacnines were depicted as being located in the hemal spaces, whence they were culled by wandering amoebocytes and digested in the digestive gland; the indigestible remains were thought to reside in the kidneys (*e.g.*, Yonge, 1936, 1953, 1975, 1980; Goreau *et al.*, 1973). However, a system of tubules, arising from one of the diverticular ducts of the stomach of *Tridacna* and ramifying through much of the clam and containing the symbionts, was described by K. Mansour (1946a, b), but forgotten. Finally, 46 years later, the "zooxanthellal tubular system" was redescribed by Norton *et al.* (1992), who proposed that the primary, secondary, and blind-ended tertiary tubes of the tubular system do not connect with the hemocoel; therefore the algae are not found in the hemolymph compartment (see Fitt, 1993, for a review).

In the heart cockle, *Corculum cardissa*, as in the giant tridacnine clams, symbiotic dinoflagellates are located in the mantle tissue; but unlike the tridacnine, *C. cardissa* has many algae located in the gills as well (Kawaguti, 1968). Early electron microscopic images, in both instances, were interpreted as indicating that the algae are within the hemal system (Kawaguti, 1966, 1968). This interpretation was consistent with the author's observations that blood cells are apparently in contact with the algae in *C. cardissa* and *Tridacna* (Kawaguti, 1966, 1968).

The occurrence of symbiotic algae in a tubular system in *Tridacna* (Mansour, 1946a, b; Norton *et al.*, 1992) raises the question of whether a similar zooxanthellal tubular system also occurs in the cockle *Corculum cardissa*, or any other related species (*i.e., Fragum* spp.). The goal of this study was to document evidence of a tubular system in *C. cardissa*, and to determine whether the tubules would penetrate the gill tissue, a conceptually difficult morphology. In the current study, ultrastructural observations indicate that a tubular system also exists in

---

Received 10 June 1999; accepted 14 February 2001.

* To whom correspondence should be addressed. E-mail: fitt@sparrow.ecology.uga.edu

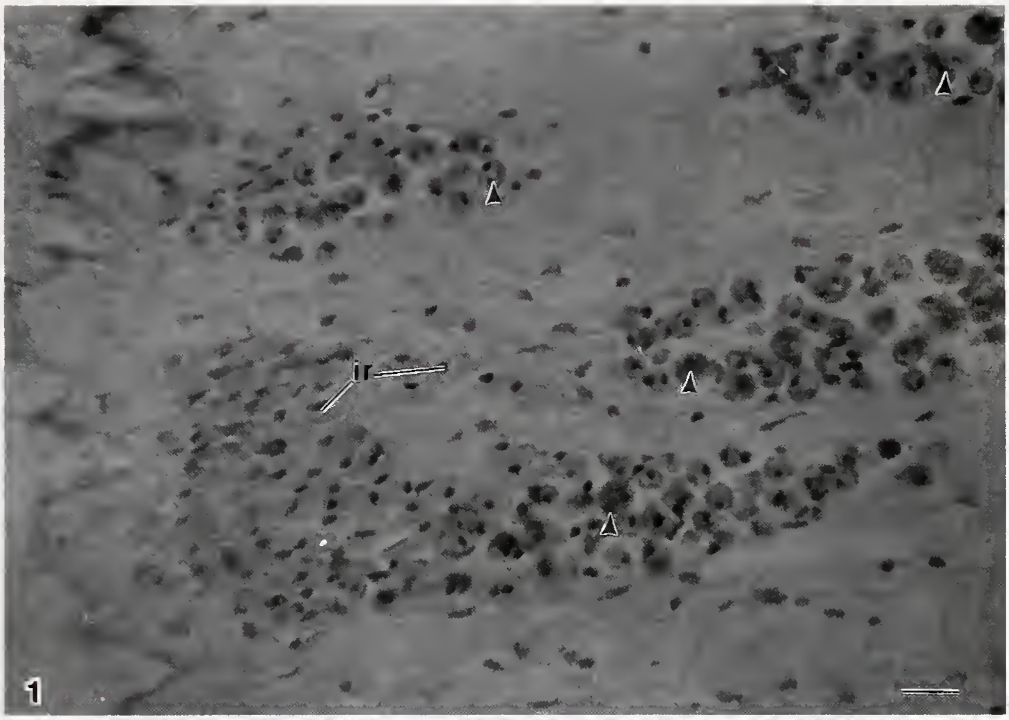

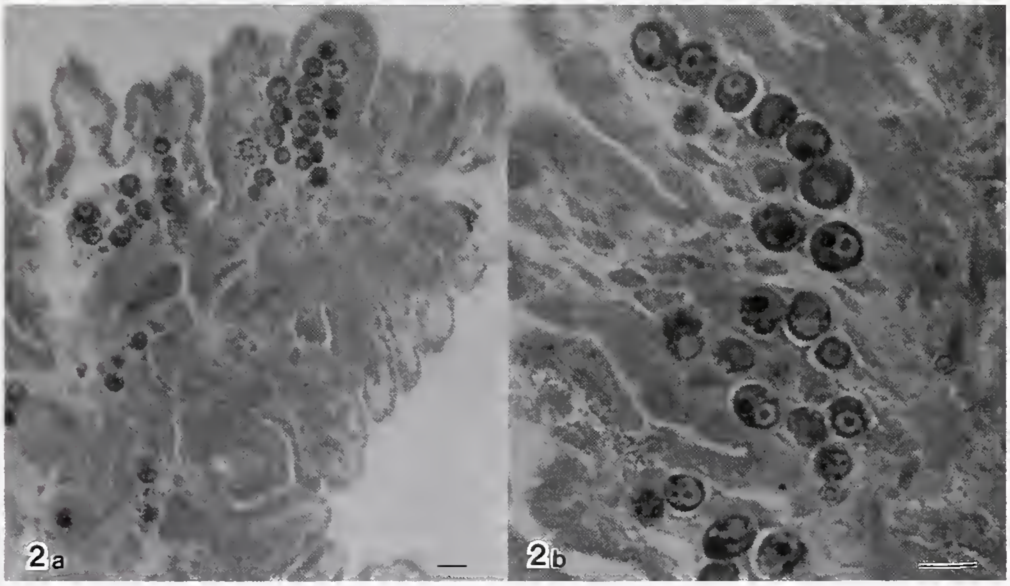

Figure 1. Light micrograph of a paraffin-embedded section through the mantle tissue of *Tridacna maxima* showing rows of symbiotic algae (arrowheads) in tertiary tubules. Iridophores (ir), animal cells with crystalline proteins that refract light, are found in the mantles of all species of clams containing symbiotic algae. Scale bar, 20 μm.

Figure 2. Light micrograph of a paraffin-embedded section through the gill tissue of *Corculum cardissa* showing rows of symbiotic algae in tertiary tubules. (a) Overview; scale bar = 12 μm. (b) Higher magnification, scale bar = 10 μm.

Corculum; that the symbiotic dinoflagellates occur within the lumina of the tubes, which themselves are located within the hemocoel; and that the algae within the tertiary tubules are separated from the hemolymph by a tissue that is mostly only one cell layer thick.

Materials and Methods

Corculum cardissa (Linne) was collected from the sandy reef flat at about 0.5 m depth in Belau (Palau), Western Caroline Islands. Animals were fixed in 6% glutaraldehyde, postfixed in 3% osmium tetraoxide, dehydrated, and embedded in Spurr's medium as previously described (Trench *et al.*, 1981). The tissues of *Tridacna* spp. were fixed, embedded, and observed as described in Trench *et al.* (1981). Thick sections (1 μm) were prepared for examination by light microscopy on an LKM Ultratome V. These were photographed with an Olympus Vanox microscope and a PM-10 camera. Ultrathin sections for electron microscopic examination were prepared on an RMC-6000 ultramicrotome, stained with uranyl acetate and lead citrate in the standard manner, and observed and photographed with a Philips 400 transmission electron microscope (TEM).

Results and Discussion

Light microscopic examination of *Corculum cardissa* revealed that, similar to observations made on symbionts living in mantle tissues of *Tridacna* (Fig. 1; Mansour, 1946a; Fitt and Trench, 1981; Norton *et al.*, 1992; Norton and Jones, 1992), algal cells are arranged in rows in both the mantle (*e.g.*, Kawaguti, 1968; Figs. 1, 2) and the gills (Fig. 2). However light microscope observations could not resolve the tertiary tubule structure in either genus of clam.

Electron microscopic examination of the gills of *Corculum* (Fig. 3) shows that the algae are indeed juxtaposed to animal blood cells. Kawaguti's (1968) early descriptions from *C. cardissa* note that algae are sometimes accompanied by "wandering cells," but he includes no figures. In contrast, TEM pictures of symbionts in *Tridacna crocea* and *T. maxima* clearly show nearby animal cells (Kawaguti, 1966; Fitt and Trench, 1981). Algal symbionts in *C. cardissa* are not in direct contact with the animal's blood cells, but are separated from the hemolymph and the blood cells

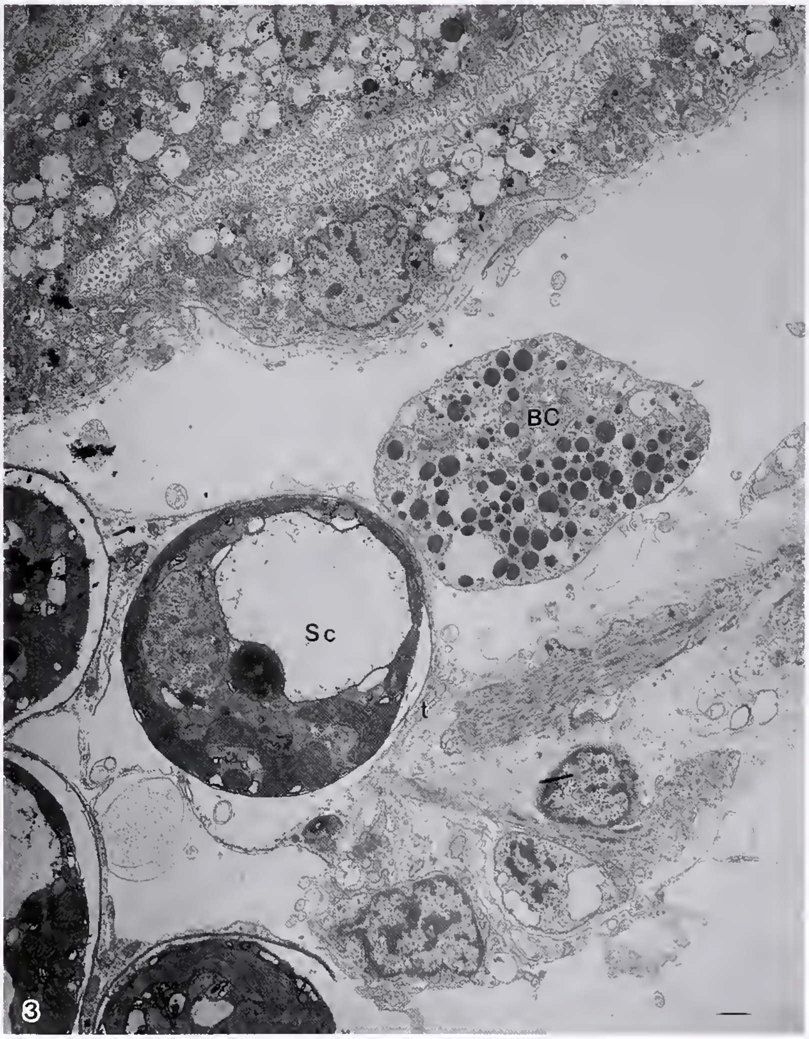

Figure 3. Transmission electron micrograph of a portion of the gill of *Corculum cardissa* showing a portion of the tertiary tubule (t), and a blood cell (BC) close to cells of the alga *Symbiodinium corculorum* (Sc) in the tubule. Scale bar, 1 μm.

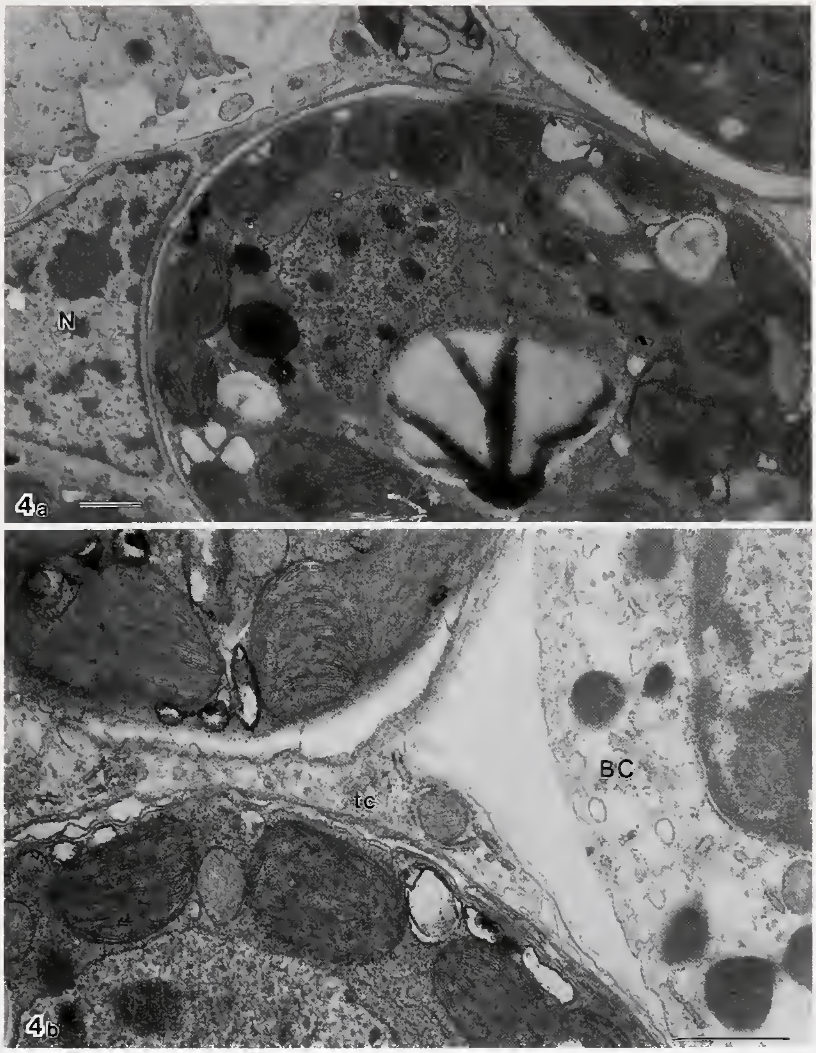

Figure 4. Transmission electron micrograph of the relation between the symbiotic algae, the tubule cells, and the blood cells in gill tissue of *Corculum cardissa.* (a) An algal cell closely appressed to a tubule cell. The algal cell wall is juxtaposed to the tubule cell plasmalemma, which can be followed around the enclosed cell nucleus, which it encloses. (b) Two algal cells in adjacent tertiary tubules, separated by the cytoplasm of the two tubule cells (tc). A blood cell is close by (bc). Scale bars, 1 μm.

by the cells of the tubules, which at the tertiary level are about one cell layer thick (Figs. 3–5). Evidence for this comes from closer examination of high-magnification TEM images of the structural relations between the algae, the cells of the tubules, and the blood cells (Fig. 4). First, algae in the lumina of the tubules are often pressed against the inner plasmalemma of the tubular cells; when nuclei of the appressed tubular cells are apparent (as in Fig. 4a), this could lead to the interpretation that the algae are intracellular (*e.g.*, Kawaguti, 1968). Second, the algae are clearly separated from the molluscan blood cells by the cells composing the tubules (Fig. 4b). Overlapping cell processes form the tertiary tubules (Fig. 5). Two or more unseparated adjacent symbionts (Fig. 6) also indicate that the algae are in tubules and not living intracellularly within host cells.

In bivalves that harbor symbiotic dinoflagellates, the structure of the tubular system, in which the tubules arise from the digestive system and are contiguous with it, suggests that the morphological and functional relation between host and symbionts in bivalves is directly analogous to that found in symbiotic cnidarians (Fitt, 1993). In both cases, the algae enter the digestive system *via* the mouth. In bivalves, symbiotic dinoflagellates enter *via* the mouth, and exit *via* the anus (Ricard and Salvat, 1977; Trench *et al.*, 1981; Maruyama and Heslinga, 1997); their entire residence in the clam is in association with the digestive system. In contrast, symbionts in cnidarians enter and exit *via* the mouth and eventually take up residence inside of host digestive cells. The location of the symbionts in bivalves and cnidarians is also analogous with respect to metabolite flux between host

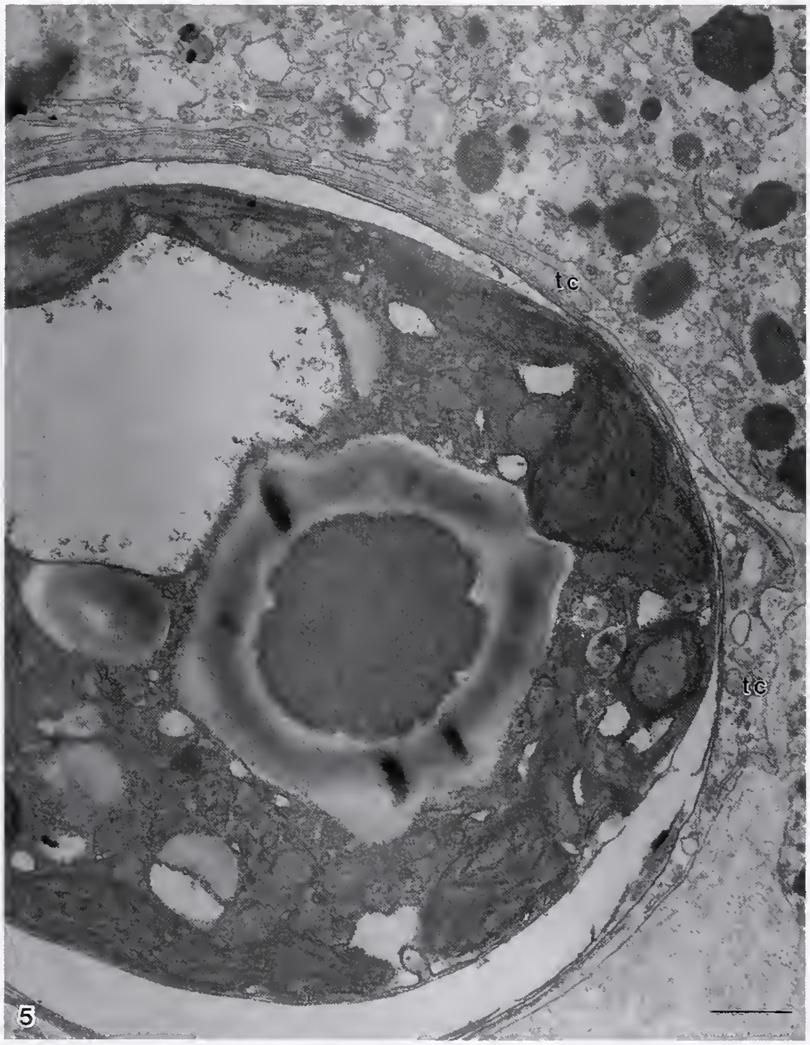

Figure 5. Transmission electron micrograph of an alga in the gill of *Corculum cardissa* surrounded by overlapping processes of tertiary tubule cells (tc). Scale bar, 1 μm.

and symbiont (Fitt *et al.*, 1985). In bivalves, where the algae are intercellular, they are separated from the hemolymph (circulating nutrients) by the proximal and distal plasmalemma of the tubule cells (Fig. 7). Hence, nutrient exchange between the algae and the hemolymph of bivalves may potentially be regulated by the tubule cells. In cnidarians, where the algae are intracellular, the symbionts are separated from their nutrient source, the gastrovascular system, by two membranes, the host cell plasmalemma and the symbiosome membrane.

The presence of the tubular system in symbiotic bivalves is also significant from ontogenetic and evolutionary perspectives. Studies of algal symbioses in tridacnines (Fitt and Trench, 1981) clearly show that the tubules develop only in the presence of dinoflagellate symbionts; the algae in the tubules are observed as "rows extending from the region of the stomach and digestive gland toward the developing siphonal tissue" (Fitt *et al.*, 1981). Juvenile clams that were allowed to develop in the absence of *Symbiodinium* did not show evidence of this feature. From the report of Norton *et al.* (1995), it is also apparent that, when the algae are lost from *Tridacna* during events of thermal "stress," the tubules atrophy. Whether the tubules are reformed should the symbiosis recover, or whether lack of recovery of bleached clams is the result of the inability of the tubular system to regenerate, is unknown.

For marine symbioses, only two other instances have been recorded in which the symbionts appear to play a significant role in the ontogenetic event in the host. One example is the process of strobilation in symbiotic scyphozoans such as *Mastigias* (Sugiura, 1964) and *Cassiopeia* (Colley and Trench, 1985); these jellyfish produce ephyrae only in the presence of *Symbiodinium*. Another example is the influence that *Vibrio fischeri*, a symbiotic luminous bacteria, has on morphogenesis of certain parts of the light organ in the squid *Eprymna scolopes* (Claes and Dunlap,

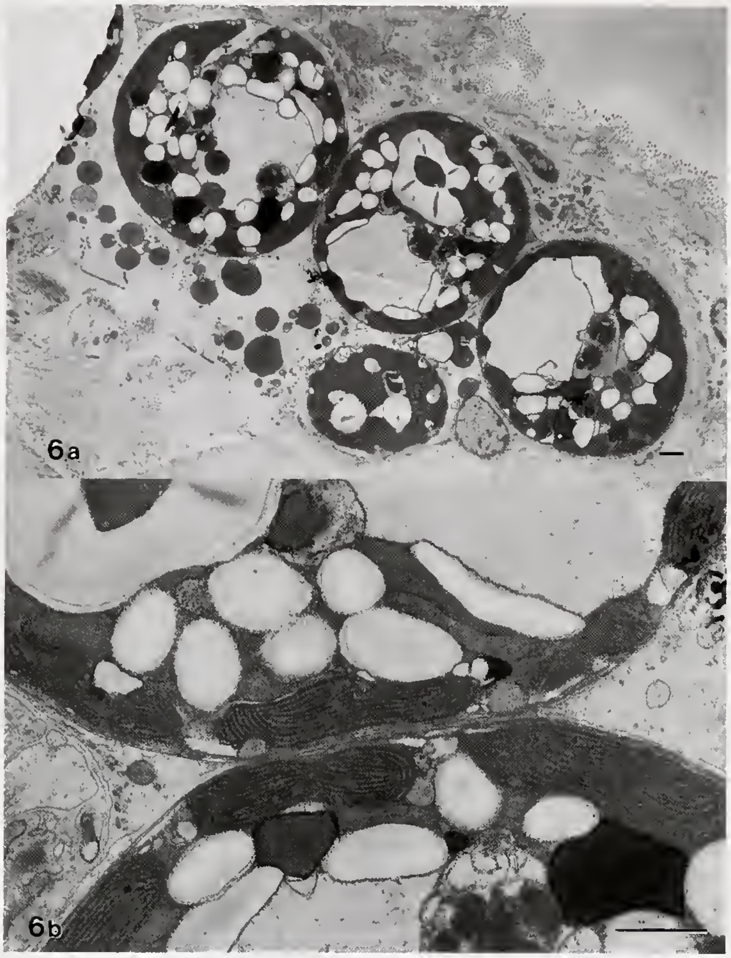

Figure 6. Symbiotic algae in tertiary tubules in the gills of *Corculum cardissa*, showing (a) several symbionts in a tubule and (b) high magnification of the two cells in 6a. Scale bar = 1 μm.

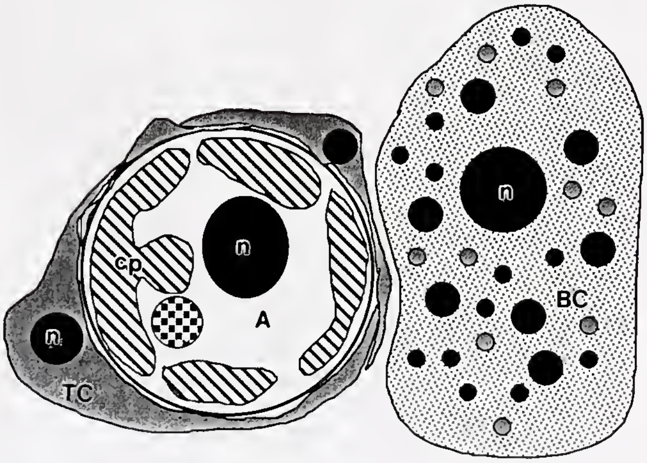

Figure 7. Schematic representation of the relation between the alga (A), the tubule cells of the tertiary tubules (TC), and the hemolymph containing blood cells (bc). n, nucleus; cp, chloroplast.

2000). In neither example are the "signals" that elicit the developmental response in the host known. In the case of the dinoflagellate associations, the exopolysaccharides exuded by *Symbiontinium* (Markell *et al.*, 1992; Markell and Trench, 1993) may be a source of the signals. For instance, in the process of root nodulation in leguminous plants, the initiation of root hair curling and infection thread formation are dependent on chemical signals from the bacterial symbionts (Brewin, 1991).

A system of tubules originating in the stomach and ramifying through the hemolymph is uncommon in bivalve molluscs and appears to be directly related to symbiosis with dinoflagellates. As far as is known, no nonsymbiotic bivalves demonstrate this feature. In addition to the tridacnine clams and *Corculum cardissa* described here, the bivalve *Fragum fragum* has also been reported to harbor symbiotic dinoflagellates (Kawaguti, 1983), and recent TEM images (Kempf, unpubl.) show morphological features similar to those presented here for *C. cardissa*. This finding supports the interpretation that all algal symbionts in molluscs occur in tubule extensions of the digestive system. Cladistic analyses based on morphological characters (Schneider, 1992, 1998) and phylogenetic relationships based on analysis of small subunit ribosomal RNA gene sequences (Maruyama *et al.*, 1998) both indicate that the known bivalves with symbiotic dinoflagellates are closely related, all belonging to Cardiidae. In addition, the available molecular genetic evidence (NcNally *et al.*, 1994) reveals that the symbiotic algae associated with *Corculum* and *Tridacna* are also very closely related (LaJeunesse, 2000), but not identical. We also suppose that freshwater bivalves, such as *Anodonta*, that are symbiotic with the green alga *Chlorella* sp. (Pardy, 1980) may demonstrate a tubular structure in which to house the algae, as these symbionts probably also enter their hosts through the digestive system.

The only other molluscan group that shows an analogous morphology is the opisthobranch gastropods: some saccoglossan opisthobranchs temporarily harbor derived chloroplasts from feeding (Trench, 1975), and eolid nudibranchs often maintain dinoflagellates for a short time after feeding on symbiotic cnidarians (Kempf, 1984). Most significantly in relation to symbiotic bivalves, in eolidacean nudibranchs "branches of the posterior aorta . . . accompany the branches of the midgut gland (digestive diverticulum) into the cerata . . ." (Hyman, 1967, p. 477), suggesting development of tubules in conjunction with development of blood vessels, or *vice versa*.

We speculate that bivalves, like their gastropod relatives, possess a suite of genes that encode the expression of the tubular system, but these genes are expressed only after activation by some "signal" produced by dinoflagellate symbionts as they enter the host digestive tract. These situations would be analogous to the production of various galls in plants following infection by bacteria, fungi, insects, or other parasitic plants (Bidwell, 1979), all of which produce chemical signals.

Acknowledgments

We thank Professor Stephen Kempf for providing us with unpublished transmission electron micrographs of tissues of *Fragum fragum*, and two anonymous reviewers for suggestions on improving the text. WKF acknowledges support from NSF and the NOAA National Undersea Research Program (UNCW and CMRC).

Literature Cited

Bidwell, R. G. S. 1979. *Plant Physiology*. 2nd ed. MacMillan, New York.

Brewin, N. J. 1991. Development of the legume root nodule. *Annu. Rev. Cell Biol.* **7:** 191–226.

Claes, M. F., and P. V. Dunlap. 2000. Aposymbiotic culture of the sepiolid squid *Euprymna scolopes*: role of the symbiotic bacterium *Vibrio fischeri* in host animal growth development, and light organ morphogenesis. *J. Exp. Zool.* **286:** 280–296.

Colley, N. J., and R. K. Trench. 1985. Cellular events in the reestablishment of a symbiosis between a marine dinoflagellate and a coelenterate. *Cell Tissue Res.* **239:** 93–103.

Fitt, W. K. 1993. Nutrition of giant clams. Pp. 31–40 in *Biology and Mariculture of Giant Clams.*, W. K. Fitt, ed. ACIAR, Canberra, Australia.

Fitt, W. K., and R. K. Trench. 1981. Spawning, development, and acquisition of zooxanthellae by *Tridacna squamosa* (Mollusca: Bivalvia). *Biol. Bull.* **161:** 213–235.

Fitt, W. K., C. R. Risher, and R. K. Trench. 1981. Larval biology of tridacnid clams. *Aquaculture* **39:** 181–195.

Fitt, W. K., T. A. V. Rees, and D. Yellowlees. 1985. The relationship between pH and the availability of dissolved inorganic nitrogen in the zooxanthella-giant clam symbiosis. *Limnol. Oceanogr.* **40:** 976–982.

Goreau, T. F., N. I. Goreau, and C. M. Yonge. 1973. On the utilization of photosynthetic products from zooxanthellae and of a dissolved amino acid in *Tridacna maxima* (Mollusca: Bivalvia). *J. Zool. Lond.* **169:** 417–454.

Hyman, L. H. 1967. *The Invertebrates. Vol. VI, Mollusca I.* McGraw Hill, New York.

Kawaguti, S. 1950. Observations on the heart cockle, *Corculum cardissa* (L), and its associated zooxanthellae. *Pac. Sci.* **4:** 43–49.

Kawaguti, S. 1966. Electron microscopy on the mantle of the giant clam with special reference to zooxanthellae and iridophores. *Biol. J. Okayama Univ.* **12:** 81–92.

Kawaguti, S. 1968. Electron microscopy on zooxanthellae in the mantle and gill of the heart shell. *Biol. J. Okayama Univ.* **14:** 1–11.

Kawaguti, S. 1983. The third record of an association between bivalve mollusks and zooxanthellae. *Proc. Jpn. Acad. Ser. B* **59:** 17–20.

Kempf, S. C. 1984. Symbiosis between the zooxanthella *Symbiodinium (=Gymnodinium) microadriaticum*. (Freudenthal) and four species of nudibranchs. *Biol. Bull.* **166:** 110–126.

LaJeunesse, T. C. 2000. Diversity, distribution and host specificity of algal symbionts of the dinoflagellate genus *Symbiodinium*. Ph.D dissertation, University of California Santa Barbara.

Mansour, K. 1946a. Communication between the dorsal edge of the mantle and the stomach of *Tridacna. Nature (Lond.)* **157:** 844.

Mansour, K. 1946b. Source and fate of the zooxanthellae of the visceral mass of *Tridacna elongata. Nature (Lond.)* **158:** 130.

Markell, D. A., and R. K. Trench. 1993. Macromolecules exuded by symbiotic dinoflagellates in culture: Amino acid and sugar composition. *J. Phycol.* **29:** 64–68.

Markell, D. A., R. K. Trench, and R. Iglesias-Prieto. 1992. Macromolecules associated with the cell walls of symbiotic dinoflagellates. *Symbiosis* **12:** 19–31.

Maruyama, T., and G. A. Heslinga. 1997. Fecal discharge of zooxanthellae in the giant clam *Tridacna derasa*, with reference to their growth rate. *Mar. Biol.* **127:** 473–477.

Maruyama, T., M. Ishikura, S. Yamazaki, and S. Kanai. 1998. Molecular phylogeny of zooxanthellate bivalves. *Biol. Bull.* **195:** 70–77.

McNally, K. L., N. S. Govind, P. E. Thome, and R. K. Trench. 1994. Small subunit ribosomal DNA sequence analyses and a reconstruction of the inferred phylogeny among symbiotic dinoflagellates (Pyrrhophyta). *J. Phycol.* **30:** 316–329.

Norton, J. H., and G. W. Jones. 1992. The giant clam: an anatomical and histological atlas. Australian Center for International Agricultural Research (ACIAR) Monograph Series, Canberra, 142 pp.

Norton, J. H., M. A. Shepherd, H. M. Long, and W. K. Fitt. 1992. The zooxanthellal tubular system in the giant clam. *Biol. Bull.* **183:** 503–506.

Norton, J. H., H. C. Prior, B. Baillie, and D. Yellowlees. 1995. Atrophy of the zooxanthellal tubular system in bleached giant clams *Tridacna gigas. J. Invertebr. Pathol.* **66:** 307–310.

Pardy, R. L. 1980. Symbiotic algae and ^{14}C incorporation in the freshwater clam *Anodonta. Biol. Bull.* **158:** 349–355.

Ricard, M., and B. Salvat. 1977. Faeces of *Tridacna maxima* (Mollusca-Bivalvia), composition and coral reef importance. *Proc. Third Int. Coral Reef Symp., Miami:* 495–502.

Schneider, J. A. 1992. Preliminary cladistic analysis of the bivalve family Cardiidae. *Am. Malacol. Bull.* **9:** 145–155.

Schneider, J. A. 1998. Phylogeny of the Cardiidae (Bivalvia): Phylogenetic relationships and morphological evolution within the subfamilies Clinocardiinae, Lymnocardiinae, Fraginae and Tridacninae. *Malacologia* **40:** 321–373.

Sugiura, Y. 1964. On the life history of rhizostome medusae. II. Indispensability of zooxanthellae for strobilation in *Mastigias papua. Embryologia* **8:** 223–233.

Trench, R. K., 1975. Of "leaves that crawl": functional chloroplasts in animal cells. *Soc. Exp. Biol. Symp.* **XXIX:** 229–265.

Trench, R. K., D. S. Wethey, and J. W. Porter. 1981. Observations on the symbiosis with zooxanthellae among the tridacnidae (Mollusca, Bivalvia). *Biol. Bull.* **161:** 180–198.

Yonge, C. M. 1936. Mode of life, feeding, digestion and symbiosis with zooxanthellae in the Tridacnidae. *Scientific Report, Great Barrier Reef Expedition* **1:** 283–331.

Yonge, C. M. 1953. Mantle chambers and water circulation in the Tridacnidae. *Proc. Zool. Soc. Lond.* **123:** 551–561.

Yonge, C. M. 1975. Giant clams. *Sci. Am.* **232:** 96–105.

Yonge, C. M. 1980. Functional morphology and evolution in the Tridacnidae. *Rec. Aust. Mus.* **33:** 735–777.

Reference: *Biol. Bull.* **200:** 344–350. (June 2001)

5-Hydroxytryptamine Stimulates Net Ca^{2+} Flux in the Ventricular Muscle of a Mollusc (*Busycon canaliculatum*) During Cardioexcitation

C. LEAH DEVLIN

Department of Biology, Penn State University, Abington College, Abington, Pennsylvania 19001

Abstract. Noninvasive, self-referencing calcium (Ca^{2+}) electrodes were used to study the mechanisms by which 5-hydroxytryptamine (5-HT) affects net Ca^{2+} flux across the sarcolemma of myocytes from ventricular trabeculae (from a marine gastropod, *Busycon canaliculatum*). Treatment of isolated trabeculae with 5-HT causes a net Ca^{2+} efflux, which is 30% blocked by verapamil. These findings suggest that the efflux is in part the result of a previous Ca^{2+} influx through L-type Ca^{2+} channels and is due to a rapid Ca^{2+} extrusion mechanism inherent to the sarcolemma of these myocytes. 5-HT-induced net Ca^{2+} efflux is also reduced by about 40% by treatment with a sodium (Na^{+})-free, lithium (Li^{+})-substituted saline, which shuts down the Na-Ca exchanger during Ca^{2+} extrusion. Cyclopiazonic acid (CPA), an inhibitor of the sarcoplasmic reticulum (SR) Ca^{2+} ATPase, almost completely abolishes the 5-HT-induced net Ca^{2+} efflux, suggesting that the SR rather than the extracellular pool is the primary Ca^{2+} reservoir serving 5-HT-induced excitation.

Introduction

The rhythmicity of molluscan cardiac muscle is regulated by numerous neurotransmitters and neuromodulatory agents, the most widely studied of these being the biogenic amine 5-hydroxytryptamine (5-HT), the tetrapeptide FMRFamide, and acetylcholine (ACh). Pharmacological application of 5-HT onto the isolated hearts of the gastropods *Busycon canaliculatum* (Hill, 1958; Huddart and Hill, 1996), *Lymnaea stagnalis* (Buckett *et al.*, 1990), and *Aplysia californica* (Liebeswar *et al.*, 1975) causes a dose-dependent increase in inotropic and chronotropic activity with a primary effect on long-duration chronotropic regulation. Underlying this potentiation in cardiac rhythmicity is an increase in the amplitude and frequency of cardiac action potentials as well as the coupled systolic force (Hill *et al.*, 1992). The combined anatomical, pharmacological, and physiological studies on the gastropods *Aplysia*, *Busycon*, and *Lymnaea* have provided overwhelming evidence that 5-HT acts as a cardioexcitatory neurotransmitter in this class of mollusc.

$^{45}Ca^{2+}$ efflux studies have been conducted on a variety of molluscan cardiac and smooth muscles to determine how Ca^{2+} ions may be mobilized by 5-HT during the process of contraction or relaxation (Bloomquist and Curtis, 1972, 1975; Koch and Greenberg, 1981; Sawada *et al.*, 1984; Ishii *et al.*, 1989). The present study uses a newer technique to study Ca^{2+} flux, noninvasive self-referencing Ca^{2+} electrodes, to determine possible mechanisms by which 5-HT affects trans-sarcolemmal net Ca^{2+} flux in the *Busycon* ventricle as a clue to understanding its role during the excitation-contraction (E-C) coupling in the gastropod heart. An earlier study focused on the action of FMRFamide on net Ca^{2+} flux in the ventricle of *Busycon canaliculatum* (Devlin, 1997), so we may be able to compare mechanisms working at putative Ca^{2+} pools accessed by 5-HT and FMRFamide to achieve the same end—enhanced cardiac performance.

Materials and Methods

Specimens of *Busycon canaliculatum*, the channeled whelk, were obtained on the day of each experiment from the Marine Resources Center of the Marine Biological Laboratory (MBL), Woods Hole, Massachusetts. All experiments were conducted at the National Institutes of Health BioCurrents Research Center located at the MBL.

Received 18 January 2000; accepted 17 February 2001.

E-mail: cld5@psu.edu

Preparation

The shell was completely cut away from the animal with bone forceps, exposing the heart and its enveloping opaque pericardium. The pericardium was opened, and the ventricle was removed by severing its connections to the aorta and atrium. The ventricle was opened and pinned down in a dish of natural seawater to expose the inner latticework of trabeculae. An individual trabecula was isolated with fine scissors from the inner wall of the ventricle and secured with minuten pins to a Sylgard well in a small recording chamber. The trabecula was bathed in a nominally Ca^{2+}-free artificial seawater (ASW) prepared according to the MBL formula (423 mM Na^{+}, 9.7 mM K^{+}, 9.9 mM Ca^{2+}, 51.2 mM Mg^{2+}, 538.6 mM Cl^{-}, 27 mM SO_4^{-2}, 2.3 mM HCO^{3-}). Magnesium was used to replace the 9.9 mM Ca^{2+} omitted from the Ca^{2+} -free ASW. The nominal (or background) amounts of Ca^{2+} ions still present in the Ca^{2+}-free ASW were typically 100 micromolar (μM) or less and were monitored continuously with a Ca^{2+} electrode throughout the experiment.

Ion flux measurement

The self-referencing ion electrode technique is used to detect *net* ion flux generated from a biological source, in this case, the sarcolemma of myocytes from a *Busycon* trabecula. The net ion flux across the membrane is the sum of both inward and outward ion movements. In the present experiments, electrodes loaded with a Ca^{2+}-specific ionophore (Fluka Chemika Ca^{2+} ionophore—cocktail A with the neutral carrier ETH 1001) were used to detect net Ca^{2+} flux (in pmol cm^{-2} s^{-1}) across the sarcolemma of the myocytes. The electrode was programmed with PC-based software (Ionprobe) to oscillate with an excursion of 10 μm and a slow frequency of 0.3 Hz; this minimized mixing of the bathing saline. The difference in voltage (μV) between the two ends of the excursion was measured and could be taken as corresponding to a Ca^{2+} concentration gradient, since the excursion was constant.

To construct the electrodes, borosilicate micropipettes were pulled from 1.5-mm-diameter glass capillaries (World Precision Instruments, Inc.), then back-filled with 100 mM $CaCl_2$ in 0.1% agar. The pipette was front-filled with calcium ionophore—cocktail A containing neutral carrier ETH 1001 (Fluka Chemika) to produce an ionophore column of 40 μm. A Ag/AgCl wire inserted into the back of the micropipette served as the coupling to the headstage. To calibrate the electrode prior to the experiment, the electrode was tested in 0.1 mM, 1 mM, and 10 mM Ca^{2+} solutions to check its Nernstian properties—that is, an approximate 28 mV difference per decade change in Ca^{2+} concentration. The return electrode was a Ag/AgCl wire inserted into a glass capillary containing 3 M KCl agar.

The electrode oscillated at right angles to the long axis of the trabecula and was positioned at two distances from the muscle surface. One electrode position was 500 μm away from the muscle surface. At this relatively great distance, Ca^{2+} flux from the ion source (*i.e.*, the muscle) cannot be detected. Thus, only the control, background levels of Ca^{2+} in the saline are recorded at this position. The second electrode position was only 5 μm from the muscle surface, so net Ca^{2+} flux could be measured directly at the sarcolemma. From the background level of Ca^{2+} ions in the bathing saline, the Ca^{2+} ion concentration gradient at the muscle surface, and the diffusion constant for Ca^{2+} ions, net Ca^{2+} ion flux was calculated using a modification of the Fick equation. The mathematical formulas used in the conversion of voltage to flux units, and other technical aspects and applications of the self-referencing electrode technique, are described by Smith *et al.* (1999).

Pharmacological agents

The neurotransmitter, 5-HT, and the L-type channel blocker, verapamil, were obtained from Sigma Chemical Company (St. Louis, MO). Verapamil was selected over other Ca^{2+} blockers because of its consistent antagonistic action on other invertebrate cardiac and smooth muscle types (Devlin 1993a, b, 1997, Devlin and Smith, 1996). Diltiazem or nifedipine, which often act as agonists in molluscan muscle preparations, were not used in this study. The Ca^{2+} channel agonist, Bay K 8644, and the sarco/endoplasmic reticulum Ca^{2+} ATPase (SERCA) inhibitor, cyclopiazonic acid (CPA), were obtained from Research Biochemicals International (Natick, MA). At the beginning of each experiment each drug was diluted in the nominal Ca^{2+}-free ASW to achieve the designated experimental concentration.

Experimental protocol

The following general protocol was used throughout the present experiments. An initial net Ca^{2+} efflux generated by 10^{-7} M 5-HT (the control) was recorded during a 3-min treatment; this net Ca^{2+} efflux immediately returns to basal levels when the 5-HT is washed from the trabecula by flushing with ASW for 20 to 30 min. Next, the trabecula was pretreated for 10 min with verapamil or Bay K 8644 (10^{-5} M) or other inhibitors (CPA or Li^{+} ASW). 5-HT (10^{-7} M) dissolved in solutions of verapamil or Bay K 8644 (10^{-5} M) or other inhibitors (CPA or Li^{+} ASW) was reapplied to the trabecula for a 3-min treatment period. The control, the initial response to 5-HT alone, was then compared to the response to 5-HT in the presence of the agonist, antagonist, or inhibitor. A *t*-test analysis was then performed.

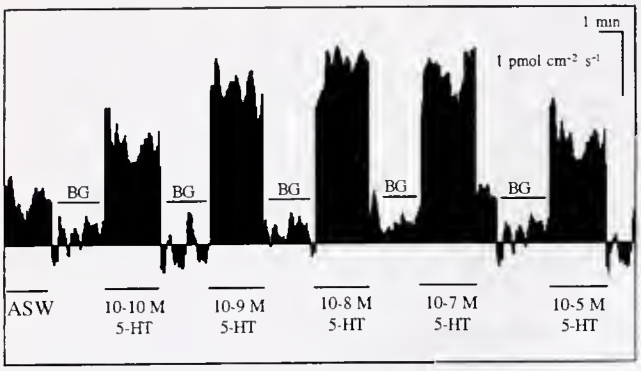

Figure 1. An experimental record showing a concentration-dependent effect of 5-HT on net Ca^{2+} efflux (in pmol cm^{-2} s^{-1}). ASW = spontaneous net Ca^{2+} flux measurement taken when the electrode was placed directly at the ion source, the trabecula, at a distance of less than 5 μm during treatment with an artificial Ca^{2+}-free seawater (ASW). 5-HT (10^{-10} *M* to 10^{-5} *M*) = net Ca^{2+} efflux measurement taken when the electrode was still placed directly at the trabecula at a distance of less than 5 μm during treatment with a range of 5-HT concentrations. Maximum net efflux was recorded between 10^{-8} *M* and 10^{-7} M 5-HT. Background (BG) = small oscillations around the baseline that were recorded when the electrode was placed 500 μm from the ion source, the trabecula.

Results

With the electrode placed 5 μm from the muscle surface, a basal net Ca^{2+} efflux of 1.21 ± 0.42 pmol cm^{-2} s^{-1} (n = 10) is recorded from the trabecula at rest in Ca^{2+}-free ASW. A range of 5-HT concentrations (10^{-12} *M* to 10^{-5} *M*) was then tested. Above a threshold of about 10^{-10} *M*, all concentrations of 5-HT enhance basal net Ca^{2+} efflux. The maximal efflux is induced at 5-HT between 10^{-8}–10^{-7} *M*; above 10^{-7} *M*, the net Ca^{2+} efflux is actually smaller than those induced by lower 5-HT concentrations (Fig. 1). Thus, the 5-HT receptor was desensitized by exposures to higher doses of its ligand. Because the effect of 10^{-7} *M* 5-HT does not desensitize the receptor and is completely reversible, it was chosen as the concentration to be challenged by various Ca^{2+} channel antagonists or agonists. A stable net Ca^{2+} efflux induced by 10^{-7} *M* 5-HT is on the order of 2.63 ± 1.01 pmol cm^{-2} s^{-1} (n = 8).

Effect of Ca^{2+}-channel antagonists or agonists on 5-HT-induced net Ca^{2+} efflux

To test the hypothesis that the Ca^{2+} ions mobilized by 5-HT during E-C coupling are from the extracellular saline, I studied the effects of two L-type Ca^{2+} channel drugs, an antagonist (verapamil) and an agonist (Bay K 8644), on the 5-HT response. In concentration-response experiments conducted with verapamil or Bay K 8644 alone, neither drug has a significant effect on net Ca^{2+} flux over the concentration range tested (10^{-12} to 10^{-5} *M*) (not shown). However, verapamil inhibits the action of 5-HT, reducing the response to 67% ± 16% (n = 3, $P < 0.025$) of the control (5-HT-induced net efflux measured prior to verapamil treatment) (Fig. 2). After verapamil was washed from the preparation, subsequent exposures to 5-HT are often enhanced. Bay K 8644 has no significant effect on the 5-HT response.

The effect of a Na^{+}-free, Li^{+}-substituted ASW on 5-HT responses

To determine whether the net Ca^{2+} efflux was mediated by the Na^{+}-Ca^{2+} exchanger, sodium (Na^{+}) ions were omitted from the bathing saline and replaced instead with an equivalent concentration (423 m*M*) of lithium (Li^{+}) ions; the rationale is that Li^{+} transverses the Na^{+} channel but cannot be substituted for Na^{+} in the Na^{+}-Ca^{2+} exchanger (Lipp and Niggli, 1994). The 5-HT-induced net Ca^{2+} efflux is reduced by the presence of Li^{+} ions to 57% ± 9% (n = 3, $P < 0.01$) that of control (the 5-HT response in normal ASW) (Fig. 3), implicating the Na^{+}-Ca^{2+} exchanger as a mechanism of Ca^{2+} extrusion during excitation by 5-HT. Li^{+} treatment alone reduced the basal net Ca^{2+} efflux to 69% ± 11% (n = 3, $P < 0.01$).

The effect of cyclopiazonic acid (CPA) on 5-HT responses

Figure 4 shows the effect of SERCA inhibitor CPA (10^{-5} *M*) on 5-HT-induced net Ca^{2+} efflux. The 5-HT response is

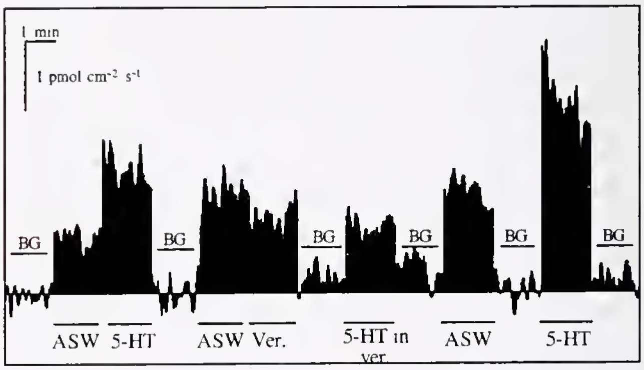

Figure 2. An experimental record showing that the 5-HT-induced net Ca^{2+} efflux signal (in pmol cm^{-2} s^{-1}) is inhibited by the L-type channel antagonist verapamil (10^{-5} *M*). ASW = spontaneous net Ca^{2+} efflux measurement taken when the electrode was placed directly at the ion source, the trabecula, at a distance of less than 5 μm. This signal was recorded prior to any drug treatment when the trabecula was bathed only in an artificial Ca^{2+}-free seawater (ASW). 5-HT (1st) = net Ca^{2+} efflux measurement taken when the electrode was placed directly at the trabecula during treatment with 10^{-7} *M* 5-HT. Verapamil = net Ca^{2+} efflux measurement taken when the electrode was placed directly at the trabecula after a 10-min treatment with verapamil (10^{-5} *M*). 5-HT in ver = net Ca^{2+} efflux measurement taken when the electrode was placed directly at the trabecula when treated with 5-HT (10^{-7} *M*) in verapamil (10^{-5} *M*). After verapamil was washed from the muscle, the final response to 5-HT (2nd) was greatly enhanced. All above recordings at the trabecula were taken at distance of 5 μm or less. Background (BG) = small oscillations around the baseline that were recorded when the electrode was placed 500 μm from the ion source, the trabecula.

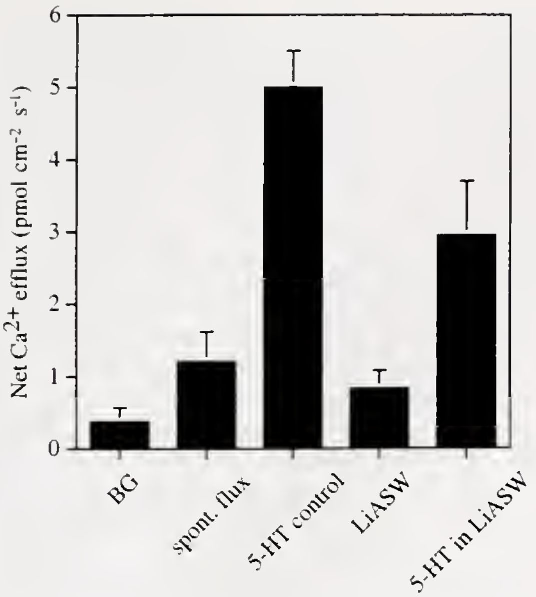

Figure 3. The inhibitory effect of LiASW on 5-HT-induced net Ca^{2+} efflux (in pmol cm^{-2} s^{-1}). First bar, background (BG): Net Ca^{2+} efflux measurement taken when the electrode was placed 500 μm from the ion source, the trabecula. Second bar, spontaneous flux: Net Ca^{2+} efflux measurement taken when the electrode was placed directly at the ion source, the trabecula, at a distance of less than 5 μm during treatment with an artificial seawater. Third bar, 5-HT control: Net Ca^{2+} efflux measurement taken when the electrode was still placed directly at the trabecula during treatment with 5-HT (10^{-7} *M*). Fourth bar: After washing the muscle for 30 min with artificial seawater, net Ca^{2+} efflux measurement was taken when the electrode was placed directly at the ion source, the trabecula, at a distance of less than 5 μm during treatment with a Na-free, Li-substituted artificial seawater (LiASW). Fifth bar, 5-HT in LiASW: Net Ca^{2+} efflux measurement taken when the electrode was still placed directly at the muscle during treatment with 5-HT (10^{-7} *M*) in LiASW. The data are means pooled from three muscles ± SD.

inhibited by CPA to 18.5% ± 10% ($n = 3$, $P < 0.005$) of the control (5-HT-induced flux prior to CPA treatment). CPA (10^{-5} *M*) alone also reduces basal net efflux to 76% ± 11% ($n = 3$, $P < 0.025$) that of the control. These data indicate that excitation by 5-HT relies more on Ca^{2+} ions from the sarcoplasmic reticulum (SR) than does spontaneous myogenicity. The inhibitory effect of CPA on 5-HT responses is completely reversible.

Discussion

The present experiments showed that 5-HT stimulates a net efflux of Ca^{2+} in the ventricular muscle of the whelk *Busycon canaliculatum*. The Ca^{2+} signal is sensitive to partial block by verapamil, which suggests that some of the Ca^{2+} movement is through sarcolemmal L-type Ca^{2+} channels. These L-type channels account for about 20% of the Ca^{2+} mobilized into the internal compartment during E-C coupling and may provide the source for Ca^{2+}-induced Ca^{2+} release from the SR, resulting in increased systolic force. The remaining 80% of Ca^{2+} ions are probably released from the SR, as shown by experiments with SERCA inhibitor CPA, which almost completely blocks the 5-HT response. Li^{+} ions, which act to block the Na-Ca exchange process, partially inhibit the 5-HT response, suggesting some reliance on the Na^{+}-Ca^{2+} exchanger during the Ca^{2+} extrusion process.

Verapamil, an L-type Ca^{2+} channel blocker, inhibits 5-HT-induced net Ca^{2+} efflux by about 30% in myocytes of the *Busycon* trabeculae. Similarly, in both gastropod (Huddart and Hill, 1996) and bivalve ventricles (Devlin, 1993)—where 5-HT enhances both inotropic and chronotropic responses—the effect of 5-HT is dependent on the movement of extracellular Ca^{2+} ions through an L-type channel, since 5-HT responses are blocked by verapamil (Devlin, 1993b). Although verapamil has no significant effect on basal net Ca^{2+} efflux in the *Busycon* ventricle, it does inhibit the 5-HT response, suggesting a use-dependent mechanism of block. This same use-dependent block by verapamil also occurs in many other invertebrate and vertebrate muscle preparations that were either chemically or electrically stimulated (Lee and Tsien, 1983; Zahradnik and Zachar, 1983; Vaghy *et al.*, 1988; Nanasi *et al.*, 1990).

Whereas verapamil inhibits the 5-HT-induced net Ca^{2+} efflux from the *Busycon* cardiac myocytes by about 30%, it

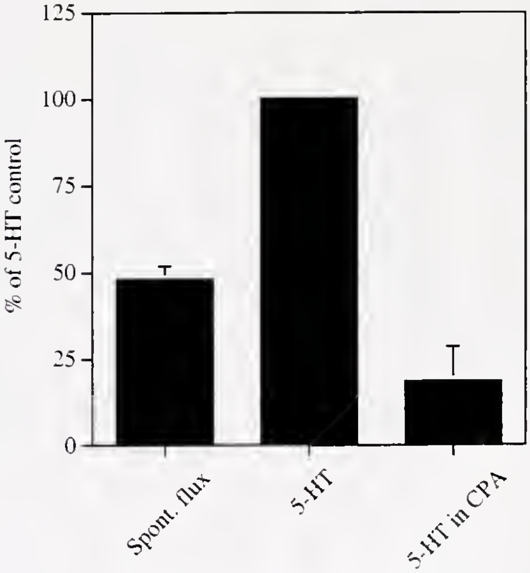

Figure 4. The inhibitory effect of SERCA inhibitor, cyclopiazonic acid (CPA) on 5-HT-induced net Ca^{2+} efflux (in pmol cm^{-2} s^{-1}). First bar, spontaneous flux: Net Ca^{2+} efflux measurement taken when electrode was placed directly at the ion source, the trabecula, at a distance of less than 5 μm during treatment with an artificial seawater. Second bar, 5-HT control: Net Ca^{2+} efflux measurement taken when the electrode was still placed directly at the trabecula during treatment with 5-HT (10^{-7} *M*). Third bar, 5-HT in CPA: Net Ca^{2+} efflux measurement taken when the electrode was still placed directly at the muscle during treatment with 5-HT (10^{-7} *M*) in CPA (10^{-5} *M*). The data are means pooled from three experiments on three ventricles ± SD.

reduces the FMRFamide response by 60% in the same preparation (Devlin, 1997). Therefore, 5-HT relies less on extracellular Ca^{2+} ions than does FMRFamide during the process of E-C coupling in the *Busycon* ventricle. The results also point to two distinct Ca^{2+} release mechanisms used by these respective neurotransmitters. However, both 5-HT and FMRFamide activate L-type Ca^{2+} channels (whether directly or indirectly remains to be determined) during cardioexcitation, since verapamil partially inhibits net Ca^{2+} efflux induced by either chemical. This finding also indicates that the net Ca^{2+} efflux is in part an effect of an earlier Ca^{2+} influx through L-type channels, possibly carried by the HVA (high-voltage activated) current described by Yeoman *et al.* (1999).

5-HT (from 10^{-9} to 10^{-6} *M*) depolarizes the heart cells from *Helix pomatia* (Kiss and S.-Rosza, 1978), *Aplysia dactylomela* (Sawada *et al.*, 1984), and *Dolabella auricularia* (Hill, 1974). This is the same concentration range in which 5-HT stimulates a net Ca^{2+} efflux from the ventricular myocytes of *B. canaliculatum.* Two depolarizing Ca^{2+} currents, designated the LVA (low-voltage activated), a T-type current, and the HVA (high-voltage activated), an L-type current, have been identified in the ventricular cells of the gastropod *Lymnaea* (Yeoman *et al.*, 1999). The sequential activation of the LVA and HVA currents provides the mechanism for pacemaking, AP generation, and a Ca^{2+} source for E-C coupling in the gastropod ventricle (Yeoman *et al.*, 1999). Since 5-HT increases the Ca^{2+}-dependent (and a Na^{+}-dependent) component of cardiac APs and coupled systolic force in bivalve ventricles (Devlin, 1993b), potentiation of an HVA-like current may be involved given that the Ca^{2+}-dependent component is sensitive to verapamil, diltiazem, and Bay K 8644. 5-HT also induces a Ca^{2+} current in *Aplysia* RB neurons (Pellmar, 1984) and mammalian neurons (Burnashev, 1998).

The relationship between the gastropod 5-HT receptor and coupled ion channels (such as the L-type channel) remains unclear because the subtypes that mediate excitatory responses in the gastropod heart are still being pharmacologically identified. However, a large body of evidence suggests that the 5-HT receptor from both gastropod (S.-Rozsa and Kiss, 1976; Kebabian *et al.*, 1979; Mandelbaum *et al.*, 1979; S.-Rozsa, 1984; Sawada *et al.*, 1984; Drummond *et al.*, 1985; Huddart and Hill, 1996) and bivalve hearts (Higgins, 1974, 1977; Higgins and Greenberg, 1974; Paciotti and Higgins, 1985) is associated with the adenylate cyclase-cAMP signaling pathway, which when stimulated produces an intracellular rise in cAMP. Higgins and Greenberg (1974) found that cAMP increases the phosphorylation of SR proteins that mediate Ca^{2+} sequestration into microsomes prepared from bivalve hearts. This then decreases the length of the diastolic phase of the cardiac cycle and primes the SR to release more Ca^{2+} ions during the next contraction. cAMP was reported to stimulate Ca^{2+} release from intracellular stores in molluscan neurons as well (Kononecko *et al.*, 1983). In contrast, FMRFamide does not appear to work through the adenylate cyclase-cAMP signaling pathway in gastropod ventricles (Drummond *et al.*, 1985; Huddart and Hill, 1996) but instead may mediate phosphoinositide hydrolysis, the process that has been implicated in some bivalve molluscs (Bayakly and Deaton, 1992).

Both 5-HT and some cAMP analogs stimulate $^{45}Ca^{2+}$ efflux from *Aplysia* ventricular myocytes during enhanced chronotropic and inotropic activities (Sawada *et al.*, 1984). In the present experiments, 5-HT also induces a large net Ca^{2+} efflux (on the order of 2.6 pmol cm^{-2} s^{-1}) from *Busycon* trabeculae that is recorded even when slow contractions of the trabecula are visible under the microscope. This net Ca^{2+} efflux is sustained over many hours. Sawada *et al.* (1984) also reported that excitatory drugs that stimulate contraction and cause simultaneous $^{45}Ca^{2+}$ efflux do not deplete cytoplasmic Ca^{2+} in the ventricular myocytes of *Aplysia.* These combined Ca^{2+} efflux data from *Busycon* and *Aplysia* ventricles suggest a substantial internal Ca^{2+} reserve such as the well-developed SR in the gastropod cardiac muscle described by Sanger (1979).

The 5-HT-induced Ca^{2+} efflux recorded from the *Busycon* ventricle is a large, stable signal that immediately returns to control levels upon washing with seawater. In contrast, in bivalve ventricles (from mussel, *Geukensia demissa*) that are excited by 5-HT, a transient $^{45}Ca^{2+}$ efflux corresponds to the onset of a 5-HT-induced contracture but is not sustained throughout the contracture (Koch and Greenberg, 1981). When 5-HT is washed from the *Geukensia* ventricle, a second large $^{45}Ca^{2+}$ efflux occurs, during which total tissue Ca^{2+} increases. Sawada *et al.* (1984) similarly noted that Ca^{2+} efflux does not necessarily reflect a reduction in cytoplasmic Ca^{2+}, because internal reserves may be available. A second application of 5-HT to the mussel heart does not induce a subsequent $^{45}Ca^{2+}$ efflux (Koch and Greenberg, 1981), whereas repeated efflux signals are stimulated by 5-HT in the gastropod heart. These findings reflect the large difference in complexity between the gastropod SR and the bivalve SR as sustainable Ca^{2+} pools.

The SERCA inhibitor, CPA, blocks 5-HT responses by 80% in the *Busycon* heart, suggesting that the SR is the major Ca^{2+} reservoir used during cardioexcitation by 5-HT. CPA acts by inhibiting the binding of Ca^{2+} ions at high-affinity binding sites on the SERCA; this shuts down both Ca^{2+} uptake and subsequent Ca^{2+} release at the SR of skeletal, cardiac (Balke *et al.*, 1994), and smooth muscle (Suzuki *et al.*, 1992). An indirect effect of inhibiting Ca^{2+}sequesteration at the SR is a reduction in Ca^{2+}-induced Ca^{2+} release; such a reduction is typically activated by the entry of extracellular Ca^{2+} through voltage-gated Ca^{2+} channels. In short, this would serve to limit the Ca^{2+}

needed to activate the contractile proteins. On the other hand, a reduction in Ca^{2+}-induced Ca^{2+} release also decreases the Ca^{2+}-dependent K^+ current ($I_{K\text{-}Ca}$), thus ultimately prolonging the excitability of vertebrate smooth muscle (Suzuki *et al.*, 1992). How CPA is affecting excitability in the mollusc ventricle warrants further investigation, especially considering its effectiveness in blocking Ca^{2+} efflux and the complete reversibility of its action.

The net Ca^{2+} efflux that was recorded during 5-HT treatment was composed primarily of Ca^{2+} released from the SR and secondarily of Ca^{2+}, from the extracellular fluid, that had previously entered the myocytes *via* an L-type current. This net Ca^{2+} efflux reflects the ability of the sarcolemma to rapidly redistribute Ca^{2+} ions outward, therefore preventing the toxic effects of Ca^{2+} overload, and reestablishing intracellular and extracellular Ca^{2+} gradients before the next successive depolarization and contraction. To determine if the net efflux was in part due to activity of the Na^+-Ca^{2+} exchanger, a Na^+-free, Li^+-substituted saline (Li^+ ASW) was used. The Li^+ ASW reduces the basal net Ca^{2+} efflux during normal, autorhythmic activity of the *Busycon* trabeculae by only 20%–30%, whereas the 5-HT and FMRFamide responses are inhibited during Li^+ treatment by 40% and 73%, respectively (Devlin, 1997). This difference in response suggests a greater reliance on the Na^+-Ca^{2+} exchanger during chemically mediated excitation than during spontaneous myogenic activity. These Li^+ substitution experiments on the gastropod trabeculae also show that Na^+ ions are a necessary stimulus for Ca^{2+} mobilization through voltage-gate channels or from an intracellular pool, perhaps during Na^+-induced Ca^{2+} release (Lipp and Niggli, 1994), and that they are also involved in the process of Ca^{2+} extrusion. The data from the present study are in agreement with studies on the Na^+-Ca^{2+} exchanger in other myocytes where the removal of extracellular Na^+ reduces Ca^{2+} efflux in guinea atrial cells (Reuter and Seitz, 1968) and in internally dialyzed myocytes (Miura and Kimura, 1989).

Acknowledgments

This work was supported by the Marine Biological Laboratory, M. G. F. Fuortes and Lucy B. Lemann Fellowships, the NASA Life Sciences Program, and a Pennsylvania State University Faculty Development Grant. Thanks are also extended to the staff of the N. I. H. BioCurrents Research Center at the MBL for their support in this research.

Literature Cited

Balke, C. W., T. M Egan, and W. G. Wier. 1994. Processes that remove calcium from the cytoplasm during excitation-contraction coupling in intact rat heart cells. *J. Physiol.* **474:** 447–462.

Bayakly, N. A., and L. E. Deaton. 1992. The effects of FMRFamide, 5-hydroxytryptamine and phorbol esters on the heart of the mussel *Geukensia demissa. J. Comp. Physiol. B.* **162:** 463–468.

Bloomquist, E., and B. A. Curtis. 1972. The action calcium-45 efflux from the anterior byssal retractor muscle of *Mytilus edulis. J. Gen. Physiol.* **59:** 476–485.

Bloomquist, E., and B. A. Curtis. 1975. ^{45}Ca efflux from anterior byssus retractor muscle in phasic and catch contraction. *Am. J. Physiol.* **229:** 1237–1243.

Buckett, K. J., G. J. Dockray, N. N. Osborne, and P. R. Benjamin. 1990. Pharmacology of the myogenic heart of the pond snail *Lymnaea stagnalis. J. Neurophysiol.* **63:** 1413–1425.

Burnashev, N. 1998. Calcium permeability of ligand-gated channels. *Cell Calcium* **24:** 325–332.

Devlin, C. L. 1993a. Acetylcholine-induced contractions in a holothurian (*Isostichopus badionotus*) smooth muscle are blocked by the calcium antagonists, diltiazem and verapamil. *Comp. Biochem. Physiol.* **106C:** 573–577.

Devlin, C. L. 1993b. An analysis of control of the ventricle of the mollusc *Mercenaria mercenaria.* II. Ionic mechanisms involved in excitation by 5-hydroxytryptamine. *J. Exp. Biol.* **179:** 63–75.

Devlin, C. L. 1997. A vibrating Ca^{2+}-selective electrode measures Ca^{2+} flux induced by the neuropeptide FMRFamide in a gastropod ventricle. *Comp. Biochem. Physiol.* **116A:** 93–100.

Devlin, C. L., and P. J. S. Smith. 1996. A non-invasive vibrating calcium-selective electrode measures acetylcholine-induced calcium flux across the sarcolemma of a smooth muscle. *J. Comp. Physiol. B* **166:** 270–277.

Drummond, G. I., S. Wernham, and K. Lukowiak. 1985. Stimulation of adenylate cyclase in the heart of *Aplysia californica* by biogenic amines. *Comp. Biochem. Physiol. C.* **80:** 129–133.

Higgins, W. J. 1974. Intracellular action of 5-hydroxytryptamine on the bivalve myocardium. I. Adenylate and guanylate cyclases. *J. Exp. Biol.* **190:** 99–110.

Higgins, W. J. 1977. 5-hydroxytryptamine-induced tachyphylaxis of the molluscan heart and concomitant desensitization of adenylate cyclase. *J. Cyclic Nucleotide Res.* **3:** 293–302.

Higgins, W. J., and M. J. Greenberg. 1974. Intracellular action of 5-hydroxytryptamine on the bivalve myocardium. II. Cyclic nucleotide-dependent protein kinases and microsomal calcium uptake. *J. Exp. Zool.* **190:** 305–316.

Hill, R. B. 1958. The effects of certain neurohumors and of other drugs on the ventricle and radula protractor of *Busycon canaliculatum* and on the ventricle of *Strombus gigas. Biol. Bull.* **115:** 471–482.

Hill, R. B. 1974. Effects of 5-hydroxytryptamine on action potentials and on contractile force in the ventricle of *Dolabella auricularia. J. Exp. Biol.* **61:** 529–539.

Hill, R. B., H. Huddart, and C. L. Devlin. 1992. Activation of a molluscan heart. Pp. 149–165 in *Phylogenetic Models in Functional Coupling of the CNS and the Cardiovascular System*, R. B. Hill and K. Kuwasawa, eds. S. Karger Medical and Scientific Publishers, Basel, Switzerland.

Huddart, H., and R. B. Hill. 1996. Modulatory mechanisms in the isolated internally perfused ventricle of the whelk, *Busycon canaliculatum. Gen. Pharmacol.* **27:** 809– 818.

Ishii, N., A. W. M. Simpson, and C. C. Ashley. 1989. Effects of 5-hydroxytryptamine (serotonin) and forskolin on intracellular free calcium in isolated and fura-2 loaded smooth-muscle cells from the anterior byssus retractor (catch) muscle of *Mytilus edulis. Pflugers Arch.* **414:** 162–170.

Kebabian, P. R., J. W. Kebabian, and D. O. Carpenter. 1979. Regulation of cyclic AMP in heart and gill of *Aplysia* by the putative neurotransmitters dopamine and serotonin. *Life Sci.* **24:** 1757–1764.

Kiss, T., and K. S.-Rozsa. 1978. Pharmacological properties of 5-HT receptors of the *Helix pomatia* L. (Gastropoda) heart muscle cells. *Comp. Biochem. Physiol. C.* **61:** 41–46.

Koch, R. A., and M. J. Greenberg. 1981. Calcium fluxes accompanying the action of 5-hydroxytryptamine on mussel hearts. *Comp. Biochem. Physiol. C.* **70:** 229–239.

Kononecko, N. I., P. G. Kostyuk, and A. D. Sherbatko. 1983. The effect of intracellular cAMP injections on stationary membrane conductance and voltage and time dependent ionic currents in identified snail neurons. *Brain Res.* **268:** 321–338.

Lee, K. S., and R. W. Tsien. 1983. Mechanism of calcium channel blockade by verapamil, D600, diltiazem and nitrendipine in single dialyzed heart cells. *Nature* **302:** 790–794.

Liebeswar, G., J. E. Goldman, J. Koester, and E. Mayeri. 1975. Neural control of the circulation in *Aplysia.* III. Neurotransmitters. *J. Neurophysiol.* **38:** 767–779.

Lipp, P., and E. Niggli. 1994. Sodium current-induced calcium signals in isolated guinea-pig ventricular myocytes. *J. Physiol.* **474:** 439–446.

Mandelbaum, D. E., J. Koester, M. Schonberg, and K. R. Weiss. 1979. Cyclic AMP mediation of the excitatory effect of serotonin in the heart of *Aplysia. Brain Res.* **177:** 388–394.

Miura, Y., and J. Kimura. 1989. Dependence on internal Ca and Na and competitive binding of external Na and Ca. *J. Gen. Physiol.* **93:** 1129–1145.

Nanasi, P. P., A. Varro, D. A. Lathrop, and M. Danko. 1990. Use-dependent action of antiarrhythmic drugs in frog skeletal muscle and canine cardiac Purkinje fiber. *Gen. Pharmacol.* **21:** 747–751.

Paciotti, G. F., and W. J. Higgins. 1985. Potentiation of the 5-hydroxytryptamine-induced increases in myocardial contractility in *Mercenaria mercenaria* ventricle by forskolin. *Comp. Biochem. Physiol. C* **80:** 325–329.

Pellmar, T. C. 1984. Enhancement of inward current by serotonin in neurons of *Aplysia. J. Neurophysiol.* **15:** 13–25.

Reuter, H., and N. Seitz. 1968. The dependence of calcium efflux from cardiac muscle on temperature and external ion composition. *J. Physiol.* **195:** 451–470.

S.-Rozsa, K. 1984. The pharmacology of molluscan neurons. *Prog. Neurobiol.* **23:** 79–150.

S.-Rozsa, K., and T. Kiss. 1976. Role of cyclic nucleotides in the effect of transmitters on the heart of *Helix pomatia* L. *Comp. Biochem. Physiol. C* **53:** 13–16.

Sanger, J. W. 1979. Cardiac fine structure in selected arthropods and molluscs. *Am. Zool.* **19:** 9–27.

Sawada, M., M. Ichinose, I. Ito, T. Maeno, and D. J. McAdoo. 1984. Effects of 5-hydroxytryptamine on membrane potential, contractility, accumulation of cAMP, and Ca^{2+} movements in anterior aorta and ventricle of *Aplysia. J. Neurophysiol.* **51:** 361–374.

Smith, P. J. S., K. Hammar, D. M. Porterfield, R. H. Sanger, and J. R. Trimarchi. 1999. A self-referencing, non-invasive, ion selective electrode for single cell detection of trans-plasma membrane calcium flux. *Microsc. Res. Tech.* **46:** 398–417.

Suzuki, M., K. Muraki, Y. Imaizumi, and M. Watanabe. 1992. Cyclopiazonic acid, an inhibitor of the sarcoplasmic reticulum Ca^{2+}-pump, reduces Ca^{2+}-dependent K^+ currents in guinea-pig smooth muscle cells. *Br. J. Pharmacol.* **107:** 134–140.

Vaghy, P. L., K. Itagaki, K. Miwa, E. McKenna, and A. Schwartz. 1988. Mechanism of action of calcium modulator drugs. Pp. 176–186 in *Calcium Antagonists: Pharmacology and Clinical Research,* Vol. 522. P. M. Vanhoutte, R. Paoletti, and S. Govoni, eds. New York Academy of Sciences, New York.

Yeoman, M. S., B. L. Brezden, and P. R. Benjamin. 1999. LVA and HVA Ca^{2+} currents in ventricular muscle cells of the *Lymnaea* heart. *J. Neurophysiol.* **82:** 2428–2440.

Zahradnik, I., and J. Zachar. 1983. Inhibitory effect of verapamil upon calcium and potassium currents in crayfish muscle membrane. *Gen. Physiol. Biophys.* **2:** 181–192.

INDEX

A

Achituv, Y., see O. Levy, 118
Adamczewska, Agnieszka M., and Stephen Morris, Ecology and behavior of *Gecarcoidea natalis,* the Christmas Island red crab, during the annual breeding migration, 305
Adamczewska, Agnieszka M., and Stephen Morris, Metabolic status and respiratory physiology of *Gecarcoidea natalis,* the Christmas Island red crab, during the annual breeding migration, 321
The adaptive bleaching hypothesis: experimental tests of critical assumptions, 51
Aerobic, 59
Aiptasia pallida, 127
Alviniconcha, 298
Amano, Shigetoyo, and Isao Hori, Metamorphosis of coeloblastula performed by multipotential larval flagellated cells in the calcareous sponge *Leucosolenia laxa*, 20
Anaerobic, 59
Analog VLSI, 243
Anemotaxis, 222
Annelida, 107
Antennae, 1
Artificial neural networks, 195
Asexual reproduction, 107
Audition, 227
Aurelia
  labiata, 92
  limbata, 92
Auditory micromechanics, 190
Axon, 252

B

Balanus amphitrite, 87
Barlow, Robert B., James M. Hitt, and Frederick A. Dodge, *Limulus* vision in the marine environment, 169
Barnacle, 87
Bartol, Ian K., Role of aerobic and anaerobic circular mantle muscle fibers in swimming squid: electromyography, 59
Beer, Amy-Jane, Claire Moss, and Michael Thorndyke, Development of serotonin-like and SALMFamide-like immunoreactivity in the nervous system of the sea urchin *Psammechinus miliaris*, 268
Behavior, 118, 160
  mating, 169
Biological sensor, 190
A biologically inspired controller for hexapod walking: simple solutions by exploiting physical properties, 195
Biomechanics, 1
Biomimetic, 227, 243
  robotics, 160
Birmingham, J. T., Increasing sensor flexibility through neuromodulation, 206
Bivalve pump, 77
Blazis, Diana E. J., and Frank W. Grasso, Introduction, Invertebrate Sensory Information Processing Workshop, 147
Body plan, 257
Bowman, John A. L., see Bernard B. Rees, 247
Brain function, 160
Breithaupt, Thomas, Fan organs of crayfish enhance chemical information flow, 150
Browne, Kenneth A., and Richard K. Zimmer, Controlled field release of a waterborne chemical signal stimulates planktonic larvae to settle, 87
Buckland-Nicks, John, see Ian G. Paterson, 261
Budding, 107

C

Ca^{2+} flux, 344
Calcification, 257
Carausius morosus, 195
Cardiac muscle, 344
Cephalopod, Antarctic, 67
Chadwick-Furman, N. E., see O. Levy, 118
Chahl, Javaan S., see Mandyam V. Srinivasan, 216
Chemical
  communication, 150
  cue, 87
  orientation, 150
  senses, 160, 211
  sensor, 222
Chemoreception, 211
Chemotaxis, 222
Christmas Island, 305, 321
Circadian rhythm, 169
Circular muscle, 59
Clam, giant, 336
Coeloblastula, 20
Coffroth, Mary Alice, see Robert A. Kinzie III, 51
COI, 92
Cold adaptation, 67
Communication, chemical, 150
Compound eye, 177
Computer simulation, 195
Constraint, 257
Controlled field release of a waterborne chemical signal stimulates planktonic larvae to settle, 87
Coral, 118
  bleaching, 51
Crab, land, 305, 321
Crayfish, 150, 201
Cricket, 184
Crinoids, 1
Cronin, Thomas W., and Justin Marshall, Parallel processing and image analysis in the eyes of mantis shrimps, 177
Cruse, Holk, see Josef Schmitz, 195
Crustacean, 211, 305, 321
Cryptic female choice, 261
Cytochrome oxidase *c* subunit I, 92

D

Dawson, Michael N., and David K. Jacobs, Molecular evidence for cryptic species of *Aurelia aurita* (Cnidaria, Scyphozoa), 92
Dean, Jeffrey, see Josef Schmitz, 195
Decapod, 281
Dendrite, 252
Derby, Charles D., and Pascal Steullet, Why do animals have so many receptors? The role of multiple chemosensors in animal perception, 211
Development, 257, 268
Development of host- and symbiont-specific monoclonal antibodies and confirmation of the origin of the symbiosome membrane in a cnidarian–dinoflagellate symbiosis, 127

Development of serotonin-like and SALMFamide-like immunoreactivity in the nervous system of the sea urchin *Psammechinus miliaris*, 268

Devlin, C. Leah, 5-Hydroxytryptamine stimulates net Ca^{2+} flux in the ventricular muscle of a mollusc *(Busycon canaliculatum)* during cardioexcitation, 344

Dodge, Frederick A., see Robert B. Barlow, 169

E

Echinoderm, 33, 268

Ecology, 305

Ecology and behavior of *Gecarcoidea natalis,* the Christmas Island red crab, during the annual breeding migration, 305

Egg size, 33

Electromyography, 59

Energy
- content, 33
- store, 321

Equilibrium pathways in crustacea, 155

Escape hatches for the clonal offspring of serpulid polychaetes, 107

Estuary, 87

Etnier, Shelley, Flexural and torsional stiffness in multi-jointed biological beams, 1

Evolution of development, 257

Evolutionary novelty, 257

Exercise, 305, 321

Eye, compound, 177

F

Factors controlling the expansion behavior of *Favia favus* (Cnidaria: Scleractinia): effects of light, flow, and planktonic prey, 118

Fan organs of crayfish enhance chemical information flow, 150

Farmer, Mark A., William K. Fitt, and Robert K. Trench, Morphology of the symbiosis between *Corculum cardissa* (Mollusca:Bivalvia) and *Symbiodinium corculorum* (Dinophyceae), 336

Favia, 118

Fujiwara, Y., see S. Kojima , 298

Finlets, 9

Fitt, William K., see Mark A. Farmer, 336

Flagellated cell, 20

Flexibility, 1

Flexural and torsional stiffness in multi-jointed biological beams, 1

Flow field, 150

Fluid mechanics, 160

Fraser, Peter J., Statocysts in crabs: short-term control of locomotion and long-term monitoring of hydrostatic pressure, 155

Fujikura, K., see S. Kojima, 298

Function and functional groupings of the complex mouth apparatus of the squat lobsters *Munida sarsi* Huus and *M. tenuimana* G. O. Sars (Crustacea: Decapoda), 281

Functional morphology, 281

G

Garm, A., and J. T. Hoeg, Function and functional groupings of the complex mouth apparatus of the squat lobsters *Munida sarsi* Huus and *M. tenuimana* G. O. Sars (Crustacea: Decapoda), 281

Gastropod, 257

Gecarcoidea, 305, 321

Gene expression, 247

GFP, 252

Giant clam, 336

Gill
- geometry, 77
- muscle, 77

Grasso, Frank W., Invertebrate-inspired sensory-motor systems and autonomous, olfactory-guided exploration, 160

Grasso, Frank W., see Diana E. J. Blazis, 147

Green fluorescent protein, 252

H

Hadfield, Michael G., see Carole S. Hickman, 257

Hashimoto, J., see S. Kojima, 298

Hearing, 190

Hemocyanin, cephalopod, 67

Hickman, Carole S., and Michael G. Hadfield, Larval muscle contraction fails to produce torsion in a trochoidean gastropod, 257

HIF-1, 247

Higgins, Charles M., Sensory architectures for biologically inspired autonomous robotics, 243

Hitt, James M., see Robert B. Barlow, 169

Hoeg, J. T., see A. Garm, 281

Honeybee, 216

Hori, Isao, see Shigetoyo Amano, 20

Hubbard, Allyn E., see David C. Mountain, 227

Hybridization, 97

Hybrids of two closely related tropical sea urchins (Genus *Echinometra*): evidence against postzygotic isolating mechanisms, 97

Hydrostatic pressure sensing, 155

Hydrothermal vent, 298

5-Hydroxytryptamine, 344

5-Hydroxytryptamine stimulates net Ca^{2+} flux in the ventricular muscle of a mollusc *(Busycon canaliculatum)* during cardioexcitation, 344

Hypoxia, 247

Hypoxia-inducible factor, 247

I

Immunocytochemistry, 127

Increasing sensor flexibility through neuromodulation, 206

Innovative biomechanics for directional hearing in small flies, 190

Insect flight, 216

Insights for robotic design from studies of the control of abdominal position in crayfish, 201

Internal transcribed spacer one, 92

Interspecific relationships between egg size and the level of parental investment per offspring in echinoderms, 33

Invertebrate sensory information processing: implications for biologically inspired autonomous systems, a workshop, 145

Invertebrate-inspired sensory-motor systems and autonomous, olfactory-guided exploration, 160

Ishida, H., T. Nakamoto, T. Moriizumi, T. Kikas, and J. Janata, Plume-tracking robots: a new application of chemical sensors, 222

ISIP-BIAS Symposium, 145

ITS-1, 92

J

Jacobs, David K., see Michael N. Dawson, 92

Janata, J., see H. Ishida, 222

Jellyfish, 92

K

Katsuyama, Y., see T. Okada, 252

Kempf, Stephen C., see Timothy S. Wakefield, 127

Kikas, T., see H. Ishida, 222

Killifish, 247

Kindermann, Thomas, see Josef Schmitz, 195

Kinematics, 9

Kinzie, Robert A., III, Michelle Takayama, Scott R. Santos, and Mary Alice Coffroth, The adaptive bleaching hypothesis: experimental tests of critical assumptions, 51

Kojima, S., R. Segawa, Y. Fujiwara, K. Fujikura, S. Ohta, and J. Hashimoto, Phylogeny of hydrothermal-vent–endemic gastropods, *Alviniconcha* spp., from the Western Pacific revealed by mitochondrial DNA sequences, 298

L

Lactate dehydrogenase, 247
Land crab, 305, 321
Landing, 216
Landing strategies in honeybees and possible applications to autonomous airborne vehicles, 216
Larva, 20, 87, 257
Larval collector, 87
Larval muscle contraction fails to produce torsion in a trochoidean gastropod, 257
Lauder, George V., see Jennifer C. Nauen, 9
Levy, O., L. Mizrahi, N. E. Chadwick-Furman, and Y. Achituv, Factors controlling the expansion behavior of *Favia favus* (Cnidaria: Scleractinia): effects of light, flow, and planktonic prey, 118
Life history, 33
Limulus, 169
Limulus vision in the marine environment, 169
Load compensation feedback control loops, 201
Lobster, 211
Locomotion, 9, 195
  central control of, 155
Lolliguncula brevis, 59

M

MacIsaac, S. Stanley, see T. Okada, 252
Macmillan, David L., and Blair W. Patullo, Insights for robotic design from studies of the control of abdominal position in crayfish, 201
Macro-video, 281
Marshall, Justin, see Thomas W. Cronin, 177
Mating behavior, 169
McEdward, L. R., and K. H. Morgan, Interspecific relationships between egg size and the level of parental investment per offspring in echinoderms, 33
Medler, Scott, and Harold Silverman, Muscular alteration of gill geometry *in vitro:* implications for bivalve pumping processes, 77
Meinertzhagen, I. A., see T. Okada, 252
Metabolic status and respiratory physiology of *Gecarcoidea natalis*, the Christmas Island red crab, during the annual breeding migration, 321
Metamorphosis, 20, 87
Metamorphosis of coeloblastula performed by multipotential larval flagellated cells in the calcareous sponge *Leucosolenia laxa*, 20
Microphone technology, 190
Microsatellite DNA, 261
Migration, 305, 321
Mitochondrial DNA, 298
Mizrahi, L., see O. Levy, 118
Modeling, 195
Molecular evidence for cryptic species of *Aurelia aurita* (Cnidaria, Scyphozoa), 92
Molecular phylogeny, 298
Mollusca, 261, 336, 344
Morgan, K. H., see L. R. McEdward, 33
Moriizumi, T., see H. Ishida, 222
Morphogenesis, 257
Morphology, functional, 281
Morphology of the symbiosis between *Corculum cardissa* (Mollusca: Bivalvia) and *Symbiodinium corculorum* (Dinophyceae), 336
Morris, Stephen, see Agnieszka M. Adamczewska, 305, 321
Moss, Claire, see Amy-Jane Beer, 268
Motor
  control, 195
  neuron, 252
Mountain, David C., and Allyn E. Hubbard, Sensing scenes with silicon, 227
Mouthparts, 281
Multiple paternity in *Littorina obtusata* (Gastropoda, Littorinidae) revealed by microsatellite analyses, 261
Munida
  sarsi, 281
  tenuimana, 281
Muscle
  circular, 59
  gill, 77
  receptor organ, 201
  smooth, 77
Muscular alteration of gill geometry *in vitro:* implications for bivalve pumping processes, 77

N

Nakamoto, T., see H. Ishida, 222
Nauen, Jennifer C., and George V. Lauder, Three-dimensional analysis of finlet kinematics in the chub mackerel *(Scomber japonicus)*, 9
Navigation, 216
Nervous system, 160
  stomatogastric, 206
Neural code, 169
Neurobiology, 268
Neuromodulation, 206
Neuromorphic, 243
Neuronal form in the central nervous system of the tadpole larva of the ascidian *Ciona intestinalis*, 252

O

Ohta, S., see S. Kojima, 298
Okada, T., S. Stanley MacIsaac, Y. Katsuyama, Y. Okamura, and I. A. Meinertzhagen, Neuronal form in the central nervous system of the tadpole larva of the ascidian *Ciona intestinalis*, 252
Okamura, Y., see T. Okada, 252
Olfaction, 150, 160, 211, 227
Optic flow, 216
Optomotor, 184
Orientation, chemical, 150
Oxygen, 247
  transport, 67

P

Panulirus, 211
Parallel processing and image analysis in the eyes of mantis shrimps, 177
Partridge, Vanessa, see Ian G. Paterson, 261
Paterson, Ian G., Vanessa Partridge, and John Buckland-Nicks, Multiple paternity in *Littorina obtusata* (Gastropoda, Littorinidae) revealed by microsatellite analyses, 261
Patullo, Blair W., see David L. Macmillan, 201
Pearse, John S., see M. Aminur Rahman, 97
Peptide, 87
Perception, 211
Pernet, Bruno, Escape hatches for the clonal offspring of serpulid polychaetes, 107
Phonotaxis, 184
Phylogeny of hydrothermal-vent–endemic gastropods, *Alviniconcha* spp., from the Western Pacific revealed by mitochondrial DNA sequences, 298
Physiology, 321
Plume-tracking robots: a new application of chemical sensors, 222
Polyandry, 261
Polychaeta, 107
Pörtner, H. O., see S. Zielinski, 67
Position control, 201
Procambarus clarkii, 150

R

Rahman, M. Aminur, Tsuyoshi Uehara, and John S. Pearse, Hybrids of two closely related tropical sea urchins (Genus *Echinometra*): evidence against postzygotic isolating mechanisms, 97
Redundancy, 211

Rees, Bernard B., John A. L. Bowman, and Patricia M. Schulte, Structure and sequence conservation of a putative hypoxia response element in the lactate dehydrogenase-B gene of *Fundulus*, 247
Representation, 184
Reproduction, asexual, 107
Robert, Daniel, Innovative biomechanics for directional hearing in small flies, 190
Robot, 184, 206, 222
Robotics, 160, 216, 243
Role of aerobic and anaerobic circular mantle muscle fibers in swimming squid: electromyography, 59

S

Santos, Scott R., see Robert A. Kinzie III, 51
Sartoris, F. J., see S. Zielinski, 67
Scene analysis, 227
Schmitz, Josef, Jeffrey Dean, Thomas Kindermann, Michael Schumm, and Holk Cruse, A biologically inspired controller for hexapod walking: simple solutions by exploiting physical properties, 195
Schulte, Patricia M., see Bernard B. Rees, 247
Schumm, Michael, see Josef Schmitz, 195
Scombrid fishes, 9
Segawa, R., see S. Kojima, 298
Senses, chemical, 211
Sensing scenes with silicon, 227
Sensor, 206
  artificial, 177
  chemical, 222
Sensory, 211
Sensory architectures for biologically inspired autonomous robotics, 243
Sensory-motor feedback, 201
Serial EM, 252
Setae, 281
Settlement, 87
Sibling species, 92
Silicon, 227
Silverman, Harold, see Scott Medler, 77
Smooth muscle, 77
Sperm
  competition, 261
  storage, 261
Sponge, calcareous, 20
Squid, 59
Srinivasan, Mandyam V., Shaowu Zhang, and Javaan S. Chahl, Landing strategies in honeybees and possible applications to autonomous airborne vehicles, 216
Statocysts in crabs: short-term control of locomotion and long-term monitoring of hydrostatic pressure, 155
Steullet, Pascal, see Charles D. Derby, 211
Stick insect, 195
Stiffness
  flexural, 1
  torsional, 1
Stomatogastric nervous system, 206
Stomatopod crustacean, 177
Stretch receptor, 206
Structure and sequence conservation of a putative hypoxia response element in the lactate dehydrogenase-B gene of *Fundulus*, 247
Symbiodinium
  bermudense, 127
  corculorum, 336
Symbiosis, 127, 336

T

Takayama, Michelle, see Robert A. Kinzie III, 51
Temperature, 67
Temperature effects on hemocyanin oxygen binding in an Antarctic cephalopod, 67
Thorndyke, Michael, see Amy-Jane Beer, 268
Three-dimensional analysis of finlet kinematics in the chub mackerel *(Scomber japonicus)*, 9
Torsion, 257
Trench, Robert K., see Mark A. Farmer, 336
Tube growth, 107
Turbulence, 160

U

Uehara, Tsuyoshi, see M. Aminur Rahman, 97
Ultrastructure, 336
Urchin, 97
Urochordate, 252

V

Vector coding in the nervous system, 155
Veliger, 257
View from the boundary, 184
Vision, 169, 216, 227
  chip, 243
  color, 177
Visual ecology, 177
VLSI, 227, 243

W

Wakefield, Timothy S., and Stephen C. Kempf, Development of host- and symbiont-specific monoclonal antibodies and confirmation of the origin of the symbiosome membrane in a cnidarian–dinoflagellate symbiosis, 127
Water pumping, 77
Webb, Barbara, View from the boundary, 184
Western Pacific, 298
Why do animals have so many receptors? The role of multiple chemosensors in animal perception, 211

Z

Zhang, Shaowu, see Mandyam V. Srinivasan, 216
Zielinski, S., F. J. Sartoris, and H. O. Pörtner, Temperature effects on hemocyanin oxygen binding in an Antarctic cephalopod, 67
Zimmer, Richard K., see Kenneth A. Browne, 87
Zooxanthellae, 51, 118, 336

'081 22

The Ultimate Deconvolution Machine.

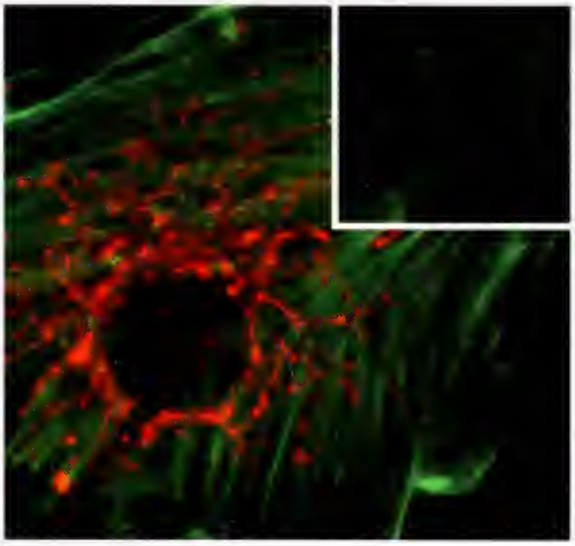

Original Widefield Image.

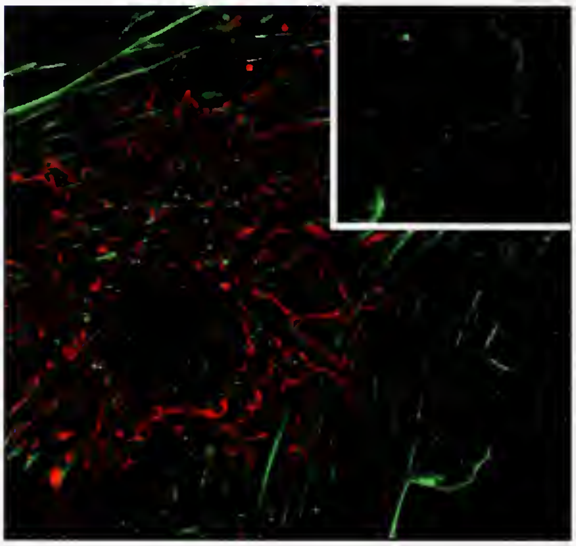

Iterative DCV (measured PSF):
Maximum Likelihood; 15 CG Iterations; Regularized.

When image quality is essential and capturing lost information is a must, Carl Zeiss 3D Deconvolution system is the answer.

Our fast, intuitive software allows reassignment of non-focal haze, noise and blur to provide image restoration to its brilliant best. Choose between theoretically calculated or measured PSF, iterative or non-iterative method, and the Zeiss 3D Deconvolution will do the rest.

Whether conventional widefield or confocal fluorescence imaging, your own 3D deconvolution system from Zeiss takes you to new heights of image fidelity.

Let us show you how!

For immediate demonstration, call **800-233-2343**.

Carl Zeiss, Inc.
Microscopy & Imaging Systems
One Zeiss Drive
Thornwood, NY 10594

800.233.2343
Fax 914.681.7446
micro@zeiss.com
www.zeiss.com/micro

ZEISS

MBL/WHOI LIBRARY
WH 1B38 T